50 Copies

NATIONAL AERONAUTICS AND SPACE ADMINISTRATION

*Technical Report 32-1203*

# *Mariner Venus 67 Final Project Report: Volume I. Launch Through Midcourse Maneuver*

GPO PRICE $ _____

CFSTI PRICE(S) $ _____

Hard copy (HC) 3.00

Microfiche (MF) .65

ff 653 July 65


FACILITY FORM 602

N68-33060 (ACCESSION NUMBER) (THRU)

114 (PAGES) 1 (CODE)

CR-96382 (NASA CR OR TMX OR AD NUMBER) 31 (CATEGORY)

SEP 1968

RECEIVED NASA STI FACILITY INPUT BRANCH



JET PROPULSION LABORATORY

CALIFORNIA INSTITUTE OF TECHNOLOGY

PASADENA, CALIFORNIA



June 15, 1968

NATIONAL AERONAUTICS AND SPACE ADMINISTRATION

*Technical Report 32-1203*

# *Mariner Venus 67 Final Project Report: Volume I. Launch Through Midcourse Maneuver*

JET PROPULSION LABORATORY
CALIFORNIA INSTITUTE OF TECHNOLOGY
PASADENA, CALIFORNIA

June 15, 1968

*TECHNICAL REPORT 32-1203*

Copyright © 1968
Jet Propulsion Laboratory
California Institute of Technology

Prepared Under Contract No. NAS 7-100
National Aeronautics & Space Administration

PRECEDING PAGE BLANK NOT FILMED.

# Preface

*Mariner V* was successfully launched from the AFETR at 02:01 EDT, June 14, 1967 On October 19, the spacecraft encountered the planet Venus; the closest approach distance during the encounter phase was 2543 miles. All systems functioned as planned.

The primary objective of the *Mariner* Venus 67 project was to conduct a flyby mission to Venus to obtain scientific information that would complement and extend the results obtained by *Mariner II*, relevant to determining the origin and nature of Venus and its environment. Secondary objectives were to acquire engineering experience in converting (and operating) a spacecraft, designed for a flight to Mars, into one flown to Venus, and to obtain information on the inteplanetary environment during a period of increasing solar activity.

The single spacecraft, prepared by converting the spare *Mariner IV* spacecraft, carried seven scientific experiments. Two of the experiments (S-band occultation and celestial mechanics) used tracking and telecommunications facilities, but no special flight instruments; the dual-frequency radio experiment required a new instrument package, and the remaining instruments were essentially as developed for the *Mariner* Mars 1964 mission.

All *Mariner* Venus 67 project objectives were fully achieved, attesting to the high degree of technical skill exercised on the part of the participating project personnel.

This volume (Vol. I) and its companion volume (Vol. II) comprise the *Mariner* Venus 67 Final Project Report which describes the formation and organization of the project, mission planning, spacecraft design and development, mission operations, and tracking and data acquisition from project inception until termination of tracking activities after encounter and data playback.

The data returned by *Mariner V* have greatly expanded the store of information about the veiled planet and will significantly deepen our insight as to the history of its evolution. It is also hoped that the operations and results documented in this report will be a useful reference to those planning future space missions.

W H. Pickering

PRECEDING PAGE BLANK NOT FILMED.

# Contents


**I. Introduction** 1

A. History of *Mariner* Projects 1

1. Related missions 1

2. *Mariner V* mission 4

B. Project Objectives 4

C. Mission Description and Characteristics 5

**II. Project Organization and Management** 7

A. General 7

B. Management Structure 7

1. National Aeronautics and Space Administration (NASA) 7

2. Jet Propulsion Laboratory (JPL) 7

3. Lewis Research Center (LeRC) 7

4. Kennedy Space Center (KSC) 20

5. Other support 20

6. Industrial management 20

C. System Responsibilities 20

D. Coordinating Bodies 24

1. Lunar and planetary projects tracking, telemetry, and communications panel 24

2. Spacecraft launch-vehicle interface working group 24

3. NASA *Atlas/Agena* launch-operations working group 24

E. Master Control Agreements 24

1. NASA management instructions 24

2. The JPL contract 24

3. Other standard practices and regulations 27

F. JPL Planning and Implementation 27

1. Interface planning and control 27

2. Meetings 27

3. Documentation 28

4. Design control 28

5. Trouble-failure reporting 28

6. Reviews 28

## Contents (contd)


G. Schedules and Progress Reports 29

1 Headquarters reports 32

2. Schedules 32

3. Flow plans 32

4. Special data banks 32

**III. Flight Path Analysis and Mission Planning** 35

A. Trajectory Design 35

1. Launch and arrival date selection 35

2. Design objectives 35

3. Arrival date characteristics 35

4. Resulting arrival date 36

5. Launch period 36

B. Aiming Point Considerations 36

1 Scientific experiments 36

2. Engineering constraints 36

3. Aiming region 36

4. Aiming point selection 37

C. Trajectory Characteristics 39

1. Near-earth trajectory 39

2. Heliocentric trajectory 41

3. Near-Venus trajectory 42

D. Effect of Antenna Design on Mission Planning 48

1. Choice of enter and exit occultation offset angles 48

2. Value functions 49

3. Description of the model 50

4. Net return from the occultation experiment 50

5. Value of the stored data 51

6. Results 51

7 Conclusions 52

E. Planetary Quarantine Analysis 53

1. General 53

2. Mathematical model description 53

3. Probability of spacecraft ejecta contaminating Venus 54

## Contents (contd)


4. Mission profile 55

5. Probability of accidental vehicle impact 56

F. Trajectory Correction Analysis 59

1. Pre-flight analysis of midcourse maneuver 59

2. Midcourse maneuver operations program 61

3. Discussion of the actual maneuver 62

**IV. Spacecraft System** 65

A. Introduction 65

B. Payload Selection 65

C. System Design and Change Control 69

1 Considerations in changing Mars design for any Venus mission 70

2. Considerations in changing design for *Mariner* Venus 67 mission 72

3. Considerations in changing basic *Mariner IV* design to enhance reliability and/or operational capability 81

4. Mechanical configuration 87

5. Project design control 88

6. Telemetry calibration 88

7 Spacecraft weight control 91

8. Redundancy techniques for increasing probability of success at system level 95

D. Science Subsystem Description and Development 100

1 Helium magnetometer scientific objective 100

2. Ultraviolet photometer scientific objective 104

3. Trapped radiation detector scientific objectives 110

4. Plasma probe scientific objectives 115

5. Dual-frequency receiver scientific objectives 118

6. Data automation subsystem 123

7 Science operational support equipment objectives and requirements 131

8. Test data handling procedures 136

E. Telecommunications Subsystem Description and Development 137

1. Dual-frequency receiver antenna subsystem 137

2. S-band antenna implementation 145

3. *Mariner V* flight command subsystem 154

## Contents (contd)


4. Tape recorder susbsystems 157

5. Flight telemetry subsystem 160

6. Radio subsystem 164

F Guidance and Control Subsystem Description and Development 181

1. Central computer and sequencer 181

2. Spacecraft control subsystems 188

3. Power subsystem 229

4. OSE modification and test operations 246

5. Star identification program 249

G. Propulsion and Pyrotechnic Subsystem Description and Development 250

1. Propulsion subsystem 250

2. Pyrotechnic subsystem 254

H. Engineering Mechanics 256

1 Structure subsystem 256

2. Fasteners 259

3. Cabling subsystem 259

4. Temperature control subsystem design 268

5. Mechanical devices subsystem 280

6. Spacecraft operational support equipment 283

7 Structure and dynamics, design, analysis, and test 285

8. Electronic packaging 289

9. Materials 296

10. Weight and center of gravity determination 299

11 Launch vehicle mechanical interface 301

12. Drawing lists 303

I. Telecommunications/DSIF Compatibility Tests 303

1 Link calibration 304

2. RF subsystem test 305

3. Telemetry subsystem test 307

4. Command system test 311

J. EMI Reductions 312

1. Integration program 313

2. Subsystem noise investigations 316

## Contents (contd)


K. Assembly and System Level Environmental Test Program 325

1 Realization of environmental test program goals 325

2. Detailed review of a typical subsystem environmental test program 326

3. Review of the electromagnetic interference program 326

4. Magnetic control program 335

L. System Test and Launch Operations 337

1 Test operations 337

2. Facilities 344

3. System test complex data system 344

4. Microbial sampling program for *Mariner V* 345

M. Reliability Program 352

1 Reliability control 352

2. Problem/failure reporting 352

3. Environmental testing 355

4. Reliability prediction and failure-mode analysis 355

5. Reliability-oriented project level reviews 355

6. Parts management 356

7 Post-launch reliability analysis 356

N. Quality Assurance Program 356

1 Organization 356

2. Requirements and reporting 356

3. Failure reporting 357

4. Subsystems 357

O. Parts Acquisition and Screening 364

1 Approach 364

2. Electronic parts failure analysis 367

3. Approved electronic parts list 371

4. Recommendations 371

P System Test Complex Data System 374

1. Evolution from *Mariner* Mars 1964 system 374

2. Configuration and system description 376

3. Development and capabilities 379

4. Performance and problem summary 379

## Contents (contd)


Q. OSE Development and Use 380

1 OSE system design changes 380

2. Grounding investigations 381

**V. Launch Vehicle Integration** 383

A. Program Initiation and Definition 383

1 Ground rules and constraints 383

2. Launch period and injection energy available 385

3. Launch readiness contingency plan 385

B. Launch Vehicle 385

1 Shroud 386

2. Adapter 386

C. Launch Vehicle Integration 386

D. Launch Pad Selection and Planning 387

1 Launch pad acoustic environment 387

2. Launch pad modifications and validation 387

E. Launch Vehicle System Problem Areas and Failures 388

F. Results 388

G. Recommendations 389

**VI. Mission Operations System** 391

A. System Definition 391

B. System Concept and Configuration 391

1 Basic design guidelines 391

2. MOS design team 391

3. Configurations 392

4. Configuration control and monitoring 392

C. Complementary Analysis Teams 392

D. Mission-Related Hardware Development 393

1 Ground command subsystem 393

2. Ground telemetry subsystem 396

3. MSA digital-to-analog converter 399

E. Computer Program Development 408

1 *Overall software development plan* 408

## Contents (contd)


2. Software system description 408

F. Mission Operations Testing and Training 417

1. Development tests 417

2. MOS–TDS integration and compatibility tests 417

3. Spacecraft–MOS compatibility tests 417

4. Operations training and readiness 417

G. FPAC Early Mission Performance 419

1. Tracking data coverage 419

2. Premaneuver orbit determination results 423

3. Midcourse maneuver analysis based on orbit information 428

4. Trajectory analysis 429

H. SPAC Early Mission Performance 430

1. Chronology 430

2. Detailed spacecraft performance 432

I. SSAC Early Mission Performance (Science Instruments) 437

1. Helium magnetometer flight results 437

2. Plasma probe flight results 437

3. Ultraviolet photometer 438

4. Trapped radiation detector 438

5. Dual-frequency receiver 438

**VII. Mission Analysis Preparations and Activities During Countdown and Launch** 439

A. Precountdown Preparation 439

B. Countdown and Launch Activities 442

C. Launch Constraints Planning and Near-Earth Coverage Analysis 442

**Appendix A.** Launch Sequence Document 449

**Appendix B.** Project Management Report 461

**Appendix C.** *Mariner* Venus 67 Launch Constraints 479

**Glossary** 483

**References** 487

## Contents (contd)

### Tables


I-1. Access difficulty in conversion of the *Mariner IV* spacecraft 4

I-2. Spacecraft changes 5

I-3. *Mariner Venus 67* principal scientific investigators 6

II-1. Composite problem (P) list 30

III-1. *Mariner V* launch period characteristics (biased aiming point) 40

III-2. Heliocentric trajectory characteristics 42

III-3. Near-Venus trajectory characteristics 43

III-4. Scientific experiment values 50

III-5. Encounter parameters of pre- and post-midcourse orbits 60

III-6. Midcourse maneuver performance 63

IV-1. Telemetry channel assignment–temperature measurements 79

IV-2. Engineering change requirement (ERC) summary 91

IV-3. Final calculated and measured spacecraft weight 97

IV-4. Final calculated M67-2 weights by subsystem 97

IV-5. Redundant equipment back-up sources for desired functions 97

IV-6. Command functions initiated by redundant signals 98

IV-7. *Mariner V* science instruments and ancillaries 100

IV-8. Instrument noise and offset 103

IV-9. Instrument calibration 104

IV-10. Frame readout identification 122

IV-11. *Data automation subsystem real-time word description* 124

IV-12. Data automation subsystem real-time status bits 127

IV-13. Test equipment functions 133

IV-14. Summary of DFR antenna parameters 139

IV-15. Comparison of *Mariner IV* and *Mariner V* TRS design specifications 157

IV-16. Sources of stop record pulses . . . 159

IV-17. Significant interferometer modes 169

IV-18. *Mariner V* radio system telemetry channel assignments 174

IV-19. Ranging phase delay of *Mariner V* RSS 178

IV-20. Spacecraft flight sequence differences 181

IV-21. Operating parameter of straylight simulator . . . . . 197

IV-22. Lens design parameters 201

## Contents (contd)

### Tables (contd)


IV-23. Solenoid operating characteristics 203

IV-24. Gas valve parameters 204

IV-25. Gas valve performance at 125 to −100°F 205

IV-26. Solar-panel response characteristics 207

IV-27 Spacecraft dynamical properties 207

IV-28. Planet sensor characteristics 213

IV-29. Launch events 219

IV-30. Attitude control cruise operating parameters 224

IV-31 Midcourse maneuver sequence 225

IV-32. Midcourse maneuver performance parameters 226

IV-33. Solar panel electrical performance summary 236

IV-34. Solar array performance 239

IV-35. Power conditioning inputs and outputs modifications 241

IV-36. Maximum power required from maneuver booster regulator 242

IV-37 Command and controls modifications 243

IV-38. Guidance and control OSE modifications 248

IV-39. *Mariner* Venus 67 electronic chassis summary 259

IV-40. *Mariner IV* to *Mariner V* flight harness conversion, comparison 264

IV-41 Comparison of flight data with predictions for science and appendages 278

IV-42. Summary of electronic assembly changes to convert *Mariner IV* to *Mariner V* 290

IV-43. Changes to *Mariner IV* electronic assembly handling and shipping containers 295

IV-44. Summary of measured weight and CG values for the M67-1 and M67-2 in the cruise configuration 303

IV-45. Results of residual phase modulation tests, *Mariner* Venus 67–DSIF compatibility test 306

IV-46. One-way to two-way RF lockup times *Mariner* Venus 67–DSIF compatibility test 307

IV-47 Two-way to one-way switchover times *Mariner* Venus 67–DSIF compatibility test 307

IV-48. Telemetry demodulator synchronization acquisition times, *Mariner* Venus 67–DSIF compatibility test 310

## Contents (contd)

### Tables (contd)


IV-49. Command acquisition test results, *Mariner* Venus 67–compatibility test 312

IV-50. Comparison of *Mariners IV* and *V* assembly level environmental test failures 325

IV-51 *Mariner* Venus 67 major environmentally-induced test failure summary, assembly level 327

IV-52. Requirements versus test external environment simulation (M67-1 system test) 333

IV-53. Requirements versus test external environment simulation (M67-1 simulated countdown) 334

IV-54. Requirements versus test external environment simulation (M67-1 pyrotechnics and shock test) 335

IV-55. Requirements versus test external environment simulation (M67-2 system test) 336

IV-56. Comparison of spacecraft perm fields 337

IV-57 Comparison of pre- and post-flight spacecraft fields 337

IV-58. Spacecraft problems during system test operations that led to spacecraft design changes 343

IV-59 Environmental fallout—mean number of aerobic spores accumulated during various spacecraft exposure periods 349

IV-60. Post-environmental teardown inspection 361

IV-61 Subsystem usage part type summary 365

IV-62. Program summary—parts acquisition and screening 368

IV-63. Part failure analyses arranged by PFR number 368

IV-64. Part failure analyses not related to specific PFR 371

IV-65. Summary of spacecraft parts count by subsystem 372

IV-66. Summary of spacecraft parts reliability ratings by subsystem 373

IV-67 Computer system reliability (up-time) 380

VI-1 Ground command subsystem PFR summary 394

VI-2. Ground telemetry subsystem PFR summary 397

VI-3. Analog recorder channel assignments 407

VI-4. DSIF tracking data used in computations of *Mariner V* premaneuver orbits 419

VI-5. *Initial conditions of Mariner V premaneuver orbits* 424

VI-6. Target parameters of *Mariner V* premaneuver orbits 425

## Contents (contd)

### Tables (contd)


VI-7 Preliminary *Mariner V* solutions for solar radiation 428

VI-8. Geocentric characteristics of *Mariner V* trajectory 430

VI-9 Chronology of *Mariner V* performance 431

VII-1 Launch phase analyst's launch plan for *Mariner V* 441

VII-2. Launch time report for June 14–17 as of June 7, 1967 442

VII-3. The figure of merit (NCV) for each station 444


### Figures


I-1 *Mariner V* spacecraft 2

I-2. Ascent trajectory profile 3

I-3. Sequence of events to Canopus acquisition 3

II-1 NASA administration chart 8

II-2. NASA space science and applications chart 9

II-3. JPL senior staff organization chart 10

II-4. *Mariner* Venus 67 project organization chart 11

II-5. *Mariner* Venus 67 detailed project organization chart 13

II-6. Space flight operations organization 13

II-7 Tracking and data systems organization 15

II-8. Lewis Research Center organization chart 17

II-9 *Agena* project office organization, NASA 19

II-10. *Agena* missions office, Lockheed Missile and Space Company 20

II-11 Summary of project responsibilities 21

II-12. *Mariner* Venus 67 project organizational relationship 23

II-13. Functional relationship of key individuals 25

II-14. *Mariner* Venus 67 work breakdown structure 26

II-15. Documentation relationships for development of *Mariner V* spacecraft system 29

II-16. Reporting structure 31

II-17 *Mariner* Venus 67 project, spacecraft system schedule 33

III-1. Injection energy vs launch date 36

III-2. Definition of aiming-zone parameters 37

## Contents (contd)

### Figures (contd)


III-3. Aiming zone and constraint regions for June 12, 1967 launch 38

III-4. Launch time vs launch date 39

III-5. Time from launch to injection vs launch date 39

III-6. Definition of spacecraft coordinate system 41

III-7 Projection of heliocentric trajectory on ecliptic plane for June 12, 1967 launch 41

III-8. Projection of heliocentric trajectory on ecliptic plane for June 27, 1967 launch 41

III-9. Isometric view of near-Venus trajectory 43

III-10. Orthographic projections of near-Venus trajectory for June 12, 1967 launch 44

III-11 Orthographic projections of near-Venus trajectory for June 17, 1967 launch 45

III-12. Orthographic projections of near-Venus trajectory for June 22, 1967 launch 46

III-13. Orthographic projections of near-Venus trajectory for June 27, 1967 launch 47

III-14. Ecliptic projection of near-Venus trajectory 48

III-15. Value function vs occultation cutoff altitude 49

III-16. Value function vs miss parameter $P$ 49

III-17 Value functions vs communications period after encounter 50

III-18. Pressure vs a function of altitude for GH-50 51

III-19. Atmosphere GH-50, beam path on antenna axis 51

III-20. Pressure at which occultation is cut off as a function of offset angle 52

III-21. Expected return as a function of $\eta$, offset angle for 10-day playback time 52

III-22. Expected return as a function of $\eta$, offset angle for 5-day recorder playback time 52

III-23. Spacecraft probability of impact 57

III-24. Launch vehicle probability of impact 58

III-25. Contours of equal impact probability at injection 60

III-26. Gradient vectors at midcourse 61

III-27 Typical capability ellipse 61

III-28. Maneuver operations program 62

# Contents (contd)

## Figures (contd)


III-29. Midcourse maneuver results 63

IV-1. *Mariner V* spacecraft configuration 84

IV-2. *Mariner V* cabling and electronic packaging 89

IV-3. Cumulative engineering change requirements (ECR) vs date summary 92

IV-4. Cumulative spacecraft engineering change requirements (ECR) vs date 93

IV-5. Cumulative operations support equipment (OSE) ECR's vs date 94

IV-6. Cumulative launch complex equipment (LCE) ECR's vs date 95

IV-7 Weight history (M67-2) 96

IV-8. Science subsystem block diagram 102

IV-9. Helium magnetometer 103

IV 10. Ultraviolet (UV) photometer 104

IV 11 Data amplifier block diagram 106

IV-12. UV photometer logic diagram 108

IV-13. Data logic differences 109

IV-14. Gate logic diagram, $33\frac{1}{3}$ bits/s 109

IV-15. *Mariner V* trapped radiation detector (side view) 111

IV-16. Trapped radiation detector functional block diagram 112

IV-17 *Mariner V* trapped radiation detector 113

IV-18. Plasma-probe sensor 115

IV-19. Plasma-probe measurement program 117

IV-20. *Mariner* Venus 67 dual-frequency receiver block diagram 119

IV-21. Dual-frequency receiver antenna subsystem functional diagram 121

IV-22. Volts output vs phase input of the modulation phase comparator 122

IV-23. Data automation subsystem 124

IV-24. Integrated circuit logic subassembly 124

IV-25. Data automation subsystem interfaces 125

IV-26. Data automation subsystem real-time data format 126

IV-27 Data automation subsystem stored-data format 128

IV-28. Data automation subsystem functional block diagram 129

IV-29. Operation and test equipment 132

IV-30. Functional block diagram of the science OSE 134

## Figures (contd)


IV-31 Science OSE simplified data-analysis process 135

IV-32. Location of DFR antennas 138

IV-33. DFR antenna patterns 140

IV-34. *Mariner* Venus 67, 1:5 and 1:85 scale model spacecraft 144

IV-35. Comparison of *Mariner V* and *Mariner IV* look angles 146

IV-36. Comparison of *Mariner V* and *Mariner IV* communication range 147

IV-37 *Mariner V* inverted sun axis plot 148

IV-38. Venus occultation experiment 148

IV-39 Earth track relative to earth polar coordinate location at encounter October 19, 1967 149

IV-40. Antenna gain required vs antenna cone angle relative to earth direction at encounter 150

IV-41 Performance near encounter for −8.2- and +9.5-deg antenna offset 151

IV-42 Venus atmosphere refracted beam paths and earth track relative to true earth direction at encounter 152

IV-43. *Mariner* Venus 67 command synchronization correlation curve 155

IV-44. *Mariner IV* video magnetic tape recorder 156

IV-45. *Mariner V* tape recorder 158

IV-46. Functional block diagram of *Mariner V* data encoder 161

IV-47 Radio subsystem block diagram 165

IV-48. Transmitter exciter to receiver mixer isolation for *Mariner V* and *Mariner IV* 167

IV-49. Radio/antenna operational modes, simplified block diagram 168

IV-50. Return loss vs exit port mismatch VSWR 169

IV-51 In-phase and out-of-phase sum of two RF signals 169

IV-52. Unfixed *Mariner* Venus 67 uplink interferometer pattern vs days from encounter 170

IV-53. *Mariner V* interferometer fix 170

IV-54. VSWR vs frequency characteristics of a $^3/_4$-wavelength shorted coaxial stub 170

IV-55. *Mariner V* uplink interferometer fix received signal level vs days from encounter 171

IV-56. Interferometer contour pattern, 18:1 effective VSWR 172

## Figures (contd)


IV-57 Clean room test area 182

IV-58. Subassembly 5A3 prior to rework 183

IV-59 Absorption and breakup of solithene by M-17 slurry 184

IV-60. Subassembly 5A3 with solithene and old components removed 185

IV-61 Finished subassembly 5A3 186

IV-62 *Mariner V* CC&S test plan 187

IV-63. Generalized single-axis attitude control subsystem 189

IV-64. *Mariner V* sun sensor system, pitch or yaw axis 190

IV-65. Attitude control electronics package, bottom view 190

IV-66. Attitude control electronics package, top view 190

IV-67 Switching amplifier preamplifier scaling resistors 191

IV-68. Primary and secondary sun sensor assemblies 192

IV-69 Aiming zone and constraint regions for June 12, 1967 launch 194

IV-70. Venus lune vs time referenced to encounter 194

IV-71 Venus isobrightness contours 195

IV-72. Canopus sensor two-stage shade 196

IV-73. Schematic of vacuum straylight test fixture 198

IV-74. Partially disassembled straylight test fixture 199

IV-75. Sample straylight data 200

IV-76. Canopus sensor straylight sensitivity, ft-c to give 1× Canopus vs cone angle 201

IV-77 Canopus sensor lens performance 202

IV-78. Canopus sensor lens schematic 202

IV-79 Sun shutter assembly 202

IV-80. *Mariner V* attitude control gas system 203

IV-81 Attitude control roll-yaw gas valve mounting 204

IV-82. Attitude control gas valve detail (modifications indicated for high-temperature operation) 205

IV-83. Spacecraft and autopilot coordinate systems 206

IV-84. Planet sensor 209

IV-85. Cutaway view of planet sensor 209

## Contents (contd)

### Figures (contd)


IV-86. Planet sensor field of view superimposed at −2 min from contact with illuminated limb of Venus 210

IV-87 Light shade assembly 211

IV-88. Planet sensor schematic 211

IV-89. Planet sensor straylight pattern 212

IV-90. Operational support equipment hood 212

IV-91 Aperture 213

IV-92. Planet sensor housing 213

IV-93. Welded module 214

IV-94. *Mariner V* terminator sensor 214

IV-95. Approximate terminator sensor encounter geometry 215

IV-96. Earth sensor 216

IV-97 Earth sensor field-of-view 216

IV-98. Earth sensor calibration 217

IV-99 *Mariner V* gyro activity (launch through start of sun acquisition) 218

IV-100. *Mariner V* spacecraft/*Agena* separation June 14, 1967 219

IV-101 Geometry of false null at initial sun acquisition 220

IV-102. Spacecraft spin rate from earth sensor data 221

IV-103. *A priori* and telemetered star maps (roll search start to earth acquisition) 222

IV-104. *A priori* and telemetered star maps (earth acquisition to Canopus acquisition) 223

IV-105. Attitude control gas weight from launch through midcourse 224

IV-106. "Best estimate" temperatures in vacuum after GCA turn-on 225

IV-107 *Mariner V* gyro commanded turn rates 226

IV-108. Jet vane positions vs time during midcourse maneuver number 1 (June 19, 1967) 228

IV-109. Jet vane drag 229

IV-110. Solar panel layout in relation to spacecraft 230

IV-111 "Folded" solar cell layout 230

IV-112. Schematic of typical electrical section 231

IV-113. Solar panel rear surface 231

IV-114. Solar panel front surface 232

## Figures (contd)


IV-115. Average individual solar cell current-voltage curve 233

IV-116. Typical solar cell submodule 233

IV-117 Typical temperature transducer installation 233

IV-118. Predicted solar panel temperature during Venus mission 234

IV-119. Predicted solar panel thermal characteristics 234

IV-120. Predicted solar panel temperature rise induced by Venus 235

IV-121 Predicted midcourse maneuver temperature history 235

IV-122. Prediction capability for a solar panel in space at some heliocentric distance 236

IV-123. Total undegraded, spacecraft solar panel, peak raw power vs heliocentric distance 237

IV-124. Variation of panel section performance with intensity 237

IV-125. Total panel power vs voltage for various conditions 237

IV-126. Raw data curve of solar panels (connected parallel) 238

IV-127 Solar array V-I curve, reduced data 238

IV-128. Prelaunch predicted power vs voltage for *Mariner V* solar array 239

IV-129. Power subsystem mechanization for *Mariner IV* 240

IV-130. Power subsystem schematic for *Mariner V* 244

IV-131 Terminal voltage profile for *Mariner V* battery (launch to Canopus acquisition) 246

IV-132. Battery charger current profile of *Mariner V* (launch to Canopus acquisition) 247

IV-133. Propulsion subsystem schematic 251

IV-134. *Mariner* Venus 67 propulsion system schedule 252

IV-135. Regular transient behavior 253

IV-136. Regulator test system 254

IV-137 APAC circuit board 255

IV-138. Circuit board installation 255

IV-139. *Mariner V* superstructure 256

IV-140. Superstructure fitting 257

IV-141 High-gain antenna structure 258

IV-142. *Mariner V* cabling block diagram 261

## Contents (contd)

### Figures (contd)


IV-143. Pyrotechnic cabling shielding backshell assembly sequence 263

IV-144. Electronic assembly I pyrotechnic harness 263

IV-145. Data encoder harness (9W6) modification 265

IV-146. *Mariner IV* electronic assembly III science harness wiring fixture 266

IV-147 *Mariner V* electronic assembly III science harness wiring fixture 266

IV-148. D&S interconnect harness assembly (9W20) 268

IV-149. View factor—bay face to solar panel 270

IV-150. Average bus temperature vs total power 271

IV-151 Upper thermal shield blanket 272

IV-152. Lower thermal shield blanket 273

IV-153. Deployable sun shade—stowed 274

IV-154. Deployable sun shade—extended 274

IV-155. Temperature control references 276

IV-156. Temperature control reference sensor schematic 277

IV-157 Black TCR predicted and actual flight temperature 279

IV-158. White TCR predicted and actual flight temperature 279

IV-159. S-13M white TCR predicted and actual flight temperature 279

IV-160. Absorptance of S-13 and S-13M white coatings vs flight time 280

IV-161 Solar panel boost damper 281

IV-162. Antenna deployment mechanism 283

IV-163. OSE cabling layout–spacecraft assembly facility (SAF) 284

IV-164. OSE cabling layout—space simulator facility (SSF) 284

IV-165. Spacecraft inverter fixture 285

IV-166. Response of tip-latched *Mariner IV* solar panels to unit acceleration 286

IV-167 STM vibration qualification test—Z-axis setup 288

IV-168. *Mariner* Venus 67 spacecraft electronic packaging and cabling documentation 291

IV-169. DAS Mark II power converter subassembly 293

IV-170. Planet sensor welded module in holding fixture 293

IV-171. Subassembly handling and storage container 294

IV-172. Modified electronic assembly shipping and handling equipment 295

# Contents (contd)

## Figures (contd)


IV-173. Battery assembly in handling fixture and container 296

IV-174. Octagon structure magnesium corrosion 299

IV-175. Electronic assembly chassis magnesium corrosion 299

IV-176. PIPS substructure translation orientation 300

IV-177 M67-2 on Z-axis CG fixture 301

IV-178. *Mariner* Venus 67 drawing tree 302

IV-179 Block diagram of RF test link *Mariner* Venus 67–DSIF compatibility test 304

IV-180. Screen room RF path final equipment configuration *Mariner* Venus 67–DSIF compatibility test 305

IV-181 Telemetry bit error test final equipment configuration *Mariner* Venus 67–DSIF compatibility test 309

IV-182. Command bit error tests final equipment configuration *Mariner* Venus 67–DSIF compatibility test 311

IV-183. Spacecraft test configuration 314

IV-184. Suspended spacecraft 315

IV-185. EMI UHF test receiver configuration 316

IV-186. S-Band transponder and DFR compatibility test setup 317

IV-187 S-Band/DFR antenna coupling measurements 319

IV-188. DFR antenna and filters 320

IV-189. DAS master oscillator harmonics 321

IV-190. Booster regulator and reverse bias recovery characteristics 322

IV-191 M67-1 flight systems history 399

IV-192. M67-2 flight systems history 340

IV-193. Typical Pasadena system test operations schedule 341

IV-194. *Mariner* Venus 67 AFETR operations schedule, Revision 1 342

IV-195. Sampling carriers attached to face of electronic chassis 346

IV-196. Sampling carriers attached to top and support rings 347

IV-197 Sampling carriers attached to handling frame spars 348

IV-198. Mockup used to simulate spacecraft positions 349

IV-199 Swab sampling of electronic chassis using template 349

IV-200. Average spare burden estimates (setting-strip techniques) 350

IV-201 Average spare burden estimates (swab-rinse technique) 351

## Figures (contd)


IV-202. Sample PFR 353

IV-203. PFR monthly sums (open and closed) vs failure date–*Mariner* Venus 67 354

IV-204. SAF disassembly inspection, M67-1 362

IV-205. SAF disassembly inspection, M67-2 363

IV-206. STCDS–CDC 3300 computer system 374

IV-207 Block diagram–system test complex data system 375

IV-208. STCDS data input subsystem 376

IV-209 Executive control program flow chart 377

V-1 Vehicle integration and *Agena* mission adaptation . . . . . 384

V-2. Variation in *Agena* performance reserves–*Mariner* Venus 67 385

VI-1 CAT equipment provision 393

VI-2. D/AC and output recorder in GCAT facility 399

VI-3. D/AC 400

VI-4. D/AC HSDL logic block diagram 401

VI-5. D/AC output control block diagram 402

VI-6. D/AC TTY logic block diagram 404

VI-7 TTY conversion control timing diagram 405

VI-8. D/A amplifier 406

VI-9 Recorded time 407

VI-10. Elements of software development and control 409

VI-11 *Data processing system for Mariner Venus 67 support* 410

VI-12. 7094 user program environment 412

VI-13. Master data library programs 414

VI-14. Program development schedule 416

VI-15. Doppler residuals during controlled roll 423

VI-16. One-way warm-up curve showing cyclic event at $21^h57^m$ 423

VI-17 B-plane plot of *Mariner* Venus 67 premaneuver orbits showing origin at Venus 426

VI-18. B-plane plot of *Mariner* Venus 67 premaneuver orbits with expanded scale 427

VI-19 Doppler tracking residuals from DSS 11 during premaneuver pitch-turn 429

## Contents (contd)

### Figures (contd)


VI-20. Doppler tracking residuals from DSS 11 during premaneuver roll-turn 429

VI-21 Doppler tracking residuals from DSS 11 during midcourse motor burn 429

VII-1 Summary chart of launch constraints 444

VII-2. Near-earth class I data requirements for *Mariner* Venus 67 445

VII-3. Earth tracks for June 14, 1967 446

VII-4. Station view periods for June 14, 1967 447

VII-5. Station view periods for June 12, 1967 448

## Abstract

This document covers the launch through the midcourse maneuver of *Mariner V*, the flight spacecraft of the *Mariner* Venus 67 project. Included in this document are a brief history of *Mariner* projects, the project objectives of *Mariner* Venus 67, and the mission description and characteristics of the *Mariner* Venus 67 project. Also included are sections on the overall project organization and management, the flight path analysis and mission planning, the spacecraft system, the launch vehicle integration, the mission operations system, and the mission-analysis preparations and activities during countdown and launch.

# I. Introduction

On June 14, 1967, a *Mariner* spacecraft, *Mariner V* (Fig. I-1), was launched on a trajectory to the planet Venus. The launch vehicle for the *Mariner V* mission was an *Atlas* (SLV-3) first stage, and an *Agena D* second stage. The ascent trajectory, as shown in Fig. I-2, was similar to that used for *Ranger* and previous *Mariner* missions. The vehicle entered a low altitude circular parking orbit, coasted for a predetermined time, and then was injected into an escape trajectory by the application of a final impulse. Figure I-3 depicts the sequence of events from launch to Canopus acquisition.

## A. History of *Mariner* Projects

***1. Related missions.*** The concept of the *Mariner V* spacecraft design traces its ancestry to the *Vega* project. At that time, a basic system was outlined that would adapt itself to an evolution of subsystem improvements and the capability to go either toward or away from the sun.

The subsystems have evolved as desired, and future missions such as *Mariner* Mars 1969, which is aimed at Mars, will draw directly upon the qualified hardware.

The *Mariner A* and *B* projects were based upon spacecraft of the 1250-lb class which were designed to make scientific investigations in interplanetary space and in the vicinity of Venus and Mars during the 1962–1964 launch opportunities. Both types of spacecraft were to be launched by a vehicle consisting of a modified *Atlas D* first stage, and a *Centaur* liquid-hydrogen/liquid-oxygen, high energy second stage. The *Mariner A* configuration was to be used on flights to Venus and *Mariner B* was to be used in exploring Mars.

During August 1961, it was apparent that the *Centaur* would not be available for the 1962 Venus launch period. Consequently, consideration was given to the possibility of using a lightweight attitude-stabilized spacecraft for these missions, since it was considered most important that the United States launch a spacecraft to the planet in 1962.

By the end of August 1961, with the completion of feasibility studies of a 1962 Venus mission, the *Mariner R* project was approved. This project was based on an *Atlas/Agena* launch vehicle and the use of a hybrid spacecraft combining features of the *Ranger* and *Mariner A* designs. In addition to the activation of the *Mariner R* project, the design and development of the *Mariner B* spacecraft was continued and scheduled for launch by the *Atlas/Centaur* with dual Mars–Venus capability in 1964 and beyond. Coincidental with the implementation of the *Mariner R* project and the shift of emphasis in *Mariner B*, *Mariner A* project was cancelled. The *Mariner B* project was subsequently cancelled.

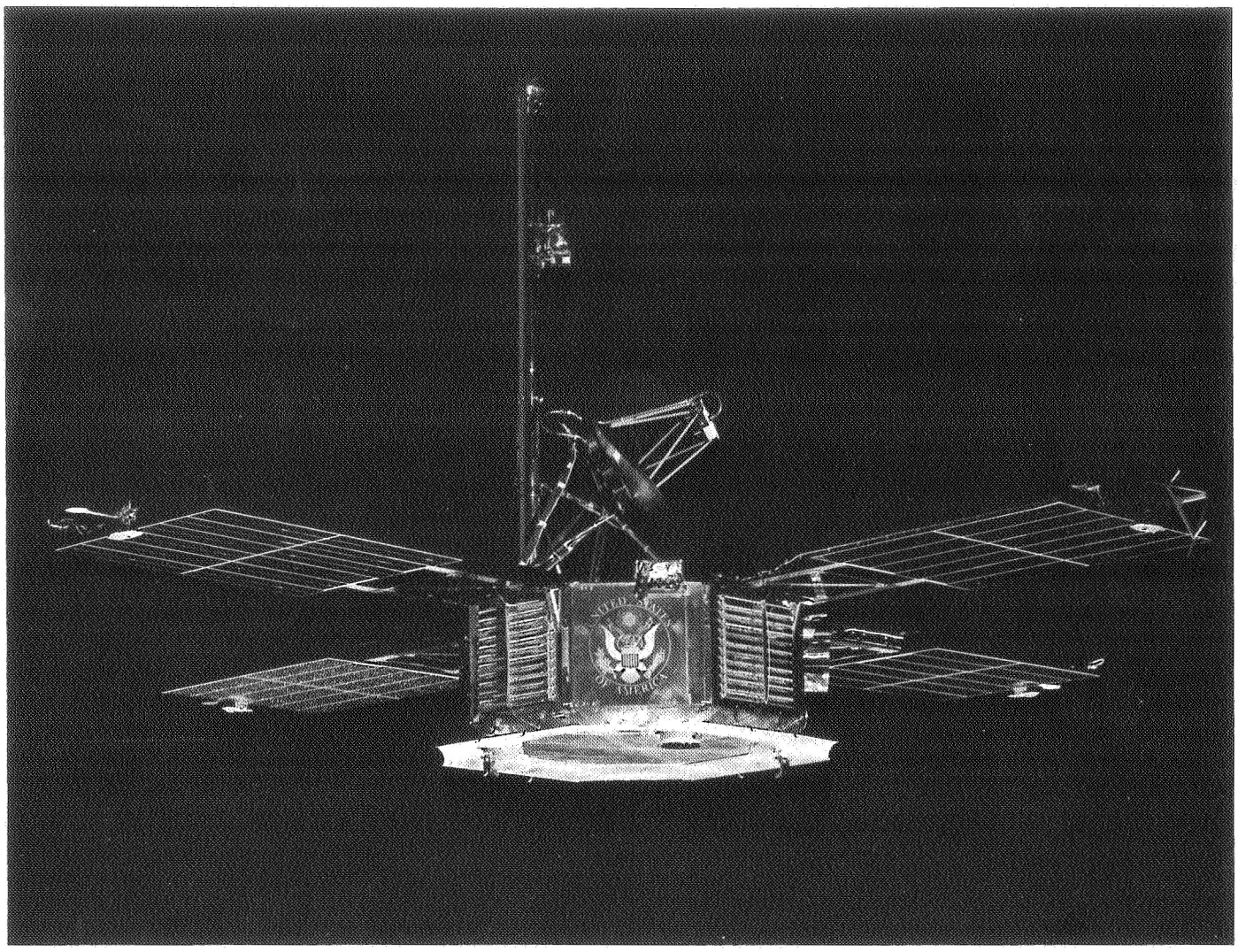


**Fig. I-1. *Mariner V* spacecraft**

The *Mariner R* project was based upon spacecraft in the 450-lb class. Two spacecraft were launched during the 1962 Venus opportunity. Much of the equipment developed for *Mariner A* was used on *Mariner R*. Lesser amounts of equipment used on *Mariner R* were original *Ranger*-type hardware.

The first *Mariner* spacecraft launched, *Mariner I*, was destroyed during the launch phase when the booster malfunctioned. *Mariner II* resulted in the first successful flyby of the planet Venus on December 14, 1962.

The *Mariner II* spacecraft, carrying six scientific experiments, obtained new data on the interplanetary environment for four months after launch, made the first scientific measurements in history near the planet Venus, and communicated to earth over a record distance of 54 million miles.

The feasibility of launching spacecraft to Mars by means of the *Atlas/Agena* launch vehicle had been under intensive study since before the launch of *Mariner II*. By the fall of 1962 it had become apparent that the *Centaur* development schedule could not support the launch of *Mariner B* spacecraft to Mars during the 1964 opportunity. Various proposals resulting from feasibility studies were reviewed, and the *Mariner C* project to be conducted by JPL was approved early in November 1962, about two years prior to the first launch opportunity.

The *Mariner C* project, later to be known as *Mariner* Mars 1964, was based upon the technological experience accumulated during *Mariner R* development and

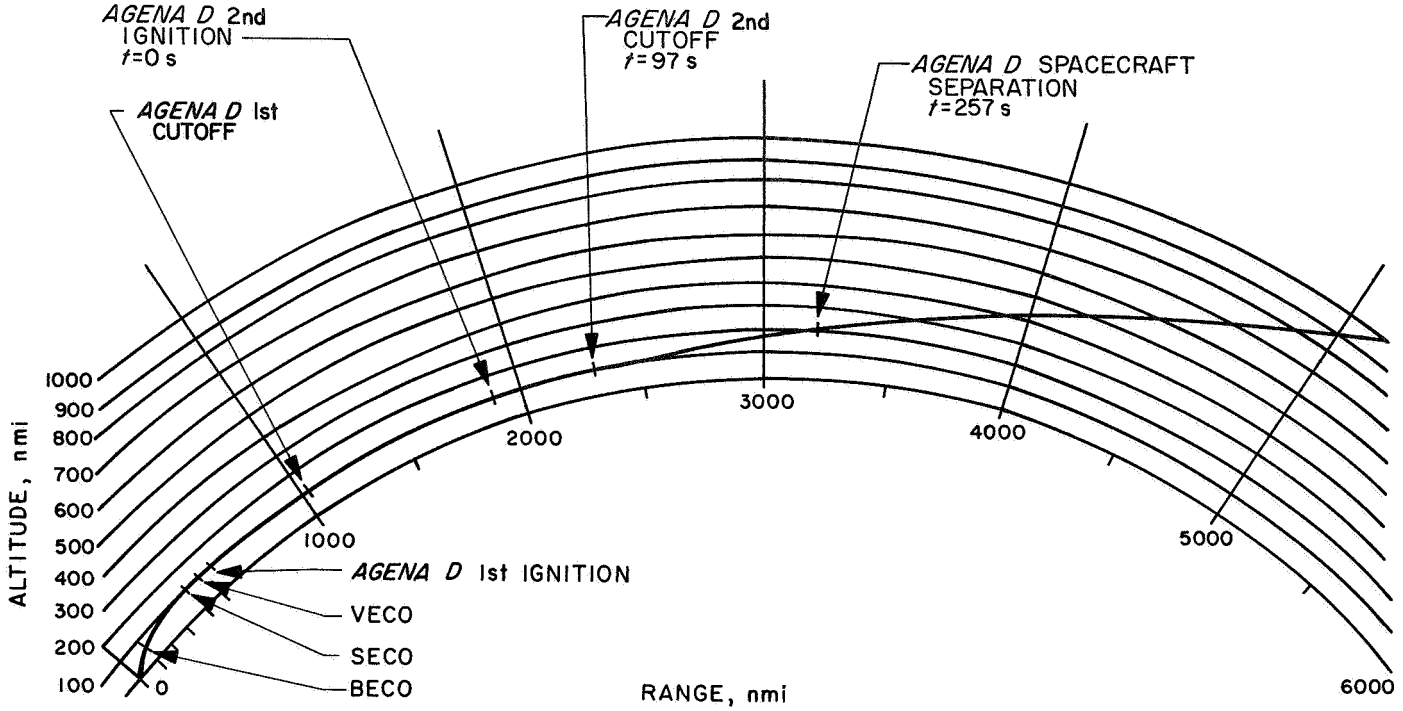



**Fig. I-2. Ascent trajectory profile**

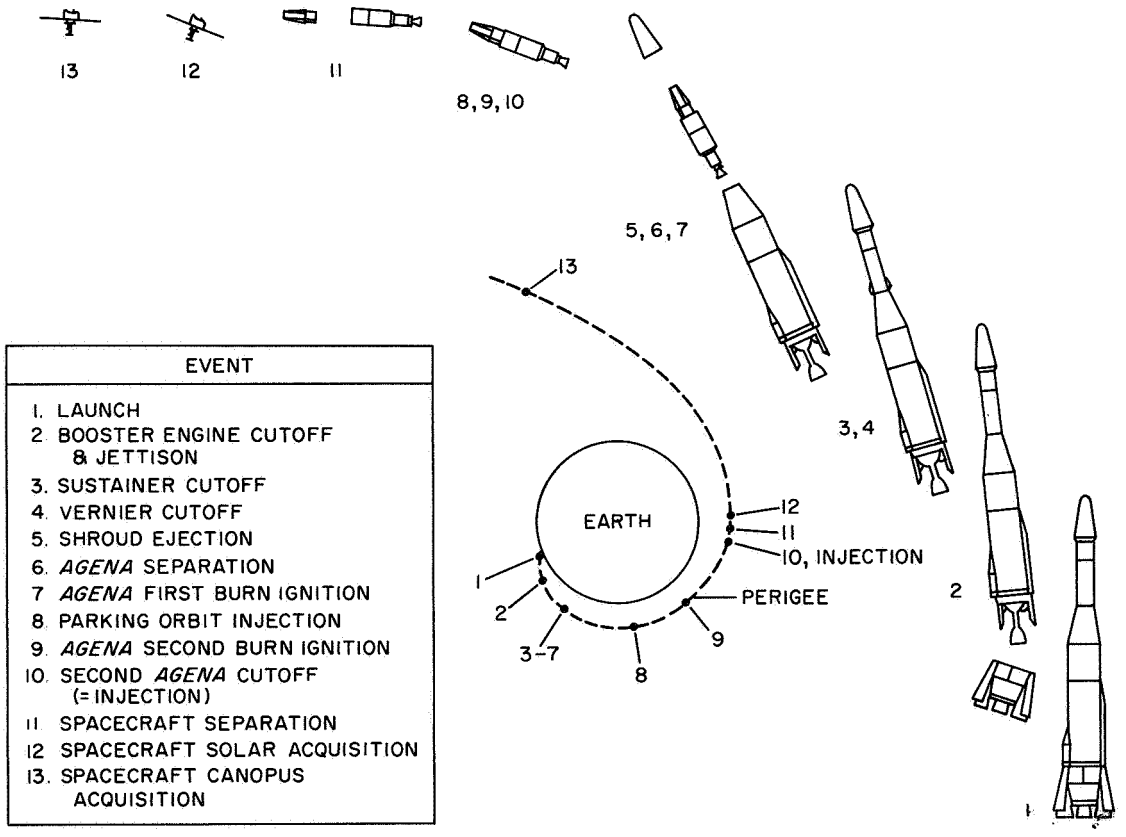



**Fig. I-3. Sequence of events to Canopus acquisition**

the *Mariner II* mission. Many design features of the *Mariner C* spacecraft were continuations and extensions of those applied on earlier *Mariners*. Rigid parts selection, screening, qualifications and controls were adopted to develop the maximum obtainable lifetime within scheduled constraints.

On November 4, 1964, *Mariner III* was launched from Cape Kennedy; however, it could not achieve the desired orbit because of the failure of the shroud to separate from the space vehicle. During the next 23 days the cause of the shroud failure was determined and a new shroud made of magnesium–thorium was designed, fabricated, and tested. On November 28, 1964, *Mariner IV* was launched and all systems performed as designed. After a 7½-month journey, the *Mariner IV* spacecraft flew by Mars on July 15, 1965, and returned the first close-up pictures and other new knowledge relating to this planet. In addition, the flight provided significant new information about the environment of the solar system and the technologies essential to interplanetary flight.

2. ***Mariner V mission.*** Authorization of the *Mariner* Venus 67 project was granted by NASA late in December of 1965. With the launch opportunity occurring in June 1967, the period available for planning, design, test, and other flight preparation was in a span between that of *Mariner II* and *Mariner* Mars 1964 (i.e., *Mariner II* was one year and *Mariner* Mars 1964 was two years) The 18-month interval between the approval of the mission and the launch opportunity necessitated the extensive application of techniques and experience garnered on prior missions.

Utilizing the spacecraft equipment that was built to support the *Mariner* Mars 1964 mission as flight spares, the *Mariner* Venus 67 project was to modify, as necessary, test, and launch one spacecraft. Modifications were to be limited to those required to accomplish the primary objective. The interplanetary scientific instruments were selected from those originally approved for the *Mariner* Mars 1964 mission. The interplanetary investigations were selected to meet the primary objectives within the time, funding, and weight constraints.

The *Mariner* Venus 67 project was, thus, to convert the *Mariner* Mars 1964 flight spares and their associated operational support equipment as necessary to accomplish the 1967 Venus mission objectives. Table I-1 is a summation of the action required to convert the *Mariner* Mars 1964 spacecraft into one suited for a mission to Venus.

**Table I-1 Access difficulty in conversion of the *Mariner IV* spacecraft**

| Item | Original estimates | Actual experience |
|---|---|---|
| Antennas | Major | Major |
| Radio | Minor | Minor |
| Command | Minor | Minor |
| Data encoder | Minor | Minor |
| Tape recorder | Minor | Major |
| CC&S | Minor | Minor |
| Attitude control | Minor | Minor |
| Autopilot | Major | Minor |
| Power converters | Minor | Minor |
| Solar panels | Major | Major |
| Spacecraft structure | Minor | Minor |
| Thermal control | Major | Major |
| Configuration | Major | Major |
| Magnetometer | Minor | Minor |
| UV photometer | Minor | Minor |
| Trapped radiation detector | Minor | Minor |
| Plasma probe | Minor | Minor |
| DAS | Major | Major |
| Propulsion | Minor | Minor |
| Pyrotechnics | Minor | Minor |
| Cabling | Minor | Minor |
| Actuators | Minor | Minor |
| New SC instrument (DFR) | Major | Major |
| Launch vehicle interface | Minor | Minor |
| Trajectory tables | Major | Major |
| Communication analyses | Major | Major |
| Flight sequence | Major | Major |
| Command list | Minor | Minor |

## B. Project Objectives

The primary objective of the *Mariner* Venus 67 project was to conduct a flyby mission to Venus in 1967 to obtain scientific information that will complement and extend the results obtained by *Mariner II* relevant to determining the origin and nature of Venus and its environment.

Secondary objectives were to (1) acquire engineering experience in the conversion of a spacecraft designed for a mission to Mars (spare flight spacecraft from *Mariner* Mars 1964 project) into one designed for a mission to Venus, and in the operation of such a spacecraft, and (2) obtain information on the interplanetary environment during a period of increasing solar activity

## C. Mission Description and Characteristics

Early in the design effort of the *Mariner* Venus 67 spacecraft (*Mariner V*), three areas were recognized as being extremely critical to the feasibility of the mission. They were (1) supporting a satisfactory scientific payload, (2) design constraints imposed by the RF occultation experiment, and (3) achieving the required electrical power at the encounter range within the weight and funding constraints imposed on the project These problems forced a departure from the *Mariner* Mars 1964 design. Other modifications were made to increase performance capability and operational flexibility (Table I-2).

Most of the *Mariner V* scientific experiments evolved from prior projects. The S-band radio occultation experiment, one of seven scientific experiments approved for this mission (Table I-3), requires the use of only the RF transmission subsystem on the spacecraft. The celestial mechanics experiment uses only the tracking doppler data derived from the RF carrier The ultraviolet (UV) photometer, helium magnetometer, solar plasma probe, and the trapped radiation detector (TRD) were slightly modified to better suit the mission to Venus. Only the dual-frequency radio propagation experiment required the incorporation of a new scientific instrument into the payload.

The *Mariner V* spacecraft is a fully attitude-stabilized system using the sun and the star, Canopus, as reference points. A two-way S-band communications system provides telemetry information, command capability, tracking, and ranging data.

The central computer and sequencer (CC&S) subsystem supplies timing, sequencing, and computational services for other spacecraft subsystems. All spacecraft events

**Table I-2. Spacecraft changes**

| Reason | Unit affected | Modification |
|---|---|---|
| To replace inferior parts or those degraded by long-term storage | Command subsystem | Decoders replaced because of corroded transformers |
| | Radio subsystem | Capacitors replaced because of poor quality—aggravated by long-term storage |
| To correct known deficiencies | Radio subsystem | Modified to permit ranging; exciters modified to eliminate spurious output mode |
| | Tape recorder | Playback analog circuitry replaced because of inadequate potting; faulty logic eliminated—potential source of relay malfunction |
| | Canopus sensor | Removed high-brightness gate to eliminate potential tracking of dust |
| To improve spacecraft performance or flight operations | Helium magnetometer | Changed sweep-vector resistors; scale factor reduced 44% |
| | Solar plasma probe | Logic altered for increased energy level sampling rate at encounter |
| | Trapped radiation detector | Changed from two-level to four-level solid-state detector; relocated detector "A" to point toward sun; increased integration time constant to improve S/N ratio |
| | UV photometer | Operation throughout cruise |
| | Battery charger | Toggling controlled by one command |
| | Temperature control reference | New instrument |
| To accommodate Venus mission | Solar plasma probe | Relocated sensor |
| | Helium magnetometer | Added heater to sensor assembly; added thermal diaper around ball part of sensor |
| | Data automation system | Complete redesign of logic and power converter; changed from pellet-type construction to integrated circuits |

**Table I-3. *Mariner* Venus 67 principal scientific investigators**

| Experiment | Principal scientific investigator | Affiliation |
|---|---|---|
| S-band radio occultation | A. J. Kliore | JPL |
| Ultraviolet (UV) photometer | C. A. Barth | University of Colorado |
| Dual-frequency radio propagation | V. R. Eshleman | Stanford University |
| Helium magnetometer | E. J. Smith | JPL |
| Solar plasma probe | H. S. Bridge | Massachusetts Institute of technology (MIT) |
| Trapped radiation detector (TRD) | J. A. Van Allen | State University of Iowa |
| Celestial mechanics | J. D. Anderson | JPL |

are implemented in three distinct sequences (i.e., launch, midcourse, and encounter).

As part of the measurements made in the vicinity of Venus, RF occultation experiments, performed with the S-band communications system and the dual-frequency receiver (DFR), will measure the atmospheric density as a function of altitude. Suggested models of the atmosphere range from a density of 2 to 200 earth atmospheres. The DFR is a low-noise, high-sensitivity receiver unit that operates with the reception of two modulated, coherent carriers. By measuring the relative phase between the two carriers and their sidebands, the electron density between the earth and the spacecraft may be determined.

The flight of *Mariner II* to Venus yielded only a rough upper limit to the planet's magnetic moment because it passed at too great a distance (20,000 miles) and on the sunny (solar) side. Since the *Mariner V* spacecraft will pass on the antisolar side of Venus at a distance of approximately 2500 miles, good measurements of the planet's magnetic field and trapped particles, if any, may be made.

A basic intent of all planetary missions is, of course, to obtain as much scientific data as possible so that our understanding of the interplanetary medium can be enhanced. The knowledge gained from these missions immeasurably contributes to the state of the art, thereby aiding in the orderly design of future spacecraft that will eventually allow man to "physically" explore the planets.

The *Mariner* Venus 67 mission promised rewards in at least three specific areas:

(1) Increased scientific data concerning Venus and the interplanetary medium between the earth and the sun.

(2) Engineering value gained by converting a spacecraft originally designed for a mission to Mars into one suited for Venus.

(3) Expected improvement to the science of orbit determination and the accuracy of space navigation.

Each of the foregoing cannot be considered trivial in their importance and, indeed, must be pursued as part of the evolution of our competence in space exploration.

# II. Project Organization and Management

## A. General

The project was undertaken essentially on the same basis as its predecessor, *Mariner* Mars 1964. Typically, the fixed limited launch opportunity was of primary concern. The unique aspects of the *Mariner* Venus 67 effort involved the use of existing hardware, the conversion of existing designs, and the single launch attempt. Accordingly, the departures taken from the *Mariner* Mars 1964 approach were intended to remedy any serious shortcoming. Adjustments were also made to accommodate the facets peculiar to the *Mariner* Venus 67 mission. In addition, budgetary constraints were regarded as strict and as immutable as any of the technical requirements for the mission.

## B. Management Structure

*1. National Aeronautics and Space Administration (NASA).* The responsibility for the *Mariner* Venus 67 project at NASA headquarters was vested in the Office of the Director of Lunar and Planetary Programs (L&PP) under the overall cognizance and direction of the Associate Administrator, Office of Space Science and Applications. Figures II-1 and II-2 show the organization of these offices. The program manager within the L&PP Division exercised the technical direction function.

*2. Jet Propulsion Laboratory (JPL).* Under the master contract between NASA and the California Institute of Technology (Caltech), JPL was assigned project management authority and responsibility for the *Mariner* Venus 67 project. They were also assigned system management authority and responsibility for the spacecraft system, the mission operations system (MOS), and the tracking and data acquisition system (T&DS). Figure II-3 shows the organization of the Jet Propulsion Laboratory, and Figure II-4 is a further breakdown of the key elements within the project organization. Figures II-5, 6, and 7 further expand upon the respective system management organizations. It should be noted that both the MOS and T&DS organizations supported the *Mariner* Venus 67 operations as well as simultaneous activities involving reacquisition of the *Mariner IV* spacecraft. Common planning and operations were applied to the latter concurrent effort.

*3. Lewis Research Center (LeRC).* Responsibility for the overall management and conduct of the launch-vehicle portion of the *Mariner* Venus 67 project was delegated to LeRC, and within the Center, to the *Agena* Project Office (Figs. II-8 and II-9). The assignment at LeRC included administrative and technical cognizance and control over the launch-vehicle system procurement and booster launch and flight operations, and analysis of flight performance and tracking information up to the time of spacecraft injection. The LeRC effort included maintenance of a branch office at the prime integration contractor's facility at Sunnyvale, California. Essentially, the LeRC organization entered into agreements with the Air Force to obtain standard military boosters for adaptation to meet mission requirements.

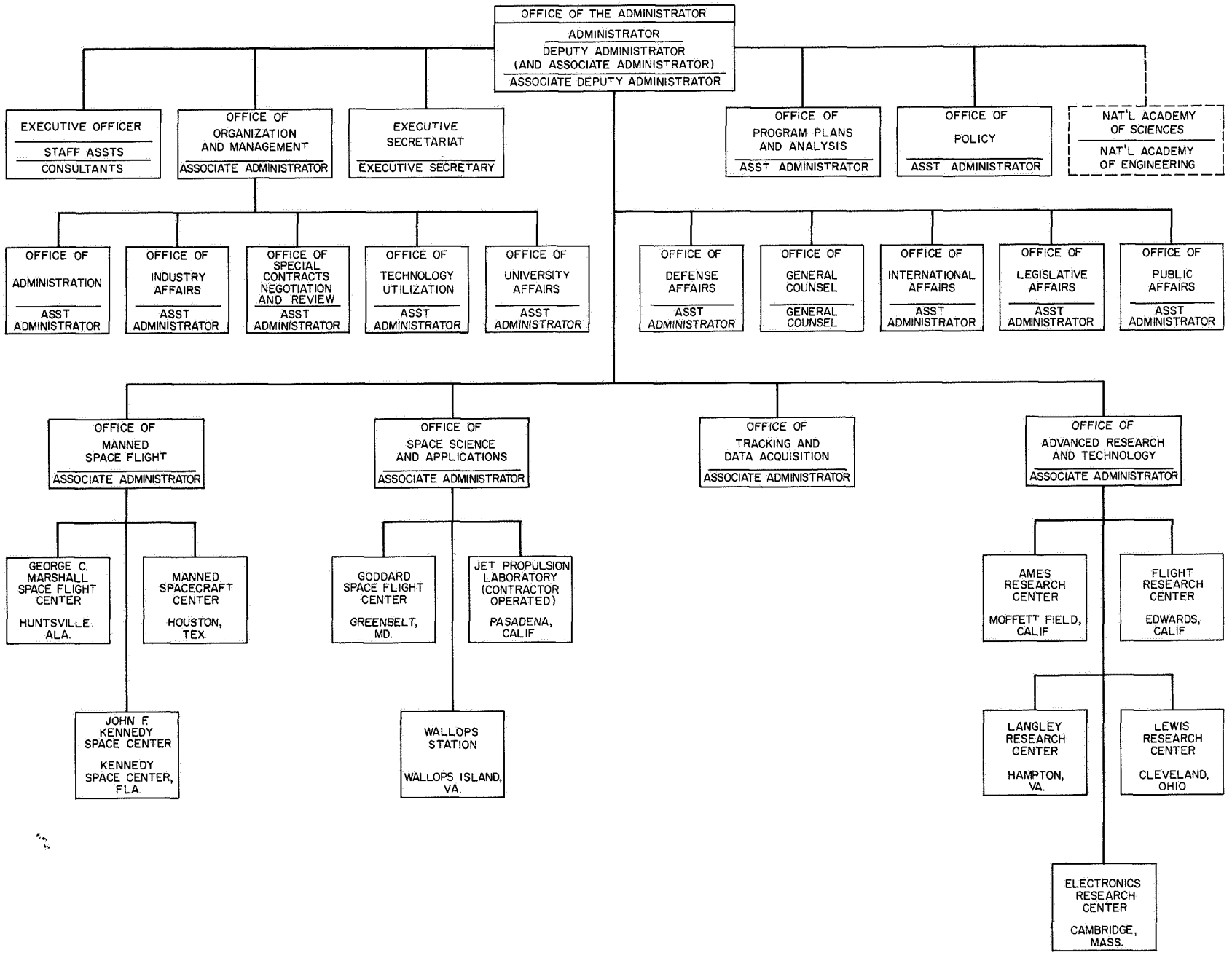



**Fig. II-1. NASA administration chart**

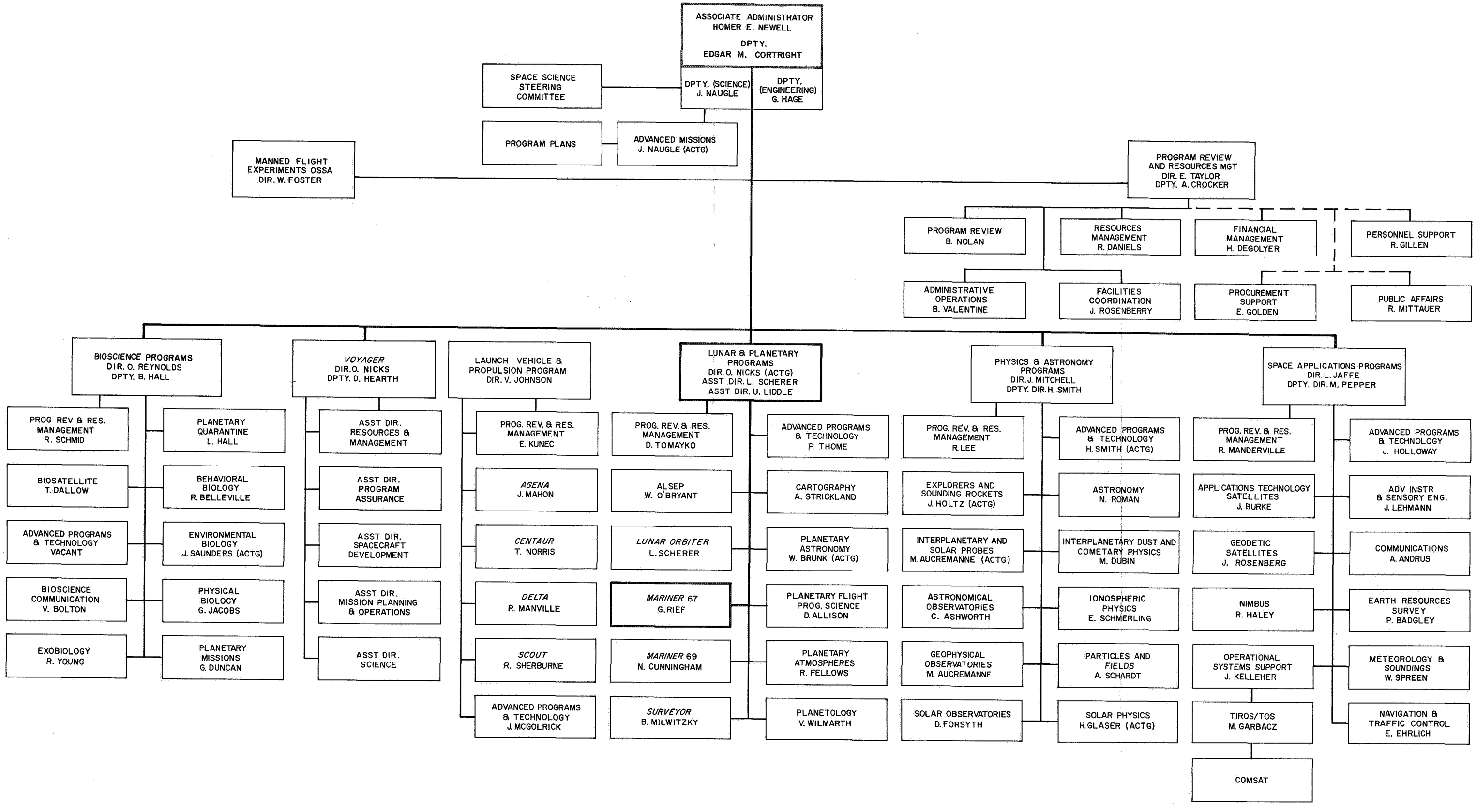



**Fig. II-2. NASA space science and applications chart**

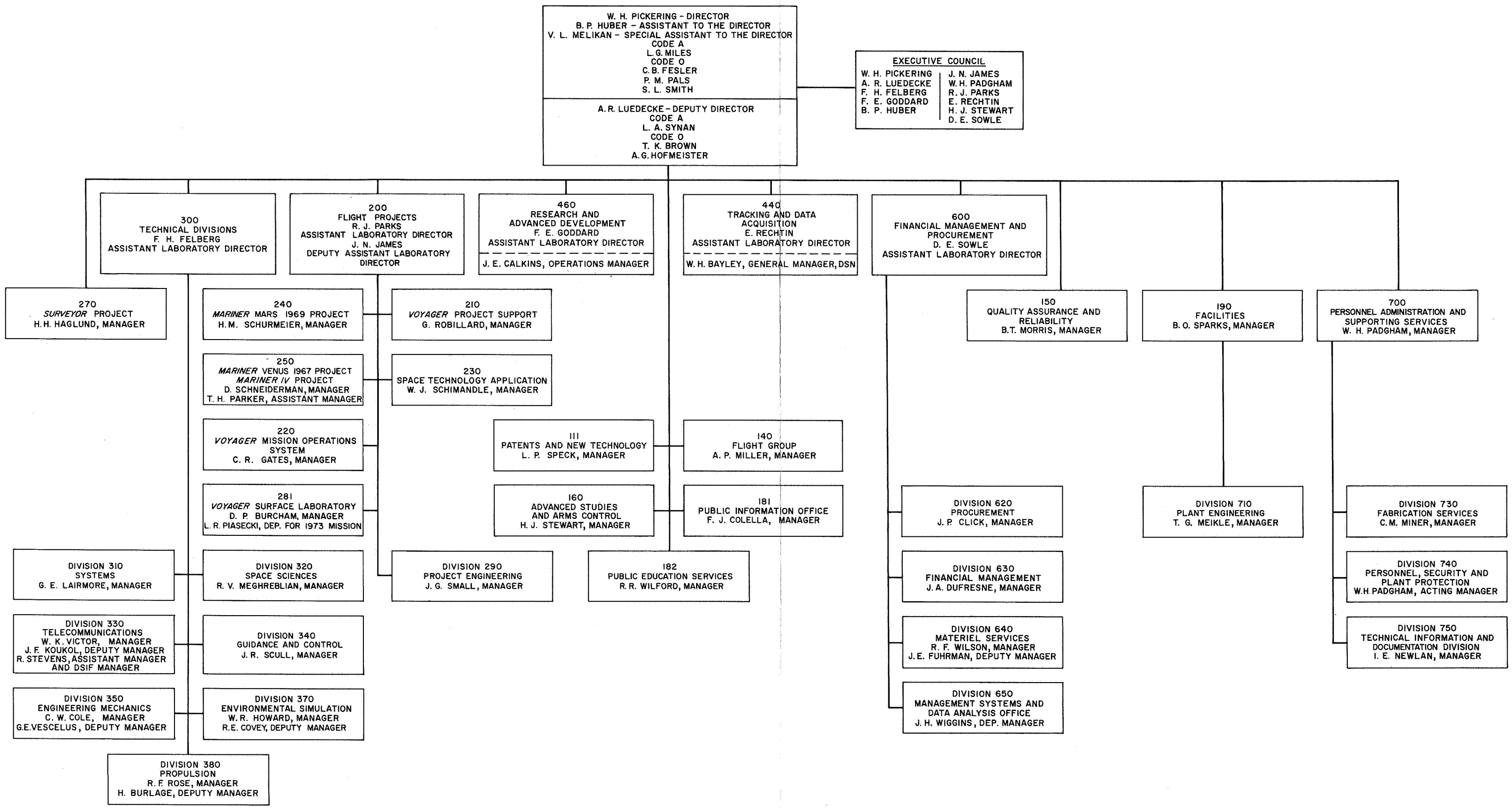



**Fig. II-3. JPL senior staff organization chart**

FOLDOUT FRAME 1

FOLDOUT FRAME 2

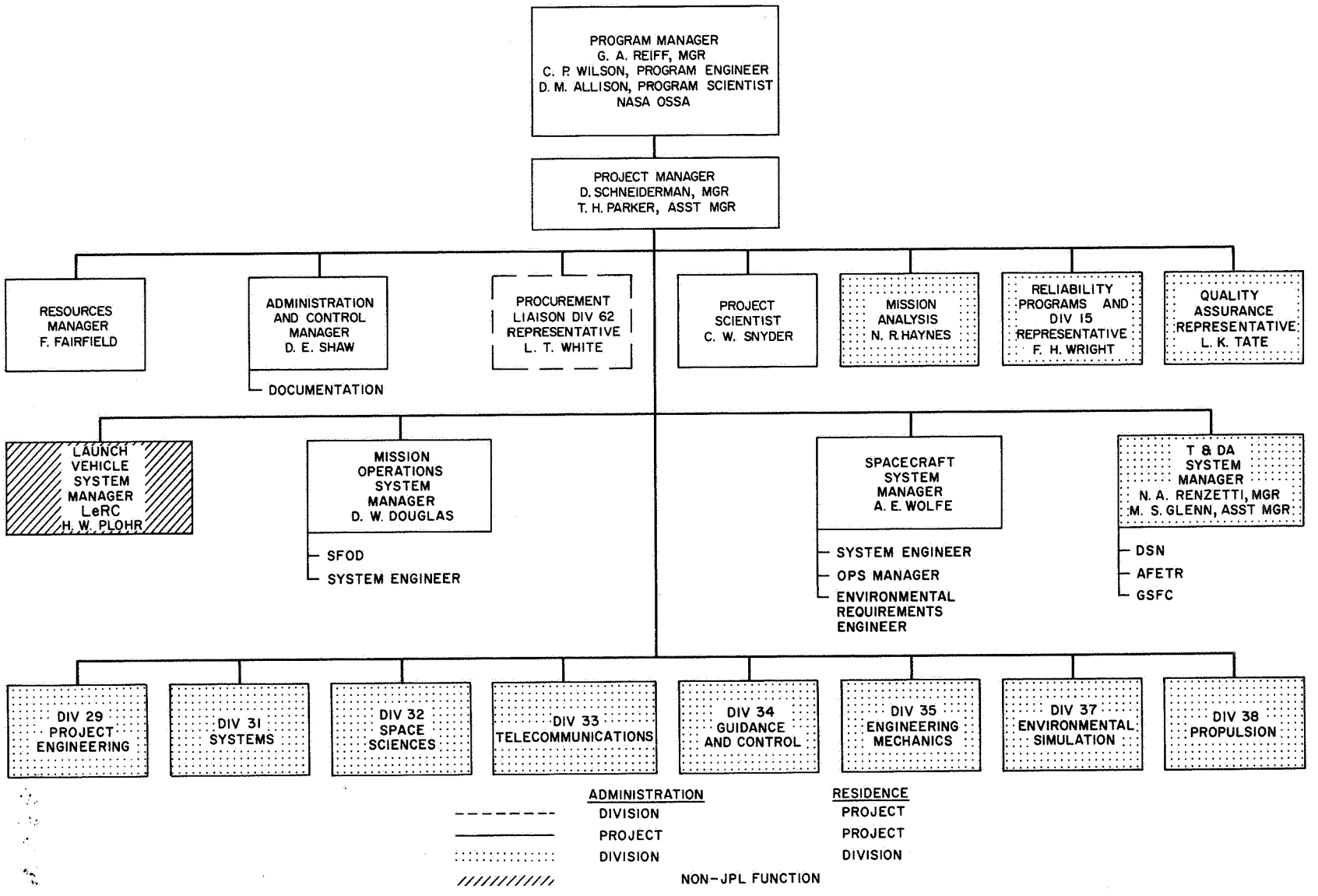



**Fig. II-4. *Mariner* Venus 67 project organization chart**

**Page intentionally left blank**

PRECEDING PAGE BLANK NOT FILMED.

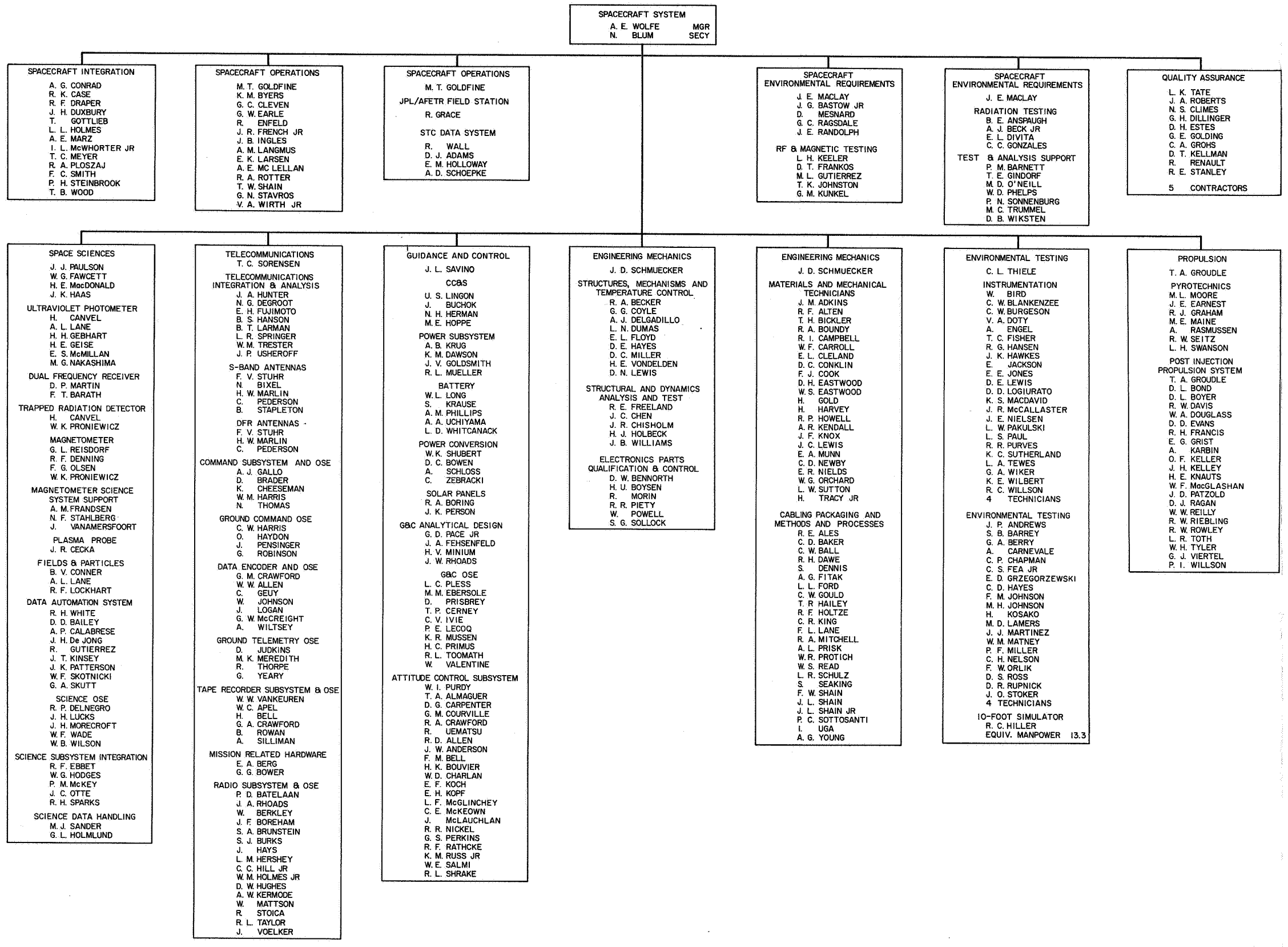



Fig. II-5. *Mariner* Venus 67 detailed project organization chart

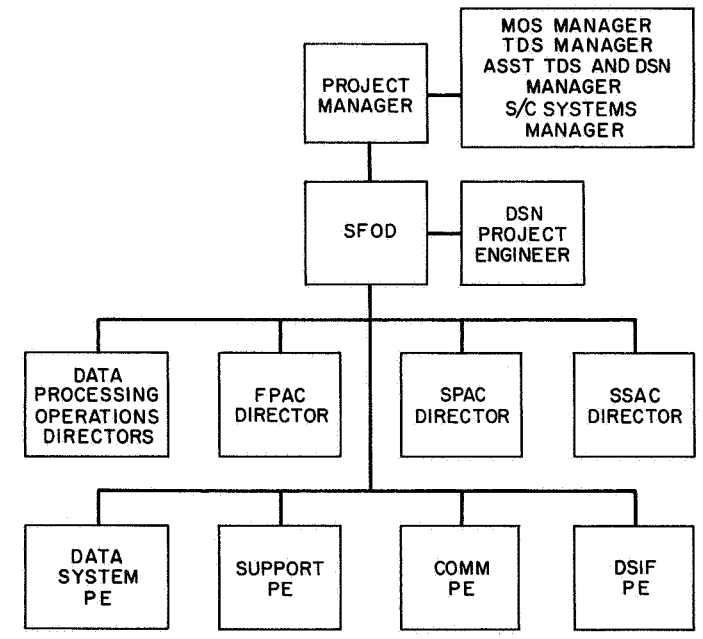



Fig. II-6. Space flight operations organization



FOLDOUT FRAME 1

FOLDOUT FRAME 2

**Page intentionally left blank**

PRECEDING PAGE BLANK NOT FILMED.

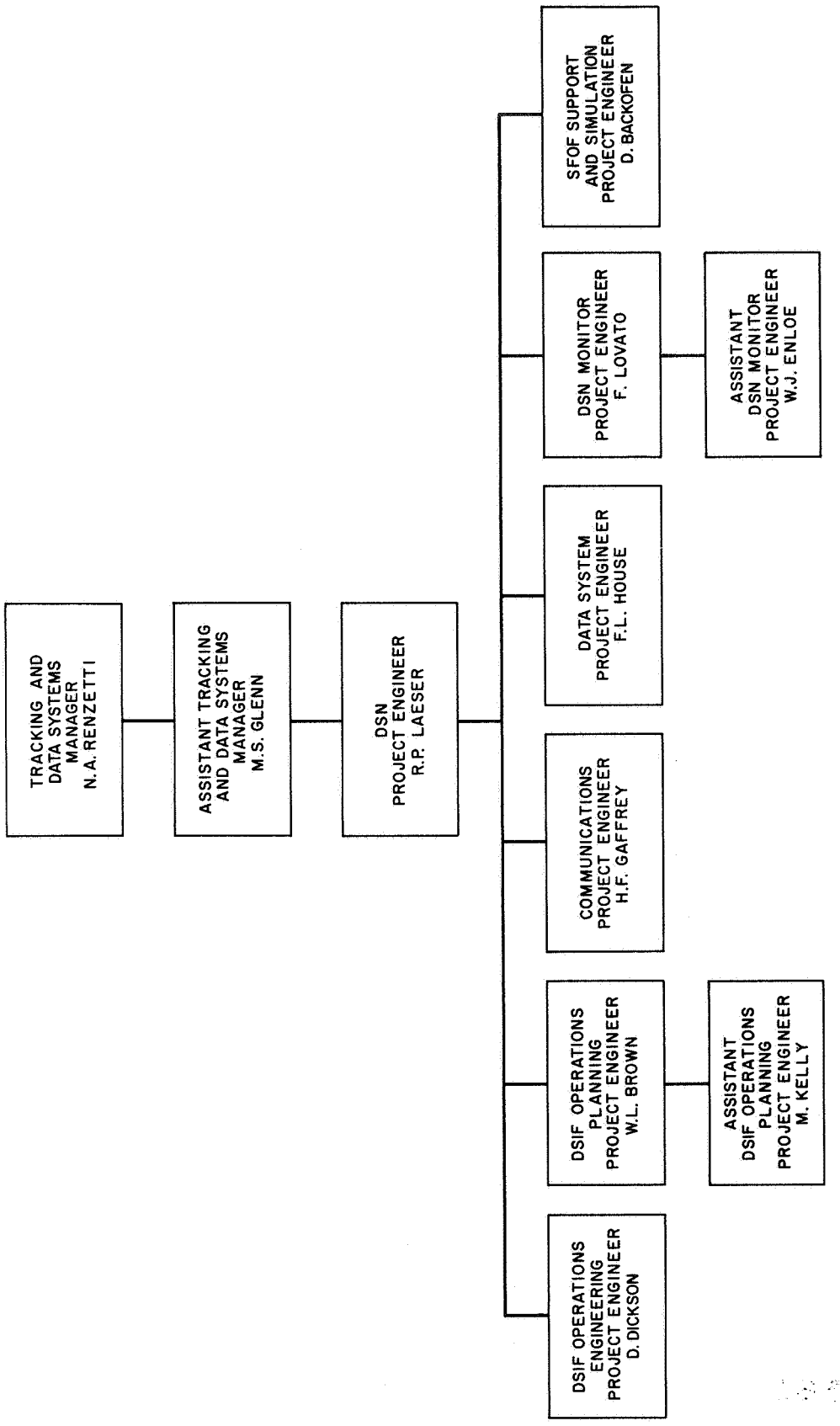



**Fig. II-7. Tracking and data systems organization**

**Page intentionally left blank**

PRECEDING PAGE BLANK NOT FILMED.

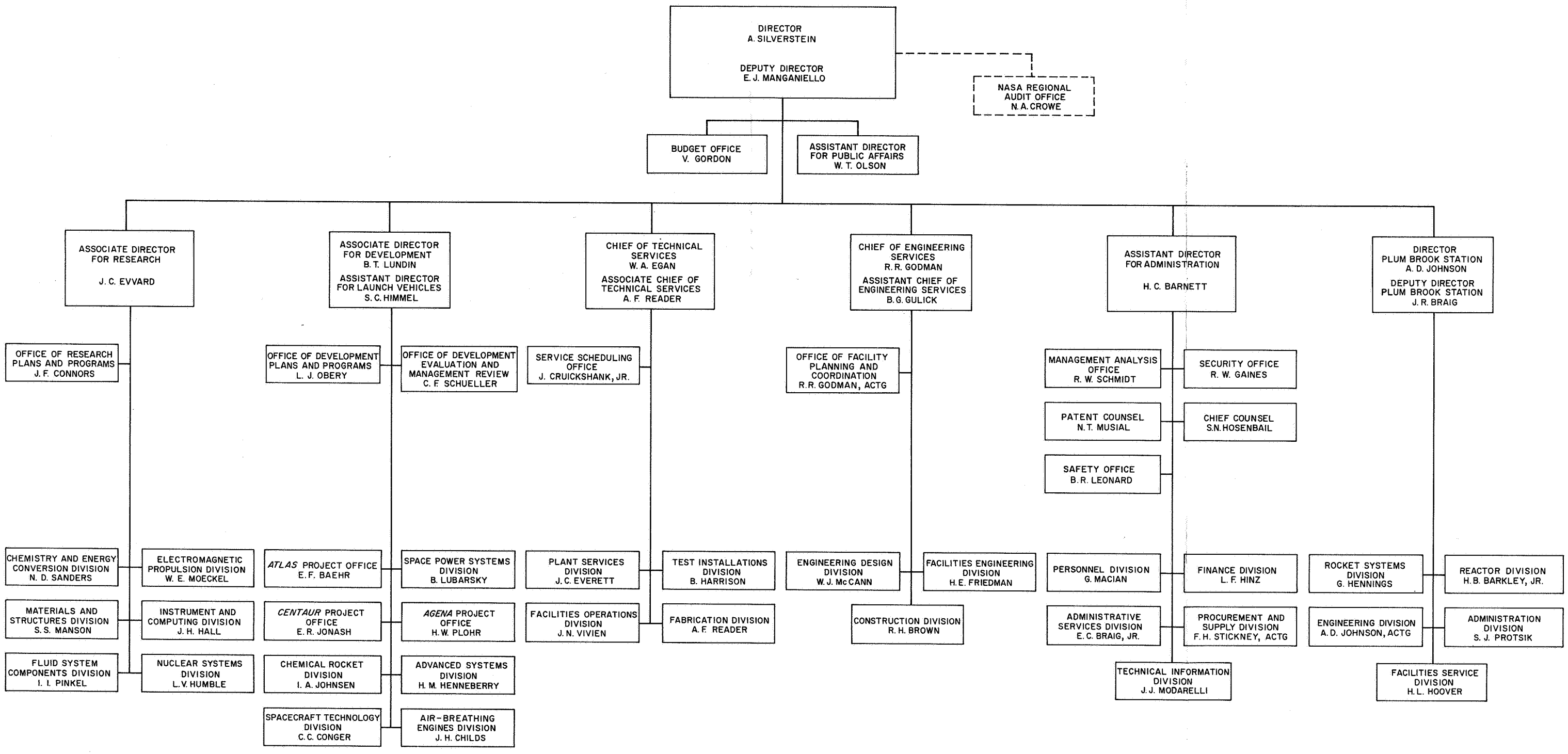



**Fig. II-8. Lewis Research Center organization chart**



FOLDOUT FRAME 1

FOLDOUT FRAME 2

**Page intentionally left blank**

PRECEDING PAGE BLANK NOT FILMED.

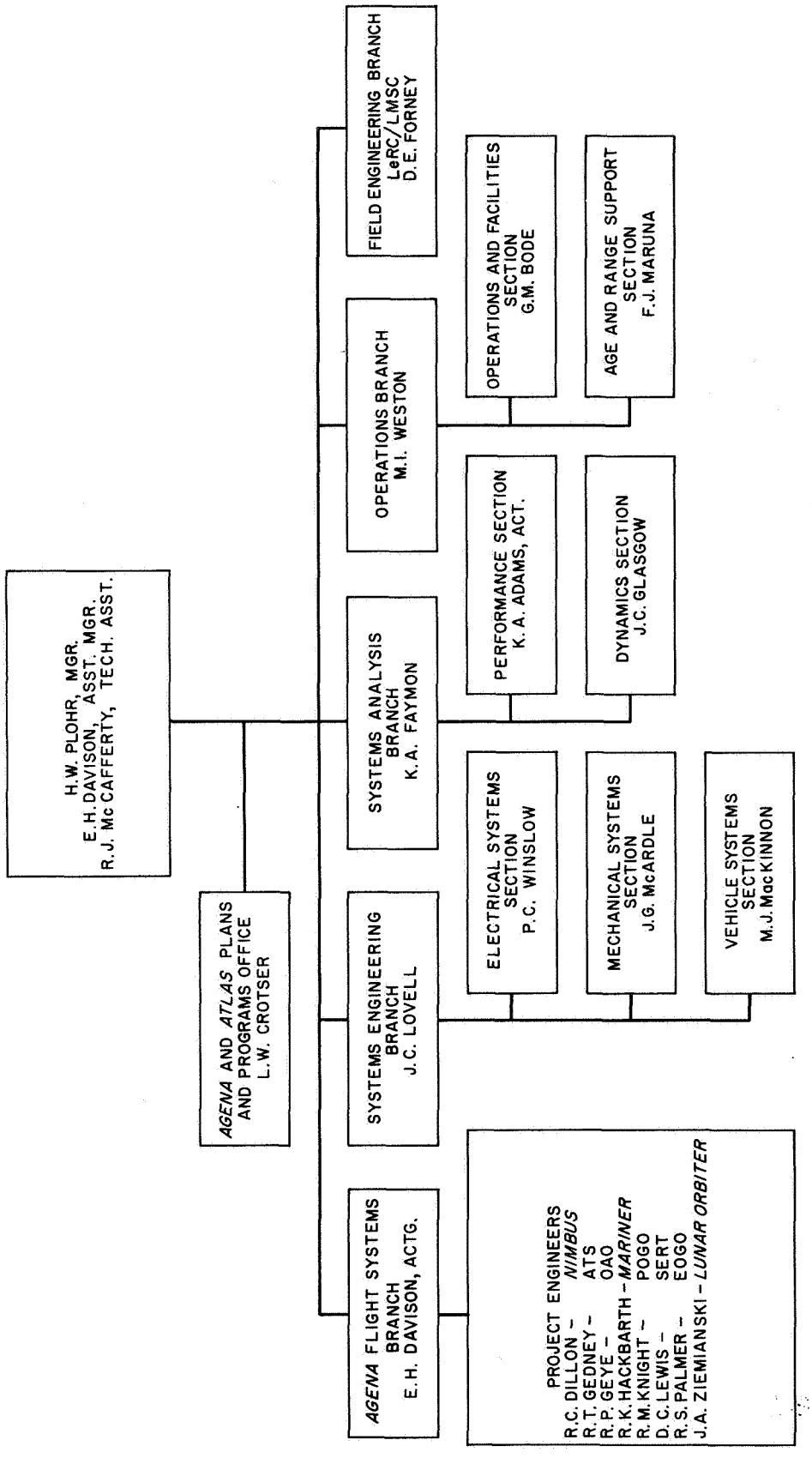



**Fig. II-9. *Agena* project office organization, NASA**

*4. Kennedy Space Center (KSC).* In accordance with interagency agreements, the Unmanned Launch Operations (ULO) Director at the NASA Kennedy Space Center is delegated the responsibility for conduct of launch preparations and countdown at the Air Force Eastern Test Range (AFETR) under the technical direction and in support of the LeRC launch-vehicle system responsibilities. Flight performance data are routed through ULO to LeRC for final evaluation.

*5. Other support.* Mission requirements of the AFETR are levied through the NASA Test Support Office at Patrick Air Force Base. Local, as well as world-wide tracking coverage is obtained through this mechanism. In addition, the Goddard Space Flight Center serves as a relay point in the world-wide data-transmission links.

*6. Industrial management.* The incorporation of mission-peculiar equipment in the *Agena D* system and the adaptation of conventional military hardware were performed by the *Agena* Missions Office within Lockheed Missiles and Space Company (LMSC), (Fig. II-10). This organization was effectively under contract to LeRC to accomplish all launch-vehicle responsibilities except for the original procurement of the basic *Agena* vehicle. LMSC performed the requisite studies and analyses appropriate to this mission and acted as an integrating contractor by interfacing with General Dynamics/Convair, producer of the *Atlas D*, and with Space Technology Laboratories, the launch-vehicle trajectory and flight-performance analysis contractor. The spacecraft encapsulating shroud and adaptor to the launch vehicle were outgrowths of those used on *Mariner* Mars 1964.

## C. System Responsibilities

Figure II-11 depicts the allocation of responsibilities and functions of the system managers. In this sense, the overall perspective of organizational relationships is an agency/system matrix that can be summarized best by reference to Fig. II-12. These organizational arrangements, however, fail to convey the dynamic nature of the situation. Indeed, as the project moved from one phase to another, there developed, or were caused to

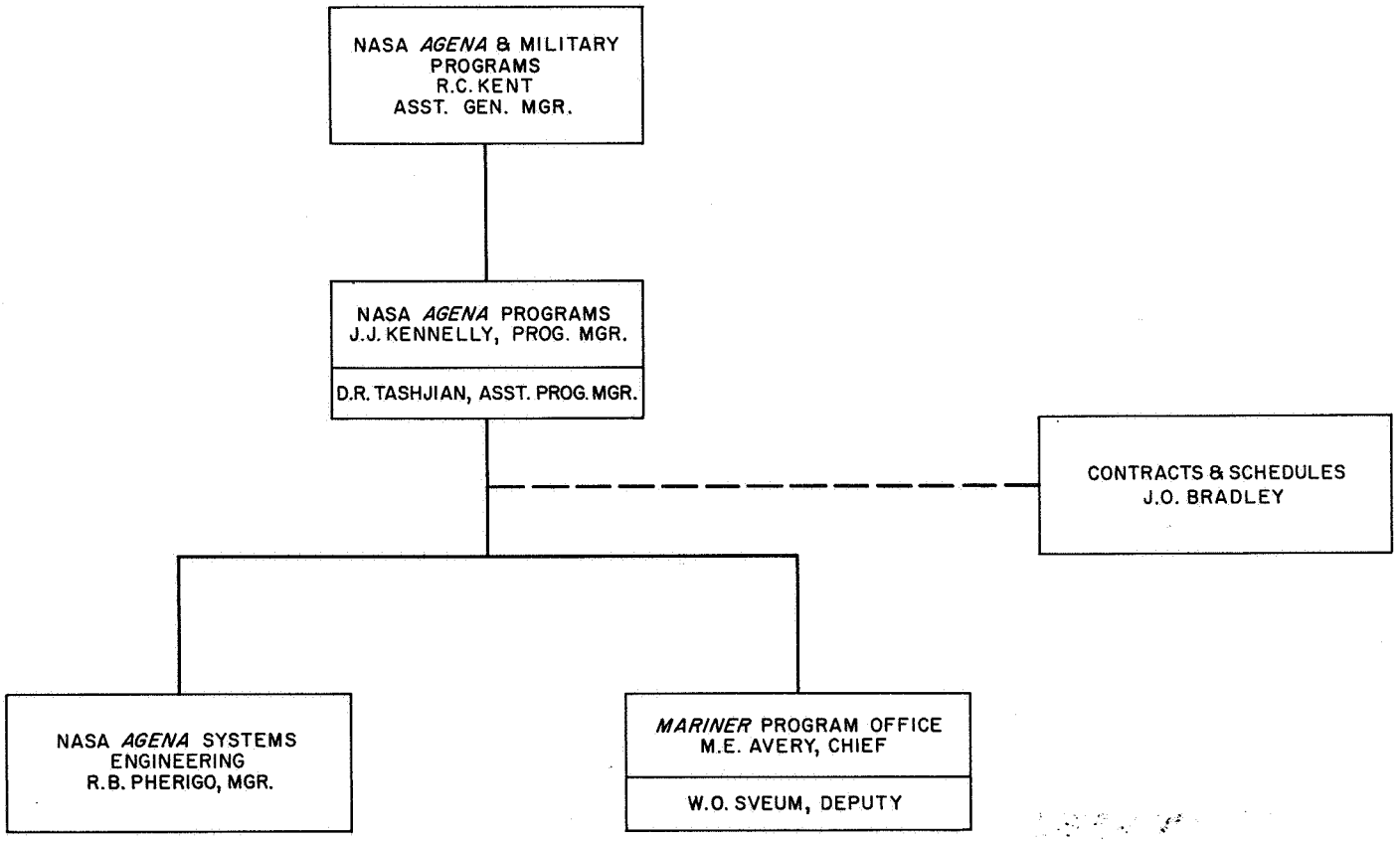



**Fig. II-10. *Agena* missions office, Lockheed Missile and Space Company**

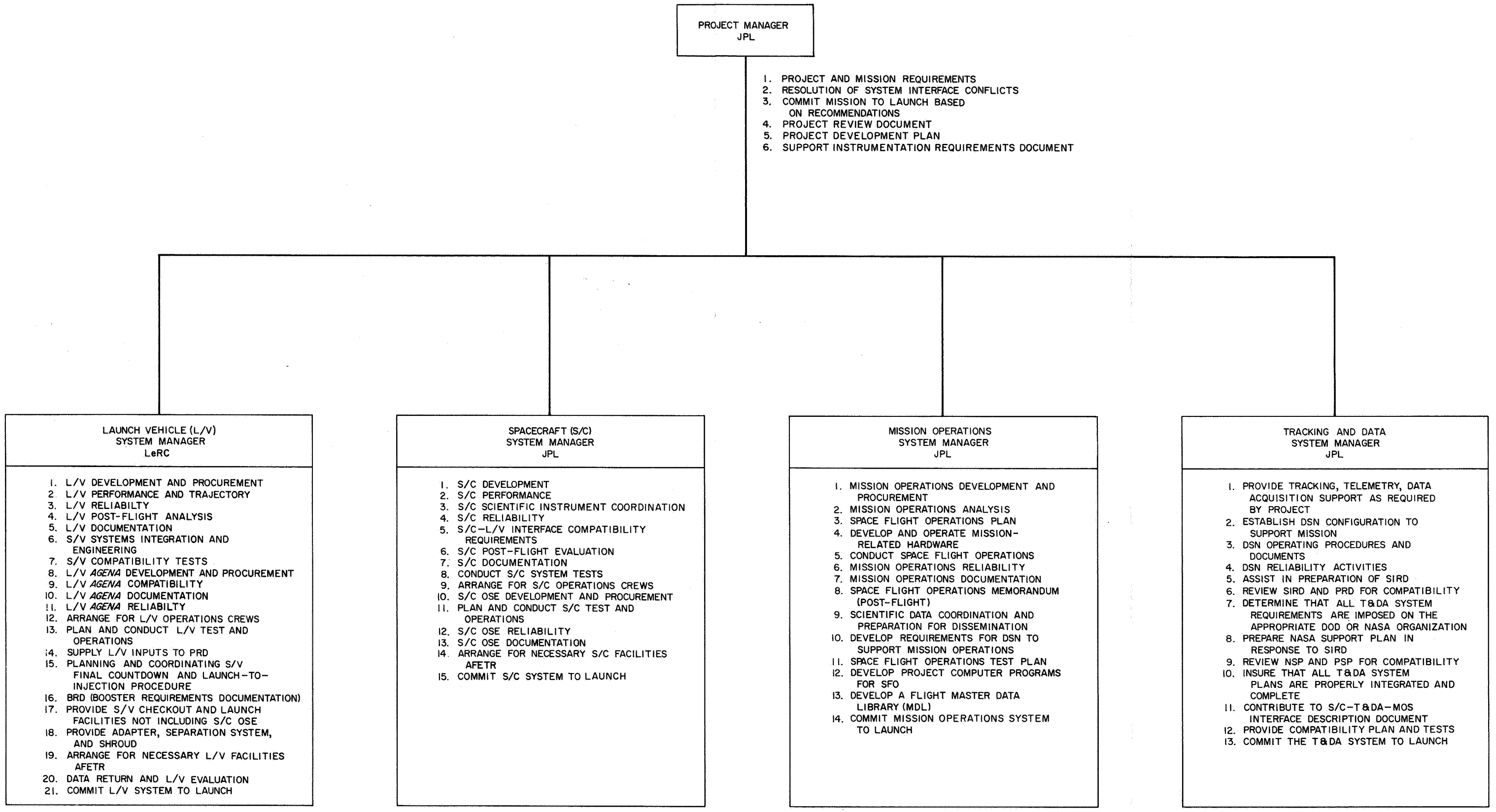



**Fig. II-11. Summary of project responsibilities**



FOLDOUT FRAME 1

FOLDOUT FRAME 2

**Page intentionally left blank**

PRECEDING PAGE BLANK NOT FILMED.

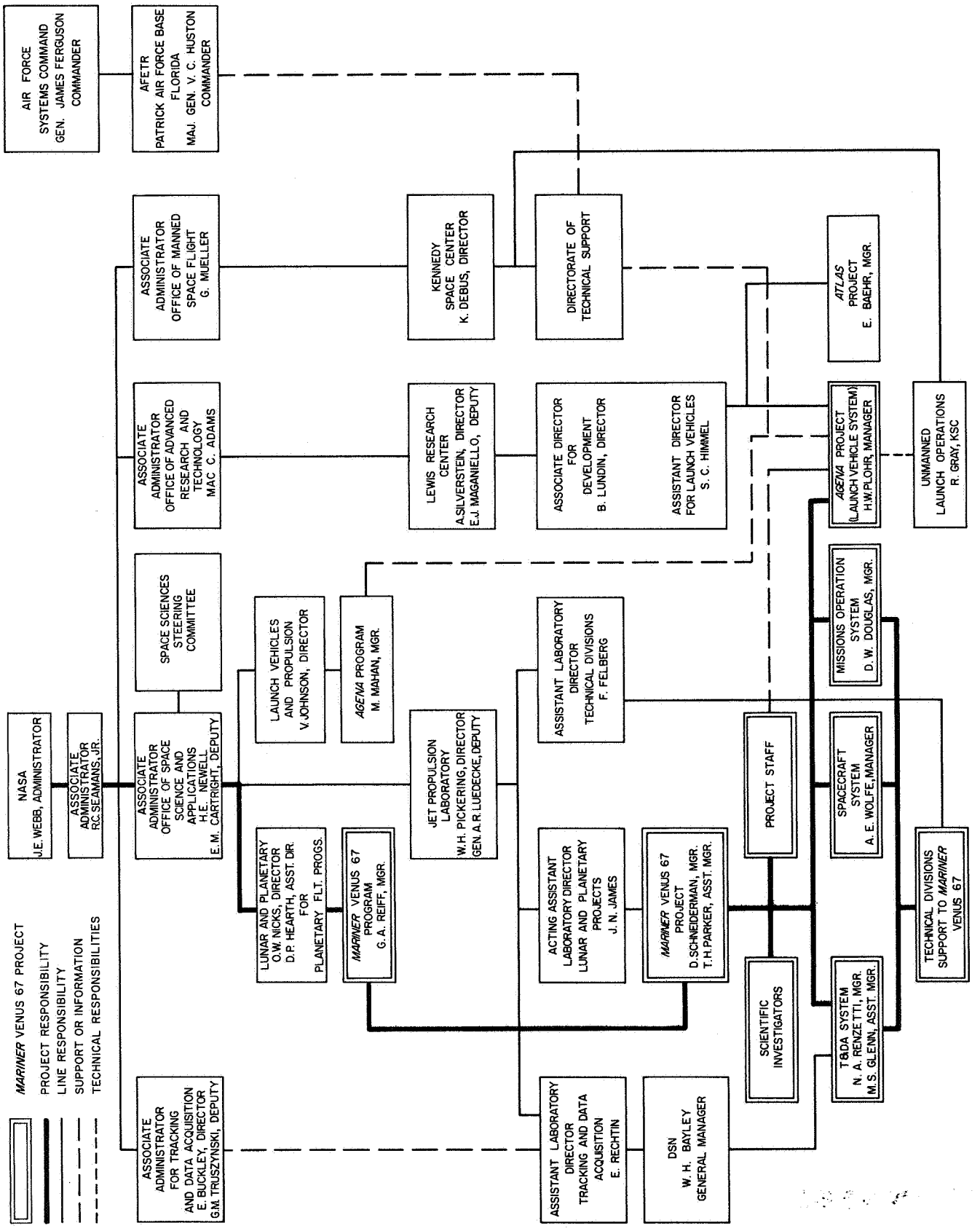



**Fig. II-12. *Mariner* Venus 67 project organizational relationship**

be developed, discrete organizational arrangements that resolved special problems or made key decisions in a timely manner. For example, when an electromagnetic incompatibility was discovered with spacecraft equipment, a special team was assigned to the task of minimizing the effects of the interference. Similarly, special, or ad hoc, groups were constituted from time to time to expedite computer program development when that effort seemed to be lagging. One of the more important special organizational entities was devised to accommodate the launch-operations phase of the mission. During this critical stage, when tremendous amounts of information had to be collected from numerous sources at different times and where various decisions and actions needed to be taken in a timely and flawless manner, an extra special organizational arrangement was devised (Fig. II-13). Even the act of diagramming and explaining the changing arrangement depicted in Fig. II-13 served to clarify the complicated and critical relationship that existed during the launch and near-earth phases of this mission.

## D. Coordinating Bodies

As with the *Mariner* Mars 1964 project, the *Mariner* Venus 67 project and system managers had available to them an additional resource of special panels to serve in an advisory and coordinating role. These panels exercised no technical direction over the responsible agencies or their contractors.

*1. Lunar and planetary projects tracking, telemetry, and communications panel.* This group continually reviewed, compiled, evaluated and interchanged data relating to tracking, telemetry, and communications as these items interacted with the launch vehicle, spacecraft, and world-wide communications systems. The panel was chaired by a representative from JPL and the Project designated one individual to coordinate and represent its interests.

*2. Spacecraft launch-vehicle interface working group.* This group was especially constituted to resolve interface activities between the launch vehicle and spacecraft systems and had representation from JPL, LeRC, and LMSC, under the chairmanship of an LeRC representative.

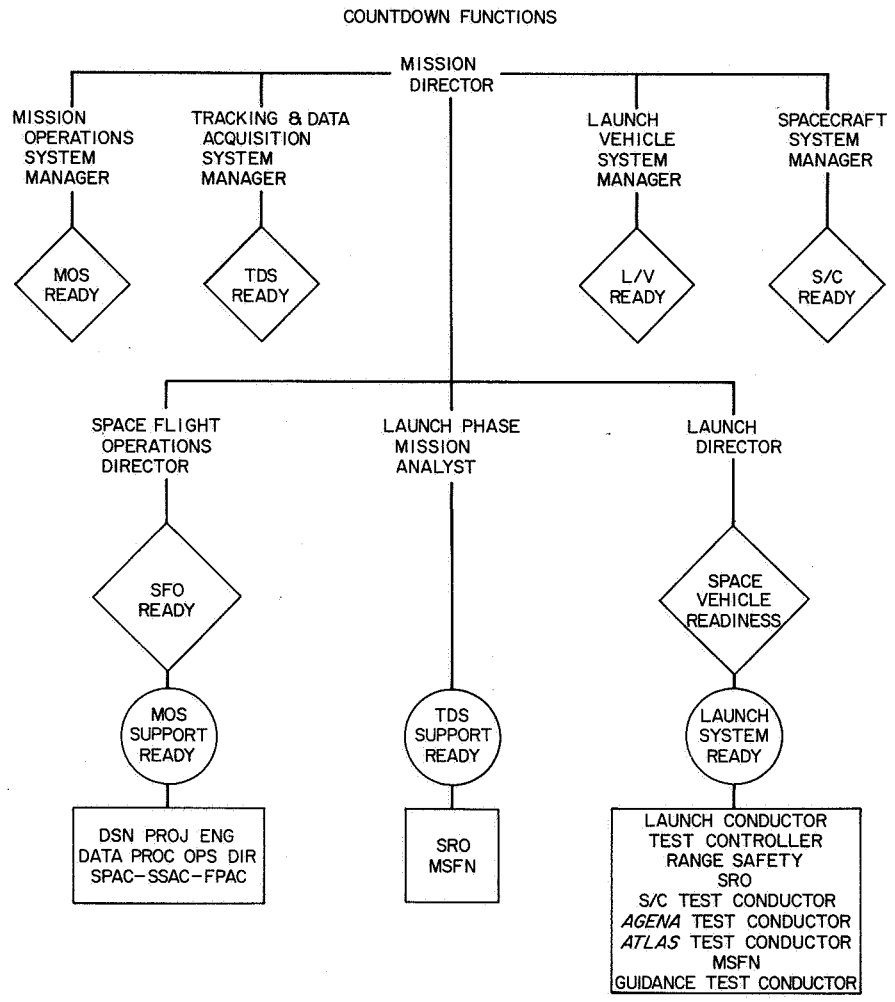
*3. NASA Atlas/Agena launch-operations working group.* This group was the prime mechanism for coordination of flight preparations at the Air Force Eastern Test Range (AFETR). Members of this group participated in mission, spacecraft, vehicle, and range readiness determinations. The group was chaired by KSC/ULO in support of the project/spacecraft/and launch-vehicle system managers.

## E. Master Control Agreements

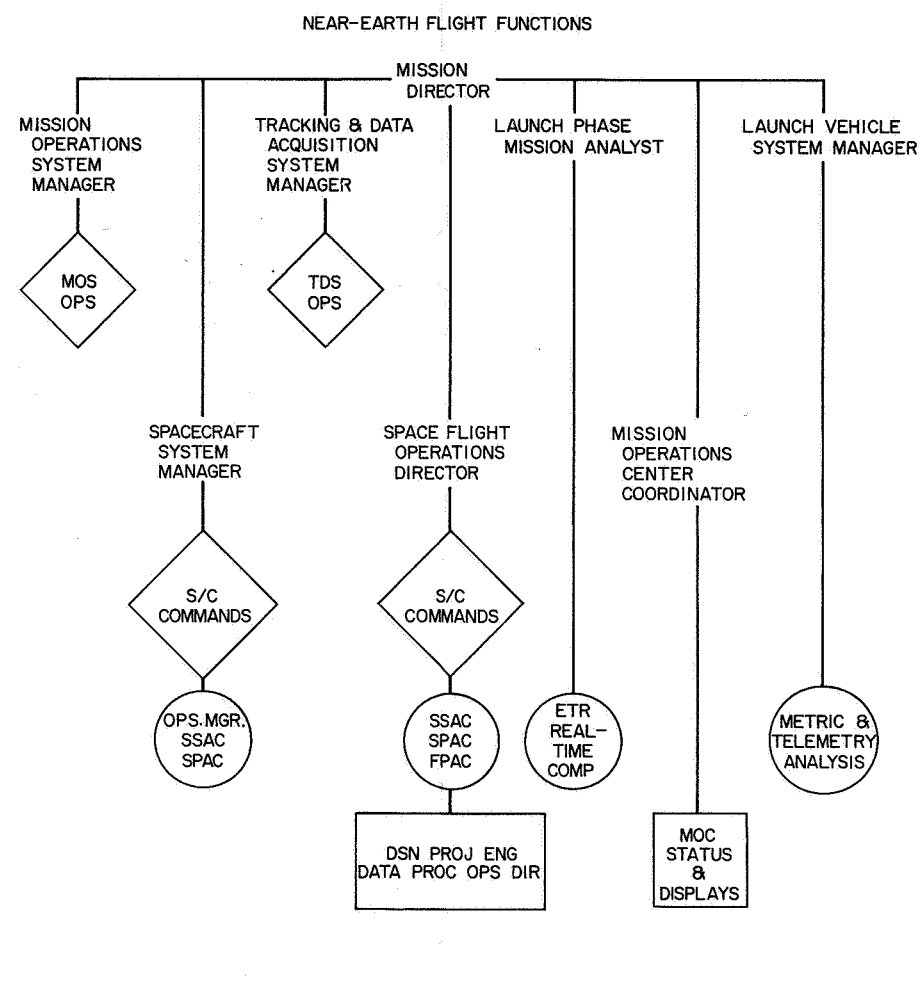
The coordinating bodies previously described were constrained in discharging their responsibilities by certain formal and informal working arrangements. The challenge of the mission and the inflexible schedule requires the project to be accomplished in a cooperative and timely fashion within these existing constraints.

*1. NASA management instructions.* The basic direction for accomplishing projects within NASA has been specified in NASA Management Instruction (NMI) 4-1-1. In fact, it is that instrument which establishes the system management approach and, in essence, provides the authorization and control mechanisms for working within a project on a multi-agency basis. Figure II-14 represents the alignment of organizational responsibilities and establishes a common framework of reference for planning, control, and for reporting of resources utilization and technical and schedule status. In general, accountability for various tasks to the subsystem level of control and the major funding categories are shown. In the case of the spacecraft, the lowest level of grouping implies assembly level of hardware as delivered for operation use. One other key NMI (NMI 8430.1) is also noted because it was without precedent on the *Mariner* Mars 1964 project. The NASA Management Instruction 8430.1 was invoked as a mechanism for levying the tracking and data acquisition support requirements and for obtaining a commitment for the tracking and data acquisition systems of the capabilities needed to meet project needs. The approach used in this NMI is analogous to the series of program and booster-requirements documents and responses or support plans long used by the AFETR for allocation of those capabilities.

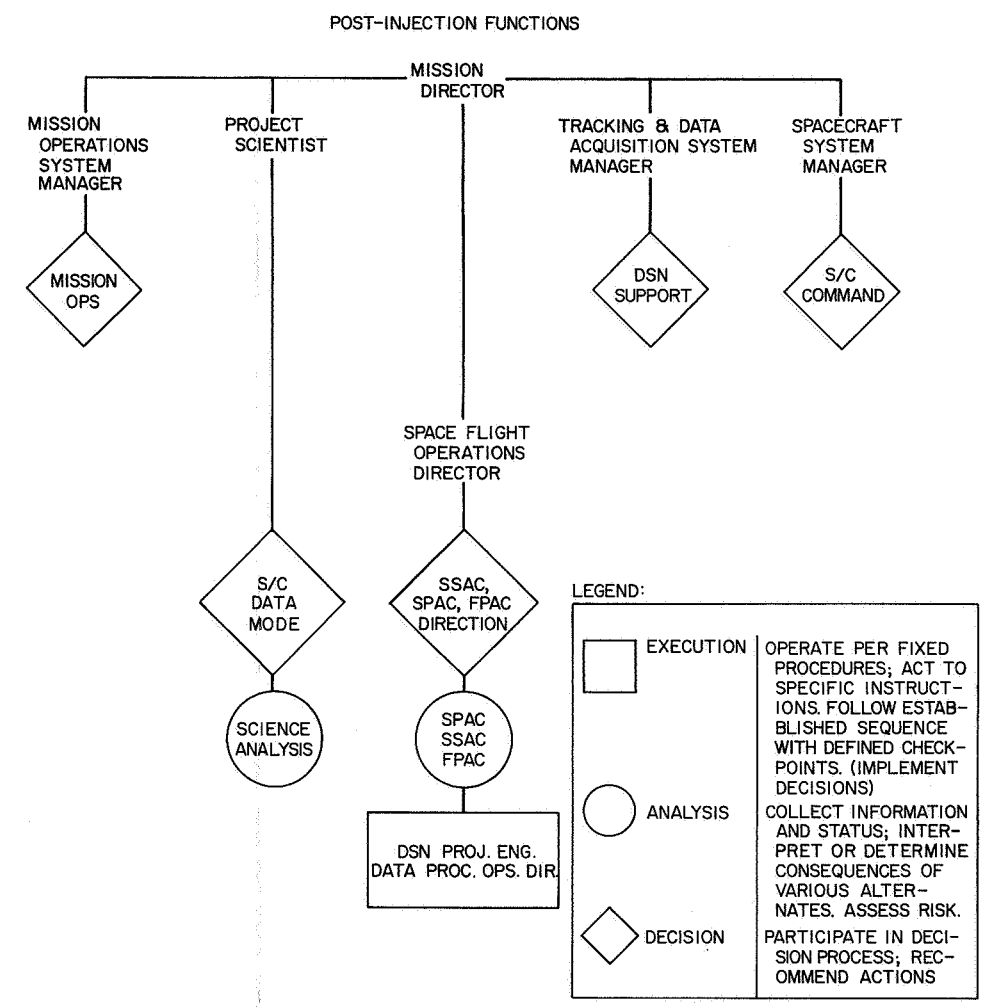
*2. The JPL contract.* Officially, the Laboratory undertakes assigned projects on the basis of task order to the basic NASA/Caltech contract. These task orders specify the mission objectives, the responsibilities for technical direction, the technical approach, the reliability and quality assurance requirements applicable to the project, and the reporting provisions. In addition to the legal "boilerplate," the task order generally uses similar wording to the project approval document (PAD), the NASA headquarters formal authorization called for in NMI 4-1-1. In practice, the working arrangements are negotiated and the technical approach is established in the PAD.




(APPLICABLE THROUGH COUNTDOWN TO LIFTOFF)




(APPLICABLE FROM LIFTOFF TO SUN ACQUISITION OR DSN CONTINUOUS TRACK)




(APPLICABLE TO POST–SUN ACQUISITION AND TRAJECTORY CORRECTION OPERATIONS)

**Fig. II-13. Functional relationship of key individuals**



FOLDOUT FRAME 1

FOLDOUT FRAME 2

RESOURCES CONTROLLED & REPORTED

——— JPL TO OSSA
– – – – LeRC TO OSSA
— — JPL TO OTDA

**PROJECT MANAGEMENT (JPL)**
- PROJECT OFFICE
- PROGRAM ENGINEERING SUPPORT
- PROGRAM ENGINEERING DOCUMENTATION
- MISSION ANALYSIS
- LAUNCH VEHICLE INTEGRATION
- RELIABILITY
- FILM REPORTS

**LAUNCH VEHICLE SYSTEM (LeRC)**
- SPACE VEHICLE INTEGRATION AND MISSION ADAPTATION
- MISSION DEFINITION, SUPPORT AND STUDIES
- SHROUD MFG AND DELIVERY
- BASIC *AGENA D* AND OPTIONAL ITEMS
- BASIC *ATLAS* AND GUIDANCE SYSTEM
- GUIDANCE EQUATIONS
- GD/C LAUNCH SERVICES
- LMSC LAUNCH SERVICES
- SUPPORTING SERVICES

**SPACECRAFT SYSTEM (JPL)**
- SPACECRAFT SYSTEM MANAGER
- QUALITY ASSURANCE
- EXPERIMENTS
  - DIVISION REPRESENTATIVE – SCIENCE
  - SCIENCE SUBSYSTEM INTEGRATION
  - DATA AUTOMATION SUBSYSTEM
  - ULTRAVIOLET PHOTOMETERS
  - PLASMA PROBE
  - HELIUM MAGNETOMETER
  - MAGNETIC SCIENCE SUPPORT
  - FIELDS & PARTICLES COGNIZANT SCIENTIST
  - TRAPPED RADIATION DETECTORS
  - DUAL-FREQUENCY RECEIVER
  - DUAL-FREQUENCY ANTENNAS
  - SCIENCE OSE
  - SCIENCE DATA HANDLING
  - S-BAND OCCULTATION
- S/C ENGINEERING & OPERATIONS
  - SPACECRAFT INTEGRATION
  - OSE INTEGRATION
  - S/C SYSTEM TEST & OPERATIONS
  - AFETR OPERATION
  - ENVIRONMENTAL REQUIREMENTS
  - RF & MAGNETIC TESTING (EMI)
  - RADIATION TESTING (NSE)
  - ENVIRONMENTAL TEST & ANALYSIS SUPPORT
  - STC DATA SYSTEM
  - STC DS PROGRAMMING
- TELECOMMUNICATIONS
  - TELECOMMUNICATIONS SUBSYSTEM INTEGRATION & ANALYSIS
  - DATA ENCODER & ASSOC. OSE
  - S/C S-BAND ANTENNAS
  - S/C COMMAND & ASSOC. OSE
  - RADIO SUBSYSTEM & ASSOC. OSE
  - TAPE RECORDER SUBSYSTEM AND ASSOC. OSE
  - GROUND TELEMETRY OSE
  - GROUND COMMAND OSE
- GUIDANCE & CONTROL AND POWER
  - DIVISION REPRESENTATIVE – G&C
  - G&C ANALYTICAL DESIGN
  - CC&S
  - POWER SUBSYSTEM
  - ATTITUDE CONTROL SUBSYSTEM
  - CC&S OSE
  - POWER OSE
  - ATTITUDE CONTROL OSE
- S/C STRUCTURES, THERMAL CONTROL & CABLING
  - PARTS SCREENING
  - PACKAGING
  - STRUCTURES, MECH. DEVICES & THERMAL CONTROL
  - CABLING
  - APPLIED MECHANICS
  - MATERIALS
- ENVIRONMENTAL SIMULATION & TEST
  - ENVIRONMENTAL TESTING – CONTRACT
  - ENVIRONMENTAL TESTING – INDUCED
  - ENVIRONMENTAL TESTING – NATURAL
  - ENVIRONMENTAL TESTING – OPERATIONS
  - SPACE SIMULATOR TECNICAL SUPPORT (10 ft SIMULATOR TESTING)
  - GROUND INSTRUMENTATION
- PROPULSION & PYROTECHNICS
  - POST-INJECTION PROPULSION SYSTEM
  - PYROTECHNICS SUBSYSTEM

**MISSION OPERATIONS SYSTEM (JPL)**
- MISSION OPERATIONS SYSTEM MANAGER
- MISSION OPERATIONS
- PROGRAM DEVELOPMENT
- FPAC PROGRAMMING
- SPAC
- FPAC
- SSAC
- GROUND TELECOMMUNICATIONS – MRH

**TRACKING & DATA ACQUISITION SYSTEM (JPL)**
- MANAGEMENT
  - OFFICE
- QUALITY ASSURANCE AND RELIABILITY
  - RELIABILITY
  - QUALITY ASSURANCE
- T&DA REQUIREMENTS
  - DSN SYSTEM
  - OTHER NASA SYSTEMS
  - DOD SYSTEM
- ANALYSIS AND ENGINEERING
  - DSN SYSTEM
  - OTHER NASA SYSTEMS
  - DOD SYSTEM
- CAPABILITIES AND SUPPORT
  - DSN SYSTEM
  - OTHER NASA SYSTEMS
  - DOD SYSTEM
- OPERATIONS
  - TRAINING AND SIMULATION
    - DSN SYSTEM
    - OTHER NASA SYSTEMS
    - DOD SYSTEM
  - FLIGHT OPERATIONS
    - DSN SYSTEM
    - OTHER NASA SYSTEMS
    - DOD SYSTEM
- SPACE FLIGHT DATA HANDLING AND PROCESSING
  - DSN SYSTEM
    - MASTER DATA LIBRARY
  - OTHER NASA SYSTEM
  - DOD SYSTEM

**Fig. II-14. *Mariner* Venus 67 work breakdown structure**



Fold out FRAME I

Fold out FRAME II

*3. Other standard practices and regulations.* All project-supporting elements are required to operate within a framework of many rules and regulations. In particular, with the fixed deadlines associated with a planetary opportunity, the procurement regulations often proved troublesome. At times it appeared that there were more legitimate constraints than degrees of freedom. However, with intensive coordination and prompt communication, it is obviously possible to devise, within guidelines, a means for accomplishing the given objective.

## F. JPL Planning and Implementation

As noted previously, the in-house mode of implementation on the *Mariner* Venus 67 project built and traded on the techniques that were developed on the *Mariner* Mars 1964 project. The following paragraphs will highlight the differences from the approach used on the *Mariner* Mars 1964 project (Ref. 1). While considerable effort was spent in keeping the approaches and tools used on the *Mariner* Venus 67 mission as similar as possible to its predecessor, this, more often than not, was not possible because the situation had changed.

The discussion below will be better understood by remembering that the Project Office, as well as the T&DS management, engaged the services and support of the JPL technical divisions (line organization) to perform the tasks appropriate to that discipline. In a manner analogous to the Project Development Plan, the Project Office issued a set of policies and requirements that were the expression of the nature and extent of the support demanded of the line organization. The policy and requirements on this project tended to be more precise and complete than those on the previous project.

*1. Interface planning and control.* Major emphasis was given to maintaining and controlling the proper flow of information and status among the interface areas within the project. Within the matrix-type organization framework, it is precisely at the intrastructure where design and management actions need to be focused. One of the more significant interfaces was handled under the auspices of the launch-vehicle/spacecraft interface working group. The other primary interfaces occurred between the spacecraft and tracking network and between the tracking network and the mission operations systems. Within this area the initiative and burden was primarily carried by the Deep Space Network (DSN). An independent subsystem interface and design integration activity was established under the cognizance of each system manager. Interface characteristics, for definition and control purposes, can normally be categorized as follows:

(1) Technical or engineering descriptions
  (a) mechanical
  (b) signal
  (c) RF
  (d) data handling
  (e) power
  (f) facility

(2) Test and validation
  (a) preparations
  (b) equipment requirements
  (c) layout or arrangements
  (d) acceptance criteria

(3) Interface transactions
  (a) layout or configuration information
  (b) performance measurements
  (c) schedule or status exchanges
  (d) hardware transfers
  (e) study and analysis reports

Even with the most rigorous attention, however, it may not be possible to avoid some mismatch at the interfaces.

The critical nature of the countdown and near-earth phase of the project has been noted. To facilitate understanding problems or status, and in making decisions in this phase, a mission director's combined launch plan was prepared. This plan summarized key elements in the master launch countdown (used at the AFETR) and also included the highlights of the JPL (Pasadena) countdown and preparations of the world-wide support provisions (Appendix A). Key action points and reports for line elements were noted. With the good fortune of a flawless count and early flight, the full potential of this device was never exploited.

The mission-related hardware (MRH) transfer agreement was first used on the *Mariner* Venus 67 effort. As has been noted, the DSN had maintenance and operational responsibility of MRH and mission-related software (MRS) deployed throughout the network, in lieu of the Project Office providing personnel for this purpose as has been done on other missions. Thus, after the design, development, test, and acceptance of MRH and MRS under project auspices, a transfer to the DSN occurs. This act and agreement for operation and maintenance is recorded on the "Transfer Agreement" over project, DSN, and technical division management signatures.

*2. Meetings.* Following established precedents, a hierarchy of conferences were held on a regular and irregular

basis. At the highest level were a series of meetings with the program personnel and others at NASA headquarters. These occurred on a quarterly basis, but with greater intensity as launch date drew near. Laboratory management was also heavily involved in the commitment of hardware to final preparations and launch at Cape Kennedy. Internal to the project, meetings were regularly held at the system level and at the project staff level. During these meetings, which served as the pulse of project activity, minutes and action items were generated and broadly distributed. One danger that had to be actively combatted was the tendency to have decisions and reports follow on this weekly cycle. In many instances, this lapse could not be tolerated, and at such times special actions were taken.

*3. Documentation.* It is clear that documentation on this project was more extensive in both variety and detail of content. While earnest efforts were made to capitalize upon existing paperwork from the *Mariner* Mars 1964 project, it was seldom feasible to use this paperwork "as is." In any event, all existing publications and design-control literature had to be given critical examination to determine the impact of the design changes.

The other primary cause of increased paperwork is attributable to additional demands for status information and attempts to exercise more thorough control over the interface areas. In addition, documents had to be generated because of newly imposed management instructions (e.g., NMI 8430.1) and other internal management requests. Indeed, there was sufficient newness in the requirements and operating approach that caused the project to prepare a documentation plan to keep personnel adequately informed as to the relationship and applicability of various publications. One is thus led to the conclusion that paperwork will grow despite real attempts to minimize it and despite the fact that fewer pieces of hardware and launches were involved as compared to *Mariner* Mars 1964. One of the other basic causes for increased documentation was the need to protect precious equipment. Considerable effort was taken to prepare very detailed procedures for the testing of flight hardware. In this instance, the extensive number of heretofore nonexisting pages proved to be well worth while. Figure II-15 shows elements of the spacecraft design documentation relationship.

*4. Design control.* Each system employed a means for controlling design changes. There were slight variations in the approach used to compensate for the nature of the particular system. Where appropriate, both hardware and software freezes and change control were applied. In the case of the spacecraft, the design was frozen at the onset and changes were authorized to remove hardware or correct designs to accommodate the new mission. The *Mariner* Mars 1964 design documentation was maintained intact as a record of that configuration. The practice was continued and extended to exercise higher level control over certain general specifications that relate to parts, materials, processes, and general requirements that were likely to be imposed on a broad basis. Some difficulty was encountered in accomplishing tight control and exerting uniform requirements because, in many instances, the original parts and processes applicable to *Mariner* Mars 1964 were no longer available. The accommodation of substitutes required considerable time to be sure that quality and flight worthiness was being adequately maintained.

*5. Trouble-failure reporting.* Complementing the design freeze and change control system were several schemes for reporting the occurrence of malfunction or misoperations. These systems shared the common characteristic of broad dissemination, early notification, notation of analysis and actions taken, acceptance by responsible line supervision, and compilation or summarization to determine the existence of trends. As with prior missions, scrupulous assessment and closeout of these reports was maintained throughout the project organization. In a few instances, thorough investigation left the failure mode and mechanism unknown so that proper corrective action was inconclusive. In such cases, higher management levels reviewed the matter and accepted the attendant risks. At the top, but not superseding the basic systems, the P-list (problem list) was again established (Table II-1). On an average, the problems required 28 days to resolve —very comparable to *Mariner* Mars 1964 experience.

*6. Reviews.* The review mechanism was extensively used as a redundant assessment of the adequacy of designs and the quality of hardware and software. Reviews were constituted by system managers or the project as appropriate to the nature and urgency of the problem under examination. Both formal and informal boards were used, again in light of the nature of the problem. In the spacecraft area, there were payload and preliminary design reviews, as well as design reviews of those subsystems considerably changed or that were new to the mission. These were followed by hardware quality reviews when the hardware was delivered to the spacecraft assembly facility (SAF). Reviews also were held at the conclusion of each major phase of testing.

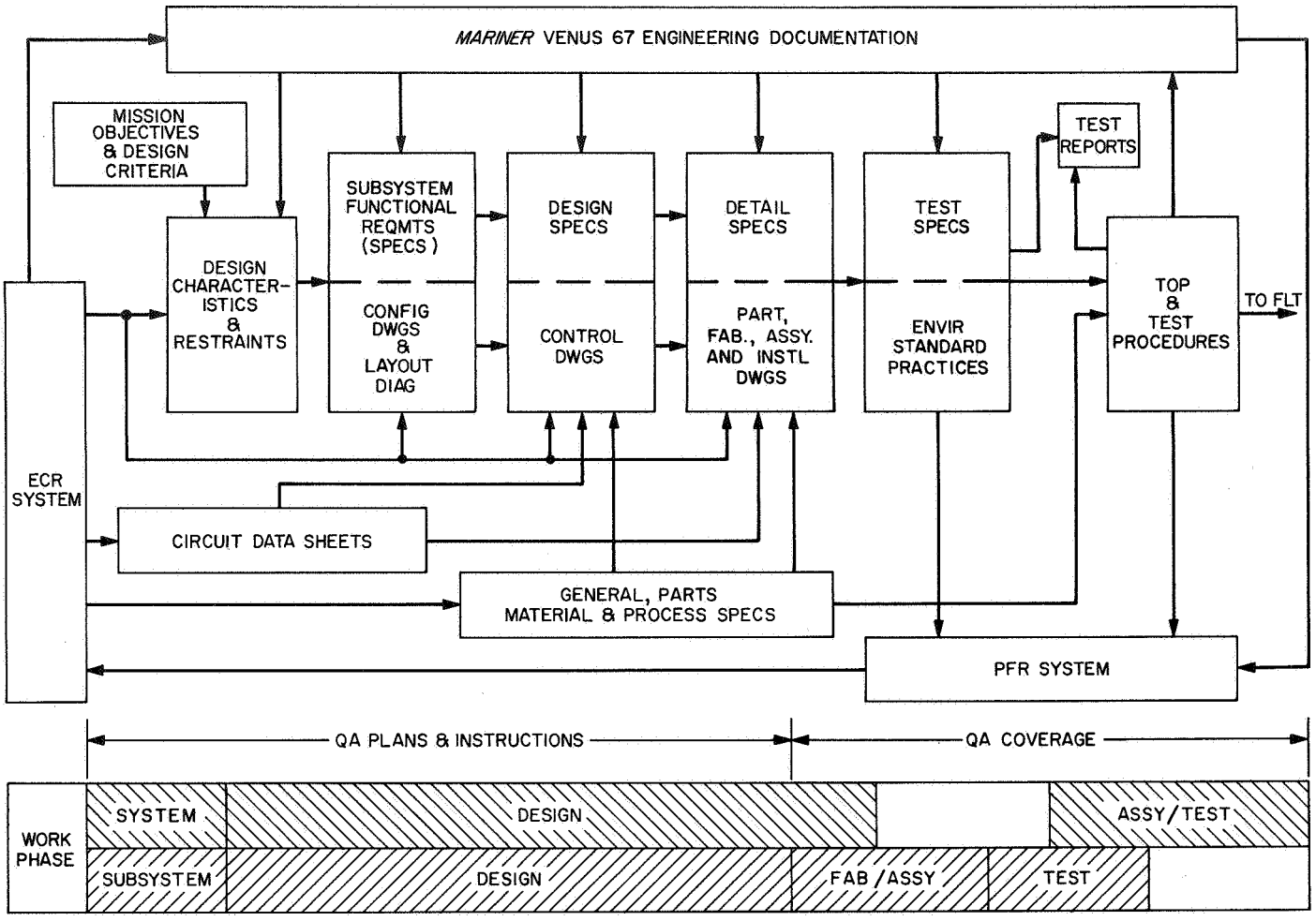



**Fig. II-15. Documentation relationships for development of *Mariner V* spacecraft system**

With respect to the mission-related hardware and software, a similar pattern was followed in the mission operations system. Launch-vehicle tracking and data system reviews were held in accordance with the normal practice of those agencies. In all instances, the related documentation and statements by the cognizant individuals were carefully recorded. Action assignments arising from these reviews were carried in the regular meeting minutes or on separate action item summaries and continually checked until satisfactory resolution was obtained. This technique proved to be valuable and well worth the effort.

## G. Schedules and Progress Reports

In addition to status monitoring that occurred in the process of regular meetings and reviews, other means of reporting were established. The system was structured generally as shown in Fig. II-16 and tailored in recognition of the irrevocable launch date. As with any goal-oriented system, but especially so with a planetary opportunity, the intermediary milestones become especially important. Thus, if there is any appreciable slip in these milestones, the implication is that greater risk is being assumed because some of the necessary steps will have to be abbreviated. In this sense, the reporting of progress against approved schedules is increasingly important as the time to launch draws near. Considerable emphasis was placed upon maintaining the credibility (and discipline) of the schedules as well as timely and accurate reporting of deviations against them. One aspect of scheduling activities that probably was not handled too well was a convenient provision for quickly requesting and acknowledging a deviation from the original plan or the necessity to invoke a significant schedule revision. Except for flow plans, emphasis was not placed on tracking slip trends, nor were the schedules or status reports an early warning system of future slips. Most delays in

the project occurred because of unexpected technical difficulties that the status system could not (and did not) detect. Thus, the initial reports of troubles or delays were first reported by the technical people through the project line organization.

The scheduling activity seemed to resolve into a dichotomy in which the initial schedules developed by the project invoked discrete milestones upon the supporting elements. The second facet was a response by the supporting elements, which culminated in the generation of

**Table II-1. Composite problem (P) list**

| P No. | System | Problem description | Person to whom primary responsibility for resolving problem was assigned | Design assistants | Date assigned | Date resolved |
|---|---|---|---|---|---|---|
| P-1 | TDS | Communications processor (C.P.). The current mechanization of the C.P. does not permit transmission of "QC" commands. Replaced by P-5. | M. S. Glenn | | 2/3/67 | 2/15/67 |
| P-2 | SC | Tape recorder delivery—late. Delivered to SAF—3/1/67. | T. C. Sorensen | | 2/3/67 | 3/1/67 |
| P-3 | SC | DAS crystal availability. All DAS crystals have been delivered. | J. J. Paulson | | 2/3/67 | 2/15/67 |
| P-4 | SC | M67-2 gyro delivery. Delivered to SAF—3/8/67. | J. L. Savino | | 2/3/67 | 3/8/67 |
| P-5 | MOS | *Mariner* Mars 1964 procedure for sending command instructions to the DSIF and acting on these instructions does not reflect the current mechanization of the DSN. Isolated to the GSFC C.P.; corrective action underway. | D. W. Douglas | W. E. Kirhofer<br>W. L. Brown | 2/15/67 | 4/3/67 |
| P-6 | SC | M67-1 DAS outputs science gates at incorrect times. This anomaly occurs only in SC system configuration and cannot be reproduced in the DAS subsystem in the lab. This problem isolated to a chip in the DAS. Failure mechanism unexplained as of 5/19/67. Chip sectioning underway as last step planned in investigation. Connector evaluation negative. | J. J. Paulson | R. H. White | 2/27/67 | 5/25/67 |
| P-7 | SC | DFR crystals are suspect and may require replacing—problem: loss of validation—crystals will be replaced. | A. E. Wolfe | J. J. Paulson<br>A. G. Conrad | 3/10/67 | 3/22/67 |
| P-8 | SC | Magnetometer toggle—filter added to eliminate toggling. | A. E. Wolfe | J. J. Paulson<br>A. G. Conrad | 3/10/67 | 3/22/67 |
| P-9 | MOS | SIPM has not achieved operational capability. | R. Stott | | 4/5/67 | 5/19/67 |
| P-10 | LV | *Agena* propellant isolation valve failure during ATS launch on 4/5/67. Oxidizer valve did not close after first burn, therefore precluding second burn. Failure mode demonstrated. Requalification completed. Flight validated by successful Lunar Orbiter injection. Expected closure 5/22 upon acceptance of reworked valves at ETR. | H. W. Plohr | R. K. Hackbarth<br>(A. N. Williams) | 4/21/67 | 5/24/67 |
| P-11 | SC | DAS frame count skip possibly results in premature antenna pointing angle change (APAC) event. This item of potential degradation to prime encounter measurements will be carried on this list at least until the consequences are better understood. Strong suggestion cause is noise of external origin. | J. J. Paulson | R. Draper | 4/24/67 | 5/25/67 |
| P-12 | MOS | RWV power supplies are experiencing excessive transistor failures. Requires timely replacement or substitute provisions throughout DSN. About one day behind on plan to re-equip primary DSN stations. First set shipped. | T. C. Sorensen | W. Trester | 4/25/67 | 6/1/67 |
| P-13 | LV | *Agena* velocity meter/chopper failed in recent Air Force launch. | H. W. Plohr | R. K. Hackbarth | 5/12/67 | 6/2/67 |
| P-14 | LV | *Agena* timer survey—possible faulty bearing installation. Prime units returned, checked out and reinstalled. Backup units enroute ETR. | H. W. Plohr<br>LeRC | H. Zweigbaum<br>(A. N. Williams) | 5/25/67 | 6/2/67 |
| P-15 | TDS | Inadequate telemetry/tracking ship commitment. Threatens to restrict launch window and shorten the launch period severely. | M. S. Glenn | A. Hirshberg | 5/25/67 | 6/14/67 |
| P-16 | SC | Radio power amplifier transfer malfunction. Initial tests suggest relay contact has welded closed. SC is being demated and returned to ESF for additional investigation and repairs. | A. E. Wolfe | T. C. Sorensen | 6/2/67 | 6/12/67 |

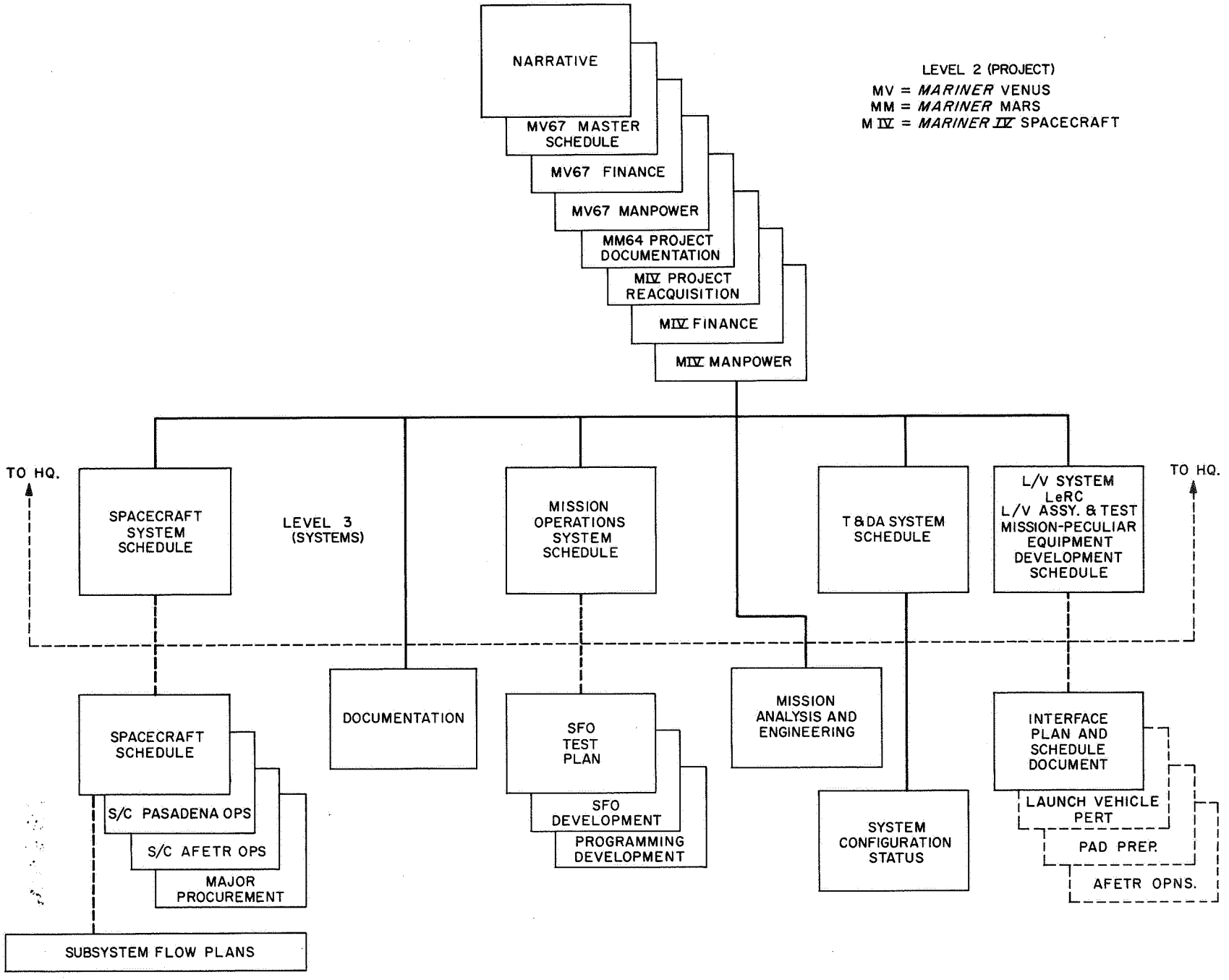



**Fig. II-16. Reporting structure**

the supporting schedules that lent credence to the original milestones.

*1. Headquarters reports.* The formal means of advising headquarters of progress and problems was the monthly submittal of the project management reports (PMR). This report (Appendix B) is part of the management information and control system developed in 1965/1966 by the Office of Space Science and Applications (OSSA). The PMR performed many of the same functions, in a more uniform and formal manner, that were accomplished by means of informal reports on the *Mariner* Mars 1964 effort. In essence, it is a standardized, unified record of schedule, manpower, fiscal plans, and status. The "headquarters" milestones shown in Appendix B were established in the Project Development Plan (PDP).

*2. Schedules.* Supporting the PMR was the layer of working schedules used within the systems and in the interfaces. An example of such a schedule is shown in Fig. II-17. This chart is an interesting case in the sense that it was never completely closed out or posted. This happened in several instances where the maintenance of the schedule no longer seemed to make sense as the work entered a different phase. In the case of the spacecraft schedule of Fig. II-17, that chart was superseded by the spacecraft operations manager's schedule which, in turn, was revised several times. Occasionally it proved difficult to track a consistent set of events.

It should be noted that special emphasis was given to a knowledge of the status of computer programming development. Indeed, a thorough schedule was prepared in that area and statused on a regular basis. The primary difficulty experienced with this new area was in the consistent interpretation of the milestone.

*3. Flow plans.* Activity and event networks similar to PERT were again used on this project, primarily in the spacecraft area. Subsystems prepared rather complete networks and the status reports extended into mission-related hardware and the system test complex data system (STCDS). With the exception of the STCDS, the flow plans were not computerized. As noted above, manipulation of these flow plans and reports seldom alerted project supervision to delays of any significance. Thus, the status reports against the plans were more often used to bring to line-management attention the fact of a slip and to suggest implications after that slip had occurred.

It was also noted again that the demands for various summaries and special breakouts of information are virtually limitless. Presentation of one particular arrangement invariably invoked questions that could not be answered by the status reports, as generated. It was recognized that automatic data processing (ADP) was one possible means of being able to generate many different sorts of status displays, and they could be placed on a call basis. However, it is the earnest recommendation of those involved in mechanizing the flow plan reporting system that ADP should not be employed until the personnel involved thoroughly understand the implications of scheduling a planetary mission so that proper emphasis and balance can be given to the depth of monitoring. It is dangerously easy to have the system swamped out by senseless trivia.

Analysis of the trends of events again proved to be of value (trend comparisons were occasionally made with *Mariner C*). But for decision purposes, such graphics or tabulations seldom showed the real cause or pointed to possible solutions.

*4. Special data banks.* There was no organized effort to initiate formal information storage or retrieval systems. However, the documentation plan, the numerous listings, the material collected for presentation at reviews, meeting minutes, etc., all reflected the reservoir of information on the project. Within the resource limitations imposed on the *Mariner* Venus 67 effort, elaborate information systems did not appear justifiable. Where, however, documentation or other information had to be conveyed to accomplish the job, there was no reluctance to produce the information and make it readily available.

In addition, a very modest configuration management effort was inaugurated. Primarily, this effort was authorized to obtain an understanding of the qualification experience of flight hardware to facilitate flight selection. In no way did this effort exercise control or direction over the design or testing activities, but rather it collected the related change history, test experience, PFR records, etc., to permit direct comparison of given subsystems. Again, a manual manipulation was employed in preference to ADP.

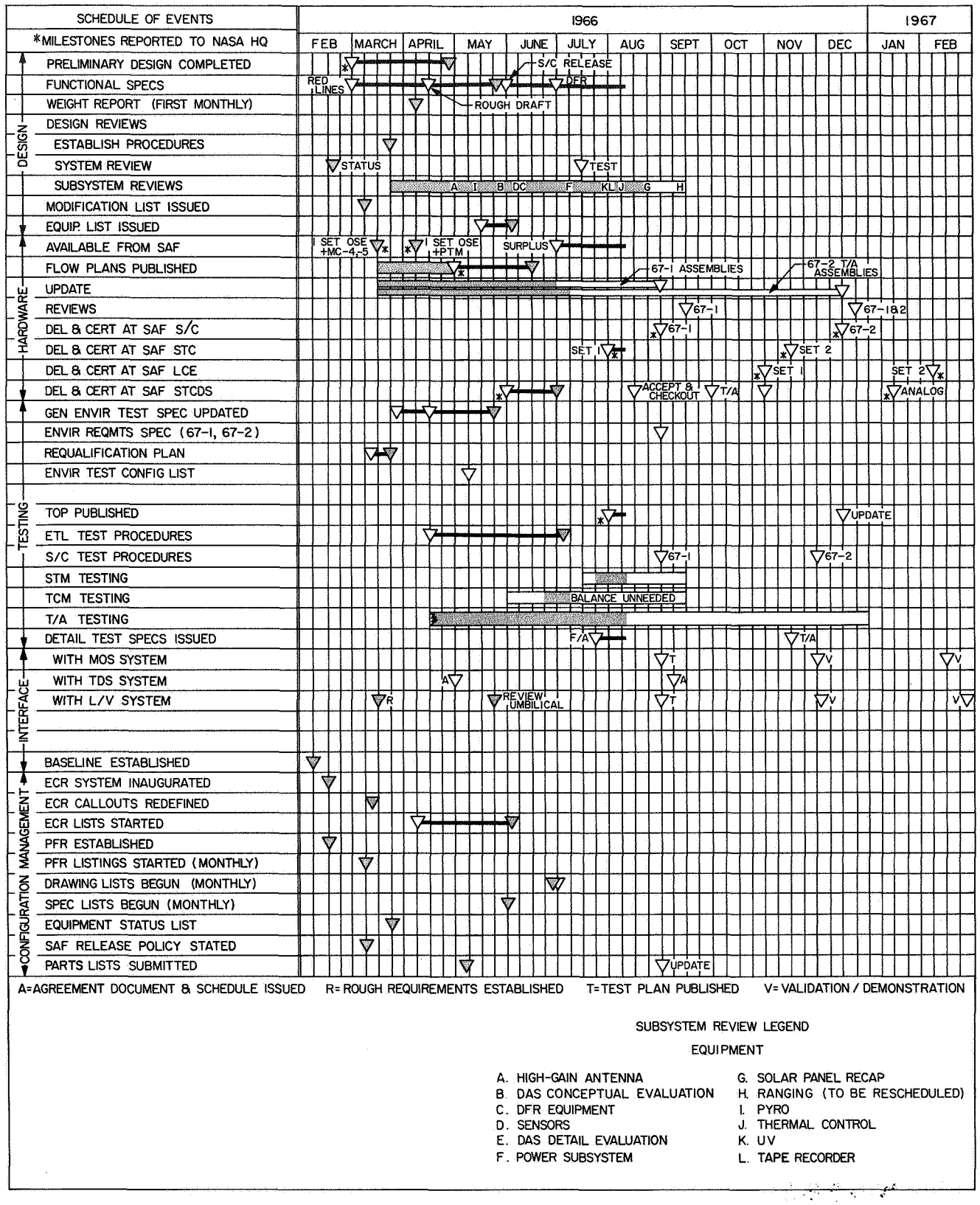



**Fig. II-17. *Mariner* Venus 67 project, spacecraft system schedule**

PRECEDING PAGE BLANK NOT FILMED.

# III. Flight Path Analysis and Mission Planning

## A. Trajectory Design

*1. Launch and arrival date selection.* Because the planets within the solar system have locations that are known functions of time, the launch and arrival date[1] for a ballistic transfer between two planets can be used to specify two-position vectors along the sun-centered transfer ellipse. From these vectors, it is possible to compute the heliocentric orbital elements that completely define the transfer ellipse. The heliocentric or sun-centered portion of an interplanetary trajectory therefore is dependent on the launch and arrival date only, and variations in the near-earth or near-Venus trajectory parameters (i.e., launch azimuth or aiming point) produce only second-order changes in the heliocentric trajectory.

*2. Design objectives.* The first objective followed in the trajectory design was to select trajectories that would simplify spacecraft configuration. Since the relative positions of the earth, sun, and Canopus are fixed for a given arrival date at Venus, the use of a launch period comprised of constant arrival-date trajectories provided similar encounter geometry for each launch date, thereby imposing less stringent antenna and planet-scan design requirements. Another objective in the trajectory design was to provide optimum geometry for the S-band occultation experiment. Satisfaction of this objective depended on the proper choice of the direction of the approach asymptote of the near-Venus hyperbola, which is a function of both launch and arrival date. Other objectives included a requirement to minimize transit time and communication distance at Venus encounter. The requirement for minimum communication distance also can be attributed to the S-band occultation experiment's need for maximum communication margin. In addition to satisfying these objectives, the selected trajectories had to provide at least a 10- to 15-day launch period with a 550-lb spacecraft.

*3. Arrival date characteristics.* A study was undertaken to determine which arrival date best satisfied the design objectives. Assuming an injection energy, $C_3 = 11.5\ km^2/s^2$, it was found that the arrival dates for Type I[2] trajectories were restricted to the month of October 1967. It was also found that later arrivals (up to October 20) were better suited for the S-band occultation experiment. Other factors associated with later arrival dates include:

(1) Encounter-communication-distance increases.

(2) Transit-time increases.

(3) Asymptotic-approach-speed-at-Venus increases.

(4) Launch-period increases.

[1]These dates correspond to the Greenwich Mean Time (GMT) of the event.

[2]Type I trajectories are defined as having heliocentric transfer angles less than 180 degrees from launch to encounter.

*4. Resulting arrival date.* Using the criteria described, an arrival date of October 19, 1967 best satisfied the trajectory design objectives. The selection of this date was based primarily on the demands of the S-band occultation experiment.

*5. Launch period.* Once the arrival date(s) is (are) selected for an interplanetary mission, the launch dates comprising the launch period are usually established by launch-vehicle performance. For the *Mariner* Venus 67 mission, however, the first day of the launch period was determined on the basis of the encounter geometry as it pertains to the S-band occultation experiment. For purposes of mission design, launch dates before June 12, 1967 were eliminated. To increase the probability of launching the spacecraft, a launch period of 16 days ($C_3 = 11.37$ km$^2$/s$^2$) was used for planning purposes. The actual launch period was slightly more than this, being ultimately determined by the final spacecraft weight and launch-vehicle performance capability. Figure III-1 depicts the increasing energy requirement as the launch period is lengthened.

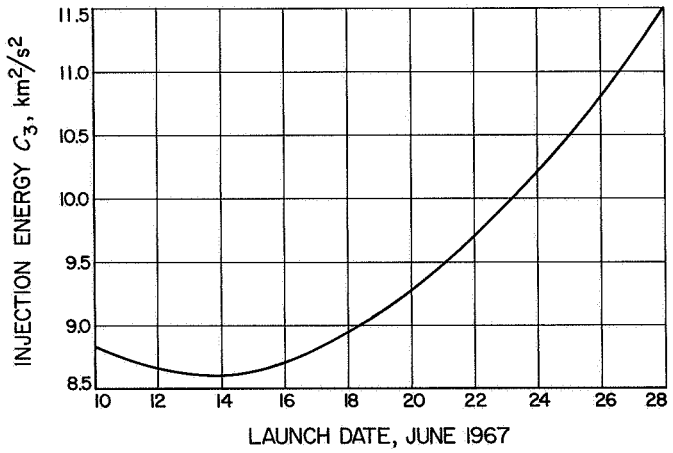



**Fig. III-1. Injection energy vs launch date**

## B. Aiming Point Considerations

The aiming points were selected to satisfy constraints imposed by the spacecraft while providing maximum return from the scientific experiments.

*1. Scientific experiments.* The science considerations used in the aiming point selection were directed toward the following:

(1) The earth occultation experiments require an aiming point that would result in the earth being occulted by Venus as seen from the spacecraft. It is necessary to have occultation occur when the spacecraft is at small distances from the planet's surface. In addition, it is extremely important that the occultation miss parameter,[3] $p$, be as small as possible.

(2) The fields and particles experiments, which consist of various instruments designed to measure magnetic fields and radiation belts (if they exist) in the vicinity of the planet, prefer trajectories with low altitudes of closest approach. In addition, a trajectory passing close to the shadow of Venus would be desirable from the standpoint of measuring the effects of the solar plasma wake.

(3) Since the UV photometer will be mounted rigidly to the spacecraft, it is important that its field of view pass nearly across the planet's center. In addition, it is desirable to have the instrument scan the terminator.

*2. Engineering constraints.* The more important spacecraft-related constraints that must be satisfied to ensure that the spacecraft will perform properly during the encounter sequence are:

(1) The sun-probe near limb of Venus angle (SPV) has to be greater than zero deg during the entire encounter phase. This constraint prohibits the spacecraft from entering the Venus shadow, thus preventing loss of the sun which is required both for solar power and as a reference body for the attitude-control system.

(2) No part of Venus should fall within a region $\pm 26$ deg in clock angle during the encounter phase. This constraint ensures that the Canopus tracker will not have sunlight, reflecting from Venus, fall within its field of view. An equivalent statement of this constraint is that the Canopus-probe near limb of Venus angle (CPV) has to be greater than 36 deg during the entire encounter phase.

(3) The spacecraft should not impact Venus. Violation of this constraint would result in the loss of most encounter science data and possible planet contamination.

*3. Aiming region.* The aiming-zone geometry may be conveniently represented on a plane that is perpendicular

[3]The occultation miss parameter, $p$, is defined as the minimum distance from the spacecraft to the planet's center as viewed from earth.

to the direction of the approach asymptote of the near-Venus hyperbola. The aiming point is defined by **B**, a vector that is perpendicular to the incoming asymptote and has a magnitude equal to the distance from the center of the planet to the asymptote. The direction of **B** is specified by the angle $\theta$ which is the angle between **B** and **T**, where **T** is in the aiming plane parallel to the ecliptic (Fig. III-2).

As shown in Fig. III-3, the contours, labeled $SPV = 0$ deg, have the property that any aiming point **B**, which lies inside this contour, will result in a planet pass such that engineering constraint (1) above is violated. Similarly, the region, labeled $CPV = 36$ deg, results in violation of constraint (2) above. The aiming point should also avoid the impact circle, so that constraint (3) above may be satisfied. To provide a trajectory that would result in earth occultation, the aiming point would have to lie within the region designated $EPV = 0$ deg (earth-probe near limb of Venus angle = 0 deg). Shown near the center of this region are lines of constant occultation miss parameter, $p$.

*4. Aiming point selection.* In selecting aiming points to be used as part of the trajectory design, careful consideration had to be given to possible aiming point dispersions caused by orbit determination and midcourse-maneuver execution errors. To provide reasonable assurance that the actual spacecraft trajectory would not violate the sun and Canopus constraint regions, in addition to not impacting the planet, prospective aiming points were established by having their 3-$\sigma$ midcourse execution error

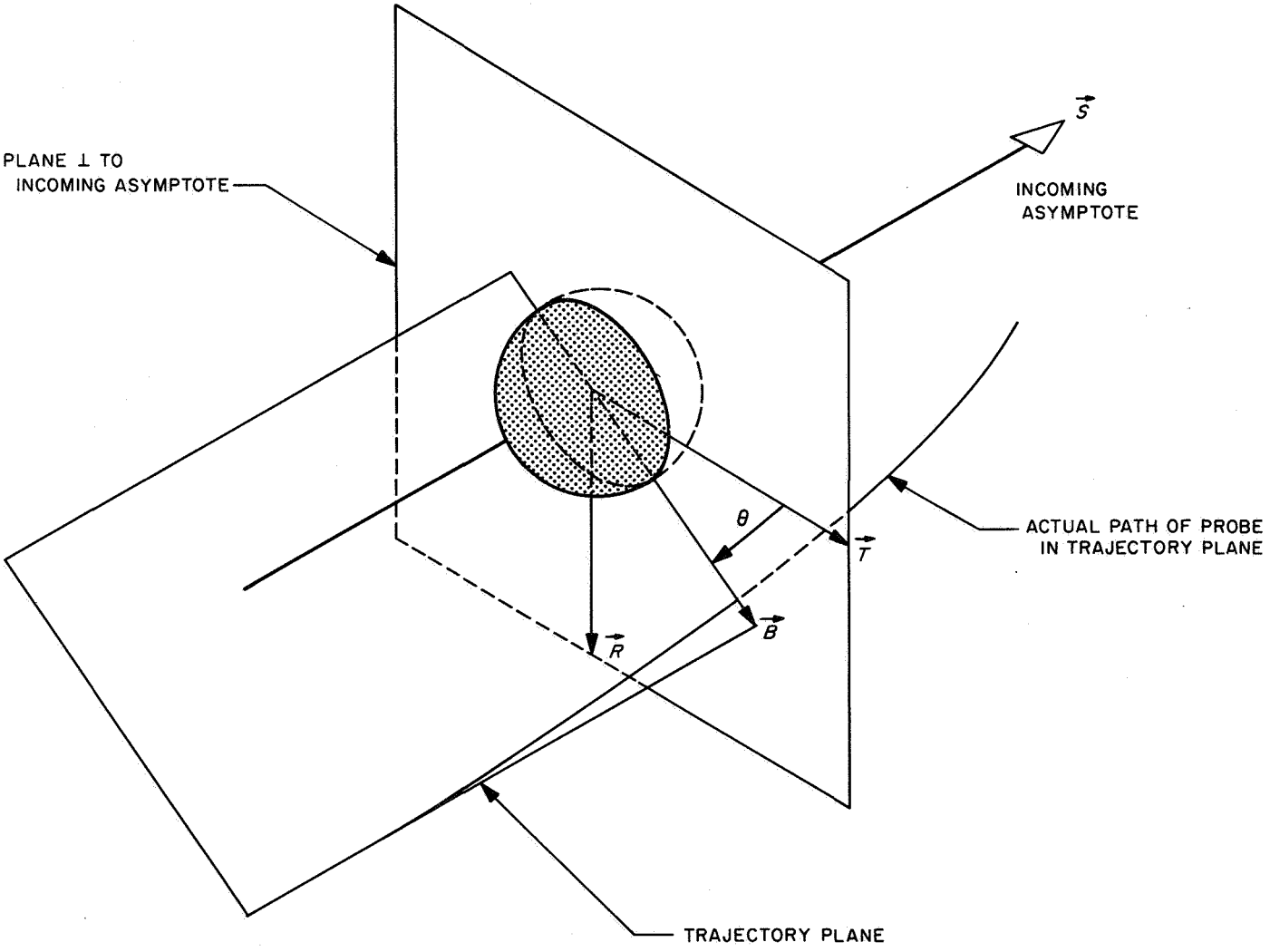



**Fig. III-2. Definition of aiming-zone parameters**

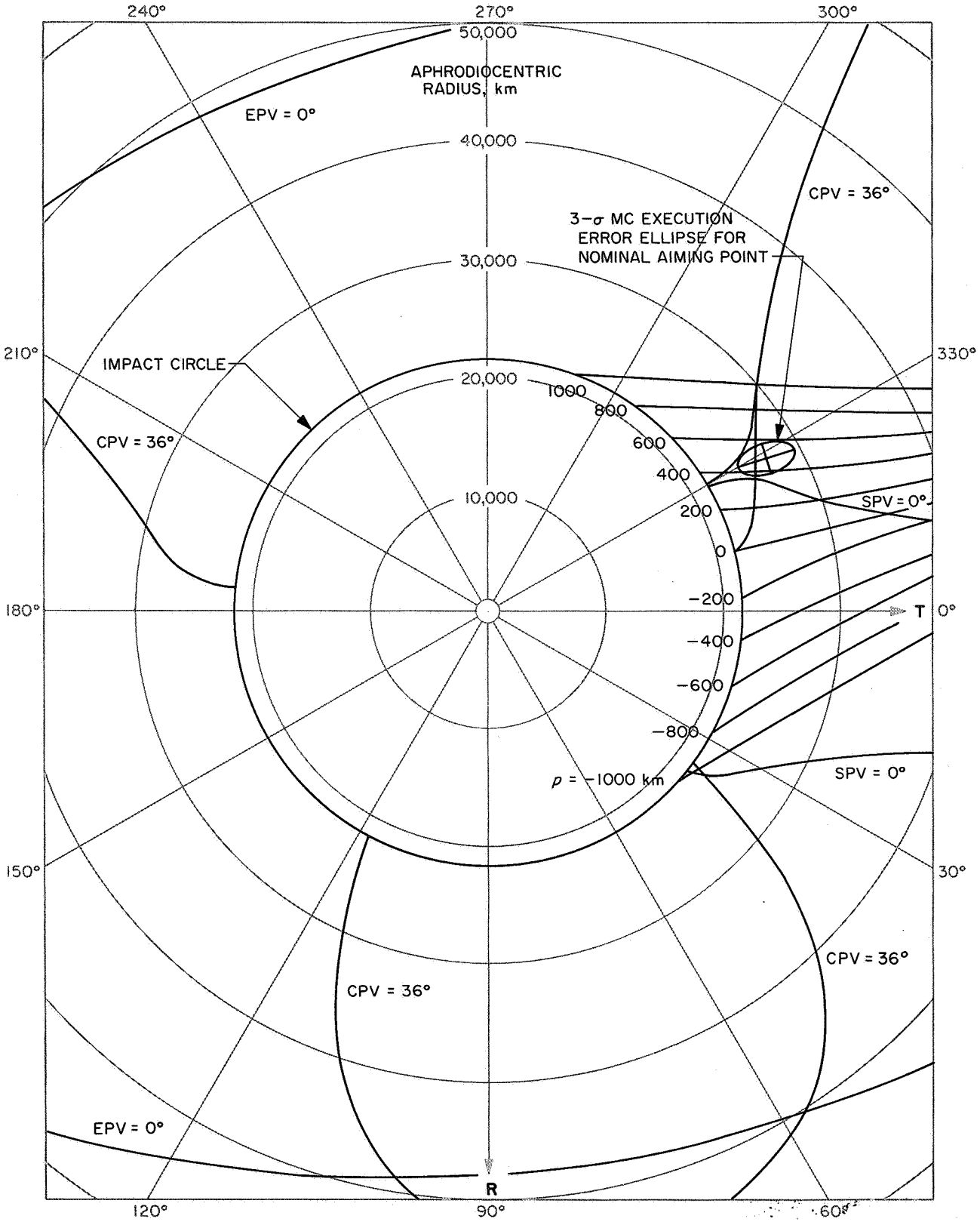



**Fig. III-3. Aiming zone and constraint regions for June 12, 1967 launch**

ellipses[4] lie tangent to the constraint regions. This provided a probability of less than $10^{-2}$ of violating the constraints. Aiming points lying on the right side of the earth occultation contour ($EPV = 0$ deg) were more desirable than those on the left because of the smaller occultation distances. Because of the requirement to minimize the occultation miss parameter, $p$, it was necessary to only consider aiming points lying above the sun occultation region. The following aiming points were chosen for a number of launch dates during the design launch period:

| Launch date, 1967 | $\|\mathbf{B}\|$, km | $\theta$, deg |
|---|---|---|
| June 12 | 27,000 | −29 |
| June 17 | 25,000 | −32 |
| June 22 | 25,000 | −33 |
| June 27 | 25,000 | −32 |

The above aiming points were used for mission design purposes. The actual injection guidance system was targeted to a biased aiming point ($\mathbf{B} \sim 100{,}000$ km, $\theta \sim -40$ deg) to maintain the total probability of violation of planetary quarantine less than $3 \times 10^{-5}$. This was necessary to assure that the contribution due to the empty *Agena* stage would be negligible, since the spacecraft with its maneuver capability could have been aimed much closer. Table III-1 lists the results of the actual targeting. Note that the first launch day listed is June 14. June 12 and 13 were eliminated because the resulting encounter geometry was not as good for those days as for the remainder of the launch period.

## C. Trajectory Characteristics

*1. Near-earth trajectory.* Near-earth trajectories can be accurately represented by a hyperbola whose perigee is nearly equal to the parking orbit radius. The orientation of the required outgoing asymptote of the hyperbola and the required injection energy stay relatively constant for a few hours on any launch day but will vary from day to day through the launch period. The launch to injection time, injection locations, and launch window for a given launch azimuth are determined by these two parameters. The injection locations move downrange as the injection energy increases and the declination of the outgoing asymptote increases in algebraic value. The launch window increases in duration as the value of the declination of the outgoing asymptote increases in algebraic value.

[4]This dispersion ellipse assumes a 1-$\sigma$ injection error.

To launch the spacecraft, a launch azimuth that will allow the spacecraft to travel in a plane containing the launch site at launch and the outgoing asymptote must be used. Since the asymptote is approximately fixed in inertial space while the launch site is rotating, it is necessary that the launch azimuth be varied continuously through the launch window. Also, since it is optimum (for maximizing payload) to inject at or near perigee, the parking-orbit coast time must be varied continuously.

Because of range safety considerations, the maximum allowable launch azimuth sector is 90–114 deg east of north from the Air Force Eastern Test Range (AFETR). With this azimuth sector, the *Mariner V* trajectories had daily launch windows ranging from 2.2 to 2.9 h for the June 12 and 27 launch dates, respectively. The launch time and time from launch to injection are given as a function of launch date in Figs. III-4 and 5.

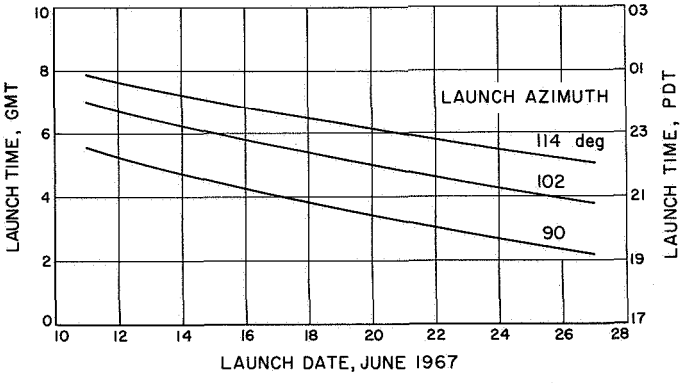



**Fig. III-4. Launch time vs launch date**

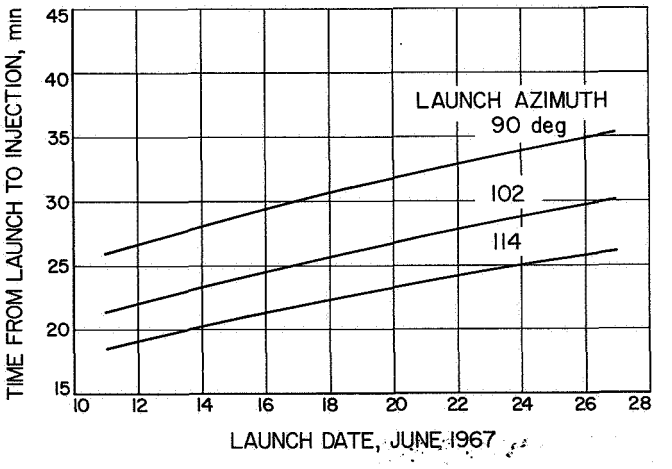



**Fig. III-5. Time from launch to injection vs launch date**

## Table III-1. *Mariner V* launch period characteristics (biased aiming point)

| Launch date, June 1967 | Launch azimuth, deg | Launch, day and time or GMT | GMT of parking orbit *injection* | GMT of transfer orbit *injection* | Injection velocity, *mph* | Nominal midcourse day and time, GMT | Distance of closest approach $R_{min}$, mi | Closest approach time, 10/19/67, GMT | Communication distance at closest approach, mi | Time of flight from injection | Nominal distance of closest approach to Venus without corrective maneuver, $R_{min}$, mi |
|---|---|---|---|---|---|---|---|---|---|---|---|
| 14 | Open 98.8<br>Close 114 | 6/14 05:47<br>6/14 07:05 | $05^h\ 56^m$<br>$07^h\ 13^m$ | $06^h\ 12^m\ 08^s$<br>$07^h\ 25^m\ 08^s$ | 25,493 | 6/19 23:00 | 5,750 | 18:00 | 49,550,000 | $127^d\ 11.5^h$ | 46,277 |
| 15 | Open 98.7<br>Close 114 | 6/15 05:31<br>6/15 06:53 | $05^h\ 40^m$<br>$07^h\ 01^m$ | $05^h\ 56^m\ 28^s$<br>$07^h\ 13^m\ 32^s$ | 25,497 | 6/20 23:00 | 5,750 | 18:00 | 49,550,000 | $126^d\ 11.7^h$ | 44,202 |
| 16 | Open 99.0<br>Close 114 | 6/16 05:20<br>6/16 06:41 | $05^h\ 28^m$<br>$06^h\ 49^m$ | $05^h\ 45^m\ 15^s$<br>$07^h\ 02^m\ 08^s$ | 25,503 | 6/21 23:00 | 5,150 | 18:00 | 49,550,000 | $125^d\ 11.9^h$ | 44,112 |
| 17 | Open 98.0<br>Close 114 | 6/17 04:59<br>6/17 06:29 | $05^h\ 07^m$<br>$06^h\ 38^m$ | $05^h\ 25^m\ 26^s$<br>$06^h\ 51^m\ 01^s$ | 25,513 | 6/22 23:00 | 5,150 | 18:00 | 49,550,000 | $124^d\ 12.1^h$ | 44,704 |
| 18 | Open 90<br>Close 93<br>Open 102<br>Close 114 | 6/18 03:47<br>6/18 04:10<br>6/18 05:13<br>6/18 06:18 | $03^h\ 56^m$<br>$04^h\ 19^m$<br>$05^h\ 22^m$<br>$06^h\ 26^m$ | $04^h\ 17^m\ 19^s$<br>—<br>—<br>$06^h\ 40^m\ 07^s$ | 25,525 | 6/23 23:00 | 5,150 | 18:00 | 49,550,000 | $123^d\ 12.4^h$ | 44,949 |
| 19 | Open 90<br>Close 95<br>Open 102<br>Close 114 | 6/19 03:34<br>6/19 04:12<br>6/19 05:00<br>6/19 06:07 | $03^h\ 43^m$<br>$04^h\ 21^m$<br>$05^h\ 09^m$<br>$06^h\ 15^m$ | $04^h\ 04^m\ 53^s$<br>—<br>—<br>$06^h\ 29^m\ 33^s$ | 25,540 | 6/24 23:00 | 5,150 | 18:00 | 49,550,000 | $122^d\ 12.6^h$ | 45,212 |

Also of interest during the near-earth phase of the mission is the position of the earth relative to the spacecraft. A convenient way to present this type of information is to relate the earth direction to the sun and Canopus-reference directions on the spacecraft. The earth direction is defined as the earth-probe-sun angle. The earth clock angle is defined as the angle between the projection of the spacecraft–Canopus vector on a plane perpendicular to the sun-probe vector and the projection of the spacecraft–earth vector on the same plane (Fig. III-6).

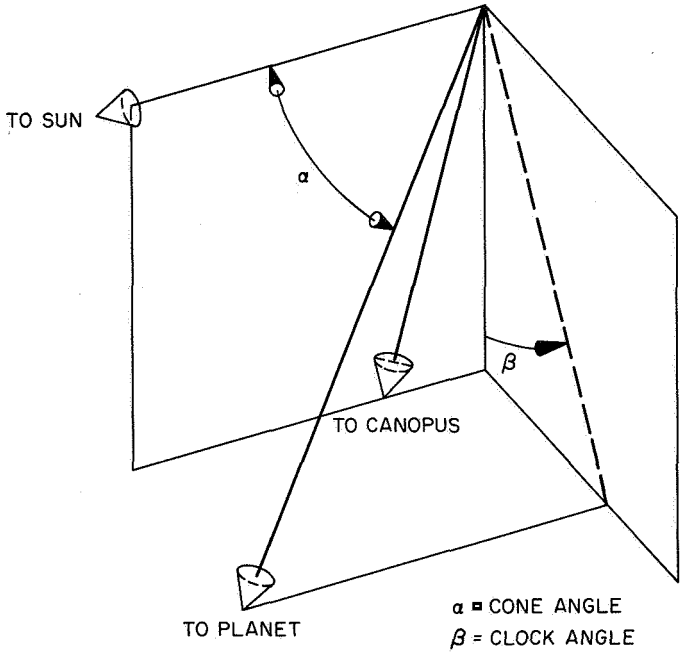



**Fig. III-6. Definition of spacecraft coordinate system**

*2. Heliocentric trajectory.* The heliocentric portion of the trajectory is an ellipse that essentially intersects the earth at launch and the planet Venus at encounter. The spacecraft escapes the earth along its outgoing asymptote at a speed determined by the energy imparted to the spacecraft at injection. The hyperbolic excess velocity vector, plus the earth's velocity vector about the sun, add vectorially to determine the velocity at which the spacecraft enters the heliocentric orbit. Since the spacecraft is launched "backward" from the earth's orbital motion, the magnitude of the resultant velocity vector is smaller (relative to the sun) than the earth's. Consequently, the spacecraft falls toward the sun (Figs. III-7, 8).

As the spacecraft falls toward the sun, it picks up speed and finally passes the earth. At this time, the earth cone

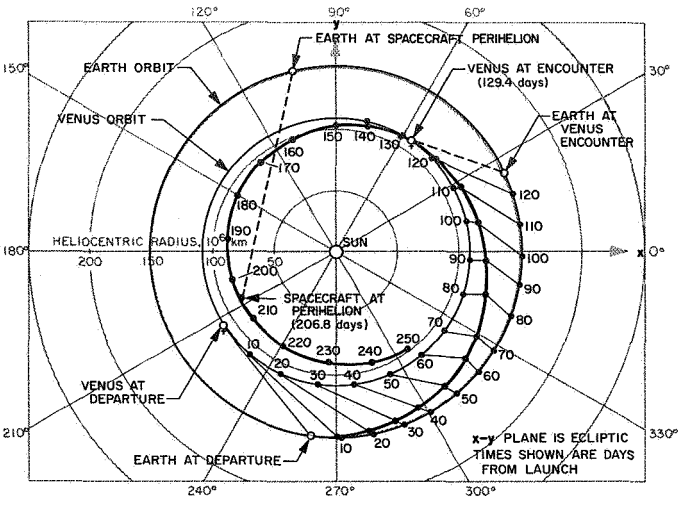



**Fig. III-7. Projection of heliocentric trajectory on ecliptic plane for June 12, 1967 launch**

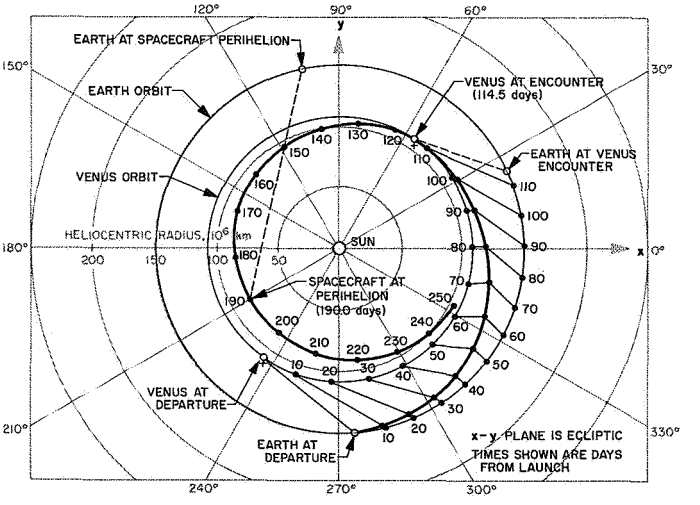



**Fig. III-8. Projection of heliocentric trajectory on ecliptic plane for June 27, 1967 launch**

angle reaches a maximum which is less than 180 deg (this angle does not reach 180 deg because the spacecraft is not in the ecliptic plane on its path to Venus).

It may be noted that the spacecraft takes up a new heliocentric orbit subsequent to its encounter with Venus (Figs. III-7, 8). The parameters of the new orbit differ greatly from those of the original orbit because of the large perturbations introduced during the Venus encounter. One significant change is the decrease in perihelion distance to approximately 0.56 AU. Table III-2

**Table III-2. Heliocentric trajectory characteristics**

| Launch date | June 12, 1967 | June 17, 1967 | June 22, 1967 | June 27, 1967 |
|---|---|---|---|---|
| Injection energy, $C_3$, km$^2$/s$^2$ | 8.668 | 8.812 | 9.715 | 11.374 |
| Declination of outgoing asymptote $\phi_s$, deg | −14.31 | −8.22 | −3.21 | 0.79 |
| Flight time, $T_F$, days | 129.40 | 124.45 | 119.50 | 114.55 |
| Communication distance at encounter, $R_E$, km | 79,726,000 | 79,726,000 | 79,726,000 | 79,726,000 |
| Sun-spacecraft distance at encounter, $R_s$, km | 108,013,000 | 108,013,000 | 108,013,000 | 108,013,000 |
| Earth cone angle at encounter, $\alpha_E$, deg | 104.02 | 104.02 | 104.02 | 104.02 |
| Earth clock angle at encounter, $\beta_E$, deg | 102.47 | 102.47 | 102.47 | 102.47 |
| Asymptotic approach speed at Venus, V, km/s | 3.020 | 3.113 | 3.215 | 3.319 |
| Pre-encounter orbit | | | | |
| Semimajor axis, a, km | 129,985,450 | 130,022,525 | 130,437,260 | 131,015,150 |
| Eccentricity, e | 0.17318665 | 0.17486428 | 0.17651082 | 0.17981485 |
| Inclination to the ecliptic, i, deg | 2.8755034 | 2.3928661 | 2.0729681 | 1.8311737 |
| Longitude of ascending node, Ω, deg | 79.825079 | 84.690343 | 89.433511 | 94.242094 |
| Argument of perihelion, ω, deg | 352.70260 | 347.98497 | 343.06508 | 337.80246 |
| Perihelion distance, $R_p$, km | 107,473,700 | 107,453,510 | 107,413,670 | 107,456,668 |
| | October 28, 1967 | | | |
| Time of perihelion passage, T, GMT | 16:52:41 | 18:36:03 | 14:45:09 | 08:36:01 |
| Post-encounter orbit | | | | |
| Semimajor axis a, km | 97,830,548 | 96,745,190 | 96,967,845 | 97,260,464 |
| Eccentricity, e | 0.12139013 | 0.13052002 | 0.13025614 | 0.13041709 |
| Inclination to the ecliptic, i, deg | 1.5076440 | 1.4624116 | 1.3671982 | 1.3417160 |
| Longitude of ascending node, Ω, deg | 107.78318 | 110.05465 | 115.78512 | 117.47809 |
| Argument of perihelion, ω, deg | 100.40705 | 102.12096 | 94.539064 | 90.254299 |
| Perihelion distance, $R_p$, km | 85,954,886 | 84,118,006 | 84,337,189 | 84,576,038 |
| | January 5, 1968 | January 6, 1968 | January 5, 1968 | January 3, 1968 |
| Time of perihelion passage, T, GMT | 01:04:12 | 01:48:23 | 02:56:07 | 17:56:01 |
| Perihelion time, days past launch | 206.8 | 202.8 | 196.9 | 190.0 |
| Perihelion time, days past encounter | 77.4 | 78.4 | 77.4 | 75.5 |
| Communication distance at perihelion, $R_{E_p}$, km | 187,966,000 | 190,007,000 | 189,191,000 | 187,126,000 |
| Earth cone angle at perihelion, $\alpha_{E_p}$, deg | 49.28 | 47.64 | 48.21 | 49.56 |
| Earth clock angle at perihelion, $\beta_{E_p}$, deg | 76.57 | 76.89 | 76.72 | 76.44 |

is a summation of the heliocentric trajectory characteristics for a number of launch dates.

3. *Near-Venus trajectory.* To an observer on Venus, the spacecraft would appear to be traveling on a hyperbola, approaching Venus from above the ecliptic and from outside the planet's orbit (Fig. III-9). Orthographic projections of the near-Venus trajectory are given in Figs. III-10 through 13. The rather large amount of bending caused by gravitational attraction of Venus is quite evident in these illustrations. One may also observe that the spacecraft, initially above the reference plane,[5] moves from left to right, passing above the planet's shadow. Assuming no atmosphere, at approximately 6 min before closest approach the occultation begins. Exit occultation occurs approximately 20 min past closest approach after a total duration of 26 min and the spacecraft is then below the reference plane. A summary of the more important planet-related trajectory parameters is given in Table III-3.

[5]The reference plane used in these illustrations is centered at Venus and oriented parallel to the ecliptic.

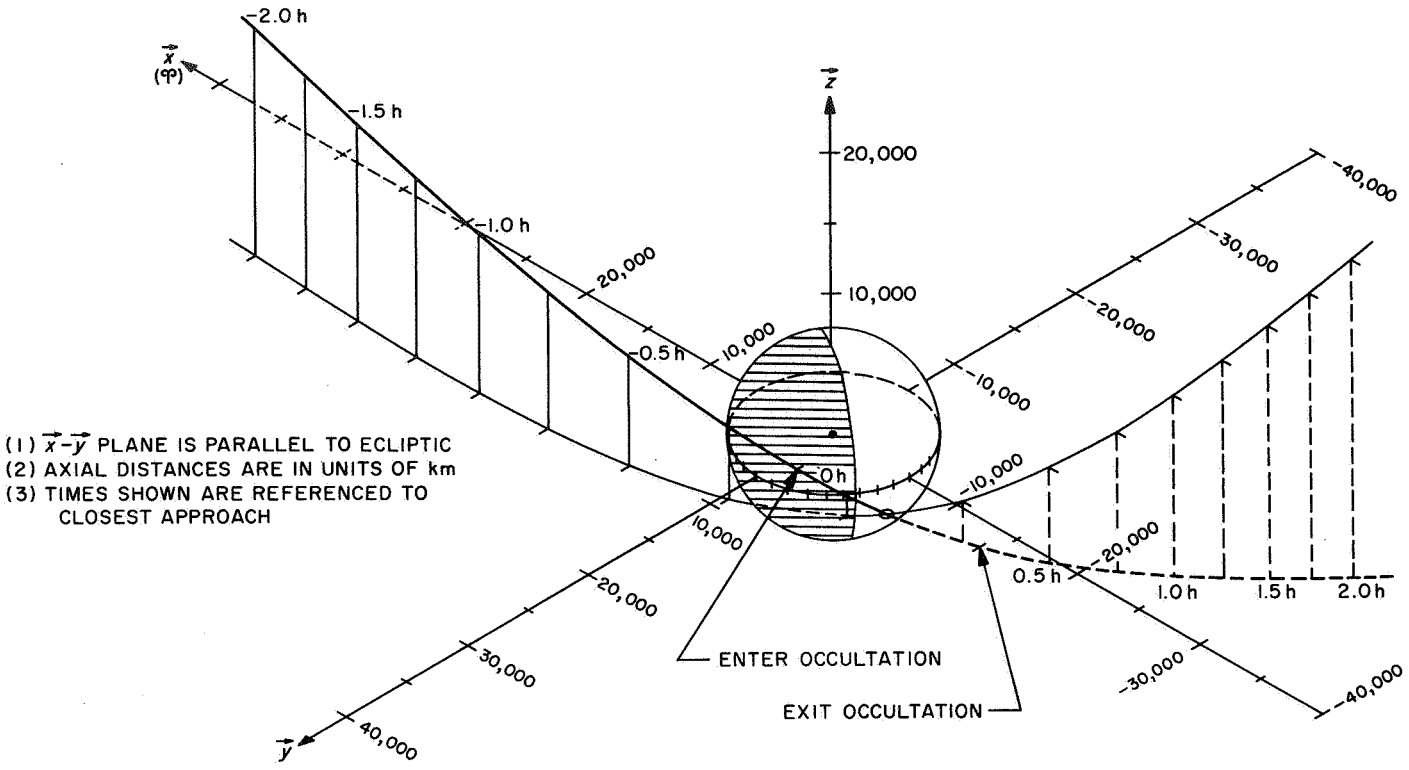



**Fig. III-9. Isometric view of near-Venus trajectory**

**Table III-3. Near-Venus trajectory characteristics**

| Launch date | June 12, 1967 | June 17, 1967 | June 22, 1967 | June 27, 1967 |
|---|---|---|---|---|
| Arrival date<br>Arrival time,* approximately 17:00 GMT | October 19, 1967 | | | |
| Radius of closest approach, km | 9,084 | 8,299 | 9,047 | 9,501 |
| Altitude of closest approach, km | 2,884 | 2,099 | 2,848 | 3,301 |
| Velocity at closest approach, km/s | 8.979 | 9.379 | 9.063 | 8.909 |
| Enter occultation time,** GMT | 16:55:19 | 16:53:52 | 16:54:29 | 16:55:16 |
| Enter occultation time, minutes from closest approach | −4.42 | −5.93 | −5.83 | −4.72 |
| Exit occultation time, GMT | 17:20:33 | 17:17:53 | 17:19:03 | 17:19:54 |
| Exit occultation time, minutes from closest approach | 20.82 | 18.08 | 19.18 | 19.92 |
| Duration of occultation, min | 25.24 | 24.01 | 25.01 | 24.64 |
| Occultation miss parameter, p, km | 498 | −220 | −767 | −1319 |
| Aphrodiocentric orbital elements | | | | |
| Semimajor axis, a, km | −35,598.055 | −33,519.747 | −31,428.807 | −29,481.032 |
| Eccentricity, e | 1.2551761 | 1.2475780 | 1.2878491 | 1.3222878 |
| Inclination to the ecliptic, i, deg | 29.188599 | 33.304917 | 35.536181 | 35.783782 |
| Longitude of ascending node, Ω, deg | 345.24683 | 336.59035 | 331.17444 | 325.90029 |
| Argument of periapsis, ω, deg | 149.90319 | 161.22310 | 165.48857 | 169.00125 |
| Time of periapsis passage, T, GMT | 16:59:44.2 | 16:59:48.4 | 16:59:52.3 | 16:59:58.7 |

*The arrival time (taken to be the time of periapsis passage) was selected to enable the spacecraft to encounter Venus during the middle of the Goldstone view period.
**Occultation times are computed here ignoring the atmosphere. Deviations from the "no atmosphere" case give information about the actual atmosphere.

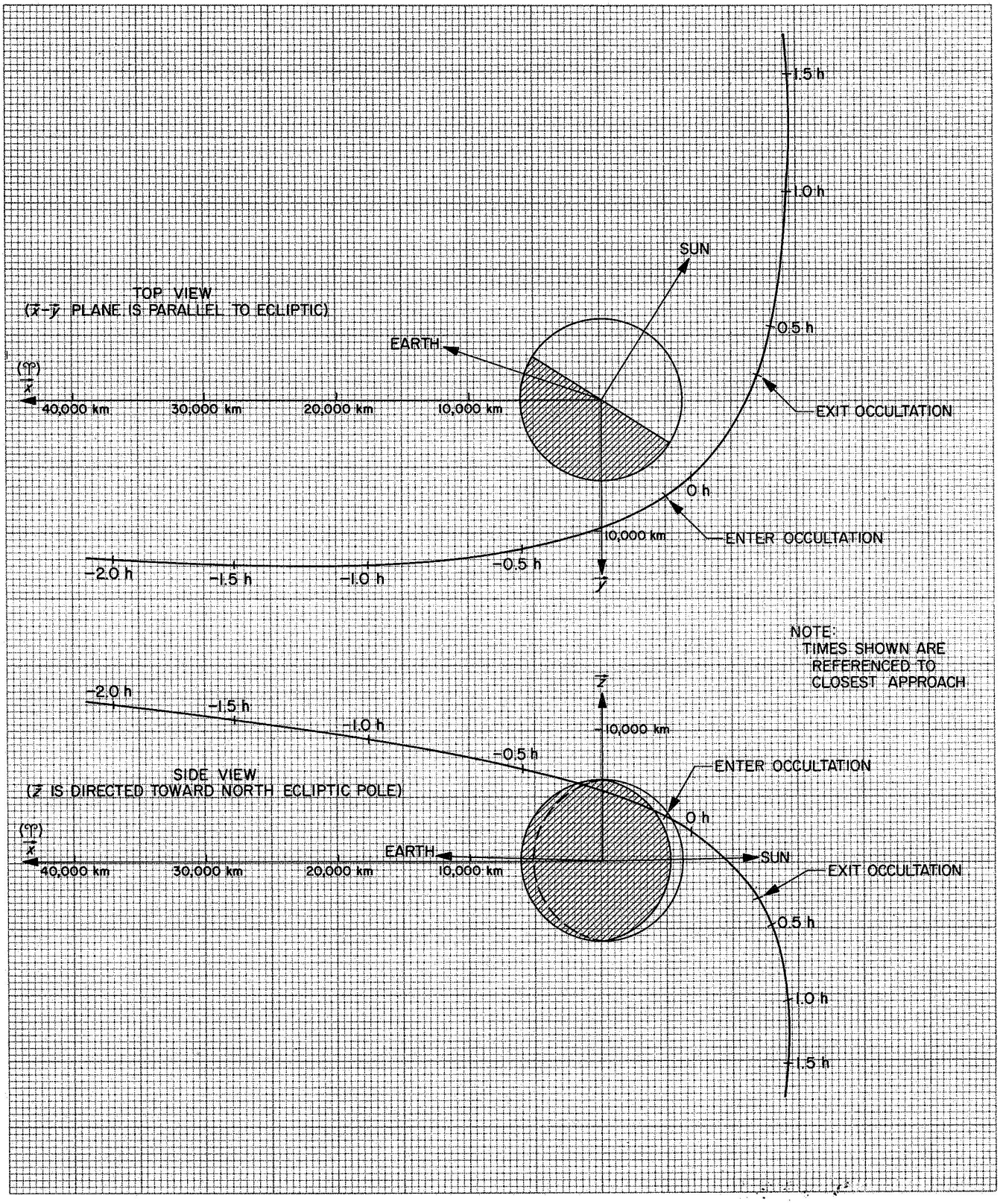



**Fig. III-10. Orthographic projections of near-Venus trajectory for June 12, 1967 launch**

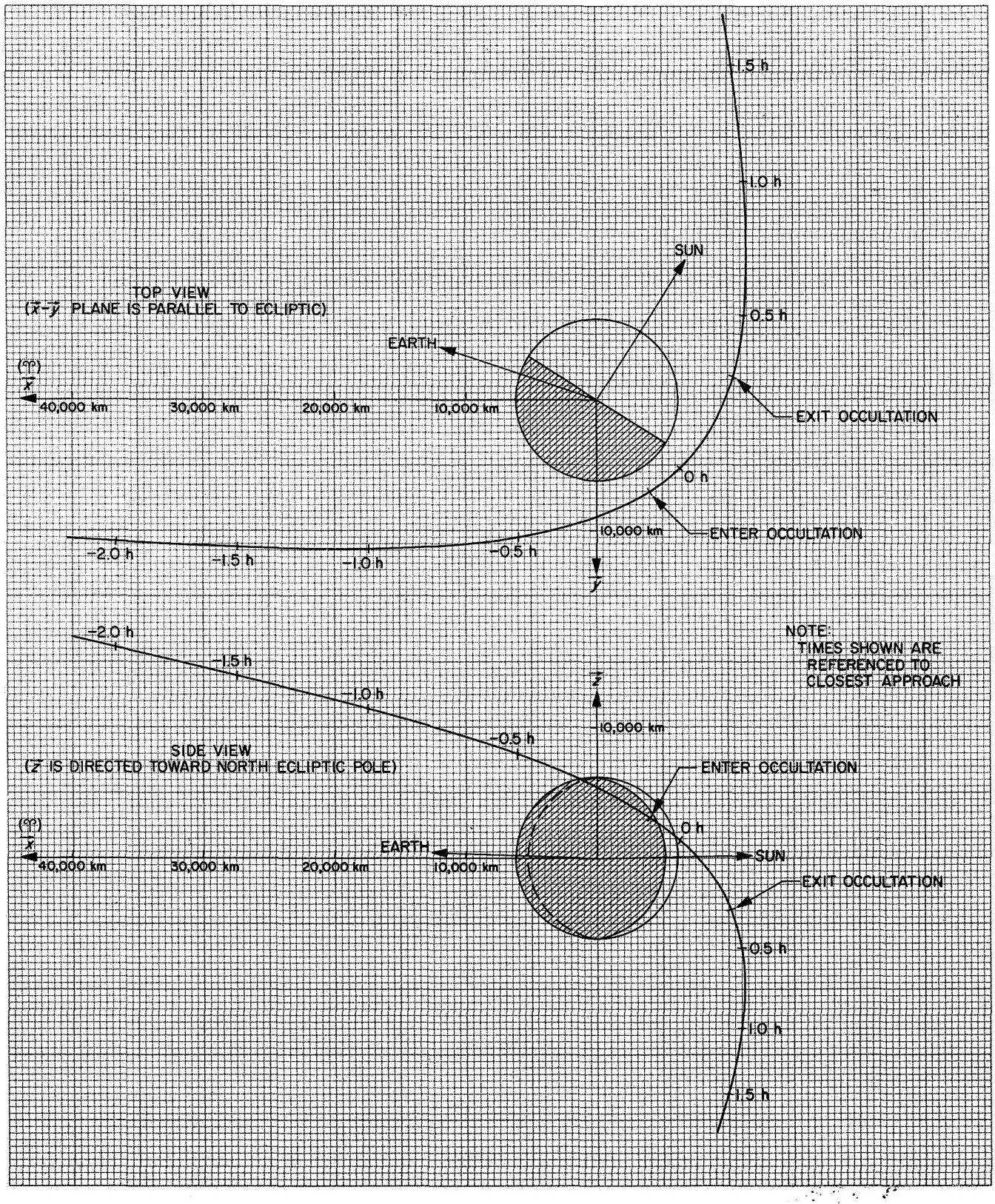



**Fig. III-11. Orthographic projections of near-Venus trajectory for June 17, 1967 launch**

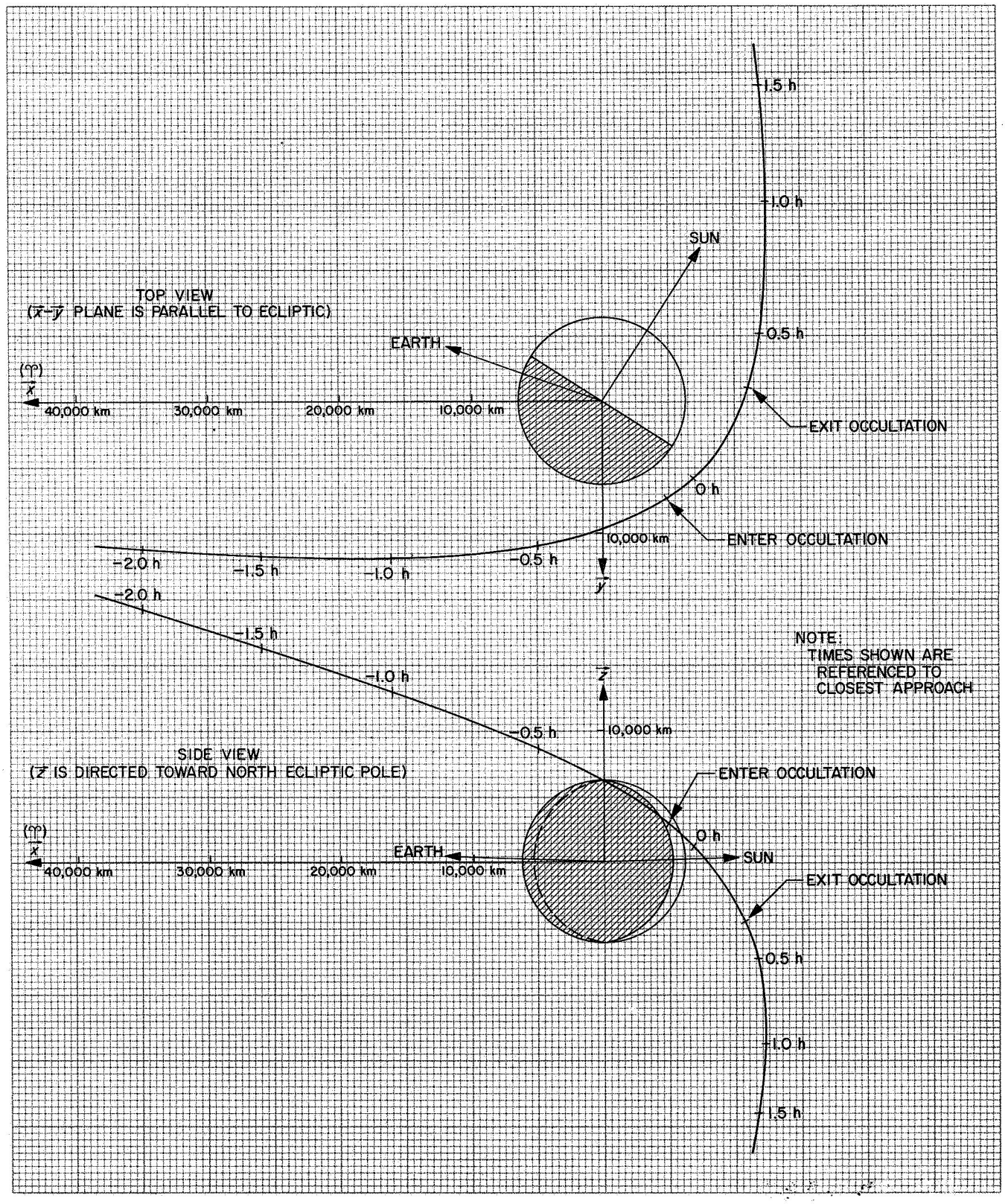



**Fig. III-12. Orthographic projections of near-Venus trajectory for June 22, 1967 launch**

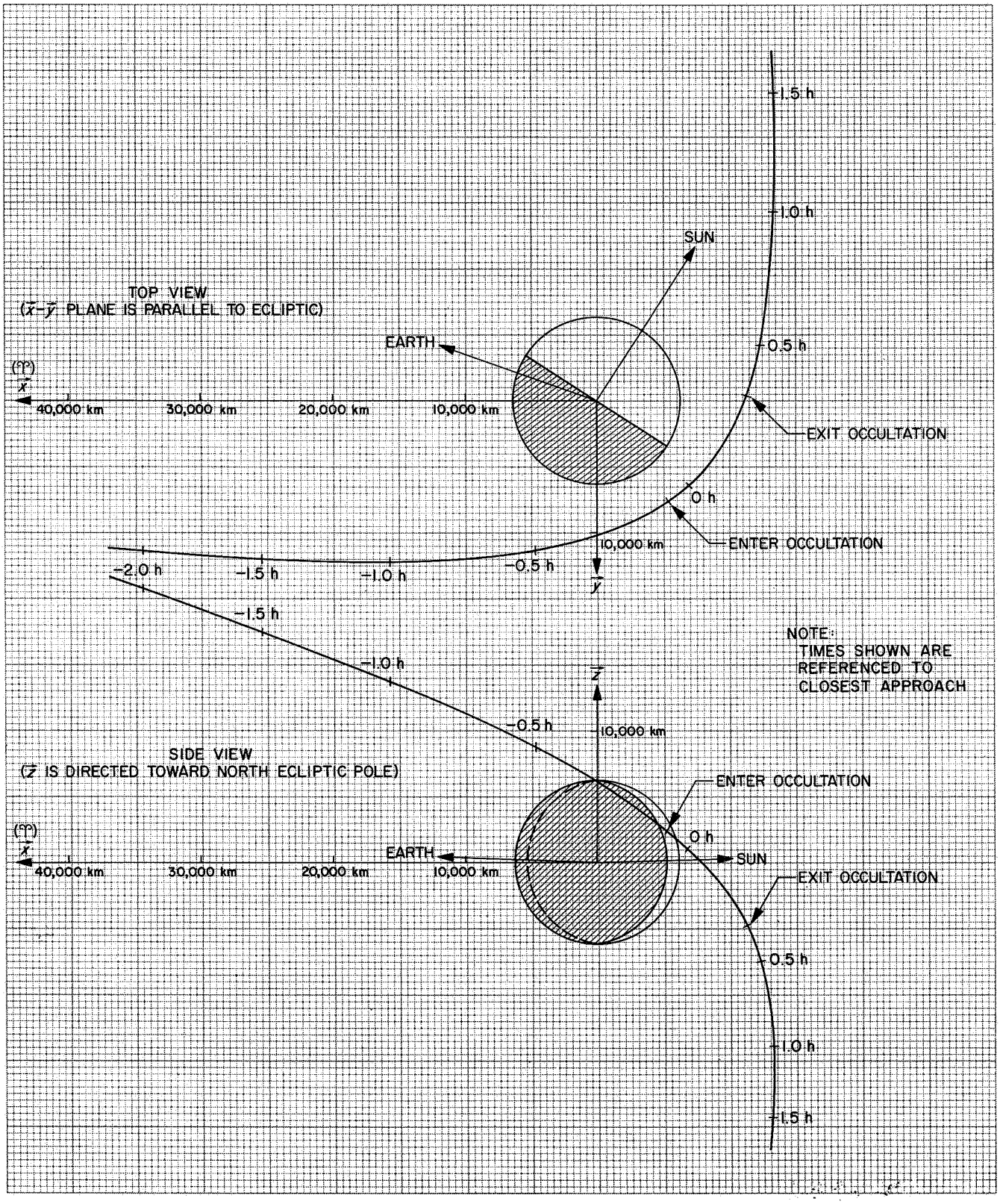



**Fig. III-13. Orthographic projections of near-Venus trajectory for June 27, 1967 launch**

## D. Effect of Antenna Design on Mission Planning

*1. Choice of enter and exit occultation offset angles.* The S-band occultation experiment is the only experiment carried by the *Mariner V* spacecraft that is directed exclusively toward the planet. Since scientific estimates of the surface pressure of the Venusian atmosphere ranged from 2 to 200 times the pressure at the earth's surface, the S-band occultation experiment had to be designed to accommodate this extreme range of estimates. The occultation experiment was designed primarily for a GH-50 model (so-called greenhouse model with a 50-atmosphere pressure). Attenuation of signal and bending of the beam are the two factors that affect the value of the occultation experiment. To minimize the degrading effects of these factors, the peak gain of the antenna was offset from the nominal earth direction by some angle $\eta_1$. In this manner, the chances of receiving entrance occultation data all the way to the surface of the planet were considerably increased. Because of the geometry, the sign of the offset angle must be reversed to improve the exit occultation (Fig. III-14).

The choice of the actual values of the enter and exit occultation offset angles ($\eta_1, \eta_2$) had a great effect upon

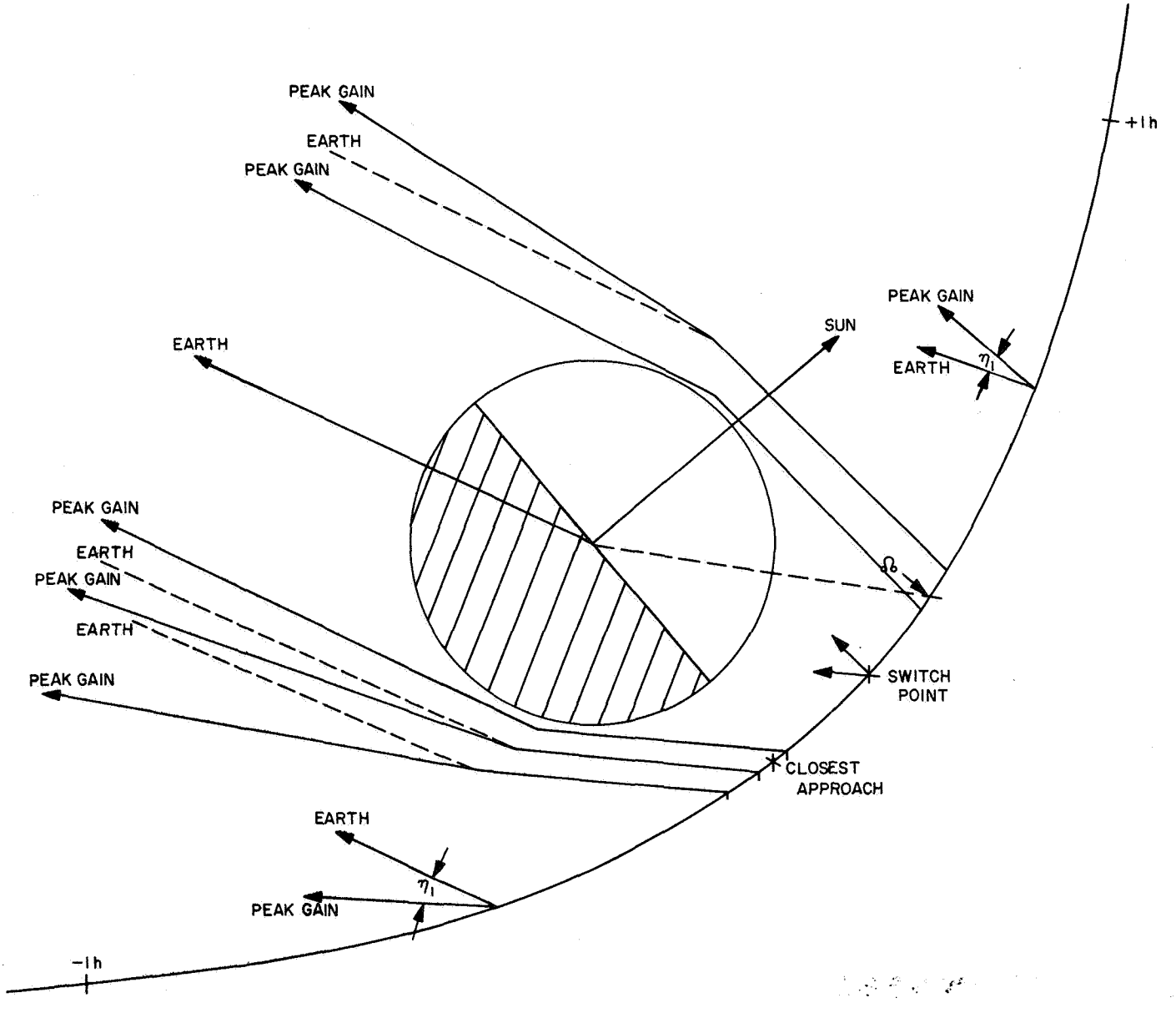



**Fig. III-14. Ecliptic projection of near-Venus trajectory**

the expected value of the occultation experiment. Since offsetting the antenna also affects the spacecraft–earth communications, the choice of the angles was to be accomplished so as to return a reasonable amount of S-band occultation data while maintaining good communications geometry. In addition, it was desirable to choose the offset positions so that even in the event of failure of the switching mechanism, the communications period of the encounter would be sufficient to return recorded scientific data.

Preliminary results indicated that, in the event of a failure, an enter occultation offset ($\eta_1$) of 5 deg would allow a 10-day post-encounter communications period. Any offsets greater than 5 deg would reduce this failure mode communications period by approximately a day per degree; therefore, for an offset of 10 deg and a 10-day recorder playback time, a failure of the switching device would allow only approximately one-half of the stored data to be transmitted to earth. If the device switched too soon, virtually no entrance occultation data would be received. In addition, if the offset angle for exit occultation ($\eta_2$) was very large (greater than 10–12 deg), this early switching failure mode could mean that no real-time telemetry would be obtained near encounter. Thus, a tradeoff had to be made between the S-band occultation experiment and the stored scientific data.

To assist in making this tradeoff, a mathematical model that used previously established techniques (Refs. 2 and 3) was developed to evaluate the problem. The model's main features included a set of value functions that reflected (roughly) the relative worth of various aspects of the tradeoff, and a set of mathematical expressions that combined these value functions into one parameter called "return," which is assumed to be a measure of the expected worth of the occultation and stored scientific data. The return was calculated for various strategies of $\eta_1$ and $\eta_2$, and the results were used to recommend an offset strategy.

*2. Value functions.* There are two major value functions for the occultation experiment and one for the communications period.

Figure III-15 gives the value function, $V_H$, for the occultation experiment as a function of the altitude at which the signal is lost. The first jump in the function occurs at 80 km and reflects the desirability of receiving data below the thick cloud layer (thought to be located at a height of 80 km). The second jump reflects the fact that obtaining occultation data all the way to the surface is much more valuable than obtaining data, for example,

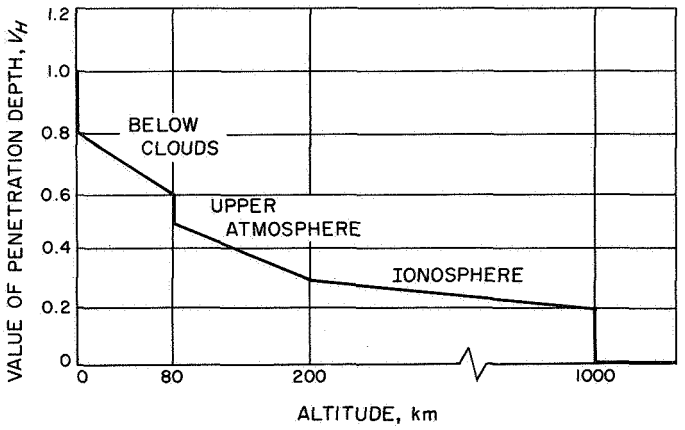



**Fig. III-15. Value function vs occultation cutoff altitude**

only to the 2-km level. This is true because unless the surface is observed, its location cannot be fixed precisely and this degrades the value of the experiment. The exit and entrance occultation value functions will not, in general, be the same. Very good exit data may be used, for example, to help interpret sketchy entrance data.

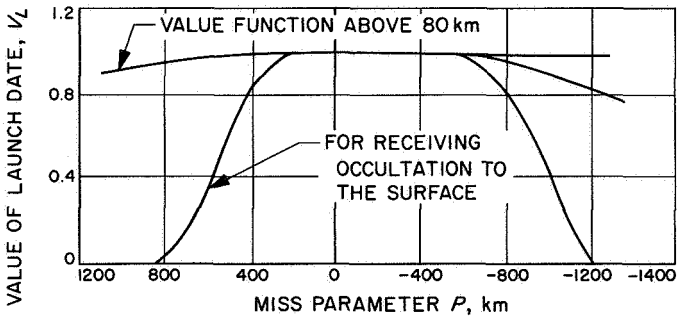



**Fig. III-16. Value function vs miss parameter *P***

The value function shown in Fig. III-16 reflects the degradation to the occultation experiment produced by the out-of-plane bending of rays caused by the failure to pass directly behind the center of the planet as viewed from earth during occultation. The distance between a center pass and the actual trajectory is the miss parameter, $P$, which varies according to the launch day. The center of the value function is not at $P = 0$ because the earth track (the apparent positions of the earth as seen from the spacecraft) has a slight curvature which makes a small amount of out-of-plane bending desirable. The out-of-plane bending is important only for the lower atmosphere (below 80 km).

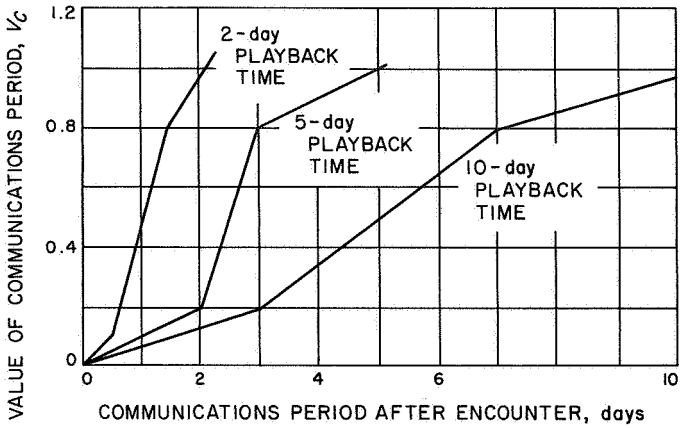



**Fig. III-17. Value functions vs communications period after encounter**

Figure III-17 reflects the expected value of the information recorded on various portions of the tape. The first part of the tape is presumably not as interesting as the middle where the near encounter ultraviolet and dual-frequency data are expected to be found.

*3. Description of the model.* The model developed used the parameter "Scientific Return," $R$, as the parameter to maximize. The objective of the model was to first display $R$ as a function of the offset strategy, i.e., $R = R(\eta_1, \eta_2)$, and then to maximize $R(\eta_1, \eta_2)$ by finding the maximizing $(\eta_1, \eta_2)$ strategy.

The function, $R$, can be resolved into the sum of three other functions: $R_o$, the return value of the occultation experiment; $R_s$, the return value of all the recorded scientific data; $R_{RT}$, the return value of all the real-time scientific data excluding the S-band data. Each of these return functions can be written as functions of the strategy $(\eta_1, \eta_2)$ and the scientific return $R$ can be calculated from the following:

$$R = W_o R_o + W_s R_s + W_{RT} R_{RT}$$

where

$W_o$ = the relative value of the occultation experiment

$W_s$ = the relative value of the recorded data

$W_{RT}$ = the relative value of the real-time data not including occultation

These weights are determined from the relative experiment values given in Table III-4.

**Table III-4. Scientific experiment values**

| Experiment | Estimate of overall value | Estimates of the fraction of scientific value obtained in case no stored data received |
|---|---|---|
| S-band occultation | 0.35 | 0.9 |
| Dual-frequency receiver | 0.20 | 0.1 |
| Ultraviolet (UV) photometer | 0.15 | 0.6 |
| Magnetometer | 0.15 | 0.5 |
| Plasma | 0.09 | 0.5 |
| TRD | 0.06 | 0.5 |

From Table III-4 the relative weights can be determined as:

$$W_o = (0.9)(0.35) = 0.315$$

$$W_s = (1 - 0.9)(0.35) + (1 - 0.1)(0.2) + (1 - 0.6)(0.15) + (1 - 0.3)(0.5) = 0.425$$

$$W_{RT} = (0.1)(0.2) + (0.6)(0.15) + (0.3)(0.5) = 0.26$$

*4. Net return from the occultation experiment.* The return from the occultation experiment depends upon:

(1) Occultation cutoff altitude ($H_{\min}$)

(2) Launch date

(3) Probability that the device switches, $P_s$

(4) Relative value of the S-band occultation

These relationships may be expressed by the following equation:

$$R_o = V_{o/s} P_s + V_{o/es} P_{es} + V_{o/ns} P_{ns}$$

where

$V_{o/s}$ = net value of the occultation if the device switches properly

$V_{o/es}$ = net value of the occultation if the device switches early

$V_{o/ns}$ = net value of the occultation if the device does not switch

The subscripted $P$'s are the probabilities associated with these respective events (the miss parameter $P$ has no subscript). The exact form of the equations are given below.

Note that the value of the entrance and exit terms are not the same if the switching device operates properly.

$$V_{o/ns} = V_p V_H(\eta_1)$$

$$V_{o/es} = V_p V_H(\eta_2)$$

$$V_{o/s} = V_p V_H(\eta_i) + (V_c + V_s) V_m$$

$$V_p = \sum_{n=1}^{K} P_L(n) V_L(n)$$

where

$P_L(n)$ = probability of launching on $n^{\text{th}}$ day of launch period which is $K$ days long

$V_L(n)$ = value of miss parameter on $n^{\text{th}}$ day

$$V_H(\eta) = V_I + V_u + (V_c + V_s) V_m$$

where

$V_I$ = 0.3 value of ionospheric occultation data only

$V_u$ = 0.2 value of upper atmosphere data only

$V_c$ = 0.3 value of data below clouds

$V_s$ = 0.2 value of data to the surface

$$V_m = \left(1 - \frac{H_{\min}}{H_o}\right)$$

where $H_{\min}$ is a function of altitude.

To simplify the expressions, $V_{o/es}$ was assumed to be equal to $V_{o/ns}$ which is true when the offset angles are symmetric. The device was assumed to have a $P_s = 0.95$ (conservative).

*5. Value of the stored data.* The expected return from all the science experiments except occultation depends upon:

(1) Recorder playback time

(2) Probability that the device switches

(3) Probability of the DAS and recorder operating

$$E_s = (V_{c/ns} P_{ns} + V_{c/s} P_s) P_R P_{DAS}$$

where

$V_{c/ns}$ = value of the communications period if no switch

$V_{c/s}$ = value of the communications period if switch

$P_R$ = probability of successful recorder operating

$P_{DAS}$ = probability of successful DAS operation

*6. Results.* Figure III-18 is a graph of pressure as a function of altitude for the GH-50 atmosphere. Figure III-19 presents the minimum altitude, $H_o$, at which

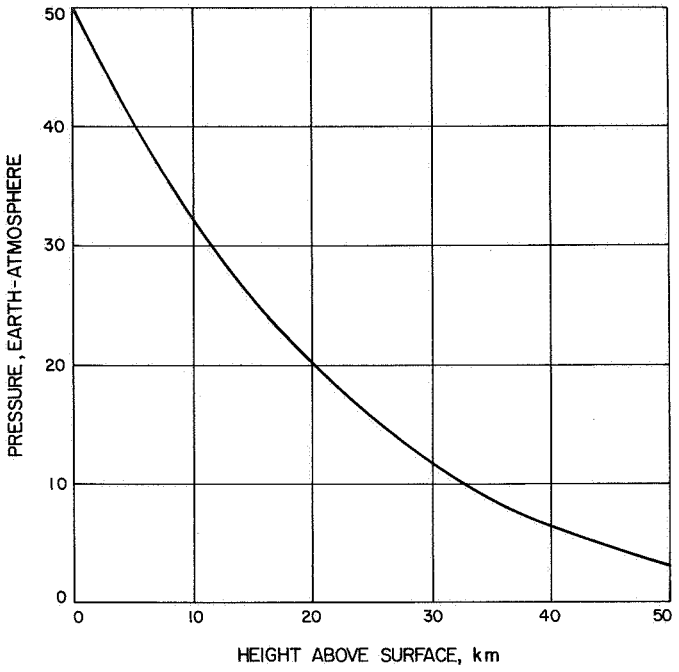



**Fig. III-18. Pressure vs a function of altitude for GH-50**

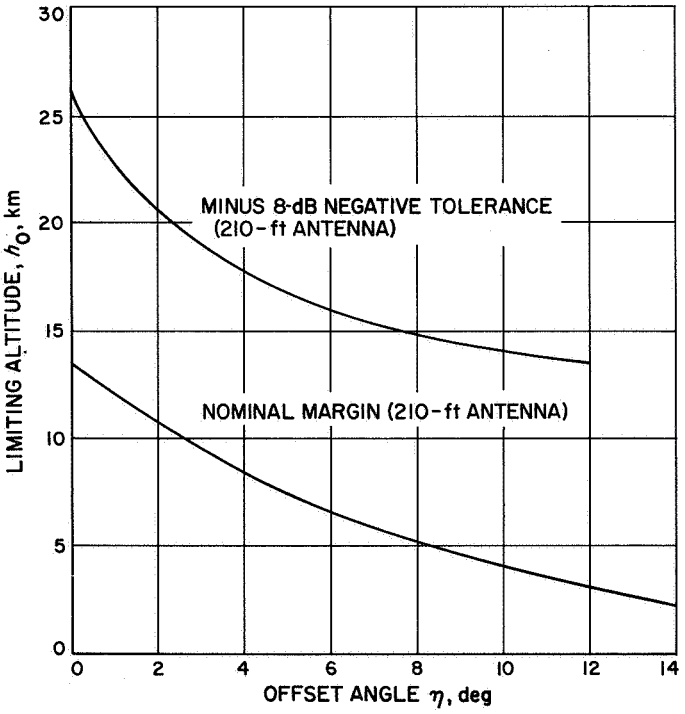



**Fig. III-19. Atmosphere GH-50, beam path on antenna axis**

occultation data can be received as a function of offset angle. Two curves are given, one using normal gain and the other using the sum of the negative tolerances. Both curves assume the use of the 210-ft antenna. These curves show that an increase in offset angle from 5 to 8 deg changes the limiting altitude more than a change from 8 to 11 deg. Figure III-20 is a cross plot of Figs. III-18 and III-19, and indicates what atmospheres can be observed all the way to the surface as a function of offset angle. This curve indicates that although a change in $\eta$ from 5 to 8 deg does not significantly alter $H_o$, it does result in observing occultation all the way to the surface for atmospheres which have about 14% higher surface pressure (that is, an increase from 35.5 to 40.5 earth atmospheres).

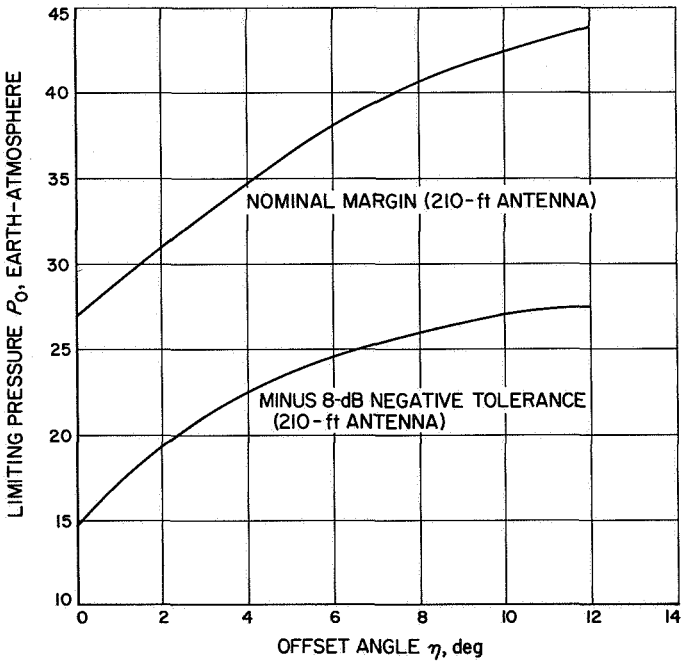



**Fig. III-20. Pressure at which occultation is cut off as a function of offset angle**

Figures III-21 and III-22 show the total return as a function of angle of offset. Figure III-21 gives the return for a 10-day recorder playback time and for relative values of the occultation experiment of 0.40, 0.60, 0.80. Each curve was calculated for equal entrance and exit offset angles. Points (7, 9) and (8, 10) are for unequal offset angles and a weight of 0.6. (In both cases $\eta_1$ is given first.) Note that these unequal offset strategies increase the total return by between 5 and 10%.

Figure III-22 gives the return for a 5-day recorder playback time. These curves are flatter indicating that

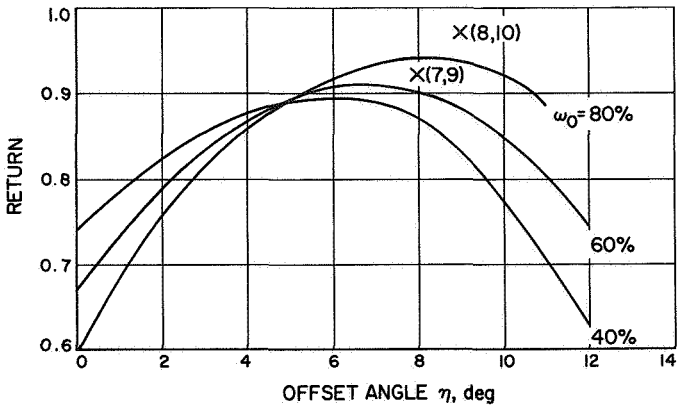



**Fig. III-21. Expected return as a function of $\eta$, offset angle for 10-day playback time**

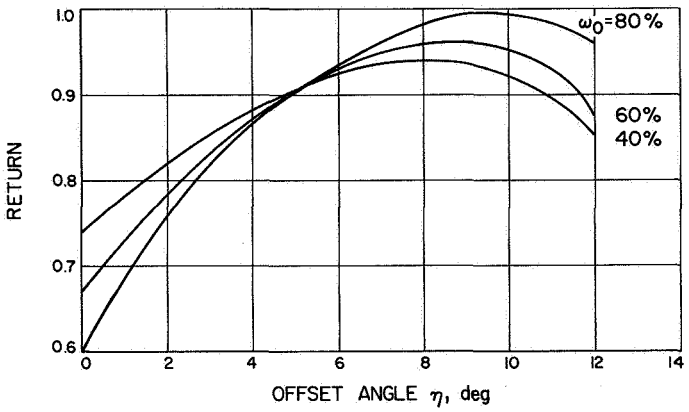



**Fig. III-22. Expected return as a function of $\eta$, offset angle for 5-day recorder playback time**

the problem tends to disappear as the playback time is decreased.

*7. Conclusions.* For a 10-day playback time, the curves peak between 6- and 9-deg offset angles. The return may be increased by going to unequal offset angles. The most attractive combination appears to be $\eta_1 = 8$ and $\eta_2 = 10$.

For playback times of 5 days or less, the offset problem tends to disappear. Offsets of $\eta_1 = 8$ deg, $\eta_2 = 10$ deg can be used without loss of failure mode coverage. In addition, offset angles which are much larger (12–14 deg) do not seem attractive because the danger exists of not receiving good occultation data in the event the Venusian atmosphere has a low surface pressure.

Overall, the (8, 10) offset position seems very attractive because it provides for: (1) 7 days of telemetry in the "no-switch" failure mode, (2) telemetry at encounter in

the event of the "early-switching" failure mode, and (3) the use of exit occultation data to interpolate to the entrance data that was not received because of the 2-deg smaller bias.

## E. Planetary Quarantine Analysis

*1. General.* To avoid altering the ecology of the planet Venus, the *Mariner* Venus 67 mission had to be constrained to limit the probability of biological contamination. In particular, the probability of accidental contamination of the planet had to be less than $3 \times 10^{-5}$.

There were two fundamental methods by which Venus could be contaminated. The first was the accidental impact of either the *Agena* stage of the boost vehicle or the spacecraft itself. To reduce the probability of impact to an acceptable level for both the *Agena* and the spacecraft, it was necessary to bias the injection trajectories away from the planet as well as to carry a retro rocket on the *Agena* to further deflect the *Agena* trajectory away from the planet.

The second method of contamination was the release of viable organisms from the spacecraft, which might impact Venus even though the spacecraft did not. Examples are organisms contained in the attitude-control gas expelled by the spacecraft, viable organisms contained in the exhaust products of the midcourse maneuver rocket propulsion system, and ejecta from micrometeorite impact.

*2. Mathematical model description.* The analytical expression for the contamination probability is

$$P = \sum_i (P_I P_R P_G)_i \tag{1}$$

where

$P_I$ = probability of impact

$P_R$ = probability that viable organisms from the spacecraft will be released onto the planet's surface or into its atmosphere

$P_G$ = probability that a viable organism, present on the planet's surface or in the atmosphere and not previously heat-sterilized, will grow and spread, contaminating the planet or its atmosphere

The summation is taken over the "$i$" sources of possible contamination.

While it is certainly possible to justify a number less than 1.0 for $P_R$, the reduction in this quantity below 1.0 (based on past analyses) would probably not be significant. The only reason for any reduction is that the vehicle, in passing through the Venusian atmosphere, would be subject to extreme aerodynamic heating because of the thick atmosphere and the high entry speed (about 35,000 ft/s). This heating would tend to destroy earth organisms if the temperature reached approximately 350 to 400°K. However, the vehicle would certainly break into pieces because of the excessive structural loads caused by the entry deceleration, and analyses have shown that pieces in certain size ranges would not be sufficiently heated to be sterilized. The question then becomes that of determining the probability of the number of pieces that are formed in the region of critical size. This probability is certainly less than 1.0, but how much less is difficult, if not impossible, to estimate. It was therefore assumed, conservatively, that $P_R = 1.0$.

The Planetary Atmospheres Subcommittee of the NASA Office of Space Sciences and Applications adopted the following resolution:

> The subcommittee agrees that, in their opinion, there is less than one chance in ten that the temperature at a random impact point on Venus would be below 400° Kelvin.

Since a temperature of this level would destroy, or at least prevent the growth and spreading of, any landed earth organism, it was assumed that $P_G$ was at most 0.10. Based on these assumptions, Eq. (1) can be written as

$$P = \sum_i (P_I P_R 0.10)_i \tag{2}$$

Since there are two basic modes of planet contamination (i.e., accidental impact of an entire vehicle, either spacecraft or launch vehicle, and spacecraft ejecta), it is useful to write Eq. (2) as

$$P = P_{I_A} P_{R_A} (0.10) + P_{I_S} P_{R_S} (0.10) + \sum_i (P_{I_E} P_{R_E} 0.10)_i \tag{3}$$

where the subscript $A$ refers to *Agena* impact, the subscript $S$ refers to spacecraft impact, and the third term represents the summation over the possible sources of ejecta contamination, with the subscript $E$ representing ejecta.

As previously mentioned, $P_{R_A}$ and $P_{R_S}$ were assumed to be 1.0 which, when substituted into Eq. (3), results in

$$P = P_{I_A} (0.10) + P_{I_S} (0.10) + \sum_i (P_{I_E} P_{R_E} 0.10)_i \tag{4}$$

This is the form of the equation used in subsequent analysis.

*3. Probability of spacecraft ejecta contaminating Venus.* Before spacecraft ejecta can contaminate Venus, they must (a) contain viable organisms, (b) achieve a trajectory that will allow them to impact the planet, (c) survive the environment in a viable condition, and (d) grow and spread in the planetary environment.

Taking item (b) first, the question to be answered is, what is the probability of achieving an impact trajectory? Of the several factors involved, the most important is the acceleration of the organism by solar pressure. For particles of small size and low density, this acceleration can be large. In fact, for particles below the region of about 25–100 $\mu$m (depending on density), it is greater than the gravitational acceleration from the sun. Since particles of biological interest are in this size range, the acceleration from solar pressure causes an enormous perturbation in the trajectory of the particle. A particle that leaves the spacecraft with a very small relative velocity will be pushed far away from it by solar pressure. To impact the planet, a particle must leave the spacecraft with just the right velocity (similar to targeting at launch). Furthermore, the particle's velocity vector must have the correct magnitude (to within a few m/s early in the trajectory and to within a few tens of m/s late in the trajectory) and the correct direction to within one degree. The probability of achieving an impact trajectory is then found by calculating the probability that an organism will be ejected from the spacecraft with a velocity vector of the required accuracy. The contamination probability is the product of the impact probability and the probability of an organism's surviving the combined effects of UV radiation and the heating of atmospheric entry.

Several studies (Refs. 4 and 5) have been made about item (c) concerning kill-rates of organisms under varying dosages of UV radiation. If the spore is unprotected (i.e., if the spore is on the outside of the ejected particle), the evidence indicates that less than 3% will survive more than a few hours of exposure. For those organisms contained inside a particle, the probability of lethality by UV is uncertain; however, to contaminate the planet, the organism must escape from inside the particle once it has landed.

A reasonable estimate of the probability of surviving the UV environment seems to be 0.10. This is consistent with past studies and estimates (Ref. 4).

Finally, the probability of surviving the entry heating pulse must be estimated. With an entry speed of 35,000 ft/s, particles from $3 \times 10^{-4}$ in. up through ½ in. in diameter will be sterilized upon entry where sterilization is defined to mean that the steady-state temperature of the entire body or particle is at least 200°C for several seconds. In addition, particles between 0.01 in. and 0.1 in. in diameter will be 100% ablated.

Past studies of the probability of organisms surviving entry conditions of Mars (Ref. 4), which are not as severe as those of Venus, have resulted in an estimate of 0.10. It therefore seems reasonable to take the probability of surviving the entry heating pulse at Venus to be 0.10.

With this background in mind, each of the sources of ejecta may be analyzed to determine their contribution to the probability of contaminating Venus.

*a. Midcourse-motor exhaust products.* The midcourse propulsion system for the *Mariner* Venus 67 spacecraft (*Mariner V*) is a liquid monopropellant (hydrazine) system. Experimental studies with hydrazine (Ref. 5) show that the hydrazine is sporicidal, and that within 4 hours after introduction of spores into hydrazine the spore count has been decreased by a factor of $10^6$. Since the system is loaded several days prior to launch, the probability of any spores being ejected from the propellant or propellant tanks must be negligible. This is consistent with Ref. 4. However, there still remains the small probability that organisms will be swept off the surface of the engine by the exhaust gases (which are 1800°R in the chamber) and ejected in a viable condition. This can occur only if the organisms are caught in the relatively cooler boundary layer and ejected. The probability of the ejection of viable organisms from the midcourse motor was conservatively taken to be 0.10.

In addition, the probability of achieving an impact trajectory is found as follows. Since the direction of the exhaust velocity at the midcourse maneuver time is random *a priori*, the probability that a particle will be ejected in a 1-deg cone is less than $10^{-3}$. The magnitude of the velocity of the particle leaving in the exhaust must be within a few m/s of the required value. This factor is estimated to have a probability of less than 0.01. Hence, the probability of achieving an impact trajectory is $10^{-5}$.

To summarize, the probability of contaminating Venus with midcourse motor exhaust products is given by

$$P_{C_{MC}} = P_E P_I P_{UV} P_{SE} P_{gs}$$

where

$P_E$ = probability of ejecting a viable organism

$P_I$ = probability of achieving an impact trajectory

$P_{UV}$ = probability of surviving the UV environment

$P_{SE}$ = probability of surviving the entry heating load

$P_{gs}$ = probability of growing and spreading on the surface or in the atmosphere of Venus

Substituting the above numbers into this equation yields

$$P_C = (0.1)\,(0.00001)\,(0.1)\,(0.1)\,(0.1)$$

$$P_C = 10^{-9}$$

for the probability of contamination from midcourse motor ejecta.

*b. Micrometeorite ejecta.* The probability of viable organisms, dislodged by micrometeorite impacts, achieving an impact trajectory is computed as follows. Since the particles would be dislodged in a random direction, the probability of being within the required 1-deg cone is less than $10^{-3}$. Since the velocity of ejecta varies randomly over several km/s, the probability of its being within a band of a few m/s is certainly less than 0.01; hence, the probability of achieving an impact trajectory is $10^{-5}$ or less.

Using the probability of surviving UV radiation and entry heating as each being 0.10, and taking the probability of growth and spreading as 0.1, results in

$$P_C = P_E P_I P_{UV} P_{SE} P_{gs}$$

$$P_C = (1.0)\,(0.00001)\,(0.1)\,(0.1)\,(0.1) = 10^{-8}$$

where it has been assumed (conservatively) that the probability of ejecting a viable organism by this means is 1.0. Reference 4 indicates the probability of contaminating Mars from an orbiter in 50 yr is of the order $10^{-5}$. A comparison of the 50-yr period near the planet Mars with a 3-mo flight (total) to Venus in 1967 makes the $10^{-8}$ estimate appear reasonable.

*c. Attitude-control gas jets.* Viable organisms ejected by the attitude-control gas jets are subject, in general, to the same reasoning as offered in *a* and *b*, above. Near the planet, however, the likelihood of the gas jets actuating is very strong. Since the attitude of the spacecraft is known relative to the planet, the probability of the jet exhaust achieving an impact trajectory can be computed. An analysis was conducted to determine the probability that organisms would escape from the attitude-control system at a time when an impact trajectory could be achieved. The results indicate that the number of organisms achieving an impact trajectory near encounter is given by

$$n = 5 \times 10^{-6} N$$

where

$n$ = number of viable organisms that achieve an impact trajectory

$N$ = total number of viable organisms in the spacecraft control system

To estimate the exact number of organisms ($N$) is difficult. The filtering system in the attitude-control system keeps the system very clean but not sterile. Past studies have disclosed that the maximum number of colonies of organisms found in ordinary commercial nitrogen tanks was 12 in 16 lb of nitrogen. The spacecraft tanks are assembled and filled in ultra-clean rooms—much cleaner than conditions under which commercial bottles are manufactured and filled. Since the spacecraft contains only 5 lb of gas, it is conservative to assume that only about four viable organisms will exist in the *Mariner V* spacecraft tanks.

In addition, all attitude-control nitrogen gas must pass through two filters, in series. The efficiency of each filter is such that less than one 0.3-$\mu$m particle in 100,000 will pass through. Laboratory experience indicates less than one failure per 100 of these filters. Therefore, the probability of ejecting a single viable microorganism times the probability of failure of the filters is $4 \times 10^{-4}$. Substituting this value for $N$ in the preceding equation yields a probability of roughly $10^{-10}$ of contaminating Venus with gas from the attitude-control system.

In summary, the probability of contaminating Venus by means of ejecta is less than $10^{-8}$, which is negligible relative to the other sources of contamination (i.e., impact of a vehicle), and to the quarantine constraint of $3 \times 10^{-5}$.

***4. Mission profile.*** The *Mariner V* spacecraft, at launch, was aimed to pass approximately 75,000 km from the surface of Venus. By aiming a relatively great distance from the surface, the probability of achieving an impacting trajectory at launch is reduced to an acceptable level.

This biased aiming point, along with the expected dispersions in the injection conditions caused by tolerances

in the launch-vehicle guidance system, results in a high (99.9%) probability of requiring a spacecraft trajectory correction maneuver. The maneuver alters the spacecraft trajectory so that it passes the planet at the nominal target point (about 3000 km from the surface), and through the earth occultation region. If the initial maneuver fails to achieve acceptable target conditions, a second maneuver is available. It is apparent that following injection, and either one or two trajectory correction maneuvers, an impact trajectory could be attained by accident; and the ability to perform a subsequent maneuver to avoid impact would not be available and would result in an eventual impact.

Following injection, the *Agena* stage of the launch vehicle, which has been injected into the same Venus trajectory as the spacecraft, is programmed to perform a 30-deg yaw maneuver and fire a solid propellent rocket to alter its trajectory away from Venus and decrease the probability of achieving an impacting trajectory. Thus, the *Agena* can achieve an impact trajectory at injection or following the retro maneuver.

*5. Probability of accidental vehicle impact.* Figure III-23 is a probability diagram of the ways in which the spacecraft can achieve an accidental impact trajectory. These ways are:

(1) The spacecraft is injected into an impact trajectory which cannot be corrected with a maneuver because of a spacecraft malfunction.

(2) Following the first maneuver, the spacecraft is on an impact trajectory which cannot be corrected with a second maneuver because of a malfunction in the spacecraft.

(3) The spacecraft performs a first maneuver which misses the planet but also misses the desired target zone. A second maneuver is performed which results in a planet impact trajectory.

(4) The spacecraft is on an impacting trajectory following the first maneuver, and a second maneuver is performed which also results in a planet impact trajectory.

The probability of the spacecraft impacting the planet can also be described as

$$P_{I_S} = [P_{I/i}\, q_1 + P_1 P_{I/1} (q_2 + P_2 P_{I/2}) + P_1 (1 - P_{I/1}) P_{2/1} P_2 P_{I/2}] P_i \qquad (5)$$

$P_{I_S}$ = probability of spacecraft impact on Venus

$P_{I/i}$ = probability of achieving an impact trajectory at injection

$P_1$ = probability of spacecraft being able to perform a first maneuver

$q_1 = 1 - P_1$ = probability of spacecraft not being able to perform first maneuver

$P_2$ = probability of spacecraft being able to perform second maneuver, given a successful first maneuver

$q_2 = 1 - P_2$ = probability of spacecraft being unable to perform second maneuver, given a successful first maneuver

$P_{I/1}$ = probability of impact following first maneuver

$P_{I/2}$ = probability of impact following second maneuver

$P_{2/1}$ = probability of requiring a second maneuver even though first maneuver did not result in an impact trajectory

$P_i$ = probability of spacecraft being injected on a Venus trajectory during the 1967 opportunity.

To compute the probability of the spacecraft impacting Venus by using Eq. (6), below, the following inputs and assumptions are made:

(1) $P_1$, the probability of the spacecraft being able to perform an initial maneuver is taken to be 0.98. This is based on the test history of the spacecraft and of the post-injection propulsion system.

(2) $P_2$, the probability of the spacecraft being able to perform a second maneuver, given a successful first maneuver performance, is taken to be 0.98. The reduction from 1.0 is basically the estimate of the small probability that the spacecraft would fail after the first maneuver but before a second maneuver and also that a second maneuver uses a different set of valves in the propulsion system than that used in the successful first maneuver.

(3) $P_{I/i}$, the probability of achieving an impact trajectory at injection was left as a variable since it could be adjusted downward by biasing the launch trajectories away from the planet and vice versa. This number was computed by mapping the injection dispersions given by the covariance matrix of injection errors to the aiming point at the planet and integrating over the capture radius of the planet.

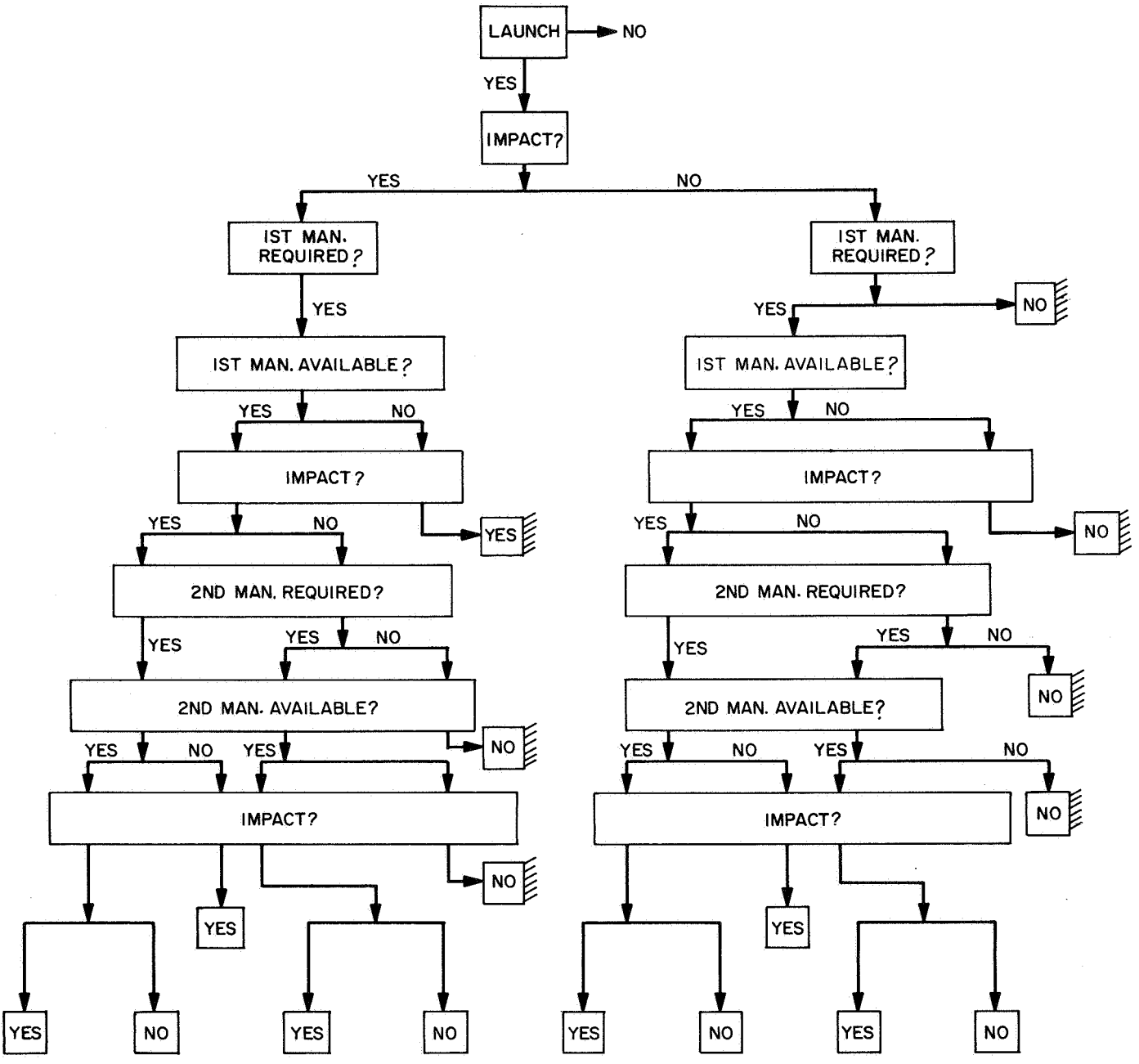



**Fig. III-23. Spacecraft probability of impact**

For unbiased trajectories, this number varied from about 0.08 for a June 12 launch date to about 0.02 for a June 27 launch date.

(4) $P_{I/1}$, the probability of achieving an impact trajectory following the first maneuver was computed by mapping the dispersions from the execution of the midcourse maneuver to the planet and integrating over the capture radius. This quantity is a function of the errors in the maneuver and the location of the target aiming point. For the *Mariner* Venus 67 mission, the aiming point was selected to result in an *a priori* probability of impact following the first maneuver of $3 \times 10^{-4}$ or less.

(5) $P_{2/1}$, the probability of performing a second maneuver even if first maneuver does not result in an impacting trajectory, was computed by finding statistically the size of the execution errors resulting from the first maneuver and mapping these to the planet and integrating over the region of acceptable encounter. For the *Mariner* Venus 67 mission this number was assumed to be 0.50.

(6) $P_{I/2}$, probability of impact following second maneuver, was determined by finding the statistical size of the execution errors resulting from the second maneuver, including orbit-determination uncertainties, and mapping these to encounter and integrating over the planet capture area. Since a second maneuver normally corrects errors from the first maneuver, it is expected to be very small and hence the errors associated with it should be small. For the *Mariner* Venus 67 mission, the second maneuver target aiming point would be selected so that an *a priori* probability of achieving an impacting trajectory would be less than $10^{-6}$.

A similar probability tree (Fig. III-24) diagram and equation for the probability of impact can be derived for the launch vehicle. The equation representing the launch vehicle probability of impact is

$$P_{I_A} = P_i \left[ P_{I/i}\, q_r + (1 - P_{I/i})\, P_r P_{I/r} \right] \qquad (6)$$

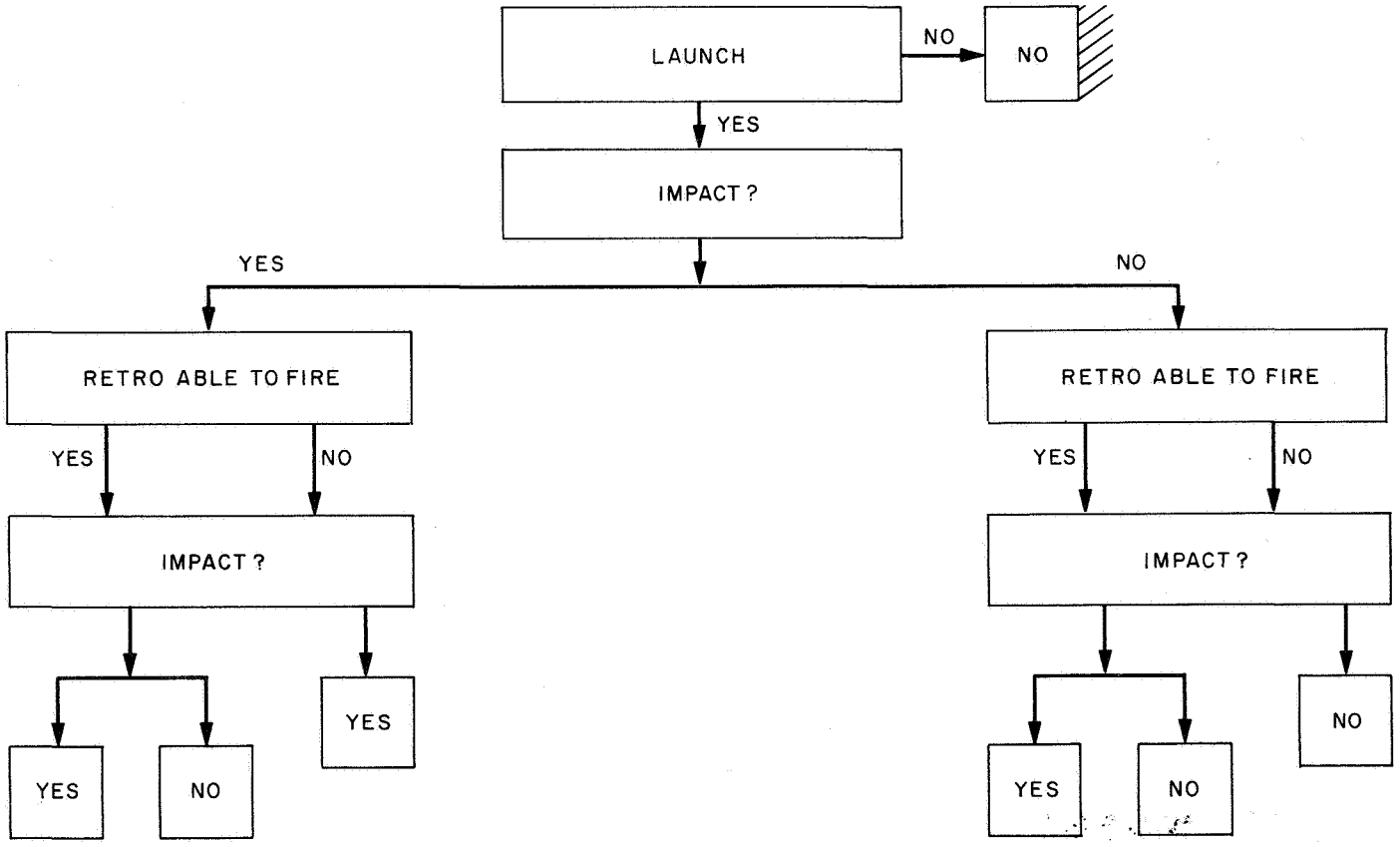



**Fig. III-24. Launch vehicle probability of impact**

where

$q_r$ = probability of the *Agena* retro-rocket not firing

$P_r = 1 - q_r$

$P_{I/r}$ = probability of achieving an impact trajectory after retro-fire, given that trajectory was non-impacting prior to retro-fire[6]

To compute the probability of the *Agena* achieving an impacting trajectory, the following assumptions were made:

(1) $P_r$, the probability of a successful retro-maneuver, given successful injection, is 0.99.

(2) $P_{I/r}$, the probability of impact following a retro-maneuver, is calculated by integrating the mapped injection errors over the capture area of the planet from an aiming point biased away from the planet by the amount the retro-maneuver moves the *Agena* trajectory.

When these numbers are substituted into Eq. (6) it can be seen that the second term in Eq. (6) is at least two orders of magnitude smaller than the first, and of the order $10^{-6}$; hence,

$$P_{I_A} = P_i P_{I/i} q_r \tag{7}$$

When analogous numbers are substituted into Eq. (5), both the last two terms are of the order $10^{-6}$ and may be neglected. Hence,

$$P_{I/S} = P_i P_{I/i} q_1 \tag{8}$$

By substituting Eqs. (7) and (8) into Eq. (4), and using the result that the third term of Eq. (4) due to ejecta is negligible (relative to $3 \times 10^{-5}$), we obtain

$$P = P_i P_{I/i} (q_r + q_1)(0.10) \tag{9}$$

Since we have already seen that $P \leq 3 \times 10^{-5}$, Eq. (9) can be rearranged, using $q_r = 10^{-2}$ and $q_1 = 2 \times 10^{-2}$, so that

$$P_{I/i} \leq \frac{0.01}{P_i} \tag{10}$$

But when we remember that for unbiased trajectories $P_{I/i}$ is between 0.08 and 0.02 depending on launch date, it is apparent that the trajectories must be biased away from the planet to reduce $P_{I/i}$ to an acceptable level.

The *Mariner V* trajectories were biased so that on each day of the launch period the probability of obtaining an impact trajectory at injection was less than 0.01.

To accomplish this it was necessary to bias the injection trajectory aiming point approximately 75,000 km away from the planet. Using the covariance matrix of launch-vehicle injection errors makes it possible to map these errors to encounter and generate loci of constant probability of impact at injection. This is shown in Fig. III-25 for both $P_{I/i} = 0.01$ and $P_{I/i} = 0.0003$ for a typical launch date. To satisfy $P_{I/i} \leq 0.01$, the injection aiming point must be on, or outside, the contour labeled $10^{-2}$; and to satisfy $P_{I/i} \leq 0.0003$, the aiming point must be on, or outside, the contour labeled $3 \times 10^{-4}$. The reason for including the contour representing $P_{I/i} = 3 \times 10^{-4}$ is as follows. If the *Mariner V* spacecraft had not been launched within the nominal (propellent margins greater than $3\sigma$ in launch vehicle) launch period, two additional launch days could have been realized by removing the *Agena* retro rocket. However, if we look at Eq. (9), this is equivalent to setting $q_r = 1.0$, with the result that $P_{I/i}$ must be lowered to approximately $3 \times 10^{-4}$ in order to still yield $P \leq 3 \times 10^{-5}$. This implies additional biasing of the injection aim point as shown in Fig. III-25.

## F. Trajectory Correction Analysis

*1. Pre-flight analysis of midcourse maneuver.* The ability to control the target-arrival parameters was necessary for two reasons. First, the purpose of the launch vehicle was to place the spacecraft on a heliocentric transfer trajectory to Venus that would achieve a prespecified set of arrival parameters. However, due to normally occurring guidance uncertainties, the *a priori* probability of achieving an acceptable set of encounter parameters is extremely low. A satisfactory encounter may be achieved by performing a midcourse maneuver with greatly reduced uncertainties at a time when the trajectory is generally less sensitive to errors. Secondly, the dispersions at the target can only be treated statistically before launch. Therefore, any set of arrival parameters that may be chosen have a certain probability of impacting Venus associated with them. To meet the planetary quarantine requirement, it was necessary to aim further from Venus at injection than was ultimately desired, and then use the more accurate midcourse maneuver to correct this biased aiming point. Table III-5 summarizes the various desired and achieved aiming points.

[6]It is assumed that if the *Agena* originally achieves an impact trajectory and the retro rocket fires, the probability of achieving an impact trajectory is zero.

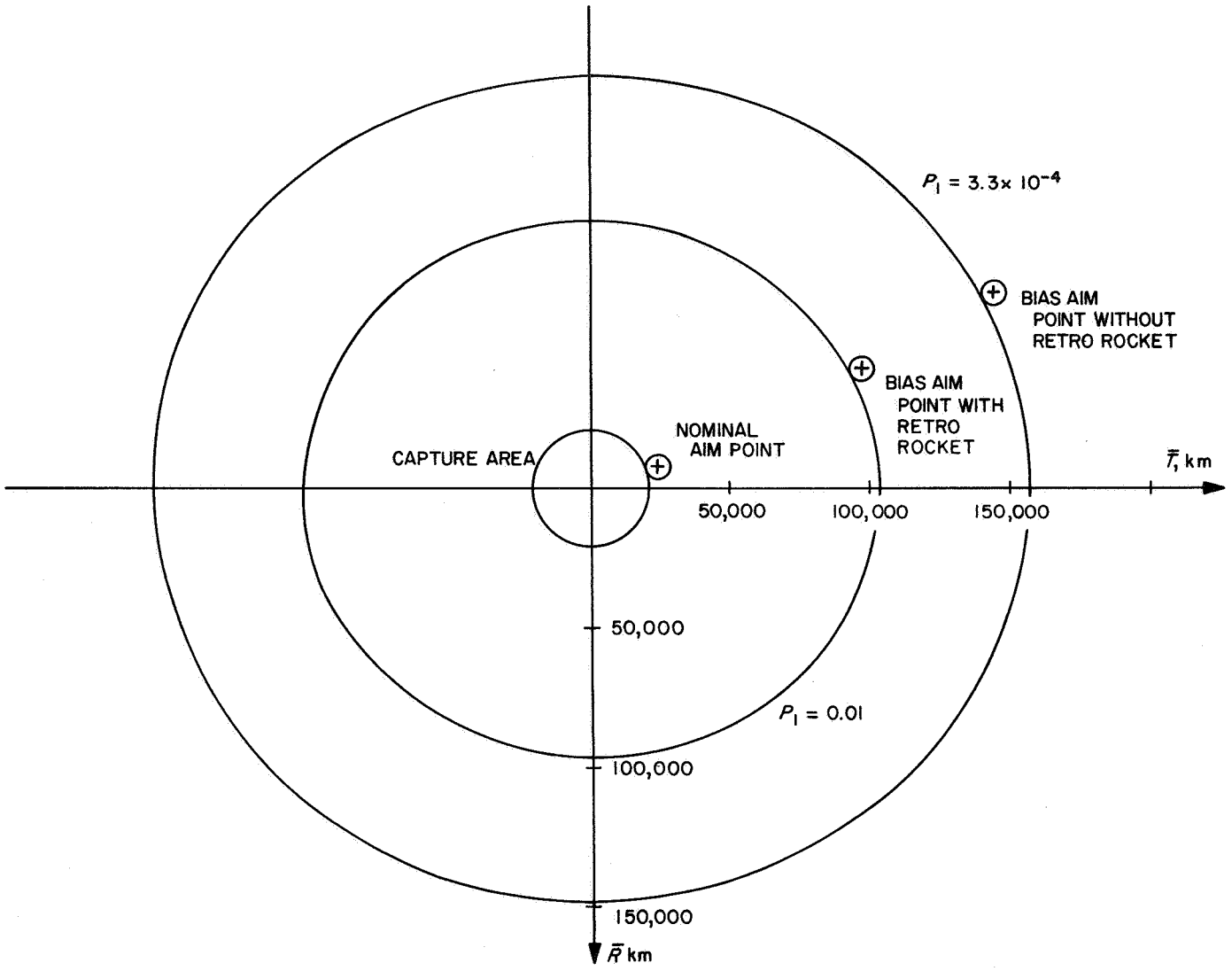



**Fig. III-25. Contours of equal impact probability at injection**

For the purpose of pre-mission studies, it is important to know how the maximum midcourse velocity maps to correction capability in terms of encounter parameters. The method by which this is determined is best explained by introducing critical plane coordinates.

**Table III-5. Encounter parameters of pre- and post-midcourse orbits**

| Aim point | B • R, km | B • T, km | $T_f$, days |
|---|---|---|---|
| Injection | achieved: −65,343 | 81,483 | 126.2451 |
| | desired: −54,275 | 87,414 | 127.1911 |
| Midcourse maneuver | achieved: −14,855 | 24,278 | 126.8152 |
| | desired: −12,761 | 21,738 | 126.8333 |

The gradients of the three encounter parameters $\mathbf{B} \cdot \mathbf{R}$, $\mathbf{B} \cdot \mathbf{T}$, and $T_f$ may be expressed as vectors in a velocity space as shown in Fig. III-26. The basis vectors $(\mathbf{u}_1, \mathbf{u}_2, \mathbf{u}_3)$, which define the critical plane coordinates, are constructed such that $\mathbf{u}_1$ is a unit vector along $\nabla \mathbf{B} \cdot \mathbf{T}$, and $\mathbf{u}_2$ is perpendicular to $\mathbf{u}_1$ and in the plane of $\nabla \mathbf{B} \cdot \mathbf{T}$ and $\nabla \mathbf{B} \cdot \mathbf{R}$. The right-hand system is completed by $\mathbf{u}_3$. The plane of $\mathbf{u}_1$ and $\mathbf{u}_2$ is called the critical plane, and the $\mathbf{u}_3$ direction is the noncritical direction. A maneuver made along $\mathbf{u}_3$ will not affect the spatial miss, and a maneuver in the critical plane will have the largest effect on the spatial miss. A velocity vector rotated in a circle around the critical plane will map to an ellipse in the B plane (i.e., capability ellipse). In a similar manner, a velocity vector that is rotated such that its projection on $\nabla T_f$ is a

constant will map to an ellipse in the B plane which is contained within the capability ellipse and represents a contour of constant flight-time change. Figure III-27 shows a typical capability ellipse for *Mariner* Venus 67 trajectories with associated ellipses of constant flight time at five days from injection.

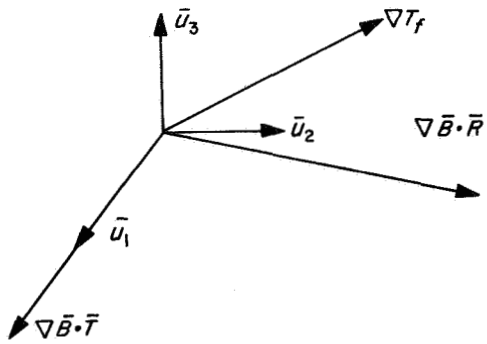



**Fig. III-26. Gradient vectors at midcourse**

*2. Midcourse maneuver operations program.* The midcourse maneuver operations program for the *Mariner* Venus 67 mission had three main functions:

(1) To determine whether an acceptable maneuver exists.

(2) To encode it in commands for transmission to the spacecraft.

(3) To provide information on the spacecraft orientation during the maneuver sequence for the purpose of evaluating spacecraft performance.

To make these calculations, three different inputs are required:

(1) The best estimate of the actual injection conditions and the uncertainties in this estimate from the orbit determination program.

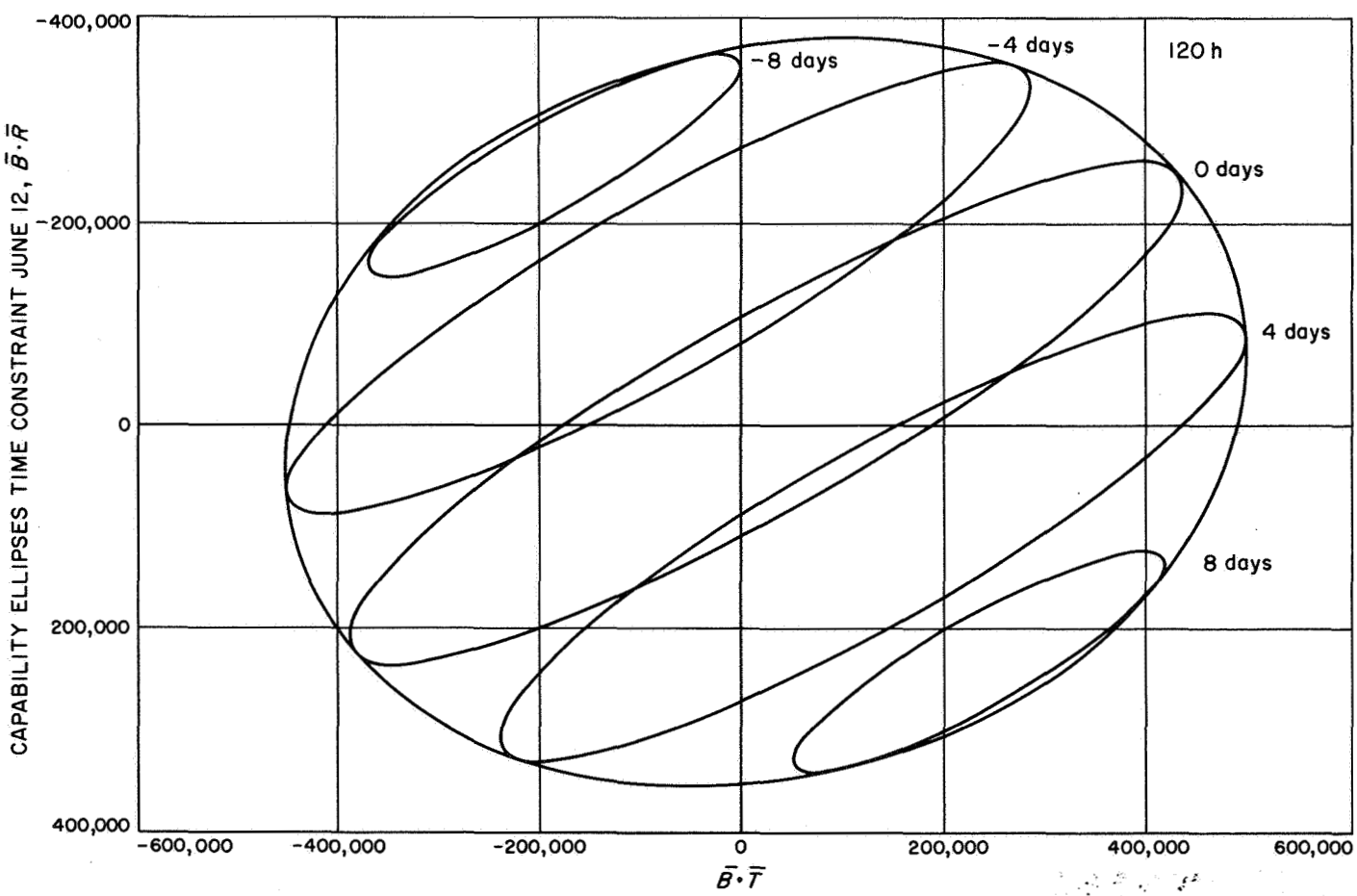



**Fig. III-27. Typical capability ellipse**

(2) Spacecraft parameters that define the spacecraft geometry and status.

(3) Control parameters, such as program controls and the desired aiming point.

The information contained in the introductory printout (Fig. III-28) describes the best estimate of the orbit obtained and an initial estimate of the quality of this orbit. Input quantities from the orbit determination program are used to estimate the error between the achieved and desired encounter parameters.

The midcourse decision program was used to calculate the required velocity increment subject to various constraints. The constraints that were evaluated were propulsion, time-of-flight, and the low-gain antenna position. The propulsion and time-of-flight constraints are absolute. If an acceptable $\mathbf{B} \cdot \mathbf{R}$ and $\mathbf{B} \cdot \mathbf{T}$ cannot be reached without violating these constraints, the program prints a statement to this effect and goes to the capability ellipse generator. However, if both of these constraints may be satisfied with some other spatial miss, the program exits to the residual miss program, which computes the minimum residual miss associated with these constraints, and then proceeds to the capability ellipse generator. If the low-gain antenna constraint is violated, the program will attempt to find a satisfactory modified maneuver. The constraint will be violated if none exists. This results in the loss of telemetry data during the turns—an undesirable but tolerable situation.

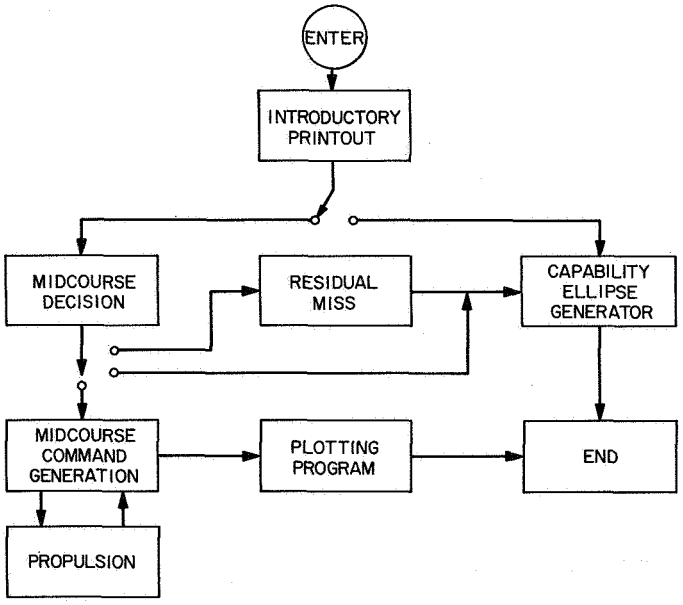



**Fig. III-28. Maneuver operations program**

The output from the midcourse decision program falls into three categories. The first specifies the trajectory conditions at which the midcourse motor would ignite. The second is a set of statements that are printed out if called for by the decision sequence that formulated the maneuver. The third contains detailed numerical information related to the test for the antenna constraint.

The purpose of the midcourse command generation program (Fig. III-28) was to convert the spacecraft turns and correction velocity magnitude into turn times and a burn time, respectively, and then encode them in a form suitable for transmission to the spacecraft. The burn time is computed from the velocity magnitude in the propulsion subroutine. The midcourse command generation program also does a complete trajectory-error analysis and computes angles of interest during the turning sequence.

The plotting program (Fig. III-28) plots the dispersion ellipses and the angles which are computed in the midcourse command generation program. This information is useful in evaluating the maneuver.

3. *Discussion of the actual maneuver.* The final maneuver calculation was performed on June 18, 1967, based on the best estimate of the orbit at that time. The midcourse decision program indicated that a maneuver existed which satisfied all the constraints in the program. The commands were transmitted to the spacecraft at $21^h\ 23^m\ 57^s$ GMT on June 19, 1967. Motor ignition occurred at $23^h\ 8^m\ 6^s$ GMT. Table III-6 shows the computed and commanded maneuver parameters, and the best estimate of the values actually achieved. The discrepancy between the computed and commanded values is due to the quantizing of the commands. The difference between the commanded and achieved values is due to hardware errors in executing the maneuver.

The estimates of the achieved values were obtained by using the post-midcourse orbit, as determined by the orbit determination program after about one month of post-maneuver tracking, and running the midcourse maneuver program to compute the maneuver parameters required to be placed on that orbit. This computation showed the turns to be very accurate, and that a significant error existed in the velocity magnitude. (Refer to

**Table III-6. Midcourse maneuver performance**

| Parameter | Pitch turn, deg | Roll turn, deg | Velocity magnitude, m/s |
|---|---|---|---|
| Computed value | 55.35 | 71.02 | 16.127 |
| Commanded value | 55.267 | 70.946 | 16.135 |
| Best estimate of achieved value | 55.12 | 70.63 | 15.412 |
| Estimated error, $\varepsilon$ | 0.15 | 0.32 | 0.723 |
| *A-priori* standard deviation, $\sigma$ | 0.7 | 0.7 | 0.121 (0.75% of commanded value) |
| Ratio of estimated error to *a priori* standard deviation, $\varepsilon/\sigma$ | 0.21 | 0.46 | 5.96 |

Volume II of TR 32-1203 for the complete analysis of the error.) The B • R and B • T values achieved by the maneuver very nearly lie on the straight line connecting the achieved injection aiming point and the desired maneuver aiming point (Fig. III-29).

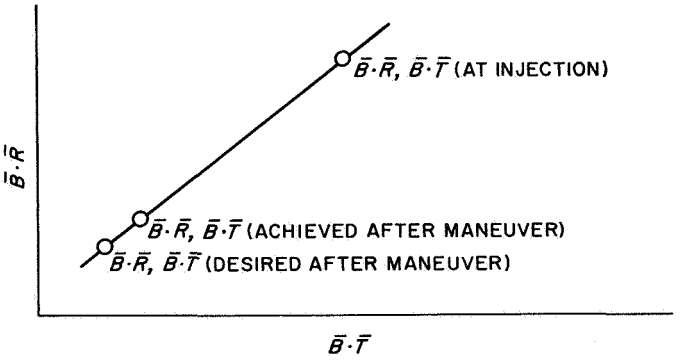



**Fig. III-29. Midcourse maneuver results**

PRECEDING PAGE BLANK NOT FILMED.

# IV. Spacecraft System

## A. Introduction

Spacecraft design fabrication and test differ in some respects from previous projects. The major innovation was the availability of existing hardware that required varying degrees of modification to accomplish a new mission. The primary advantage of this approach was that the basic elements of the spacecraft were inherently in good shape, allowing concentration upon new elements and modifications to old. The associated disadvantage and of new concern was that of age. In considering age to be a problem (or at least the understanding of whether it was a problem), the availability of qualified manpower on a timely basis, the resource constraints, and the substance of the mission itself all combined in making a considerable task of readying a spacecraft for flight.

Basic techniques and experience from the successful *Mariner* Mars 1964 and *Ranger* Projects were welded together to make a highly effective team effort. The time and resource limitations plus the *Mariner* Mars 1964 test history of existing hardware led to several major changes from previous project undertakings. Of major importance were the single team concept and using the flight support spacecraft as a pseudo proof test model (PTM). These approaches worked and, in so doing, resulted in reduced project cost and, for these particular circumstances, a more reliable end product. The chief consideration here is believed to be more effective use of time and manpower in concentrating on one spacecraft at a time, rather than the dilution of effort had there been another spacecraft.

## B. Payload Selection

At the time of the authorization of the *Mariner* Venus 67 project in December 1965, a Planetary Sciences Strategy Group was formed within the NASA Office of Space Science and Applications (OSSA). One of the first recommendations of this group was a canvass of the *Mariner IV* interplanetary investigators. Accordingly, on December 30, 1965, a teletype message was dispatched from Dr. Newell, NASA Associate Administrator, Space Science and Applications, to the Principal Investigator for each of the six so-called interplanetary experiments on *Mariner IV*. This message began: "Please advise your *Mariner IV* investigator team that NASA is planning to launch the spare *Mariner* spacecraft (MC-4) on a flight to Venus in 1967. It has been tentatively decided to retain the same set of interplanetary scientific instruments as were flown on *Mariner IV* for this new mission." It requested information on the suitability of the *Mariner IV* instrument for the new mission and the interest of the *Mariner IV* team in continuing as investigators, a restatement of the scientific objectives and a projected cost estimate. In every case the replies indicated that the experiments were considered appropriate and that the investigators were interested, although some reorganization of the investigator team or some modification of the instrument was suggested in several instances.

Also on December 30, the Project Scientist was appointed, and he immediately organized an experiment-evaluation committee consisting of JPL and Caltech

personnel. This committee agreed upon a procedure for arriving at a recommendation of a science payload for the mission, listed people whose advice on the matter was likely to be valuable, and compiled a preliminary list of experiments and categorized each. It concluded that the best course of action would be to convene for a one-day discussion a group of scientists who had been studying the planet Venus. More than 25 people from all over the country were contacted by telephone, and on January 8, 1966 at Caltech this discussion was held with approximately 30 people attending. Of these one third were out-of-town guests, one fifth were Caltech faculty members, and the rest were JPL personnel.

The Project Scientist explained the nature of the proposed spacecraft orbit and the possible encounter geometries, stated the constraints under which the mission was being planned (to wit, that restrictions on time, money, and manpower required the reflight of some of the *Mariner IV* experiments, and that additional or replacement experiments would have to be essentially flight-ready in order to be considered). Finally, he defined the purpose of the conference to be to arrive at a consensus on the most scientifically useful payload that could be accommodated within these constraints.

In the following general discussion, it was agreed that the high temperature of the surface of Venus had been well substantiated, that the most important single thing the mission could do would be to establish the value of the density or pressure of the atmosphere at the surface, that this measurement could best be made by dropping an atmospheric probe onto the planet's surface, but that such a probe did not appear feasible for this mission. Every Venus-oriented experiment that anyone could think of was discussed. Listed as probably feasible were the following experiments:

(1) Infrared radiometers similar to that on *Mariner II*.

(2) A two-frequency microwave radiometer.

(3) An ultraviolet radiometer similar to the one that was supposed to have flown on *Mariner IV*.

(4) Television pictures of the clouds in the near ultraviolet.

(5) An S-band occultation experiment.

(6) A dual frequency radio occultation experiment.

(7) An optical occultation experiment.

(8) A search coil magnetometer to detect very low frequency electromagnetic radiation near the planet.

Listed as interesting but probably requiring a crash effort to get them aboard were the following:

(1) Ultraviolet (UV) spectrometer.

(2) Infrared spectrometer.

(3) Radar mapping of the surface.

(4) Top side ionosphere sounder.

(5) Thermosphere sampler.

There were, of course, disagreements regarding the relative value of the various experiments, but at the end of the afternoon a near unanimous consensus was evident on the following three points:

(1) The S-band occultation experiment was of major importance.

(2) Television pictures of the clouds were highly desirable and should be obtained with polarizing filters, if possible.

(3) An optical occultation experiment (which had not been suggested prior to the meeting) was generally approved as a very important supplement to the S-band occultation experiment.

On January 11, 1966 the *Mariner* Venus 67 program manager requested that the *Mariner* Venus 67 project and a few prospective scientific investigators meet at NASA Headquarters for a conference on the payload selection the following week. The Headquarters list of candidate experiments was the following:

(1) The *Mariner IV* complement of interplanetary investigations.

(2) The *Mariner IV* occultation experiment with the following improvements listed in order of preference:

  (a) With a phase-locked subharmonic frequency.

  (b) With the two-frequency *Pioneer VI* radio propagation experiment package.

(3) The *Mariner IV* UV photometer experiment.

(4) One of the following instruments:

  (a) The microwave radiometer of Barrett and Barath at wavelengths of 30, 13.5, and 8 mm.

  (b) An infrared spectrometer, either the rotating filter-wedge type being developed by Pimentel or the interferometer type being developed by Hanel.

(c) The UV spectrometer of Barth.

(5) The optical occultation experiment that had been suggested by Hunten.

(6) The modified *Mariner IV* television experiment.

The project was requested to present its findings on the state of development and the spacecraft compatibility of each of these experiments and to present suggested payload variations, recommendations, and alternatives. Proposed scientific investigators were requested to discuss the scientific objectives of their investigations and their capability to produce flight hardware.

The possibility of including an atmospheric entry probe on the spacecraft was also being considered at headquarters, and JPL and the Ames Research Center were directed by the Associate Administrator for Space Science and Applications to investigate jointly the problem of the interface between the spacecraft and such a probe.

The official JPL recommendation for the science payload was transmitted to NASA Headquarters on January 17. It was based upon the recommendation of the Project Scientist's experiment selection committee and the conference of January 8, and proposed the following complement of experiments:

(1) The fields and particles experiments as flown on *Mariner IV*.

(2) The S-band occultation experiment.

(3) The UV photometer as originally planned for *Mariner IV*.

(4) The television system modified for the near-UV region.

(5) The cosmic dust detector from *Mariner IV*.

(6) The celestial mechanics experiment using the spacecraft tracking data.

(7) The optical occultation photometer if its feasibility could be demonstrated.

The reasons for not recommending the other experiments that appeared on the NASA headquarters list were set forth. Briefly they were as follows:

(1) Various suggestions for altering the spacecraft communications system, so as to obtain additional information above that which would be given by the simple S-band occultation experiment were rejected because the required redesign would be extensive and would not be compatible with the mission constraints, either from the standpoint of system reliability, system performance margins, or redesign cost.

(2) The *Pioneer* dual-frequency radio propagation experiment proposed by Stanford University was not recommended because the information that it could obtain about the ionosphere of Venus was deemed to be of less interest scientifically than the information obtainable by the recommended experiments.

(3) The microwave radiometer experiment was not recommended primarily because the weight, power, and size of the instrument would make its integration into the spacecraft difficult.

(4) These same considerations applied to the UV spectrometer, but in addition it was considered that the cost of producing the flight hardware would be high and the probability that it could meet the schedule was low.

(5) Several proposed infrared spectrometers were rejected because the information obtainable by the simpler and smaller instruments did not appear to be sufficiently valuable, whereas the development of the more complex and capable instruments was not sufficiently advanced to meet the schedule even if the formidable problems of integration on the spacecraft could be solved.

At the meeting in Washington on January 18 and 19, under the chairmanship of Dr. John Naugle, Acting Associate Administrator for Space Science and Applications (Science), presentations on behalf of the following experiments were made:

(1) The atmospheric entry probe, by several people from AVCO.

(2) The television experiment, by Professor G. J. F. MacDonald of UCLA.

(3) The UV photometer, by Professor Charles A. Barth, University of Colorado.

(4) The microwave photometer, by Professor Alan Barrett, MIT.

(5) The infrared spectrometer, by Dr. Rudolf A. Hanel, Goddard Space Flight Center.

(6) The infrared spectrometer, by Professor George C. Pimentel, University of California, Berkeley.

(7) The optical occultation experiment, by Dr. D. M. Hunten, Kitt Peak National Observatory.

(8) The S-band occultation experiment, by Dr. Arvydas J. Kliore, JPL.

(9) The dual-frequency occultation and related experiments, by Professor Von R. Eshleman, Stanford University.

At the end of the meeting, after extensive discussion, the *Mariner* Venus 67 project still advocated the payload that had been recommended on January 17, but the project was directed by Dr. Naugle to make a firsthand investigation of the flight readiness and the spacecraft compatibility of two additional instruments, namely, Professor Pimentel's infrared spectrometer and the dual-frequency radio propagation experiment proposed by Professor Eshleman. Accordingly, a group of six JPL engineers and the Project Scientist visited these two investigators on January 21, examined their instrumentation and facilities, and discussed the problems of flight hardware fabrication, spacecraft integration, and schedule. The conclusion of this group was that the infrared spectrometer was in such an early stage of development that the cost of a crash program necessary to produce flight hardware for *Mariner* Venus 67 would be excessively high and that meeting the schedule at any cost would be unlikely. In the case of the Stanford experiment, the group concluded that, since flight hardware for the *Pioneer* spacecraft was already available, a modified version of this instrument could probably be integrated into the *Mariner* Venus 67 spacecraft, but that it would be a formidable task because of the antenna problems and the high probability of electromagnetic interference between the instrument and other spacecraft subsystems. The Project Manager therefore recommended to the Program Manager that no further consideration be given to the infrared spectrometer for this mission.

During the next few days, the *Mariner* Venus 67 project staff and the JPL Technical Divisions conducted extensive budgetary studies, on the basis of which the Project Manager determined that the full list of experiments that had been considered feasible technically could not be accommodated within the funding limits established by NASA. Consequently, the *Mariner* Venus 67 project staff and the Space Sciences Division gave consideration to the choice of a smaller number of experiments which would yield a maximum amount of scientific information without costing more than the budget analyses indicated to be available. It was concluded that the science payload would have to be restricted to the following:

(1) The S-band occultation experiment, included because it was the only feasible experiment that promised to yield definitive information about the lower atmosphere of Venus.

(2) The celestial mechanics experiment, included because it would yield information of importance for spacecraft navigation on subsequent planetary flights and because the instrumentation required for it was already on board the *Mariner IV* spacecraft.

(3) The UV photometer, included because it had the promise of providing a complete temperature and density profile of the upper atmosphere of Venus which could not be obtained in any other way and because flight hardware was available from the *Mariner* Mars 1964 project.

(4) One additional major planetary experiment: the TV experiment and the dual-frequency occultation experiment were considered alternatives here because the volume of data required, the cost, the complexity, and the effort required for testing and integration of either were judged to be so great that both could not be accommodated within the schedule and funding constraints.

(5) The minimum complement of particles and fields experiments that would yield definitive information about the environment of the planet, i.e., the interaction of the planet with the solar wind. Since three phenomena were involved, the choice of three experiments was clear. The plasma probe would measure the solar wind, the magnetometer would measure the magnetic field, and the trapped radiation detector would search for radiation belts or other associated high-energy charged particles. The trapped radiation experiment was chosen over the other two *Mariner IV* charged-particle experiments (cosmic ray telescope and ion chamber) because it had a capability of detecting a greater variety of particles, was sensitive to particles of lower energy, and had greater directional coverage.

The above five-point recommendation was transmitted from the Project Manager to the Program Manager on February 2, 1966. The preference of JPL for the TV over the dual-frequency occultation was reaffirmed.

On February 4, the OSSA Space Science Steering Committee met to consider the payload. The recommendation presented by Mr. Oran W. Nicks, Director, Lunar and Planetary Programs, corresponded to the restricted payload mentioned above, with dual-frequency occultation included and TV excluded. The result of the deliberations of the committee was a teletype from Dr. Newell

to the Director of JPL, dated February 4, which is quoted here in full, as follows:

"This is in reply to the JPL letters of January 17 and February 2, 1966 containing recommendations regarding the scientific payload to be carried on the *Mariner* Venus 67 spacecraft [*Mariner V*].

"Based upon your recommendations and the recommendation of the Space Science Steering Committee, I have approved the following set of investigations to be conducted as part of the mission: UV Photometer (Barth, Principal Investigator); S-band Occultation (Kliore, PI); Dual-Frequency Occultation (Eshleman, PI); Trapped Radiation Detector (Van Allen, PI); Magnetometer (Smith, PI); Plasma Probe (Bridge, PI); and Celestial Mechanics (Anderson, PI), subject to the following comments:

(1) We would like to add the TV investigation to the above list. If a means can be found to overcome the difficulties in providing adequate buffer storage in the data automation system to support both television and dual frequency occultation without exceeding the primary power capacity of the spacecraft, we should be advised and provided with your recommendations.

(2) The Celestial Mechanics Experiment is approved with regard to the collection of the data. Ranging is considered highly desirable but not mandatory. Funding of data analysis may be deferred as required by budgetary constraints.

(3) Since the Radio Occultation Experiments are closely interrelated, special attention shall be given by project management to the proper coordination of the requirements of each investigation in consonance with the overall mission objectives and to the exchange of data. Since the Stanford group is also interested in S-band Occultation it may be desirable that we recommend the addition of Stanford representatives to the S-band Occultation team.

(4) Even though we can currently fund ground operations associated with the Dual Frequency Experiment for only a few days bracketing the Venus encounter, cruise data formats should be arranged to include the possibility of obtaining interplanetary data from this experiment should additional funds become available. Also the possibility of obtaining additional ground support in cooperation with the *Pioneer* Project should be investigated.

(5) Attempts should be made in conjunction with Hunten to obtain a less expensive earth sensor which can provide a rudimentary optical experiment. If, as the mission design progresses, this experiment becomes feasible, please advise.

(6) If means can be obtained to add more interplanetary experiments, the Cosmic Ray Telescope is desired first, the Cosmic Dust Experiment second. However, the priority of these experiments is lower than TV or Optical Occultation. We realize that the current funding estimates of the above payload slightly exceed the present money allocations, however, further effort should be applied toward supporting this set of investigations within the funding bound as other segments of the total project costs are resolved. JPL is authorized to proceed with contractual support of the approved investigations."

The Director's reply on February 15, 1966 stated that JPL would like very much to add the TV experiment to the list (and indeed would still prefer to replace the dual-frequency occultation experiment with it) but that it was not considered possible to do so without seriously jeopardizing the probable success of the mission. Furthermore he stated that with only 14½ months remaining until launch, an all-out effort on the primary system was mandatory, and continued studies of alternate systems could not be afforded.

The principal investigators of the seven selected experiments were notified by Dr. Naugle on February 17.

## C. System Design and Change Control

Changes to the *Mariner* Mars 1964 design to achieve the mission objectives of the 1967 Venus opportunity can be divided into three categories:

(1) Those required to convert the *Mariner* Mars 1964 design to accommodate the requirements of any Venus mission.

(2) Those required to convert the design to accommodate the requirements of this specific 1967 Venus mission.

(3) Those required to enhance the reliability and operational capability of the basic spacecraft system.

The changes being discussed will be identified with the above categories. The mission design, trajectory parameters, and experiment requirements interact heavily with the spacecraft system design. Understanding such interactions relative to the encounter phase of the mission

delayed the completion of the preliminary design for two reasons:

(1) The planetary atmosphere's large dispersive affects on the RF signal when performing the occultation experiment.

(2) The questionable ability to provide ground command back-ups for spacecraft events in the proximity of the planet because of the high doppler rates resulting from the close planet pass.

*1. Considerations in changing Mars design for any Venus mission.* Adapting the Mars spacecraft design to be compatible with the requirements of a Venus mission primarily involved the accommodation of the increased solar intensity and the accompanying effects. Typical of the effects considered were the operation of solar cells at increased temperatures which required revision of the series-parallel wiring of the solar cells. Also, the brightness of the planet Venus as seen by the Canopus sensor necessitated a redesign of the baffle box mounted in front of the sensor to increase its stray light rejection capability. A discussion of those changes relative to the modification of the Mars design to accommodate a mission approaching the sun closer than the orbit of Venus is presented. More detailed information is available in the subsystem reports contained in this volume.

*a. Solar panel.* Most obviously, the alteration of the solar panels had to be considered to accommodate the increased solar intensity. Assuming an unchanged spacecraft power demand, the solar panel area ratio of about 0.65:1:1.86 was required for operation at Venus, earth, and Mars, respectively. This assumption considered nominal heliocentric distances for the planets and the corresponding variation in efficiency of the solar cells at the respective operating temperatures. *Mariner V* solar panel area was 43.6 $ft^2$ as compared to 70.4 $ft^2$ for *Mariner IV*. The performance of the solar panels at earth and at Mars were the governing factors for the Venus and Mars missions respectively.

Solar panel area was not the only consideration; the operating characteristics of the solar cells at different temperatures demanded that the series-parallel arrangement of the cells be altered. The *Mariner IV* design used *P* on *N* cells, 84 in series *X*, 84 in parallel per panel. *P* on *N* cells, 105 in series *X*, 42 in parallel per panel were used in the *Mariner V* design (refer to Guidance and Control, and Engineering Mechanics sections for additional detail).

The output voltage of the panels decreased with temperature, making it necessary to assure that the lowest expected solar panel voltage did not decrease below the battery voltage or the spacecraft load would be shared between the solar panels and the battery. This decreasing voltage also forced the consideration of the change in efficiency of the booster regulators and the radio power amplifier power supplies. This effect was small enough to be of minimal concern.

Weight and packaging considerations resulted in the deletion of the solar panel boost-phase dampers used on *Mariner IV* to control the motion of the solar panels during the launch vibration environment. There was some delay in defining the high-gain antenna configuration and pointing directions. The severe interaction between the superstructure, to which these dampers attached, and the high-gain antenna supports for the movable antenna resulted in the decision to adopt a tip-latching technique of restricting the solar panel motion during launch. This method of joining adjacent solar panel tips together had, as its basis, some analytical and developmental experience achieved during a previous advanced developmental activity.

The solar cells had to be mounted in such a way that they did not face in-board, as on *Mariner IV*, but outboard, making them susceptible to damage if the shroud impacted them due to some malfunction of its jettison maneuver; however, extensive analysis of the shroud–spacecraft dynamics during the jettison maneuver revealed that a worst-case situation would not result in an impact to the solar panels. It was still desirable to protect the solar cells from this potential failure mode because of its unknown effects should it, in fact, occur. Adaptation of some type of bumpers to deflect the shroud under these conditions was considered but discarded for several reasons:

(1) Bumpers increased the probability of shroud–spacecraft contact.

(2) Mounting of bumpers through the celled area of the panels would have required special mechanical consideration and complicated manufacture of the panel structure.

(3) The shadow cast by bumpers would have an adverse effect on the performance of the panels; a solution would require a more sophisticated cell layout.

*b. Sun shade.* The experience acquired during the thermal testing and flight of *Mariner IV* validated the technique of isolating the spacecraft from the solar input as a means of maintaining a reasonable temperature profile on the spacecraft. Isolation from the solar heat input precluded devising another solution to the problem. It was desirable to continue this technique of spacecraft temperature control on the *Mariner* Venus 67 mission also. Because of the requirements of a Venus mission, the *Mariner* Mars 1964 spacecraft configuration had to be "turned-over" to point the low-gain antenna and high-gain antenna at the earth. This resulted in the "shaded-side" (referenced to cruise orientation) becoming the "sun-side." The periphery of the lower octagon structure contained the interface areas needed for attachment and electrical connection to the launch vehicle adapter. In the *Mariner V* configuration these areas, which must of necessity be free from obstruction prior to separation, are free to absorb energy and conduct it then into the spacecraft electronic compartments—unless they are shaded following separation.

A sun shade was developed (refer to Engineering Mechanics section for details) which was deployed at the time of solar panel deployment to cover these peripheral regions and make them independent of the varying solar intensity. The sun shade aided the thermal control of the spacecraft bus to the extent that the bus would run 30° F cooler at Venus with the shade deployed.

The sun shade had potential interactions with the celestial sensors in the spacecraft, particularly under failure mode conditions. Special tests were conducted to evaluate these interactions to assure the elimination of any interference with the celestial sensors. Equipment could not be located on the sun-side of the spacecraft if it would in any way interfere with the deployment or effectiveness of the deployable sun shade. The plasma probe was the only instrument mounted on the sun-side of the spacecraft bus; this was in-board of the movable portion of the shade. Other instruments, mounted on the shaded-side of the trapped radiation detector looking for low energy solar X-rays, necessitated cutting a hole in the outer portion of the shade to eliminate the attenuation of the X-rays.

*c. Celestial sensors.* Reconsideration of the adequacy of celestial sensor location and design was a requirement when reconfiguring the Mars spacecraft for the Venus mission. As a consequence of inverting the spacecraft as discussed in the previous section, the primary sun-sensors were on the shaded-side of the spacecraft. These sensors and the acquisition sun sensors had to be relocated to the proper side of the bus.

The increased solar intensity associated with the Venus mission resulted in increased solar heat inputs to the sensors themselves; without design modification, they would have been unable to survive the mission. Zener diodes were added to the attitude control electronics to reduce the voltage supplied to the primary sun sensors from 16 V to 12 V. The reduction in internal dissipation now made it possible to keep the sun sensors within design bounds by using conventional thermal control techniques.

Possible stray light interference is a necessary consideration in any design effort employing celestial sensors. The most significant area of concern was that of light from the planet Venus reflecting off portions of the spacecraft into the optics of the Canopus sensor and confusing the optical lock on the star Canopus. This could lead to an undesirable roll orientation of the spacecraft. An occurrence of this near the planet could cause operational problems and severely jeopardize the achievement of the primary mission objectives. Damage to the sensor might also ensue if the sensor were pointed directly at the planet during this roll mis-orientation.

Accommodation for this difficulty existed in the attitude control/command logic of the spacecraft but it was not desirable to depend on this for mission success for a variety of reasons. A new baffle box was designed, fabricated, and extensively tested to assure that it was adequate to maintain the reflected light levels below allowable limits as long as geometrical constraints of the spacecraft relative to the planet could be guaranteed by the trajectory path chosen. A constraint was imposed to maintain the Canopus-spacecraft-near-limb-of-Venus angle greater than 36 deg during the entire encounter phase.

Prior to the development of the baffle-box, the concern for light reflected from the solar panels or DFR antennas into the Canopus sensor optics resulted in changing the location of the Canopus sensor. It was located mid-way between the $+X$ and $-Y$ axes, whereas on *Mariner IV* it was located in the same quadrant but 57 deg from the $+X$ axis. The *Mariner V* location was the best that could be adopted, but development of the Canopus sensor baffle-box was still a prime requirement for the system design.

Testing was accomplished to verify that the nominal configuration of the spacecraft did not result in narrow margins of light rejection capability at each of the celestial sensors. Not only was the nominal configuration tested but various failure mode configurations, particularly of the deployable sun shade, were also thoroughly tested.

*d. Shaded elements.* The reversal of the basic sun–probe–earth geometry from the Mars mission necessitated that many elements which were developed to operate under conditions of solar heating for *Mariner IV* now had to operate in shaded conditions for *Mariner V*. These elements were the magnetometer, the high-gain antenna, and the low-gain antenna.

Preliminary results of the investigation of the magnetometer thermal response to being in the shade indicated that without some change to the thermal control of this instrument, it would be operating at −89°F during encounter (*Mariner IV* operated at −35°F during encounter). Use of a heater element to compensate for the lack of solar heating was considered early in the project. A reflective thermal blanket was added around the magnetometer sensor to isolate the sensor from sunlight when the spacecraft was not sun-acquired. This thermal blanket effectively prevented thermal leakage to outer space as well, reducing the quantity of heat required.

Power for heating the magnetometer sensor was taken directly from the dc output of the solar panels through a fuse. It was mandatory to use this fuse to prevent catastrophic damage to the spacecraft power subsystem in the event of a heater short. Raw dc power was used because insufficient capability existed in the inverters or booster regulators. The heater consisted of 48 resistors in a series/parallel arrangement with an effective resistance of 795 Ω. Operating from the variable with heliocentric-range dc-voltage source caused the power dissipated at earth to be 2.9 W and the power dissipated at Venus to be 2.1 W.

Anticipated magnetometer temperatures during cruise were expected to range from −16°F at earth to −25°F at Venus. During midcourse maneuvers, the anticipated temperatures were +54°F for a worst-case near-earth maneuver and +103°F for a worst-case near-Venus maneuver. The latter condition is nearly beyond the desired operating range of the instrument; consequently, as the spacecraft approached the orbit of Venus, the midcourse turns were limited to angles which prevented overheating the instrument.

Another shade-side element of the spacecraft was the high-gain antenna. It was anticipated that the high-gain antenna would have to operate at temperatures as low as −151°F for the *Mariner* Venus 67 mission as compared to the +50°F for the *Mariner* Mars 1964 mission.

Areas of concern in placing the high-gain antenna in the shade included (1) possible stresses on the honeycomb structure bonds while at the low temperatures and during the antenna deployment, and (2) stresses on the feed which would distort the antenna pattern. A change of temperature of this magnitude had not been assessed in the *Mariner* Mars 1964 testing.

The method of deploying the antenna was such that the loads were not carried directly through the honeycomb structure. Additionally, the coaxial cable which had to flex at the time of deployment added some resistance to the motion of the antenna, removing high deceleration loads at deployment. Warping the laminated feed ground plane on the antenna feed required a change of mounting screws from nylon to titanium. This modification had negligible effects on the antenna pattern.

Temperature sensitivity of the low-gain antenna was not judged to be a difficult problem. There was, however, an anomaly noted when testing the type approval (TA) low-gain antenna. Small cables bonded to the antenna waveguide loosened when the epoxy cracked at low temperatures. A fix was developed in the event this problem re-occurred during flight-acceptance testing. The objective of these periodic bonds along the antenna waveguide was to limit the movement of the cables during vibration; their ability to sustain the launch environment had been proven. Should the bonds fail at the flight temperatures, no spacecraft damage would ensue. If the bonds did not crack during ground testing at low temperatures, it was judged advisable not to break the existing bonds intentionally to replace the epoxy used for bonding. After the TA anomaly, no additional bonds were found to fail.

***2. Considerations in changing design for Mariner Venus 67 mission.*** Achievement of the objectives of this mission necessitated the largest number of system design changes. Many subsystems of the spacecraft had to undergo some change to achieve the system design which was constrained to change the *Mariner IV* design as little as possible. The existence of the *Mariner IV* hardware at the time of the preliminary design forced solutions to

system design problems which might not otherwise have been chosen had the basic system design been in an embryonic state.

*a. Deployable high-gain antenna.* Since the S-band occultation experiment was the primary means of probing the Venus atmosphere, it was necessary to optimize the pointing of the high-gain antenna to achieve the best results possible. Implementation of the occultation experiment for a Venus mission was a more complex problem than the Mars radio occultation experiment conducted with the *Mariner IV*. Acknowledging that the radio signals would be refracted and attenuated orders of magnitude more by the atmosphere of Venus than they were by the atmosphere of Mars, some compensation for this phenomenon had to be made. There were large uncertainties as to what the density profile of the atmosphere was. The one thing known was that the refraction of the radio signals would tend to extend the periods of communication to the earth when entering and leaving the occultation zone behind the planet. The direction of bending of the signals for entry and exit were opposite; also, the deeper the radio signals penetrated the atmosphere, the larger the attenuation became. Consequently, the decision was made to point the antenna in different directions for the entry and exit condition. The precise direction was chosen in such a manner as to have the high-gain antenna oriented with its peak gain in the direction of the most refracted signal. Since the refraction is a function of the density profile of the planet, the uncertainty in the expected density had to be considered. The performance of the radio link under the various conditions of refraction and attenuation also had to be considered in making the final choice. Limiting factors, of course, were the peak gain and the expected antenna pattern of the spacecraft's high-gain antenna. Study revealed that the *Mariner* Mars 1964 high-gain antenna pattern was as practical an antenna pattern as one could expect to find to do this experiment. The final selection of the pointing direction was made in consultation with the principal investigator of the S-band occultation experiment. The selection necessarily had to be a tradeoff between the ability to transmit a signal through a dense atmosphere without forfeiting the ability to transmit through a less dense atmosphere because of improper antenna orientation. The atmospheric models utilized in the preliminary design studies when considered against the spacecraft performance capabilities yielded answers that the radio signal tangent to the surface of the planet could be received at earth if the surface pressure was no greater than 35 earth atmospheres. For the same models, critical refraction (the signal never emerging from the atmosphere) was expected to occur at about 50 earth atmospheres surface pressure. Thus, there was sufficient margin to obtain a successful occultation experiment for a reasonable range of atmospheric surface pressures, provided that critical refraction did not occur before the "surface-tangent" ray was received at the earth. In either case, a more significant knowledge of the atmosphere would be obtained at the conclusion of the experiment.

Change of antenna pointing direction would have to occur after entry and before exit of occultation. The method selected for achieving the deployment was the use of a pyrotechnics-actuated pin-puller which retained the high-gain antenna in the pre-entry position from launch until mid-occultation. This pin puller was activated by a command signal from an optical sensor, called the terminator sensor, or the data automation subsystem, while the spacecraft was in occultation. Following pin-puller activation, two coiled clock springs pivoted the antenna to its exit position. The angular displacement of the antenna was 17.7 deg.

*b. Encounter sequence.* Specific mission requirements influence the encounter sequence in a very direct manner. Only minimal similarity exists between the encounter sequences of the *Mariner IV* and *Mariner V* missions. Many aspects of the Venus mission sequence are different, including:

(1) No TV experiment.

(2) No scan platform requirement.

(3) Questionable command capability in the vicinity of the planet because of expected high doppler rates.

(4) Refraction of radio signals by atmosphere.

(5) Longer record sequence.

(6) All instruments acquire cruise and encounter data.

The basic requirements of the *Mariner V* encounter sequence are summarized below:

(1) Provide capability to obtain entry and exit occultation data for S-band occultation experiment.

(2) Acquire high-rate sampling of selected science instruments.

(3) Modify mode of operation of selected science instruments.

(4) Provide redundant command signals for key encounter sequence events.

(5) Provide capability to compensate for failure modes if such should occur during the encounter phase.

(6) Provide capability to achieve encounter sequence without the aid of commands from earth.

(7) Establish an all-science telemetry mode early enough to observe the interaction of the planet with the interplanetary magnetic field.

Design of the encounter sequence had to take all of the above requirements into consideration. It is apparent that not only was there concern for the successful execution of the various command functions at the correct time, but there was also concern that an inadvertent or erroneous command must be counteracted before disastrous consequences develop. The most crucial of all events in this sequence was the antenna pointing angle change (APAC) function. If it occurred prematurely, due to some failure, nothing could be done to prevent the loss of the entry occultation data. Other key events could be inhibited and re-cycled on a reasonable time scale to salvage some of the encounter experiment objectives.

The use of failure mode effect analysis was very prevalent in the design of the encounter sequence. Choice of the antenna positions was predicated in part on the consideration that should the antenna fail to deploy, the signal strength from the high gain antenna would be sufficient to allow playback of the recorded data before threshold was reached. Also, in the case of premature deployment, the received signal level would be sufficient to assure satisfactory telemetry signal levels to evaluate the spacecraft prior to the initiation of the encounter sequence. In other words, it was necessary that there be overlap of the high-gain antenna patterns in both positions during the encounter phase of the mission. The final design provided telemetry capability at encounter minus two days when in the deployed position, and up to encounter plus two days, assuming use of the cavity power amplifier. Use of the traveling-wavetube (TWT) power amplifier (the expected radio configuration) adds about three days of additional coverage in each position.

The final sequence chosen for the encounter phase provided for turn-on of tape-recorder electronics and the terminator sensor at encounter minus 12⅔ h by the CC&S MT-7 command backed up by a direct command (DC-V25) from earth. At encounter minus 6⅔ h, the CC&S MT-8 command signaled the data automation subsystem (DAS) to do a number of functions. The spacecraft telemetry mode was changed to an all-science format, except for two words necessary for command link information. At this time the plasma-probe instrument would also be switched to an encounter mode in which the three detectors were sampled simultaneously instead of sequentially. The DAS also turned on the planet sensor and enabled Clock "B" outputs. A direct command (DC-V24) was available as a backup. Selection of the time of this event was based upon the desire on the part of the scientists to be in the all-science telemetry mode at the time the spacecraft passed through the magnetopause. CC&S command resolutions and trajectory uncertainties had to be considered.

As the spacecraft approaches the planet, the recording sequence will be initiated by the planet sensor field of view intersecting the lighted limb of the planet. The planet sensor signal will also inhibit the UV photometer calibrate signals from being generated. (The concern was the possible loss of significant scientific data due to a calibrate cycle being in effect.) Track 1 data recording will be initiated at the time of the planet sensor signal. Thirteen minutes later, the recording on Track 2 of the dual-frequency-receiver (DFR) data will be initiated.

Approximately one hour through the record sequence, the terminator sensor will observe the transition from dark to light as the trajectory carries the sensor field-of-view across the planet. This signal activates the antenna position change. 107.5 minutes after Track 2 recording has been initiated, data to that track will terminate. The end of Track 1 recording will be commanded thirteen minutes later by the DAS. Sometime between the end of Track 2 and Track 1 recording (nominally 127 minutes after the planet sensor signal), the tape recorder will automatically turn itself off after reaching its end of tape (EOT) foil.

The command signals controlling the recording of data will be generated by a clock initiated by the planet sensor signal. This clock, Clock B, has a back-up, Clock A, which will be initiated by direct command (DC-V16) at 3 h 8 min prior to the center of occultation. As Clock A counts, it generates commands in close proximity to the Clock B commands to provide the command signal redundancy desired. An additional back-up capability for the APAC event is provided by Clock A. Since the antenna will not be deployed prior to center of occultation, all of its times will be measured relative to that event. The time of center of occultation will be determined from trajectory predictions and the time for its initiation by DC-V16 will thereby be selected. Consequently, dependent upon the trajectory characteristics predicted for

encounter day, the outputs from Clock A may or may not precede the outputs from Clock B.

As a consideration of the possible failure modes, the direct commands (DC-V16 and DC-V24) were mechanized to be toggle commands; after initial transmission, subsequent alternate transmissions turned off and turned on the respective clocks affected by these commands. Thus, in the case where one clock counts improperly and consequently issues its commands at an incorrect time, the clock and its outputs will be inhibited to prevent destruction of the encounter sequence.

After the close approach to the planet, the playback of the recorded data will be initiated by another CC&S command, MT-9. This command has a DC-V4 backup. One playback will require approximately 35 h. Two playbacks are planned.

*c. Terminator sensor.* The *Mariner* Venus 67 mission requirement to change the position of the high-gain antenna during the occultation period lent itself to the use of an optical sensor that could sense the planet's terminator. With the trajectory being a dark side approach, the transition from dark to light was easily sensed by a cadmium sulfide detector. The pointing direction of the sensor axis was the variable which permitted the sensor to see the terminator at mid-occultation. Orientation of the sensor was chosen to be 110-deg cone angle and 110-deg clock angle. The field of view measured 1.5 by 2.5 deg.

An optical sensor very similar to this terminator sensor was used in the *Mariner IV* design to initiate the TV recording sequence. Only minor redesign was required to properly orient the sensor and adjust its threshold over temperature.

*d. Planet sensor.* Consistent with the philosophy that the spacecraft be capable of executing the encounter sequence without ground commands, it was necessary to automatically initiate the recording sequence approximately one hour prior to closest approach. A planet sensor was again considered as a possible candidate. The requirements for this sensor were more stringent than those for the terminator sensor.

Use of a cadmium sulfide detector was desirable because of previous experience with such a device. Potential problems with this approach were the intensity of the signal which must be detected at one hour before closest approach and the temperature range over which it had to function. The trajectory was such that the view of the planet available to the planet sensor was that of a slender crescent. The operating temperature influenced the threshold of the sensor.

Consideration was given to the use of an infrared detector, but the final choice, based primarily on simplicity and schedule constraints, was an optical sensor using a cadmium sulfide detector. It was necessary to design more temperature compensation into this device than into the terminator sensor to prevent false triggering of the output.

Choice of the pointing direction necessitated an iterative process of looking at all variations in the trajectories to assure that the direction selected did not result in excessive variations of output as a function of time to closest approach. Working with a requirement to issue an output at $60 \pm 15$ min prior to closest approach, a pointing direction was selected which gave an output, considering 3-$\sigma$ trajectory dispersions, at $60 \pm 13$ min from closest approach. The field of view of the planet sensor was selected to be at 24.9-deg cone and 0-deg clock.

To prevent an output signal at the time of the planet sensor turn-on, the recipient of the signal, the DAS, had a built-in time delay to allow any turn-on transient signal to be ignored effectively.

*e. Tape recorder.* Modifications to the design of the *Mariner IV* tape recorder were a mandatory requirement for this mission. A record data rate of 66⅔ bps was selected for this mission as compared with a 10,700 bps record rate for *Mariner IV*. Although the packing density remained the same, the record interval changed from 25 min of intermittent recording to 129 min of continuous recording. The length of the *Mariner V* tape was 53.5 ft as opposed to the length of 330 ft for the *Mariner IV* tape (refer to the Telecommunications section for further details).

The shortened length of tape increased the number of passes over the tape while in the launch mode. As an attempt to reduce this number, the launch mode speed of the tape was reduced approximately 55%. The choice of this value was a compromise between the speed required to prevent the tape from looping off the reel during vibration and the angular momentum of the tape pack at the post-separation turn-off of the launch mode motor.

*f. Science overload inhibit.* An additional bit of logic was built into the power subsystem at an early stage to

prevent an untoward overload of the maneuver booster regulator in the power subsystem. A short discussion of some of the power subsystem logic is in order at this point. The power subsystem had two booster regulators (B/R), one of which, the main B/R, was on all the time while the second, the maneuver B/R, was on only when the gyros were to be turned on. In the event of a main B/R failure, the maneuver B/R was turned on to supply the spacecraft loads normally handled by the main and maneuver B/R's. The maneuver B/R was sized to handle all the spacecraft loads for the *Mariner IV* design.

In the course of the preliminary design, the power loads anticipated for the science subsystem were judged to be in excess of the *Mariner IV* science loads. The inclusion of a TV camera in the complement of science instruments was a distinct possibility for some time. Also, the *Mariner V* DAS was expected to consume a large amount of power compared to the *Mariner IV* DAS. These circumstances resulted in the condition that with a failure of the main B/R and with the requirement for gyros-on to maintain attitude control (also a non-standard situation), the loads on the maneuver B/R would exceed the design of that equipment. It was recognized that the equipment might be able to operate at load levels beyond the design limit for short periods if the temperature of the power transistors were low enough. Internal logic to preclude overload of the maneuver B/R by the simultaneous occurrences of main booster failure, gyros on, and science on was built into the early design. This logic would switch off the science loads to permit the maneuver booster to safely handle all other spacecraft loads, including the gyros. A direct command was available to override this logic if the conditions in the spacecraft warranted such action. Even when the maneuver B/R was supporting all the spacecraft loads, this technique permitted the decision "to turn on science" to be made on the ground. Deciding to send this science inhibit override command required better knowledge of the exact characteristics of the maneuver booster regulators. Data to support this decision were to be obtained in a series of tests to be conducted during the course of the project. At the time of launch, there was reasonable confidence that the B/R could handle the entire spacecraft loads including the science if the situation demanded it. This was based, in part, on the expected flight temperatures. Only after the flight data were considered could a final decision be made.

*g. Inverter redesign.* The initial power estimates for the science loads caused the loads on the main 2.4 kHz inverter to exceed the design limits. A new design for these inverters was incorporated which increased its steady-state load capability from 80 to 105 W. Its peak load capability was increased from 120 to 150 W. An additional precautionary design change was incorporated to preclude interchanging the previously identical main and maneuver 2.4 kHz inverters. Whereas the inputs to the main and maneuver inverters were on identical pins in the *Mariner IV* design because they were to be interchangeable, the wiring was re-arranged so the inputs to each were now on different pins. Even if the inverters became interchanged, no damage could be incurred by the maneuver inverter because the connector for the main inverter would have the input power on pins not coincident with the pins on the maneuver inverter subassembly.

System design considerations of this nature were required to decrease the chance of damage to equipment and subsequent schedule delays while repairs were being made. A program with such stringent schedule constraints could not afford needless delays as this situation may have presented.

*h. Command list modifications.* Conversion of the spacecraft to accomplish the mission certainly required a review of the existing spacecraft direct command (DC) list. New mission requirements called for new direct command capability to be added to the system design. There were a total of 29 DC's available from the command subsystem. Many of these commands were required to maintain the basic engineering system back-up capability originally designed into the *Mariner IV* spacecraft (Ref. 1).

There was the possibility that the mission requirements for the *Mariner* Venus 67 mission would force the deletion of some basic engineering commands. Obviously, this was not desirable but there had to be a complete review and understanding at an early date to map out the command capability required to handle the many possible strategies which might be required should in-flight anomalies occur. Since the spacecraft flight sequence is intimately associated with the final command list, these two items were developed in parallel. A difference between the construction of the command list was that there were spare commands in the early *Mariner* Mars 1964 command list which permitted added capability as the system design progressed. Early in the design of the *Mariner V* system it was recognized that there was little room for growth should unforeseen problems arise at a later date. Fortunately, the *Mariner V* command list did

not have to be amended to achieve a satisfactory flight sequence.

Review of the *Mariner IV* command list revealed that only two commands were readily available for use in the *Mariner V* design:

(1) DC-V16—Narrow Angle Acquisition: This command was utilized in the *Mariner IV* design as the backup to initiate the TV recording sequence.

(2) DC-V24—Inhibit Scan Search: This command was utilized in the *Mariner IV* design as the backup for stopping the planetary scan platform.

The most immediate need for command capability was to implement the encounter sequence. Clock A, the back-up timer for the record start/stop functions, and the antenna pointing angle change (APAC) were initiated via DC-V16. DC-V24 was used to back up the turn-on of the planet sensor and to enable Clock B command outputs. These functions used up the available commands.

Further examination of the encounter sequence revealed that there was little need for maintaining the DC-V3 command capability to command a switch to telemetry mode 3 (all science). This was to be done by the data automation subsystem (DAS) at the time of receipt of the MT-8 command from the CC&S. The DAS could easily be designed to send the signal to switch the data encoder to telemetry mode 3 at the receipt of the DC-V24 command, the back-up to the MT-8 command for planet sensor turn-on and plasma probe encounter mode switch. This approach was adopted leaving the DC-V3 command open for other uses. The only reasonable suggestion for use of this command was to effect the antenna-pointing angle change after occultation, should it not occur during occultation.

There were already two means of commanding the antenna change, so the addition of a third path protected against an unlikely occurrence. However, the antenna-pointing angle change not only permitted attainment of the exit-occultation data but extended the post-encounter communications time with the spacecraft by about one month. The importance of data in the post-encounter period was significant because the spacecraft would be closer to the sun than any spacecraft has ever been. Since there were no alternatives for the spare command, it was allocated to the APAC function.

A detail of the command subsystem forced the exchange of this function with the tape track change function which used DC-V22. The command subsystem has two types of output signals: an isolated step, or an isolated pulse signal. The former has a characteristic duration of 100 ms with a maximum current capability of 100 mA. The latter has a characteristic duration of 6 ms with a maximum current capability of 10 mA. DC-V3 had an isolated pulse output wavefom which was not capable of reliably activating the pyrotechnic circuitry associated with the APAC function. An isolated step waveform was being used for the tape track change command on DC-V22. The tape recorder circuitry would operate satisfactorily with the DC-V3 output, and thus the exchange was made. This change also provided an isolated step capability for another function if it were to replace the APAC function on the DC-V22 command output. This capability was desirable because there was now a high probability that any demand for a command at a later date could be satisfied.

*i. Telemetry channel assignments.* Redesign of a spacecraft system has associated with it the redesign of the telemetry channel assignment list. This list represented the areas of interest to engineers and scientists. The content of the telemetry subcarrier from the spacecraft was controlled by the data encoder. This subsystem permitted the following telemetry data modes:

Mode 1: All engineering (real-time)

Mode 2: 2/3 science, 1/3 engineering (real-time)

Mode 3: All science (real-time)

Mode 4: All recorded data playback (non-real time)

The engineering data were subcommutated internal to the data encoder to provide the required sampling rates. Science data were acquired by the DAS and serially shifted to the data encoder which gated it to the radio subsystem for the transmission to the earth. The recorded data were played back through the data encoder from the tape recorder. These data went to the tape recorder from the DAS.

Changes to the engineering telemetry channel assignment list were the result of the desire for information relative to:

(1) The spacecraft command capability while in mode 3.

(2) The use of an earth sensor as a roll reference back-up during the pre-midcourse phase of the mission.

(3) The prevention of an inadvertent terminator sensor excitation from causing catastrophic mission results.

(4) The thermal profile of this new configuration.

Deletion of some equipment from the *Mariner IV* design permitted the availability of enough channels to accommodate the measurements required in the *Mariner V* design.

Science telemetry modifications resulted from the different complement of science instruments aboard the spacecraft and also the new status information required to evaluate and conduct such a mission. The science requirements caused a new DAS to be designed and built. The generation of the science telemetry format will not be discussed here (refer to the Science Subsystem section for details).

The most significant modification to the engineering telemetry list was caused by the need for direct commands after the time desired for the establishment of telemetry mode 3 (all science). Without sufficient data on the performance of the spacecraft command link, the reliability of command transmission was jeopardized. A method for inserting some appropriate data into the mode 3 format was found. This required that, while in mode 3, the spacecraft receiver static-phase error and command detector should monitor telemetry words to be inserted between science words. Two science words were utilized for this function. In order to place these words in sequential order and still permit compatibility with the desired science data format and the existing data encoder design, the following modifications to the telemetry list were adopted:

| *Mariner IV* channel number | Function | *Mariner V* channel number |
|---|---|---|
| 105 | Pitch gyro/fine sun sensor | 103 |
| 106 | Yaw gyro/fine sun sensor | 104 |
| 104 | Command detector monitor | 105 |
| 111 | Receiver SPE | 106 |
| 103 | Receiver AGC | 111 |

Provisions for a backup roll reference to establish the spacecraft attitude before initiating the spacecraft turns during the midcourse maneuver were supplied by modifying the field of view of the earth sensor on the spacecraft. A high-rate telemetry channel was required to achieve this backup capability. In the *Mariner IV* design, the earth sensor output was only visible with the gyros off, which was not compatible with this use of the earth sensor. The only available telemetry channel was channel 118. Additional changes were also required to accommodate this capability, as follows:

| *Mariner IV* channel number | Function | *Mariner V* channel number |
|---|---|---|
| 107B | Earth sensor | 118 |
| 118 | MC $N_2$ pressure | 228 |
| 228 | Oxidizer pressure | 305 |
| 305 | Solar vane position, $+X$ | NA |

Acknowledging that one of the most detrimental mission failure modes would be to have the high-gain antenna be deployed prematurely, a review of ways to avoid this was conducted. Should the terminator sensor be prematurely energized, the antenna would be deployed whenever the sensor saw a light stimulus. During the midcourse maneuver was one time when the spacecraft would be intentionally changed in attitude. A constraint could be placed on the allowable turns to preclude looking at the sun with the terminator sensor if it were energized. Therefore, a means of determining the terminator sensor state was desired.

Originally, the use of an event counter indication had been chosen to denote the excitation of the terminator sensor. It was noted that occurrence of an early terminator sensor excitation could not be uniquely determined by a telemetry event register indication because the occurrence of extra counts at the time of redundant pyrotechnic events was a distinct possibility (Ref. 6). The pyrotechnic subsystem, the source of the terminator sensor power, was modified to provide an analog output indicating the presence of excitation voltage to the terminator sensor. Channel 306 was chosen for this measurement. It had become available when the solar vanes were deleted from the design.

Temperature measurements were added to obtain an improved understanding of the spacecraft thermal profile. Critical components, temperatures, operationally important temperatures, and additional thermal control evaluation measurements were included on the temperature measurement change list.

Critical components which were instrumented for temperature readout during this mission were the high-gain antenna, the omni-antenna mast, the plasma probe, and a primary sun sensor. The antennas were now in the shade during cruise whereas they previously were in the sun. Concern about materials and distortion at the expected low temperatures in the event of flight anomalies caused these measurements to be made. Also, the accuracy of prediction based upon space simulator tests could be evaluated. The plasma probe and primary sun sensors were anticipated to become precariously hot as the spacecraft heliocentric range decreased to a minimum. Monitoring their temperature would yield valuable information on their performance.

Temperature measurements of the two auxiliary oscillators and the spacecraft receiver VCO were important to the conduct of the occultation experiment. Lock-up time for the DSN receivers could be reduced if an accurate prediction of the downlink frequency could be made. Since the auxiliary oscillator frequency was a function of temperature, the knowledge of this temperature throughout the cruise phase would permit a more accurate prediction of its temperature near the planet. Knowledge of the spacecraft receiver VCO temperature would aid in determining the best lock frequency to be set into the ground transmitter.

New temperature measurements for thermal control evaluation were divided into the areas of solar panels, attitude control gas jets and thermal control materials. The solar panels were instrumented to permit evaluation of the temperature profile on a single panel by multiple measurements rather than a single measurement on all panels. Solar panel 4A5 was capable of providing information on the temperatures of the panel substrate, a point in the vicinity of the standard cell transducer, and the solar panel spar near a zener diode. These measurements were selected to provide information on the temperature gradients in the solar panel and also permit more precise analysis of the standard cell data.

The attitude control gas jets were redesigned to be more compatible with the expected high temperatures of this mission. Extreme temperatures could cause their performance to deviate from specifications. Monitoring of their temperature in flight also provided data useful to the evaluation of the temperature control references (TCR's). The response of various paint materials to exposure to the UV radiation from the sun affects the thermal control effectiveness on this and subsequent spacecraft. The TCR's results depended upon the solution of a heat-balance equation. The amount of heat conducted to the solar panel was inferred from the gas jet assembly temperature measurements which were made at the base of the TCR mounting bracket.

A summary of the changes to the assignment of telemetry channels for temperature measurements is given in Table IV-1.

*j. MT command changes.* As mission requirements change from mission to mission, the master timer (MT) matrix in the central computer and sequencer (CC&S) must be modified. The times for the MT commands must be hardwired into the equipment; the actual command times are determined during the countdown based upon the expected time of flight to encounter.

The functions of MT-1, 2, 3, 4, 5, 6 were the same for the *Mariner V* mission as for the *Mariner IV* mission. MT-7 was used to energize the encounter science instruments; however, in the *Mariner V* mission there were no solely-encounter oriented instruments. All the instruments yield data during the cruise phase as well as the encounter phase. However, the instruments would be turned on by the MT-7 if they had been turned off for some reason during the mission. Previously the MT-8 command turned off the encounter instruments following encounter. The *Mariner V* MT-8 command turns on the planet sensor, switches the data encoder to telemetry

**Table IV-1. Telemetry channel assignment—temperature measurements**

| Channel number | *Mariner V* measurement | *Mariner IV* measurement |
|---|---|---|
| 403 | SP4A5 $I_{sc}$ VCO temp. | Spare |
| 406 | +X — R&Y jet assy temp. | Bay VII louvre pos. |
| 411 | Spare | Scan actuator temp. |
| 412 | TCR +X | Abs. std. #1 |
| 413 | TCR −Y | Abs. std. #2 |
| 414 | Aux. osc. #1 temp. | Science cover deployment |
| 418 | Aux. osc. #2 temp. | TV temp. |
| 419 | HG dish temp. | Ion chamber temp. |
| 422 | Plasma probe temp. | Bay III louvre pos. |
| 424 | VCO temp. | Crystal osc. temp. |
| 425 | −Y pitch jet assy temp. | Bay I louvre pos. |
| 427 | SP4A5 spar/zener temp. | Spare |
| 430 | Primary sun sensor temp. | Lower ring harness temp. |
| 431 | Omni mast temp. | Upper ring harness temp. |
| 432 | TCR −X | Abs. std. #3 |
| 433 | −X R&Y jet assy temp. | Abs. std. #4 |

mode 3 and establishes the plasma probe encounter phase data sequencing. A function of the MT-9 for the Mars mission was to turn off the cruise science to conserve power in addition to initiating the recorded data playback. In the Mars case, the available power was decreasing each day as the heliocentric range increased. For *Mariner V* the heliocentric range would be decreasing each day, thereby increasing the available solar panel power. Consequently the science instruments were to be left on during data playback.

*k. Temperature control references.* As an aid to the evaluation of the thermal control performance of this spacecraft, and for future applications, three temperature control references (TCR's) were added to the design (refer to Engineering Mechanics section for further details). Briefly, the effects of the UV radiation from the sun on the paint material coating each TCR are indicated by examining the changing temperature as a function of time and evaluating this curve against a theoretical $1/R^2$ curve.

Originally, four TCR's, one on each panel tip, were planned to be flown. As the dual-frequency receiver (DFR) antenna design concept developed, it was judged more expedient to eliminate the TCR on the end of the $+Y$ solar panel over Bay III than to go into a special program to assess the effects of such a device on the antenna pattern of the 423.3 Mc antenna mounted on the end of the $+Y$ solar panel.

There was also potential physical interference between the TCR and the antenna during the launch environment which would have to be considered.

*l. Dual-frequency receiver.* The complement of science instruments for this mission included a dual-frequency receiver (DFR). The DFR measured the differential refraction of 49.8 Mc and 423.3 Mc radio waves between the transmitter on the earth and the receiver on the spacecraft.

This instrument represented the most significant addition to the design of the *Mariner* spacecraft system. Integration into the spacecraft required the design of antennas and extensive system testing to identify, assess and eliminate sources of RF interference with this receiver. The integration effort was successfully accomplished following many modifications to the spacecraft hardware (refer to the Telecommunications section for details).

The data from this instrument had to be sampled at a high rate and recorded during the encounter period in order to get satisfactory data resolution relative to the ionosphere of the planet Venus. The entire Track 2 of the two-track tape recorder was devoted to the recording of DFR data. Additional DFR measurements were recorded on Track 1.

*m. Ultraviolet photometer.* The incorporation of the ultraviolet (UV) photometer instrument into the spacecraft design represented an addition to the complement of science instruments flown on the *Mariner IV* spacecraft. This instrument had been under development for the *Mariner* Mars 1964 launch, but technical problems caused it to be eliminated from the design prior to launch. The difficulties had been eliminated in the interim.

Modifications to the instrument were made to permit it to operate as a cruise phase instrument to investigate the concentration of hydrogen in outer space as the spacecraft moved along its trajectory. A look angle of 90 deg to the sun direction was chosen to give the desired look angles to the planet during the encounter phase of the mission. There was also the possibility that a UV star might come into the field-of-view of the instrument permitting some inflight calibration data to be acquired.

It was possible to mount the instrument on the spacecraft structure, thus eliminating the requirement for a scan platform, actuator and electronics. By selecting the clock angle orientation appropriately, a satisfactory crossing of the planet's atmosphere could be obtained. A clock angle of 95.5 deg was selected. This location placed it just above the rocket motor used for the trajectory correction. Analysis had to be performed to assure that the exhaust products from the nozzle would not contaminate the optics of the instrument. The analysis showed that there would be no contamination of the optics because the instrument is mounted approximately three inches in back of the nozzle exit plane, outside the predicted plumefield.

A constraint was placed on the midcourse maneuver turns, i.e., not allowing the sun to come within 5 deg of the field of view of the detectors. The concern for the instrument was that the intense UV radiation of the sun would cause damage to the photomultiplier tubes.

The data requirements of the UV instrument were such that the data had to be recorded during the encounter phase of the mission. These data constituted the majority of data on Track 1 of the tape recorder.

*n. Plasma probe.* The plasma probe instrument was modified for the Venus mission to correct the difficulties that occurred during the *Mariner* Mars 1964 mission. In addition, the internal sequencing was modified so that at encounter the individual measurements from each of the three sectors of the sensors' collector were eliminated and replaced by a measurement which included the sum of all three sectors of the collector. This mode of operation remained in effect from the receipt of the MT-8 or DC-V24 commands until the end of the recording sequence.

Having been designed for an earth-to-Mars mission, the sensor would be exposed to severe solar intensities as the heliocentric range decreased. The highest temperature to which the sensor had been previously exposed was 257°F measured at the flight temperature transducer. Under solar radiation, internal portions of the sensor were hotter. Nominal temperatures for this mission were expected to be 220°F at encounter and 300°F at perihelion. Additional testing disclosed that the limit of the design was approximately 348°F (the melting point of the solder on the high-voltage ring within the sensor itself). Tests showed that this temperature would be reached when the plasma probe sensor temperature transducer read 275°F.

*o. Trapped radiation detector.* The requirement to have one detector of the trapped radiation detector (TRD) experiment observe the soft X-ray intensities from the sun was satisfied by a design change to the instrument. Detector A was mounted so its look direction relative to the sun-line was changed from 135 deg to zero. A hole was cut in the deployable sun shade to permit the 10-deg field-of-view of Detector A to be unobstructed.

***3. Considerations in changing basic Mariner IV design to enhance reliability and/or operational capability.*** Experience with the *Mariner IV* spacecraft system was the basis for a number of system design changes which increased reliability or operational capability of the spacecraft. Such changes were desirable regardless of the type of mission being conducted.

As with any design change, the cost and risk being assumed had to be weighed against the advantages to be gained. A ground rule for evaluating suggested design changes was: satisfactory performance during the *Mariner IV* mission was adequate proof of reliability of the subsystems flown.

All design changes which may have increased reliability of the spacecraft were not approved, although each suggested modification was evaluated on its own merit. Those changes which were approved to increase system reliability and operational capability are presented in subsequent paragraphs.

*a. Ranging.* Shortly before the launch of the *Mariner IV* spacecraft, a receiver self-lock condition was noted. In this circumstance, the spacecraft receiver would lock onto a spurious signal emanating from the power amplifier and then track it. Under this condition the spacecraft receiver would not respond to any uplink signal from the ground transmitter unless its signal strength were extremely high. Self-lock never occurred when the ranging receiver in the transponder was off.

The self-lock could be overpowered by a signal from the ground transmitter in the test configuration. A sufficiently high signal level could not be expected in flight. The consequence of such an anomaly in flight would be the inability to obtain phase-lock between the ground station and the spacecraft, precluding the attaining of two-way doppler data or transmitting commands. Since a direct command would be ineffective in eliminating this problem should it occur in flight, a decision was made never to activate the ranging receiver during the Mars mission.

Since ranging data would enhance the celestial mechanics experiment, the *Mariner* Venus 67 mission required ranging capability. A two-pronged approach was initiated: the radio subsystem to eliminate the self-lock problem, and a mechanized subsystem to effect an automatic turn-off of the ranging receiver should the problem occur in flight even after the radio design modifications were incorporated.

Changes to the *Mariner IV* radio configuration which were to eliminate the ranging problem were (refer to the Telecommunications section for further details):

(1) Add low-pass filter to receiver input

(2) Add low-pass/band-pass (LP/BP) filter between exciters and power amplifiers

(3) Replace 4-port circulator switch between exciters and power amplifiers with a dual 3-post device to allow incorporation of the LP/BP filter

(4) Delete notch filter on cavity amplifier input

(5) Replace a transistor in the mixer preamplifier which was prone to oscillation

In-flight automatic turn-off of the ranging receiver was achieved. The self-lock anomaly was not a necessary condition for turning off the ranging receiver, however. It was turned off at the time of the CC&S cyclic commands which occurred every 66⅔ h. This CC&S function went to the radio subsystem to switch exciters or power amplifiers in the case of failure or excessive degradation. A direct command (DC-V9) was used to activate the ranging receiver whenever desirable. Command lock could be established after each cyclic command if the self-lock condition occurred between cyclics. The strategy to be used in activating the ranging receiver had to be evolved after some flight experience was obtained with the system. This was particularly important in the near encounter phase where command capability for backup of critical events was needed; this same period was the most important to the celestial mechanics experiment. If there was any question about the reliability of the radio operation with the ranging receiver on, the near encounter ranging data to support the celestial mechanics experiment would have had to have been forfeited. The CC&S sequence was designed so the ranging receiver would be commanded "off" 19⅓ h before closest approach. Therefore, a decision to turn-on the ranging receiver could be made on the earth if all looked well.

*b. Battery charger toggle command. Mariner IV* flight experience indicated that it was desirable to be able to turn off the battery charger without having to turn off the cruise science also. Although two commands (DC-V25 and DC-V26) turned off the battery charger, only the latter was a reasonable choice during the cruise phase. The DC-V25 command was primarily an encounter-oriented command. Use of DC-V26 to turn off the battery charger caused the science instruments and the DAS to be turned off also. Recognizing that there was some added risk of failure associated with turning this equipment off and on, there was a reluctance to exercise this command.

For this mission, the turn-off of the battery charger during cruise was recognized as a required and anticipated mission event. A design change was made within the power subsystem which allowed the battery charger to be turned off with DC-V28, the command which was used to turn on the battery charger previously. The change required the addition of command steering logic which caused each successive DC-V28 to change the state of the battery charger. This toggle capability of DC-V28 removed any consideration of potential science failure modes at the time it was judged advisable to turn off the battery charger.

*c. Battery charger telemetry transducer.* One unresolved anomaly of the *Mariner IV* flight was the continuing increase in the battery voltage telemetry output following the turn-off of the battery charger. Subsequent to the turn-off of the charger in flight, a trickle charge, theoretically less than 2 mA, flowed into the battery, supplied by the battery voltage transducer circuitry. No answer was available to the question of the damage, if any, induced into the battery by this continual changing current. Also, there was the possibility that the battery was developing an open cell, resulting in an increase in internal battery resistance and consequently higher battery voltage readings.

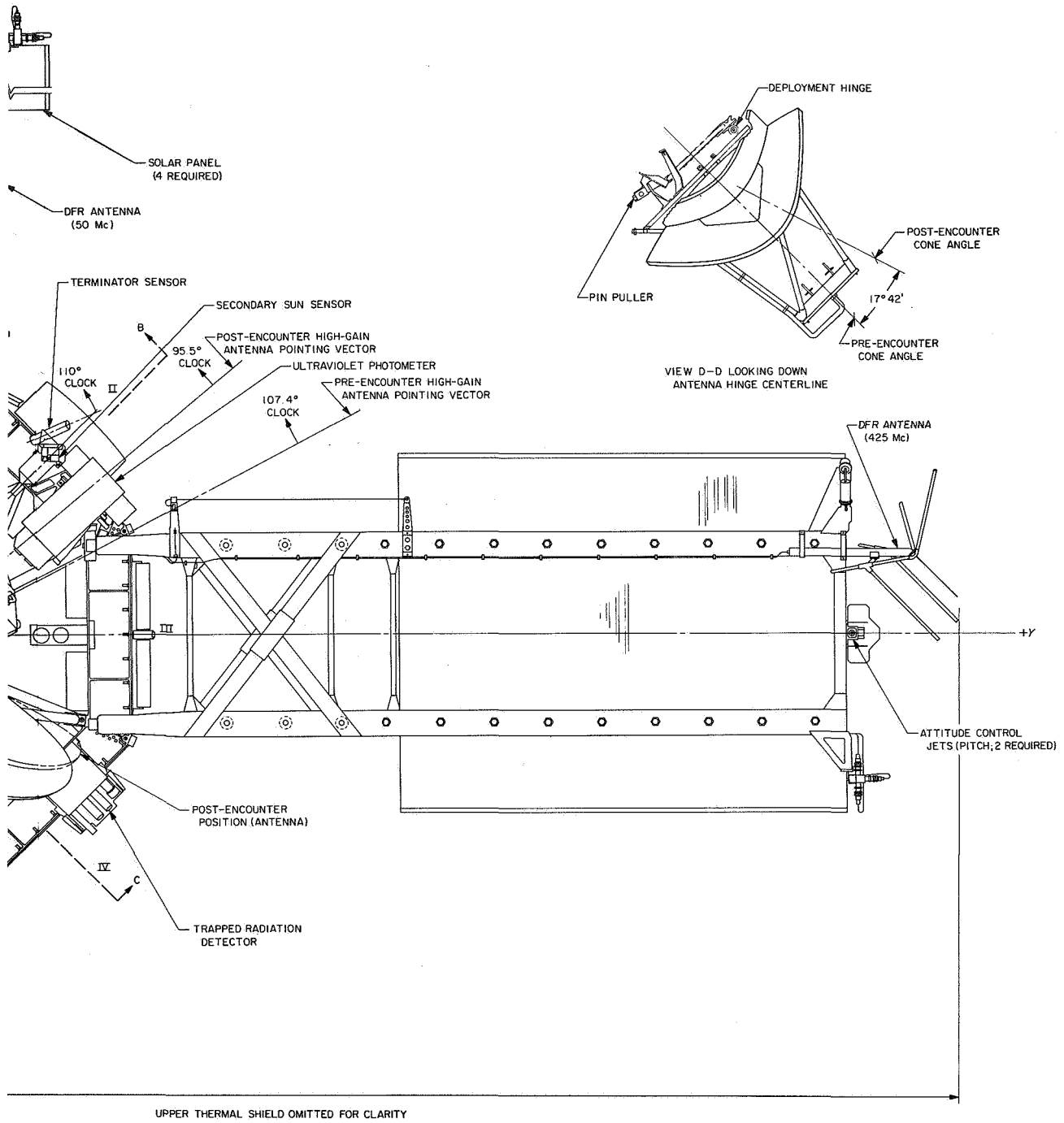
The battery voltage telemetry transducer trickle charge current was eliminated in the design of this spacecraft preventing this potential cause of increasing battery voltage telemetry readings after charger turn-off. An emitter follower isolation stage was employed. A recurrence of such anomalous readings of battery voltage during the *Mariner* Venus 67 mission would certainly be indicative of an anomaly within the battery and its ability to supply power if required.

*d. Earth sensor roll reference backup.* One deficiency of the *Mariner IV* system design was the lack of an adequate means of determining the roll attitude of the spacecraft without the Canopus sensor early in the mission. Should this device experience an anomaly which rendered it useless, the capability to achieve a successful midcourse maneuver would be severely curtailed because of the added pointing errors which would be present.

The roll attitude of the spacecraft in inertial space was known to within 5 mrad when the Canopus sensor was used in determining the orientation. Orientation determined from successive observations of the lobes on the low-gain antenna pattern during rolls is accurate to within several degrees. Use of magnetometer data permitted estimates of roll orientation to within 7 deg. It was determined that the use of an earth sensor with a restricted field of view in clock would give an accuracy of prediction to within 1 deg.

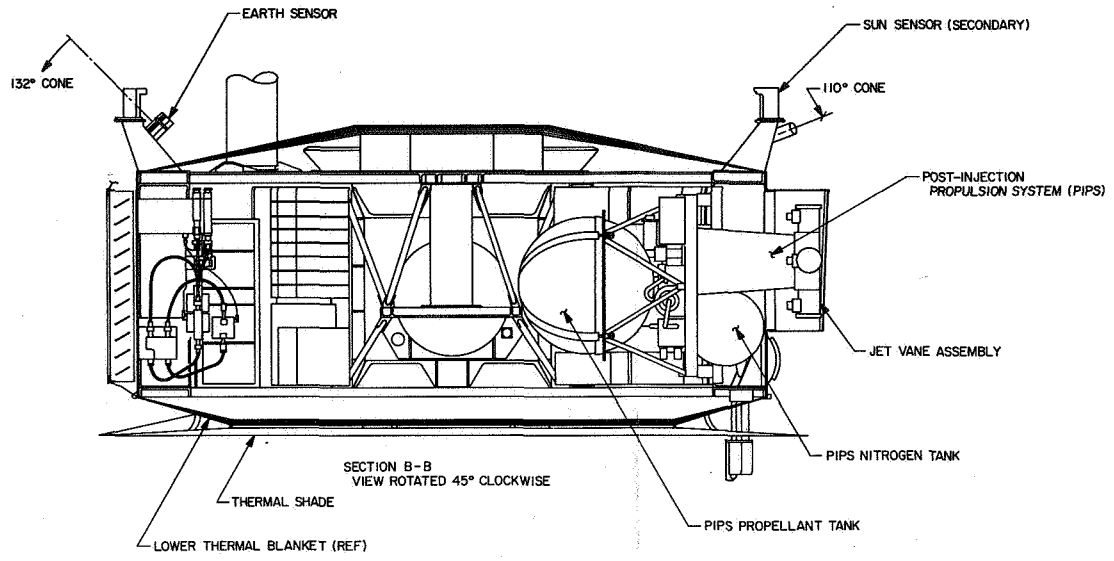
This latter technique required rolling the spacecraft and observing the passage of the earth's limb across the leading and trailing edges of the sensor's field of view. To be effective, the output from the sensor had to be observed as frequently as possible. This necessitated relocating the earth sensor telemetry channel to position 118 (as previously discussed) in the telemetry channel assignment list, replacing the midcourse nitrogen

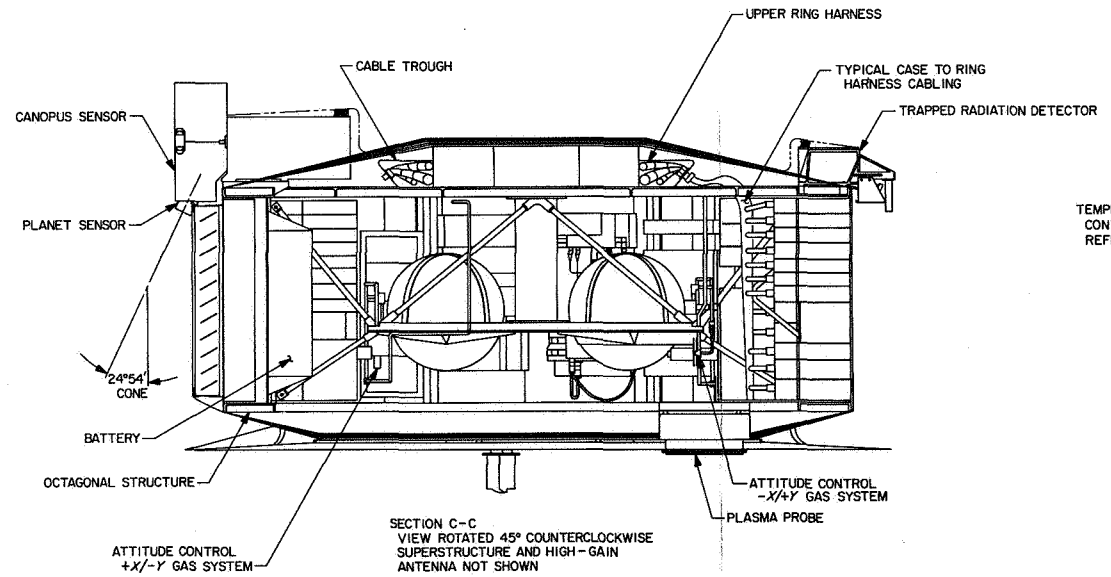
**Page intentionally left blank**

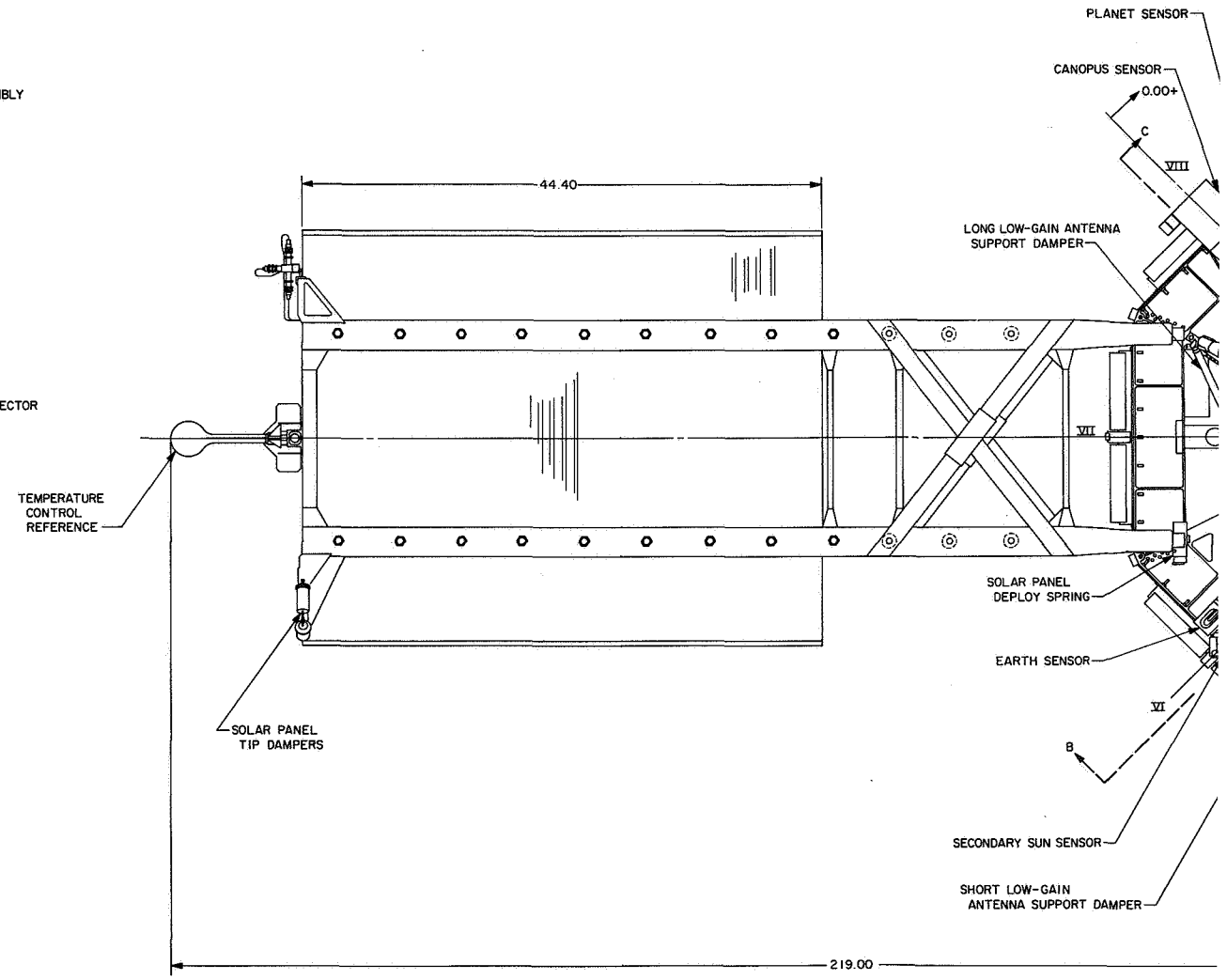



IE CONTROL
LL AND YAW, 2 REQUIRED)

PRECEDING PAGE BLANK NOT FILMED.






FOLDOUT FRAME 1

FOLDOUT FRAME

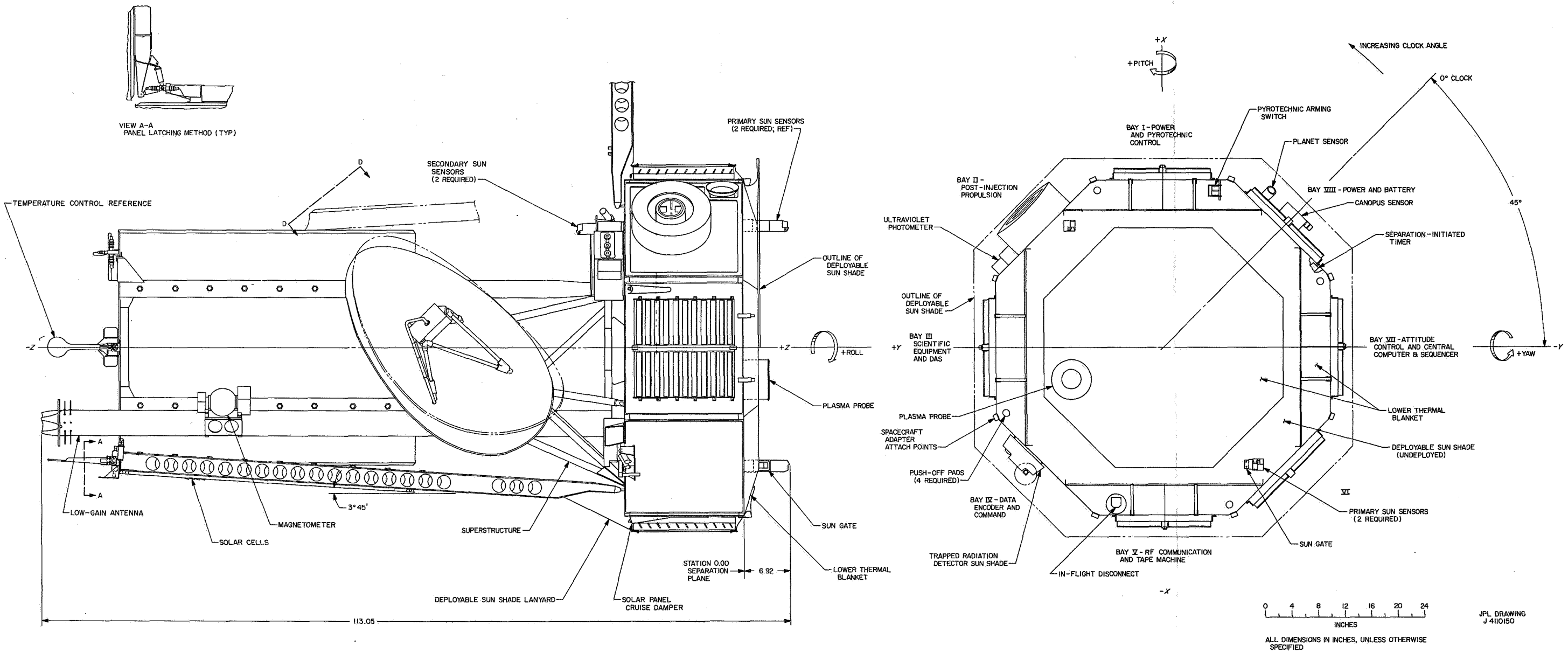



**Fig. IV-1. *Mariner V* spacecraft configuration**



FOLDOUT FRAME 1

FOLDOUT FRAME 2

**Page intentionally left blank**

PRECEDING PAGE BLANK NOT FILMED.

pressure reading which moved to position 228. In the *Mariner IV* design, the earth sensor output was used only as a check on the acquisition of the star Canopus by the Canopus sensor. Its field of view was then quite large by comparison to the field of view in *Mariner V*: 26-deg clock × 86-deg cone, as compared to 3-deg clock × 50-deg cone.

*e. Tape recorder.* A design deficiency noted during the *Mariner IV* spacecraft development could potentially prevent the switching of the two tracks of the tape recorder for recording or playback. Should this condition occur in flight, as it had on the ground, only one-half the anticipated data would be received on the earth. Mechanical hang-up of the relay in a null position was the reason for this potential anomaly. Relay change of state was dependent upon one set of the track change relay contacts being closed. The design did not provide a means of recovery from the relay hang-up condition which had both sets of contacts open.

The *Mariner* Venus 67 design was modified to use a flip-flop to determine the charge on the energy storage capacitors. Having no null state, the flip-flop controlled the charge on the capacitor banks to permit recovery from the relay hang-up condition. The flip-flop utilized was already in the system, being available from circuitry no longer required for the *Mariner V* mission.

As a preventive measure during the *Mariner IV* encounter, the tape-recorder record motor was turned off by direct command immediately following the end of the record sequence. This action was to protect against a failure which might cause the record sequence not to terminate automatically. The means by which this was accomplished also resulted in the undesirable turn-off of the science instruments.

Because the tape recorder did not use a 400-Hz single-phase power supply, the use of DC-V26 could not accomplish this same result. The logic of the tape recorder was modified so a DC-V4, an initiate playback command, also caused the record sequence to be terminated. This command could be used as a backup to an automatic termination on the spacecraft without requiring that the science loads be turned off. With the reduced record speed and the shortened round-trip transmission time, the use of this capability as part of the standard encounter sequence was doubtful; however, its presence as a backup was desirable.

*4. Mechanical configuration.* The mechanical configuration of the *Mariner V* spacecraft retained as much of the *Mariner IV* hardware elements as possible while still reliably satisfying the *Mariner* Venus 67 mission requirements. The basic spacecraft configuration (Fig. IV-1) is the same as *Mariner IV*. The changes are discussed below.

*a. Antennas.* To satisfy earth-pointing requirements, the omnidirectional and high-gain antennas were required to be oriented in the anti-sun direction. In addition, the size of these antennas dictated that the under-shroud orientation could not differ greatly from *Mariner IV* without imposing serious design changes to the spacecraft and launch vehicle. These restrictions, plus the desirability of not articulating the antennas, made it necessary to locate physically the antennas as before by orienting the *Mariner V* spacecraft in-flight attitude "upside down" as compared to *Mariner IV*. Sun-oriented equipment such as sun sensors, certain science experiments, and solar panels were then re-oriented as required.

The high-gain antenna support structure was redesigned to provide proper pointing direction and mechanization to step-change the pointing direction of this antenna for improved coverage during occultation and after Venus encounter.

*b. Solar panels.* Reversed sun-line attitude of the spacecraft required the solar panels to be mounted on the same hinges with the celled surfaces reversed on the supporting spars. Maintaining the original panel length and locating the celled area away from the bus allowed for the use of the remaining *Mariner IV* attitude-control gas systems and much of the existing panel structure tooling and fixtures, and served to provide needed thermal decoupling of the panels from the faces of the electronic bays. Temperature-control references were mounted on the gas jet manifolds in Bays I, V, and VII, and attached at the interface previously occupied by the *Mariner IV* solar vanes. Panel deployment springs and cruise dampers were unchanged. The boost latching and dampers were replaced with orthogonal pairs of dampers that tied the panels together at the tips. Four pinpullers, instead of the eight used in *Mariner* Mars 1964, were used to release the panels.

*c. Attitude control sensors.* The reversed sun attitude required that primary and secondary sun sensors be interchanged. Secondary sensors were mounted on the existing primary sensor pedestals, and the primary sensors were mounted on pedestals of sufficient height above the sun-side thermal shield to obtain an unobstructed view.

To provide an improved field of view, the Canopus tracker was also relocated from the bottom ring of Bay VIII to a centerline location on the top ring of the same bay.

A modified *Mariner IV* earth sensor and planet terminator sensor were adapted with suitable bracketry to mount on the Bay VI and Bay II secondary sun sensor pedestals, respectively. In addition, a new planet sensor was located on the upper ring in Bay VIII.

*d. Octagon electronics compartment. Mariner V* used the same general equipment arrangement within the octagon as *Mariner IV*. The attitude control gas bottles are the same as for *Mariner IV*. The post-injection propulsion system was in Bay II. The cabling and electronics arrangement in the other seven bays (Fig. IV-2) is the same as *Mariner IV* except in Bay III, the scientific equipment bay. The change in the science payload and the new data automation subsystem required that a new layout be used.

*e. Science instrument sensors and antennas.* The scientific instrument sensors are mounted on the spacecraft to satisfy their look-direction requirements. The magnetometer is mounted on the low-gain antenna, identical to *Mariner IV*. The trapped radiation detector is mounted at the same location as for *Mariner IV* with the instrument itself reversed to provide the same orientation as before. The UV photometer is rigidly mounted on the top ring over Bay II at a cone angle of 90 deg to allow a field of view compatible with the planet encounter geometry.

The DFR antennas consist of two 50-Mc antennas mounted to the Bay I and III solar panel spars and a 423-Mc array mounted at the outboard end of the Bay III panel. Orientation and phasing is such as to provide peak gain in the direction of earth at encounter. The plasma probe relocation involved mounting it on an auxiliary support structure inboard of the lower ring on the sun side of the spacecraft.

*f. Temperature control hardware.* Shield philosophy and temperature control louver hardware remained unchanged from *Mariner IV* with the exception of the sun-side thermal blanket. Concern over heat leaks at Venus intensities has dictated a shield design with a minimum of penetrations for sun-side mounted equipment. The mechanization selected to satisfy these thermal requirements consisted of a deployable shade erected following launch-vehicle separation. All hardware interfacing with the launch vehicle adapter is shielded from the solar input by this shade.

***5. Project design control.*** At the onset of the *Mariner* Venus 67 project, the design of the *Mariner IV* spacecraft and OSE were considered to be frozen. That is to say, the designs were under engineering change requirement (ECR) control; all design changes required authorization by an ECR. In regard to new hardware, the interfaces were frozen in all respects, but internal details became subject to ECR control upon delivery to the spacecraft assembly facility (SAF). Hardware deleted from the *Mariner IV* design was also handled by ECR in order to authorize the requisite changes to drawing lists, specifications, etc.

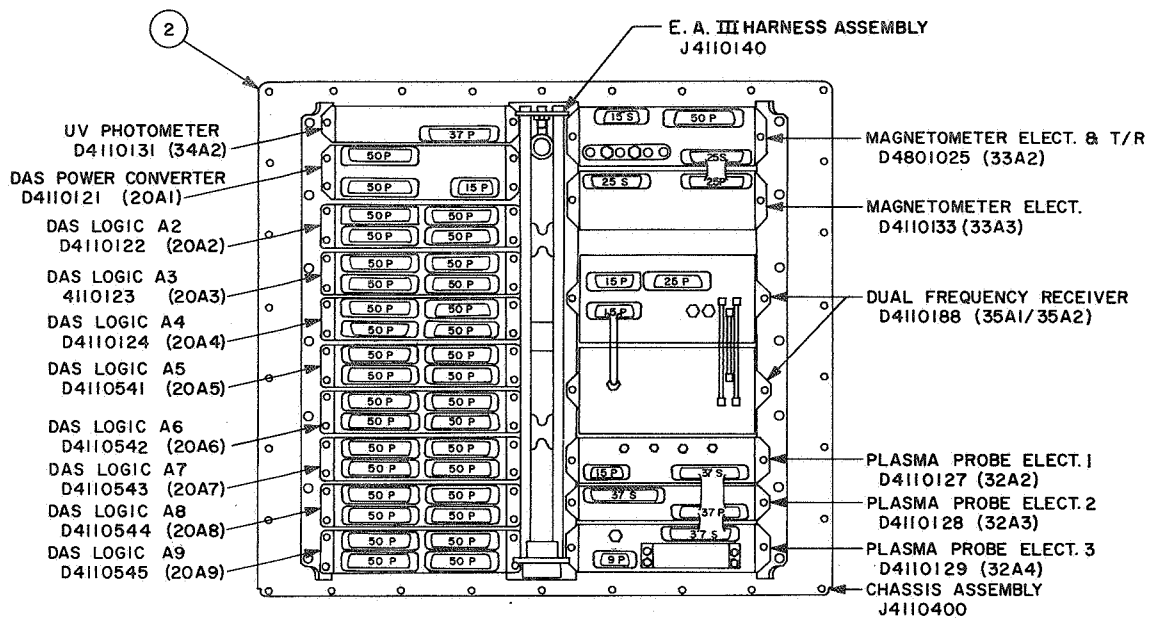
The number of approved ECR's was 789, of which 359 were solely authorized changes to documentation. A summary of the *Mariner* Venus 67 ECR's by subsystem is shown in Table IV-2. The area codes are: 0 = Spacecraft; 1 = OSE; 2 = LCE. Standard subsystem reference designators are used in the second column. Note that OSE-to-OSE interfaces are included in the system (00) category of the spacecraft area (0).

A time rate of ECR generation by the three areas is shown in Figs. IV-3, 4, 5, 6: summary, spacecraft, OSE, and LCE. These graphs also show the breakdown by the two categories of changes: (1) hardware changes, plus changes to associated documentation, and (2) documentation changes only, which do not affect hardware.

***6. Telemetry calibration.*** Successful analysis of spacecraft performance during pre-launch spacecraft testing and during flight depends upon the correct conversion of digital data numbers (DN) to engineering units. This is achieved through the use of telemetry calibration curves; these are generated at the time of hardware delivery to SAF and are updated as required.

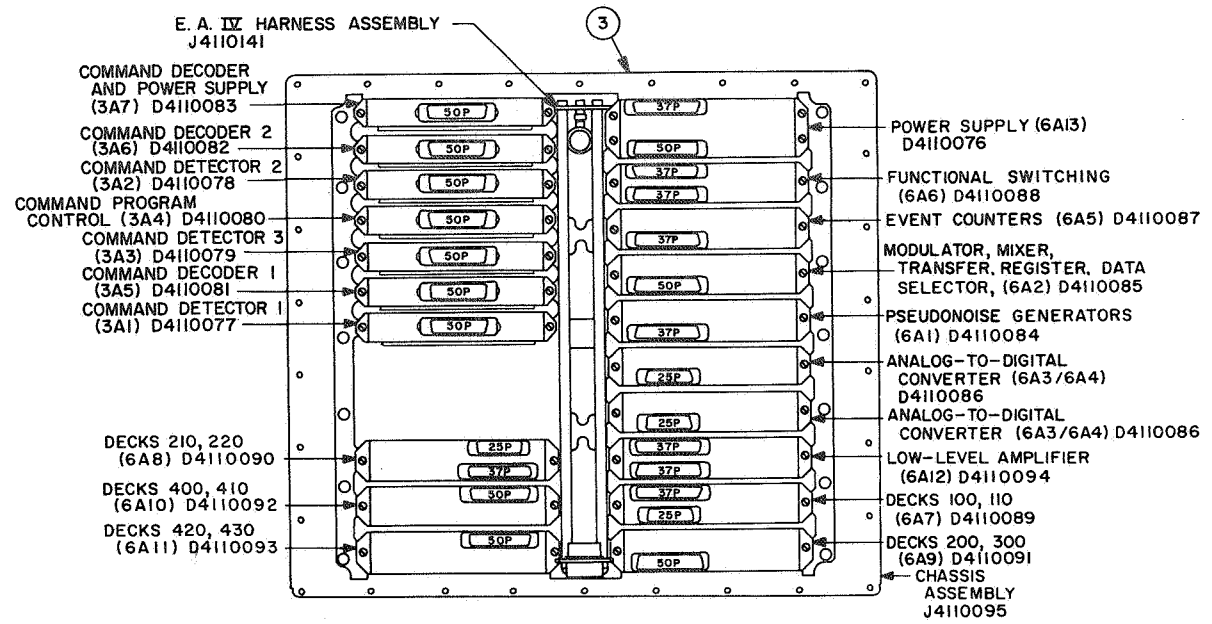
A calibration curve for a particular telemetry channel will change whenever a piece of hardware generating the telemetry analog voltage is replaced on the spacecraft, or if the data encoder is replaced. A program of matching individual equipment characteristics to provide the required calibration curves was effected.

The data encoder subsystem receives all analog engineering data from the various spacecraft equipment in one of three voltage ranges: 0 to 100 mV; $\pm 1.5$ V, or 0 to 3 V. These data are then digitized into seven-bit binary words through an analog-to-digital converter. The digitized data are transmitted to the earth for analysis.



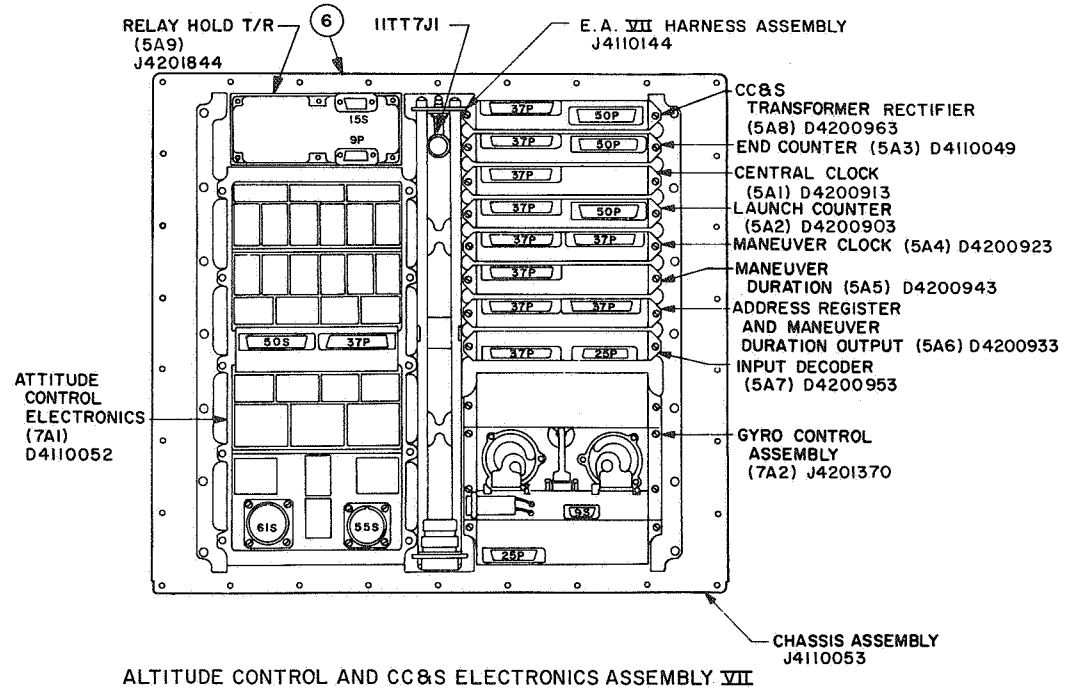

SCIENTIFIC EQUIPMENT ELECTRONICS ASSEMBLY III

REF. J4110120



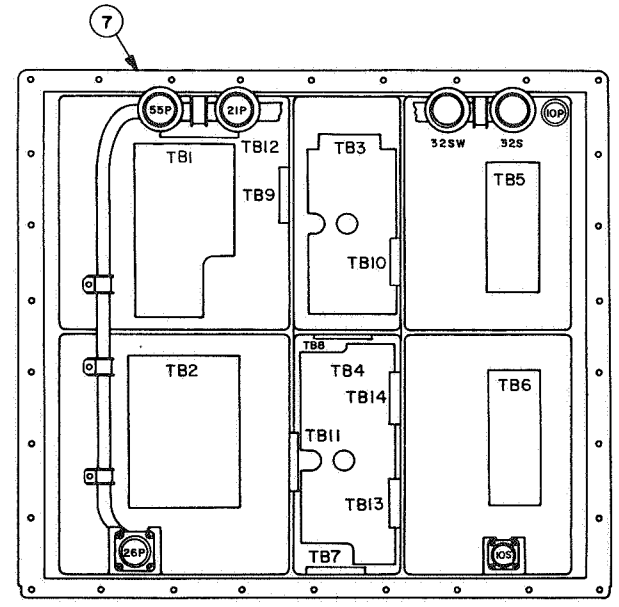

DATA ENCODER AND COMMAND ELECTRONICS ASSEMBLY IV

REF. J4110075




ALTITUDE CONTROL AND CC&S ELECTRONICS ASSEMBLY VII

REF. J4110041




POWER REGULATOR ASSEMBLY ELECTRONICS ASSEMBLY VIII

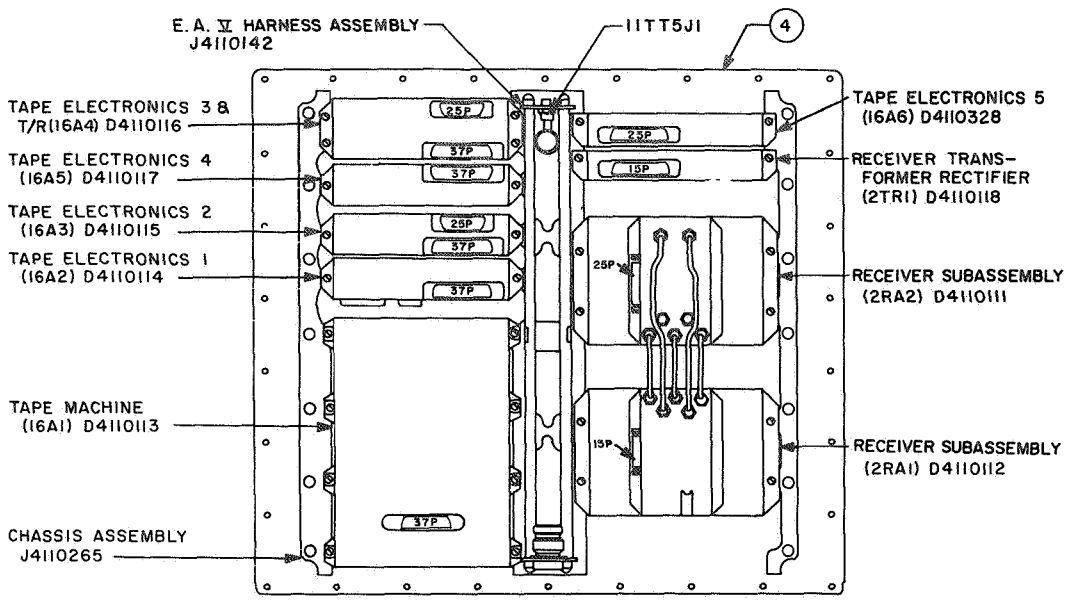
REF. J4120172



FOLDOUT FRAME

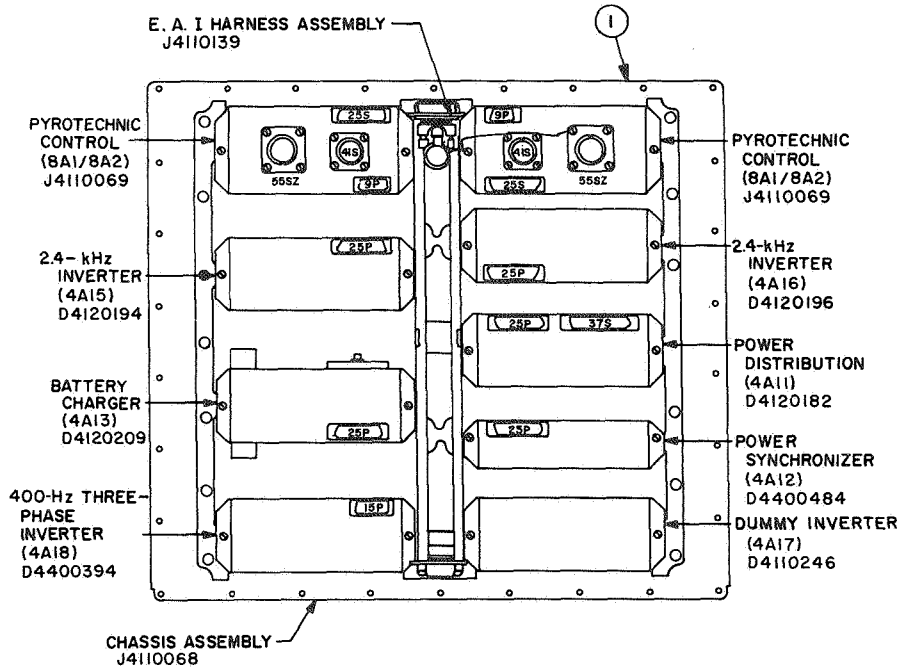
FOLDOUT FRAME

FOLDOUT FRAME 2




RECEIVER AND TAPE MACHINE ELECTRONICS ASSEMBLY V

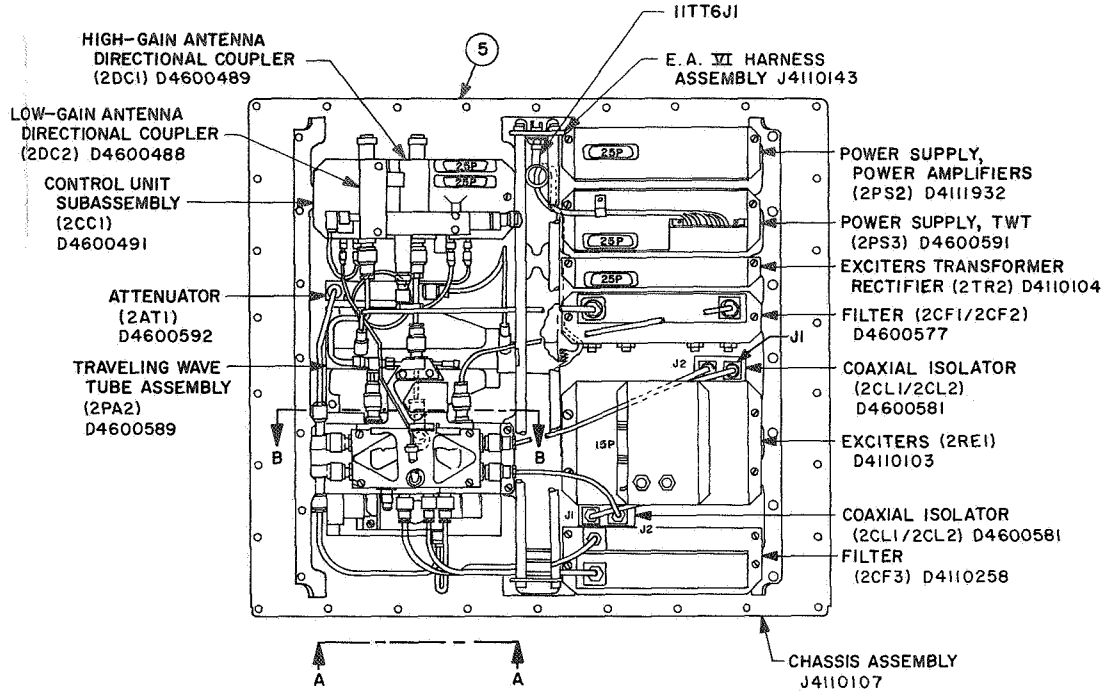
REF. J4110110




POWER SUBSYSTEM ELECTRONICS ASSEMBLY I

REF. J4110062

FOLDOUT FRAME 3




RF COMMUNICATIONS ELECTRONICS ASSEMBLY VI

REF. J4110100

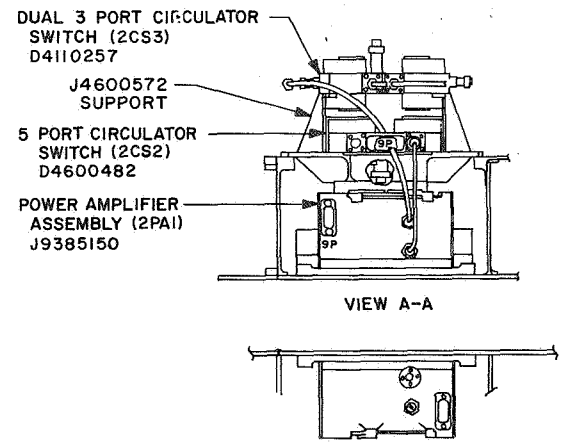



Fig. IV-2. *Mariner V* cabling and electronic packaging



FOLDOUT FRAME 4

**Page intentionally left blank**

PRECEDING PAGE BLANK NOT FILMED.

Table IV-2. Engineering change requirement (ECR) summary

| Area | Subsystem | Total approved |
|---|---|---|
| 0 | 00 | 146 |
| 0 | 01 | 62 |
| 0 | 02 | 43 |
| 0 | 03 | 10 |
| 0 | 04 | 31 |
| 0 | 05 | 4 |
| 0 | 06 | 17 |
| 0 | 07 | 39 |
| 0 | 08 | 11 |
| 0 | 09 | 53 |
| 0 | 10 | 15 |
| 0 | 11 | 22 |
| 0 | 12 | 17 |
| 0 | 15 | 1 |
| 0 | 16 | 27 |
| 0 | 20 | 23 |
| 0 | 21 | 1 |
| 0 | 24 | 3 |
| 0 | 25 | 9 |
| 0 | 26 | 3 |
| 0 | 31 | 4 |
| 0 | 32 | 15 |
| 0 | 33 | 8 |
| 0 | 34 | 13 |
| 0 | 35 | 9 |
| 0 | 36 | 3 |
| Sub-total | | 589 |

| Area | Subsystem | Total approved |
|---|---|---|
| 1 | 01 | 3 |
| 1 | 02 | 10 |
| 1 | 03 | 20 |
| 1 | 04 | 22 |
| 1 | 05 | 6 |
| 1 | 06 | 7 |
| 1 | 07 | 14 |
| 1 | 08 | 4 |
| 1 | 09 | 29 |
| 1 | 16 | 3 |
| 1 | 20 | 9 |
| 1 | 90 | 2 |
| 1 | 94 | 1 |
| 1 | 96 | 2 |
| 1 | 97 | 10 |
| 1 | 98 | 2 |
| 1 | 99 | 17 |
| Sub-total | | 161 |
| 2 | 02 | 5 |
| 2 | 04 | 13 |
| 2 | 05 | 1 |
| 2 | 06 | 3 |
| 2 | 09 | 13 |
| 2 | 17 | 3 |
| 2 | 20 | 1 |
| Sub-total | | 39 |
| Grand total | | 789 |

The engineering data format contains 86 analog measurements, each requiring a calibration curve which combines the data encoder and measurement characteristics. Each analog channel in the data encoder is calibrated from 0 to 126 data numbers (DN) vs analog voltage input. Engineering subsystem measurements of analog voltage output vs source input in engineering units are made.

*7. Spacecraft weight control.* A weight-control program was initiated to provide all rigid-body mass parameters and consistent weight data from one official source. A weight goal of 550 lbs was established which included a 10-lb contingency allowance to cover expected discrepancies between the sum of the weights of the individual spacecraft subassemblies and the total weight of the assembled spacecraft. The weight control function included:

(1) Derivation, both computationally and experimentally, of rigid-body mass parameters characterized by weight, c.g., moments of inertia and products of inertia.

(2) Acquisition and compilation of data required for weight distributions in accordance with stipulated requirements for structural and dynamic analyses.

(3) Maintenance of records of current weight status reflecting improved knowledge of design and development progress.

(4) Preparation of periodic weight status reports.

(5) Acquisition of actual weights, centers-of-gravity, centroidal moments of inertia and centroidal products of inertia for system components or subsystems.

(6) Generation and maintenance of records of actual weight data paralleling those for calculated or estimated weight data.

(7) Analysis of weight status and presentation of relevant design recommendations.

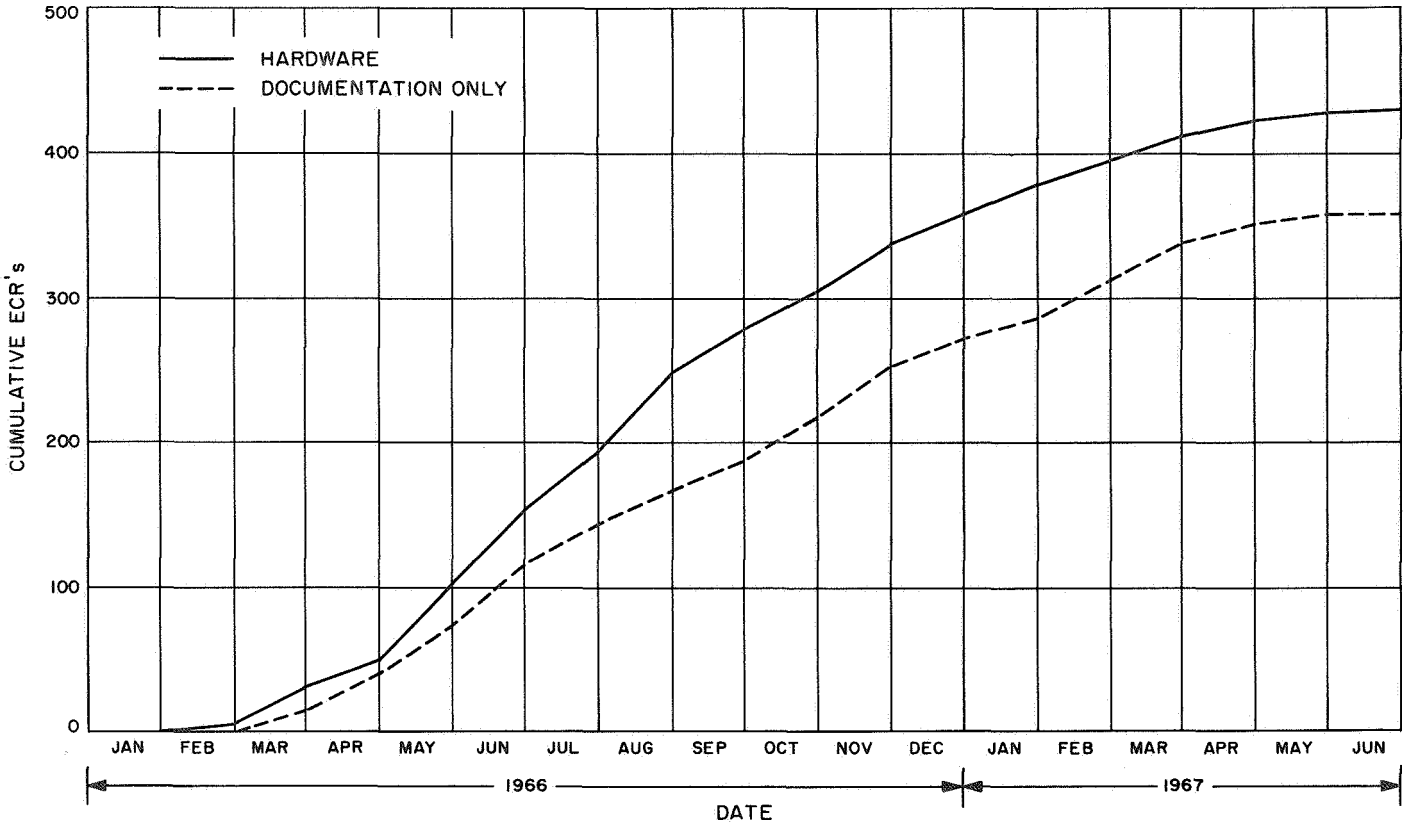



**Fig. IV-3. Cumulative engineering change requirements (ECR) vs date summary**

Accumulation of data relative to spacecraft weight, c.g., moments of inertia, and products of inertia, began concurrently with the preliminary design. The best estimates of configuration and weight were obtained, based upon *Mariner IV* actual weights, and modified for consistency with the design goal. The modified weight estimates were reviewed to ensure the inclusion of weight for mounting hardware, wiring, and related structures.

Actual weights of *Mariner V* hardware were initially obtained by re-weighing *Mariner IV* components certified for *Mariner V* flight. As component designs solidified, calculated weights were used to replace corresponding estimated weights. This process of iteration continued throughout the program with calculated values replacing estimated values and actual weights replacing calculated weights. Prototypes were weighed, and any discrepancies between the prototype actual weight and the corresponding estimated or calculated weight were investigated and resolved. As the flight hardware was completed, the actual weights were obtained, and any discrepancies encountered were reconciled. A careful account of attachment hardware weight utilization was maintained to prevent double-entry errors from occurring. Spacecraft assemblies were weighed and c.g.'s were experimentally determined. Each spacecraft was re-weighed at Cape Kennedy just prior to launch.

Computer programs provided weight reports in several formats, using sequencing codes for subsystem, assembly, and effectivity. Tab cards were used to input the program with updating data. Magnetic tape was used for data storage. The weights for each spacecraft were carried in the computer program as separate entities, and actual weight variations between serial-numbered components assigned to specific spacecraft were reflected in the current weight report.

Another computer program using magnetic tape data storage and tab card data updating provided moments of inertia, c.g.'s, inertia tensor, and inverse J-matrix data as a function of current weight changes.

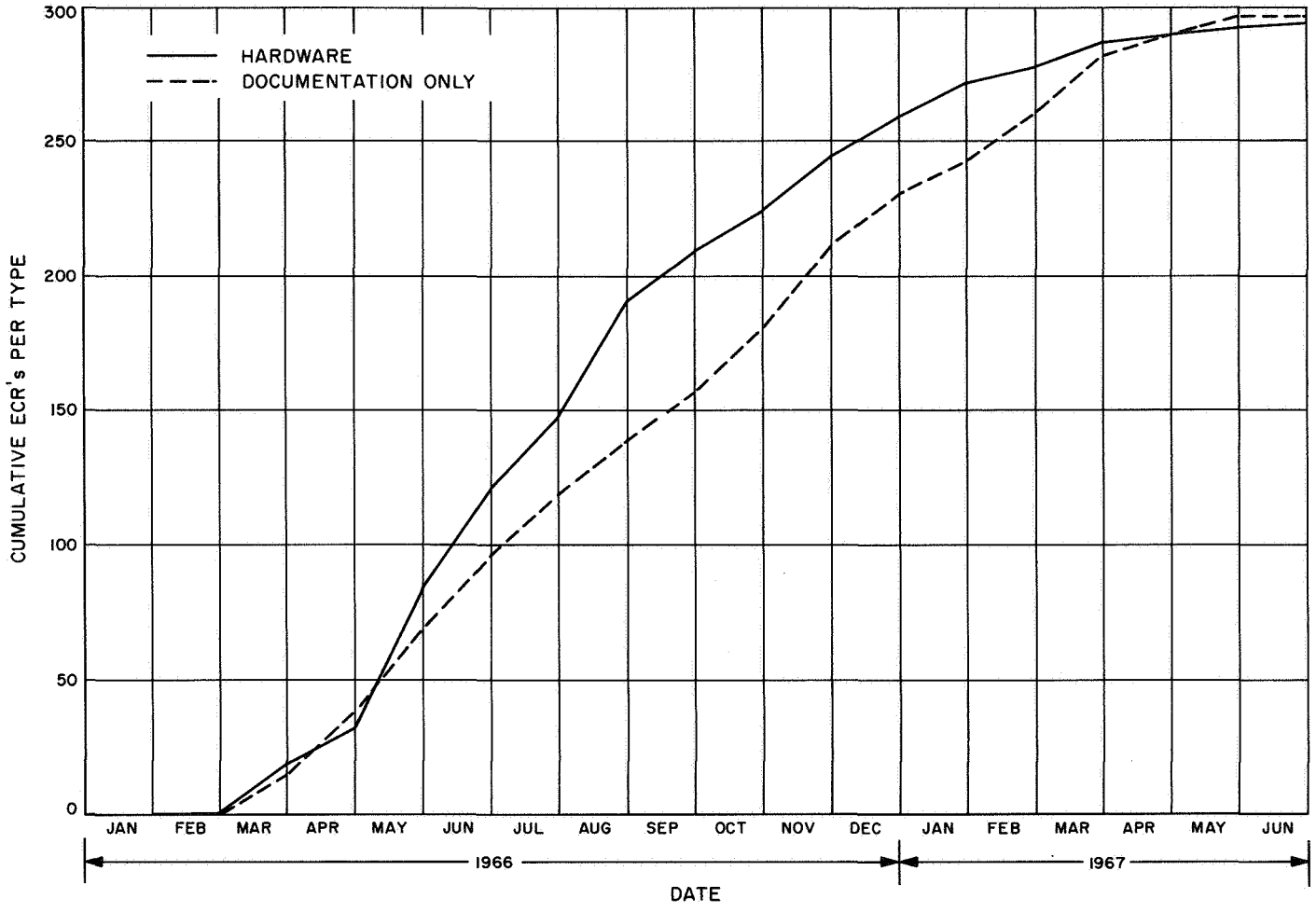



**Fig. IV-4. Cumulative spacecraft engineering change requirements (ECR) vs date**

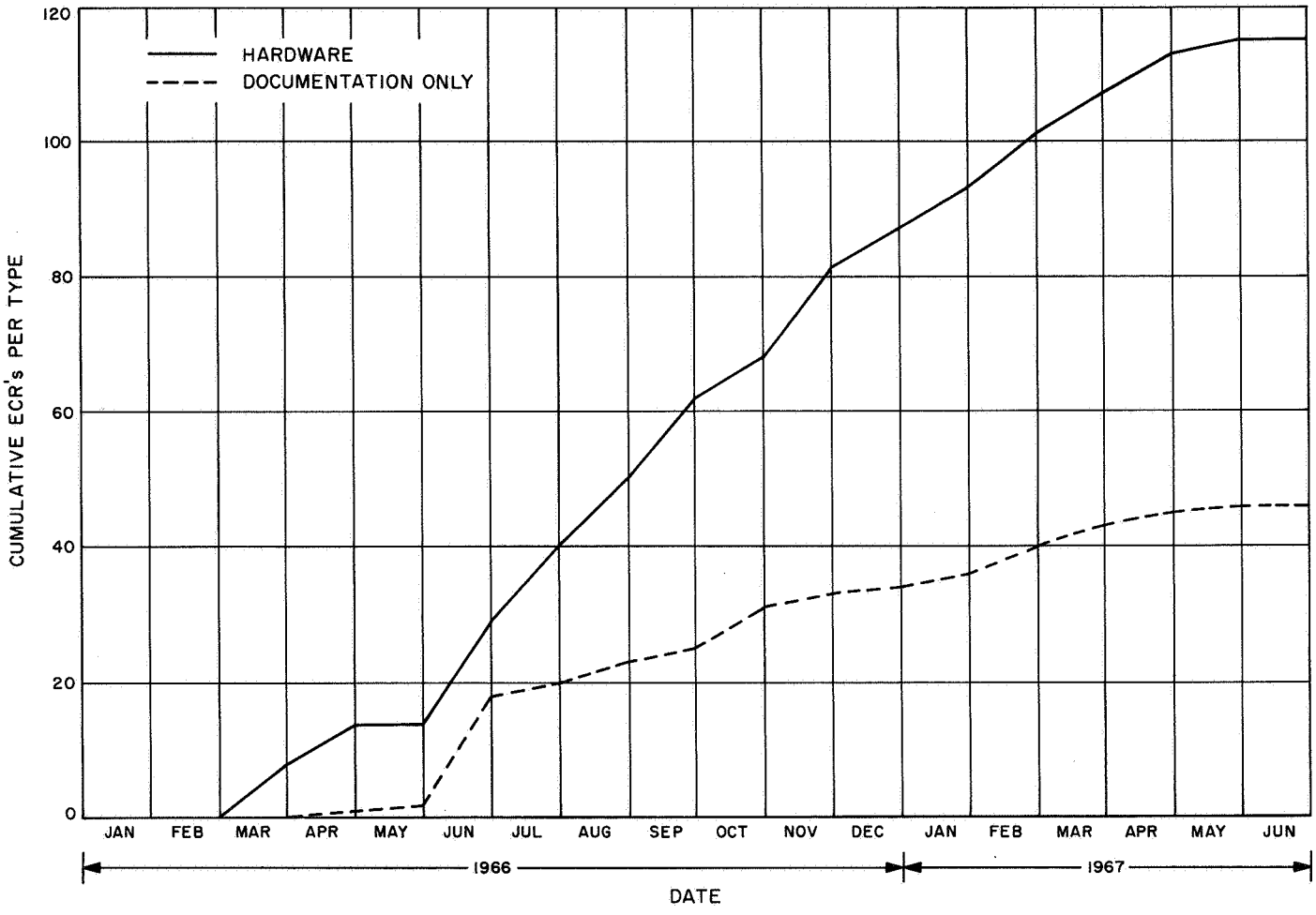



**Fig. IV-5. Cumulative operations support equipment (OSE) ECR's vs date**

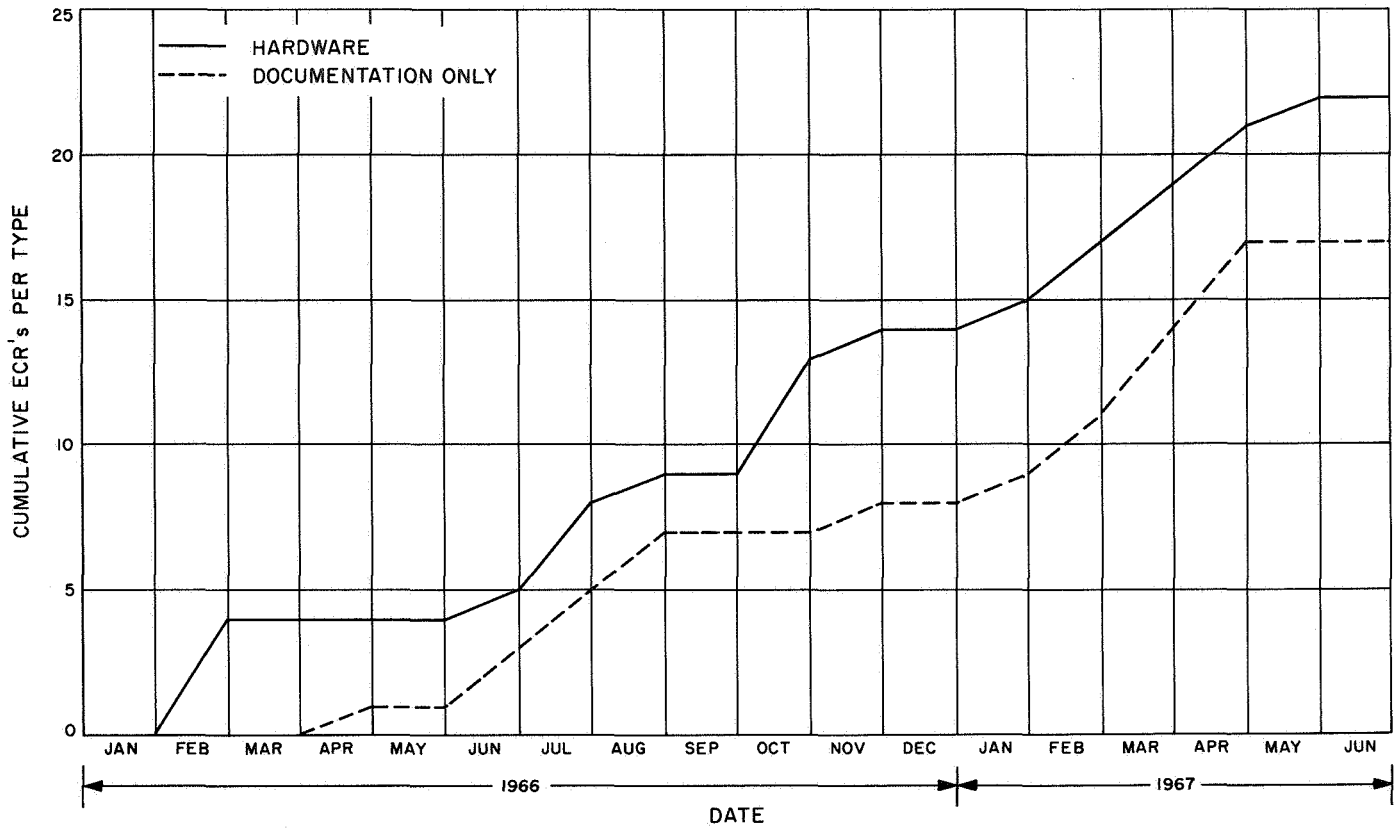



**Fig. IV-6. Cumulative launch complex equipment (LCE) ECR's vs date**

The input to this program consisted of component current weight, centroidal coordinates $\bar{x}$, $\bar{y}$, and $\bar{z}$, local moments of inertia, and local products of inertia for each component. Each component was identified by reference designator, drawing number, title, and an effectivity code. The coordinates were obtained by analysis of existing drawings; the local moments and products of inertia of each component about centroidal axes were computed manually, using existing drawings.

Periodic reports presented the current weight, c.g., moments of inertia, products of inertia, inertia tensor; and inverse J-matrix for each of three phases of the trajectory, namely: launch, before midcourse correction maneuver, and after midcourse correction maneuver. The variation of spacecraft total weight as a function of time is shown in Fig. IV-7.

The flight-support spacecraft (M67-1) was weighed at JPL. The final measured values are shown in Table IV-3. The calculated weight proved to total 1.25 lbs less than the measured value of 539.89. The calculated weight was therefore adjusted to agree with the measured value in order to produce the most realistic values of calculated moments and products of inertia, since no actual measured values of moments and products of inertia were obtained.

The flight spacecraft (M67-2) was weighed at JPL. The final calculated weight of 540.31 lbs was reduced by 1.14 lbs to agree with the measured value as explained in the previous paragraph. The spacecraft was again weighed at the Cape just prior to launch. In the interval between weighings, several modules had been replaced with similar modules which weighed somewhat more. This exchange resulted in an increase in spacecraft weight of +0.57 lbs for a total of 539.74 lbs. The calculated weight was not re-adjusted to account for this small increase. The final calculated and measured values are shown in Table IV-3. A subsystem breakdown of the final calculated weight for the M67-2 spacecraft is presented in Table IV-4.

*8. Redundancy techniques for increasing probability of success at system level.* Several methods of redundancy were employed in the design of the *Mariner V* spacecraft.

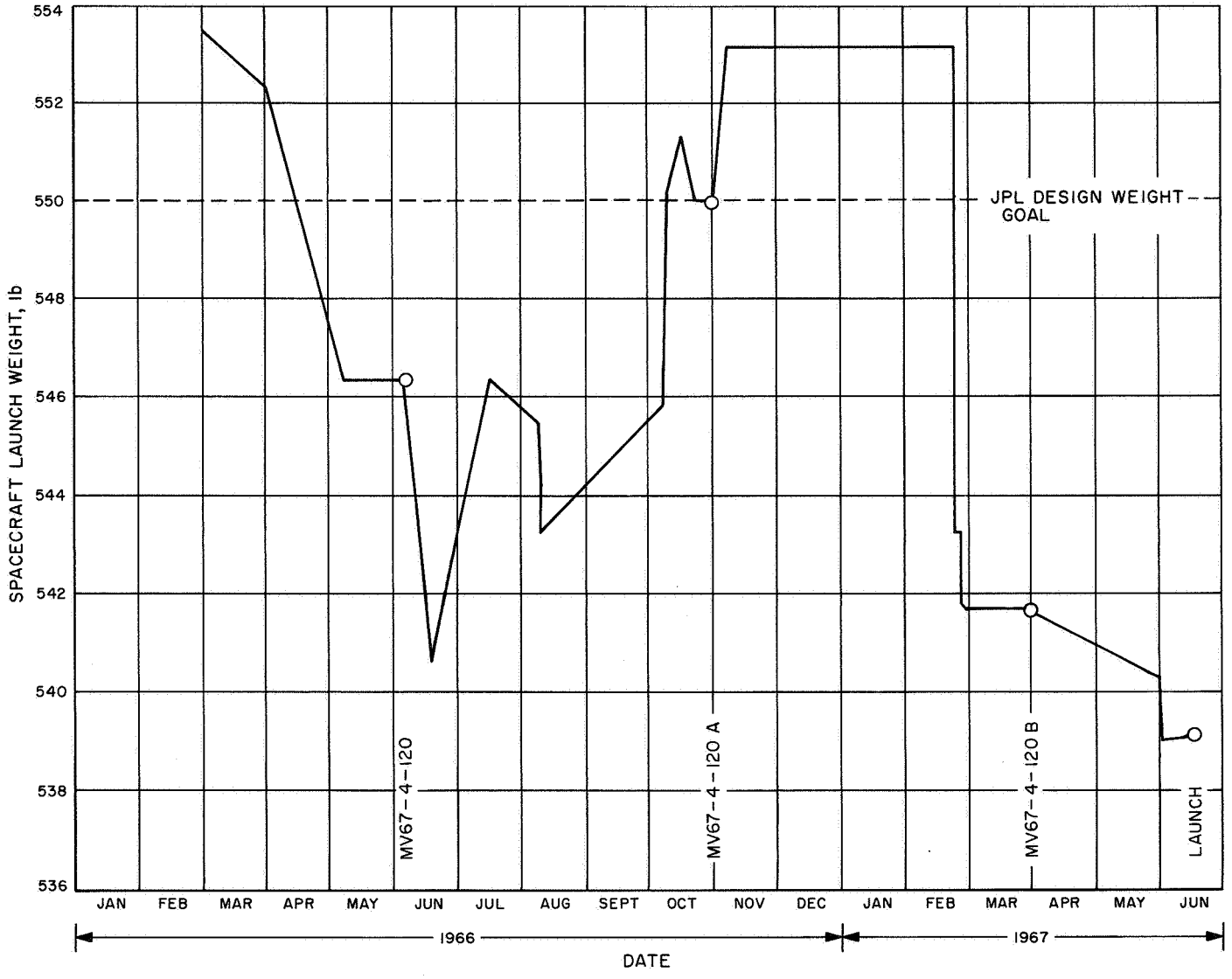



**Fig. IV-7. Weight history (M67-2)**

**Table IV-3. Final calculated and measured spacecraft weight**

| Parameter (before midcourse correction) | Spacecraft | | | | | |
|---|---|---|---|---|---|---|
| | M67-1 (flight support) | | | M67-2 (flight) | | |
| | Calculated | Measured | Δ | Calculated | Measured | Δ |
| Weight (lbs) | 539.89 | 539.89 | 0 | 539.17 | 539.74 | +0.57 |
| $\bar{x}$ (in.) | 0.78 | 0.778 | −0.002 | 0.77 | 0.777 | +0.007 |
| $\bar{y}$ (in.) | 0.31 | 0.305 | −0.005 | 0.29 | 0.329 | +0.039 |
| $\bar{z}$ (in.) | − 12.18 | − 12.180 | 0 | − 12.14 | − 12.133 | −0.007 |
| $I_x$ (slug ft$^2$) | 75.720 | — | — | 73.604 | — | — |
| $I_y$ (slug ft$^2$) | 74.250 | — | — | 71.083 | — | — |
| $I_z$ (slug ft$^2$) | 128.643 | — | — | 124.485 | — | — |
| $I_{xy}$ (slug ft$^2$) | − 1.949 | — | — | − 3.236 | — | — |
| $I_{yz}$ (slug ft$^2$) | 0.405 | — | — | 0.957 | — | — |
| $I_{xz}$ (slug ft$^2$) | 0.275 | — | — | 1.028 | — | — |

Most of the redundancy was present in the *Mariner IV* design (Ref. 1). Those new elements of redundancy are indicated in Tables IV-5, 6 by an asterisk. Definitions of the redundancy techniques used in the tables are required:

*Block:* Paralleling two identical units to achieve the desired function. This technique protects against a loss of function as a result of component or piece part failure. It is not effective if the failure is causal, such as a design failure or an overstress of all components due to an external environment.

**Table IV-4. Final calculated M67-2 weights by subsystem**

| Subsystem | Weight, lbs | |
|---|---|---|
| Structure | | 68.34 |
| Radio: | | 47.51 |
| Electronics | 39.18 | |
| Antennas | 8.33 | |
| Command | | 10.37 |
| Power: | | 130.88 |
| Electronics | 69.77 | |
| Solar panels | 61.11 | |
| CC&S | | 12.23 |
| Data encoder | | 23.40 |
| Attitude control | | 56.98 |
| Pyrotechnics | | 8.53 |
| Wiring | | 43.63 |
| Propulsion | | 45.87 |
| Thermal control | | 17.25 |
| Mechanical devices | | 5.46 |
| Tape recorder | | 19.35 |
| Science: | | 49.37 |
| DFR antennas | 0.94 | |
| Data automation | 14.60 | |
| Trapped radiation detector | 2.63 | |
| Ion chamber* | 0.24 | |
| Plasma probe | 6.88 | |
| Magnetometer | 8.04 | |
| UV photometer | 9.21 | |
| Dual-frequency receiver | 6.83 | |
| Total | | 539.17 |

*This is the weight of a bracket on the low-gain antenna mast which could not be removed in converting the *Mariner* Mars 1964 design.

**Table IV-5. Redundant equipment back-up sources for desired functions**

| Redundant equipment | Type of redundancy employed | Discussion |
|---|---|---|
| RF exciters | Block | Two identical exciters switchable either by internal logic or by ground command. Only one operates at any time. |
| Pyrotechnic control assemblies | Block | Two identical half systems both on line continuously after separation. |
| Midcourse propulsion valves | Block | Duplicate pyrotechnic actuated valves provide the capability for two midcourse maneuvers. |
| Power booster regulators | Block | Failure sensing circuit detects over/under voltage condition at main booster output. Switches maneuver booster on and main booster off. |
| Science power relays | Block | Three relays can supply power to the science loads. One operated at separation or DC-V2; one operated at DC-V2 or MT-7; one operated at DC-V25, overriding science inhibit logic. |
| Analog-to-digital converter and pseudonoise code generator | Block | Two identical units switchable by ground command. Only one operating at any time. |

## Table IV-5 (contd)

| Redundant equipment | Type of redundancy employed | Discussion |
|---|---|---|
| Attitude control gas system | Block | Two half systems and pressure vessels. Both operate continuously after attitude control turn-on. |
| DAS encounter clocks* | Block | Two clocks count in parallel to achieve recording sequence control. Clocks A and B initiated by DC-V16 and planet sensor, respectively. |
| DAS oscillators* | Block | Two crystal oscillators are on continuously. Failure of prime oscillator causes backup to be gated into countdown circuit to obtain required internal frequencies. |
| RF power amplifiers | Functional | Cavity and TWT power amplifiers plus associated power supplies switchable either by internal logic or by ground command: Only one operates at any time. |
| Pyrotechnic arming devices | Functional | Two separation-activated switches: pyrotechnic arming switch, and separation-initiated timer. Either one can power both pyrotechnic half systems. |
| Power frequency sources | Functional | Primary control is a 38.4-kc synchronization signal from the CC&S. In the absence of this signal, synchronization is derived from an oscillator internal to power, or the inverters will free-run at approximately 2.4 kc. |
| Roll attitude sensors* | Functional/ alternate mode | A Canopus sensor and an earth sensor are used. The latter is useful only during the first three weeks of the mission. Accuracy of roll attitude determination is somewhat reduced. |
| Roll orientation controls | Alternate mode | Normally initiated at L-3 or DC-V13. Canopus sensor on with brightness gate in effect. This mode may be restored after use of an alternate by DC-V19.<br>DC-V15. Canopus sensor on; brightness gate removed from circuit. Canopus sensor will track any detectable light source. Gyros disabled.<br>DC-V18. Inertial roll control. Canopus sensor off, gyros on. Pitch and yaw gyros in rate mode; sun sensors unaffected.<br>DC-V20. No roll control. Canopus sensor off; gyros off. |

*New elements of redundancy.

## Table IV-6. Command functions initiated by redundant signals

| Command function | Redundancy type | Redundant command signals |
|---|---|---|
| RF power up | Alternate mode | Removal of separation connector releases holding circuit.<br>Turn-off of gyros releases holding circuit. Power up/down will cycle with gyros. |
| TRS launch mode OFF | Alternate mode | Removal of separation connector activates count one end of tape and stop logic.<br>Gyro turn-off removes tape drive power. |
| CC&S relay hold OFF | Alternate mode | Removal of separation connector interrupts holding current.<br>Gyros off turns off holding current. Relays will reset if gyros are turned on again. |
| Attitude control ON | Functional | Pyrotechnic arming switch.<br>CC&S L-2 event.<br>DC-V13, which also turns on Canopus sensor and sets maneuver inhibit logic. |
| Science ON | Functional/ alternate mode | Power switched on at separation when holding current removed from power subsystem relay.<br>DC-V2, which also switches encoder to Data Mode 2.<br>DC-V25*, which also turns on terminator sensor and overrides science inhibit logic.<br>Gyro turn-off prior to separation. |
| Solar panel deployment | Functional | Separation-initiated timer.<br>CC&S L-1 event. |
| Canopus sensor ON | Functional | CC&S L-3.<br>DC-V13, which also turns on attitude control and sets maneuver inhibit logic. |
| Switch data modes | Functional | To Mode 1: attitude control signal at start of midcourse maneuver.<br>DC-V1.<br>To Mode 2: attitude control signal at end of midcourse maneuver.<br>DC-V2 which also turns on science.<br>DAS signal at end of tape recording phase.<br>To Mode 3*: DAS signal at receipt of MT-8 or DC-V24.<br>To Mode 4: CC&S MT-9.<br>DC-V4. |

Table IV-6 (contd)

| Command function | Redundancy type | Redundant command signals |
|---|---|---|
| Switch power amplifiers | Functional | DC-V7.<br>Internal logic signal at receipt of CC&S CY-1 when power output is too low. |
| Battery charge OFF | Functional | DC-V28* toggles battery charger state, also turning TRS 2.4 kc electronics OFF.<br>DC-V25 which also turns on the terminator sensor and tape recorder electronics and overrides science inhibit logic.<br>CC&S MT-7 which also turns on the terminator sensor and tape recorder electronics.<br>DC-V26, which also turns off science. |
| Switch data rates | Functional | CC&S MT-6 switches to 8⅓ bps.<br>DC-V5 switch bit rates (toggle). |
| Canopus cone angle update | Functional | CC&S MT-1, MT-2, MT-3, MT-4.<br>DC-V17. |
| Antenna selection | Functional/ alternate mode | CC&S MT-5 switches to transmit via high-gain antenna and enables CY-1 logic.<br>DC-V10 switches to transmit via high-gain antenna and to receive via low-gain antenna.<br>DC-V11 switches to transmit and receive via high-gain antenna.<br>DC-V12 switches to transmit and receive via low-gain antenna.<br>Gyros on switches to receive via low-gain antenna.<br>Two consecutive CC&S CY-1 signals with the receiver continuously out of lock will switch receiver to other antenna. Each subsequent consecutive CY-1 with receiver remaining out of lock will switch receiver to other antenna. |

Table IV-6 (contd)

| Command function | Redundancy type | Redundant command signals |
|---|---|---|
| Ranging OFF | Functional | CC&S CY-1.*<br>DC-V9 which toggles ranging ON/OFF. |
| *Terminator sensor ON/tape recorder ON | Functional | CC&S MT-7, which also turns off battery charger if on, and turns on science if off.<br>DC-V25, which also overrides science inhibit logic and turns off battery charger, if on. |
| *Planet sensor ON/establish DAS encounter mode | Functional | CC&S MT-8.<br>DC-V24, which also enables or disables clock B on alternate commands. |
| Recording sequence initiation | Functional | Planet sensor output.*<br>DAS Clock A signal.* |
| *Antenna-pointing angle change | Functional | Terminator sensor output.<br>DAS Clock A signal.<br>DC-V22. |
| Record sequence stop | Functional | End of tape signal interval to TRS.<br>Stop record signals from DAS initiated by Clock A or Clock B signal.* |
| Initiate playback | Functional | CC&S MT-9.<br>DC-V4. |
| Switch tracks | Functional | End of tape signal internal to TRS.<br>DC-V3.* |
| Switch exciters | Functional | Internal logic signal at receipt of CC&S CY-1 when exciter power output is too low.<br>DC-V8. |

*New elements of redundancy.

*Functional:* Paralleling functionally identical units having different physical characteristics to achieve the desired function. This technique protects against causal failures, frequently at low cost in terms of weight, power, volume and complexity. A prime objective of this redundancy form is to provide at least two separate and independent paths by which a critical function could be performed.

*Alternative mode:* Use of a non-primary mode of operation to achieve the same or nearly the same level of performance as the primary mode. This technique frequently exploits equipment in the system for another purpose to keep the spacecraft operating even in the event of some failure. Some increase in operational complexity or mission risk must be acceptable to utilize this technique.

## D. Science Subsystem Description and Development

The *Mariner* science subsystem consists of five scientific instruments and the data automation system. The experiments to be conducted with these instruments are shown in Table IV-7. All the instruments are capable of making measurements during the cruise portion of the flight as well as during the Venus encounter.

Three of the instruments carried on the *Mariner V* spacecraft are identical to those of *Mariner IV* with the exception of the necessary modifications and design improvements required to meet the different environmental conditions (see Table I-1, Section I). Figure IV-8 is a functional block diagram of the science subsystems.

*1. Helium magnetometer scientific objective.* The helium magnetometer (Fig. IV-9) was designed to measure the intensity and direction of magnetic fields that originate on the sun and are convected out through the solar system by the solar wind. The magnetometer operates on the principle of detecting the amount of light absorption, of the proper wavelength, in a helium gas cell.

*a. Modifications.* The modifications to the *Mariner* Mars 1964 unit changed the scale from $\pm 360$ ($0.7\gamma$/DN) to $\pm 204.8$ ($0.4\gamma$/DN) and increased the sweep vector to approximately $300\gamma$. By increasing the sweep vector, the signal-to-noise ratio was significantly improved (Table IV-8).

Functionally, the operation of the *Mariner V* magnetometer was identical to that of *Mariner IV*. All parts, with the exception of the resistors needed to effect the scale and sweep vector changes (Ref. 7), were identical.

**Table IV-7. *Mariner V* science instruments and ancillaries**

| Description | Spacecraft unit number | Weight, lbs | Power, W | Look angle | Purpose | Number of sensors | Output data |
|---|---|---|---|---|---|---|---|
| Trapped radiation detector | 25 | 2.63 | 0.500 | Detectors B, C and D have look-angle axis directed 70 deg to probe-sun line. Full look angle of 60 deg for B and C. Full look angle of 80 deg for D. | To search for magnetically trapped particles in the vicinity of Venus and, if found, make preliminary determination of their distribution in space, their energy spectra and their identities. To monitor the occurrence of solar cosmic rays and energetic electrons in interplanetary space and study their angular distributions, energy spectra and time histories. To monitor soft X-rays from the sun throughout the flight. | 4 | Digital |
| Solar plasma probe | 32 | 6.88 | 2.7 | 15-deg half angle cone, zero deg from probe-sun line. | To determine the positive ion flux density in the range $5 \times 10^{-5}$ to $5 \times 10^{-9}$ particles, $cm^{-2}$ $sec^{-1}$. To measure the energy spectrum in the range 30 eV to 10 keV. To determine the arrival direction of the plasma flux within a cone of 15-deg half angle centered on the probe-sun line. To measure the temporal and spatial variations of the above quantities. To correlate above measurements with measurements of the magnetic field. | 1 (3 sections) | Pulse width |
| Helium magnetometer | 33 | 6.41 | 7.21 | One sensor along spacecraft Z axis, one sensor along Y axis, one sensor along X axis. | To establish whether a planetary field exists and, if so, to determine the characteristics of the field (magnitude, directional, multipolarity, orientation relative to the planetary rotational axis). To investigate the nature of the interface between planetary and interplanetary magnetic fields. To measure the magnitude and direction of the steady and slowly varying components of the interplanetary magnetic field and to determine its variation with heliographic latitude and longitude. | One | Pulse width |

## Table IV-7 (contd)

| Description | Spacecraft unit number | Weight, lbs | Power, W | Look angle | Purpose | Number of sensors | Output data |
|---|---|---|---|---|---|---|---|
| UV photometer | 34 | 9.21 | 3.5 avg. @33⅓ bps. 4.5 avg. @8⅓ bps. | Detectors A, B, and C have look-angle axis directed 90 deg to probe-sun line. The field of view of detectors A and B are cones with a half angle of 0.5 deg @ half sensor input amplitude. The field of view of detector C is a cone with a half angle of 1.25 deg at half sensor input amplitude. | To measure atomic hydrogen resonance radiation at 1216 Å and atomic oxygen resonance radiation at 1304 Å in the outer atmosphere of Venus during the phase and in interplanetary space during cruise. | 3 | Pulse width |
| Dual-frequency receiver | 35 | 5.1 | 2.0 | Not applicable. | To monitor the average interplanetary electron density between the earth and the spacecraft. To provide information to correct the tracking data for plasma propagation effects, and supplement the data from the plasma probe. The DFR will make it possible to separate dispersive ionosphere effects from the nondispersive refractive effects of the neutral atmosphere. This will provide more detailed information on both the neutral and the ionized region of the atmosphere. | Not applicable | Digital and pulse width |
| Ancillaries* | | | | | | | |
| Data information system | 20 | 14.6 | 11.0 avg. during cruise. 11.0 avg. during encounter. | Not applicable. | To control and synchronize the science instruments in accordance with a preset timing and format structure. To provide the necessary sampling rates to ensure meaningful science data. To buffer science data and to send it to the data encoder or the tape recorder. To issue and receive commands from other spacecraft subsystems which pertain to the operation of the science subsystem. | None | See data automation system |

*Mariner Venus 67 modifications.

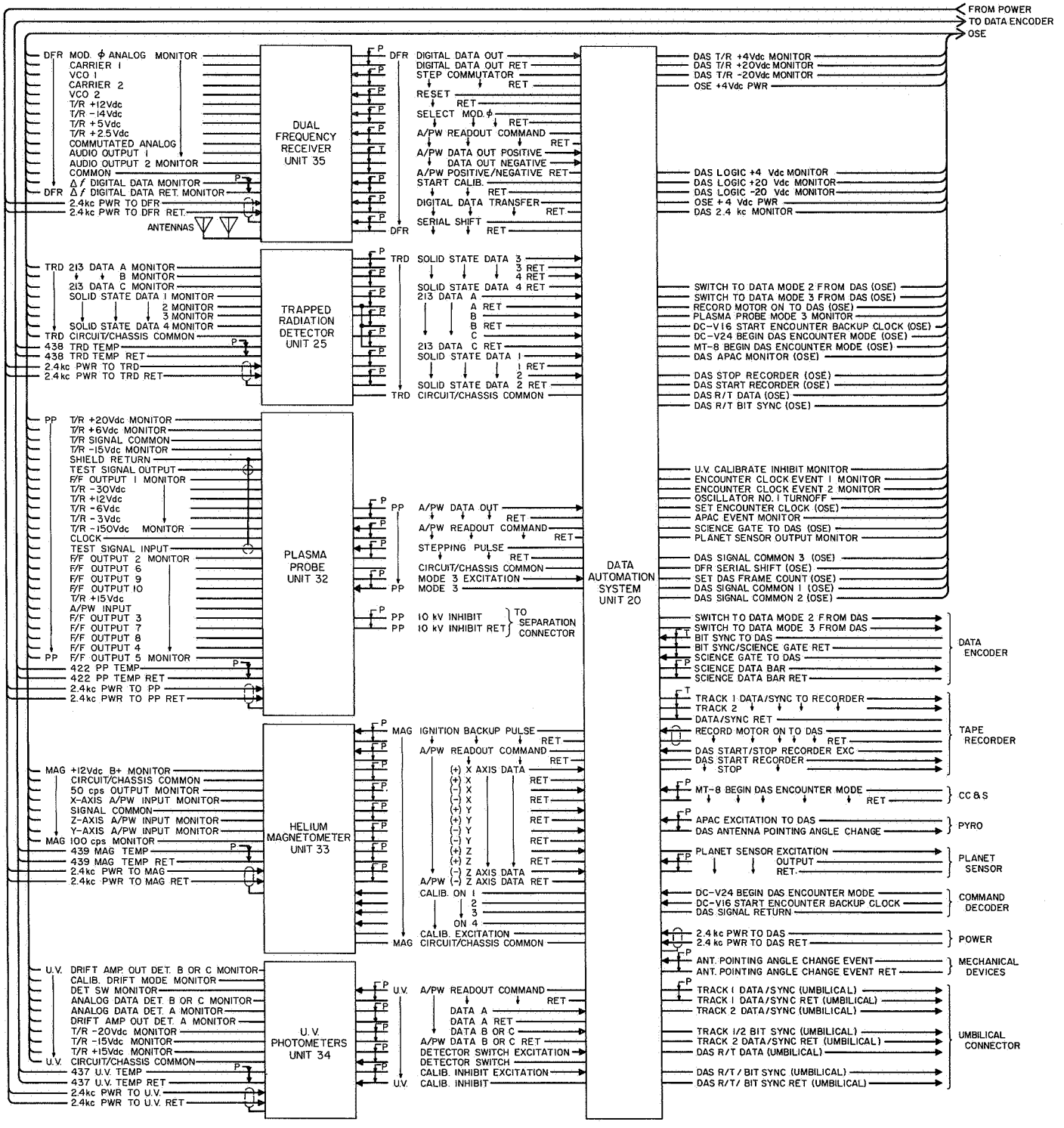



**Fig. IV-8. Science subsystem block diagram**

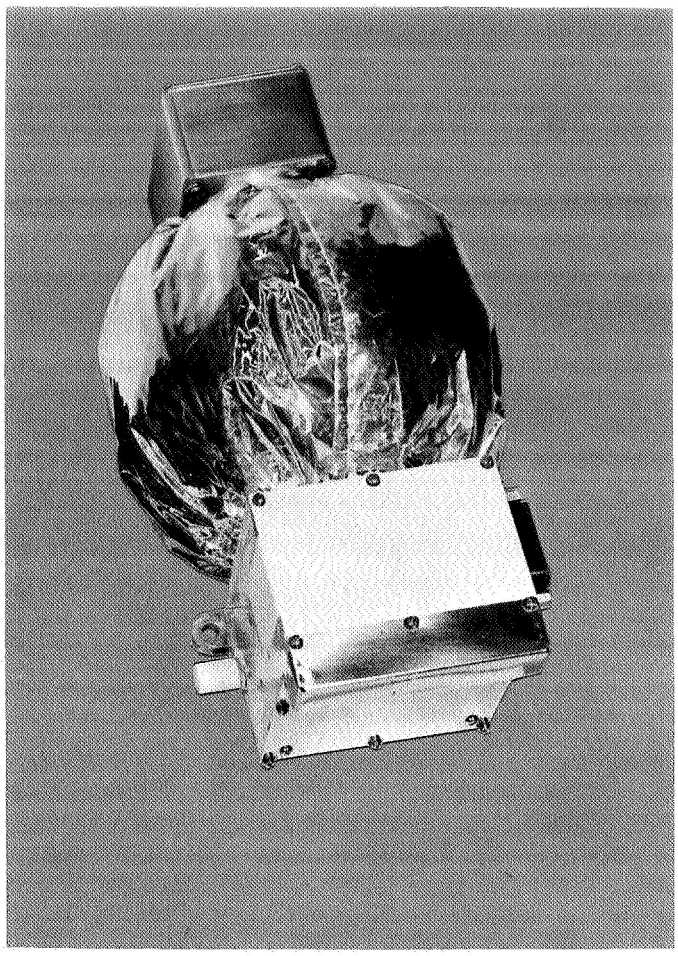


**Fig. IV-9. Helium magnetometer**

Additionally, a sensor heater was required because of the inverted orientation of the spacecraft.

To provide better temperature control/stability, especially during the midcourse correction maneuver, a thermal "diaper" was added to the ball and 3¼ in.² of JPL PV100 white paint were applied to the ignitor end of the sensor.

*b. Problem areas.* The problems encountered fell into three basic areas:

(1) Analog noise, related to cell, lamp, and polarizer deficiencies.

(2) Variable offset, related to permiable components in the sensor.

(3) Sign changes (toggling) in the digital output from the DAS to the data encoder.

**Table IV-8. Instrument noise and offset**

| Parameter | Axis | | |
|---|---|---|---|
| Noise (100 samples @ ≈ 1 per sec): | x | y | z |
| Maximum deviation (γ) | ±0.15 | ±0.15 | ±0.12 |
| Standard deviation (γ) | 0.090 | 0.100 | 0.074 |
| Analog zero-offset: | | | |
| Instrument offset (γ) | −0.4 | −2.7 | +0.8 |
| Heater-current offset (γ) | +0.2 | +0.2 | +0.1 |
| Total offset (γ) | −0.2 | −2.5 | +0.9 |

The first problem area was encountered immediately upon removal of the two flight instruments from the spacecraft assembly facility (SAF) storage area. It was found, due to long term storage of the instruments, that the helium cells had become contaminated by the internal re-emission of the mono-molecular layer of $H_2O$ driven into the wall during manufacture and burn-in of the cells. This contamination interferes with the ordered population of the metastable states and results in a decrease in the system signal-to-noise ratio. New cells were tested, burned in, and installed.

The variability of offset, discovered during calibration, was confined to the M67-1 unit. Exposures of 1 to 100 G caused changes in the offset as high as 9γ. Since no completely nonmagnetic capacitors could be found, for a replacement preamplifier, the effect of 1, 2, 3, 5, 10, etc. gauss fields on the existing preamplifier were accurately calibrated. The prime flight unit (M67-2) exhibited no variance in offset as a function of field temperature (Table IV-8).

The analog noise problem reappeared during the calibration of M67-2. Extensive testing indicated a defective circular polarizer that lowered the amount and quality of light transmitted to the cell from the lamp. Since there is an optimum operating point for light transmitted in relationship to signal/noise ratio (S/N), the analog noise increased from the normal $<10$ mV (⅝ DN) to approximately $>40$ mV (3 DN). Replacement of the polarizer and certain parts in the RF supply (to optimize RF power delivered) brought the noise down to 6 mV (¼ DN).

The third problem area was that of toggling. This anomaly would cause sign changes not necessarily accompanied by a DN change. Extensive testing, on and off the spacecraft, indicated the presence of 55 to 110 kHz noise pulse that would increase the occurrence of toggling from the normal 3–10 times per day to as high as 6 times per frame. Further off-spacecraft testing revealed an inherent

instability in the analog-to-pulse width (A/PW) converters. As little as 6 pF, from input to output, would allow the A/PW's to oscillate between read-out commands. The presence of 55 to 110 kHz pulses accentuated the problem. A positive solution was made by the addition of a low-pass filter to the input of each A/PW. The filter, which shunted all signals or extraneous noise above 10 kHz to ground, consisted of a 1-kΩ resistor in series with the input, and a 0.1-$\mu$F capacitor to ground.

*c. Environmental testing.* All environmental testing was successfully completed. Only one problem, related to thermal-vacuum testing, was encountered: the ability to relight the lamp and cell at the hot temperature. This was remedied by adoption of a new tuning procedure which took into account the variation in component value change, cell and lamp pressure change, and variations of RF output at various temperatures.

*d. Systems testing.* Systems testing produced no anomalous behavior, other than items noted above, and was greatly simplified and enhanced by the replacement of the helmholtz coil (used on *Mariner* Mars 1964) with a spacecraft-mounted flux tank. This tank permitted easy nulling of the instrument and long periods of quiet data.

*e. Calibration.* Scale factor, linearity, in-flight calibrates, noise and offsets were all measured (Tables IV-8 and IV-9) and found highly repeatable. Additional calibration was performed on the A/PW's.

***2. Ultraviolet photometer scientific objective.*** The *Mariner* Venus 67 ultraviolet (UV) photometer (Fig. IV-10) was designed to measure atomic hydrogen resonance radiation at 1216 Å and atomic oxygen resonance radiation at 1304 Å in the outer atmosphere of Venus and in interplanetary space. The UV photometer was originally designed to measure a part of the hydrogen and oxygen density distribution in the vicinity of Mars (*Mariner* Mars 1964). One set of data readings, synchronized with the data automation system (DAS), was to be telemetered during each frame at the rate of 8⅓ bits per second (bps). Once every eighth frame, UV photometer data were substituted by an alternately presented internal mid-scale calibration or a data zero reference level.

**Table IV-9. Instrument calibration**

| Parameter | Axis | | |
|---|---|---|---|
| | x | y | z |
| Scale-factor: | | | |
| ΔV/ΔB (mV per γ) | 29.55 | 29.47 | 29.63 |
| ΔT/ΔB (μsec per γ) | 45.43 | 45.34 | 45.51 |
| Quantization (γ per DN) | 0.397 | 0.398 | 0.396 |
| Flux density at ±511 DN (γ) | ±202.9 | ±203.3 | ±202.6 |
| Gross non-linearity: | 0.3% or less all axes | | |
| In-flight-calibrate increments (analog outputs): | | | |
| Step 1 (γ) | −39.80 | −40.16 | −38.44 |
| Step 2 (γ) | −79.52 | −80.30 | −77.91 |
| Step 3 (γ) | +38.90 | +38.76 | +38.95 |
| Step 4 (γ) | +78.31 | +78.50 | +78.21 |

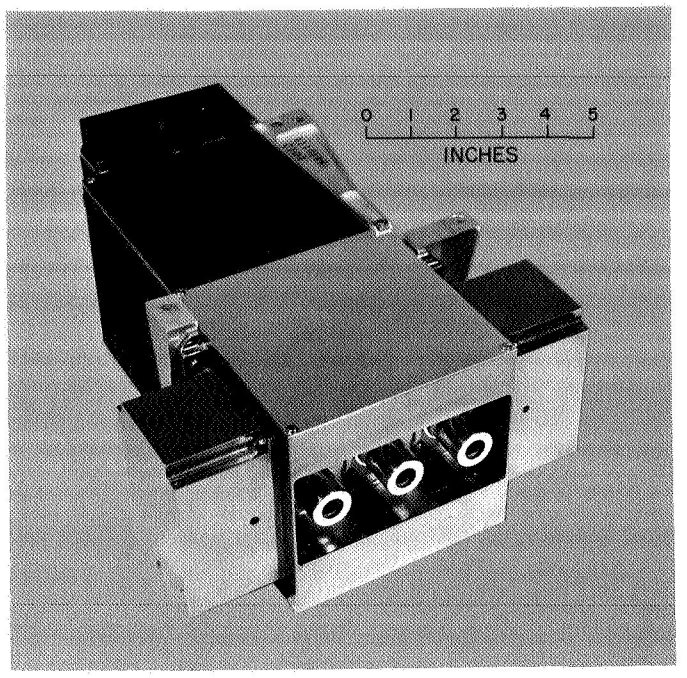



**Fig. IV-10. Ultraviolet (UV) photometer**

The *Mariner* Mars 1964 UV instruments were modified to meet the scientific requirements of the mission and the new spacecraft configuration.

*a. Configuration.* The three UV sensors were identical 18-stage photomultiplier tubes with cesium iodide photocathodes and lithium fluoride windows. The photocathode material determines the wavelength response rejection characteristics toward visible light. The window material determines the shorter wavelength response cutoff point. Each solar blind phototube has a relatively flat spectral response from 1050 Å to 1900 Å. At the mercury line, 2537 Å, the output of each tube with equal source intensities, is less than $1 \times 10^{-3}$ lower than the output at Lyman Alpha wavelength (1216 Å).

Optical filters were used to modify the windows of two of the phototubes (detector tubes A and B—tube C had no external filter), increasing the wavelength response cutoff point. Tube A views through a cleaved calcium fluoride filter resulting in a sensor bandpass of 1250 to 1900 Å. Tube B views through a cleaved barium fluoride filter resulting in a sensor bandpass of 1350 to 1900 Å. The atomic hydrogen density measurement is proportional to the intensity difference between tubes A and C. The atomic oxygen density measurement is proportional to the intensity difference between tubes A and B.

A collimating aperture, in front of each phototube and filter, was used to restrict the field of view. Detectors A and B each have a field of view of a cone with a half angle of 0.5 deg at an aperture output of half amplitude. Detector C has a field of view of a cone with a half angle of 1.25 deg at an aperture output of half amplitude. The latter view cone was measured with collimated light to have a half angle of 15 deg at an aperture output of $1 \times 10^{-5}$.

The apertures for detectors A and B are alternately stacked discs of 0.001- and 0.004-in. thickness and have chemically etched patterns of hexagonal holes, 0.020 in. between opposite edges and 0.028 in. between hole centers. The aperture for detector C is alternately stacked discs of 0.003- and 0.012-in. thickness, which have a chemically etched pattern of hexagonal holes, 0.050 in. between opposite edges and 0.070 in. between hole centers. Each stack of aperture discs has a total length of one inch and has a light transmission of 60%.

Dynamic range of the UV photometer is such that it will measure a source brightness in the range from about 500 Rayleighs to 100,000 Rayleighs. The voltage across the phototube without optical excitation is about 3250 V (phototube output of about $1 \times 10^{-12}$ A) decreasing to about 2600 V with $10^3$ times equivalent dark current excitation on the photocathodes.

Figure IV-11 is a block diagram of channel A analog data system. The phototube anode current is connected to a single-end dc amplifier (amplifier A) that has a voltage output amplitude proportional to the input current amplitude, having a trans-resistance of $10^9$ Ω. With high voltage applied across the phototube, the amplifier A analog output (between 0 and 6 V) is divided to about half amplitude (by $R_3$ and $R_4$) to excite the high-voltage control amplifier (HVC). The HVC amplifier has a voltage gain of 120 dB.

The dc output voltage of HVC, which is inversely proportional to the input voltage, provides a supply voltage up to 46 for the high-voltage inverter collector circuits. The high-voltage inverter is synchronized to 2.4 kHz, and the output transformer has a voltage gain of about 10. The output of the transformer drives latter-connected rectifiers, having a voltage gain of about 8 that provides a potential output capability of about 3600 V.

A differential amplifier is used at the input of the HVC, and the input signal is used as a reference voltage. The opposite input to the differential amplifier is the high-voltage supply scaled down by the PMT bleeder resistor string, having an overall feedback of 60 dB.

A negative dc voltage level from the high-voltage keying logic saturates $Q_1$ which inserts about +10 V into the HVC input, derived from the voltage divider $R_4$ and $R_5$, resulting in a PMT potential of about 200 V. The gain of the PMT is reduced to zero at about 600 V. While $Q_1$ is in the off position, the analog output signal, divided down by $R_3$ and $R_4$, drives the PMT potential proportionally to the analog signal level to between 2600 and 3250 V.

The analog output signal also provides drive to the drift correct amplifier (Amplifier G) when $Q_2$ is in the off state. While $Q_2$ is saturated by a positive level from the drift correction keying logic (which always occurs while $Q_1$ is in the off state), the amplifier G input signal is inhibited and the FET switch is held open. $R_6$ provides enough isolation between $Q_2$ and amplifier A output to prevent analog signal degradation.

While $Q_1$ is saturated, the PMT is essentially cut off; therefore, the presence of an analog output voltage would be caused by a dc offset within amplifier A. During this time $Q_2$ is in the off state and the FET switch is held closed. Amplifier G amplifies the offset of amplifier A to provide the necessary amount of voltage into the feedback loop, $R_1$ and $R_2$, to nullify the offset. The drift correction circuitry has the dynamic capability to compensate for positive or negative offsets to the saturation point of amplifier A (analog output of 11 V). While full high voltage is applied to the PMT ($Q_1$ in the off state), $Q_2$ will be saturated (amplifier G input inhibited), and the FET switch will be held open. During this time, amplifier A will be held drift corrected by the correction voltage stored in $C_1$.

Internal calibration of amplifier A gain occurs once every 16th DAS readout. During the data collection

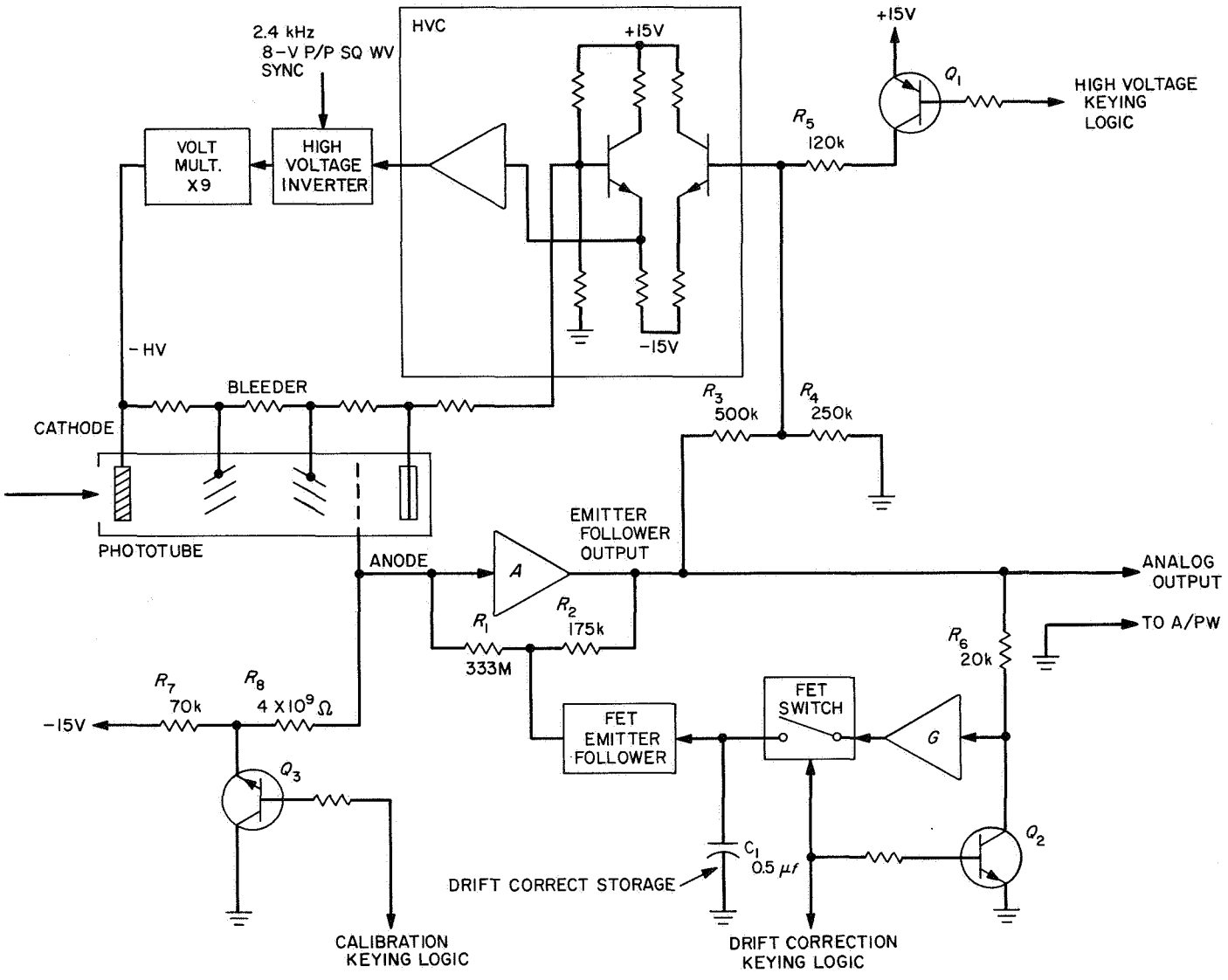



**Fig. IV-11. Data amplifier block diagram**

periods, $Q_3$ is held saturated by the calibration keying logic, thereby grounding $R_8$. During the calibration period $Q_3$ is held in the off state allowing a known current to pass into the input of amplifier A provided by $R_7$ and $R_8$. The analog output voltage during calibration is about +3 V. While the instrument is in the calibration mode, the PMT gain is cut off and amplifier G is inhibited.

The second analog channel is similar to channel A except that two phototubes (detectors B and C) with separate high-voltage power supplies share one channel. The anodes of the two phototubes are connected together, and sensor switching is accomplished by selective application of high voltage. The sum of the on and off times of the two detectors occurs in coincidence with detector A. The one HVC drives both phototube supplies simultaneously to the appropriate amount of high voltage. The instrument logic determines which power supply is operative. NPN transistor switches are connected to the push–pull high-voltage inverter transistor bases that inhibit base drive when the switches are saturated by logic command.

Even though the rise and fall times of the high voltages during switching are controlled to about 50 ms, the resulting switching transients from the phototube anodes are of sufficient amplitude to saturate amplifier A, and in turn, drive the high voltage in a non-linear fashion to a lower value. The settling time of the system would therefore be far too great to be useful. Compensation was employed to minimize the switching transient amplitude by inserting a superimposed pulse of opposite polarity into the input of amplifier A. The compensation pulse is derived by differentiating, in opposite polarity, the high-voltage turn on and turn off at the lowest dc potential point in the high-voltage power supply. The net effect reduces the switching transient amplitude at amplifier A output to 1.5 V or less at the 8⅓ bps data rate.

*b. Amplifier input modification.* Past experience has shown that high-voltage arcing, or any mode of operation such as the instrument viewing the sun, could emit voltages from the phototubes anode in excess of the −30-V rating of the amplifier A input transistor (the anode voltage could go to −200 V). Four ½-W, 5.1-MΩ carbon resistors were connected in series between the PMT anode and the amplifier A input in each channel. Series redundant diode clippers were then connected at the amplifier A input. NPN transistors employing the base emitter junctions were used as the diodes. Leakage of the diode devices was measured to be about $10^{-9}$ A at 70°C. The base of the devices was biased to about −5 V derived from a voltage divider connected between the existing −15-V bus and common. The resistance value from the transistor base to common is 10,000 Ω. The clipping level of the diode circuit is −4 V in which a 2000:1 voltage divider is effective.

The time constant of the analog signals at the input of the APW's was changed from 3 ms to between 100 and 120 ms to allow a longer integrating time of random short duration pulses, such as that caused from the sensors sensitivity to radiation and thermal agitation, to reduce the UV data error. The time constant was increased by increasing the shunt value of C from 0.68 to 39 μF.

*c. Logic.* Figure IV-12 is a block diagram of the original logic of the instrument. The detector switch command, originating from the DAS, is fed through three stages of saturable amplifiers, each having filter rejection to noise. While the amplifier output is in the one state, detector C high voltage is inhibited via $OR_1$ gate, the high voltages are held on via $OR_3$ and $OR_4$ gates, and the drift correction circuits are held off via $OR_3$. When the output of the amplifier swings from a "1" state to a "0" state, the one-shot $Q$ is triggered and the $Q$ output would go to and remain in a "1" state for 3.5 s (the $\bar{Q}$ output is the reciprocal of $Q$). During the regeneration period of the one-shot, the drift correction amplifiers are held in the off state via $OR_3$ gate, and the high voltages are held on via $OR_3$ and $OR_4$ gates. Detector C high-voltage inhibit is removed by the "0" state of the amplifier output via $OR_1$ gate, and the detector B high voltage is inhibited by the "0" state of $\bar{Q}$ via $OR_2$ gate. The binary counter counts each time that the one-shot $Q$ output swings from a "1" to a "0" state. After the one-shot $Q$ output has returned to a "0" state, and while the amplifier output remains in "0" state, detectors B and C high-voltage inverters are held uninhibited via $OR_1$ and $OR_2$ gates, and the high voltages are held off via gates $OR_3$ and $OR_4$. The drift correction amplifiers are held in the *on* state via $OR_3$ gate. The logic switching cycle is completed when the amplifier output returns to a "1" state.

During the time that the first three binaries are in coincidence, the high voltages are suppressed through $AND_1$ and $OR_4$; however, the drift correction amplifiers remain turned *off*. If only the first three binaries of the counter are in coincidence, the analog amplifier A output drift status is presented to telemetry. While all four binaries are in coincidence, the high voltages are suppressed via $AND_1$ gate, and the calibration signals are applied into the analog amplifier A inputs via $AND_2$ gate.

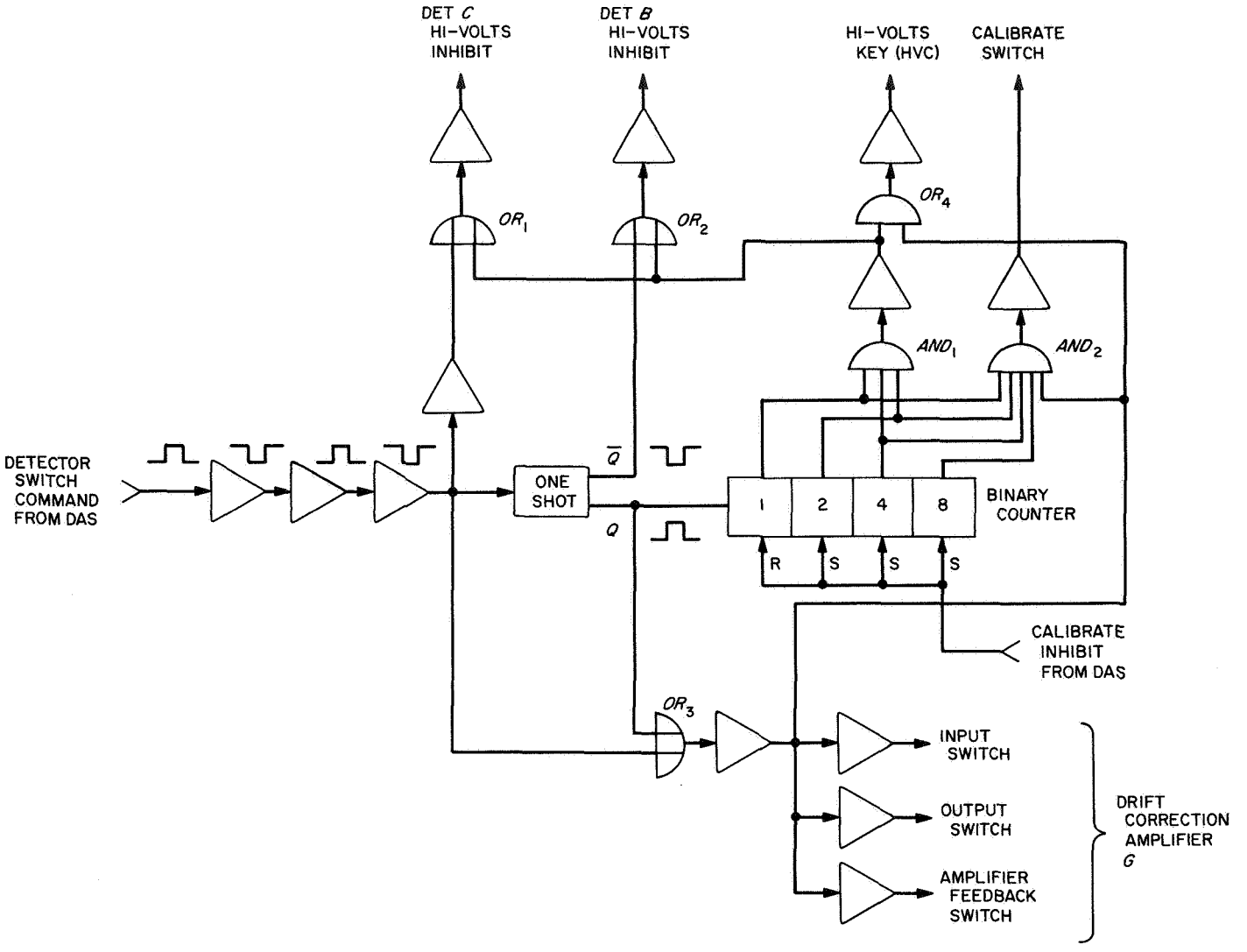



**Fig. IV-12. UV photometer logic diagram**

The drift correction switching signal has been included as one of the inputs to the $AND_2$ gate to assure that the drift correction amplifier will be *off* during the calibration period.

*d. Logic modifications.* The instrument can remain in the calibrate or drift check mode for as long as 19 s, and all the oxygen data about Venus will be taken within a 10-s period. It is therefore necessary to inhibit calibrate and drift check in the vicinity of Venus.

The original design of the instrument provided for holding the binary counter in the calibrate state by inserting +3 V through the test connector for test purposes. This binary "set" bus was moved from the "set" side to the "reset" side of the first binary and connected to the DAS calibrate inhibit interface. During the data recording phase of the encounter mode, the DAS provides a continuous signal that applies +10 V to hold the first binary in a zero state preventing coincidence of gates $AND_1$ and/or $AND_2$.

*e. Original data logic.* Figure IV-13 shows the basic data logic differences between *Mariner* Mars 1964 and *Mariner* Venus 67. The detector switch command was inverted so that detectors B and A (oxygen data) would remain *on* for most of the time. The one-shot period had to be shorter so that amplifier A drift correction could occur. Measurements were made of all three instruments, and the drift-correcting period was found to consistently

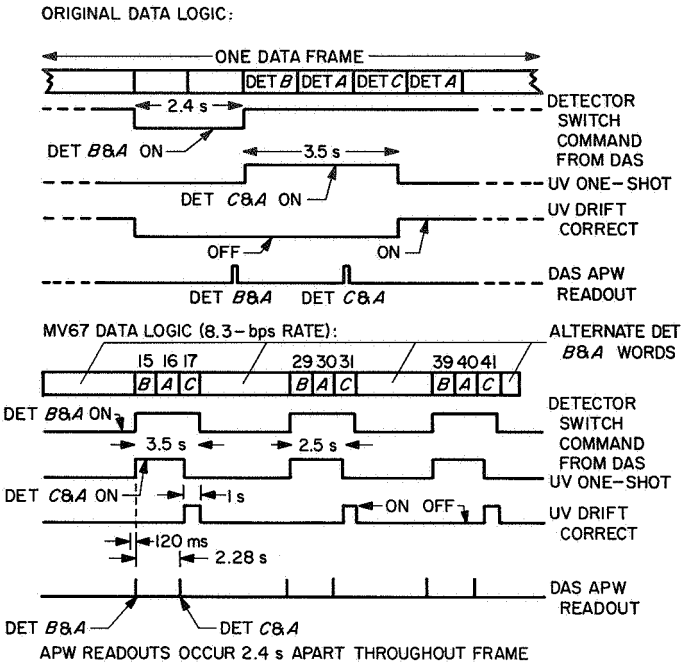



**Fig. IV-13. Data logic differences**

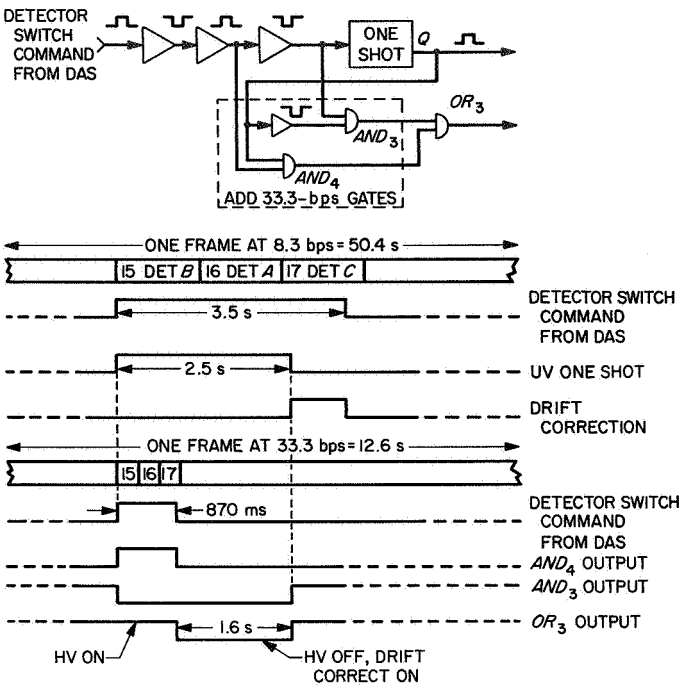



**Fig. IV-14. Gate logic diagram, 33⅓ bits/s**

require between 650 and 700 ms. The one-shot period was changed from 3.5 s to 2.490 s, allowing a 1-s drift-correcting time and a margin of 200 ms holding *on* time of detector C for data readout. The one-shot was temperature cycled over the range of −50°C to +80°C with the correct loads, including the 33⅓-bps gate to be described later. The repeatable period was 2.44 s at −50°C and 2.71 s at +80°C.

At the 33⅓-bps data rate, the one-shot period exceeds the "1" state of the detector switch command (Fig. IV-14). Under such conditions, the high voltages would not switch *off* (detectors B and C would switch alternately, however, by command from the one-shot) and drift correction could not occur. If the analog amplifiers are allowed to drift, the analog offsets could not only be great but could be of negative polarity. Any amount of negative analog output will display a data number of zero at the DAS output. The amounts of high voltages and, hence, the phototube gains are proportionally affected by the amounts of amplifier offsets. Degradation, if any, of the drift correction systems at the 33⅓ bit rate may not be seen. The circuit shown in the block diagram in Fig. IV-14 was added to the logic board to command drift correction at the faster data rate. The $AND_4$ gate was added to hold on high voltages during the detector switch command "1" state (870 ms duration). The $AND_3$ gate was added to hold *off* high voltages and hold *on* drift correcting circuits for the remainder of the one-shot period (1.6 s).

*f. DAS/UV interface modification.* The detector switching command was dc-coupled between the DAS and the UV photometer on *Mariner IV*. The *Mariner V* interface was modified to provide isolation of circuit commons between the two instruments with the use of a DAS IS switch. The added calibration inhibit command also uses the new IS switch interface. The UV portion of the IS switch is located in the power supply chassis, and the signal is taken from the IS transistor emitter. The UV +15 V regulated bus is used as the supply for the IS switch.

*g. Instrument calibration.* All three instruments were calibrated at several wavelengths between 1216 Å and 2537 Å. The output of selected UV sources was translated to the photometer sensors through a monochromator and referenced to a calibrated standard phototube in vacuum at ambient temperature. Source amplitudes were controlled at the monochromator output by adjustment of slit size. The optical filters were calibrated independently for wavelength transmission. The calibration curve for the flight unit shows an absolute calibration at 1216 Å for 6 V analog output of: detector A, 200 kilorayleighs; detector B, 140 kilorayleighs; detector C, 64 kilorayleighs. The optical filter calibration curves show: calcium fluoride, 60% transmission at 1300 Å and 0% at 1245 Å; barium fluoride, 60% transmission at 1400 Å and 0% at 1360 Å. All

three photometers were calibrated before and after environmental testing. All three instruments, after environmental testing, were checked for analog drift with respect to temperature in a vacuum chamber and a Krypton source (1235 Å). In addition, all APW's were recalibrated with respect to FA temperatures.

*h. UV/systems performance.* The *desiccant* cover was left on the MC2 photometer when the M67-2 spacecraft was first put in a vacuum environment. As a result, the UV analog channels were driven off scale by either a high voltage arc or corona across the phototube faces caused by *desiccant* outgassing. The instrument was inspected and recalibrated and found not to have been degraded.

Another anomaly occurred in the explosive safe area at EMR after pyro arming and prior to installing the shroud. Basically, the anomaly was that about 200 mV appeared on detector C readout at the 33⅓ bit rate in lieu of a normal 10 to 30 mV level. The prime suspect was an aerostat ionizer that was used in the vicinity of the spacecraft to cancel electrostatic charges. The analog output waveform parameters were recorded and the MC4 photometer was reassigned to be the primary flight unit. The MC2 unit was vacuum tested to FA levels; the anomaly did not reoccur. Special tests were conducted for three days with no firm explanation of the anomaly. An aerostat ionizer, similar to the one used at EMR, was purchased and subjected to the MC2 unit. The analog waveform parameters then agreed with the EMR anomaly.

*3. Trapped radiation detector scientific objectives.* The trapped radiation detector (TRD) was designed for the support of further studies on geomagnetically trapped particles.

The Van Allen Radiation Belts are believed to contain charged particles emanating from solar eruptions which ultimately are trapped in the magnetic field of the earth. There are essentially two belts: the inner and the outer belts. The inner belt consists primarily of protons and is at a distance of approximately 5,000 km from the earth at the equator. The outer belt is composed primarily of electrons and is approximately 10,000 to 15,000 km from earth at the equator.

*a. An improved search for a radiation belt around Venus.* If the actual aphrodiocentric radial miss distance is as small as the intended value of 9,000 km (vs 41,000 km for *Mariner II*), it will be possible to detect a radiation belt, due to a planetary magnetic moment, as small as $10^{-3}$ to $10^{-4}$ of that of the earth. A negative result will establish such a value as an upper limit.

*b. A search for low-energy particle effects in the magnetohydrodynamic wake of Venus.* The intended passage of the approach trajectory across the antisolar wake of the planet will provide another sensitive test of the interaction of the planet (even if intrinsically unmagnetized) with the solar wind.

*c. The study of the occurrence, intensity, and energy spectra of solar protons, electrons, and alpha particles, separately identified in the following energy ranges:*

(1) Electrons: $E_e > 45$ KeV
$E_e > 95$ KeV
$E_e > 150$ KeV

(2) Protons: $0.30 < E_p < 12$ MeV
$0.50 < E_p < 5.3$ MeV
$0.98 < E_p < 2.2$ MeV

(3) Alpha particles: $2.1 < E_a < 18$ MeV

Such measurements are of special interest during the period of anticipated high solar activity during the flight of *Mariner V*. The measurements will be made throughout the interplanetary flight for some 120 days. It is hoped that the observations can also be continued after encounter for as long a period of time as physically possible. Comparison of such observations with those of other spacecraft widely distributed in solar longitude will contribute further to the understanding of interplanetary propagation of solar-emitted particles.

*d. The observation of soft X-ray ($\lambda < 10$ Å) intensity from the sun throughout interplanetary flight.* Such X-ray emissions are related in an essential way to the occurrence of solar flares and to the emission of particles. The spacecraft will be able to view portions of the sun which are not visible from the earth.

*e. Constraints and characteristics.* Of necessity, spacecraft instruments must meet weight, power and size constraints. The volume of the TRD chassis was approximately 82.5 in.$^3$, with a total weight of 2.67 lbs. The power consumption was 450 MW or less, and the input voltage was 50 V, rms ± 2% 2400 Hz (square wave). Turn-on and short circuit current were limited to 200% of the normal operating current. Further protection to the spacecraft power subsystem was provided by two 50 mA fuses in parallel (1/10 A) in the 2400 Hz input power line. The input rise time requirements were 5 $\mu$s ± 4 $\mu$s.

The thermal requirements for the operating temperature limits of the entire unit were −20 to +50°C and the nonoperating temperature limits were −30 to +60°C.

The look-angle axis of detector A was directed along the sun-probe line (Fig. IV-15). Soft X-rays, electrons and protons will be detected within a solid aperture angle of 10 deg. The unidirectional and omnidirectional geometric factors were $1.7 \times 10^{-3}$ cm² sterad and approximately 0.15 cm², respectively.

Detectors B, C, and D shared the same look-angle axis (70 deg to the sun-probe line) and had full aperture angles of 60, 60, and 80 deg, respectively. Detectors B and C had unidirectional and omnidirectional geometric factors of 0.13 cm² sterad.

*f. Modification of the* Mariner *IV* TRD. A four-channel solid-state detector was substituted for the two-channel detector. The electronic components for the additional two channels were packaged in modules and were mounted on the available space in the existing instrument. The look-angle axis of detector A was changed from 135 to 0 deg to the sun-probe line of the spacecraft, and a beryllium foil was added. The full-aperture angle of the detector was decreased from 60 to 10 deg to prevent saturation during periods of high solar activity.

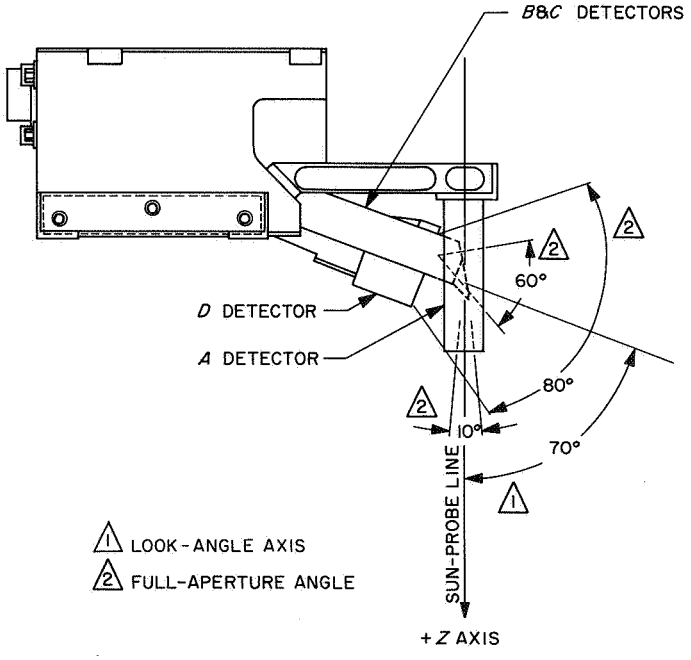



**Fig. IV-15. *Mariner V* trapped radiation detector (side view)**

Detector A was mounted on the instrument so that no part of the spacecraft would obscure its conical field of view.

The aperture angle of detector D was increased from 60 to 80 deg to increase the total collecting area and thus raise the count for a given flux density.

Three Geiger-Mueller (GM) tubes were used for proton and electron detection. Detectors A, B, and C are EON type 6213 GM end window counters, which measure the total number of charged particles passing through their sensitive volumes. The sensitive volume of each tube was shielded so that low-energy particles could enter only by passing through the window at the end of the tube. By allowing for omnidirectional flux of higher-energy particles, a directional measurement of the low-energy particles could be made.

The window of detector A was covered by approximately 1.4 Mg/cm² of mica. Detector A measured electrons > 95 KeV and protons > 2.7 MeV. A beryllium (9.4 Mg/cm²) shield defines the energy threshold of the flux that enters the window. The window of detector B was covered by approximately 1.6 Mg/cm² of mica. Detector B measured electrons > 45 KeV and protons > 0.65 MeV. A sun shade was incorporated on the end of each tube housing to protect the detectors from exposure to direct sunlight during the cruise mode.

The window of detector C was covered with 1.6 Mg/cm² of mica, and an aluminum foil of approximately 20 Mg/cm² is placed behind the aperture of the detector. This increased the threshold energy to 150 KeV for electrons and 3.1 MeV for protons. The GM counter outputs are shaped by means of saturating current amplifiers before being sent to the data automation system (DAS).

The solid-state detector (detector D) was a totally-depleted silicon surface-barrier diode with a thin (0.2 Mg/cm² air equivalent for alpha particles) nickel foil for light shielding. The sensor was 31.7 $\mu$ thick and had a normal sensitive area of 12 mm². The detector, used as a four-channel (D1-D2-D3-D4) proton and alpha particle spectrometer, was capable of detecting protons and alpha particles in a high flux of electrons. Sensitivity to electrons is minimized by making the detector too thin to stop energetic electrons, and setting the discrimination level much higher than the expected electron energy loss.

Figure IV-16 is a block diagram of the TRD electronics.

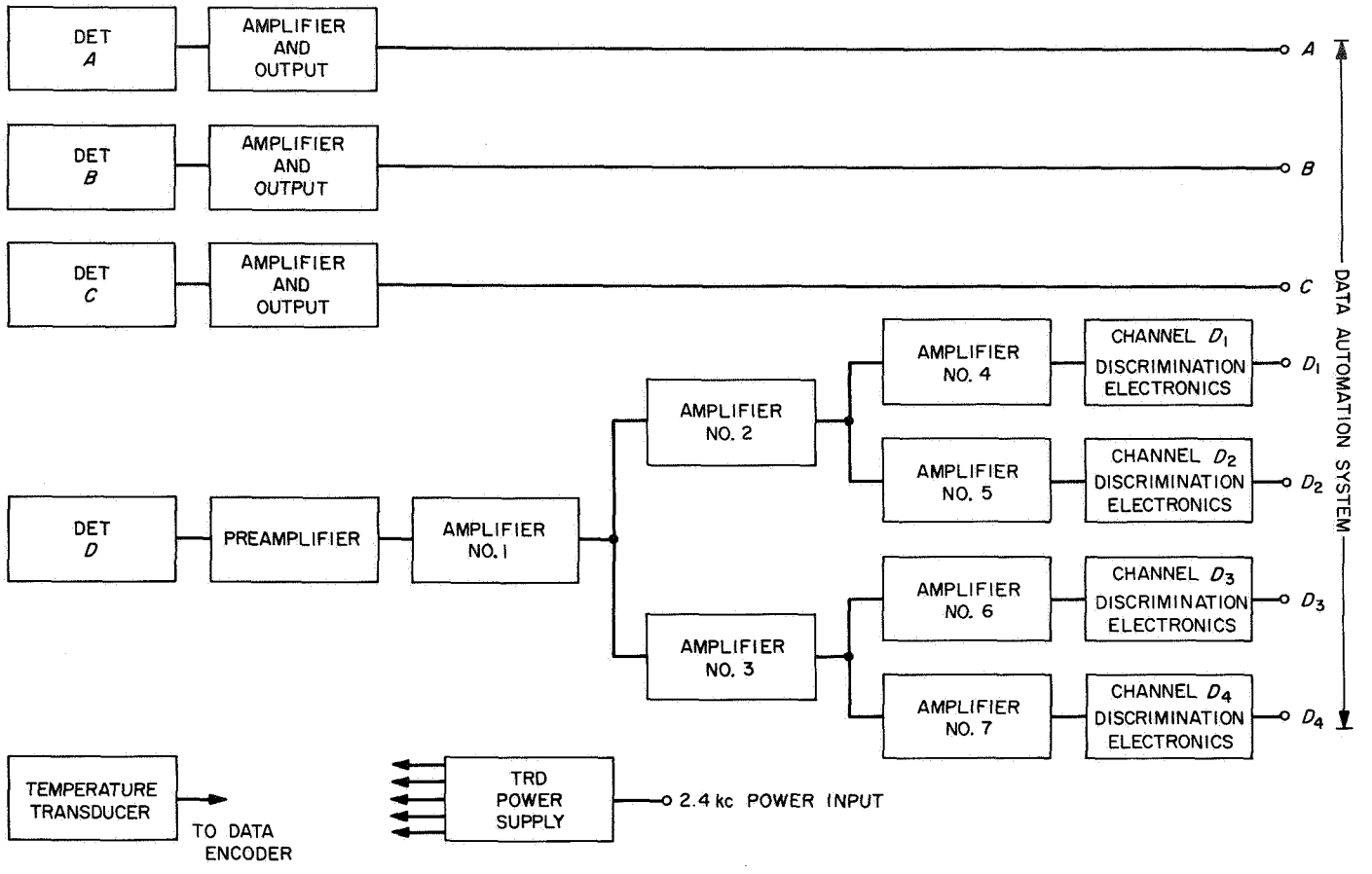



**Fig. IV-16. Trapped radiation detector functional block diagram**

A summary of detector characteristics is contained below.

| Detector | Shielding | Energy for penetration | Dynamic range in true counts/ps |
|---|---|---|---|
| A | magnesium | electrons $E_e > 95$ KeV | 0.6–$10^7$ |
| | teflon | protons $E_p > 2.7$ MeV | 0.6–$10^7$ |
| | beryllium foil | X-rays $\lambda < 10$ Å | 0.6–$10^7$ |
| B | magnesium | electrons $E_e > 45$ KeV | 0.6–$10^7$ |
| | teflon | protons $E_p > 0.65$ MeV | 0.6–$10^7$ |
| C | magnesium | electrons $E_e > 150$ KeV | 0.6–$10^7$ |
| | teflon | protons $E_p > 3.1$ MeV | 0.6–$10^7$ |
| | aluminum foil | | |

Electrons insensitive to any energy are:

| *Protons:* | *Range:* |
|---|---|
| D1 $0.30 < E_p < 12$ MeV | 0.05–$10^7$ |
| D2 $0.50 < E_p < 5.3$ MeV | 0.05–$10^7$ |
| D3 $0.98 < E_p < 2.2$ MeV | 0.05–$10^7$ |

*Alpha particles:*

D4 $2.1 < E_a < 18$ MeV

Figure IV-17 shows the physical configuration of the four detectors.

*g. Data flow.* At the 8⅓ bps data rate, the output data channels were commutated so that each output was sampled for 37.2 s out of every 403.2 s. If the total count during this 37.2-s period exceeds $2^{19}$, the number transmitted to earth is $2^{19}$ plus one-fourth of the number of counts in excess of $2^{19}$.

At the 33⅓ bps data rate, the above times are reduced by a factor of four. The commutation order of the data channels are A, C, B, D1, D2, D3, D4, D1. In addition to the commutation sequence of the seven data channels, detector B output is sampled for 31.2 s out of every 50.4 s at the low bit rate and for 5.4 s out of every 12.6 s at the high bit rate.

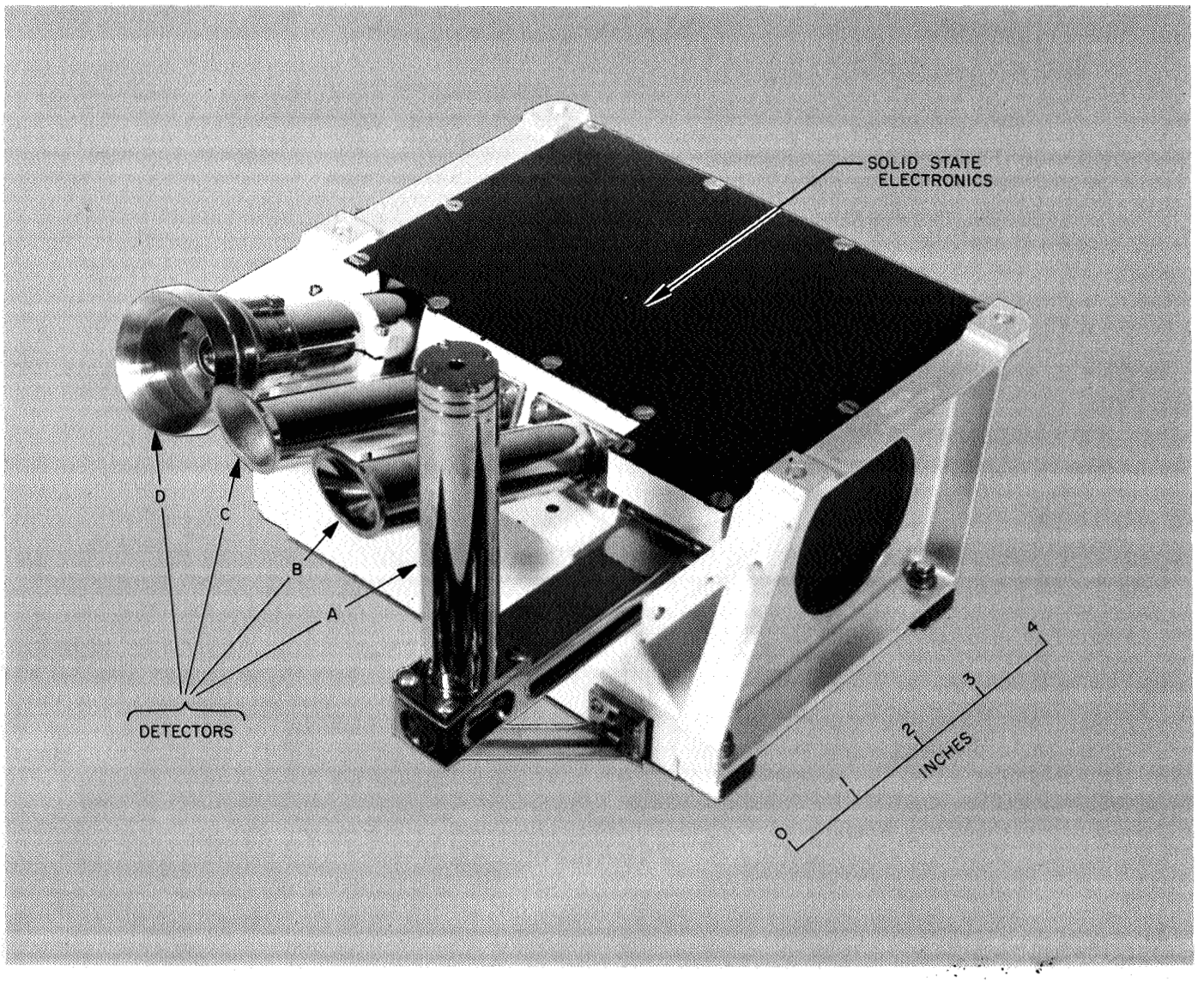



**Fig. IV-17. *Mariner V* trapped radiation detector**

The data telemetered in real time are the total count that occurs during the first 21.6 s of this 31.2-s period. In addition, during the encounter recording sequence the count accumulation is recorded on tape every 1.2 s during the 31.2-s period. In either case, this additional detector B data has a maximum value of 512 counts due to the DAS limitations.

*h. Test and calibration history.* A modified *Mariner IV* TRD was used as the TA unit for *Mariner V*. The unit passed TA vibration and magnetic environmental testing on August 24, 1966.

*The flight instrument (S/N MC-1).* This instrument was received at JPL from the University of Iowa (U.I.). After the flight acceptance test was completed, the unit was returned to U.I. for modifications to eliminate the cross-talk problem noted during DAS compatibility tests. During rework, the GM window of detector B was fractured. The instrument was repaired and returned to JPL. FA requalification was completed. The unit was again carried to U.I. for PFR modification and returned to JPL three days later. MC-1 was again sent to the U.I. for the scheduled calibration. The experiment was returned to JPL and installed on the M67-1 spacecraft on the following day. Upon certification into SAF, MC-1 had 1310 *Mariner IV* operating hours and 296 *Mariner V* hours for a total of 1606 h of operating time.

*Flight instrument S/N MC-5.* The MC-5 instrument was received and successfully passed flight acceptance testing. Final calibration was completed at U.I. MC-5 was certified into SAF with 158.35 h operating time. The TRD was installed on the M 67-2 spacecraft and launched on June 14, 1967.

*Critical problem failure reports (PFR's).* The major concern during the testing phase was in the area of solid-state detector data channels. Cross-talk problems were encountered. Under certain conditions, the solid-state detector data channel would count the GM pulses and the 2.4 kHz power supply. These problems were solved by the addition of decoupling networks in the +8 V line of the internal power supply. By the addition of power supply decoupling, the experiment became very stable and the cross-talk anomaly was completely eliminated.

The window thicknesses of the GM tubes were determined at the University of Iowa through the use of an electron gun. The relationship between apparent and true counting rates (i.e., that which would be observed by a GM counter with zero dead time) was measured on the completed instruments. An X-ray machine was used to provide the high radiation flux necessary for this calibration.

Through selection of a thin detector, and high discrimination levels, to minimize electron sensitivity, the sensor was capable of detecting protons in a high proton flux. A linear pulser and alpha source (Polonium$^{210}$) of known value were used to set these discrimination levels. Calibrations were verified by placing the unit in a proton beam from a Van de Graaff accelerator.

Calibrations on the spacecraft were used primarily to verify the correlation between the instrument counting rates and the science data (DAS) output. The sources used were of sufficient flux to produce an overflow condition in words 10 and 11 of the science DAS (bit 1 of word 10, binary 1).

A Strontium$^{90}$ 1 curie source was used to stimulate the GM tubes to saturation. Readouts were recorded at both 8⅓ bps and 33⅓ bps rates. The source was placed successively on all 3 GM tubes.

In the same manner, a Polonium$^{210}$ source of approximately 80 millicuries was placed on the solid-state detector. Data were recorded at 8⅓ and 33⅓ bps. The saturation levels with the Polonium$^{210}$ and the Strontium$^{90}$ were as follows:

| | |
|---|---|
| Solid-state detector | 100 kHz |
| Detector A | 37 kHz |
| Detector B | 30 kHz |
| Detector C | 33 kHz |

A 300-W flood lamp was held at the detector D aperture to check for damage to the nickel foil, and data were recorded from the DAS. No increase in counting rate was observed, indicating that the foil had not been damaged. The nickel foil was used to prevent detector contamination through direct exposure to the sun. This foil was 0.2 Mg/cm$^2$ of air equivalent for alpha particles (approximately $12.5 \times 10^{-6}$-in. thick).

Counting rates of the detectors were taken over one-hour periods, using the sources associated with the instrument throughout the FA, and systems testing phase of the program. These sources were approximately 200 microcuries of cobalt$^{60}$ for the GM tubes, and approximately 1 microcurie of Americium$^{241}$ for the solid-state detector. The counting averages were compared with data from previous tests for degradation indications—none were noted.

Quiet tests were made for 7 h with no sources on the instruments to verify the background count rates of the detectors (on both M 67-1 and M 67-2 spacecraft).

In-flight calibration consisted of an Americium$^{241}$ source (0.01 microcuries) mounted in detector D housing assembly to establish background counting rates. This source produced 3–4 counts per minute in the D1 channel and 2–3 counts per minute in the D2 channel.

***4. Plasma probe scientific objectives.*** The plasma probe was designed to measure the energy (velocity), direction, and density of positive particles (i.e., protons and alpha particles) contained in the solar wind, both in interplanetary space and near Venus. These data will be used in conjunction with information from the helium magnetometer, and perhaps, with simultaneous data from the comparable instruments on *Mariner IV*, to better understand the characteristics of the magnetic field and solar wind in interplanetary space and near the planets.

*a. General theory of operation.* The *Mariner V* plasma probe is essentially identical to that flown on *Mariner IV* with the exception of the modifications to be presented. For this reason, only a brief description of the instrument will be provided. (See Refs. 1 and 7 for additional detail.)

Basically, the instrument consists of a sensor mounted outside of the spacecraft, facing the sun, and a set of electronics located in three modules within the spacecraft. The sensor (Fig. IV-18) is a cup-like structure with an aperture through which the solar wind enters, a series of grids, and a segmented collector plate. All of the grids, with the exception of the modulation grid, are used to establish desired dc field conditions within the sensor. The modulator grid is the second grid from the input and, being always positive, causes incoming positive particles to experience a repelling field, since the first grid is maintained at instrument ground potential. Only those positive particles having sufficient initial velocity to pass the modulator grid will reach the collector plate. This allows the sorting out of particles, according to velocity, by the adjustment of modulator grid voltage. Actually, the instrument makes measurements of particle concentration in 32 overlapping velocity ranges (otherwise known as energy windows). This is accomplished by driving the modulator grid with a 2 kHz square wave (added to a dc voltage) whose upper value is a voltage sufficient to repel all particles having velocities within the desired window, and a lower value which passes all particles within the window. At the collector plate, therefore, there will be a modulated beam of those particles within the selected energy window. This is sensed as an ac current and processed by the electronics to finally result in an output that is related to the density of particles within the particular energy window. The nominal modulating voltage ranges from a square wave between 30 and 40 V to one between 7700 and 10,000 V.

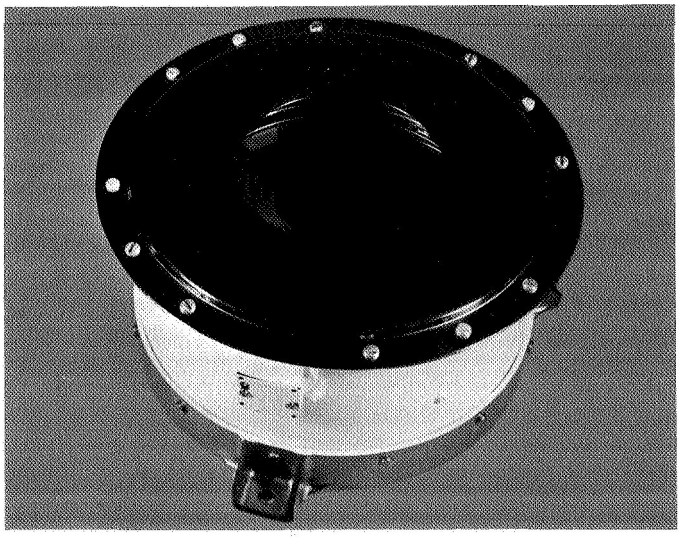


**Fig. IV-18. Plasma-probe sensor**

The instrument sequences through the energy windows under the control of the DAS which provides one stepping pulse every 2.1 s at the high data rate and every 8.4 s at the low rate. At each step, the DAS provides an interrogate pulse which reads the density at that step.

As previously mentioned, the collector plate is segmented, actually consisting of three 120-deg pie-shaped, electrically isolated sections. Each of these is provided with an independent signal processing channel up to a sampling point. By sampling each segment independently, it is possible to determine the direction of the incoming solar wind. The manner in which the instrument sequences through the energy windows was modified for the *Mariner V* mission, and is discussed in a later section.

*b. Changes from Mariner IV to Mariner V.* A number of modifications were made to the plasma probe to make it suitable for the different requirements of the Venus mission, and to take advantage of information gained from the *Mariner IV* flight. The flight unit (M67-2) was built from the *Mariner IV* flight spare which had operated for approximately 1000 h prior to modification.

*Configuration.* Since the *Mariner V* spacecraft is essentially inverted, with respect to sun direction, from the *Mariner IV* spacecraft, it was necessary to relocate the sensor with respect to the spacecraft. This, in turn, made it necessary to relocate the plasma electronics within the spacecraft so that proximity to the sensor could be maintained. For scientific reasons, the plasma sensor look direction was directly along the sun line rather than being tilted at a 10-deg angle as on *Mariner IV*.

*Temperature.* Since the solar intensity for a Venus mission is much greater than for a Mars mission, thermal control considerations became very important to the plasma sensor. Analysis and testing showed, however, that the plasma sensor could tolerate much higher temperatures than that to which it had previously been exposed, and that the temperature could be held within this range through the use of gold plating and thermal control paint.

*Sequencing.* The manner in which the instrument sequences through the energy windows was modified for the *Mariner V* mission. Two different sequencing modes were used, one for the cruise portion of the flight and the other only during encounter. The cruise mode sequencing is quite similar to that used in *Mariner IV* except that it is rearranged slightly. On *Mariner IV*, half of the energy windows were examined first with the collectors summed, then with independent collectors (Fig. IV-19(a)). The remaining half of the energy windows, interlacing the first, were then examined in the same manner. The *Mariner V* technique samples all of the energy windows with the collectors summed, then all with separate collectors (Fig. IV-19(b)). In this way, it is felt that there is less chance of solar wind conditions changing appreciably between overlapping summed collector readings. The calibration part of the sequence, which consisted of two groups of eight readings on *Mariner IV*, is one continuous set of sixteen readings on *Mariner V*. Because of this, a few of the steps in the calibration sequence are either redundant or unnecessary. These include the second noise measurement, the second temperature reading, the first reset zero, and both markers (retained in the measurement program to avoid modification of the calibration sequence logic).

The encounter mode sequencing was designed to provide increased energy information at the expense of direction information. This was accomplished by eliminating all separate collector sampling. A complete encounter mode sequence consists of two complete common collector samples followed by an eight-step calibration sequence (Fig. IV-19(c)). This sequence is identical to the second half of the cruise mode calibration sequence.

*Performance and reliability.* A number of modifications were made to improve the basic performance and/or reliability of the instruments. The *Mariner IV* instrument has operated properly well beyond its design lifetime with the exception of the failure of the high voltage bleeder resistor. This failure has been traced to a characteristic of the particular type resistor used. For *Mariner V*, this resistor was replaced with a series string of 15 resistors of a type known to be reliable. In addition to the use of existing reliability data, a test program was conducted which stressed the components in a manner similar to that encountered in flight, with no failures.

The design of the grids and their supporting structure within the sensor was changed to provide increased high voltage safety margins. This design effort included both analytical and experimental work. In addition, a few minor changes were made to the electronics to obtain small improvements, such as increasing the integration time constant to reduce the noise level.

*c. Test results.* During type-approval thermal-vacuum testing of the non-flight unit, a minor design problem was discovered. At low temperature the instrument failed to sequence properly. The problem was traced to a buildup of logic voltage due to diode voltage drops, and corrected through the addition of two compensating diodes. This modification was made to the flight units prior to flight acceptance testing.

No test-related problems were encountered during the flight acceptance testing of the two flight units. It was, however, necessary to partially repeat the FA test of the flight backup unit (M67-1) because the high-voltage cable was short.

Except for the high-voltage cable length, no integration problems were encountered between the plasma probe instruments and the spacecraft or other subsystems. At certain times during spacecraft testing, a condition arose which caused some concern as to the high voltage breakdown margins in the instruments. During these times, the instruments indicated high collector currents at the steps corresponding to the highest voltages on the modulator grid. This condition was seen during space simulator testing and also occasionally during normal spacecraft testing. In the simulator, high vacuum conditions existed, while in normal testing very dry air was provided for the sensor. After a number of special tests

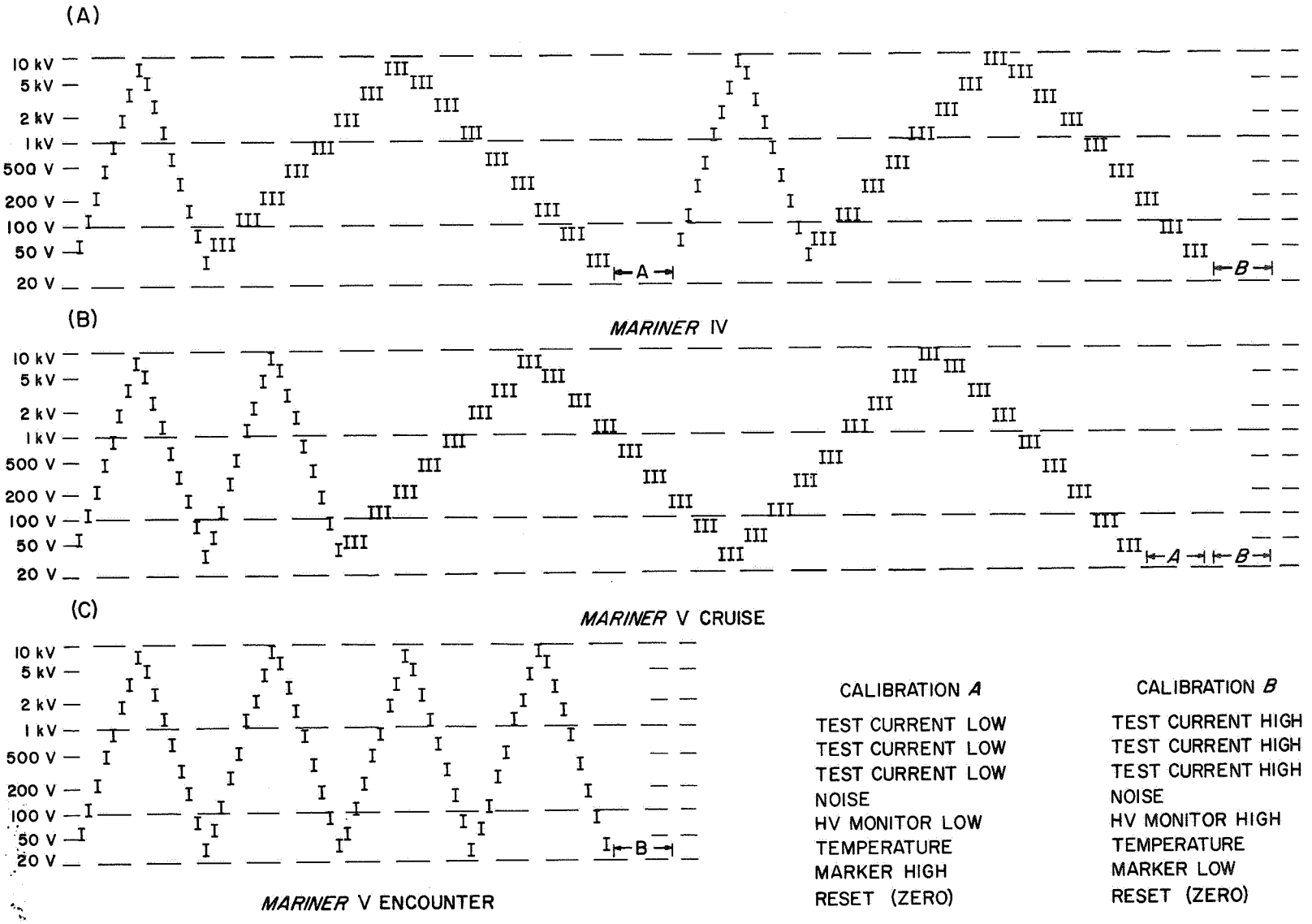



**Fig. IV-19. Plasma-probe measurement program**

it was concluded that the most likely cause of the anomaly was that under the test environments there was sufficient contamination within the sensor to give these results, and that, once in space, this condition would not exist.

***5. Dual-frequency receiver scientific objectives.*** The dual-frequency receiver (DFR) is the spacecraft instrument for measuring radio propagation effects in the dual-frequency radio occultation experiment. The experiment will measure the average interplanetary electron density and the characteristics of the atmosphere of Venus. Freqencies of 49.8 MHz and 423.3 MHz are transmitted from the 150-ft diameter antenna at Stanford University to the DFR. The receiver will measure the differential doppler frequency, differential group path, signal amplitudes and frequencies. Similar instruments are on *Pioneer VI* and *VII* spacecraft and are described in Ref. 8. A preliminary report on the *Pioneer* radio propagation experiment has been published (Ref. 9).

*a. Functional description.*

*Propagation parameters measured by the DFR.* Figure IV-20 is a functional block diagram of the receiver. Two phase locked loops with the same reference oscillator detect and track the received frequencies. The phase of the radio waves passing through an ionized medium is advanced by an amount directly proportional to the integrated electron density and inversely proportional to the frequency. The 423.3 MHz is relatively unaffected by the amount of ionization in interplanetary space. Thus, the relative phase shift due to the propagation path is determined by comparing the output of the voltage controlled oscillator (VCO) in each loop. The dispersive doppler frequency is determined by counting the VCO's beat cycles with the $\Delta f$ phase detector. The doppler frequency due to path length change must also be taken into account since it is additive to this effect. The frequency is counted and read out as word 20 of the science data format.

The two RF carriers are phase-modulated with an audio frequency of either 8692 or 7692 Hz. The modulation envelope is delayed by the dispersive medium so that a measure of the differential group delay is obtained from the phase shift of the modulation. The modulation phase detector contains two low-frequency phase locked loops. The low-frequency VCO outputs are phase compared to obtain the modulation-phase analog voltage. This voltage is subcommutated with four other analog voltages and read out as word 21 in the science data format.

The two carrier amplitudes' VCO frequencies are determined from the other subcommutated analog voltages. The analog voltage is changed to digital by an analog-to-pulse width converter in the DFR. Radio propagation effects on the amplitude and VCO voltages during the encounter will be observed at a higher data rate, stored by the spacecraft tape recorder, and played back after encounter.

*423.3 MHz channel.* The 423.3 MHz phase locked loop is shown in the upper left quadrant of Fig. IV-20. The antenna is a quarter wave stub with two reflector elements. The received signal is filtered by a low pass filter which isolates the DFR from the S-band telemetry subsystem. The signal is amplified and converted to the intermediate frequency of 24.9 MHz. The IF amplifier has a crystal filter with a $-3$ dB bandwidth of 45 kHz and a $-60$ dB bandwidth of 500 kHz. The filter determines the bandwidth of the IF amplifier and must be phase matched with an identical filter in the 49.8 MHz receiver to prevent introducing spurious phase shifts. A second mixer converts the signal to the second intermediate frequency of 7 MHz. This 7-MHz frequency is amplified, limited, and applied to the loop phase detectors. The audio frequency component goes to the modulation phase comparator, while the dc voltage is amplified in the loop amplifier and used to control the frequency of the local oscillator (i.e., the 31.9 MHz VCO).

*49.8 MHz channel.* The 49.8 MHz phase locked loop functions in the same manner as the 423.3 MHz loop. The 49.8 MHz antenna operates by shunt feeding the two adjacent spars of the spacecraft Bay I and Bay III solar panels. The antenna functional diagram is shown in Fig. IV-21. This band pass filter provides greater than $-30$ dB isolation from the S-band telemetry and IF amplifier frequencies. There is greater than $-50$ dB isolation from interfering signals at the image frequency. The 49.8 MHz signal is amplified and converted to the intermediate frequency of 24.9 MHz. The signal goes through the IF switch which is used to calibrate the receiver. When actuated by a calibrate pulse from the DAS, the IF switch connects the 24.9 MHz IF signal from the 423.3 MHz first mixer to the input of the 49.8 MHz IF amplifier. Calibrate occurs every 512 frames. The VCO in each loop should then be at the same frequency so the $\Delta f$ count goes to zero. There should also be no phase shift of the modulation so the zero degree point of modulation phase is calibrated. The IF amplifier, second mixer, loop phase detector, and VCO circuits are the same for both loops. The loop amplifiers have an appropriate lead-lag network for each loop.

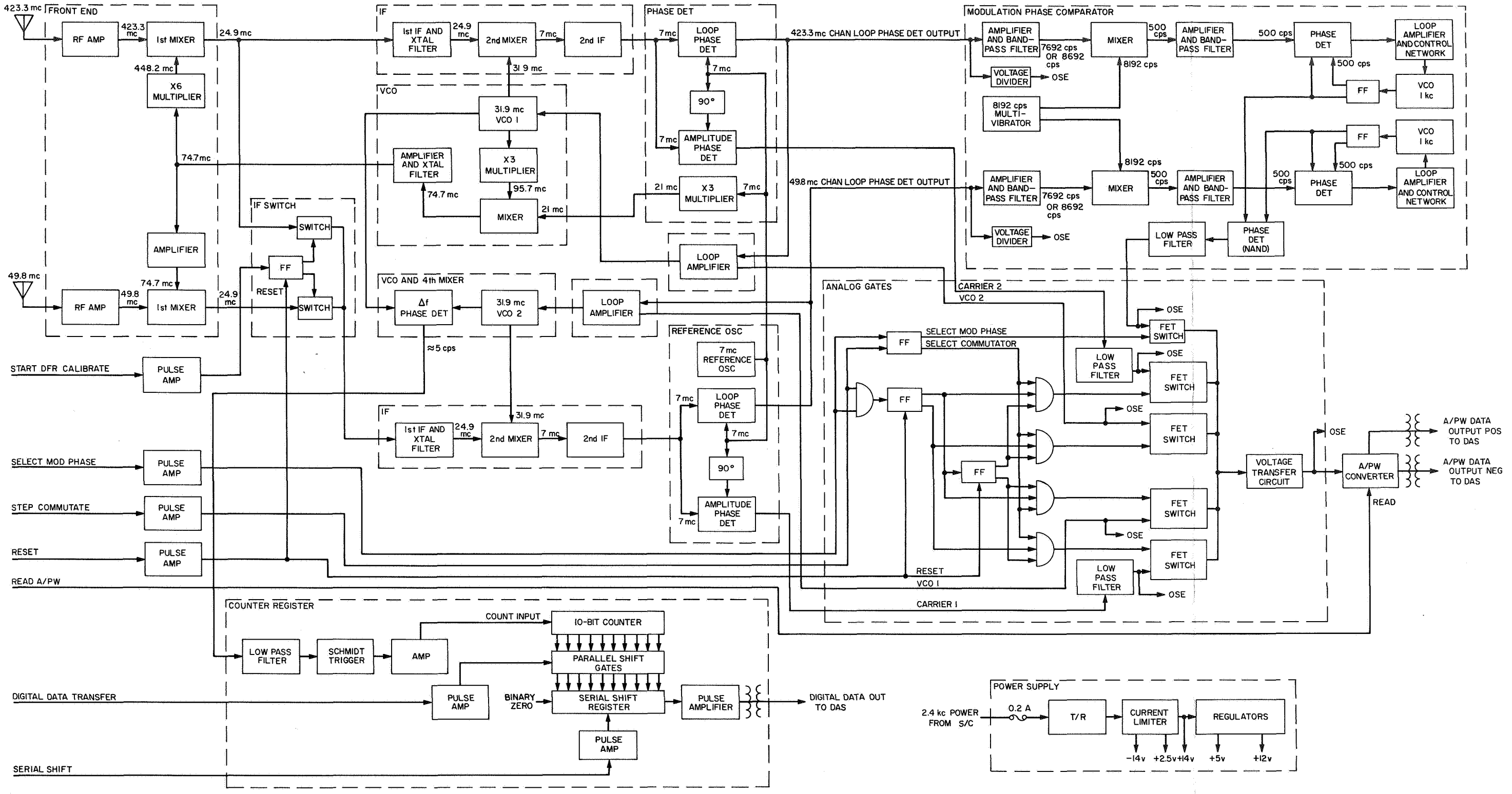



**Fig. IV-20. *Mariner* Venus 67 dual-frequency receiver block diagram**

**Page intentionally left blank**

PRECEDING PAGE BLANK NOT FILMED.

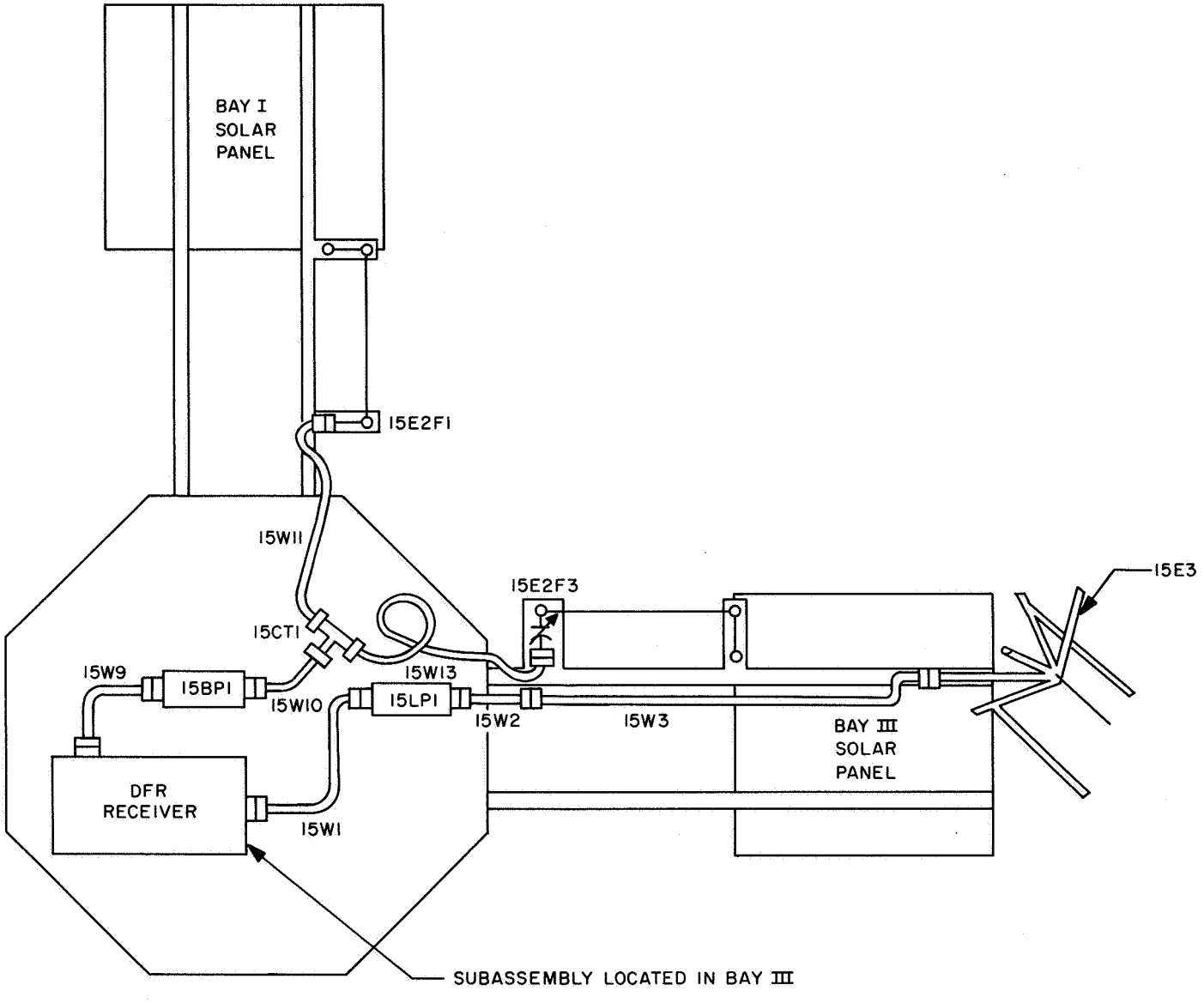



**Fig. IV-21. Dual-frequency receiver antenna subsystem functional diagram**

*Differential doppler frequency counter.* The output of the VCO in each loop is compared by the $\Delta f$ phase detector. This output is shaped by the Schmitt trigger and counted with the 10-bit counter. The content of the counter is transferred to the serial shift register where it is read-out by the DAS serial shift pulses. The 10-bit counter is not reset but simply recycles when the count $(2)^{10}$ is exceeded. The rate at which the counter overflows can be adjusted by adjusting the carrier frequencies at the ground transmitters. Normally $\Delta f$ will be offset by 5 Hz to enable detection of positive and negative excursions of $\Delta f$.

*Modulation phase comparator.* The block diagram of the modulation phase comparator appears in the upper right hand corner of Fig. IV-21. This circuit measures the relative phase of the detected modulation and provides an output proportional to the relative phase. An amplifier and band pass filter centered at 8 kHz precedes the mixer which converts the modulation signal to 500 Hz. The 500-Hz signal is filtered, amplified and fed to the phase detector. The phase detector output goes through the loop filter and dc amplifier to a 1 kHz voltage controlled oscillator. The VCO frequency is divided by two in the flip-flop which provides a 500 Hz signal for the phase detector and for phase comparison with the other channel. The 500-Hz signal from the phase locked flip-flop in each channel is compared in a digital NAND gate. The output is filtered to provide a dc voltage which is proportional to the relative phase of the modulation. When the modulation signal level approaches the threshold of locking the carrier loops, the comparator voltage changes as shown in Fig. IV-22.

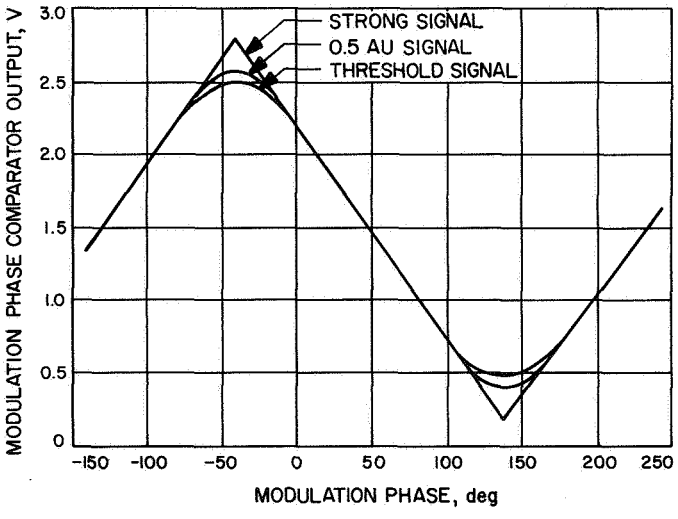



**Fig. IV-22. Volts output vs phase input of the modulation phase comparator**

*Subcommutator and analog data converter.* The subcommutator makes it possible to read out five analog voltages in one DAS word position. The select modulation phase and step commutator pulses from the DAS advance the subcommutation through the flip-flops and diode gates shown on Fig. IV-20. During the interplanetary cruise phase of the mission, the readout in each frame is identified by the three least significant bits of the DAS frame count in octal as follows (see Table IV-10):

**Table IV-10. Frame readout identification**

| DAS frame count | DAS word 21 |
|---|---|
| 1 | Carrier 1 (49.8 MHz) |
| 2 | Modulation phase |
| 3 | VCO 1 |
| 4 | Modulation phase |
| 5 | Carrier 2 (423.3 MHz) |
| 6 | Modulation phase |
| 7 | VCO 2 |
| 0 | Modulation phase |

During encounter, the DAS sends the DFR data to both the telemetry and the tape recorder. The tape recorder receives eight DFR analog words per real time DAS word. The subcommutation pulse sequence is the same for both cruise and encounter. The select modulation phase pulse occurs every other frame while the step commutator pulse occurs eight times per word. This allows every other frame to be a modulation phase and the intervening frames to sequentially read out the other DFR analog words in real time and to send DFR data at a higher rate to the tape recorder.

Field effect transistors are used for switching the analog voltages in response to the commands from the DAS. The command pulses are 120 ms apart (in groups of four) with a 240-ms interval following each fourth pulse. The analog voltage level is changed by the voltage transfer circuit so that the 3.0 to 6.5 V range is translated to a 6.0 to 0 V range. The voltage transfer circuit is required so that the maximum input to the analog-to-pulse width converter is not exceeded.

The analog-to-pulse width converter uses the ramp comparison technique (Ref. 10). The sweep begins when the trigger command is received. The sweep voltage is compared with the analog input in one comparator and with zero volts in the other channel. When equivalence is detected, an output pulse is generated in the appropriate channel. The time difference between the pulses is proportional to the analog voltage.

*Power supply.* The power supply converts the spacecraft supplied 2.4 kHz square wave power to the dc voltages required by the DFR. A current limiter circuit is required to reduce the peak turn on and short circuit current to less than 150% of the normal current. A series regulator in the +14 V supply is controlled by a resistor on the center tap of the power transformer and a balanced amplifier. The −14 and 2.5 V supplies have series regulators which control the current by comparing the voltage drop across the emitter resistance with the voltage across reference diodes. At turn on, the control amplifier is held off until the −14 V supply is on. This reduces the turn on transient since most of the load is on the +14-V supply. Series voltage regulators provide +12 and +5 V regulated sources.

*b. Vibration and thermal vacuum tests.* No major problems were encountered during the vibration and thermal vacuum testing.

*c. Electromagnetic interference tests.* Electromagnetic interference tests were performed with other subsystems and with the assembled spacecraft. The tests with the S-band transponder demonstrated the need for filters to ensure sufficient isolation between the two subsystems. The transponder traveling wave tube (TWT) power supply generated noise at 49.8 MHz but did not couple enough noise to cause a significant degradation on the spacecraft.

Special spacecraft tests were made to identify noise sources that would degrade the DFR performance. The power subsystem booster regulator (B/R) and battery charger, the DAS timing oscillator, the magnetometer ignition generator, the gas jet actuator, and the transponder power converters were noise sources at 49.8 MHz. Changes were made in the subsystems to decrease the noise. Subsequent system electromagnetic compatibility tests demonstrated that the sensitivity at 49.8 MHz was degraded by less than 1 dB. Thus, the EM compatibility development effort resulted in a lower RF noise level and acceptable performance for all the subsystems.

*d. System tests.* The system tests revealed two characteristics of the DFR operation that had to be taken into account when analyzing the data. The differential doppler frequency counter has a bit error rate of less than 0.5% which is due to the mechanization. If the counter receives a $\Delta f$ input pulse during the data transfer pulse, then, as the $\Delta f$ pulse ripples through the counter, it will transfer ones to the serial shift register. Thus, this reading will be $2^n - 1$ greater than it should be; however, the number in the counter is correct so the following readings are correct until the next simultaneous occurrence of the two pulses. The bit errors can be recognized and removed from the data so no design changes were made.

A cyclic variation in the DFR analog data was observed in the Track 2 or encounter mode. The design of the subcommutator and level converter causes the variation. Because the fourth commutation step is twice as long as the preceding three, there is a greater average load placed on the high impedance analog voltage source. Thus, the voltage readout in the fourth position will differ from that in the other three subcommutation positions. The observed variation matches the calculated value for the circuit. No design changes were made since the effect can be accounted for in analyzing the data.

***6. Data automation subsystem.*** The primary functions of a science data automation subsystem (DAS) are to control the operation of the scientific instruments, collect the data generated by the instruments, and format the data for transmission to earth via the telemetry channel and/or storage on the spacecraft tape recorder subsystem.

The spacecraft requirements placed upon the *Mariner V* DAS were originally the same as those on *Mariner IV*. Project constraints dictated a minimum change between the two missions. The data rates of 33⅓ bps in the near earth environment and 8⅓ bps in the near Venus environment remained the same.

The *Mariner V* DAS (Fig. IV-23) consisted of five integrated circuit logic subassemblies (Fig. IV-24), three discrete component subassemblies, one power converter subassembly, and ten analog-to-pulse width converter (A/PW) modules located in the scientific instruments. A total of 1114 discrete components and 566 integrated circuits were packaged in a volume of 565 cubic inches and weighed 15.35 lbs for a component density of 3 parts per cubic inch and 6.84 parts per ounce. Considering the specific discrete component equivalents for the integrated circuits used, the system had 41.5 parts per cubic inch and 95.5 parts per ounce. The DAS internal harness, not included in the above figures, contained 750 wires and weighed 4.50 lbs.

A diagram of the DAS and its interface with the various subsystems on-board the spacecraft is shown in Fig. IV-25. The inputs and outputs will be discussed only in general terms.

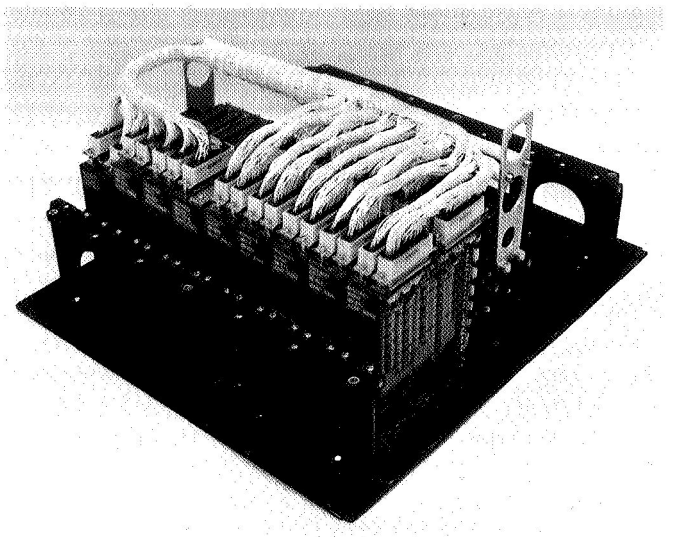


**Fig. IV-23. Data automation subsystem**

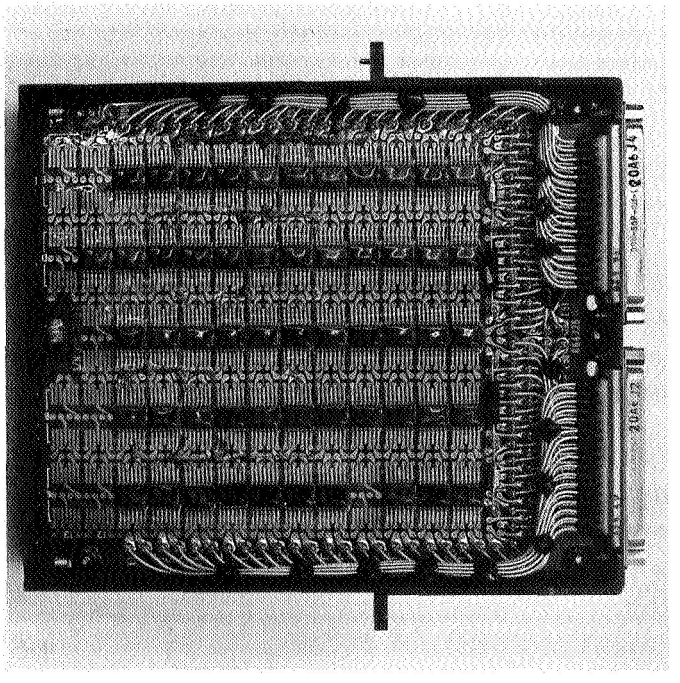


**Fig. IV-24. Integrated circuit logic subassembly**

*a. Inputs.* The major inputs to the DAS are data from the five scientific instruments shown on the left side of Fig. IV-25.

*b. Outputs.* The major outputs from the DAS consist of data which have been sampled from the various instruments and properly formatted. The two destinations for the data from the DAS are the data encoder, and the tape recorder subsystems.

**Table IV-11. Data automation subsystem real-time word description**

| Abbreviations | Data format word | Description |
|---|---|---|
| PN | 1, 2 | The 15-bit pseudo-noise sequence used to identify the beginning of each real-time data frame. The sequence is 000011101100101. |
| TRB | 23 | The readout of the B-channel count of TRD data accumulated in the 10-bit W-register. |
| TRH | 10 | The ten high-order bits (bits 11–20) of the T-counter assigned to the TRD. |
| TRL | 11 | The ten low-order bits (bits 1–10) of the T-counter assigned to the TRD. |
| UVA<br>UVB<br>UVC | 16, 30, 40<br>15, 29, 30<br>17, 31, 41 | The three sets of A/PW data from the UV photometer. |
| DFA | 21 | The A/PW data from the DFR. |
| DFD | 20 | The binary whole word digital data from the DFR. |
| FCH | 22 | The 9 high-order bits (bits 11–19) of the frame counter. Clock B is substituted in this word on alternate frames. |
| FCL | 28 | The 10 low-order bits (bits 1–10) of the frame counter. |
| MX | 7, 13, 25, 34, 37 | The A/PW data from the helium magnetometer X-axis. |
| MY | 8, 14, 26, 35, 38 | The A/PW data from the helium magnetometer Y-axis. |
| MZ | 9, 18, 27, 36, 42 | The A/PW data from the helium magnetometer Z-axis. |
| PL1<br>PL2<br>PL3<br>PL4<br>PL5<br>PL6 | 6<br>12<br>19<br>24<br>4<br>5 | The six sets of A/PW data from the plasma probe. |

*c. Telemetry data modes.* The four spacecraft data modes were designated as follows:

*Mode 1:* All transmitted data during this mode are of spacecraft engineering functions. No science data are present.

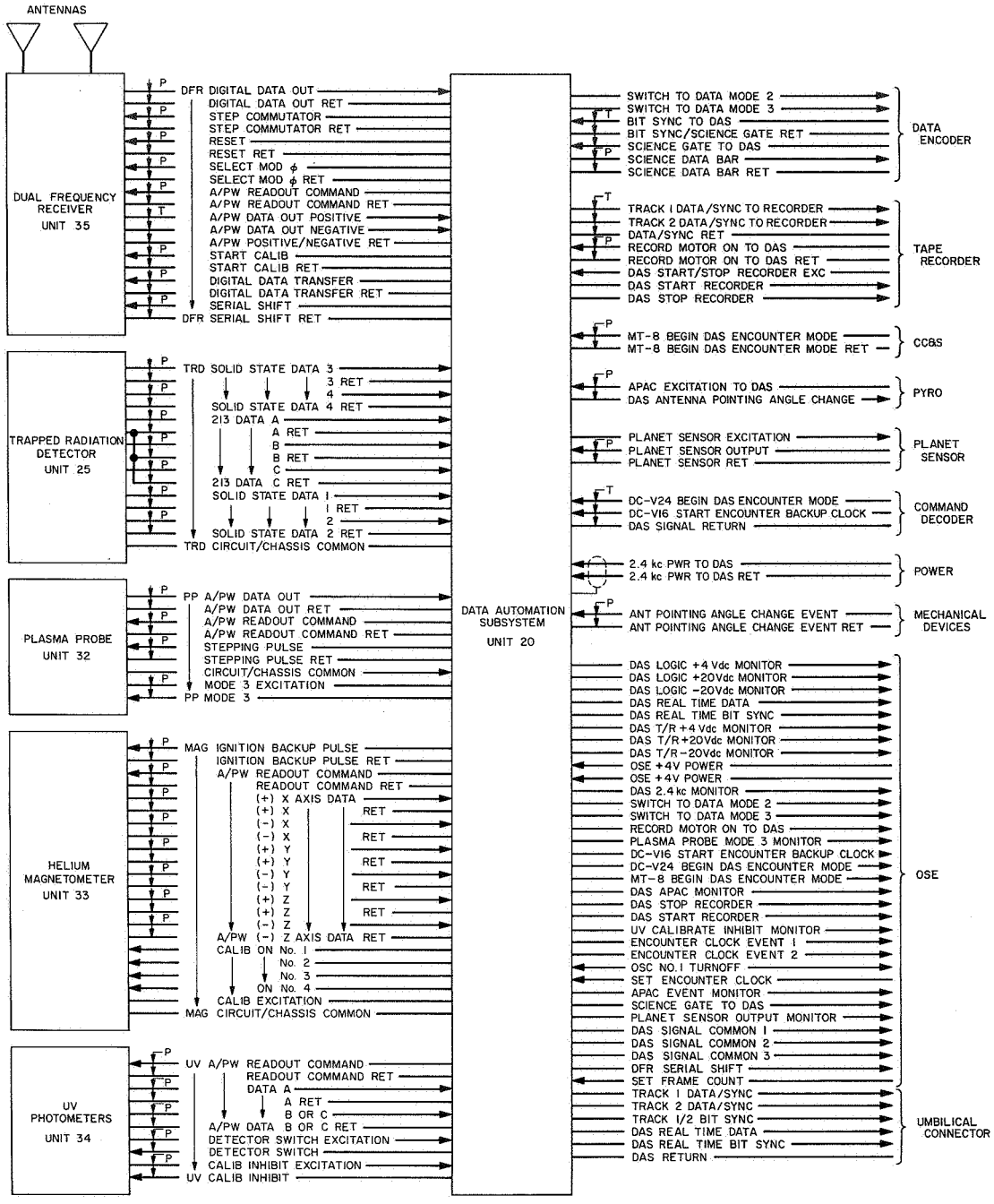



**Fig. IV-25. Data automation subsystem interfaces**

*Mode 2:* Cruise: Science and engineering share the telemetry channel during this mode. Each master data frame consists of 420 bits: 280 science and 140 engineering.

*Mode 3:* Planet encounter: Science has 96.9% of the available telemetry channel capacity; the remainder is used for engineering telemetry necessary to retain ground command capability near Venus.

*Mode 4:* Playback (post-encounter): The science data recorded during the encounter phase are played back from the tape-recorder subsystem during this mode.

*d. Real-time data format.* The DAS real-time (RT) data format is shown in Fig. IV-26. A description of the RT words is given in Table IV-11. The science data words are from 1 to 20 bits in length. However, the DAS word

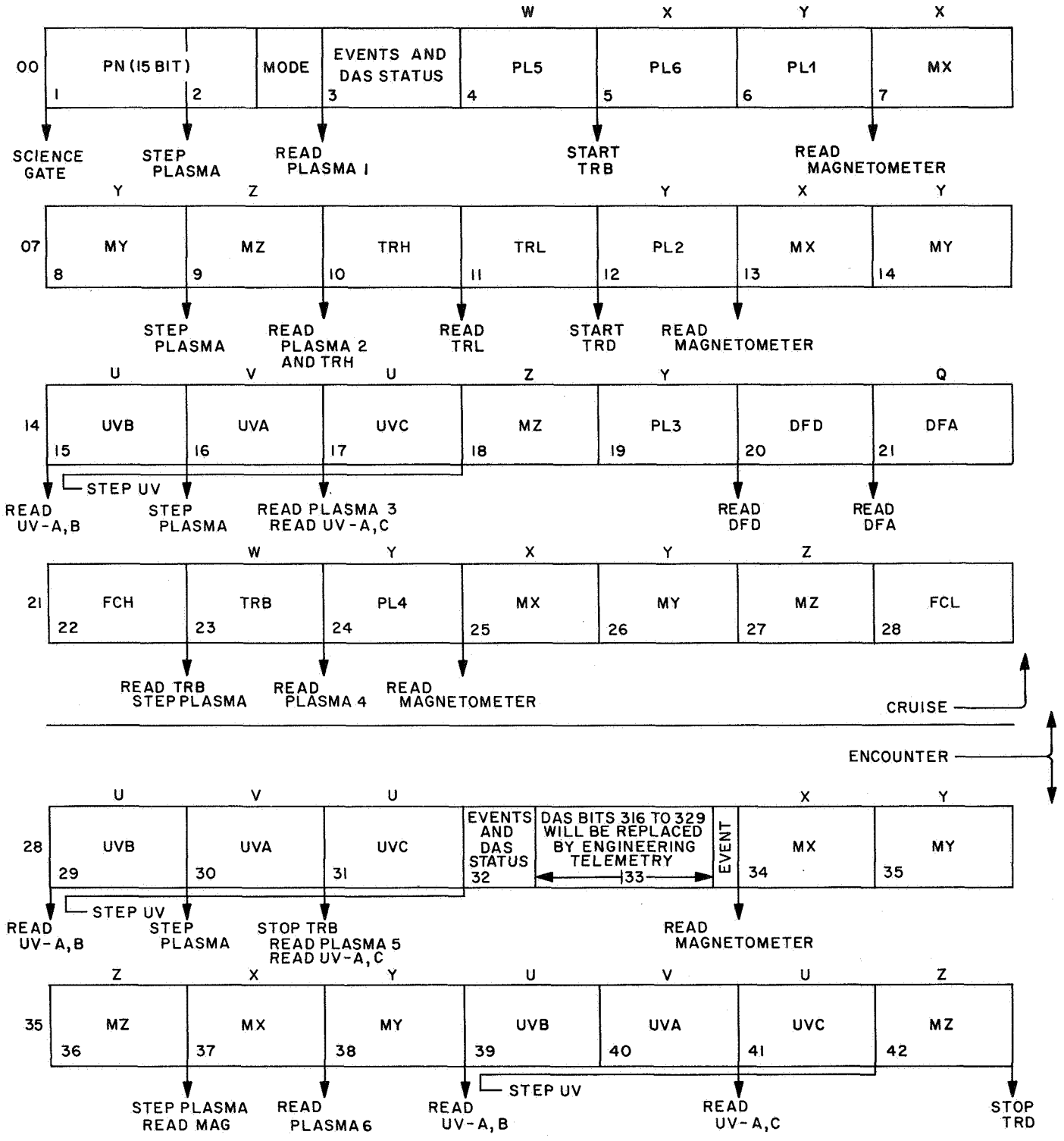



**Fig. IV-26. Data automation subsystem real-time data format**

length is 10 bits. There are 28 DAS words in the Mode 2 format and 40.5 DAS words in the Mode 3 format.

The DAS is mechanized in such a fashion that it always operates as though it were in Mode 3. Thus, the dormant encounter channels are sampled throughout Mode 2 even though the data encoder does not accept these 12.5 words. In this manner, the DAS operation need not be changed for Mode 3; the format is merely expanded by appending the 12.5 encounter oriented words.

Status bits are included in the RT format to indicate the time of receipt or transmission of certain functions and to permit evaluation of the DAS performance throughout the mission. A description of the DAS real-time status bits is given in Table IV-12.

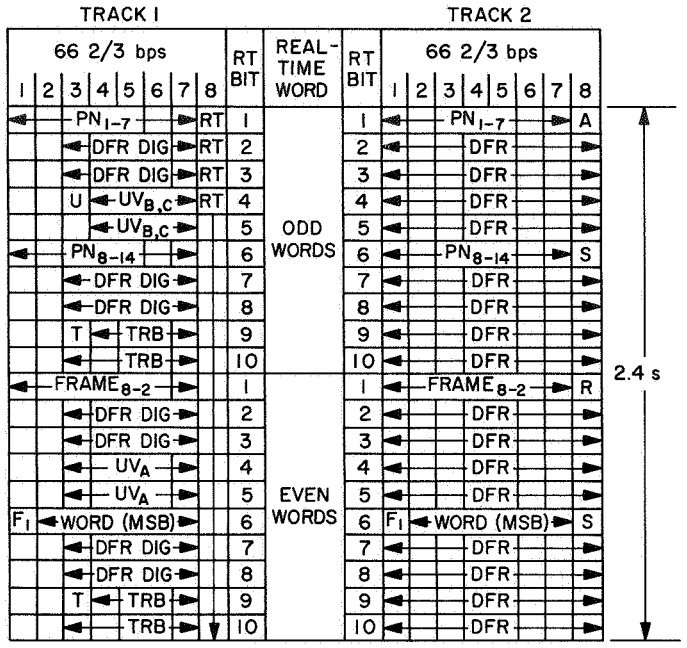
*e. Stored data format.* The type of information sent to the tape recorder subsystem and its format is shown on Fig. IV-27. The real-time telemetry words are shown in the vertical column in the center, and the ten real-time bits contained in each of the 42 words are shown in the columns to the left and right of center. To the left and right of the real-time bit columns are the eight recording bit intervals, shown horizontally.

*f. Internal system operation.* A block diagram of the overall internal system operation of the DAS is presented in Fig. IV-28. The flow of data in the DAS is generally from left to right on the block diagram. Most input signals are shown on the left side of the diagram as entering one of the 4 input-oriented functional blocks, i.e., sync interface, power converter, master controller, and input interface. In general, all inputs of the controlling type feed into the timing counter, where they govern the basic sequencing of the various counters.

The data inputs generally lead into pulse accumulators and counter registers, where the data are collected for

**Table IV-12. Data automation subsystem real-time status bits**

| Bit | Function | Notes |
|---|---|---|
| 16 | MT-8 | "1" indicates receipt of MT-8 |
| 17 | Clock "B" enabled | "1" indicates clock B will start upon receipt of PSO |
| 18 | DC-V16 | Toggles for each DC-V16 received during Mode 3 |
| 19 | PSO | "1" indicates PSO received |
| 20 | Mode 3 | "1" indicates DAS in Mode 3 |
| 21 | Magnetometer cal. #1/2 | Starts every 2049 frames; set cal. #1 (on for 4 frames), reset cal. #2 |
| 22 | Magnetometer cal. #3/4 | Set cal. #3 (on for 4 frames); reset cal. #4 |
| 23 | Power supply monitor high | 4 V supply > approximately 4.4 V |
| 24 | Power supply monitor low | 4 V supply < approximately 3.6 V |
| 25 | Magnetometer ignition | Status bit on for 64 frames; starts at 64 frames and repeats every 128 frames |
| 26 | Record motor ON | "1" indicates tape-record motor excitation ON |
| 27 | DFR calibrate | "1" during cal. (8 frames); repeats every 512 frames |
| 28 | DFR digital transfer | Change each frame |
| 29 | Not used | Always "0" |
| 30 | Not used | Always "0" |
| 31 | APAC event | "1" = antenna in post-encounter position |
| 41 | DFR step commutator | Change each frame |
| 51 | Step UV | Change each frame |
| 111 | Step plasma probe | Change each frame |
| 141 | DFR reset | Change each 8 frames |
| 151 | Read plasma probe | Change each frame |
| 161 | Read magnetometer | Change each frame |
| 181 | Read UV | Change each frame |
| 201 | DFR mod $\phi$ | Change each frame; "1" = DFA is mod $\phi$ "0" = DFR housekeeping |
| 211 | FCH/clock "B" | Change each frame; "1" = FCH, "0" = clock B |
| 231 | Read DFR | Change each frame |
| 281 | Clock "A" decode enabled | "1" = clock A decodes enabled |
| 291 | Planet sensor excitation | "1" = excitation applied to PS |
| 301 | Oscillator status | "0" = OSC A, "1" = OSC B |
| 311 | Start tape | Changes each frame when function active |
| 312 | Stop tape | Changes each frame when function active |
| 313 | Track 1 data | "1" = DAS sending data to Track 1 |
| 314 | Track 2 data | "1" = DAS sending data to Track 2 |
| 315 | Plasma probe mode 3 | "1" = PP Mode 3 |
| 330 | Not used | Always "1" |
| 381 | Not used | Always "1" |
| 391 | APAC | "1" = Command sent to pyro |
| 401 | UV calibrate inhibit | "1" = UV cal. inh. on |




THE DATA FOR DFR, UV AND TRB IS RECORDED MSB FIRST, LBS LAST.

$PN_{1-7}$ = BITS 1-7 OF 15-BIT PN SEQUENCE (0000111)
$PN_{8-14}$ = BITS 8-14 OF 15-BIT PN SEQUENCE (0110010)
$FRAME_{8-2}$ = FRAME COUNTER, LEAST SIGNIFICANT BITS 8-2
$F_1$ = FRAME COUNTER, LEAST SIGNIFICANT BIT 1
TRB = TRAPPED RADIATION DETECTOR, DATA B
DFR DIG = DFR DIGITAL DATA
DFR = DFR ANALOG DATA
$UV_A$ = UV, DATA A
$UV_{B,C}$ = UV, DATA B OR C
RT = REAL-TIME DATA
S = APAC STATUS BIT
A = ONE IF DFR-A IS NEXT RECORDED WORD
U = "1" IF $UV_{B,C}$ IS $UV_C$
T = "1" IF TRB IS TRB:
"0" IF TRB IS PL-5
WORD (MSB) = COARSE WORD COUNT:

| RT WORDS | WORD (MSB) |
|---|---|
| 1 - 7 | 100000 |
| 8 - 14 | 010000 |
| 15 - 21 | 001000 |
| 22 - 28 | 000100 |
| 29 - 35 | 000010 |
| 36 - 42 | 000001 |

BLANK SPACES = ONES ON TRACK 1
R: STATE CHANGE INDICATES LAST 8 DFR ANALOG WORDS WERE ACDE BCDE AND THAT THE NEXT 664 WORDS ARE IN THE BCDE SEQUENCE

**Fig. IV-27. Data automation subsystem stored-data format**

further processing. The various states of the controlling timing counters are decoded in the timing matrix. The outputs of the timing matrix, which represent decoded states of various control counters, are then routed either to the command matrix or directly to the dump matrix. The function of the command matrix is to provide the required combinations of the various decoded counter states. The control signals which constitute the outputs of the command matrix are generally routed back to the dump matrix. The function of the dump matrix is to use the control signal originating in the timing and command matrixes to sequence the data being routed to the shift register. The data in the shift registers are then serially shifted out to the data encoder and the tape recorder subsystem.

*g. Payload requirements.* Encounter constraints required the DAS to acquire approximately 16 times as many bits as could be transmitted to earth in real time (RT). This required modifications to enable the spacecraft tape recorder to record two parallel channels at 66⅔ bps. The data sampling rates for the various instruments were as follows (samples per RT frame of 50.5 s):

| Instrument | Cruise (Mode II) | Encounter (Mode III) | Recorded |
|---|---|---|---|
| TRD | 2 | 2 | 42 |
| Plasma | 6 | 6 | None |
| DFR | 2 | 2 | 420 |
| Magnetometer | 3 | 5 | None |
| UV photometer | 1 | 3 | 42 |

The DAS was also required to send commands to the scientific instruments and other spacecraft subsystems to change their mode of operation between cruise and encounter. These commands included inhibiting the ultraviolet photometer calibrate sequence, placing the plasma probe in Mode III, switching the data encoder to Mode III, starting and stopping the tape recorder, supplying power to the planet sensor, and a back-up command for the antenna pointing angle change at mid-occultation.

*h. Functional design.* The functional design of the *Mariner V* DAS was directed by the decision that there be one DAS vs the separate real-time and non-real-time DAS's on *Mariner IV*. Since the same instruments are operated during cruise and encounter, the DAS would always sample the instruments as though it were in the encounter phase of the mission and only output some of the data during cruise. Therefore, the only additional functions required of the DAS during encounter have to do with switching instrument modes and data storage, plus a back-up command (to that from the terminator sensor) to reposition the high-gain antenna during occultation.

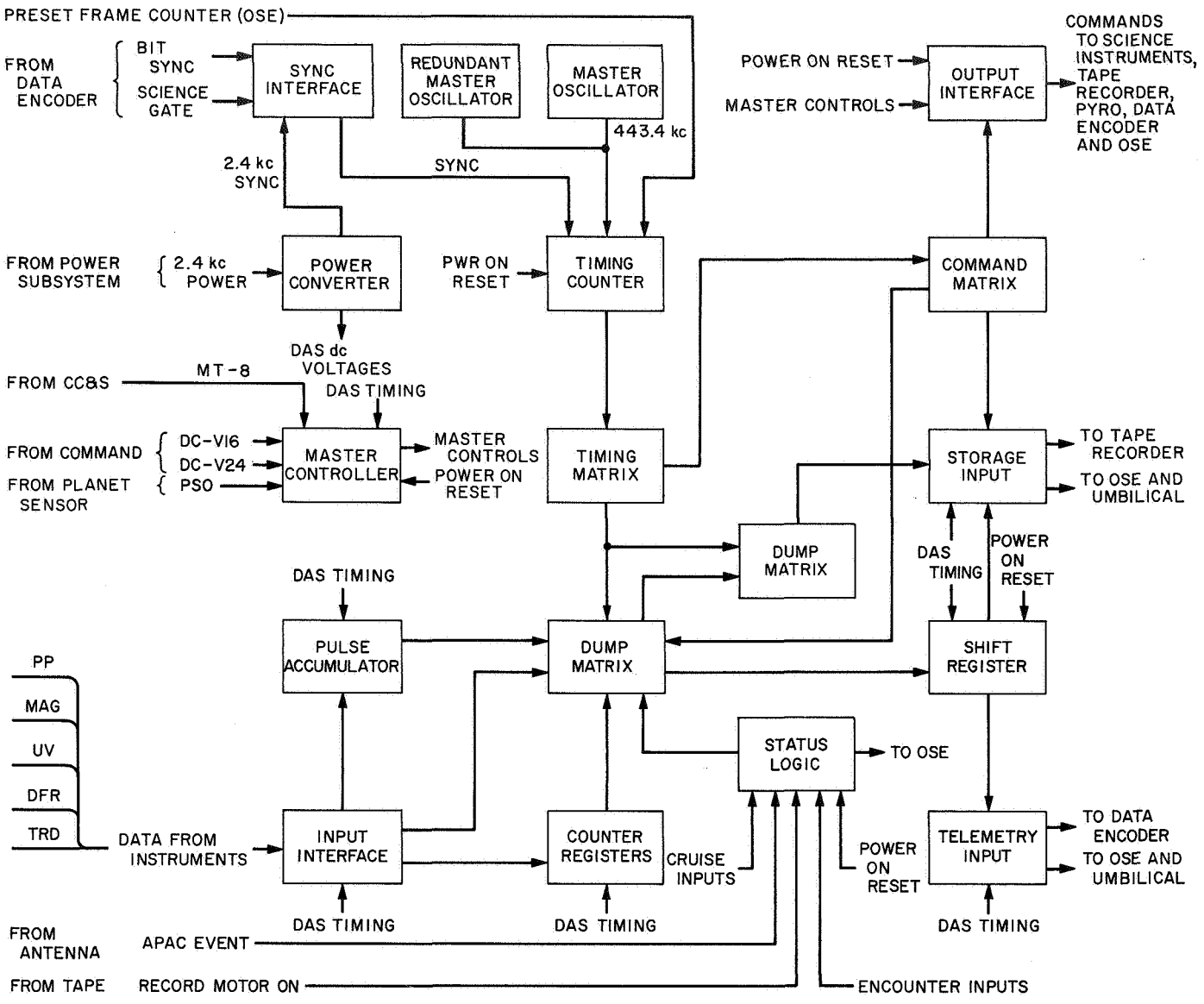



**Fig. IV-28. Data automation subsystem functional block diagram**

*i. Logic type.* The *Mariner IV* weight and volume requirements of 34 components per cubic inch and 56 components per ounce dictated a logic family of 29 module types and the resulting procurement and spares logistic problems. The development of a standardized logic family was initiated at the close of *Mariner IV*. This approach increased the system part count by 50% over *Mariner IV* due to a buffered output flip-flop which doubled the part count to achieve more drive and noise immunity. The replacement of "AND" and "OR" gates by "NAND" gates for uniformity of circuit and logic design techniques also added to this increase. The standardized discrete component circuits selected were similar to "off the shelf" integrated circuit designs. This standardized logic family was proposed for use on *Mariner V*.

*j. Integrated circuits.* The *Mariner IV* DAS used pellet components for the RT DAS and miniature components for the NRT DAS. The above parts were considered undesirable and in the case of pellets were unavailable for use on the *Mariner V* DAS. The number of discrete components to be procured, 23,446 per system for each of 5 systems plus spares (plus yield losses through screening) was staggering and considered impractical within the DAS schedule. Integrated circuits were considered to be inherently more reliable than the sum of the parts and

interconnects they replaced. It was estimated and later verified that the procurement and screening of integrated circuits would cost 1/10 that of discrete components. Based on the above constraints, the use of integrated circuits was proposed for the *Mariner V* DAS.

The implications were far reaching and included DAS contractor selection, system design constraints, electronic packaging, component procurement/screening, assembly processes, handling, troubleshooting and failure analysis.

Integrated circuit problem solving was a continuing effort throughout the DAS fabrication and test cycle. Twenty-three problem/failure reports were written against integrated circuits. These problems included:

(1) Handling problems which were solved by tooling and training.

(2) Static discharge and troubleshooting problems which were reduced through education and control.

(3) Failure verification problems, some of which were never solved.

(4) Product uniformity and physics problems which were identified and partially understood.

Recommendations on this subject include:

(1) More positive design constraints.

(2) In-circuit testing as a trouble-shooting aid.

(3) More powerful failure analysis tools.

(4) Process visibility as well as inspection at the manufacturer.

(5) Static discharge control requirements.

(6) A course for JPL engineers on "the care and feeding" of integrated circuits.

*k. Multilayer printed circuit boards.* A packaging scheme for an integrated circuit DAS required an approach tailored to accept close lead spacing and device form factor as well as a means for interconnecting discrete component interface circuits and satisfy weight, volume and maintainability requirements. Historically, data automation subsystems have been packaged in many varied configurations to satisfy mission dependent requirements of DAS functional design, technology and weight and volume requirements. However, none of the previous packaging schemes would satisfy integrated circuit packaging constraints.

Integrated circuit packaging approaches were studied which included: magnetwire sticks, welded cordwood modules, multilayer printed circuit boards and double-sided printed circuit boards. Multilayer printed circuit boards were selected as an integrated circuit interconnection scheme for the *Mariner V* DAS.

A program was initiated to qualify multilayer boards that satisfied DAS design requirements. Mechanical design constraints were documented and enforced which "designed in" the capability of changing interconnections after assembly by making all internal functions accessible. Etch cut and magnetwire rework processes were developed to incorporate changes. Development tests were conducted to demonstrate the ability of DAS designed boards to satisfy the environmental requirements.

*l. Multilayer printed circuit board process control.* The use of photomicrograph acceptance of plated-through holes was instituted to identify and control process variables. Holes were sectioned around the periphery of each board, two photomicrographs of the worst-case holes were submitted for acceptance.

During process verification, plated-through hole process problems became apparent. This was traced to excessive "etch back" and inadequate controls over tooling, solutions and current density during plating. The process variables were then investigated, fine tuned and controlled, and did not present a problem during flight fabrication.

Photomicrographs were demonstrated to be a powerful tool in the control of multilayer board reliability. There were no multilayer board problems at the subassembly level on the *Mariner V* DAS program.

*m. Subsystem testing.* System acceptance tests were conducted at ambient temperature with the DAS in a flight configuration.

Acceptance was verified by the bench checkout equipment (BCE). Temperature margin testing (0 through +55°C) was then initiated using the BCE and the PDP-4 computer checkout system. The PDP-4 provided a more comprehensive and timely test of the DAS by comparing actual events and measurements with their expected time of occurrence and values.

Upon the completion of the initial margin tests, all units underwent TA or FA testing as required and were again margin tested to detect any changes. After system level

testing, the two flight DAS systems were margin tested again prior to delivery to the Cape. The results of these tests showed that the system margins had changed by less than the resolution of the test equipment used.

*n. System testing.* Spacecraft level testing of the science subsystem began before delivery of a flight configuration DAS to JPL. Therefore, it was necessary to mate the breadboard DAS to the spacecraft. These initial tests revealed two major interface problems with the data encoder: (1) the leading edge of the bit sync at 8⅓ bps was too slow for proper DAS response (the data encoder side of the interface was modified to correct this problem), and (2) the DAS generated redundant bit sync was incompatible with the data encoder (this signal was removed from the DAS).

The most serious problem revealed during system tests was that the 112th harmonic of the DAS oscillator interfered with the 49.8 MHz channel of the dual frequency receiver. Because of this, the DAS crystal frequency was changed from 444.444 kHz to 443.406 kHz.

The integrated circuits used in the *Mariner V* DAS proved to have adequate noise margin. Two noise margin problems were experienced. One was minor and required a resistor change on a line from the OSE. The second problem was more serious and was the result of routing the expander modes of several gates through the DAS interconnect harness which caused significant noise pickup. This problem was overcome by R-C filtering of the expander nodes at the gate terminals.

During system testing, there were times when the status bits for some DAS generated functions would not change as predicted. The source of this difficulty was traced to nonstandard timing on science gate signals from the data encoder. These early science gates were caused by data encoder deck skips which shortened the frame time in increments of seven bits.

There was one integrated circuit failure. This integrated circuit failure was on M67-1 where the failure of a flip-flop caused the data stream to contain mostly zeros and also output an incorrect P/N sequence.

***7. Science operational support equipment objectives and requirements.*** The science operational support equipment (OSE) is nonflight hardware used to provide an overall check on the performance of the spacecraft science payload.

The science OSE objectives were:

(1) To verify that the science subsystem functions properly.

(2) To verify that there are no detrimental interactions with other spacecraft subsystems.

(3) To verify that the signal outputs of the science subsystem do not degrade from test to test.

(4) To provide basic troubleshooting instrumentation.

The primary requirements of the science OSE were:

(1) To provide stimuli for the science instruments which, as nearly as possible, simulate flight conditions.

(2) To monitor and record the outputs of the science DAS directly or through the spacecraft telemetry link.

(3) To record spacecraft science data in a format suitable for real-time analysis and for a permanent record.

(4) Display the science DAS output and the science instrument outputs independently for evaluation and comparison.

(5) Provide data outputs formatted for computer data reduction.

The secondary requirements of the science OSE were:

(1) To supply the spacecraft power and conditioned signals necessary for independent operation of the science subsystem.

(2) To time-tag or event-correlate all science data.

*a. Physical and functional description.* The science OSE consists of five consoles containing operational and test equipment plus peripheral equipment (Fig. IV-29). Table IV-13 lists all of the operational and test equipment that is used for the science operations.

More than 50% of the individual pieces of equipment were used in the *Mariner C* science OSE. A few noncommercial pieces were modified, and some were new designs to meet the *Mariner* Venus 1967 science data requirements. The same construction techniques developed during the *Mariner C* program (Ref. 11) were used for the modified and new equipment.

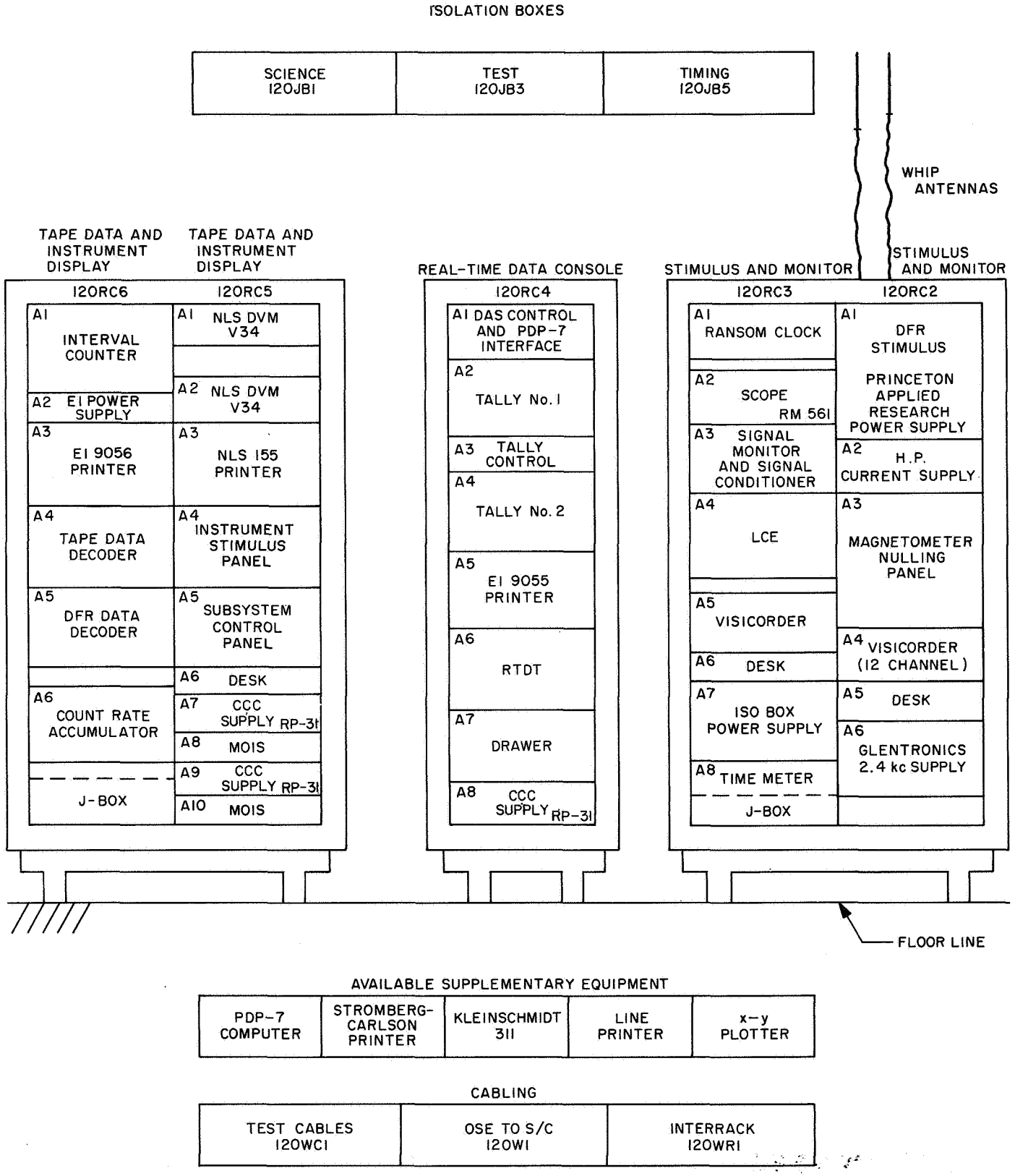



**Fig. IV-29. Operation and test equipment**

## Table IV-13. Test equipment functions

| Console chassis | Type of equipment | Used in conjunction with | Purpose |
|---|---|---|---|
| 120RC2 | Operational | DFR and magnetometer | Stimulus and monitor console |
| A1 | Operational | DFR | Stimulus |
| A2 | Test | All experiments | HP current supply |
| A3 | Operational | Magnetometer | Nulling panel |
| A4 | Test | Analog and UV | Visicorder (12 channel) |
| A6 | Test | All experiments | 2.4 kc power supply |
| 120RC3 | Operational | Function-monitoring | Stimulus and monitor console |
| A1 | Operational | Interval | Clock/step chassis provides timing to OSE |
| A2 | Test | Signal monitoring | Scope—RM561 |
| A3 | Test | All science function | Test jack panel for scope or DVM |
| A4 | Operational | LCE | Amplifiers |
| A5 | Test | DAS | Visicorder-event display |
| A7 | Operational | Isolation box | Power supply |
| A8 | Operational | DAS T/R voltages | Running time meters |
| A10 | Operational | S/C–OSE | Junction box |
| 120RC4 | Operational | DAS | Real-time data console |
| A1 | Test | DAS | DAS control and PDP-7 interface |
| A2 | Test | DAS | Tally No. 1 |
| A3 | Test | DAS | Tally control panel |
| A4 | Test | DAS | Tally No. 2 |
| A5 | Operational | DAS | *E1* 9055 printer |
| A6 | Operational | DAS | Real-time data translator |
| A8 | Test—OSE | DAS–OSE | CCC supply RP-31 |
| 120RC5 | Operational | Instrument monitoring | Tape data and instrument display console |
| A1 | Test | Signal monitoring | DVM-NLS V34 |
| A2 | Test | Signal monitoring | DVM-NLS V34 |
| A3 | Test | Signal monitoring | Dual printer-NLS 155 |
| A4 | Operational | Plasma probe and UV | Instrument stimulus panel |
| A5 | Operational | All experiments | Subsystem control panel |
| A7, A9 | Operational | CRA | CCC power supply RP-31 |
| A7, A10 | Test | Operations | MOIS-end instrument |
| 120RC6 | Operational | Instrument monitoring | Tape data and instrument display console |
| A1 | Operational | Trapped radiation | Interval counter |
| A2 | Operational | TRD DFR | *E1* power supply |
| A3 | Test | TRD DFR | Dual printer *E* 19056 |
| A4 | Operational | Encounter data | Tape data stripper |
| A5 | Operational | DFR | DFR data decoder |
| A6 | Operational | TRD | Count rate accumulation |
| A10 | Operational | Experiment–OSE | Junction box |
| 120JB1 | Operational | OSE to experiment | Science isolation box |
| 120JB3 | Test | OSE to DAS interface | Test isolation box |
| 120JB5 | Operational | TIU to OSE | Timing isolation box |
| 120SB2 | Test | UV photometer | UV stimulus |
| 120SB5 | Test | DAS | Data encoder and command decoder simulator |

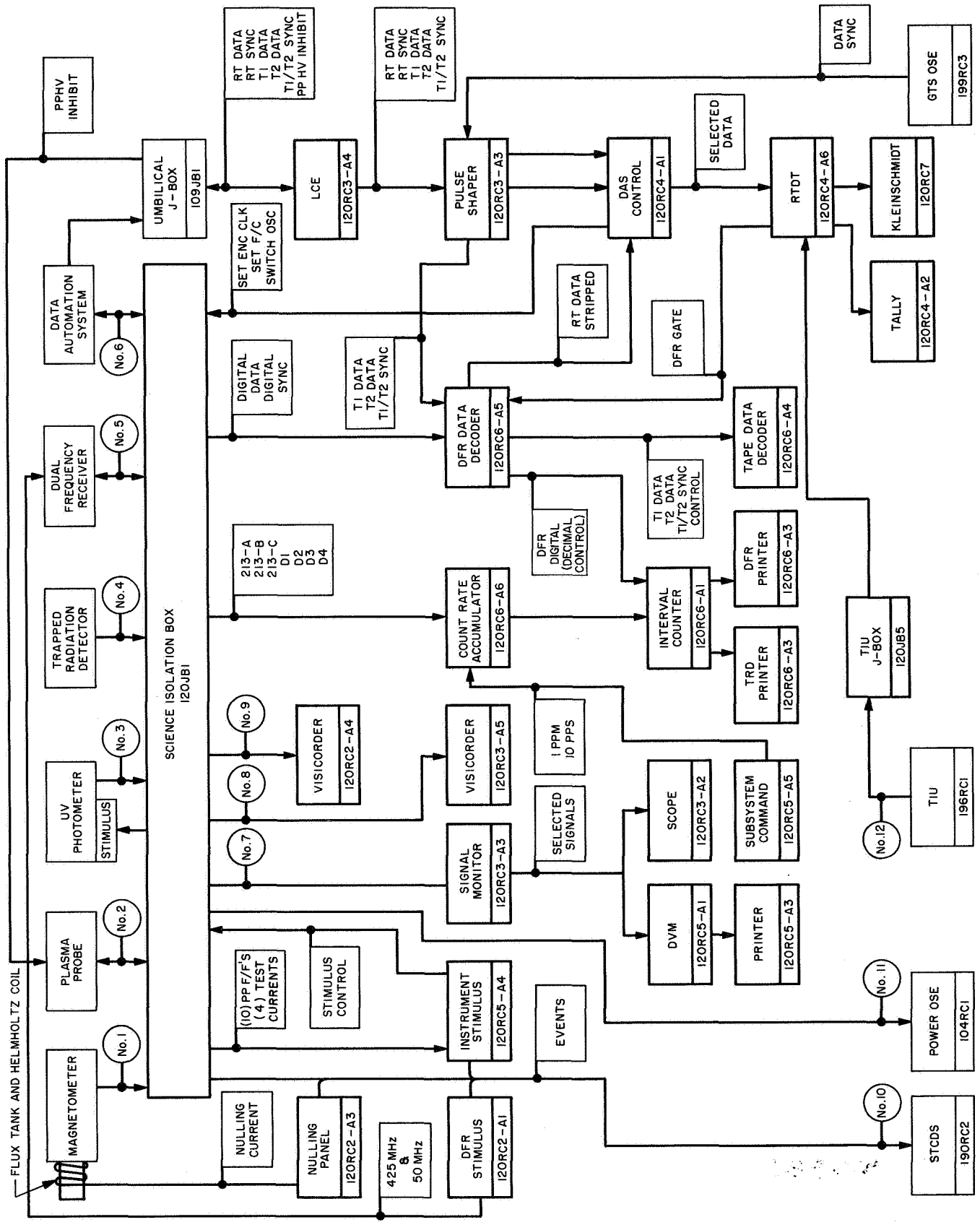



**Fig. IV-30. Functional block diagram of the science OSE**

The science OSE uses approximately 5 kVA of 120 V, 60-cycle power. Figure IV-30 is a functional block diagram of the science OSE that shows the flow paths of data, monitoring functions, commands, and the telemetry loop. Figure IV-31 is a simplified block diagram of the data compression process (provides an overall check of the science subsystem's performance).

*b. Design evolution.* A few changes in the science OSE were caused by modifications in the spacecraft data configuration, such as encounter science, and some were made because of experience gained from the *Mariner C* program.

*New designs.* The tape data decoder and DFR data decoder were designed to handle the new tape data configuration. These chasses, in conjunction, decoded and displayed the track 1 and track 2 data from the DAS umbilical or from the ground telemetry system (GTS). These chasses function mainly during encounter and playback.

A simple status display panel was designed to display visually the spacecraft status, especially during the encounter mode.

The change in the signal monitor panel was made primarily for simplification. The previous chassis that performed monitor switching functions used crossbar switches that were a source of many problems. The functions to be monitored by the modified panel were wired to test points and simple selector switches.

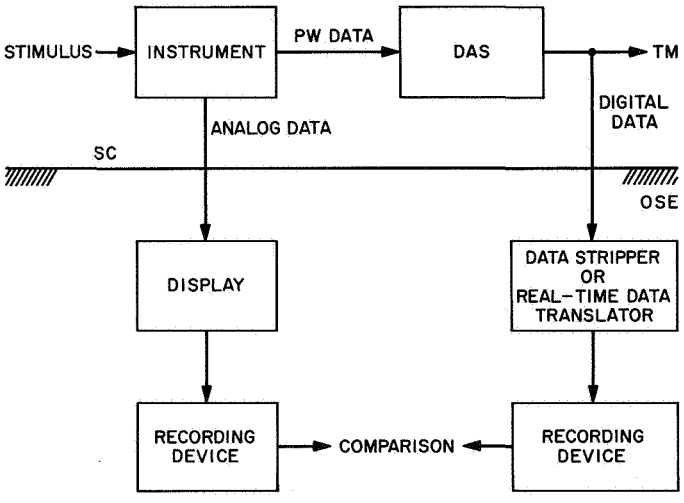



**Fig. IV-31. Science OSE simplified data-analysis process**

The isolation box and power supply were completely changed because of previous experience and because of the environmental requirements imposed by the *Mariner* Venus 67 program. The isolation amplifiers had a higher input impedance, and used silicon rather than germanium transistors.

The subsystem command panel and test isolation box were new designs because the equipment used on *Mariner C* was not suitable for modification.

Other newly designed equipment was the launch complex equipment (LCE) and the DAS control and PDP-7 interface. A new LCE was required because of the changes in the data that was routed through the umbilical cables. The DAS control and PDP-7 interface allowed the frame count and encounter clock functions of the DAS to be reset. The PDP-7 computer was never used for processing of science data, but the interface was used to tie two science OSE together during playback to allow one OSE to process real-time data while tape data was processed by the other.

*Modified designs.* Minor design modifications were performed on the instrument stimulus, interval counter and count rate accumulator chassis to update the equipment to the *Mariner* Venus 1967 instrument monitoring requirements. The design of the RTDT was modified and simplified because of the experience gained on the *Mariner C* program.

*c. Testing summary.* There were no major breakdowns or delays in spacecraft testing due to the science OSE.

*Subsystem testing.* Subsystem testing with the individual instruments was performed before interfacing with the spacecraft. The capability of operating the instruments without a DAS was not tried because of the early availability of the breadboard DAS. The PDP-7 computer processing of the science data was not used because of programming problems with the computer.

*Spacecraft operations.* Mechanical breakdown of the Kleinschmidt Printers was the main problem that kept occurring with the science OSE during operations. Four of these units were available and they were all used on the *Mariner C* program. Three of the units were sent back to the manufacturer to be rebuilt. There were still breakdowns, however, after they were rebuilt.

During early operations with the M67-1 spacecraft, the DAS had the frame count inadvertently reset several

times. The triggering threshold of the input circuit of the DAS was increased to reduce susceptibility to noise. The OSE driver circuits had to be modified to increase drive capability. Sometimes during operations the process of switching Kleinschmidt Printers would cause a power transient that would reset the DAS frame count.

A grounding interface problem existed during the entire program between the science OSE and the STCDS. Whenever the spacecraft was a distance away from the testing complex, it became necessary to tie the DAS common at the science OSE to the chassis common to accommodate the STCDS. Another grounding problem existed between the OSE and STCDS. Whenever any of the remote teleprinters touched the OSE consoles, the data in the computer would be garbled.

A noise pickup problem existed during operations in the ESF facility at AFETR. Four-hundred hertz spikes appeared on the umbilical real-time bit sync line. The noise caused the line drivers in the science LCE to trigger, creating extra or missing bit sync pulses. This problem had not been discovered before, nor did it exist later during operations on the launch pad. The science bit sync line is an unshielded conductor that lies next to the 400 hertz external power conductor in the umbilical cable. The noise spikes were reduced in amplitude below the triggering level of the line drivers by installing a 1 $\mu$F capacitor from the DAS common to chassis common at the LCE. The spacecraft grounding scheme used at the launch pad was different, and also the cables were not coiled together as at ESF.

A data-handling problem existed between the DFR instrument and the DAS. A modification was made to the DFR data decoder in the science OSE that allowed a more rapid display of the DFR digital data. This source of data was then compared with the DAS real-time output and the computer-processed data. A determination was then made of the source of the problem between the two subsystems.

*8. Test data handling procedures.* Processing during testing was accomplished by the real-time data translator (RTDT). The RTDT produced, via a high-speed character printer, an octal display of all the real-time science data. This was monitored for changes and events by the science data monitor whose duties included both data monitoring and keeping a complete log of science related events.

A data package that included the following was assembled at the end of each test:

(1) CDC 3300 console printout.

(2) CDC 3300 system test experimenters tape (STET).

(3) CDC 3300 alarm printout from the complex line printer.

(4) CDC 3300 science data listing from the off complex line printer.

(5) CDC 3300 character printer output.

(6) RTDT printout.

(7) Test director's log and science data monitor's log.

A log of the test complex events was assembled from items 1, 3, 5, and 7, punched on IBM cards and listed for multiple copies. Items 1, 3, 4, 5, 6, and 7 were booked and logged into the science data library. The STET tape was taken to the PDP-7 and used to produce further off-line outputs which, along with the log, were distributed to science personnel for subsystem performance evaluation.

*a. Experimenter's data tapes.* At intervals of approximately one week, data tapes were assembled for the experimenters. The tapes recorded after each test were stacked onto a single tape, duplicated and distributed.

*b. Experimenter's extract program.* To provide the experimenters with a tool for reading the test and flight-data tapes, a program was written which allows any computer capable of operating a Fortran IV program to extract any binary bit, or group of bits from the original data tapes onto a second tape which then contains only the data each experimenter decides he needs. Because the data tape formats were different in each case, slightly different versions for flight data and test data were necessary.

*c. Test data processing at Cape Kennedy.* The science data processing at Cape Kennedy, a phase of test data handling that presented a great problem during the *Mariner* Mars 1964 Project, resolved into almost a routine phase of activities. The reason was that the same computer system used for JPL test support also was used for AFETR test support. The magnetic tapes were stacked and sent to the experimenters as usual. One copy also was mailed to JPL where it was processed and distributed. The turn around for this was about 2 to 3 days.

*d. General discussion of science data processing.* The support provided science for system testing has been

very good. There remain, however, areas where improvement is yet called for.

*Non-Real time-computing.* The system test situation requires that data from experiments be processed, reduced, or re-formatted to provide adequate information for proper performance analysis. In general, a go/no go decision can be made with very little software and OSE outputs alone, but the detection of subtle problems requires either a massive, highly specialized OSE or proper software and computing support. The PDP-7 effort was the first such *Mariner* non-real-time system test data reduction support other than re-formatting.

*Suppressed data displays.* With the concepts used during the *Mariner* Venus 67 project, the processing of spacecraft data at 33⅓ bps represented a major problem. The key to handling other similar missions with doubled, quadrupled, or even higher rates is data suppression type displays and real-time computer alarm monitoring. As mechanized on the *Mariner* Venus 67 project, the system presented an excellent real-time capability; however, review of the real-time displays in non-real time was very difficult. The established format on the test complex line printer made it very difficult to maintain continuity between printouts of alarms on the same parameter.

The philosophy of displaying everything together on a one line printer to obtain correlation between events is valid, but a distinction should be drawn between data alarms and messages relating to hardware manipulation.

*Test logs.* One major problem area lay in providing the cognizant scientists and engineers with a complete log of spacecraft-system test complex events. A number of logs were available, all overlapping to some extent. A very real need exists for one complete log that does not contain any data-derived alarms or status. The CDC 3300 printout on the science TTY's was a start toward such a log. Unfortunately, when all OSE functions, commands, and other log items available as 3300 outputs were assigned to the TTY's, they were immediately swamped and lost messages. The design of future systems should take into account the fact that the times when an anomaly takes place are of greatest interest, and at such times computer event messages and alarms, etc. are generated at a much higher rate.

*Digital log tape.* Two log tapes were generated by the CDC 3300. The first contained a variety of messages including raw data word/time pairs. The second contained a de-commutated data frame (rather than data word) oriented format of science telemetry only.

## E. Telecommunications Subsystem Description and Development

*1. Dual-frequency receiver antenna subsystem.* The dual-frequency receiver (DFR) antenna subsystem was designed for the reception of signals at 49.8 and 423.3 MHz transmitted from earth to the dual-frequency radio propagation experiment on the spacecraft. This experiment was not included on the *Mariner IV* spacecraft and, consequently, the DFR antenna subsystem is new for *Mariner V* spacecraft. The subsystem consists of an antenna, transmission lines, and a filter for each frequency.

*a. Implementation of 49.8- and 423.3-MHz antennas.* The 49.8-MHz antenna consists of shunt feeding the two adjacent spars of the spacecraft Bay I and Bay III solar panels simultaneously through a power divider "tee" element. Unequal lengths of flexible coaxial cable connect the two arms of the "tee" element across the solar-panel hinges and along the adjacent spars to the feed units. Each feed unit is fixed relative to the respective solar panel, and the antenna is, therefore, deployed with the panels.

The tuning of the antenna was determined by the relative coaxial line lengths connecting the "tee" to the feed units, and by the adjustment of the series capacitor on the Bay III solar-panel feed unit. The tuning was such that the maximum antenna gain at 49.8 MHz was most nearly in the direction of earth at encounter. This direction is 104.0 and 102.5 deg in spacecraft cone and clock angle, respectively.

The 49.8-MHz antenna was connected to the dual-frequency receiver through two lengths of flexible coaxial cable and a bandpass filter. The 49.8-MHz antenna on a full scale spacecraft model is shown in Fig. IV-32.

The 423.3-MHz antenna consists of a stub radiator with two reflector elements over four ground plane radials. The ground plane radials are at 90-deg angles to each other and form a 120-deg conic angle with the stub. A dielectric bar extends from the antenna mast to the two radials with reflector elements for mechanical support.

The 423.3-MHz antenna is mounted on a mast at the tip of Bay III solar-panel spar. The entire antenna assemblage remains in a fixed position, relative to the solar panel, and is, therefore, deployed with the panel. The mast consists of aluminum tubing with an inner conductor, which connects to the coaxial cable center conductor to the antenna stub.

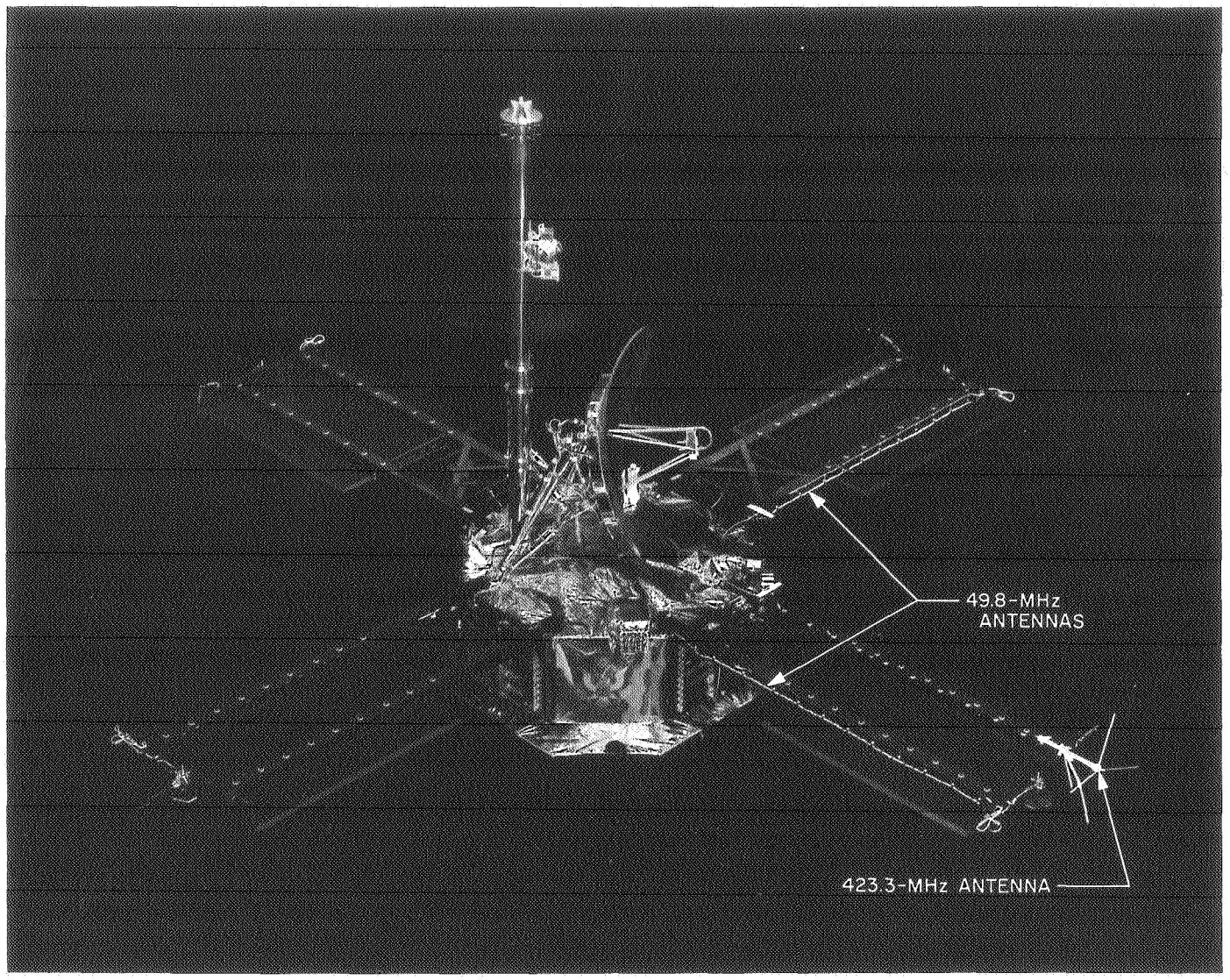



**Fig. IV-32. Location of DFR antennas**

The antenna was implemented such that the maximum gain at 423.3 MHz was most nearly in the direction of earth at encounter. The received 423.3-MHz antenna signal is passed along the solar panel through a length of semirigid coaxial cable and across the panel hinge through a length of flexible coaxial cable. The received signal is then passed through a low-pass filter and another length of flexible cable to the dual-frequency receiver. The 423.3-MHz antenna on a full scale spacecraft model is shown in Fig. IV-32.

*b. Electrical performance.* The final electrical parameters of the 49.8- and 423.3-MHz antennas are listed in Table IV-14. Radiation patterns for each antenna are shown in Fig. IV-33.

*c. Development.* During the preliminary design phase, the requirements and constraints were defined and different approaches were considered.

*Requirements.* The performance desired by Stanford University for the DFR antenna subsystem is summarized as follows:

(1) Gain (in the direction of earth at encounter, relative to linear isotropic).

  (a) 49.8-MHz antenna $\geqq 0$ dB.

  (b) 423.3-MHz antenna $\geqq +4$ dB.

(2) Pattern coverage. The primary pattern coverage requirement for each antenna is the minimum gain

**Table IV-14. Summary of DFR antenna parameters**

| Parameter | 49.8-MHz antenna | 423.3-MHz antenna |
|---|---|---|
| Gain (in direction of earth at encounter relative to linear isotropic) | +0.5 dB | +5.5 dB |
| VSWR (at center frequency) | 1.15:1 | 1.13:1 |
| Bandwidth (2:1 VSWR) | 0.95 MHz | 21.0 MHz |
| Cabling insertion loss (from gain measurement point to receiver, including filters) | 0.8 dB | 0.95 dB |
| Polarization | Linear | Linear |
| *Mutual coupling (minimum isolation* between antenna terminals) | | |
| at 2297.6 MHz from high gain | 57 dB | 62 dB |
| at 2115.7 MHz from high gain | 56 dB | 54 dB |
| at 423.3 MHz from high gain | NA | 79 dB |
| at 49.8 MHz from high gain | 70 dB | NA |

at encounter specified in item (1). The following was also requested: "The antenna pattern should contain no rapid variations or nulls within the envelope of expected look angles predicted for the period after one month after launch."

(3) Impedance.

(a) 49.8-MHz antenna: VSWR $\leq$ 2.01:1 over a bandwidth of at least 2%.

(b) 423.3-MHz antenna: VSWR $\leq$ 1.5:1 over a bandwidth of at least 2%.

(4) Mode of operation. Each antenna will be used for receiving only.

(5) Mutual coupling. The S-band power at the terminals of either DFR antenna should not exceed +20 dBm.

The experiment includes operation during occultation, which involves the change in the apparent direction (amplitude and frequency) of received signals due to refraction by the planet's atmosphere. It is desired that signals incident at the spacecraft from both sides of the planet be received at the dual-frequency receiver. Hence, a broad antenna radiation pattern was required. Since bending due to refraction is greater at 49.8 MHz than at 423.3 MHz, the pattern for the 49.8-MHz antenna must be broader than that for the 423.3-MHz antenna.

*Constraints.* The implementation of the DFR antennas could not degrade the spacecraft system in any way. This implementation included consideration of the S-band antenna operation and the maintenance of clear fields of view for the spacecraft attitude control and instrument sensor. In addition, the time allowed for design, development, fabrication, and testing severely limited the time available for investigation of various approaches. It was necessary to choose a design approach as quickly as possible so that schedule dates could be met.

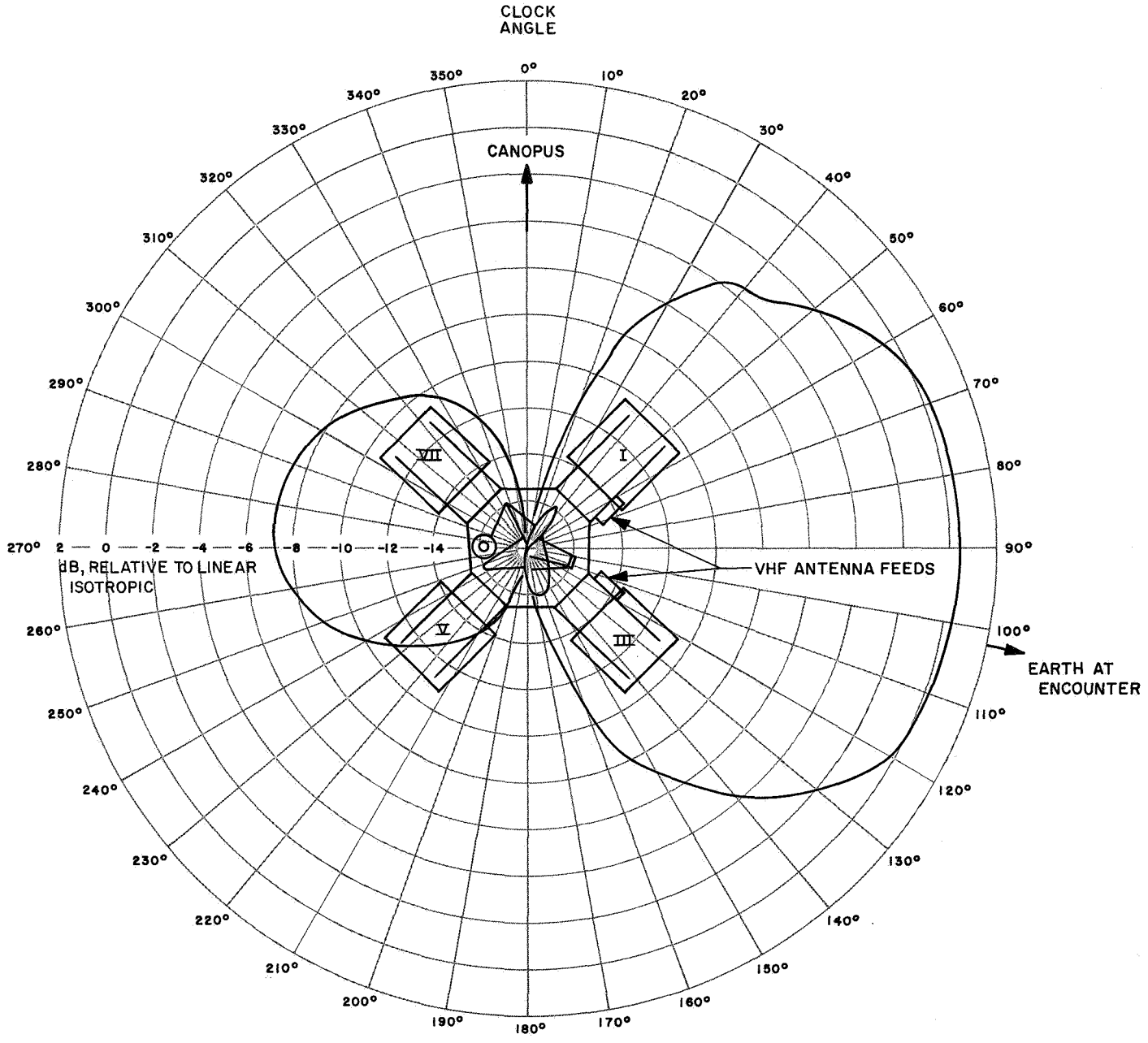
*Scaled model measurements.* Scaled models were used in the feasibility investigation and in the early design and development of the DFR antennas. During the initial phase, a 1:8.5-scale model spacecraft was used. Selection of the preferred approach was made during this phase. Later, a 1:5-scale model spacecraft was used for additional development and for comparison of results with those of the 1:8.5-scale model (Fig. IV-34).

The scaled model measurements could then be compared against the full-scale model results when they were obtained. This approach allowed a correlation between three sets of results, thereby increasing confidence in the final flight performance.

*Preliminary full-scale model measurements.* At the beginning of the final stages of the design development, measurements were made using a full-scale antenna test model (ATM) spacecraft. This model was a full-scale mock-up of the *Mariner V* spacecraft, but it had no flight parts. The fabrication of the full-scale test antennas was accomplished according to preliminary design drawings generated from the scale model results. A selection of coaxial cabling was also made at this time.

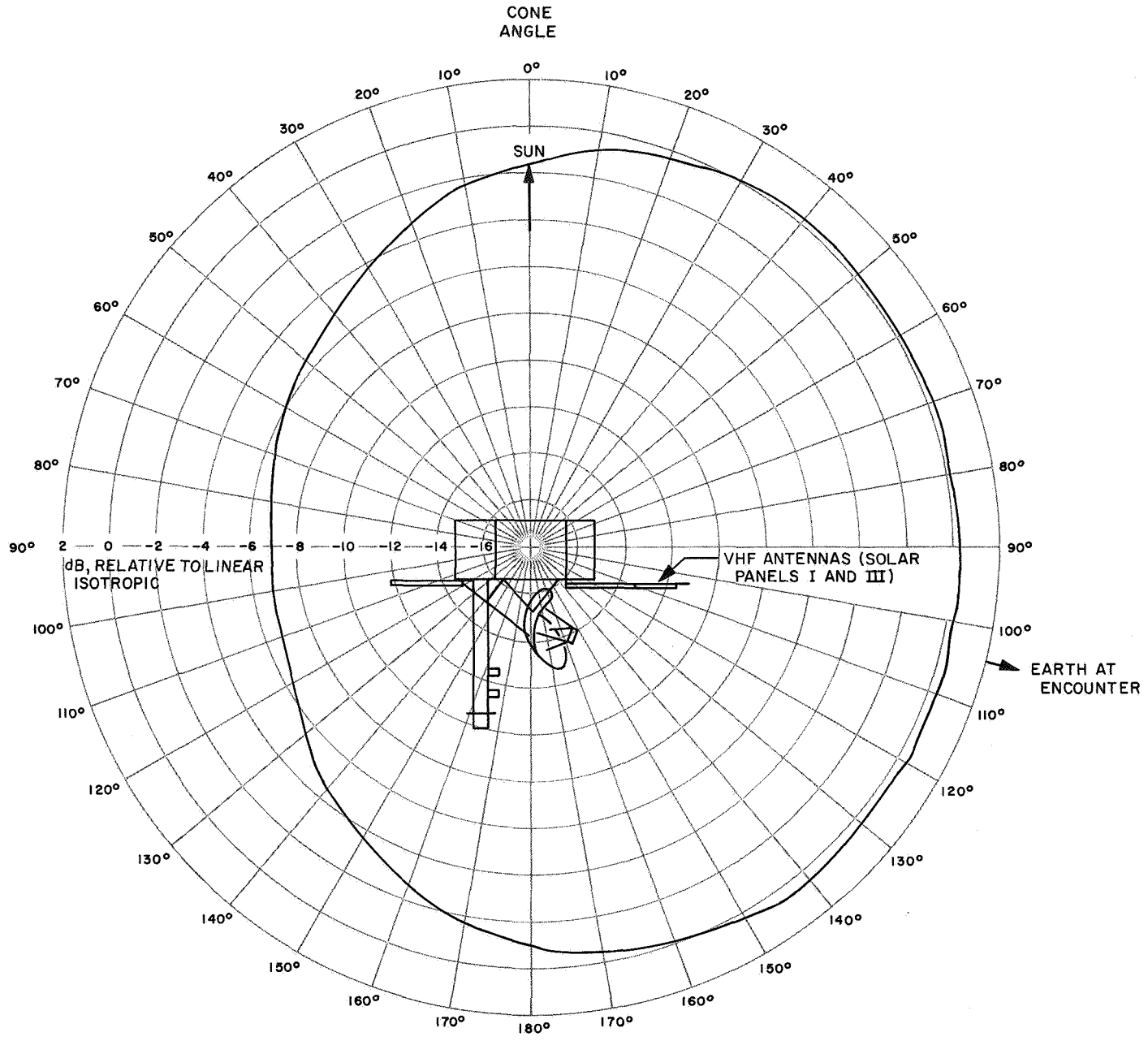
*d. Measurements of 49.8- and 423.3-MHz antennas, ATM spacecraft.* Because of the questionable value of full-scale measurements (other than VSWR) and the complexity involved in these measurements at 49.8 MHz, only VSWR measurements were initially planned. However, in view of the variable-tuned, dual-panel antenna selected, it was decided that full-scale gain and pattern measurements as well as VSWR would be accomplished. Linearly polarized illumination was used for the pattern measurements because of the unavailability of a circularly polarized antenna at 49.8 MHz.

The VSWR of the 423.3-MHz antenna was measured and the proper VSWR across the required bandwidth was achieved. A great deal of difficulty was encountered in obtaining 423.3-MHz pattern measurements free from severe multipath problems. Measurements of sufficient quality were made and the results showed satisfactory correlation with the 1:8.5- and 1:5-scale results. Circularly polarized illumination was used for the 423.3-MHz pattern measurements.



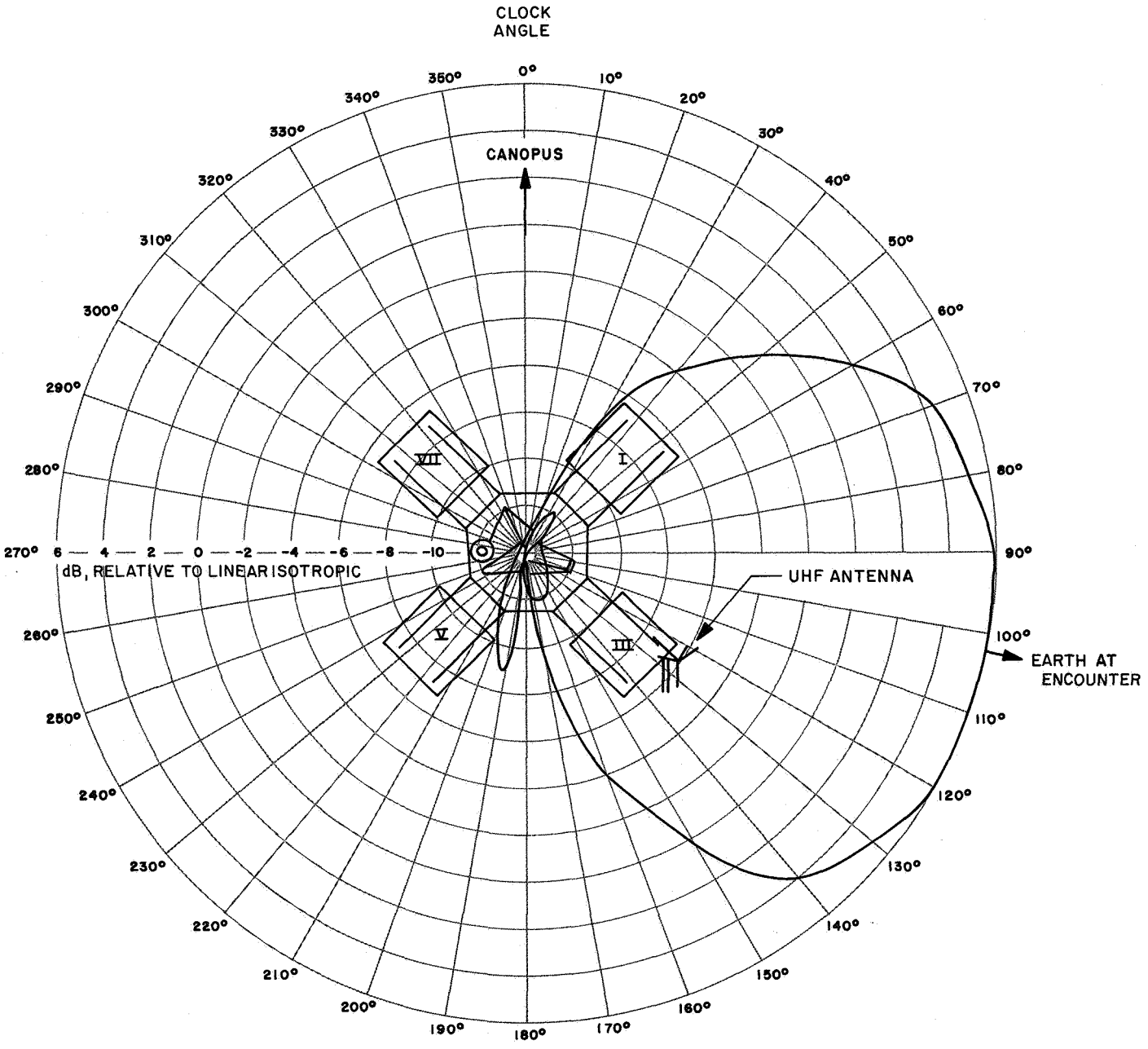

$f$ = 49.8 MHz
RIGHT-HAND CIRCULAR ILLUMINATION
PLANE OF PAPER AT CONSTANT SPACECRAFT
CONE ANGLE OF 90 deg

**Fig. IV-33. DFR antenna patterns**



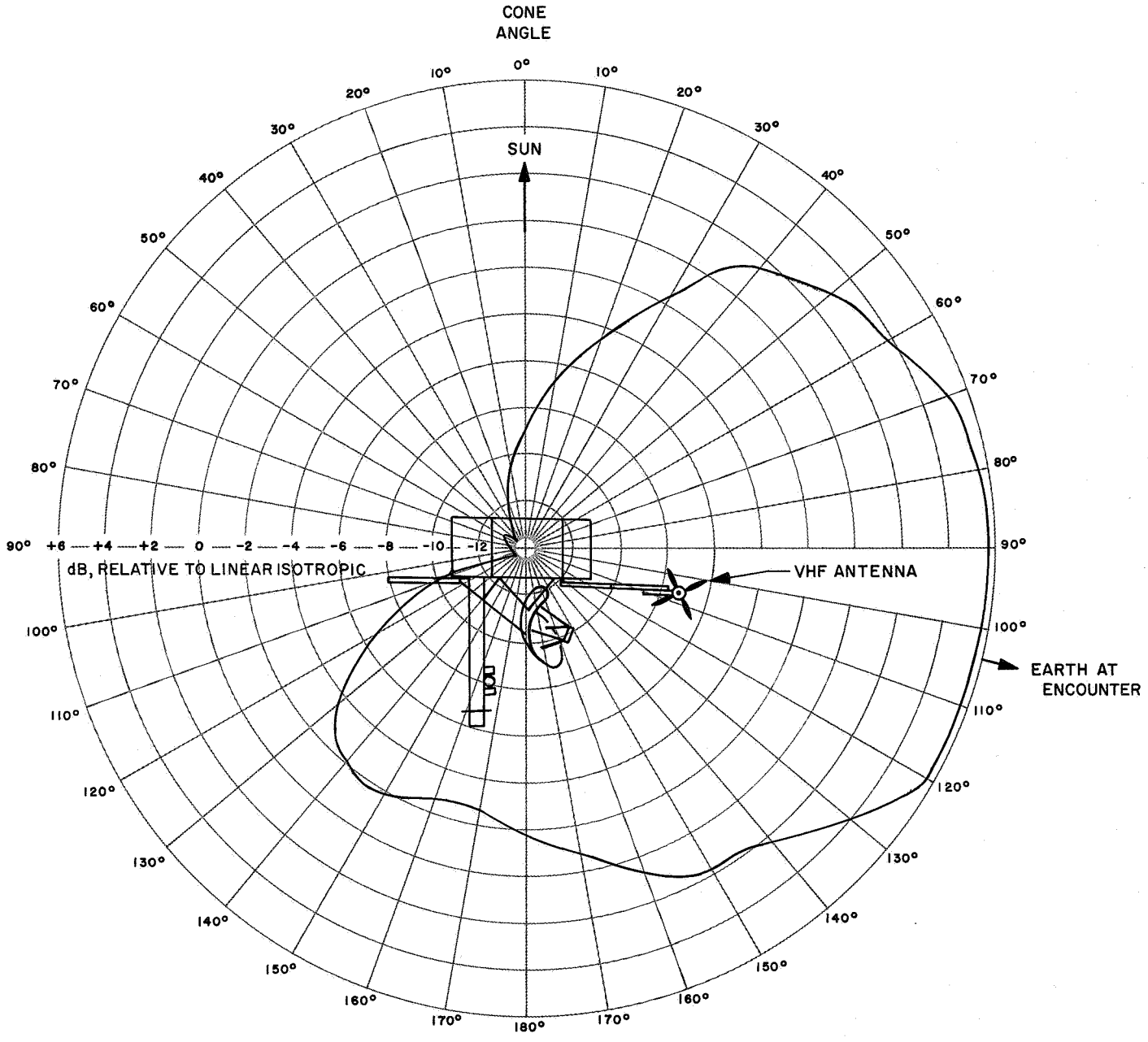

$f$ = 49.8 MHz
RIGHT-HAND CIRCULAR ILLUMINATION
PLANE OF PAPER AT CONSTANT SPACECRAFT
CLOCK ANGLES OF 100 AND 280 deg

**Fig. IV-33 (contd)**




$f$ = 423.3 MHz
RIGHT-HAND CIRCULAR ILLUMINATION
PLANE OF PAPER AT CONSTANT SPACECRAFT
CONE ANGLE OF 90 deg

**Fig. IV-33 (contd)**




$f$ = 423.3 MHz
RIGHT-HAND CIRCULAR ILLUMINATION
PLANE OF PAPER AT CONSTANT SPACECRAFT CLOCK ANGLES OF 105 AND 285 deg

**Fig. IV-33 (contd)**

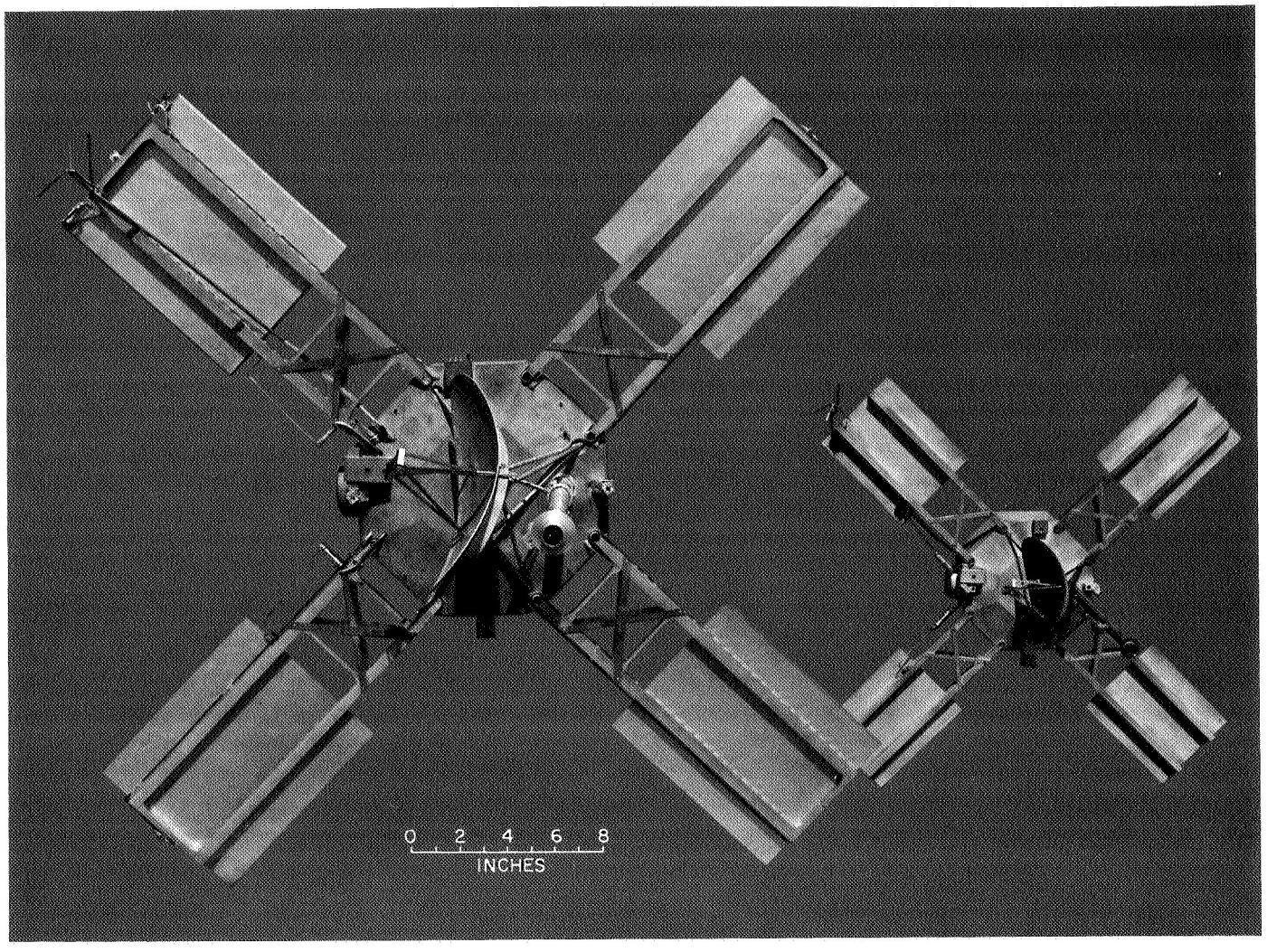



**Fig. IV-34. *Mariner* Venus 67, 1:5 and 1:85 scale model spacecraft**

*e. Mutual coupling measurements.* During the development phase, measurements of the isolation between the S-band and DFR antennas were made. The results of these measurements are presented in Table IV-14.

*f. Final full-scale measurements, DTM spacecraft.* Following antenna fabrication and completion of the required environmental tests, the flight-type antennas were measured on the developmental test model (DTM) spacecraft.

*Measurements of 49.8-MHz antenna.* Each of the four flight feed units was tuned on the DTM spacecraft. VSWR, gain, and pattern data were recorded for each set of feeds. The VSWR for each flight unit was equal to or better than 2.0:1 over a bandwidth of 0.95 MHz.

The gains varied from −0.2 to +0.6 dB, relative to linear isotropic. The patterns were recorded with linearly polarized illumination and were recorded only over a sector. These patterns showed that the peak of the beam was properly pointed and that there were no deep nulls in the vicinity of encounter. The flight gain data (Table IV-14) and the pattern data (Fig. IV-33) were estimated, based on the combined results of all model measurements.

The data recorded on the DTM spacecraft demonstrated repeatability in results between the ATM and a more flight-like DTM spacecraft.

*Measurements of 423.3-MHz antenna.* VSWR, gain, and pattern data were recorded for each of four flight antennas on the DTM spacecraft. The VSWR in each case was better than the required 1.5:1 over the desired bandwidth. Gain and pattern measurements were in good agreement with other model results. The gain of the flight antennas varied between +5.8 and +7.5 dB, relative to linear isotropic. Patterns were recorded with circularly polarized illumination to accurately represent the flight condition. The flight data recorded in Table IV-14 and Fig. IV-33 were determined from the measurements on the DTM spacecraft.

*g. Special tests.* Several residual problem areas existed following delivery of the flight qualified antennas. In the case of the 49.8-MHz antenna, verification of the proper tuning on the flight spacecraft and overall system operation was of concern. In the case of the 423.3-MHz antenna, verification of proper operation on the flight spacecraft was of concern.

*Tuning of 49.8-MHz antenna on flight spacecraft.* The method of exciting the spacecraft structure created the problem of obtaining performance repeatability between the scaled models and the flight spacecraft. This method further involved the problem of obtaining sufficiently accurate and repeatable measurements for verification of the performance.

The full-scale gain, VSWR, and pattern measurements for the ATM and DTM spacecraft provided a relative comparison between test model feeds on a rough spacecraft and the flight feeds on a more flight-like spacecraft. In particular, the method of tuning to place the peak of the beam in the proper direction was verified. This verification also indicated that performance obtained on the full-scale spacecraft model would be repeatable on the flight spacecraft. Therefore, the flight feeds were to be installed on the flight spacecraft after being tuned on the developmental test model spacecraft.

After the flight feeds were tuned at the antenna range, it was necessary to verify the tuning on the flight spacecraft. A preliminary check of the VSWR was made on the flight spacecraft in spacecraft assembly facility (SAF) during electromagnetic interference (EMI) testing. A set of test feeds was tuned on the DTM spacecraft at the antenna range and then installed on the flight spacecraft in SAF. The VSWR measurements were made with the flight spacecraft suspended 15 ft above the floor. These tests included the monitoring of the VSWR bandwidth on a scope with a reflectometry set-up. The VSWR in all cases remained the same as that measured at the antenna range.

*Final verification.* VSWR and radiative coupling measurements were made at the Cape for the 49.8-MHz antenna to verify that the feeds and cables were properly connected and that the tuning had not changed. VSWR and radiative coupling measurements were also recorded for the 423.3-MHz antenna at the Cape to verify proper cable connections and operation.

The coupling measurements were performed by radiating 49.8- and 423.3-MHz signals at varying levels to the appropriate spacecraft antenna from a test antenna located close to the spacecraft. The received signals were translated to data numbers and retrieved from the spacecraft via the S-band telemetry link for evaluation.

***2. S-band antenna implementation.*** At the inception of the *Mariner* Venus 67 project, it was clear that the

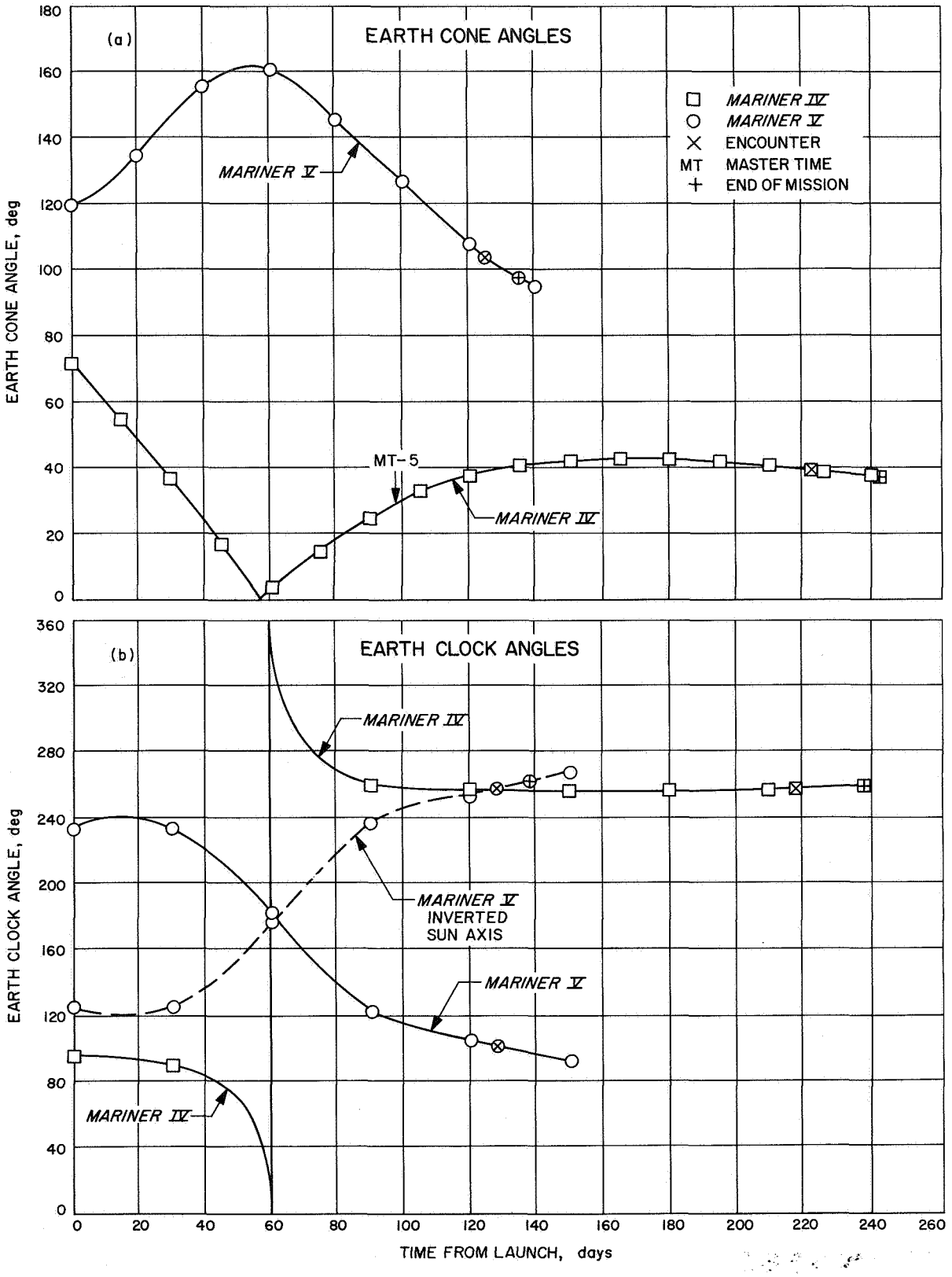



**Fig. IV-35. Comparison of *Mariner V* and *Mariner IV* look angles**

antenna subsystem implementation would present a difficult design problem primarily due to the incompatibility of the directionality of the spacecraft antenna patterns of the *Mariner IV* antennas and the *Mariner* Venus 67 mission trajectory look angles to earth (Fig. IV-35). From this figure, it may be seen that the *Mariner IV* and *V* trajectories put the earth look angles on opposite sides of the spacecraft.

This placement of these angles would not have been a difficult problem if only telemetry and command requirements had to be met, since the encounter range (Fig. IV-36) of Venus is only 80 million km, whereas it was 222 million km for Mars in 1965. Hence, for the Venus encounter, the antenna gain required would be about 9 dB less than that for *Mariner IV* at Mars. If this antenna gain, then, was the only requirement, the encounter antenna coverage could be accomplished by a relatively small antenna that could have been packaged on the opposite side of the *Mariner IV* type spacecraft. However, the S-band occultation experiment had to be considered as a key element. Hence, the predicted properties of the Venus atmosphere played a large part in the selection and location of the S-band antennas.

The atmospheric model chosen by the occultation experimenter as the design goal for antenna selection is called the GH50 ("greenhouse" model with 50 earth atmospheres surface pressure). For this model atmosphere, the ray bending and the attenuation experienced by the ray passing closest to the planet's surface is 26.5 deg and 26.6 dB, respectively. To determine the antenna gain required, the last number must be adjusted so as to account for the fact that only the RF carrier is tracked and that the 210-ft antenna (DSIF 14) would be used for the occultation experiment. Hence, the nominal peak antenna gain required to accommodate these conditions is 21.5 dB, which is approximately the gain required for telemetry return from Mars by *Mariner IV*. This fact sizes the *Mariner V* high-gain antenna to something approximately the same as the *Mariner IV* high-gain antenna.

Since an antenna of this size would be impossible to position between the spacecraft and *Agena* or between the bus and the shroud adapter, the antenna would have to be stowed above the bus during launch and deployed after planetary injection or the solar axis of the spacecraft would have to be reversed. Of these two choices, the reversal of the solar axis appeared to be not only inherently the most reliable but also the easiest to implement.

In this configuration, the present *Mariner IV* low-gain antenna could be used as is for *Mariner V*, since the cone angle variations of earth with time from launch to loss of low-gain antenna signal would now be similar (Fig. IV-37). Clock angle variations are not of significance in

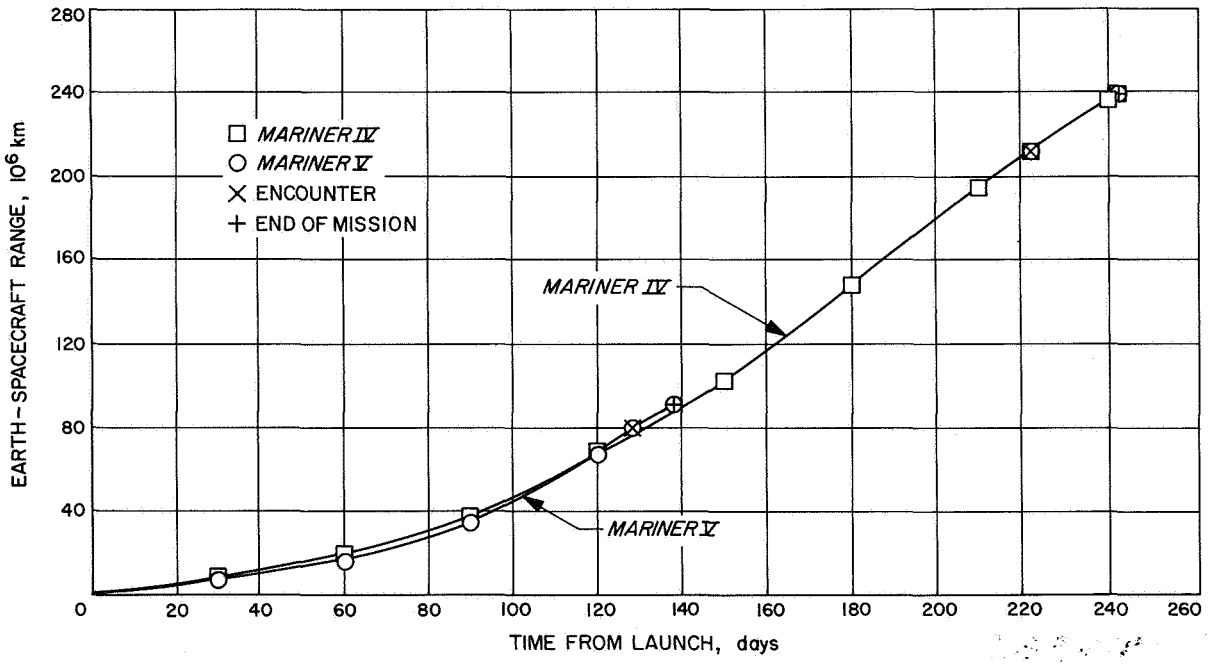



**Fig. IV-36. Comparison of *Mariner V* and *Mariner IV* communication range**

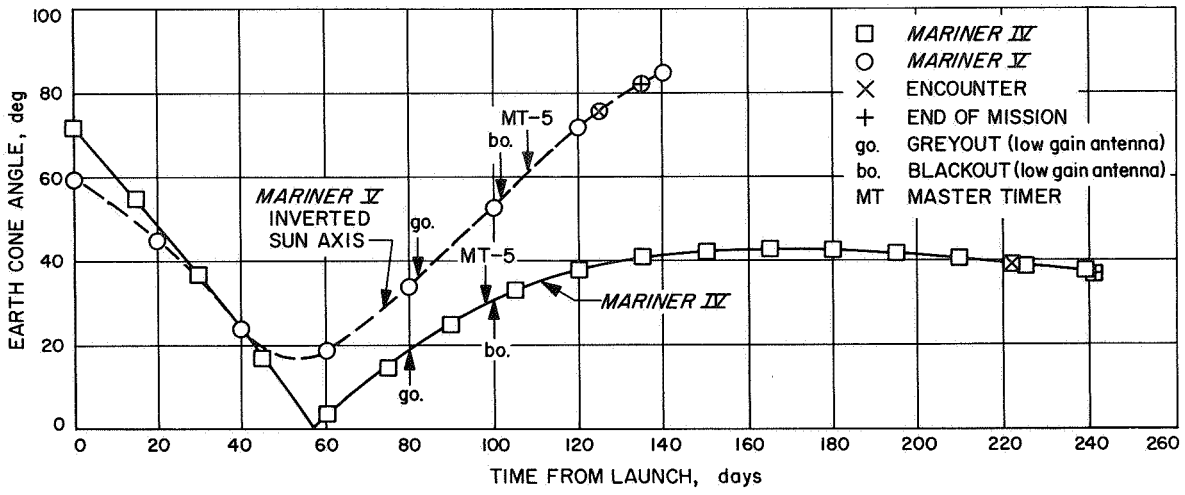



**Fig. IV-37. *Mariner V* inverted sun axis plot**

the low-gain antenna selection, since its pattern is essentially symmetrical about the roll axis. Loss of down link signal from the low-gain antenna can occur as early as the point marked go. (greyout) in Fig. IV-37 and would be most certain to occur at the point marked bo. (blackout). The down link is switched to the high-gain antenna as soon as the earth look angles intersect the main lobe of the high-gain antenna. Switchover is accomplished automatically by a stored CC&S command (MT-5 in Fig. IV-37). A backup direct command is also available.

It was necessary to accept a longer period of cruise mode communications uncertainty (approximately 26 days) in the *Mariner* Venus 67 mission primarily due to the rapid variation of the earth cone angle from low-gain greyout to encounter.

Since three flight-spare low-gain antennas were in bonded stores, no low-gain antenna development was required for the *Mariner* Venus 67 project. However, since the antenna would now be on the shady side of the spacecraft, the antenna's tolerance to extreme low temperatures had to be checked. These tests are detailed later in this report (subsection IV-H, Engineering Mechanics).

*a. High-gain antenna implementation.* Figure IV-38 shows a view of the spacecraft passing behind the planet. As the signal starts to skim the top of the atmosphere (position 1), the ray is slightly bent and attenuated. As the spacecraft moves to position 2, the ray penetrates further into the atmosphere and is thereby bent and attenuated more. This effect continues as the S-band radio ray further penetrates the atmosphere until, finally, the

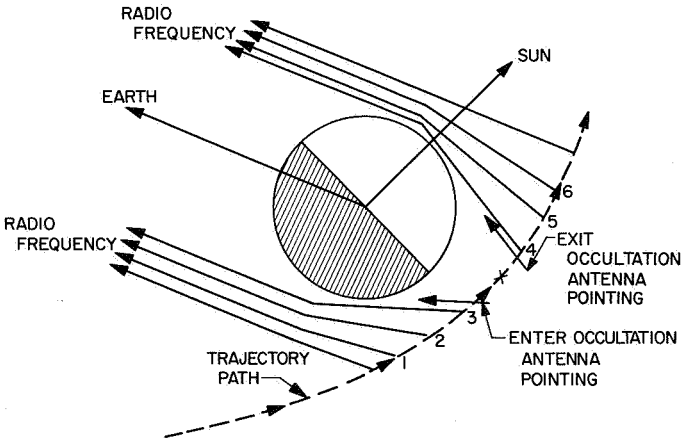



**Fig. IV-38. Venus occultation experiment**

spacecraft arrives at position 3, where the ray strikes the planet's surface and total RF occultation occurs. This phenomenon repeats itself in reverse as the spacecraft begins to emerge from behind the opposite limb of the planet (positions 4, 5, and 6).

Figure IV-39 shows the net effect of this apparent movement of earth to an observer on the spacecraft along with the earth's normal look angle variation before and after encounter. The reason that the occultation "whiskers" do not remain in a plane is explained by the fact that, for a fixed arrival date (November 19, 1967), the spacecraft only passes directly behind the planet as seen from earth when launched on June 17, 1967 (not shown in Fig. IV-39). For a June 12, 1967 launch, since the spacecraft passes below the earth-Venus vector, the earth

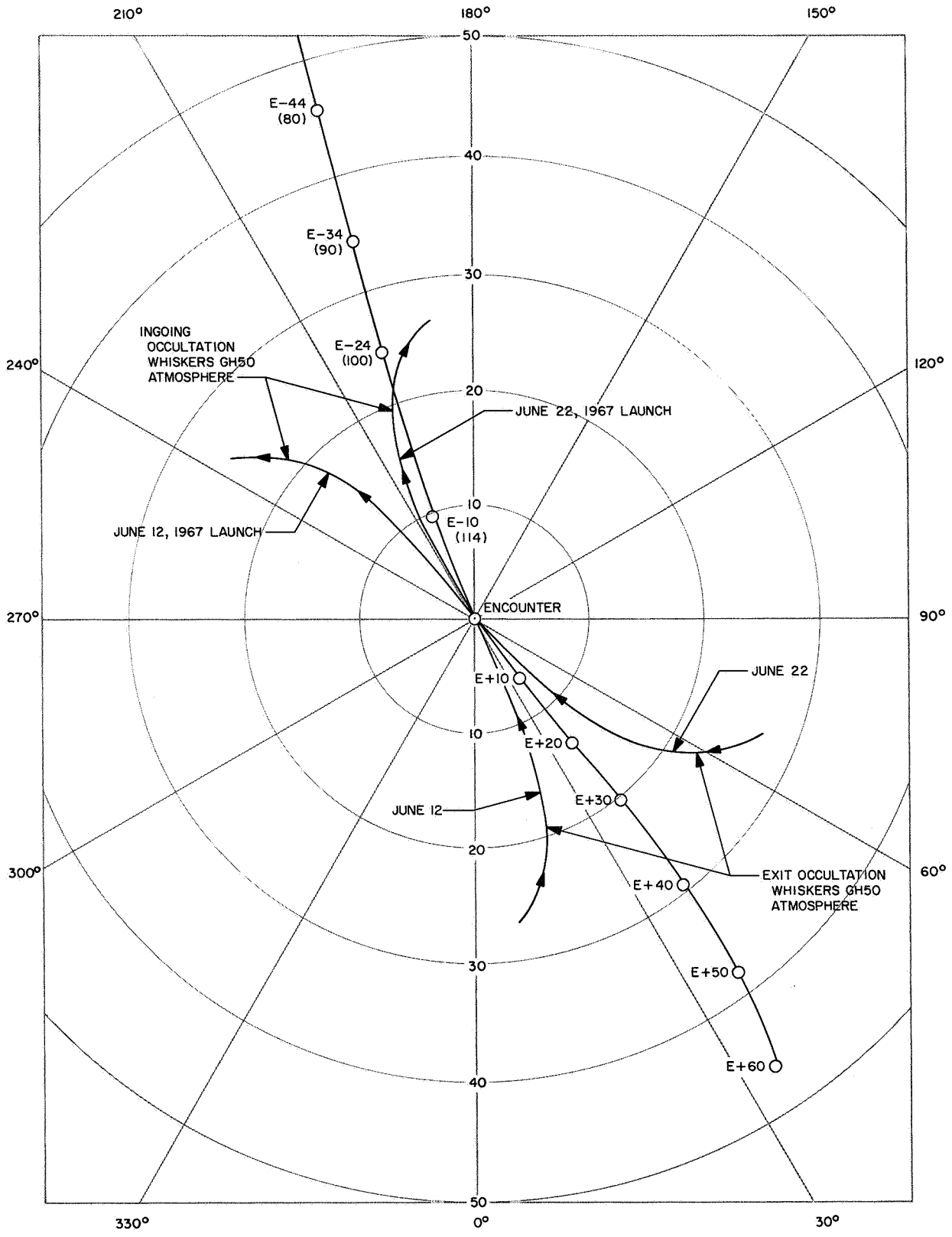



**Fig. IV-39. Earth track relative to earth polar coordinate location at encounter October 19, 1967**

appears to move up and out to the left going into occultation and up from below going out of occultation. Although a June 17 launch optimizes the occultation experiment, a launch period from June 12 through June 22 with an October 19, 1967 arrival was determined to represent the best compromise of all spacecraft constraints (more details of these constraints and on the trajectory selection are found in Section III: Systems Analysis and Mission Planning of this report).

*b. High-gain antenna requirements.* As previously stated, the selection of the high-gain antenna was based primarily on the attenuation and bending of the radio signal (during occultation) with secondary consideration given to telemetry before and after encounter. The attenuation parameter can best be presented (Fig. IV-40) as the antenna gain required as a function of the ray bending relative to earth's true direction at encounter. Figure IV-40 also presents the antenna gain required for telemetry return to earth as a function of cone angle from encounter and days from launch.

*c. High-gain antenna selection.* From the foregoing requirements, it is clear that the optimum high-gain antenna would have two peaks with approximately 28.5 dB gain (21.5 dB nominal plus 7 dB assumed without negative tolerance), each spaced 53 deg apart in the plane containing the earth track (Fig. IV-40), and with a sufficient cross earth track width to account for the out-of-plane bending of the occultation whiskers (Fig. IV-39). However, if a realizable antenna could be made to meet the first two requirements, the cross earth track beamwidth would be only 0.7 deg rather than the 25 deg required.

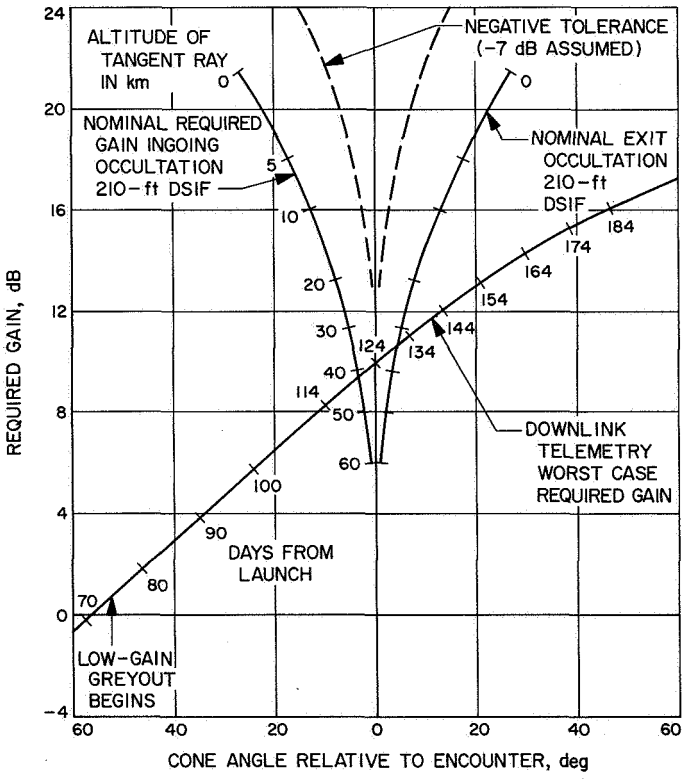



**Fig. IV-40. Antenna gain required vs antenna cone angle relative to earth direction at encounter**

Hence, it was obvious that the design goal could not be met by a simple split beam antenna, or even an antenna with a subantenna (one optimized for ingoing and the other for outgoing occultation), since the narrow beamwidth would only be doubled. Therefore, the antenna selection proceeded on a best level-of-effort basis with several design approaches studied.

Among the approaches studied, but rejected for cause, were:

(1) Split beam antennas on the basis of too low realizable peak gain.

(2) Fan beam antennas with reflector aspect ratios greater than 2:1 on the basis of too narrow cross earth track beamwidth.

(3) Symmetrical beam antennas on the basis that they did not take advantage of the higher angular variations in the plane of earth track.

These studies narrowed the logical choice to the *Mariner IV* high-gain antenna with its 23.2-dB peak gain and 2.06:1 beamwidth aspect ratio, along with a simple one-step position change to be made while the spacecraft was behind the planet. This choice would allow optimum pointing of the antenna back along the earth track when entering occultation, then, allow it to be placed to a second position behind the planet allowing optimum pointing for the outgoing occultation. The offset angle chosen for the first position of the high-gain antenna was a compromise between occultation optimization and telemetry return to earth after encounter in the event that the antenna pointing angle change did not occur. Hence, the first offset angle was −8.2 deg, while the exit occultation offset was 9.5 deg. Figure IV-41 shows the gain performance characteristics for the in-plane (no whisker bending) case, while Fig. IV-42 shows the out-of-plane bending and occultation performance in a polar plot presentation.

*d. S-band antennas description.* The spacecraft antenna subsystem included a low-gain antenna, a high-gain antenna, and their transmission lines. The function of the

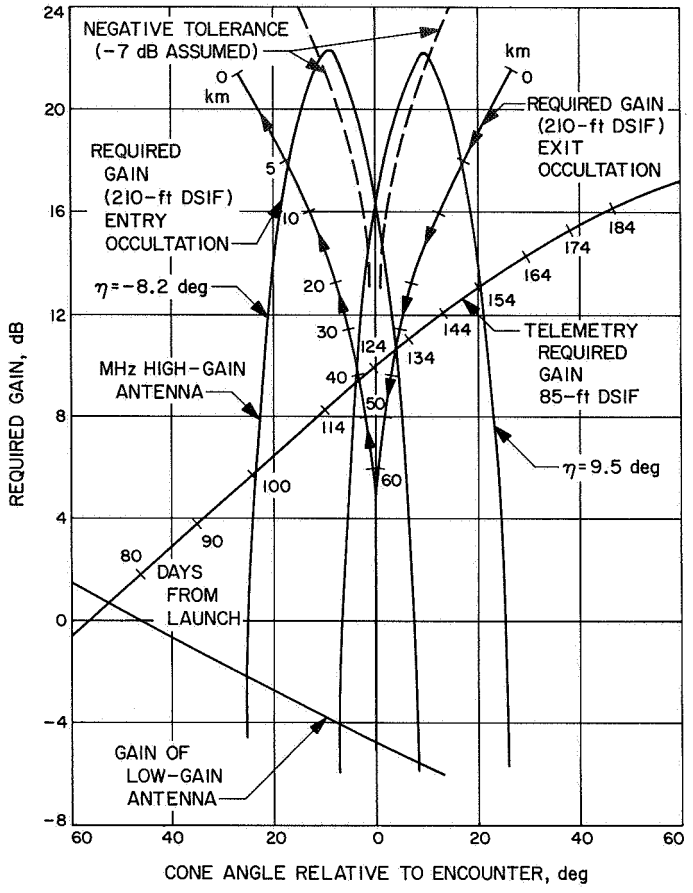



**Fig. IV-41. Performance near encounter for −8.2- and +9.5-deg antenna offset**

low-gain antenna was to receive commands from earth and transmit telemetry to earth during the first half of the mission as well as during the midcourse maneuver. The earth look angles were somewhat different than those for the *Mariner* Mars 1964 mission. In particlular, the look angles in the case of Venus continue away from the low-gain peak after encounter, while those at Mars reverse and retrace through the low-gain beam. The primary function of the high-gain antenna was to transmit telemetry to earth during the last half of the transfer orbit and for a period after planetary encounter.

The S-band antennas fabricated for *Mariner IV* were used for *Mariner V* with only minor changes. The low-gain antenna consisted of a right-hand circularly polarized mode launcher in the base of an 84-in. long, 4-in. diameter circular aluminum waveguide, with a crossed slot radiator and ground plane system at the other end. The base of the antenna was mounted in a fixed position on the spacecraft structure with the waveguide extending parallel to the spacecraft −Z axis.

The high-gain antenna consisted of a reflector and feed. The reflector was a sectoral paraboloid, having an elliptic aperture with a major axis of 46.0 in. and a minor axis of 21.2 in. The feed was an array of two turnstile elements driven in phase through a stripline power divider and matching network. The high-gain antenna was right-hand circularly polarized. Unlike the *Mariner IV*, the *Mariner V* high-gain antenna had two separate positions.

The changes to the antenna to accommodate the two positions included the addition of a new mounting interface structure and revision of the coaxial cabling between the antenna and the electronics cases. An additional change in the design included the insertion of a tuned mismatch in the low-gain antenna transmission line. This change was done as a partial fix for the interferometer problem that occurred on the *Mariner IV* as a result of insufficient isolation between the high-gain and low-gain antennas (a detailed discussion may be found in the following radio subsystem section).

*Environmental testing.* The environmental requirements for a Venus mission were different than those for a Mars mission. Primarily, the Venus mission exposed the antennas to a cold environment, whereas the Mars mission involved high temperatures.

*Type approval testing.* In the case of the low-gain antenna, thermal-vacuum and magnetic field testing were the only type approval (TA) level tests performed. Since the antennas had been qualified for *Mariner IV* and no changes in mounting or design were made, no vibration testing was required. Electrical checks were made before and after the TA tests and no performance degradation occurred. However, inspection of the antenna, following exposure to −200°F for 2 h, revealed that the bonding of the cable clamps had become loose. Developmental tests were run with a section of antenna tubing for investigation of several bonding agents and techniques. It was decided not to rework the cable clamps on the flight antennas unless failure occurred during spacecraft simulator tests. The cable clamps of the M67-1 and M67-2 antennas were inspected following simulator tests and found to be unaffected.

Thermal-vacuum, magnetic field, and TA vibration testing were accomplished for the *Mariner V* high-gain antenna. In addition, TA models of the antenna and applicable coaxial cables were utilized in the performance of low-temperature deployment testing. The vibration testing was required due to the change in the mounting

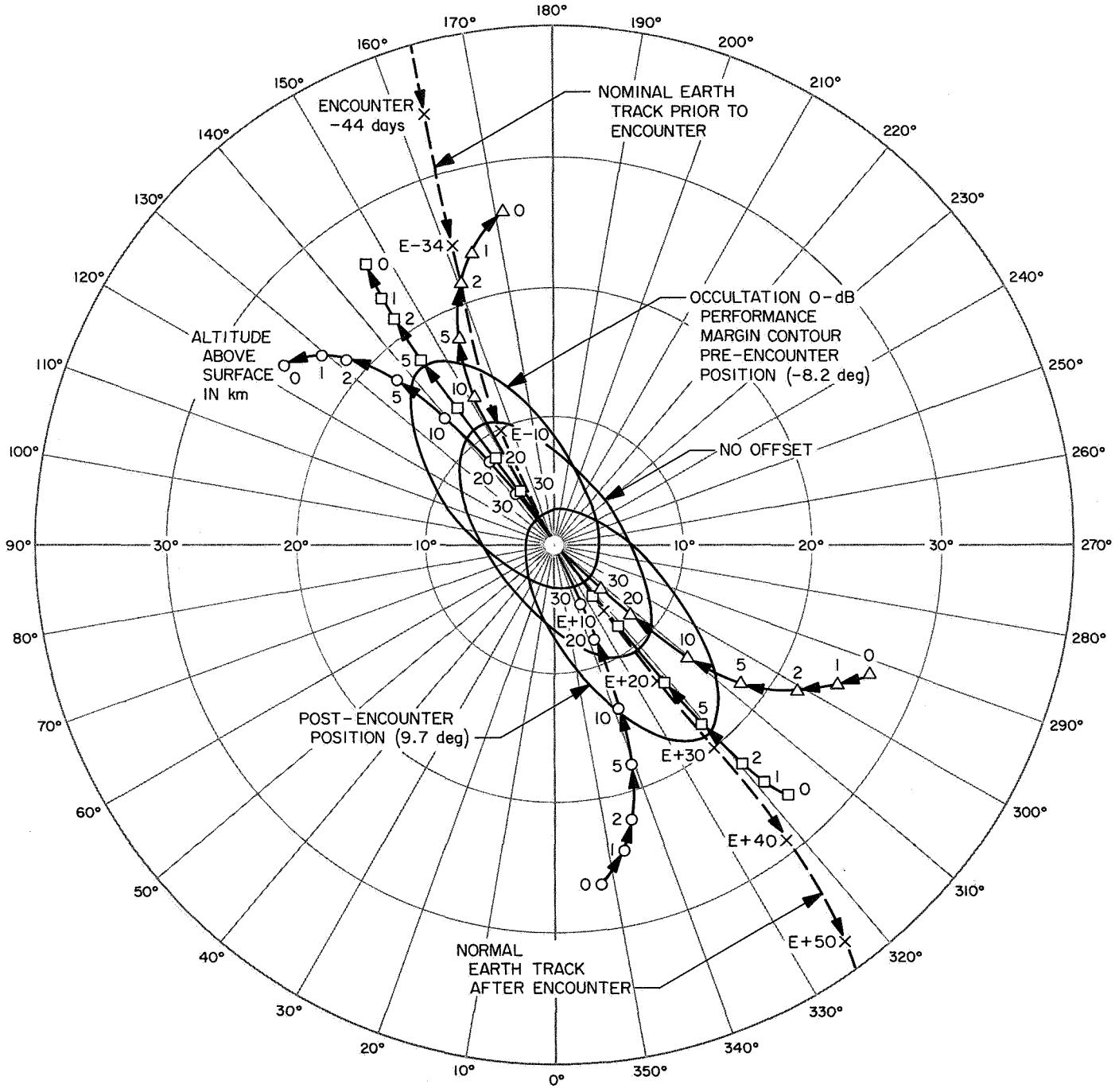



**Fig. IV-42. Venus atmosphere refracted beam paths and earth track relative to true earth direction at encounter**

of the antenna from *Mariner IV* and was accomplished on the structural test model (STM) spacecraft. Electrical tests before and after magnetic field and vibration testing showed no performance degradation.

A TA high-gain antenna was subjected to a low-temperature environment of −285°F for 6 h. The VSWR following the test was higher than when measured before the test. Investigation determined that the ground plane in the antenna feed was warped upward at the edge opposite the coaxial connector.

The ground plane is a laminate of copper foil on a sheet of Rexolite (polystyrene), with the copper foil surface exposed. Since the coefficient of thermal expansion of Rexolite is greater than that of copper, the Rexolite shrinks more rapidly than copper when the ground plane is cooled. The common bond interface restrains free contraction, thereby placing the copper in compression and the Rexolite in tension.

Cooled to the extreme TA temperature, the copper was compressed to the yield point and the length of the copper was permanently reduced by plastic deformation. After being returned to room temperature, the copper remained at a reduced length. Hence, there was a hysteresis effect in the change of the differential lengths of the copper and Rexolite with changes in temperature beyond the point where plastic deformation occurred. This effect placed the Rexolite in compression and the copper in tension, and warpage occurred in the opposite direction from that seen at the low temperature.

The threads of the nylon screws, which extend through the feed surfaces and the ground plane, were stripped by the stress of the warpage and as a result of differential coefficients of expansion. The TA and flight antenna feeds were reworked and the nylon screws in the feed were replaced by titanium screws. In addition, the paint was removed at the interfaces between the feed and the connector to avoid paint chipping in the event of ground plane warpage at low temperatures. The new screws were intended to restrict the warpage of the laminate such that the VSWR would not be affected.

As the temperature is lowered from room temperature, the pre-stress placed on the ground plane by the titanium screws relaxes as the ground plane warpage begins to reduce. At some lower temperatures near that occurring in flight, the board will become flat. As the temperature is further lowered, the board will attempt to warp in the opposite direction. However, since the Rexolite surface is restricted by the interface with the feed assembly, the ground plane will attempt to rise in the center. The center will be restricted by the titanium screws and little warpage will occur.

The VSWR of a reworked TA antenna was then checked before and after low-temperature deployment testing. An additional check of this problem was made on a reworked flight antenna before and after the system level, solar simulator test. In both cases, the performance was found to be satisfactory.

The VSWR measured at room temperature is not necessarily the value that will occur in flight. An accurate measurement of VSWR at low temperatures is not possible. However, it is felt that, due to the hysteresis effect, warpage will occur at the actual flight temperature in an opposite direction, but with no greater amplitude than at room temperature.

Ground plane warpage should be considered in any future plans to use the high-gain antennas that were low-temperature tested for *Mariner V*. In particular, missions that involve high-temperature environments (i.e., components placed on the seeing side of the spacecraft) are of concern. Due to the hysteresis effect, ground plane warpage of the *Mariner V* antennas at high temperatures will occur by a greater amount than if the antennas had not been subjected to extremely low test temperatures. It is noted that ground plane warpage may have occurred during the *Mariner* Mars 1964 mission. However, since the test temperature levels did not result in plastic deformation of the copper, measurements at room temperature did not indicate the problem.

Low-temperature deployment testing of the high-gain antenna was accomplished with the mounting superstructure, deployment mechanism, antenna, and associated cabling in a vacuum chamber at −240°F. Approximately 5 W of RF power was transmitted through the coaxial cable to the antenna to simulate the minimum power anticipated in flight. At this power level, 0.15 W was dissipated in the cable, thereby increasing its flexibility due to increased temperature. Difficulty was encountered in obtaining proper deployment. Initially, a mechanical failure of the latch mechanism occurred. After solution of this problem, it was determined that the cables across the hinge were inhibiting proper deployment. Rearrangement of the cable routing was accomplished, and successful low-temperature deployment was then achieved.

*Flight acceptance testing.* Vibration testing was accomplished for each flight low-gain antenna because of the fix being attempted for the interferometer effect. It was necessary to determine if impedance changes occurred for any of the antennas as a result of the launch environment. This check was required because the mismatch, added as part of the fix, was tuned for a specific impedance range. The performance could, therefore, be degraded by excessive changes in antenna impedance. Measurements made before and after vibration indicated that no changes occurred.

Vibration testing of each flight high-gain antenna was accomplished because of the new mounting configuration for *Mariner V*. Thermal-vacuum testing consisted of subjecting the high-gain antenna to −245°F for 2 h. Electrical checks before and after testing indicated that the performance was within the specified limits. These checks included VSWR, gain, patterns, and boresight alignment.

*e. Full-scale spacecraft model measurements.* A full-scale antenna test model spacecraft was used early in the mission analysis to determine the adequacy of the high-gain and low-gain antenna patterns. Since these measurements were accomplished for *Mariner IV*, the changes in spacecraft structure for *Mariner V* were of primary interest. The change that could most feasibly affect the patterns involved the solar panels. The solar cell area was reduced for *Mariner V* and the panels were inverted. Inversion of the panels exposed the corrugated backside to the antennas. Pattern data were measured on the ATM spacecraft and indicated that no performance degradation would occur as a result of the *Mariner V* configuration changes.

Data were recorded prior to launch as an estimate of the actual in-flight performance. These data were recorded on magnetic tape, using a full-scale developmental test model spacecraft. The primary purpose of recording final flight patterns on a full-scale spacecraft model was to include the multipath distortion effects caused by the spacecraft structure.

The antennas were TA models, chosen to have performance characteristics as nearly identical to the flight antennas as possible. These differences were accounted for with correction factors and tolerances.

The patterns recorded on magnetic tape included a set for the low-gain antenna and for both positions of the high-gain antenna, each at the transmit and receive frequencies. In addition, three interferometer mode patterns were recorded. This recording was a secondary purpose for utilizing a full-scale spacecraft model in the final pattern measurements. That is, a well-aligned spacecraft is required to provide the proper relative orientation of the low-gain and high-gain antennas for a proper interferometer effect. The interferometer modes recorded were transmit-low/receive-low mode (launch mode) at both the transmit and receive frequencies, and transmit-low/receive-high mode at the receive frequency. The interferometer effect is negligible for the transmit-low/receive-high mode at the transmit frequency. The isolation between the high-gain and low-gain antennas was adjusted to a value determined by measurements made on the flight spacecraft. The exact phasing of the signals was not determined prior to launch. An arbitrary phasing was, therefore, used for the recording of each mode. The envelope of the pattern expected in flight was obtained. That is, the locations of these recorded interferometer pattern peaks and nulls in spacecraft angular coordinates were not necessarily those that would occur in flight.

***3. Mariner V flight command subsystem.*** The *Mariner V* flight command subsystem was, with minor exceptions, identical in design to the *Mariner IV* command subsystem. In some cases, it was necessary to use components that differed from those used on *Mariner IV*. Some interface changes between the command system and various users also were required.

The *Mariner V* command subsystem employs a phase shift key modulation technique. Basically, this technique assigns the weight of a binary 1 or zero to a cosine wave. If a binary 1 is assigned to the cosine function, then a binary zero would be represented by the negative cosine function (bi-phase modulation).

It is necessary to know the polarity of the received command data to distinguish "ones" from "zeroes." This is accomplished in the command detector, whose functions are:

(1) Establish phase coherence between the ground command subsystem and the spacecraft command subsystem.

(2) Once coherence is established, determine the phase of the transmitted data.

Once the phase of the incoming data channel is determined, the data are converted back to binary form. The detector transmits the information to the second functional unit of the command subsystem, the decoder.

The primary purpose of the decoder is to look at the data emanating from the detector and to determine if valid information is being transmitted. Once it is established that a valid command is being sent, the decoder deciphers the incoming data and routes it to the subsystem requiring the command. All interfaces between the command subsystem and its users are isolated through either IP (isolated pulse) or IS (isolated step) switches.

*a. Design changes.* Essentially, there were no design changes between the *Mariner IV* and the *Mariner V* flight command subsystem. There were some component parts used on the *Mariner IV* command subsystem that were not manufactured in 1967. In addition to the component changes, it was also necessary to change the potting material used in two types of transformers (transformer design not changed). Both the IP and IS switches utilized transformers that, as a result of life testing the *Mariner IV* flight command subsystem, became suspect parts. The transformers used in the *Mariner IV* spacecraft used a potting compound that contained chlorine and bromine (corrosive elements). Investigation revealed that it was possible for these elements, over a period of time, to attack and corrode the fine wire used in the transformer windings.

*b. Development and production problems.* One of the production problems encountered was related to the previously mentioned transformers. The new transformers did not meet the inductance and resistance parameters. The change in parameters was due to using a different grade of wire in the transformer windings than that used for *Mariner IV*. Inasmuch as it was impossible to build new transformers in time to meet schedule requirements, the systems were built with the transformers as received. A worst case analysis was performed on both the IP and IS switches, using the new worst case conditions for the transformer. After performing the analysis, it was concluded that the transformers would not have a detrimental effect on the performance of the system.

A second major production problem encountered was one pertaining to the VCO (voltage-controlled oscillator) used in the flight command detector. Information first received revealed that one of the critical components, the field-effect transistor (FET), in the VCO was no longer commercially available. Further, to replace the FET with another component would require a major redesign. A sufficient number of the transistors was located eventually. By this time, it was too late to build a new VCO and to incorporate it in the new system and still meet schedule requirements. The solution was to use one of the residual *Mariner IV* life test VCOs in the new system. This VCO had approximately 10,000 h of data on it, all of which indicated it would be able to meet mission requirements.

*c. Critical problems.* During FA testing, one of the IS switches used in the command subsystem exhibited characteristics different from all other switches. The suspect module was removed and carefully checked. The transformer used in the switch contained a direct primary to secondary short, the result of a poor manufacturing technique. After replacing the switch, the module was requalified and all switch parameters were consistent and appeared normal.

*d. Testing.* During SAF testing, it was noted that the command subsystem was difficult to lock up at signal levels greater than −125 dBm. Subsequent testing showed that at high signal levels, the radio subsystem introduced distortion in the command subsystem composite signal, which could cause a false lock.

Figure IV-43 shows the error voltage produced by the command phase lock loop. There is a definite distortion on one side of the −110-dBm correlation curve. However, no distortion is shown on the opposite side. Since one side of the curve represents obtaining correlation with a positive offset of the RWV $8f_s$ frequency and the

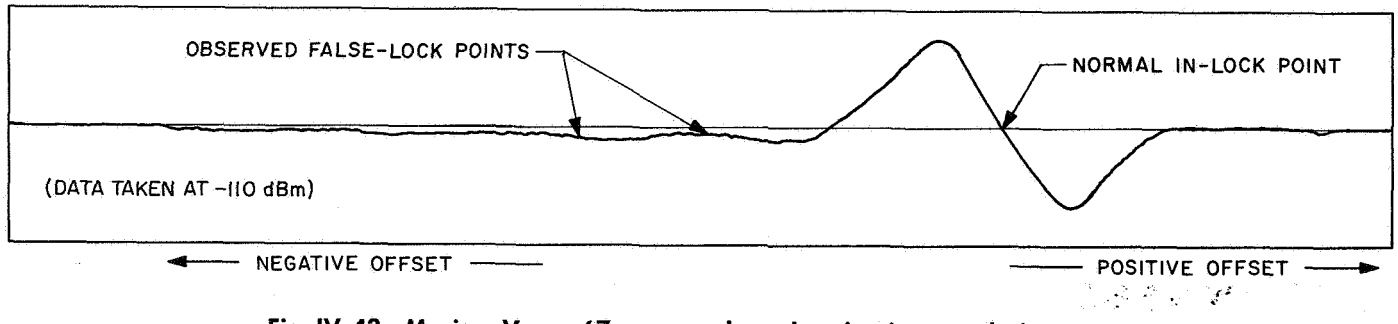



**Fig. IV-43. *Mariner* Venus 67 command synchronization correlation curve**

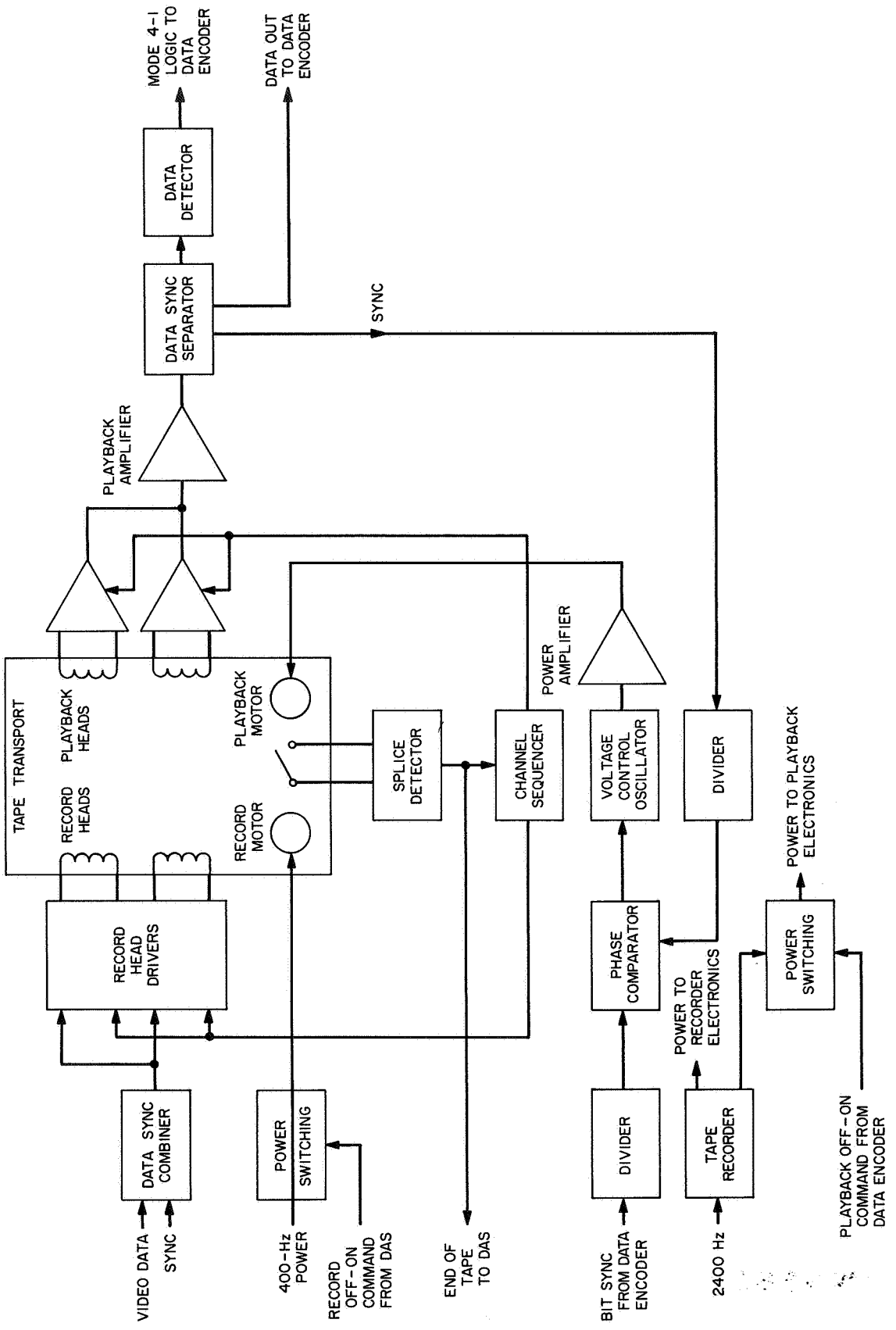



**Fig. IV-44. *Mariner IV* video magnetic tape recorder**

other represents obtaining correlation with a negative offset, a positive offset is always used while securing command lock. Inasmuch as the distortion appears on only one side of the correlation curve, it is most likely that a false lock will occur while attempting correlation from the negative offset.

*e. Command package design.* The *Mariner IV* and *Mariner V* command packaging was basically a "sandwich" contained in a frame. This type of design made both sides of a "sandwich" easily accessible to inspection and to reduce handling and disturbance of sections of the subsystem not affected by the modification, or repair, being accomplished on other sections. However, the first reason was partially invalidated when a requirement was made to place a web across the frame to give greater package rigidity.

***4. Tape recorder subsystems.*** The *Mariner V* tape recorder subsystems (TRS) were modified flight systems left over from the *Mariner* Mars 1964 Program. To better understand the nature and scope of these modifications, a brief review of the *Mariner IV* TRS is presented.

The *Mariner IV* tape recorder was designed to record digital data from the data-automation subsystem at a rate of 10,700 bits/s and to play back synchronously through the data encoder at a rate of 8⅓ bits/s. The operation of the TRS consisted of 21 start/stop cycles to record the 21 video pictures. Figure IV-44 is a block diagram of the *Mariner IV* TRS.

**Table IV-15. Comparison of *Mariner IV* and *Mariner V* TRS design specifications**

| Parameter | *Mariner IV* | *Mariner V* |
|---|---|---|
| **Record mode** | | |
| Data rate | 10,700 bits/s | 66⅔ bits/s |
| Tape speed | 12.86 in./s | 0.08 in./s |
| Storage capacity | $5 \times 10^6$ | $10^6$ |
| Packaging density | 833 bits/in. | 833 bits/in. |
| Simultaneous data channels | One | Two |
| Power (2400 Hz) | 4.0 W av | 7.3 W av |
| Power (400 Hz) | 3.5 W av | 0 W |
| Record time | 5 min/track | 127 min |
| **Playback mode** | | |
| Data rate | 8⅓ bits/s | 8⅓ bits/s |
| Tape speed | 0.01 in./s | 0.01 in./s |
| Power (2400 Hz) | 4.0 W av | 6.1 W av |
| Playback time/track | 8 days | 17 h 48 min |
| **Launch mode** | | |
| Tape speed | 12.86 in./s | 5.796 in./s |
| Power (400 Hz) | 3.5 W av | 3.5 W av |
| Tape pass time | 308 s | 111 s |
| **Other** | | |
| Tape length | 330 ft | 53 ft |

The acceleration and deceleration of the tape recorder during the record start/stop periods was adjusted so that the amount of tape used in each stop/start cycle was 3–5 ft. This amount of tape took from 1 h to 1 h 40 min to play back. This time was the amount of "dead" time required for engineering data between pictures during playback (Telemetry Mode 4).

The prime function of the *Mariner V* TRS was to record science data in the vicinity of the planet Venus. The TRS was required to record 2-data streams of digital data from the data-automation subsystem, each at a rate of 66⅔ bits/s and to play back synchronously through the data encoder at a rate of 8⅓ bits/s.

Figure IV-45 is a functional block diagram of the *Mariner V* TRS. Table IV-15 is a comparison of the *Mariner IV* and *Mariner V* TRS design specifications.

*a. Design modifications and qualification.* The design modifications were of two classes: (1) those necessary to meet the mission requirements, and (2) those that were design problems inherited from *Mariner IV* and logically could be integrated into the modification-refurbish efforts.

*Operation of playback motor at 8000 rev/min.* In the *Mariner IV* system, separate motors were used for record and playback. The *Mariner V* configuration used the *Mariner IV* playback motor for both record and playback. This synchronous motor was designed to operate over a range of 1000–8000 rev/min. To avoid changes to the data reconstruction circuitry and the phase-locked playback servo system, the *Mariner IV* playback rate of 8⅓ bits/s was retained. Nominal playback motor speed was 947 rev/min for this data rate. Motor speed in the record mode was $8 \times 947$ rev/min = 7576 rev/min.

The required motor drive voltage for operation at the new record speed was determined from test data obtained from the breadboard transport. Operation with a 35-V dc input to the motor drive circuit was selected as the best compromise between obtaining fast acceleration time and minimum power consumption.

Since the playback motor also had to operate in the record mode, steps were added to the motor test procedure to measure stall torque, no load input current, and

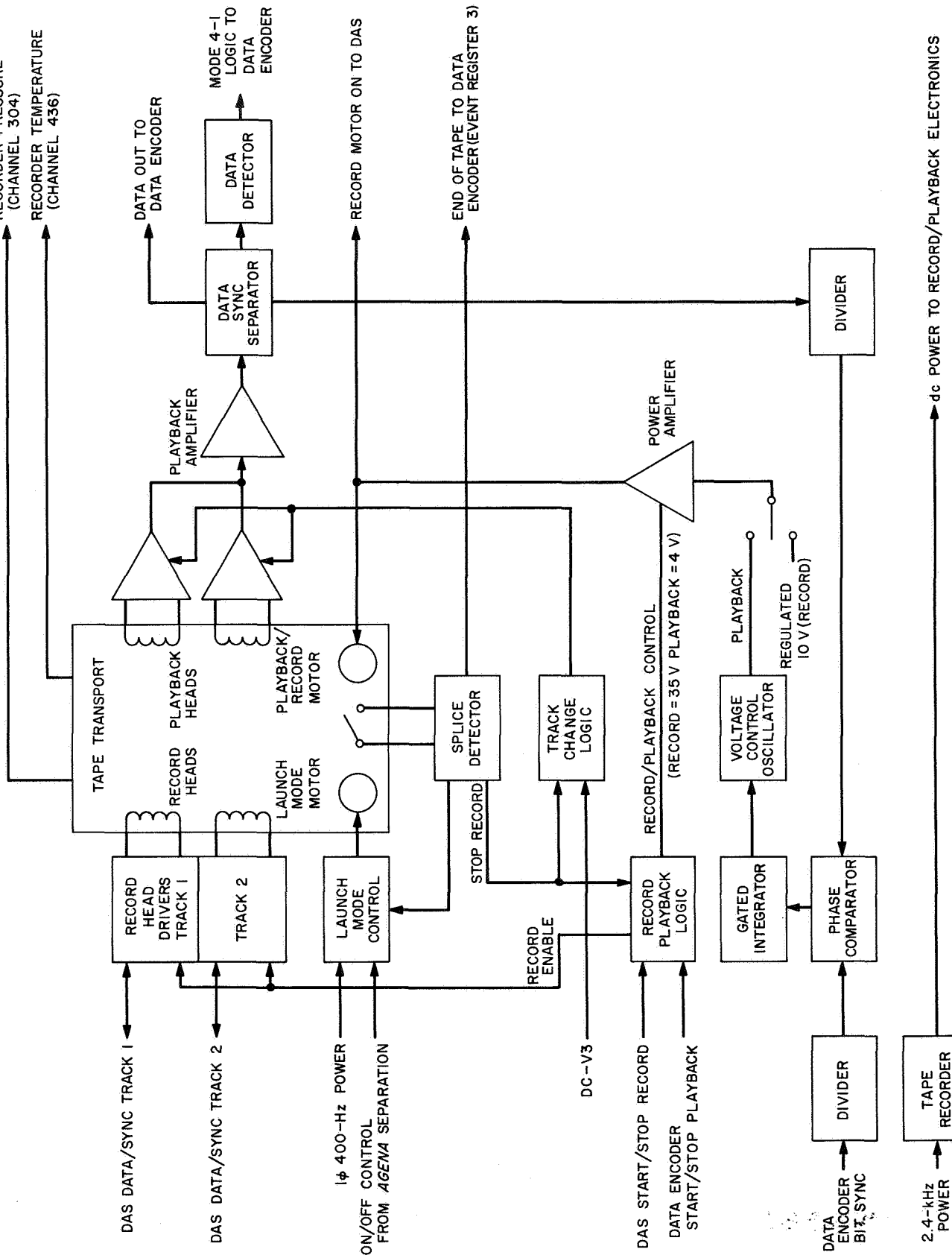



**Fig. IV-45. *Mariner V* tape recorder**

maximum synchronous torque at 7576 rev/min. The only modification required to the existing motor driver circuit was the replacement of a few transistors and diodes. These changes were required because of the higher operating voltages in the record mode.

*Record/playback switching.* Care was taken in the design of the motor speed switching circuits to avoid application of high voltage (35 V) in the presence of the low-frequency playback clock. This combination could result in large and destructive currents flowing in the motor and driver. The original circuit approach for *Mariner V* employed a voltage sensing circuit to inhibit the application of low-frequency drive if high voltage (over approximately 10 V) was present at the input to the motor driver. This approach worked fine except for power turn-on. It was possible to turn on with low-frequency playback clock drive and the 35-V supply switched to the motor driver. Under these conditions, the overload was so severe that the 35-V supply would not develop the required voltage (approximately 10 V) to actuate the voltage sensing circuit.

To solve this problem, a relay was used to generate the record and playback logic. In the record position, the relay provided a record enable signal that enabled the motor driver, and provided high-speed clock to the input of the motor driver. The second set of contacts switched either 4 or 35 V to the driver. During the transition between relay contacts when switching between record and playback, the high speed clock was enabled.

*Record clock source.* In selecting the clock source, consideration was given to deriving a source that would allow the maximum chance of surviving a shift in the basic 2.4-kHz spacecraft clock.

The effect of a shift in 2.4 kHz, using a record clock referenced from 2.4 kHz, was analyzed as follows. Consider the case of 2.4 kHz shifting 10% low. Since the input data rate is derived from 2.4 kHz, both the input data rate and the motor speed will slow and the packing density of information recorded on the tape will be the same as if no shift in 2.4 kHz had occurred. During playback, the master clock derived from 2.4 kHz will be low; therefore, the playback servo will need to reduce the tape speed by the same percentage that 2.4-kHz frequency shifted.

Using a record motor clock independent of 2.4 kHz was analyzed as follows. A 10% reduction in 2.4 kHz lowers the input data rate, but not the motor speed. Information is recorded on the tape at a reduced packing density. During playback, the master clock will be low, but the reduced packing density tends to compensate and the playback tape velocity will be identical to the nominal case. Because of the compensation for shifts in 2.4-kHz frequency afforded by a record clock independent from the 2.4-kHz spacecraft clock, it was decided to use a separate clock.

Using the existing VCO in the playback servo for a record clock source required clamping the VCO input during the record mode. The reference voltage is derived from 35 Vdc and is set to obtain a VCO frequency of 1512 Hz.

The compensating effect derived by using an independent clock source was verified by test. The tape recorder will record and maintain synchronous playback between 1.8 and 2.8 kHz.

*Record motor ON to DAS.* To provide an indication of the tape recorder operation during encounter such that corrective action could be taken if required, the end of tape (EOT) pulse was replaced with an IS switch closure that indicates when the record motor power is applied.

*Record stop mechanization.* In the *Mariner IV* configuration, there were three sources of a stop record pulse: (1) DAS, (2) direct access, and (3) count 2 and stop circuit. As both tracks of data are recorded in a single tape pass on *Mariner V*, the count 2 circuit was not needed and was replaced by an encounter automatic stop circuit that sends a stop record pulse at EOT.

To provide a backup stop record, an extra IP switch was employed to issue a stop record pulse when the data encoder switched to the playback mode (Mode IV).

The sources of stop record pulses in *Mariner IV* and *Mariner V* are compared in Table IV-16.

**Table IV-16. Sources of stop record pulses**

| *Mariner IV* | *Mariner V* |
|---|---|
| Count 2 & stop | EOT pulse |
| DAS stop (IP switch closure) | DAS stop (IS switch closure) |
| OSE direct access | Transition to Mode IV (DC-V4) |

*Track change relay hang-up.* In the *Mariner IV* configuration, if the steering contacts of the track change relay floated open, both energy storage capacitors would become fully charged, making recovery impossible without breaking conformal coat on the subsystem. In the

*Mariner V* version, the state of a flip-flop determined the charge on the energy storage capacitors. The flip-flop had no middle state; hence, even if the contacts hung up, the next track change command will cause them to recover. With the relay contacts hung up, track selection was determined by the state of the flip-flop. Tests on the prototype subsystem verified that the track selection logic will operate from the flip-flop only in case of relay hang-up.

*Record input mechanization.* In the *Mariner IV* configuration, data and bit sync came into the tape recorder system on two separate lines and were mixed in the video storage subsystem. For *Mariner V*, the mixing of data and bit sync occurred in the DAS. The additional flip-flop required for parallel recording was made available by the deletion of the *Mariner IV* count 2 circuit. Two simultaneous data tracks were required for *Mariner V*.

The *Mariner IV* record head drivers were enabled whenever the system was not in Mode IV (playback). For *Mariner V*, the record head drivers were energized only when the system was recording. Enabling the record head drivers with the record enable logic rather than the playback command eliminated a spot erasure problem that occurred in the standby mode.

*Changes to improve bit error performance.* The error rate of the *Mariner IV* TRS was about five times the specified rate of 1 error per $10^5$ bits required in the design specification. A logic change to improve the bit error performance was incorporated in the *Mariner V* design. Bit error tests on the modified unit revealed that the change was not sufficient to correct the problem. To eliminate a time race condition, the functions of a high-speed and low-speed NAND gate were interchanged; the modification was effective.

*New reel design.* Because of the reduced amount of data to be stored by *Mariner V*, the tape length was reduced from 330 ft to about 53 ft. The major change involved a decrease in the outside diameter of the reel assembly. The original hub diameter was retained.

*Launch mode.* Because of the reduced tape length, a large number of tape passes are accumulated during the launch phase. As it is desirable to minimize these passes, the launch-mode running speed was changed from 12.86 to 5.796 in./s by removing the flywheel assembly. The new belt was run off the motor shaft instead of the integral pulley. With the flywheel removed, it was observed that the EOT foil came to rest on the downstream capstan. Long term storage of the EOT foil on the capstan was deemed dangerous.

A new flywheel without an integral pulley was designed to provide a coast down time of about 15 s resulting in the EOT foil being stored about 3 turns into the tape pack after launch-mode run down. The dead space on the tape provided by this flywheel action is equivalent to approximately 58 min during playback.

*b. Rework of analog modules.* During FA testing of the tape recorder subsystem, an oscillation was observed at the output of the main playback amplifier. Investigation of the failure revealed poor filling of the semicordwood module with Eccofoam potting compound. This poor filling resulted in a lack of structural support for the component parts that, as a result of vibration testing, had produced several cracked solder joints in the area of the printed circuit pads.

Investigation of the system revealed that the preamplifier and differentiator also were potted with the same compound. The differentiator was decanned and found to have potting voids also. All other modules in the TRS were potted with Stycast 1090.

Rework and requalification were done in a serial fashion so that the one flight tape recorder subsystem could support the spacecraft system test operations. Rework/rebuild of hardware started on February 1, 1967 and all rework requalification was complete on March 27, 1967.

***5. Flight telemetry susbsystem.*** The flight telemetry subsystem is composed of the data encoder and the telemetry transducers (temperature and pressure).

*a. Data encoder.* The function of the *Mariner V* data encoder is to accept spacecraft measurement data in the form of analog voltages and digital information, to convert the data into 7-bit NRZ words in serial form, to modulate a subcarrier with the binary data, and to add synchronization information, which forms a signal to be presented to the radio transmitter.

The *Mariner V* flight data encoder was essentially the same as the *Mariner IV* flight data encoder with certain modifications. These modifications can be grouped into the following categories:

(1) Mode III modification.

(2) Component part substitutions.

(3) DAS interface modification.

*Mode III modification.* In the data encoder operational Mode III, engineering words 105 and 106 are inserted into the data train in lieu of science data. These two words are inserted as words 46 and 47 after issuance of the science gate pulse to the DAS.

*Component part substitutions.* The following part substitutions were made for the *Mariner V* data encoder:

| *Mariner V* | *Mariner IV* |
|---|---|
| Ultronics 202 A resistor | Kilvin 3-HR resistor |
| Angstrohm J51 resistor | IRC MEA-T resistor |
| 2N2946 transistor | 2N2185 transistor |
| 2N338 transistor | MM2N338 transistor |
| VK 37/27 capacitors | VK 36/26 capacitors |

*DAS interface modification.* The interface between the data encoder and the DAS was modified to provide bit sync with a rise time of less than 5 $\mu$s. The rise time of the *Mariner IV* data encoder bit sync pulse was approximately 400 $\mu$s, which was incompatible with the new DAS integrated circuit requirement of a rise time of less than 10 $\mu$s.

The data encoder operates at two data rates (8⅓ and 33⅓ bits/s) and four data modes. Figure IV-46 is a functional block diagram of the data encoder system.

Two system rates are derived from the 2400-Hz main power frequency. This basic signal is divided down by binary dividers to furnish frequencies termed $4f_s$ and

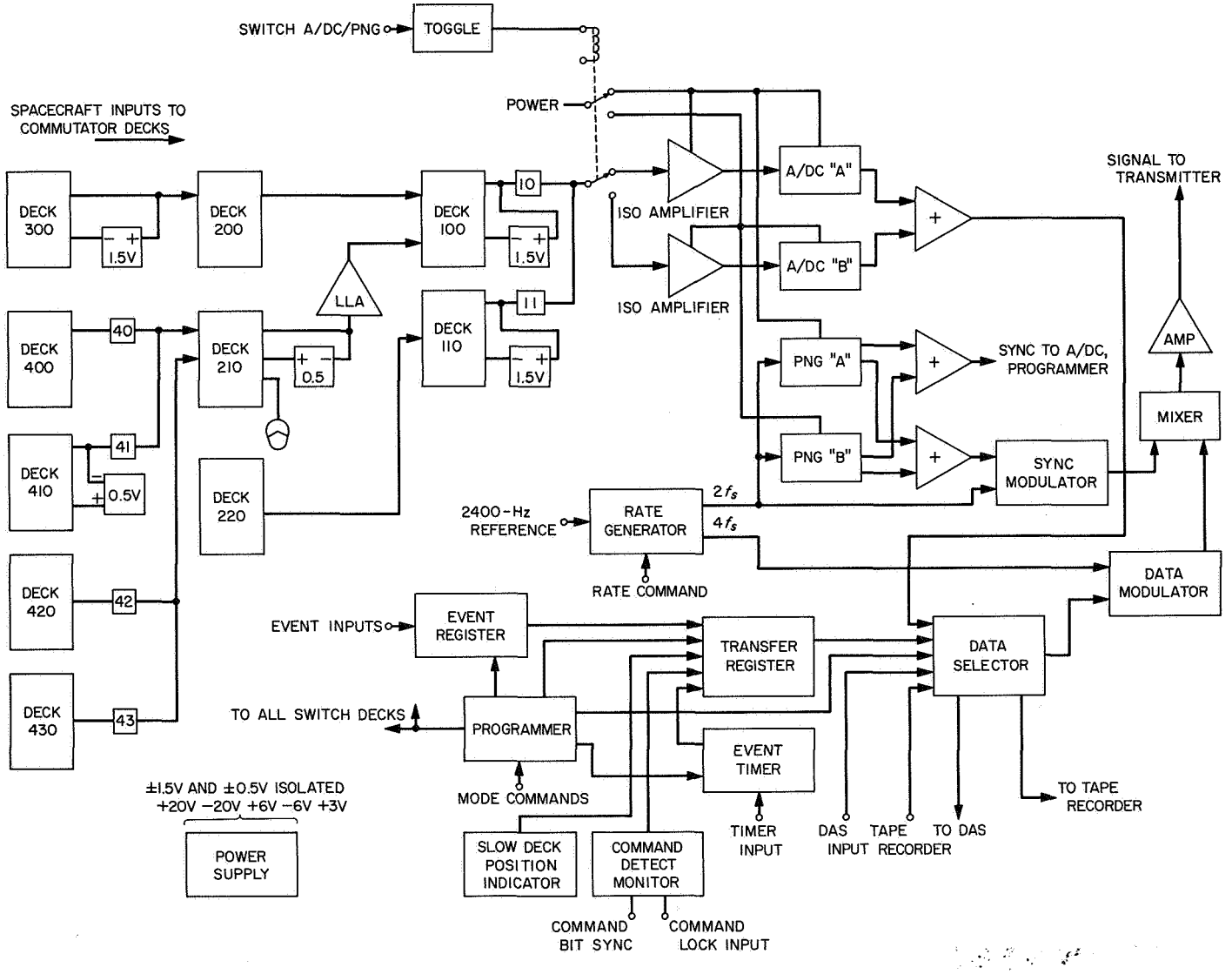



**Fig. IV-46. Functional block diagram of *Mariner V* data encoder**

$2f_s$, which are the data and sync subcarriers, respectively. Two sets of $4f_s$ and $2f_s$ are selected to provide two system rates. The $2f_s$ frequency is used to clock the pseudonoise sync-code generator which generates bit sync, word sync, P-N code, and an additional timing pulse for the data encoder.

Ninety analog and digital engineering and ten subcommutation and frame synchronization channels are accommodated on the completely solid-state commutator. The switches are arranged in a three-layer subcommutator (Fig. IV-46) to allow four basic sampling rates. Inputs on decks 100 and 110 are sampled at 1/20 the basic word rate. Inputs on decks 200, 210, and 220 are sampled at 1/200 the basic word rate. Inputs on deck 300 are sampled at 1/2000 the basic word rate. Inputs on decks 400, 410, 420, and 430 are sampled at 1/4000 the basic word rate.

All high-level analog signals were normalized to a 0- to 3-V range. All low-level analog inputs were normalized to a 0- to 100-mV range and then amplified by 30. Digital inputs were handled in the transfer register, which is a seven-stage storage register, and clocked to the data selector by the programmer.

Event inputs, consisting of switch closures, are sensed and stored in four event registers. The programmer reads out these registers into the data selector.

In the modulator, the 7-bit NRZ data are used to biphase modulate the $4f_s$ data subcarrier. The sync channel of the modulator combines the pseudonoise code and $2f_s$ clock in EXCLUSIVE OR addition. The data channel is mixed with the sync channel at the proper voltage ratio. This mixed signal is then routed through output isolation amplifiers to the spacecraft transmitter, *Agena* transmitter, and the ground support equipment.

The data encoder provides four modes of operation, each creating a different data format. These formats are as follows:

| *Mode* | *Format* |
|---|---|
| I (maneuvers) | Decks 100 and 110 are sampled sequentially. |
| II (launch and cruise) | Decks 100 and 110 are sampled sequentially with a 280-bit science DAS read-in occurring after deck 110. |
| III (encounter) | Science DAS read-in with engineering words 105 and 106 inserted in lieu of science data as words 46 and 47 after issuance of the science gate pulse to the DAS. |
| IV (tape recorder data playback) | Data storage read-in only, in presence of "data present" signal from recorder, otherwise the data encoder reverts back to the Mode I format. |

*Temperature measurements.* A 1-mA constant-current generator supplies current to each transducer. A parallel resistor shunts the transducer resistance change to a standard 100-Ω change for all ranges. A series resistor is included to transform the total network resistance to 500-Ω at the low-temperature end. The total network resistance at the high-temperature end is 600-Ω. With a constant current of 1 mA applied to the network, the voltage across the network varies from 0.5 to 0.6 V from low-band to high-band temperature. This network voltage is then bucked down by a series 0.5-V bucking supply, presenting signals between 0 and 100 mV to the low-level amplifier. This system presents an advantage over the bridge, in that a transducer shorted to ground does not upset all temperature measurements.

*Power supply.* The primary power provided is a 2400-Hz 100-V peak-to-peak square wave. The data encoder power supplies transform this ac signal to the following dc voltages and currents:

(1) +20-Vdc, regulated ±0.5%, 50-mA load.

(2) −20-Vdc, regulated ±0.5%, 30-mA load.

(3) +6-Vdc, unregulated ±5%, 500-mA load.

(4) −6-Vdc, unregulated ±5%, 30-mA load.

(5) +3-Vdc, regulated ±0.1%, 12-mA load.

(6) +1.5-Vdc, zener-stabilized, negligible load; isolated (bucking supply).

(7) +0.5-Vdc, zener-stabilized, negligible load; isolated (bucking supply).

*Manufacturing problems.* Staking problems caused the loss of certain terminals and carrier printed wiring boards. This loss created a serious terminal shortage. Another terminal shortage was caused by improper cleaning procedures. It was suggested that only pure alcohol be used to clean terminals prior to tinning them.

During the final fabrication of data encoder modules, several areas were necessary to be covered by contractor material review board (MRB) action. There were three MRB actions involving the following solutions:

(1) Foreign matter was observed on the outer edge of certain modules. X-rays were taken of these modules to ascertain the depth of penetration of these impurities imbedded in the potting material. The X-ray films verified that the impurities were only on the surface of the modules. A possible explanation of this contamination problem was that the same emery cloth used to clean the backside of the carrier boards was also used to rough up the sides of the modules. It was decided not to reject any of the modules, a clean emery cloth would be used to rough up the sides of new potted modules.

(2) A second MRB action pertained to the leads protruding through the potting material of the potted modules. It was decided that modules with protruding leads on the bottom were to be rejected. Modules with protruding leads on the top were to have a protective coating applied over the exposed leads.

(3) The third MRB action provided for the symbolization defects. It was decided that, although a light white film over the symbolization was not aesthetically pleasing, it would be acceptable if the symbolization was legible.

A problem of carrier board delamination around the terminals was caused by excessive heating of the printed wiring board during the tinning of the terminals. The amount of delamination experienced did not warrant scrapping the boards.

*Testing.* Data encoder subsystem tests included margin tests, analog-to-digital converter checks, calibrations, environmental tests, and data encoder subsystem tests.

The margin test was intended to show whether any degradation was occurring during subsystem or spacecraft tests. The tests included checks on input regulation, load regulation, modulator, low-level amplifiers, bucking supplies, commutator channel offsets, and A/DC linearity.

The calibration tests were conducted during the thermal-vacuum portion of the flight acceptance test at ETL (Environmental Test Laboratory). A complete five-point calibration of each analog telemetry channel was run at 0, 25, and 55°C. A precision voltage source and a field-effect transistor were used to simulate inputs to the appropriate channels. The voltage was set such that the A/DC was on an indecision point rather than a solid data number. By using this indecision point rather than a solid data number, more accurate calibrations were possible. No significant problems were encountered during environmental testing.

*System problem areas.* Deck skips have been observed on all *Mariner* spacecraft. A deck skip/reset (any improper commutation sequence) is caused by spacecraft power transients. It is worthwhile to note that after transfer of the spacecraft from SAF to AFETR, prior to launch, very few deck skips were observed during extensive system testing.

During the buildup of MV67-2 spacecraft, it was discovered that the system test complex data system (STCDS) was not capable of working with the data encoder OSE (operational support equipment) interface. The operational schedule was not hindered however, since the STCDS was capable of working with its inputs from GTS (ground telemetry subsystem). An investigation of this problem revealed a common mode voltage of 7 V between the data encoder OSE and the STCDS, which prevented the STCDS from working off this interface.

A Problem Failure Report was written against homing of the flight data encoder with the launch complex equipment (LCE), which brought about an intensive investigation of the problem.

As a "quick fix," an IP switch in the LCE (which furnished the commutator control pulses) was modified to provide a low-output impedance amplifier. This modification apparently solved the problem, but ground isolation was broken between the LCE logic ground and the line amplifier ground (located in the umbilical tower).

In an attempt to restore ground integrity, an isolation amplifier, driven by the low-output impedance amplifier, was used to provide the commutator control pulses. Subsequently, the problem reoccurred in SAF operations.

Investigation revealed that the blockhouse to spacecraft cabling combined functions in twisted shielded pairs and provided only one return. Each data encoder function in the cable was combined with its own separate return in a twisted pair shielded cable.

Upon implementation of the modifications, no further problems were experienced with homing operations at

AFETR. There were no data encoder problems during the entire testing program conducted at AFETR. The data encoder subsystems on both spacecraft performed normally. It might be noted that the deck skip problem was noticeably less frequent and pointed to a better testing environment.

*b. Telemetry transducers (temperature and pressure).* There were twenty-five 500 Ω and twenty-four 125 Ω temperature transducers used on the *Mariner V* spacecraft. The transducers consisted of platinum wire sensors capable of measurement over the range from −300 to +300°F with an approximate sensitivity of 1 Ω/°F.

The solar-panel temperature transducers were electrically equivalent, miniaturized, extended range (−425 to +400°F) versions that were designed specifically for solar panel measurements; twelve were used on the *Mariner V* spacecraft. The design of the solar-panel temperature transducers was changed to incorporate Teflon tape rather than Mylar tape because of the higher temperatures predicted.

There were no problems in installation, testing, or flight. The pressure tranducers were potentiometric devices of 300-turn resolution, employing a Ni-Span-C Bourdon tube for high-pressure application (i.e., ≤ 300 psi), or bellows as sensing element. Seven pressure transducers were used on the *Mariner V* spacecraft (i.e., two 4000-psi A/C nitrogen, one 4000-psi PIPS nitrogen, one 500-psi PIPS propellant, one 500-psi PIPS oxidizer, one 300-psi motor chamber, and one 40-psi tape recorder transport).

There were no design changes nor procurement required for the *Mariner* Venus 67 program. During cape operations, one PIPS oxidizer transducer developed an external leak and was replaced. This failure was of a critical nature and cast doubt on the flight integrity of the other flight units. The problem was, however, determined to be specific to this unit, not generic. Through midcourse, there were no pressure transducer anomalies.

***6. Radio subsystem.*** The *Mariner V* radio subsystem (RSS) was basically the same as the *Mariner IV* system. There were some modifications of the *Mariner IV* system to make it compatible with the *Mariner* Venus 67 mission requirements; however, these changes did not greatly change the design or functional requirements of the RF subsystem.

The *Mariner V* RSS was required to provide for phase-coherent two-way tracking, for reception and demodulation of command signals, for transmission of the telemetry data, for reception and transmission of a pseudo-random sequence for ranging information, and for an RF signal for the occultation experiment.

A block diagram of the *Mariner V* RSS is shown in Fig. IV-47 (*Mariner V* differences to the *Mariner IV* RSS are also indicated). The description of the *Mariner IV* RSS (Refs. 1 and 11) is valid for the most part. Only those areas in which changes were made for *Mariner V* RSS will be covered in detail.

*a. Modifications of Mariner IV radio subsystem.* Because the *Mariner* Venus 67 project was constrained to use the *Mariner IV* design and hardware where possible, the only acceptable design changes were those necessary to accomplish mission requirements. Thus, the only changes made were those that, if not accomplished, would have adversely affected the RSS mission performance. These changes were in two categories:

(1) Elimination of the probability of self-lock, thereby providing the capability for ranging throughout the mission.

(2) Utilization of the interferometer effect to maintain two-way tracking and command capability at encounter without antenna design changes.

*Prevention of self-lock to enable the use of ranging.* The ability to use the ranging channel of the *Mariner V* RSS was a very desirable feature for both tracking and scientific reasons. Ranging provided a significant improvement in orbit determinations. Also, by using recently developed ground-based ranging equipment, it became possible to range at planetary encounter distances. This ranging would provide valuable scientific information when used in conjunction with the two-way doppler and occultation measurements made at encounter.

Although turnaround ranging was a built-in capability of the *Mariner IV* RSS, it was not possible to use ranging unless the problem of self-lock was solved. When the problem was found, just prior to the launch of *Mariner IV*, it was not possible to fully analyze the problem and provide a solution. Since the capability for ranging was desirable, an extensive analysis was performed to better define the self-lock problem so that modifications to the *Mariner IV* RSS could be made.

Self-lock can be defined as the acquisition of phase lock by the transponder receiver on an internally (self) generated signal that is not dependent upon external (earth generated) signals. Self-lock in flight could effectively negate the two-way tracking capability of the

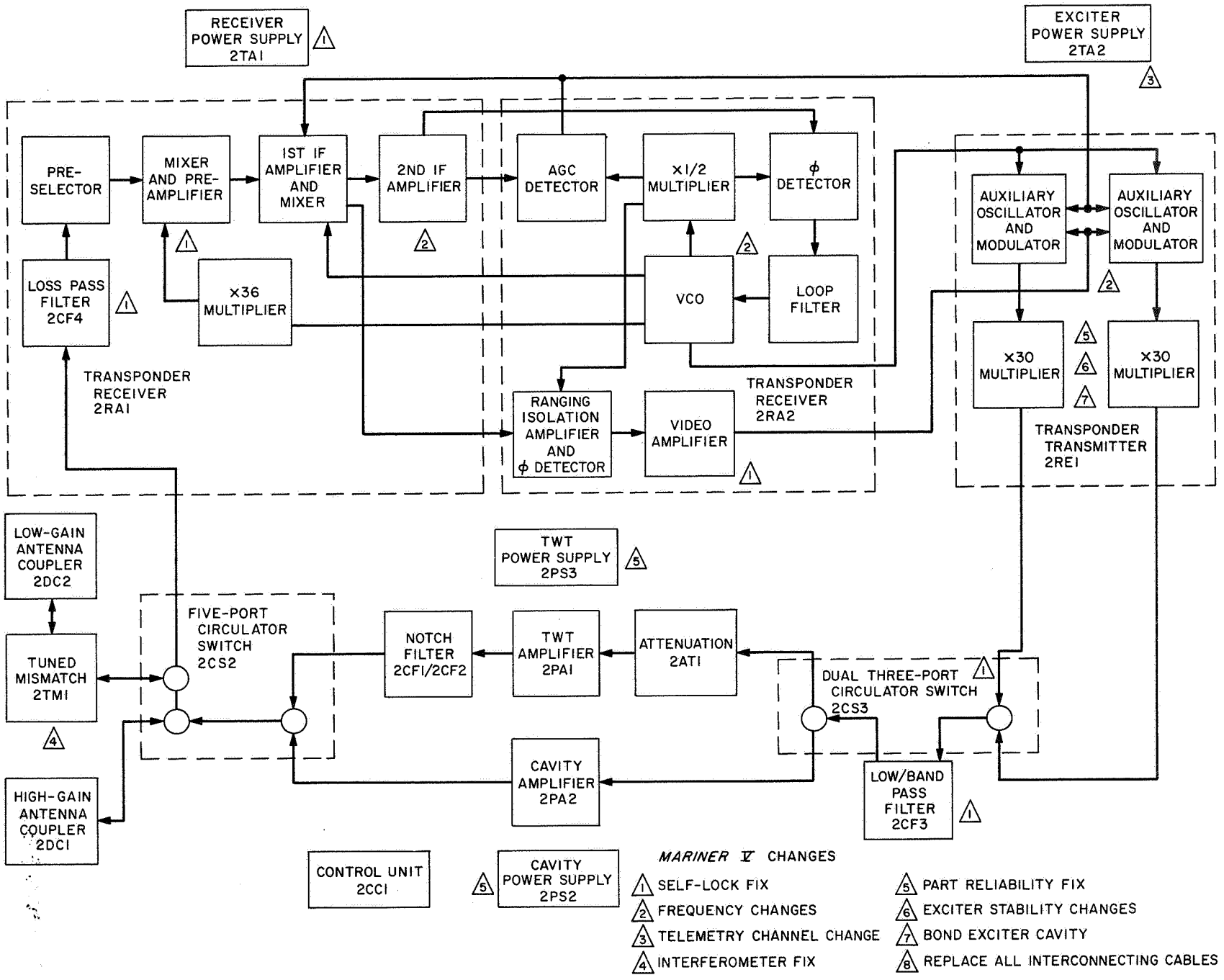



**Fig. IV-47. Radio subsystem block diagram**

transponder and prevent the reception and demodulation of ground transmitted commands, since the receiver can only respond to the signal to which it is locked.

Self-lock is the result of an unwanted spurious signal that is generated in the transponder and that is not harmonically related to any of the transponder primary frequencies. Through various mixing modes and paths this signal can enter the ranging channel within its bandpass (approximately 3 MHz). The signal is then detected by the ranging channel modulation detector and is amplified and limited. Then the signal is remodulated onto the transmitted carrier, as is a normal ranging signal. Using the broadband amplification properties of the TWT and/or its nonlinear mixing capability, these signals are then passed into the receiver. These self-lock signals, which are at about 4 GHz in frequency, then pass through the receiver preselector (bandpass) filter, which does little to reject signals above 3.5 GHz, into the receiver input and through various mixing products result in a frequency to which the transponder can acquire phase lock. Although this explanation is somewhat oversimplified, several requirements for self-lock become apparent:

(1) The ranging channel must be on.

(2) The receiver preselector (bandpass) filter must pass the unwanted signal with little attenuation.

(3) The TWT broadband amplification characteristics (800 MHz to 4.6 GHz with positive gain) may be required to pass the signal and/or mix the various exciter output frequencies.

(4) A spurious signal not harmonically related to the transponder primary frequencies must be generated.

These items define the requirements for ranging-on self-lock. If it is possible to limit or eliminate some of these requirements, self-lock can be prevented. The solutions used for *Mariner V* are shown in Fig. IV-47.

Item (1) could not be eliminated, since the desire was to use the ranging channel. However, a relatively minor fix was available that would automatically turn the ranging channel off, if it were on, whenever the CC&S issued a CY-1 pulse. This fix would prevent the failure of the receiver, if the transponder did go into self-lock with ranging-on, through some other mechanism that the other fixes did not prevent. This fix was accomplished by the addition of a diode in the power supply that controls ranging-on and ranging-off. The diode was placed in the turn-off logic of the ranging control such that, whenever the CC&S CY-1 66⅔-h cyclic interrogated the RSS, ranging would be automatically turned off if it were on.

Item (2) was the result of the fact that the preselector filter at the receiver input is a true bandpass filter only up to 3.5 GHz. The filter provided about 100 dB of rejection to frequencies except at its bandpass (2116 $\pm$ 20 MHz) below 3.5 GHz. However, above its passband, the filter began to act as a waveguide that propagated frequencies above 3.5 GHz with little attenuation.

The problem was solved by the addition of a lowpass filter with a 3.5-GHz cutoff frequency. This filter would provide rejection to frequencies above 3.5 GHz, with little insertion loss (less than 0.2 dB) at and below the receiver input frequency.

The preselector was mounted in one of the module spaces in the 2RA1 six pack. Since the six pack had one unused module space, the lowpass filter was added by fabricating it with an external mechanical configuration similar to the preselector. Because of the proximity of the two filters, little cabling insertion loss was added to the receiver input.

The net result of the preselector-bandpass/lowpass filter combination was to provide a true bandpass characteristic at the receiver input with very high rejection to frequencies above and below its bandpass (2116 $\pm$ 20 MHz). For signals below and above 2116 $\pm$ 180 MHz to somewhat above 10 GHz, the rejection is about 100 dB.

Item (3) is a typical broadband amplification characteristic of a traveling wave tube amplifier (TWTA). The only way of reducing this effect is to limit the band of possible input frequencies, or by limiting the band of possible output frequencies. By placing a bandpass/lowpass filter at the output of the exciters, a very high rejection to frequencies outside of the filter bandpass (2298 $\pm$ 20 MHz) could provide true bandpass filtering at the input to the TWTA.

This filter installation was accomplished by replacing the *Mariner IV* four-port circulator switch at the output of the exciters with a dual three-port circulator switch. The new switch permitted the installation of the single bandpass/lowpass filter in the common line between the switch sections, as shown in Fig. IV-47. Thus, the one bandpass/lowpass filter would filter the output of both exciters and the input to both power amplifiers. This filter accomplished the same type of function at the transmitted

2298-MHz frequency that the preselector/lowpass filter combination achieved at the received frequency. That is, a true bandpass characteristic was created by combining both types of filters to achieve a very high rejection of frequencies outside of its bandpass (2298 ± 20 MHz). For signals above and below 2298 ± 180 MHz the rejection is about 100 dB.

It was necessary to retain the 2116-MHz notch filter at the output of the TWTA, since the exciters could generate signals within the receiver bandpass. The notch filter characteristics complemented those of the receiver bandpass and, hence, added about 100 dB more isolation between the TWT and the receiver. The narrowband cavity amplifier, by the nature of its high-Q tuned RF cavity design, provided high rejection to frequencies near 2116 MHz. For this reason, and the fact that the exciter bandpass/lowpass filter increased 2116-MHz rejection about 100 dB, the cavity notch filter was removed from the input to the cavity. Without the cavity notch filter about 160 dB of exciter-to-receiver isolation is achieved.

The overall improvement by the additional RF filtering is shown in Fig. IV-48. This figure represents the total isolation of the receiver mixer input from the transmitter exciter output using the TWT power amplifier for both the *Mariner IV* and the *Mariner V* RSS. The gradually decreasing and increasing isolation shown on both curves (from about 800 MHz to 4.6 GHz) is the result of the positive gain of the TWTA in this region. The important characteristic is the substantially increased rejection in the 4-GHz region, which is the major area of self-lock frequencies. This area shows a 100–200 dB improvement in receiver isolation. Spurious signals below the 2116-MHz region also can cause self-lock, and the filtering has increased this isolation by about 100 dB. This improvement includes a 100-dB increase in isolation at the receiver input frequency (2116 MHz).

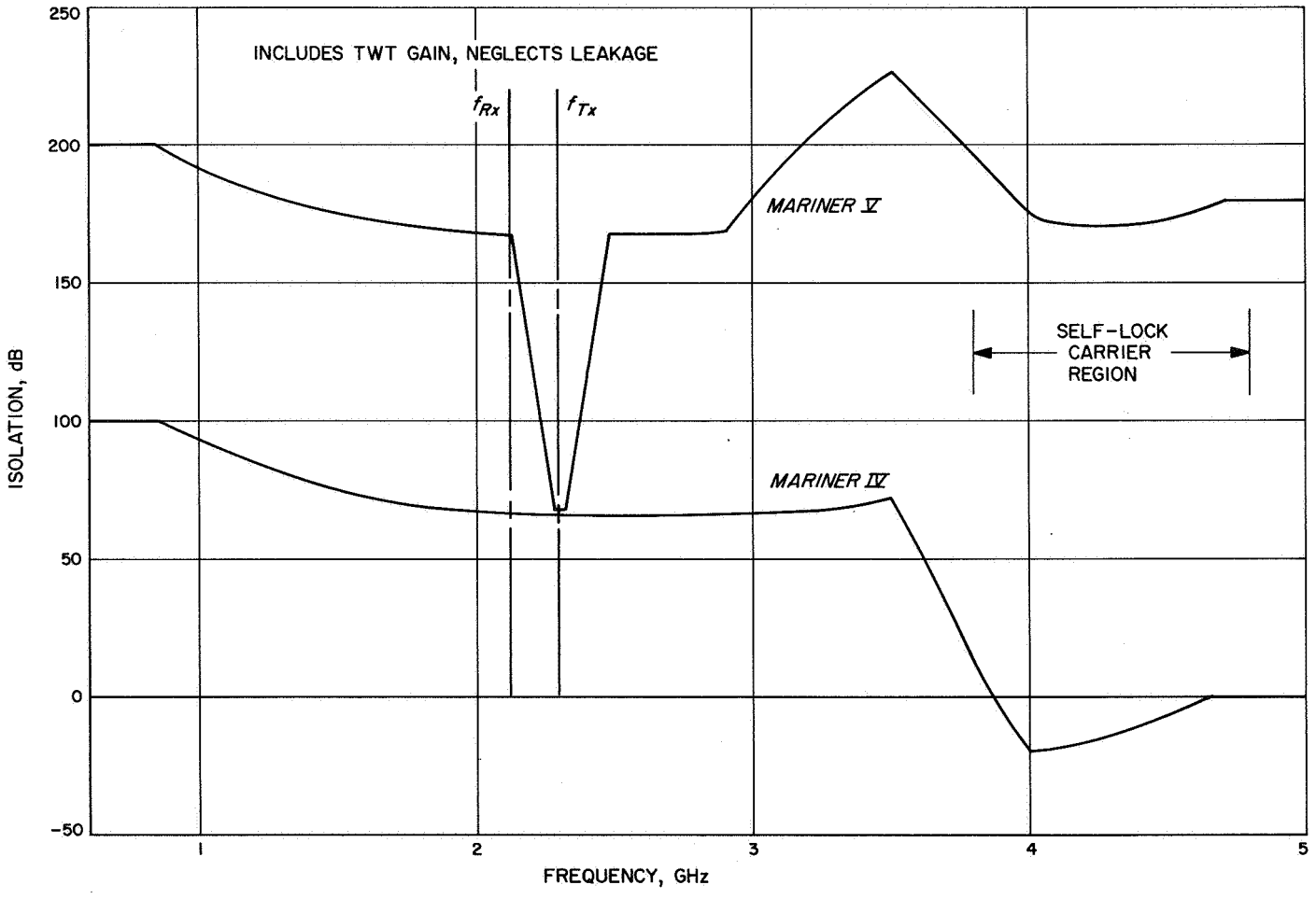



**Fig. IV-48. Transmitter exciter to receiver mixer isolation for *Mariner V* and *Mariner IV***

Item (4) in the list of self-lock requirements was the generation of spurious signals. The self-lock study revealed that only two modules were major generators of self-lock spurious signals. These modules were the preamplifier-mixer and the exciter X30 frequency multiplier. These modules had fundamental design problems that could, under certain conditions, generate spurious signals. Other modules in the transponder were also capable of generating spurious signals; however, a failure resulting in severe detuning was required.

The preamplifier mixer was found to have a low-level instability in its cascode amplifier stages (caused by the high-frequency transistors). Under certain input voltage and temperature conditions, this instability could sustain the generation of a spurious signal. The problem was corrected by replacing two of the high-frequency transistors with those of a lower frequency. They were then cycled over the temperature range and the voltage varied while observing the output spectrum. No spurious signals were observed.

To eliminate spurious generation, the X30 frequency multiplier would have required complete redesign. However, through very careful tuning and testing of the multiplier, the possibility of spurious signal generation could be minimized. Further investigation into the ranging performance characteristics revealed that the modulation response of the exciter was highly unstable, resulting in ranging modulation distortion and large ranging phase delay changes with temperature. This instability limited the ranging accuracy of the transponder and reduced the overall reliability of the exciter. With relatively minor changes to the X30 input stages and the auxiliary oscillator phase modulator, and by reducing the modulation bandwidth from 1.8 to 1.0 MHz, the ranging delay stability of the transponder was greatly improved. The stability improvement also reduced the chances of the generation of self-lock spurious signals by the X30 frequency multiplier.

*Interferometer problem and solution.* During the *Mariner* Mars 1964 program, a phenomenon known as the interferometer effect was recognized. This effect manifests itself as a periodic, large variation in the uplink or downlink signal during the portion of the flight when the spacecraft-to-earth vector intersects the main lobe of the high-gain antenna, and when reception or transmission is attempted over the low-gain antenna. This signal variation is caused by the circulator switches used to connect the radio transmitter and receiver to the high- and low-gain antennas.

Ideally, all RF energy entering a particular port of a circulator switch would exit at the adjacent port (in the direction of the arrow shown in Fig. IV-49). However, there are two effects that upset this ideal case. These effects are junction leakage and reflected energy.

Junction leakage, inherent in all circular switches, allows a finite amount of energy to circulate in the opposite direction and exit at the third port. This leakage, known as intrinsic isolation, is typically 18–36 dB below the normal path signal for the type of switches used in the *Mariner IV* radio subsystem.

Reflected energy occurs when the exit port is not perfectly matched (VSWR = 1.00:1), since energy reflected from this port will be circulated to the next adjacent port. Figure IV-50 shows the magnitude of the reflected signal relative to the normal signal as a function of the exit port VSWR. This exit port mismatch is the resultant of all component mismatches downstream of the port.

In the case of the *Mariner IV* circulator switch, if the exit port is the common leg between the two switches (Fig. IV-49), the effect must be traced through the next circulator switch and its mismatches.

For example, assume that the switches are set in the transmit-low/receive-low mode (Fig. IV-49) and that both

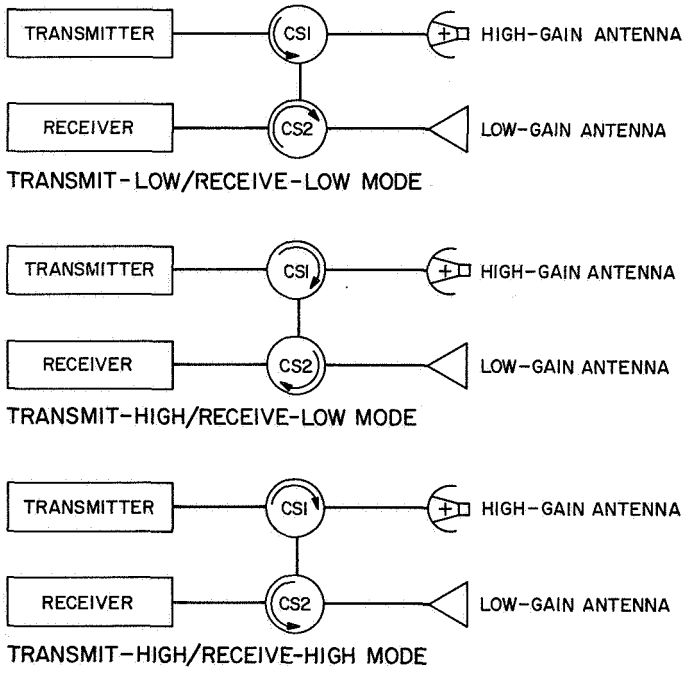



**Fig. IV-49. Radio/antenna operational modes, simplified block diagram**

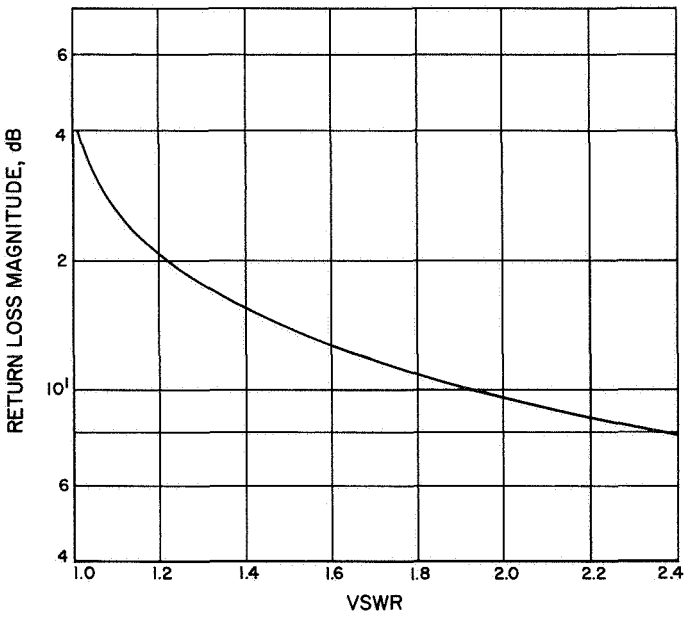



**Fig. IV-50. Return loss vs exit port mismatch VSWR**

switches have infinite intrinsic isolation, the normal 2116-MHz uplink signal will be received by the low-gain antenna and circulated directly into the receiver. In addition, any uplink energy entering the high-gain antenna circulates first through the upper switch to the transmitter (which is effectively an infinite mismatch at the receive frequency), then back through the upper switch, then down to the lower switch and finally out toward the low-gain antenna. However, since the low-gain antenna is not perfectly matched at the uplink frequency, a portion of the signal will be reflected back through the lower switch to the receiver.

This example demonstrates that, even with perfect circulator switches, an interferometer effect can be generated. In reality, both junction leakage and reflected energy exist; for simplicity, their resultant is called the effective isolation of the system. The magnitude of this resultant, as well as the resultant high- and low-gain received or transmitted signals that produce the interferometer, are dependent on the magnitude and phase differences between the two signals. In general, the greatest sum and the least difference relative to the larger signal will occur when the signals are in-phase and out-of-phase, respectively. Figure IV-51 represents the magnitude of the interferometer effect relative to the larger signal as a function of the difference in magnitude of the two interfering signals. For two signals of equal magnitude, the gain would be 6 dB when in-phase, and the loss would be infinite when out-of-phase.

Table IV-17 lists the radio mode in which an interferometer effect exists and indicates whether the effect is significant or not.

**Table IV-17. Significant interferometer modes**

| Radio/antenna mode | | Interferometer exists | |
|---|---|---|---|
| Transmit | Receive | Uplink | Downlink |
| Low | Low | Yes | Yes |
| High | Low | Yes | No |
| High | High | No | No |

Operationally, the transmit-low/receive-low interferometers are only of consequence during the midcourse maneuver where the desired thrust vector might place the spacecraft-to-earth vector within the main lobe of the high-gain antenna, and during cruise just prior to switchover to transmit high-gain antenna. These two isolated problems are of relatively minor consequence when compared with the transmit-high/receive-low interferometer (which was the prime planetary fly-by mode for *Mariner V*).

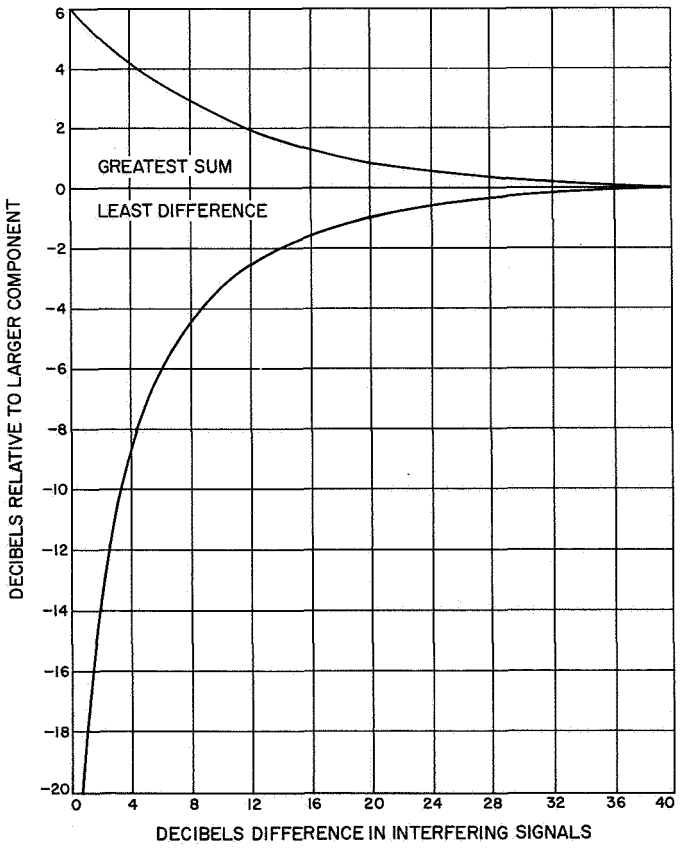



**Fig. IV-51. In-phase and out-of-phase sum of two RF signals**

An analysis of the telecommunications parameters for the *Mariner V* spacecraft at encounter revealed that the nominal uplink received signal strength through the low-gain antenna alone would be at command threshold for the DSIF 85-ft antennas transmitting 10 kW (the basic mission configuration). To be able to encounter Venus in the transmit-high/receive-low mode, it was decided to enhance the interferometer effect such that at no time from 10 days before to 2 days after encounter would the uplink signal level come within the sum of the negative tolerances of command threshold.

This approach was possible because all critical flight hardware components were in existence and their complex impedances easily determined. The two critical components involved were the five-port circulator switch and the low-gain antenna. Upon measurement of these components, it was determined that without enhancement the most likely effective VSWR of a flight system would be 1.30:1 or an effective system isolation of 18 dB. An analysis of the uplink interferometer for this condition in the encounter region revealed the uplink spacecraft-received signal-strength prediction as shown in Fig. IV-52. Only the locus of maximums and minimums could be determined exactly. The received signal pattern is shown only for illustration with an assumed worst-case phasing at encounter.

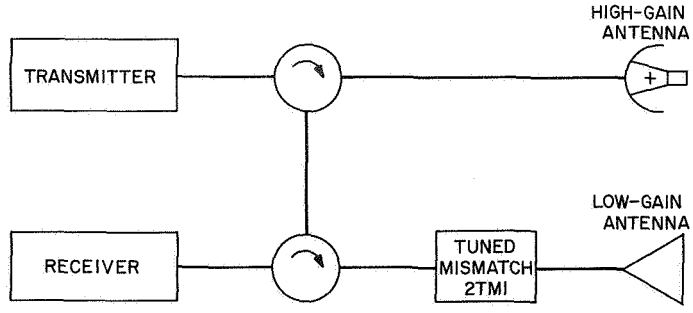



**Fig. IV-53. *Mariner V* interferometer fix**

Further analysis showed that if the effective isolation was reduced to $9.5 \pm 1.5$ dB, the mission uplink requirements would be satisfied. This effective isolation reduction corresponds to an effective low-gain VSWR at the five-port circulator switch of 2.0:1.

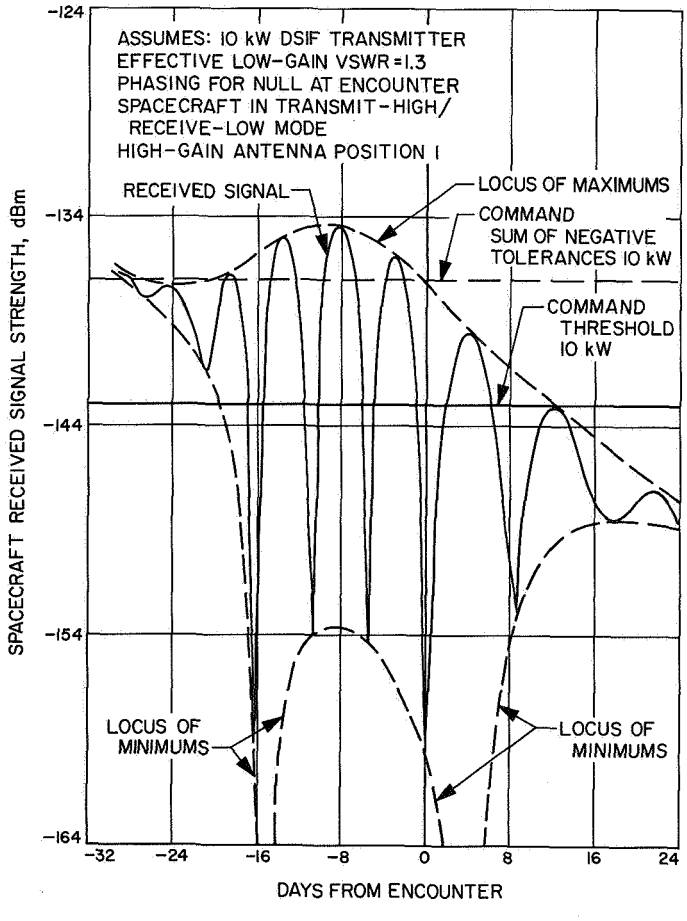



**Fig. IV-52. Unfixed *Mariner V* uplink interferometer pattern vs days from encounter**

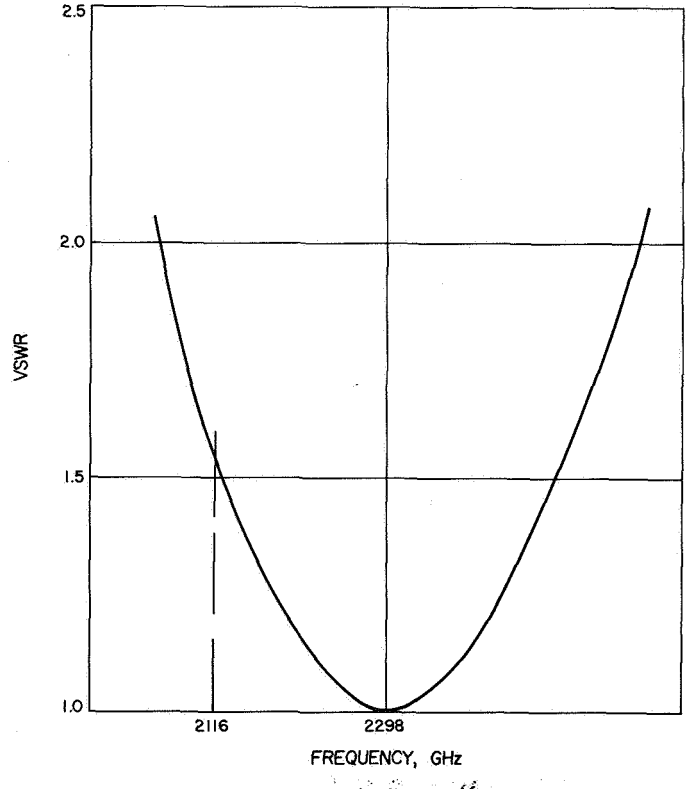



**Fig. IV-54. VSWR vs frequency characteristics of a ¾-wavelength shorted coaxial stub**

This design requirement resulted in the addition of a tuned mismatch at the low-gain antenna port of the five-port circulator switch, as shown in Fig. IV-53. The tuned mismatch is a ¾-wavelength shorted coaxial stub that has a 1.53:1 VSWR at the uplink frequency, yet it is a perfect match at the downlink frequency and, hence, does not affect the low-gain transmitted signal (Fig. IV-54). When this mismatch is properly phased with the other components in the low-gain antenna leg of the five-port switch, the prescribed 2.0:1 effective VSWR is obtained. The mismatch increases the uplink circuit loss from the low-gain antenna to the receiver by approximately 0.5 dB; however, this loss only increases the uplink grey-out by approximately three days prior to entering the interferometer region. The expected worst-case uplink interferometer patterns for the *Mariner V* near encounter for the pre- and post-encounter high-gain antenna positions are shown in Figs. IV-55.

A computer analysis of the problem produced an output of antenna gain versus cone and clock angles from which a three-dimensional contour plot of the 1.8:1 case could be generated (Fig. IV-56). This plot also shows the earth track as a parameter. The area shown in dark gray is the region below command threshold as determined by the cone angle and range to earth versus time to encounter. Similarly, the light gray area depicts the region where the nominal received signal is above threshold but below the sum of the negative tolerances. The white area is the region of guaranteed uplink communications where the received signal level is above the sum of the negative tolerances.

It is obvious that the interferometer nulls still exist. However, they exist along the earth track well before and well after the period of guaranteed communications. They also exist on either side of the white region and, hence, present a precariously small roll drift margin.

*b. Telemetry.* When the *Mariner* Venus 67 program was initiated, only critical or potential failure items were considered for changes.

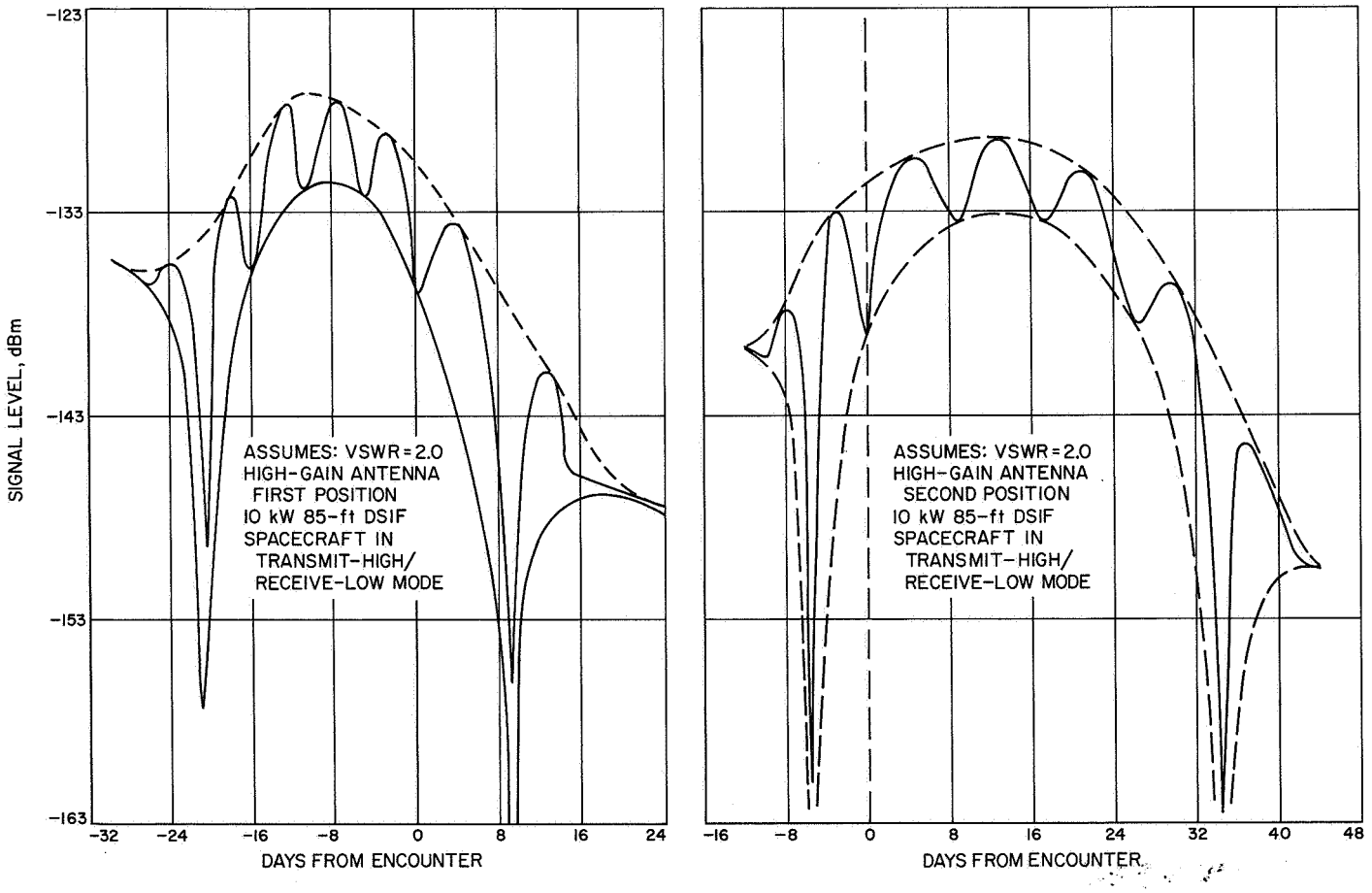



**Fig. IV-55. *Mariner V* uplink interferometer fix received signal level vs days from encounter**

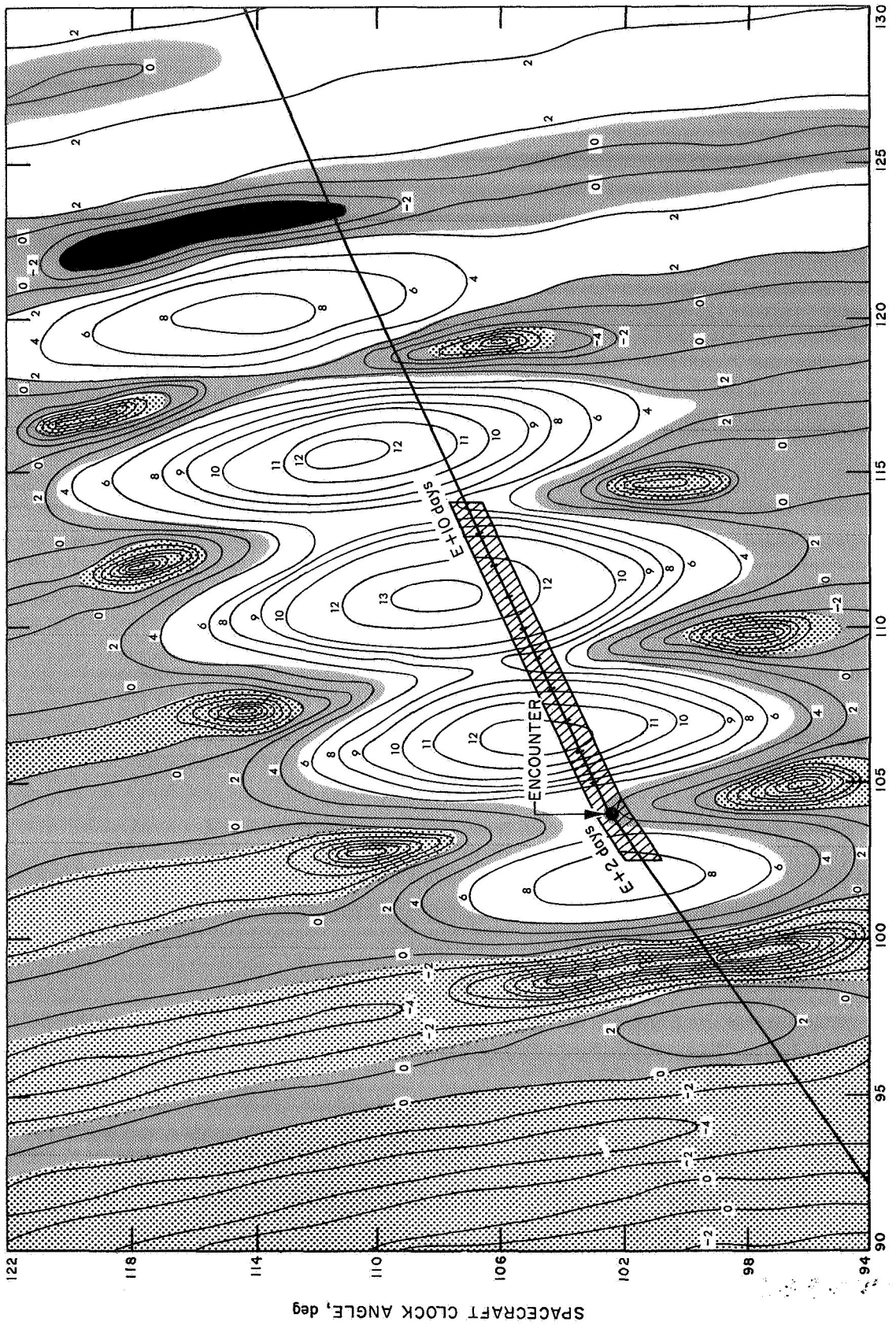



Fig. IV-56. Interferometer contour pattern, 18:1 effective VSWR

Two temperature transducers were added to the auxiliary oscillator modules in order to more accurately predict the downlink frequency when operating in the noncoherent mode. Since the auxiliary oscillator frequency is mostly dependent upon temperature changes of the crystal, the addition of the two transducers made it possible to calibrate frequency over the entire temperature range expected during the mission.

A second change to the radio subsystem telemetry (TLM) channels made it possible to determine whether exciter A or B is operating. Channel 302 (exciter − 15V) was used to monitor the −15V supply voltage for both exciters (only one exciter and associated power supply was on at any time). By changing one of the resistors in the voltage divider network, the voltage output to the data encoder was different depending on which exciter was operating.

The last change improved the operating characteristic of the TLM channel 229 (exciter drive). This improvement was done by changing the power monitor design in the new dual three-port circulator switch, which provides the voltage for telemetry. This switch provides 30-dB isolation between the diode monitor and the output of the circulator switch. *Mariner IV* had little or no isolation; hence, when the power amplifiers were switched, the mismatch between the power amplifiers and the output of the circulator switch caused this TLM voltage to vary as a function of which power amplifier was operating.

By employing better calibration techniques and calibrating over small temperature increments, greater resolution and accuracy was achieved in the radio subsystem telemetry. Table IV-18 gives a brief description of the TLM channels and their associated problems.

*c. Utilization of residual Mariner IV hardware.* The *Mariner* Venus 67 project required the utilization of as much of the *Mariner* Mars 1964 residual hardware as was possible with a minimum procurement of new hardware. From the residuals, it was hoped that the equipment would be available to meet the project requirements of having one flight, one flight spare, and one TA radio subsystem, as well as the test sets and test equipment that would be required. These objectives were met.

In addition to the four radio subsystems available for use, there were three OSE flight test sets, one LCE launch checkout rack, one DSIF equivalent OSE, and miscellaneous test equipment. Based on this hardware availability, two flight systems and a TA system were chosen to be used. The OSE and the LCE available were felt to be sufficient, with minor modifications, for most testing requirements. However, it was necessary to purchase some specialized test equipment and to build in-house a power amplifier test set to complete the test equipment required for *Mariner* Venus 67.

The M67-2 RSS was used on the *Mariner C* flight spare spacecraft during the *Mariner* Mars 1964 program. At the end of the *Mariner* Mars 1964 operations, the spare spacecraft was placed in bonded storage. When the M67-2 RSS was returned, it was maintained as flight hardware and was selected as the *Mariner V* flight RSS. This choice was made because of the excellent past history of the system and the fact that the system had been handled as flight hardware at all times. Because of its past environmental test history, the M67-1 RSS was questionable for use as the *Mariner V* flight spare.

To use the M67-1 and M67-2 as the *Mariner V* flight units, a decision was required as to the operating frequencies that would be used. The M67-2 RSS frequencies were being used by *Lunar Orbiter*, leaving the M67-1 RSS frequencies for possible use. However, if the M67-1 RSS were to be used, DSIF would have to acquire new VCOs for all the DSN stations. Also, the use of these frequencies would increase the operational complexity of the stations in tracking the *Mariner V* and *Mariner IV* spacecraft on separate frequencies. After careful analysis of the trajectories of the two *Mariner* spacecraft, it was found that the differences in view periods, doppler frequency separation, and expected signal levels would allow the *Mariner IV* frequencies to be used with little risk involved.

*d. Conversion of residual Mariner IV radio subsystems to Mariner V flight hardware.* The following section will describe the new hardware designed to accommodate the self-lock and interferometer fixes, as well as the retrofit of the transponders. It will also cover the rework of a more minor nature, the individual component retest, and the reassembly of the subsystem up to, but not including, flight acceptance requalification.

*Filters and dual three-port switch.* Design, fabrication, and testing were accomplished on a very tight time schedule; however, critical delivery dates were met.

*RF cables.* One of the most frequent types of problems and failures during the *Mariner* Mars 1964 program was the failure of RF cables. At the outset of the *Mariner*

## Table IV-18. *Mariner V* radio subsystem telemetry channel assignments

| Channel | Measurement | Measurement range Eng units | Measurement range Voltage | Importance to in-flight performance | Importance to failure analysis | Problem areas |
|---|---|---|---|---|---|---|
| 106 | Receiver SPE (static phase error) | ±600 Hz | ±1.5 Vdc | Indicates receiver VCO frequency and best lock frequency | Indicates overall performance of phase lock receiver | Not enough resolution; very sensitive to temperature changes |
| 111 | Receiver AGC (coarse) | −90 to −150 dBm | 0–3 Vdc | Indicates received signal strength | Indicates overall performance of phase lock receiver (back up for channel 215) | Too sensitive to temperature; lowers accuracy of channel |
| 210 | Local oscillator drive | ±3 dBm | 0–100 mV | Indicates local oscillator drive to balanced mixer of receiver | Indicates performance of receiver multiplier (X36) and first mixer | [a] |
| 215 | Receiver AGC (fine) | −115 to −145 dBm | 0–100 mV | Indicates with greater resolution the received signal level | Indicates overall performance of phase lock receiver (back up for channel 111) | [a]; sensitive to temperature; makes resolution useless and limits accuracy |
| 213 | High-gain antenna drive | +23 to +41 dBm | 0–100 mV | Indicates RF drive power to high-gain antenna | Indicates performance of downlink signal | [a]; not enough isolation between diode and output of coupler, thus making output voltage sensitive to VSWR changes |
| 214 | Low-gain antenna drive | +23 to +41 dBm | 0–100 mV | Indicates RF drive power to low-gain antenna | Indicates performance of downlink signal | [a]; not enough isolation between diode and output of coupler, thus making output voltage sensitive to VSWR changes |
| 229 | Exciter drive | +12 to +29 dBm | 0–3 Vdc | Indicates RF drive power to TWT or cavity | Indicates performance of X30 multiplier in transponder | Output impedance too high, causes loading |
| 300 | Helix Current<br>Cathode Current | 0–18 mA<br>0–148 mA | 0–3 Vdc | Indicates amount of helix or cathode current flowing in TWT or cavity | Indicates performance of TWT or cavity power amplifier | No problems |
| 301 | Exciter voltage 1 | 0 to −30 Vdc | ±1.5 Vdc | Indicates exciter −25 Vdc power supply voltage | Indicates performance of exciter power supply | Poor resolution, only utilizing 20% of TLM channel |
| 302 | Exciter voltage 2 | 0 to −18 Vdc | ±1.5 Vdc | Indicates exciter −15 Vdc power supply voltage; identifies which exciter is operating | Indicates performance of exciter power supply | Poor resolution, only utilizing 20% of TLM channel; level changes when going from VCO to AUX OSC |
| 404 | Bay V temperature | +25 to +150°F | NA | Indicates average temperature Bay V | NA | No problems |
| 405 | Bay VI temperature | +25 to +150°F | NA | Indicates average temperature Bay VI | NA | No problems |
| 414 | Aux osc A temperature | +25 to +150°F | NA | Enables ground station to acquire downlink quickly | NA | Not enough resolution |
| 418 | Aux osc B temperature | +25 to +150°C | NA | Enables ground station to acquire downlink lock quickly | NA | Not enough resolution |
| 424 | VCO crystal temperature | +25 to +150°C | NA | Enables ground station to acquire uplink lock quickly | NA | Not enough resolution |

[a] All 100-mV channels are too sensitive to noise generated on the spacecraft.

Venus 67 program, this problem was thoroughly reviewed and all residual cables reinspected. Numerous deficiencies were noted concerning the cable design, connector assembly, and hardware quality.

To eliminate these deficiencies, all RF cables were redesigned, new assembly instructions were generated, and close quality assurance was performed during manufacture. These cables were fabricated on-lab primarily due to the extremely tight delivery schedule. As a result of this closer attention to cable quality, only two noncritical failures concerning the new cables occurred. Neither of these failures was traced to manufacturing quality.

*Tuned mismatch.* As previously described, the tuned mismatch was used to effectively lower the isolation between the high-gain antenna and the receiver so that the interferometer effect could be used to accomplish planetary fly-by in the transmit-high/receive-low mode. The device consisted of a shorted section of semi-rigid, 0.141-in. coaxial line that was three quarters of a wavelength (2.71 in.) long, a coaxial tee, an adapter, and a special length of semi-rigid coaxial cable.

*Rework and requalification of Mariner IV residual RF components.* The *Mariner IV* RF components were electrically tested, mechanically inspected, and where necessary, retuned or reworked on-lab. In general, the rework of these components was limited to internal and external cleanup and paint touchup. Upon completion of the rework, all RF components were recalibrated and requalified at 0, 25, and 55°C.

The five-port circulator switch, the triode cavity and TWT amplifiers, and the TWT and cavity power supplies were electrically reworked.

*e. Transponder rework and requalification.* The residual transponders to be used in the *Mariner V* RSS were reworked and requalified. The rework, changes, and additions to the transponder were made because of the *Mariner* Venus 67 mission requirements and to enhance the overall reliability and performance of the transponder.

The requalification of the transponders (to insure they met flight performance requirements) included a complete revision in the previously used test techniques. In particular, changes were made in the test procedures used and the method of recording data for the final acceptance testing. This improved the quality of the data, as well as making it more easily interpreted. The transponders were also calibrated by using smaller temperature increments and specifying test equipment calibration standards and procedures used. By doing this calibration and standardization, the radio subsystem functions such as static phase error (SPE), signal level versus AGC voltage, auxiliary oscillator frequency, and ranging phase delay were calibrated to a higher degree of accuracy than had been obtained previously.

In the case of the ranging phase delay, automatic test equipment was available to rapidly make accurate delay measurements over the full temperature range and at different transponder receiver input signal levels.

*f. Radio subsystem flight acceptance and type approval testing.* In comparison to the *Mariner* Mars 1964 program, the *Mariner* Venus 67 FA testing was relatively trouble free. Many of the FA testing problems had been previously resolved, and by use of personnel familiar with the *Mariner* Mars 1964 program, potential problems were recognized early in the testing.

One of the more significant changes made in the FA testing was in the method of data taking and evaluation. Although the techniques for making the various measurements had not been greatly changed, the modification of the data sheets and the testing sequence resulted in a more meaningful consolidation of the data, shorter test time per sequence, more data accumulated in a format more easily evaluated, and a fixed number of measurement modes representative of flight operating modes.

Vibration testing was accomplished by mounting both cases on a single shake fixture so that the RSS could undergo vibration as a system. This method resulted in more meaningful results, since the cases previously had to undergo vibration separately.

The vacuum-temperature tests were conducted in much the same way as in the *Mariner* Mars 1964 program, except that the test modes used provided a more stable system at the time the measurements were made. However, unlike the *Mariner* Mars 1964 program, no attempt was made to calibrate the RSS telemetry channels for only three discrete temperature ranges. The test was a performance evaluation only. The measurements were used to compare against the more refined calibrations taken over several discrete temperatures prior to the vacuum-temperature test. However, comparison of the vacuum-temperature test results to calibrations indicated small discrepancies. An even higher degree of calibration accuracy could be attained if the entire RSS is

calibrated in its flight environment over the FA temperature range, using small temperature increments and adequate stabilization time. The test did indicate more clearly what was already known: the RSS performs differently in a vacuum environment than in air where convection cooling provides different thermal gradients. Protective devices were added to prevent possible thermal runaways and loss of vacuum through critical pressure (as happened during the *Mariner* Mars 1964 program).

The TA radio subsystem was tested to a *Mariner V* RSS type approval specification, which was similar to the *Mariner* Mars 1964 TA specification. Since a similar system had undergone full TA testing on the *Mariner* Mars 1964 program, the TA testing would provide verification of the new components and configuration of the *Mariner* Venus 67 system.

Many of the components making up the TA system were not handled as flight hardware after the end of the *Mariner* Mars 1964 program. The new hardware and components that were changes from the *Mariner IV* radio subsystem were, however, fully flight qualified. Thus, the primary test objective was to verify that these items would function properly during TA testing.

*g. Systems testing.* Once the radio subsystem has successfully passed FA testing, it is delivered to SAF for installation on the flight spacecraft. Almost exclusively from this time on, the RSS is evaluated as an integral part of the total spacecraft system. The many tests performed allow evaluation of the subsystem performance when interfaced with other spacecraft subsystems and ground support equipment. Prior to this time, these interfaces could only be simulated with the OSE used for subsystem testing. During these tests, the compatibility with other subsystems is evaluated, as well as the basic performance characteristics of the RSS.

The system testing was similar to the *Mariner IV* spacecraft testing. However, because of the knowledge gained from the *Mariner* Mars 1964 program, the procedures and quality of the testing were greatly improved. The RSS tests performed and the test sequence used in system testing permitted using the same test techniques used for the subsystem bench testing performed during FA testing. Because of this similarity, most of the test technique improvements were incorporated in the systems testing. Also, the measurements made, the data taken, and the data evaluation could be accomplished in a shorter time period with more meaningful results.

Although many other tests were performed on the spacecraft system, the only ones to be described are those that indicated specific problem areas or were of special significance to the RSS.

The system test essentially simulates various types of actual mission sequences and the various spacecraft operational modes expected in flight. However, for the RSS, only the mission uplink signal performance characteristics can be simulated. The downlink telemetry and ranging performance cannot be adequately simulated. The present OSE is not capable of simulating a DSIF receiving function, making it nearly impossible to make more than basic downlink performance measurements. The downlink telemetry threshold simulation and ranging performance at low-signal levels could only be accomplished during special tests with a DSIF station.

*Space simulator test.* The spacecraft vacuum-temperature testing performed in the space simulator provided the most valuable data concerning the expected RSS flight performance characteristics. These tests provided an extremely stable test environment, as well as sufficient time for making more accurate and refined measurements and for conducting special tests. The various other system type testing performed in other areas did not provide this stable environment, because of the changing spacecraft operating modes and the changing thermal environment. Also, the time available for special tests was usually limited. This limitation meant that, even though the RSS performance could be evaluated, the more accurate and refined measurements made in the simulator were not possible.

The space simulator testing allowed accurate measurement of auxiliary oscillator (AO) and voltage controlled oscillator (VCO) best lock frequencies as a function of temperature. The measurement of the VCO to AO warm-up frequency change was also measured as was the effect of the CC&S CY-1 pulse on the AO frequency. The calibrations of spacecraft receiver VCO frequency (SPE) and uplink signal level (AGC) as a function of the telemetry outputs were also more accurately determined.

Several other tests were made and, in general, the measurement results were superior to those in general system testing. However, the several ranging phase delay measurements made in the chamber resulted in data that could not be used. While the data were being taken, it appeared to indicate the expected results. However, when a closer analysis was performed using several crosschecks

available, the data indicated that the RSS phase delay was higher than previous measurement indicated, including subsystem vacuum-temperature tests. The increase in delay was not actually a RSS delay increase, but was due to the test setup used while in the chamber.

Besides the improved accuracy in the measurements taken because of the stability of the system and the greater time allowed for measurements, the expected in-flight performance was more clearly defined. As mentioned previously, the radio subsystem did not perform exactly the same in a vacuum as it did in an air ambient set of conditions, where convection cooling is available. The thermal gradients set up in the RSS were different in the two environments. Because of this difference, some of the telemetry channels showed changes where none occurred, or indicated changes greater or smaller than had actually taken place.

Because of the space simulator tests, an apparent cavity-amplifier output-power degradation indication experienced just after the launch of *Mariner V* was shown to be a characteristic of the cavity in a vacuum. The space simulator data showed the same telemetry indications experienced in flight, but hardline measurements confirmed there was no power change.

*S-band/DFR electromagnetic compatibility test.* Another system type test of specific interest to the RSS was the S-band/DFR electromagnetic compatibility (EMC) test. The object of the test was to verify that neither subsystem affected the performance of the other. The spacecraft was in a simulated flight condition and flight signal levels were simulated. The test was performed on both flight spacecraft, and no performance degradation was observed on either system.

As with any spacecraft system using independent radio receivers and/or transmitters, it was necessary early in the development of the *Mariner V* spacecraft to insure compatibility between the DFR and the RSS. These tests were first performed in a screen room using a prototype DFR and the engineering model RSS. The initial prototype tests performed in the lab and subsequent tests on the spacecraft indicated the presence of 50-MHz noise from the RSS power amplifier power supplies, as well as other spacecraft sources that interfered with the DFR VHF receiver. The investigation resulted in a bandpass filter being added to the VHF receiver and additional spacecraft filtering to reduce the level from the spacecraft 50-MHz sources.

The final S-band/DFR EMC tests performed on the two flight spacecraft verified that the problems encountered during the initial design phases were eliminated.

*DSIF/radio compatibility tests.* To establish compatibility between the DSIF stations and the *Mariner V* spacecraft telecommunications subsystems, the DSIF compatibility tests were performed. The purpose of these tests was to evaluate the spacecraft telecommunications subsystems performance with a DSIF station providing the spacecraft received signal and receiving the spacecraft transmitted signal. Two such tests were performed, one at Goldstone and the other at AFETR using DSIF 71.

Since the Goldstone tests were conducted with the nonflight engineering model RSS and the results were comparable to the tests on the two-flight spacecraft by DSIF 71 at AFETR, only the AFETR compatibility tests will be discussed.

The compatibility tests were performed over a calibrated RF air link between the spacecraft location in Building A0 and later in ESF (explosive safe facility). The RF links were very stable and, outside of one case of RFI, the link provided meaningful results. The RSS/DSIF compatibility tests performed were:

(1) Spurious radiation and false-lock check.

(2) Uplink and downlink thresholds.

(3) One-way and two-way frequency measurements and frequency stability.

(4) RSS receiver tracking rate capabilities at various uplink signal levels (i.e., ability to track a linearly varying input frequency) and receiver tracking range.

(5) Downlink telemetry threshold, modulation level, and phasing.

(6) Uplink command threshold and phasing.

(7) Ranging phase delay of the RSS.

(8) Ranging uplink and downlink thresholds, and downlink ranging modulation suppression and phasing.

The search for spurious signals and/or false-lock signals from the RSS transmitter proved that the RSS had no observable spurs that could cause DSIF difficulty. However, during the testing, several spurious signals were observed; they had a jamming effect on the DSIF receiver. Investigations revealed that these signals at about

2 GHz were being radiated by an RF path loss measurement being conducted elsewhere. Although the signal source was turned off for the remainder of the test, the problem of making these types of measurements over an RF link in an area such as AFETR was indicated; preventive measures were taken against possible future interference.

The threshold of the RSS receiver was measured by DSIF and found to be the same as that previously measured in system testing. The downlink signal to the DSIF receiver from the RSS transmitter indicated the same threshold as that measured using the station transmitter.

One- and two-way frequencies measured by DSIF showed good correlation to the predicted values and the values measured in system testing. The frequency and phase stability of the RSS transmitted signal in both one- and two-way lock showed the RSS to be a stable source.

The uplink command modulated signal transmitted by DSIF to the spacecraft receiver proved that the modulation from the station to the receiver and then to the command subsystem was of the correct polarity. At the same time, the command acquisition threshold was measured. These results indicated good correlation to both the theoretical value and the value measured in system testing. This correlation indicated that there was no command performance degradation by the RSS.

The telemetry signal transmitted on the downlink carrier from the RSS was found to have the correct modulation index and the proper phase polarity. The telemetry threshold measurements by DSIF were close to theoretical values, indicating no problems in transmission from the RSS. No comparable measurement was available from system testing, since the present OSE receiver is not capable of making telemetry threshold measurements.

The measurement of the RSS turnaround ranging performance indicated the downlink phase of the ranging modulation was inverted. This indication confirmed previous subsystem measurements, and was in no way detrimental to ranging performance. The uplink and downlink ranging thresholds showed good correlation with both the theoretical values and the Goldstone tests. No corresponding subsystem test data were available, since this capability does not exist in the present test equipment used for subsystem and system testing. The ranging phase delay of the RSS measured by DSIF was very close to the values measured in system testing.

**Table IV-19. Ranging phase delay of *Mariner V* RSS**

| Radio subsystem mode | | | | | | |
|---|---|---|---|---|---|---|
| Power amplifier | Exciter | Antennas | | DSIF 71 phase delay measurement, ns | RSS system phase delay measurement, ns | Difference, ns |
| | | XMT | RCV | | | |
| Cavity | A | Low | Low | 937.6 | 934 | +3.6 |
| TWTA | A | Low | Low | 914.6 | 914 | +0.6 |
| TWTA | B | Low | Low | 885.1 | 890 | −4.9 |
| Cavity | B | Low | Low | 908.7 | 910 | −1.3 |
| TWTA | B | Hi | Hi | 881.5 | 886 | −4.5 |

Table IV-19 shows the DSIF and system test measurement values for the same uplink signal levels. These measurements are remarkably close considering the limitations of the measurement equipment used in the subsystem phase delay measurements.

The transponder tracking rate and tracking range tests were somewhat hampered by both equipment problems and erroneously predicted values. As was expected, the tracking range was found to be somewhat greater than specified and, of course, was adequate for mission requirements. However, values published for the tracking rate of the transponder for given input signal levels were higher than the theoretical tracking capability of the transponder. When the rates were reduced to realistic values, the transponder tracked well for rates near the maximum theoretical limit. One major difficulty was found in performing the test. This difficulty was an apparent phase or frequency transient that occurred whenever the frequency ramp was applied by DSIF 71. This initial glitch was large enough so that the transponder receiver would not track it and thus would drop lock. Apparently, it was a marginal condition; since after several tries at initiating the ramp, the transponder did maintain lock and tracked the changing frequency without any trouble.

The DSIF compatibility tests were especially valuable in three ways. First, the tests verified that both flight radio subsystems were fully compatible with the DSN stations under the static (no doppler) conditions of the test and should present no outstanding difficulties during the mission.

Second, DSIF performed several measurements that were not possible to make by the radio group with the equipment available. Specifically, these measurements were the ranging uplink and downlink thresholds, telemetry threshold, and tracking rates. These parameters can only be estimated on the basis of other subsystem and

system tests, which only indicated expected or anticipated performance.

Third, the tests pointed out the need for making these measurements during the system tests with updated system test equipment and during the subsystem tests in a telecommunications evaluation laboratory.

*Mariner V spacecraft/Agena interface and antenna verification tests.* The *Mariner V* spacecraft/*Agena* (RF matchmate) and the antenna verification tests were conducted to verify the operational readiness of the *Mariner V* S-band radio subsystem. The objective of the radio subsystem portion of the *Mariner V* spacecraft/*Agena* interface tests performed at JPL-Pasadena was to establish the electrical compatibility between the spacecraft and shroud. The radio subsystem umbilical functions, coupling between antennas, and changes in antenna VSWR were all measured with the shroud installed. The *Mariner V* spacecraft/*Agena* interface tests were conducted twice, once with the M67-1 and nonflight shroud, and later with the M67-2 flight spacecraft and flight shroud. A faulty RF connector in the spacecraft portion of the umbilical connector was detected and repaired. No other problems were noted. While the spacecraft was removed from the spacecraft area to perform the interface tests, the tuning of the M67-1 and M67-2 VHF DFR antennas was also measured.

The antenna verification tests were performed at AFETR. The impedance of the flight low-gain antenna, the exact value of which is critical to the interferometer fix, was measured in Building A0. No measurable change had occurred as a result of transportation of the spacecraft from Pasadena to AFETR. The spacecraft was moved to the ESF for the remaining antenna verification tests. These tests were conducted to ensure that all RF transmission lines and antennas were properly installed and that all RF connectors properly mated during the final spacecraft assembly operations. A special low-gain RF pickup probe and the flight umbilical cable were installed, and the RF paths between the antennas and test probes were calibrated. The assembly of the radio subsystem was then completed. The RF power level at the low-gain probe and at the umbilical connectors via the high-gain probe and precision coupler was measured with the spacecraft operating. The measured power levels were as expected from previous data, verifying that the antenna and RSS interface was correct. The UHF and VHF DFR antennas were also measured at this time.

Upon completion of the antenna verification tests, the shroud was installed and the radio subsystem RF umbilical functions were remeasured just prior to the spacecraft being transported to the launch complex.

The antenna verification tests were rerun after the spacecraft failure on the pad required that the spacecraft be returned to ESF. Only the S-band portion of the antenna verification tests was rerun. The test results agreed with previous test data.

Relatively few RSS problems were found during the system tests. Two of the RSS problems occurring during the spacecraft system tests were a result of changes to the spacecraft design. Only one failure occurred during testing; the other problems were noncatastrophic to the RSS performance.

*DFR/RSS compatibility.* The addition of the DFR receivers to the *Mariner IV* design could be expected to present compatibility problems with the RSS. This problem area was anticipated and, as previously described, problems did exist, but they were solved prior to the late delivery of a flight RSS to the *Mariner V* spacecraft.

*Automatic CY-1 failure mode switching.* A second spacecraft interface problem occurred in the automatic failure mode switching logic because the addition of a diode in the RSS receiver power supply to turn off ranging (if on) with the CC&S CY-1 cyclic. This change prevented the CY-1 cyclic from switching from a simulated failed cavity to the TWT when ranging was on.

The CC&S CY-1 cyclic pulse is used by the radio subsystem for automatically switching the power amplifiers or exciters in the event of a reduction or failure of output RF power. This 200-ms, relay contact closure, CY-1 pulse also is used to control the antenna state by switching the receiver antenna between the low-gain and high-gain antennas, if two-way lock has not occurred between two consecutive CY-1s. For *Mariner V*, an additional function was added to allow the CY-1 to turn off ranging (if on). It was this change that caused the anomaly. Various tests revealed the mechanism causing the failure to switch.

A simple fix was proposed and tested and was found to produce satisfactory switching over all operating conditions. This fix involved the addition of a 0.22-$\mu$f capacitor to the CY-1 input to eliminate the pullup effect of the +15-Vdc ranging on voltage. This fix made the effective CY-1 first-bounce contact closure appear longer to the control-unit logic circuitry. To prevent the generation of excessive current transients when this capacitor was shorted to ground with the CY-1, a 10-$\Omega$ resistor was added in series with the capacitor.

Although the capacitor/resistor fix did solve the problem, it did not completely eliminate the marginal switching condition. At temperatures above the FA limit of 130°F, the problem could occur even with the fix. This occurrence indicated the need for redesign of the 2CC1 control unit, if the unit were to be used on any future systems.

*h. Flight performance up to switchover to TWT.* The radio subsystem performed in a normal manner from launch up to and during TWT cruise. Both the uplink and downlink level performance has been as predicted. The cavity and TWT have functioned as predicted.

The following items of specific interest were noted:

(1) RF power-up. Shortly after RF power-up, the cavity power output to the low-gain antenna began to decrease from an initial DN (data number) of 75. After the radio subsystem temperatures stabilized, the power output stabilized at a DN of 70 to 71. Based on space simulator data, this operational sequence was normal cavity behavior. The power output change observed was due to decreasing temperature in Bay VI and to the time required for the cavity power output to stabilize. Channel 300 cavity cathode current also behaved normally during this period.

(2) Frequency predictions for first DSIF acquisition. Predictions of DSIF acquisition frequencies for both uplink and downlink were made based on predicted spacecraft temperatures and curves of spacecraft transmitter and receiver frequencies versus temperature. The actual frequencies observed agreed well with the predictions, and the first DSIF acquisition was accomplished smoothly.

(3) Midcourse maneuver. During the midcourse maneuver, the radio system temperatures increased by 8°F, which is within the range considered normal. Also during the midcourse maneuver, the spacecraft power was switched from solar panels to battery due to the spacecraft pitching away from the sun. While on the battery, channel 214 transmitter power output and channel 300 cavity cathode current decreased by 1 DN. This decrease was a result of the cavity power supply voltage dropping slightly, due to the lower primary input voltage from the spacecraft battery. After sun acquisition, channel 300 and channel 214 returned to their normal DN readings.

During the three rolls performed for ultraviolet photometer calibration after the midcourse maneuver, additional data were acquired pertaining to the antenna interferometer pattern on the flight spacecraft. The data are presently being analyzed and will be used with data previously obtained to try to pinpoint the locations of the peaks and the nulls in the spacecraft low-gain antenna pattern. After the midcourse maneuver, radio subsystem temperatures returned to their pre-midcourse values and all radio subsystem telemetry functions returned to normal.

(4) First use of spacecraft ranging channel with DC-V9 command. Prior to the launch of the *Mariner V* spacecraft, the only indications of spacecraft ranging-on observed during testing were small glitches in the spacecraft SPE and AGC when the DC-V9 (ranging-on) was received. In the quieter environment of space, several other small changes were noted that served to indicate that spacecraft ranging was on.

(5) Switch to TWT amplifier. The switch to TWT amplifier was accomplished normally by a DC-V7. After the switch, the Bay VI and the VCO crystal temperatures increased by 15°F and 12°F, respectively. These temperature changes were within 1°F of the predicted change and within the resolution of the telemetry. The TWT power output to the low-gain antenna and the input power to the TWT power supply were as predicted. TWT helix current came up 2 DN higher than originally predicted, but within the limits of data observed prior to launch. It is expected that, as the TWT ages, the helix current will increase in a similar manner to that observed during the *Mariner* Mars 1964 mission.

(6) TWT helix current variations. TWT amplifier helix current varied 2 or 3 DN as predicted. It is expected that these small variations will continue and that the helix current will slowly increase as the TWT ages.

*i. Conclusions and recommendations.* Briefly, the *Mariner* Venus 67 mission proved the feasibility of using planetary spacecraft hardware for more than one uniquely designed mission. As far as the radio subsystem was concerned, the *Mariner IV* subsystem design was adequate for this mission with the exception of the self-lock and interferometer problems, and a few components of suspect reliability. The frequency change required on both

transponders, to be compatible with *Mariner IV* tracking operations, did not fall into a design change category.

The fact that very little in the nature of basic subsystem redesign (other than those previously mentioned) was required for the *Mariner* Venus 67 mission did not preclude the necessity for an assessment of its adequacy on a requirement by requirement basis. The primary basis for its basic compatibility was the fact that both missions were to the earth's two closest planetary neighbors and, therefore, have similar communications requirements. Hence, the problems involved with the conversion from a Mars to a Venus mission, as far as the RSS was concerned, were related primarily towards flight space hardware and additional test equipment resurrection and requalification in support of the *Mariner IV* spare spacecraft equipment.

In future similar situations, a large amount of start-up effort can be conserved if the "mothballed" project will take a little more time and care in the closedown operation. That is, adequate protection and safe storage of records, unique test equipment, and any hardware of flight quality whether component parts or assemblies.

## F. Guidance and Control Subsystem Description and Development

*1. Central computer and sequencer.* Conversion of the *Mariner IV* flight central computer and sequencer (CC&S) subsystems for use on the *Mariner V* spacecraft is presented in four main parts:

(1) Initial preparations.

(2) Redesign.

(3) Modifications.

(4) Testing.

*a. Initial preparations.* Certain preparations were necessary prior to actual work on the flight equipment. A laboratory clean area was set up (Fig. IV-57) to modify and test the flight subsystems.

In addition to the two flight subsystems, two prototypes, and the type approval subsystems, spares from the *Mariner* Mars 1964 program, were reactivated for support of the *Mariner* Venus 67 CC&S development. The electrical prototype (EP) was set up as a breadboard to check out all modifications prior to their incorporation into the flight subsystems. The electrical prototype was not encapsulated; therefore, the mechanical prototype (PR) and the type approval (TA) subsystems (both encapsulated with solithane) were used as the production models for practice in reworking encapsulated equipment. A clean bench was installed for the rework of these two test subsystems as well as the flight subsystems.

*b. Redesign.* Changes made to the CC&S were those necessitated by the differences in the spacecraft flight sequence between a mission to Mars and a mission to Venus. The differences between the two are associated with the master timer (MT) events and are listed in Table IV-20.

The MT times are determined by the placing of diodes within a diode matrix; the changing of the matrix was the extent of the redesign. There was some tolerance ($\pm$0.5 day) associated with most of the MT events and this tolerance was used to:

(1) Minimize the number of diodes needed for each command.

(2) Optimize the time of day when each command would occur.

Minimizing the number of diodes took precedence; therefore, not all of the events occurred in the middle of the day (PDT) as desired.

As a result of this redesign, a total of 26 diodes were used in the matrix of *Mariner V*; whereas, 42 diodes were used for *Mariner IV*.

**Table IV-20. Spacecraft flight sequence differences**

| Event | *Mariner IV* time | *Mariner V* time |
|---|---|---|
| L1 | L[a] + 53 min | L + 53 min |
| L2 | L + 57 min | L + 57 min |
| L3 | L + 16⅔ h | L + 16⅔ h |
| MT-1 | E[b] − 137 days | E − 56.4 days |
| MT-2 | E − 103 days | E − 39.7 days |
| MT-3 | E − 68 days | E − 23.0 days |
| MT-4 | E − 30 days | E − 9.2 days |
| MT-5 | E − 131 days | E − 18.5 days |
| MT-6 | E − 192 days | E − 87.0 days |
| MT-7 | E − 6⅔ h | E − 12⅔ h |
| MT-8 | E + 6⅔ h | E − 6 h |
| MT-9 | E + 13⅓ h | E + 14 h |

[a]L = launch.
[b]E = encounter.



Fig. IV-57. Clean room test area

*c. Modification.* After the changes to the CC&S were determined, they were incorporated first into the electrical prototype for testing. The changes were subsequently incorporated into the mechanical prototype and the type approval subsystem for practice in reworking encapsulated equipment. The type approval subsystem was modified under QA surveillance. Generally, an attempt was made to duplicate the efforts to be expended on the flight equipment as closely as possible.

The rework to each subsystem (MC-04 and MC-05) consisted of removal of the solithane encapsulating material from the rework area in the 5A3 subassembly, removal of the old components, installation of the new components, and re-encapsulation. This rework is illustrated in Figs. IV-58–IV-61.

*d. Testing.* Some rework was necessary before the electrical prototype was ready for use as a breadboard. The *Mariner V* redesign was incorporated in the electrical prototype and subsequent tests indicated that there were no problems with the redesign.

The test procedures developed for requalification testing were as follows:

(1) Voltage/temperature margin test. This test exercised the CC&S subsystem under various combinations of temperature ($-10$ to $+75$°C) and voltage ($\pm 20\%$).

(2) Magnetic counter signal compatibility test. This test verified that the critical interstage counter signals had the correct phase relationship.

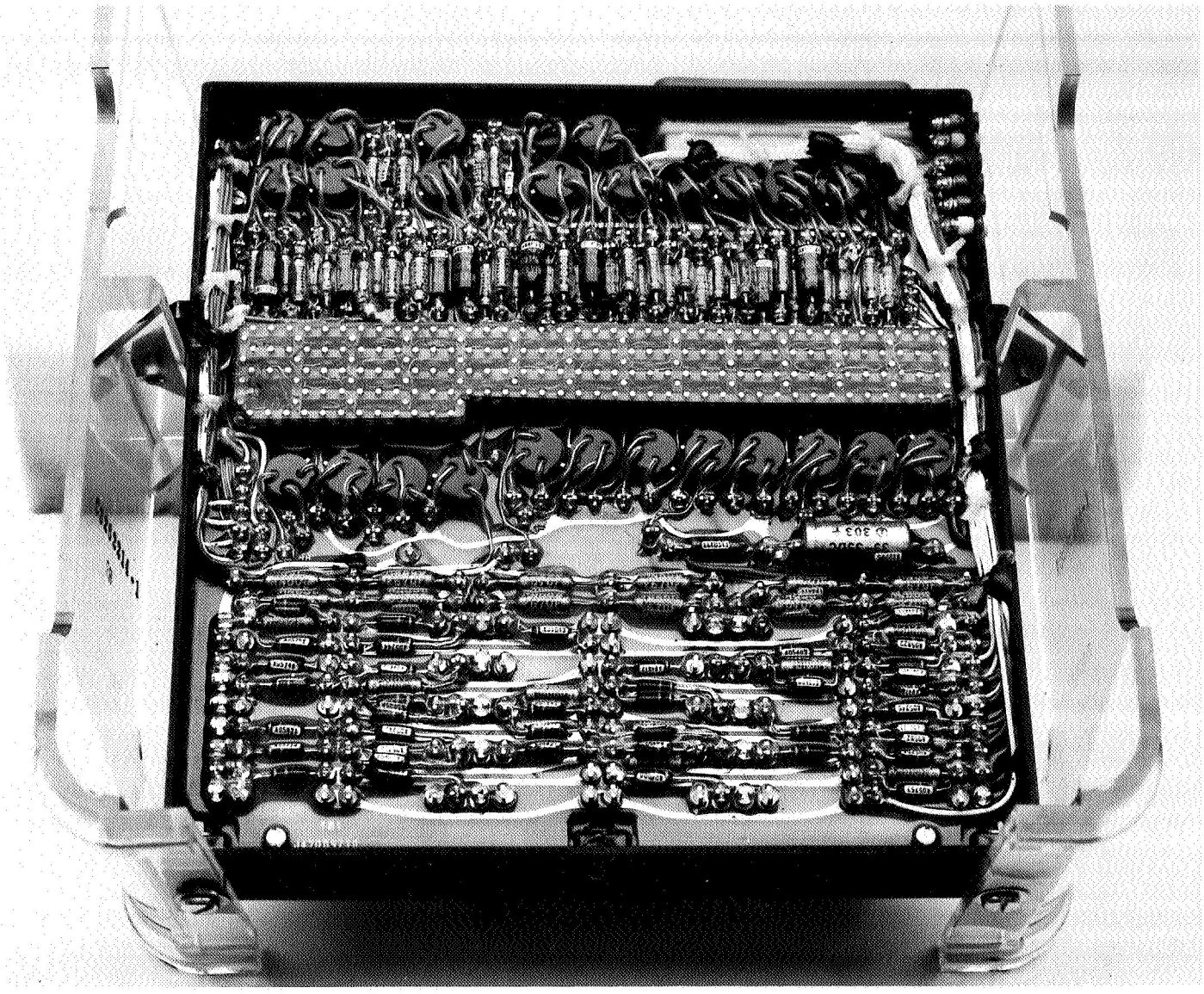


Fig. IV-58. Subassembly 5A3 prior to rework

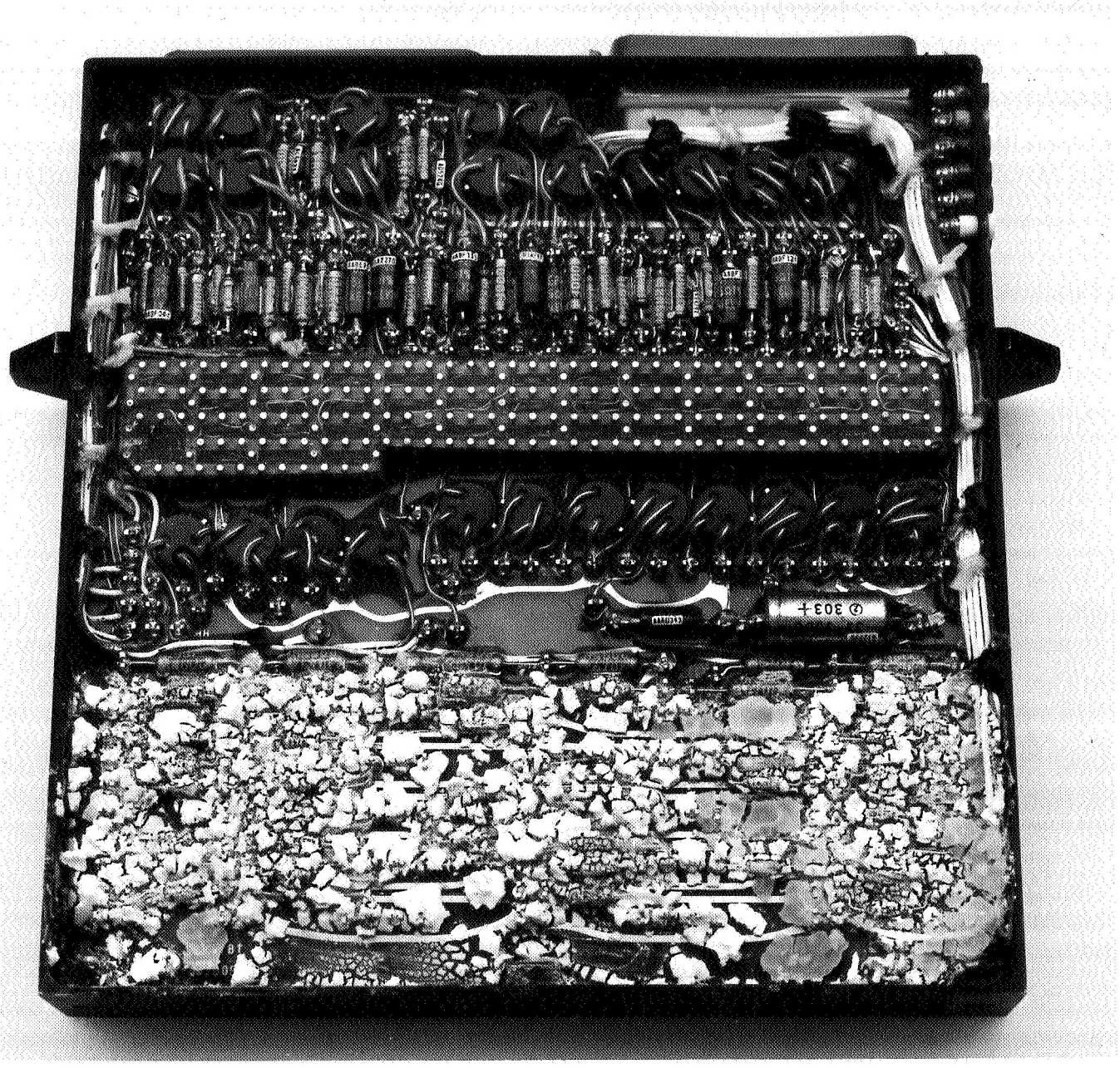


Fig. IV-59. Absorption and breakup of solithene by M-17 slurry

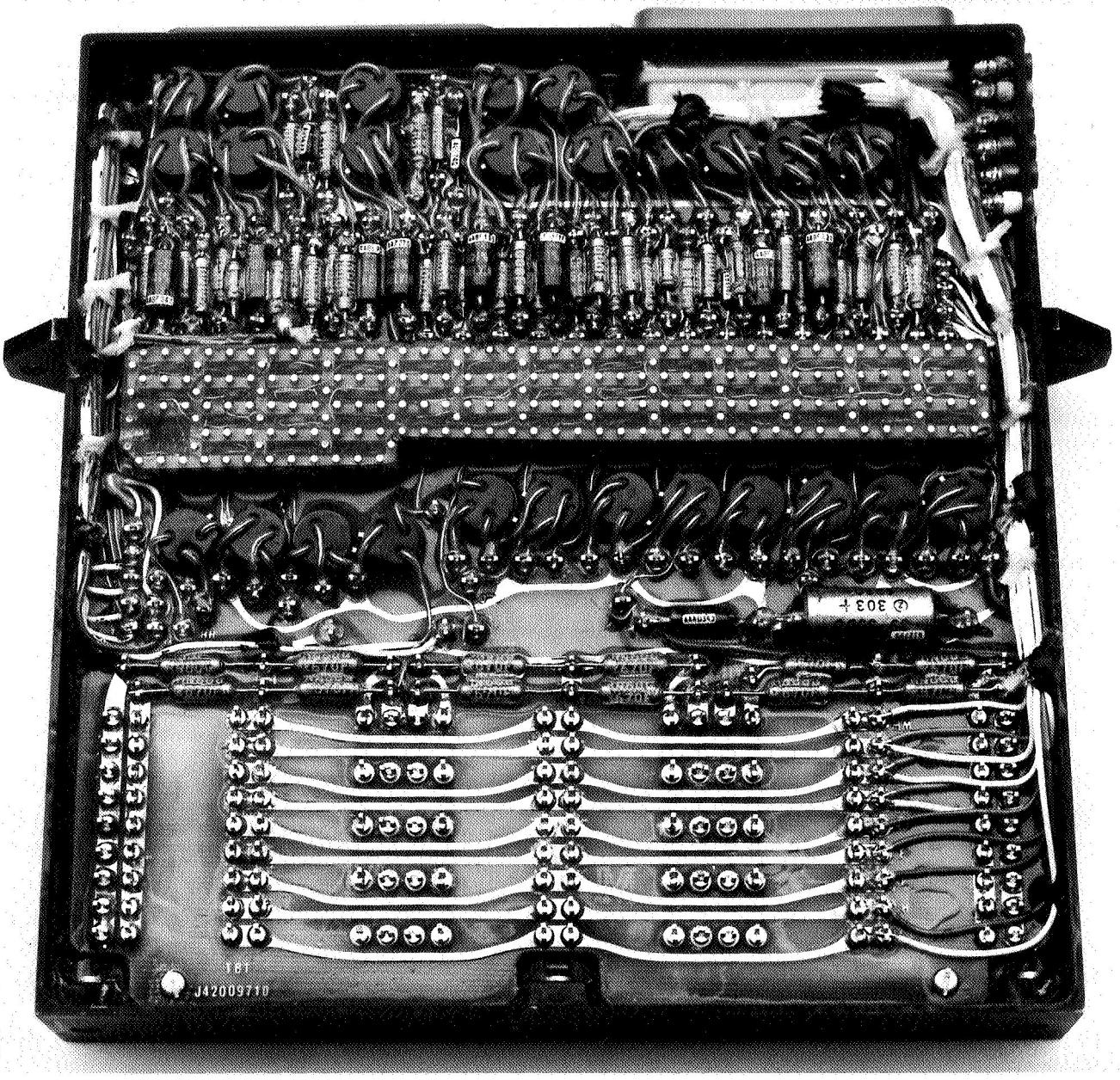



Fig. IV-60. Subassembly 5A3 with solithene and old components removed

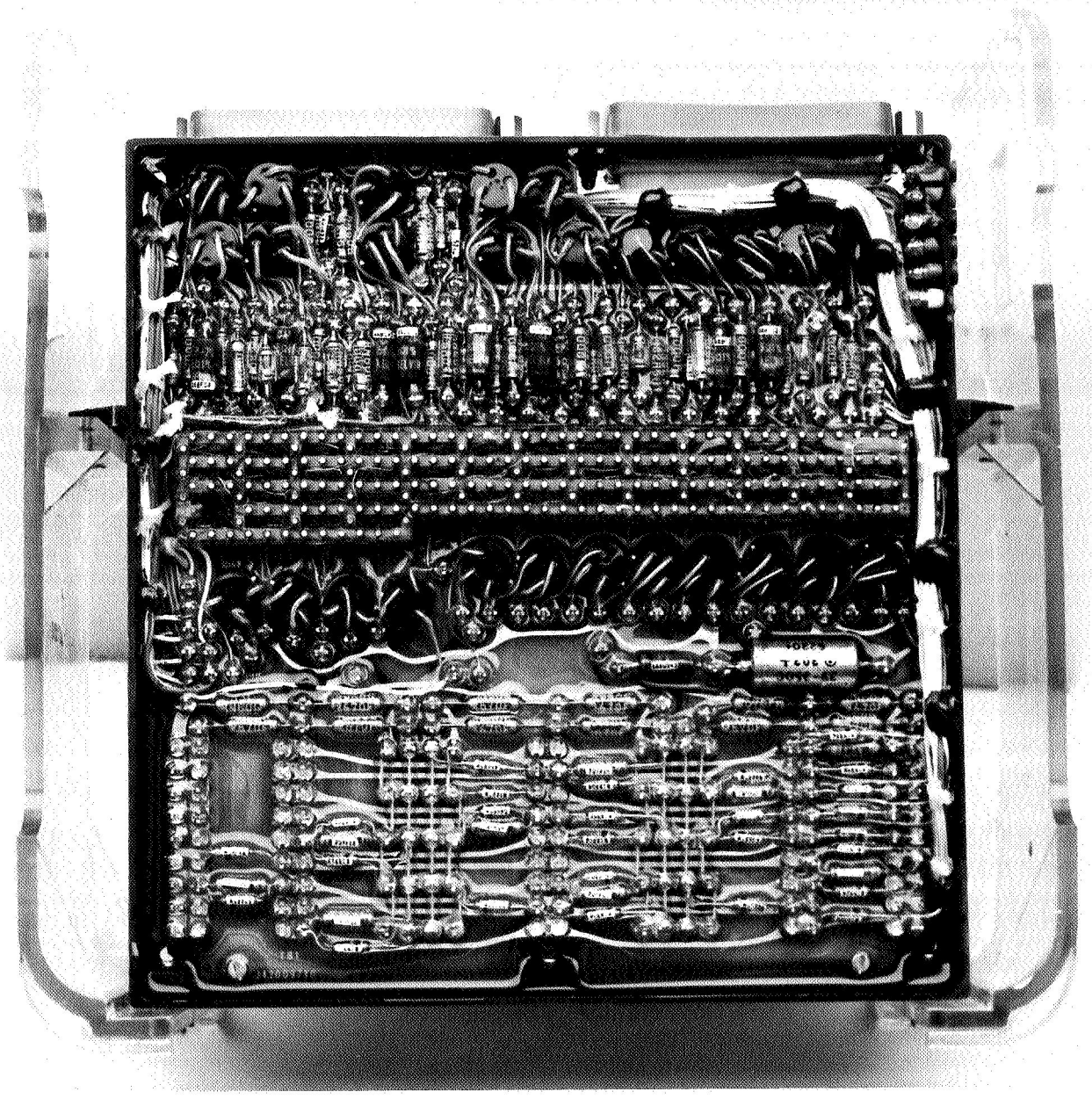


Fig. IV-61. Finished subassembly 5A3

(3) Relay driver capacitor leakage test. This test measured the leakage current associated with the Tantalum capacitors that couple the relay drivers to the output relays.

(4) Shift register margin test. This test determined the lowest 2.4-kHz power voltage at which the midcourse maneuver circuitry will operate at room temperature. Results were then compared with previous data to check for any degradation.

The test plan for requalification of the CC&S subsystems is shown in Fig. IV-62.

In support of the proton tests conducted at Harvard University, three typical CC&S subassemblies were combined with a special harness and test set. The assembly, irradiated with various proton densities and energy levels, performed normally.

During the magnetic counter signal compatibility test of the MC-04 subsystem, a marginal condition was noted between two counter signals in the 5A3 subassembly (end counter). The marginal condition did not, however, cause abnormal operation of the CC&S.

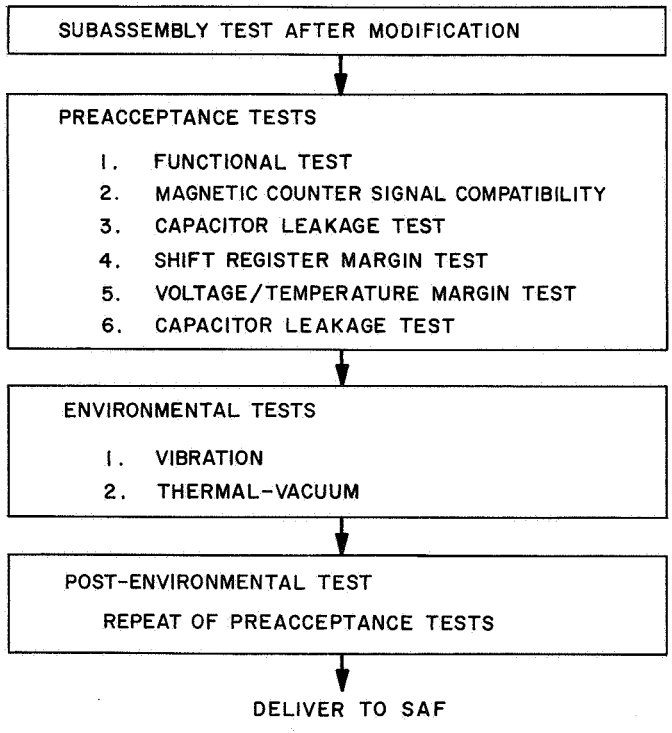



**Fig. IV-62. *Mariner V* CC&S test plan**

During the magnetic counter signal compatibility test of the MC-05 subsystem, a marginal condition was noted between the same two counter signals as with the MC-04 subsystem. The situation with this subsystem was such that abnormal operation of the CC&S subsystem could be expected, and, therefore, a fix was added to the 5A3 subassembly to correct this condition. A decision was also made at that time to correct the marginal condition with the MC-04 subsystem. The fix for this problem was the addition of a 15-ohm resistor in parallel with an existing 5-ohm resistor, which widened the marginal counter signal. The marginal counter signal was then compatible with other signals within the counter.

The MC-04 subsystem vibration test and the thermal-vacuum portion of the environmental test were completed with no problems. Post-environmental tests were completed on the MC-04 subsystem and it was delivered on schedule to SAF.

Testing of the MC-05 subsystem resumed after the delivery of the MC-04 subsystem to SAF. Environmental and post-environmental tests were conducted without incident, and the subsystem was placed on life test until delivery to SAF. Placing the subsystem on life test was done to accumulate extra operating time on this subsystem, which saw limited use during the *Mariner* Mars 1964 program. The MC-05 subsystem was delivered to SAF at the end of the life test cycle.

The MC-04 CC&S subsystem was installed as part of the M67-1 spacecraft. CC&S operation during subsequent tests at SAF was normal. The series of tests conducted at SAF included the following:

(1) Subsystem and interface tests.

(2) EMI tests.

(3) System tests.

(4) Parameter variation tests.

(5) Telemetry calibration.

(6) Simulated countdown.

(7) Pyro shock tests.

(8) Vibration.

(9) Space simulator tests.

(10) Magnetic mapping.

The MC-05 subsystem was installed as part of the M67-2 spacecraft. Performance of the subsystem during SAF tests was normal with the following exceptions:

(1) During interface tests between the CC&S and command subsystems, all CC&S MT commands were set when an oscilloscope that was connected between ground and the alert signal was turned off. The exact cause of this phenomenon was not found, but it was believed to be due to a ground line transient induced by turning off the oscilloscope while it was still connected to the subsystem. A recommendation was made that equipment of this type be disconnected from electronic equipment before it is turned off.

(2) While participating in the simulated countdown, the CC&S clear release function occurred earlier than normal. Subsequent tests disclosed that cable capacity associated with the inhibit interface with the CC&S was causing a magnetic counter signal to widen and become incompatible with another signal within the counter. The signal widening was analyzed as inherent with the inhibit function in the CC&S. A conclusion was reached that this subsystem was adversely affected by the signal widening; whereas, previous subsystems were not. The fix for this problem was to shorten the affected signal pulsewidth to allow for the widening when the inhibit interface was connected to the CC&S. Subsequent tests at SAF proved the fix to be effective; however, when checking the clear release function for the first time after the spacecraft was installed on the shake table preparatory to vibration testing, the clear release occurred early again. This early clear release could not be duplicated and it was assumed that the problem was probably associated with the environmental laboratory environment.

Prior to the preshipment systems tests to be conducted at SAF, both CC&S subsystems were subjected to final qualification tests. The tests included an oscillator frequency check, a shift register margin test, a capacitor leakage test, and a check to verify that the fixes for the magnetic counter signal incompatibility problem were still effective. The qualification tests verified the flight worthiness of both subsystems.

Because of the problems with the inhibit interface on the MC-05 subsystem, it was decided to use the MC-04 subsystem on the flight spacecraft (M67-2). The two subsystems were subsequently interchanged and preshipment tests conducted.

During the preshipment systems test on the M67-2 spacecraft (CC&S MC-04), the launch clamp function appeared to be inoperative. The inoperative condition was evidenced by the TM39F (cyclic) relay being periodically set and reset during the encounter update insertion. The loss of the launch clamp was traced to connectors that apparently were not making proper pin contact. The connectors involved were cleaned and remated with no subsequent reoccurrence of the problem.

*2. Spacecraft control subsystems.* Spacecraft control subsystems for *Mariner* Venus 67 consist of the attitude control subsystem, the autopilot, and the planet, terminator, and earth sensors. The concept and design of the attitude control and autopilot subsystems was unchanged from *Mariner* Mars 1964, but some modifications due to mission-peculiar requirements were necessary and some modifications arising from mission experience with *Mariner IV* were desirable. However, the major portion of the subsystems were usable without change on the *Mariner V* spacecraft. The planet sensor was a newly designed item; the terminator sensor and earth sensor were modifications of the *Mariner IV* narrow angle mars gate and earth detector, respectively.

The function of the attitude control subsystem is to positionally orient the spacecraft to a preselected set of references and to maintain that orientation throughout the cruise and planetary encounter phases of the mission. Additionally, the attitude control subsystem has the capability, during the midcourse maneuver phase, of repositioning the spacecraft to any given orientation in space. This temporary spacecraft attitude is maintained during the firing of the post-injection propulsion subsystem by the autopilot subsystem. The attitude control can then automatically reorient the spacecraft to its references; the subsystem also has the capability of automatic reacquisition of these references in the event a noncatastrophic disturbance should cause a loss of attitude control.

The function of the planet sensor is to detect the sunlit edge, or limb, of the planet Venus and to then signal the data automation subsystem (DAS) to begin the science encounter sequence. During the planetary encounter, the terminator sensor detects the terminator of the planet and signals the pyrotechnic subsystem to initiate the high-gain antenna pointing-angle change. The earth sensor serves as a backup method of obtaining a reference in spacecraft roll coordinates for purposes of the midcourse maneuver.

*a. Attitude control subsystem.* The attitude control subsystem is functionally composed of the control electronics, the gyro control assembly, the Canopus sensor, the cruise and acquisition sun sensors, the sun gate, and the gas system. All of these units were used unchanged in form, and modified only slightly in content from the *Mariner IV* design.

The spacecraft attitude is controlled on three orthogonal axes, called spacecraft pitch, yaw, and roll. The spacecraft roll axis is (ideally) oriented along the spacecraft–sun line, and attitude control pitch and yaw is referenced to the sun. Deviation of the roll axis from the spacecraft–sun line is sensed in pitch or yaw by a cruise sun sensor; the error signal generated is fed to the control electronics. If the error signal exceeds a given level (either positive or negative: the range, positive to negative, is termed the "deadband"), a device called a switching amplifier in the electronics activates a solenoid valve in the gas subsystem. Opening this valve permits dry nitrogen gas at low pressure to flow through a small nozzle located at the end of a solar panel, thus applying torque to the spacecraft in a direction that tends to reduce the error signal. Hence, sun-line orientation is maintained in pitch and yaw within the deadband, and the spacecraft is said to limit cycle within the deadband.

The spacecraft roll axis is referenced to the star Canopus, and the Canopus sensor senses angular deviation from the star and generates an error signal for roll control in the same manner a sun sensor does for pitch and yaw control. Spacecraft position is thus controlled by the sun and Canopus sensors.

Spacecraft rate, in the cruise mode, is controlled by feeding back to the switching amplifier input a voltage proportional to the time a solenoid valve has been activated. This "derived rate" feedback permits the gyros in the gyro control assembly to be turned off when all celestial references have been acquired. Prior to cruise mode acquisition, these pitch, yaw, and roll rate gyros provide rate damping to the spacecraft, enabling rapid acquisition of the sun and Canopus. Should sun or Canopus acquisition be lost, the gyros will normally be turned on to expedite the reacquisition process. Figure IV-63 shows a generalized single-axis attitude control subsystem.

The acquisition sun sensors augment the limited field of the cruise sun sensors, providing a full $4\pi$ sr field-of-view, enabling sun acquisition regardless of the initial orientation of the spacecraft. When the roll axis of the spacecraft is within a cone of given half-angle from the

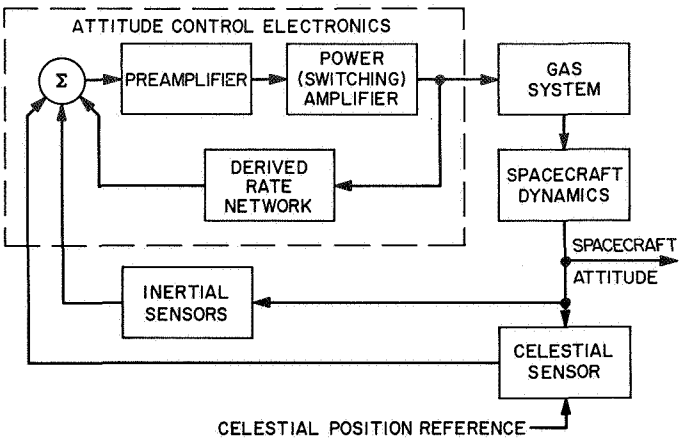



**Fig. IV-63. Generalized single-axis attitude control subsystem**

spacecraft–sun line, the sun gate disables the acquisition sun sensors and initiates (upon initial sun acquisition only) the magnetometer calibrate constant spin rate about the roll axis or, subsequently, the Canopus search constant spin rate about the roll axis.

The modifications to the attitude control subsystem for the *Mariner* Venus 67 mission are summarized for each item.

*Control electronics.* There were three modifications to the control electronics package; in addition, thirteen scaling resistors in the autopilot, which is physically housed in the same case, were replaced. Only the changes to the attitude control portion of the unit will be discussed.

The *Mariner IV* control electronics provided the dc excitation voltage to the cruise and acquisition sun sensors; these voltages were $\pm 16$ and $\pm 26$ V, respectively. Figure IV-64 depicts a complete single-axis sun sensor system; for *Mariner V*, the cruise sensor excitation was reduced to $\pm 12$ V, as shown. This modification reduced the $I^2R$ losses of the photo conductive cell, helping compensate for increased operating temperatures due to the decreased spacecraft–sun distance.

To implement the change in excitation voltage, 12.0V zener diodes (1N759A) were placed across the excitation supply. It was possible to physically and electrically connect these diodes by soldering them into welded terminals that projected from the matrix circuit board of the proper cordwood module of the electronics package (careful attention had to be paid to the cleaning and soldering process, however, to avoid damaging the insertable

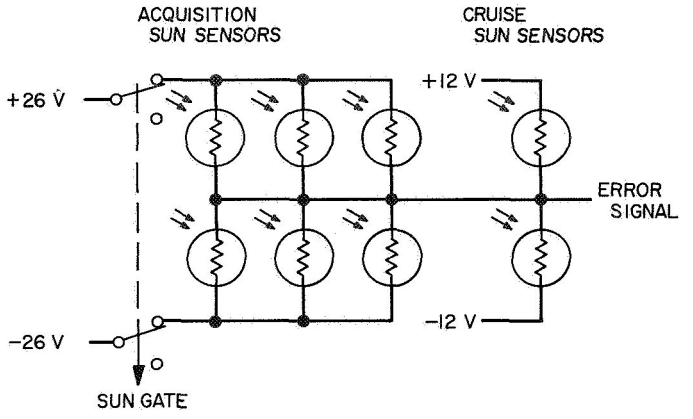



**Fig. IV-64. *Mariner V* sun sensor system, pitch or yaw axis**

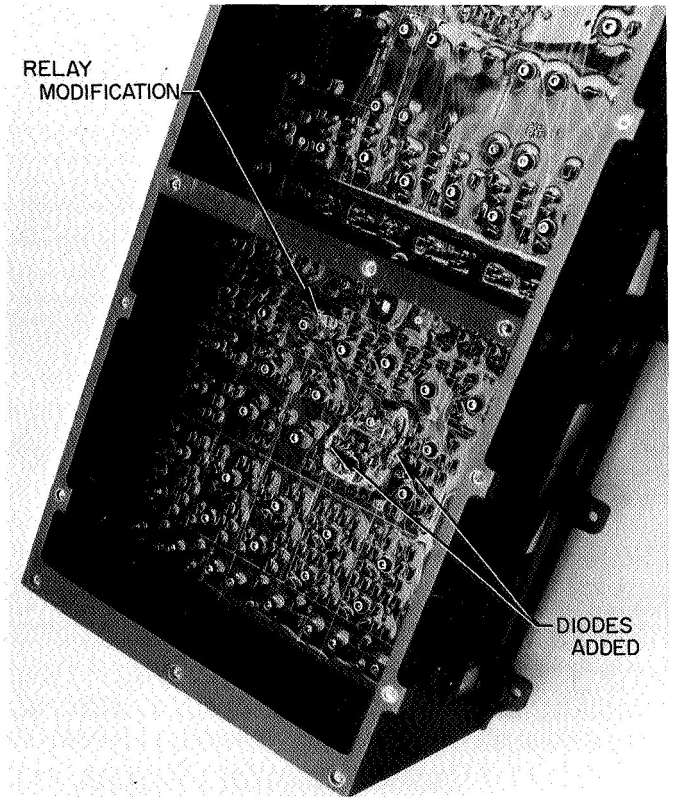



**Fig. IV-65. Attitude control electronics package, bottom view**

pins of the boards). Figure IV-65 shows the location of the diodes on the underside of the control electronics package.

Associated with the change in excitation voltage was the necessary change in scaling. As shown in Fig. IV-63,

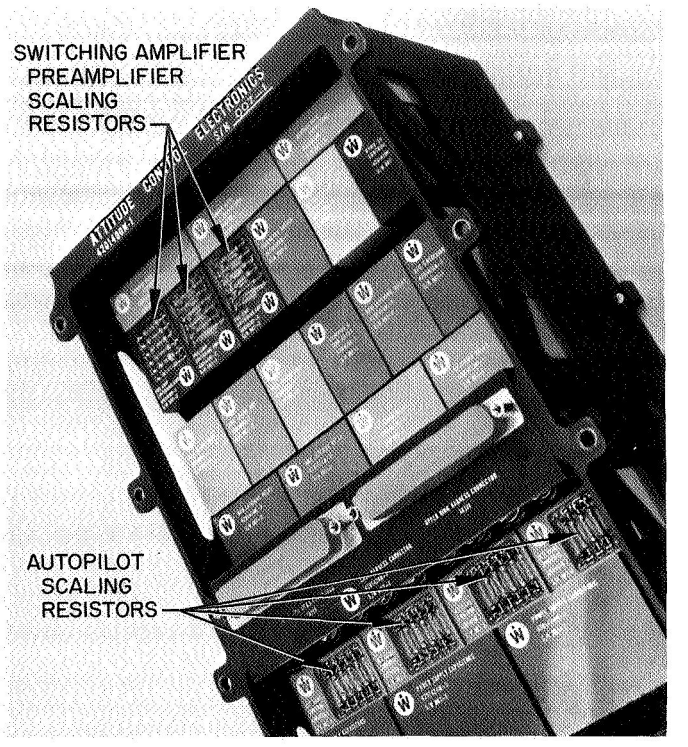



**Fig. IV-66. Attitude control electronics package, top view**

there are three inputs to the preamplifier of the forward servo control loop: the position, rate, and derived rate feedback. These inputs are scaled to help optimize the control equation, and in order to maintain the relative position scaling with the voltage change, the 442-kΩ sun sensor scaling resistor was jumpered. This resistor is readily accessible, as shown in Fig. IV-66, and it was only necessary to remove the existing solithane coating, solder the jumper into place, and recoat the assembly. An enlarged view of the modification is provided in Fig. IV-67.

The third modification to the control electronics was the functional (but not physical) removal of a relay in the telemetry buffer. In the *Mariner IV* design, this relay had allowed the sharing of telemetry channel 107 between the roll gyro output and the earth detector output. When the gyro was not on, the earth detector output was telemetered; when the gyros were turned on, this relay was energized and the telemetry input was switched to the roll gyro output. For *Mariner V*, the earth sensor was intended to be used as a backup instrument to establish a roll reference during the midcourse maneuver if the Canopus sensor should fail. It was, therefore, necessary to remove the sensor output from a sharing mode with

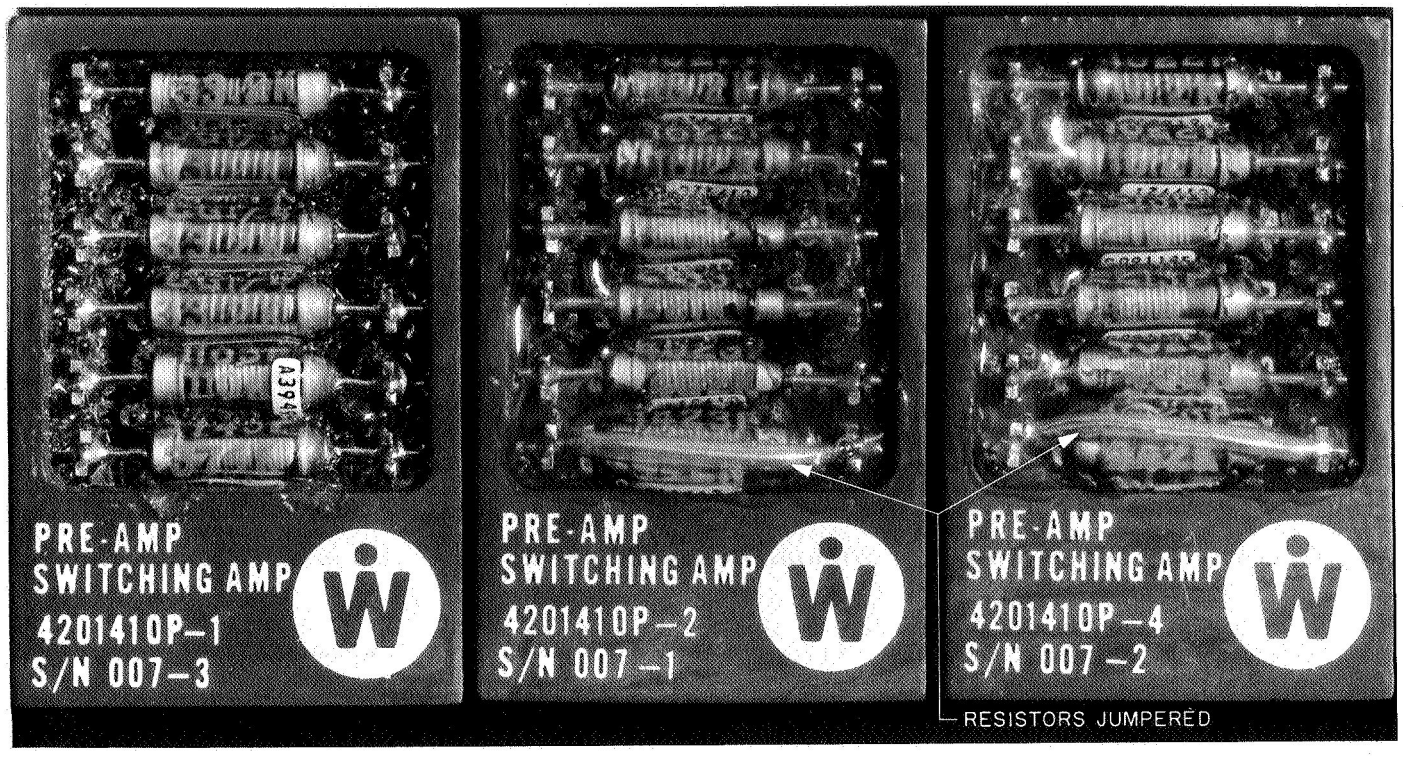



**Fig. IV-67. Switching amplifier preamplifier scaling resistors**

the gyro. This was accomplished by removing the connections to the relay coil, the relay contact arm, and the normally open and normally closed contacts, and by connecting a jumper between the arm and the normally open contact. The effect of this modification was to connect the roll gyro output to channel 107. The earth sensor was connected to telemetry channel 118 by modifying the spacecraft upper ring wiring harness and the data encoder case harness to provide wiring directly from the earth sensor to the data encoder.

Testing on the control electronics consisted of functional bench testing at the flight acceptance (FA) temperature limits of 32 and 131°F. The tests included evaluation of control loop performance and measurements of essential and critical performance parameters. The only environmental testing deemed necessary was single-axis FA vibration in a plane normal to the matrix board, which contained the added jumper and diodes.

The attitude control and autopilot subsystems were additionally tested together functionally before delivery to the Spacecraft Assembly Facility (SAF). This integration test included the control electronics, the gyro control assembly, the Canopus sensor, the gas system, and the jet vane actuators. The sun sensors were not included because the spacecraft cabling to these sensors was soldered to terminal boards on the sensor assemblies at the time of installation to the spacecraft, making a test on the spacecraft more meaningful in terms of the correctness of phasing and polarities. The primary purpose of the test was to validate the electrical interfaces of the subsystem. The secondary purposes were to verify the correct phasing of the several components with respect to each other and the performance of a gross functional test. The tests were successful and most of the equipment involved was delivered to the spacecraft immediately after the test.

*Gyro control assembly.* There were no modifications to the *Mariner IV* gyro control assembly (GCA). The units were removed from bonded storage in SAF to be functionally tested to ensure that there was no significant change from the 1964 test data and that both GCAs were still within all specification limits, recalibrated, and then returned to the spacecraft. No FA testing was planned.

At the beginning of the subsystem and system testing in SAF, the GCA S/N 016, in the flight spacecraft M67-2, was noticed to have an unusual pitch channel output. The voltage output of the gyro amplifier was observed to vary between 0 and 110 mV at about 2 Hz and was in phase

with a variation in gyro spin motor current. The GCA was returned to the Spacecraft Control Inertial Sensors Laboratory where, after extensive analysis and testing, it was determined that the spin motor was faulty. A replacement gyro was available; it had been stored in the Inertial Sensors Laboratory and specifically designated as a spare for the *Mariner* Venus 67 program, but pre-replacement testing disclosed that it was also defective. An immediate time and materials contract was negotiated with the manufacturer and both gyros, along with a third known defective gyro, were returned to the factory immediately, the goal being to recover two usable gyros from the three available. Fortunately, spare parts were available for these instruments, and by working on a 24 h per day basis at the manufacturers and in the Inertial Sensors Laboratory the replacement gyro was repaired, tested, installed in the flight GCA, functionally tested, FA tested (vibration only), calibrated, and replaced in the spacecraft in time to participate in all systems and environmental testing with the exception of the first spacecraft systems test. No further problems were encountered with the gyro control assembly.

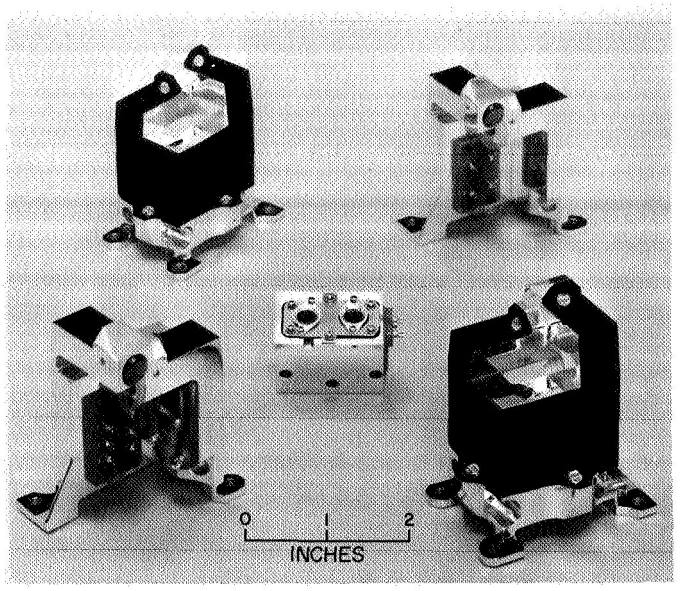



**Fig. IV-68. Primary and secondary sun sensor assemblies**

*Sun sensors and sun gate.* The sun sensors and the sun gate were physically unchanged from the *Mariner IV* design. However, since the spacecraft flight attitude was such that the side that had faced away from the sun for the 1964 mission faced toward the sun for the 1967 mission, it was necessary to relocate the sun gate and the primary and secondary sun sensor assemblies on the spacecraft bus.

Each of the two primary sun sensor assemblies contain two cruise detectors and two acquisition detectors; each of the two secondary assemblies contain four acquisition detectors. Accordingly, the primary assemblies are mounted on the side of the bus facing the sun, and had to be so relocated for *Mariner V*. As shown in Fig. IV-68, the primary and secondary assemblies are identical in physical construction, and the arrangement of the fields-of-view is such that it was only necessary to actually interchange primary and secondary assembly positions.

The extent of formal testing on the sensors was the recalibration of the cruise sensors, since their excitation voltage had been changed. No FA testing was necessary. The excitation voltage change was designed to keep the power dissipated at Venus–sun distances the same as that dissipated by the *Ranger* and *Mariner IV* sensors.

There were several areas of concern attributable to the closer approach to the sun during this mission. The first was the offset caused by Venus light on the sensors at or near planetary encounter. The offset is a function of distance from the planet, and cursory tests performed in the Celestarium indicated that the offset could be as great as 56 arc-min in pitch and yaw. Since there was no remedy for this situation, the effects had to be investigated. It was determined that the only significant effect due to this offset would be on the high-gain antenna pointing angle and that the ½-deg offset expected would actually increase the value of the S-band occultation experiment. The conclusion was, therefore, that Venus light on the sun sensors causing an offset in spacecraft attitude would not be a problem.

A second area of concern involved sun sensor offsets due to reflected light from the newly designed deployable sun shade. Should the shade deploy prematurely or incorrectly, or should it become damaged, the possibility existed that a cruise or acquisition sensor would be covered or have its field-of-view partially obscured, or that light would be reflected from the shade to the sensors, causing an offset. No remedy was available for this situation, either; therefore, the closest attention was paid to the details of deployment and storage of the shade to ensure that it operated as planned.

The third mission-peculiar effect investigated was high-temperature operation. Although the excitation voltage had been lowered to reduce dissipation, the sensors would

still have to operate at elevated temperatures. It was determined that no significant degradation occurred when the sensors were operated at temperatures as high as 160°F and, thus, that no action was necessary because of the higher temperatures expected during flight. However, a thermocouple was added to the primary assembly on Bay III of the spacecraft to monitor this temperature during flight.

No change was made to the sun gate for the Venus mission, except to move it to the other side of the spacecraft bus. No testing other than functional testing was required or performed.

*Canopus sensor.* The greatest change to a component of the attitude control subsystem was the modification of the *Mariner IV* canopus tracker to the *Mariner V* Canopus sensor. The changes were generated by the relocation on the spacecraft bus of the sensor, the higher straylight levels to be expected at Venus encounter, and mission experience with dust particles entering the sensor field-of-view.

*Canopus sensor electronics modifications.* Because of the closer approach to the sun of the *Mariner V* spacecraft, predicted operating temperatures throughout the bus and structure increased. To reduce the effect of generally higher temperatures on the Canopus sensor, the unit was relocated to the shady side of the bus.

No mechanical changes to the sensor were necessary because of this location change, other than the removal of the 1.4-deg mounting bias on the feet of the sensor. The two electronic changes necessary were the reversal of the phasing of the roll error signal and the adjustment of the cone angle generator to provide the correct range and steps for cone angle field-of-view adjustments. The phasing reversal was accomplished by interchanging the leads from the 1-kHz sweep oscillator to the deflection plates of the image dissector. The net effect was a 180-deg phase reversal in the demodulator, with no effect on the intensity information (it was also necessary to interchange two leads from a voltage balancing circuit). The cone angle generator was modified by changing the value of two trimming resistors in the high-voltage deflection circuitry. The effect was to increase the value of a cone angle change from 4.6 to 5.125 deg and to change the cone angle range from the 71.9–105.7-deg range to a 74.5–111.1-deg range.

The final change to the electronics of the sensor was the effective removal of the "high gate." The *Mariner IV* unit would automatically initiate a roll search when the intensity of the object being viewed was outside the range of ¼ to 8 times Canopus intensity. However, particles that were from the spacecraft and illuminated by the sun and passed through the field-of-view of the tracker caused violations of the 8× gate, thereby initiating a roll search. The solution proposed was to bias the high gate from 8× Canopus to "infinity." This solution was accomplished by removing a resistor in the brightness gate circuitry.

*Canopus sensor straylight modifications.* The major effort to convert the *Mariner* Mars 1964 Canopus tracker design for the *Mariner* Venus 67 mission centered around the requirement to retain acquisition of Canopus in the proximity of Venus. The illumination of the sensor due to Venus, at the time of maximum illumination, exceeds 8 billion times the illumination due to Canopus. Venus light coming from outside the 5 deg × 32 deg secondary field-of-view of the sensor is scattered off the various optical components and onto the image dissector photocathode area defining the field-of-view.

The exact illumination from Venus and the geometry of Venus relative to Canopus are a function of the trajectory that is ultimately flown. Although the actual trajectory depends on many parameters, for determination of Venus illumination near planetary encounter, these parameters can be reduced to two that are the most important: the launch date and the aiming point.

Four trajectories for each of the first, the middle, and the last days of the launch window were investigated to determine the worst case illumination condition. These trajectories were chosen to be representative of 3-$\sigma$ midcourse error cases.

Figure IV-69 is the aiming zone and constraint region diagram for a June 12, 1967 launch. Impact and occultation constraints on the aiming point are indicated by areas on this diagram. The figure shows the aiming points selected for the study of Venus illumination. The trajectory aimed at $B = 24{,}000$ km, $\theta = 330$ deg for a June 12, 1967 launch has the worst illumination condition.

Figure IV-70 shows the Venus lune geometry relative to the Canopus sensor for this trajectory at 5-min intervals near Venus encounter. A spherical coordinate system with the Z axis aligned to the sensor optical axis is used to show the relative geometry.

The straylight sensitivity for a Canopus sensor will have a higher degree of symmetry about its optical axis

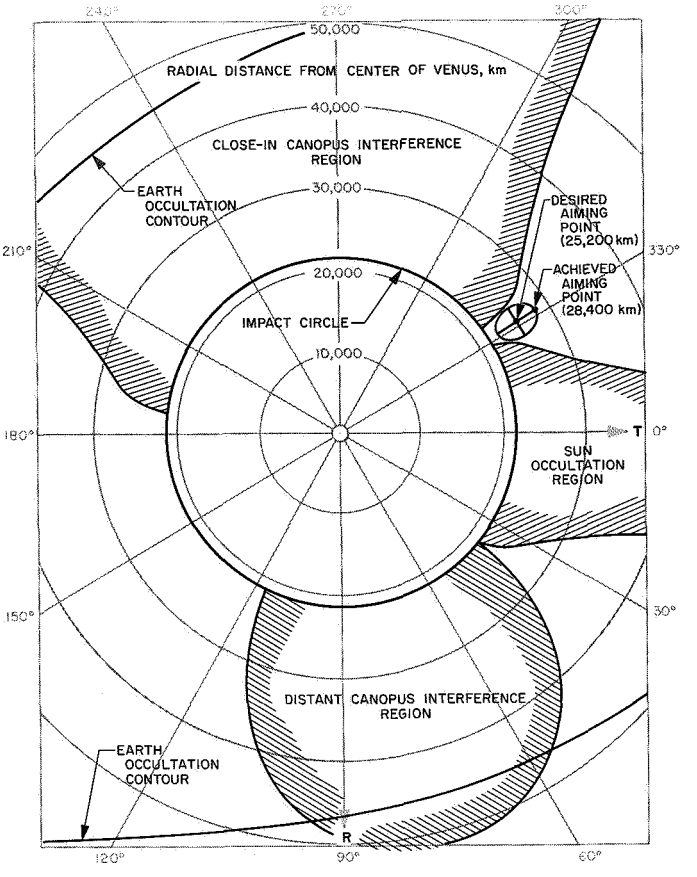



**Fig. IV-69. Aiming zone and constraint regions for June 12, 1967 launch**

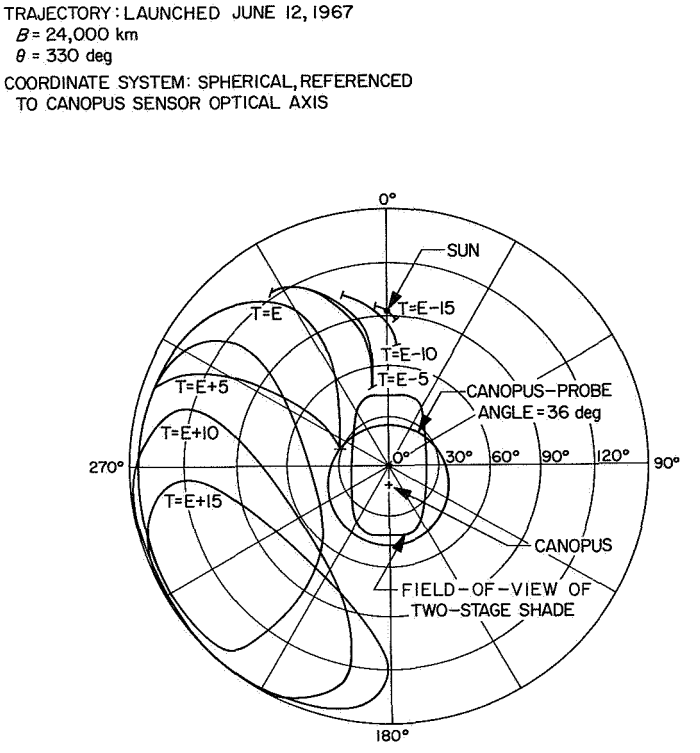



**Fig. IV-70. Venus lune vs time referenced to encounter**

than about the star being tracked. However, the software used for preliminary trajectory design was only capable of handling conical constraints symmetrical about the Canopus–probe line. The 36-deg Canopus–probe–Venus limb cone indicated in Fig. IV-70 was used to generate the Canopus constraint region shown in Fig. IV-69. The 36-deg cone adequately covered the sensitive region of the sensor on the side subject to a lit Venus limb, while allowing the dark limb of Venus to encroach slightly into the more sensitive region.

A surface brightness model that takes into account the nonlambert character of the planet's reflectance was developed for use with the *Mariner V* celestial sensors. Three assumptions are made:

(1) The reflectance of the planet is independent of surface location.

(2) The reflectance of the surface is a function of the scattering angle $\gamma$ only.

(3) The brightness and distribution on the planet when viewed from a long distance away is the same as a lambert planet.

For the model to be plausible, it must fit the observed phase function for distant observation. This fit requires that the reflectance vary with scattering angle in the same manner as the ratio of the planet phase function to the lambert phase function varies with phase angle.

This model was mechanized on the 7094 computer. The surface brightness distribution is computed and displayed as isobrightness contours in the spacecraft fixed cone-clock angle coordinate system. Figure IV-71 shows the brightness distribution of Venus at encounter on the worst case trajectory selected (i.e., June 12, 1967). The total illumination on the Canopus sensor can be obtained by integrating the brightness over the area where the clock angle is less than 90 deg. The worst case illumination is 1260 ft-cd.

*Straylight shade design.* A two-stage shade was designed to improve the straylight sensitivity of the Canopus sensor.

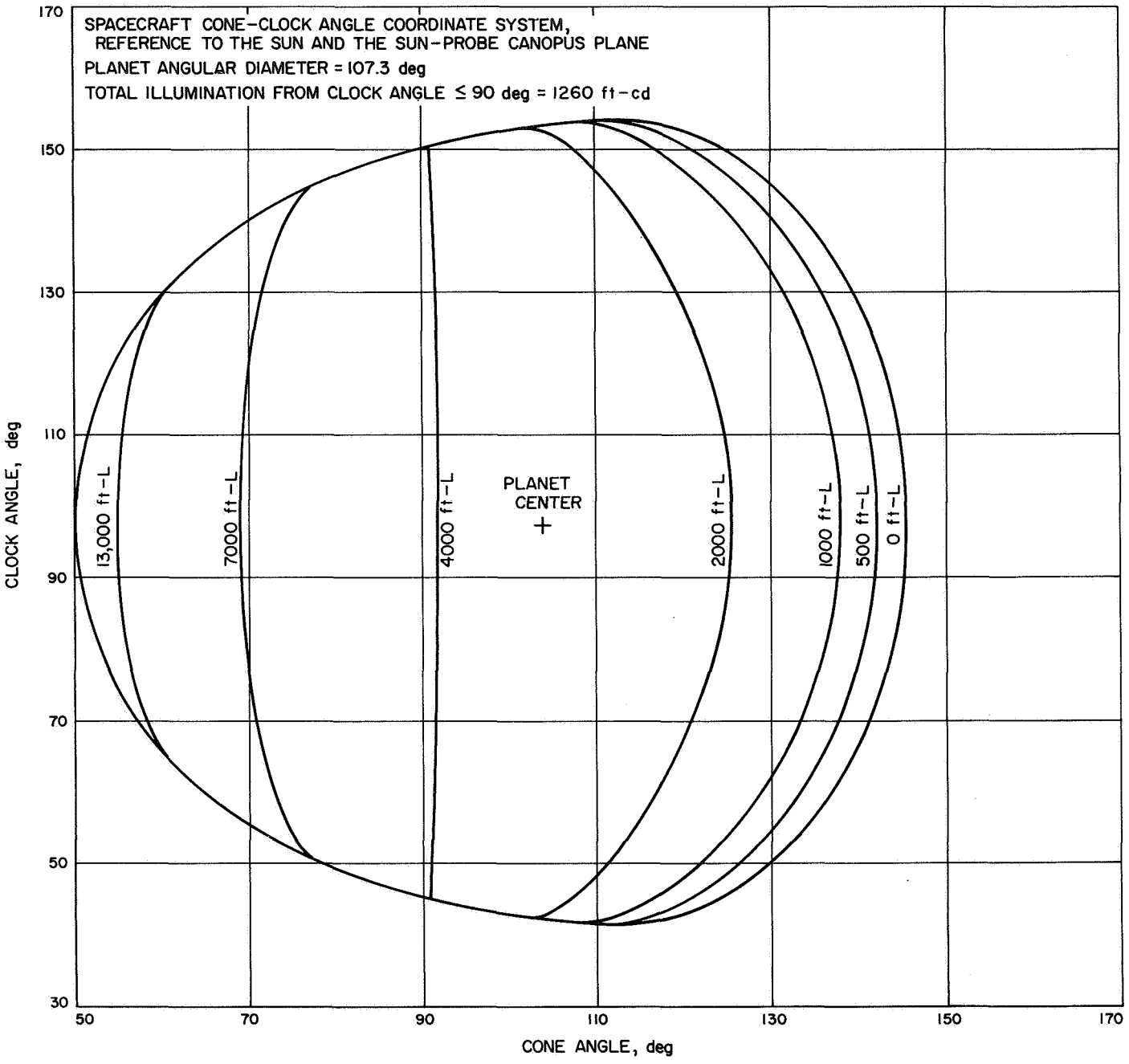



**Fig. IV-71. Venus isobrightness contours**

To make clear what is meant by a two-stage shade, the function of a single-stage shade must be understood. The idea behind a single-stage shade is that it prevents light from outside a critical field-of-view from falling directly on the sensor lens. In a two-stage shade, a second shade is built to prevent light emanating from outside a second critical field-of-view from falling directly onto the first-stage shade defining aperture. The second-stage defining aperture must be located so that it is not visible from any point on the sensor lens.

There is no limit to the possible configurations of two-stage shades, which protect to a given angle. However, there is a choice of design that minimizes the overall length, given a required field-of-view and a required angle of two-stage protection. The Canopus sensor shade was designed with these constraints as an optimum two-stage shade. As a practical matter, the aperture defining the second stage is set back slightly from the calculated value to allow for manufacturing tolerances, distortion, and possible minor damage. The two-stage shade used on the *Mariner V* sensor is shown schematically in Fig. IV-72.

The sun detector was relocated from the lower right corner of the face of the sensor to the right-hand side

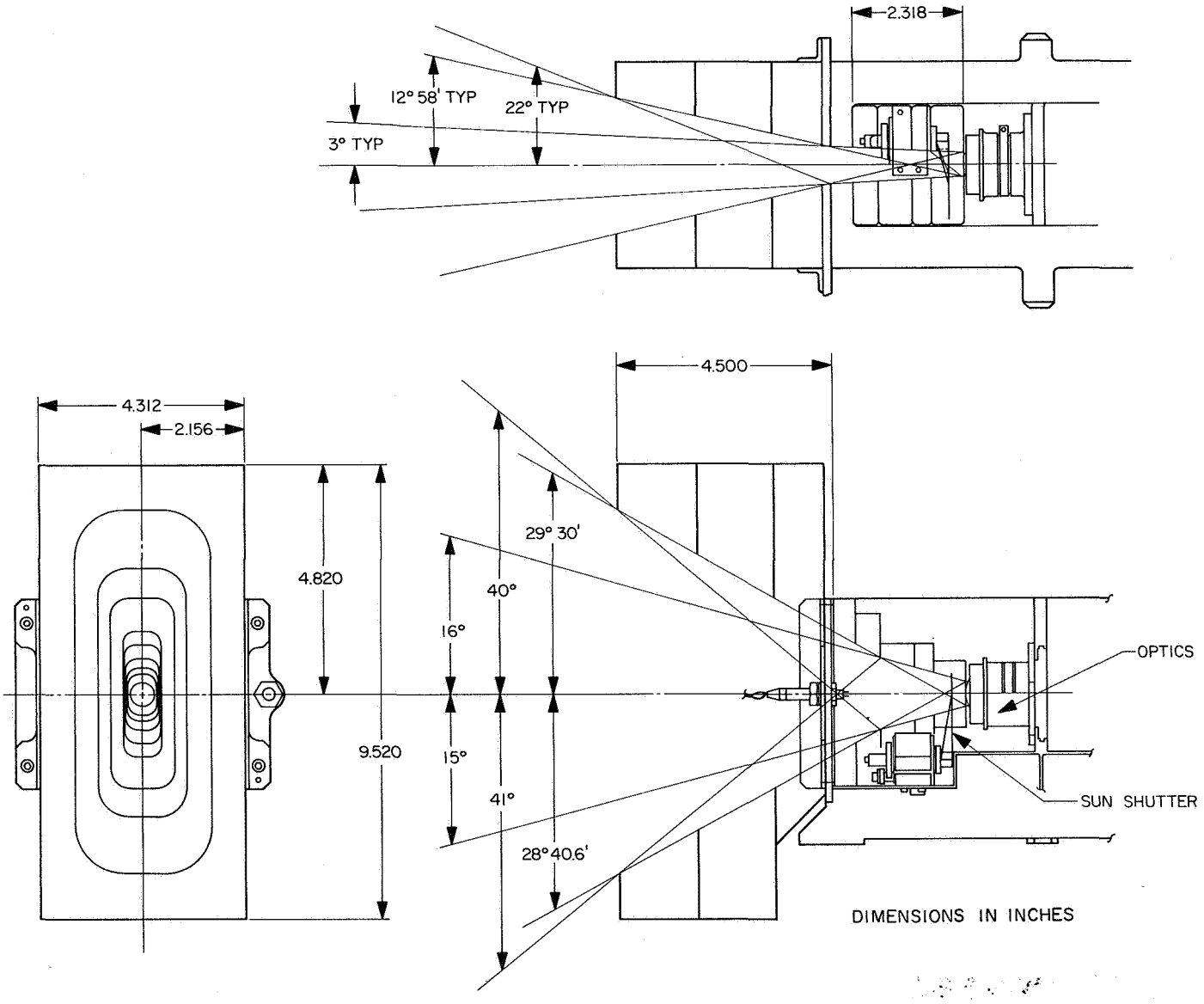



**Fig. IV-72. Canopus sensor two-stage shade**

of the shade, since the new shade would obscure part of the field-of-view of the detector. In addition, since the new shade extended beyond the edge of the spacecraft bus, it was necessary to thermally isolate it from the sensor. This was accomplished by mounting a thermal isolation plate between the shade and the sensor. The sun detector was thermally isolated from the shade in the same manner, but thermally connected to the sensor by a strap.

*Straylight testing.* The straylight performance of a sensor can be described by plotting an isofailure contour in illumination vs geometry space. If the interfering source of light plots above the isofailure contour, the sensor will be inoperative; if it plots below the contour, the sensor will work. Although this concept is simple enough, determination of the isofailure contour and interpretation of the isofailure contours in terms of large angular diameter planets present some practical problems.

The main problem is determining the isofailure contour. A definition of "failure" must be decided upon, and a test facility that will give adequate results must be provided. In general, "failure" occurs when the sensor does not perform adequately. Therefore, "failure" changes during the mission.

For the *Mariner* Venus 67 mission inadequate alignment at planetary encounter was the most constraining failure criteria. Before Canopus acquisition, the intensity channel threshold must be low enough to generate an adequate star map. Near planetary encounter and at midcourse maneuver, the sensor must remain accurately aligned to and acquired to Canopus. During cruise, alignment is less critical with maintenance of acquisition being of primary importance. In general, it is necessary to conduct the straylight test before deciding exactly what failure criteria should be used for the isofailure contour.

During the *Mariner* Mars 1964 project, the complete straylight sensitivity test was conducted in the JPL celestial sensor 40-ft darkroom. However, dust and molecular scattering limited the usefulness of this facility to illumination levels below 100 ft-cd. A preliminary estimate of the worst possible illumination level to be expected from Venus was 4500 ft-cd. The calculated background brightness due to molecular scattering in STP air exceeded the background brightness required to conduct a meaningful test by a factor of 20. Helium was experimented with as a medium in which to conduct the test, but was quickly dropped because of difficulty with high-voltage arcing. Ultimately, the test was conducted in a vacuum, using a fixture designed to fit a $7 \times 14$-ft chamber.

The test fixture is shown schematically in Fig. IV-73. A control panel outside the chamber controls remotely all indicated articulation. The sensor gimbal and illuminator gimbal allow the light source to be located anywhere in the forward hemisphere of the sensor, outside of 36 deg from the optical axis. The light sink is constructed so that the sensor field-of-view looks into black carrara glass. Black carrara glass was chosen because it has a diffuse reflectance that is a factor of 10 less than honeycomb. The star source is located so that an error signal may be generated and the sensor field-of-view tracked with a single gimbal axis. The star source is located on a honeycomb disc. The honeycomb disc and the black carrara glass are the essential components of the light sink. Black anodized 0.0007-in. honeycomb is used liberally throughout the fixture to reduce extraneous light in the fixture. The complete fixture is shown in Fig. IV-74.

The capabilities of the fixture are tabulated in Table IV-21. The star source in the fixture remains a problem. Of necessity, the sensor being tested is the brightest light source in the fixture. The star source uses a 3-in. lens to form a collimated source. Ghost images of the sensor are formed in each surface of the 3-in. lens. At a straylight level of 1500 ft-cd of Venus illumination, these ghost images look like a star whose brightness is $1.5 \times$ Canopus. Therefore, the star source had to be rotated out of the sensor field-of-view to successfully

**Table IV-21. Operating parameter of straylight simulator**

| Parameter | Quantity |
|---|---|
| Illuminator intensity at minimum background and source diameter | 100–5500 ft-cd |
| Maximum illuminator intensity source | 20,000 ft-cd |
| Illuminator source | 100-W quartz-iodine sealed beam lamp |
| Gimbal about sensor optical axis | 3- to 375-deg pot readout |
| Illuminator gimbal relative to optical axis | 36- to 90-deg pot readout |
| Star source gimbal | 360-deg synchronous drive |
| Light sink | 32-deg half-angle dark area |
| Background brightness for illuminator set at 5000 ft-cd of Venus illumination | equivalent to $7 \times 10^{-4}$ cd/ft$^2$ at 2870°K |

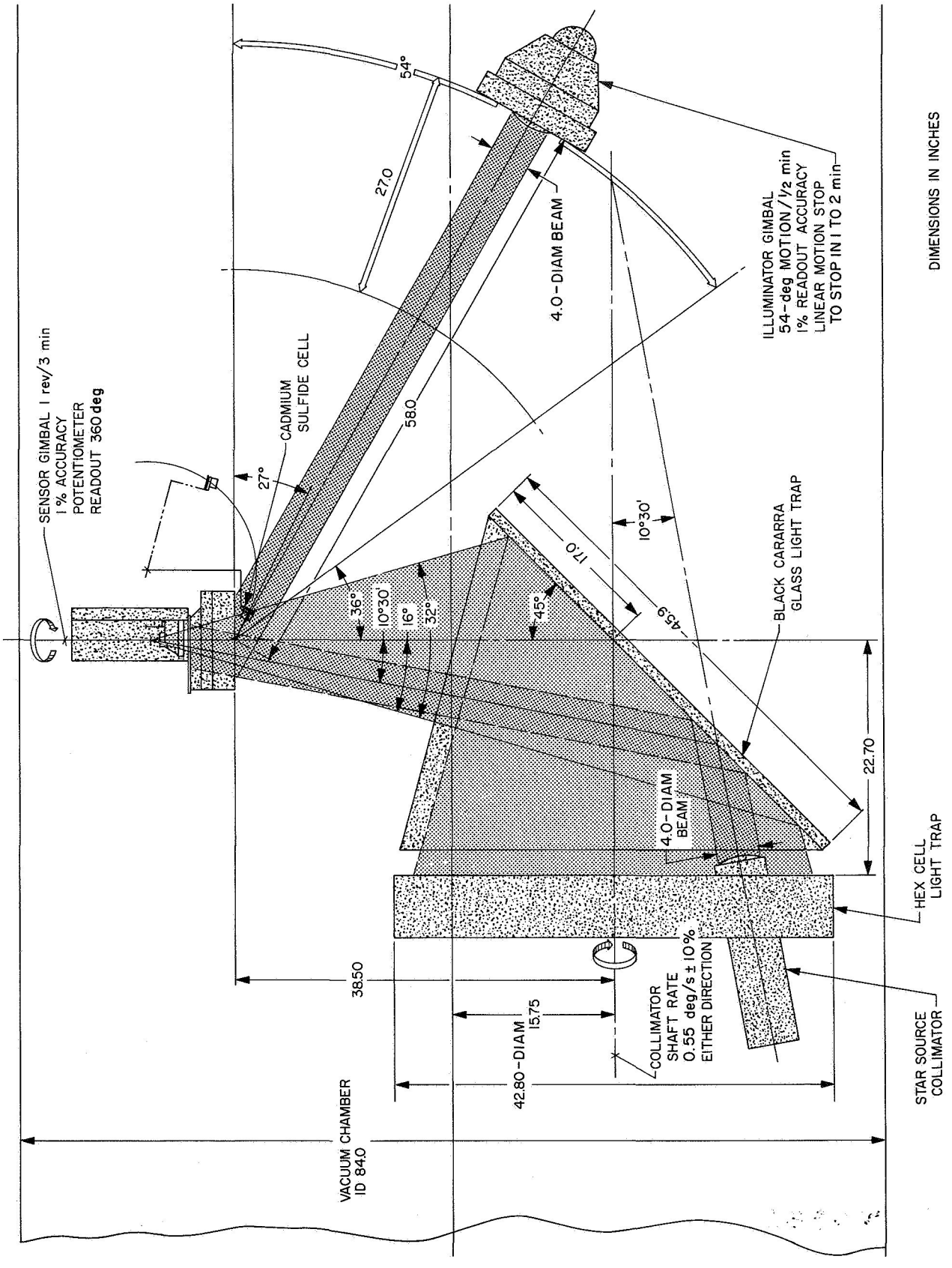



**Fig. IV-73. Schematic of vacuum straylight test fixture**

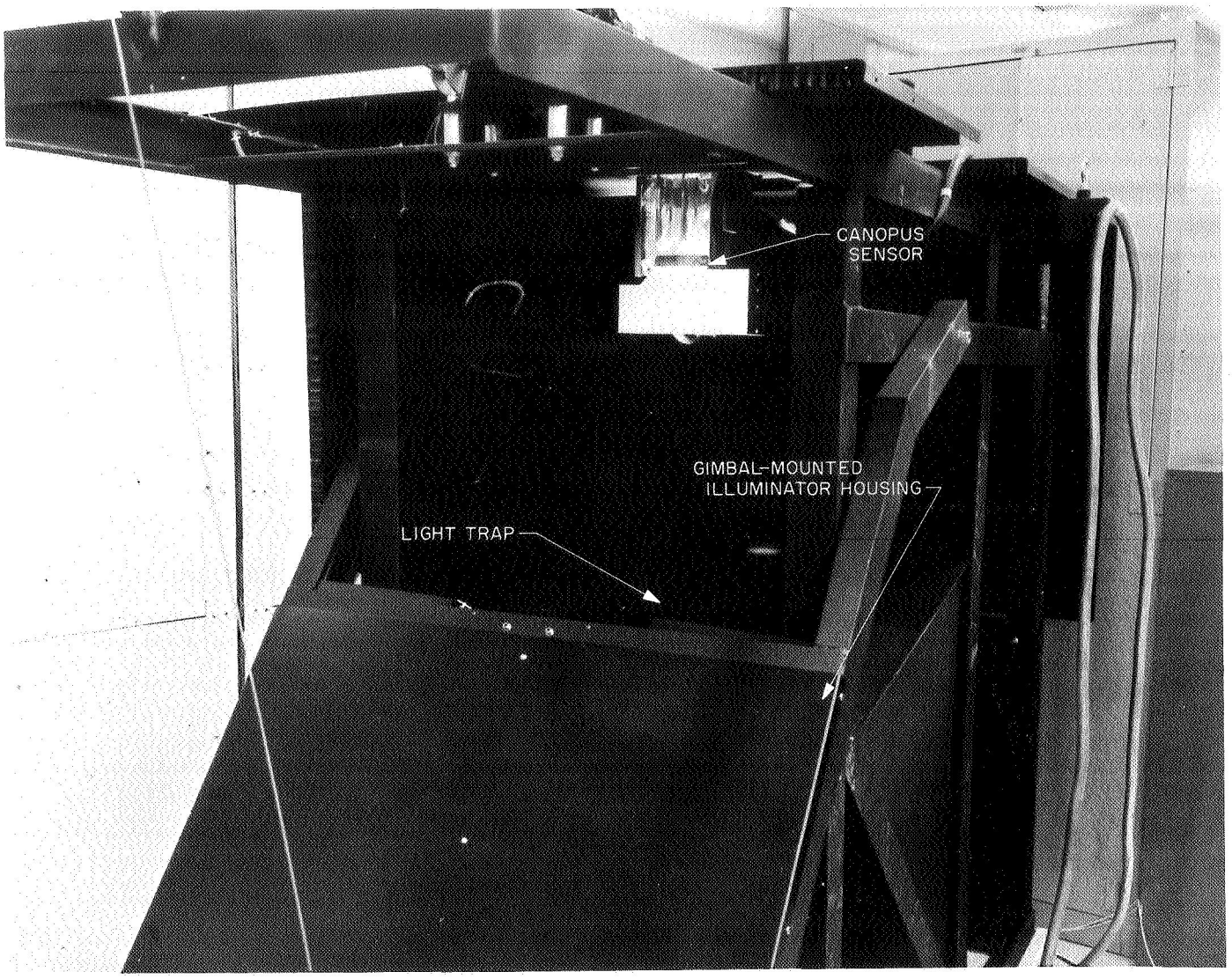



**Fig. IV-74. Partially disassembled straylight test fixture**

conduct the test. The star source collimator could probably be replaced with an uncollimated point source for most applications. With careful design of point source, the problem with the present design can be eliminated.

The data-taking operation was partially mechanized. The intensity signal and the roll error signal were plotted vs straylight angle for constant illumination. An *X-YY* plotter was used to record a family of curves with illumination as a parameter. Data were taken at 30-deg intervals in azimuth around the sensor. A sample of the data taken is presented in Fig. IV-75.

Analysis of this type of data led to a choice of failure criteria. The illumination level to 1 × Canopus intensity at a given angle was chosen as a reasonable definition of failure. This choice yielded smooth isofailure contours and guaranteed that null offsets were less than a few tenths of a degree.

The angular diameter of Venus approaches 120 deg at closest *a priori* trajectories. It is not easy to simulate a source with this diameter. The sources used to simulate straylight are relatively small with angular diameters between a few tenths of a degree to a few degrees in diameter. A conservative approach to this problem is taken by plotting the total illumination from Venus at the angle to the near limb of Venus. The total illumination is calculated by integrating the brightness up to 90 deg from the optical axis. This procedure is probably

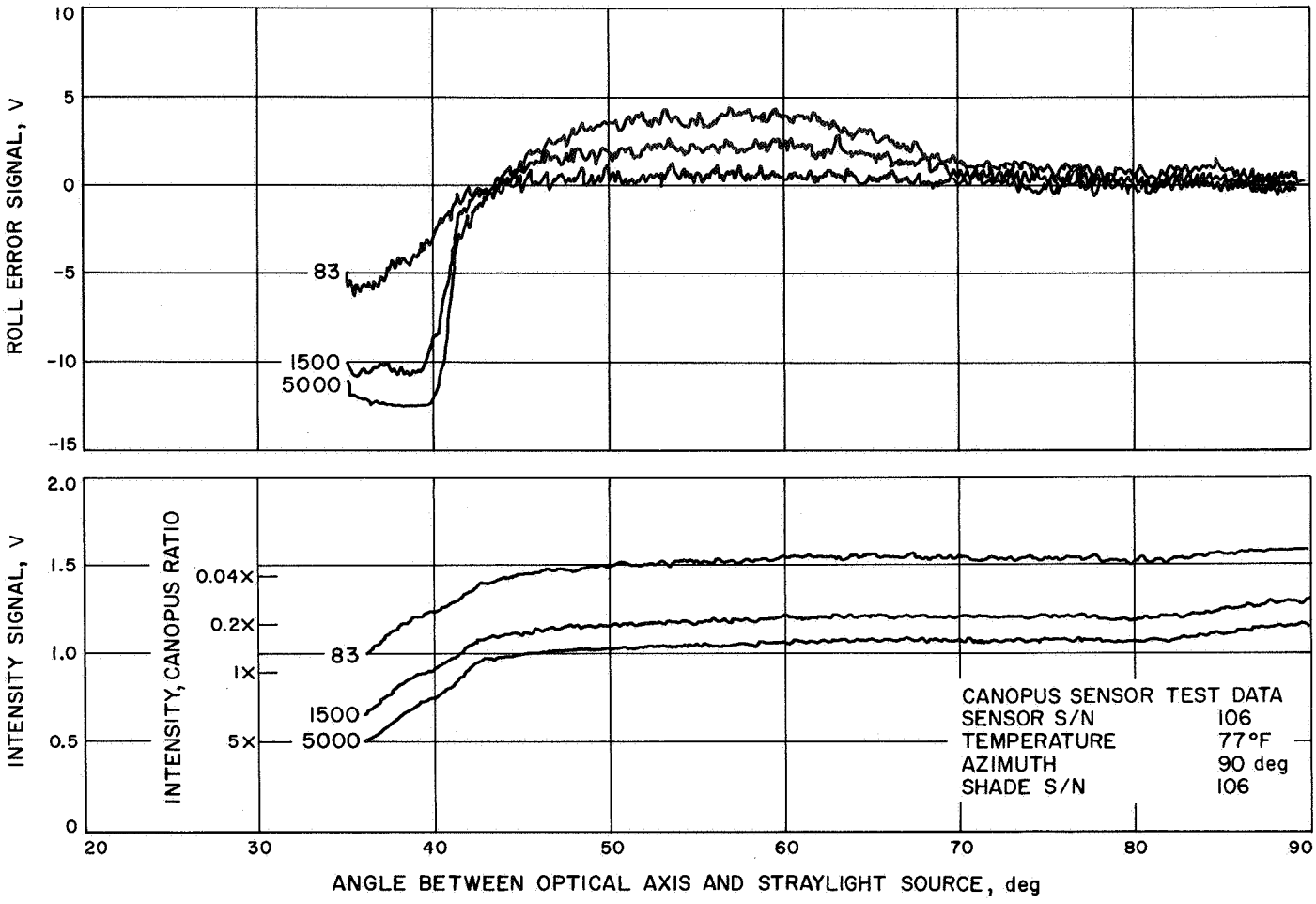



**Fig. IV-75. Sample straylight data**

conservative by a factor of 2 or more depending on the nature of the straylight response curve.

Any straylight test is in some degree conservative, since extraneous illumination will always be scattered into the sensor by the test facility. Because of the iso-failure contour slope, the extraneous illumination is only serious if it comes in to the sensor closer to the optical axis than the test source. It is very difficult to estimate exactly how conservative the test is in this respect, but 2–5 deg in angle would be a reasonable estimate.

The performances of the *Mariner IV* and *Mariner V* straylight shades are shown in Fig. IV-76. The worst case straylight from Venus is also indicated in this figure. The diagram indicates over a factor of 10 safety margin for the *Mariner V* sensor, while the *Mariner IV* sensor had a factor of 50 from being adequate.

*Canopus sensor optics.* The requirement for two-stage shade made the *Mariner IV* lens design unsuitable for use in the *Mariner V* Canopus sensor. The volume required to construct the necessary shade on the *Mariner IV* lens was not available on the spacecraft.

Although the effective diameter of the *Mariner IV* lens is 0.8 in., the actual diameter is 1.3 in.; this is due to occultation of the central rays by the aperture compensator and secondary reflector. Shade length is proportional to lens diameter; therefore, a considerable penalty in shade size and weight is involved in using the catadioptric lens used on *Mariner IV*.

The shroud dynamic envelope limited the length of the *Mariner V* shade. The lens diameter was fixed at 0.500 in. once the maximum shade length was determined by the shroud dynamic envelope, and the 42-deg requirement for two-stage shading was established. Refracting optics were needed to maximize the lens area within the 0.500-in. aperture allowed.

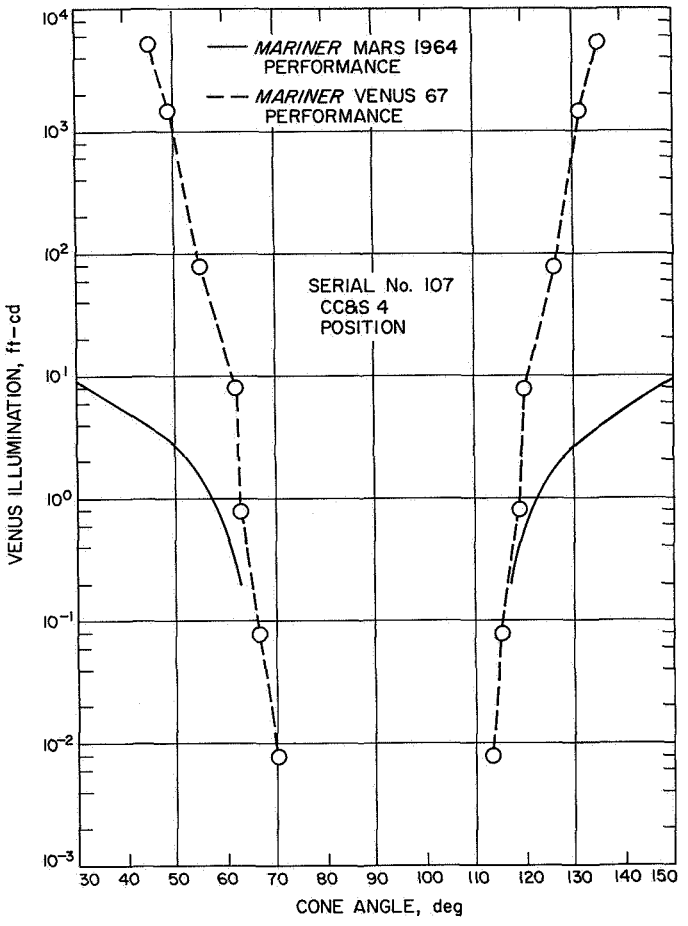



**Fig. IV-76. Canopus sensor straylight sensitivity, ft-cd to give 1 × Canopus vs cone angle**

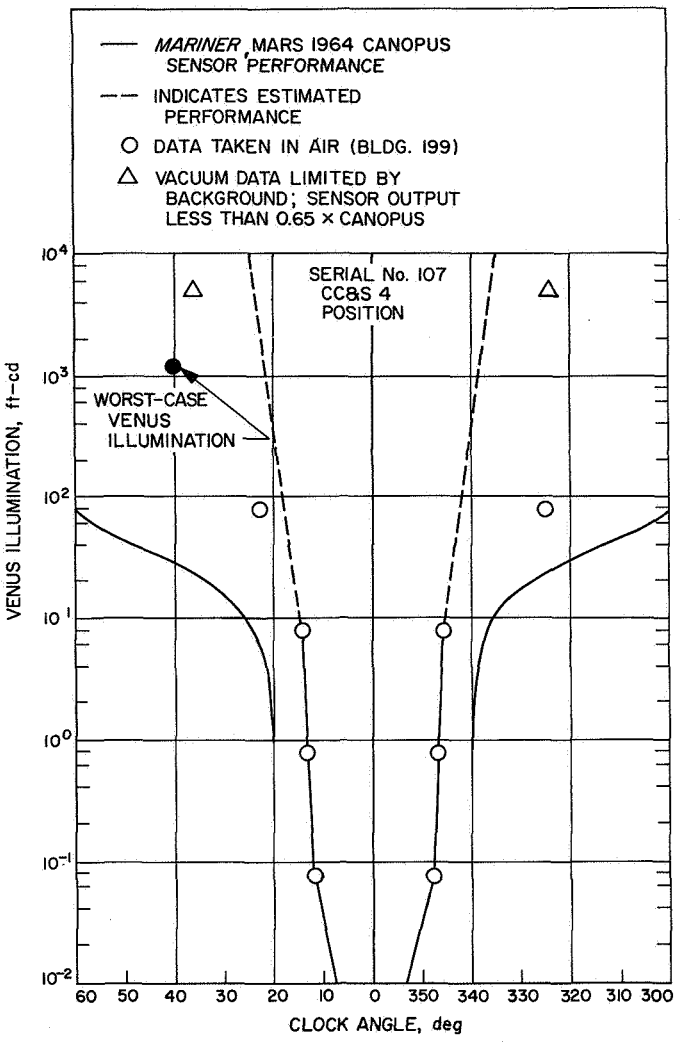



**Fig. IV-76 (contd)**

A four-element lens system was designed using the JPL-LASL lens design program. The constraints imposed on the design are listed in Table IV-22.

**Table IV-22. Lens design parameters**

| Parameter | Specification |
|---|---|
| Entrance pupil | 0.500-in. diameter; located in front of first element |
| Focal length | 0.8 in. |
| Image plane | Flat fiber optics of image dissector |
| Useful area | ± 3 deg primary field-of-view; ± 16 deg straylight field-of-view |
| Special transmission and chromatic correction | 0.37 to 0.58 μm minimum |
| Image intensity | Uniform to 90% within useful area |
| Front element to be insensitive to radiation | Quartz |
| Overall length | 1.625 in. |

The computer optimized the lens design with respect to resolution in the clock angle direction. The resolution in the cone angle direction was uncontrolled because the sensor is a single-axis device, sensitive to resolution in the clock angle direction only. A 32-ray pattern intercepting ½ the entrance pupil was used to determine the resolution. Resolution is determined by calculating the rms distance between the mean intercept and the intercepts of the 32 rays in the pattern.

Twice the rms spot size is approximately equal to the point source image size. The image size in each direction is plotted vs cone angle in Fig. IV-77. Figure IV-78 shows a schematic of the lens.

The edges of the elements were polished and painted with cata-lac black paint to minimize stray reflections.

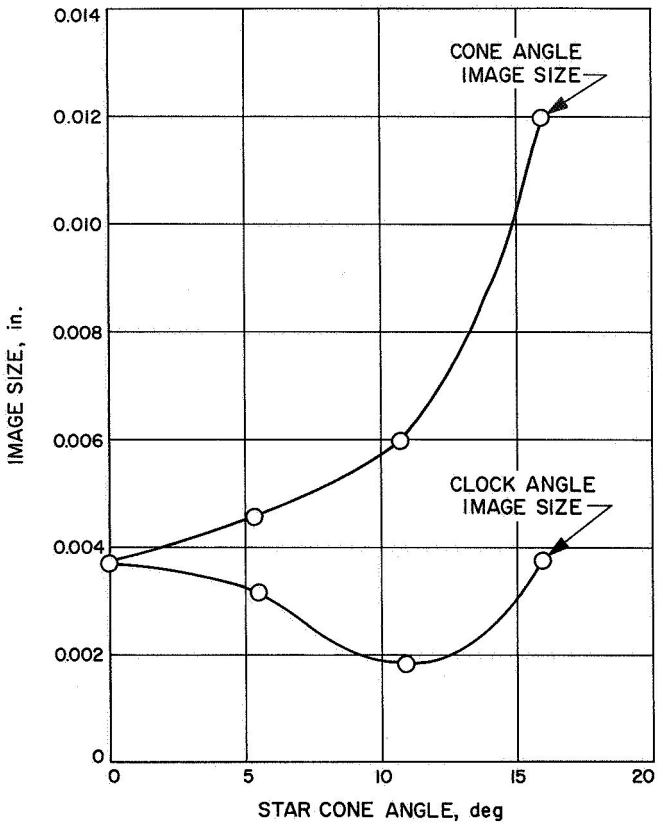



**Fig. IV-77. Canopus sensor lens performance**

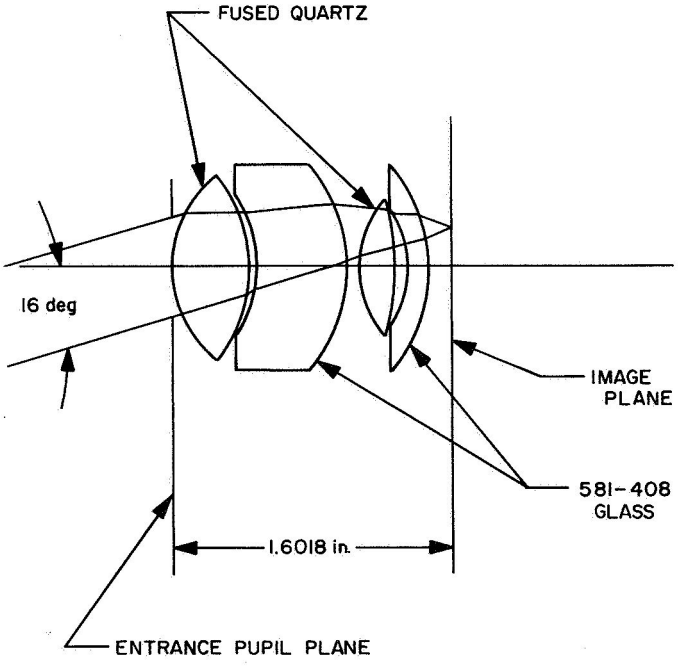



**Fig. IV-78. Canopus sensor lens schematic**

The unused area on the last surface was also painted black. In general, an attempt was made to use oversized elements to minimize edge reflections as a source of stray-light.

When mounted in the sensor, the lens optical axis must be aligned to the electrical center of the image dissector, which is uncertain to 0.040 in. Also, the entrance pupil must be aligned accurately to the shade to minimize shade length. It was, therefore, necessary to design the lens with an oversized entrance pupil of 0.580 in. The 0.580-in. diameter entrance pupil attached to the shade could then be off center on the lens by 0.040 in. without compromising lens performance. By allowing the entrance pupil to be off center in this way, the length of the shade was effectively reduced by 16%.

*Canopus sensor sun shutter.* The *Mariner IV* sun shutter could not be used on the *Mariner V* sensor, because it was too large to go inside the two-stage shade and too small to be used externally. An internal shutter was designed using a JPL-developed rotary solenoid. The shutter assembly is shown in Fig. IV-79. The solenoid uses a balanced helical magnetic structure to generate a stroke of 36 deg. The operating characteristics of the solenoid are tabulated in Table IV-23.

Armco magnetic iron was selected for the solenoid, because it has low retentivity. Low retentivity was important for two reasons: general spacecraft magnetic

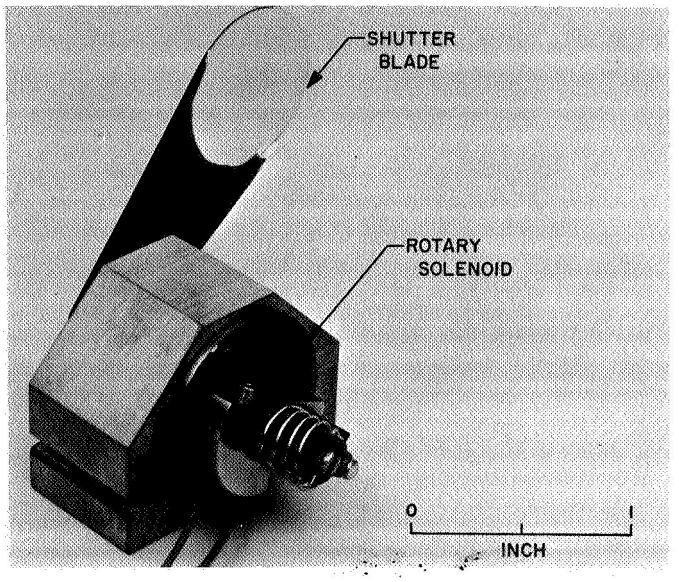



**Fig. IV-79. Sun shutter assembly**

**Table IV-23. Solenoid operating characteristics**

| Parameter | Value |
|---|---|
| Volts | 21.5 V |
| Room temperature resistance | 95 Ω |
| Starting torque | 1.0 in.-oz |
| Return spring preload | 0.500 in.-oz |

cleanliness, and Canopus sensor null accuracy. Since the image dissector (being an electron optical device) was sensitive to magnetic fields, it was necessary to locate the solenoid 3 in. from the image dissector to limit null offsets to less than 0.05 deg.

This design has proven very reliable. In life testing at room ambient conditions, the prototype shutter assembly has been operated 6 million cycles without a malfunction. A unit equivalent to the flight units was also subjected to simulated space temperature environments. During a 15-day test, 1500 shutter cycles at 0°F and ½ million cycles at 170°F were completed without a malfunction.

*Gas system.* The *Mariner IV* gas system was used virtually unchanged for *Mariner V*. The only changes were removal of the solar vanes and internal modifications to the solenoid operated gas valves to improve operation over an expanded temperature range. Figure IV-80 shows one of the two identical half-gas systems mounted on its carrying frame.

The solar pressure control system was physically incorporated into the gas system; each solar vane and actuator was mounted on a boss on the manifold that housed the four gas valves, Fig. IV-81. With the decision to eliminate the system for the *Mariner V* design, it was only necessary to dismount the actuator and vane from the manifold, and sever and tie back the wiring (which was contained in the same cable with the wiring to the gas valves). Temperature control reference (TCR) assemblies were mounted on the $+X$, $-X$ and $-Y$ manifolds (on the bosses that had held the solar vanes and actuators). The 0–300°F temperature sensors were mounted on the $-X$ and $-Y$ TCRs to provide a measurement of the $-X$ roll and yaw and of the $-Y$ pitch valve and manifold assembly temperatures.

The presence of the temperature sensors underscored the concern over the temperature range that the gas system was expected to be exposed to and to operate over

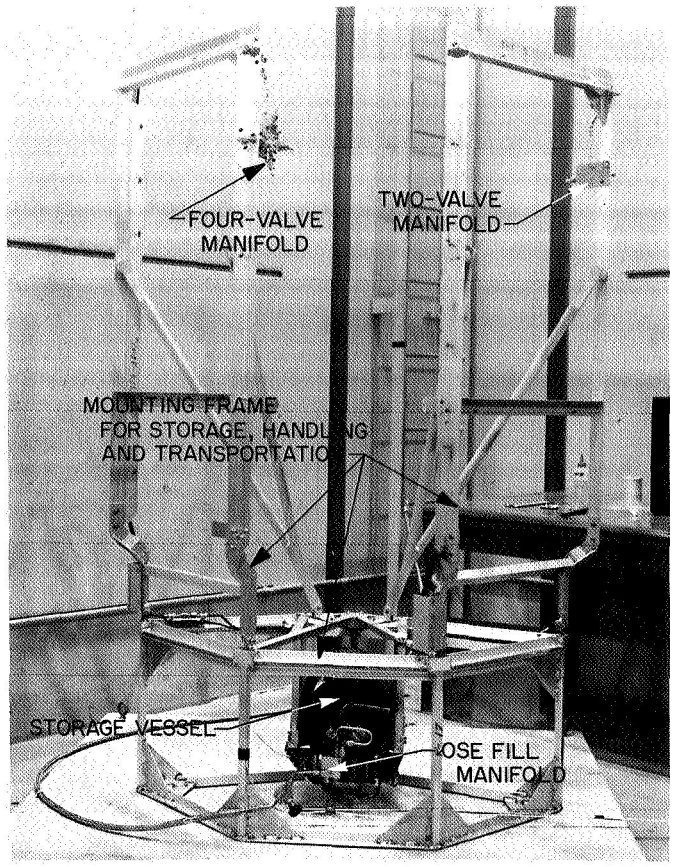



**Fig. IV-80. *Mariner V* attitude control gas system**

during flight. Initial estimates of the jet valve temperatures at encounter and perihelion (245 ±30°F and 290 ±30°F, respectively) led to an investigation of the operation of the valves at elevated temperatures.

The *Mariner IV* design was qualified for operation up to 167°F, but testing showed that their operation at 245°F was completely unsatisfactory. Accordingly, a valve redesign effort was begun. Initially, a thermal shield was added to protect the valve from circuit sunlight; this shield reduced the design maximum temperature to 215°F. The rework on the valve itself centered on reducing the effort involved in opening the valve. Figure IV-82 is an exploded view of the valve illustrating the modifications, which were: removal of material from the end of the pushrod to reduce the travel of the pushrod to a minimum consistent with the gas flow rate required; removal of a large radius on the guide pin that interfered with proper seating of the return spring; addition of a 1-mil tantalum shim between the clapper and the valve body to reduce the effects of residual magnetism in the clapper assembly; and substitution of a spring with a spring constant of 82 lb/in. for the existing 164-lb/in. spring.

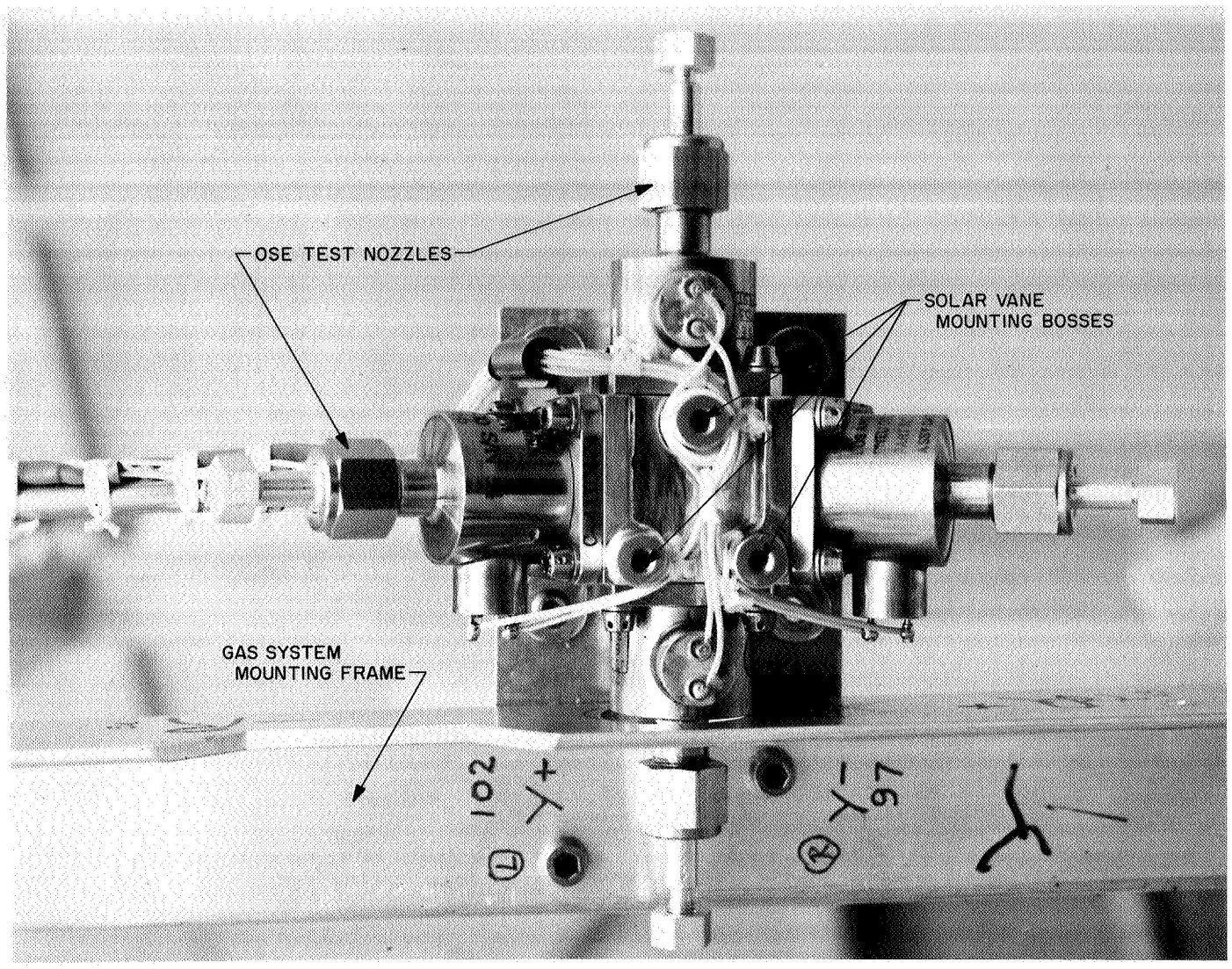



**Fig. IV-81. Attitude control roll-yaw gas valve mounting**

The purpose of these modifications was to measurably increase the performance of the valve at high temperatures. Table IV-24 compares the performance of a non-flight valve at 72°F before modification, 75°F after modification, and 250°F after modification.

**Table IV-24. Gas valve parameters**

| Performance parameter | Before modification 72°F | After modification | |
|---|---|---|---|
| | | 75°F | 250°F |
| Coil resistance, Ω | 312.4 | 311.8 | 430.8 |
| Pull-in current, mA | 38.0 | 19.5 | 18 |
| Opening time, ms | 18.4 | 5.8 | 6.4 |
| Closing time, ms | 1.7 | 3.9 | 3.1 |
| Valve travel, in. | 0.0085 | 0.0038 | 0.0038 |

The dramatic improvement in opening time (i.e., the time between application of the signal to open and the cessation of valve movement) is evident. There appeared to be a problem with high-leakage rates, but a combination of relapping the valve seat by the manufacturer and a slight increase in the valve relief pressure reduced leakage to an acceptable level. The specification for each valve is 3.0 $cm^3/h$ (at STP) leakage; the average delivered leak rate was less than 1 $cm^3/h$.

The first opportunity to actually test the valves in a flight configuration occurred when a *Mariner V* solar panel became available for TA testing in the 10-ft space simulator. The results of the test showed that the temperatures at encounter and perihelion would be much

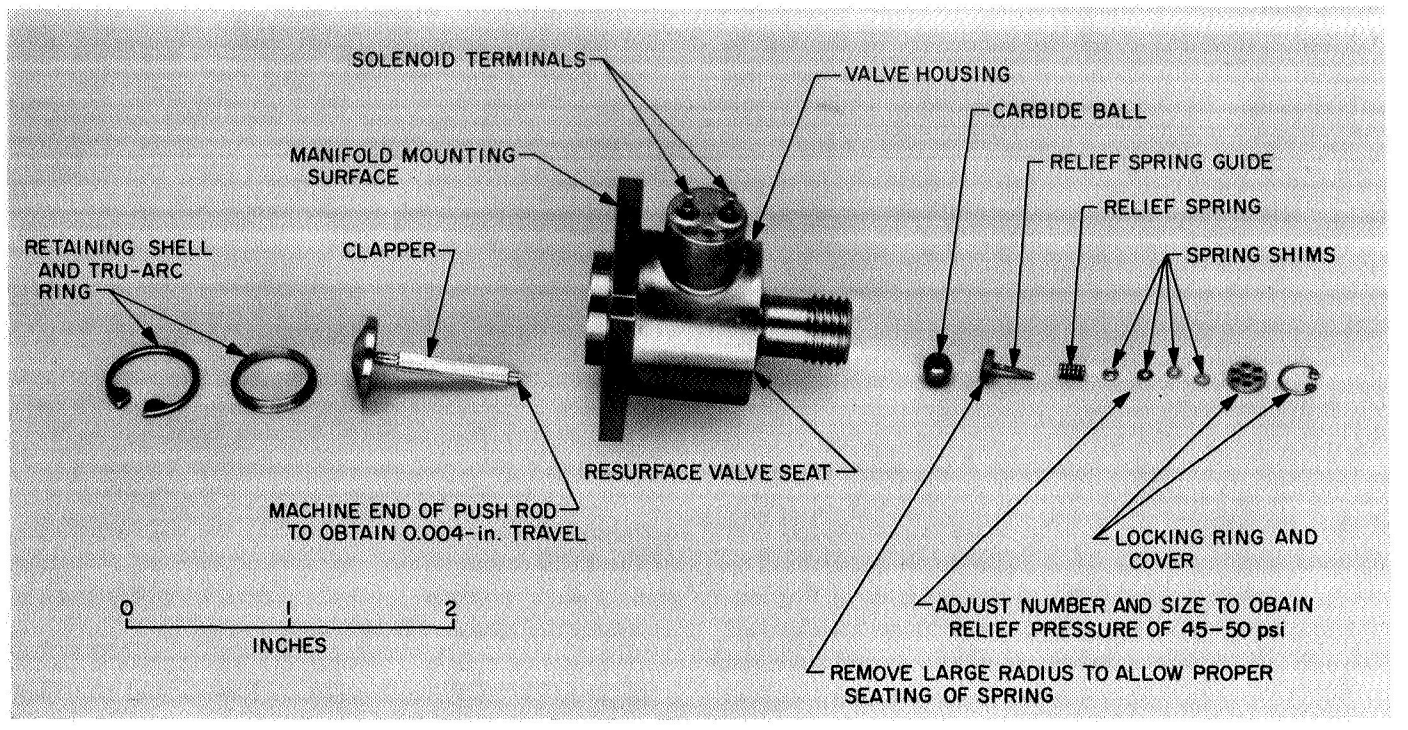



**Fig. IV-82. Attitude control gas valve detail (modifications indicated for high-temperature operation)**

lower than those predicted; in addition, the worst-case cooling transient during a midcourse maneuver could cool portions of the manifold, valve, and nozzle assembly to −75°F. Since there were no data on the valve operation at temperatures below approximately 0°F, two valves were tested in the Actuator Laboratory for operation at −75°F and −100°F; the results are summarized in Table IV-25.

**Table IV-25. Gas valve performance at 125 to −100°F**

| Operation | Valve | Temperature, °F | | | | | |
|---|---|---|---|---|---|---|---|
| | | +75 | −100 | −75 | 0 | +75 | +125 |
| Opening time, ms | A | 8.9 | 9.0 | 8.0 | 7.9 | 7.8 | 8.2 |
| | B | 9.8 | 9.5 | 9.0 | 9.2 | 9.7 | 9.3 |
| Closing time, ms | A | 1.4 | 1.8 | 1.7 | 1.7 | 1.5 | 1.4 |
| | B | 1.3 | 1.6 | 1.7 | 1.6 | 1.3 | 1.3 |
| Pull-in current, mA | A | 35 | 34 | 34 | 33 | 36 | 31 |
| | B | 40 | 41 | 45 | 42 | 44 | 48 |
| Drop-out current, mA | A | 8 | 8 | 5 | 7 | 10 | 10 |
| | B | 12 | 9 | 8 | 8 | 11 | 11 |
| Leak rate, $cm^3/h$ | A | 1.6 | 1.0 | 1.6 | 1.4 | 1.5 | 2.0 |
| | B | 1.8 | 1.2 | 4.8 | 5.5 | 3.7 | 3.5 |

The dewpoint of the dry nitrogen used in the gas system is −65°F. Condensation or deposition of ice or water in the manifold or valve body at these low temperatures did not seem to interfere with the operation of the system. As a result of the revision of the expected operating temperature range, the temperature transducer range was changed to −75 to 150°F.

Formal testing on the gas system was limited to a TA, and FA tests on the valves inasmuch as they were the only component of the system changed from the *Mariner IV* configuration. (A pressure regulator was vibration tested to FA levels; it had been a *Mariner IV* spare, and was intended for use as a *Mariner V* spare.)

The initial requirements for the TA test were: a vacuum-temperature test over the temperature range 14–255°F, a thermal shock test, and a vibration test would be required. With the revision of expected mission temperatures, the thermal shock requirement was eliminated and the temperature range changed to −65 to 167°F for the TA vacuum-temperature test.

The FA testing required was a vibration test and a vacuum-temperature test over the range 32–215°F. This range was subsequently modified to −45 to 131°F.

The changes in TA and FA temperature limits did not occur, however, until after 18 valves had been FA tested to the original range. Consequently, the two TA valves

were tested at 225°F for five of the required 12-day test duration and at 167°F for the remainder of the test to maintain the relation between the FA and TA tests embodied in the testing concept. Therefore, of the thirty attitude control gas valves intended for use as flight and flight spare equipment, twelve (the valves intended for the M67-1 spacecraft) were FA tested to the range of 32–215°F, twelve (the valves intended for the M67-2 spacecraft) were tested to the range of −45 to 215°F, and the remaining six spares were tested to the range of −45 to 215°F. A waiver of FA testing at −45°F of the first twelve was granted, based on the performance of the latter eighteen valves.

During all functional testing in SAF, only one valve was found to be leaking consistently at a rate in excess of the allowable 3 $cm^3/h$. The valve was removed and replaced with one of the spare flight-qualified valves. The leaking valve was examined microscopically in the laboratory and some contamination was found on the ball and seat. It is characteristic of these valves that the greatest source of contamination comes from within the valve itself, generated by valve actuation.

*b. Autopilot.* The spacecraft autopilot was functionally composed of the gyro control assembly, the autopilot electronics assembly (physically located within the control electronics package), and the thrust vector control assembly (TVCA), which in turn was composed of the four jet vane actuators (JVA) and a mounting ring. These three assemblies were used unchanged from the *Mariner IV* design, except for a gain adjustment in the electronics to compensate for the change in spacecraft moments and products of inertia and PIPS (post-injection propulsion system) mounting angle, and a shaft seal lubricant change in the JVA.

The function of the autopilot is to maintain a stable and accurate spacecraft orientation during the engine burn portion of the midcourse maneuver. To accomplish this orientation, the autopilot electronics processes the three gyro "rate plus position" outputs, transforming these error signals into appropriate deflection commands for the four JVAs. Each actuator controls the position of an aerodynamically neutral jet vane in the exhaust stream of the PIPS engine; these vanes then generate, as a function of their position, corrective torques which tend to maintain the spacecraft attitude.

Because the PIPS is located in Bay II and the PIPS thrust vector is not collinear with the spacecraft coordinate system, a system other than the spacecraft *X-Y-Z* coordinate system is employed for autopilot description and analysis. The spacecraft reference *X-Y-Z* coordinate system and the autopilot reference *a-b-c* system are depicted in Fig. IV-83, along with the orientation and

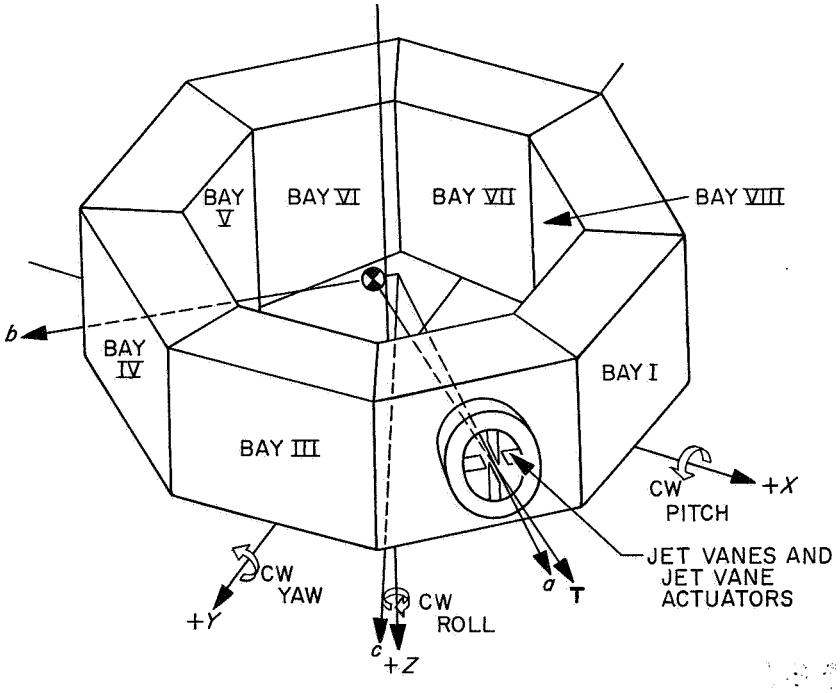



**Fig. IV-83. Spacecraft and autopilot coordinate systems**

approximate location of the gyros, vanes, and engine thrust vector T. It is readily apparent that the autopilot must convert from the inertially referenced *X-Y-Z* to the *a-b-c* system; further, since the cross-products of inertia are not, in general, zero, there is coupling between the spacecraft *X*, *Y*, and Z axes such that rotation about one axis causes torques about the other two axes. Finally, the center of gravity of the spacecraft is not necessarily located at the origin of the *a-b-c* system, although an attempt is made to optimize the PIPS location to minimize any CG displacement, and the autopilot must continually correct for any CG offset or migration.

Extensive autopilot analysis was done for the *Mariner V* configuration; the autopilot was simulated in a six-degree-of-freedom program on the 7094 computer using DSL/90, and the effects of solar-panel dynamics, dynamic cross-coupling between axes, solar-panel cruise damper characteristics, and solar-panel deployment failures were investigated and analyzed in detail. The results of the analyses of the autopilot operation indicated that no basic changes to the autopilot were necessary, but for best performance, some care in selecting the solar-panel cruise dampers should be exercised. Accordingly, the dampers were selected so that the M67-2 flight spacecraft had the most nearly optimum solar-panel response characteristics. Table IV-26 lists these characteristics.

**Table IV-26. Solar-panel response characteristics**

| Response | M67-1 | M67-2 |
|---|---|---|
| Damping coefficient | 0.12–0.3 | 0.4–0.6 |
| Damped frequency, Hz | 3.0–3.4 | 2.4–2.8 |

*Autopilot electronics (mix matrix resistor selection).* As previously mentioned, the only modification necessary to the autopilot electronics was a gain adjustment necessary because of the changes from *Mariner IV* in spacecraft moments and products of inertia and PIPS mounting angle. This adjustment was accomplished by selection of the resistance of the resistors in the autopilot mix matrix. Each of the three gyros feed each of the four JVA amplifier inputs through a scaling resistor: these twelve resistors, plus one additional roll scaling resistor and three differential input balancing resistors, make up the mix matrix that transforms the spacecraft gyro-referenced *X-Y-Z* coordinate system to the PIPS-autopilot referenced *a-b-c* coordinate system.

The CG of the *Mariner V* spacecraft was closer to the geometrical center of the bus (as measured along the Z axis) than that of *Mariner IV*. Since the PIPS can be tilted slightly to optimize the location of the centerline of the exhaust nozzle (and thus the undeflected thrust vector) with respect to the CG, this tilt angle was changed from the *Mariner IV* value of 88 deg to 88.5 deg for *Mariner V*. (This angle is the angle between the geometrical centerline of the exhaust nozzle and an intersecting line parallel to the spacecraft Z axis. Equivalently, the angle may be measured as the angle between the geometrical centerline of the exhaust nozzle and the spacecraft *X-Y* plane, in which case the angles become, respectively, 2 deg and 1.5 deg.) Since it was not possible to tell, *a priori*, what the final PIPS tilt angle would be for the fully assembled and flight ready spacecraft, five sets of resistors corresponding to the PIPS tilt angles of 88, 88.5, 89, 89.5 and 90 deg were purchased and screened.

When the M67-2 flight spacecraft was weighed and the location of its CG defined, the optimal PIPS tilt angle of 88.5 deg was established and the C/E (control electronics) package was removed; the scaling resistors were replaced and the necessary functional tests were performed; and the C/E replaced in the spacecraft. Table IV-27 illustrates the change in spacecraft dynamical properties that necessitated the changes.

Since the autopilot electronics is contained within the C/E package, it received the same environmental testing as the C/E: the single-axis FA vibration and functional bench testing at the FA temperature limits of 32 and 131°F. The functional testing measured the gains, nulls, saturation levels, and phase shift of the electronics in an open-loop configuration, and, using a TVCA, measured the closed-loop gain and phase shift from the gyro input to the JVA vane position output.

**Table IV-27. Spacecraft dynamical properties**

| Spacecraft (pre-M/C configuration) | Weight, lb | Center of gravity, in. | | | Moment of inertia, slug-ft$^2$ | | | Product of inertia, lb-ft-s$^2$ | | |
|---|---|---|---|---|---|---|---|---|---|---|
| | | $\bar{X}$ | $\bar{Y}$ | $\bar{Z}$ | $I_{xx}$ | $I_{yy}$ | $I_{zz}$ | $I_{xy}$ | $I_{yz}$ | $I_{zx}$ |
| *Mariner IV* (MC-3) | 574.74 | 0.66 | −0.05 | −12.32 | 82.22 | 82.51 | 136.94 | −2.39 | 0.88 | 1.50 |
| *Mariner V* (M67-2) | 539.17 | 0.77 | 0.29 | −12.14 | 73.6 | 71.08 | 124.48 | −3.24 | 0.96 | 1.03 |

In addition, there was a series of autopilot tests in the system configuration to verify the phasing and gain of the gyro–autopilot–JVA interface. These tests were:

(1) Using the attitude control (AC) OSE and the spacecraft mounting fixture, the spacecraft was rotated about each principal axis separately at a prescribed rate, and the JVA positions (i.e., potentiometer voltage) were checked against a recorded table in the system test procedure.

(2) Using the AC OSE alone, simulated rates about each principal axis were introduced by feeding an OSE integrator output into the gyro torquing coil input, and the JVA positions were checked against a recorded table in the system test procedure.

(3) Using the AC OSE, spacecraft fixture, and SAF computer data system (CDS), the spacecraft was rotated about either a principal axis or the autopilot *b* axis. The CDS measured and recorded the gyro output voltages and computed the corresponding JVA position potentiometer voltage; the measured potentiometer voltage then provided an indication of the error. Suitable averaging techniques were employed.

(4) Using the AC OSE and the CDS, simulated rates about each principal axis were introduced as in test (2), and the testing technique of test (3) was used.

The *Mariner* Venus 67 system test program was the first to successfully employ the CDS for SAF system testing of the autopilot. Tests, such as test (3), were able to measure dynamic autopilot gains that agreed with calculated gains to within 5%.

*Thrust vector control assembly.* When the jet vane actuators were removed from storage, it was found that all had excessive breakaway friction, i.e., stiction above the specification limit of 0.6 oz-in. The actuators were reworked by renewing and relubricating the shaft seals. The actuators were then FA tested. All actuators again failed due to binding of the shaft at the lower FA temperature of 32°F. Investigation and analysis of the problem showed that the shaft-seal lubricant used was hardening enough at 32°F to cause marginal or unsatisfactory performance. Replacing this lubricant with one whose viscosity was more nearly constant across the expected temperature range, in conjunction with the selective fitting of the seal O-rings, resolved the problem. This change of shaft-seal lubricant was the only modification to the JVA.

The actuators were completely disassembled for the rework; consequently, any previous FA vibration testing was invalidated, and replacement of the O-rings and shaft-seal lubricant was cause for a FA vacuum-temperature test. Functional testing was performed on the unit before and after FA testing.

The following problems arose during the flight qualification testing period:

(1) The JVAs operated erratically at low temperature (32°F); this problem was the cause of the modification previously described. After the modification, when the FA requirement was lowered to 20°F as a result of the TCM (thermal control model) tests, all actuators passed without incident.

(2) The null on one actuator potentiometer shifted as a result of the FA vibration. Although this shift was believed to be due to improper assembly of the potentiometer wiper to the actuator shaft, a procedure to check and verify the null position of the actuator was devised. All actuators were checked before and after shipment to AFETR to ensure transportation vibration had not affected the units. No null shifts occurred.

(3) The torque gains of the JVAs on the M67-2 TVCA were below specification after FA vibration; after remagnetization of the rotor, the ring passed FA testing and was delivered to the spacecraft. On-spacecraft testing of the M67-1 TVCA and a subsequent test of the M67-2 TVCA disclosed that the torque gains of all the JVAs were apparently degraded.

This last problem, the apparent loss of torque gain of the actuators, was at first thought to be caused by marginal magnetization of the JVA rotors. Since the rotor had no keeper, whenever the actuator was disassembled (e.g., to renew or rework the shaft seal), it was necessary to remagnetize the rotor after reassembly. Theoretically, the rotor was magnetically saturated; the field-of-strength of the rotor was then "trimmed" to produce the specified torque gain ($0.0336 \pm 0.050$ in.-oz output torque per mA input current) by applying a current to the stator coils. To ensure that the rotor was indeed being magnetically saturated during remagnetization, another magnetizing facility with a more powerful magnetizing machine ($10^5$ A-t as contrasted to $5 \times 10^4$ A-t) was utilized.

Concurrently, the procedure used to trim, or stabilize, the actuator was being examined along with the methods

and instruments used to determine the torque gain of an actuator. The solution to the problem was found in these two operations: the stabilization procedure was revised so that the stabilization current was applied to the torque coil as the rotor was rotated from stop to stop. This step ensured that the opposing magnetic field generated by the stabilizing current was effectively distributed throughout the rotor. The torque gain measuring instruments were recalibrated and the measuring procedure altered to measure gains at the center-of-travel of the rotor instead of the mechanical stop. With these revisions, the torque gains measured were acceptable and constant.

*c. Planet, terminator, and earth sensors.* The following discussion of the *Mariner V* sensors includes a description with any modification and testing in relation to the *Mariner* Mars 1964 program.

*Planet sensor.* The *Mariner V* planet sensor (Figs. IV-84 and IV-85) was designed to sense the illuminated limb of Venus and initiate the spacecraft encounter sequence. The planet sensor output (PSO), backed up by an onboard timer, would provide a start signal approximately 1 h before planet encounter.

The initial design concept was that the narrow-angle Mars gate (NAMG) flown on *Mariner IV* was to be utilized with as little modification as necessary. The following general requirements were designated:

(1) Fixed pointing angle and field-of-view (FOV).

(2) The angle and FOV were to be selected on the basis of providing a PSO at a minimum of 38 min before encounter and a minimum PSO time dispersion, relative to encounter, for any of the planned combinations of trajectories and launch dates. Timing was also to be optimized relative to midocculation as a secondary consideration.

(3) The unit must have a high straylight rejection, since preliminary estimates placed the pointing angle near the sun.

(4) The unit should interface with existing DAS excitation (+20 Vdc at $\leq$5 mA) and the PSO should operate directly into existing DAS logic inputs.

In addition, a search was to be made for a suitable spacecraft location. An area near the Canopus sensor was considered primarily and was ultimately selected.

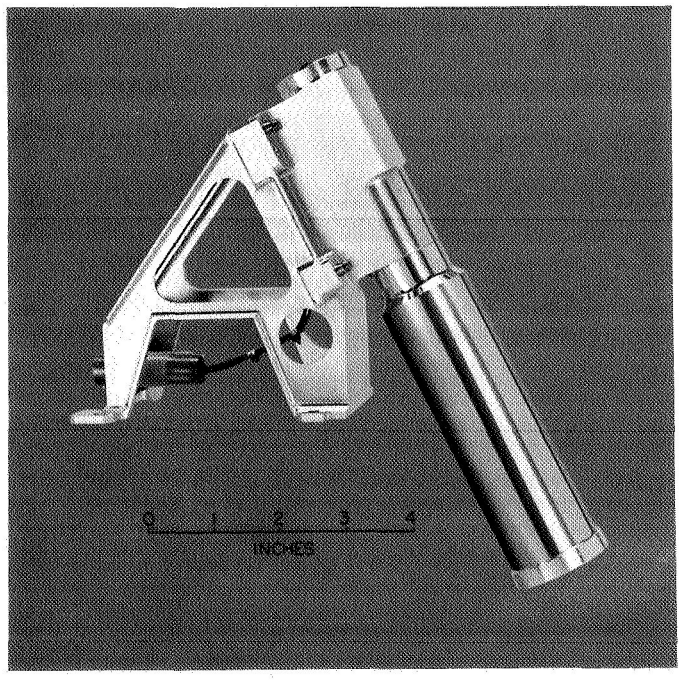



Fig. IV-84. Planet sensor

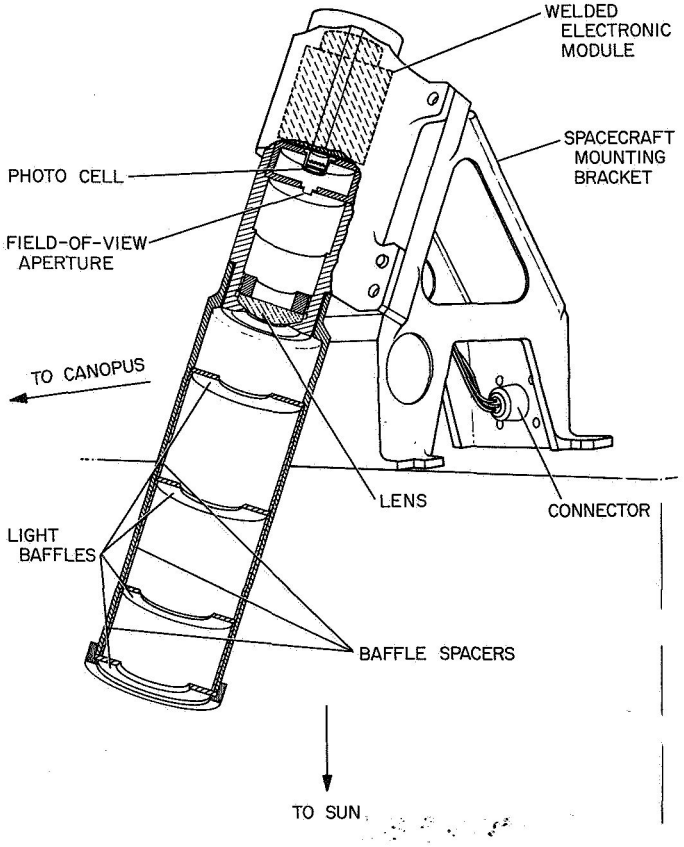



Fig. IV-85. Cutaway view of planet sensor

*Planet sensor design fabrication and testing.* The preliminary design steps were required for a prototype to be fabricated and tested as follows.

(1) PSO timing. Determination of the optimum field-of-view with consideration to previously outlined requirements was undertaken. This determination was primarily accomplished by hand-drawn plots of the illuminated limb of Venus. The plots, as in Fig. IV-86, were drawn for each 3 min of flight in the vicinity of encounter minus 1 h, and for each of five points (limits and center) in the 3-$\sigma$ trajectory dispersion pattern. This plotting was repeated for the total span of launch dates from June 12–27. As a result of these graphical iterations, a "leading edge"* for the FOV was selected. A computer program was modified to determine contact time of the illuminated limb with the leading edge of the FOV and the results, which were in agreement with graphically tabulated data, are:

(a) PSO relative to encounter $= 60^{+12}_{-13}$ min.

(b) PSO relative to midoccultation $= 60^{-8}_{+16}$ min.

(c) PSO relative to enter–exit occultation $= 60^{-18}_{+40}$ min.

The next step was to determine the angular width of the field back of this leading edge. This width would have little effect on timing, but was controlled by the conflicting considerations of viewing as much of the planet as possible (to keep the light level threshold maximized) and limiting the straylight susceptibility. Based on these considerations, the angular width was optimized at 1°30′.

(2) Light level threshold. Determination of optimum light level threshold to achieve PSO was next accomplished. The trajectory that placed the planet sensor FOV nearest to the illuminated horns of Venus (Fig. IV-86) was chosen as worst case (i.e., lowest illumination). An overlay of the selected FOV onto a calculated intensity map of this sector provided a conservative value of 0.07 ft-cd to the detector. This value included the effects of effective lens aperture, detector spectral response, and a conservative calculation of Venus spectral irradiance and intensity. The threshold for PSO was then set at 0.01 ft-cd, which provides a safety factor of 7. A larger safety factor was considered undesirable because of increased susceptibility to straylight, and a less stable control of threshold point. The stability decreases at the lower light levels due to the characteristics of the CdS detector, and the electronics module "seeing" a higher (dark) impedance.

(3) Location. Optimum location was next determined. A prime area near the Canopus sensor was available. This area afforded the clearest view into the desired direction, since the 0-deg clock angle of Canopus coincided with the planet sensor clock angle axis, and straylight sources were already minimized for the Canopus sensor. The other choices afforded less shading from the sun and spacecraft straylight sources, or less space for orientation of the sensor baffle tube. A further consideration, at the time, involved a possible change in trajectories. This change may have required repositioning of the sighting angle which could be accomplished in the selected area.

(4) Light baffles. Planet sensor straylight baffles were next designed on the basis of maximum straylight rejection consistent with simplicity of design and the shroud clearance, which limited the light baffle

*Leading edge is defined by a line (41°4′ away from 0-deg clock angle that is 4°33′ in length) that first intercepts the planet limb. This line is identified in Fig. IV-86.

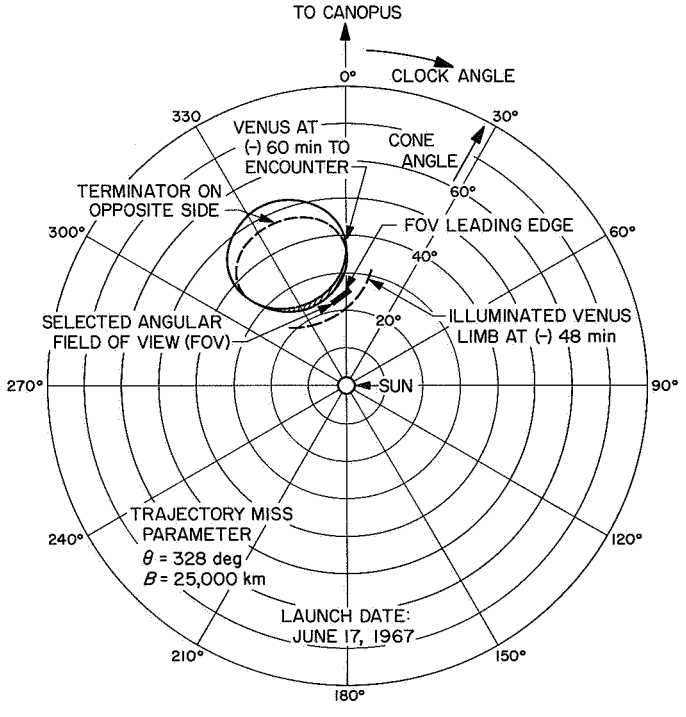



**Fig. IV-86. Planet sensor field of view superimposed at −2 min from contact with illuminated limb of Venus**

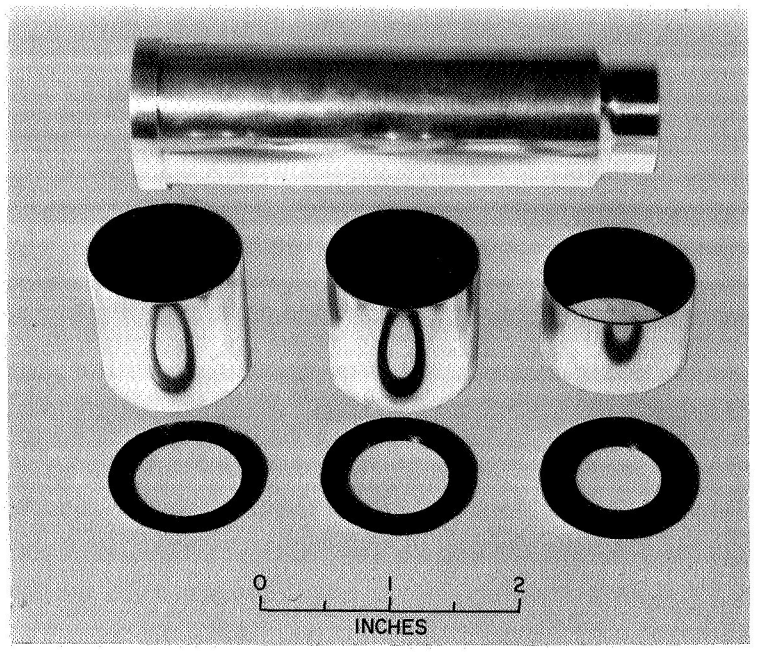



**Fig. IV-87. Light shade assembly**

tube length. The baffles (Fig. IV-87) were carefully machined, liquid honed, and anodized to provide effective light trapping and a minimum of scattering by virtue of their sharp edges.

(5) Detector and electronics module. In parallel with the optical–mechanical considerations, a test program on the CdS detector and electronics module was conducted. A 100 Clairex (CL705L) CdS photoconductive cells from the same production run were obtained; 50 of these passed a preliminary visual examination and were selected for screening. After all screening tests, five were deemed suitable for the planet sensor, i.e., they had consistent high dark resistance, a similar resistance versus light level, and the least deviation of characteristics during screening. The selected CdS cells also exhibited a negative 15% temperature characteristic at the desired threshold level.

The electronics module under test demonstrated a compensating positive temperature characteristic with the result that the combination of CdS cell and electronics provided a constant light level threshold over the environmental TA temperature range. The final circuit, as shown in Fig. IV-88, being arranged in the form of a bridge, also compensated for ±20% excitation voltage change and up to 50% ripple on the excitation line. Provision was made to adjust the light level threshold of the module after encapsulation by the addition of an external shunting resistor (RX).

The circuit functions similarly to a Schmitt trigger. When the CL705L CdS photoconductive cell is illuminated sufficiently to cause the voltage on the base of Q1 to exceed its reverse bias, both

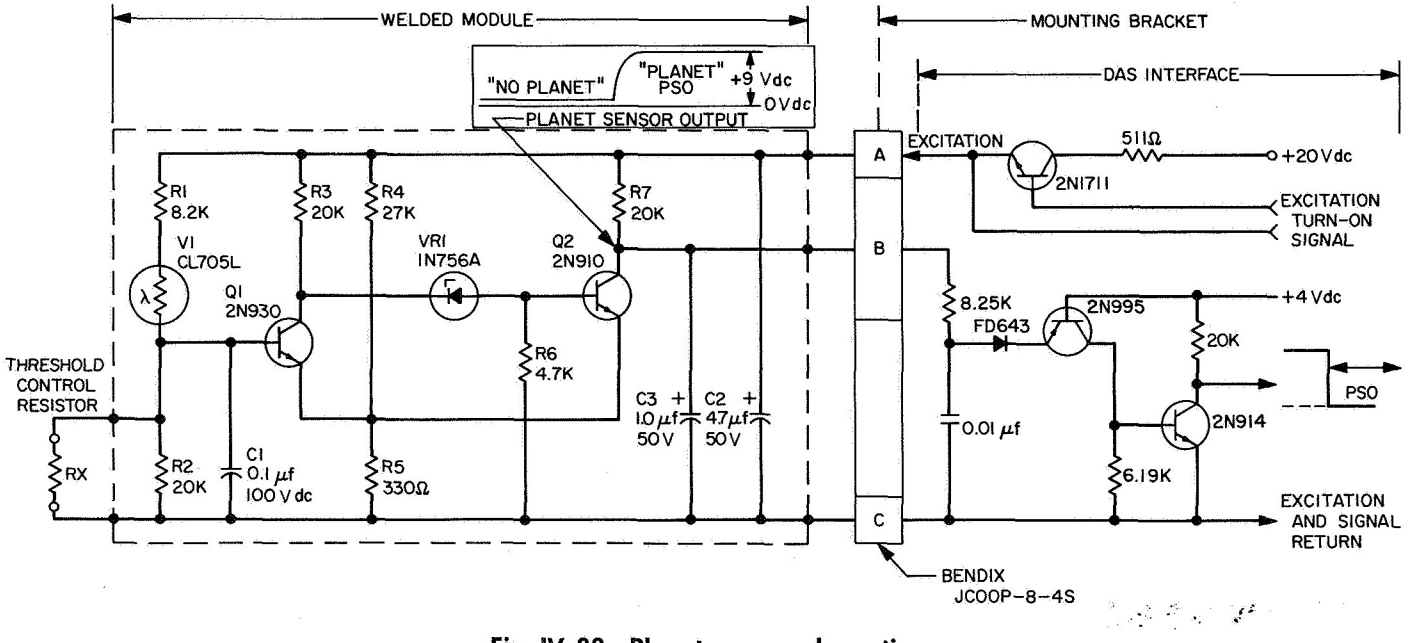



**Fig. IV-88. Planet sensor schematic**

transistors switch state. The collector potential of the output transistor Q2, which is now in the *off* state, rises to approximately 9 V. The switching time, after threshold, is less than 10 ms. Filtering on the base of Q1, the excitation load line, and the PSO load line provides a low-noise susceptibility. Additionally, the DAS input is reverse biased five times the normal "no planet" output voltage.

(6) Development. In early August 1966, a prototype planet sensor was assembled and subjected to extensive TA testing. During TA vibration, the sensor was inadvertently exposed to a level 20 to 50 times normal vibration level. The unit was then functionally tested and showed no change in performance. It was then completely disassembled, inspected, and reassembled. The prototype was redesignated as the TA unit and passed all TA tests. Two more units were fabricated, tested, and delivered to the M67-1 and M67-2 spacecraft in late August and December 1966, respectively. During the interim, an intensive test program subjected the CdS cells and spare welded modules to a wide range of long-term extremes in environmental conditions. As a result, the stability of the CdS cells and electronics was encouraging in establishing long-term reliability.

A measured survey of straylight sources from the sun shade, Bay VIII thermal louvers and solar panels, etc., established a probable 200 ft-cd maximum intensity, no closer than 9 deg from the mean planet sensor optical axis. Measured performance of the planet sensor indicated that the unit could reject in excess of 30,000 ft-cd, 8.5 deg off axis, thereby assuring proper operation even if the sun shade should not deploy. A plot of the straylight rejection characteristics is shown in Fig. IV-89. Each "constant intensity contour" represents the intensity required to cause PSO, or the intensity required at that angle to allow the equivalent of 0.04 ft-cd to fall on the CdS detector (lens to detector gain = ×4).

(7) OSE hood. The OSE hood was designed as an aid to environmental testing, but primarily for spacecraft subsystem checkout. The principal configuration is a closed hood (Fig. IV-90) that fits over the entrance aperture of the planet sensor to the exclusion of all other light. It consists of a miniature lamp with a diffused surface placed behind a partially transmitting and diffusing Teflon screen.

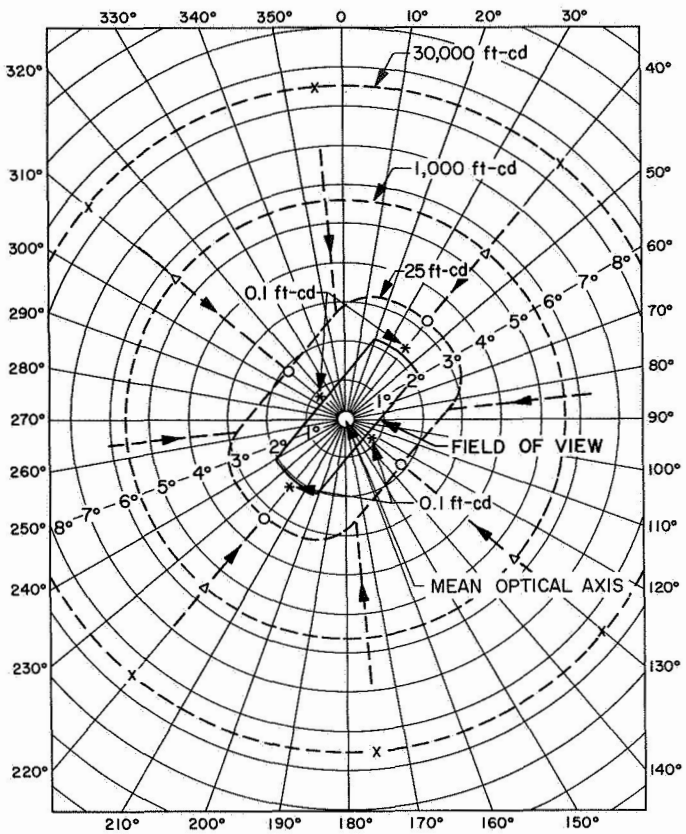



**Fig. IV-89. Planet sensor straylight pattern**

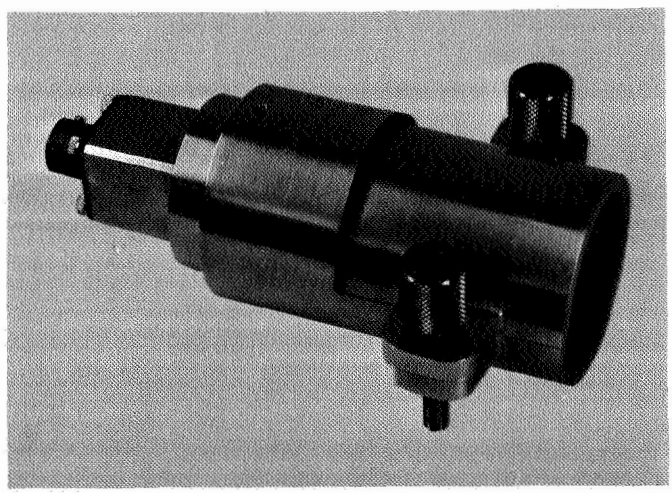


**Fig. IV-90. Operational support equipment hood**

This screen provides an even surface brightness of approximately 0.5 cd/ft² at the required planet sensor threshold level and is large enough so that alignment is not critical.

For testing in an environmental chamber, the lamp is supplied a variable current. This is monitored during test to ascertain changes in threshold by noting changes in lamp current required to cause PSO. For spacecraft checkout, the lamp will operate (on OSE command) at a current sufficient to provide three times planet sensor threshold. Each OSE hood is serialized and mated to a particular planet sensor.

*Planet sensor functional details.* The outline of planet sensor characteristics is given in Table IV-28. A detailed breakdown of these characteristics follows.

**Table IV-28. Planet sensor characteristics**

| | |
|---|---|
| Weight | 257 g |
| Power | 42 mW (20 Vdc at 2.1 mA) |
| Electronics (welded module) | 2 transistors, 1 zener diode, 8 resistors, 3 capacitors, 1 CdS photoconductive cell |
| Dimensions | Maximum length: 8 in.<br>Maximum dimensions ⊥ to this: 6.25 in. |
| Spacecraft pointing angle | Plane of constant clock angle equal to zero and 24°54′ away from sun |
| Field-of-view | 4°33′ × 1°30′<br>(clear field assured by front light baffles 6 deg circular) |
| Lens | Single element plano convex crown glass |
| Detector | Cadmium sulfide, Clairex CL705L (visible) |
| Straylight rejection | $3 \times 10^6$ (30,000 ft-cd) at 8.5 deg off axis |
| Input | Light level threshold: 0.01 ft-cd at 5500 Å peak response |
| Output | 9-V step to data automation subsystem when input exceeds threshold; starts timer B to initiate encounter sequence |

(1) The excitation is 20 Vdc ±5% at 5 mA maximum with 4% peak-to-peak ripple. The maximum current is supplied only if the CdS cell should look directly at the sun.

(2) The field-of-view is 4°33′ × 1°30′ as determined by a small rectangular aperture on the focal plane of the lens. The aperture dimensions are closely controlled to minimize light scattering and to maintain an accurate FOV. This aperture allows illumination of approximately 50% of the CdS cell active area. The rear view of the aperture is shown in Fig. IV-91, and a front view (facing lens) is shown in Fig. IV-92.

(3) The lens is optical-quality crown glass, especially selected to be free of scattering strains and bubbles.

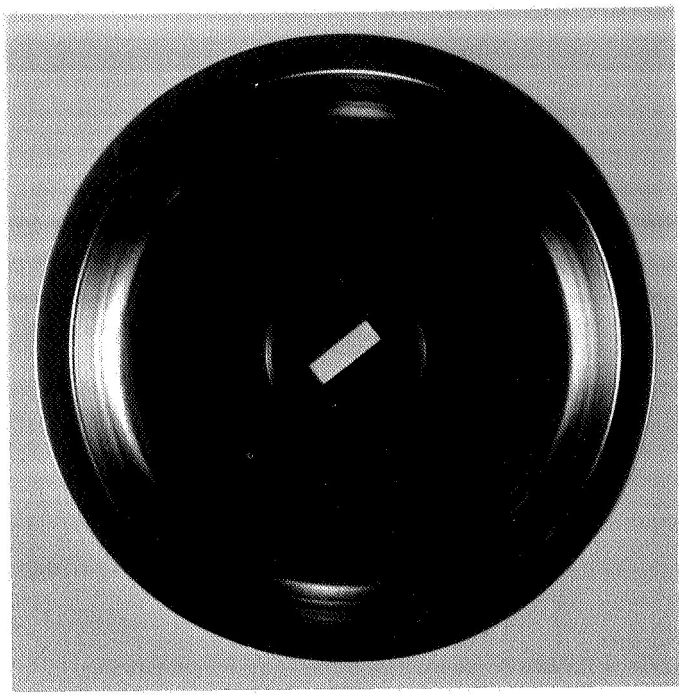


**Fig. IV-91. Aperture**

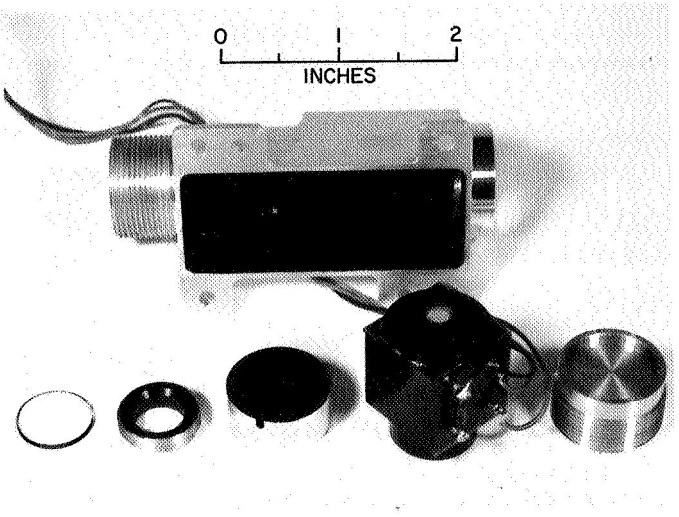



**Fig. IV-92. Planet sensor housing**

The edge is ground and coated with a light absorber, and only the central 60% of its diameter is utilized.

(4) The housing assembly, shown in Fig. IV-93, contains the lens, lens retainer ring, aperture (front view), welded module (CdS cell facing up), and module retainer plug.

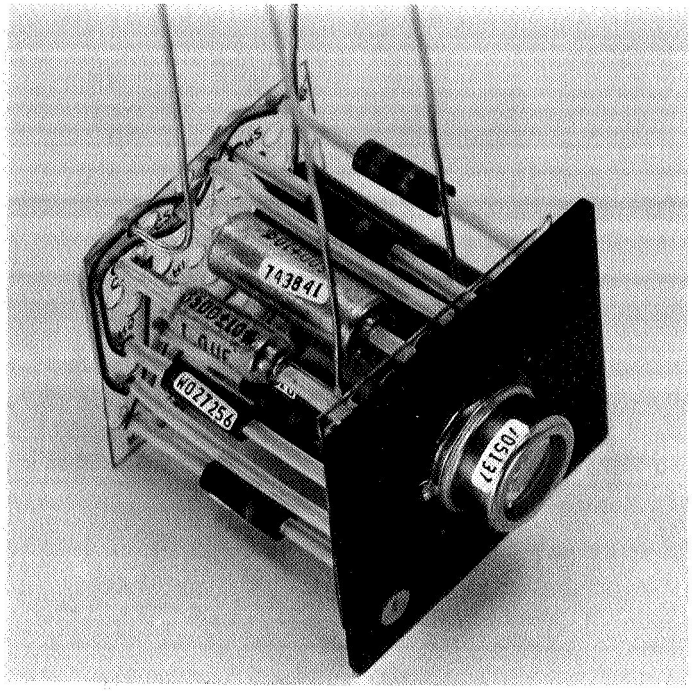


Fig. IV-93. Welded module

(5) The electronics of the unpotted welded module is shown in Fig. IV-93. The CdS cell is bonded to the face with its sensitive pattern aligned at 41-deg clock angle to match the tilt of the leading edge of the FOV. All components are welded except threshold setting resistor RX, which is added during preenvironmental functional tests. The threshold is set for 0.01 ft-cd incident on the planet sensor lens. The lens provides a gain of 4 to the detector. The electronics will reverse state if this threshold intensity is reduced 30% (switch hysteresis). The cell may look directly at Venus–sun without damage (22,000 ft-cd) to the CdS cell or electronics. A limiting resistor is placed in series with the CdS cell to limit peak current.

*Terminator sensor.* The terminator sensor (Fig. IV-94), an electrically modified *Mariner IV* narrow-angle Mars gate, was used as the primary signal source for activation of the high-gain antenna pointing angle change (APAC) by providing a signal to the pyrotechnic subsystem when the Venus terminator entered its 1.5 × 2.5-deg field-of-view. The sensor was mounted on Bay II of the

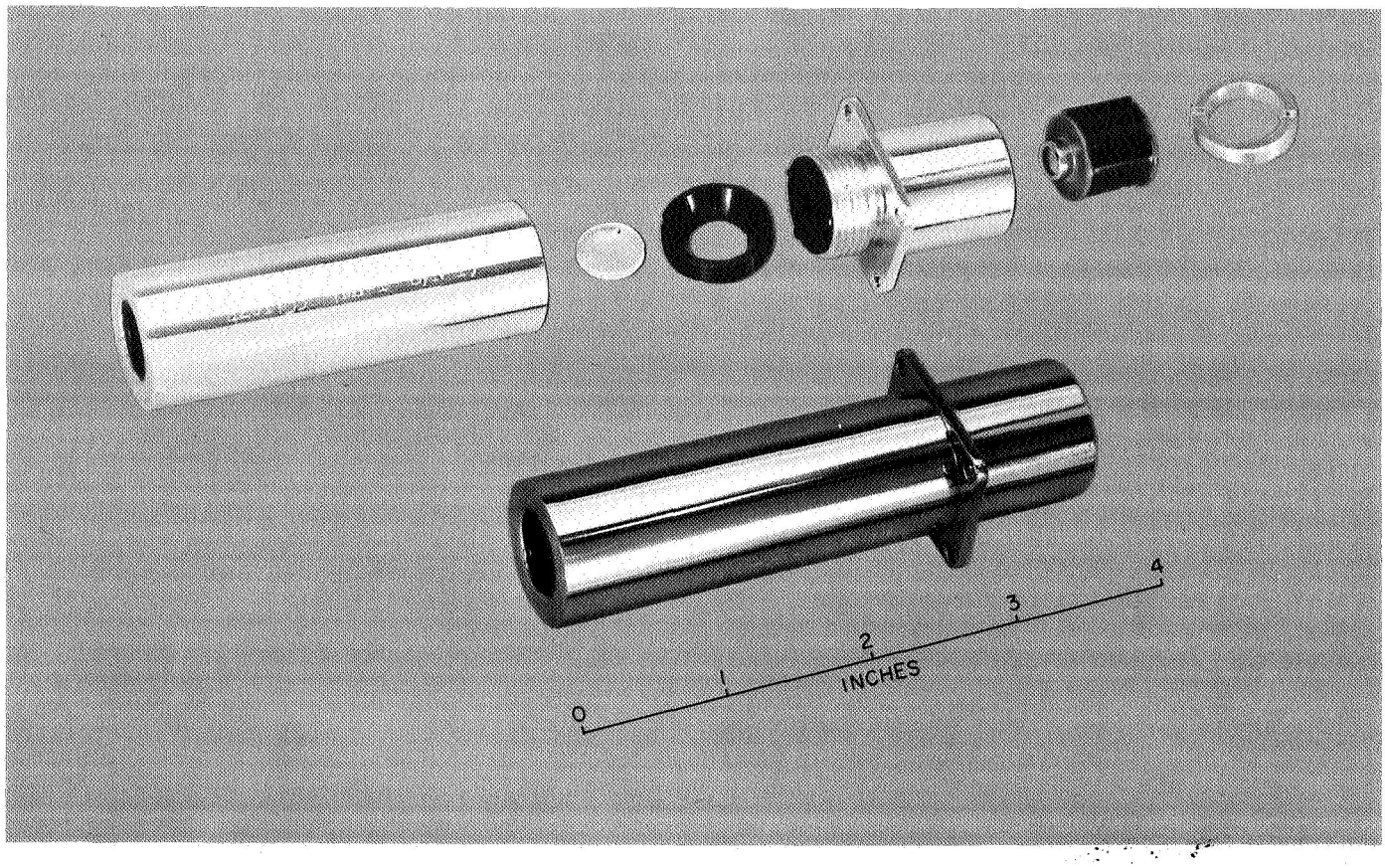



Fig. IV-94. *Mariner V* terminator sensor

spacecraft, and had look angles of: 110-deg clock and 110-deg cone. These angles were determined by the geometrical relationship between the spacecraft and the terminator at the desired time of APAC. Figure IV-95 depicts the encounter geometry. These angles were analyzed with the *Mariner* Mars 1964 MARCAM program, adapted for the *Mariner* Venus 67 mission, to verify the dispersion of terminator sensor output (TSO) times shown in Fig. IV-95. As is evident, all times fall within the cone of radio occultation, indicating APAC would occur at the desired time.

The threshold level was selected by first constructing intensity contours for Venus covering all trajectories and launch dates, and then accounting for forward light scattering. Using the predetermined look angles, an average brightness of 300 cd/ft² was set as the intensity threshold. The field-of-view of the sensor will sweep across Venus from the dark side of the lit side and TSO will occur when the field-of-view is completely filled with an object of 300-cd/ft² brightness corresponding to an intensity of 0.1 ft-cd at the entrance pupil of the sensor.

The terminator sensor, being mechanically equivalent to the *Mariner IV* NAMG, did not require a TA test. The FA testing consisted of vibration and vacuum-temperature testing; as a result of the TCM testing, the lower FA temperature for the sensor was changed from 32 to 0°F.

Extensive testing of the interface with the pyrotechnic subsystem was performed. It was shown that the sensor

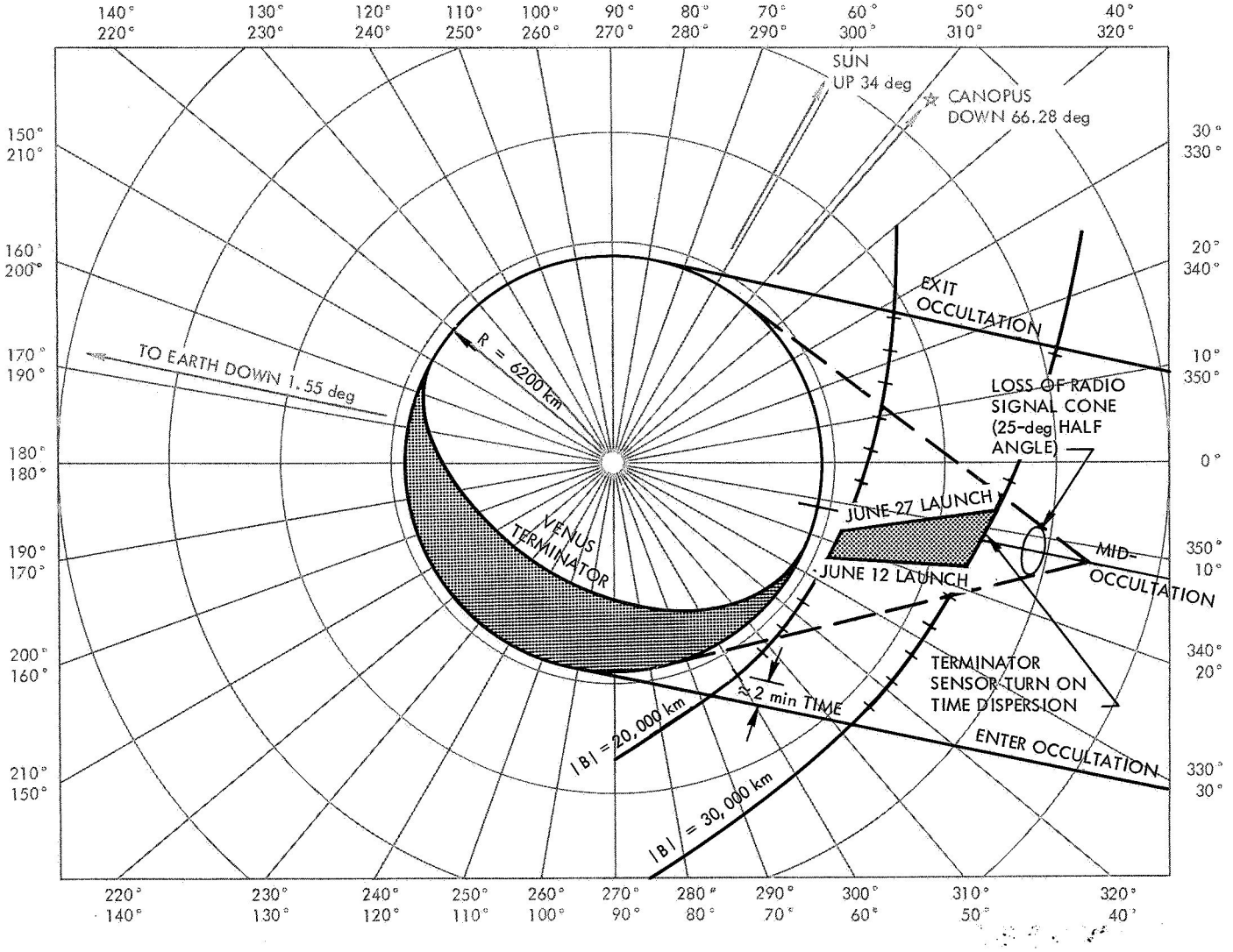



**Fig. IV-95. Approximate terminator sensor encounter geometry**

would deliver the required output over the sensor temperature range of 160 to −40°F with a ±25% variation in threshold sensitivity, and that the sensor would fire the two pyro loads that it interfaces with over the range of 10–160°F, with worst-case sensor supply voltages from the pyro of 12.43–13.8 Vdc.

*Earth sensor.* On the *Mariner IV* spacecraft, the earth detector was used as an aid in verifying the acquisition of Canopus by the Canopus tracker: when Canopus was acquired, the earth would appear in the field-of-view of the instrument. Flight operations experience with star acquisitions showed that a backup of this type was not necessary, and it was decided to employ the *Mariner V* earth sensor (Fig. IV-96) as a backup to the Canopus sensor. In the event of a Canopus sensor failure prior to the midcourse maneuver, the spacecraft would be placed in the roll inertial control mode and incrementally stepped until the earth appeared in the field-of-view of the earth sensor, or placed in the roll search mode until the earth appeared in the sensor field-of-view. Spacecraft roll position would subsequently be controlled using the roll inertial control mode. The earth instead of the star Canopus would then serve as the roll position reference, albeit the accuracy of the reference is degraded to ±1 deg.

The modification necessary to convert the *Mariner IV* earth detector to the *Mariner V* earth sensor was the replacement of the baffles with a set of baffles designed to produce a field-of-view of 50 deg in cone angle and 3 deg in clock angle. Figure IV-96 shows the defining aperture; Fig. IV-97 illustrates the field-of-view of the instrument.

Environmental testing on the earth sensor was limited to FA vibration and vacuum-temperature; as with the terminator sensor, the lower FA temperature limit was changed from 32 to 0°F as a result of TCM testing.

Thorough calibration of the earth sensors output versus simulated earth size and clock angle was performed. Figure IV-98 is a typical set of sensor calibration curves utilizing varying earth sizes, intensities, and cone angles. The dots represent static values, and the solid lines represent the response obtained when the stimulus sweeps through the field-of-view at the spacecraft search rate, 2 mrad/s.

*d. Flight performance of the spacecraft control subsystems (launch through midcourse maneuver).* The *Mariner V* spacecraft was launched at 06:01:00.176 GMT on June 14, 1967, from Cape Kennedy. The events from launch through sun acquisition occurred as expected and

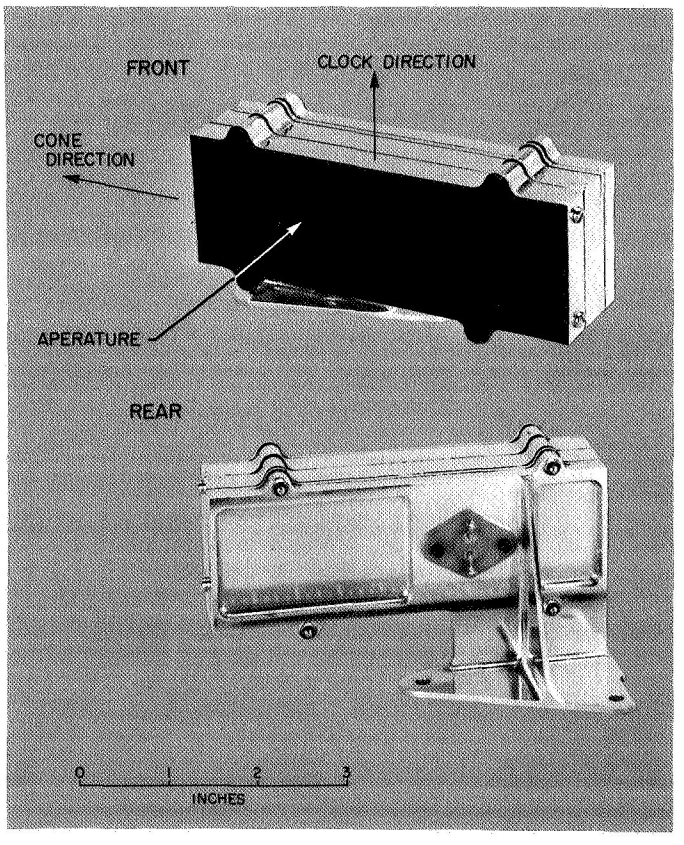



**Fig. IV-96. Earth sensor**

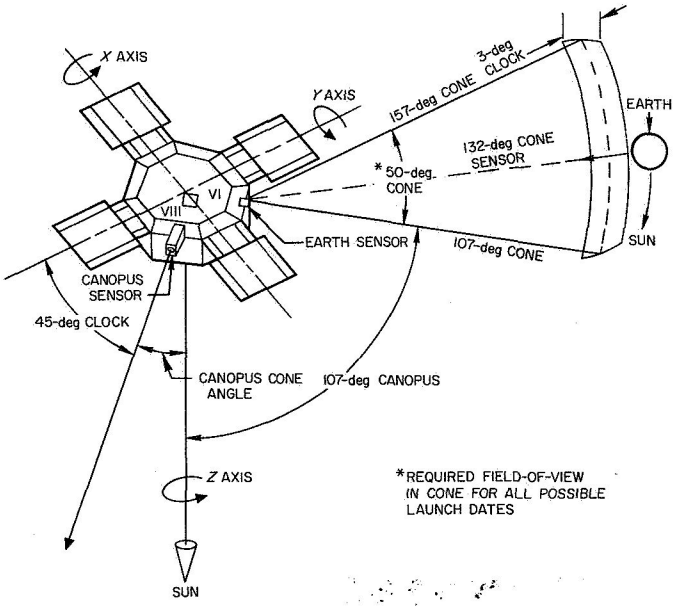



**Fig. IV-97. Earth sensor field-of-view**

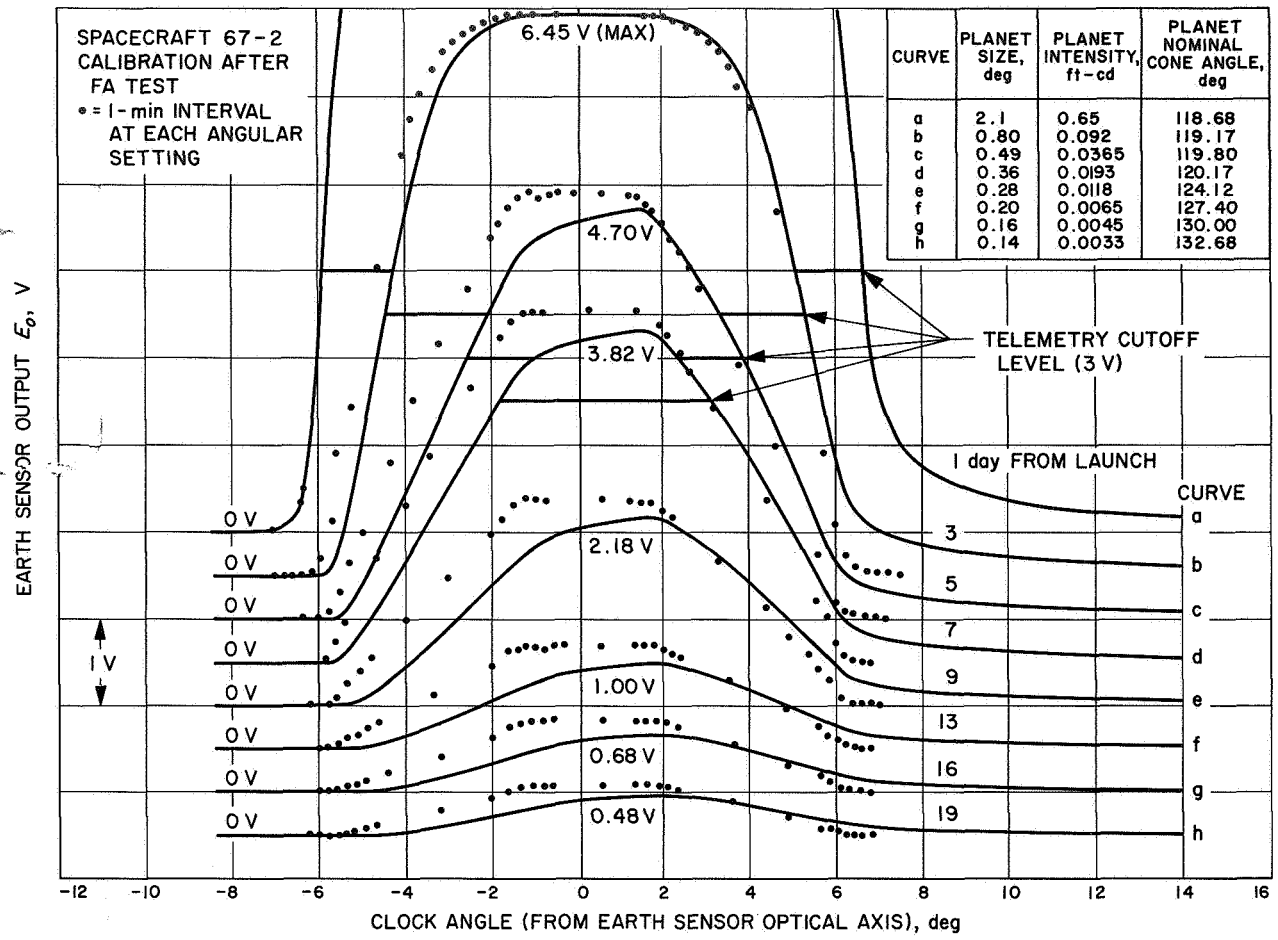



**Fig. IV-98. Earth sensor calibration**

were normal. Table IV-29 summarizes the performance of the gyros during the launch; the event number is keyed to the corresponding event number on Fig. IV-99. An expanded plot of the gyro telemetry received at spacecraft/*Agena* separation is shown in Fig. IV-100. The separation rates were:

| | |
|---|---|
| Pitch: +7.5 mrad/s | (0.43 deg/s CW) |
| Yaw: −17.2 mrad/s | (0.99 deg/s CCW) |
| Roll: −4.1 mrad/s | (0.23 deg/s CCW) |

The vector sum of these rates is 19.2 mrad/s (1.1 deg/s).

*Sun acquisition.* The sun acquisition process began at spacecraft/*Agena* separation, at 06:27:16.2 GMT, when the pyro arming switch (PAS) turned on the attitude control subsystem. The initial acquisition rates were $4.92 \pm 0.15$ mrad/s in pitch and $-4.84 \pm 0.15$ mrad/s in yaw. The separation initiated timer event occurred at 06:30:11.6 ± 4.9 s GMT, 175.4 ± 4.9 s after separation. The four solar-panel deployment events were recorded by 06:30:19.2 GMT, and the acquisition rates decreased to $3.46 \pm 0.15$ mrad/s pitch and $-3.02 \pm 0.15$ mrad/s yaw (although conservation of angular momentum considerations would indicate the angular velocity should increase when the panels deployed, since the moment of inertia about both the pitch and yaw axes decreases, the moment arm for the pitch and yaw gas jets increased from about 1 ft to about 8 ft at deployment and acted to decrease the acquisition rate).

The sun sensors were activated at PAS and initially showed saturated outputs. The spacecraft was driven CW in pitch and CCW in yaw to acquire the sun, but earthlight on the secondary sun sensors biased the electrical null at least 78 mrad (4.5 deg) off the probe–sun line. Figure IV-101 depicts the geometry of the acquisition. The false null had to be acquired in both pitch and yaw to trigger the sun gate. (This figure depicts the observer as being on the spacecraft; therefore, the sun–probe and false null–probe vectors are represented as points in a plane containing the sun. The sun gate field-of-view is

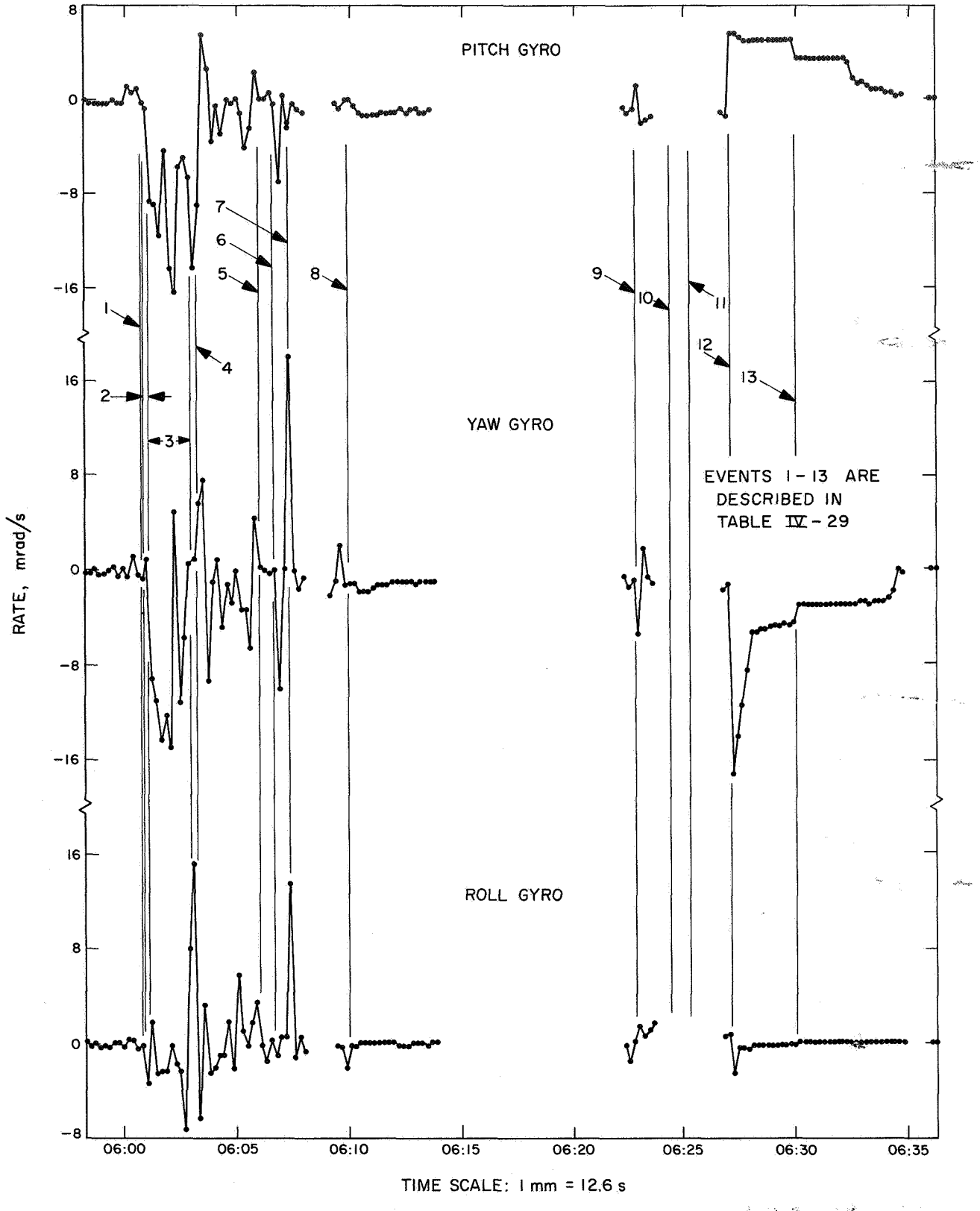



**Fig. IV-99. *Mariner V* gyro activity (launch through start of sun acquisition)**

Table IV-29. Launch events[a]

| No. | Event[b] | Time, GMT | Gyro activity |
|---|---|---|---|
| 1 | Launch | 06:01:00.176 | |
| 2 | *Atlas* roll maneuver | 06:01:02–06:01:15.2 | CCW roll maneuver |
| 3 | *Atlas* pitch maneuver | 06:01:15.2–06:03:08.6 | CCW pitch and yaw maneuver |
| 4 | BECO and booster separation | 06:03:09–12 | CCW pitch and yaw, CW roll transient |
| 5 | SECO | 06:05:57 | |
| 6 | VECO and shroud separation | 06:06:18–20 | CCW pitch and yaw transient |
| 7 | *Agena* first burn ignition | 06:07:22 | CW yaw and roll transient |
| 8 | *Agena* first burn cutoff | 06:09:45 | |
| 9 | *Agena* second burn ignition | 06:23:01.2 | CCW pitch and roll, CW yaw transient |
| 10 | Injection | 06:24:25.6 | No data |
| 11 | *Agena* second burn cutoff | 06:24:35.5 | No data |
| 12 | *Agena*/spacecraft separation: PAS, AC on | 06:27:16.2 | CW pitch, CCW yaw and roll transient, sun acquisition begins |
| 13 | SIT: solar panels deploy | 06:30:11.6 ± 4.9 | All rates decrease |

[a]Shown in Fig. IV-99.

[b]BECO = booster engine cutoff; SECO = sustainer engine cutoff; VECO = vernier engine cutoff; PAS = pyro arming switch; AC = attitude control; and SIT = separation initiated timer.

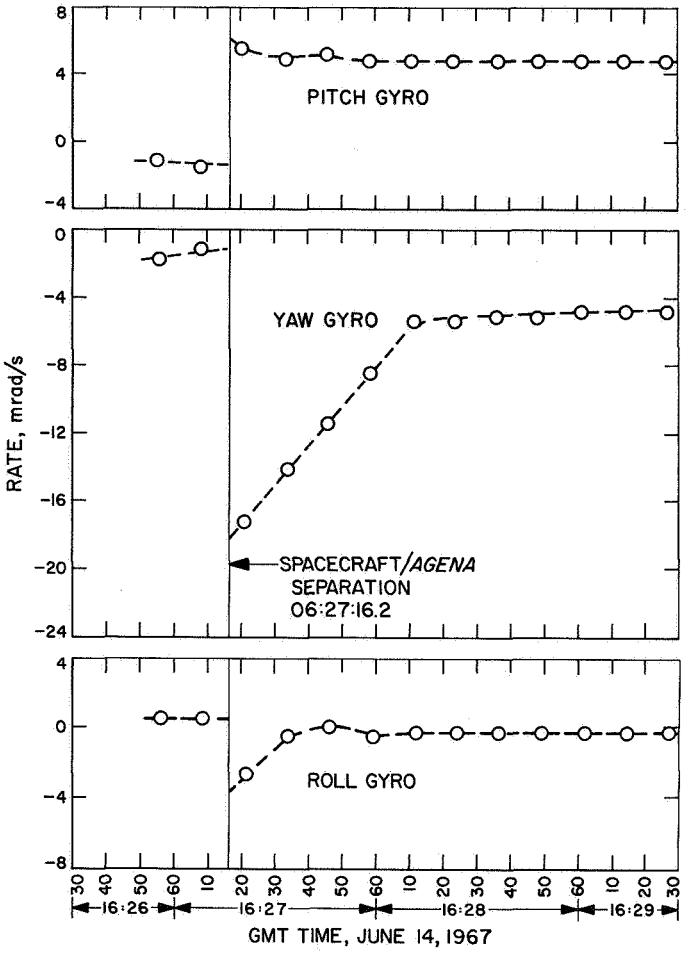



**Fig. IV-100. *Mariner V* spacecraft/*Agena* separation June 14, 1967**

shown centered about the sun for convenience, instead of about the spacecraft +Z axis.) The sun gate event occurred at 06:43:25.4 ± 4.9 GMT. Fortunately, the location of the false null was such that all points of a normal limit cycle within the deadband placed the sun in the sun gate field-of-view, so that the sun gate event, in removing the power to the secondary sun sensors, also removed the false null.

*Magnetometer calibration.* The sun gate event initiated the magnetometer calibration, in which the spacecraft, sun-acquired in the *X* and *Y* axes, spins CCW about the Z axis at a constant rate. The specified spin rate is −3.5 mrad/s, plus or minus the roll rate deadband of 0.37 mrad/s; it was expected that the actual rate would be near the upper edge of the deadband, i.e., between −3.5 and −3.87 mrad/s. The rate determined from the roll gyro telemetry was initially −3.45 ± 0.13 mrad/s, but within a few minutes, the telemetry settled at −3.72 ± 0.13 mrad/s.

An independent measure of roll rate was available from the earth sensor. The earth sensor would view the planet during each roll for an amount of time that was a function of the spacecraft roll rate, the brightness of the earth, and the relative earth–spacecraft motion. Once a model of the sensor response to the earth is defined, then the spacecraft roll rate can be determined very accurately.

Figure IV-102 is a plot of rate versus time for the magnetometer calibration period. The exponential increase in rate corresponds closely to the exponential decrease in the Bay VII temperature over this period. The change in rate is probably due more to temperature effects in the control electronics than in the GCA or in the gyros themselves, since a similar change at similar temperatures only changes a typical commanded turn rate by 0.001 mrad/s, approximately 0.03%.

During the roll spin, after the initial acquisition transient, the pitch and yaw axis motions were sinusoidal

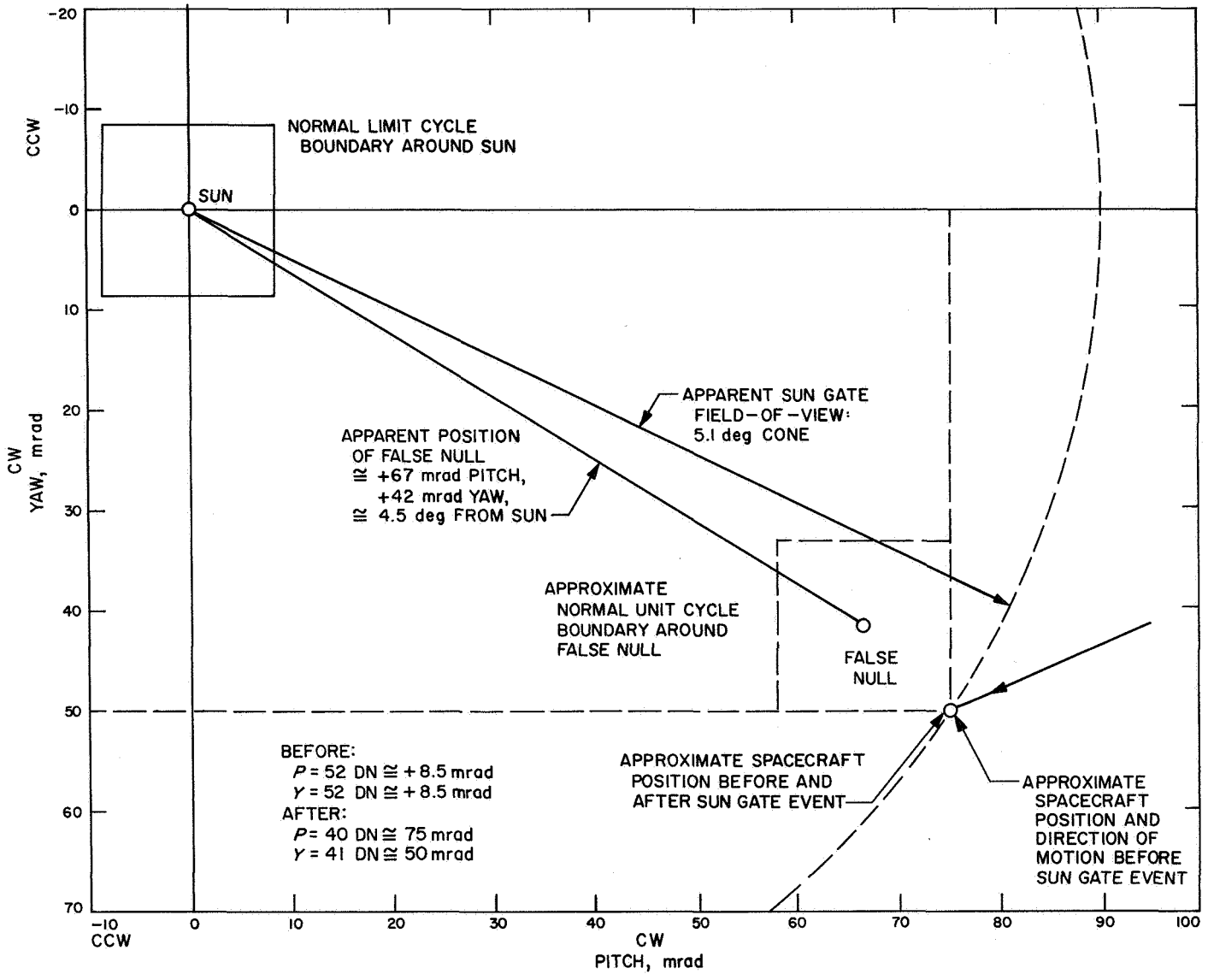



**Fig. IV-101. Geometry of false null at initial sun acquisition**

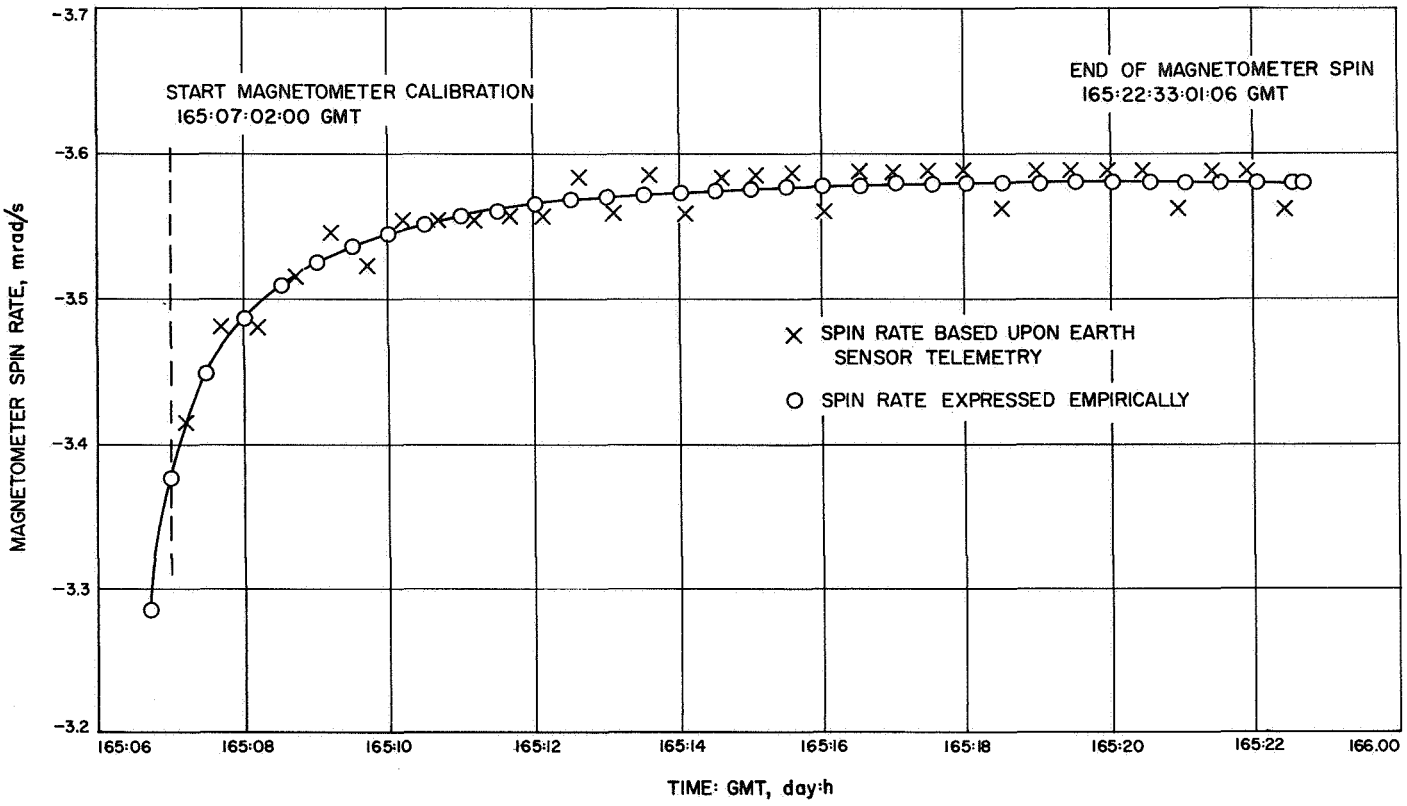



**Fig. IV-102. Spacecraft spin rate from earth sensor data**

with a period of about 35 min and an amplitude in pitch of +7.2 to −4.9 mrad and in yaw of −8.5 to 9.3 mrad.

*Canopus acquisition.* The CC&S event L-3 terminated the magnetometer calibration at 22:38:00.5 ± 0.7 GMT, after 33 revolutions. The Canopus sensor was turned on for the first time at a spacecraft clock angle of approximately 312 deg (as determined from the earth sensor output).

Figure IV-103 is the *a priori* star map for the time of the L-3 occurrence, showing both the *a priori* and the telemetered Canopus intensity. Although the cone angle of the earth at this time is about 110 deg and the cone angle field-of-view of the sensor is 74.5–85.5 deg, the earth is bright enough for the sensor to acquire on straylight.

The "earth" acquisition occurred at 22:46:30.6 ± 5.6 GMT, when the roll error signal from the Canopus sensor was switched into the roll control channel. Acquisition of the earth had been predicted, based on the *a priori* map, but the earth was brighter than expected. The model of the earth was not affected, however, and the decision was made to continue the roll search by sending two DC-V21 roll override commands, 4 min apart.

Two commands were necessary because the straylight model predicted two stable nulls, either of which would fulfill the acquisition logic and enable the sensor to assume roll position control of the spacecraft. The spacing between the commands would allow initiation of search from the first stable null by the first command, a short period of search followed by acquisition of the second stable null and subsequent initiation of search from the second stable null by the second command.

If the search lasted more than approximately 45 s, the second command would prevent the gyros from being turned off between commands. Accordingly, the first DC-V21 command was sent to the spacecraft and received in the data at 00:30:40.2 ± 4.9 GMT on June 15, 1967; the second command was received in the data at 00:34:39.6 ± 4.9 GMT. The second stable null was acquired at 00:31:30.8 ± 5.6 GMT when the roll error signal from the Canopus sensor was switched into the roll error channel, but the second command reinitiated the roll search, as planned.

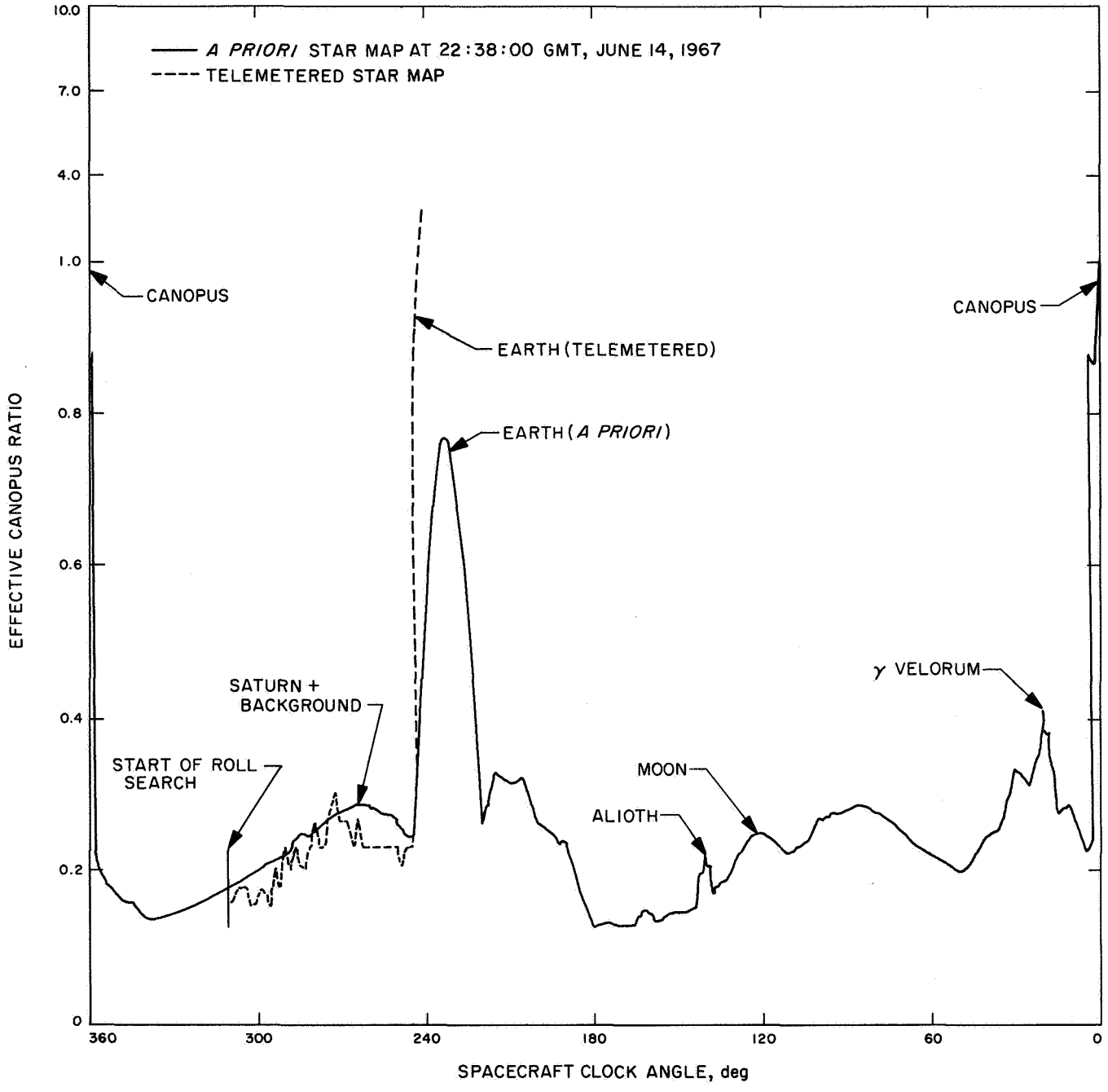



**Fig. IV-103. *A priori* and telemetered star maps (roll search start to earth acquisition)**

Figure IV-104 shows the *a priori* and telemetered star map for the period from earth deacquisition to Canopus acquisition. Based on the unexpected brightness of the earth, acquisition of straylight from the moon was predicted, and the moon was acquired at 00:46:57.6 ± 5.6 GMT when the roll error signal from the Canopus sensor was again switched into the roll control channel. However, the moon did not possess a stable null, and roll search was resumed at 00:49:14.8 GMT. Search continued until 01:09:12.6 ± 0.7 GMT, when Canopus was acquired. The spacecraft gyros turned off at 01:12:26.4 ± 6.2 GMT, 193.8±6.9 s after the sensor assumed roll position control of the spacecraft.

*Earth cruise.* Attitude control performance through the earth cruise phase of the mission was normal. Table IV-30

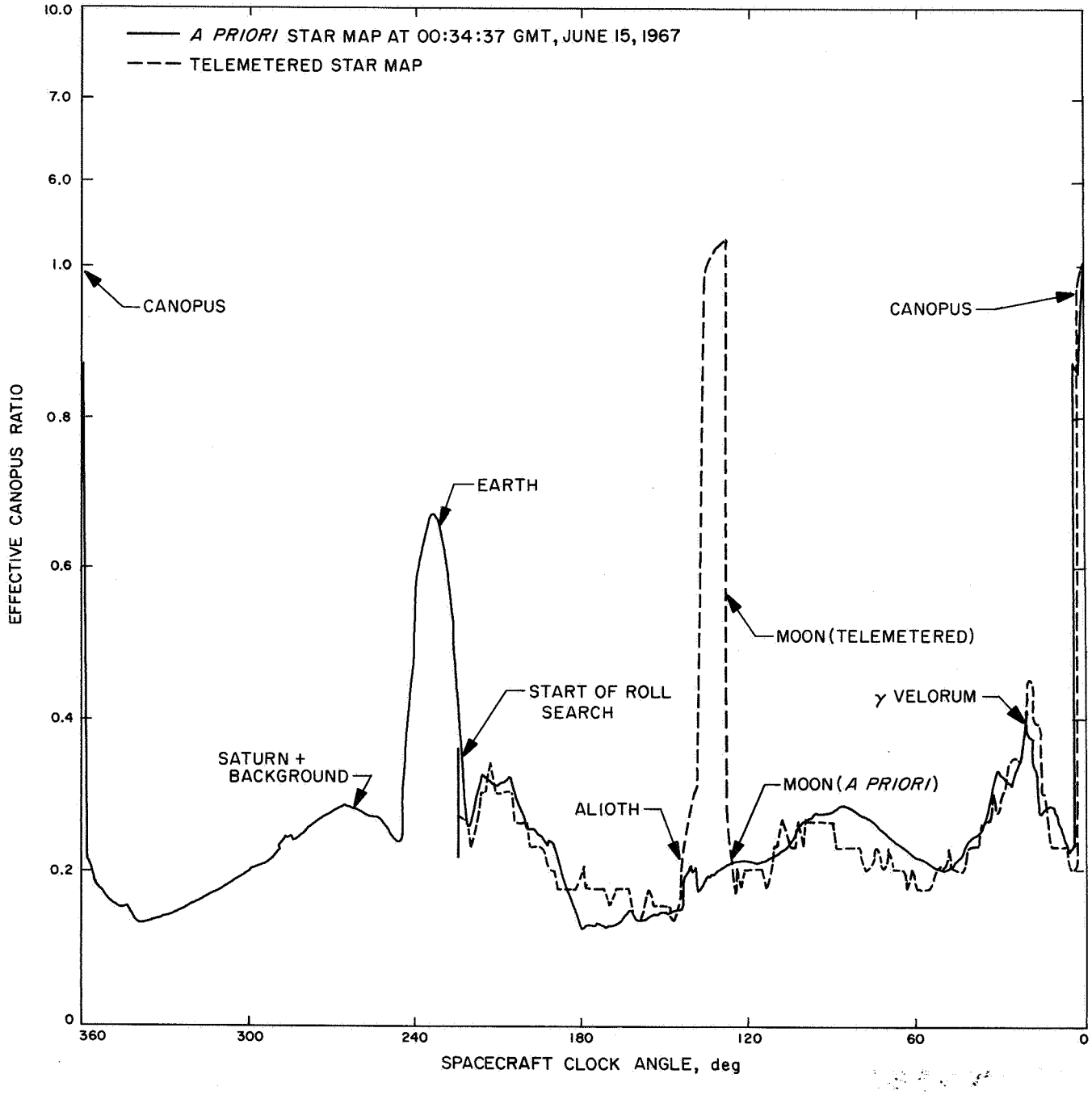



**Fig. IV-104. *A priori* and telemetered star maps (earth acquisition to Canopus acquisitions)**

**Table IV-30. Attitude control cruise operating parameters**

| Axis | Pitch | Yaw | Roll |
|---|---|---|---|
| Deadband, mrad | +7.6 ± 0.1 | +8.4 ± 0.05 | +6.3 ± 0.4 |
| Size, mrad | −7.9 ± 0.1 | −8.69 ± 0.16 | −3.0 ± 0.5 |
| Minimum rate, mrad/s | +17.8 ± 0.4 | +18.1 ± 0.4 | +18.0 ± 1.7 |
| Increment, mrad/s | −18.8 ± 0.7 | −18.4 ± 0.5 | −16.8 ± 1.5 |
| External torque, dyn-cm (typical) | −1 to 2 | −8.5 | — |

summarizes the operating parameters of the subsystem. Two roll transients were noted in the non-real time data analysis, but neither caused more than a momentary disturbance in the limit cycles.

Attitude control gas usage through the midcourse maneuver was negligible. Figure IV-105 shows the calculated $N_2$ gas weight in each half system. The transients at launch and midcourse maneuver were due primarily to thermal effects, as the temperature of the gas vessels reached equilibrium (the resolution of gas weight is 0.006 lb/DN in temperature, but a change in temperature may cause a change in the telemetered pressure DN and that resolution is 0.015 lb/DN).

*Midcourse maneuver.* The midcourse maneuver sequence was initiated on June 19, 1967 with the transmission of QC-V1-1, pitch turn duration, to the spacecraft. The commanded turn rates for the pitch and roll turns were predicted about one day in advance of the maneuver by obtaining an estimate from the thermal control analysts of the temperature of Bay VII at the start of the pitch turn. The average gyro case temperature during the turn was then calculated from Fig. IV-106, and finally the average turn rate during the pitch turn was obtained from Fig. IV-107. The effects of heating on Bay VII due to the post-pitch turn orientation were estimated by the thermal control analysis to be small, and so the roll turn rate was calculated in the same manner as the pitch turn rate.

These turn rates determined the quantitative commands (QC) for pitch and roll turn durations to achieve the desired turns. The opportunity existed to make a vernier correction to the engine burn duration QC to account for the effects of jet vane drag in the exhaust stream, but pre-maneuver autopilot simulations indicated this correction to be negligible.

After the reacquisition of Canopus terminated the maneuver sequence, three roll searches were performed to provide additional data to aid in the evaluation of the performance of the ultraviolet photometer. Table IV-31 summarizes the sequence of operations from the beginning of the midcourse maneuver sequence to the final reacquisition of Canopus.

*Post-maneuver analysis.* At the time of the maneuver, a preliminary indication that the velocity increment was smaller than desired was obtained from the doppler tracking data. Post-maneuver orbit determination determined that the velocity increment was indeed less than commanded by 4.56%, but that the commanded turns were quite accurate. Table IV-32 lists the significant maneuver parameters.

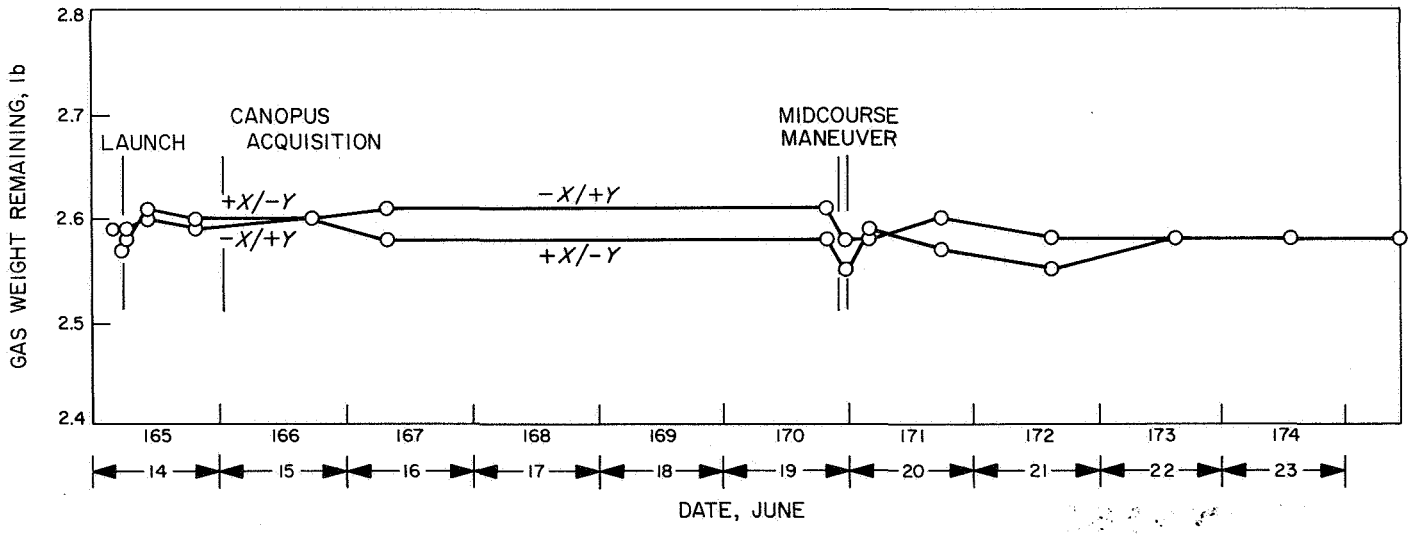



**Fig. IV-105. Attitude control gas weight from launch through midcourse**

## Table IV-31. Midcourse maneuver sequence

| Event | Spacecraft time, GMT | Description |
|---|---|---|
| QC-V1-1 received | 170:20:18:55.42 ± 6.3 | 304-s duration pitch turn command |
| QC-V1-2 received | 20:23:45.23 ± 6.3 | 380-s duration roll turn command |
| QC-V1-3 received | 20:28:37.64 ± 6.3 | 17.66-s duration motor burn command |
| DC-V29 received | 20:38:52.45 ± 6.3 | Arm first burn engine squibs command |
| DC-V14 received | 20.48:44.66 ± 6.3 | Remove maneuver inhibit command |
| DC-V27 received, CC&S M-1, gyros on, mode 1 data | 21:24:46.03 ± 0.42 | Initiate midcourse maneuver command |
| CC&S M-2, M-3, and M-4, pitch turn start | 22:24:10.87 ± 0.00 | Gyros to rate + position mode, start CW pitch turn |
| CC&S M-4 reset, stop pitch turn | 22:29:14.8 ± 0.42 | |
| CC&S M-5 and M-3, start roll turn | 22:46:10.8 ± 0.42 | Start CW roll turn |
| CC&S M-5 reset, stop roll turn | 22:52:31.1 ± 0.2 | |
| CC&S M-6, start motor burn | 23:08:11.3 ± 0.2 | |
| CC&S M-7, stop motor burn | 23:08:28.0 ± 1.6 | |
| CC&S M-1, M-2 reset, begin sun acquisition | 23:14:10.9 ± 0.3 | Gyros to rate mode |
| Sun gate event, initiate roll search | 23:21:24.2 ± 5.3 | Sun acquired |
| Canopus acquisition | 23:32:19.2 ± 5.7 | |
| DC-V21 No. 1 received | 23:34:06.4 ± 0.6 | Initiate first post-maneuver roll search |
| Canopus acquisition | 171:00:23:58.4 ± 5.7 | |
| DC-V21 No. 2 received | 00:25:52.4 ± 5.4 | Initiate second post-maneuver roll search |
| Canopus acquisition | 01:16:54.2 ± 5.7 | |
| DC-V21 No. 3 received | 01:18:35.1 ± 5.2 | Initiate third post-maneuver roll search |
| Canopus acquisition | 02:06:15.2 ± 5.7 | |
| Gyros off | 02:09:48.9 ± 5.2 | |

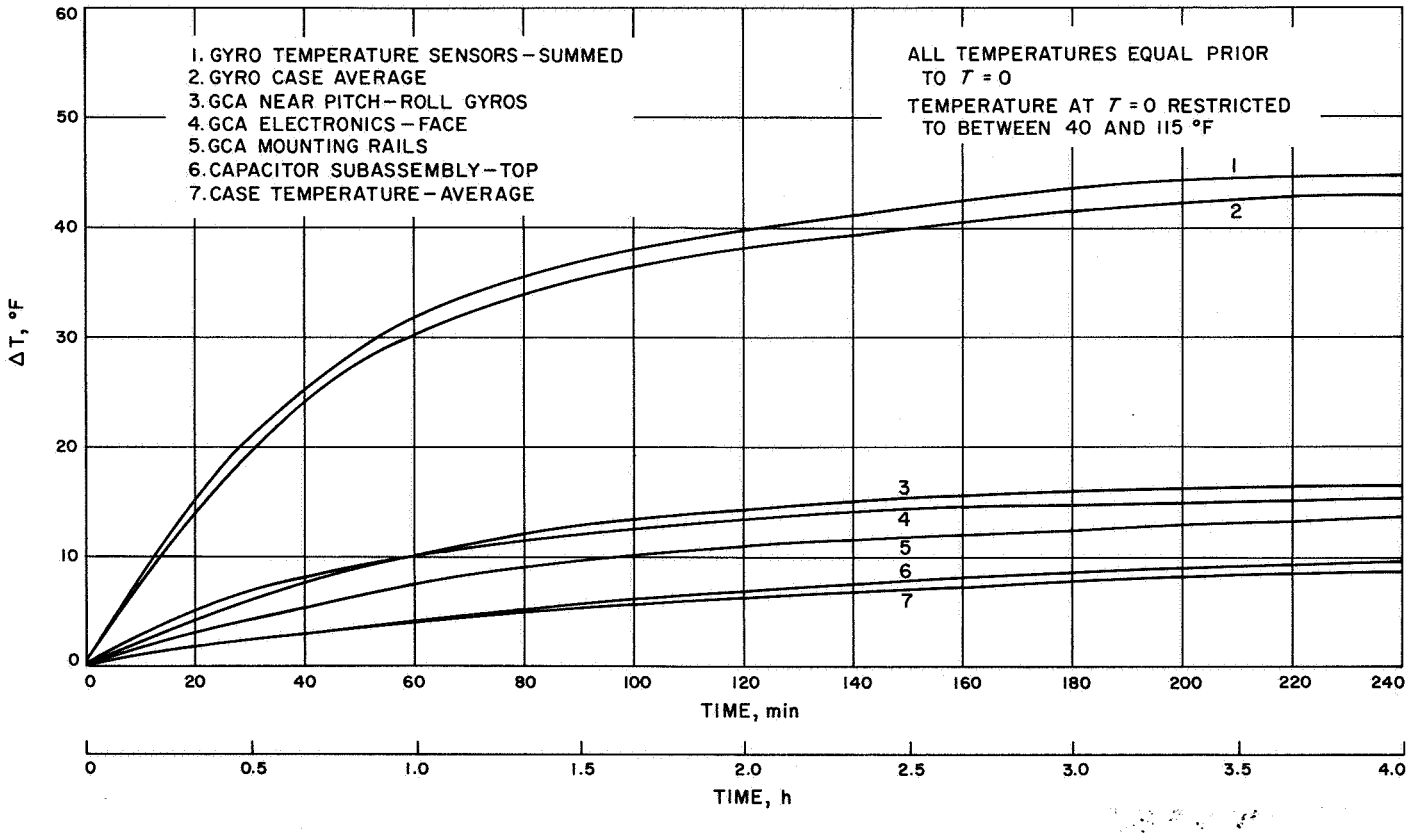



Fig. IV-106. "Best estimate" temperatures in vacuum after GCA turn-on

Table IV-32. Midcourse maneuver performance parameters

| Parameter | Required[a] | Commanded, deg | Achieved[a] | Standard deviation, $\sigma$ |
|---|---|---|---|---|
| Pitch turn (rate = 0.1818 deg/s) | 55.3503 | 55.267 | 55.18 | 0.2 |
| Roll turn (rate = 0.1867 deg/s) | 71.0248 | 70.946 | 70.93 | 0.04 |
| Motor burn | 16.127 m/s | — | 15.392 m/s | 6.0 |

[a]In deg except as noted.

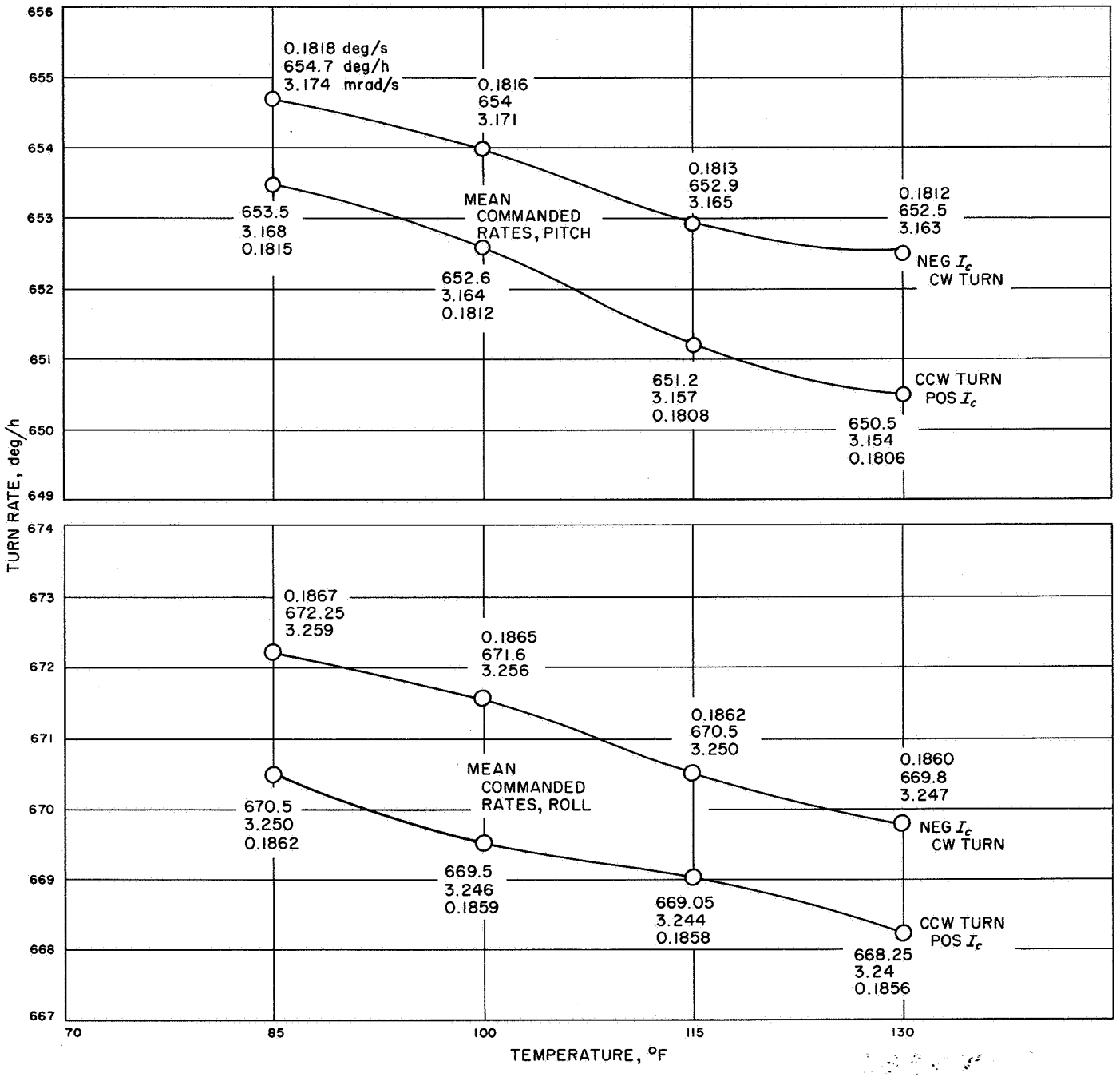



Fig. IV-107. *Mariner V* gyro commanded turn rates

An analysis effort was immediately started by the Propulsion and Guidance-and-Control groups to determine the cause of the degradation in velocity increment. It was obvious from the commanded turn results that the autopilot performed its task of maintaining the spacecraft attitude during the motor burn. The only interface that the autopilot had with the magnitude of the velocity increment, however, was the drag associated with the jet vanes. There was no direct telemetry on the vanes themselves, and the vane position must be calculated by a transformation from the inertially referenced system to the thrust vector system. Vane positions were not immediately obvious from the gyro telemetry outputs, and neither was autopilot performance.

During the midcourse, the observed gyro readings were small deviations from zero; a later attempt was made to fit the observed gyro telemetry to the known behavior of the control system, as described by a six-degree-of-freedom simulation. After an extensive attempt at such a fit, it was determined that this technique would need more effort and time than was currently available to produce viable results. An alternate technique (one that involved using steady-state analysis in a dynamic system) was to transform the gyro telemetry readings directly into jet vane positions.

The results of this analysis are summarized in Figs. IV-108 and IV-109. Figure IV-108 shows calculated jet vane positions as a function of time for the three gyro telemetry samples prior to motor ignition, the four samples obtained during the motor burn and the first two samples after shutoff. The drag force produced by the jet vanes is plotted in Fig. IV-109. The range of values shown at each discrete telemetry point is a consequence of the quantized nature of the telemetry. Another error is introduced because the gyros are operating in the rate-plus position mode and neither the instantaneous rate nor the position are obtained from the telemetry.

These figures are derived under the assumption that the instantaneous rate is zero. The lines connecting the discrete telemetry point range end values are also not necessarily representative of the dynamic situation; however, the conclusion drawn from this simplified analysis was that the degradation in velocity increment could have been caused by an unexpected jet vane force. As is evident from Fig. IV-109, the range of average drag forces and their associated velocity decrements brackets the observed value of 0.735 m/s, and the nominal value, 0.68 m/s, is very close to this value.

This crude analysis indicated that the autopilot could be oscillating. An immediate effort to determine the cause of the oscillation was begun, starting with an examination of the six-degree-of-freedom simulation. The simulation of the gyros, autopilot mixing resistor matrix, autopilot electronics, and the jet vane actuators was scrutinized, and transfer functions re-derived where necessary. Concurrently, propulsion system analysts were analyzing the energy and mass distribution of the exhaust plume to evaluate the possibility of plume impingement upon the spacecraft (specifically, on the solar panels), generating an unexpected external torque and, thereby, causing the observed autopilot performance. This analysis showed that the effect of plume impingement on the solar panels was to produce a torque about the spacecraft CG that was about 8% of the control torque available from the autopilot, but the worst-case and conservative factors in the analysis led to an estimated value of torque that was lower by an order of magnitude. This effect was, therefore, considered to be negligible.

The only area not amenable to immediate re-evaluation was the model of performance of the JVA in the exhaust of the motor. To validate the existing model or to develop a new one, several firings of a *Mariner* engine were scheduled, with the actuators mounted and instrumented. The first firing was designed to gather data on the stiction model of the actuator; four actuators were exercised through a preprogrammed series of deflections during the engine burn to gather data on their thermal shock and stiction characteristics during the 100-s burn. The second through sixth firings were conducted with the engine and actuators mounted in a newly designed six-degree-of-freedom test stand, developed expressly for this test program. This stand was able to measure forces and moments about three orthogonal axes to provide data on the interaction between the jet vanes in the exhaust stream.

The second firing disclosed that there was an unexpected force produced that was a function of the square of vane deflection angle. This force was along the axis of the vane being rotated, normal to the direction of thrust, and its magnitude, at the maximum vane deflection angle of 25 deg, was about 26% of the drag force produced by the vane. The third firing used the smaller *Ranger* jet vanes to determine if reduction in the size of the vanes would decrease the interaction effects, but the magnitude of the effect was approximately the same. The fourth firing used two modified vanes to determine if the side force was being developed on the vane thermal shield; the fifth firing used a single *Mariner* vane for the same reason. These two tests revealed that the side force

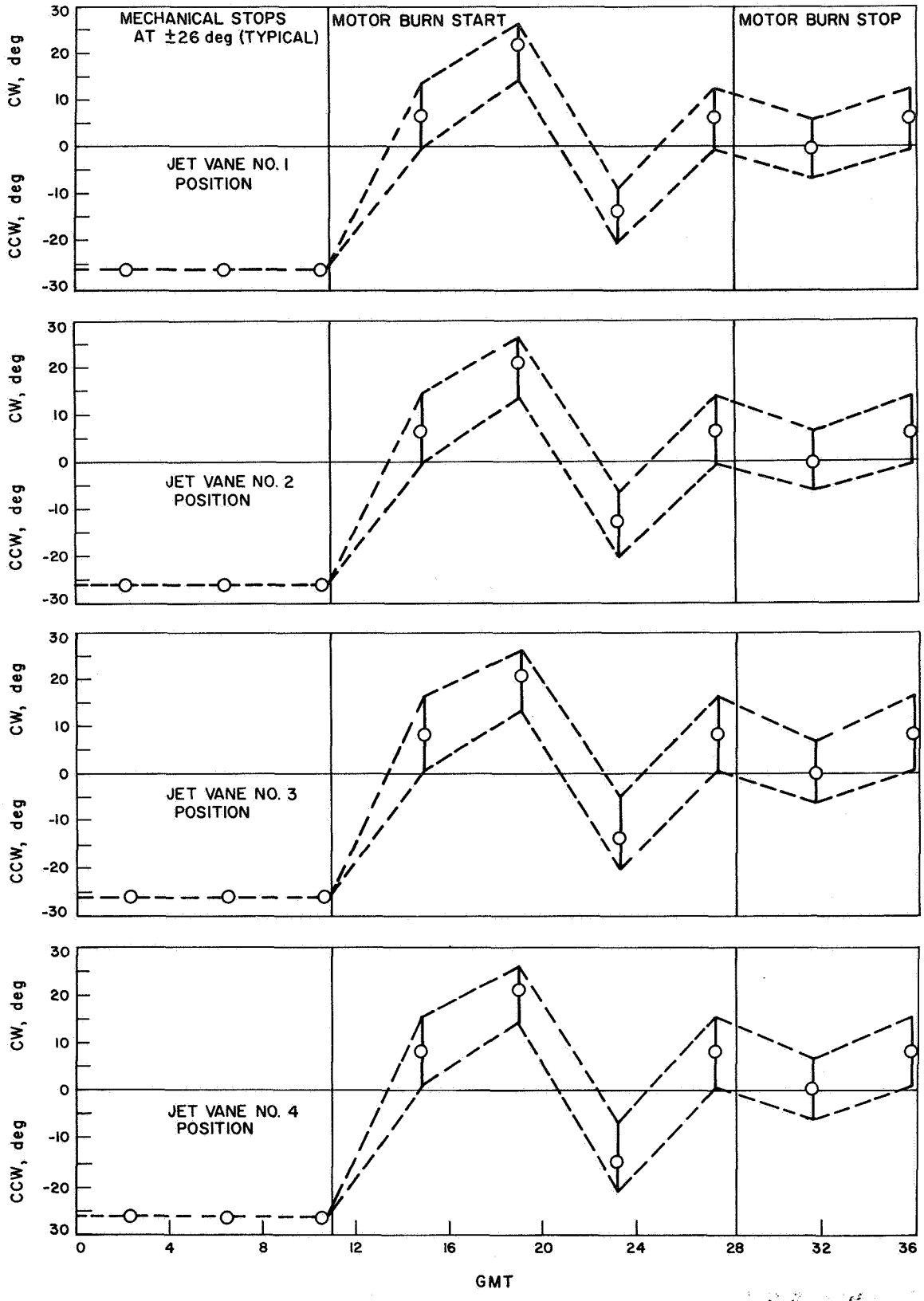



**Fig. IV-108. Jet vane positions vs time during midcourse maneuver number 1 (June 19, 1967)**

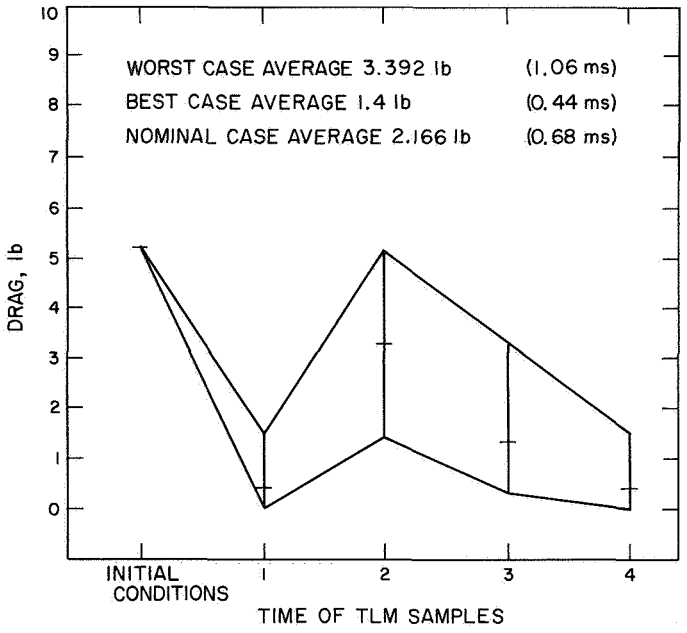



**Fig. IV-109. Jet vane drag**

was relatively independent of the vane thermal shield. The sixth and last firing used a larger support ring (the ring the actuators are mounted on); the test results showed the side force to be reduced to about one third of the previous values. The conclusion then drawn was that a redesign of the ring could minimize the side forces, but not eliminate them.

To summarize the status of the autopilot anomaly investigation, the simulation has been modified to include the jet vane interaction characteristics. Even with this change, however, the observed telemetry data cannot be exactly duplicated from the given initial conditions, and the performance of this particular *Mariner* autopilot under the in-space conditions of the midcourse maneuver is suspect. The obvious noncatastrophic failure modes (e.g., a failed resistor in the mixing matrix, a failed actuator feedback potentiometer, or an open actuator winding) have been investigated, but a complete solution describing the exact cause and effects of the anomaly has not been, and in all probability cannot be, formulated.

3. ***Power subsystem.*** The *Mariner* Mars 1964 spare power conditioning units and newly fabricated solar panels and batteries provided the flight and flight spare units of the power subsystem for *Mariner* Venus 67. The fact that the spacecraft was to fly toward rather than away from the sun caused the redesign and fabrication of new solar panels. Since new batteries would be required for the flight and flight spares, they were slightly redesigned to provide some improvement. The power conditioning required modification and fabrication of new main 2.4-kHz inverters because of increased power requirements and revised load switching sequences.

*a. Solar panel design and test.* The *Mariner V* solar array was designed to meet the raw electrical power requirements and environmental extremes that would be experienced during the mission to Venus. A basic ground rule associated with this design was that it would employ *Mariner IV* technology wherever possible. Functional requirements of the design of the solar array were that it provide a minimum of 360 W of power at a space solar intensity of 135 mW/cm$^2$ and 58°C, the voltage output from the array be limited to 50 V, the voltage at maximum power should be $44 \pm 2$ V, and the panel weight less than 15.7 lbs.

The *Mariner V* solar array consisted of four oriented solar panels, each having 10.9 ft$^2$ of area available for solar cell mounting. The cell layout on each solar panel consisted of a "folded" string (Figs. IV-110 and IV-111) that, after deployment, was maintained in a plane perpendicular to the Z-axis of the spacecraft. Each panel was divided for improved reliability into three isolated electrical sections of two "folded" strings of 105 cells in series and 14 cells in parallel. The cells used in the design were $1 \times 2$-cm P-on-N (P-N) silicon solar cells interconnected into seven cell submodules with gold-plated kovar bus bars. The output of each electrical section of the array was shunt regulated by a string of six zener diodes to limit the voltage output to less than 50 V. The electrical schematic of a typical electrical section is shown in Fig. IV-112. Basically, the electrical design was the same as that employed on *Mariner IV*. Similar materials, submodules, and techniques were incorporated wherever possible.

The cell layout and cable routing was designed to minimize the magnetic fields caused by solar-panel current flow and materials. The use of the folded electrical section concept minimized the magnetic field generated by the solar cell current through cancellation caused by positioning adjacent current paths flowing in opposite directions. In addition, all voltage strings terminated at the inboard edge of the panel, thereby greatly simplifying the cabling required. The longitudinal string orientation also reduces the possibility of the loss of a complete panel (three voltage strings) resulting from shroud damage during the shroud separation event. To provide good heat sinking and radiation to space, the zeners were mounted on the supporting spars of the array structure.

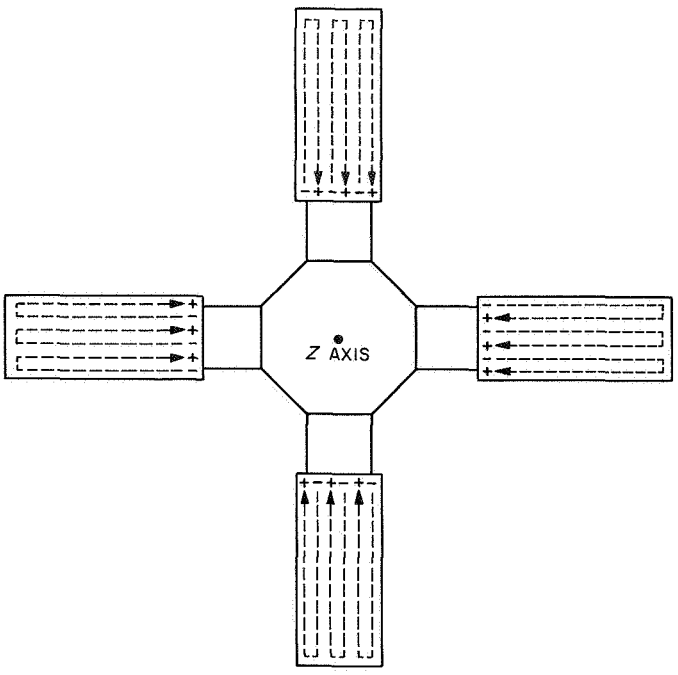



Fig. IV-110. Solar panel layout in relation to spacecraft

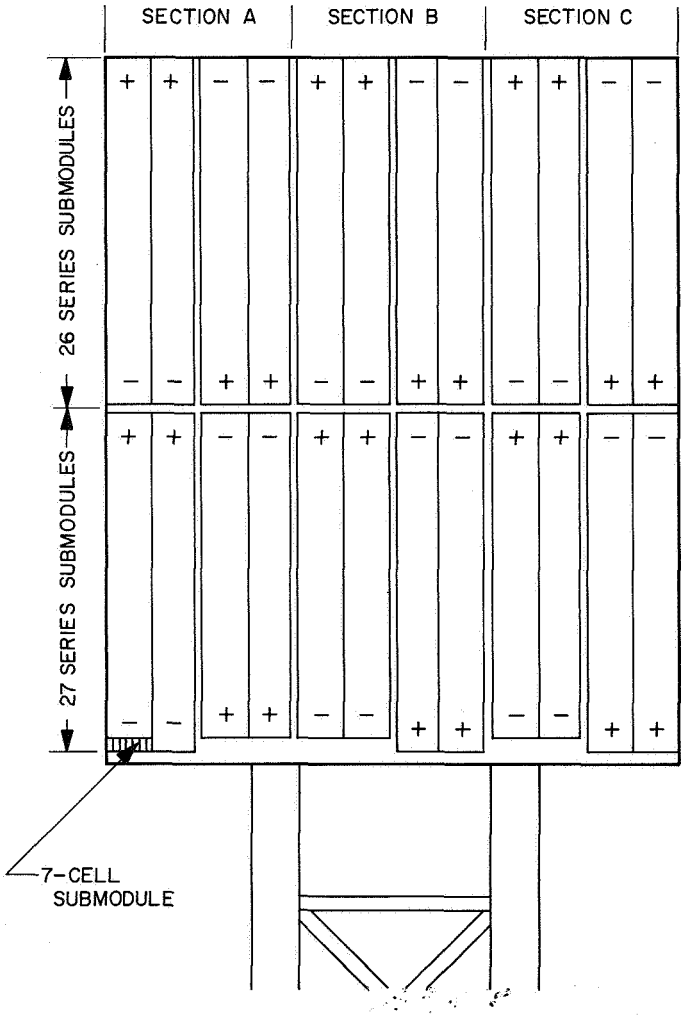



Fig. IV-111. "Folded" solar cell layout

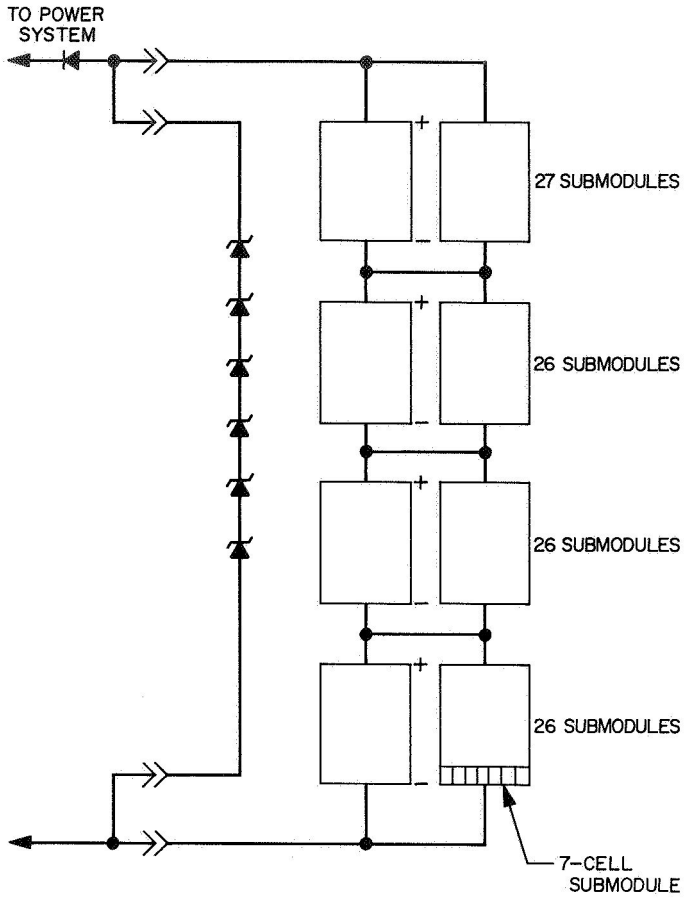



**Fig. IV-112. Schematic of typical electrical section**

Additional features of the *Mariner V* solar array included four transducers to aid in monitoring the array operating temperature and a short-circuit current and open-circuit voltage transducer (Figs. IV-113 and IV-114).

*Solar panel substrate design.* The *Mariner V* solar panel substrate (Figs. IV-113 and IV-114) consisted of a 4-mil aluminum skin reinforced with lateral 3-mil corrugations. The vertical elements of the corrugation and the spars were pierced with flanged lightening holes to minimize weight and to aid in heat radiation from the back side of the skin. The entire back surface of the panel was coated with a high emissivity gloss black paint. The cell surface of the substrate skin was covered with a 3-mil-thick epoxy-impregnated fiberglass to provide an electrically insulating layer upon which to mount the solar cells. The resulting solar panel substrate weighed approximately 9 lbs.

*Zener diode shunt regulator.* The flight configuration of the *Mariner V* solar array shunt regulator required six Zener diodes connected in series for each electrical section of a panel. The diodes were torqued to the under-

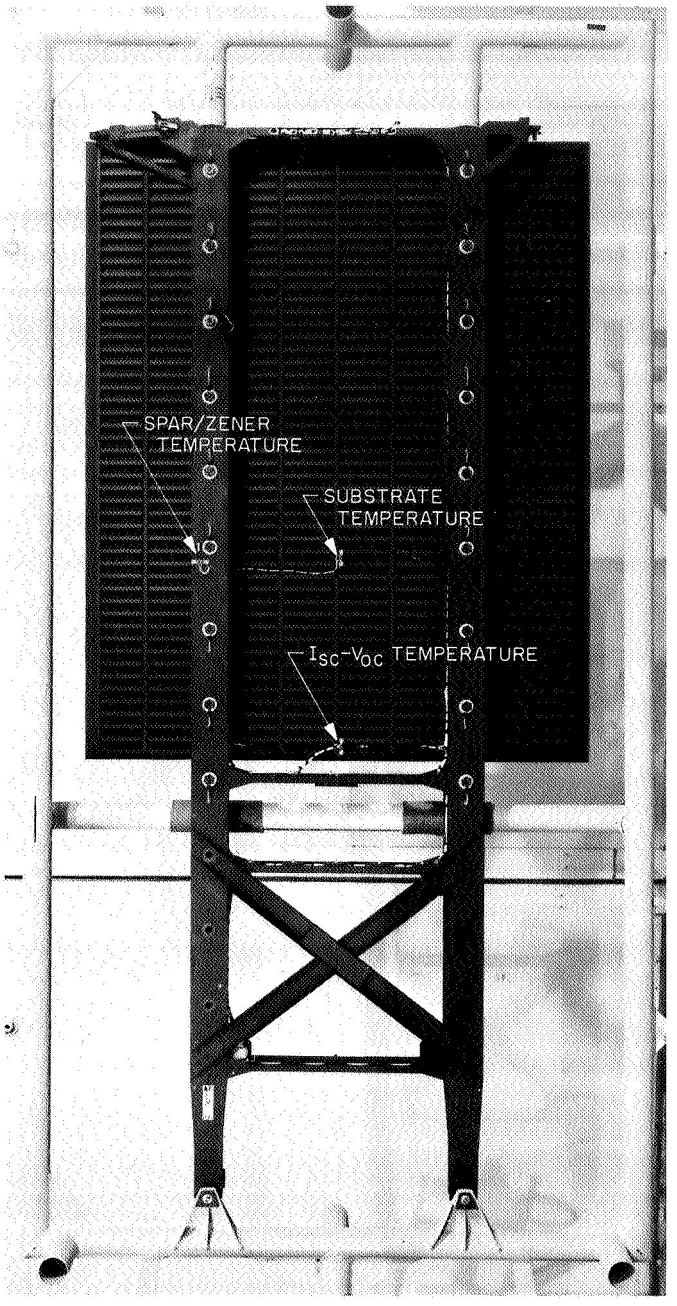



**Fig. IV-113. Solar panel rear surface**

side of the panel box-beam spars, which provide heat sink for controlling diode temperature in excess of the anticipated worst-case power dissipation of 10.5 W per diode. The diodes were electrically insulated from the spars with 6-mil mica washers and, after installation, were coated with nonconductive black paint to improve their surface emissivity.

*Solar cell assembly.* Boron-diffused silicon solar cells were employed in the *Mariner V* array fabrication. Most

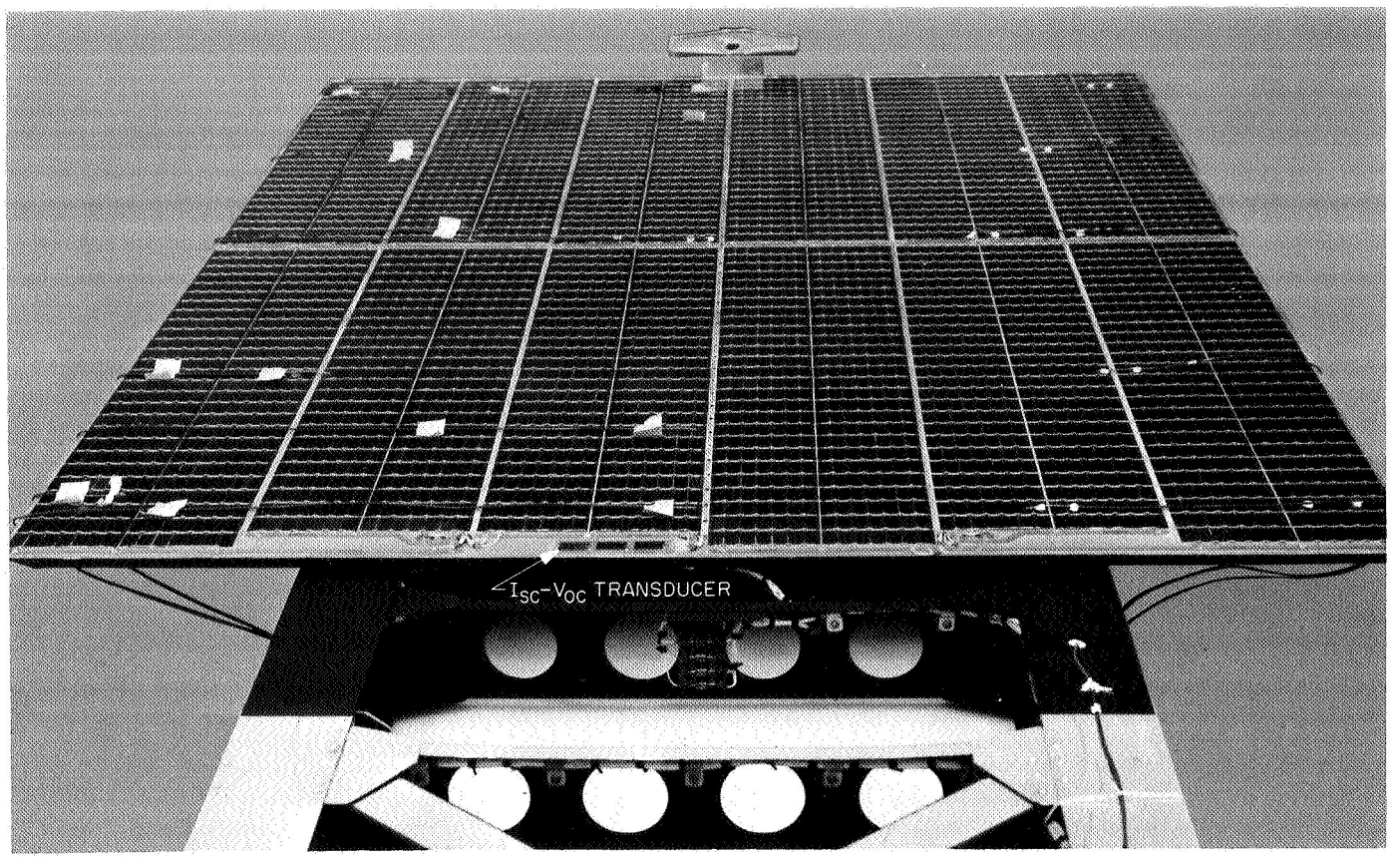



**Fig. IV-114. Solar panel front surface**

of these cells were procured during the *Mariner* Mars 1964 program; some additional cells were required for *Mariner V*.

Figure IV-115 is a plot of the *Mariner V* mean solar cell characteristics prior to and after filtering and assembly. These data are reduced to 100 mW/cm² tungsten data and are intended to show power loss due to assembly.

*Solar cell submodule.* The solar cell submodule was the smallest subassembly of the solar array and consisted of solar cells, filter covers, filter adhesive, and bus bars. The *Mariner V* submodule (Fig. IV-116) was designed such that all soldering connections could be made directly to the cells before assembly of the submodule to the panel. This design was employed on *Mariner IV*. The individual solar cells were electrically interconnected on the P side with a 20-mil wire, and on the N side with a 3-mil-thick ribbon, each of which was gold-plated kovar. (Kovar is employed because of its similar thermal coefficient to the silicon solar cell.)

Each solar cell was covered with a glass filter to protect it from space low-energy radiation and to aid in temperature control of the cells during flight. The filter covers were fabricated from a 6-mil-thick microsheet substrate with a 0.410-$\mu$m cutoff filter vacuum-deposited on one surface.

*Solar array temperature monitoring.* Four temperature transducers were employed to aid in the evaluation of the space performance of the solar array. The temperature transducer selected for use was a small resistive element encased in a thin electrically insulating Mylar jacket, approximately 2-mil thick. The transducer exhibited a relatively linear resistance versus temperature range from plus to minus 300°F.

Three transducers are actually bonded to each panel, one in the center of the panel, one under the $I_{sc}$-$V_{oc}$ transducers, and one on the spar of the structure close to a Zener diode (Figs. IV-113 and IV-117). In flight, only a total of four temperature transducers are monitored.

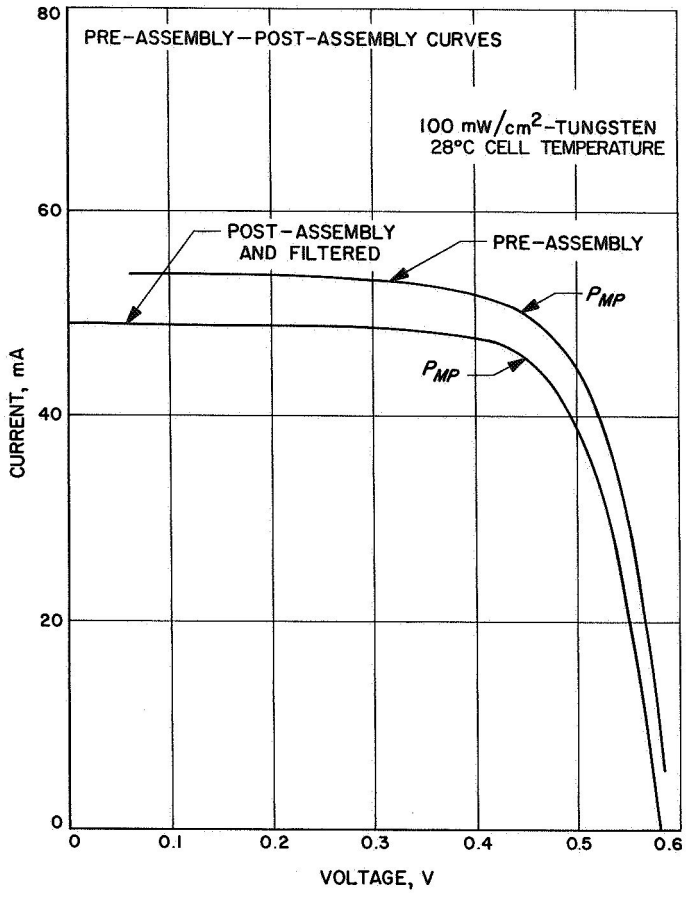



**Fig. IV-115. Average individual solar cell current-voltage curve**

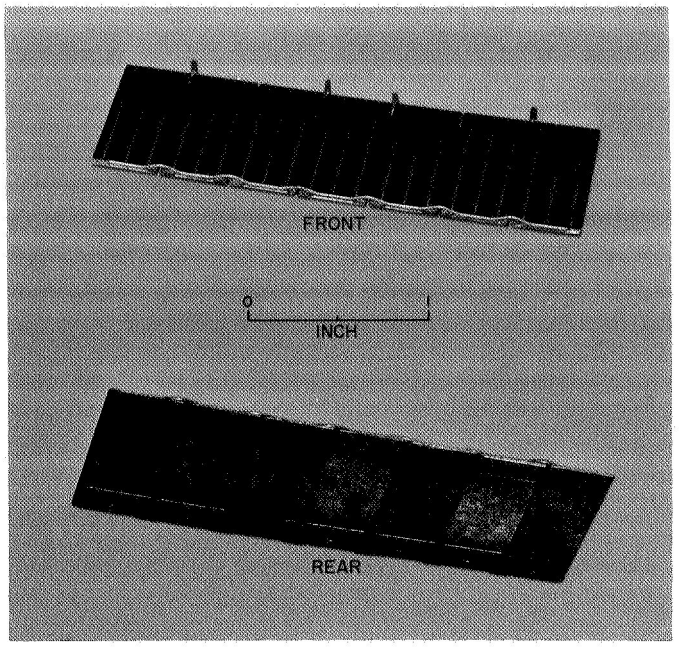



**Fig. IV-116. Typical solar cell submodule**

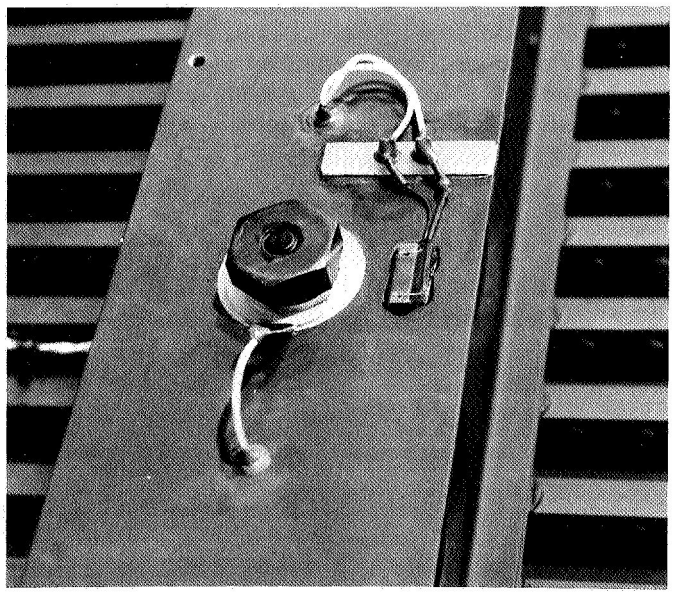


**Fig. IV-117. Typical temperature transducer installation**

There are two other temperature-dependent outputs that can be used in evaluating the thermal equilibrium characteristics of the array: the open-circuit voltage cell of the $I_{sc}$-$V_{oc}$ transducer, and the operating points of the solar array when the array is not limited by the Zener diode shunts. These outputs, when compared to the pre-flight calibrated $V_{oc}$ cell and V-I characteristics of the array, help to give a relative setting to the space array temperature.

*Solar array assembly.* The submodules were bonded to the front surface of the panel with a silicon adhesive, and interconnected in three sections. The three electrical sections per panel represented a total of 1470 solar cells per section, and 4410 cells per panel.

To minimize the requirement for feedthrough holes in the panel and to reduce mechanical stress associated with the attachment of the harness cable directly to the submodules, a conformal-coated printed-circuit board concept was developed. The circuit boards provided all the inter-submodule redundant wiring required and were bonded to the front surface of the substrate.

*Environmental qualification testing.* All solar panels to be designated as flight hardware had to successfully complete a vibration and thermal-vacuum FA test program. Evaluation of the effects of the test on a solar panel was

through a comparison of the normalized electrical performance characteristics made in sunlight before and after each test, and by 10× microscopic inspection of all the panel assemblies and solder connections.

The TA solar panel successfully passed the TA vibration and acoustic tests; however, during the thermal-vacuum test, a loss of electrical power to the solar simulator occurred. At this time, the panel had been subjected to thermal shocks simulating midcourse maneuver at two sun–spacecraft distances less than L + 30 days, and was being exposed to a 100-h soak at 280°F. The failure of the light source power occurred after 85 h of the high-temperature soak. This failure caused a severe thermal shock to be induced into the panel. An electrical and mechanical inspection of the panel after removal from the chamber revealed that 16% of the solar cells showed P contact delamination and that the electrical power output capability of this panel had decreased approximately 27%.

An extensive testing program was conducted to provide additional information to evaluate the mechanism and mode of failure. The resulting data indicated that the TA panel would have successfully survived the thermal-vacuum tests with probably no broken cell contact if the power to the solar simulator had not failed. A thermal shock of the type that the TA panel was exposed to would not normally occur in flight. Subsequent real-time life test of two 1-ft² solar panels in a thermal-vacuum environment profiled to look like the anticipated *Mariner V* mission to encounter plus 30 days showed no failures or design inadequacies.

The spacecraft vibration test was used to certify the mechanical integrity of each solar panel because it was not possible to vibration test individual panels with confidence. No difficulties or abnormalities were encountered in employing this process.

*Predicted array thermal characteristics.* The solar panel design of *Mariner V* is very similar in construction and materials to that of *Mariner IV*. Therefore, it was believed that the preflight and flight temperature data and analysis of *Mariner IV* would be, in most cases, directly applicable. Because of the spacing between the inboard edge of the substrate and the spacecraft bus, it was also believed that the lengthwise temperature gradient due to bus–substrate interaction would be negligible. Figures IV-118 to IV-121 are the predicted flight temperature conditions of the array.

*Mariner IV* flight data generally supported the fact that this array could be nominally described as following a simple flat-plate thermal analysis, where the area of the

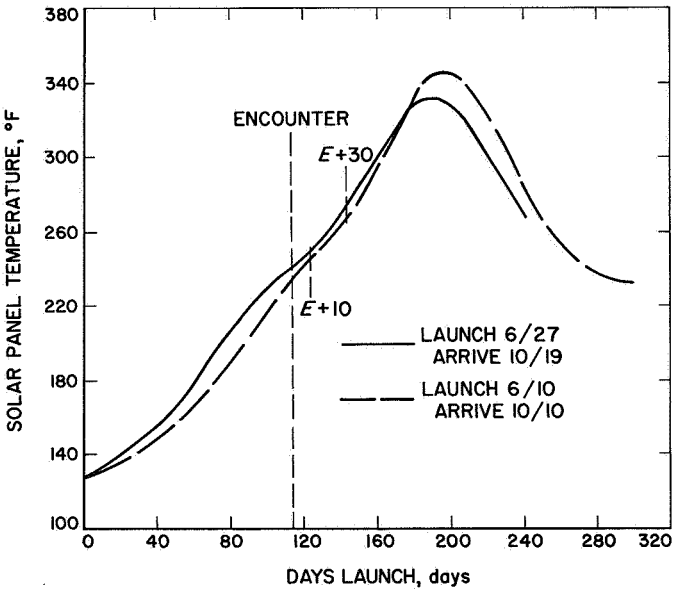



**Fig. IV-118. Predicted solar panel temperature during Venus mission**

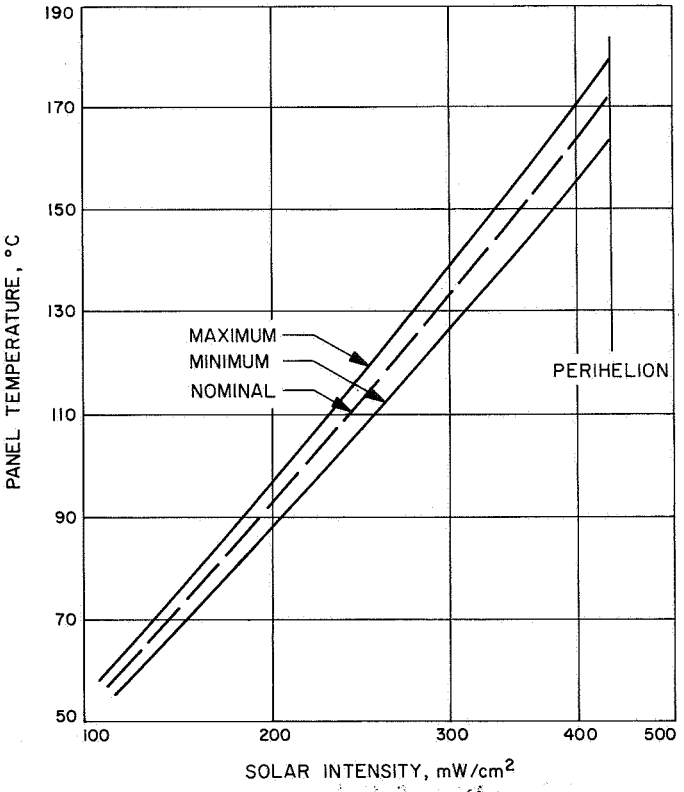



**Fig. IV-119. Predicted solar panel thermal characteristics**

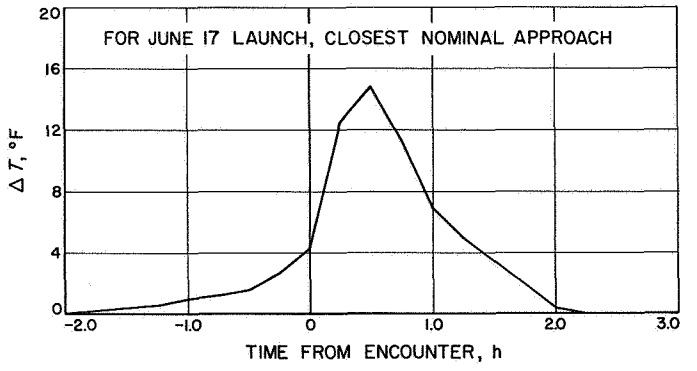



**Fig. IV-120. Predicted solar panel temperature rise induced by Venus**

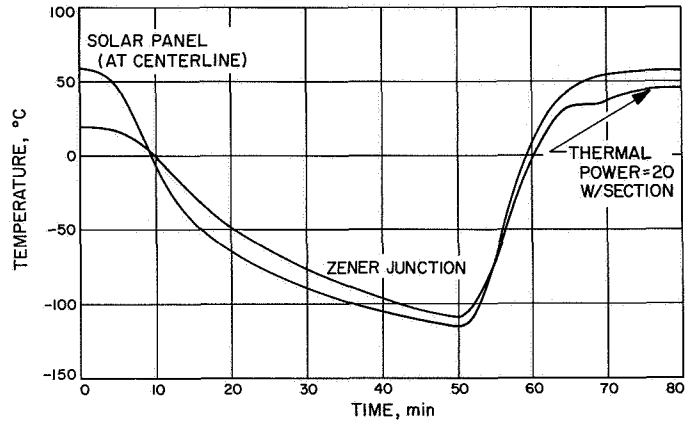



**Fig. IV-121. Predicted midcourse maneuver temperature history**

front surface of the panel effectively equals the area of the rear.

$$T = \left[\frac{H\alpha - P}{\sigma(E_f + E_r)}\right]^{1/4}$$

where

$T$ = temperature in °K

$H$ = normal solar intensity

$P$ = solar energy converted to electrical energy

$\sigma$ = Boltzmann's constant

$\alpha$ = hemispherical absorptivity of panel front

$E_f$ = hemispherical emissivity of panel front

$E_r$ = hemispherical emissivity of panel rear

Based on *Mariner IV* experience $\alpha$ is assumed to be 0.83, $E_f = 0.79$, and $E_r = 0.90$.

*Electrical performance testing.* The panels were oriented normal to sunlight, and the current-voltage characteristics of each of the electrical sections was measured in the ambient temperature–humidity environment. The relative space intensity of the sunlight at the time of testing was monitored by a balloon-flight standardized calibrated solar cell, which had similar spectral response characteristics to the solar cells on the panel. The temperature of the panels was determined from the open-circuit voltage output normalized to some nominal intensity and compared to calibration curves relating voltage and temperature. The equation employed to reduce solar panel data to space conditions is:

$$I_2 = I_1 + I_{sc_1}\left(\frac{L_2}{L_1} - 1\right) + \alpha(T_2 - T_1)$$

$$V_2 = V_1 - \beta(T_2 - T_1) - \Delta I_{sc} R_s - K(I_2 - T_1) I_2$$

$$\Delta I = \Delta I_{sc} = I_{sc_1}\left(\frac{L_2}{L_1} - 1\right) + \alpha(T_2 - T_1)$$

$$P_2 = I_2 V_2$$

where:

$$\alpha \equiv \left.\frac{dI_{sc}}{dT}\right| \text{ intensity constant}$$

$$\beta \equiv \left.\frac{dV_{oc}}{dT}\right| \text{ intensity constant}$$

$I_1$ = reference current coordinate

$V_1$ = reference voltage coordinate

$I_{sc_1}$ = short-circuit current of the reference data

$I_2$ = extrapolated current coordinate

$V_2$ = extrapolated voltage coordinate

$L_1$ = reference incident solar intensity

$L_2$ = equivalent solar intensity to be investigated

$T_1$ = reference cell temperature

$T_2$ = cell temperature to be investigated

$R_s$ = panel effective series resistance

$K$ = series resistance correction function for temperature

$\alpha$ = short-circuit current temperature coefficient

$\beta$ = open-circuit voltage temperature coefficient

Table IV-33. Solar panel electrical performance summary[a]

| Panel | Section | Power (Maximum power point), W | Voltage (Maximum power point), V | Short-circuit current, A | Open-circuit voltage, V |
|---|---|---|---|---|---|
| 003 (spare) | A | 32.59 | 43.74 | 0.833 | 56.73 |
| | B | 33.31 | 45.26 | 0.832 | 56.73 |
| | C | 33.42 | 43.88 | 0.849 | 56.64 |
| 004 (spare) | A | 34.00 | 44.84 | 0.857 | 56.69 |
| | B | 33.80 | 44.51 | 0.851 | 56.69 |
| | C | 33.56 | 44.96 | 0.847 | 56.68 |
| 005 (4A5) | A | 34.02 | 44.73 | 0.844 | 56.69 |
| | B | 33.90 | 45.03 | 0.848 | 56.69 |
| | C | 34.01 | 45.42 | 0.850 | 56.69 |
| 006 (4A7) | A | 33.55 | 44.16 | 0.841 | 56.67 |
| | B | 33.67 | 44.84 | 0.843 | 56.69 |
| | C | 34.00 | 44.42 | 0.848 | 56.69 |
| 007 (4A1) | A | 34.09 | 44.56 | 0.852 | 56.69 |
| | B | 34.17 | 45.29 | 0.854 | 56.69 |
| | C | 34.05 | 44.93 | 0.854 | 56.67 |
| 008 (4A3) | A | 34.04 | 45.22 | 0.845 | 56.69 |
| | B | 34.12 | 45.73 | 0.849 | 56.69 |
| | C | 34.16 | 44.42 | 0.850 | 56.69 |

[a]Data reduced to 135 mW/cm² and 58°C.

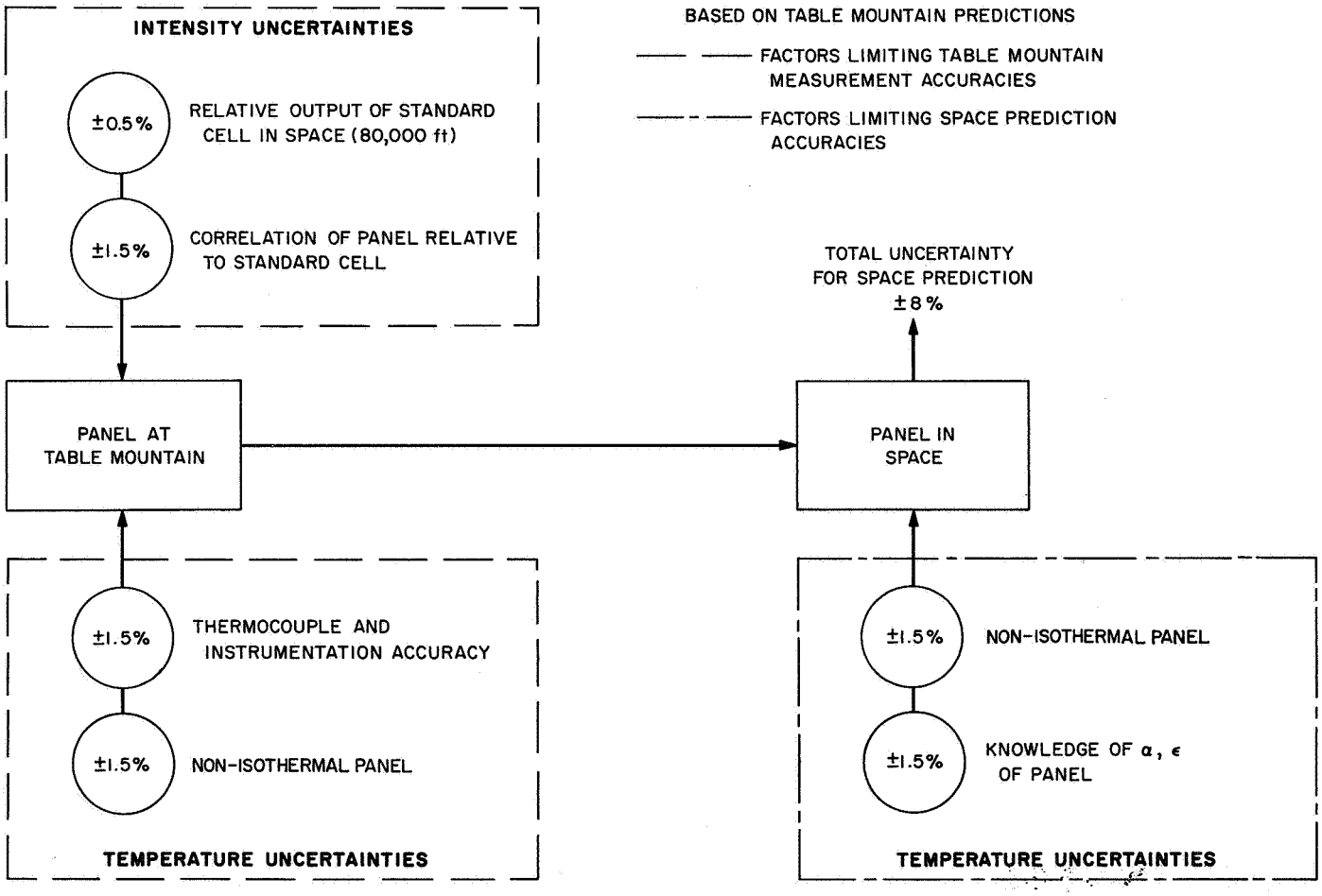



Fig. IV-122. Prediction capability for a solar panel in space at some heliocentric distance

A summary of the electrical performance of the six flight panels is presented in Table IV-33. The data indicate that the panels, particularly the four flight panels, are relatively uniform. The uncertainty in predicting the performance characteristics of a solar panel in space is assumed to be 8%. The causes of this uncertainty are displayed graphically in Fig. IV-122 and are primarily associated with measuring and predicting solar panel temperature.

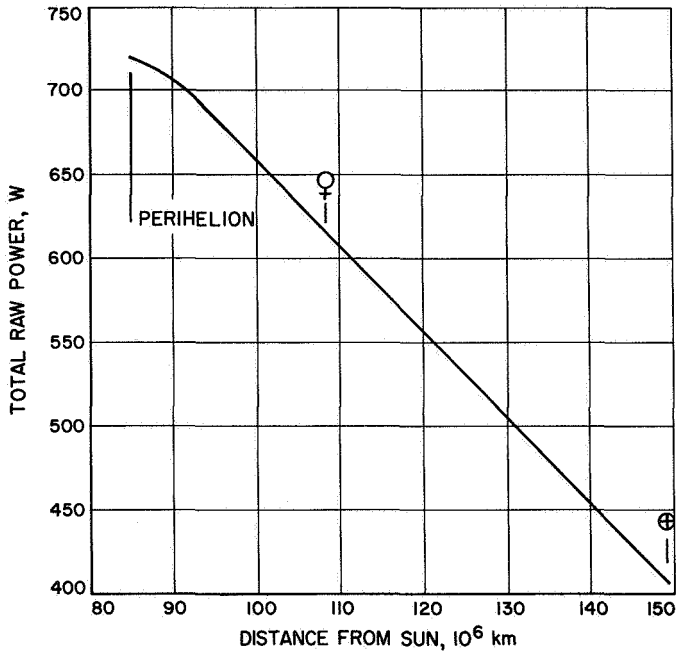



**Fig. IV-123. Total undegraded, spacecraft solar panel, peak raw power vs heliocentric distance**

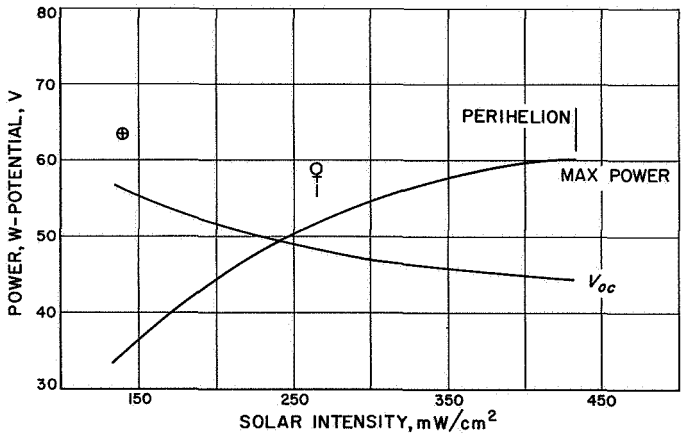



**Fig. IV-124. Variation of panel section performance with intensity**

*Electrical performance characteristics.* The predicted preflight electrical characteristics of the array are shown in Figs. IV-123 to IV-125. It was calculated that incident solar intensity at the time of launch would be 135 mW/cm$^2$, and that the resulting temperature, based on *Mariner IV* data, would be 56°C. From preflight measurements, it was determined that an undegraded *Mariner V* solar array should have a power temperature correction factor of approximately 0.32%/°C. Curves of an undegraded *Mariner V* array showing maximum power output and voltage at maximum power as a function of heliocentric distance are presented in Figs. IV-123 to IV-125.

Prior to launch, a last electrical check of the solar array was made at the AFETR. A raw data curve of the solar panels obtained from these measurements is shown in Fig. IV-126. The data were normalized to space sunlight conditions, and the output capability was compared to

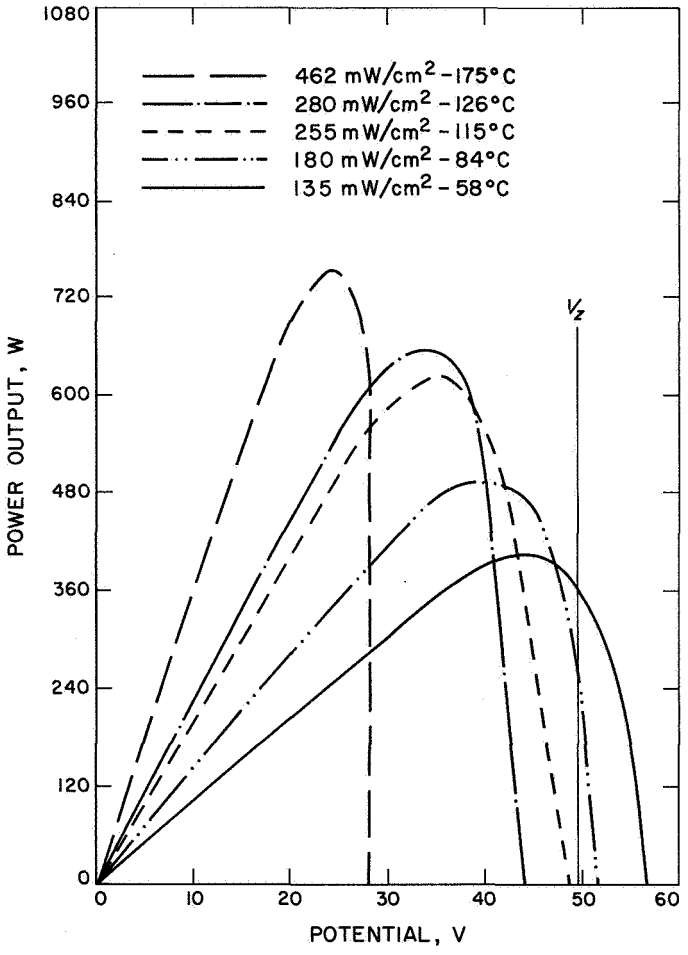



**Fig. IV-125. Total panel power vs voltage for various conditions**

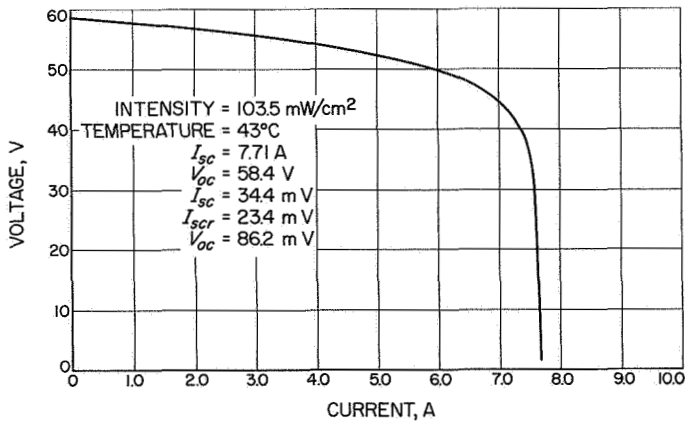



**Fig. IV-126. Raw data curve of solar panels (connected parallel)**

reduced data of the solar panels when last measured at Table Mountain. Figure IV-127 shows agreement to within 2%.

*Launch through midcourse performance summary.* The *Mariner V* solar array appeared to perform well. There were, however, three parameters that initially appeared to be performing at values other than those predicted. The solar panel temperature was approximately 7 deg lower than predicted and the short-circuit current and radiation resistant short-circuit current cells of the $I_{sc}$-$V_{oc}$ transducer were producing approximately 4% more output than predicted. The temperature offset apparently was due to the additional power being dissipated in the Zener diodes. The diodes were effectively loading the panel at near the panel's maximum power point. This loading would mean that the solar array was converting solar energy to electrical energy at better than 9 W/ft². The difference of 6 W/ft² plus the poor thermal path that the additional power dissipated in the diodes would have in providing heat back to the panel region around the temperature transducer would probably well account for most of the offset.

The $I_{sc}$-$V_{oc}$ transducer difference from nominal was traceable to the calibration technique used to standardize the cells. The technique used to perform the standardization required that different load resistors be used on the balloon flight and on the spacecraft. The sizes of these resistors were relatively small, 1.00 and 0.715 Ω, respectively, so that small variations in these resistors plus handling and interconnection techniques could well account for variation.

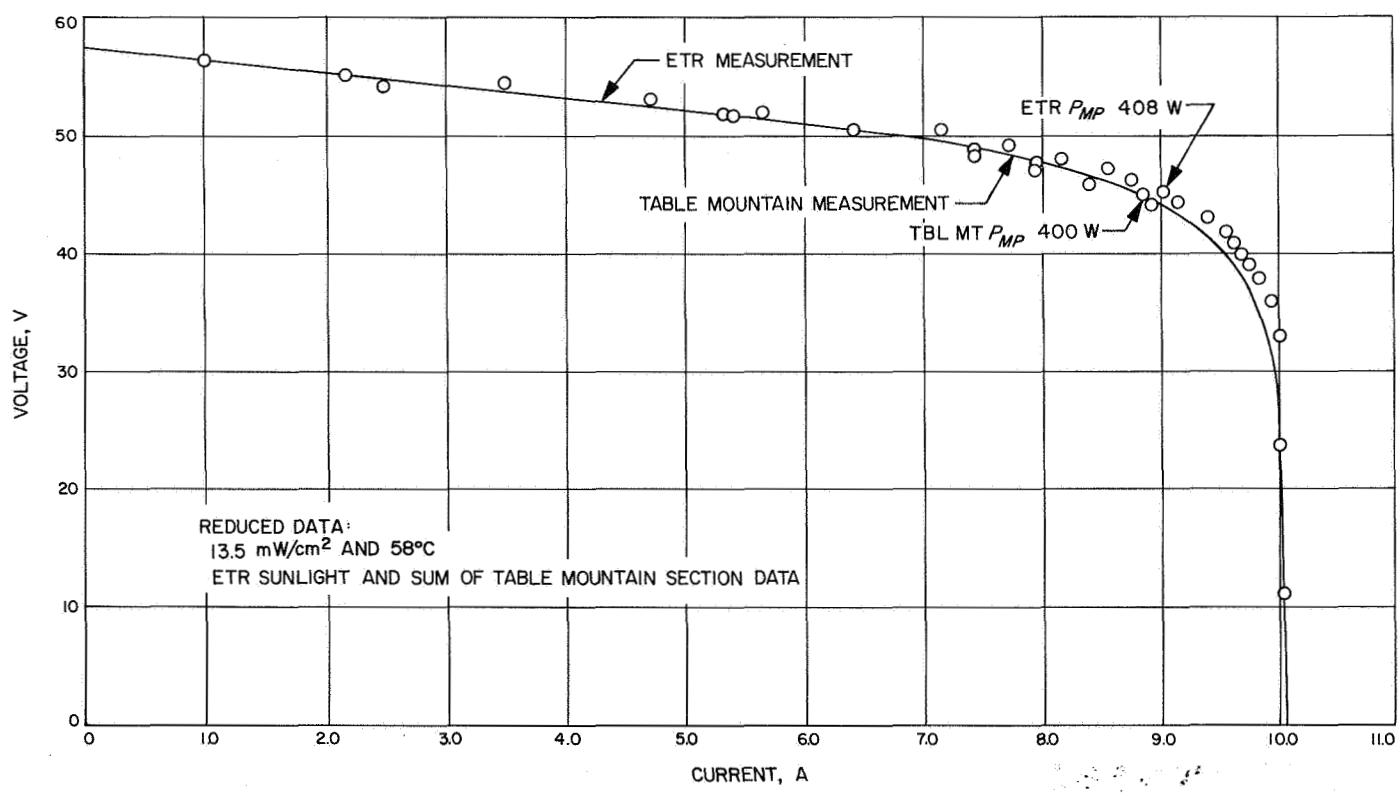



**Fig. IV-127. Solar array V-I curve, reduced data**

The relative effect of the 7°C lower temperature on the power output capability of the solar panel is shown in Fig. IV-128. Table IV-34 indicates the solar array performance to date.

*b. Power conditioning equipment modification and test.* The basis for the *Mariner V* power conditioning equipment (PCE) was the *Mariner IV* equipment. Spare *Mariner IV* hardware was modified to perform the *Mariner* Venus 67 mission. To appreciate the design changes required, the *Mariner IV* PCE configuration will be described and compared with the *Mariner V* PCE.

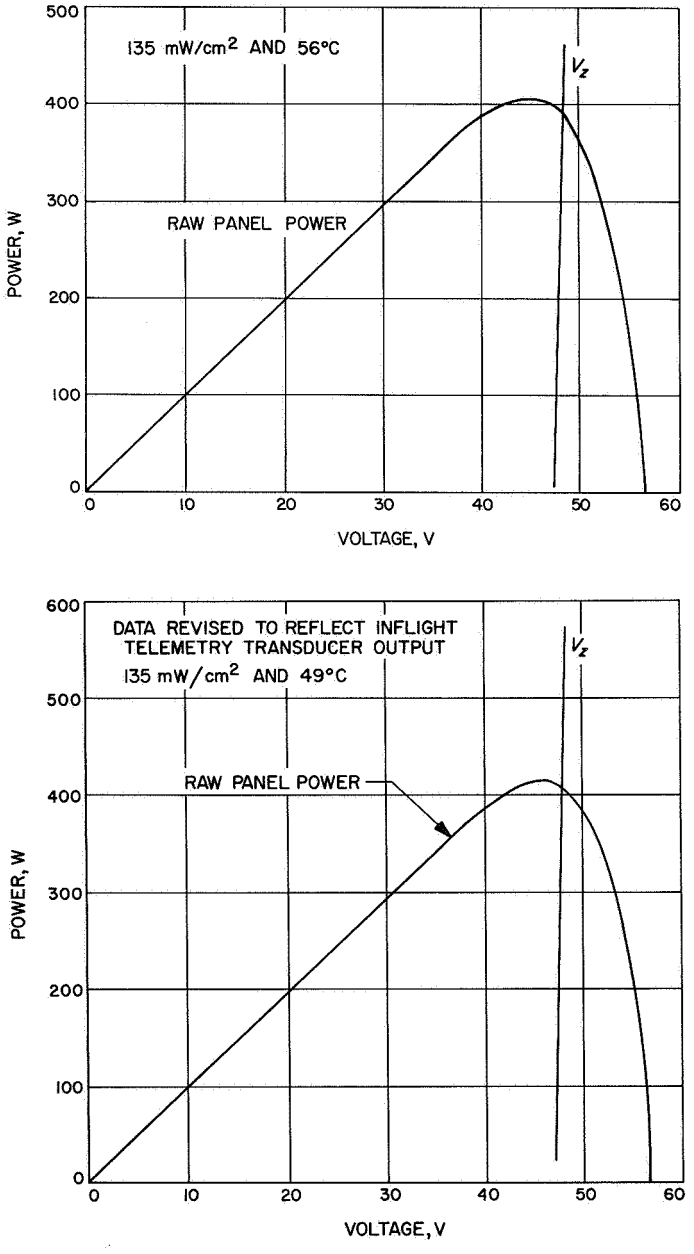



**Fig. IV-128. Prelaunch predicted power vs voltage for *Mariner V* solar array**

**Table IV-34. Solar array performance[a]**

| Day[b] | Heliocentric distance, $10^6$ km | Solar intensity, mW/cm² | Array maximum power, W | Voltage at maximum power, V | Temperature, °C |
|---|---|---|---|---|---|
| L | 151.0 | 135 | 410 | 45.5 | 49 |
| L + 30 | 146.0 | 144 | 423 | 45.2 | 55 |
| L + 60 | 134.6 | 173 | 481 | 42.0 | 70 |
| L + 90 | 120.5 | 212 | 555 | 36.0 | 93 |
| E | 108.5 | 255 | 615 | 32.8 | 115 |
| E + 10 | 105.0 | 290 | 630 | 32.5 | 122 |
| E + 30 | 99.0 | 317 | 660 | 30.2 | 132 |

[a]Based on early flight measurements.
[b]L = launch; E = encounter.

*Mariner IV configuration.* The *Mariner IV* PCE block diagram is shown in Fig. IV-129. It is physically and functionally divided into two cases: Case VIII, the power regulator assembly (also called 4A8) and Case I, the power conditioning assembly. Case VIII is one large integral module, and Case I consists of a frame and seven individual modules with an interconnecting harness.

The *Mariner IV* Case VIII can be functionally divided into the power switch and logic (PS&L), two electrically identical booster regulators (B/R), a booster regulator failure sensing circuit, and battery charger control relays. The PS&L includes the following:

(1) Solar panel and battery logic diodes.

(2) Current and voltage telemetry monitors.

(3) A motor-driven switch that transfers the battery power input from a ground support power supply to the spacecraft battery.

The booster regulators are identical; input power to the regulators is provided by the solar panels and/or battery in a range of from 25 to 50 Vdc. The output power is a regulated 52 Vdc supplying the inverters at loads of 27–150 W. The B/R efficiency is greater than 72% at 120-W load. One B/R (main booster regulator) provides power for cruise and encounter loads while the other one (maneuver booster regulator) provides power to the maneuver loads. The maneuver B/R is also used to provide standby redundancy for the main B/R, and must, therefore, be capable of providing power to both the maneuver and main loads.

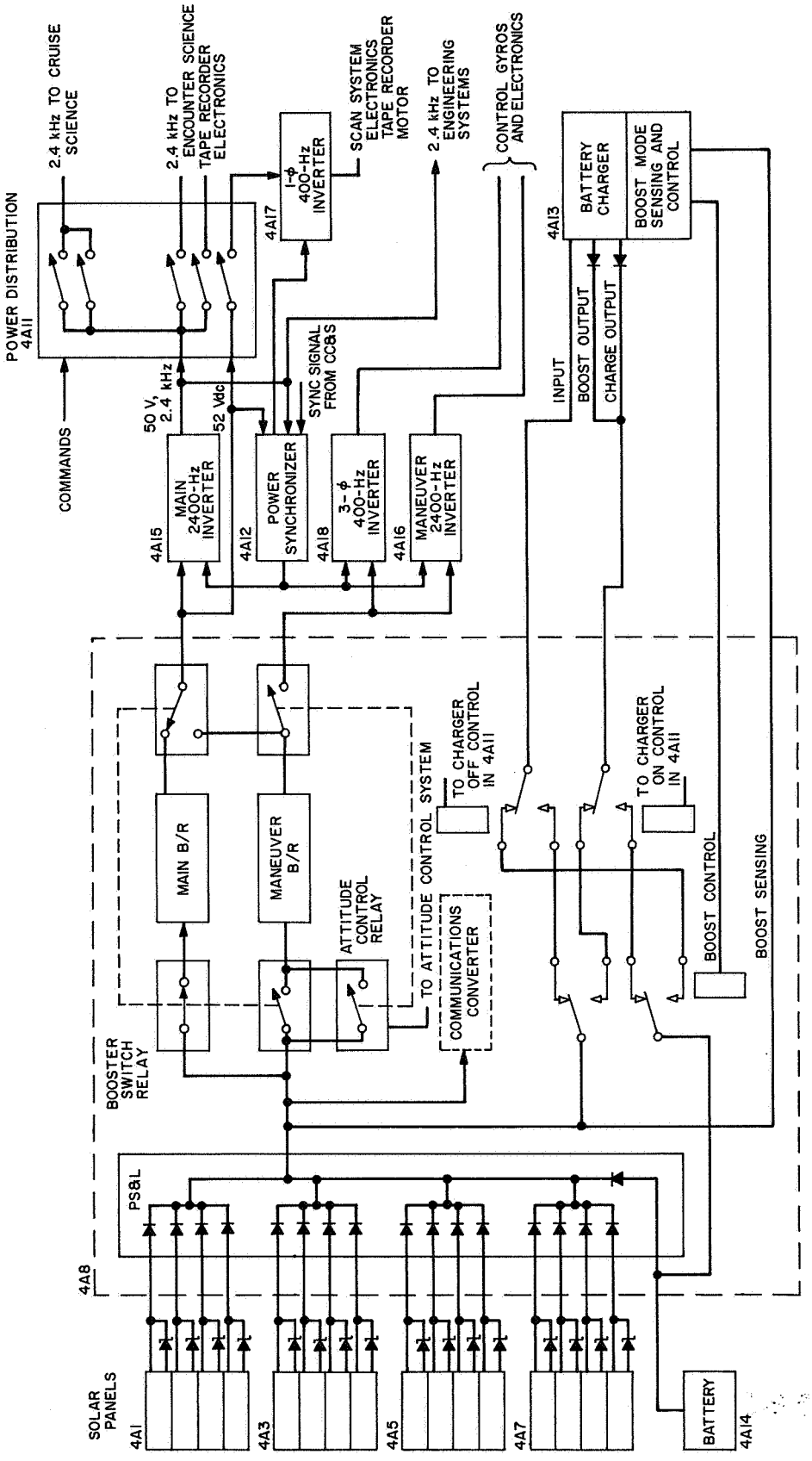



**Fig. IV-129. Power subsystem mechanization for *Mariner IV***

The *Mariner IV* Case I modules are described in the following paragraphs.

*Power distribution module (4A11).* This module accepts signals from the command decoder and central computer and sequencer (CC&S) and performs power switching as directed, using magnetic latching relays.

*Power synchronizer (4A12).* The power synchronizer receives a 38.4-kHz frequency reference signal from the CC&S. Internal countdown stages provide two 2.4-kHz output signals (used by the 2.4-kHz power inverters) and one 400-Hz 3-phase output signal (used by the 400-Hz 3-phase inverters). If the 38.4-kHz signal from the CC&S doubles in frequency or disappears, the power synchronizer will operate on its own 38.4-kHz oscillator at a reduced accuracy of 2%.

*Battery charger (4A13).* The battery charger performs two separate functions (battery charging and share protection) and can only perform only one at a time. Battery charging is accomplished basically by the constant potential method. Its current output is limited, however, so charging occurs in two modes: constant current and constant voltage.

The share protection function is performed by a circuit called the booster (not the booster regulator). A sharing condition can occur when a transient causes the primary system voltage to equal the battery voltage and the solar panels and battery both provide current to the load (share). This condition is unnecessary if the panel power capability is equal to or slightly greater than the load required, but at some voltage higher than the battery voltage.

Two conditions must be met before the booster can attempt to correct the condition. One condition is that it be "enabled" (the charger is off), and the other condition is that the share sensor has detected a share condition from the primary system voltage (it is inhibited from detecting this condition if the spacecraft gyros are on). The booster then raises the primary system voltage to a point where the panels should supply all of the power. If the panel *can* handle the entire load, the boost circuit, after removing the share condition, will turn off automatically. If the panels *cannot* handle the load (power required is greater than the capability), the booster will continue to attempt to correct the share condition until commanded off from the ground.

*Main 2.4-kHz inverter (4A15).* This inverter is powered from the Case VIII main B/R regulated 52-V line. Its 2.4-kHz 50-V rms square wave is the source of the spacecraft main power. The inverter is synchronized by the power synchronizer, but is capable of free running. Its minimum efficiency at 105-W load is 86%.

*Maneuver 2.4-kHz inverter (4A16).* For *Mariner IV*, this inverter is identical to the main 2.4-kHz inverter. Its input power is obtained from the maneuver B/R 52-V line; it powers the attitude control subsystem maneuver electronics.

*400-Hz single-phase inverter (4A17).* This inverter is powered from the main regulated 52-V line, and provides 400-Hz square wave to the scan platform motor and the tape recorder motor. It is synchronized from the power synchronizer. (This unit is not used on *Mariner V*.)

*400-Hz three-phase inverter (4A18).* This inverter is a driven amplifier with signal inputs from the power synchronizer and power from the maneuver 52-V line. Its quasi-square wave output runs the gyro motors.

*Changes from Mariner IV PCE due to changed power requirements.* Table IV-35 provides a comparison between the inputs and outputs of the *Mariner IV* and the *Mariner V* power subsystems. The significant changes are:

(1) The main 2.4-kHz inverter (4A15) maximum output power has increased from 80 to 105 W.

**Table IV-35. Power conditioning inputs and outputs modifications**

| Input/Output | *Mariner IV* | *Mariner V* |
|---|---|---|
| Number of diode isolated solar panel sections | 16 | 12 |
| Battery charger output voltage | 34.6 V | 34.6 V |
| Primary system voltage | 25–50 V | 25–50 V |
| Main 2.4-kHz output voltage | 50 V rms | 50 V rms |
| Main 2.4-kHz output power | 50–80 W | 50–105 W |
| Maneuver 2.4-kHz output voltage | 50 V rms | 50 V rms |
| Maneuver 2.4-kHz output power | 5–33 W | 5–33 W |
| 400-Hz single-phase inverter output voltage: No. 1 | 32.6 V rms | Not required |
| No. 2 | 28.0 V rms | Not required |
| 400-Hz three-phase inverter voltage (line-to-line) | 27 V rms | 27 V rms |
| 400-Hz three-phase inverter power total | 10 W | 10 W |
| Magnetometer heater power | Not required | 3 W |
| Synchronizing signal from CC&S | 38.4 kHz | 38.4 kHz |

(2) For *Mariner V*, no 400-Hz single-phase power is required.

(3) Raw power is required to keep the magnetometer warm.

The change (1) requirement had the most impact on the modification of the *Mariner IV* PCE. To maintain the 50-V output within a 2% lower tolerance, a new power transformer had to be installed in the main 2.4-kHz inverter. This transformer was bonded to the chassis making it almost impossible to remove without damaging the unit. Therefore, new main 2.4-kHz inverters were fabricated.

The increased loads on these inverters also required changes to the power regulator (4A8). If the main B/R failed, these loads would be automatically applied to the maneuver B/R by the failure sense circuitry. These loads, in addition to the maneuver loads, would be greater than the 150-W maximum load for the B/Rs (Table IV-36).

**Table IV-36. Maximum power required from maneuver booster regulator**

| Unit | Maximum output power, W | Efficiency, % | Input power, W |
|---|---|---|---|
| 4A15 | 105 | 86 | 122.0 |
| 4A16 | 33 | 80 | 41.3 |
| 4A18 | 10 | 78 | 12.8 |
| 4A8 TMO[a] | NA[a] | NA | 3.6 |
| | | | 179.7 |

[a]TMO = telemetry monitor oscillator; NA = not applicable.

The problem was corrected by the addition of a circuit that would automatically remove part of the 4A15 load (the science loads), if the overload condition should occur. The conditions for an overload are:

(1) Main B/R failed.

(2) Maneuver loads required.

(3) Science on.

Actual test and analysis showed that, if the B/R input voltage is high (over 40 V) and maneuver loads are on only for spacecraft stability (as opposed to an actual maneuver), the load is reduced to a more acceptable 155–160-W range. Under these conditions science could be left on. Therefore, the science inhibit can be overridden by ground command (DC-V25).

Since no 400-Hz single-phase power was required, this inverter was removed and a dummy module put in its place for structural stability in Case I.

A separate fused (0.2 amps) line was added to the communications converter power output to provide raw power to the magnetometer.

*Command logic changes from Mariner IV PCE.* Except for the maneuver loads signal, all external command signals to the PCE are sent to the power distribution assembly (4A11). Circuitry inside this assembly controls magnetic latching relays to provide the correct response. The changes in command and response logic are shown in Table IV-37. These changes required significant modification to the power distribution module.

*Battery-voltage telemetry circuit.* Flight telemetry from *Mariner IV* indicated that the spacecraft battery continued to be charged after the flight battery charger was turned off. A current of 1.3–2.5 mA was flowing into the battery from the battery voltage telemetry monitor. For *Mariner V*, an amplifier with high input impedance and unity gain was added to correct the problem.

*Mariner V PCE configuration.* The *Mariner IV* PCE, along with the previously described modifications, formed the basic configuration of the *Mariner V* PCE. The overall power subsystem configuration is shown in Fig. IV-130.

*Detail design changes to Mariner IV PCE.* The following is a list of the changes required to convert the *Mariner IV* PCE:

(1) The power regulator (4A8) required the addition of several small circuits.

(2) The power distribution assembly (4A11) required extensive rework of the logic.

(3) The power synchronizer (4A12) required no changes.

(4) The battery charger (4A13) required the addition of a sense lead to determine whether it was on or off for the DC-V28 command toggling.

(5) The main 2.4-kHz inverters (4A15) for *Mariner IV* were used as spares for the *Mariner V* maneuver 2.4-kHz inverters (4A16), and new modules were fabricated for the main inverter.

(6) The maneuver 2.4-kHz inverter (4A16) was modified very slightly so that no power could be applied to it if it was accidentally used as a main inverter.

(7) The 400-Hz single-phase inverter (4A17) was removed.

(8) The 400-Hz three-phase inverter required no changes.

Table IV-37. Command and controls modifications

| *Mariner IV* | | *Mariner V* | |
|---|---|---|---|
| **Command** | **Required action by power system** | **Command** | **Required action by power system** |
| CC&S MT-7 | (a) Connect planet science to primary 2.4 kHz<br>(b) Connect cruise science to primary 2.4 kHz<br>(c) Turn on 400-Hz single-phase supply<br>(d) Connect tape machine to primary 2.4 kHz<br>(e) Turn off battery charger | CC&S MT-7 | (a) Connect science to primary 2.4 kHz<br>(b) Connect tape machine to primary 2.4 kHz<br>(c) Turn off battery charger |
| DC-25 | (a) Connect planet science to primary 2.4 kHz<br>(b) Connect cruise science to primary 2.4 kHz<br>(c) Turn on 400-Hz single-phase supply<br>(d) Connect tape machine to primary 2.4 kHz<br>(e) Turn off battery charger | DC-V25 | (a) Connect science to primary 2.4 kHz<br>(b) Connect tape machine to primary 2.4 kHz<br>(c) Turn off battery charger<br>(d) Will allow operation of science and maneuver attitude control if main B/R fails |
| CC&S MT-8 | (a) Disconnect planet science from 2.4 kHz<br>(b) Disconnect redundant cruise science from 2.4 kHz<br>(c) Turn off 400-Hz single-phase supply | Not required | |
| DC-26 | (a) Disconnect planet science from 2.4 kHz<br>(b) Disconnect redundant cruise science from 2.4 kHz<br>(c) Turn off 400-Hz single-phase supply<br>(d) Disconnect main cruise science from 2.4 kHz<br>(e) Turn off battery charger | DC-V26 | (a) Disconnect main science from 2.4 kHz<br>(b) Turn off battery charger<br>(c) Rescind DC-V25 override |
| SC separation connector | (a) Connect cruise science to primary 2.4 kHz<br>(b) Provide RF power-up signal by opening NC relay contact (irreversible in flight) | SC separation connector | (a) Connect cruise science to primary 2.4 kHz<br>(b) Provide RF power up signal |
| DC-2 | (a) Connect cruise science to primary 2.4 kHz | DC-V2 | (a) Connect science to primary 2.4 kHz<br>(b) Connect alternate science to primary 2.4 kHz |
| DC-28 | (a) Turn on battery charger<br>(b) Turn off tape electronics | DC-V28 | (a) Turn on battery charger (or)<br>(b) Turn off battery charger, depending on last state of charger<br>(c) Turn off tape electronics |
| Data encoder Mode 4 | (a) Disconnect cruise science from 2.4 kHz | Not required | |

*Design changes required because of systems testing.* Two problems were observed in the PCE during the spacecraft testing. The first was found during RFI testing for the DFR subsystem. The DFR experiment used two sensitive receivers at 50 MHz and 420 MHz. The B/R generated considerable noise at 50 MHz, degrading the signal-to-noise ratio of the DFR at that frequency. The B/R design changes reduced the noise to an acceptable level.

The second problem had to do with the toggling operation of the battery charger. When the battery charger turned on in the boost enable mode, it would switch itself to the charge mode rather than boost as desired. A design change to the 4A11 unit was required to eliminate this difficulty.

*c. Battery modification and test.* The capacity of the battery is dictated by the system energy requirements at various critical phases of the mission. Both the *Mariner IV* and *Mariner V* capacity requirements for the battery during launch and encounter were the same, 1200 and 900 Wh, respectively. Since the system requirements were the same as the previous mission and the battery performed well during the *Mariner IV* mission, it was decided that no basic design changes were necessary, other than minor improvements that would increase reliability without altering performance characteristics.

*Design and testing.* The only problem noted with the *Mariner IV* battery was the increasing terminal voltage after termination of charge. However, this problem was attributed to the trickle charging by the voltage monitor

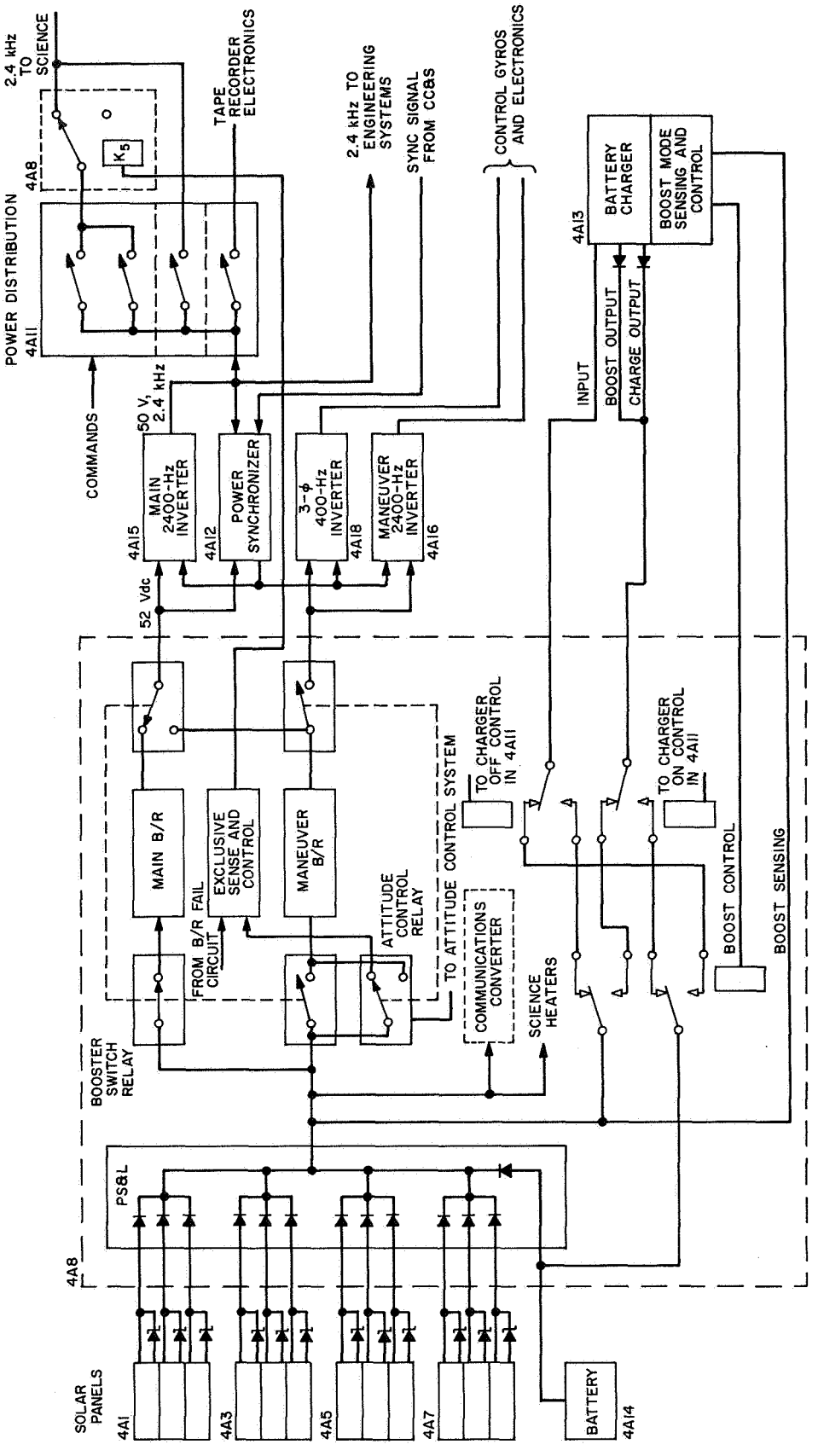



**Fig. IV-130. Power subsystem schematic for *Mariner V***

circuitry. Because new batteries had to be fabricated, some minor improvements were instituted into the design.

The active material mix of the negative plate for the *Mariner IV* battery consisted of 90% ZnO, 7% HgO, and 3% PVA binder. This binder had been changed from Teflon powder to PVA for *Mariner IV* in the expectation of some improvement. It was found that the improvement was not measurable and that the recombination rates of oxygen on the negative plate could be increased by a return to the Teflon powder. This return was done for *Mariner V*.

Another improvement made was not a change in materials, but in processes. It was found on the *Surveyor* battery program that the uniformity and quality of the cellophane separator used in the plate wrap tended to vary significantly from lot to lot. To assure uniformity and quality, an improved acceptance specification was used for *Mariner V*.

The battery chosen for flight did not undergo testing with the other spacecraft elements until the spacecraft was ready to be installed on the *Agena*. Batteries identical in design were used during the spacecraft vibration and space simulator testing. Spare batteries from the *Mariner* Mars 1964 program were used during the SAF testing. This spare usage was necessary because the average lifetime of a battery in use is six discharge-charge cycles. By only using the flight battery on the last system test, assurance was provided that the battery flown was in the best condition possible.

Because of this last system test of the flight battery, the acceptability of the battery design and capability of the flight battery must be based on the tests of the TA batteries, the spacecraft tests using system test batteries, and the FA tests and manufacturing data of the battery chosen for flight. One battery was initially procured as an engineering battery and underwent TA testing as well as some additional special testing to determine specific battery characteristics.

Three batteries were used for TA testing on the *Mariner* Venus 67 program. These were used to verify the design and the manufacturing capability. The batteries performed nominally during the testing, but all had some occurrence of plate wire breakage as did the TA batteries on *Mariner IV*. However, two of the three batteries were accidentally shocked during vibration. Because of the shock, it was difficult to determine whether the plate wire breakage was entirely a result of the vibration or an effect of the shocking. The plate wire breakage had not been observed on any battery as a result of the FA vibration tests. Even with the broken plate wires, the capacities of the TA batteries were above the specification requirements at both 32 and 140°F.

*Battery performance during launch and midcourse maneuver.* Spacecraft power was switched from an external supply to the battery for a test at launch minus 100 min and then for the final time at launch minus 7 min. At the time of launch, the battery was capable of providing at least 54.5 A-h.

At the time of liftoff, the total amount of current that the battery was supplying to the spacecraft was 5.6 A, at a voltage of 27.65 V (32DN). By launch plus 1 min, the spacecraft load had increased to 5.8 A, and the battery terminal voltage was steady at 27.65 V. Just before sun acquisition at launch plus 30 min the battery terminal voltage was 27.5 V, with the load still at 5.8 A. This voltage was the lowest value noted during launch.

The spacecraft load was removed from the battery at sun acquisition. The total capacity removed from the battery during the launch period was 4.3 A-h, assuming a nominal 55-A-h capacity prior to the launch minus 100 count, and adding in the capacity returned between launch minus 100 min and launch minus 7 min. A total of 3.2 A-h was used between liftoff and sun acquisition.

Since the battery charger is on during the launch, the battery began to be recharged as soon as the solar panels acquired the sun. The initial charge rate was 270 mA (37 DN) at 28.9 V, gradually tapering down to 30 mA at 34.45 V and 134.05 h after the start of charge. The number of A-h replaced up to this time (at the start of the midcourse maneuver) was 4.81 A-h; the battery then having a total capacity of 55.51 A-h.

The pitch portion of the midcourse maneuver started 135.5 h after launch. As expected, when the solar panels were partially shaded by the spacecraft bus, the battery began to share with a load voltage of 27.9 V and a discharge current averaging approximately 3 A. The total sharing time was 46 min. Battery load voltage remained fairly constant, the lowest voltage being 27.8 V, only 100 mV less than at the beginning of the pitch. The battery capacity was depleted by 2.33 A-h during the midcourse maneuver.

The battery charger, on during the maneuver, began to recharge the battery at the conclusion of the share

mode when the panels reacquired the sun. The initial charge rate was 270 mA at 29.0 V, dropping gradually to 50 mA at 34.2 V, at Canopus acquisition after the midcourse. The total input to the battery up to that time was 0.35 A-h, providing available capacity of 53.84 A-h at Canopus acquisition, approximately 139 h after launch.

Figure IV-131 shows the battery terminal voltage profile from launch to Canopus acquisition, while Fig. IV-132 presents the battery charger current profile for the same period of time.

*4. OSE modification and test operations.* The basic guidelines for the OSE modifications and test operations for the *Mariner* Venus 67 project were:

(1) The design was "frozen" at the *Mariner IV* configuration and all changes to this configuration required an Engineering Change Requirement (ECR).

(2) ECRs were approved only for those modifications that were considered necessary to accomplish the mission and that were critical to mission success.

In addition to these guidelines, all ECRs were evaluated with respect to their cost. Table IV-38 lists all of the ECRs and PFRs (Problem Failure Report) for the guidance and control OSE.

*a. Attitude control OSE.* The major improvement in the attitude control OSE was the new Canopus sensor hood and control circuit. The *Mariner IV* hood had 15 collimators for simulating clockwise, counter-clockwise, and null errors. Each hood had to be calibrated for the particular Canopus sensor in use, and part of the calibration was done in the hood and part in the OSE. This method of calibration caused many problems and, in addition, some of the Canopus sensors had warm-up drift characteristics such that the hood fixed offsets would not enable the acquisition logic until the sensor had warmed up. The result was many delays during the spacecraft testing.

In contrast, the new hood had five collimators (mounted on a bar) that could be driven clockwise and counter-clockwise in the Canopus sensor clock angle. In addition,

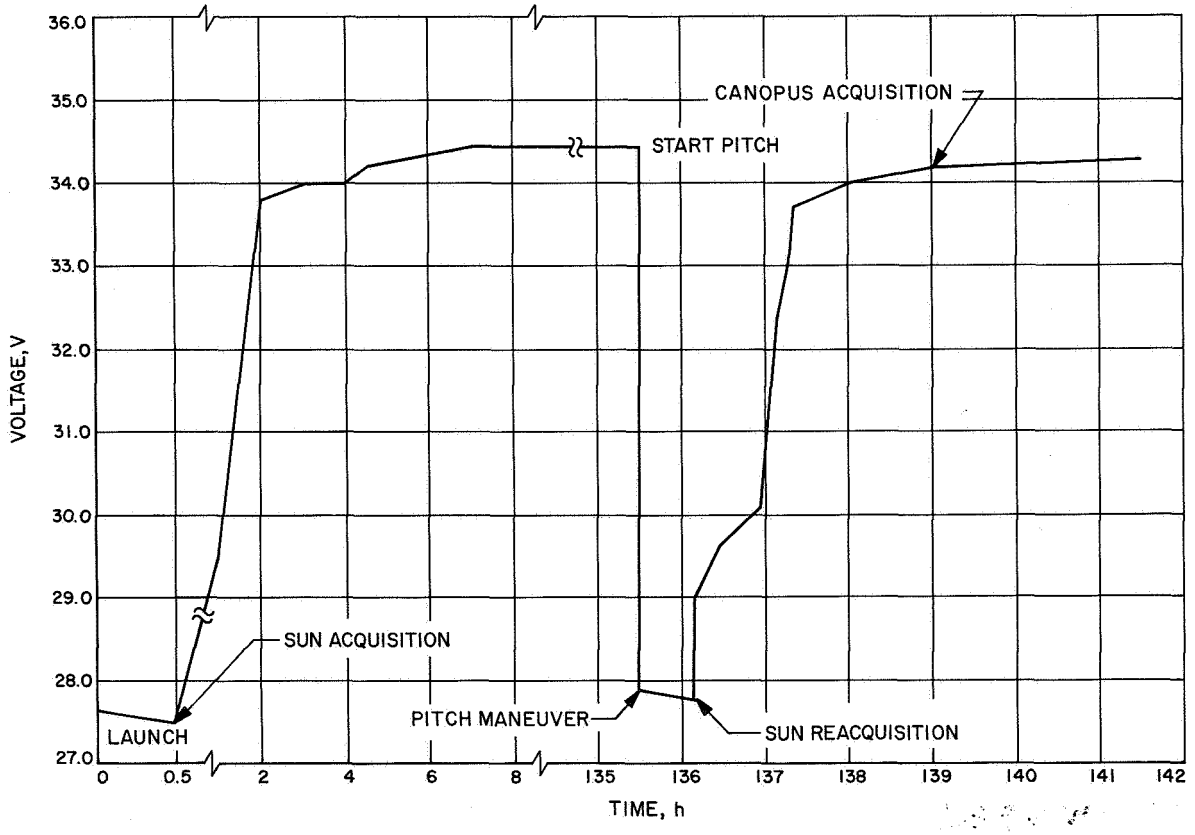



**Fig. IV-131. Terminal voltage profile for *Mariner V* battery (launch to Canopus acquisition)**

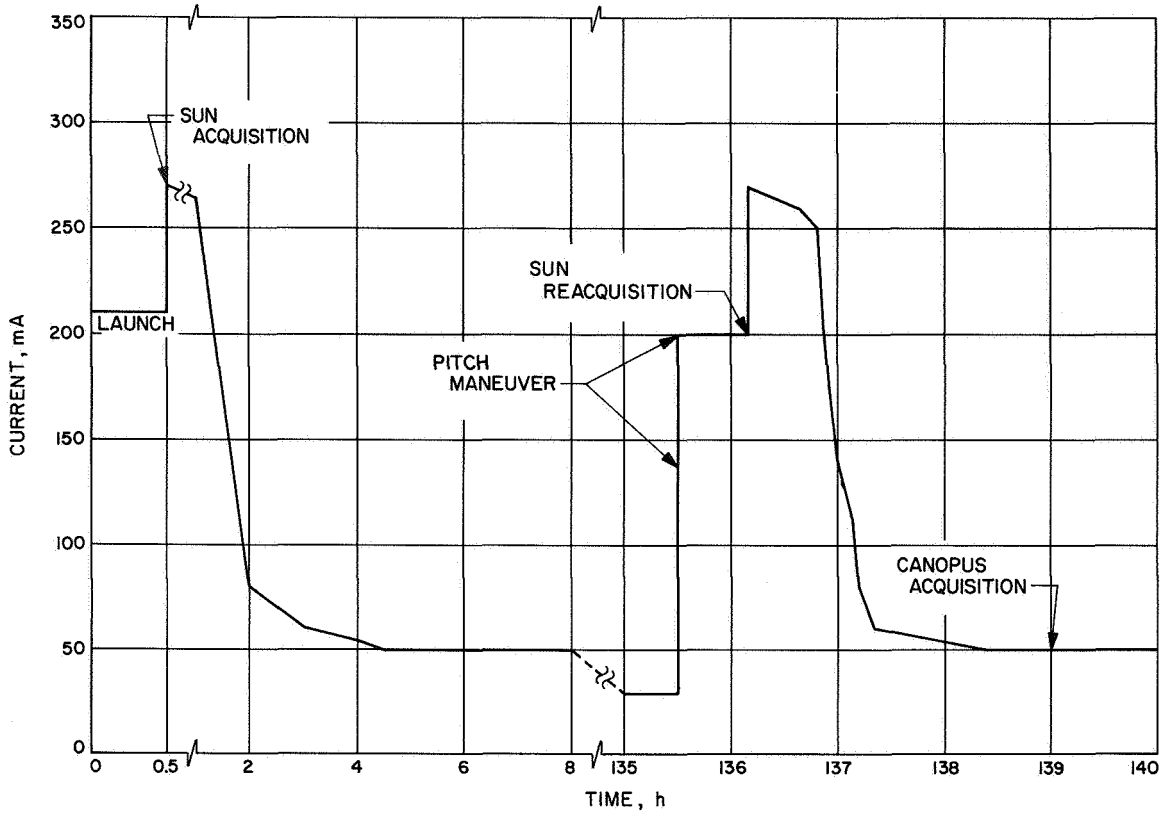



**Fig. IV-132. Battery charger current profile of *Mariner V* (launch to Canopus acquisition)**

the intensity of each collimator was controlled by a current generator located in the OSE. There were no calibration components in the hood itself.

The new hood and control circuit worked well; there was one problem with the control circuit that required redesign and rework.

Another problem that continually slowed operations was verification and adjustment of the lamp current. The current was sensed by a 5-Ω resistor, and the intensity output of the Canopus sensor was proportional to the seventh power of the lamp current. The dynamics meter in the OSE could not resolve a 5-mV change (out of approximately 250 mV). A good digital voltmeter should be installed in the OSE.

One other continual problem was the sun gate hood. This hood had one lamp and a collimator, and illuminated both sun gate photocells at the same time. The lamp was not very reliable, and the hood could not be used during space simulation tests. Also, if one of the sun gate cells failed, it probably would not be detected until the final AFETR operations. A new hood should be developed that illuminates each cell individually, and that is reliable enough so that it can be used in the space simulator.

The rest of the changes made to the OSE were required because of the spacecraft redesign and presented no problems.

An innovation that was informally related to the OSE was the fabrication of an attitude control simulator for training the test team and systems test-set checkout. It was not completed in time to serve as a training aid, but did serve very well as a test-set checkout aid.

*b. CC&S OSE.* Most of the troubles encountered in this OSE were concerned with trigger circuits being sensitive to noise. One case was interrelated with the source impedance and pulse waveshape from the flight CC&S; no change was made to this circuit, since the problem appeared only in the space simulator, and the testing there was completed by the time that the problem was completely understood.

*c. Power OSE.* There were no major changes made to the power OSE. A small number of minor changes was

Table IV-38. Guidance and control OSE modifications

| Subsystem | ECR | | PFR | |
|---|---|---|---|---|
| | Reason for ECR | No. | Reason for PFR | No. |
| Attitude control | Redesign | 4 | Manufacturing and workmanship | 3 |
| | Improvement of OSE | 5 | Design | 2 |
| | Documentation | 3 | Commercial equipment failures | 3 |
| | OSE failure or problem | 2 | Procedural problems | 1 |
| | To improve OSE and because of redesign | 1 | Documentation | 2 |
| | | | Undetermined | 2 |
| | | | End of life | 1 |
| | | | Transportation | 1 |
| | | 15 | | 15 |
| CC&S | Redesign | 1 | Manufacturing and workmanship | 2 |
| | Improvement of OSE | 3 | Design | 2 |
| | Testing problems | 2 | Commercial equipment failures | 2 |
| | Project requirement | 1 | End of life | 1 |
| | | 7 | | 7 |
| Power | Redesign | 17 | Design | 1 |
| | Improvement of OSE | 14 | Commercial equipment failure | 10 |
| | Documentation | 4 | Procedural problems | 1 |
| | OSE failure or problem | 3 | Documentation | 1 |
| | | | Undetermined | 5 |
| | | | End of life | 1 |
| | | 38 | | 19 |

made because of the spacecraft redesign, and a large number to increase the reliability and ease of operation.

One change made to the launch complex set was very important. From T-5 to launch, the blockhouse operator must release the inhibit and relay hold, time the clear event pulse, and monitor the battery voltage and the gyros. The battery monitor voltmeter originally used was a manual balance type, and balancing this instrument distracted his attention from the rest of the OSE. A digital voltmeter was installed in the OSE for monitoring the battery to allow the operator to concentrate upon the OSE, with only a glance at the battery monitor required.

Table IV-38 shows that the main cause of the power OSE problems was related to commercial instruments (the data recording subsystem).

Some of the repairs made to these instruments involved replacing semiconductors. This fact should be of concern, since one can expect a relay or chopper to fail after 2–4 yr, but good semiconductors should not fail. However, the manufacturers of such instruments used components that enabled them to have a minimal failure rate (for minimum cost) and one could expect the semiconductors that they use to begin degrading by this time. The voltmeters should be replaced for future missions.

The other troublesome instrument in this system is the printer. Unless replaced, they should be put on a short (1 mo) maintenance cycle.

*d. Test operations.* The following discussion of test operations for the guidance and control OSE concentrates on those aspects of the operations that caused the most problems and should be corrected for future missions.

One of the continuing problems during the program was involved with procedures. There were really two problems here. One problem was that the procedure for a test was often unavailable until the day of the test. The main concern with this problem is that the procedures were unavailable for review by the division personnel, and this lack of review could cause problems. The other part of the problem was connected with the JPL policy on the amount of detail contained within the procedure. In the past, the system level procedures have been written in an outline form, with the subsystem operators expected

to know the detail steps necessary to perform the test. This method has worked well in the past, with a pool of experienced operating personnel available and a PTM spacecraft to learn the basic techniques. Neither of these was available (in the attitude control and CC&S areas) for the *Mariner* Venus 67 program. A master procedure with subprocedures for each subsystem is the most likely alternative.

A second continuing problem was the system test complex data system (STCDS). Both the hardware and the STCDS programs caused many problems. The hardware was finally disconnected from the OSE and the STCDS was then used as a telemetry decommutator.

The problems with the STCDS outputs were largely concerned with programming. The normal problem was that the data suppression did not permit analyzing a problem from the STCDS outputs. Many times, a shift in data number of one would be significant, but would be suppressed (not printed) by the STCDS. The standard technique was to review the STCDS outputs for obvious problems, and to use the direct telemetry outputs for analyzing the problems.

Another problem that occurred, particularly during the launch and launch-type operations at the AFETR, was involved with the alarm limits placed on the computer outputs. An attempt was made to set the limits for two different spacecraft operating modes and to change these limits as a function of time. This attempt did not work well, since the limits were based upon the launch criteria. There were many times when the spacecraft mode was different from the launch mode, and some functions were incorrectly marked as being out of specification.

The spacecraft mounting fixture serves mainly as an assembly and holding fixture for the spacecraft. In addition, it is being used as a rate input device for the autopilot gain test for which it is unsuited. The rate is not independent of position, and there is enough "gear noise" so that an accurate autopilot test is almost impossible. The fixture should be replaced with one that will rotate the spacecraft smoothly.

The new 10-ft space simulation chamber was used for the spacecraft tests. Since the spacecraft had to be suspended (to point the spacecraft sun side toward the sun simulator), there were more problems encountered than there would have been had the spacecraft been hard mounted.

*5. Star identification program.* The star identification program (**SIPM**) was developed to support operations for *Mariner V* during Canopus acquisitions. This support was essentially the same as that provided for the *Mariner* Mars 1964 mission (Ref. 11). A few changes were made to improve that support for the *Mariner* Venus 67 mission.

These changes were based on experience gained during the *Mariner* Mars 1964 mission. For example, *Mariner IV* attempted to acquire reflected light caused by the earth during its initial attempt to acquire Canopus. Because the Canopus sensor response to this type of light had not been modeled, the attempted acquisition was not predicted. As a result, the spacecraft analysts were not able to provide an estimate of what had been acquired until some time after the acquisition. To avoid this, a model of the Canopus sensor response to this type of reflected light was constructed and incorporated into **SIPM**. The estimated Canopus sensor intensity output could then be used to indicate when these acquisitions might occur. During the mission, this model allowed the analysts to predict that *Mariner V* would acquire reflected light from the earth if roll search started when the clock angle of the Canopus sensor was between 225 and 357 deg. During the flight, this was indeed the case.

The map-matching technique was made somewhat more efficient for this mission. Instead of hand plotting the estimated, telemetered intensity output of the Canopus sensor, this plot was made to a specified scale by **SIPM**. This method made it possible to vary the size of the plot to match the real-time strip chart plot of telemetry data. It also became practical to make new versions of this plot as knowledge of the *Mariner V* trajectory improved.

In addition to **SIPM**, a new technique was used to support the operations for *Mariner V*. This technique made use of the intensity output of the *Mariner V* earth sensor during the roll spin used to calibrate the helium magnetometer. The outputs from the earth sensor were used to estimate the clock angle of the Canopus sensor at the time *Mariner V* started its attempt to acquire Canopus. This estimate was done by observing the time at which the earth passed through the earth sensor field-of-view on each revolution of the spacecraft. These times were correlated with the orientations of the Canopus sensor to obtain an indication of how the Canopus sensor clock angle varied with time. This technique proved very useful

in estimating what would be acquired. In fact, it was this estimated clock angle that allowed the acquisition of reflected light from the earth to be predicted.

This estimated clock angle was also useful in making an estimate of the clock angle of the Canopus sensor at the time of acquisition. This estimate was made using two methods. The first method was to take the amount of roll between the start of roll search and acquisition, and add it to the clock angle of the Canopus sensor at the start of roll search. This method provided a quick estimate of the sensor clock angle at acquisition. The second method consisted of matching the estimated intensity output of the Canopus sensor with the intensity output telemetered from *Mariner V*—the map-matching technique. The estimated clock angle of the Canopus sensor at the start of roll search was used to indicate which part of the estimated output plot should match best with the telemetered output. The map-matching technique was more accurate because it was not affected by uncertainties in the estimated clock angle of the Canopus sensor at the start of roll search, and most of the variations in the roll rate of *Mariner V* could be taken into account.

Preparations for this operational support were made more efficient by another modification to the **SIPM** computer program. Prior to the launch of *Mariner V*, it was desirable to make the plots of the estimated intensity output for different times during the mission (e.g., for the initial attempt to acquire Canopus and for the reacquisition of Canopus after the midcourse maneuver). At other times during the mission, it was desirable to have these plots for several different locations of the probe along the trajectory (usually for planning purposes). During the *Mariner* Mars 1964 mission, it would have taken many runs of **SIPM** to produce these plots, since the program could only consider one point on the trajectory per run. For the present mission, the program was modified so that up to 31 points along the trajectory could be considered in a single run of the program. This modification made the program much more efficient for making pre-flight runs and runs for planning purposes.

**SIPM** was used in flight to determine what star the ultraviolet (UV) photometer viewed during the three rolls after midcourse. This determination was done by matching the *a priori* brightness data from **SIPM** with the telemetered output of the Canopus sensor and noting the spacecraft orientation at the time of the UV output. **SIPM** was also used to predict what stars would pass through the UV field-of-view during the cruise portions of flight.

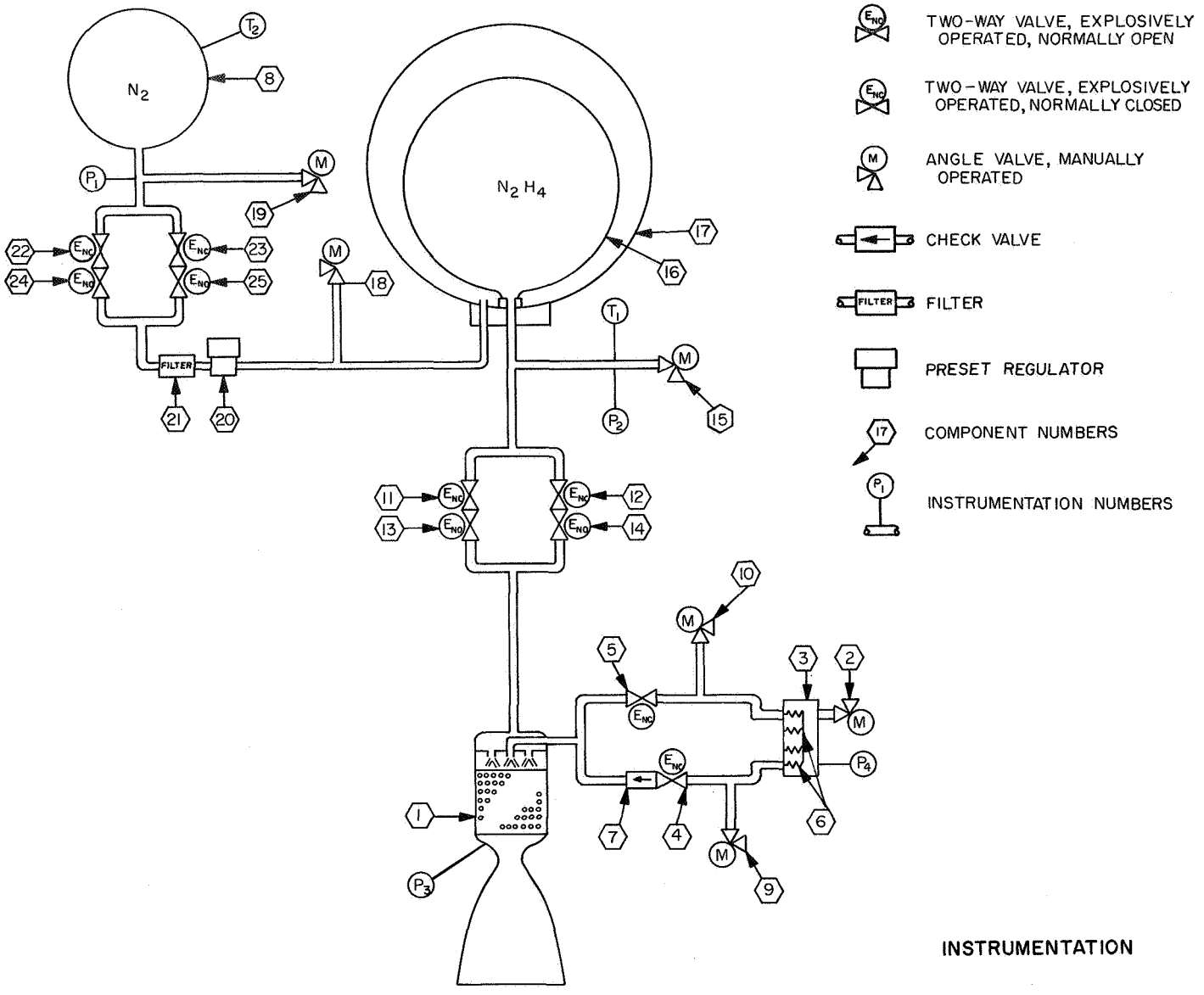
## G. Propulsion and Pyrotechnic Subsystem Description and Development

*1. Propulsion subsystem.* The primary function of the propulsion subsystem is to remove or reduce launch vehicle injection dispersion errors, and to remove biased trajectories of the launch vehicle caused by contamination constraints. This function is performed during the two possible spacecraft post-injection maneuvers during which the spacecraft is directed to turn to a prescribed position in space and impart a corrective impulse via the propulsion subsystem.

*a. Subsystem description.* A schematic of the propulsion subsystem is shown in Fig. IV-133. The subsystem design is identical to the *Mariner IV* subsystem, except for a modification of the pyrotechnic cable harness. The subsystem utilizes a liquid monopropellant, anhydrous hydrazine, as a propellant. It is functionally a regulated-gas-pressure-fed constant-thrust rocket. Principal subsystem components consist of a high-pressure gas reservoir, a pneumatic pressure regulator, a propellant tank and propellant bladder, an oxidizer ignition cartridge, and a rocket engine. The rocket engine contains a quantity of catalyst to accelerate the decomposition of hydrazine.

The subsystem concept shown in Fig. IV-133 is predicated on the basis that it satisfies the long-term space storage (maximum of 250 days) and multiple start (maximum of 2 starts) requirements imposed by the *Mariner IV* mission. The propulsion system required no major changes to accomplish the Venus mission.

To better fulfill the long-term storage requirement, pressurization by nitrogen gas was used instead of gaseous helium, the latter being more prone to leakage. In a similar manner, welded and brazed tubing and fittings were used wherever possible to minimize the number of potential leak sources. Metal seals were used (where welding and brazing was impractical) in place of elastomeric seals to alleviate the effects of radiation, hard vacuum, and long-term storage on the critical system seals. Multiple start capability is realized by the inclusion of "ganged" explosive valves with two parallel branches of normally closed (start) and normally open (shutoff) valve groups in the nitrogen and fuel circuits, and two normally closed valves in parallel in the oxidizer circuit. Individual oxidizer cartridges (13 $cm^3$ of nitrogen tetroxide, $N_2O_4$) are used for each of the two starts, both cartridges being pressurized by a common source.




## COMPONENTS

| No. | DESCRIPTION |
|---|---|
| 1 | ROCKET ENGINE |
| 2 | $N_2$ FILL VALVE, IGNITION CARTRIDGE |
| 3 | $N_2$ RESERVOIR, IGNITION CARTRIDGE |
| 4 | OXIDIZER VALVE, START 1 |
| 5 | OXIDIZER VALVE, START 2 |
| 6 | OXIDIZER RESERVOIR, IGNITION CARTRIDGE |
| 7 | CHECK VALVE |
| 8 | NITROGEN TANK |
| 9 | OXIDIZER FILL VALVE 1, IGNITION CARTRIDGE |
| 10 | OXIDIZER FILL VALVE 2, IGNITION CARTRIDGE |
| 11 | PROPELLANT VALVE, START 1 |
| 12 | PROPELLANT VALVE, START 2 |
| 13 | PROPELLANT VALVE, SHUTOFF 1 |
| 14 | PROPELLANT VALVE, SHUTOFF 2 |
| 15 | FILL VALVE, PROPELLANT |
| 16 | PROPELLANT BLADDER |
| 17 | PROPELLANT TANK |
| 18 | PREPRESSURIZATION VALVE, NITROGEN |
| 19 | FILL VALVE, NITROGEN TANK |
| 20 | PRESSURE REGULATOR, NITROGEN |
| 21 | NITROGEN FILTER |
| 22 | NITROGEN VALVE, START 1 |
| 23 | NITROGEN VALVE, START 2 |
| 24 | NITROGEN VALVE, SHUTOFF 1 |
| 25 | NITROGEN VALVE, SHUTOFF 2 |

## INSTRUMENTATION

### PRESSURE TRANSDUCERS

- $P_1$ NITROGEN TANK
- $P_2$ PROPELLANT TANK
- $P_3$ THRUST CHAMBER
- $P_4$ IGNITION CARTRIDGE $N_2$ RESERVOIR

### TEMPERATURE TRANSDUCERS

- $T_1$ PROPELLANT
- $T_2$ NITROGEN TANK

NOTE:
EVENT REGISTER DATA (BLIP DATA) ON EXPLOSIVE VALVE START AND SHUTOFF CURRENT

**Fig. IV-133. Propulsion subsystem schematic**

The design and operational philosophy of the subsystem is directed toward maximizing system reliability and reproducibility, minimizing pre-flight handling and spacecraft interactions, minimizing in-flight electrical signals and sequencing, and minimizing the number of subsystem components. The propulsion subsystem can be fueled, pressurized, and monitored for several weeks prior to emplacement within the spacecraft and actual launch. In the pressurized and fueled condition, the subsystem is safe for personnel to work near the temperature range of +35 to +125°F (burst pressures of the pressure vessels are a factor of 2.2 greater than maximum working pressures at 125°F). No spacecraft umbilicals or hardlines are required to maintain the propulsion subsystem in the "ready" condition.

*b. Test and fabrication.* The existing *Mariner IV* propulsion subsystem design was determined to be adequate for this mission. It was decided to fabricate one new subsystem for the flight unit and to utilize the existing *Mariner IV* spare as the *Mariner* Venus 67 spare, subsequently designated M67-1. No additional development or type approval (TA) tests were performed before fabrication of the new flight unit. Flight acceptance (FA) tests were performed on flight components in accordance with JPL testing procedures. A schedule representing the planned milestones up to the time of delivery to the spacecraft is shown in Fig. IV-134.

The first engine vacuum calibration test was performed at the JPL Edwards Test Station. A flight-type

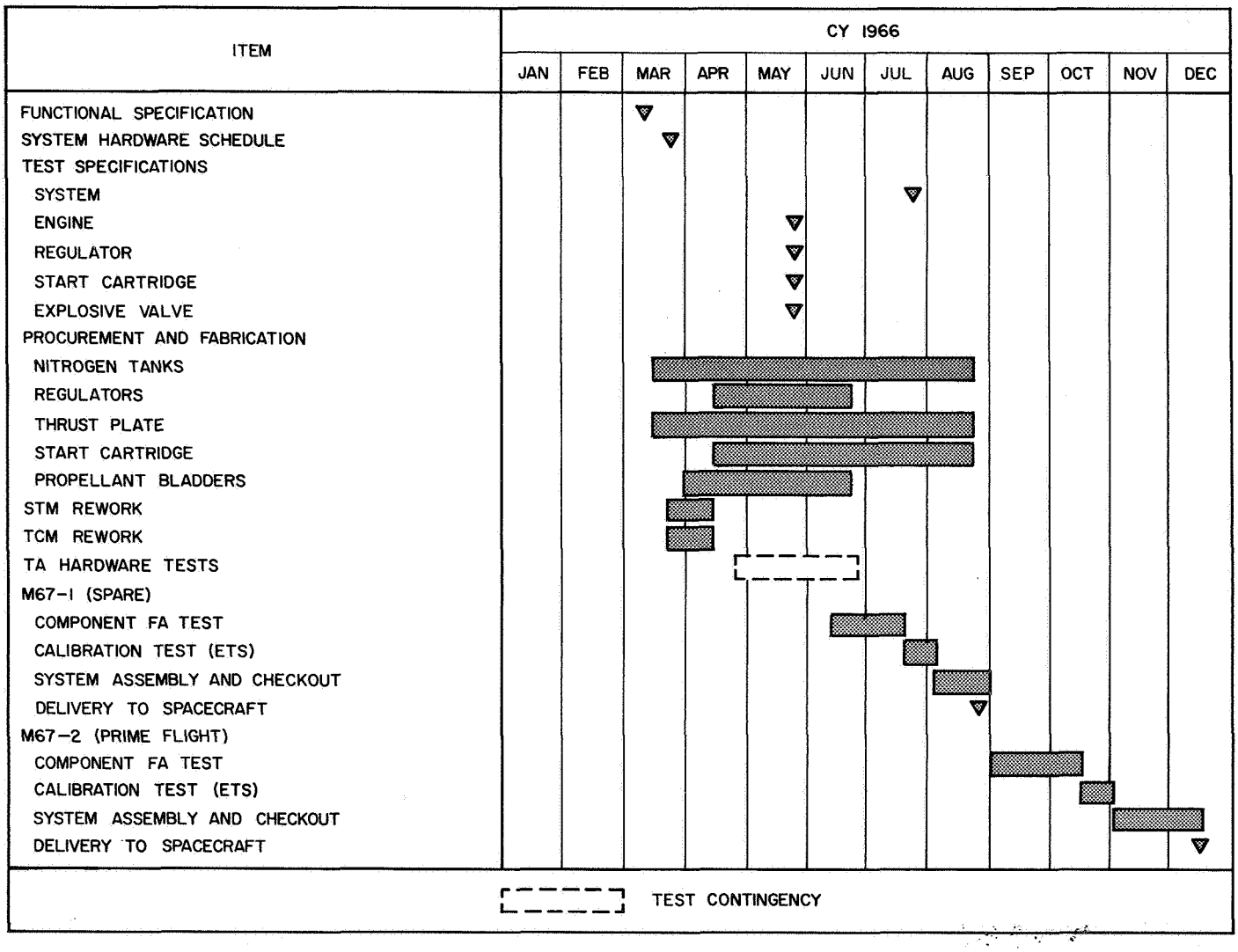



**Fig. IV-134. *Mariner* Venus 67 propulsion system schedule**

unit was assembled (i.e., assembled of flight quality hardware) with the actual M67-1 engine and regulator mounted on the subsystem. Test data from this firing indicated that the performance of this engine/regulator assembly was within 3% of the previous performance obtained in 1963. Because this subsystem had been built in 1963 as the *Mariner IV* spare subsystem, and the regulator was considered one of the shelf-life limited components, it was decided to replace the regulator with a new one. This decision resulted in another calibration test to determine the new regulator performance. A significant event occurred during this test which led to a detailed investigation of the regulator dynamics in a vacuum environment.

It appears that this particular regulator design exhibits a characteristic that permits the regulator to shut off gas flow momentarily at near regulator set pressure during start transient operation. The sequence of events for a given regulator would be as follows:

| Initial conditions | Value |
|---|---|
| Vacuum environment | −0.03 psia to 5 $\mu$m |
| Regulator set pressure | −305 psia |
| Regulator upstream pressure | −305 psia |
| Regulator downstream pressure | −305 psia |

As the propellant valve and the gas circuit valve are opened (Fig. IV-133), the regulator does not immediately respond, but, instead, shuts off the flow of gas until an imbalance occurs in the regulator diaphragm/spring package. The result of this condition is a "blowdown" of the propellant tank pressure for the duration of the shutoff condition (Fig. IV-135). The duration of the shutoff period is a function of the propellant tank ullage at the time of valve opening.

The ramification of this anomaly, because of the timer shutoff system in the spacecraft, was an uncertainty in the total impulse of the propulsion subsystem due to the "blowdown" characteristic. It was determined that the previous history had not revealed any indication of this problem when the propellant tank pressure (regulator downstream ullage pressure) was significantly *less* than regulator set pressure. Therefore, because the flight subsystem propellant tank is prepressurized to 290 psia at final launch preparation (regular set pressure ≈310 psia), it was expected that this characteristic would not be a problem for the first propulsion subsystem firing in space. However, the accuracy of the second firing, if there was one, could be jeopardized.

To better understand and verify this regulator anomaly, tests were performed with a dynamically similar system (Fig. IV-136). The system consisted of all the components of the flight configuration except for a

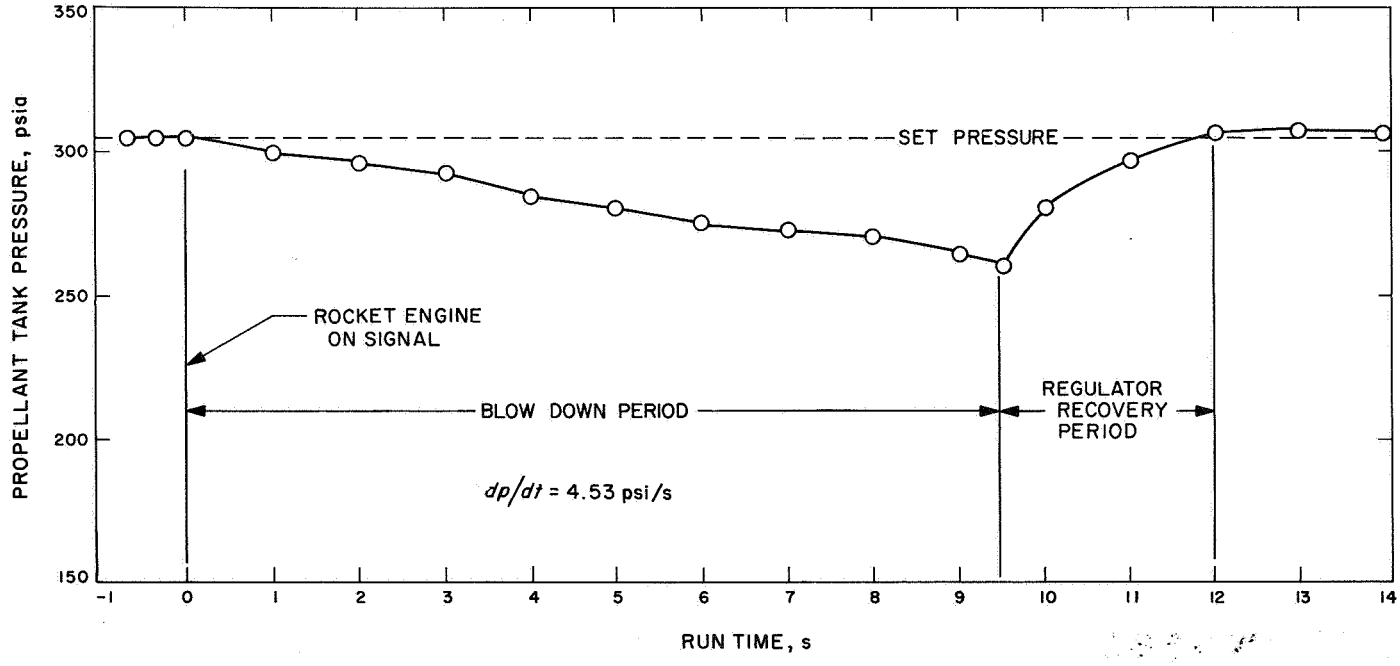



**Fig. IV-135. Regular transient behavior**

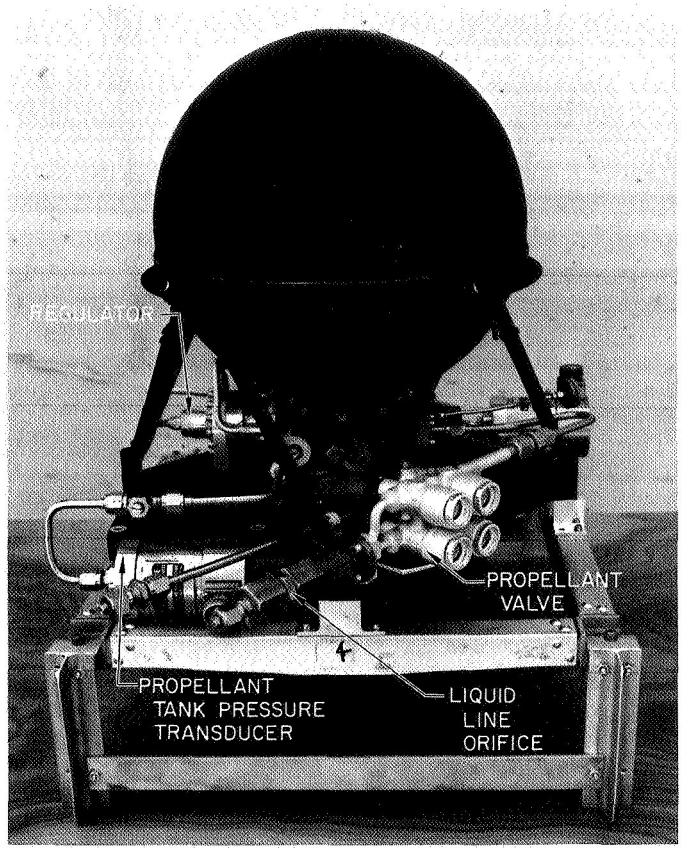



**Fig. IV-136. Regulator test system**

rocket engine (an orifice was used to simulate the pressure drop) and flight transducers. Distilled water was used to simulate the propellant.

From these tests, it was determined that the regulator did not close when the downstream ullage pressure (propellant tank pressure) was 5 psi, or more, below the regulator set pressure. In addition, a boundary of shutoff characteristics along with a prediction and uncertainty of the minimum blowdown pressure was determined. This information was used to generate a curve of regulator performance to provide a burn-time prediction if a second firing in space became necessary.

A second series of engine/regulator calibration firings was initiated for the prime flight (M67-2) subsystem. During this series of tests, the flight engine was destroyed in an explosion caused by the failure of the oxidizer start system to inject the nitrogen tetroxide starting fluid at the proper time. An intensive investigation was conducted to determine the cause of the failure. The investigation revealed that an electrical ground had occurred in the facility firing circuit causing a power drop to the oxidizer start squib valve, resulting in an oxidizer injection delay of approximately 0.6 s. Since the failure was attributed to ground-support equipment, not flight hardware, a backup flight engine was calibrated successfully using the flight prototype pyrotechnic control assembly instead of the facility-type firing circuit.

*c. Mission performance.* Telemetry data obtained during launch and cruise indicated that the propulsion subsystem remained leak tight. A $\Delta V$ capability of 92.1 m/s was available following injection. Performance during the trajectory correction maneuver was nominal except for a slightly lower than expected thrust chamber pressure. Analysis of maneuver data indicates that motor performance could have been as much as 3% lower than predicted. However, this cannot be confirmed because of the low-resolution and low-sampling rate of the spacecraft data system, coupled with inaccuracies inherent in the potentiometer-type pressure transducer used. Analysis is continuing, and further results will be published in Volume II of this report.

In summary, there were no special adaptations required of this subsystem to permit its use on the *Mariner* Venus 67 mission. During the actual flight, a successful post-injection maneuver was performed.

To improve in-flight performance evaluation, two changes should be made in the following areas:

(1) The potentiometer pressure transducer should be replaced with an improved design, such as a transducer incorporating strain-gage elements. This would eliminate the mechanical friction inherent in the present design, resulting in increased accuracy and repeatability.

(2) Better resolution and a higher sampling rate for propulsion parameters are desirable during trajectory correction maneuvers.

***2. Pyrotechnic subsystem.*** The *Mariner* Venus 67 pyrotechnic control assembly (PCA) was required to provide squib firing current for six spacecraft functions:

(1) Pin retraction of four solar panel latches.

(2) First start, PIPS motor.

(3) First stop, PIPS motor.

(4) Second start, PIPS motor.

(5) Second stop, PIPS motor.

(6) Pin retraction of one high-gain antenna latch.

In addition, the firing units had to contain switching circuitry which, upon command, would inhibit firing of the propulsion subsystem, release the inhibit, and transfer the command to fire the propulsion subsystem to either of the two groups of ON–OFF squibs.

A detailed development history of the *Mariner IV* pyrotechnic control unit, the remaining units of which were modified for this mission, is presented in Ref. 1.

*a. Subsystem redesign.* The *Mariner* Mars 1964 PCA, in its original configuration, could have performed all the required MV-67 pyrotechnic functions except for the added antenna pointing angle change (APAC). To accommodate that function, a circuit board was fabricated that includes a solid-state switch which, upon command, supplies excitation to the terminator sensor and data automation subsystem. Because of the high output impedance of the terminator sensor, an integrating circuit with unijunction transistor was provided to supply an adequate gate signal to trigger the antenna pin-puller squib firing circuit. The added circuit board is shown in Fig. IV-137. Figure IV-138 shows the board installed in the PCA.

Redesigned solar panel latches required that the pins in the pin-pullers be lengthened. The surplus pin-pullers were reworked.

To satisfy firing cable requirements for category A squibs, new cables having continuous no-gap circumferential shielding were fabricated for the PIPS. Since it was necessary to provide new firing cables to pin-puller squibs because of the relocation of the solar panel latches, these cables were also fabricated with continuous circumferential shields.

*b. Pre-flight test performance.* Type approval tests were conducted after the modification on two flight PCA units. The units were removed from the *Mariner* Mars 1964 prototype test model (PTM) spacecraft. During vibration, an internal failure in one of the energy storage capacitors occurred. The failure was caused by the methods used in the internal construction of the capacitors. The failure mode was corrected by the manufacturer subsequent to the fabrication of these units. The failure, had it occurred during spacecraft flight, would not have been catastrophic. Because of the redundancy of the flight PCA and method of capacitor failure detection, it was decided not to change the capacitors in the flight system. In addition, the necessary rework in the PCA chassis would have decreased the overall reliability of the PCA.

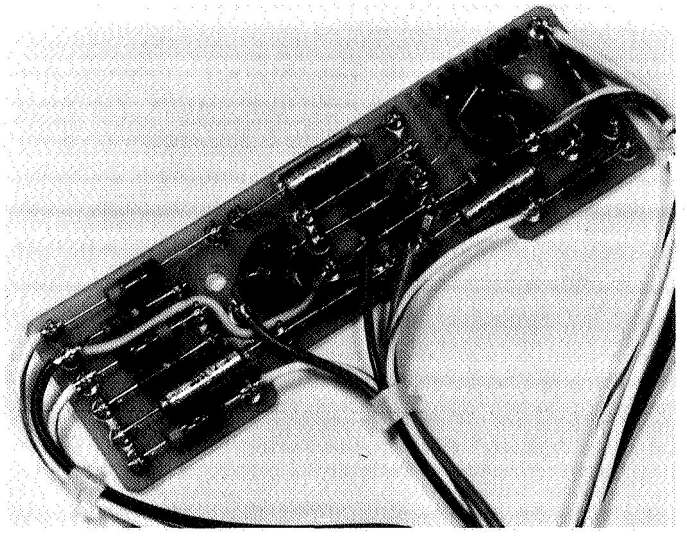


**Fig. IV-137. APAC circuit board**

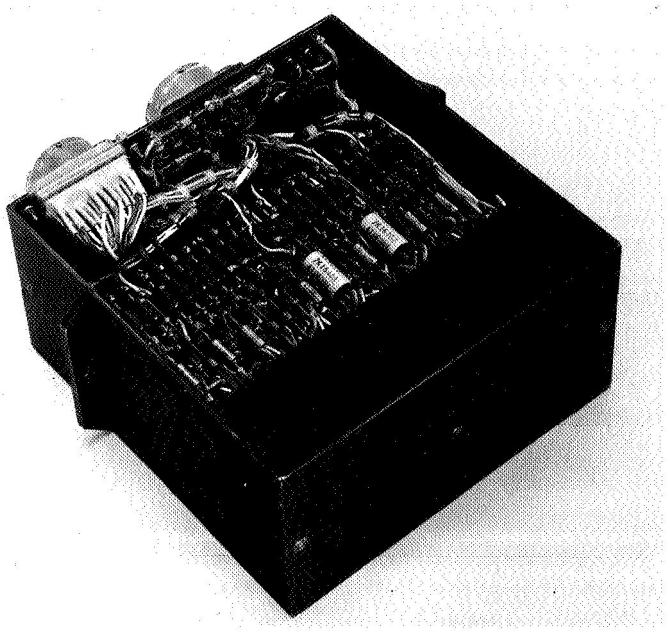


**Fig. IV-138. Circuit board installation**

Flight acceptance tests were conducted on four PCA units. No anomalies were detected.

*c. Mission performance through midcourse maneuver.* The subsystem operated normally and as expected. The pyrotechnic arming switch armed the subsystem at *Agena*/spacecraft separation. The solar panel squibs were fired when commanded from the separation-initiated timer, and the propulsion subsystem squibs were fired when commanded from the CC&S.

## H. Engineering Mechanics

*1. Structure subsystem.* The structure subsystem provides the structural elements that enable the many elements comprising a functional spacecraft to withstand the boost environment and to maintain geometric relationships, alignments, and orientations from initial assembly to mission completion. The hardware elements comprising the subsystem are discussed in the following subsections.

*a. Octagon structure.* The basic spacecraft structure, consisting of the primary octagon and internal secondary structure, utilized the *Mariner* Mars 1964 structure virtually intact (see Ref. 12 for a description of the development of this structural configuration). Modification of the *Mariner* Mars 1964 basic structure was limited entirely to the category of add-on bracketry to support relocated equipment. No structural resizing was required to accommodate packaging revisions.

Specifically, brackets that were added to the bus structure to form equipment mounts were (1) Canopus sensor mount, (2) planet sensor mount, (3) UV photometer adapter, (4) plasma probe mount, (5) dual-frequency receiver (DFR) filter mounting, and (6) a relocated primary sun sensor attachment. In all cases, the primary concern was not structural adequacy, but the ability to provide proper alignment at the assembly interface.

Canopus and planet sensor attachments consisted of aluminum alloy adapter brackets. Necessary alignment was provided by machining tolerances and locating shoulders on the piece-part adapters which allowed overall alignment tolerances to be automatically satisfied upon assembly to the octagon structure. Attachment of the UV photometer was accomplished by the addition of blank mounting brackets. The necessary instrument alignment and attach pattern was provided by a simple indexed drill template. This permitted accurate instrument placement without concern for the tolerances within the individual adapter brackets.

The plasma probe mount consisted of a magnesium alloy support frame. In-plane alignment was provided by location to the plane of the lower ring. Out-of-plane stiffness was provided by a tie-rod connecting the instrument support to the spacecraft secondary structure through monoball rod ends, thus decoupling the secondary structure response modes from the instrument.

*b. Superstructure.* The *Mariner* Venus 67 mission design required that the pointing direction of the high-gain antenna at planet encounter be changed. Prior to encounter, the antenna has a pointing direction of 110.7-deg cone and 107.4-deg clock. The *Mariner IV* elliptical dish was skewed about the boresight axis 38°44′ relative to the *X-Y* plane. To communicate with the spacecraft after planet encounter, the antenna boresight must be shifted by specific cone, clock, and skew angles. Given these angle constraints, plus the folded solar panel, sun sensor view clearances, and low-gain antenna location, the antenna position with respect to the spacecraft could be predetermined.

The superstructure was developed from three of the *Mariner IV* superstructure attach points on the octagon structure top ring and a triangular structure mounted on the back of the high-gain antenna reflector. The resulting strut arrangement is shown in Fig. IV-139.

Response acceleration levels of the high-gain antenna dish obtained from the *Mariner* Mars 1964 structural test model (STM) Structural and Environmental Vibration Qualification Test Report were used as a basis to develop a mathematical idealization of the antenna dish. This model was used in static and dynamic response analyses of the new superstructure. The analysis indicated that member buckling and local member resonance were the governing design parameters of the truss members. Proper member tube sizes were then selected and

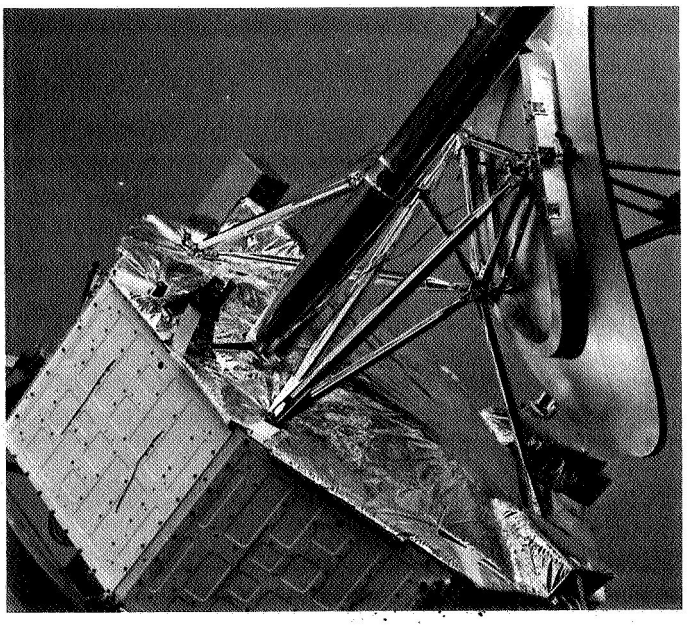


**Fig. IV-139. *Mariner V* superstructure**

member joints designed using the results of the forced response analyses.

The superstructure for *Mariner IV* was fabricated from welded aluminum tubing. Because of the fabrication problems encountered as a result of welding on *Mariner IV*, riveted aluminum tubular construction with machined end fittings was selected. Dynamic considerations sized the tubes at 1.375, 1, and 0.75 in. in diameter, depending on their positions in the assembly. To minimize end fitting weight, the tube ends were swaged, where required, to 1 in. in diameter at the bus attachment end, and 0.75 in. in diameter at the upper attachments. The weight of the superstructure was 3.25 lb.

Fabrication of the end fittings was somewhat difficult because of the complexity of the configuration (i.e., five tubes terminated at a single junction in one instance — Fig. IV-140); however, the time consumed in machining was compensated for in assembly time. Typically, a superstructure was assembled in approximately 6 h.

Type approval testing of the superstructure was performed on the STM spacecraft. Flight acceptance tests were conducted with the superstructures mounted on the flight spacecraft.

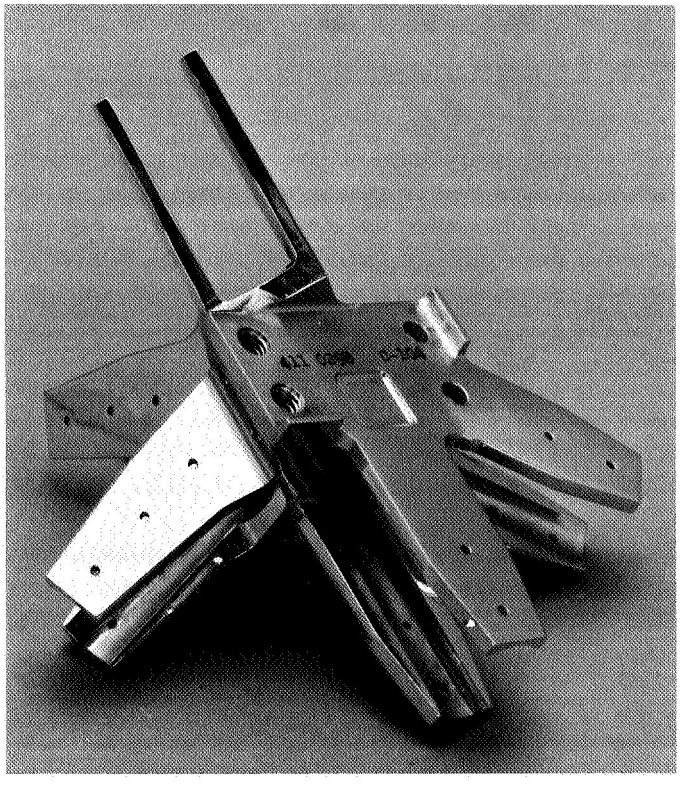


**Fig. IV-140. Superstructure fitting**

*c. High-gain antenna structure.* The existing *Mariner* Mars high-gain antenna reflector, feed support truss, feed, and attached RF coaxial cable were used for the *Mariner* Venus 67 mission. Trajectory geometry made it necessary to reposition the antenna at the planet encounter so as to maintain earth communication. This required that the antenna employ a new support structure on the rear of the reflector (Fig. IV-141). The coaxial cable from the antenna feed to the rear of the dish remained unchanged from the *Mariner IV* configuration; however, an additional section of hardline was formed along the back of the antenna to the vicinity of the deployment hinge. A new hardline cable was formed from the radio subsystem to the hinge area. The RF link was completed by a section (approximately 7 in. long) of 0.25-in. OD flexible coaxial cable across the hinge.

Orientation of the spacecraft for the *Mariner* Venus 67 mission placed the high-gain antenna on the shade side of the spacecraft. In this configuration, the antenna acts as a thermal radiator for the spacecraft and must be thermally isolated. As a result, the antenna was subjected to extremely low temperatures, on the order of −200°F. A series of tests was successfully conducted on the antenna to evaluate the effects of cold temperatures on the antenna both as a static unit and when subjected to deployment shock.

*d. Low-gain antenna structure.* The low-gain antenna design remained nearly unchanged from the *Mariner IV* configuration (Ref. 1). Although the ion chamber was removed, the instrument mounting bracket, which was bonded to the mast, was not removed because of the possibility that bracket removal might distort the wave guide. The ion chamber honeycomb shade was removed by peeling the foil face skin from the support bracket. The temperature control paint was removed from the ground plane to minimize heat losses from the antenna.

Because of its orientation on the spacecraft, the antenna was requalified to meet more stringent low-temperature vacuum requirements. As a result, a few of the Viton cable clamps, which were not properly bonded, became detached from the TA antenna during the low-temperature TA test. The clamps were rebonded after a test determined the cause of the problem. The problem did not recur.

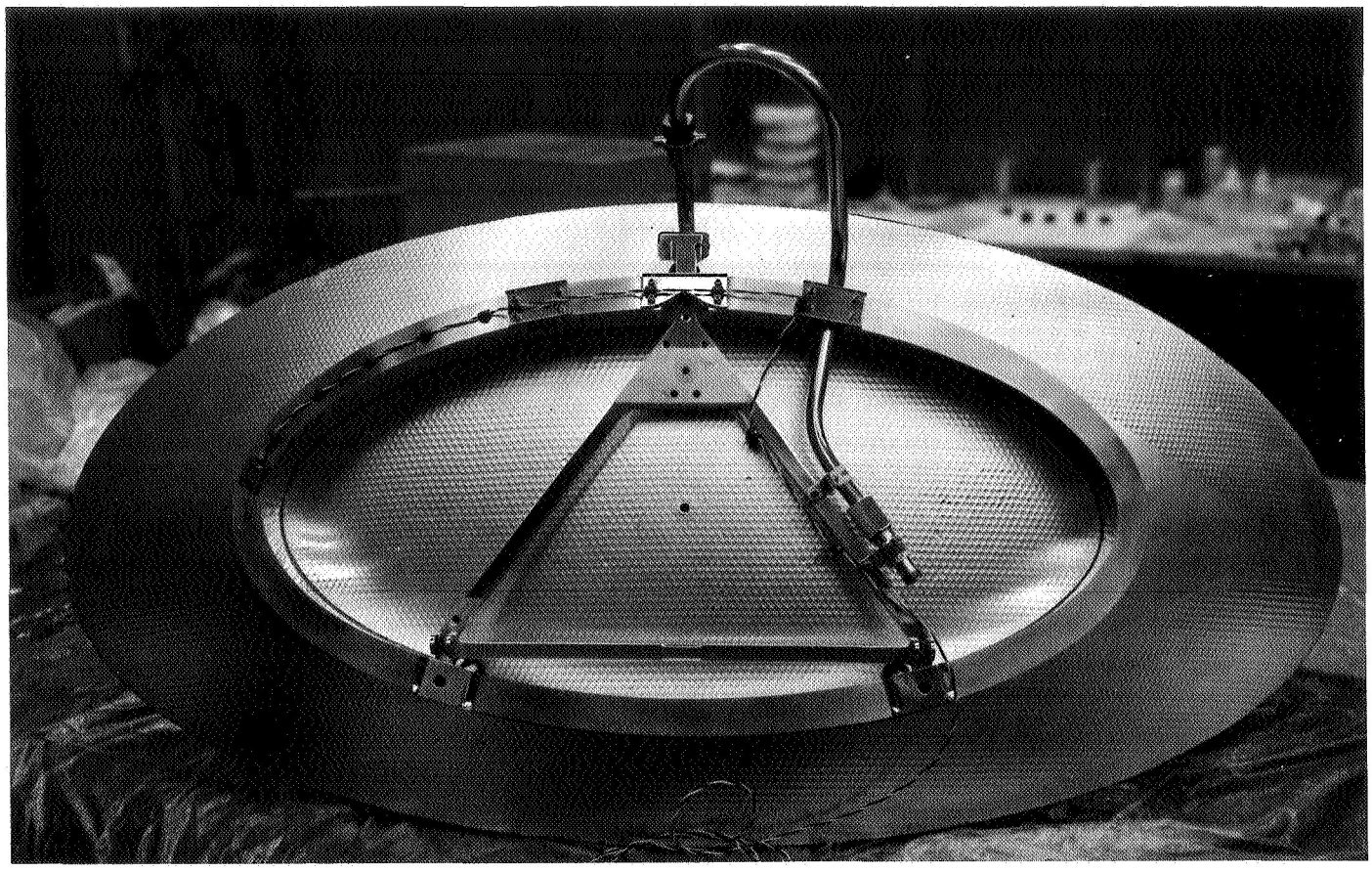


**Fig. IV-141. High-gain antenna structure**

The only structural problem encountered was the discovery of elongated mast-base mounting holes, which had resulted from *Mariner IV* testing. This problem was remedied by reaming the holes to a larger size and installing precision bushings.

*e. Solar panel structure.* The solar panel configuration remained as similar as possible to the *Mariner IV* configuration (Ref. 12). The *Mariner* Venus 67 approach was to minimize the number of changes in interfaces between the panel structure and interacting subsystems, while still satisfying the area requirements, temperature control requirements, and structural dynamics requirements of the Venus mission.

The *Mariner V* solar panels were mounted to the same hinge points as the *Mariner IV* panels, but were attached to each other at the tips during boost rather than to the antenna support structure as on *Mariner IV*. The panel's back-beam structure is the same as in *Mariner IV* except for two brackets at the tips which attach the tip dampers, and an added set of cross braces about halfway up the back beams. Retention of the *Mariner IV* back-beam structure made possible the utilization of the *Mariner IV* attitude control gas systems, solar panel cruise dampers, solar panel deployment hardware, and solar panel open switches without design modifications. The corrugated substrate aluminum foil thickness was increased to raise structural reliability and to reduce the possibility of handling damage. The corrugations are mounted on the side of the spars opposite that of the *Mariner IV* panel, because of the spacecraft's reversed solar orientation. This change resulted in some rerouting of panel power cabling and in moving the diode mounting surface to the side opposite that of *Mariner IV* panel back beam (see Section IV-F).

All adhesives used in the *Mariner IV* panel were requalified for use at the elevated temperatures to be encountered by *Mariner V*. Some of these adhesives are permanently degraded in strength after extensive aging

at temperatures greater than 300°F; however, high-temperature aging is of no real concern because it occurs in the flight sequence after the high stresses of launch.

A *Mariner IV* polymer that was not acceptable at elevated temperature was the SMP 62/63 dielectric used on the cell-mounting surface to electrically isolate the solar cells from the structure. High-temperature testing revealed drastic softening of that material, which made it unacceptable as a mechanical barrier for the Venus mission. An alternate material (EPON 956), which does not soften at high temperature, was selected. This alternate material was sprayed on the panel in the same way as the original dielectric. As the panel surface was sprayed, a layer of 2-mil glass cloth was "laid into" the resin, thereby placing a mechanical spacer between the solar cells and the panel surface. The glass cloth also simplified visual inspection of the dielectric thickness by presenting an unwet appearance when too little resin was used.

*f. Electronic assembly chassis.* The universal and flexible characteristics of the *Mariner IV* chassis and subchassis design demonstrated the soundness of the electronic packaging concept for *Mariner* Venus 67 applications. Changes required for *Mariner* Venus 67 were made with a minimum of difficulty (Table IV-39).

The *Mariner V* electronic assembly chassis were slightly modified versions of those used in *Mariner IV* (Ref. 12). The residual hardware from *Mariner* Mars 1964 was reinspected and all inserts that were damaged or failed the specification torque-out test were replaced with the longer capped inserts.

**Table IV-39. *Mariner* Venus 67 electronic chassis summary**

| Electrical assemblies | *Mariner* Mars 1964 | | New fabrication | |
|---|---|---|---|---|
| | Test[a] | Flight | Test | Flight |
| I | 3 | 2 | | |
| III | 5 | | 4 | 2 |
| IV | 3 | 2 | | |
| V | 5 | | | 3 |
| VI | 3 | 3 | | |
| VII | 3 | 2 | | 1 |
| VIII | 3 | 3 | | |
| Battery | 11 | | | 4 |
| Spare basic | | | | 1 |

[a] Includes STM, TCM, and DTM chassis.

The electronic assemblies and chassis were handled by continuing the same philosophy of handling fixtures and containers. The fixtures were modified to ensure a better fit in the containers. The inner containers were modified by sealing, providing a desiccant holder, and were provided with a harness that allowed hand carrying without danger of dropping the container.

Table IV-39 summarizes the *Mariner* Venus 67 electronic assembly chassis procurement, rework, and usage.

*g. PIPS substructure.* The propulsion system support structure was of the same design as *Mariner IV*. Existing flight spare frames were utilized and fitted with 1.5-deg tilt blocks to replace the 2-deg blocks optimum for thrust axis positioning on *Mariner IV*. Since the structure design originally allowed for tilt blocks from 0 to 4 deg, the slight change in angle did not constitute a design modification. No requalification testing was required.

***2. Fasteners.*** At the beginning of the *Mariner* Venus 67 program, a residual supply of structural fasteners was available from the *Mariner* Mars 1964 program. An inventory of these fasteners was taken and recorded. Also available from the *Mariner* Mars 1964 program was an installation hardware list that had been compiled from all drawing documentation used at the spacecraft assembly facility (SAF). These two lists were reviewed for predicted structural fastener requirements. Predictions were based on past experience (i.e., requirements for certain sizes and/or types of fasteners were established at higher levels based on greater usage). Requirements were also established from reviews of assembly drawings, particularly for new design requirements. Where insufficient quantities of hardware existed in the *Mariner* Mars 1964 inventory, new parts were ordered. A certain number of fasteners of various sizes, for which no requirements were currently known, was also ordered. This was done to make available a more complete range of fastener sizes that might satisfy unknown requirements.

Only one significant change was made in the type of fasteners used on *Mariner V*. The screws used to attach the subchassis to the chassis were changed from nonlocking to self-locking "long-lok" screws.

***3. Cabling subsystem.*** The design and fabrication of a cabling subsystem requires a certain knowledge of the

system elements (subsystems) that are to be interconnected. A complete knowledge of the external electrical and mechanical interfaces of each subsystem is required to establish the cable design. At least a partial knowledge of the internal circuitry is required to confirm the design and reconcile discrepancies that occur during its evolution. The modification of existing hardware to incorporate new design details requires the additional knowledge of the exact configuration and condition of the hardware to be changed.

There were two major differences between the *Mariner* Mars 1964 mission and the *Mariner* Venus 67 mission that caused virtually all of the cabling changes. These differences were in the science payload and the reversed sun attitude.

Changes in the science payload consisted of the deletion of four experiments, the addition of a new experiment, relocation of the electronics for three experiments, and a complete redesign of the science data automation subsystem. These changes caused the deletion of the lower science signal harness, a complete redesign of the upper science signal harness, science electronic assembly harness, and data automation system (DAS) interconnect harness, and minor change to the magnetometer signal harness and coaxial cables, and the plasma probe interconnect harness. The changes to the science payload made it necessary to modify the science portion of the power cabling and certain aspects of the data storage subsystem cabling.

The new "sun direction" and its effect on spacecraft geometry had a large mechanical effect on the cabling. Generally, this caused many spacecraft items which had been at the bottom of the spacecraft to be moved to the top. It also indirectly changed the superstructure and the method of latching the solar panels. Devices such as sun sensors, which had been interconnected by cabling on the lower portion of the bus, now had to be wired on the top, and vice versa.

The *Mariner* Venus 67 cabling design was established by modifying the known *Mariner IV* configuration in accordance with project-approved engineering change requirements (ECRs). All of the spacecraft design changes were reviewed for a possible effect on the cabling subsystem. Cabling changes were made as a result of:

(1) ECRs initiated by other areas which changed some aspect of the spacecraft system (either functional or physical).

(2) ECRs initiated by cabling personnel or other areas for a detailed change to a spacecraft cable, usually as required by item (1).

ECRs described in item (1) had the indirect effect of making cabling design changes necessary. These cabling changes were incorporated by authority of an ECR, which was usually written, incorporated into the hardware, and closed out by the cabling group. Changes that were merely functional (nomenclature), or that had a specifically desired solution, were initiated by the project engineering group. When a change required an involved analysis of several cables, the design was worked out by cabling personnel, reviewed with all affected areas, and then incorporated into the system by an ECR originated in the cabling area.

Approximately 45 ECRs that fall under item (1) were received. These changes resulted in a total of approximately 85 ECRs that fall under item (2), which changed some aspect of cables or cable installation.

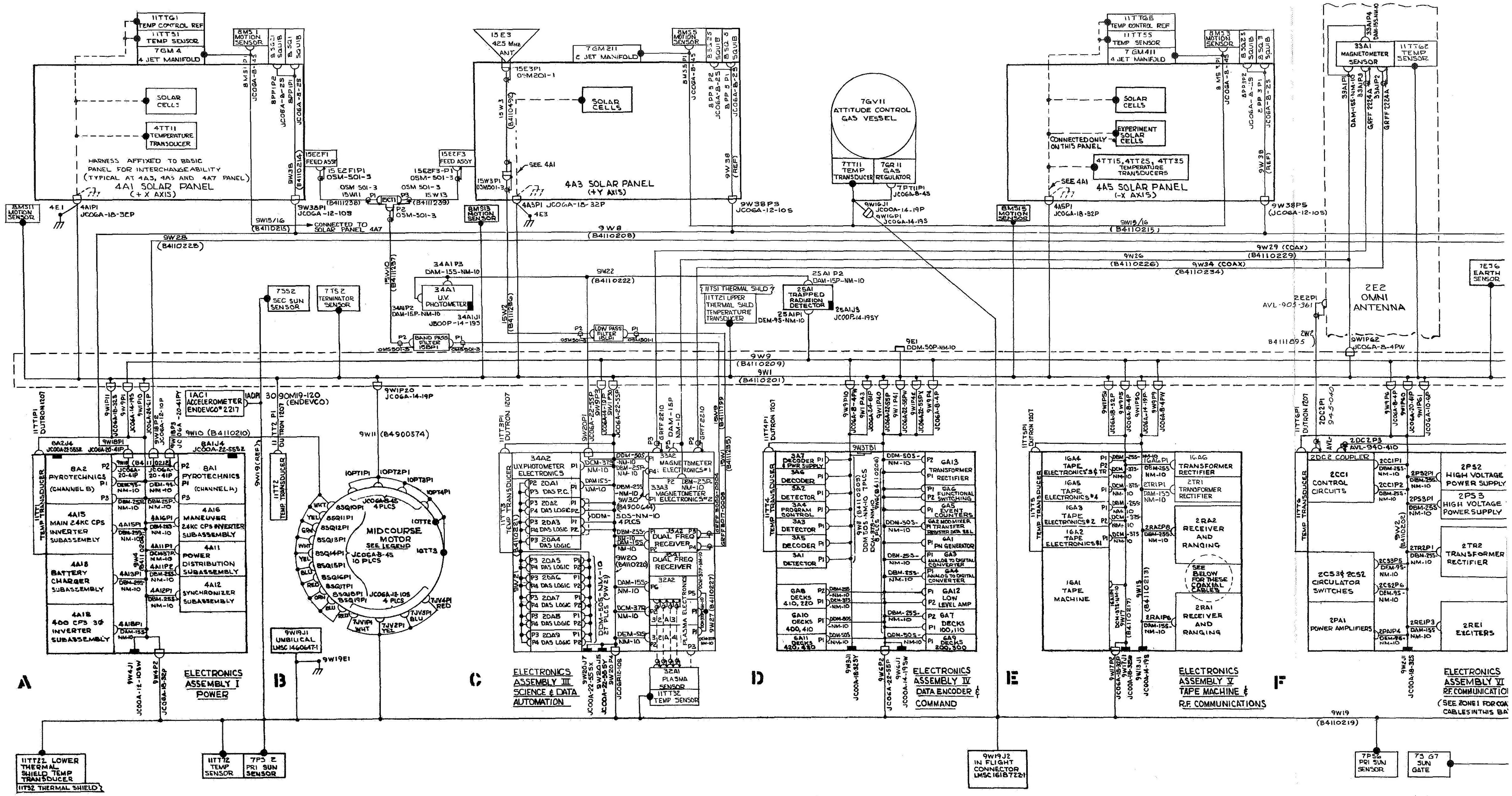
*a. Design description.* The general arrangement and design of the *Mariner* Venus 67 cabling is essentially the same as that of the *Mariner* Mars 1964. As shown in Fig. IV-142, the system includes 12 subsystem harnesses, 3 system ring harnesses, 8 pyrotechnic cables, 1 midcourse motor harness, 2 attitude control gas system cables, and 4 science signal cables. Three of these 30 cables are identical to the *Mariner* Mars 1964 hardware and 4 are new requirements. The remaining 23 items are modifications of the *Mariner* Mars 1964 design. Features of the system that are different from the *Mariner* Mars 1964 system are:

(1) A squib firing cable was added to each solar panel to accommodate the new tip latching. A connector interface, with the panel connector "hard mounted," was provided at the solar panel hinge line.

(2) The pin-puller motion sensor harness was deleted and this function performed by wiring in the gas system harness.

(3) The AC solar sail assemblies were removed from the ends of the solar panels, allowing the use of identical gas system harnesses and leaving unused wires for wiring of the motion sensors.

(4) Temperature control references (TCRs) were added to the ends of the panel and wired into the upper ring through circuitry added to the solar panel wiring for access to the telemetry channels formerly used by the absorptivity standard.



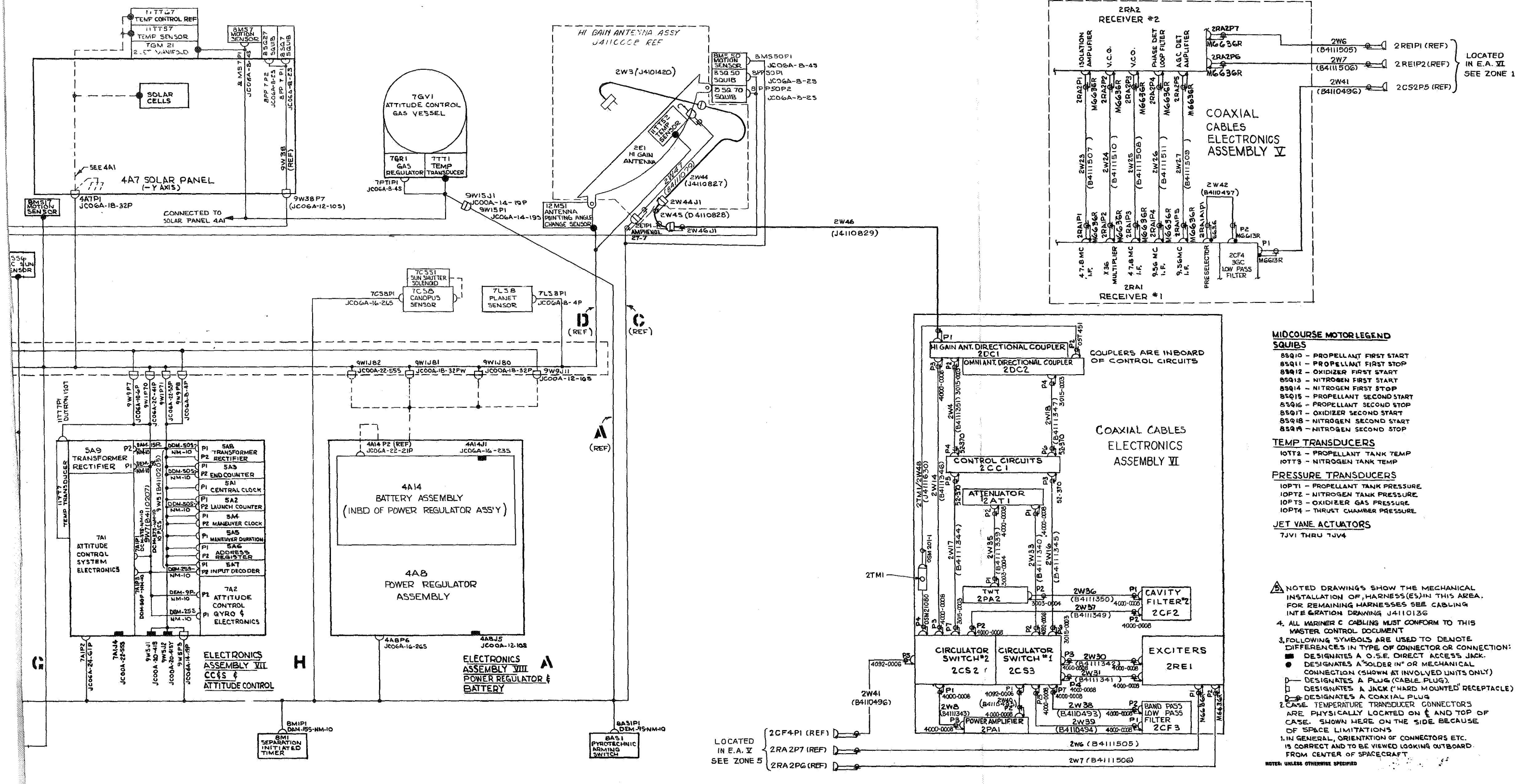

JPL TECHNICAL REPORT 32-1203

FOLDOUT FRAME 1

FOLDOUT FRAME 2

FOLDOUT FRAME 3

1




**MIDCOURSE MOTOR LEGEND**

**SQUIBS**

- 8SQ10 – PROPELLANT FIRST START
- 8SQ11 – PROPELLANT FIRST STOP
- 8SQ12 – OXIDIZER FIRST START
- 8SQ13 – NITROGEN FIRST START
- 8SQ14 – NITROGEN FIRST STOP
- 8SQ15 – PROPELLANT SECOND START
- 8SQ16 – PROPELLANT SECOND STOP
- 8SQ17 – OXIDIZER SECOND START
- 8SQ18 – NITROGEN SECOND START
- 8SQ19 – NITROGEN SECOND STOP

**TEMP TRANSDUCERS**

- 10TT2 – PROPELLANT TANK TEMP
- 10TT3 – NITROGEN TANK TEMP

**PRESSURE TRANSDUCERS**

- 10PT1 – PROPELLANT TANK PRESSURE
- 10PT2 – NITROGEN TANK PRESSURE
- 10PT3 – OXIDIZER GAS PRESSURE
- 10PT4 – THRUST CHAMBER PRESSURE

**JET VANE ACTUATORS**

- 7JV1 THRU 7JV4

5 NOTED DRAWINGS SHOW THE MECHANICAL INSTALLATION OF HARNESS(ES) IN THIS AREA. FOR REMAINING HARNESSES SEE CABLING INTEGRATION DRAWING J4110136

4. ALL MARINER C CABLING MUST CONFORM TO THIS MASTER CONTROL DOCUMENT
3. FOLLOWING SYMBOLS ARE USED TO DENOTE DIFFERENCES IN TYPE OF CONNECTOR OR CONNECTION:
   - ■ DESIGNATES A O.S.E. DIRECT ACCESS JACK.
   - ● DESIGNATES A "SOLDER IN" OR MECHANICAL CONNECTION (SHOWN AT INVOLVED UNITS ONLY)
   - ▷— DESIGNATES A PLUG (CABLE PLUG).
   - □ DESIGNATES A JACK ("HARD MOUNTED" RECEPTACLE)
   - ▷—◁ DESIGNATES A COAXIAL PLUG
2. CASE TEMPERATURE TRANSDUCER CONNECTORS ARE PHYSICALLY LOCATED ON ¢ AND TOP OF CASE. SHOWN HERE ON THE SIDE BECAUSE OF SPACE LIMITATIONS
1. IN GENERAL, ORIENTATION OF CONNECTORS ETC. IS CORRECT AND TO BE VIEWED LOOKING OUTBOARD FROM CENTER OF SPACECRAFT

NOTES: UNLESS OTHERWISE SPECIFIED

**Fig. IV-142. *Mariner V* cabling block diagram**

FOLDOUT FRAME 4

FOLDOUT FRAME 5

**Page intentionally left blank**

PRECEDING PAGE BLANK NOT FILMED.

(5) The scan platform and its cabling were deleted. The platform latch squib firing cable was rerouted to the top of the spacecraft to perform the antenna pointing angle change. The UV photometer was moved to the top of the spacecraft. Its functions were added to the upper science signal harness.

(6) Several items (Canopus sensor, sun gate, and sun sensors) were interchanged from top to bottom on the spacecraft. The ring harness wiring was rerouted and lengthened accordingly.

A third major change, not required by the mission change, was the addition of a 100% shield on all pyrotechnic firing lines. This was incorporated to satisfy range safety requirements. Although most of the pyrotechnic firing cables had to be replaced because of new routing, the shield requirement added the task of developing a technique for incorporating this feature into the design. A metal backshell developed for this application during the *Ranger* program was used. This backshell was used directly for the "singly" shielded cables at squib connectors, and was modified for use at the larger connectors where several shields had to be connected.

Full-circle shielding of several individual shields was accomplished by distributing the shield strands around a single large crimped ferrule. This ferrule was then potted into the metal backshell, and the shield strands clamped to the shell with a locking nut. Figure IV-143 shows various phases of the backshell assembly. Figure IV-144 shows a completed electronic assembly I pyrotechnic auxiliary harness with the flight version of the backshell.

Table IV-40 lists the *Mariner V* cables in the order of their difference from *Mariner IV*. Also shown is the percentage of the total number of connector pins in the harness that were involved in the reworked connectors. This tabulation assumes that the addition of one wire to a potted connector required the total replacement of that connector.

*b. Documentation.* The drawings that required changes from the *Mariner* Mars 1964 condition were given new drawing numbers, even if the hardware was not affected. An approved ECR was required for the

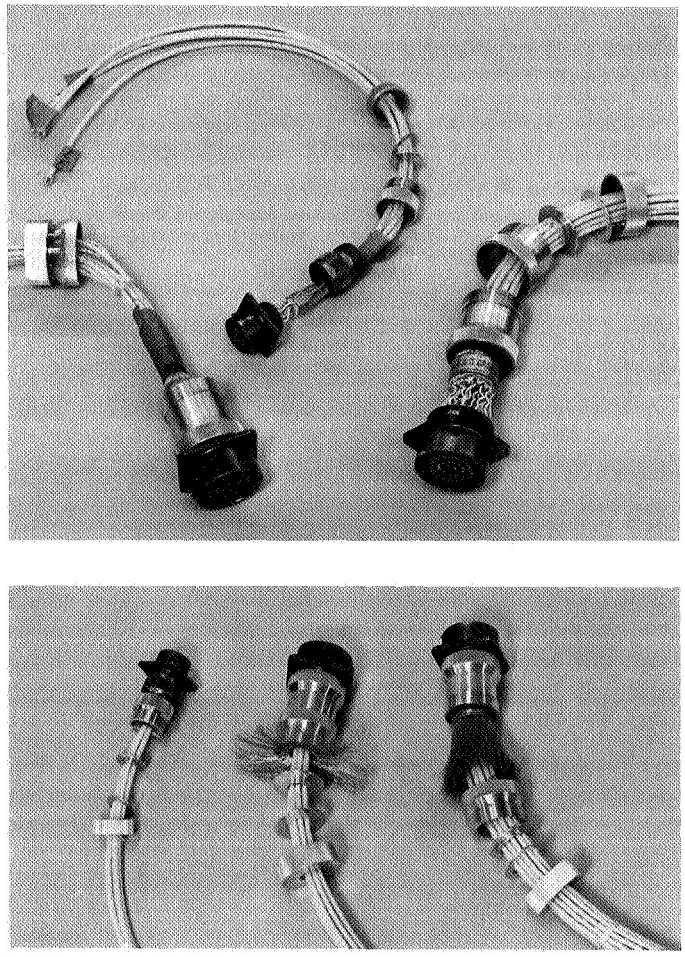


**Fig. IV-143. Pyrotechnic cabling shielding backshell assembly sequence**

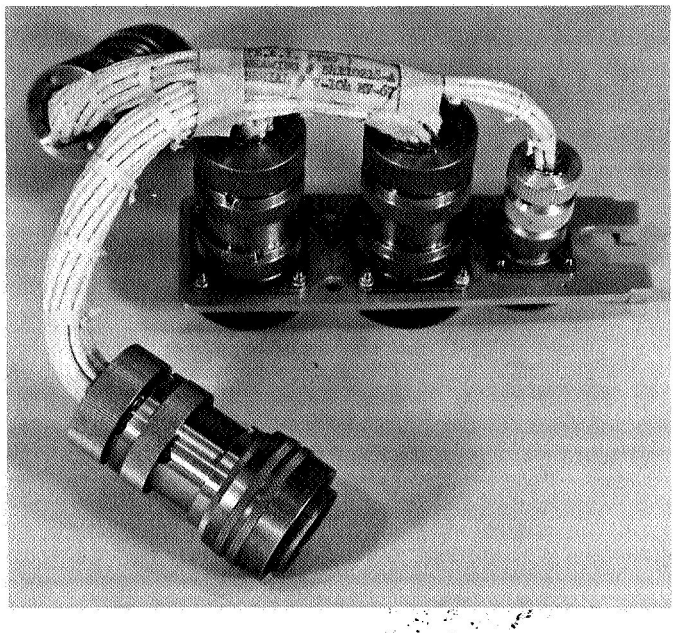


**Fig. IV-144. Electronic assembly I pyrotechnic harness**

Table IV-40. *Mariner IV to Mariner V* flight harness conversion comparison

| No. | Item | Percent change | | Extent of change | Quantity replaced | Quantity modified |
|---|---|---|---|---|---|---|
| | | Connections | Circuits | | | |
| 9W21 | Science (data automation system) | 100 | 100 | total | 6 | 0 |
| 9W20 | Science (electronic assembly III) | 100 | 100 | total | 4 | 0 |
| 9W22 | Science (upper) | 100 | 100 | total | 7 | 0 |
| 9W26 | Science (mag) | 80 | 82 | total | 3 | 1 |
| 9W27 | Science (plasma) | 67 | 70 | total | 5 | 0 |
| 9W17 | Tape machine | 100 | 100 | total | 3 | 1 |
| 9W8 | Pyrotechnic (S/P) | 100 | 100 | total | 4 | 0 |
| 9W10 | Pyrotechnic (PIPS) | 100 | 100 | total | 3 | 0 |
| 9W18 | Pyrotechnic (electronic assembly I) | 100 | 100 | total | 5 | 0 |
| 9W28 | Pyrotechnic (antenna pointing angle change) | 100 | 100 | total | 4 | 0 |
| 9W38 | Pyrotechnic S/P inter | 100 | 100 | total | 20 | 0 |
| 9W1 | Upper ring | 88 | 94 | major | 0 | 3 |
| 9W4 | Power (electronic assembly I) | 69 | 63 | total | 4 | 0 |
| 9W9 | Power (upper ring) | 38 | 64 | total | 3 | 0 |
| 9W6 | Data encoder (electronic assembly IV) | 50 | 68 | major | 0 | 5 |
| 9W19 | Lower ring | 47 | 62 | major | 0 | 2 |
| 9W3 | Command (electronic assembly IV) | 40 | 46 | major | 3 | 2 |
| 9W15/16 | Gas system | 34 | 24 | minor | 0 | 4 |
| 9W13 | Communications (electronic assembly V) | 34 | 39 | minor | 1 | 4 |
| 9W2 | Communications (electronic assembly VI) | 23 | 17 | minor | 2 | 3 |
| 9W7 | Attitude control (electronic assembly VII) | 20 | 21 | minor | 0 | 2 |
| 9W5 | CC&S (electronic assembly VII) | 0 | 0 | none | 0 | 2 |
| 9W11 | PIPS instrumentation | 0 | 0 | none | 3 | 0 |
| 9W30 | Magnetometer interconnect | 0 | 0 | none | 0 | 2 |
| 9W29 | Mag coax | 50 | 50 | major | 0 | 4 |
| 9W34 | Mag coax | 50 | 50 | major | 0 | 4 |

release of each new drawing. Since ECRs were received from several sources and over a considerable length of time, there was a period when the design of some cables was quite fluid. This was handled by withholding the release of some of the larger drawings until a majority of the changes were known, and then incorporating as many of the changes as possible into the first release.

Most of the cable wiring drawings were made from vellums which were reproducible copies of the *Mariner* Mars 1964 vellums. These reproducibles were modified to become *Mariner* Venus 67 masters by changing the drawing number and the face of the drawing as necessary. No official "modification" or "make from" type of drawings were made for cables.

The cable installation drawings, of which three were in the *Mariner* Mars 1964 system, were completely redrawn and combined into one drawing for *Mariner* Venus 67. This combination was accomplished to simplify the documentation of areas where several cables utilized the same installation hardware.

*c. Fabrication.* A total of approximately 120 cables was used for test, the flight support, and flight spacecraft. About two-thirds of these cables were fabricated especially for this program. The remainder had been originally fabricated for *Mariner* Mars 1964, and were modified to some extent for *Mariner* Venus 67. In general, the modification from *Mariner* Mars 1964 to *Mariner* Venus 67 involved approximately 70% of the cabling subsystem connectors, which carry approximately 72% of the spacecraft circuits.

The decision of whether to modify existing hardware was based on many factors, the most demanding of

which were: (1) the extent of the change, (2) availability and condition of hardware to be modified, (3) complexity of the harness, and (4) delivery schedules.

Each cable was reviewed on the basis of these factors to determine the best approach. Cables that were reworked were given a complete visual and electrical inspection to determine their condition prior to modification.

Rework of existing hardware was handled differently from new fabrication. The primary difference was in the working drawing used in the shop. Minor rework was performed to a drawing of the existing harness, with changes marked in red on the drawing. For major rework, an informal drawing (e.g., Fig. IV-145) was made showing the "before" and "after" conditions of areas which required changes. These manufacturing drawings were provided to the shop along with a released drawing of the new harness configuration. In all cases, the released drawing was used for inspection.

Eleven of the spacecraft cables required design changes that could be modified from the *Mariner* Mars 1964 hardware. In five of these cables, the rework involved from 50 to 90% of the harness connectors or circuits, and was considered a major modification. The other six cables required rework of 20 to 50% of the harness connectors or circuits. Typically, the major rework required from 30 to 60% of "new fabrication" manhours,

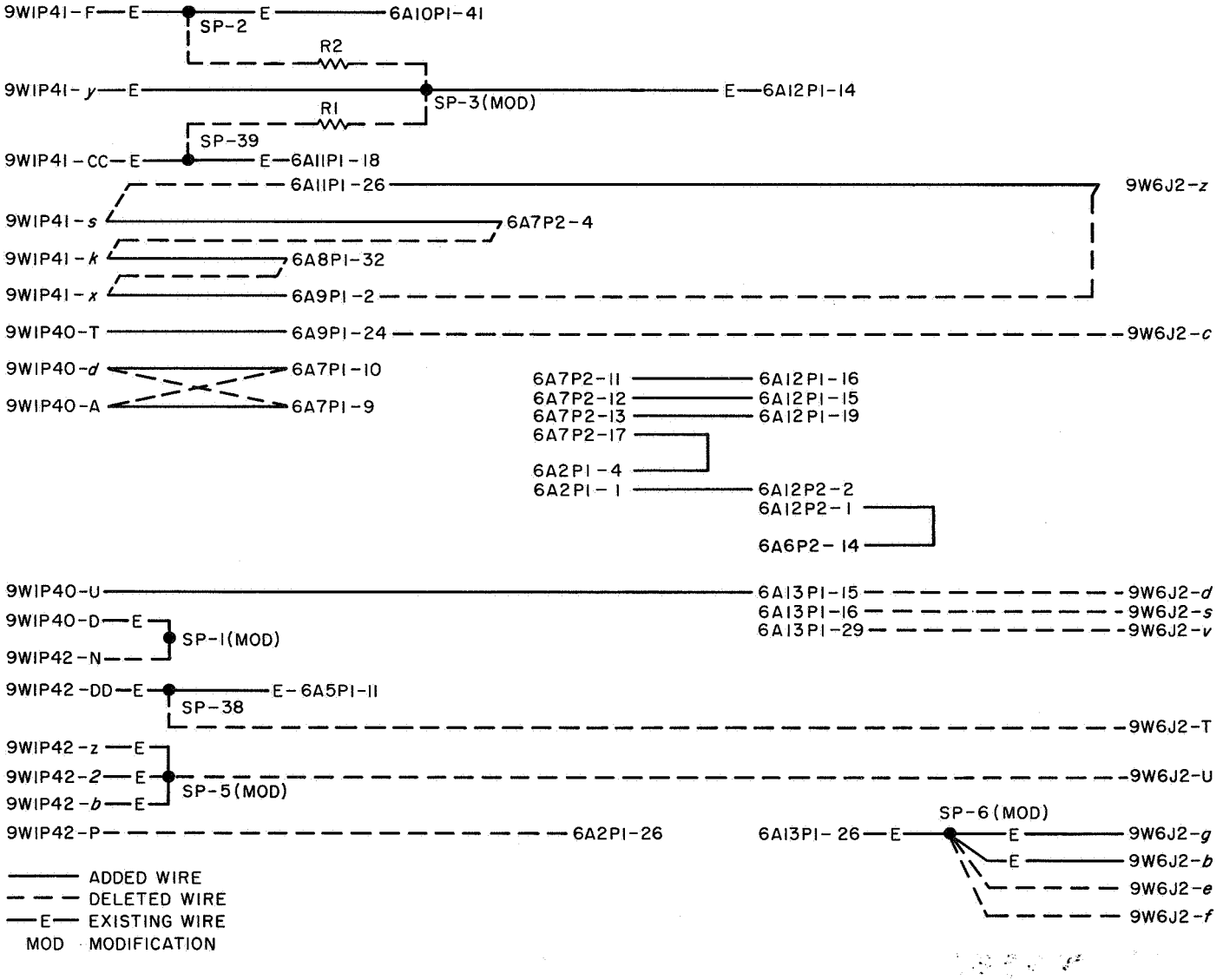



**Fig. IV-145. Data encoder harness (9W6) modification**

and minor rework required from 10 to 50%. The percentages for minor rework appear high because even small jobs require certain fixed fabrication times.

Sixteen spacecraft cables (all power, all pyrotechnic, and most science cabling) required so much modification that use of existing hardware was not attempted. These cables were replaced, using the same fabrication technique developed for *Mariner* Mars 1964. The system cables were made on the spacecraft cabling mockup, and smaller cables were made on modified *Mariner* Mars 1964 wiring fixtures. Four of the harnesses did not require the spacecraft mockup and, theoretically, could be procured from sources other than JPL. Lack of time prevented this in most cases, however, and only two flight cables for the *Mariner* Venus 67 program were obtained from sources outside JPL.

A total of 33 electronic assembly harnesses wiring fixtures were fabricated for the *Mariner* Mars 1964 program. From four to six fixtures were made for each of the six electronic assembly configurations. Two fixtures for each bay were left in the *Mariner* Mars 1964 configuration for reinspection of the harnesses prior to rework. The remaining fixtures were modified to the *Mariner* Venus 67 configuration. The fixture modification usually consisted of replacing or relocating connector mounting brackets. Because the capability for such changes was designed into the fixture, the fixture rework presented no problems. The science Bay III harness wiring fixture was the most seriously affected by system redesign. Figures IV-146 and IV-147 show the *Mariner IV* and *Mariner V* versions of the electronic assembly III science wiring fixture.

The details of the routing and installation of all system (ring) and peripheral cables were developed on the spacecraft cabling mockup. Mounting hole locations, insert sizes, etc., were established on the mockup, coordinated with the spacecraft integration group, and incorporated into the flight equipment.

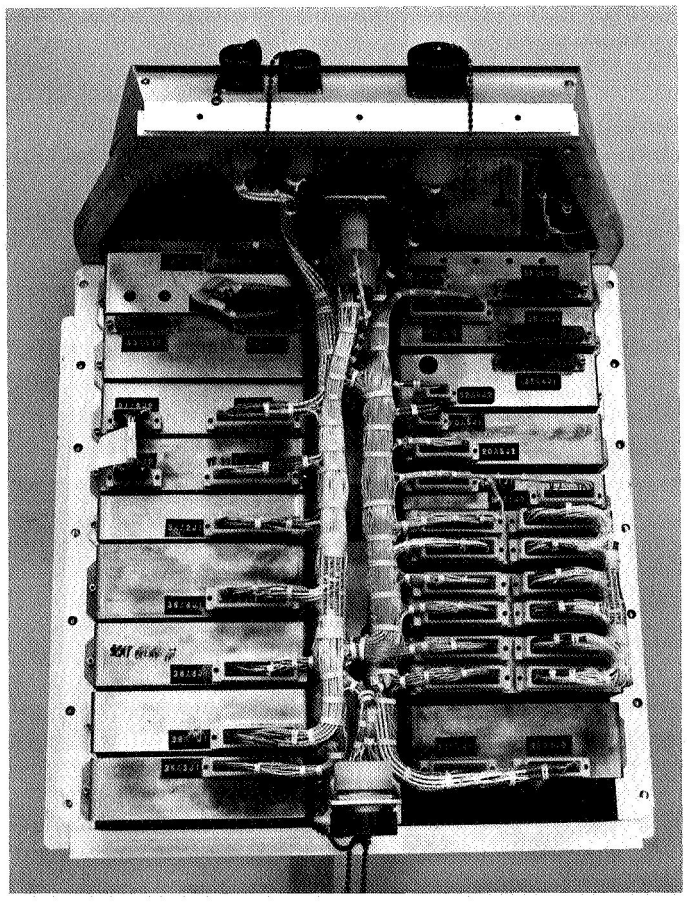


**Fig. IV-146. *Mariner IV* electronic assembly III science harness wiring fixture**

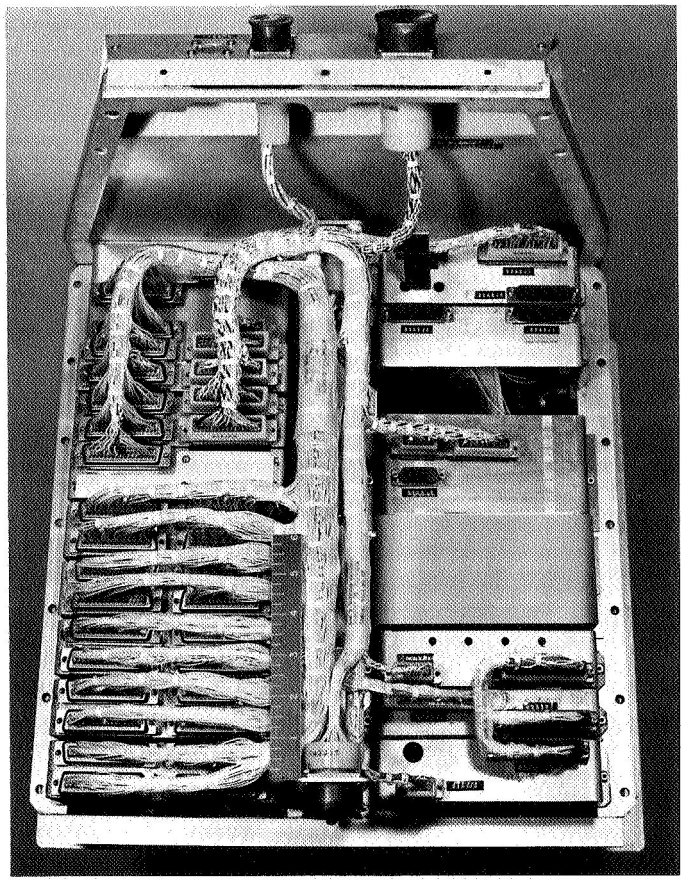


**Fig. IV-147. *Mariner V* electronic assembly III science harness wiring fixture**

All processes used in fabrication of the flight cables were the same as on *Mariner* Mars 1964, with the exception of the soldering procedure. The soldering process used on *Mariner* Mars 1964 was modified to include tinning of the inside of the connector solder cups. This was done to improve inspectability and provide more reliable solder joints on the contacts of the rectangular connectors procured for *Mariner* Venus 67.

*d. Cabling materials.* The wire used on *Mariner* Venus 67 was of the same basic construction as that used on *Mariner IV*.

Limited quantities of *Mariner IV* wire still on hand were rescreened to the new specification and used in early harness fabrication while new wire was being procured. All newly procured hookup wire was 100% screened after receipt from the supplier. Approximately 15% of the wire was rejected. Typical discrepancies included a spiral discoloration referred to as "barberpole," foreign matter inclusions in the insulation, and work-hardened conductors.

The connectors used on *Mariner V* were the same as those used on *Mariner IV*, even though the documents used on new procurements were revisions of the *Mariner IV* documents. The availability of connectors from the residual stock was an important factor in meeting the *Mariner* Venus 67 development and fabrication schedules.

Residual stock of all circular and rectangular connectors, except the "socket" configuration of rectangular connectors, was rescreened and used on *Mariner* Venus 67. The rectangular socket connectors used on *Mariner IV* were not installed in rework of *Mariner* Venus 67 hardware because of a known problem with the socket contact (Ref. 1). Only the *Mariner* Venus 67 procurements in this configuration were used in new installations.

New D series of rectangular connectors for *Mariner* Venus 67 were procured. No verified electrical failures occurred in the new connectors during *Mariner* Venus 67 operations. The new connectors were much more difficult to solder, however, and the JPL soldering process was changed to improve solderability. These changes helped the situation; however, high-rejection rate and longer fabrication times continued throughout the program.

The circular connectors remaining from *Mariner IV* were reinspected. These connectors were used to meet flight requirements on *Mariner* Venus 67, except for approximately 1.5% of these connectors, which were scrapped, and approximately 5%, which were downgraded to non-flight classifications.

The upper ring harness trough and other mechanical harness support hardware were residual *Mariner IV* hardware, modified as required to change connector size or location. The titanium screws and special nuts used in *Mariner* Mars 1964 were reused as available. Appropriate substitution of A-286 stainless steel was made and documented when necessary.

All cable clamps, ty-raps, insulation sleeving, lacing tape, and other fabrication materials used were the same as on *Mariner IV*. All nylon and silicone-covered cable clamps underwent thermal–vacuum cleaning prior to installation on the flight spacecraft, in accordance with a project requirement to prevent contamination of the spacecraft and of the space simulator facility.

*e. Problems.* The major problems in *Mariner* Venus 67 cabling occurred in areas where new designs, processes, or techniques were being used. These problems are discussed in the following paragraphs.

The design of the DAS was such that the connector density was much greater than had been previously used. Pin utilization was also much higher than normal. The complexity of this harness created problems in fabrication, installation, and inspection techniques.

System testing on the DFR experiment revealed a crosstalk problem that was solved by changing the DAS interconnect harness (9W21) and science electronic assembly harness (9W20). The following changes were made after initial harness fabrication to reduce noise outputs from the DAS subsystem into the science cabling:

(1) The entire DAS harness (9W21) was shielded by wrapping it with double-sided aluminized Mylar tape.

(2) Ferrite beads were installed on all of the wires in the science harness connectors (9W20) which enter the DAS subassemblies.

Although these changes (Fig. IV-148) produced the desired electrical results, they required new techniques

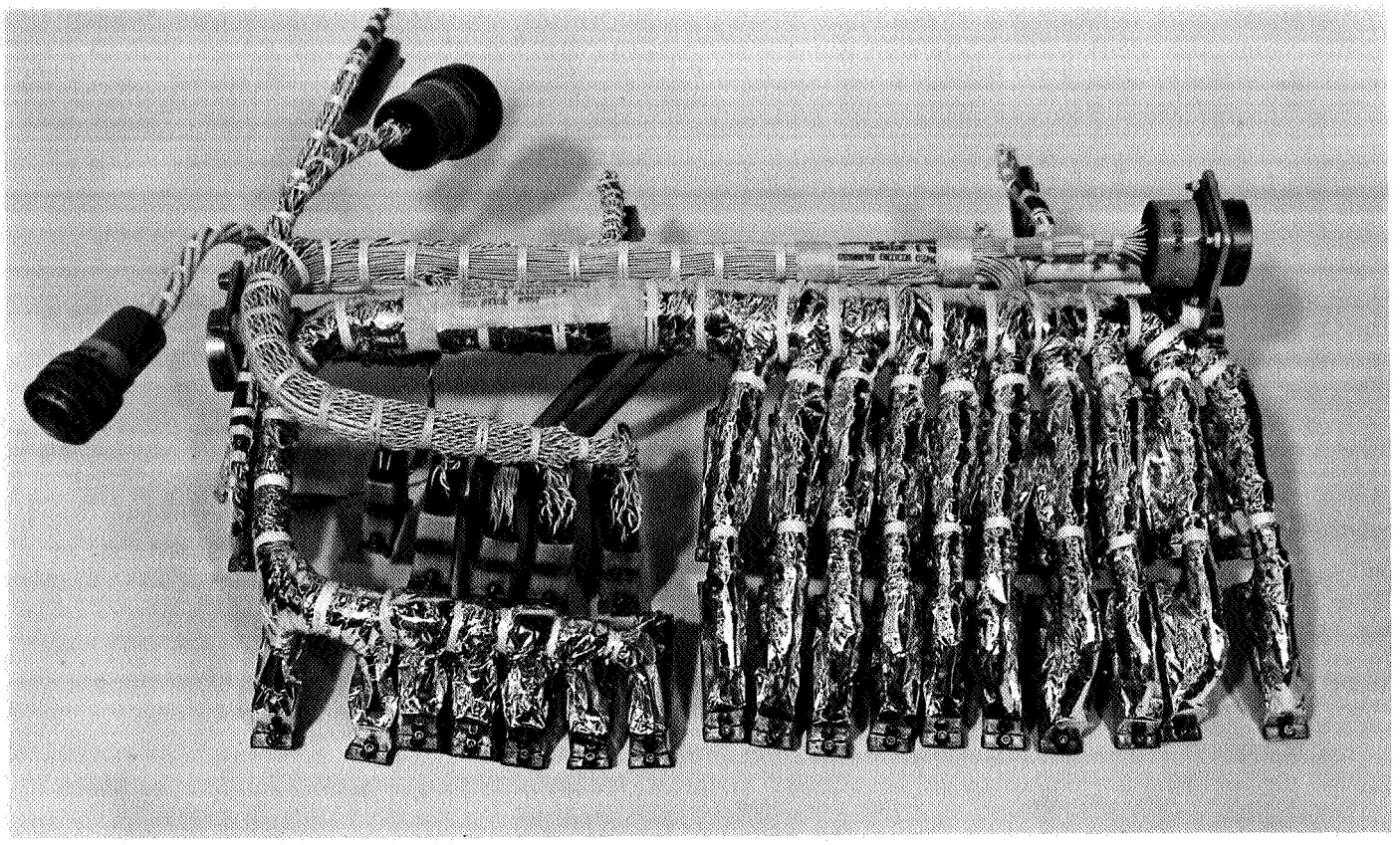


**Fig. IV-148. D&S interconnect harness assembly (9W20)**

that had not been proven in flight and additional development tasks.

The wrapping of the DAS harness (9W21) was of particular concern, because it decreased the harness flexibility even further. This condition could have been improved if the harness had been designed and fabricated with this requirement. The reduced flexibility aggravated the harness installation and caused concern about the possibility of open circuit in the connectors. It was concluded that the harness stiffness was undesirable but acceptable.

*4. Temperature control subsystem design.* Technically, the temperature control subsystem is comprised of the hardware necessary for maintaining acceptable spacecraft temperatures throughout flight. In reality, temperature control reaches beyond this definition as a "cosmetic" subsystem into the details of spacecraft configuration, structural design, and component placement. Tradeoffs are required at a system level when electronic subsystems have competing temperature requirements. In these latter senses, then, temperature control is a spacecraft system function implemented partially within the temperature control subsystem proper, and partially within the spacecraft structure and configuration.

The major changes to be accommodated by the temperature control subsystem were the reversal of the sun–spacecraft orientation and the higher solar intensities encountered. Several thermal design changes were required; however, the basic approach and much of the hardware was unchanged.

The *Mariner V* temperature control subsystem was functionally similar to that of *Mariner IV*. Some design changes were required, however, because of the nature of the mission and the "upside down" configuration. The solar intensity for this mission was approximately 125 W/ft$^2$ at launch, 248 W/ft$^2$ at Venus encounter, and 386 W/ft$^2$ at perihelion. The *Mariner IV* range was from 133 to 53 W/ft$^2$. This extreme variation in solar intensity made effective solar isolation an absolute requirement for spacecraft survival. The necessary improvements in isolation were provided by two design changes. First, the solar input to the bus by infrared

(IR) radiation from the solar panels was reduced below *Mariner IV* levels by eliminating 27 in. of the inboard celled area of the panels. Second, the efficiency of the solar shield was greatly improved by deploying a sun shade over known leaks.

The reversal of the solar vector shaded most of the science and appendages. With the exception of the helium magnetometer and the antennas, these components were conductively coupled to the bus. The helium magnetometer required approximately 2 W of electrical heating to remain above the lower temperature limit.

*a. Description of major changes.* The most significant single change in the *Mariner IV* thermal design was the addition of a deployable sun shade. This shade protected the bus from sun heat inputs by shading three areas of potential solar heating:

(1) Components mounted on the lower ring which functionally must penetrate the lower shield. Included are the pyrotechnic arming switch (PAS), separation-initiated timer (SIT), adapter attach feet, in-flight disconnect, and pushoff pads.

(2) Components which extend outboard of the bay faces. Included are the midcourse motor thermal can, Canopus tracker baffle box, trapped radiation detector (TRD), planet sensor, louver cages, and the umbilical connector.

(3) Thermal shorts in the lower thermal shield caused by seams, edge attachments, support structure pressure, and other compromises necessary for fabrication.

It was estimated that approximately 15 in.$^2$ of black absorbing area would be contributed by items in the first category, or approximately 26 W input at Venus. An input this size is not serious except for localized overheating problems. Of more serious concern were the potentially much larger leaks in the latter two categories. Uncompromised multiple-layered radiation shields are virtually perfect insulators; however, this perfection is never realized in practice. Furthermore, shielding efficiency can only be estimated until tests are run on the specific configuration in question. This uncertainty stems from imperfect understanding of the mechanism of the leaks (e.g., through a stitched seam) and from the smallness of the individual leaks.

The sun shade, in combination with the lower shield, virtually eliminated solar inputs to the bus except from solar panels, primary sun sensors, and the solar plasma probe, which, because of their functions, had to be located in the sun. This shield eliminates conduction to the bus through shielding leaks, as noted above in item (3), and by shading items otherwise exposed or imperfectly shaded as noted above in items (1) and (2). The resulting benefits are listed below:

(1) Reduction of variable heat input to bus, hence reduction of earth-to-Venus temperature rise.

(2) Prevention of local hot spots in lower ring, thus reduction of temperature gradients and improved heat-sinking ability for sun sensors.

(3) Reduction of design effort by elimination of separate shades over midcourse motor, etc., and by relaxation of isolation requirements at the periphery of lower thermal shield.

(4) Elimination of the need to redesign SIT to take higher temperatures.

(5) Reduction of stray light.

(6) Reduction in thermal design uncertainty.

On the other hand, care was required in the shade design to eliminate or minimize the effects of the following potential problems:

(1) Launch vehicle hang-up caused by in-shroud deployment.

(2) Sun sensor interference when deployed, nondeployed, or failed.

(3) Non-deployment, causing out-of-tolerance flight temperatures.

In addition, the incorporation of the sun shade required relocation of the primary sun sensors on pedestals to provide adequate view angles.

The solar intensity for each of the *Mariner* missions is given below:

| Spacecraft | Solar intensity, W/ft$^2$ |
|---|---|
| *Mariner II* | 130 at earth<br>250 at Venus<br>260 at perihelion |
| *Mariner IV* | 133 at earth<br>53 at aphelion |
| *Mariner V* | 125 at earth<br>248 at Venus<br>386 at perihelion |

*Mariners II* and *IV* each had the equivalent of one black square foot of absorbing area. Inspection of the above solar intensity changes will show that this figure had to be halved for *Mariner V* to reproduce the earth-to-encounter temperature change of *Mariner IV*.

The radiant flux falling on an electronic bay face from the corresponding solar panel is directly proportional to the bay-to-panel form factor and to the solar intensity. For *Mariner V*, the solar intensity at encounter is approximately twice the maximum *Mariner IV* level, and the irradiation of the bay face would have scaled up proportionately had the *Mariner IV* panel design been retained. The removal of side shielding to cool the bay would have aggravated the problem by exposing more area to the variable radiation from the panels. To reduce the bay face-to-panel form factor, the celled area of the solar panel was cut back from the bus. The effect of this cutback is shown in Fig. IV-149. The irradiation of the near bay from each solar panel is only approximately 4 W/ft² at encounter.

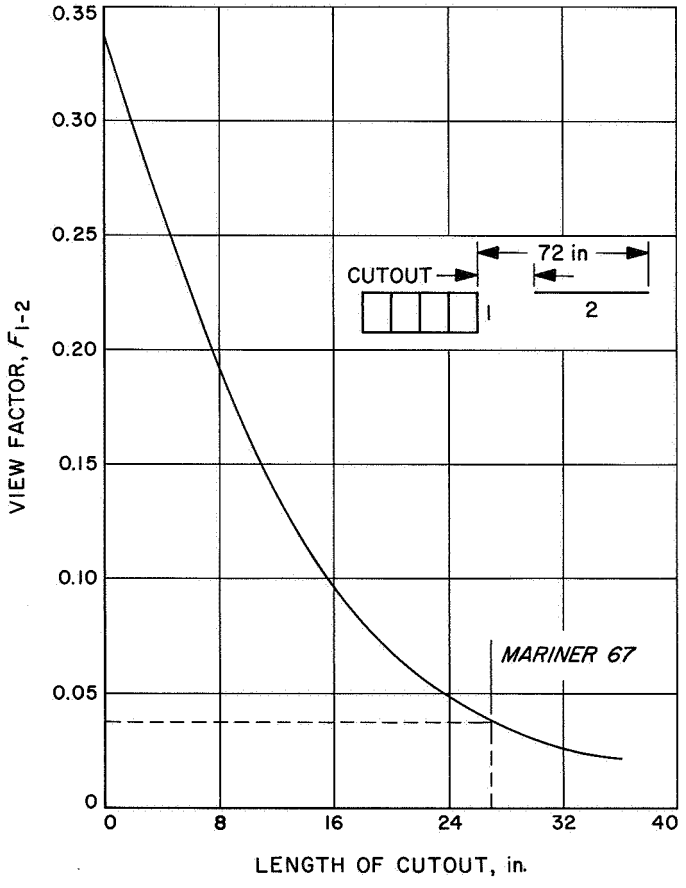



**Fig. IV-149. View factor — bay face to solar panel**

*b. Design evolution and test experience.* In all *Mariner* projects, thermal tests have constituted an integral part of the design process. Tests of the TCM and flight spacecraft are expected to result in refinements of the thermal design. Thus, it is appropriate to examine the design evolution as a consequence of the results of the more important thermal tests.

An important result of *Mariner IV* experience was the recognition that the environment in which the spacecraft was tested was imperfectly understood. An initial radiometer comparison test was performed in the 10-ft simulator that, together with earlier data obtained for *Surveyor*, checked the calibration of solar simulator monitoring devices and yielded information on the level of background radiation.

Preflight temperature predictions for both *Mariners II* and *IV* were incorrect because of solar heating test inputs which differed from flight. For the Venus probe (*Mariner II*), this error was nearly disastrous. For *Mariner V*, efforts were made both to minimize this input and to understand its effects. During the TCM testing, two modes were run in which the solar simulator lights were turned off and the TCM heater power was increased to reproduce the temperature profiles for the earth cruise mode and the gyroscopes on encounter mode. The difference in internal power with the lights off is equivalent to the solar heating input. Excluding the conductive input from the sun sensors and the radiative input from solar panels, the solar input at earth was 18.5 W and at Venus, 36 W. These inputs are small compared to the 150- to 250-W bus internal power dissipation.

With no solar input and the spacecraft's lowest cruise mode power, the midcourse propellant tank just dropped to freezing. A solar intensity increase from 250 to 286 W/ft² caused only a 1.3°F average increase in bus temperature at Venus. An extrapolation to perihelion showed that bus survival was not a problem.

The thermal effects of a catastrophic sun shade failure were investigated in TCM test III. The shade was completely stowed, and earth cruise and encounter modes were run. Analysis of the test data indicated that the bus absorbed an incremental 150 W at Venus with the shade stowed. This heat input raised the bus temperature 32.5°F at encounter and caused an undesirably high, but probably tolerable, temperature level.

*Mariner V* is thermally a power-dependent spacecraft. Therefore, this parameter is of interest in design studies and in the evaluation of the effect of simulator error sources. For these reasons, tests were performed in which internal power was reduced 20% at earth and increased 20% at Venus. The power variation produced a negligible effect for the Venus "power up" case, but brought the midcourse propellant near freezing for the earth "power down" mode. Thus, the power margin at the cold end is approximately 30 W. The hot end margin was deduced by a "louvers open" mode in which internal power was increased to force all louvers open and drive temperatures near the upper limits. The power increment above the gyroscopes on encounter level was approximately 125 W. The spacecraft operates near its lower power limit to provide margin for midcourse heating and solar heating after encounter (Fig. IV-150).

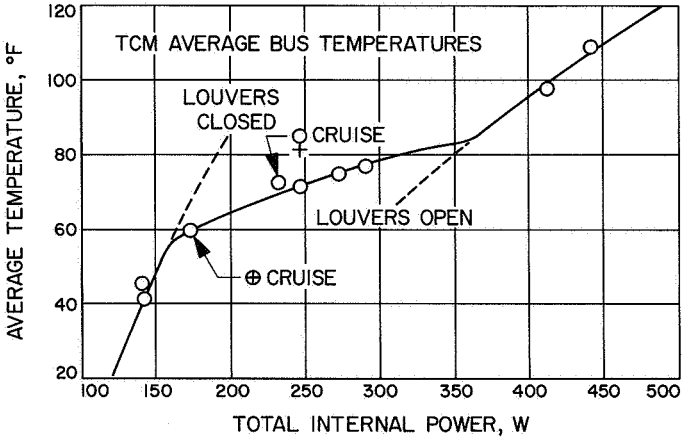



**Fig. IV-150. Average bus temperature vs total power**

The timely upgrading of the solar simulator to produce a Venus sun for this test, combined with the demonstrated thermal margins, satisfied most of the test objectives which were to have been met in a second TCM test. The second test was therefore cancelled. A radiometer calibration test was scheduled to resolve a 15% discrepancy in the readings of the two test radiometers at Venus intensity. The resolution of this anomaly was not crucial to the use and interpretation of the test data because the spacecraft had demonstrated an insensitivity to solar intensity.

During the TCM test in the 10-ft space simulator, the Eppley and absolute cavity (cone) radiometers, used to monitor solar intensity, differed by approximately 15% at Venus levels. Although the cone radiometer had been believed to be the more accurate instrument, it was observed that the ratio of the measured intensity to the lower thermal shield absolute temperature to the fourth power was not constant over the intensity range of the test. To resolve this anomaly, and to increase the assurance that the flight spacecraft would be tested at the correct solar intensities, a radiometer comparison test was conducted in the 10-ft space simulator.

The lower thermal shield data were in considerably better agreement with the cone during this test than during the TCM test. Also, there had been scatter in shield temperatures for the TCM test at 125 W/ft² intensity. This, combined with the agreement among plates, TCRs, and the shield in the comparison test, suggested that the comparison test data were more reliable. It was therefore concluded that the TCM test levels, as measured by the cone, were substantially correct, and the cone radiometer was used to set intensity levels for the flight spacecraft tests.

*c. M67-1 space simulator test. Mariner* 67-1 underwent system tests in the JPL 10-ft space simulator. Two test sequences were performed: a system test (Part I) and a thermal test (Part II). Part I of the test was intended to exercise the spacecraft system test configuration in a space environment. The thermal test was accomplished with minimum cables and operational support equipment (OSE) so as to provide a flight-like thermal configuration.

The test objective for Part II was to verify the ability of the temperature control subsystem (TCS) to maintain spacecraft temperatures within allowable bounds for all combinations of operating mode and flight environment. Secondary objectives were to check the accuracy of flight temperature transducers and to obtain more accurate flight temperature predictions. The M67-1 bus was initially 7°F cooler than the TCM; the addition of 0.5 ft² of polished aluminum side shields reduced this difference to 2°F. The temperature difference was caused by a high power estimate for use in the TCM test. For the earth cruise mode, a total of 158 W was dissipated in the TCM bus; the corresponding value measured on M67-1 was 141 W.

All test objectives were met. Satisfactory operation at the coolest and warmest modes was demonstrated, and adequate margins of safety were shown to exist.

*d. M67-2 space simulator test.* The system test in the 10-ft space simulator was similar to that performed with M67-1. The average bus temperature was approximately 2°F cooler than M67-1, which was within

the expected temperature variation from spacecraft to spacecraft.

This test, together with the corresponding M67-1 test, resulted in the following conclusions:

(1) The thermal design was adequate for all anticipated combinations of spacecraft operating mode and flight environment.

(2) All flight telemetry temperatures were within design accuracy.

(3) OSE installed in the simulator during the system portion of the test (Part I) had only a minor influence on bus temperature.

(4) Discrepancies (6 to 12%) still existed between the various intensity monitors used, although this disagreement was less for M67-2 than that observed during the M67-1 test.

(5) M67-2 had thermal characteristics that were similar to those of M67-1.

*e. Analysis.* An essential adjunct to the above test program was calculations based on an analytical thermal model of the spacecraft. This model was useful in initial design studies and for the prediction of temperature transients for launch, midcourse, and encounter. Early in the program, an 80-node computer model was devised. After the TCM test, the model was revised to agree with test data, and minor corrections and modifications were later made to suit the needs of the particular calculations being performed. This feedback of test data for correcting the computer model is a valuable experience for the thermal designer, for it forces a reconciliation of preconceived notions with reality. In the case of *Mariner V*, the original model agreed reasonably well with TCM test data (usually within 10°F), but the louvers appeared to be less effective than previous test data had indicated. If time and manpower had allowed, further tests on the TCM louvers could have been performed to confirm or disprove the theories advanced to explain this behavior. It is significant, however, that the anomaly would have passed unnoticed if the computer model had not been available.

*f. Thermal shields and sun shade.* The temperature control shielding for *Mariner V* contained approximately the same number of components as *Mariner IV*; however, all the multilayer thermal shield blankets were revised.

The removal of the scan platform and relocation of science instruments necessitated a configuration change in the upper and lower thermal shield blankets. The solar intensity of the Venus mission required a material change to the outer layer of the sun-exposed thermal shield blanket to reduce the surface temperature. A deployable sun shade was mounted on the sunlit side of the spacecraft to reduce the solar input to the bus by shading the peripheral hardware on the spacecraft from direct sunlight.

Additional shields required for the Venus mission included four attitude control jet shields, one TRD shield, and one magnetometer shield. The polished aluminum side shields used were *Mariner IV* spares with minor revisions.

The *Mariner V* shield (Fig. IV-151) is in the shade during the flight except for a possible short exposure to the sun during a midcourse maneuver. The sunlit shield on *Mariner IV* was covered with an outer layer of black Dacron cloth. The black cloth was replaced with 1-mil Teflon, aluminized on one side with the Teflon side out. The interior of the blanket was composed of multiple layers of aluminized Mylar. The shield area and seams were reduced by not covering the high-gain antenna superstructure. The blanket was secured to the spacecraft around the periphery by a nylon hook and pile closure strip. *Mariner IV* used metal attach angles sewed to the blanket. The *Mariner V* attachment method reduced the installation time and the probability of damage during installation of the upper shield late in the spacecraft assembly sequence (i.e., after final systems test and solar panel installation). The addition of the UV photometer, and the relocation of the Canopus sensor and planet sensor to the upper ring on the bus, offset the simplification to the blanket by forcing the removal of the *Mariner IV* cosmic dust detector and

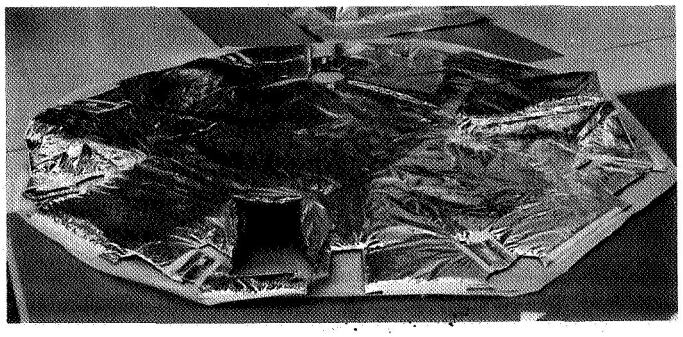


**Fig. IV-151. Upper thermal shield blanket**

absorptivity standard, and the relocation of the plasma probe.

The lower thermal blanket (Fig. IV-152) remained much the same as *Mariner IV* in configuration except for the revisions that were necessary to delete the scan platform and relocate the plasma probe. The total effect was a cleaner, more efficient shield with fewer seams. The lower shield on *Mariner V* is in the sun for the total mission vs shade on *Mariner IV*. Both *Mariners IV* and *V* used 1-mil aluminized Teflon with the Teflon side out for the outer layer. Multilayer Mylar super insulation is used in the rest of the blanket.

The aluminized films used for the *Mariners IV* and *V* thermal blankets were a combination of Mylar and Teflon. A difference between the two projects was the use of a pre-dimpled aluminized Mylar for *Mariner V*. This material was first investigated because it provided a greater thickness with the same number of layers in comparison with the hand-crinkled material used on *Mariner IV*. Although the lower shield (sunlit) on *Mariner V* did not require as many seams to construct and was, therefore, a more efficient shield, the thermal resistance had to be high, known, and repeatable. The new material was selected because it could withstand handling and preloading upon installation and still retain a known minimum thickness which would yield the desired properties. It was especially desirable to improve the properties of the shield because of the nearly disastrous solar dependence encountered during the *Mariner II* Venus mission.

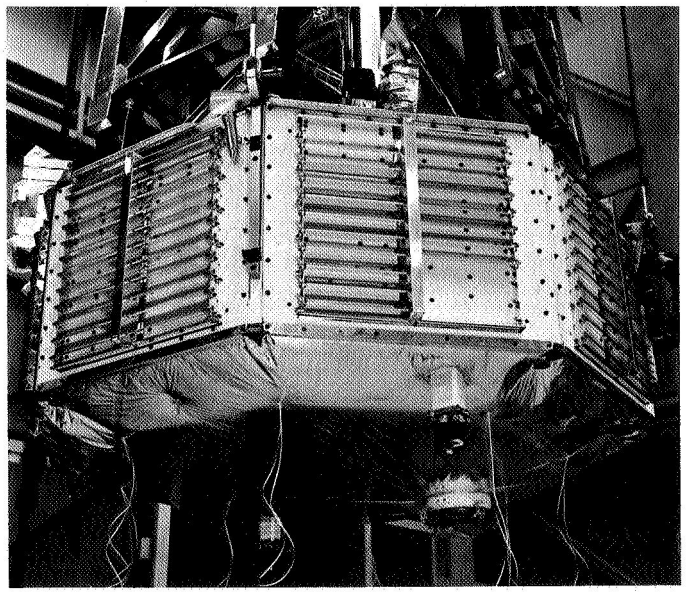


**Fig. IV-152. Lower thermal shield blanket**

The gross difference in thermal environment of a mission to Venus rather than Mars dictated a major change in the sunlit outer layer of the thermal shield (multilayer blanket).

An $\alpha/\varepsilon$ ratio significantly lower than the black fabric used on *Mariner IV* was required to avoid exceeding the upper temperature limit of materials in the shield.

Of the films available, Mylar and Tedlar were known to darken under solar ultraviolet irradiation; Kapton and FEP Teflon have been reported to be acceptably stable. Kapton has a higher initial solar absorptance, its availability in requisite widths was uncertain, and metallizing techniques were less proven at the time. Aluminized FEP Teflon, type A, has been more extensively tested and was successfully used on *Mariner II*, *Ranger*, *Surveyor*, and *Mariner IV*. This film can be aluminized; although adhesion is not high, it is suitable for use as a shield layer. The film is available in standard thickness from 0.5 to 20 mils and the aluminized second surface mirror yields emittance values between 0.5 and 0.8 mil, increasing with thickness and $\alpha_s$ values in the range of 0.12 to 0.20 mil.

Minimum temperatures and minimum degradation would be expected for the thicker film. However, the design was fairly insensitive to outer layer temperature. Therefore, the 1-mil film was selected for the blanket and sun shade for mechanical reasons (deployment and handling).

The pre-dimpled Mylar is 0.5 mil thick. The Mylar is processed with heat to form a permanent dimple in the material. Several depths of dimpled material were investigated. Material in the 3 to 6% "take up" had the best mechanical properties. Material in 5 to 6% "take up" had the best unit loading capability, while that in the 3 to 4% retained its configuration best. For comparison, a shield of nine layers (alternating dimpled and flat) material was 0.62 to 0.75 in. thick, while a 30-layer shield of hand-wrinkled 0.25-mil Mylar was approximately 0.35 in. thick. In one test, after compressing the two samples to approximately a 0.062-in. thickness, the pre-dimpled material returned to its original height while the hand-wrinkled material returned only to 50% of its original height. The unit loading to compress the samples was approximately ten times more for pre-dimpled samples.

The pre-dimpled and the flat 0.5-mil Mylar materials used were aluminized on both sides. This eliminated inspection during fabrication to determine which side was aluminized. The 0.5-mil material was much easier to handle during the blanket fabrication although difficulties were encountered in finishing operations because of the thickness. The blankets were fabricated of alternating layers of pre-dimpled and flat Mylar sheets. The pre-dimpled construction also improved the venting capability of the blankets.

Although detailed thermal properties, such as effective conductivity or emittance of the thermal blankets as used on the spacecraft, were not evaluated, some conclusions can be made from spacecraft test data. Tests show that the hand-wrinkled shield conductivity changes more rapidly with compressive loading than the pre-dimpled shield. The mean apparent thermal conductivity of various types of pre-dimpled super insulation shields ranges between $10^{-4}$ to $5 \times 10^{-3}$ $\frac{\text{Btu in.}}{\text{h-ft}^2 \cdot ^\circ\text{F}}$, which was more than adequate for *Mariner* Venus 67 requirements. Therefore, the final selection among these various types of materials was based on minimizing the effect of unit loading on effective conductivity.

The pattern and detail fabrication techniques developed for the *Mariner* Mars 1964 program were used for the *Mariner* Venus 67 shield construction. An area requiring close attention was the limited capability of the paper pattern to contour as the thicker and more flexible finished thermal shield would. In many cases, a small sample of the actual blanket material was used to arrive at the proper flat pattern necessary for fabrication.

*g. Deployable sun shade description.* The sun shade design and concept was new. It was designed to reduce the solar input to the bus by shading the spacecraft–*Agena* interface hardware and spacecraft equipment outside the octagon periphery. Because of its configuration resulting from the necessary shadow pattern, the shade had to be retracted and stowed during the boost phase so as to clear the *Agena* adapter and separation hardware (Fig. IV-153). When deployed by means of lanyards attached to the solar panels, the shade forms an octagonal-shaped awning approximately 10 in. wide and 1900 in.$^2$ total area on the periphery of the spacecraft on the sunlit side. A 4-in. diam clearance hole was provided at Bay IV so that the X-ray tube of the trapped radiation detector could have an unobstructed view of the sun. In the deployed position (Fig. IV-154), the shade extends approximately 3 in. beyond the edge of the bus in Bays I, III, V, and VII, and 5 in. beyond the edge of the bus in Bays II, IV, VI, and VIII. Although not required by the equipment shadow pattern, the shade was symmetrical to balance solar pressure and simplify construction.

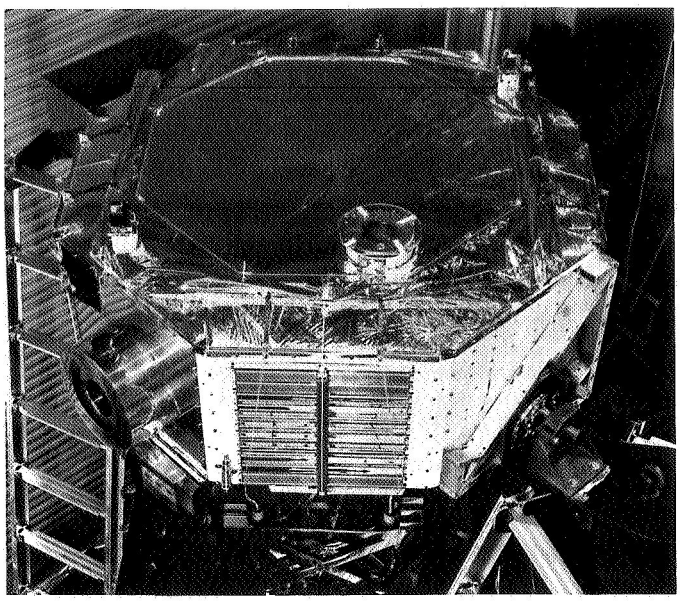


**Fig. IV-153. Deployable sun shade — stowed**

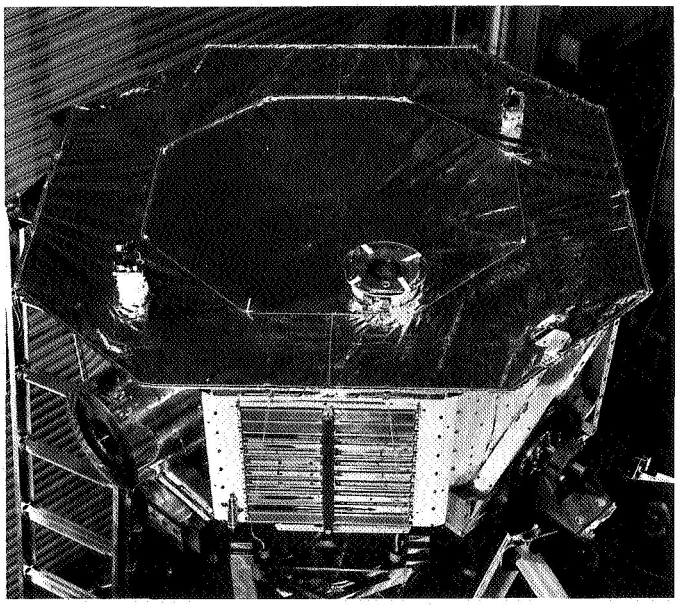


**Fig. IV-154. Deployable sun shade — extended**

The shade was constructed of a single sheet of 1-mil Teflon aluminized on one side. An octagonal tubular support ring was sewn to the shade at the inner perimeter. The outside edge of the shade was hemmed to contain the four support tubes and a Dacron cord around the shade outer perimeter. All of the shade edges were reenforced with a glass-backed aluminum tape to prevent tearing. Eight pieces of nylon hook (0.625 × 1 in.) were sewn to the Teflon. When the shade was stowed, these eight pieces mated with nylon hook retainers that prevented the shade from slipping from its stowed position.

The deployment and support of the shade was performed by eight spiral-wound spring assemblies located in pairs that attached to shade support tubes. Each spring assembly contained a nonmagnetic, high-strength Elgiloy steel spring mounted on an adjustable center arbor. Prior to installation on the spacecraft, the spring assemblies were pre-set to a torque of 1 in.-lb ± 2 in.-oz. The torque increased to 2 in.-lb when the spring was rotated 150 deg to fix the shade in the stowed position. Each of four shade support tubes, to which the shade was attached, was allowed to deploy independently by the relaxation of a Dacron release lanyard attached through a series of eyelets to the solar panel in that bay. The sun shade was deployed at a rate limited by the solar panel deployment. Full deployment of the shade occurred when the solar panel was three-quarters deployed. The shirttail release occurred during the shade deployment when the shade perimeter cord tightened between the two adjacent support tubes. Full deployment was achieved when the perimeter Dacron cord was taut.

The release lanyard was a multi-filament untreated Dacron cord with a breaking strength of approximately 20 lb. Prior to installation, the lanyards were tested and pre-stretched by applying 14 lb tension for 1 h at 70°F. The lanyards were then tied to the center of each shade support tube and the knot spot-bonded.

*h. Attitude control jet shields.* Shields were required to shade each of the four attitude control gas jet assemblies that were mounted at the ends of the panels. The shields each consisted of (1) a multilayer blanket that contained a clearance hole for the pitch or yaw jet exhausts, and (2) a sheet metal blanket support structure that was mounted by sandwiching it between the solar panel and the manifold.

*i. Trapped radiation detector shield.* This shield, intended to shade the instrument detectors, was similar to the attitude control jet shields. The shield support structure was polished aluminum sheet metal with the multilayer thermal shield attached to the sunlit side. The support was attached directly to the instrument mounting brackets.

*j. Magnetometer shield.* A multilayer shield with stable thermal properties was required to protect the coils of the helium magnetometer. The vacuum-deposited aluminum on the ball had degraded and exhibited variations in surface emittance that could not be tolerated in the temperature control of the instrument. A shield was constructed from nine layers of aluminized Mylar to cover the ball.

*k. Side shields.* The same side shielding approach used for *Mariner IV* was used on *Mariner V*. In particular, thin-gage aluminum (0.016 in.) shield elements were used. These elements were bolted to the sides of the octagon as required. No new hardware was required because sufficient *Mariner IV* side shields were available.

*l. Shade and shield testing.* The thermal shields and sun shades were subjected to a complete series of qualification and acceptance tests. In addition to the flight vibration and space simulator tests, the hardware was qualified during the STM vibration tests and TCM space simulator tests. The blanket tests included launch pressure profile tests in a vacuum chamber. The deployable sun shade was subjected to a series of deployment tests on the TCM, STM, and flight spacecraft, a long-term storage test, adapter hangup tests (in the event of a lanyard failure prior to separation from the booster), and stray light reflectance tests.

Although several problems were encountered during the development of the shielding, especially the sun shade, they were capably solved and eliminated.

*m. Louvers.* The louvers that remained from the *Mariner* Mars 1964 program were used for *Mariner* Venus 67. The only change to the louvers was the inclusion of sun-shade lanyard guides. These guides were bonded to the upper and lower corners of the bimetal housing cover to prevent the lanyards from becoming entangled in the louvers. The *Mariner IV* louver design is discussed in Ref. 1. The louvers were disassembled, cleaned, inspected, and subjected to the thermal portion of the FA test prior to redelivery to the SAF.

The *Mariner* Venus 67 louvers were mounted in the same bays as in *Mariner IV*. Because of the questionable nature of the *Mariner IV* louver position indicator telemetry, these measurements were omitted.

*n. Temperature control references.* The purpose of the TCRs is to compare preflight estimates of solar thermal input (solar intensity × absorptance) to thermal input in actual flight. The TCRs have provided a means of comparison between the results obtained with solar simulation and those encountered in space.

The equilibrium heat balance equation for a sun-dependent item in space can be written:

$$S\alpha A_S + P = \varepsilon A_\varepsilon \sigma T^4$$

where

$S$ = solar intensity

$\alpha$ = absorptance

$\varepsilon$ = emittance

$\sigma$ = Stefan-Boltzmann constant

$A_s$ = sunlit area

$A_\varepsilon$ = emitting area

$T$ = absolute temperature

$P$ = internal power

This is a grossly simplified equation for spacecraft temperature control; however, it illustrates the significance of solar input.

The TCR measures the temperature of a sun-dependent item for which $P$ (internal power) is zero, and thus, because the geometrics are known, allows the quantity $S\ \alpha/\varepsilon$ to be computed. For purposes of spacecraft temperature control, the three terms ($S$, $\alpha$, and $\varepsilon$) are used often. Separate measurements of these terms are subject to sizable uncertainties. Although it is impossible to separate the three quantities in the TCR results, the net product $S\ \alpha/\varepsilon$ is of significant interest to the spacecraft thermal designer.

The TCR also determines the variation in solar absorptance of painted surfaces with time in space.

The TCRs consist of three assemblies, one located at the tip of each of three solar panels. (One assembly is not located on the $+Y$ panel because of potential interactions with the DFR UHF antenna which is located there.) Each assembly is identical except for the coating used on the sunlit side and the sensor range selection.

Physically, each TCR (Fig. IV-155) consists of a 3-in.-diam sensor area, a tee section fiberglass epoxy laminate support, and an aluminum bracket which attaches to the attitude control gas jet manifold at the tip of the solar panel.

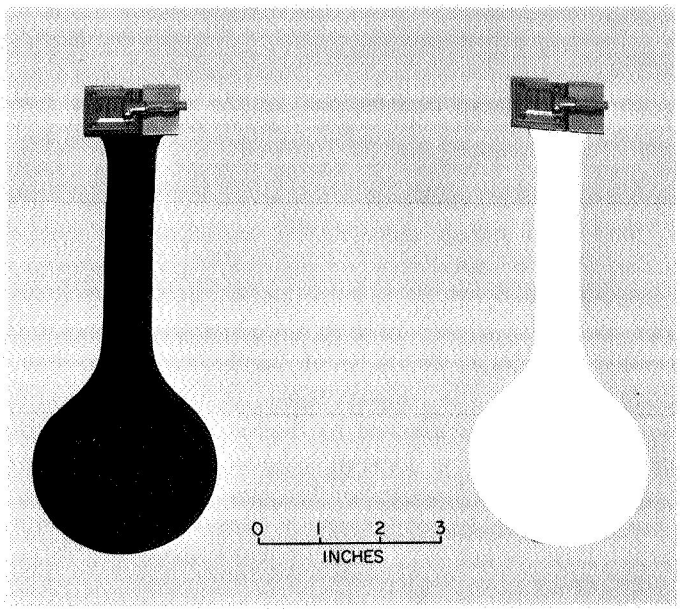



**Fig. IV-155. Temperature control references**

A standard flight transducer is mounted on the TCR bracket to measure the temperature of the attitude control manifold.

The sensor is encapsulated in the center of the 3-in.-diam area at the outer end. This sensor is a platinum resistance thermometer consisting of three separate coils. The sensors are identical and the coils are used in combinations of series arrangements to provide the proper temperature range for the coatings used. These combinations are shown in Fig. IV-156.

Spacecraft engineering temperature measurements utilize 500-Ω transducers with appropriate scaling resistors in the data encoder to provide a range of 500 to 600 Ω that the encoder can sense.

The TCR sensor resistance values were selected to be compatible with standard data encoder mechanization.

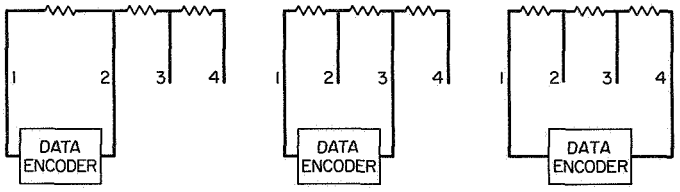



**Fig. IV-156. Temperature control reference sensor schematic**

For maximum sensitivity and accuracy, the TCRs present the range of 500 to 600 Ω without scaling resistors to the data encoder.

Encapsulated in the center of the sensor area with the sensor is a 2-in.-diam copper mesh disc that provides temperature uniformity over the center of the sensor area.

The remaining 0.5-in. annulus, having low conductivity and the same coatings, acts as a passive "guard." Similarly, the tee section support acts as a guard for the sensor leads that are encapsulated in it and run down to terminals adjacent to the assembly bracket.

Thermally, each TCR approximates a thin, flat, infinite plate normal to the sun, radiating from both sides. The effects of conduction losses and of thermal gradients through the assembly have been determined analytically and experimentally. Appropriate corrections for these effects are used for data reduction.

The TCR location at the ends of the solar panels results in negligible radiation coupling to the spacecraft.

Sensor resistance ranges were such that each sensor was near 500 Ω in the vicinity of earth and increased as the solar intensity increased during the mission. The requirements for data early in the mission and for maximum sensitivity will result in resistance values exceeding 600 Ω before perihelion.

The TCR surfaces are coated to provide engineering information of significance to spacecraft thermal designers. The shaded sides of all assemblies are painted black for similar response to simulator background radiation and for handling and maintenance simplicity. The coatings selected for the sunlit surfaces were:

(1) Flat black.
(2) S-13 white.
(3) S-13 (modified) white.

The black paint is CAT-A-LAC[7] flat black epoxy, a widely used spacecraft coating whose properties have been as well established as possible with current radiation measurements technology. It was used on, and its space stability apparently verified by, the *Mariner IV* absorptivity standard. Results provide a comparison to space simulator total absorbed energy with that in space, independent of spectral distribution mismatch.

The S-13 white is the best usable engineering spacecraft white paint available at this time. This paint will provide a basis for energy absorption by white surfaces as well as engineering data on the change in absorptance with time in space. S-13 is a zinc oxide pigmented methyl silicone paint. It is used on some continuously sunlit surfaces on *Mariner* Venus 67.

The modified S-13 is an experimental white that is similar to S-13, but is formulated with a treated zinc oxide for improved stability. It was undergoing laboratory development and evaluation at the time of the *Mariner V* mission and the results were expected to be of engineering interest for future missions.

*o. Flight results.* With minor exceptions, the in-flight performance of the temperature control subsystem from launch through midcourse was very close to nominal. Launch transients were mild, and midcourse transients were normal for the maneuver performed. Cruise temperatures within the bus typically ran 1 to 2°F above predictions; external items range from 10°F cool to 25°F warm, in relation to predicted levels. These discrepancies are within expected limits and are considerably less than those observed on previous flights.

The nearness of bus temperatures to expected values clearly indicates that the temperature control hardware is performing as designed and that the sun shade deployed properly.

Results from the TCR during the early portion of the *Mariner V* mission verified equipment design, implementation and sensitivity. These same results raised some questions about the performance of coatings in space and laboratory testing.

*Launch.* Because the spacecraft was in telemetry mode II at launch and there were time gaps in received data during the parking orbit, relatively few temperature data are available prior to sun acquisition. All the

[7]Finch Paint and Chemical Company, Torrance, California.

data observed were entirely normal, however. Very little temperature change was observed in the bus during ascent and parking orbit. Temperatures at sun acquisition were on the cool side of nominal, but within expected tolerances. Cooling of external items occurred during boost because of gas expansion under the shroud, then further cooling occurred while the spacecraft was in the earth's shadow. No extreme transients were observed, however, and all spacecraft components remained well within allowable limits.

*Cruise temperatures.* All components operated well within design limits. The average bus temperature was 2°F above the predicted level during pre-Canopus acquisition cruise and 1°F above the predicted level after Canopus acquisition. No bus temperature was more than 4°F from prediction during pre-Canopus acquisition, nor more than 2°F from prediction after Canopus acquisition.

As expected, temperatures external to the bus showed larger deviations from predictions. A brief discussion for these channels is presented in Table IV-41.

First TCR data were obtained approximately 30 min after sun acquisition. Subsequent decrease in data number (DN) values during the following 3 h indicated a thermal input from the earth early in the mission. (A similar effect was noted for the solar panels which faced the earth, but not on the lower thermal shield which faced away from the earth.)

*Midcourse maneuver.* Bus temperatures generally agreed with predictions. The Bay II primary sun sensor reached a maximum temperature of approximately 98°F during the maneuver, as compared with the predicted value of 110°F. The difference in predicted and actual $\Delta T$ was almost totally caused by a less severe "soakback" from the motor burn than had been expected.

During the midcourse maneuver, all TCR assemblies were cold and off scale, but returned to expected DN values after sun reacquisition.

*p. Results, conclusions, and recommendations.*

*Spacecraft temperature control design and hardware.* On the whole, it must be concluded that the conversion of an existing spacecraft was less difficult than producing the entire design and development from scratch. The *Mariner* thermal design for the bus depends on solar isolation. After this isolation was provided, the louver and side shielding arrangement was usable intact. With one or two minor exceptions, subsystem hardware was unaffected by age.

**Table IV-41. Comparison of flight data with predictions for science and appendages**

| Channel | Location | Comments |
|---|---|---|
| 422 | Plasma probe | Exact agreement with predictions |
| 403 | Standard cell | 23°F below prediction. Prediction did not account for nontypical position on panel |
| 425 | −Y pitch jet | 15°F warmer than prediction, because of geometric differences from 4-jet assembly, upon which prediction was based |
| 406, 433 | ±X roll and yaw jets | 5°F warmer than prediction, well within accuracy of prediction |
| 427 | S/P spar | 40 to 50°F above prediction. This measurement was included to determine whether zener diodes on spars are firing. Prediction is nominal spar temperature with no heat input from zeners. Therefore, zeners were firing |
| 409, 429 | S/P 4A1 and 4A5 | 8 to 10°F below prediction, mostly because of energy withdrawn from cells and dissipated in zeners |
| 431 | Low-gain antenna mast | 15°F warmer than prediction. Discrepancy caused by incorrect assessment of chamber effects; however, prediction is within normal uncertainty range |
| 434 | Upper thermal shield | 5°F below prediction |
| 435 | Lower thermal shield | 10°F below prediction, when uncorrected for solar simulator spectrum. Apparently caused by far IR in chamber |
| 419 | High-gain antenna | 25°F above prediction, which was based on radiation analysis only. Poor modeling, but with ±30°F accuracy estimate |
| 439 | Magnetometer | 23°F above prediction, a surprising but not frightening $\Delta T$. Analysis is continuing |

The new techniques used to isolate the bus from solar heating proved effective. *Mariner V* had to be less affected by solar heating than previous spacecraft. The lower thermal shield, the deployable sun shade, and the solar panel cutouts all contributed to this sun-independence.

The success of the thermal design depends greatly on the space simulator in which it is tested. For this program, the timely upgrading of the solar simulator, and an improved understanding of the test environment, produced quite accurate flight temperature predictions. The importance of thorough simulator checkout and solar intensity monitor calibration can hardly be overstressed.

Simplifications in the heater circuitry of the TCM did not degrade the quality of the test data.

A small test facility for space simulation testing of individual assemblies would be valuable. Isolated appendages, such as the magnetometer, cannot be adequately tested during TCM and system level space simulator tests. A fifth-scale version of the 10-ft space simulator would solve this dilemma.

The 10% error in the estimate of dissipated power for the TCM was costly. Future programs should take every precaution to prevent such an error; however, parametric data and design margin must be provided in case a late "fix" is required.

*Temperature control reference.* Pre-flight nominal temperature profile curves with flight results plotted are shown in Figs. IV-157 to IV-159. These original curves did not include correction for edge losses and thermal gradient (~6°F for the black at earth). The excessive degradation of the whites is obvious.

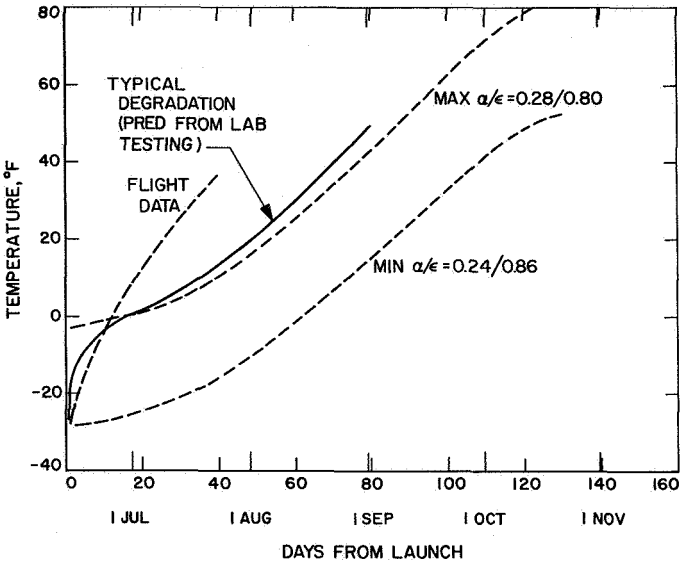



**Fig. IV-158. White TCR predicted and actual flight temperature**

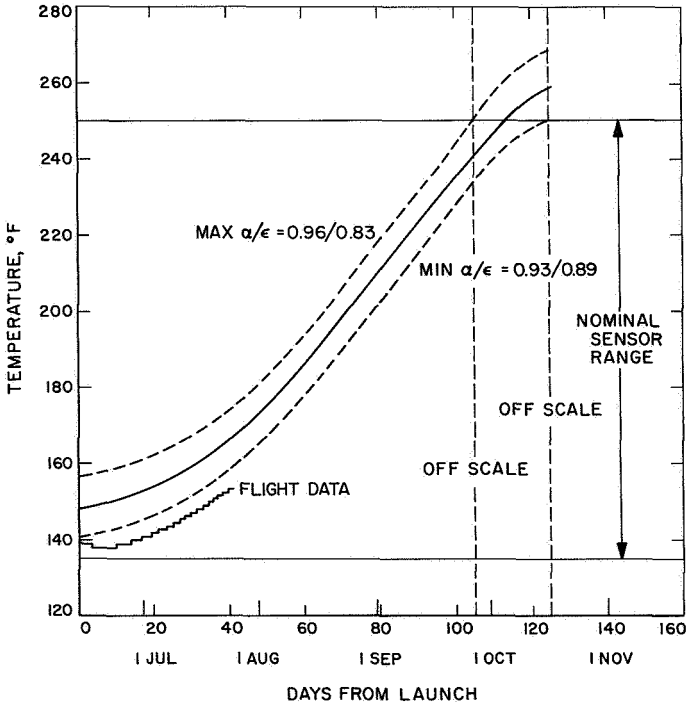



**Fig. IV-157. Black TCR predicted and actual flight temperature**

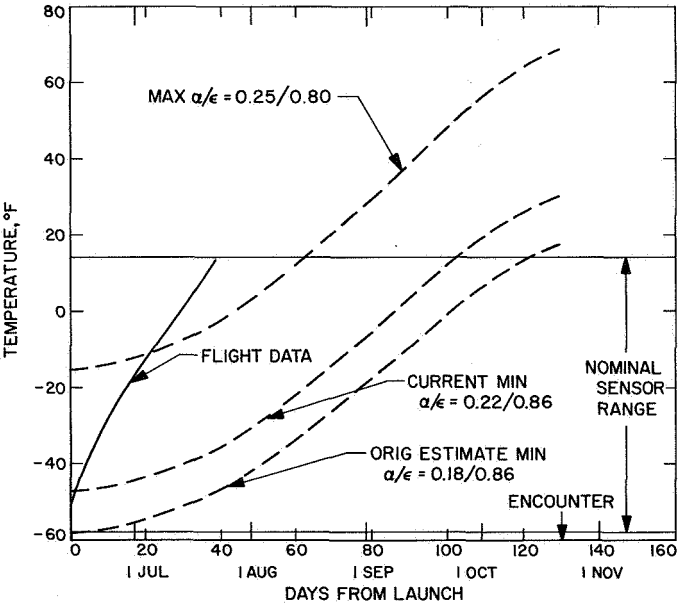



**Fig. IV-159. S-13M white TCR predicted and actual flight temperature**

The decrease in DN following launch and subsequent delay in temperature increase with changing solar distance indicate a change of approximately 3% in $S\ \alpha/\varepsilon$ during the first month of the mission. This may be a change in S, $\alpha$, $\varepsilon$, or some instrumentation or equipment change. The most likely explanation is a change in $\alpha_s$.

Bleaching of CAT-A-LAC black has been observed in air, and bleaching of approximately 1% when irradiated with ultraviolet in vacuum has been reported. The magnitude observed on the TCR is unexplainable at this time.

Laboratory results with S-13 white show rapid degradation of the S-13 during the first few hours. Because data were not expected during the first few hours, the range of the sensor was biased upward. The coating was expected to degrade causing the sensor to come on scale within 10 to 15 h after launch. This degradation did not occur until $L$ + 30 h, indicating either a lower initial $\alpha_s$ or slower initial degradation.

The $\alpha_s$ at launch of the S-13 white is estimated (from laboratory measurements) to have been 0.20. From the data obtained 30 min after launch and the apparent earth thermal input to the black and S-13 white it can be shown that the initial $\alpha_s$ was less than 0.23.

The temperature of the sensor coated with S-13 modified white was on scale from the beginning; the first four values showed a temperature decrease, indicating thermal input from the earth. The first increase in DN (assumed caused by degradation) appeared 6 h after launch. Degradation has continued at a slowly decreasing rate since that time. The calculated solar absorptance of the two whites is shown in Fig. IV-160.

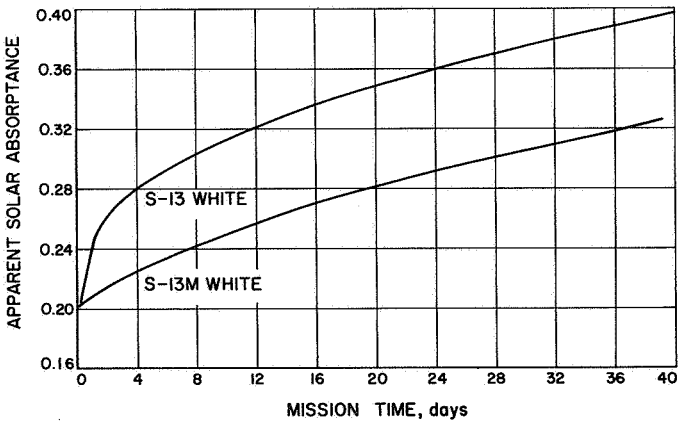



**Fig. IV-160. Absorptance of S-13 and S-13M white coatings vs flight time**

Figure IV-161 shows that the degradation rate decreased as the degradation progressed. This behavior is similar to that observed in the laboratory. The rate for the S-13 white has been decreasing more rapidly than that for the S-13 modified white. At the time channel 432 went off scale, the rates were nearly equal. If this trend continues, the absorptance values for the two white coatings will tend to converge.

*5. Mechanical devices subsystem.* Mechanical devices include those items associated with the latching, structural damping, and nonservoed activations of the various spacecraft elements. The devices included in the subsystem are:

(1) Solar panel boost dampers.

(2) Low-gain antenna support dampers.

(3) Solar panel deployment springs and switches.

(4) Cruise dampers and latches.

(5) Antenna pointing angle change deployment mechanism.

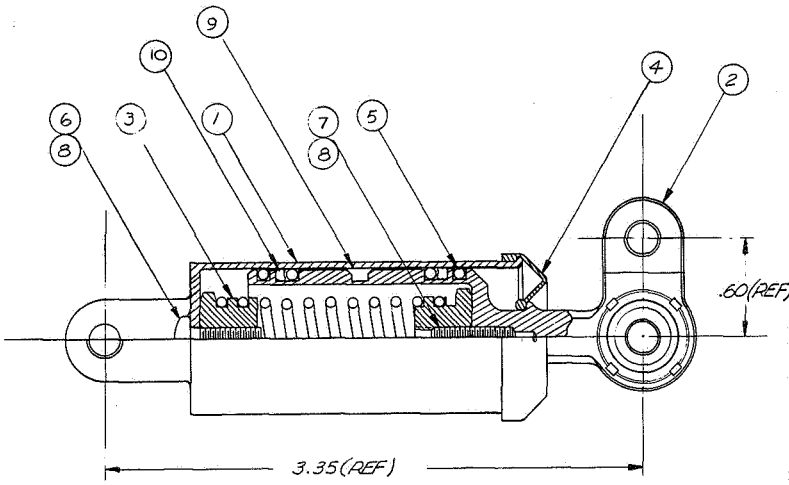
(6) Pyrotechnic arming switch.

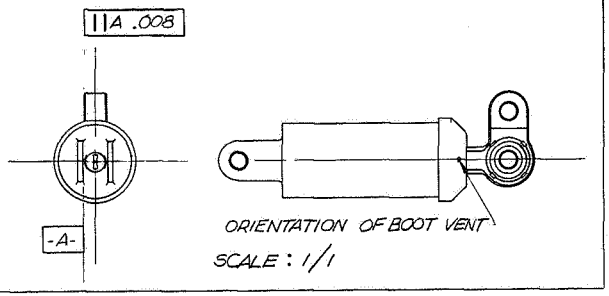
(7) Separation initiated timer.

*a. Solar panel boost dampers.* The primary structural innovation made on the solar panels was the use of tip latching to support the panels during boost. This scheme cleared the center area of the spacecraft by removing the need for panel support struts, thus decoupling, to a greater extent, the design of the panels from that of the antenna system.

The panels were interconnected through damped struts which absorbed vibrationally induced energy, thereby preventing the buildup of damaging structural resonances. The location of these dampers at the panel tips gave positive control of more panel resonances than was the case with *Mariner IV*, although smaller, lighter dampers were used.

Prototype dampers were fabricated and subjected to a series of vibration tests in conjunction with four *Mariner* Mars 1964 panels modified to include prototype tip latching. Lateral excitation was introduced and data were obtained for comparison with the analytical model. The test results compared favorably giving confidence in the adequacy of the design.




| REV | CHANGE DESCRIPTION | EFFECTIVITY | DL | RELEASE DATE | DWN | CHK | STRU | MATL PROC | T C | PKG ENGR | ENGR | DES CHIEF |
|---|---|---|---|---|---|---|---|---|---|---|---|---|
| A | RELEASED FOR FLIGHT MV-67 PER E.C.R.# 8236 | | | | GLM | | | | | | | |
| A | AND W.D./CONTRACT # 00775 . E.C.I.# NONE | | | | GLM | | | | | | | |
| A | INCORPORATED. THIS DWG. REPLACES/MODIFIES | | | | GLM | | | | | | | |
| A | M-C-I DWG# J-415-575. | | | | GLM | | | | | | | |
| B | (8) INCORP. ECI # 25595 EXCEPT ITEM (FIND NO)5— | | | | JCR | EDS | KMB | | | | | CEA |
| B | NO CHANGE, (9) ADDED ITEM (10), PER ECR 8555. | | | 11-21-66 | JCR | RCE | RMA | | | | | CEA |

| JPL SPEC | IDENTIFICATION | | | BAG & TAG | | |
|---|---|---|---|---|---|---|
| | | ZPO-20002-PRS | | | | 14 |
| | SOLAR PANEL BOOST DAMPER ASSEMBLY AND INSPECTION PROCEDURE | QAI-10-35-6 | | | | 13 |
| | | | | | | 12 |
| | | | | | | 11 |
| 8-017-N300-9 | PARKER SEAL CO. "PARBAK" RING | | | BUNA N SHORE 90 | 2 | 10 |
| 200 | DOW CORNING OIL | MIL-S-21568 | | 30,000 CENTI-STOKE VISCOSITY | A/R | 9 |
| | AMERICAN SEALANT CO. ADHESIVE | | | LOCKTITE GRADE C | A/R | 8 |
| AN565BC6H8 | SETSCREW, HEX SOCKET, CONE PT. | | 6-32NC-3A x 1/2 LG | A151303 SS | 1 | 7 |
| DS84-06-7 | SCREW, HI-TORQUE PAN HEAD | | 6-32UNC-3A x 7/16 LG | TITANIUM | 1 | 6 |
| D90568-017-1015 | "O" RING | | | VITON A SHORE 70 | 4 | 5 |
| C411 0174 | BOOT | | | | 1 | 4 |
| B411 0173 | SPRING ASSY | | | | 1 | 3 |
| C411 0170 | PISTON ASSY | | | | 1 | 2 |
| D411 0169 | CYLINDER | | | | 1 | 1 |

| DWG OR PART NO. | DASH NO. | DESCRIPTION | SPECIFICATION | STOCK SIZE / REF DESIGNATION - ELEC DWG | MATERIAL | NO. REQD | FIND NO. |
|---|---|---|---|---|---|---|---|

RELEASE DATE OF DRAWING 2-21-67
DWN JC Carter ENGR Engineer
CHK P. Bassett PKG ENGR
STRU Bamford DES SUPV
MATL PROC DL
TC

UNLESS OTHERWISE SPECIFIED DIMENSIONS ARE IN INCHES
TOLERANCES DECIMALS XX ±.03 XXX ±.010 ANGLES ±1/2°

INTERPRET DRAWING IN ACCORDANCE WITH STANDARDS PRESCRIBED BY MIL-D-70327

BOOST DAMPER ASSEMBLY, SOLAR PANEL

JET PROPULSION LABORATORY
CALIFORNIA INSTITUTE OF TECHNOLOGY
RELEASED THROUGH SECT. 356

C 411 0009

| J411 0000 | MV 67 | CROSS REFERENCE | | | |
|---|---|---|---|---|---|
| NEXT ASSY | USED ON | CLASSIFICATION UNCLASSIFIED | SCALE 1/1 & 2/1 | SHEET 1 OF 1 | REVISION B |

NOTES: UNLESS OTHERWISE SPECIFIED

**Fig. IV-161. Solar panel boost damper**

Boost dampers of the flight-type design were subjected to TA tests during the first series of STM vibration tests. Excessive excursion resulting in "bottoming out" at the end of travel was observed at approximately 10 Hz during the ultimate load level portion of the test series. Following the STM tests, the dampers were removed and tested on a force response machine to compare damping characteristics with data obtained prior to the STM environment tests. This test indicated a 40% loss in damping. Visual inspection revealed gross oil leakage and extensive O-ring seal damage.

The dampers were modified to eliminate O-ring wear and improve oil sealing ability (Fig. IV-160).

Flight dampers were retrofitted with these same modifications and subjected to qualification tests on their assigned spacecraft with satisfactory performance. Several months following the completion of qualification testing, these dampers were removed from bonded stores for further bench tests and visual inspection to determine the effect of storage. No appreciable deterioration in performance was noted in comparison to initial predelivery data and there was no evidence of oil leakage.

*b. Low-gain antenna dampers.* Flight spare antenna dampers remaining from the *Mariner* Mars 1964 program were utilized virtually unchanged. Sufficient damper assemblies were available to provide all required test hardware and existing flight spare assemblies were requalified for use. Existing spare parts were assembled to obtain new flight and flight spare assemblies.

Rework required to adapt these parts to the *Mariner* Venus 67 configuration was minimal. The reversed sun attitude altered the dampers' thermal environment such that a low emissivity surface was required. This modification was accomplished by bonding a polished aluminum sleeve over the existing damper body. The second modification, which affected the short damper only, required shortening of the overall damper length for compatibility with the attach point provided on the *Mariner* Venus 67 superstructure. This modification consisted of removing a section of the existing strut extension and reattaching the end fitting with no change to the damper. Qualification of new hardware and requalification of existing damper assemblies proceeded without difficulty; no problem/failures occurred, and no equipment rework or replacement was required for the duration of the program.

*c. Solar panel deployment springs and switches.* The residual *Mariner* Mars 1964 solar panel deployment hardware and solar panel open switches were used for *Mariner* Venus 67 after they had been reinspected and their performance verified. A solar panel deployment test verified that the different solar panel mass characteristics and sun shade lanyard attachment did not degrade panel deployment. The design of the solar panel deployment springs and switches is discussed in Ref. 1.

*d. Cruise dampers and latches.* The *Mariner V* cruise damper and latches were residual *Mariner IV* hardware. The damping characteristics of the cruise dampers were found out-of-tolerance from the $0.25 \pm 0.10$ damping coefficient specification. Using the same test equipment that was used to qualify this hardware for *Mariner* Mars 1964, with adjustment for the revised solar panel inertia, damping ratios from 0.16 to 0.63 were measured. An investigation into the effect of this apparent degradation revealed that higher damping coefficients were acceptable if the properties within the set could be matched within the specified $\pm$ 0.10. Further tests were conducted utilizing an actual solar panel, more nearly simulating the interaction, with all available cruise dampers being catalogued according to damping coefficient. Two complete sets of dampers were qualified and matched to give an acceptable $0.5 \pm 0.1$ range of damping coefficients for the flight set, and $0.23 \pm 0.07$ for the flight spares.

*e. Antenna pointing angle change deployment mechanism.* The *Mariner V* high-gain antenna must be repositioned at planet encounter to optimize the RF occultation experiment and maintain post-encounter earth communication. This was achieved by rotating the antenna 17°36′ about an axis parallel to the major axis of the antenna reflector (Fig. IV-162). The antenna reflector was mounted on a triangular structure which was fastened to the reflector at three points. The deployment hinge line was located across the base of the triangle (parallel to the reflector major axis) providing a 14.5-in. separation between the superstructure-mounted hinge bearings.

The top of the triangle provided an attach point for the antenna rigid coaxial cable and a latch, which was fastened to the superstructure by a pyrotechnic pin-puller. A short section of flexible coaxial cable across the hinge, joined on each side by rigid coaxial cable, formed the hinge coaxial link. An adjustable stop was provided, near the latch point, to position the antenna in the deployed orientation. A switch at the full deployed position is used to telemeter the APAC event.

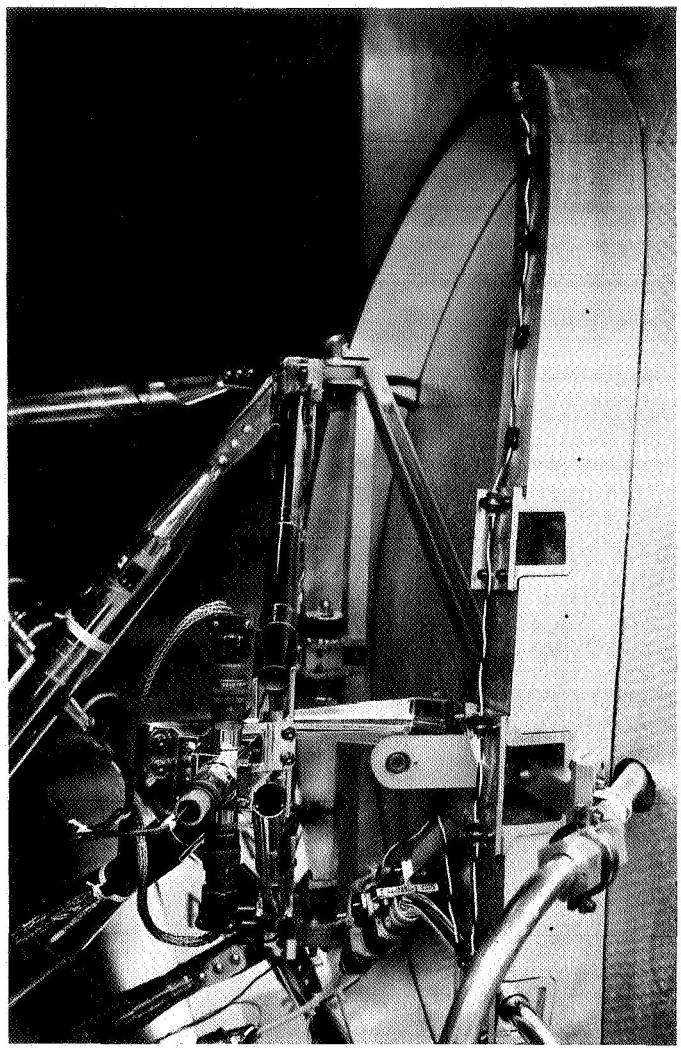


**Fig. IV-162. Antenna deployment mechanism**

The antenna was deployed by two clock-type power springs mounted on the hinge line, midpoint between the hinge bearings. The power springs were selected because of the small decrease in the 16-in.-lb initial torque for the 17°36′ angular displacement.

To prevent bending loads from being transmitted into the antenna from the superstructure, each of the attach points (two at the hinge and one at the latch) was made through monoball bearings. These bearings were lined with a Teflon fabric and had a rotational torque of less than 1 in.-lb. Bearings of this type were flown on the *Mariner IV* science cover hinge.

Because the antenna was located in the shade and was a large thermal radiating surface, it was necessary to thermally decouple it from the superstructure. This was accomplished by using Kel-F as an insulating material for the bearing pillow blocks.

The APAC deployment mechanism was TA vibration tested on the STM and FA vibration qualified on the flight spacecraft. Deployment TA thermal-vacuum testing was performed as a subassembly in a cold-wall vacuum chamber. Flight approval deployments were performed during the spacecraft thermal-vacuum tests and final preflight checks.

*f. Pyrotechnic arming switch. Mariner IV* PAS hardware was used for the *Mariner* Venus 67 program without modification. Sufficient assemblies were available so that no new units were fabricated or assembled. Qualification tests were performed on all flight PAS assemblies and redelivered without reference to previous test history.

Switch adjustment was required on three flight assemblies as a result of contact chatter noted during vibration testing. Following proper adjustment of the switches' overtravel, the units were FA retested without further difficulties. System level testing also proceeded with no performance anomalies reported.

*g. Separation initiated timer.* As for the PAS, the SIT was utilized without design change. Existing units were disassembled, cleaned, and refurbished with new O-ring seals and filled with new, filtered silicone oil. Conformal coating was added to all exposed terminals, and microswitch overtravel adjusted.

To ensure sufficient spares, several switch-deck subassemblies were fabricated and subjected to complete qualification tests along with the rebuilt units.

Unlike the system test history associated with the SIT during the *Mariner* Mars 1964 program, no handling damage and resultant equipment replacement was necessary for the duration of the *Mariner* Venus 67 system test operation.

An analysis of *Mariner V* telemetry data indicated completely nominal performance of the SIT. Proper arming occurred at separation, and solar panel deployment was indicated at separation + 172 ± 2 s. Event register readings were nominal and consistent with both pyrotechnic A and B channels having applied firing current.

### *6. Spacecraft operational support equipment.*

*a. OSE cabling.* The purpose of the OSE cabling is to route power and signals to the spacecraft from the OSE,

generally known as the systems test complex (STC), in a manner compatible with the requirements of both the spacecraft and OSE.

The design of the OSE cabling for *Mariner* Venus 67 was governed by electrical and physical restraints (i.e., IR drops in grounds, and insulation electrical characteristics; insulation strength, moisture resistance, abrasion resistance, and conductor tensile strength).

The direct access receptacles on the spacecraft were female. All connector junctions between the OSE and spacecraft were required to comply to the following: each cable in a series had a male connector on the end nearest the spacecraft and a female connector on the end nearest the OSE.

Another requirement was that shielded wires were to be grounded at the end of the cable nearest the spacecraft.

The OSE cables, shown in Figs. IV-163 and IV-164 can be divided into three categories:

(1) Console cables which interconnected the OSE consoles of two or more subsystems.

(2) Umbilical cables running from the spacecraft umbilical connector, through the simulator plate, into the umbilical junction box. The junction box acted as a distribution center from which the umbilical cables ran to the various OSE consoles.

(3) Direct access cables routed from the spacecraft's direct access connectors to the OSE consoles. These comprised the majority of the cables involved in the *Mariner* Venus 67 OSE cabling effort and were divided into two groups (i.e., cables that ran from the spacecraft to the simulator feed through plates, or interface plates, and cables that ran from the simulator plates to the OSE consoles).

The OSE cabling functions were further classified into two groups: one containing power leads and other switching transient leads, the other consisting of signal and monitor leads. All interface and simulator feedthrough plates were designed to separate physically the two functional groups as much as possible.

The OSE cables remaining from the *Mariner* Mars 1964 program were reviewed to verify that they met the previously mentioned design requirements and restraints. They were cleaned, repaired, relabeled and inspected.

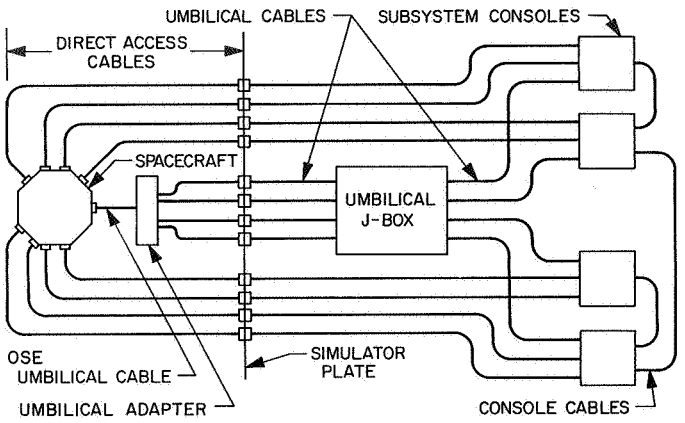



**Fig. IV-163. OSE cabling layout — spacecraft assembly facility (SAF)**

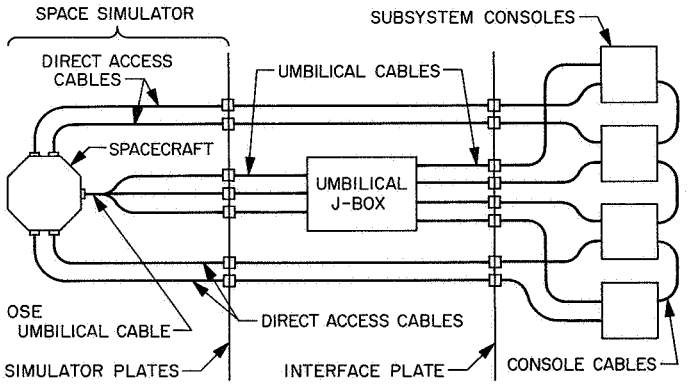



**Fig. IV-164. OSE cabling layout — space simulator facility (SSF)**

Approximately 50% of the *Mariner* Mars 1964 OSE cabling design required changes. Most of the changes consisted of revising the cable assembly drawing wire functions.

Two complete sets of OSE cables for the STC and for use in the space simulator were provided.

In addition to the fabrication and documentation of OSE cables, this effort included the documentation and hardware modification of all junction boxes and interface plate assemblies considered to be part of the STC.

*b. Ground-support equipment.* The ground-support equipment used to hoist, ship, environmentally protect and support *Mariner V* is the same used during the *Mariner* Mars 1964 program. This hardware, including the magnetometer mapping fixture, is discussed in detail in Ref. 1. Two new items were designed and built for

*Mariner* Venus 67. These are described in the following paragraphs.

Special guide rails were fabricated during the *Mariner* Mars 1964 program to guide the shroud when it was lowered over the spacecraft. This prevented the shroud from inadvertently damaging the spacecraft. The guides worked so well that a similar set (that attached to the U-ring) was built to guide and align the spacecraft shipping cover when it was lowered over the spacecraft.

*c. Spacecraft inverter fixture.* The spacecraft inverter fixture was fabricated for installing and removing the spacecraft in an inverted position from the 10-ft space simulator. Other conditions that influenced the design were the possibilities that this fixture could also be used as a spacecraft support fixture during the free-mode test and the spacecraft light reflectance studies.

The inverter basic structure is a U-shaped steel tubular weldment which is supported in the vertical position by three welded-on steel pads. A monoball bracket is bolted to each pad and fits compatible mounting brackets of a four-wheel transport trailer as well as mounting brackets on the spacecraft support ring of the end bell of the 10-ft space simulator (Fig. IV-165).

The height of the inverter was governed by the length of the spacecraft and the prescribed distance between the spacecraft and the end bell while the spacecraft was suspended in the space simulator. The weight of the inverter was approximately 1100 lb.

The spacecraft was supported between the two vertical tubular columns of the fixture. Two pivot shafts, which were secured to the approximate CG location of the spacecraft, rested on welded pads at the ends of the vertical columns. The pivot shafts are modified *Mariner* Mars 1964 simulated midcourse interaction test (SMIT) gimbal assemblies. These assemblies were attached to Bays VIII and IV and were bolted in place directly over the electronic chassis. The pivot shaft on the Bay IV assembly was allowed to move axially as well as radially (floating shaft) in a monoball bearing while the pivot shaft on the Bay VIII assembly was locked to the drive mechanism.

Counterbalance arms with adjustable weights were attached to the SMIT test gimbal assemblies. They were installed to compensate for a spacecraft CG condition that fell out-of-range of the adjustable pivot shafts.

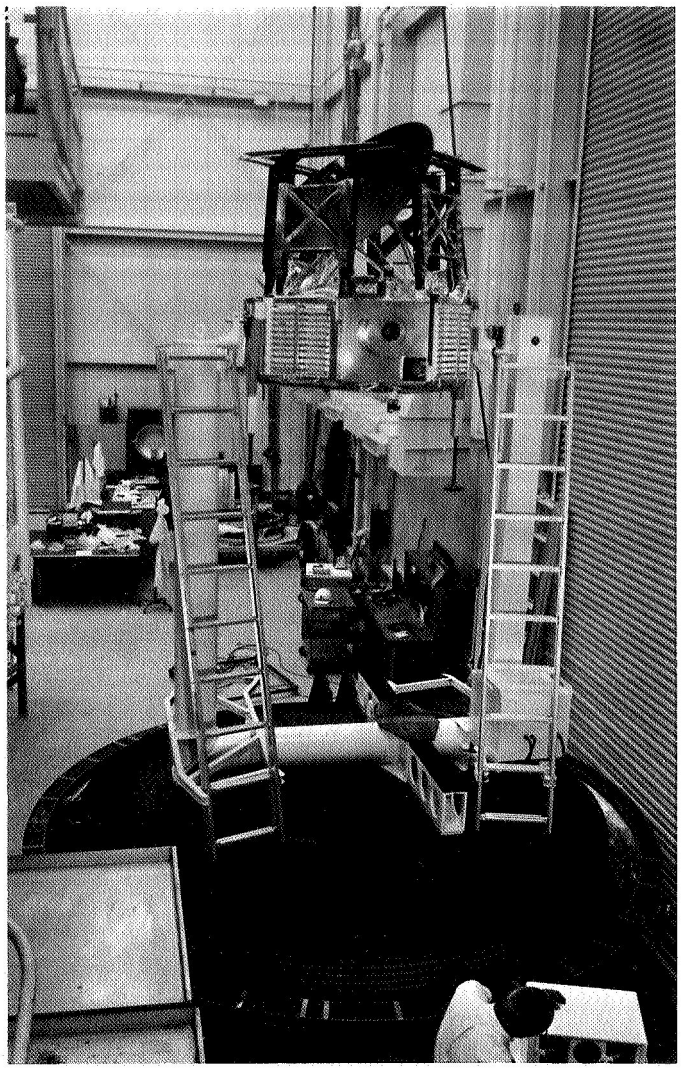


**Fig. IV-165. Spacecraft inverter fixture**

A drive mechanism that provided a variable turning rate was selected. This mechanism is primarily a link chain drive assembly and is composed of link chains, chain sprockets, a series of reduction gear boxes, two electrical motors, and two clutch assemblies. The speed control power supply is mounted on a rollaway cart. The control power supply can energize either electrical motor in the drive mechanism. Two ranges of spacecraft overturning speeds can be selected by engaging either of the clutch assemblies, and, with the aid of the speed control power supply, overturning speeds from 0 to 0.18 rev/min can be achieved.

*7. Structure and dynamics, design, analysis, and test.* Static and dynamic structural analyses of major spacecraft components were utilized during the *Mariner* Venus 67

program from preliminary design to test evaluation. Results from early analyses were used to establish structural configuration and to provide load estimates from which more detailed analyses of structural components and elements were made. Analyses using more refined structural idealizations were then made to obtain analytical predictions which were compared to, and updated by, modal test results. Improved response analyses were used as a basis for evaluating test results and for determining the effects of any structural modifications.

Geometric changes to some of the major elements of the *Mariner V* spacecraft resulted in an entirely different set of dynamic responses that were characteristic of *Mariner IV*. This is especially true of the solar panels, the high-gain antenna and superstructure, and somewhat true of the secondary structure, PIPS, and omnidirectional antenna. The structural design and test criteria were basically the same for both programs.

*a. Mariner Mars 1964 to Mariner Venus 67 analysis comparison.*

*Solar panels.* Differences in configuration between *Mariner* Mars 1964 and *Mariner* Venus 67 are primarily the interconnection of the four solar panels during boost. This results in significant differences in solar panel dynamic response when subjected to lateral and torsional loads. Only minor differences exist when the panels are subjected to axial loads.

The forced response solution of the tip-latched *Mariner V* solar panels was initiated by performing a forced response analysis of four tip-latched *Mariner IV* panels to verify the structural integrity of the proposed configuration.

The model was developed with each panel represented by an out-of-plane analysis of the panel idealized as a planar structure. The panel idealization was modified by moving the damper attachment points to the panel top corners. The panels were interconnected by spring-dampers and the in-plane support was represented by a spring chosen so that the in-plane rigid body frequency matched *Mariner IV* test data.

The composite analysis retained six out-of-plane modes and one in-plane mode for each panel, and eight modes corresponding to the dampers, for a total of 36 elastic modes. Modal damping of 1% critical was used for all normal modes. The constraint modes of the panels and all rigid body modes, except that of the base, were dependent modes.

There were two sets of 18 undamped eigenvalues with associated eigenvectors that were completely decoupled. (This was true only because the in-plane loads on the panels were applied by the dampers at the shear center.) Because the two sets had corresponding frequencies and mode shapes the problem was reduced to the solution of one 18-degree-of-freedom system.

Results of the preliminary analysis indicated that the proposed tip-latch configuration was reasonable and the analysis continued to improve the in-plane model, to evaluate the true in-plane modal damping, the effect of a change in damping coefficients, and the effect of the in-plane load not at the shear center.

A development test was conducted on a set of four *Mariner* Mars 1964 panels to obtain a comparison between analysis and test.

The test results were compared with analytical results in Fig. IV-166. The analytical model was based on a

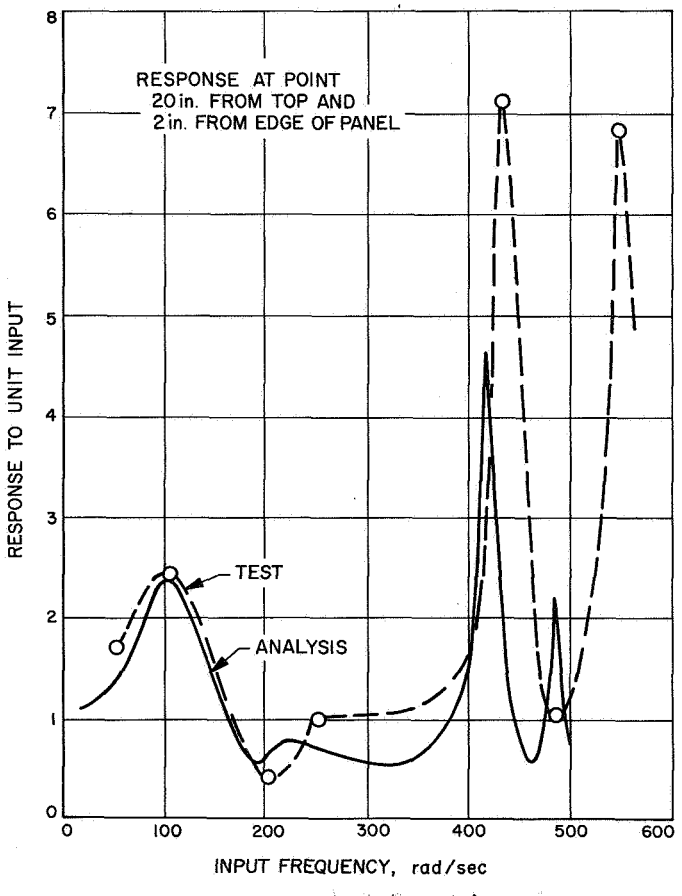



**Fig. IV-166. Response of tip-latched *Mariner IV* solar panels to unit acceleration**

four-panel configuration with in-plane interconnecting spring damper loads applied at the shear centers of the panels. The test model had these loads applied two to four inches from the shear center. The analytical model had the panels vertical while the test model had the panels sloping inward approximately 3½ deg. The modal damping of the analytical model was assumed to be 1% for all modes, except the in-plane mode. This was approximately the average of that measured in the *Mariner* Mars 1964 configuration. The method of analysis was such that good results were expected only at frequencies below 80 Hz. The values plotted as test values in Fig. IV-166 are the ratio of the output amplitude to input amplitude after both had been processed to retain only their fundamental content. The comparison between analysis and test was very good at low frequencies where the model was good.

Frequency prediction was quite good at the higher frequencies, but the response prediction was low. This was very sensitive to the structural damping coefficient used in the analysis and could be much improved by a better approximation of panel structural damping which must be obtained by test.

The relocation of the dampers from the superstructure to the tips of the panels, a position three times as effective when considering pinned-free modes of the panel, required using spring dampers with stiffness and damping coefficients approximately 1/9 that of the *Mariner* Mars 1964 values. This resulted in damper dynamic excursions three times as great as those in *Mariner* Mars 1964.

The coupling between torsion and translation that was so dramatic in the *Mariner* Mars 1964 was entirely missing, while *Mariner* Venus 67 had coupling between out-of-plane bending of one panel with in-plane shear of the adjacent panel.

*High-gain antenna and superstructure.* The dynamic response of the high-gain antenna and superstructure was somewhat different than the dynamic response of the *Mariner IV* high-gain antenna and support structure.

The first two natural modes of vibration of the *Mariner V* antenna were a function of the antenna support structure geometry. The first and second modes are a rigid body rocking motion about the major and minor axes of the antenna, respectively. The three-point support connection of the *Mariner V* antenna to its superstructure allowed this type of rigid body motion about both the major and minor axes of the antenna dish. The *Mariner IV* antenna was constrained from rotating about its major axis because of the five-point support connection of the antenna to its support structure. The frequency of the first natural mode of the *Mariner* Venus 67 antenna is substantially higher than the frequency of the first natural mode of the *Mariner IV* antenna because of the much stiffer structure.

*Post-injection propulsion system.* The PIPS structure was identical to that of *Mariner* Mars 1964. The removal of the planet scan platform from the bus secondary structure, however, changed the dynamic response characteristics of the PIPS. On the *Mariner* Mars 1964, dynamic coupling existed between the PIPS and the planet scan platform support structure at 55 Hz. Removal of the platform reduced the effective mass participating in the secondary structure response mode and caused a shift in its natural frequency, thereby uncoupling its modal response from the PIPS.

*Low-gain antenna.* Changes to the antenna structure that affected its dynamic response included a geometric change to one damper reaction point and removal of the ionization chamber experiment from the antenna. These factors caused a significant decrease in the dynamic amplification to the tip of the mast and an increase in the natural frequency for the first mode of response. The changes had little effect on the dynamic amplification of the second response, but the frequency of response was increased.

*b. Shroud separation dynamic analysis.* A possible collision between the shroud and the spacecraft caused by a nonfunctional shroud separation spring bank was analytically investigated to aid in the definition of the requirements for solar panel protective devices.

Two cases were considered. For Case 1, the manufacturing and assembly tolerances (i.e., spring stroke, preload, stiffness, and alignment and center of mass offset), and the maximum residual vehicle rate were applied in a manner which was considered to maximize the chance for the shroud aft ring to collide with the solar panels. For Case 2, these parameters were applied in a manner which was considered to maximize the chance for a collision between a solar panel tip and an intermediate point on the shroud.

The JPL-developed separation dynamics computer program was used to carry out the required dynamic analyses, and hand calculations served to translate the

computer output into useful shroud–spacecraft relative position data. The spacecraft envelope was conservatively taken to be an axisymmetric figure whose radius at any axial station is equal to the maximum spacecraft radius at that station.

For both cases, it was determined that at least 1 in. of clearance remained. Therefore, results of this analysis did not justify the need for solar panel protective devices to prevent damage caused by one bank out condition.

The STM vibration tests were intended to provide a verification of the ability of the spacecraft to structurally withstand the boost environment. The STM was composed of flight structural items and structural simulations of all spacecraft components (Ref. 13).

*Initial vibration test.* The test objectives were:

(1) To determine dynamic response characteristics of the STM for input loads.

(2) To determine adequacy of primary structure when subjected to qualification dynamic loads.

(3) To determine the effect of the PIPS fuel pressure/configuration on dynamic response characteristics of spacecraft.

(4) To evaluate the performance of the new equalization equipment for its application to FA testing at the system level.

(5) To qualify one celled solar panel at the system level.

Low-frequency structural developmental and design ultimate load tests were run for torsional, lateral, and axial axes of excitation with a test structure containing four uncelled solar panels. A typical test setup is shown in Fig. IV-167. Tests were performed to qualify one celled solar panel at the system level for low frequency and complex wave excitation along one axial and two lateral axes. Additional low-level runs were made to determine the dynamic response characteristics of the PIPS for fuel pressure/configurations along its most critical axis of response. For this portion of the test, the STM contained four uncelled solar panels.

*Final vibration test.* A followup spacecraft composite vibration test of the modified *Mariner* Venus 67 STM was performed. The purpose of this STM test was to obtain supplemental dynamic response data required by late design changes in the basic spacecraft structure and to qualify structural hardware which was either not included on the previous STM or was modified since the previous tests. The tip dampers are an example of hardware that was extensively redesigned between tests. The followup STM test also provided an opportunity to verify the complex wave vibration control equipment operational procedure to be used on flight spacecraft testing. Verification of flight operational test procedures on the STM was mandatory because no PTM was allocated for the purposes of structural dynamic testing.

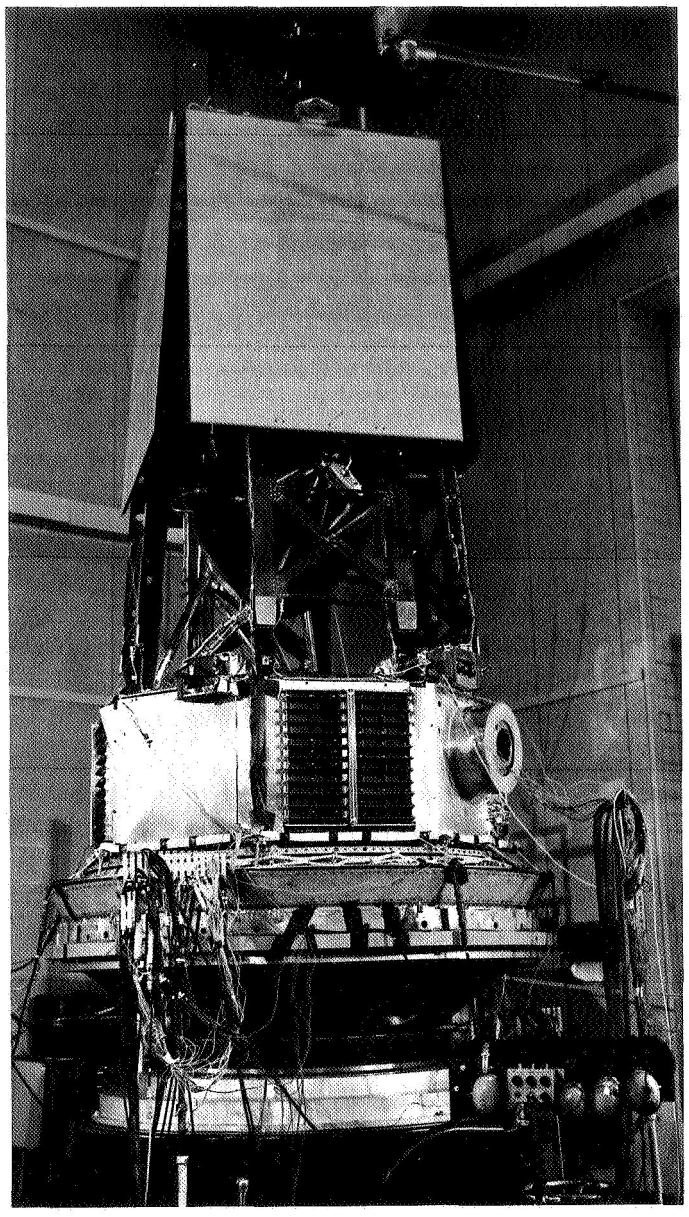


**Fig. IV-167. STM vibration qualification test — Z-axis setup**

Low-frequency structural developmental and qualification dynamic load tests were conducted for two lateral and one axial axes of excitation. Analysis of reduced test data indicated no major changes in the dynamic response characteristics of the modified test structure.

*c. Conclusions and recommendations.* The feasibility, from a structural point of view, of modifying an existing spacecraft design for purposes of performing a different mission is dependent on the following factors:

(1) The boost vehicle on which the spacecraft is supported.

(2) Any additional dynamic maneuver requirements.

(3) Increases or additions in critical masses.

(4) Any additional constraints imposed on the dynamic shroud envelope.

(5) The dynamic effects of changing any major structural elements of the spacecraft.

The *Mariner* Venus 67 structure utilized the *Mariner* Mars 1964 basic design criteria and structural dynamic test specification, with minor modifications, because both spacecraft use the same type of boost vehicle.

Structural changes were made to the secondary structure, solar panels, superstructure, high-gain antenna support structure, and low-gain antenna. This resulted in a completely different set of dynamic response characteristics, both for these elements and also for the elements affected by them.

Structural analyses were required to support design of the new and revised elements to determine their effect on supporting structures prior to qualification testing. The utilization of the *Mariner* Mars 1964 octagonal bus structure and V-band adapter configuration eliminated the need for a static test to demonstrate the adequacy of the *Mariner* Venus 67 to withstand ultimate shear static overturning moment.

The STM successfully demonstrated its ability to withstand structural qualification dynamic loads in the most critical test configuration. The dynamic response characteristics of the test structure when subjected to qualification level loads were well established. The magnitudes of response were within acceptable limits and the test structure demonstrated a minimum amount of dynamic coupling. The pressure-sensitive dynamic response at the PIPS, and its effect on the spacecraft, were well within the design constraints of the overall structure.

*8. Electronic packaging.* The objective of the *Mariner* Venus 67 electronic packaging was to ensure the transition of electronic schematics into functional equipment for reliable operation during testing, launch, and flight environments.

*a. Bus electronics.* The bus electronics configuration and integration support included the definition of the electronic assemblies and the establishment and control of interface requirements for the subassemblies. The packaging assembly drawing called out the electronic assemblies and the battery for spacecraft installation. When a subassembly was under JPL control, interface information was defined on the subassembly drawing. In instances where JPL did not have drawing cognizance, a control drawing was generated. This drawing served as the top subassembly drawing and defined the structural, thermal and envelope characteristics, and listed the contractor's top assembly drawing.

Table IV-42 gives a summary of the changes required on each assembly.

*b. Science instruments.* Control drawings were generated for the helium magnetometer, the TRD, the solar plasma probe, the ultraviolet photometer, and the dual-frequency receiver.

*c. Documentation.* The *Mariner* Venus 67 packaging documentation effort consisted of rewriting the *Mariner IV* functional packaging specification and completely rewriting the general specification covering electronic packaging.

A complete documentation tree covering design, fabrication, handling equipment materials, and hardware was defined (Fig. IV-168). The documentation tree included:

(1) Seventeen *Mariner* Mars 1964 documents used on *Mariner* Venus 67 with no change.

(2) Ten revised *Mariner* Mars 1964 documents with new document numbers.

(3) Nine combinations of *Mariner* 1964 documents having change of number and/or type with new document numbers for *Mariner* Venus 67.

(4) Nine new documents generated for *Mariner* Venus 67.

## Table IV-42. Summary of electronic assembly changes to convert *Mariner IV* to *Mariner V*[a]

| Electronic assembly | Subassembly | Prototype | Test | MV67-1 | MV67-2 |
|---|---|---|---|---|---|
| Electronic assembly I, power subsystem | 4A11 | R | | R | R |
| | 4A12 | MC | | MC | MC |
| | 4A13 | MC | | MC | MC |
| | 4A15 | ND | | ND | ND |
| | 4A16 | ND | | ND | ND |
| | 4A17 | ND | | ND | ND |
| | 4A18 | MC | | MC | MC |
| | 8A1/2 | MCR | | MCR | MCR |
| | EA I, chassis | MCR* | 2MCR* | MCR* | MCR* |
| | EA I, harness | ND* | ND* | ND* | ND* |
| Electronic assembly III, scientific equipment | 20A1 through 20A9 | ND | | ND | ND |
| | 32A2, 32A3, 32A4 | MCR | MCR | MCR | MCR |
| | 33A2 | MC | MC | MC | MC |
| | 33A3 | MCR | MCR | MCR | MCR |
| | 34A2 | ND | ND | ND | ND |
| | 35A1/2 | ND | ND | ND | ND |
| | EA III, chassis | ND* | 84ND | ND* | ND* |
| | EA III, harness | ND* | 2ND* | ND* | ND* |
| Electronic assembly IV, data encoder and command | 3A1 through 3A7 | | RT* | MCR* | MCF |
| | 6A1 through 6A13 | | RT* | MCR* | MCF |
| | EA IV, chassis | RT* | RT* | MCF* | MCF* |
| | EA IV, harness | MCF* | 2MCR* | MCF* | MCF* |
| Electronic assembly V, receiver and tape machine | 2RA1 | RT* | RT* | MCR* | MCR |
| | 2RA2 | RT* | RT* | MCR* | MCR |
| | 2TR1 | RT* | RT* | MCR* | MCR |
| | 16A1 through 16A5 | RT* | RT* | MCR* | MCR* |
| | 16A6 | ND | ND | ND | ND |
| | EA V, chassis | RT* | RT* | ND* | ND* |
| | EA V, harness | ND* | 82R | ND* | ND* |
| Electronic assembly VI, RF communications | 2DC1 | MC | MC | MC | MC |
| | 2DC2 | MC | MC | MC | MC |
| | 2CC1 | MC | MC | MC | MC |
| | 2AT1 | MC | MC | MC | MC |
| | 2PA1 | MC | MC | MC | MC |
| | 2PA2 | MC | MC | MC | MC |
| | 2CS3 | ND | ND | ND | ND |
| | 2CS2 | MC | MC | MC | MC |
| | 2PS2 | RT* | RT* | MCR* | MCR* |
| | 2PS3 | MC | MC | MC | MC |
| | 2TR2 | RT* | RT* | MCR* | MCR |
| | 2CF1/2 | MC | MC | MC | MC |
| | 2RE1 | RT* | RT* | MCR* | MCR |
| | 2CF3 | ND | ND | ND | ND |
| | EA VI, chassis | RT* | 2RT* | MCR* | ND* |
| | EA VI, harness | ND* | 82R | ND* | ND* |
| Electronic assembly VII, attitude control and CC&S | 5A1, 5A2, 5A4 through 5A9 | MC | | MC | MC |
| | 5A3 | R | | R | R |
| | 7A1 | R* | R* | R* | R* |
| | 7A2 | MC | MC | MC | MC |
| | EA VII, chassis | | | MCR* | MCR* |
| | EA VII, harness | | | MC* | MC* |
| Electronic assembly VIII | 4A8 | R | R | R | R |
| | EA VIII, chassis | MCR* | | MCR* | MCR* |
| Battery assembly | 4A14 | | 8RT* | 2MCF* | 2MCF* |
| | Battery, chassis | | | | |

[a]Rework Code

MC = No change from *Mariner IV* hardware.
MCR = *Mariner IV* hardware reworked for FA.
MCF = New fabrication of existing *Mariner IV* design.
ND = New design and fabrication required by *Mariner* Venus 67.
R = *Mariner IV* design electrically changed and reworked.
RT = *Mariner IV* hardware reworked for subsystem test.
* = Denotes rework by Section 357.

J 4110135
MARINER VENUS 67 SPACECRAFT CABLING MASTER BLOCK DIAGRAM
(2)

MV67-4-560
FUNCTIONAL SPECIFICATION, MARINER VENUS 67 FLIGHT EQUIPMENT FLIGHT CABLING
(2)

J 4900550
CABLING INTEGRATION INSTALLATION
(2)

MVW-50572-GEN
GENERAL SPECIFICATION MARINER VENUS 67 FLIGHT EQUIPMENT SPACECRAFT SYSTEM CABLING CABLE AND HARNESS ASSEMBLIES
(2)

MVO-50561-FAT
ENVIRONMENTAL SPECIFICATION, MARINER VENUS 67 FLIGHT EQUIPMENT FLIGHT ACCEPTANCE TEST REQUIREMENTS AND PREACCEPTANCE TEST LIMITS (ASSEMBLY LEVEL)

MVO-50560-TAT
ENVIRONMENTAL SPECIFICATION, MARINER VENUS 67 FLIGHT EQUIPMENT TYPE APPROVAL TEST REQUIREMENTS (ASSEMBLY LEVEL)

20030 A
ENGINEERING DRAWINGS, ASSOCIATED LISTS AND SPECIFICATIONS DATA REQUIREMENTS FOR

MV67-4-550
FUNCTIONAL SPECIFICATION, MARINER VENUS 67 ELECTRONIC FLIGHT EQUIPMENT PACKAGING
(2)

J 4110040
MARINER VENUS 67 PACKAGING ASSEMBLY
(2)

MVU-50573-GEN
GENERAL SPECIFICATION, MARINER VENUS 67 FLIGHT EQUIPMENT ELECTRONIC PACKAGING
(2)

J 4110030
SCIENTIFIC INSTRUMENTS INSTALLATION
(2)

MV67-4-130
FUNCTIONAL SPECIFICATION, MARINER VENUS 67 FLIGHT EQUIPMENT ELEMENT IDENTIFICATION

30274
JET PROPULSION LABORATORY QUALITY CONTROL REQUIREMENTS FOR MARINER PROGRAM PROCUREMENT

20016 C
GENERAL SPECIFICATION, WORKMANSHIP REQUIREMENTS FOR ELECTRONIC EQUIPMENT

(1)

(1) MARINER MARS 1964 DOCUMENTS USED ON MARINER VENUS 67 WITH NO CHANGE.

(2) REVISED MARINER MARS 1964 DOCUMENT WITH NEW DOCUMENT NUMBER.

(3) COMBINATION OF MARINER MARS 1964 DOCUMENTS HAVING CHANGE OF NUMBER OR TYPE WITH NEW DOCUMENT NUMBER FOR MARINER VENUS 67.

(4) NEW DOCUMENT GENERATED FOR MARINER VENUS 67.

(5) OTHER PROGRAM DOCUMENT REVISED FOR MARINER VENUS 67.

## MATERIALS, HARDWARE AND PARTS

MVU-50575-GEN
GENERAL SPECIFICATION, MARINER VENUS 67 SPACECRAFT MATERIAL AND HARDWARE FOR PACKAGING OF SPACECRAFT ELECTRONIC EQUIPMENT
(4)

ZFP-2061-PPL
JPL PREFERRED PARTS LIST

ZCF-4010-0002
GENERAL SPECIFICATION, JPL FLIGHT HARDWARE PREFERRED POLYMERIC MATERIALS AND PRODUCTS

ZFP-2022-APL
PRELIMINARY APPROVED PARTS LIST MARINER VENUS 67

### MATERIAL ACCEPTANCE

#### POLYMERIC MATERIAL

ZME-1061-0002
MATERIAL PACKAGING AND CONTROL DOCUMENT, CONFORMAL COATING JPL NO. 1002
(1)

ZME-1061-0001-A
MATERIAL PACKAGING AND CONTROL DOCUMENT, CONFORMAL COATING JPL NO. 1001
(1)

ZME-1061-0004
MATERIAL PACKAGING AND CONTROL DOCUMENT SOLITHANE 113/300 CONFORMAL COATING (FLUORESCENT AND NONFLUORESCENT)
(3)

ZME-1071-0001
MATERIAL PACKAGING AND CONTROL DOCUMENT, EMBEDMENT COMPOUND, LOW DENSITY
(4)

ZME-1091-0001
MATERIAL PACKAGING AND CONTROL DOCUMENT TAPE, LACING, FLAT, BRAIDED, IMPREGNATED WITH SYNTHETIC RUBBER
(1)

#### MECHANICAL PARTS

ZPH-2239-0160-A
DETAIL SPECIFICATION, PRECISION HOOKUP WIRE ELECTRICAL FLUOROCARBON INSULATED
(2)

ZPH-2245-0300
DETAIL SPECIFICATION, ELECTRICAL CONNECTORS, CIRCULAR, MINIATURE, QUICK-DISCONNECT (MI-REL DS311 THROUGH DS319)
(3)

20045/200 E
DETAIL SPECIFICATION, D SERIES, MARK 1, CONNECTORS (MINIATURE TYPE) (MI-REL)
(1)

## DESIGN

MVU-50581-DSN
DESIGN SPECIFICATION, MARINER VENUS 67 FLIGHT EQUIPMENT TERMINAL CONNECTED PLANAR ELECTRONIC PACKAGING
(4)

MVU-50584-DSN
DESIGN SPECIFICATION, MARINER VENUS 67 FLIGHT EQUIPMENT ELECTRONIC PART INSTALLATION
(4)

20018 J
GENERAL SPECIFICATION FLIGHT EQUIPMENT ELECTRICAL INTERCONNECTIONS
(1)

GMO-50571-GEN
GENERAL SPECIFICATION, DESIGN AND FABRICATION REQUIREMENTS FOR RESISTANCE WELDED ELECTRICAL CONNECTIONS
(3)

30262
GENERAL SPECIFICATION SOLDERED CORDWOOD ELECTRONIC MODULE, FABRICATION
(1)

MVU-50586-DSN
DESIGN SPECIFICATION FLIGHT EQUIPMENT HIGH VOLTAGE PROTECTION
(4)

## STANDARD CONFIGURATION

D 4110500
TYPICAL ASSEMBLY

J 4901046
CHASSIS BASIC ASSEMBLY

C 4110499
TYPICAL SUBASSEMBLY

D 4901045
SUBCHASSIS OUTLINE

## ASSEMBLY SHIPPING AND HANDLING EQUIPMENT (OSE)

MVU-50582-PRS
PROCESS SPECIFICATION MARINER VENUS 67 FLIGHT ASSEMBLY HANDLING AND TRANSPORTATION SYSTEM
(5)

20064
GENERAL SPECIFICATION FOR PACKING FLIGHT EQUIPMENT FOR SHIPMENT WITHIN THE CONTINENTAL UNITED STATES.

ZBE-1070-0001
PROCESS BULLETIN ELECTRONIC SUBASSEMBLY HANDLING AND STORAGE EQUIPMENT
(4)

HARNESS FABRICATION FIXTURES

ASSEMBLY HARNESS

| | |
|---|---|
| BASIC FIXTURE | J 8901854 |
| EA-I | J 4110948 |
| EA-III | J 4110949 |
| EA-IV | J 8901899 |
| EA-V | J 4110950 |
| EA-VI | J 4110951 |
| EA-VII | J 8901855 |

RING HARNESS

| | |
|---|---|
| UPPER RING | J 4111035 |
| LOWER RING | J 4111036 |

## QUALIFIED PROCESSES

### INSTALLATION

ZBE-1051-0003
PROCESS BULLETIN INSTALLATION OF TEMPERATURE TRANSDUCERS
(4)

ZBE-1041-0007
BONDING OF PRINTED WIRING TERMINAL AND INSULATION BOARDS WITH ECCO BOND 55/9
(3)

ZBE-1091-0001
PROCESS BULLETIN, FABRICATION AND USE OF LACING TIES
(1)

GMO-20514-PRS-A
PROCESS SPECIFICATION, INSTALLATION OF THIN WALL INSERTS IN ALUMINUM AND MAGNESIUM
(3)

20001
PROCESS SPECIFICATION RIVET AND SCREW HOLE PREPARATION

MVU-50583-PRS
PROCESS SPECIFICATION MARINER VENUS 67 FLIGHT EQUIPMENT INSTALLATION OF ELECTRONIC ASSEMBLIES AND SUBASSEMBLIES
(3)

GMW-50344-PRS-B
PROCESS SPECIFICATION INSTALLATION OF RETENTION SLEEVE ON "D" SERIES CONNECTORS
(5)

20014 F
GENERAL SPECIFICATION SOLDERING PROCESS

A 90314 C
CONNECTOR INSTALLATION DEM 9 THROUGH DDM 50, MODIFIED ASSEMBLY
(1)

20013
PROCESS SPECIFICATION INSPECTION OF RIVETED JOINTS

### POLYMERIC MATERIAL USAGE

ZBE-1061-0006
PROCESS BULLETIN APPLICATION OF SOLITHANE 113/300 CONFORMAL COATING (FLUORESCENT AND NONFLUORESCENT)
(3)

ZBE-1041-0008
PROCESS BULLETIN, SPOT BONDING OF ELECTRONIC PARTS WITH STYCAST 1095/9
(3)

ZBE-1072-0003
PROCESS BULLETIN CONFORMAL ENCAPSULATION OF ELECTRICAL CONDUCTORS
(3)

ZBE-1072-0004
PROCESS BULLETIN, COATING OF ELECTRICAL CONDUCTORS EXPOSED TO ULTRAVIOLET RADIATION

ZBE-1041-0009
PROCESS BULLETIN SPOT BONDING ELECTRONIC PARTS WITH SOLITHANE 113/300 FILLED POLYURETHANE
(5)

A 90539 D
PROCEDURE TO INSULATE AND SEAL BACKSIDE OF CANNON (D) CONNECTORS
(5)

A 3172895 A
IMPREGNATION AND ENCAPSULATION PROCEDURE FOR TRANSFORMERS AND CHOKES
(5)

20060 B
PROCESS SPECIFICATION ADHESIVES, COATINGS, AND ENCAPSULANTS FOR ELECTRONIC PACKAGING
(1)

ZBE-1071-0003-A
PROCESS BULLETIN EMBEDMENT OF ELECTRONIC MODULES IN STYCAST 1090/11
(2)

20015 F (1)
PROCESS SPECIFICATION FLIGHT AND GROUND EQUIPMENT POTTING OF CONNECTORS
(1)

20015/1A (1)
PROCESS SPECIFICATION FOR POTTING COMPOUND SILASTIC RTV 881 - SILICONE RUBBER
(1)

20015/3A (1)
PROCESS SPECIFICATION FLIGHT EQUIPMENT POTTING COMPOUND PR-1527 POLYURETHANE
(1)

### INTERCONNECTION

MVU-50585-PRS
PROCESS SPECIFICATION, PRINTED WIRING AND TERMINAL BOARD FABRICATION MARINER VENUS 67 SPACECRAFT
(4)

GMO-50571-GEN
GENERAL SPECIFICATION, DESIGN AND FABRICATION REQUIREMENTS FOR RESISTANCE WELDED ELECTRICAL CONNECTIONS

30262
GENERAL SPECIFICATION, MODULE, FABRICATION

20014 F
GENERAL SPECIFICATION, SOLDERING PROCESS
(1)

20500 A (1)
PROCESS SPECIFICATION SPLICING OF ELECTRICAL HOOK-UP WIRE GROUND AND FLIGHT

20501 A
PROCESS SPECIFICATION, SHIELDING TERMINATIONS GROUND AND FLIGHT
(1)

20502
PROCESS SPECIFICATION, ELECTRICAL INTERWIRING FOR FLIGHT EQUIPMENT
(1)

GMW-50343-TST-B
TEST SPECIFICATION, CONTACT SEPARATION FORCE FOR "D" SERIES CONNECTORS
(5)

ZBE-1081-0006
PROCESS BULLETIN HAND SOLDERING OF STRANDED WIRE INTO ELECTRICAL CONNECTOR CONTACT SOLDER CUPS
(4)

### SURFACE FINISHES

B 90433
SURFACE TREATMENT A31 AND ZF640 FOR MAGNESIUM SUBCHASSIS
(1)

GPF-20229-PRS-B
PROCESS SPECIFICATION, SPACECRAFT FLIGHT EQUIPMENT, TEMPERATURE CONTROL SURFACES, GOLD PLATING (ELECTRODEPOSITED) FOR MAGNESIUM AND MAGNESIUM ALLOYS

ZBE-1061-0005-B
PROCESS SPECIFICATION, SPACECRAFT FLIGHT EQUIPMENT, TEMPERATURE CONTROLLED SURFACES, GOLD PLATING (ELECTRODEPOSITED) FOR ALUMINUM AND ALUMINUM ALLOYS

A 90302-1
SURFACE TREATMENT AND HANDLING TEMPERATURE CONTROLLED ITEMS (FOR ALL METALS)

A 90302-3
SURFACE TREATMENT AND HANDLING TEMPERATURE CONTROLLED ITEMS (FOR WROUGHT MAGNESIUM)

A 90302-4
SURFACE TREATMENT AND HANDLING TEMPERATURE CONTROLLED ITEMS (FOR BUFFED PLATING)

A 90302-5
SURFACE TREATMENT AND HANDLING TEMPERATURE CONTROLLED ITEMS (FOR WROUGHT ALUMINUM)

A 90302-6
SURFACE TREATMENT AND HANDLING TEMPERATURE CONTROLLED ITEMS (FOR WROUGHT ALUMINUM)

### GENERAL

MVU-50584-DSN
DESIGN SPECIFICATION MARINER VENUS FLIGHT EQUIPMENT ELECTRONIC PART INSTALLATION

MVU-50581-DSN
DESIGN SPECIFICATION MARINER VENUS 67 FLIGHT EQUIPMENT TERMINAL CONNECTED PLANAR ELECTRONIC PACKAGING

ZPO-20002-PRS-C
PROCESS SPECIFICATION IDENTIFICATION REQUIREMENTS PARTS AND ASSEMBLIES
(1)

ZBE-1061-0005-B
PROCESS BULLETIN, MODIFICATION AND REWORK OF PLANAR ELECTRONIC SUBASSEMBLIES
(5)

20018 J (1)
GENERAL SPECIFICATION FLIGHT EQUIPMENT ELECTRICAL INTERCONNECTIONS

= SECTION 357 CONTROLLED DOCUMENT.

(1) APPLIES TO CABLING ONLY.

**Fig. IV-168. *Mariner* Venus 67 electronic packaging and cabling documentation**



FOLDOUT FRAME 1

FOLDOUT FRAME 2

**Page intentionally left blank**

PRECEDING PAGE BLANK NOT FILMED.

(5) Eight other program documents revised for *Mariner* Venus 67.

*d. Subsystem support.* Rework was done at JPL because of (1) the unavailability of the contractor who had manufactured the equipment, (2) the inability to get the contractor to rework it in a given scheduled period, (3) the high cost of minor rework items that were required, and (4) the contractor's performance capability for the type of rework involved. Table IV-42 gives a summary of the rework performed.

*Fabrication and modification.* Electronic fabrication was performed at JPL for reasons similar to those given in subsection d above. In addition, it was performed as a backup for a contractor fabrication.

A backup power supply for the DAS subsystem was designed in support of the science division. One prototype and one flight unit were fabricated and delivered (Fig. IV-169). This entire effort was accomplished in a three-month period. As part of this effort, a design and fabrication technique for transformers and inductors was developed.

The mechanical design and packaging for the planet sensor electronic welded module was performed. Three

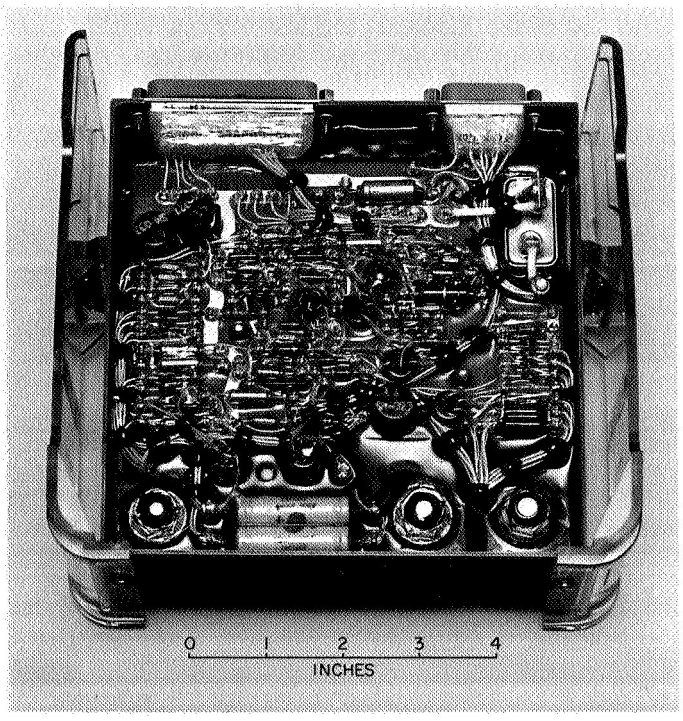



**Fig. IV-169. DAS Mark II power converter subassembly**

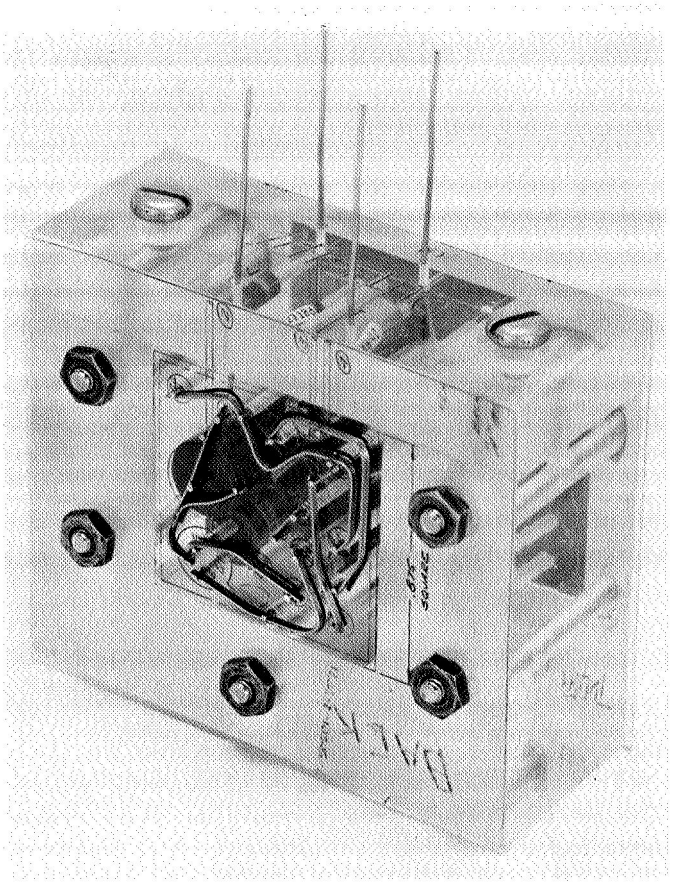


**Fig. IV-170. Planet sensor welded module in holding fixture**

flight and two test modules were fabricated (Fig. IV-170). Four terminator sensor welded modules also were fabricated.

*Subsystem rework.* A review of all residual subsystem subassemblies that were candidates for the *Mariner* Venus 67 mission was made. Deviations with recommendations were then submitted to the cognizant personnel for evaluation. When deemed possible, rework was performed to incorporate the items that were agreed upon, using the latest electronic packaging techniques. The majority of rework was accomplished at JPL.

The rework in support of the subsystems is very extensive and detailed. Therefore, only the tasks involved for one subassembly are summarized herein.

One such subassembly was the 2PS2 cavity power supply. While this subassembly was being reviewed for possible acceptance, a leak around the base of the terminal of capacitor C3 in TB8 was found.

Although the amplifier checked out satisfactorily according to the TA test, it was decided to replace TB8 with an amplifier from a selected flight quality 2PS1 from *Mariner* Mars 1964.

After environmental test, during final cleanup, it was noted that the replacement capacitor was leaking. Therefore, another TB8 was selected and installed in the subassembly. After checking all components in the subassembly, the power supply was returned to Division 33.

After evaluating the capacitors, two ECRs were generated. The quantity, size, and shape of the recommended capacitor type required to replace the capacity and voltage of the old capacitor were changed. To fit the new capacitor in the same location, it was necessary to design and fabricate two new capacitor modules and molds.

Normally, a large number of drawings, many of which were not under JPL control, would have to be altered to incorporate this capacitor change. However, to reduce the magnitude of this operation, a procedure was generated which called out in detail all of the work required. This procedure enabled the necessary detailed documentation and control of the rework with a minimum amount of new drawings and changes to existing documentation.

All the rework on three subsystems was completed satisfactorily.

*Subsystem contractor support.* The following types of support were given:

(1) Instruction and demonstrations were provided to ensure proper soldering of wire into connector cups.

(2) Demonstration or supervision of specific phases of the fabrication was enforced to meet JPL packaging standards. As an example, the contractor of the DAS power supply was brought to the Laboratory and the prototype was rewired under JPL direction and supervision.

(3) Support for the cordwood welded module was furnished for several contractors. Many instances required the survey of facilities, recommendations on equipment, setup calibration, and weld verifications.

(4) Support was furnished to contractors in the design of equipment, review of design, troubleshooting of fabrication problems, verification or recommendation of manufacturing processes to meet the requirements for a given design, and recommendations required to implement the processes for given contractor support.

(5) The largest block of manpower to contractor support was provided for review of the new DAS subsystem. This consisted of the review of the design, a study of its principles, a review of the processes required to ensure repetitive fabrication, and numerous consultations on minor process difficulties.

*e. Handling, shipping and storage equipment.* All of the subassembly handling frames and containers used for *Mariner* Mars 1964 (Fig. IV-171) were cleaned, modified, and made into subsystem lots. Two hundred-fifty sets were modified and reworked. Fifty new sets of frames and containers were fabricated. Each subsystem received at least two sets. A process bulletin was also generated to ensure proper application in the use of the subassembly handling equipment.

To protect the electronic equipment during assembly and bench testing, hard-anodized aluminum handling fixtures were provided in *Mariner IV*. These fixtures were required to hold the chassis in accurate alignment during installation of the subassemblies. The chassis attached to the fixture at the existing spacecraft mounting points and supported the cable harnesses. Protection

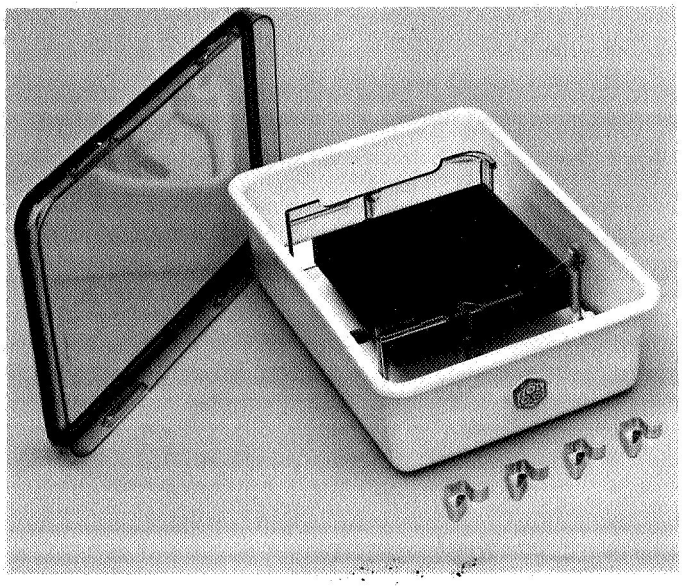


**Fig. IV-171. Subassembly handling and storage container**

of assemblies in storage and shipment was provided by a double plastic container. Inner boxes were made to accommodate the assembly handling fixture and rested inside the outer container on foam plastic blocks.

The acceptability of this system was in doubt because the *Mariner IV* environmental test data on the container design were inconclusive. A series of tests performed on the *Mariner IV* system proved that the system did not adequately protect the electronic equipment. A program was generated to upgrade all old containers and to design new fixtures and containers whenever necessary. A parallel effort was followed to modify the existing hardware and to procure the replacement parts with the necessary changes presented in Table IV-43.

The shipping system exceeded all *Mariner* Venus 67 specifications when the modifications (Fig. IV-172) were environmentally tested.

To incorporate the new shipping system, a transportation and handling specification was generated. Because this specification was not widely known, a training program was conducted.

Because the batteries were handled and shipped more frequently than the electronic assembly, JPL decided to design a separate handling and shipping system that was



**Fig. IV-172. Modified electronic assembly shipping and handling equipment**

**Table IV-43. Changes to *Mariner IV* electronic assembly handling and shipping containers**

| Handling fixtures | Inner container | | Outer container | |
|---|---|---|---|---|
| | Modify and refurbish | New procurement | Modify and refurbish | New procurement |
| 1. Install thermofit on four rails of handling fixture | 1. Install gasket seals on opening and seal rivets | 1. Same | 1. Delete humidity indicator and desiccant holder | 1. Same |
| 2. Replace all existing fasteners with new ones | 2. Install desiccant holder | 2. Same | 2. (a) Reinforce the polystyrene corner supports for the inner container and eliminate the 1/2 dynamic non-linear decoupling | 2. (a) Not applicable |
| 3. Radius edges of end supports and reanodize | 3. Install two-way breather valve | 3. Same | | |
| | 4. Install humidity indicator | 4. Same | | |
| | 5. Provide web harness for clamping and hand carrying | 5. Install latches with lockwire provisions and carrying handles | (b) Design and install a two-piece polyurethane liner to support inner container | (b) Same |
| | 6. Coated fairing inside surfaces to eliminate powdering | 6. Change material from ABS to high-density polyethylene | 3. Not applicable | 3. Increase gage of ABS material from 3/16 to 3/8 in. to eliminate need for corner reinforcement |

easier to transport. The new handling fixture was to fit into a modified *Ranger* shipping container. The following were accomplished:

(1) Twenty old *Ranger* containers were located, cleaned, and modified as follows:

  (a) All existing rubber pads, paint, and nomenclature were removed.

  (b) New rubber pads made up of 80% Neoprene and 20% Neoprene foam were bonded to their respective mounting areas.

  (c) All latches, handles, and seals were reworked. Containers were repainted and identified.

(2) A new fixture was designed to carry 1 or 2 batteries. This fixture was a frame of welded aluminum construction (Fig. IV-173). Twenty fixtures were fabricated for the program.

(3) The existing *Mariner* Venus 67 outer container was used for shipping with a specially designed two-piece polyurethane foam liner bonded to the inside.

The shipping system exceeded all *Mariner* Venus 67 specification requirements when the modifications were tested.

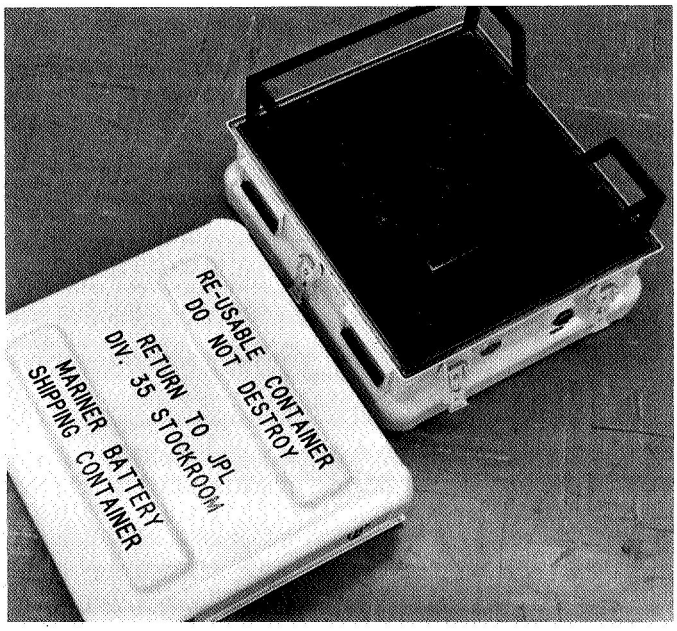



**Fig. IV-173. Battery assembly in handling fixture and container**

*f. Environmental thermo-vacuum plates.* Subassembly mounting inserts were damaged during the initial environmental testing of one of the subsystems. Improper hardware use during the installation of the heat-transfer plate to the electronic assembly for thermal-vacuum testing was established as the cause of this damage. The following were accomplished in support of the environmental test area:

(1) A drawing defining the thermo-vacuum plate requirements was generated and proper fasteners were procured.

(2) The existing thermo-vacuum plates defined for each assembly were inspected and reworked, where necessary, to the revised drawings.

(3) The thermo-vacuum plates were Teflon-coated to eliminate the separate Teflon sheet in the installation.

(4) The installation and removal procedure was incorporated into the specification for the installation of electronic assemblies and subassemblies.

During the interim period required to implement the changes, a packaging engineer assisted in each installation and removal of the thermo-vacuum plate.

As a result of this exercise, a universal thermo-vacuum plate that could be used for all the electronic assemblies without requiring the removal and replacement of the subassembly mounting screws was defined.

***9. Materials.*** The materials support activities were restricted to materials applications for new items and equipment, the solution of materials problems which arose, and the investigation of potential problem areas associated with the different mission environment.

In general, materials selected for use were those which have been demonstrated to have low outgassing rates and reliable performance. In addition, an attempt was made to reduce the number of materials on the spacecraft (e.g., to eliminate situations where two different adhesives are used in similar applications).

*a. Solar panels.* An epoxy polyamide dielectric coating, SMP62/63 (Western States Lacquer Corp.), had been successfully used on the *Mariner* Mars 1964 solar panels. For *Mariner* Venus 67, the maximum solar panel temperature was predicted to be from 275 to 300°F as opposed to 135°F for *Mariner IV*. An investigation was undertaken to determine the suitability of this dielectric

for the new mission. It was established that SMP62/63 lacked sufficient hardness to resist penetration by sharp objects (i.e., solder projections) at the higher temperatures.

Six other candidate dielectric materials were selected for experimental evaluation. Of the six, Epon 956 and PT-401 had adequate penetration resistance at 300°F. Epon 956 had better outgassing characteristics (lower volatile condensable content) and was, therefore, recommended for use on *Mariner V*. It was established that glass fabric reinforcing of the dielectric coating is a good method of obtaining high reliability in penetration resistance and for thickness control. Although this method imposed a weight penalty, it was not considered excessive.

During thermal testing of the *Mariner* Venus 67 TA solar panel in the 10-ft simulator, a severe thermal shock occurred as a result of power failure. Tests of panel power output, following the shock and subsequent visual examination, revealed extensive delamination of solder contact from the solar cells. Although the thermal shock was far more severe than anything that could reasonably be expected during the mission, an investigation was undertaken to establish the relationship between the failure and mission reliability.

Several potential contributors to the problem were identified but no one factor, or readily identifiable combination of factors, provided correlation to the failures. Because the solar cells used for *Mariner V* had been in storage, detailed processing information was unavailable. This information can be used to establish, or at least indicate, the cause of an apparently random failure of this type.

Metallographic examination of the solder–silicon interface revealed three distinct phases: (1) the solder, (2) the silicon cell, and (3) intermediate nickel-rich phase. Observed delaminations occurred most frequently between the nickel-rich phase and the silicon. Microprobe analysis confirmed that diffusion had occurred in the cells heated during the test.

Some evidence of cracking parallel to the interface plane was detected in some of the cells examined. A hypothesis of off-plane cutting or fracture during the grinding operation as the cause of failure was developed. This hypothesis was not pursued but should be considered in any future investigation.

Considerable variation was observed in solder thickness. Like other variables observed, this could not be directly correlated to delamination failures.

Two silicone adhesives that were known to produce significant volatile condensable material at elevated temperature were used on the *Mariner* Mars 1964 and *Mariner* Venus 67 solar panels. RTV-40 was used as the cell adhesive and RTV-602 as the cover glass adhesive. At the temperature encountered by *Mariner IV*, this condensability was not a serious problem, but could become serious at the significantly higher temperatures expected on *Mariner V*.

Volatile condensable materials can be significantly reduced by proper thermal or vacuum-thermal conditioning of the solar panels. However, extended thermal exposure of the solar cells results in decreased performance and reliability. A sequence of treatment, compatible with minimum hazard to solar panel performance, which would result in the minimum outgassing during flight, was required. A series of pre- and post-thermal treatments coupled with simulated flight acceptance vacuum-thermal tests was conducted and the effect on outgassing measured. It was established that the FA vacuum-thermal treatment reduced outgassing to a rate nearly equal to that achievable by any acceptable combination treatment. Therefore, no additional treatment was recommended. The hazard associated with residual outgassing following FA thermal-vacuum was minimal.

*b. Outgassing and corona-arcing of high-voltage equipment.* Special emphasis was placed on the evaluation of the outgassing characteristics of all material used in subsystems containing voltages in excess of 250 V. This was necessary because of the potential effect of outgassing products on corona-arcing. The best available information was obtained from the cognizant engineers and from available drawings and other documents for all science experiments and for all areas known to contain potentials of 250 V or greater. The areas surveyed were the UV photometer, trapped-radiation detector, plasma probe, helium magnetometer, dual-frequency receiver, data automation subsystem, science cabling, Canopus sensor, and spacecraft radio subsystem.

The factors considered were: (1) voltage levels involved, (2) type and quantity of materials used and their outgassing characteristics, (3) instrument venting and calculated pumpout rate, and (4) time from launch to instrument turn-on.

Three general criteria of acceptability were used:

(1) Use only of materials which have been found satisfactory with respect to outgassing.

(2) Use of designs previously proven successful on missions such as *Mariner IV* and *Pioneer* with no material changes from these models.

(3) Sufficient venting and elapsed time between launch and application of power such that the pressure in the vicinity of high voltage did not exceed $10^{-4}$ torr.

All of the instruments surveyed meet at least one of these criteria; most meet two. No evidence was found of a corona-arcing problem as a result of material outgassing in any of the areas surveyed.

*c. Outgassing of spacecraft cabling and simulator operational support equipment.* Historically, there is concern about spacecraft temperature control surfaces and subsystems which might be degraded by outgassing products during the space simulator test. In addition, the optics in the JPL 10-ft simulator are sensitive to contamination. If contamination had occurred during the M67-1 test, it would have degraded or delayed the test of M67-2 (flight spacecraft). As a result, considerable effort was expended to ensure that OSE cabling and hardware in the chamber was as free of outgassing products as possible. All available OSE cabling and hardware were preconditioned in vacuum at 125°F prior to installation in the solar simulator.

As permitted by schedule, all spacecraft cabling hardware, particularly silicone rubber grommets and cable clamps, were preconditioned in vacuum at elevated temperature prior to assembly on the spacecraft.

As was noted with the solar panels, considerable vacuum-thermal cleaning of most spacecraft subsystems is achieved during the vacuum-thermal portion of the FA test. In future programs, improved materials and processing control should be instituted to reduce the outgassing hazard from both flight and OSE hardware.

*d. PIPS nitrogen tanks.* At least one additional $N_2$ pressure vessel had to be fabricated and qualified for the *Mariner* Venus 67 PIPS.

The best available stock consisted of ends of several bars, all from the same heat. The material had a higher oxygen content than allowed by the specification (0.16 to 0.19% compared to 0.15% allowable) and, as a result, had higher tensile yield and tensile ultimate strength than allowed. However, since the elongation and reduction of area values were within specified limits, these higher values were acceptable and the material approved for use.

Considerable effort and coordination were required to meet satisfactory qualification requirements of material heat, bar stock, forging, welding, and proof test (a single tank was proof-tested), and to provide a qualified tank for the project.

*e. Battery wire work hardening.* As a result of failures of *Mariner* Venus 67 battery plate wires during vibration testing, an investigation was undertaken to determine susceptibility of silver wire to work hardening by bending. Samples of silver wire in similar geometry were bent in the annealed condition in an effort to simulate bending that would result from handling of battery plates during assembly of the battery. The limited number of tests performed clearly indicated that the silver work-hardens very rapidly. Therefore, it was recommended that extreme care be taken to minimize bending of the wires during assembly of the battery.

*f. Magnesium coatings and corrosion.* Magnesium parts for *Mariner IV*, and similarly for *Mariner V*, were coated for both corrosion protection and temperature control. When low emittance was required, gold plating was used. For high emittance, a conversion coating (Dow 7) was used. The Dow 7 coating is intended as a temporary coating or paint base and provides only moderate corrosion protection over long periods of time.

Several instances of serious magnesium corrosion occurred during the *Mariner* Venus 67 program. The first serious occurrence was on the M67-1 basic structure in the thermal control paint shop when temperature and humidity conditions overloaded the air-conditioning unit. At the end of one working day, there was no evidence of corrosion; the next morning the structure had seriously "flowered" (Fig. IV-174). The corrosion products were removed and affected areas were retreated with the Dow 19 coating.

Subsequently, during spacecraft buildup and test in the SAF, corrosion recurred (Fig. IV-175). Again, it was necessary to remove the corrosion products and re-treat the surface. This recurrence of corrosion was associated with increases in relative humidity in the spacecraft area. The corrosion appears to be associated with relative humidity levels of 50% and higher.

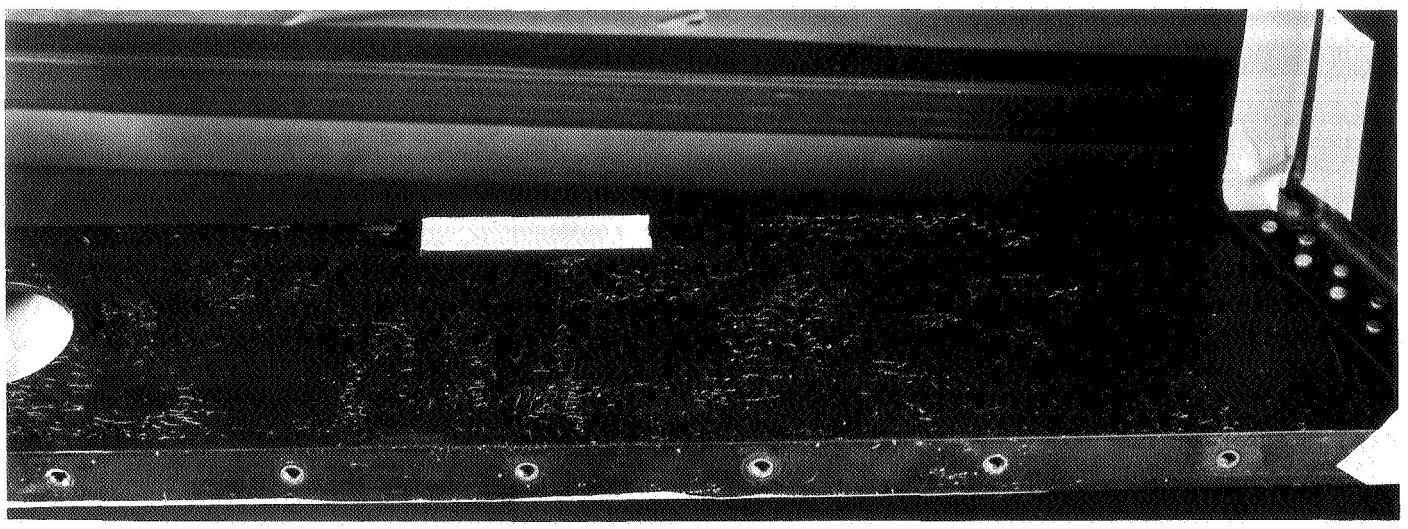


**Fig. IV-174. Octagon structure magnesium corrosion**

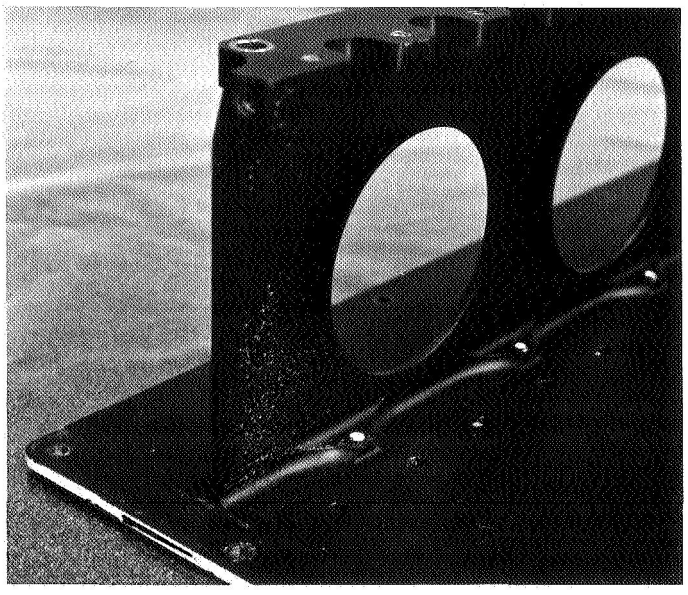


**Fig. IV-175. Electronic assembly chassis magnesium corrosion**

The most serious incident of corrosion occurred on the M67-1 (spare) at Cape Kennedy. The vehicle was in the explosive safe facility (ESF) undergoing checkout when the air conditioning failed. The gross relative humidity in the area never exceeded 73%. There was severe corrosion of most exposed magnesium surfaces on the vehicle. Since the vehicle was completely assembled, and had partially completed systems tests, it was decided to only remove the loose debris and not attempt to thoroughly clean the vehicle.

The problems of magnesium corrosion cannot be ignored though fabrication, assembly, and test are carried out in controlled environments. Coatings that offer a greater degree of corrosion protection should be used.

Anodic coatings (such as Dow 17) can be applied to controllable thicknesses much more readily than the conversion-type coatings (Dow 7), and thus provide reproducible emittance for radiant thermal control as well as provide a greater corrosion protection.

*g. High-gain antenna feed.* Several minor problems were encountered which were associated with equipment expected to operate at temperatures significantly different from that for which they were designed. Appendage items which were on top of *Mariner IV* and operated at moderate temperatures were now in the shade and expected to experience extremely low temperatures. Differential thermal expansion of dissimilar materials for *Mariner IV* was a source of potential problem for the extremely low temperatures expected for equipment in the shade and decoupled from the bus on *Mariner V*. The high-gain antenna feed assembly includes a polymer-copper laminate which distorted during low-temperature testing. It was impractical to redesign the feed to eliminate this laminate and the problem was solved by providing physical restraint and thus preventing distortion.

***10. Weight and center of gravity determination.*** The method used to align the *Mariner V* PIPS thrust axis and the procedure used to determine the spacecraft weight

and CG location were basically the same as that used for *Mariner IV*. In spite of the several changes to spacecraft configuration, all the existing CG fixtures and load cell equipment were utilized without change. Revisions to the written procedure were limited to corrections resulting from differences in the spacecraft configuration and some changes in the step-by-step calculation format to simplify the process of weight and CG determination. The latter revisions proved useful in that it allowed personnel who were relatively unfamiliar with the procedure to double-check the final calculations.

*a. Initial alignment estimates.* During the spacecraft preliminary design phase, it was necessary to determine if the adjustment capability in the *Mariner IV* substructure design was sufficient to properly align the PIPS thrust axis. As shown in Fig. IV-176, the available adjustment consisted of:

(1) Rotation of the PIPS mounting plane about a pivot point such that the thrust axis is parallel to the $X$-$Y$ plane ($\alpha = 0$ deg) to 4 deg out-of-plane ($\alpha = 4$ deg).

(2) Translation of the mounting pattern in plane C by as much as 0.375 in. up ($-Z$) to 0.25 in. down. Various combinations of this translation and the above rotation could be used for vertical CG adjustment.

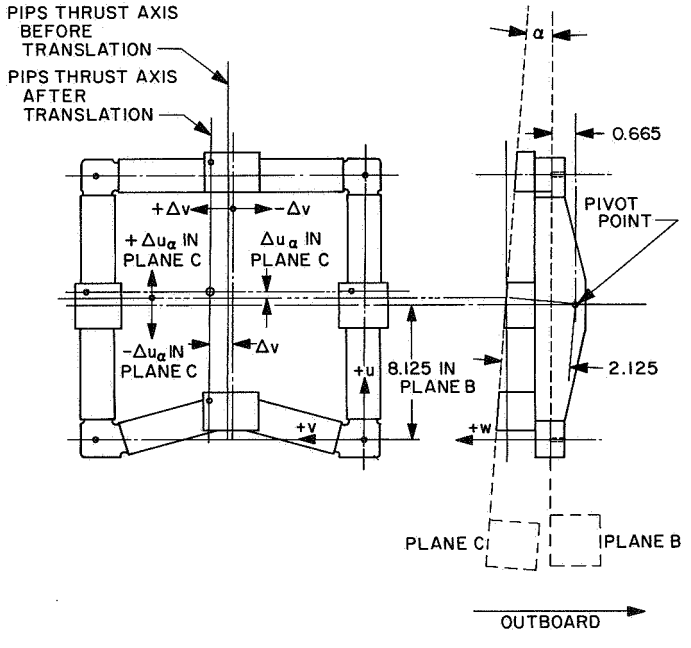



**Fig. IV-176. PIPS substructure translation orientation**

(3) Translation of the mounting pattern in plane C by $\pm 0.500$ laterally from the centerline of Bay II.

By tabulating the estimated weights of the proposed spacecraft changes, an initial estimate of spacecraft weight was determined to be approximately 550 lb with a CG location somewhat closer to the separation plane but within range of the present capability. Further investigation, however, indicated that the combination of rotation and vertical translation necessary, although within the stated range, would cause a possible interference between the PIPS propellant tank and a portion of the spacecraft secondary structure. The spacecraft structure was, therefore, reworked to ensure acceptable clearance for the entire adjustment range.

To gain further assurance as to the expected location of the flight spacecraft CG, the STM spacecraft was ballasted, to represent the best estimate of final equipment weight, and was subjected to a weight and CG exercise utilizing a rough-draft procedure. In addition to obtaining an early estimate of CG location, the rewritten procedures and existing CG fixtures were given a trial run to ensure their adequacy. Based on this exercise, it was estimated that the flight spacecraft would weigh approximately 535 lb and the CG location could be accommodated with a tilt angle of between 1 and 2 deg. This is in good agreement with the final values of approximately 540 lb and a tilt angle of 1.5 deg.

*b. Flight spacecraft measurements.* Before the decision was made as to the optimum tilt angle, a weight and CG determination was performed on M67-1. A full complement of flight spare equipment was available at this time with the notable exception of flight solar panels. Ballasted STM panel structures were utilized with the weight and CG of each panel carefully measured so that flight panel properties could be analytically substituted. After the flight panels had been individually weighed and the corrections entered into the determination, the optimum tilt angle, which allowed the maximum range of translation, was chosen to be 1.5 deg. The flight and flight spare autopilots were then modified with the equivalent biasing networks and all existing flight-type PIPS substructures were retrofitted with 1.5-deg blocks.

At the time the flight spacecraft (M67-2) was being measured at SAF, a full complement of flight solar panels was still not available. Two STM panels and two flight spare panels were substituted with corrections

made in the same manner as with the flight spare vehicle. Following the incorporation of corrected data for missing flight equipment on the two vehicles, M67-1 and M67-2 PIPS substructures were prepared with their respective thrust axis alignment translations and delivered for final assembly.

At AFETR, the flight spacecraft was subjected to a final CG determination to check the adequacy of the previously defined motor position and to provide an accurate number for thrust axis offset. Since this was the first time that the spacecraft was assembled with a full complement of flight hardware, it also allowed a direct comparison of actual position data with the answer derived from the previous incomplete weighing with substitution of properties for missing hardware.

Since the purpose of this final determination was to check motor location, an abbreviated procedure was used. This procedure required the spacecraft to be mounted on the Z-axis fixture only (Fig. IV-177). This minimized spacecraft handling, allowed an accurate determination of spacecraft weight and the measurement of CG position components in a plane parallel to the Bay II mounting plane. Because the PIPS thrust axis was only 1.5 deg from perpendicular to this plane, this allowed offsets to be interpreted directly from these data with minimum error (a 0.038-in. error in assumed location of the out-of-plane CG component would factor as only 0.001-in. offset error). Measurement errors were also minimized by using two sets of load cells. This resulted in the recorded load for each spacecraft reaction point being the average of data from six different load cells.

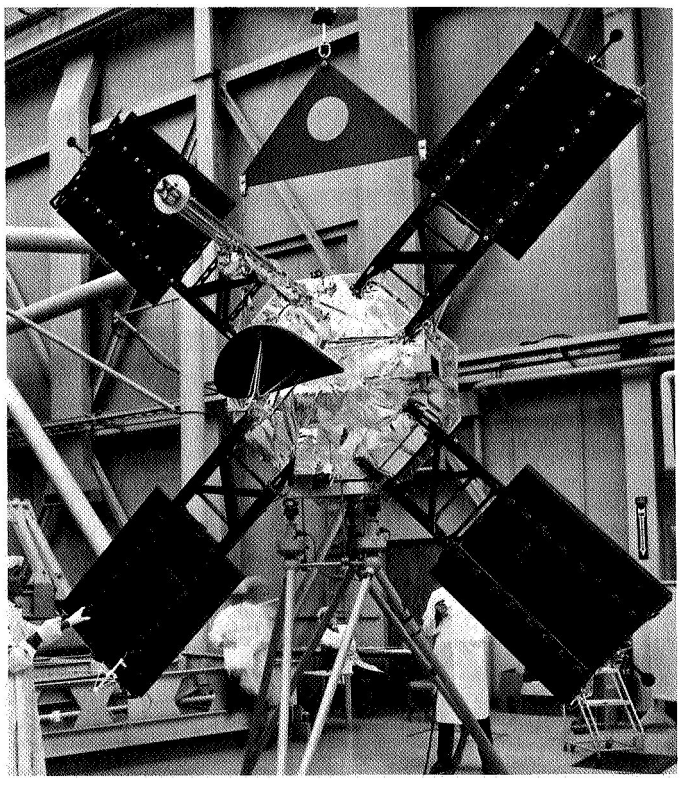


**Fig. IV-177. M67-2 on Z-axis CG fixture**

*c. Measurement and alignment results.* Table IV-44 summarizes measured weight and CG values for the M67-1 and M67-2 vehicles in the cruise configuration. It should be noted in the table that the differences in properties of the two vehicles is quite small, which is a tribute to the consistency in fabrication and assembly. A comparison of values for the separate determinations of the flight spacecraft also demonstrates the degree of accuracy that can be obtained by the correction of measured values for missing or substituted equipment. In particular, the solar panels represented approximately 11% of the total spacecraft weight and had significant CG moment arms; yet the difference in spacecraft CG between measurements was approximately 0.012 in. To further refine the probable contribution due to solar panel measurement errors, corrections were made to the data based on equipment changes recorded in the quality assurance (QA) status log. These corrections resulted in a residual CG error of approximately 0.004 in., which can be allocated to measurement errors and such small contributors as final cable splices and connector bonding.

*d. Analytical weight and CG determination.* In conjunction with the method of actually weighing an assembled spacecraft in the cruise configuration, a tabulation of piece-part weights, CG locations and estimated inertias was generated. This tabulation proved valuable early in the design for determining the adequacy of the *Mariner* Mars 1964 PIPS adjustment capability. As design and fabrication progressed, actual weights were substituted in the tabulation until, when hardware deliveries were complete, good agreement was realized with the actual measured spacecraft weight and CG location. Although not of the accuracy required to align the PIPS thrust axis, sufficient confidence was gained in the comparison to be assured of a satisfactory prediction of launch configuration CG and inertia properties of both launch and cruise configurations.

*11. Launch vehicle mechanical interface.* The *Mariner* Venus 67 effort in the launch vehicle mechanical interface

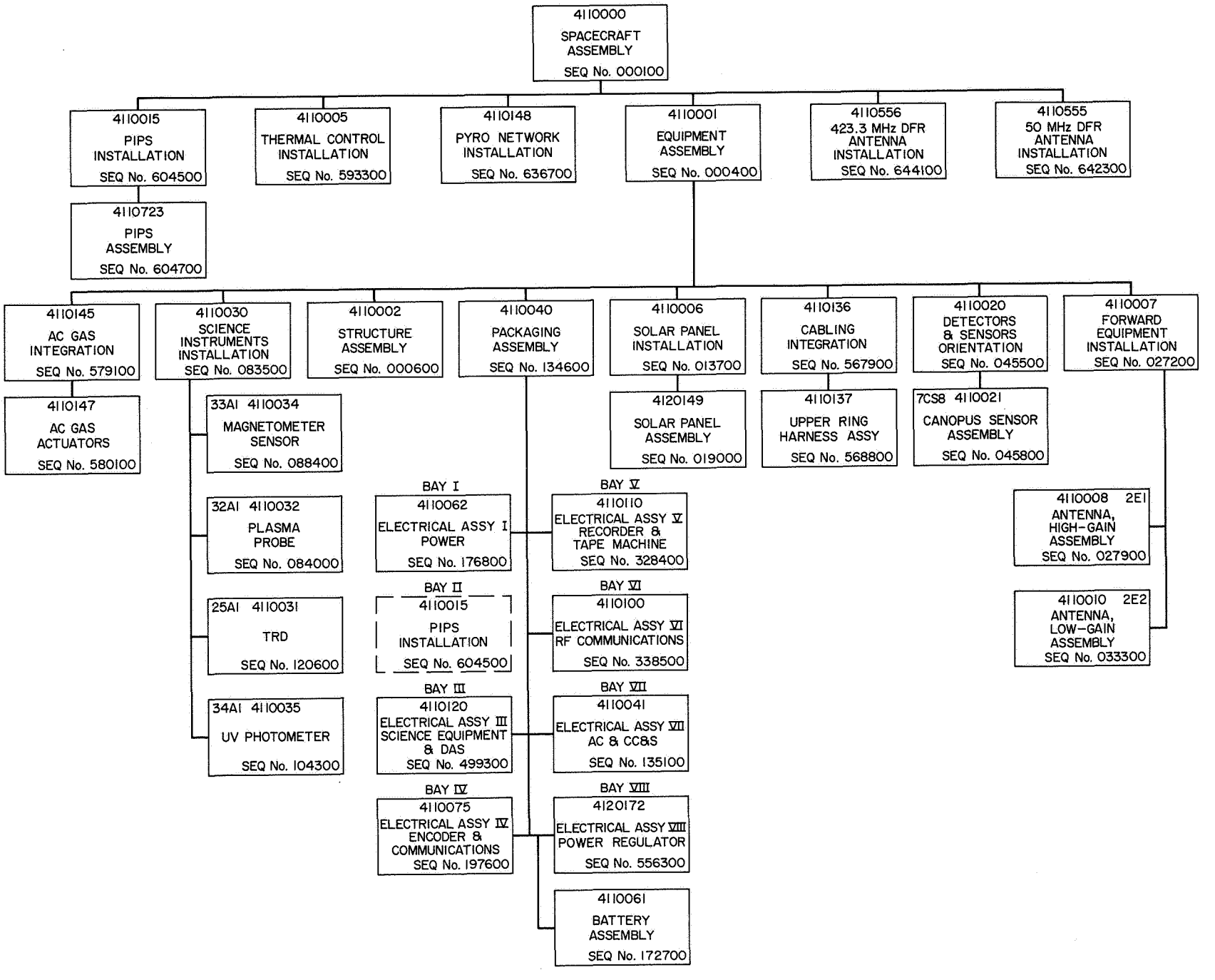



**Fig. IV-178. *Mariner* Venus 67 drawing tree**

Table IV-44. Summary of measured weight and CG values for the M67-1 and M67-2 in the cruise configuration

| Spacecraft | Weight, lb | CG location | | | PIPS translations | | Thrust axis offset | |
|---|---|---|---|---|---|---|---|---|
| | | X | Y | Z | ΔU | ΔV | Vertical | Horizontal |
| M67-1 (SAF) | 539.96 | +0.784 | +0.273 | −12.192 | +0.010 | +0.360 | 0 | 0 |
| M67-2 (SAF) | 540.00 | +0.761 | +0.301 | −12.145 | −0.038 | +0.324 | 0 | 0 |
| M67-2 (AFETR) | 539.17 | +0.768 | +0.293 | −12.145 | −0.037 | +0.336 | +0.001 | +0.012 |

area was small compared to that in *Mariner* Mars 1964. The major tasks included:

(1) Generating and updating the spacecraft *Agena* interface control drawing.

(2) Maintaining cognizance of the Lockheed-supplied interface flight, test, and ground-support hardware at JPL.

Several small changes and additions were required in the adapter to eliminate the possibility of sunshade hanging up on the adapter if a premature shade deployment occurred. These changes included relocating the shroud cavity pressure transducer and installing small skids in the inflight disconnect and PAS support bracket areas.

Although several hardware changes were made in the adapter, the *Mariner* Venus 67 design, in general, successfully avoided significant changes in the spacecraft booster interface area, which required extensive redesign and retesting.

*12. Drawing lists.* The *Mariner* Venus 67 drawing list consists of three publications:

(1) Offset. A listing in indentured form of all flight drawings. All part drawings that comprise an assembly are listed under that assembly drawing number (Fig. IV-178).

(2) Numeric. A numerical listing of all flight drawings.

(3) OSE. A numerical listing by cognizant division of all OSE drawings.

The list was published periodically during the program. The two flight lists each contain 6300 listings, involving 4100 drawings. Of the 4100 drawings used, 1900 were generated at JPL and 2200 were generated by vendors. Twenty-six different vendors furnished drawings.

The *Mariner* Venus 67 operational support equipment list contained 7300 listings. JPL generated 3800 drawings and vendors generated 2450. Fourteen vendors are represented in the OSE list.

## I. Telecommunication/DSIF Compatibility Tests

The objectives of the compatibility tests were to demonstrate compatibility between the spacecraft telecommunications system (STS) and the GSDS ground stations of the DSIF. Further objectives were to compare telecommunications systems operating performance characteristics with the predicted characteristics and to provide the DSN personnel with a limited amount of experience in operating *Mariner* Venus 67.

The STS used for this test was electrically equivalent to that flown for the *Mariner* Venus 67 mission. It was set up, along with its associated OSE, in the spacecraft test facility screen room located between DSS-11 and DSS-12 at the Goldstone tracking station. An S-band RF link between the screen room and DSS-11 was established and calibrated for use during the test. Both the spacecraft and DSIF systems were exercised under various operating conditions designed to uncover any incompatibilities between the spacecraft and the ground station, and to demonstrate that the performance of each was adequate to meet mission requirements. The test plan and schedule are shown in Appendix C. The results of each test, including a discussion, and any problem areas discovered, are presented as a summary of each test. With few exceptions, it was possible to follow the predicted schedule quite closely.

The DSIF station had two full crews during these tests, one during the day and the other during the evening shift. Spacecraft personnel worked both shifts because of the limited number of personnel available for this task.

In general, the test results were satisfactory and all of the major objectives were achieved. The tests successfully demonstrated that the STS and the DSIF ground stations were compatible, and that their performance was adequate to meet mission requirements.

*1. Link calibration.* The objectives of the link calibration were:

(1) To compare measured RF link attenuation with the attenuation derived by summing the individual components of the link. This will verify that all significant components of the link have been considered.

(2) To demonstrate repeatability of measured RF link attenuation over the complete range of signal levels from maximum to RF threshold. This will verify that the isolation of the screen room is adequate to perform repeatable tests at near threshold signal levels.

(3) To check out all pads and attenuators that will be used during the test and verify that they will provide the required dynamic range of signal levels.

A block diagram showing the configuration of the RF link between the ground stations and the screen room is shown in Fig. IV-179. Figure IV-180 shows the additional losses due to cables, attenuators, and pads within the screen room. The calculated path loss between the screen room and the DSIF station receiver at 2295 MHz was 90 dB and the loss from the DSIF transmitter to the screen room input at 2113 MHz was 92 dB.

During link calibration, the average measured path loss was 90 dB for the spacecraft to ground station channel at 2295 MHz and 94 dB for the ground station to spacecraft channel at 2113 MHz. These numbers agree closely with the computed path losses and were considered acceptable for use during the test. It should be noted that the spacecraft AGC was re-calibrated after some discrepancies were noted during the first few days of the test. During the remaining 2½ weeks of the test, this calibration remained good.

During the first two days of the test, link calibrations were performed by DSIF personnel, using their own path loss measuring equipment. Beginning with the third day, and for the duration of the test, enough confidence had been gained in the RF link calibrations and in the spacecraft and ground station AGC calibrations to allow the link to be calibrated each morning using the spacecraft and the ground receiver AGC.

RF leakage within the screen room caused some problems until the 2113-MHz notch filter was placed on the line immediately following the diplexer (Fig. IV-180). The effect of the leakage was that at low uplink and high downlink signal levels, the uplink-received AGC varied when the downlink attenuator varied. After trying several configurations, the notch filter was found to solve the 2113-MHz leakage problem without inducing additional problems, such as 2295-MHz leakage.

The screen room and RF communication link from the screen room to DSS-11 performed satisfactorily during the test. Modifications to the screen room facility

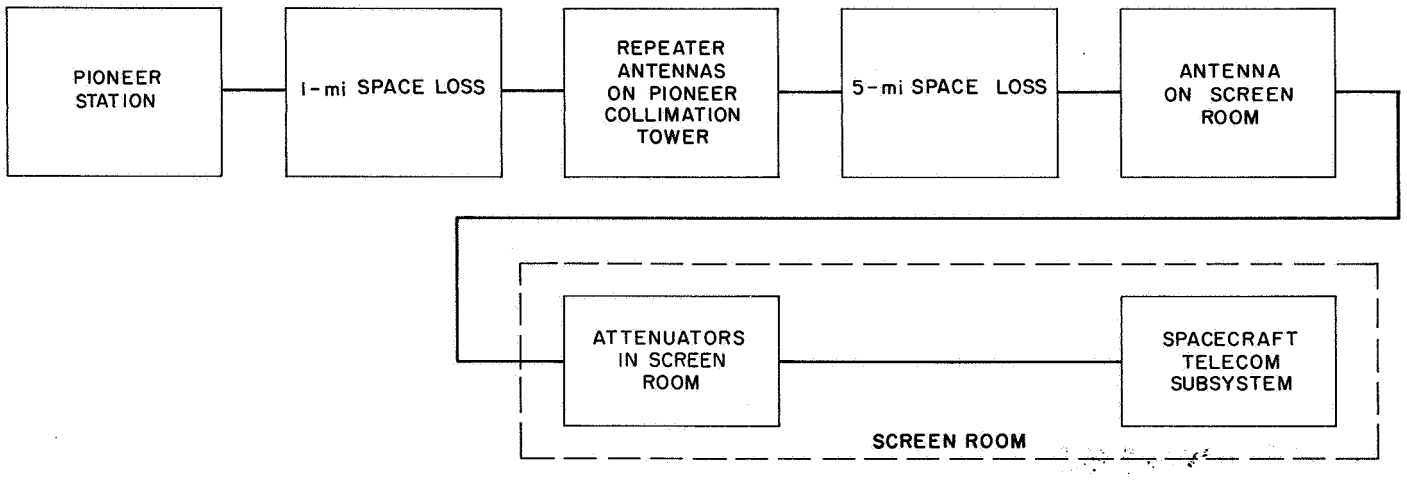



**Fig. IV-179. Block diagram of RF test link *Mariner* Venus 67 — DSIF compatibility test**

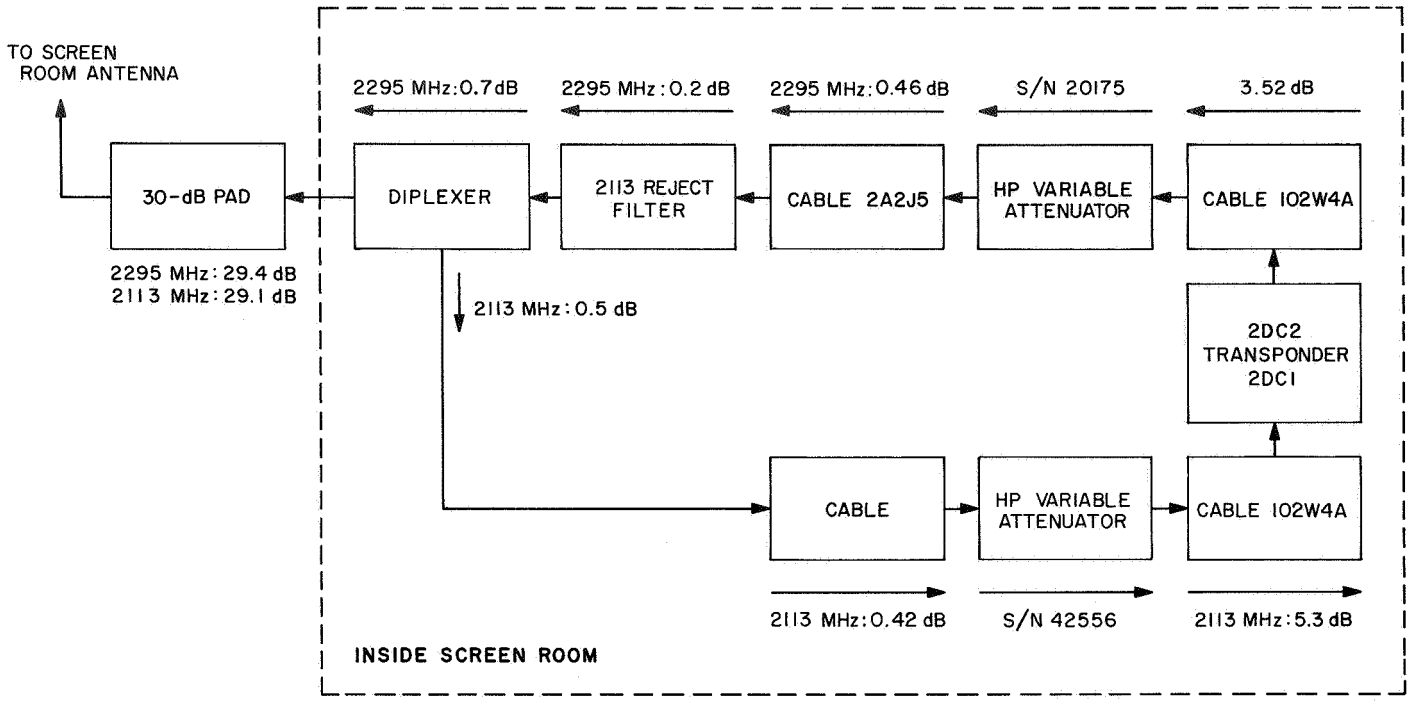



**Fig. IV-180. Screen room RF path final equipment configuration *Mariner* Venus 67 — DSIF compatibility test**

since the *Mariner IV* tests provided greatly improved conditions for setting up the spacecraft and its OSE. The only significant problem concerned with the screen room was the temperature control. It was difficult to maintain an even temperature during an entire testing day.

A return data link was established between the screen room and DSS-11 over telephone lines from the screen room to the DSS-12 communications center and over the intersite microwave from the communications center to DSS-11. This link was used for the command bit error tests with good results.

However, the link was not adequate to support the telemetry bit error tests. It was necessary to modify the link, using FM voltage-controlled oscillators (VCOs) and discriminators to pass telemetry data and bit synchronization for these particular tests.

In general, the test facility was adequate for tests of this type, and no problems were encountered that could not be overcome.

***2. RF subsystem test.*** The objectives of the RF subsystems test were:

(1) To verify all RF operational modes between the spacecraft and the DSIF stations.

(2) To demonstrate that the spacecraft RF system will perform within required specification limits with the DSIF station.

(3) To verify both spacecraft and ground receiver threshold in an operational configuration.

(4) To discover and investigate any spurious lockup modes between the spacecraft and the DSIF receiver, or between the DSIF transmitter and the spacecraft receiver.

(5) To measure residual phase modulation for both the spacecraft and the ground station receivers in both one- and two-way lock.

(6) To measure spacecraft receiver static phase error (SPE) pull range with varying DSIF transmitter frequencies.

(7) To familiarize station personnel with the operation of the *Mariner* transponder, and to note any unique characteristics of the *Mariner* transponder for use in preparing operational procedures.

*a. Results.* With one exception, the spacecraft RF system used for these tests was equivalent to that flown on *Mariner V*. This concerned the bandpass/lowpass filter, which was included in the flight system as a part of the ranging fix. The system used for the compatibility test

had a simulation of the filter, and would have been more susceptible to spurious lockup with ranging than on a flight system. However, no evidence of spurious ranging lockup was observed during the test. Initial acquisition of the spacecraft by the ground station was easily accomplished by the DSIF operators once they learned the spacecraft receiver best-lock frequency, and spacecraft exciter auxiliary oscillator frequencies. It was noted that at high downlink signal levels, the ground receiver would easily lock onto the telemetry sidebands at 8⅓ bits/s. The ground receiver operator soon became adept at identifying the correct carrier lock point; however, this problem should be called to the attention of all receiver operators around the net.

During the first few days of the test, variations in temperature in the screen room were observed, and corresponding variations in spacecraft receiver best-lock frequency and auxiliary oscillator frequencies resulted. The screen room air conditioner was adjusted and daily temperature variations became much less. This condition did not cause any major problems.

Also, during the first few days of the test RF leakage problems inside the screen room were observed, and some testing delay was necessary until these problems could be resolved. After several attempts, the test configuration shown in Fig. IV-180 was chosen. No further leakage problems were noted.

Both spacecraft and DSIF receiver RF thresholds were verified on numerous occasions during the test. The measured levels were always consistent with predicted levels. During the spurious radiation tests, the spacecraft receiver detected no spurious signals at any level within its bandwidth. The ground receiver observed numerous spurious signals radiating from the spacecraft; however, all signals were within specifications (i.e., more than −30 dB below the carrier). Results of the residual phase modulation tests are presented in Table IV-45.

A trial to determine the spacecraft receiver maximum pull range was attempted at a signal level of −100 dBm on the uplink and −93 dBm on the downlink. The ground transmitter VCO was slowly varied until it was 1034 cycles at the VCO frequency above spacecraft receiver best-lock frequency. The spacecraft receiver was still in lock. Since the receiver would never be required to track this far in an actual operation, and inasmuch as

**Table IV-45. Results of residual phase modulation tests, *Mariner* Venus 67—DSIF compatibility test**

| Spacecraft | | | | DSIF | | | Uplink | Downlink |
|---|---|---|---|---|---|---|---|---|
| Power amplifier | Exciter | Telemetry modulation | Received carrier power, dBmW | Transmitter power, kW | Receiver 2 $B_{LO}$, Hz | Received carrier power, dBmW | Residual phase mod (P−P), deg | Residual phase mod (P−P), deg |
| A | A | Off | — | — | 12 | −100 | — | 12 |
| A | B | Off | — | — | 12 | −100 | — | 10.5 |
| B | A | Off | — | — | 12 | −100 | — | 20 |
| B | B | Off | — | — | 12 | −100 | — | 11 |
| A | A | Off | — | — | 48 | −100 | — | 9 |
| A | B | Off | — | — | 48 | −100 | — | 9.5 |
| B | A | Off | — | — | 48 | −100 | — | 15 |
| B | B | Off | — | — | 48 | −100 | — | 8 |
| A | A | On | — | — | 12/48 | −100 | — | TLM signal |
| — | — | — | −80 | 0.2 | — | — | 2.8 | — |
| — | — | — | −80 | 1 | — | — | 2.8 | — |
| — | — | — | −80 | 10 | — | — | 3.0 | — |
| A | A | Off | −100 | 10 | 12 | −100 | — | 7.5 |
| A | A | Off | −100 | 10 | 48 | −100 | — | 6.0 |
| A | A | Off | −100 | 10 | 152 | −100 | — | 5.0 |

this far exceeds the functional specification tracking range, it was decided to terminate the test at this point. Because of the length of time these tests took, it was decided not to perform any more pull range tests and to devote the time to more useful tests.

A series of operational tests was conducted to familiarize the DSIF personnel with the behavior of the *Mariner V* transponder under various operating conditions, and to furnish information for mission planning.

The first of these tests was for the ground transmitter operator to activate the transmitter at a frequency displaced a known amount from the spacecraft receiver best-lock frequency, and to observe the spacecraft receiver lockup. This test demonstrated that unless the best-lock frequency is known quite accurately, it will take a long time for the spacecraft receiver to lock up (acquisition might never occur if the uplink frequency were displaced far enough). The most reliable way to achieve uplink lock in a minimum time is for the uplink transmitter frequency to be slowly swept through spacecraft receiver best-lock frequency.

The second set of operational tests was to determine typical downlink receiver lockup times when going from one-way to two-way lock. Table IV-46 lists the results of these tests. The average lockup times were 4 to 5 s, except when the spacecraft or ground receivers were near (within 10 dB) the threshold. Under these conditions, average lockup times were 15 to 22 s.

To evaluate the time required for the spacecraft transmitter exciter to switch from VCO reference to auxiliary oscillator reference, the ground transmitter was turned off, and the time required for the ground receiver to drop lock at the two-way frequency was noted. The

**Table IV-46. One-way to two-way RF lockup times *Mariner* Venus 67–DSIF compatibility test**

| Spacecraft-received signal level, dBmW | Ground-received signal level, dBmW | Average lockup time, s |
|---|---|---|
| −100 | −100 | 4 |
| −100 | −120 | 5 |
| −120 | −120 | 4.5 |
| −120 | −140 | 5.5 |
| −140 | −140 | 15 |
| −140 | −160 | 22 |

**Table IV-47. Two-way to one-way switchover times *Mariner* Venus 67–DSIF compatibility test**

| Spacecraft-received signal level, dBmW | Ground-received signal level, dBmW | Average switchover time, s |
|---|---|---|
| −100 | −120 | 21 |
| −120 | −120 | 19 |
| −140 | −120 | 13 |

results of this test are listed in Table IV-47 as a function of spacecraft-received signal level.

During the *Mariner* Mars 1964 mission, it was noted that the occurrence of CY-1 events from the spacecraft CC&S would cause a small shift in spacecraft auxiliary oscillator frequency if the spacecraft receiver was out of lock. This was analyzed and explained as a small change in an exciter voltage, due to the RF system switching logic changing states when a CY-1 is received and the spacecraft receiver is out of lock. This frequency shift was also noted to be a function of the individual auxiliary oscillator, and was not consistent between exciters.

During this test, several CY-1 were sent under varying conditions of downlink signal level; no frequency shift was noted for either exciter. This does not mean that a frequency shift would not be observed with the flight spacecraft, but merely indicates that the particular system under test did not have this phenomenon.

*b. Conclusions.* This series of tests successfully demonstrated that the spacecraft RF system and the GSDS ground stations were completely compatible. Ground receiver operators should be made aware of the ease with which the RF receiver will lock onto a telemetry sideband and the means of verifying the correct lock condition. No problems requiring modifications to either spacecraft or ground station hardware were discovered.

*3. Telemetry subsystem test.* The objectives of the telemetry subsystem test were:

(1) To demonstrate real-time decommutator and telemetry and command processor (TCP) readout of telemetry measurements in a system configuration, including the spacecraft and the DSIF station.

(2) To check polarity compatibility of DSIF and mission-related hardware (MRH) with the spacecraft telemetry subsystem.

(3) To verify telemetry modulation indices.

(4) To perform bit-error tests on the telemetry system through the complete ground station receiving and telemetry distribution systems.

(5) To verify relative thresholds for data subcarrier and synchronization channels.

(6) To observe demodulator synchronization correlation curves at various received signal levels.

(7) To measure average acquisition times for the telemetry demodulator at various received signal levels.

(8) To provide familiarization and experience with *Mariner* Venus 67 equipment for station personnel.

*a. Results.* The spacecraft data encoder used for these tests was equivalent to the *Mariner* Venus 67 flight unit, except that there was no input data from the science subsystems used during the test. The test did not include a switch to the second ground station TCP string, as called out in the test procedure. This was because the beta TCP did not have an operational millisecond clock at the time of the test. Otherwise, the overall system was compatible for all spacecraft bit rates, amplifiers, exciters, and DSIF receiver combinations.

The polarity of the DSIF receiver signal into the ground telemetry subsystem (GTS) is in accordance with the convention agreed upon in the DSN/*Mariner* Venus 67 compatibility document when the ground station receiver phase shifter is at zero degrees. The operational procedures utilized regarding this phase shifter should be carefully defined to prevent a telemetry data inversion.

The modulation index, with the spacecraft data encoder as a source, did not vary between exciters or A to D converter/PN generator (ADC/PNG). The carrier suppression, as measured by DSIF receiver AGC, was 0.3 dB less at 8⅓ bits/s than at 33⅓ bits/s when measured through the RF system.

Bit error tests were attempted, using the test configuration defined in the test plan. This required passing the composite telemetry signal from the encoder simulator at DSS-11 via microwave to the DSS-12 communication center, then via telephone lines to the screen room. The signal was then used to modulate the spacecraft S-band carrier, which was transmitted over the RF link back to DSS-11.

Considerable time was spent in attempting to stabilize this link and to improve its frequency characteristics so that it could support the bit error tests. Because of several problems with the response characteristics of this link, it was finally decided that it could not be used in its present configuration. Among the reasons for this decision were amplitude variations of nearly 3 dB that resulted in carrier suppression variations and precluded an accurate setting of the subcarrier modulation index.

After much experimentation, a new configuration (Fig. IV-181) was found to be adequate for the test. Although this arrangement was a good deal more complex than that originally proposed, it proved stable, and had satisfactory linearity and frequency response to support the bit-error tests.

The original test plan called for a long sequence of bit-error tests requiring approximately 2⅔ days of testing for completion. Because of the time consumed in setting up test links, it was necessary to shorten the test sequence, and to eliminate tests designed to gather many data points on only one configuration. It was decided that overall compatibility could be shown by one successful test for each particular combination of spacecraft and ground station operating mode. These tests were conducted and their results compared to theoretical bit-error rates.

Data points fell within 1 dB of theoretical, except at the threshold points, where the noise on the ground receiver signal made it difficult to control the signal level to within 1 dB. The long-term stability of the test link during the period of the bit-error test was not as stable as required for laboratory quality bit-error test, and the test results are within the experimental tolerances. These tests demonstrated overall compatibility of the spacecraft–DSIF system as a whole, and the results of laboratory bit-error tests must be used to demonstrate theoretical performance capabilities.

Relative threshold tests showed the GTS demodulator would lose synchronization correlation and drop lock at the signal levels predicted within the accuracy of the test configuration. With signal levels very near threshold (within 3 dB), precision in operating the GTS demodulator is necessary to reach the theoretical limits of the telemetry system.

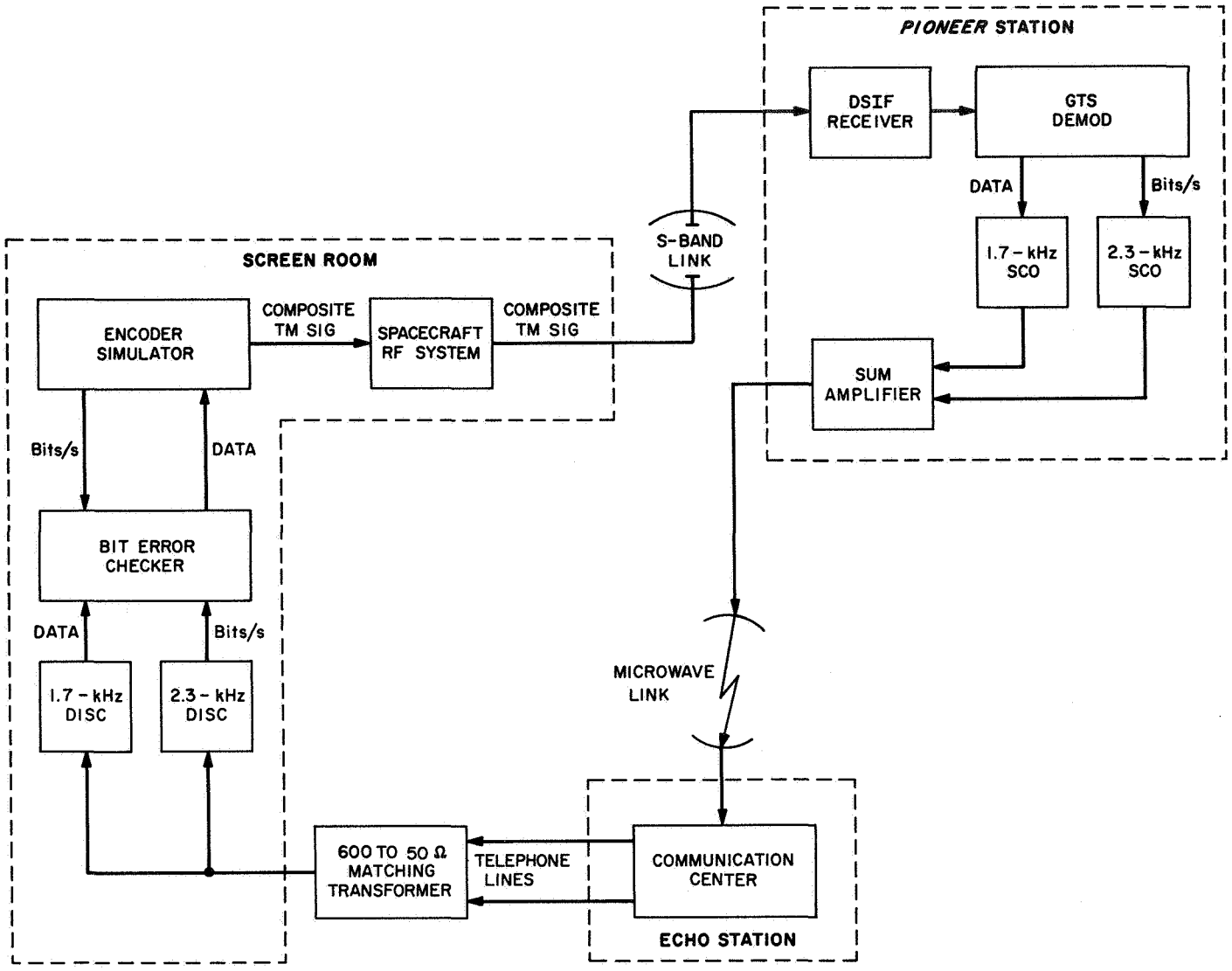



**Fig. IV-181. Telemetry bit error test final equipment configuration *Mariner* Venus 67 — DSIF compatibility test**

Table IV-48 shows average demodulator acquisition time at various receiver bandwidths, signal levels, and bit rates. These are average times and should be considered rough, since few samples were taken. The only area of concern observed during these tests is that of false lock points. At 8⅓ bits/s, with the ground receiver $2B_{LO}$ at 48 Hz, part of the synchronization spectrum falls within the bandwidth of the RF loop and is tracked out by the receiver. This causes a shift in the synchronization correlation curve toward the quarter PN bit out point. This results in the demodulator looking up a quarter PN bit away from the center and a subsequent incorrect data bit presentation. This should not be a problem during an operation, since the GTS operator can readily identify the false lock point and achieve correct lock. Also, the ground receiver will normally be set to 12 Hz, $2B_{LO}$ when the spacecraft is operating at 8⅓ bits/s.

Real-time decommutator and TCP readouts of the engineering telemetry were demonstrated, and data were sent to the SFOF via teletypewriter (TTY) and high-speed data line (HSDL) in a test of the overall system.

*b. Conclusions.* The objectives of the test were met and systems compatibility proven. To realize optimum GTS performance and eliminate operation at false lock points, operations procedures must be carefully defined and followed. No incompatibilities or other problems were uncovered that will require modification of either the spacecraft or ground station hardware.

**Table IV-48. Telemetry demodulator synchronization acquisition times, *Mariner* Venus 67–DSIF compatibility test[a]**

| Run No. | 33⅓ bits/s | | | | | | 8⅓ bits/s | | | | | |
|---|---|---|---|---|---|---|---|---|---|---|---|---|
| | $2B_{LO}$ = 12 Hz | | | $2B_{LO}$ = 48 Hz | | | $2B_{LO}$ = 12 Hz | | | $2B_{LO}$ = 48 Hz | | |
| | −120 dBmW | −140 dBmW | −158 dBmW | −120 dBmW | −140 dBmW | −156.5 dBmW | −120 dBmW | −140 dBmW | −160.5 dBmW | −120 dBmW | −140 dBmW | −160 dBmW |
| 1 | 55 s | 53 s | 1 min 26 s | 54 s | 52 s | 1 min 13 s | 225 s | 79 s | 144 s | 218 s | 156 s | |
| 2 | 55 s | 55 s | 1 min 00 s | 55 s | 51 s | 3 min 53 s | 216 s | 188 s | 180 s | 225 s | 205 s | |
| 3 | 55 s | 53 s | 2 min 36 s | 53 s | 51 s | 16 s | 217 s | 186 s | 176 s | 206 s | 193 s | |
| 4 | 55 s | 55 s | 1 min 56 s | 55 s | 51 s | 51 s | 217 s | 179 s | 176 s | 213 s | 186 s | |
| 5 | 55 s | 55 s | 1 min 58 s | 54 s | 51 s | 1 min 6 s | 216 s | 171 s | 188 s | 240 s | 178 s | |
| 6 | 55 s | 54 s | 17 s | 54 s | 52 s | 28 s | 217 s | 163 s | | 218 s | | |
| 7 | | 54 s | 1 min 52 s | | 52 s | 46 s | | 210 s | | 211 s | | |
| 8 | | 52 s | 2 min 21 s | | 52 s | 1 min 10 s | | 209 s | | | | |
| 9 | | 53 s | 2 min 51 s | | 51 s | 26 s | | 199 s | | | | |
| 10 | | 53 s | 28 s | | 51 s | 1 min 45 s | | 194 s | | | | |
| 11 | | | | | 50 s | | | | | | | |
| 12 | | | | | 51 s | | | | | | | |
| Average | 55 s | 53.3 s | 1 min 40 s | 54.18 s | 51.52 s | 65.4 s | 218 s | 177.8 s | 172.8 s | 218.7 s | 183.6 s | |
| AGC, V | −5.72 | −4.11 | — | −5.72 | −4.08 | — | −5.76 | — | — | −5.79 | — | |
| dBmW | −120 | −138.9 | −158 | −120 | −139.3 | −158 | −120.3 | −140 | −160.5 | −120.0 | −140 | |

[a]Spacecraft power amplifier A and exciter A.

*4. Command system test.* The objectives of the command system test were:

(1) To verify polarity compatibility of DSIF and read-write-verify (RWV) with the spacecraft command system.

(2) To verify command modulation indices.

(3) To perform command bit error tests through an RF link.

(4) To observe synchronization correlation curves at various received signal levels to verify satisfactory system performance over the range of signal levels predicted for the mission.

(5) To measure acquisition times for the command system at various 8 $f_s$ frequency offsets.

(6) To demonstrate the display of RWV operator information on the TTY printer next to the RWV in the MRH area.

(7) To demonstrate telemetry indication of command reception by real-time decommutator and TCP readout.

(8) To verify command synchronization threshold through the RF link.

(9) To provide operational experience with the spacecraft command system for station personnel.

*a. Results.* The polarity of the command signal, as generated by the RWV and transmitted by the DSIF transmitter, is in accordance with the convention agreed upon in the *Mariner* Venus 67/DSIF compatibility document.

With the RWV modulation output, it was not possible to suppress the uplink carrier the required 3.2 dB. This problem was recognized and a fix implemented at all stations. The suppression during the test was approximately 2.7 dB and was adequate to allow the remainder of the compatibility tests to be run.

Figure IV-182 shows the configuration used for the command bit-error test. The telephone line and microwave link from the spacecraft OSE in the screen room to the RF phase modulator at the ground station passed the composite command signal with negligible distortion and appeared to be stable on the days the tests were run.

Results of these tests were compared to data from command bit-error tests run in the laboratory. Results of these comparisons showed that the maximum deviation from laboratory data was 0.6 dB, which is within the tolerances associated with the test configuration.

Command synchronization correlation curves, plotted at three RF input levels, showed that it is possible to obtain a false lock point at high-signal levels when the 8 $f_s$ offset used for acquisition is below the nominal frequency. No false lock problems were observed when the 8 $f_s$ offset was above nominal. Operating procedures should be written so as to always offset the 8 $f_s$ frequency high for acquisition during a mission to eliminate this potential problem.

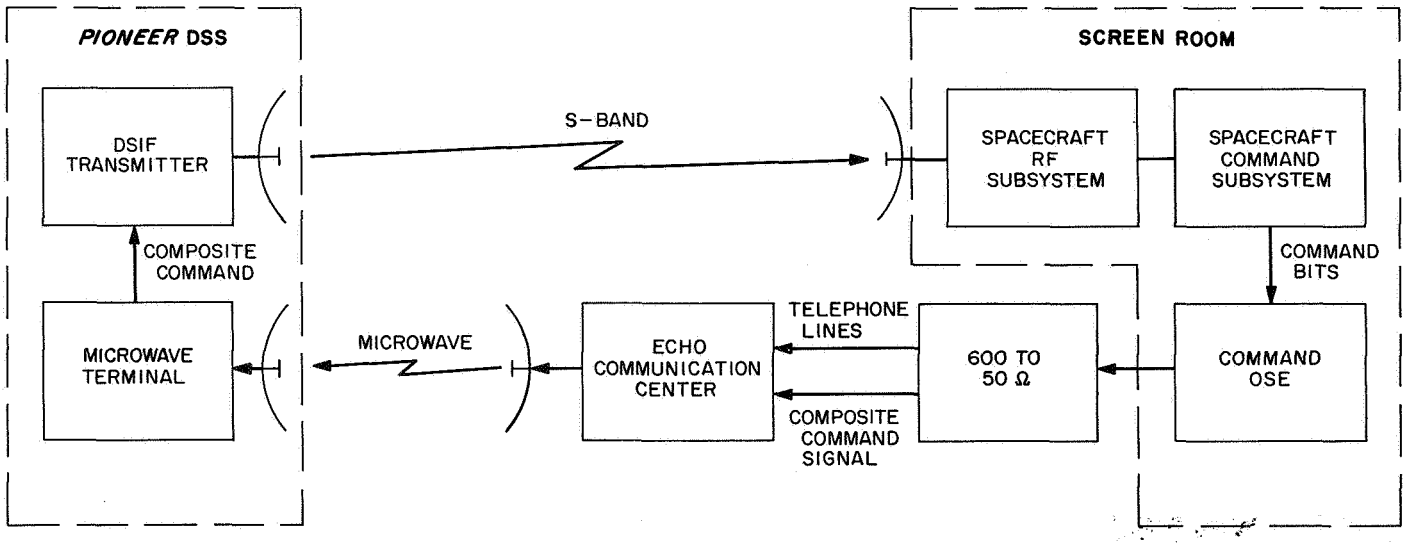



**Fig. IV-182. Command bit error tests final equipment configuration *Mariner* Venus 67 — DSIF compatibility test**

Table IV-49. Command acquisition test results, *Mariner* Venus 67–DSIF compatibility test

| Test[a] | 8-$f_s$ offset | | | | Test[b] | 8-$f_s$ offset | | | |
|---|---|---|---|---|---|---|---|---|---|
| | 3 Hz, s | 4 Hz, s | 5 Hz, s | 6 Hz, s | | 2 Hz, s | 4 Hz, s | 5 Hz, s | 6 Hz, s |
| 1 | 426 | 347 | 358 | 252 | 1 | | 994 | 1229 | 238 |
| 2 | 1085 | 366 | 303 | 209 | 2 | | 1710 | 192 | 345 |
| 3 | 1812 | 383 | 638 | 306 | 3 | | 116 | 439 | 888 |
| 4 | | 701 | 463 | 378 | 4 | | | 814 | 1075 |
| 5 | | 845 | 415 | 224 | 5 | | | 553 | 1072 |
| 6 | | | | | 6 | | | | |
| 7 | | | | | 7 | | | | |
| 8 | | | | | 8 | | | | |
| 9 | | | | | 9 | | | | |
| 10 | | | | | 10 | | | | |
| Average | 1108 | 528 | 435 | 274 | Average | | 940 | 645 | 723 |

[a]Command acquisition time test, $P_{total} = -135$ dBmW.
[b]Command acquisition time test, $P_{total} = -137$ dBmW.

Table IV-49 shows results of acquisition time tests run at various signal levels and 8 $f_s$ offsets. These times, although not enough runs were made to accurately define average lockup time, are comparable to times achieved in the laboratory. Synchronization acquisition by the spacecraft command system appeared to be normal in all respects. The telemetry displays on the RWV console as driven by the GTS decommutator, are operational and functioned normally throughout the tests.

Numerous commands were transmitted from the RWV to the spacecraft and successfully performed switching functions within the telecommunications system. Verification of command reception was demonstrated by real-time TCP and GTS decommutator readout of event channel data.

*b. Conclusions.* The RWV–DSIF–spacecraft interface was compatible and functioned within specification. The only significant problem noted during the test was that the RWV output was not adequate to suppress the carrier's 3.2 dB as required. Modifications were made to all RWVs around the net to overcome this difficulty.

## J. EMI Reductions

Because *Mariner V* was a modification of the adequately qualified *Mariner IV* design, electromagnetic compatibility verification requirements were focused primarily on those areas where design changes or additions had occurred. An addition to the *Mariner IV* design was a sensitive DFR. The DFR is the receiving element of a radio wave propagation experiment. The experiment consists of measuring amplitude, frequency, and phase changes of 49.8 and 423.3 MHz signals from a ground transmitter.

Because interference is a distinct possibility for radio subsystems in close proximity to electronic devices and because radio receivers can be seriously degraded by RF noise, a formal electromagnetic interference assessment was initiated on the compatibility of the DFR with *Mariner V*.

Specifically, there were three principal areas of concern for the ability of the DFR experiment to perform satisfactorily on *Mariner V*. First, although the DFR is a phase-locked receiver, its sensitivity can be degraded by low-level RF energy in its frequency band. Any RF noise coupled into the receiver will decrease the signal-to-noise ratio and thereby decrease receiver sensitivity. A reduction in receiver sensitivity could jeopardize the instrument's capability to perform its scientific mission objectives. The second area of concern was the power levels of the fundamental and harmonics of the DFR ground transmitters. The fifth harmonic of 423.3 MHz is 2116.5 MHz while the *Mariner V* S-band receiver frequency is 2115.7 MHz with a 7-MHz intermediate frequency amplifier bandwidth. With the 423.3-MHz

ground transmitter operating at its 30-kW output level, there was the possibility that the fifth harmonic would be of sufficient magnitude to acquire phase lock with the S-band receiver, particularly during the near-earth portion of the mission. In addition, the 49.8-MHz ground transmitter operating at its 300-kW output might interfere with the 47.8-MHz intermediate frequency of the S-band receiver. Finally, reports of DFR performance degradation on two sun-orbiting spacecraft caused apprehension for the successful operation of the instrument on *Mariner V*.

The objective of the DFR integration effort, then, was to develop as compatible an environment as possible between the DFR and the other subsystems on *Mariner V*. During this investigation, it became necessary to establish levels of maximum permissible noise degradation to the DFR. The principal investigator for the experiment contributed to this effort by specifying that no more than a 3-dB degradation should occur to the 49.8-MHz channel and no more than a 1-dB degradation to the 423.3-MHz channel.

*1. Integration program.* The integration program for the DFR consisted of both analysis and testing to determine incompatibilities between the DFR and the other spacecraft subsystems. The analysis served to select areas that required special tests to determine integration problems. Spacecraft subsystem and system level tests, as well as tests of the DFR ground transmitter harmonic content, subsequently were performed to establish the necessary corrective action for compatibility between the DFR experiment and *Mariner V*. During the investigation, specific recommendations were made and spacecraft redesign changes were incorporated to reduce or eliminate RF noise interference. The last phase of the integration effort consisted of system level verification tests using a flight-assembled spacecraft suspended from nylon ropes to simulate flight conditions. The suspension tests demonstrated that acceptable DFR performance was possible if the spacecraft were modified according to the recommendations of the DFR integration team.

*a. Analysis summary.* The DFR integration analysis began by reviewing DFR data obtained from another space program. Personnel at the cognizant NASA center were interviewed to determine problem areas. The results of subsystem level electromagnetic interference tests performed on the DFR were obtained and reviewed. Examination of the electromagnetic interference (EMI) data showed some frequencies to which the DFR was susceptible and others at which it emitted RF energy. A calculation of the expected RF power density levels of the DFR ground transmitter (a potential problem area) indicated that, in the event of maximum DFR ground transmitter power emission during the first view of the spacecraft, no interference would be expected. It was also estimated that harmonics from the transmitter would be sufficiently suppressed; however, because of unknown parameters, no definite conclusions could be drawn about the actual power levels. It was recommended that measurements be performed on the harmonics of concern (specifically $5 \times 423.3 = 2116.5$ MHz) to verify that the radiated levels would not affect the spacecraft transponder. A computer program was written as part of the investigation to determine possible intermodulation products on the spacecraft that would cause interference to the DFR or the S-band transponder. Several potentially disruptive frequencies were determined through usage of the computer program.

*b. Test program.* A series of tests was performed at the subsystem level as well as at the spacecraft system level with both completely and partially assembled systems. The approach was to evaluate questionable areas as soon as possible with the equipment available, taking advantage of fluctuations in the schedule of spacecraft equipment. The goal was to obtain as much information as possible about DFR/spacecraft incompatibility early in the program to allow maximum time to solve the problems encountered.

Figure IV-183 shows the spacecraft configuration for the first and second tests performed. Neither a science subsystem nor a DFR was available for these tests. Because a DFR was not available, the degradation levels had to be calculated based on measurements taken by the test receiver. These tests were preliminary in nature, but were useful in establishing the techniques and direction for further testing. Three significant facts were learned from these early tests:

(1) A 50-MHz noise generated by spacecraft subsystems was present at the VHF antenna at a level sufficient to seriously degrade the VHF channel of the DFR. The source of this 50-MHz noise was the power subsystem booster regulators, battery charger, and the radio subsystem RF amplifier power supplies. Calculated values of DFR degradation from these noise sources ranged from 3 to 6 dB, depending on what combination of noise sources were operating.

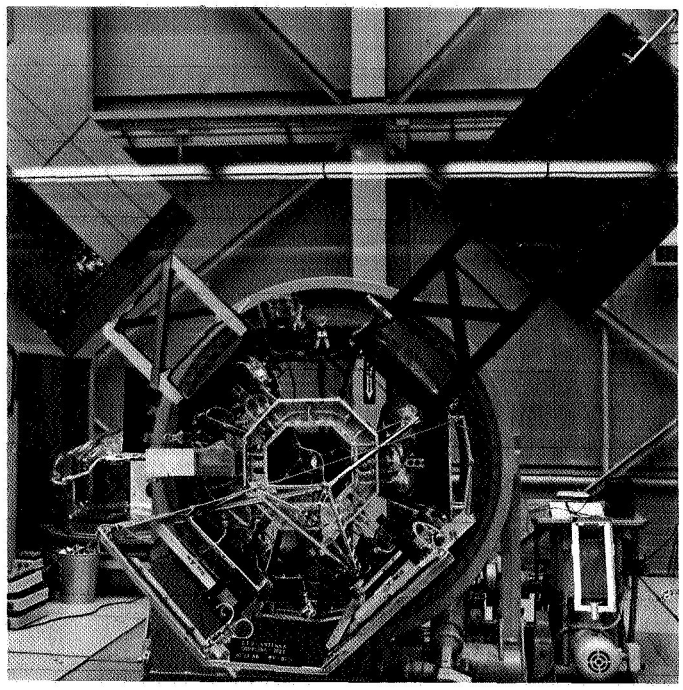


**Fig. IV-183. Spacecraft test configuration**

(2) No significant amount of noise existed in the 423.3-MHz frequency band of the UHF channel of the DFR.

(3) The background noise level during the daylight hours was too high and too unstable to permit noise tests to be performed during the day. It was discovered that to obtain a noise background low and stable enough required testing between the hours of 2300 and 0600 PST.

Another interesting result from these spacecraft tests was the discovery of a 4-dB difference in the near-field gain of two different sets of 50-MHz antenna feeds. The spacecraft solar panels serve as the antenna for the VHF channel of the DFR. Feed wires are connected to adjacent solar panel spars to couple the RF energy from the panels to the receiver. The original design of the 50-MHz antenna feeds called for stainless steel wire. However, antenna tests indicated that the resistive losses of the stainless steel seriously reduced the antenna's efficiency. To decrease the resistance of the feeds, the feed wires were silver-plated and then covered with a layer of gold. Using the gold feeds the 50-MHz antenna was able to meet its gain requirements. An increase in the spacecraft noise level at the 50-MHz antenna was expected using the gold-plated feeds. However, EMI tests showed that the near-field gain of the stainless steel feeds was 4 dB higher than the gold-plated feeds. This rather fortunate situation provided a much-needed effective increase in test receiver sensitivity.

Following the identification of noise sources, subsystem investigations were initiated to develop means of suppressing the generation of RF noise, or its coupling, into the DFR. To verify that the fixes developed in the laboratory to reduce the level of 50-MHz noise would result in the required reduction of noise seen by the DFR, a third systems test was performed in conjunction with the subsystem tests on the DAS. This third test showed that changing the output diodes of the power subsystem booster regulators, reducing the frequency of the DAS master oscillator, installing filters at the input to the DFR, installing ferrite bead filters on the interconnecting cables of the DAS, and wrapping the intraconnecting cables of the DAS with a metallic foil reduced the 50-MHz noise level to within the limits necessary for proper operation of the DFR. No degradation to the 423.3-MHz channel of the DFR was observed during any of the testing.

Because the noise investigation tests were performed on a partially assembled spacecraft in a test configuration (Fig. IV-183), an acceptance test with a fully assembled spacecraft in a flight configuration was necessary to adequately verify that the DFR was compatible with the spacecraft electromagnetic environment. A test envisioned as feasible for the acceptance testing was one with the spacecraft suspended by nylon lines from a hoist in the spacecraft assembly facility (Fig. IV-184). The spacecraft would be completely assembled into a flight configuration with no connecting cables. A suspended spacecraft test was performed on both the flight and backup spacecraft. With the spacecraft powered by its battery and suspended in a flight configuration, approximately 15 ft above the floor, the DFR was degraded from 0.5 to 1.0 dB with a measured antenna noise temperature of 5400°K. Since the lower range of expected antenna noise temperatures in space was on the order of 6000°K, the level of degradation expected for flight should be no worse than that measured in the suspended spacecraft test.

*Test instrumentation.* The noise susceptibility analysis had determined that three frequency bands should be examined. There were two bands for the UHF channel, one centered at the receiver frequency (423.3 MHz), and the other centered at the image frequency (473.1 MHz). For the VHF channel, only a band centered at 49.8 MHz

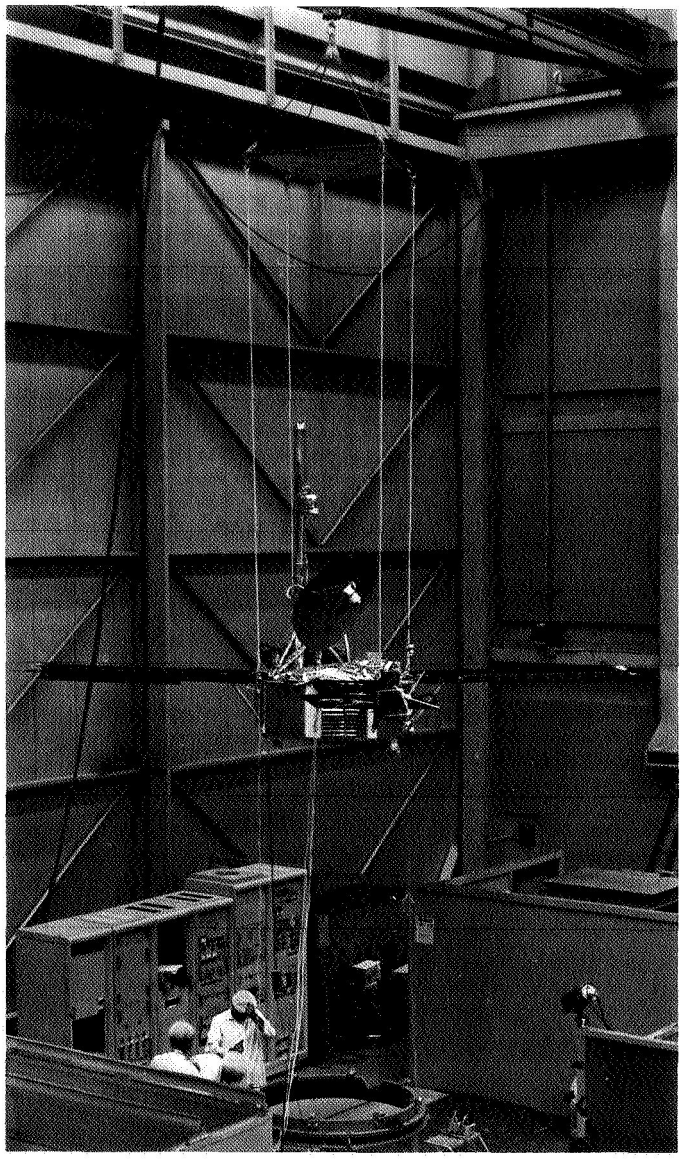


**Fig. IV-184. Suspended spacecraft**

was deemed critical. Definition of critical bands was based on the requirement, demonstrated in a subsystem compatibility test, that filters were necessary at both DFR channel inputs. By the time the final low-noise instrumentation was assembled, the incorporation of the two filters on the flight spacecraft was ensured. The final design of the test receivers was based on commercially available low-noise RF amplifiers that could meet the required delivery time. An additional requirement imposed on the instrumentation was that a sufficiently wide range of frequencies, centered at the test frequency, should be scanned with a narrow bandwidth receiver. The narrow bandwidth capability was desired to provide a resolution of the noise spectra in the 45-kHz intermediate frequency (IF) noise bandwidth of each DFR channel. These requirements were met by employing a military R390A/URR HF receiver (0.5 to 32 MHz) with narrow bandwidth mechanical filters and accurate frequency readout. The receiver was incorporated into the instrumentation along with low-noise VHF and UHF preamplifiers and frequency converters. An output of the R390A/URR receiver is the 455-kHz IF at selectable bandwidths of 0.1, 1, 2, 4, 8, and 16 kHz. The IF output was monitored with a true rms voltmeter and a spectrum analyzer operating at a center frequency of 455 kHz. The rms voltmeter measured the true rms value of complex waveforms with all significant components in the range of 5 Hz to 500 kHz. The spectrum analyzer enabled an examination of the noise spectra of the signal received by the R390A/URR. The stability of the local oscillators for the frequency converters was desired to be sufficient to maintain the center frequency within a bandwidth of 1000 Hz on the R390A/URR receiver during a measurement period of approximately 20 min. The local oscillator stability satisfied this requirement. Because a frequency counter was used to monitor the local oscillator frequency, the capability existed for determining the frequency of discrete RF signals to the accuracy of the R390A/URR receiver.

The instrumentation assembled for the UHF channel to measure noise at 423.3 and 473.1 MHz is shown in Fig. IV-185. The preamplifier was a commercially available low-noise module with a noise figure of 2.0 dB. By placing this unit on the spacecraft at the DFR location during tests, an overall low-noise figure of approximately 2.4 dB was obtained. The mixer was also a commercially available unit. The bandwidths of the UHF preamplifier and mixer were wide enough to permit an investigation of the 473.1-MHz image frequency without the need for an additional preamplifier and mixer. However, it was necessary to use two local oscillators. The local oscillator frequencies were selected to translate 423.3- and 473.1-MHz frequencies to the frequency range of the R390A/URR HF receiver. Consideration was given in the design for adequate filtering on all power leads, reduction of spurious outputs, and IF selection for image rejection.

An interim preamplifier/mixer/local oscillator low-noise assembly with a noise figure of 3 dB was made available by Stanford University to permit immediate noise measurements in the VHF band. The local oscillator of this device was relatively stable and it permitted measurements of the science data automation system basic oscillator harmonics at the DFR VHF passband.

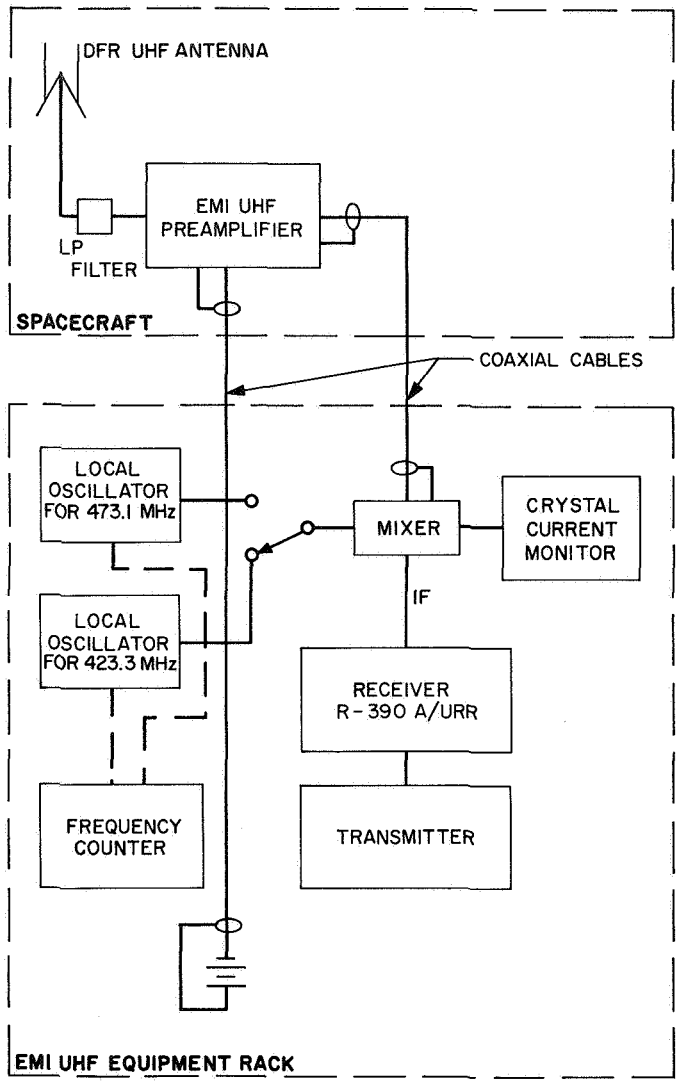



**Fig. IV-185. EMI UHF test receiver configuration**

This device was later replaced with a commercially available preamplifier/mixer/IF amplifier/local oscillator combination with an overall noise figure of only 1 dB. The output of this unit is a 30.0 ±5 MHz signal that can be examined directly with the R390A/URR receiver.

A portable receiver was used extensively in the noise investigation. Although the use of the receiver did not permit accurate noise measurements, the low-noise figure of the unit at 49.8 and 423.3 MHz, and its portability (the size was approximately 2 × 10 × 12 in.) allowed it to be used as a "sniffer" in a variety of applications. The receiver was very useful in the spacecraft test area prior to each test to search out and identify noise sources external to the spacecraft. By this "sniffing" process, the background ambient noise temperature could be substantially reduced by turning off equipment that the receiver showed to be a noise source. The unit also proved valuable in providing qualitative information on noise levels of subsystems in laboratory tests.

*2. Subsystem noise investigations.* A key test in the early portion of the investigation was a bench compatibility test using an engineering model S-band transponder and a prototype DFR. The DFR used was a *Pioneer* spacecraft model, the only unit available at the time of the investigation. Although the frequencies of the engineering model transponder differed from the flight transponders by more than 2 MHz, the interactions discovered during this test also existed in the flight transponder during a similar test. Sufficient time was obtained as a result of this test to permit the procurement of the necessary hardware to eliminate the interference between the RF subsystems and to plan and perform special tests prior to the formal spacecraft acceptance test.

The S-band/DFR subsystem compatibility test was performed with the subsystems placed next to each other on a conducting surface in a shielded enclosure. Figure IV-186 shows a typical test configuration. This configuration was selected to provide a worst-case condition for interaction between the subsystems. The results obtained in this test are discussed in the following paragraphs.

*a. Interaction of local oscillator harmonics.* The *Pioneer* prototype/S-band compatibility (PP/S-B) tests indicated a −3.5-dB change in the sensitivity of the 423.3-MHz channel of the DFR when the S-band and the DFR receivers were connected. Three decibels of attenuation eliminated the apparent interference.

It should be pointed out that the 3.5-dB reduction in receiver performance could have resulted from an impedance mismatch between the receiver and transmitter in the test setup. Regardless of the cause, more than 3 dB of isolation existed between the DFR and S-band antennas; therefore, interference of this type would not exist with the subsystems operating on the spacecraft.

*b. Intermodulation interference.* A computer program that determined whether linear combinations of pairs of local oscillator frequencies and other frequencies fell within the RF or IF passbands of the receiver was used

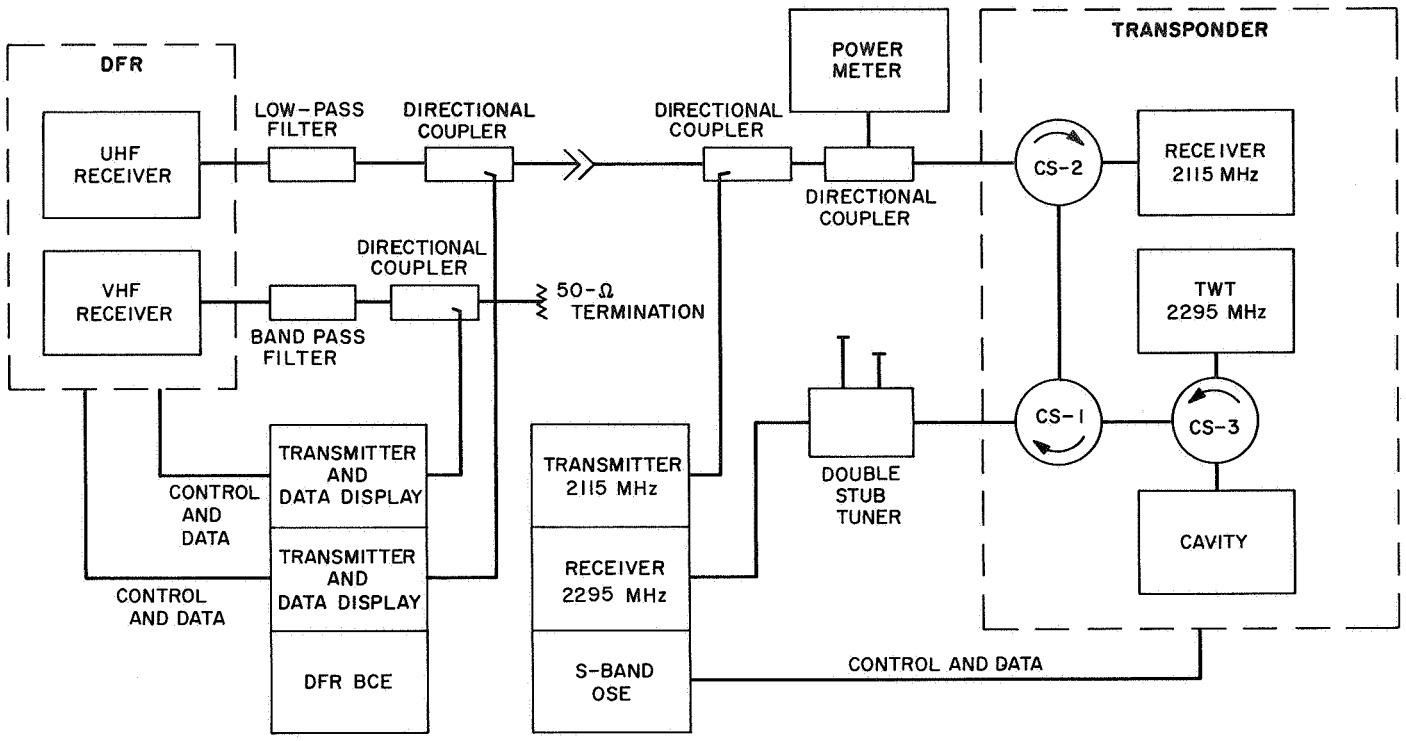



**Fig. IV-186. S-Band transponder and DFR compatibility test setup**

to determine possible intermodulation products. Two possible intermodulation products were discovered:

S-band receiver frequency = 2115.699800 MHz

DFR receiver frequency = 423.300000 MHz

2115.699800 MHz − 4 (423.300000 MHz)
= 422.499800 MHz

6 (423.300000 MHz) − 2115.699800 MHz
= 424.100200 MHz

While connected to the S-band receiver, the DFR was caused to drift ±7.5 kHz about 423.3 MHz in search of an output of the S-band receiver upon which to lock; no interfering signals were found.

*c. Interaction between S-band transmitter outputs and the DFR.* The PP/S-B tests indicated that both channels of the DFR were degraded approximately 27 dB when a low-level output of the traveling wave tube (TWT) amplifier is coupled into the DFR. It was determined that 60 dB of isolation were required to eliminate the interference.

*d. Interaction between DFR outputs and the S-band receiver.* The PP/S-B tests indicated that the 50-MHz channel of the DFR could reduce the S-band receiver sensitivity. With the 50-MHz channel of the DFR connected through circulator switch CS-2, a slight increase in S-band static phase error and a 1.3-dB decrease in signal strength were observed. An attenuation of 20 dB was required to eliminate the interference.

When the 423.3-MHz channel of the DFR was connected to the S-band receiver operating at a signal level of −130 dBmW with the ranging receiver and the traveling wave tube amplifier on, an S-band signal was generated that would take control of the S-band phase-lock loop. Thirteen decibels of attenuation between receiver inputs were required to eliminate this interference. No jamming signal was generated when the 50-MHz channel and the S-band receiver, operating with the ranging receiver and TWT amplifier, were connected.

Based on the results of this test the following recommendations were made:

(1) RF filters, preferably bandpass, should be installed at the input to each DFR channel to prevent noise in the 2297.5-MHz frequency band from degrading the DFR sensitivity. Such filters would

attenuate any noise outside the filter passband, thereby preventing noise at other frequencies (including the image frequency), from interfering with the DFR. A bi-directional filter in the 423.3-MHz channel would also isolate the spurious signals within the DFR from the S-band receiver.

(2) A filter should be added at the output of the S-band transmitters to prevent radiation of noise at 49.8 and 423.3 MHz, thus ensuring that the DFR channels would not be degraded in sensitivity.

(3) The following measurements should be made to determine the coupling coefficients between the antennas of the spacecraft RF subsystems:

(a) The level of a 2297.5-MHz signal transmitted from the S-band antennas and received by the DFR antennas.

(b) The coupling of a 49.8- and a 423.3-MHz signal transmitted from the S-band antennas and received by the respective DFR antennas.

(c) The level of a 2115.7-MHz signal received by the S-band antennas when transmitted from the 423.3-MHz DFR antenna.

The results of the recommended antenna coupling measurements would be a determining factor in the procurement of the filters. Because the DFR did not possess preselector filters, the installation of bandpass filters would ensure that each channel would be relatively insensitive to frequencies outside its intended bandpass. The recommended DFR filters could not eliminate noise at the operating frequencies. Therefore, if noise were originated on the spacecraft, this noise would have to be reduced at its source or the coupling suppressed; the recommendation for a noise suppression filter at the TWT output was intended for that purpose but its procurement depended on the antenna coupling measurements. If the noise coupled between the S-band transmitter and the DFR through the antennas was adequately attenuated, then a filter at the output of the TWT would not be required.

Antenna RF coupling tests were subsequently performed (Fig. IV-187). Based on the results of the antenna coupling tests, it was determined that a sufficient decoupling margin existed for noise from the S-band RF power amplifiers at 49.8 and 423.3 MHz, but that the decoupling between the S-band and DFR antennas at 2297 MHz was marginal. To provide sufficient isolation between the DFR and the 2297-MHz signal from the S-band power amplifiers, it was necessary to add filters at the inputs to the DFR (Fig. IV-188). Ideally, from the standpoint of noise isolation, bandpass filters should be used. However, in the case of the 423.3-MHz channel a low-pass filter with an insertion loss of 0.05 dB was used instead of a bandpass with an insertion loss of 0.5 dB. Tests showed that a low-pass filter provided the necessary isolation for the 423.3-MHz channel without significantly reducing the already marginal signal level at the 423.3-MHz receiver frequency. Concern about the receiver signal level for the 423.3-MHz channel of the DFR was a result of the limited ground transmitter output power at this frequency.

*DAS noise investigation.* While the first production model of the data automation subsystem was being interfaced on *Mariner* Venus 67, a cursory examination of the noise level of the science system, consisting of the DAS and those instruments other than the DFR (e.g., magnetometer, trapped-radiation detector, and ultraviolet photometer), was performed with the portable 49.8- and 423.3-MHz test receiver. This check indicated that the 49.8-MHz noise emanating from the DAS was greater than that of any other subsystem investigated. Spacecraft tests using the DFR indicated that the threshold of the 50-MHz channel was degraded by more than 16 dB as a result of RF noise radiated by the DAS. Further investigations revealed that the major source of interference from the DAS was the 112th harmonic of the DAS master oscillator (Fig. IV-189). The DAS master oscillator frequency was 444.444 kHz; the 112th harmonic of this frequency is 49.777728 kHz. The 112th harmonic is, therefore, 228 Hz inside the 45-kHz, 3-dB IF bandwidth of the DFR. This discrete RF signal, only 33.277 kHz from the receiver frequency of the 49.8-MHz channel of the DFR, was the major source of noise from the DAS. Also, in the DAS, the 444.444-kHz master oscillator frequency is brought down to 55.555 kHz and used as the timing signal for the DAS logic. Therefore, there were eight other discrete signals 55.555 kHz apart between every harmonic of the 444.444-kHz signal. The harmonics of the 55.555-kHz signal, although 40 dB lower in amplitude than the harmonics of the 444.444-kHz signal, also interfered with DFR operations. To reduce the interference from the DAS master oscillator, the obvious solution was to move the 112th harmonic out of the IF passband of the DAS by changing the master oscillator frequency. However, the 3-dB IF bandwidth of the DFR is 45 kHz wide; therefore, the 55.555-kHz harmonics would be separated by no more than

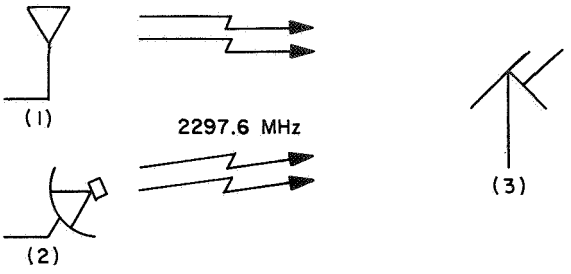
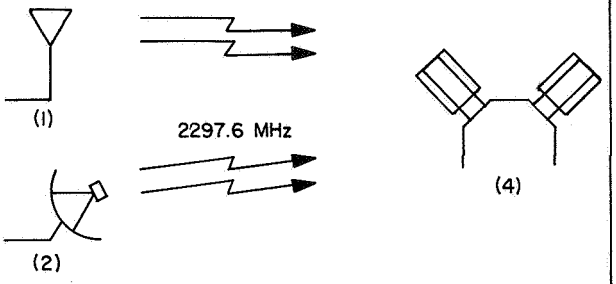
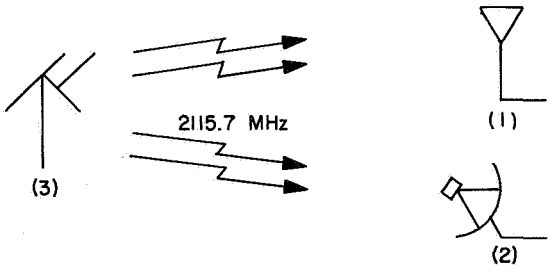
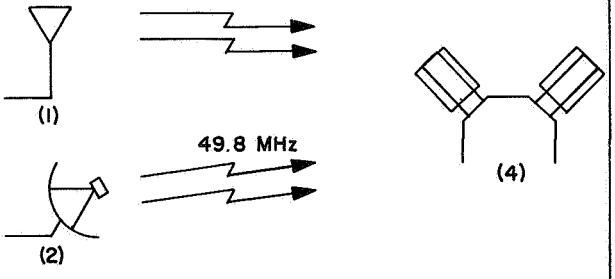
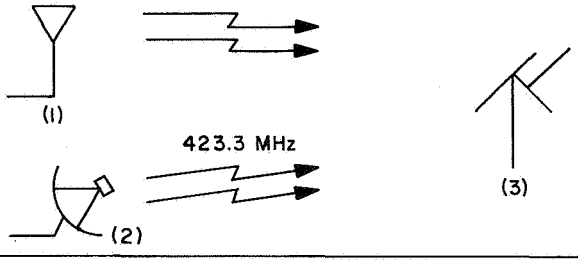
| | | ISOLATION | |
|---|---|---|---|
| | | MEASURED, dB | REQUIRED, dB |
|  | (1) TO (3)<br>(2) TO (3) | 68.0<br>62.5 | 60 (ESTIMATED)<br>60 |
|  | (1) TO (4)<br>(2) TO (4) | 68.0<br>57.5 | 60<br>60 |
|  | (3) TO (1)<br>(3) TO (2) | 69.2<br>54.5 | 13<br>13 |
|  | (1) TO (4)<br>(2) TO (4) | 78.0<br>73.0 | 40 (ESTIMATED)<br>40 (ESTIMATED) |
|  | (1) TO (3)<br>(2) TO (3) | 93.0<br>79.0 | 40 (ESTIMATED)<br>40 (ESTIMATED) |

**Fig. IV-187. S-Band/DFR antenna coupling measurements**

5.277 kHz from the 3-dB points by a reduction in the DAS master oscillator frequency to eliminate the interference from the 112th harmonic.

Drastic changes could not be made to the DAS master oscillator frequency because DAS logic was based on timing signals generated from the 444.444-kHz oscillator. Small changes in the master oscillator frequency could be tolerated; however, large changes would seriously affect DAS operation. Tests showed that a 1-kHz reduction in the frequency of the master oscillator eliminated the major portion of DFR interference from the DAS without degrading operation. The selection of a new frequency for the DFR master oscillator was based on three constraints. First, the change in oscillator frequency should be as small as possible. Because the 112th harmonic lies on the lower frequency side of the DFR IF bandwidth, a reduction in oscillator frequency would provide the greatest reduction in signal strength for the smallest change in oscillator frequency. Second, the 112th harmonic should be moved from the 3-dB DFR IF amplifier bandwidth by approximately 110 kHz – two 55-kHz harmonics. Third, the 898th and 899th harmonics of the 55 kHz should be centered approximately at the 49.8-kHz DFR receiver frequency. These constraints resulted in the following equation used to determine the new DAS master oscillator frequency:

$$112\,x + \frac{2}{8}x + \frac{1}{16}x = 49.8\ \text{MHz}$$

$x$ = desired DAS master oscillator frequency

$x = 443.406$ kHz

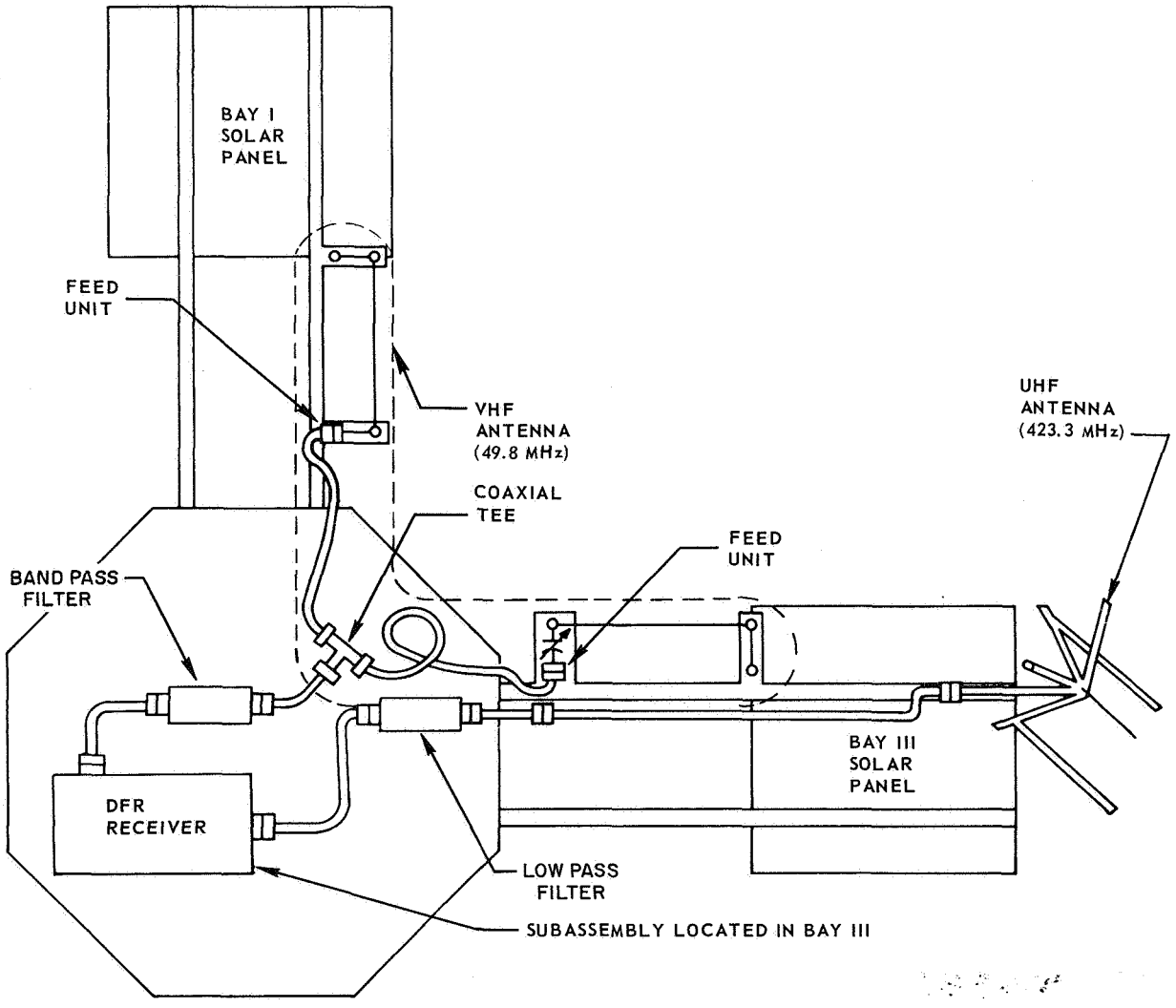



**Fig. IV-188. DFR antenna and filters**

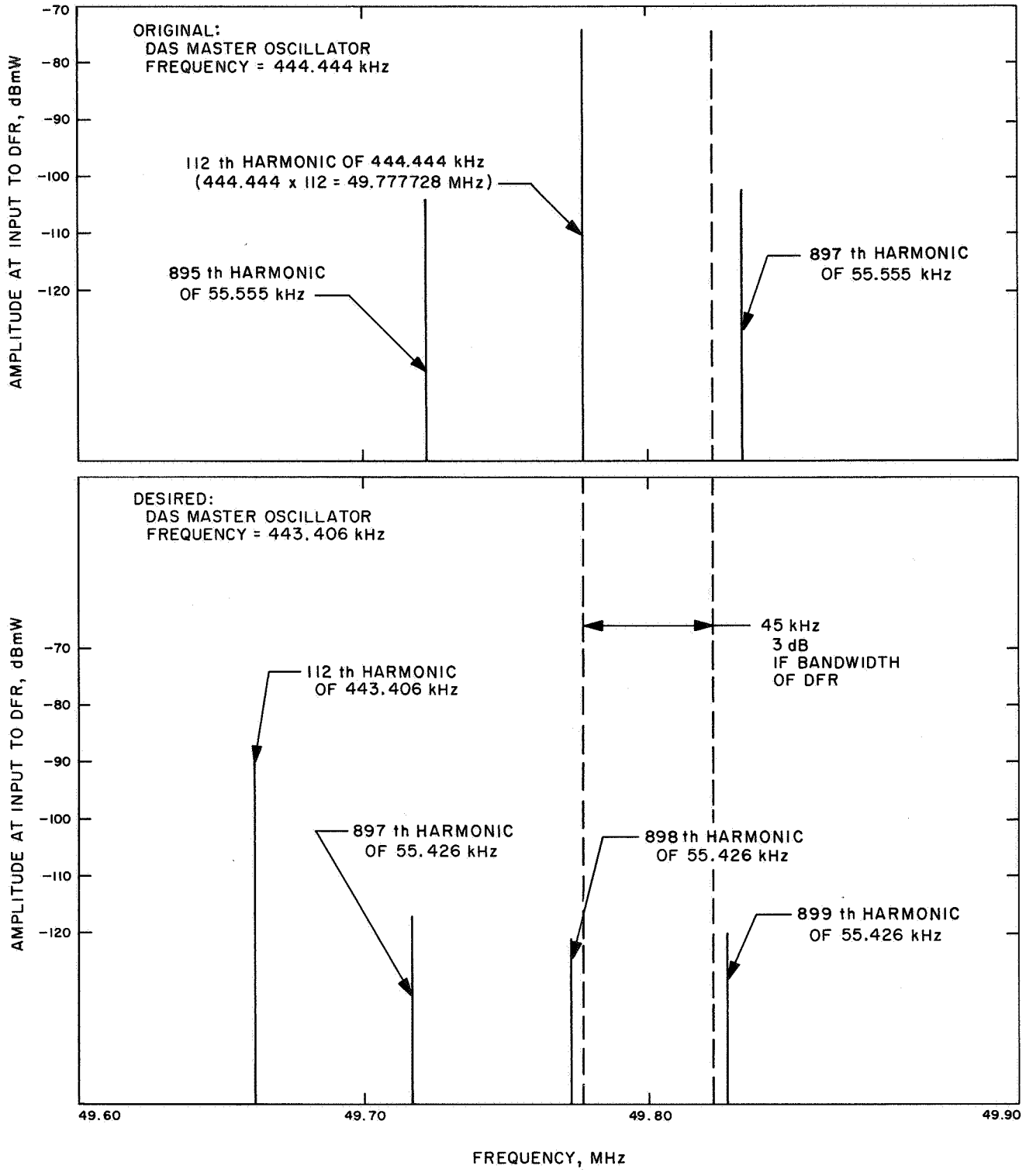



**Fig. IV-189. DAS master oscillator harmonics**

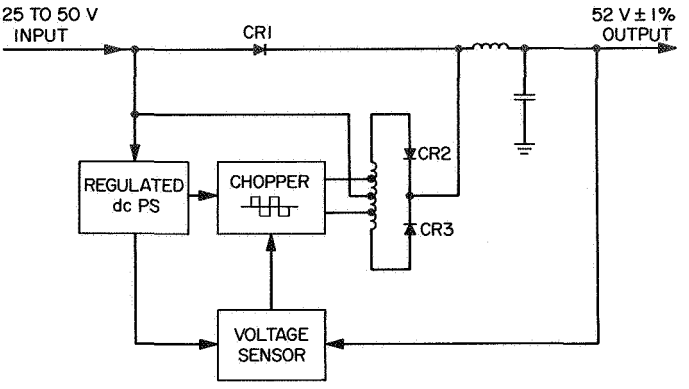
Changing the frequency of the DAS master oscillator to 443.406 kHz placed the two 55.426-kHz harmonics 5.213 kHz away from each side of the 45-kHz 3-dB IF bandwidth of the DFR. The only approach for further decreasing the interference from the 55.426-kHz harmonics was to contain this noise within the DAS, thereby preventing it from coupling into the VHF antenna. The noise from the DAS timing circuitry was suppressed by shielding the intraconnecting cables with aluminized Mylar to prevent radiation of signals from the cabling. Ferrite beads that act as low-pass filters were installed on each wire of the interconnecting cables to reduce the conduction of noise of the DAS.

Further spacecraft testing indicated that the corrective actions had reduced the interference between the DFR and DAS to less than 1 dB.

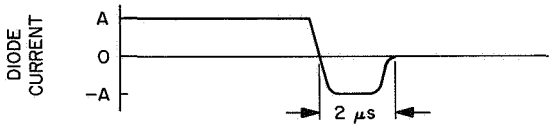
*Booster regulator noise investigation.* The function of the power subsystem booster regulators is to take a variable dc voltage input and to generate a regulated 52-V dc output. The input to the booster regulator is the solar panels and spacecraft battery connected in parallel through isolation diodes. Various factors such as sun–spacecraft distance, battery charge level, solar panel temperature, and solar cell damage from radiation and micrometeorites can cause the booster regulator input voltage to change. The booster regulator is designed to operate with input voltage variations between 25 and 50 V. The power subsystem includes two booster regulators: (1) a maneuver booster regulator to power a 2.4-kHz single-phase inverter and a 400-Hz three-phase inverter for attitude control and gyroscope power during spacecraft maneuvers, and (2) a main booster regulator that drives a 2.4-kHz single-phase inverter that supplies power to all spacecraft and science instruments throughout the mission.

A simplified diagram of a booster regulator is shown in Fig. IV-190a. The booster regulator maintains voltage regulation by comparing its output voltage to a reference in the voltage sensing circuitry. The sensing circuit in turn controls the duty cycle of the chopper so that the output of the rectifier, when added to the input voltage, produces 52 V at the booster regulator output.

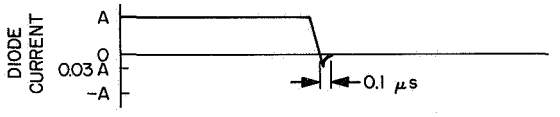
Tests performed on the spacecraft identified the power subsystem booster regulators as generators of 50-MHz noise at a level that, coupled into the VHF receiver, caused a threshold degradation of 5 dB. The source of noise generation was discovered to be large




(a) SIMPLIFIED DIAGRAM FOR BOOSTER REGULATOR




(b) GI IN1583 REVERSE BIAS RECOVERY CHARACTERISTICS




(c) WESTINGHOUSE IN3892 REVERSE BIAS RECOVERY CHARACTERISTICS

**Fig. IV-190. Booster regulator and reverse bias recovery characteristics**

current spikes produced each time diodes CR-1, CR-2, and CR-3 were reverse-biased. When a diode is switched from forward to reverse bias, the storage of minority carriers in the body of the device can cause large transient reverse currents. This effect is expected because of the diode junction capacitance. However, the magnitude of reverse current that develops when a diode is reverse-biased is much larger than would result from junction capacitance. The large reverse current at the instant of switching results from the high density of minority carriers near the junction that must be depleted before the diode reaches its steady state reverse current. For the GI 1N1583 diodes used in the booster regulator, Fig. IV-190b shows that, after a reverse bias is applied, a reverse current equal in magnitude to the forward current exists. These reverse current spikes occur on the order of every 200 μs. The amplitude of the frequency components of the spikes is directly related to the total energy contained in the spike. The amplitude of the components in the 50-MHz range for the spike produced by the GI 1N1583 diodes was sufficient to couple into the DFR at a magnitude that degraded the VHF receiver by 5 dB. It is not too surprising that noise

generated in the booster regulators would interfere with the DFR since the booster regulators are connected to the solar panels, two of which serve as the 50-MHz antenna.

To eliminate the noise problem, diodes CR-1, CR-2, and CR-3 were replaced with faster diodes. A faster diode reduces the reverse bias recovery time (Fig. IV-190c) by reducing the lifetime of the carrier, thereby reducing the total energy contained in the noise spike. The incorporation of faster diodes in the booster regulator reduced the 50-MHz noise level such that the spacecraft booster regulators contributed less than 1 dB of degradation to the DFR.

Spacecraft tests also showed the battery charger to be a 50-MHz noise source. Because the battery charger uses the same type of diodes in the same fashion as the booster regulator, the diodes were the suspected noise generators. Noise generated by the battery charger was not as detrimental as booster regulator noise because the spacecraft flight sequence can be controlled so that the battery charger cannot operate during those critical periods of DFR operations. Therefore, it was decided not to change these diodes.

*S-band transmitter power supply noise investigation.* Preliminary noise measurements made during spacecraft noise investigation tests with a 50-MHz test receiver indicated that noise originating in the engineering model S-band transmitter power supplies would degrade the VHF receiver sensitivity by as much as 11 dB. Cognizant radio personnel initiated a noise-reduction investigation and verified that an envelope of noise containing harmonics of the power supply switching frequency, 11 kHz, existed at 50 MHz. Noise reduction methods such as shielding, ferrite bead filters, and bypass capacitors were evaluated in an effort to reduce the 50-MHz noise level from the power supplies.

A check of the level of degradation of DFR sensitivity resulting from electromagnetic interference emanating from the S-band transmitter power supplies showed that no more than 1 dB of degradation occurred to the DFR from either the modified or unmodified power supplies. Subsequent testing with a power supply and the DFR removed from the spacecraft and operating in an anechoic chamber showed DFR degradation levels of as much as 28 dB. However, no more than 1 dB of degradation was ever observed by the DFR as a result of noise generated by the power supplies when the subsystems were operating on the spacecraft.

The inconsistency in the noise level measurements is not completely understood. Other tests have shown a close correlation between test receiver data and DFR degradation levels. A possible source of inconsistency would be a varying coupling coefficient between the DFR antenna and the noise sources. The fact that the spacecraft was in several states of buildup during the tests would help support this hypothesis. Because of the magnitude of effort required to make noise measurements on the spacecraft and lack of time, further investigation into this discrepancy was not possible.

Noise reduction efforts were continued to accumulate data on the feasibility of various noise reduction schemes. Various combinations of ferrite beads and capacitors were evaluated. However, because no appreciable degradation was observed by the DFR, no modifications for noise suppression were made to the flight S-band transmitter power supplies.

*e. DFR noise reduction analysis.* It was required to determine the amount of degradation experienced by the DFR from noise generated by the spacecraft in a space environment. In space, cosmic noise is present and forms part of the receiver background noise. In tests performed in the SAF, the noise ambient is contributed from sources other than cosmic noise. It was necessary, therefore, to determine the noise contributed by the spacecraft (for various operating modes) and then to calculate the level of degradation for given values of cosmic noise.

If the background noise is assumed to be uniform flat noise, the magnitude of spacecraft noise may be determined by forming a ratio of unknown to known noise levels (Eq. 1). With the test receiver connected to the spacecraft DFR antenna terminals, the magnitude of the background noise level can be determined. If the antenna is then replaced by a standard noise source, a second reading can be obtained as a reference level. In practice, it is convenient to use 50-Ω input terminations at room temperature (approximately 290°K), or at the temperature of liquid nitrogen (approximately 77.5°K), to establish a reference level. The lower temperature is provided by submerging a standard impedance termination in liquid nitrogen. When the unknown noise level is low, the liquid nitrogen termination is preferred because it yields greater test receiver output changes for a given unknown input noise level. Because the test receiver readings are directly proportional to the input power levels (at least for the ranges of interest) a ratio

may be formed and then used to calculate the unknown noise level.

$$\left\{\begin{matrix}\text{Noise}\\ \text{Power}\\ \text{Ratio}\end{matrix}\right\} = \frac{\text{test receiver internal noise + unknown input noise}}{\text{test receiver internal noise + reference noise}} \quad (1)$$

The test receiver internal noise can be determined in laboratory calibrations.

At radio frequencies, it is convenient to express the noise power available at the terminals of a receiving antenna or from a resistive load in terms of noise temperature, a concept based on Planck's radiation law for thermodynamic black bodies, and Nyquist's theorem for the noise power generated in dissipative electric circuit elements. The relation between temperature and noise power is:

$$P_k = kTB \ W \quad (2)$$

where

$k$ = Boltzmann's constant ($1.38 \times 10^{-23}$ J/°K)

$B$ = the receiver bandwidth over which the noise power is measured in Hz

$T$ = the temperature in °K

Using Eq. (2), Eq. (1) can be written as

$$\left\{\begin{matrix}\text{Noise}\\ \text{Power}\\ \text{Ratio}\end{matrix}\right\} = \frac{kT_eB + kT_AB}{kT_eB + kT_0B} = \frac{T_e + T_A}{T_e + T_0} \quad (3)$$

where

$T_e$ = the test receiver effective noise temperature

$T_0$ = the reference noise source temperature

$T_A$ = the unknown noise temperature

Expressing the noise power ratio as $\delta$ and solving Eq. (3) for $T_A$ results in

$$T_A = \delta\,(T_e + T_0) - T_e \quad (4)$$

The unknown noise temperature ($T_A$) is either the test area background noise or the combined spacecraft and test area background noise level, depending on the test conditions. With spacecraft power off, a noise temperature of $T_{A1}$ is obtained. With spacecraft power on, a second value, $T_{A2}$, will result. The increase in noise temperature from $T_{A1}$ to $T_{A2}$ is caused by spacecraft noise.

Therefore,

$$T_{sc} = T_{A2} - T_{A1} \quad (5)$$

where $T_{sc}$ is the effective antenna noise temperature as a result of spacecraft noise.

Because DFR performance is directly related to the background noise level in which it operates, DFR degradation levels measured in spacecraft tests will not be the same as in space unless the testing background noise temperature is the same as the cosmic noise temperature. This is because spacecraft noise can be masked by high levels of cosmic noise. Whereas spacecraft noise becomes the predominant factor if the cosmic noise level is of the same order of magnitude as spacecraft noise, the amount of degradation to the DFR from spacecraft noise for a given value of cosmic noise can be determined from

$$\begin{matrix}\text{DFR degradation}\\ \text{above cosmic (dB)}\end{matrix} = 10 \log \left[\frac{T_r + T_c + T_{sc}}{T_r + T_c}\right] \quad (6)$$

where

$T_r$ = the DFR noise temperature, approximately 300°K for the 49.8-MHz channel

$T_c$ = the cosmic noise temperature

$T_{sc}$ = the measured value of spacecraft noise temperature

*f. Conclusions and recommendations.* The final test results demonstrated that the DFR degradation levels were below the permissible values. Tests performed during flight operations have shown that noise contributed by spacecraft subsystems has not been observable in DFR data analysis.

During the testing period, it became evident that an early delivery of a prototype subsystem would have

helped considerably in the integration effort. It is recommended that, in future programs, a breadboard or prototype model of any new addition to a spacecraft system be made available for intersubsystem evaluation tests. Since time is a vital element in planetary programs, the time gained in the early portions of a test program is of great value in successful spacecraft equipment integration.

An adequately shielded test facility would be a valuable asset for future radio subsystem integration efforts. The merits of such a facility should be evaluated by considering its overall effectiveness to a test program. Experience on the *Mariner V* program has shown that a stable, low-noise environment cannot be obtained during any given 24 h. Consequently, test sequences had to be modified to accommodate the available time during which noise measurements could be taken. Modifications to test sequences were often accomplished with a resulting sacrifice in the amount of test data that could be obtained.

## K. Assembly and System Level Environmental Test Program

At the start of the project, goals for the environmental test program were established. The project policy was to have a flight spacecraft (M67-2) and a flight support spacecraft (M67-1) completely FA-tested, both at the subsystem and system levels. Further, the design was to be adequately TA-tested at the assembly level (there was to be no PTM for system level TA testing).

The goal of the environmental test program, then, was to ensure that these policies were realized, and that the effect of no PTM would be minimized, if possible. The general approach was to consider the *Mariner V* to be a derivative of the adequately qualified *Mariner* Mars 1964 design and to make maximum use of the test experience previously obtained. Requalification requirements would then arise from the assessment of design changes and mission differences.

The first step was a re-examination of the general TA and FA test levels. It was felt that these levels were still appropriate, but procedural changes were made to facilitate testing, which had negligible effect on test level.

As a result of the subsystem assessments, of the 38 assemblies environmentally tested as entities, 25 underwent re-TA to some extent (10 because they were a new design, 12 because their design was changed, and 3 because their new environment would transcend the *Mariner IV* levels). Because there was no PTM, several items whose environments were strongly influenced by the spacecraft system were partially or wholly qualified for vibration aboard the STM (e.g., solar panels, solar panel tip dampers, DFR antennas, temperature control reference, high-gain antenna deployment assembly, and numerous thermal control shields and blankets).

Both spacecraft were FA-tested to conservative levels for vibration, thermal/vacuum and EMI, and all important pyrotechnic devices were fired. Of the 38 testable entities on each spacecraft, all but 3 (on each spacecraft) were FA-tested before delivery to SAF (*Mariner IV* testing still valid). In the event of subsequent rework because of ECRs or PFRs, each assembly was carefully reviewed to determine the degree of re-FA required.

*1. Realization of environmental test program goals.* One way of evaluating an environmental test program is by examining the failures that occurred and their effect on the hardware flown. During the system level FA environmental tests of M67-1 and M67-2, seven significant anomalies or failures were noted. The numerical results of the subsystem level testing for vibration and thermal/vacuum are presented in Table IV-50, where they are compared with *Mariner IV* results.

**Table IV-50. Comparison of *Mariners IV* and *V* assembly level environmental test failures**

| Spacecraft | Type | Vibration | | | Thermal/vacuum | | | Overall failure rate, % |
|---|---|---|---|---|---|---|---|---|
| | | No. of Tests | Failures | Failure rate, % | No. of tests | Failures | Failure rate, % | |
| *Mariner V* | TA | 21 | 4 | 19.0 | 22 | 7 | 32.0 | 25.0 |
| | FA | 117 | 7 | 6.5 | 81 | 5 | 6.2 | 6.0 |
| *Mariner IV* | TA | 244 | 30 | 12.3 | 95 | 19 | 20.0 | 14.5 |
| | FA | 538 | 26 | 4.8 | 310 | 28 | 9.0 | 6.3 |

It should be noted that the percentage failure rates for FA tests were fairly close. Also of interest is that the TA failure rate was higher for both vibration and thermal/vacuum on *Mariner* Venus 67. Because the test levels were the same for *Mariners IV* and *V*, this most likely reflects the use of old hardware.

The assembly level environmental test failures on *Mariner* Venus 67 are briefly described in Table IV-51. It should be noted that none of the assembly level environmental test failures recurred during system level environmental testing. Also, although it is not explicitly stated, all subsystem FA failures were followed by a successful re-FA test.

***2. Detailed review of a typical subsystem environmental test program.*** To illustrate the general process used to progress from *Mariner IV* qualification status to *Mariner V* flight status, the attitude control jet valves can be looked at in detail. These valve assemblies are chosen as being representative of the methodology followed for all subsystems.

Preliminary estimates of maximum valve temperature was 215°F. However, at this temperature, the valve opening time was not satisfactory; therefore, the valve's pintle assembly was modified slightly. A possible need for requalification testing arose from a change in design and a change in expected assembly environment.

Two of these valves were successfully TA-tested to general test levels for humidity, shock, and vibration, and tested to special thermal/vacuum test levels of 14 and 225°F. Twelve of the valves designated for use on the M67-1 were FA-tested to vibration and special thermal/vacuum test levels of 32 and 215°F.

Before testing began on the valves for the M67-2 and spare valves, it was learned (from solar panel tests in the space simulator) that the operating temperature range would run low, not high. The TA valves were successfully retested to the revised lower thermal/vacuum temperature of −65°F (thermal/vacuum only), and the 18 valves for M67-2 (and spare valves) were FA-tested to vibration and thermal/vacuum temperatures of −45 and 131°F.

The valves should then have been removed from M67-1 for new FA tests to the new low temperature. Because there was no problem during any temperature testing (2 TA valves and 12 flight valves to extra high temperature; the same 2 TA valves and 18 flight valves to extra low temperature), retesting of the 12 valves for M67-1 to the new lower FA temperature was waived.

This assembly illustrates several typical characteristics of the *Mariner* Venus 67 environmental test program:

(1) The mission change necessitated a design change. This led to requalification requirements because *Mariner* Mars 1964 testing had been compromised.

(2) Independent of the design change, the mission change resulted in an expected environment sufficiently different from *Mariner* Mars 1964 to warrant augmenting the *Mariner* Mars 1964 tests with tests to new levels.

(3) For lack of a PTM, this item went aboard the solar panel for a portion of its qualification testing. There it was tested for acoustics and thermal shock. Although it experienced a thermal/vacuum environment, the main output of this facet of test was a better estimate for assembly level testing (i.e., its formal TA thermal/vacuum test was as an assembly).

(4) With many things moving in parallel rather than series (e.g., assembly level thermal/vacuum tests slightly preceded the above tests in the space simulator), late information had to be incorporated into the test levels in the midst of the environmental testing program. Hence, the question of whether to repeat previous tests arose, and was settled by careful consideration of the circumstances.

(5) Units passed tests that were to deliberately conservative levels with no difficulty.

***3. Review of the electromagnetic interference program.*** In the area of EMI, the general approach was that expressed for other environmental tests. *Mariner V* was considered a derivative of the adequately qualified *Mariner* Mars 1964 design, and requalification requirements were based on an assessment of design changes and mission differences. The EMI effort can be classified in three main categories: (1) subsystem qualification, (2) spacecraft system qualification, and (3) special investigations and support.

## Table IV-51. *Mariner* Venus 67 major environmentally induced test failure summary, assembly level

| No. | Subsystem | Test in which failure occurred | | Cause of failure | | | | Description of failure | Concern over failure |
|---|---|---|---|---|---|---|---|---|---|
| | | TA | FA | Design deficiency | Workmanship | Procedural | Old age | | |
| 1 | Plasma probe | Thermal/ vacuum | | X | | | | At low temperatures, the unit did not sequence properly. The problem was also noted on a flight unit prior to delivery from the vendor. The problem was corrected by a design change to the circuitry | No concern since the design change was verified as curing the problem. All flight units were modified accordingly |
| 2 | Pyrotechnic control assembly | Thermal/ vacuum | | | | | X | The assembly passed TA testing on *Mariner IV*, but for *Mariner* Venus 67, was modified by the addition of a terminator sensor amplifier. In TA thermal/vacuum, a partial failure of an energy storage capacitor was noted. The *Mariner* Venus 67 TA unit is not the *Mariner IV* TA unit, but is one of the leftover *Mariner IV* flight units. Even though this problem has not been noted in any flight units, this TA unit was dissected to analyze the failed capacitor, since all flight units are of the same age | Because this portion of the pyrotechnic control passed TA testing on *Mariner IV*, there is no real concern over the adequacy of the design. There is concern, however, over the possibility that the energy storage capacitors are being affected by age, hence flight units are being frequently examined. Further, multiple redundancy exists in this function |
| 3 | Radio | Vibration | | X | | | X | The *Mariner* Venus 67 TA unit is the old *Mariner IV* PTM unit. It was not rebuilt to eliminate a design problem with Johansen capacitors. Its TA testing has been plagued by capacitor problems and by problems which are attributed to its age and excessive test history. These problems are localized to the receiver only and the RF amplifiers have experienced no problems during *Mariner* Venus 67 testing | There is no concern over the radio because the RF amplifier portions have experienced no difficulty during *Mariner* Venus 67 testing and the receiver passed TA testing on *Mariner IV*. The problem with Johansen capacitors was expected. The other problems in the receiver are not surprising for a unit with an excessive history of qualification level testing |

## Table IV-51 (contd)

| No. | Subsystem | Test in which failure occurred | | Cause of failure | | | | Description of failure | Concern over failure |
|---|---|---|---|---|---|---|---|---|---|
| | | TA | FA | Design deficiency | Workmanship | Procedural | Old age | | |
| 4 | Low-gain antenna | Thermal/ vacuum | | X | | | | On the *Mariner* Venus 67 mission, this item will experience much lower temperatures than it was designed for. During testing to these low temperatures, cable clamp bonding failed. Developmental work was conducted to find a different bond material that would sustain lower temperatures. A new material was found. The bonding on flight antennas cannot be changed because, at room temperatures, the bonds have full strength and cannot be removed. Should any bonds fail on flight antennas, they will be repaired with the new bond material. To date, none have failed | This failure is not a cause for concern. If these bonds should fail on a flight antenna, it will be past the launch phase when they experience a low-temperature environment, and the support of the cable clamps is no longer needed |
| 5 | Battery | Vibration | | X | | | | At very low frequencies (approximately 2 Hz), the battery plates go through a slosh mode which broke some header wires inside the battery. The same condition was known to exist on the *Mariner IV* batteries | This is not felt to be a serious problem because the failures occur under very unique vibration conditions (slowly swept low-frequency sine) which do not exist in flight. Further, the battery has sufficient capability so that it could still function if a similar failure would occur in flight |
| 6 | Tape recorder | Thermal/ vacuum | | X | | | | Following test, failure of a discrete component was noted. This component is one which the component parts personnel had recommended should be changed. The problem is felt to be caused by the wrong choice of parts rather than a circuit design deficiency | This item has since been successfully re-TA tested. After review, the project office decided that replacement of the part was not warranted |
| 7 | DFR | Vibration | | X | X | | | During vibration, a spot bond on a lead broke loose and allowed motion of the wire to break the solder terminal. The unit was satisfactorily repaired and more attention given to the spot bonding on flight units | No concern over this failure since the TA unit was satisfactorily reshaken, no flight unit has exhibited this problem, and the flight units are verified as being better quality bonding |

## Table IV-51 (contd)

| No. | Subsystem | Test in which failure occurred | | Cause of failure | | | | Description of failure | Concern over failure |
|---|---|---|---|---|---|---|---|---|---|
| | | TA | FA | Design deficiency | Workmanship | Procedural | Old age | | |
| 8 | DFR | Thermal/ vacuum | | | X | | | At high temperature, the unit exhibited improper data readout. This was traced to two discrete components which were not within tolerance | No concern because, following replacement of components, the unit was satisfactorily retested |
| 9 | Solar panel | Thermal/ vacuum | | | | X | | During TA testing in the space simulator at Venus intensities, the lamps went off because of a Laboratory-wide power failure. The resulting thermal transient damaged the solar panel beyond repair | This failure is of no concern. Prior to the accident, it had been established that the panel was not affected by thermal transients that would be experienced during midcourse maneuvers when solar intensity is nearer to that of earth. Immediately following the accident, extensive work was done on samples of panels and reconfirmed that thermal transients appropriate for midcourse maneuver conditions would not affect the panel and that thermal transients appropriate for Venus intensity conditions degraded the panel. This test is considered to have been passed in spite of the accident |
| 10 | Radio | | Vibration | X | | | | An L-shaped tuning cavity was not supported at its ends. The overhanging end contacted the chassis under vibration and caused a crystal mounted adjacent to it to fluctuate in frequency. This design condition exists on all radios but was not as noticeable on others as on this particular radio. A fillet of bonding was put around the perimeter of the cavity and verified that it cured the problem | There is no concern over this failure. At one time, a decision had been reached to launch with it. It was known to occur only under certain levels of vibration and always return to its original condition at the end of vibration. Since the design fix was simple, however, it was instituted on all units |

Table IV-51 (contd)

| No. | Subsystem | Test in which failure occurred | | Cause of failure | | | | Description of failure | Concern over failure |
|---|---|---|---|---|---|---|---|---|---|
| | | TA | FA | Design deficiency | Workmanship | Procedural | Old age | | |
| 11 | DFR-UHF antennas | | Vibration | X | | | | Following vibration, a crack between a phenolic fitting and the aluminum mast was noted. It was determined that differences in expansion coefficients between the fittings and the mast caused separation during curing, and a fiberglass dowel pin was added to the design to retain the fitting on the mast | Since TA tests had occurred prior to FA, this failure should have been noted at that time. It was not, but after the FA failures, when the TA was re-examined, a crack was found which had not been previously noted. An antenna test model which had experienced no environmental testing was examined and it also exhibited the same crack. The addition of the dowel pin was felt to be an adequate fix and no concern exists over this failure |
| 12 | Thrust vector control assembly | | Vibration | | X | | | The potentiometer brush block came loose on the shaft during vibration | Although the unit successfully passed the test following retightening of the locking screw, enough concern exists to institute null position checks during Pasadena and ETR operations |
| 13 | Thrust vector control assembly | | Thermal/ vacuum | X | | | | At low temperatures, the shaft motion was erratic. The cause of the problem was traced to the lubricant used which was replaced with a lubricant with better low temperature properties | Following this design change, it was learned that the flight environment of the TVCAs was even lower than the test temperature at which problems occurred. Tests were run at 0°F with the new lubricant and experienced no problem; hence, there is no concern over this problem |
| 14 | Thrust vector control assembly | | Thermal/ vacuum | | X | | | This unit lost torque gain during thermal/vacuum test. The problem was ultimately traced to a defective magnet in the unit | No concern. The actuator was rejected |
| 15 | Temperature control reference | | Thermal/ vacuum | | X | | | This unit exhibited excessive thermal gradients across its sensor surface during test. This unit had been reworked once before for the same problem | No concern. This unit was scrapped and no other unit has exhibited this problem |

## Table IV-51 (contd)

| No. | Subsystem | Test in which failure occurred | | Cause of failure | | | | Description of failure | Concern over failure |
|---|---|---|---|---|---|---|---|---|---|
| | | TA | FA | Design deficiency | Workmanship | Procedural | Old age | | |
| 16 | Tape recorder | | Vibration | | X | | | Erratic performance during test was noted. This was traced to a potted module which was only partially filled with potting compound. On further checking, this same condition existed in several potted modules. This condition also existed in the TA unit but did not give any problems when the TA unit was satisfactorily tested | All modules which were suspected were replaced with newly-fabricated modules. An abbreviated TA was rerun to verify that the modules (3 in each tape recorder subsystem) are still qualified; hence, there is no concern over this failure |
| 17 | Separation-initiated timer | | Vibration | | X | | | A dimensional problem on a bracket allowed switch contacts to chatter in vibration. The bracket was replaced and the unit successfully retested | No concern |
| 18 | Separation-initiated timer | | Temperature | X | | | | The timing was not within specifications due to viscosity of oil in the damper | This unit will be flown as is since it was determined that the specification time limits were needlessly tight |
| 19 | Thrust vector control assembly | | Vibration | | | X | | Following vibration it was noted that all four actuators in the vane assembly had experienced a loss of torque. This problem was ultimately traced to a procedural error in magnetizing the torquer magnets in the actuators | The new magnetizing procedure gave superior results to the procedure used on *Mariner IV*. This new procedure results in adequate gain under all conditions and therefore there is no concern |
| 20 | Magnetometer | | Thermal/vacuum | | | X | | Unit did not function properly at low temperatures. This was traced to an improper tuning condition of an RF section. It was retuned correctly and passed the test | The proper way to tune this device is somewhat at variance to the instruction manual. The test temperature had been lowered from *Mariner IV* test temperature because of change in mission from Mars to Venus. There is no concern now that the proper tuning method is known |

## Table IV-51 (contd)

| No. | Subsystem | Test in which failure occurred | | Cause of failure | | | | Description of failure | Concern over failure |
|---|---|---|---|---|---|---|---|---|---|
| | | TA | FA | Design deficiency | Workmanship | Procedural | Old age | | |
| 21 | Pyrotechnic arming switch | | Vibration | | X | | | During vibration, contact chatter was observed. This was traced to improper adjustment of spring load on switch levels. Discrepancy was corrected and item satisfactorily retested | No concern |
| 22 | DAS | Thermal/ vacuum | | | X | | | All magnetometer Z-axis works in the DAS 420-bit format indicated that the seventh most significant bit was always a one. This problem disappeared for approximately 16 h, then reappeared | No concern. The failure was isolated to a flat pack, which was replaced. The DAS was then subjected to TA level and duration high-temperature thermal/vacuum test. The failed flat pack was tested separately, but in the same chamber and at the same time as the DAS. The DAS operated normally throughout the test and failure was repeated in the flat pack |
| 23 | Plasma probe | Vibration | | | | | X | Following the special repeat of TA sine and random vibration of module 32A3 only, the plasma probe failed to sequence properly | No concern. This module had previously passed TA vibration. The test was repeated to check the integrity of the diode board added as a result of PFR 011071. The failure was in old circuitry which had been successfully TA-tested twice before and does not affect the validity of this test |
| 24 | DFR | | Thermal/ vacuum | | | X | | A crystal had been replaced as a precaution for a potential manufacturing defect. Spurious outputs from the multiplier circuits caused the receiver to lose lock. Unit No. S/N2 appears to be extremely sensitive to multiplier circuit alignment | No concern. After adjustment of the multiplier, the unit was successfully retested |

*a. Subsystem qualification program.* The majority of spacecraft subsystems were adequately qualified by virtue of compatible performance on the *Mariner* Mars 1964 mission. Three subsystems, however, were new to the spacecraft and their compatible operation after integration was unascertained. EMI subsystem tests performed on *Mariner* Venus 67 were not arbitrary requirements of an existing specification. The test levels selected for qualifying tests were based on available data of measured noise levels on *Mariner IV* PTM. Basic to the subsystem testing was the goal of performing an extensive electrical circuit analysis to classify each interface circuit by degree of susceptibility. It was not until after this analysis was complete that a detailed test procedure was formulated. A realistic and comprehensive test was thus possible on each subsystem.

The three subsystems that were new in whole or in part because of additional circuitry were the DFR, the DAS, and the PCA. Each of these subsystems successfully passed the qualification tests. In summarizing the EMI qualification test program, two points should be made:

(1) The *Mariner* Venus 67 EMI philosophy of performing a thorough circuit analysis on subsystems prior to the generation of a test procedure resulted in a test program superior to previous programs.

(2) It became apparent during this work that greater in-depth understanding of noise levels on a spacecraft would have resulted in an improved qualification program.

*b. Spacecraft system qualification.* Both M67-1 and M67-2 were subjected to an RF environment similar to that expected at the AFETR launch complex and during launch to ensure RF compatibility of the spacecraft. On M67-1, three RF simulation tests were performed. The RF simulation level requirements and the actual test levels are shown in Tables IV-52, IV-53, and IV-54. One RF simulation test was performed with M67-2. Table IV-55 gives the RF levels.

**Table IV-52. Requirements versus test external environment simulation (M67-1 system test)**

| Radio frequency source simulated | RF simulation requirements | | | | Test levels for system test procedure | | | |
|---|---|---|---|---|---|---|---|---|
| | Frequency, GHz | Peak power density, dBmW/m² at spacecraft | Average power density, dBmW/m² at spacecraft | Minimum pulse width, μs | Frequency, GHz | Peak power density, dBmW/m² at spacecraft | Average power density, dBmW/m² at spacecraft | Minimum pulse width, μs |
| *Agena* radar transmitter (FPS-16) | 5.690 | +59 | +21 | 1.0 | 5.690 | See note 1 | +20 | CW |
| *Atlas* guidance track ground transmitter | Classified | +20 | −12 | 2.0 | Classified | See note 2 | −12 | CW |
| *Atlas* guidance rate ground transmitter | Classified | NA | +14 | NA | Classified | NA | +15 | CW |
| Command destruct ground transmitter | Classified | NA | + 4 | NA | Classified | NA | + 4 | CW |
| *Agena* telemetry | 0.2443 | NA | +23 | NA | 0.2443 | NA | +25 | Subcarrier modulated |
| *Agena* radar transponder | 5.765 | + 7 | − 8 | 0.7 | 5.765 | +7 | − 8 | See note 2 |
| *Atlas* telemetry | 229.9 | NA | − 6 | NA | 229.9 | NA | − 6 | Subcarrier modulated |
| *Atlas* guidance track transponder | Classified | +30 | − 1 | 2.0 | Classified | See notes 1 and 3 | +30 | CW |
| *Atlas* guidance rate transponder | Classified | NA | − 5 | NA | Classified | NA | − 5 | CW |

NA = not applicable.

1. Equipment limitations prevented simulation of specification requirements for the peak levels.
2. Two sources used, one on pulse to meet peak requirement and one continuous wave (CW) to meet average level requirements.
3. The required peak level was simulated with a CW signal level.

Table IV-53. Requirements versus test external environment simulation (M67-1 simulated countdown)

| Radio frequency source simulated | RF simulation requirements | | | | Test levels for simulated countdown procedure | | | |
|---|---|---|---|---|---|---|---|---|
| | Frequency, GHz | Peak power density, dBmW/m² at spacecraft | Average power density, dBmW/m² at spacecraft | Minimum pulse width, μs | Frequency, GHz | Peak power density, dBmW/m² at spacecraft | Average power density, dBmW/m² at spacecraft | Minimum pulse width, μs |
| *Agena* radar transmitter (FPS-16) | 5.690 | +59 | +21 | 1.0 | 5.690 | See note 1 | +20 | CW |
| *Atlas* guidance track ground transmitter | Classified | +20 | −12 | 2.0 | Classified | See note 1 | 0 | CW |
| *Atlas* guidance rate ground transmitter | Classified | NA | +14 | NA | Classified | NA | +15 | CW |
| Command destruct ground transmitter | Classified | NA | + 4 | NA | Classified | NA | + 4 | CW |
| *Agena* telemetry | 0.2443 | NA | +23 | NA | 0.2443 | NA | +25 | Subcarrier modulation |
| *Agena* radar transponder | 5.765 | + 7 | − 8 | 0.7 | 5.765 | +7.5 | − 8 | See note 1 |
| *Atlas* telemetry | 229.9 | NA | − 6 | NA | 229.9 | NA | − 3 | Subcarrier modulation |
| *Atlas* guidance track transponder | Classified | +30 | − 1 | 2.0 | Classified | See notes 1 and 2 | +30 | CW See note 2 |
| *Atlas* guidance rate transponder | Classified | NA | − 5 | NA | Classified | NA | − 5 | CW |

NA = not applicable.

1. Equipment limitations prevented simulation of specification requirements for the peak levels.

2. The required peak level was simulated with a CW signal level.

The average power levels were met in the test; however, the peak power levels for two of the sources were not met because of equipment limitations. The omission is not considered serious because each of the two simulated sources is a ground-based RF transmitter.

The spacecraft systems were monitored by cognizant personnel and no adverse effects from any RF source were reported to the test director.

Part of the spacecraft EMI qualification program included formal compatibility tests of the DFR experiment, the S-band transponder, and the spacecraft. These tests were the culmination of a series of investigative tests and spacecraft modifications made to suppress interference to the DFR VHF channel. Acceptable DFR and spacecraft performance was demonstrated in these tests. The DFR integration effort is discussed elsewhere in this report.

Measurements of noise at the S-band transponder and image frequencies at the spacecraft antenna terminals were part of EMI testing. On M67-1 and M67-2, these tests were performed in the SAF. The decision to omit S-band noise measurements in the space simulator chamber was based on the test and flight results of *Mariner IV*, and on an analysis that compared the test receiver sensitivities for each location. An analysis (Ref. 14) has shown that no increase in sensitivity would be gained by performing the test in the space chamber. No extraneous noise levels were measured in the receiver band when examined with a 100-Hz bandwidth of the low-noise test receiver.

*c. Special investigations and support.*

*Pinpuller pyrotechnic susceptibility to S-band transmitter.* The objective of this test was to determine whether the radiation from the *Mariner V* omnidirectional antenna would be hazardous to the pinpuller squibs. The solar panel pinpuller locations are closer to the low-gain antenna on *Mariner V* than they were on *Mariner IV*. This test was performed to determine the margin of safety for the new configuration without conducting a test on M67-1 that would require test time and

Table IV-54. Requirements versus test external environment simulation (M67-1 pyrotechnics and shock test)

| Radio frequency source simulated | RF simulation requirements | | | | Test levels for pyrotechnics and shock test procedure | | | |
|---|---|---|---|---|---|---|---|---|
| | Frequency, GHz | Peak power density, dBmW/m² at spacecraft | Average power density, dBmW/m² at spacecraft | Minimum pulse width, μs | Frequency, GHz | Peak power density, dBmW/m² at spacecraft | Average power density, dBmW/m² at spacecraft | Minimum pulse width, μs |
| *Agena* radar transmitter (FPS-16) | 5.690 | +59 | +21 | 1.0 | 5.690 | | +20 | CW |
| *Atlas* guidance track ground transmitter | Classified | +20 | −12 | 2.0 | Classified | | −12 | CW |
| *Atlas* guidance rate ground transmitter | Classified | NA | +14 | NA | Classified | NA | +15 | CW |
| Command destruct ground transmitter | Classified | NA | + 4 | NA | Classified | NA | + 4 | CW |
| *Agena* telemetry | 0.2443 | NA | +23 | NA | 0.2443 | NA | +25 | Subcarrier modulated |
| *Agena* radar transponder | 5.765 | + 7 | − 8 | 0.7 | 5.765 | +11 | − 6 | See note 2 |
| *Atlas* telemetry | 229.9 | NA | − 6 | NA | 229.9 | NA | − 6 | Subcarrier modulated |
| *Atlas* guidance track transponder | Classified | +30 | − 1 | 2.0 | Classified | | +30 | CW |
| *Atlas* guidance rate transponder | Classified | NA | − 5 | NA | Classified | NA | − 5 | CW |

NA = not applicable.

1. Equipment limitations prevented simulation of specification requirements for the peak levels.
2. Two sources used, one on pulse to meet peak requirement and one continuous wave (CW) to meet average level requirements.
3. The required peak level was simulated with a CW signal level.

manpower. One of the objectives was to obtain data at an early date in case a redesign was necessary.

Special instrumentation was devised for this investigation to measure RF power dissipated in a squib. This series of tests demonstrated that there was no hazard to the pinpuller squibs in their new locations.

*Umbilical lines conducted EMI susceptibility study.* A susceptibility analysis of spacecraft umbilical line interface circuits was performed to attempt to identify marginal conditions. A comprehensive analysis would have involved considerable time and manpower. The work performed on this program was an expedient limited by the program deadlines. No inordinate circuit susceptibilities were discovered.

*Support of AFETR launch operations.* The primary tasks of the EMI support were as follows:

(1) Perform noise measurements at the AO hangar, the Explosive Safe Facility (ESF), and Launch Complex 12 at the spacecraft transponder frequencies to ensure that the communications links would not be degraded because of electromagnetic interference during the pre-launch phase of the mission.

(2) Perform noise measurements at the AO hangar, ESF, and Launch Complex 12 at the DFR frequencies to provide data relevant to the normal background noise at the DFR frequencies.

(3) Provide assistance in investigations where electromagnetic interference could be a factor.

*4. Magnetic control program.* The *Mariner* Venus 67 project policy required that the magnetic quality of the spacecraft should be at least equal to that of *Mariner IV*, and that an attempt should be made to improve this quality with techniques compatible with the schedule and fiscal restraints. Based on these requirements, and post-launch demagnetization tests made on the *Mariner IV*

Table IV-55. Requirements versus test external environment simulation (M67-2 system test)

| Radio frequency source simulated | RF simulation requirements | | | | Test levels for system test procedure | | | |
|---|---|---|---|---|---|---|---|---|
| | Frequency, GHz | Peak power density, dBmW/m² at spacecraft | Average power density, dBmW/m² at spacecraft | Minimum pulse width, μs | Frequency, GHz | Peak power density, dBmW/m² at spacecraft | Average power density, dBmW/m² at spacecraft | Minimum pulse width, μs |
| *Atlas* radar transmitter (FPS-16) | 5.690 | +59 | +21 | 1.0 | 5.690 | See note 1 | +20 | CW |
| *Atlas* guidance track ground transmitter | Classified | +20 | −12 | 2.0 | Classified | See note 1 | −12 | CW |
| *Atlas* guidance rate ground transmitter | Classified | NA | +14 | NA | Classified | NA | +14 | CW |
| Command destruct ground transmitter | Classified | NA | +4 | NA | Classified | NA | +4 | CW |
| *Agena* telemetry | 0.2443 | NA | +23 | NA | 0.2443 | NA | +23 | Subcarrier *modulated* |
| *Agena* radar transponder | 5.765 | +7 | −8 | 0.7 | 5.765 | +7.5 | −8 | See note 2 |
| *Atlas* telemetry | 0.2299 | NA | −6 | NA | 0.2499 | NA | −6 | CW |
| *Atlas* guidance track transponder | Classified | +30 | −1 | 2.0 | Classified | See notes 1 and 3 | +30 | CW |
| *Atlas* guidance rate transponder | Classified | NA | −5 | NA | Classified | NA | −5 | CW |

NA = not applicable.

1. Equipment limitations prevented simulation of specification requirements for the peak levels.
2. Two sources used, one on pulse to meet peak requirements and one on continuous wave (CW) to meet average level requirements.
3. The required peak level was simulated with a CW signal level.

PTM, a magnetic control plan was developed covering the following specific points:

(1) Review ECRs and consult with cognizant engineers to ensure that *Mariner V* hardware is magnetically equivalent to *Mariner IV* hardware.

(2) TA testing is to include tests for compatibility of a demagnetization procedure.

(3) Flight hardware is to be demagnetized on the subsystem level at the conclusion of vibration and shock testing.

*a. Magnetic control plan.* The control plan outlined the magnetization and demagnetization tests and the magnetic mappings that would be performed on the TA or prototype hardware to qualify each assembly or subassembly for demagnetization of the flight hardware. These procedures included two demagnetizations: one at the same field level as to be used on the flight hardware (40-G peak), one at twice this level; and a magnetization at a 25-G exposure level. The hardware was mapped "as received," again, following each of the above three tests, and to determine the effect of an inducing field.

Solar panels, being too large to test in the same manner as other hardware, were tested in the earth's field as was the case with the *Mariner IV* panels. With the major changes in the solar panel design necessitated by a Venus mission, *Mariner V* solar panels did not acquire a residual magnetization as easily as *Mariner IV* panels. Consequently, the flight solar panels did not require demagnetization.

Flight hardware was demagnetized and mapped at the assembly or subassembly level during the final disassembly and inspection of the spacecraft prior to shipment to Cape Kennedy. Following demagnetization of the flight hardware, magnetic cognizance of the hardware was maintained until launch. If the hardware was removed from the spacecraft assembly area, it was remapped. If the demagnetized field had changed by more than 10%, the hardware was redemagnetized.

The magnetic control plan also called for control of tools which might come in contact with the spacecraft after the spacecraft had been demagnetized. All tools were initially tested and those having a residual magnetization were demagnetized. Subsequent rechecks were

made to ensure that the tools did not re-acquire a residual field.

*b. Program results.* Program results cannot be precisely stated because, at present, there is no meaningful measure of spacecraft magnetic quality. Table IV-56, which gives the components of the residual field of the spacecraft at the science magnetometer sensor prior to launch, shows that the field was materially reduced.

**Table IV-56. Comparison of spacecraft perm fields**

| Spacecraft | | X | Y | Z |
|---|---|---|---|---|
| *Mariner* Mars 1964 | MC-2 | 2.5 | 21.0 | 17.4 |
| | MC-3 | 5.0 | 11.5 | 30.1 |
| *Mariner* Venus 67 | M67-1 | −1.2 | 3.5 | 7.1 |
| | M67-2 | −1.2 | 2.8 | 7.3 |

Although it appears from this comparison of M67-1 and M67-2 that the spacecraft magnetic stability was improved, a comparison of the in-flight calibration of *Mariner V*, launched on June 14, 1967, and the prelaunch measured fields demonstrates a significant difference in two of the field components. This comparison is shown in Table IV-57. Because of the large time interval between these two field determinations, the results are not indicative of the source or cause of the apparent instability.

**Table IV-57. Comparison of pre- and post-flight spacecraft fields**

| Pre- and post-flight fields | X | Y | Z |
|---|---|---|---|
| April 13, 1967, pre-flight mapping at JPL | −1.3 | 0.3 | 6.6 |
| June 14 to 30, 1967, in-flight calibration | 3.7 | 0.9 | 8.5 |

Generally, the change in scientific experiments on *Mariner V* and the redesign of the DAS and solar panels have resulted in hardware with lower magnetic fields at the magnetometer. At the same time, demagnetization resulted in a spacecraft with a much lower residual field and, to some extent, improved magnetic stability. A considerable amount of magnetic mapping data was obtained in this program. These data will benefit future programs because they were obtained under more controlled conditions.

## L. System Test and Launch Operations

In general, *Mariner* Venus 67 system test and launch operations planning, philosophy, and management techniques were based on experience gained on the *Mariner* Mars 1964 project and other previous JPL programs.

Because of the similarity between the test programs, only areas of significant difference in concept, attainment, or experience are described. As shown in Figs. IV-191 and IV-192, M67-1 had been tested for 752 h at the system level and M67-2 had undergone 710 h of testing before launch. The total 1462 h of system test experience gained on two spacecraft by one test team in 1967 compares satisfactorily with 3910 h of system test experience accumulated on four spacecraft by three test teams in the 1964 test program.

Throughout the program, system operations were completed on schedule (Figs. IV-193 and IV-194).

*1. Test operations.*

*a. Use of a single test team.* A significant difference between the *Mariner* Venus 67 program and the *Mariner* Mars 1964 system test program was the use of a single test team for both spacecraft (M67-1 and M67-2). In the 1964 program, three test teams were used for a four-spacecraft test program. The one-team approach was made possible by the serial scheduling of major spacecraft activities (Figs. IV-193 and IV-194) and the interleaving of mechanical and electrical operations.

Besides reducing manpower requirements, the single-team method promoted a higher level of test proficiency by the team members and simplified performance analysis and comparison between the two spacecraft. The test effort was further enhanced when test personnel were able to make use of experience gained on *Mariner* Mars 1964 test program and were able to rely upon system test complex data system (STCDS).

*b. Role of the flight-support spacecraft.* M67-1 was designated the flight-support spacecraft. In this role, it acted as a pseudo PTM for design verification, procedure and facility checkout, personnel training, special problem research, and spares qualification. The spacecraft was not a true PTM because test levels were not significantly different from the FA levels used on M67-2. If all considerations, such as reliability, performance, and qualifying test history, had indicated that a change would have been advantageous, the flight-support spacecraft could have been redesignated the flight spacecraft.

*c. Magnetic control.* Magnetic control techniques were somewhat less stringent during the early part of the *Mariner* Venus 67 test program than they were during a comparable period in 1964. However, once the post-environmental testing demagnetization of spacecraft assemblies had been completed,[8] strict magnetic control of system hardware and operations was enforced to prevent magnetic contamination of the spacecraft through the use of improper tools, fasteners, or parts. These measures gave high confidence that the spacecraft magnetic background was minimized, stabilized, and well understood.

*d. DFR interface problems.* Addition of the DFR to the science payload was the major system interface problem to affect the system test program. The interface problems resulted from the susceptibility of the DFR to electrical noise generated by various elements of the spacecraft system in its different operating modes. A major test effort was required to identify the sources of the noise, to select efficient design solutions, and to incorporate and verify the adequacy of the changes.

The system-level test program was coordinated with major subsystem-level test programs to solve the interface problems. Flight experience to date shows that the design changes and interface verifications were adequate and that the DFR was successfully integrated into the science package.

*e. Cleanliness.* One of the major objectives of the system-level assembly and test program was the fabrication of a clean, dust-free spacecraft. Basic emphasis was given to the protection of surfaces and the elimination of loose dust particles that could float near the spacecraft during its flight in space. These aims were largely met by use of a large, portable, laminar downflow clean room. Whenever feasible, the spacecraft was enclosed in the clean room.

Use of the portable clean room was an important factor in producing a cleaner spacecraft in 1967 than was possible in 1964. Experience gained during the 1967 program will lead to better cleanliness techniques on future programs.

*f. Launch pad operations.* In previous JPL missions, two sequences of launch pad operations were performed. The first sequence verified all launch complex interfaces and procedures using the flight spacecraft without pyrotechnics or propellants installed. The second sequence of operations used the flight-ready spacecraft and culminated in launch. For the 1967 launch opportunity, the spacecraft was scheduled for only one trip to the launch complex. The considerations leading to the one-trip decision were as follows:

(1) The launch pad (Launch Complex 12) and the launch vehicle system (*Atlas/Agena*) had been used on past programs and their characteristics were well understood.

(2) Schedule time availability would make it very difficult to accommodate two launch-pad sequences.

(3) Detailed preliminary checkout of launch complex and launch complex equipment (LCE) links from the spacecraft interface to the blockhouse and the spacecraft checkout facility could be performed in greater detail and to greater depth through the use of spacecraft and subsystem simulators.

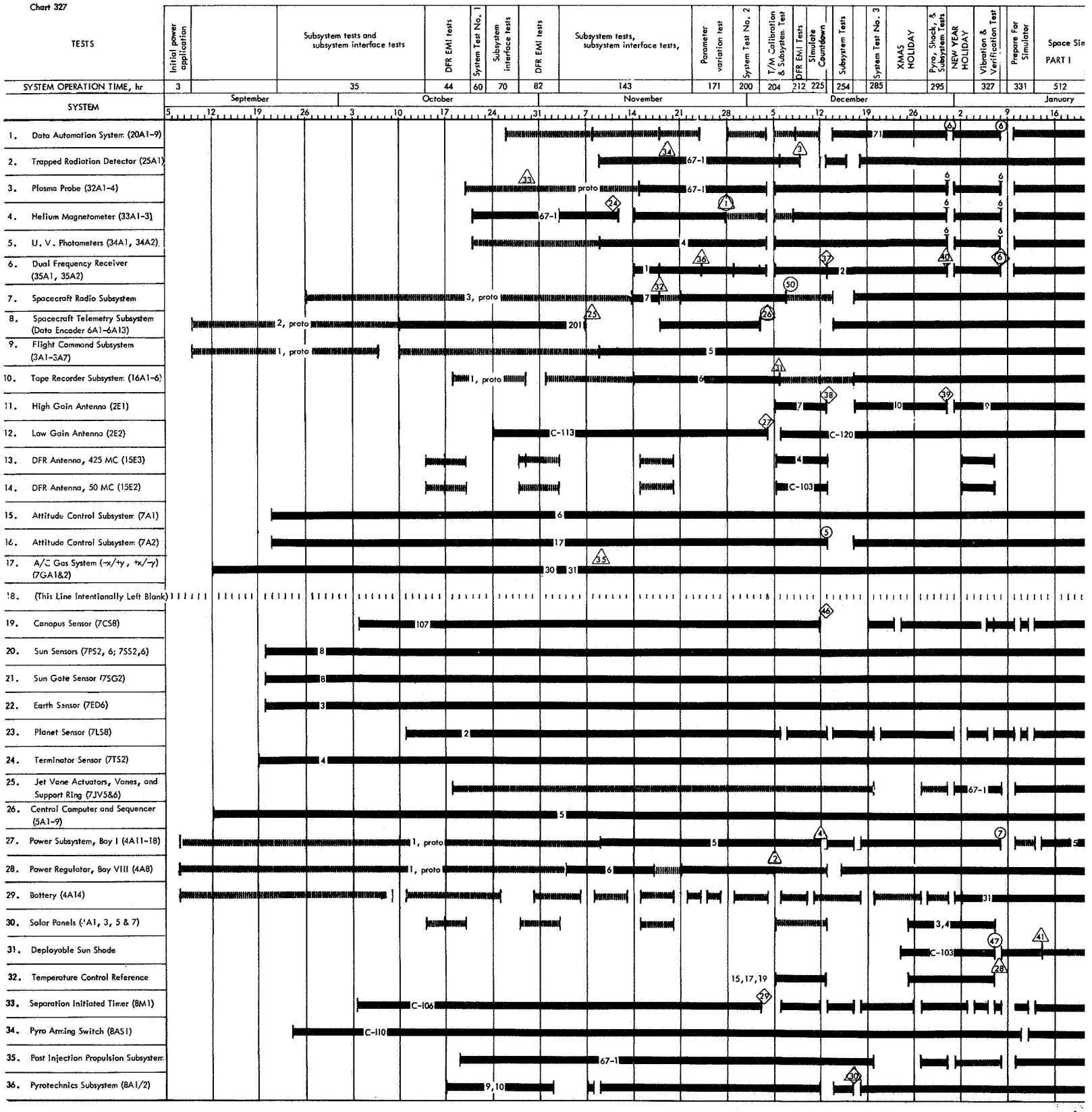
The spacecraft was successfully interfaced with the launch vehicle and launch complex. The smoothness of the interfacing operation was attributable to the familiarity with the launch complex and launch vehicle gained on previous missions and the accuracy with which spacecraft functions were simulated for the calibration and adjustment of control and monitor lines.

*g. Spacecraft removal from Launch Complex 12 for problem investigation.* During a simulated pre-countdown, spacecraft telemetry indicated that radio power amplifier A (traveling-wave tube) did not turn off when power amplifier B (cavity) was turned on by a DC-V7 command. After extensive analysis and discussion, it was decided to de-mate the spacecraft from the launch vehicle and return it to the JPL ESF for more detailed examination.

Return of the spacecraft to ESF meant that the spacecraft would not be able to participate in the joint FA composite test (J-FACT). Absence of the spacecraft did not compromise the launch vehicle test objectives for the J-FACT. From the spacecraft standpoint, it was determined that all spacecraft test objectives could be met by participation in the simulated launch. Furthermore, if difficulty in intersystem operations were encountered, a second simulated countdown exercise could be scheduled.

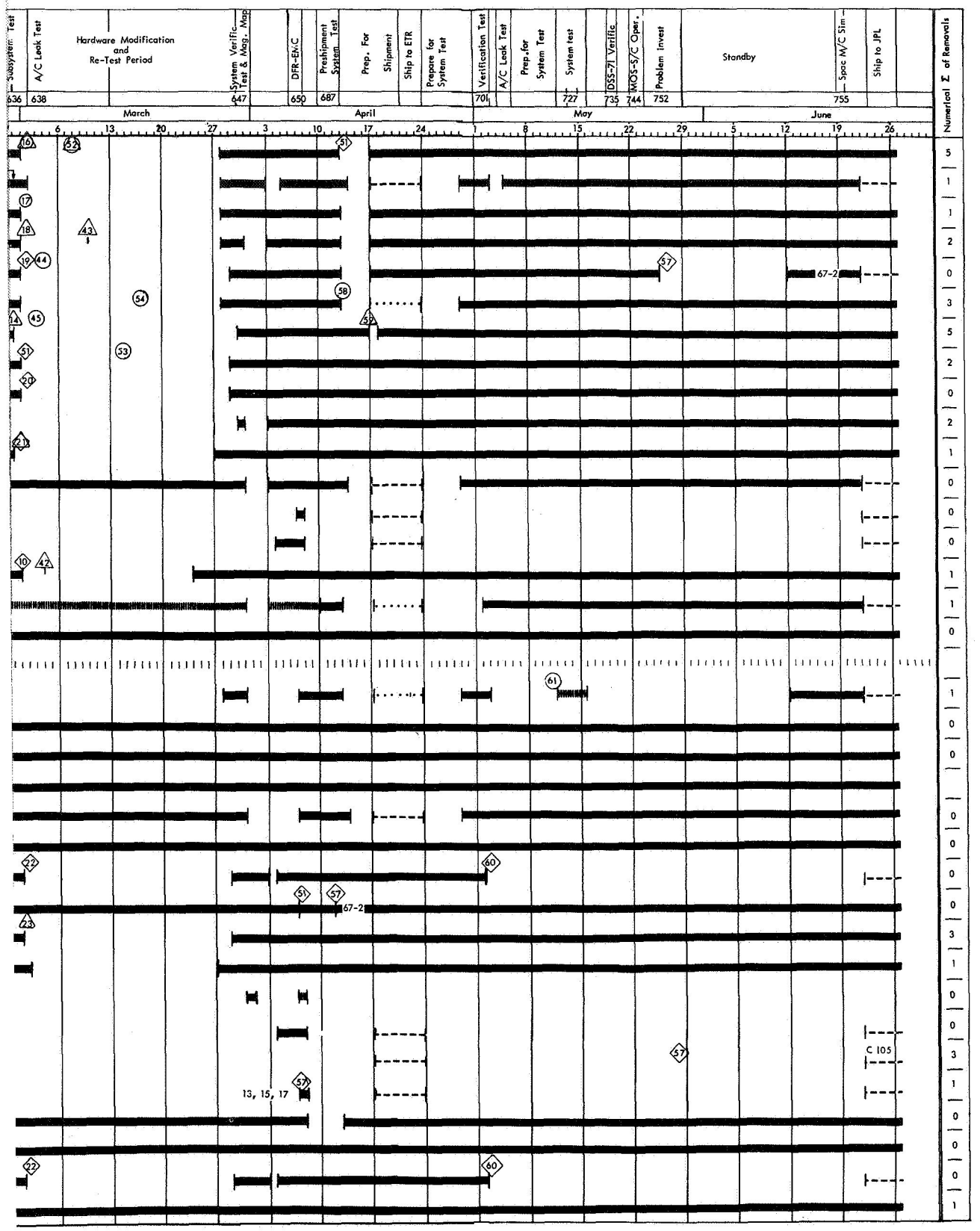
[8] *Mariner V* was the first JPL flight spacecraft to be demagnetized as a part of its system test program.

Chart 327






FOLDOUT FRAME 1




LEGEND:

- Flight System installed
- Prototype, STM T. A., Spare
- Removal of system for storage, protection access to other system
- P/FR, Removal of system for
- E. C. R., removal of system for
- System removed for Independent Test and/or Calibration
- Unit shipped to ETR with S/C in separate container.
- Unit shipped to ETR by separate shippment.

Summary of Removals:

1. Returned to Div. 32 to evaluate Y-Axis flipping problem (P/FR-10643), Sensor (33A1) painted (ECR-8646).
2. Returned to Div. 34 to change diode to reduce noise. (ECR-8651).
3. Returned to Div. 32 to install inductor in +8v line to eliminate Data channel D1 (ECR-8671).
4. Returned to Div. 34 to modify time constant in charger toggle circuitry (ECR-8680).
5. Returned to Div. 34 to evaluate rate movement exceeding limits (P/FR-10663).
6. Removed to evaluate DAS bad rate data (P/FR-11047). DFR had X-former X-rayed.
7. Returned to Div. 34 to replace resistor in 4A11, damaged by C-Clamp (P/FR-10690).
8. Removed for seperate wt & c.g.
9. Returned to S.U.I. for calibration.
10. Removed to use on S/C 67-2.
11. Stored to avoid excessive use.
12. Removed (34A1) to remove thermocouples.
13. Removed to evaluate DAS P/N sequence (P/FR-010718).
14. Returned to Div. 33 for cavity bonding & capacitor replacement. (ECR-8714, 8715).
15. Returned to Div. 33 to replace analog modules & tape; fix end of tape sensor, & investigate degradation in bit error rate.
16. Returned to Div. 32 for rework per ECR-8659: change crystals, ECR-8746: set framecount, and P/FR-010718: P/N sequence evaluation.
17. Removed to evaluate P/FR-10655: high voltage step noise, and/or P/FR-11083: high noise during vacuum test.
18. Returned to Div. 32 to change cover on 33A1 (ECR-8774).
19. Removed to pot flight connectors.
20. Returned to Div. 33 for bit error degradation & lock up bench check.
21. Returned to Div. 33 for Pattern Check and repainting to eliminate peeling (P/FR-8304, ECR-8727).
22. Returned to Div. 38 for leak test & preshipment check-out.
23. Returned module 4A18 to Div. 34 to replace capacitors (ECR-8728).
24. Returned to Div. 32 for EMI test with power PTM.
25. Returned 6A12 to Div. 33 to change bit sync. rise time to DAS (ECR-8601).
26. Returned 6A10, 6A11 to Div. 33 to change Temp. Control Signal conditioning. (ECR-8613) (P/FR-010631)
27. Returned to Div. 34 for gain measurements. Reassigned to 67-2 S/C.
28. Returned to Div. 35 for terminal I.D. & conformal coating (ECR-8743).
29. Returned to Div. 35 to seal connectors & insulate terminals.
30. Removed to insulate and seal backside of Pyro connectors (ECR-8623).
31. Returned to Div. 33 to replace tape, complete margin test, correct Bit error rate (ECR-8642), change transistor type in 16A5 (ECR-8668), & to replace diodes (ECR-8669).
32. Returned to Div. 33 to add coaxial tee and tuned stab to eliminate interferometer null near encounter (ECR-8524) and replace x-ponder exciter output cables with cables having connectors potted (ECR-8722).
33. Replaced short H. V. cable (ECR-8603).
34. Washer configuration revised to isolate TRD from S/C (ECR-8621).
35. Replaced fasteners for attaching A/C gas system plumbing to solar panel spar (ECR-8622).
36. Upper ring structure above Bay III modified to accommodate mounting of DFR filters (ECR-8656).
37. Returned to Div. 32 and reassigned as T. A. unit.
38. Returned to Div. 33 & reassigned to 67-2 S/C
39. Returned to Div. 33 & reassigned as spare
40. Removed to change digital data serial shift pulse generator circuit to reduce temp. effect (ECR-8690).
41. Removed to modify lanyard ties (ECR-8700), add polished aluminum side shields and multi-layered insulation boot (ECR-8730).
42. Returned to Div. 34 to install flight resistors in Auto Pilot (ECR-8787).
43. Aadition of R/C filter circuit to A, PW converter (ECR-8801).
44. UV fell 6" while potting connectors (P FR-010719)
45. A transistor shorted during electrical testing of 2PS3 TWT Power Supply, S N 14346 & seven transistors were replaced as a pre cautionary measure (IR-83205) (P FR-00832).
46. Returned to Div. 34 for "stray-light" test.
47. Removed to evaluate operation; shade did not fully deploy during test (P/FR-010691).
48. Harness 2W2 connector binds (P/FR-010715).
49. Removed after simulator test & damaged (P/FR-010717). Replaced by S/N C-104.
50. Removed to evaluate cross talk with command (P FR-010658).
51. Returned to Div. for Margin Test.
52. Module 20A8 Etch Cut & Hay-Wired (ECR-8799) to eliminate DFR Serial Shift out of phase pulses (P/FR-10844).
53. Threaded inserts in subchasses 6A3,4,5 damaged & replaced (IR-91257).
54. Returned to Div. 32 to measure digital out put data. (P/FR-011067).
55. Returned to Div. 33 for Margin and Vacuum Test
56. Returned to Div. 34 to evaluate: "Sensor lost canopus durring cruse mode" 21 Oct 66 (P/FR-010635).
57. Reassigned to 67-2 S/C
58. Returned to Div. to replace 7MH$_2$ crystals (P/FR-11076)
59. Returned Receiver 2TR1 to Div. to add resistor and capacitor
60. Removed to fuel.
61. Returned to JPL to evaluate intensity variation without a light stimulus. (P/FR-10896).

**Fig. IV-191. M67-1 flight systems history**



FOLDOUT FRAME 2

FOLDOUT FRAME 3

CHART 329

| TEST | Assembly | Initial Power Application | Subsystem Interfaces And Subsystem Tests | Telemetry Chan Calibration And Special Tests | System Test No. 1 | Parameter Varia And Special Tests Preamble | Subsystem Test DFR EMI Test | Prepare for Wt. & C.G. | Wt. & C.G. | Sim. Countdown | DFR EMI Test | Match Mate | SFAC to S/C Loop 3 Test | System Test No. 2 | Subsystem Test | Vibration & Verification Test | Prepare for Simulator | Space Simulation Test - PART I | PART II | Sys. Verific Test | S/C Disas/C Leak Test & Reassembly | S/C Mag. Map Ground Interf. Test & Prelnpment Sys. Test | Prep for Shipment | Ship to ETR | System Test | DSS-71 Verific | Final A.C. Elect. Test | WT. & C.G. | DSF-71 Compat. | A/C Leak test | DSF Elect. test | Sim Precountdown L.V.C. Func. R.F. | Radio prob. Invest | Sim. Pre.-Count Mate with L.V. Simulate Launch | Count down Sequence | LAUNCH 11:01 p.m. PDT |
|---|---|---|---|---|---|---|---|---|---|---|---|---|---|---|---|---|---|---|---|---|---|---|---|---|---|---|---|---|---|---|---|---|---|---|---|
| SYSTEM OPERATION TIME, | 0 | 2.4 | 60 | 75 | 109 | 129 | 141 | 155 | 161 | | | 170 | 197 | 213 | 217 | 242 | | 422 | | 515 | 523 | 535 | 561 | | | 589 | 611 | 624 | | 640 | | 648 | 657 | 665 | 682 | 691 | 696 | 710 |
| SYSTEM | DECEMBER | | JANUARY | | | | FEBRUARY | | | | | | | | | MARCH | | | | | | APRIL | | | | MAY | | | | | | | | | | JUNE |

1. Data Automation System (20A1-9)
2. Trapped Radiation Detector (25A1)
3. Plasma Probe (32A1-4)
4. Helium Magnetometer (33A1-3)
5. U. V. Photometers (34A1, 34A2)
6. Dual Frequency Receiver (35A1, 35A2)
7. Spacecraft Radio Subsystem
8. Spacecraft Telemetry Subsystem (Data Encoder 6A1-6A13)
9. Flight Command Subsystem (3A1-3A7)
10. Tape Recorder Subsystem (16A1-6)
11. High Gain Antenna (2E1)
12. Low Gain Antenna (2E2)
13. DFR Antenna, 425 MC (15E3)
14. DFR Antenna, 50 MC (15E2)
15. Attitude Control Subsystem (7A1)
16. Attitude Control Subsystem (7A2)
17. A/C Gas System (7GA1/2)
18. (This Line Intentionally Left Blank)
19. Canopus Sensor (7CS8)
20. Sun Sensors (7PS2,6; 7SS2,6)
21. Sun Gate Sensor (7SG7)
22. Earth Sensor (7ED6)
23. Planet Sensor (7LS8)
24. Terminator Sensor (7TS2)
25. Jet Vane Actuators, Vanes, and Support Ring (7JV5&6)
26. Central Computer and Sequencer (5A1-9)
27. Power Subsystem, Bay I (4A11-18)
28. Power Regulator, Bay VIII (4A8)
29. Battery (4A14)
30. Solar Panels (4A1, 3, 5 & 7)
31. Deployable Sun Shade
32. Temperature Control Reference
33. Separation Initiated Timer (8M1)
34. Pyro Arming Switch (8AS1)
35. Post Injection Propulsion Subsystem
36. Pyrotechnics Subsystem (8A1/2)

**Fig. IV-192. M 67-2 flight systems history**



Fold Frame I

Fold out Frame

- - - - - - Unit shipped to ETR with S/C
in separate container

. . . . . Unit shipped to ETR by separate shipment

to change crystals (ECR-8659)

seal crystals.

10833

ors in Auto Pilot (ECR-8787)

o output (P/FR-10802).

S.

istor in SA2 (P/FR 010834)(ECR-8783)

ice resistor (P/FR-10690).

ice capacitor

#2.

and hav-wire (ECR-8799), to
pulses (P/FR-10844)

ter circuit to A/PW converter

des (ECR-8789).

) mode

ator
ked
e.

e problem
C Y-1

ement &

of
10876)

leak rate

ibration

n without a light stimulus (P/FR-10896).

nput stimulus. (P/FR-010514)
in off position (P/FR-10518)

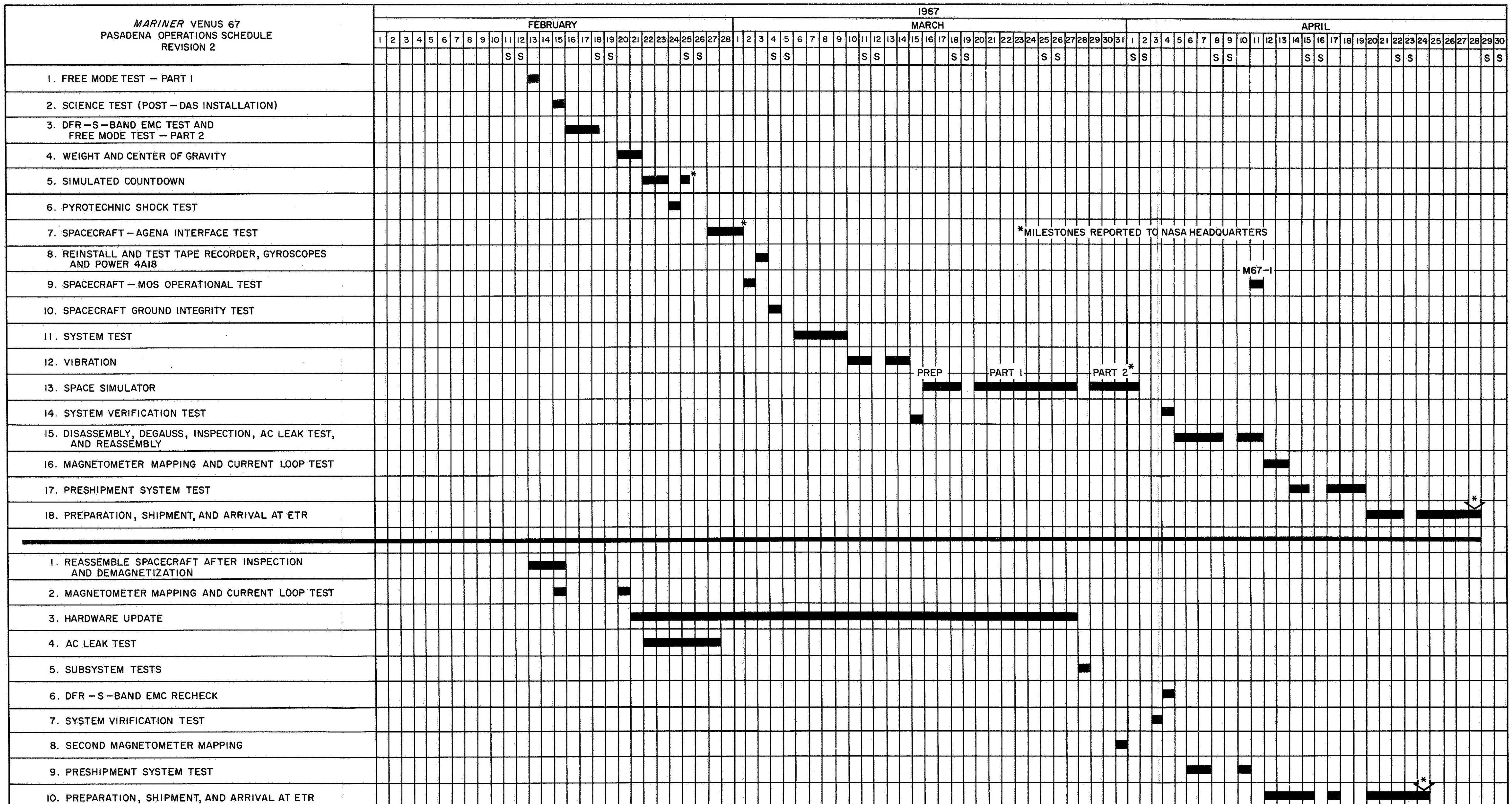



Fig. IV-193. Typical Pasadena system test operations schedule



FOLDOUT FRAME 1

FOLDOUT FRAME 2

*MARINER* VENUS 67
AFETR OPERATIONS SCHEDULE
REVISION 1

APRIL: 1 2 3 4 5 6 7 8 9 10 11 12 13 14 15 16 17 18 19 20 21 22 23 24 25 26 27 28 29 30
MAY: 1 2 3 4 5 6 7 8 9 10 11 12 13 14 15 16 17 18 19 20 21 22 23 24 25 26 27 28 29 30 31
JUNE: 1 2 3 4 5 6 7 8 9 10 11 12 13 14 15 16 17 18 19 20 21 22 23 24 25 26 27 28 29
S S S S S S S S S S S S S S S

1. SPACECRAFT AND OSE ARRIVAL, EXAMINATION, AND ASSEMBLY
2. CALIBRATION VERIFICATION
3. SYSTEM VERIFICATION TEST
4. FINAL SYSTEM TEST
5. SPACECRAFT–MOS OPERATIONAL TEST
6. MECHANICAL PREPARATION AT BLDG AO — INCLUDES WEIGHT AND CENTER OF GRAVITY
7. MOVE TO ESF
8. MECHANICAL PREPARATION AT ESF
9. ELECTRICAL TEST AT ESF
10. AC GAS LEAK TEST
11.° SPACECRAFT MATE WITH AGENA ADAPTER AND SHROUD
12. MOVE TO LC–12
13. SPACECRAFT/LC–12/AO/DSS–71
14.* RF INTERFERENCE TEST
15. SPACECRAFT SIMULATED PRECOUNTDOWN
16.°* JOINT FA COMPOSITE TEST
17. SIMULATED LAUNCH
18. SPACECRAFT PRECOUNTDOWN
19.* COUNTDOWN

INTERFACE MILESTONES

20. SPACECRAFT SUPPORT EQUIPMENT INSTALLED BY LMSC ON LC–12 — TENTATIVE
21. JPL PRELIMINARY TEST OF AO, ESF, AND LC–12 COMPLETE
22.* MISSION READINESS REVIEW
23.* *AGENA* MATE WITH *ATLAS*
24.° LAUNCH READINESS

HOLIDAY

* PROJECT MILESTONES APPEARING IN LSD
° MILESTONES REPORTED TO NASA HEADQUARTERS
M67–1
M67–2
TIME IN EST

**Fig. IV-194. *Mariner* Venus 67 AFETR operations schedule, Revision 1**



FOLDOUT FRAME 1

FOLDOUT FRAME 2

PRECEDING PAGE BLANK NOT FILMED.

Two failure models were initially proposed to explain the failure: (1) a set of relay contacts had stuck together in relay K2 of subassembly 2CC1, or (2) there was a short circuit in the 2CC1 connector or in the EA VI harness.

Operations at building AO included X-ray photography of the suspected relay and surge current measurements of the cavity and traveling-wave tube power supplies. The suspected relay was removed from subassembly 2CC1 and de-canned. Microscopic examination showed that the failure was probably caused by anodic transfer from one contact to the other under heavy current loading.

The M67-2 radio was repaired by installing a screened equivalent and returned to ESF for reinstallation on the flight spacecraft. The M67-2 radio was repaired instead of being replaced by the M67-1 spare radio because of previous test history on the M67-1 radio.

A reverification of all functions passing through connectors that had been de-mated for the removal of EA VI was performed, and a series of electrical and mechanical operations required to prepare the spacecraft for its return to Launch Complex 12 was completed. The spacecraft was returned to the launch pad and normal prelaunch testing operations were resumed.

*h. Spacecraft–DSN compatibility verification.* Spacecraft–DSN compatibility tests were performed in two phases. The first series of tests was conducted at the Goldstone tracking station approximately 4 months before the spacecraft was scheduled to be launched. This test series involved extensive compatibility testing and performance parameter measurement (refer to Section IV-I for further details).

The second series of tests was conducted at AFETR and involved both *Mariner* Venus 67 and Deep Space Station 71. These tests successfully verified spacecraft telecommunications performance parameters.

*i. Launch pad S-band parameter measurements.* The same technique used to measure *Mariner IV* S-band characteristics under the shroud in 1964 was used to determine *Mariner V* performance on the launch pad. The *Mariner IV* method evolved from the *Mariner III* approach after the elimination of the low-gain antenna coupler and *Agena* parasitic slot antenna that were used in the *Mariner III* shroud.

*j. Safety.* AFETR range safety personnel exercised considerably more control over the safety aspects of the *Mariner* Venus 67 project than in 1964. All procedures dealing with hazardous operations, or involving the spacecraft while it was in a hazardous condition (e.g., pyrotechnics installed), had to be submitted to AFETR range safety for review 1 month before use. Revisions of the most minor nature had to be incorporated in the procedure before use would be permitted.

*k. Spacecraft problems and failures.* The *Mariner* Venus 67 spacecraft system test program produced 248 problem failure reports (PFRs) in the period starting with the assembly of M67-1 and ending with the launch of M67-2 (*Mariner V*). A total of 146 of the PFRs were concerned with actual spacecraft problems; the remainder involved operational support equipment. Table IV-58 lists problems detected during the system test program that resulted in changes in spacecraft design.

**Table IV-58. Spacecraft problems during system test operations that led to spacecraft design changes**

| No. | Problem | Design change |
|---|---|---|
| 1 | Placement of sun sensors on *Mariner* 67 was different than on *Mariner* Mars 1964. Cable harnesses made to fit 1964 configuration | Wiring harnesses corrected and documentation corrected |
| 2 | Radio power amplifiers and exciters switched anomalously | Resistors changed |
| 3 | Open connection found between 9W20J1-D and 34A2P1-31 | Connector 9W20J1 rewired |
| 4 | High-voltage cable to plasma probe sensor too short | Cable lengthened 1 in. |
| 5 | Sun sensor mounting screw interfered with UV photometer installation | Screw length shortened |
| 6 | DAS generated extra bit snyc pulses | Data encoder modified to drive isolation pulse switch off hard |
| 7 | Radio power converts the power subsystem regulator, and the DAS clock generated EMI affecting the DFR | Diodes in the power regulator were changed and the frequency of the DAS clock was altered |
| 8 | Magnetometer Y-axis data polarity reversed with no change in stimulus | Extra triggering by magnetometer analog-to-pulsewidth converters eliminated |
| 9 | Battery charger toggled to boost mode when OSE boost-mode inhibit was released | Resistor values increased |

Table IV-58 (contd)

| No. | Problem | Design change |
|---|---|---|
| 10 | DAS frame count jumped because of noise from attitude control gas valve operation | OSE set frame count interface desensitized |
| 11 | Sun shade did not deploy completely | Lanyard restrictions removed and aluminum tape cut at fold points for greater flexibility |
| 12 | Magnetometer sensor operated 15°F cooler than expected | Thermal paint removed from top igniter housing |
| 13 | Low-gain antenna cable connector was found to bind | New cable fabricated with connectors having hard-anodized nuts |
| 14 | Maneuver booster-regulator was accidentally overloaded | OSE interlocked to prevent power subsystem overloading |
| 15 | Interference between octagon angle and channel structures | Velco configuration on angle changed |
| 16 | CC&S short counted with LCE-2 | Resistor added to compensate for loading of the inhibit input |
| 17 | Science data was garbled by DC-V6, switch ADC/PNG command to data encoder | DAS reset serial shift logic rewired |
| 18 | Magnetometer data fluctuated with no apparent change in input | R–C networks added to each analog-to-pulsewidth converter |
| 19 | Radio power amplifiers failed to switch upon CC&S CY-1 command | R–C circuit added to suppress the effects of CY-1 contact bounce |

*2. Facilities.*

*a. Spacecraft assembly facility.* JPL assembly and system test facilities used for *Mariner* Venus 67 were essentially the same as those for the *Mariner* Mars 1964 program, with the addition of the laminar downflow portable clean room that maintained a protective environment for the spacecraft (see Section IV-L-4). Equipment layout approaches and control were essentially the same as those used previously.

*b. Environmental facilities.* The vibration facilities were the same as those used in 1964. However, in 1967, the operations approach differed. The spacecraft was under local control using LCE in a trailer and an S-band RF airlink to the SAF evaluation center. The test mode was essentially the same as used for spacecraft launch pad operations at AFETR.

The 1967 operations mode was the same as the *Mariner* Mars 1964 method; however, the 10-ft space simulator was used because the 25-ft simulator was not available. *Mariner* Venus 67 was the first planetary spacecraft to use the 10-ft chamber. Spacecraft installation and configuration buildup was difficult because of space limitations. Functional operation was smooth and straightforward in terms of safely coordinating spacecraft, test team, and facility operators to pumpdown or return the simulator to ambient temperature and pressure. A problem was encountered in the design and operation of a suspension and damping system that could effectively isolate the spacecraft from mechanical motion. Suspension system modifications were made. These modifications yielded a system quiet enough to allow operation of the spacecraft gyroscopes without undue mechanical inputs.

*c. AFETR facilities.* The facilities and layout approaches used for *Mariner V* were essentially the same as for *Mariner IV*. During the *Mariner* Venus 67 project residency at AFETR, the *Surveyor* project was engaged in the SC-4 AFETR operations. Both operations shared building AO and ESF facilities. This was the first time two projects had operated in these facilities simultaneously. The two projects carried out their independent operations and interface management very smoothly and with no real handicap to either effort.

*3. System test complex data system.* After *Mariner IV* launch, the Univac 1218 computer data system was released to support the *Surveyor* spacecraft system test program. A new computer system had to be acquired to support the *Mariner V* system test program. A Control Data Corporation (CDC) 3300 computer system was leased by the project. To bring the new system *on line* required a major software development effort. This development effort was not completely successful because of schedule limitations.

The capability for processing engineering and science telemetry data was completely developed on the *Mariner* Venus 67 system test complex data system (STCDS). Of the hardline (nontelemetry) data available to the STCDS, only the events and status input data and the spacecraft autopilot data were processed. The types of hardline data that were interfaced with the STCDS, but not processed because of hardware deficiencies, included: (1) analog functions, (2) counters, (3) radio frequency counter input, (4) the spacecraft clock, and (5) the plotting capability.

The real-time support program was iterated a number of times. These iterations included eight major assemblies and numerous modifications to each. The major assemblies were primarily for the purpose of adding new capabilities and secondarily for incorporating accumulated program changes. The final assembly took place two weeks before shipment of the STCDS to AFETR.

A nonreal-time support program was available for *off line* processing of data stored on magnetic tape during spacecraft support.

*4. Microbial sampling program for Mariner V.* As part of a continuing NASA/JPL effort (see Section III-E) to determine the microbial burden on spacecraft, microbial assays were performed during all phases of the assembly and test operations of the *Mariner* Venus 67 project. This program was conducted on a noninterference basis with project operations. The only NASA requirement for sampling of the spacecraft was a final swab assay for the NASA inventory of outbound contamination.

The NASA-recommended sampling methods (Ref. 15) were followed throughout assembly, testing, and prelaunch operations of M67-2. The assays were limited to sampling specific surfaces which were adaptable to the techniques being utilized. Supportive environmental fallout data were obtained from assembly and test areas in an attempt to correlate spacecraft environmental exposure to the observed burden.

The microbial sampling program was conducted during a 137-day period. Samples were obtained on a regularly scheduled basis throughout all operational phases, terminating with the procurement of final samples just prior to shroud encapsulation of the spacecraft.

*a. Environments.* Most assembly and test operations at JPL were conducted in the SAF. The high-bay area was utilized for assembly and testing of the spacecraft, as well as for housing related ground and operational support equipment. Air makeup in the SAF was 80% internal and 20% external, with filtration by Farr HP-2 filters.

Whenever feasible, the spacecraft was maintained in a 168-ft$^2$, Class 100, portable, laminar-downflow, clean room housed within the SAF high-bay area. The walls consisted of plastic drop curtains with zipper corner closures. Constraints for those working on, or near, the spacecraft included cleaning shoes and wearing head covers, gowns, and cotton gloves. The number of personnel in the high-bay area varied between 10 and 30, while the level in the portable downflow clean room was maintained between 3 and 6 persons.

The spacecraft was transported to the JPL environmental laboratory for vibration and space simulation tests. Air makeup, filtration, and personnel constraints were the same as those in the SAF high-bay area. The vibration laboratory is a sound-proof area used to simulate noise, shock, and vibration spectra. During test periods, personnel levels varied between 5 and 15. The spacecraft was exposed to the vibration laboratory environment for 3 days.

Housed within a 4250-ft$^2$ area, the 10-ft space simulator was used to simulate the thermal/vacuum spectrum encountered during interplanetary cruise. Except for the pre- and post-test inversions, the spacecraft was maintained in this simulator. Air exchange between the simulator and facilities occurred during interim test periods; however, during tests the simulator was sealed, purged with dry nitrogen, and then back-filled and maintained with air filtered through two layers of an air-mat filtration system. The spacecraft was subjected to the thermal/vacuum environment for 15 days.

Following the completion of assembly, testing, and preshipment activities at JPL, the spacecraft was placed in a vacuum-cleaned, alcohol-decontaminated canister for shipment to AFETR. Upon arrival at AFETR, the spacecraft was transferred to the JPL clean room in Hangar AO and maintained there for 14 days. Air makeup in this facility was 80% internal and 20% external, with filtration through high-efficiency particulate air (HEPA) filters. Personnel constraints were similar to those employed in the SAF high-bay area at JPL. Personnel levels varied between 10 and 30; however, many of these persons were working on *Surveyor IV* which was housed within the same facility.

The final testing area for the spacecraft, prior to placing it on the gantry, was the north bay of the Explosive Safe Facility (ESF), where attitude-control tank pressurization, pyrotechnics, midcourse motor installation, and final shroud encapsulation were accomplished. Air makeup, filtration, and personnel constraints were the same as those listed for Hangar AO. The number of personnel was limited to a maximum of 15. The spacecraft was maintained in this environment for 16 days.

*b. Sampling procedures.* The microbial profile relative to fallout contamination for all of the facilities was derived from data obtained from 1- × 2-in. stainless steel settling strips and Reyniers air samplers. Settling-strip and swab-rinse methods (Ref. 15) were used for the burden estimation of the spacecraft.

*c. Settling-strip samples.* The settling strips were contained in Teflon-backed units that were nonmagnetic, self-contained, portable, and sterilizable. The units were attached directly to the spacecraft or its support equipment to obtain a distributive effect around, above, and below the structural octagon.

The carriers varied in shape and size according to their location on the spacecraft. Those attached to the faces of the electronic chassis (Bay I and Bays III through VIII) contained fifteen 1-in.$^2$ strips (Fig. IV-195). Other carriers were attached to the top ring by a stainless steel plate. The plate held six carriers, each of which contained nine 1-in.$^2$ strips (Fig. IV-196). The remaining carriers were placed on the attitude-gas-control handling frames. Three (two vertical and one horizontal) carriers were attached to each of four frames. Each carrier contained nine 1-in.$^2$ strips (Fig. IV-197).

When the nature of a specific test dictated removal of the carriers, the carriers were transferred to a mockup (Fig. IV-198) and maintained in proximity to the spacecraft. Exposure times and positions of the carriers were correlated with the normal times and positions on the spacecraft.

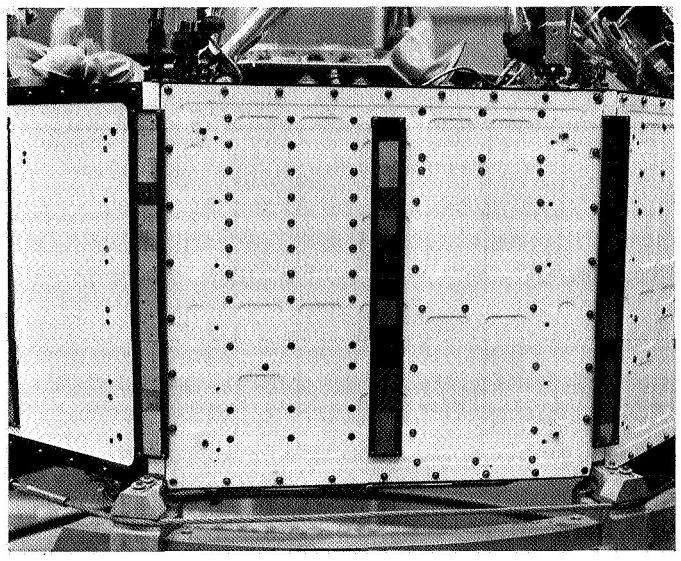


**Fig. IV-195. Sampling carriers attached to face of electronic chassis**

All carriers contained strips that were retrieved on both weekly and monthly bases. Additionally, each carrier held strips that remained throughout the JPL or AFETR phase of the program and strips that remained throughout the entire program. At each sampling period, a minimum of 72 strips was assayed.

*d. Swab-rinse samples.* Swab samples were obtained using the techniques presented in Ref. 15. Individual surface areas of 4-in.$^2$ were sampled using templates (Fig. IV-199) on a weekly basis. A minimum of 45 samples was taken at each sampling period from both ground-support and flight equipment. The ground-support equipment swab-sampling sites were:

(1) Attitude-gas-control handling frames.

(2) Pressure switches.

(3) Umbilical breakout box.

(4) Universal ring.

(5) Louver covers.

(6) Light hood, Canopus sensor.

(7) Shipping canister.

The flight equipment swab-sampling sites were:

(1) Face, electronic chassis.

(2) Canopus sensor.

(3) Low-gain antenna (omnidirectional antenna).

(4) Superstructure, high-gain antenna.

(5) Pedestals, secondary sun sensors.

(6) Ultraviolet photometer.

(7) Thermal blanket (TFE side).

(8) Struts, solar panels.

(9) Flight shields.

(10) Adapter.

(11) Shroud.

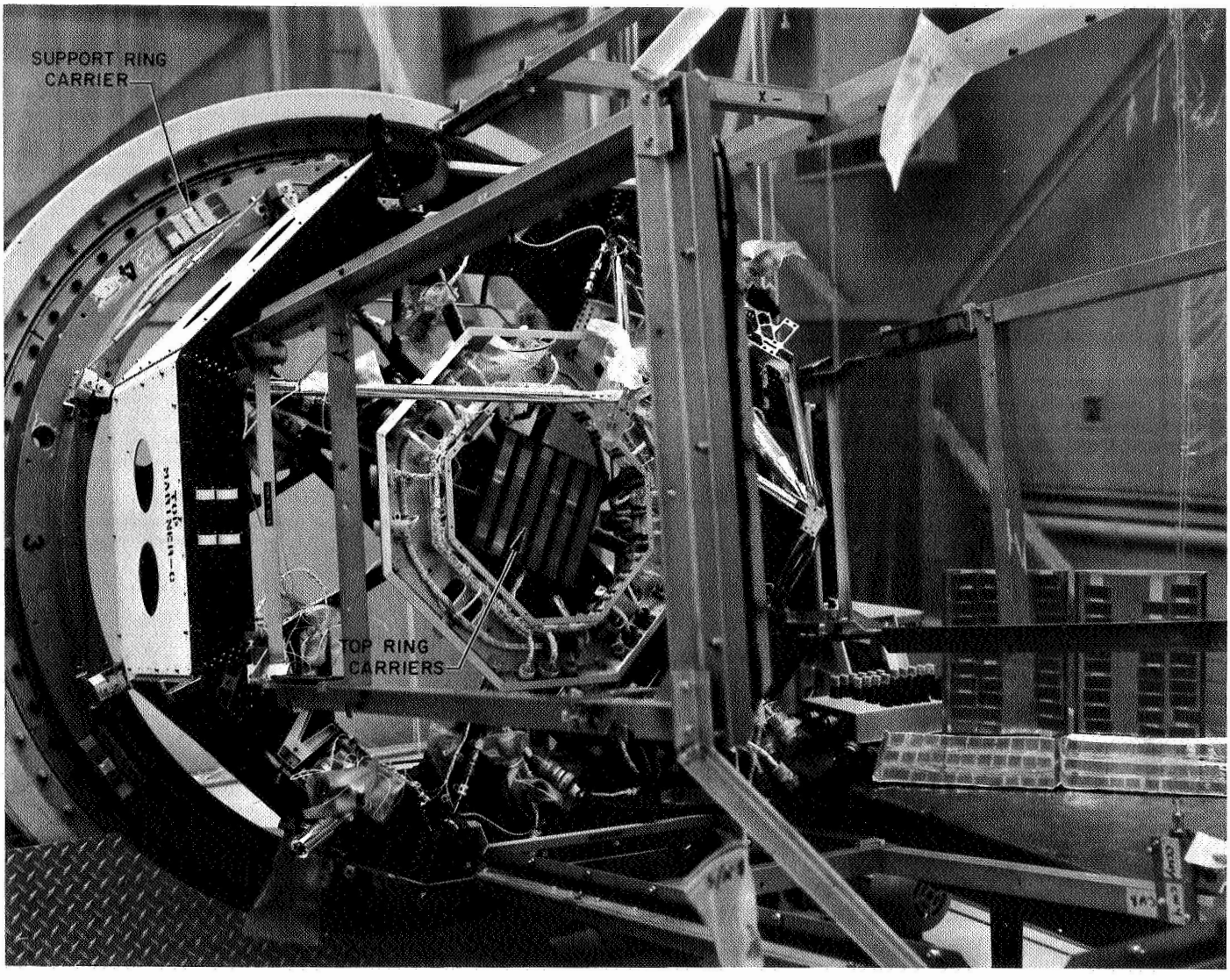



**Fig. IV-196. Sampling carriers attached to top and support rings**

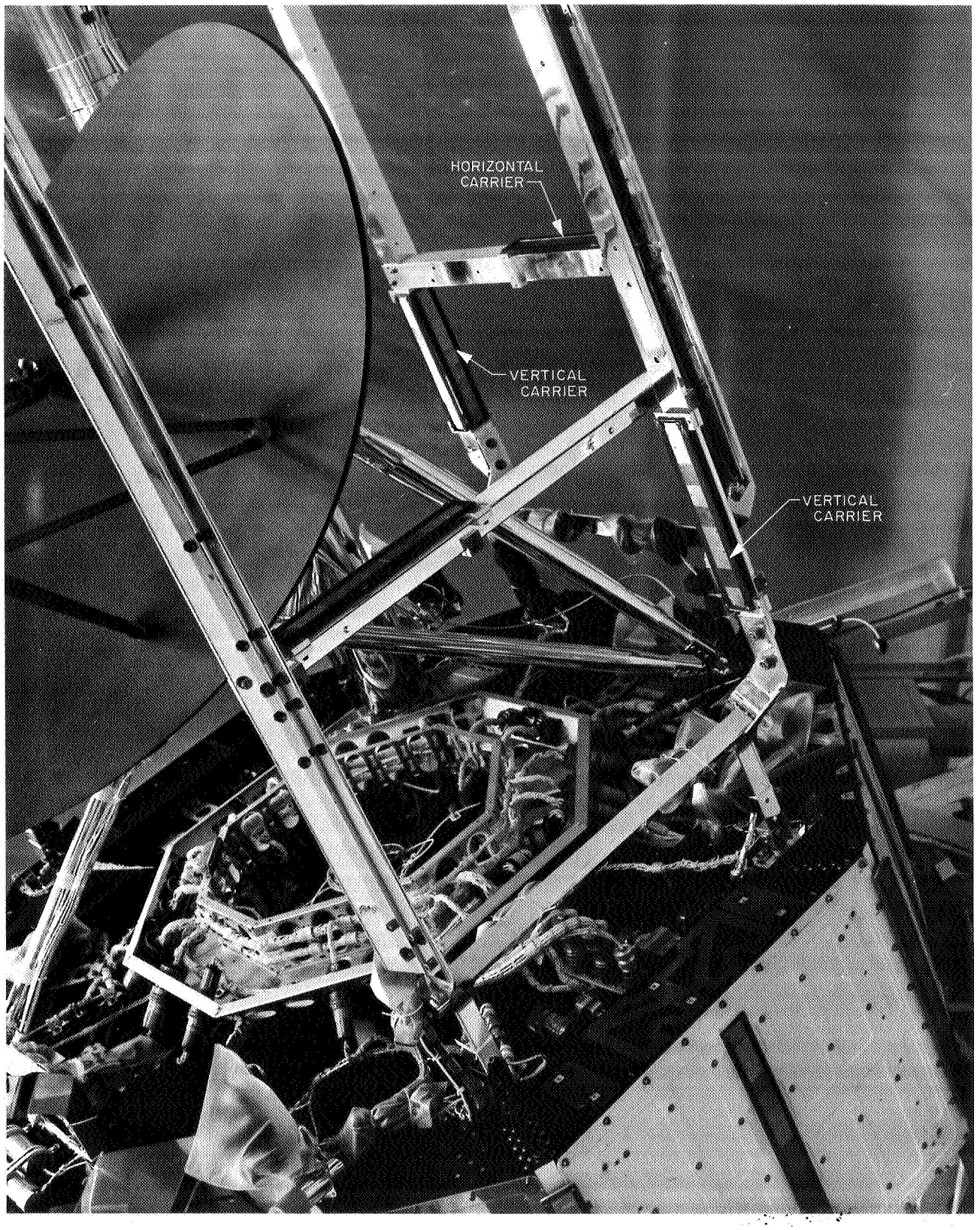



**Fig. IV-197. Sampling carriers attached to handling frame spars**

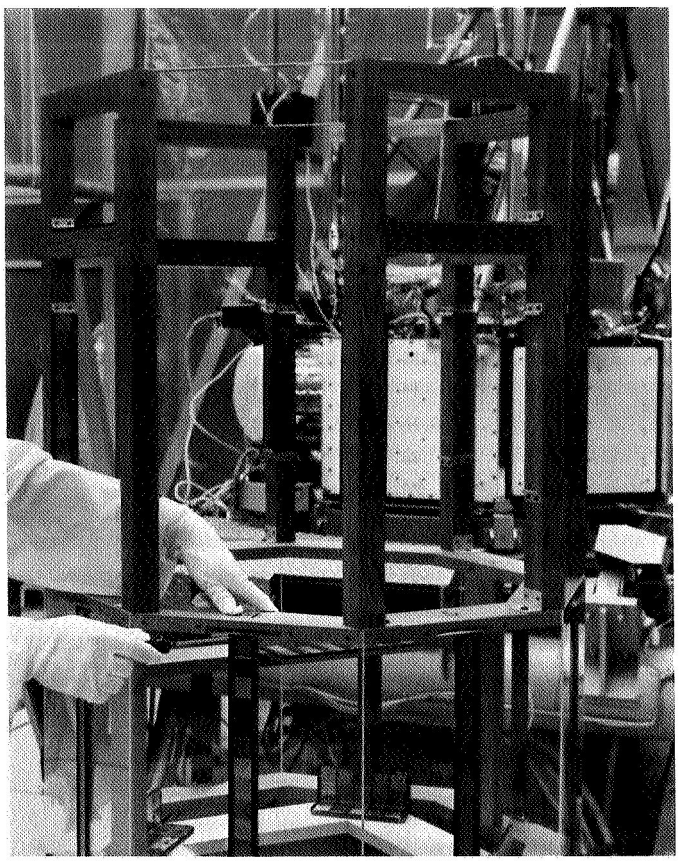


**Fig. IV-198. Mockup used to simulate spacecraft positions**

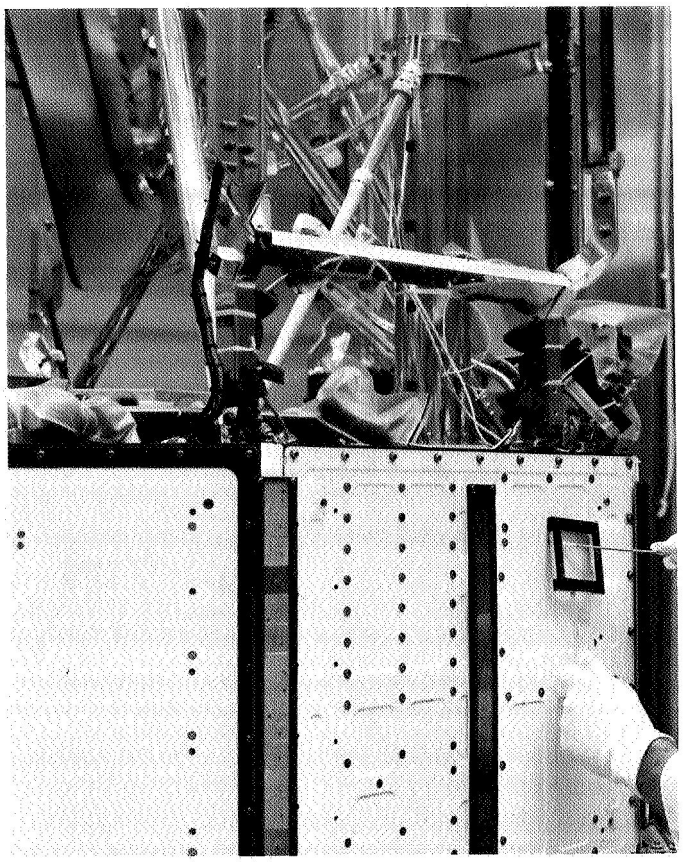


**Fig. IV-199. Swab sampling of electronic chassis using template**

**Table IV-59. Environmental fallout—mean number of aerobic spores accumulated during various spacecraft exposure periods**

| Environment | Operation | Period, 1967 | Mean number of aerobic spores accumulated |
|---|---|---|---|
| SAF high bay (JPL) | Assembly | Jan 15–Feb 4 | 520 |
| SAF high bay and clean room (JPL) | Assembly and testing | Feb 4–Feb 16 | 620 |
| | | Feb 16–Feb 28 | 1700 |
| Clean room (JPL) | Testing | Feb 28–Mar 9 | 517 |
| Environmental laboratory (JPL) | Vibration testing | Mar 9–Mar 16 | 360 |
| 10-ft space simulator (JPL) | Thermal/vacuum testing, Phase I | Mar 16–Mar 25 | 240 |
| | Thermal/vacuum testing, Phase II | Mar 25–Apr 6 | (in chamber) |
| Clean room (JPL) | Disassembly and cleaning | Apr 6–Apr 20 | 720 |
| Within shipping canister | Shipment | Apr 20–Apr 29 | (shipment) |
| Hangar AO (AFETR) | — | Apr 29–May 12 | 1250 |
| ESF (AFETR) | — | May 12–May 28 | 1990 |

*e. Results.* The results reported herein are limited to the data obtained for heat-resistant spores. The mean environmental contamination levels for the areas of spacecraft activity are presented in Table IV-59. Settling-strip data are presented in Fig. IV-200. Figure IV-201 shows burden levels obtained with the swab technique.

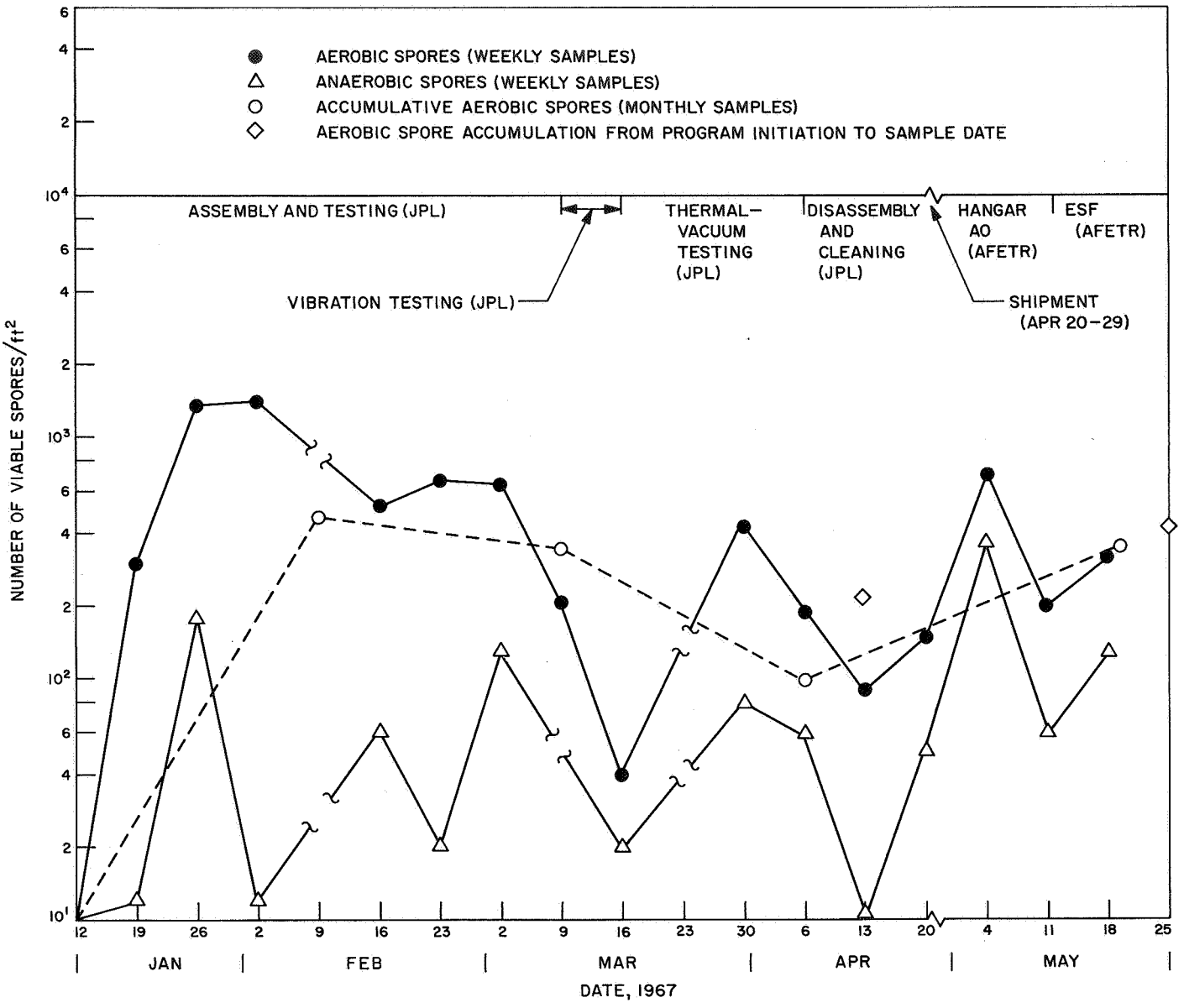



**Fig. IV-200. Average spare burden estimates (setting-strip techniques)**

A 30% efficiency recovery factor has been incorporated into the swab data. Continuity breaks in the curves represent periods when the spacecraft was unavailable for sampling.

*f. Discussion.* Comparison of the results from swab-rinse and settling-strip sampling indicates that the strip may be a more sensitive method for the enumeration of accumulative contamination. The lower recovery percentage observed for the swab method is probably the result of various contributing factors. The swab technique requires removal of the organisms from the spacecraft and then removal from the swab for enumeration. Additionally, large areas of spacecraft surfaces were removed from the environment for short periods and cleaned; on various occasions, the entire exposed surface of the spacecraft was cleansed with isopropyl alcohol. The strips were not subjected to these procedures.

Weekly data obtained from both methods of sampling indicate a relationship between personnel activity and the level of microbial accumulation (Figs. IV-200 and IV-201). Both swab and strip data reflect the higher

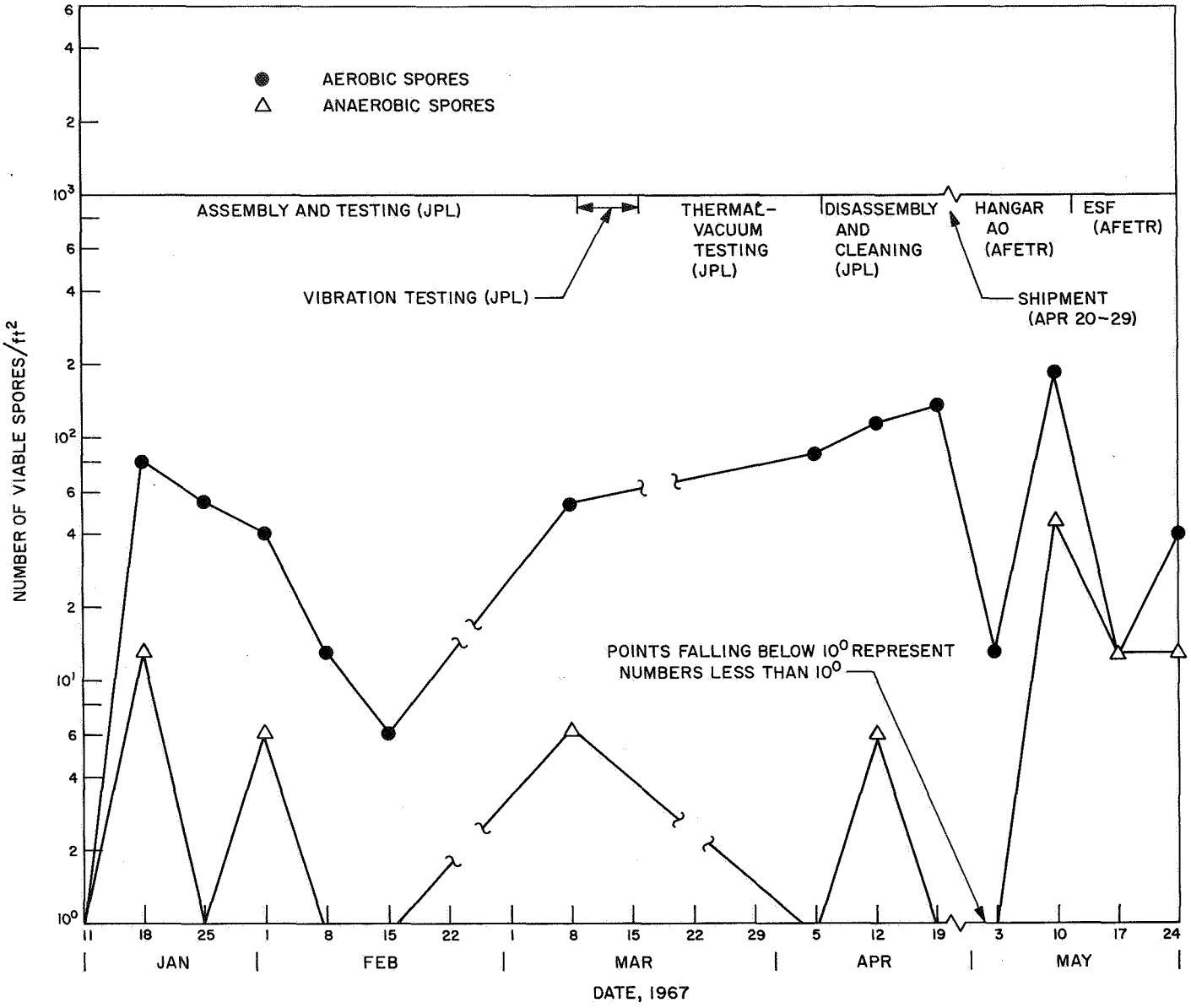



**Fig. IV-201. Average spare burden estimates (swab-rinse technique)**

levels of personnel activity that occurred during the spacecraft assembly operations. This relationship is also noted when the spacecraft was being prepared for movement to the ESF.

The effect of environmental factors in the absence of activity is indicated in Fig. IV-200 from March 2 through 16, 1967. At that point in the operations, the thermal/vacuum tests of the spacecraft were being performed in the space simulator, and the strips were attached to the mockup located in the laminar downflow clean room where activity was minimal. The clean room appeared to be the closest simulation of the space simulator environment. The procedure was repeated between March 30 and April 13, during which the spacecraft was disassembled in the clean room following environmental tests.

Although weekly accumulative levels fluctuated, burden estimates from monthly and long-term settling strips (Fig. IV-200, broken line and encircled points) indicate a leveling of the microbial burden. Under the prevailing conditions, the plateau occurred at approximately 400 aerobic spores/ft².

Assuming 645 $ft^2$ of exposed surface area on M67-2 and an equal distribution of microorganisms on all exposed surfaces, the estimate of 400 aerobic spores/$ft^2$ represents a total burden of $2.6 \times 10^5$ aerobic spores on spacecraft surfaces. This compares to a total aerobic spore burden of approximately $6 \times 10^3$ if the data from the swab-rinse method are used. These estimates are based on averages of the data and assume an equal distribution of organisms on the spacecraft. (Distribution functions will be determined and reported with the conclusion of the data analysis.) The level of anaerobic spores has not been included in the estimate, since a high percentage of the anaerobic organisms is facultative and would be included in the aerobic count. Therefore, the two are not cumulative. The anaerobic spore counts, although lower, show similar trends.

Computer analyses (using analysis of means by variance) of all data are presently being conducted to:

(1) Submit the data to analysis for a comparison of microbial distribution (i.e., horizontal versus vertical accumulation, and top rings versus support ring versus electronic bays, etc.).

(2) Compare levels of accumulation at various working areas with levels of personnel activity and types of work being accomplished.

The information provided by the above operation will enable a revised estimate of the burden of the spacecraft. In addition, the analyses will provide a basis for the selection of sampling areas for the estimation of microbial burden on future spacecraft.

## M. Reliability Program

*1. Reliability control.* In recognition of the stringent constraints imposed by the guidelines of the *Mariner* Venus 67 mission, the reliability responsibilities for the project were disseminated among several groups, such as the design sections, the parts and packaging sections, hardware subcontractors, and the *Mariner* Venus 67 project office. To maintain a central cognizance over the total project reliability activity, a reliability monitoring group was organized. The main tasks performed by this group were: surveillance and coordination, including participation in hardware, design, and system reviews; maintenance and control of the PFR system; assistance in project level parts management; and monitoring of the information flow between the subsystem fabrication groups, the subsystem and system test complexes, the space flight operations area, the launch vehicle area, and system management.

*2. Problem/failure reporting.* The PFR system used on *Mariner V* was a logical follow-on of the successful system used on the *Mariner IV* program. It provided a closed-loop system that allowed effective collection, distribution, analysis, and corrective action of all reported anomalies. Since *Mariner V* did not involve the quantities of hardware and paperwork usually associated with a full-scale production program, it was decided to keep the reporting system on a more personal manual level rather than to automate the paper flow. This became an effective method of keeping failure reporting on a responsible technical working level for analysis and corrective action by allowing anyone who believed a problem or failure existed to originate a report. The PFR was used to record failures and problems occurring during TA testing or FA testing of the flight system and the flight spare. It was also used during bench testing of subassemblies, assemblies, and subsystems commencing with the first application of power. These reports were written at JPL and at Cape Kennedy during preflight activities. During the *Mariner V* flight the reports were written on the flight spacecraft from telemetry data monitored at SFOF. (A record of in-flight anomalies is considered especially useful in planning for future programs, both from a standpoint of hardware and procedure.) A typical PFR is shown in Fig. IV-202. Figure IV-203 shows the number of these reports versus calendar time and project development. There were 811 PFRs written on tests, flight performance, and operational support equipment through midcourse.

The actual mechanization of the PFR system hinged on the relationship between each subsystem's cognizant engineer (who had the final responsibility for analysis and corrective action on each report), his section manager, the reliability project representative, and the spacecraft systems engineer, who had final authority for evaluating the significance of the analysis and corrective action before PFR closeout. This interaction enabled each cognizant engineer to determine the amount of corrective action needed on a specific subsystem, such as having parts failure analysis performed or starting a design change action to modify the design of the subsystem. Concurrently, the cognizant engineer's section manager was aware, through his sign-off responsibility, of the problems or failures occurring on the subsystems under his control. In making their final sign-offs, the

☒ Flight (S/C Ser. No. TA) ☒☒ **PROBLEM / ☐ FAILURE REPORT** **Nº 106069**

☐ OSE (Complex Ser. No. )

1. PROJECT ☐ Ranger ☒☒ Mariner '67 ☐ Other | 2. PROBLEM/FAILURE DATE 3/14/67 | 3. LOG NO. DAS 109-3

| | A) REFERENCE DESIGNATIONS | B) NOMENCLATURE | C) SERIAL NUMBER | D) OPERATING TIME |
|---|---|---|---|---|
| 4. SUB-SYSTEM | 20 | Data Automation Subsystem | 73 | 124.5 hours |
| 5. ASSEMBLY | 20A5A2 | #2 data shift module | 5 | 84.5 hours |
| 6. SUB-ASSEMBLY | | | | |

7. REPORTING LOCATION ☒☒ JPL Sec. 324 ☐ Vendor ☐ SAF ☐ AMR Other

8. PROBLEM/FAILURE NOTED DURING — INITIAL DISTRIBUTION DATE

☐ Bench Testing ☐ In-Process Testing ☒☒ TA Testing ☐ FA Testing ☐ Systems Testing

☒☒ Specific Environment subsystem thermal vac in bldg 248 ☐ Other

**I**

9. DESCRIPTION OF PROBLEM/FAILURE

U-status bit in the Track #1 tape data was starting to come on at the wrong time as temperature was increased. As the temperature approached the TA limit of 75° C the repetition of the U-status bit increased exponentially. At 75° C (with the voltage nominal) the status bit was always wrong. When temperature was ambient and +Vcc (~~+4~~ volts) was increased to above ~~+4.6~~ volts, the same problem appeared. IDN50* was always at the 4 volt level during this +4.6 voltage application, and never went low. The output of A-12 in 20A6A1 was then measured and found to be in a similar state. A-12, a DAE 480 I/C, was found to be causing the measured bit conditions.

Originator James D. Allen Date 3/14/67 Cognizant Engineer Robert White

**II**

10. VERIFICATION & ANALYSIS

The DAE 480 was replaced, but it was found that this did not cure the problem. A detailed investigation was then conducted on the logic involved. This investigation revealed that a logic design error is the cause of the problem, and that the DAE 480 integrated circuit was not the cause of the problem, as originally suspected. Never-the-less, the I/C was sent to the failure analysis labs as a double check.

11. CAUSE OF PROBLEM/FAILURE

☒☒ Design ☐ Piece Part Failure ☐ Operator Error ☐ Damage (Mishandling) ☐ Adjustment

☐ Workmanship ☐ Manufacturing ☐ O.S.E. Failure ☐ Other

12. FOLLOW-UP ASSIGNMENT

☒☒ Cognizant Engineer ☐ Design Review ☐ Vendor ☒☒ Components Evaluation Group

☐ Material Review Board ☐ Quality Assurance ☐ Other

| 13. PART DATA | A) PIECE PART NAME & NUMBER | B) SERIAL NO. | C) CIRCUIT SYMBOL | D) MANUFACTURER | E) DEFECT | F) PRI. | G) SEC. |
|---|---|---|---|---|---|---|---|
| | DAE 480 I/C (B) | 2353 | IDN*50 | Signetics | not a failure | N/A | |
| | | (lot 66176) | | | (see Box 14) | | |
| | | | | | | | |

PERSON COMPLETING SECTION II Signature Dan D. Bailey Date 4/04/67

**III**

14. CORRECTIVE ACTION TAKEN

Lab failure analysis by Section 354 (attached to this P/FR) found the DAE 480 to be in a non-failed state, both by measurement and subsequent dissection. The original I/C (S/N 2353) was replaced by a DAE 480, S/N 1342, lot #66216. An ECR was written (8724) to change the design as required. It appears that a wire was incorrectly connected to point A-12. This wire was removed by the ECR. The unit went back into TA test, both thermal vac and vibration, on 4-10-67, and successfully passed re-test.

15. DISPOSITION ☒☒ Reworked ☒☒ Redesigned ☐ Readjusted ☐ Scrapped ☐ Other

16. EFFECTIVITY ☐ This Unit ☒☒ All Units ☐ Other ECR No. 8724

Signature Cognizant Engineer s/Robert White Sec. 324 Date 4/30/67 Signature Cognizant Sec. Chief s/John Joseph Paulson

**IV**

17. REVIEW CONCURRENCE

Reliability Coordinator: s/Frank H. Wright Date 5/15/67

Space Project Engineer: s/Allan G. Conrad Date 5/12/67

18. CLASSIFICATION ☒☒ Critical ☐ Non-Critical

**V**

19. STANDARD & SPECIAL DISTRIBUTION

MV67 20

P/FR RELIABILITY STAFF JPL 1798 APR 64

**Fig. IV-202. Sample PFR**

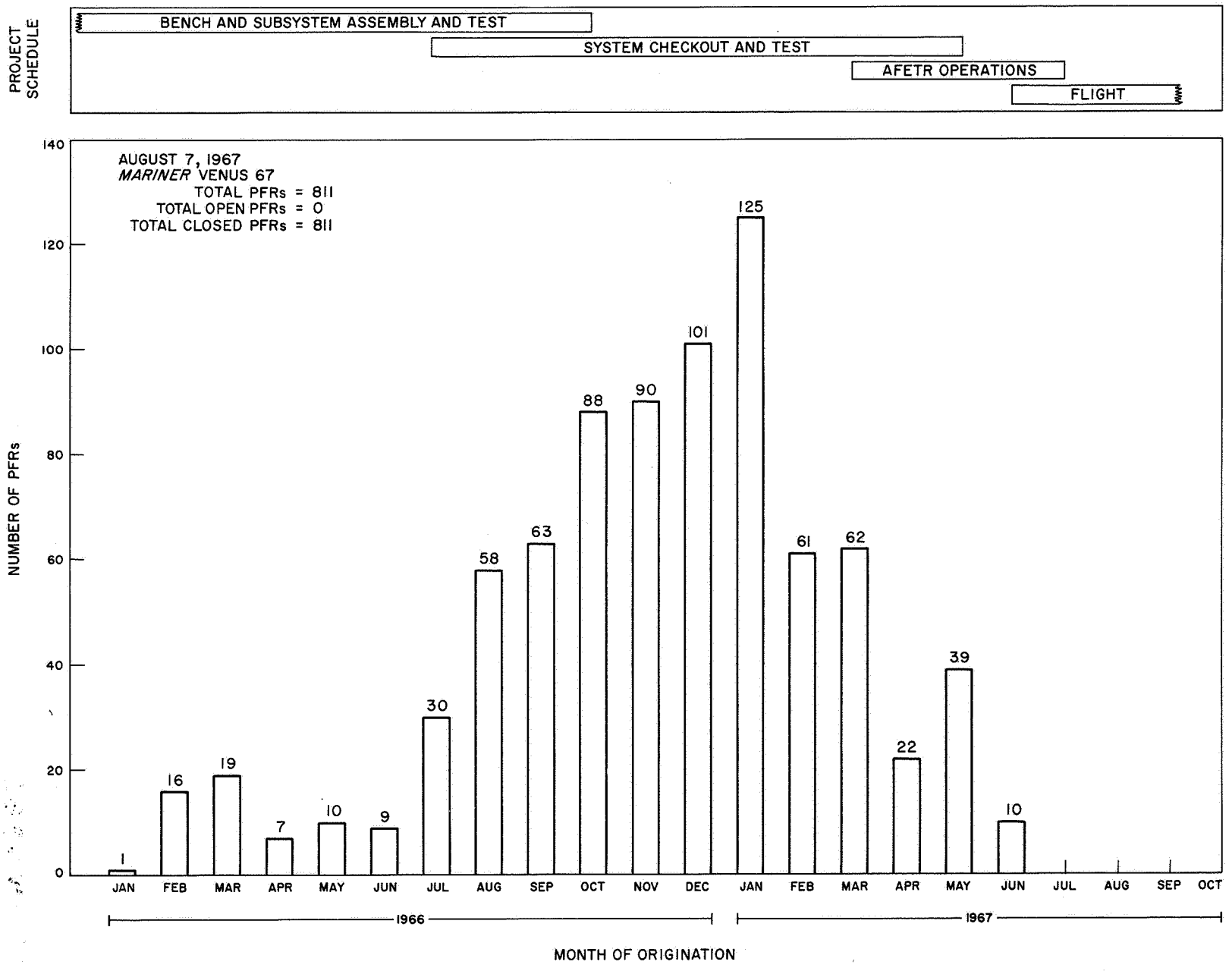



**Fig. IV-203. PFR monthly sums (open and closed) vs failure date—*Mariner* Venus 67**

reliability project representative and the spacecraft systems engineer incorporated their knowledge of the overall spacecraft system and how each individual PFR, failure analysis, or design change might affect the total spacecraft system.

*3. Environmental testing.* Although environmental testing on the spacecraft was performed and supported by separate test groups, it was an integral part of the reliability program. The two classes of reliability-oriented tests of most significance performed on *Mariner V* equipment were the TA and the FA tests. These tests were performed at the subsystem and system levels on flight configuration hardware. The combination of these two levels of environmental testing proved successful, especially in the indication and elimination of design deficiencies and quality problems.

*4. Reliability prediction and failure-mode analysis.* A reliability prediction and failure-mode assessment was originally made for the *Mariner* Mars design in 1963. Most of the design changes recommended then concerned increasing subsystem reliability through redundancy. Conventional techniques were used in modeling the assessment. These techniques employed the functional block diagram method of analysis. The assessment covered typical failure modes and design interfaces, and gave success probabilities for each functional unit. Because *Mariner V* used the basic *Mariner IV* design with a minimum of changes, no formal updated prediction analysis was made. However, failure-mode effects and analysis were closely reviewed by the Design Review Board on those subsystems undergoing design reviews during the program.

*5. Reliability-oriented project level reviews.* A complementing series of project level reviews was conducted during the months prior to launch of *Mariner V*. These reviews were especially useful in focusing the proper level of management attention, not only on reliability problem areas, but also on other key technical and administrative problems. These reviews were:

(1) Design review. Design reviews were conducted on those subsystems that were entirely new in design or were involved in a major redesign effort. These reviews were performed on hardware designed and fabricated both at JPL and by prime hardware subcontractors, and were conducted by a Spacecraft Design Review Board. The board was headed by the Spacecraft Systems Manager and was composed of parts personnel, packaging and cabling personnel, reliability and quality assurance personnel, subsystem section managers, system design personnel, and other members of the project. The procedure was to have cognizant technical personnel conduct a review on their subsystem before the Design Review Board, with special attention given to the subsystem design and their consistency with subsystem interfaces, using such typical techniques as check lists and circuit analyses.

(2) Hardware review. These reviews were conducted on all flight and flight spare hardware at the time of their delivery to SAF. The reviews verified that all applicable tests and inspections had been performed with acceptable results, that drawings and specifications were current and correct, and that the quality and reliability of hardware under review met required standards. The impact and status of open PFRs connected with the hardware were also reviewed. The hardware reviews were chaired by the Spacecraft Systems Manager. The manager was assisted by project personnel similar in technical depth and content to a Design Review Board.

(3) Pre-shipping acceptance reviews. These reviews were held just prior to the shipment of the flight and flight spares to Cape Kennedy. The purpose of these reviews was to evaluate flight readiness of each spacecraft and to measure the extent to which flight qualification criteria were attained. All contributors to the design, fabrication, and testing of each spacecraft system participated in these reviews, and committed their hardware to flight or made other appropriate recommendations.

(4) Launch readiness review. This review was held at Cape Kennedy approximately two weeks prior to launch. Its purpose was to determine the acceptability of the flight spacecraft for launch, evaluate mission risks, and to review project test and malfunction histories, at both the subsystem and system levels. At this review the status of open PFRs and ECRs was closely analyzed as to mission significance. This meeting was chaired by the Systems Manager, and attendance included top level technical personnel from supporting JPL Divisions, as well as NASA Headquarters and supporting NASA Centers.

*6. Parts management.* The parts management program was very similar to that initiated on the earlier *Mariner* Mars program. It included parts selection, acquisition, screening, and failure analysis.

In addition, because of the advanced age of much of the hardware, a special analysis activity called the suspect parts team was initiated at the start of the program. This team made recommendations to the Spacecraft Systems Manager as to those electronic and electromechanical parts that were candidates for replacement because of age, or reliability considerations. This team was composed of members of the quality and reliability organization, parts specialists, materials specialist, and a packaging specialist. In reviewing the parts considered "suspect," the team talked with technical cognizant subsystem personnel to truly define the status of the parts in question. Final resolution on replacement of suspect parts involved part usage, screening history, replacement availability, functional criticality, packaging, and resources. In many cases, this investigation pointed out that parts that had been considered as possible "suspect" parts were not potential reliability hazards. In summation, 104 parts were changed in 7 *Mariner V* subsystems, and many spare parts were purchased and screened for emergencies.

*7. Post-launch reliability analysis.* Reliability analysis studies are being performed on testing and failure data collected from both ground-based activities and the flight spacecraft during flight of *Mariner V*. These studies are intended to supply information that will be valuable in establishing the reliability of future JPL space efforts. A summation of the results of these studies and the final results of the reliability activities for the *Mariner* Venus program will be presented in Vol. II of this report.

## N. Quality Assurance Program

The *Mariner* Venus 67 quality assurance (QA) program utilized proven techniques to monitor and control the quality and reliability of the test and flight spacecraft. The QA effort was carefully planned to maximize the desired benefits of the mission objectives while minimizing the cost of the program. Significant activities of the QA effort were:

(1) Selection of procurement sources (vendor surveys).

(2) In-process source inspection and control.

(3) Receiving inspection.

(4) Failure reporting.

(5) Procedure review.

(6) SAF, hardware, and spacecraft control.

*1. Organization.* To meet the requirements of the project for quality control and inspection, a QA engineer was assigned to each hardware fabrication division. Each of these engineers supervised a permanently assigned group of inspectors. This organization enabled QA personnel to continue the same pattern of endeavor which had been applied successfully to the *Mariner* Mars 1964 program. Because the *Mariner* Venus 67 program required updating of *Mariner* Mars 1964 hardware, the learning curve for QA personnel was virtually nonexistent. Because the hardware suppliers for *Mariner* Venus 67 were, for the most part, the same suppliers who had built the hardware for *Mariner* Mars 1964, QA was able to assign residents who had intimate knowledge of the peculiarities of suppliers as well as their manufacturing and inspection techniques. These resident inspectors were assigned to supplier facilities according to the volume of work, criticality of task, and prior quality history of each manufacturer.

QA personnel in the field were supported by QA groups at JPL; i.e., Parts QA, Mechanical Inspection, Systems and Procedures, and SAF QA.

*2. Requirements and reporting.* QA utilized the quality document used for *Mariner* Mars 1964 to outline vendor quality activities. QA also generated QA instructions (QAIs) for each subsystem or special requirement. These QAIs identified the requirements for each subsystem and were approved by the technical manager for the respective subsystem, or the spacecraft manager, prior to implementation.

When fabrication of hardware began, each of the QA engineers submitted weekly activity reports which included hardware status and significant problems. These reports were distributed to the technical managers and were the basis of the weekly status reports. This reporting network continued, after arrival of the hardware at JPL, to report all significant events until launch. These reports were not statistically organized and, at times, permitted the subject matter to be opinionated and controversial. In retrospect, the reports would have been of more value had they been oriented toward, and supported by, some simple statistics (i.e., percentage

defective, quantitative defects by characteristic, MRB summary, etc.).

3. *Failure reporting.* Failure reporting on the *Mariner* Venus 67 program was handled similarly to that of *Mariner* Mars 1964. PFRs were generated for each problem. These were submitted to engineering for action and to JPL reliability for analysis and distribution.

4. *Subsystems.*

*a. Science.* The QA effort performed in the science area consisted of monitoring the refurbishment of *Mariner* Mars 1964 hardware to the new *Mariner* Venus 67 configuration, and also the fabrication of the new hardware. The helium magnetometer, DAS, UV photometer, plasma probe, DFR, and the TRD were all under QA surveillance.

The helium magnetometer was of the *Mariner* Mars 1964 configuration, and was modified and re-tested at JPL. No significant problems were encountered. A new DAS was manufactured for *Mariner* Venus 67. Problems were encountered in the software because red-lined drawings were changed without proper notification or authorization. The DAS units, when delivered to SAF, needed additional conformal coating. Some conformal coating had purposely not been applied to provide accessibility for rework if necessary. During the post-environmental teardown inspection of the vehicles, the encapsulant was applied to the DAS modules.

Connected with the DAS was the procurement and fabrication of the integrated circuits (ICs). In an effort to produce an adequate method of microscopic inspection, QA utilized the 600-power microscope. Results of this method are still under investigation because of difficulties involved in correlating the statistical data available with the visual criteria.

The plasma probe experiments were left over from *Mariner* Mars 1964. These units were refurbished to the new *Mariner* Venus 67 configuration. During the initial rework of these units, it was necessary for QA to monitor the cleanliness of the assembly area in which the units were being reworked. Calibration of bench checkout equipment and cleanliness was a continuing problem throughout the program. During the conformal coating cycle, the units became excessively dirty, and this contamination was sealed in the encapsulant. It was concluded that, because of the nonmetallic nature of the contaminants, the units in question were not degraded.

The DFR was a new procurement and experiment for the *Mariner* Venus 67 project. There were no significant problems for QA in this area.

The UV photometer units were of the *Mariner* Mars 1964 configuration, and were refurbished to the *Mariner* Venus 67 configuration. During the rework period, the filters for one of the flight units were broken due to mishandling. Better work habits and improved storage facilities prevented recurring damage.

The science OSE transition, from *Mariner* Mars 1964 to *Mariner* Venus 67 configuration, was, in the opinion of QA, accomplished smoothly and without major problems.

*b. Telecommunications.* The fabrication of new hardware for the *Mariner* Venus 67 project was unique in that *Mariner* Mars 1964 processes and specifications were utilized whenever possible. The subsystems developed were the command, data encoder, radio, tape electronics, and tape transport.

The new command and data encoder subsystems, as well as the reworked *Mariner* Mars 1964 units, utilized the *Mariner* Mars 1964 specifications and processes. The QA effort in these specific areas was to monitor all phases of assembly of new hardware being fabricated, in addition to rework of *Mariner* Mars 1964 hardware. Because of the three-year time differential between the *Mariner* Mars 1964 and *Mariner* Venus 67 projects, problems arose in processing and materials availability. Techniques and methods had changed during the three-year interruption in manufacturing; therefore, close surveillance of these subsystems was required to ensure that hardware was compatible with the desired requirements. Problems with new and better specifications arose, but were soon resolved.

In the radio subsystem, two *Mariner* Mars 1964 subsystems were withdrawn from SAF bonded stores, and delivered to the contractor for refurbishment and updating to the new *Mariner* Venus 67 configuration. During the rework cycle, it was necessary to procure new components. This caused problems because the lead time was insufficient for proper screening of parts. As a result, components installed in the radio system contained screening deviation liens.

The coax cables were included in the RF system. It was the opinion of JPL QA that existing *Mariner* Mars 1964 cables should not be used, because microscopic

inspection showed signs of degradation. After exhaustive tests, new cables were fabricated.

The tape transport for the *Mariner* Venus 67 project underwent a major modification by two suppliers. During the refurbishment of this subsystem, hardware problems arose. Because of the lack of potting in the submodule located in the tape transport, the unit had to be disassembled. The tape transport problem was found late in the program, and a general effort was necessary to meet the *Mariner* Venus 67 launch date. During this period of rework, because of a test failure, a torque value for the assembly of the tape transport had to be established. This value had not been established during the *Mariner* Mars 1964 project.

Problems encountered with the transducers produced under the cognizance of the telecommunications division and used throughout the spacecraft were felt insignificant by QA, except for a transducer utilized in the propulsion subsystem (see Section IV-G-1 for details).

*c. Guidance and control subsystems.* The attitude control electronics package was fabricated during the *Mariner* Mars 1964 program. Problems were encountered by QA in the attempted modification of the prototype unit. New jet vane actuators (JVA) were built for the *Mariner* Mars 1964 mission, and 12 usable units were left over. These units were reworked for use on *Mariner* Venus 67. Problems were encountered in process control during the refurbishment cycle. All actuators showed excessive stiction and reworking and relubricating the actuators with Apiezon-N did not resolve the problem. Investigation showed that the lubricant DC-11 would alleviate the stiction problem. This anomaly did not recur following the use of the new lubricant. A point of concern for QA was that no design or detail specification had been released for this area of activity. All procedure and specification changes correcting the stated problems have been incorporated in the *Mariner* Mars 1969 specification and will be invaluable to participating contractors.

The attitude control gas systems were also of *Mariner* Mars 1964 vintage. Two systems, each composed of two identical valves, were modified per ECRs and subjected to quantitative leak tests prior to redelivery to SAF. Source inspection was performed on all the reworked valves.

The Canopus sensors were of *Mariner* Mars 1964 manufacture, except for the optical system, baffle assemblies, sun detectors, and shutter which were fabricated for the *Mariner* Venus 67 mission. Improper screening of resistors was one of the problems encountered. Because screening was not performed by the parts QA group, traceability was difficult. Excessive noise during testing was another anomaly encountered during system test at AFETR. The sensors were switched between M67-1 and M67-2 to further advance the investigation of the problem. Recalibration and exhaustive testing revealed nothing of value. The units were re-installed on their respective spacecraft, and from that point on the noise ceased. During this trouble-shooting and recalibration effort, the sensors were hand-carried between AFETR and JPL. QA provided surveillance during all testing and evaluation of this activity in both areas.

The gyroscope control assemblies (GCA) were also from the *Mariner* Mars 1964 program. The remaining units were removed from SAF, and returned to the technical division for analysis and recalibration. During the testing phase, a pitch gyroscope in one unit failed. Upon disassembly, a broken pivot was found on the bellows end of the gyroscope. QA provided constant surveillance at the suppliers' facility during the disassembly, rework, and reassembly of all gyroscope assemblies used for the *Mariner* Venus 67 program. Because of the gyroscope shortage during this program, it was necessary to maintain the flight unit in bonded stores under QA surveillance until authorization for its issue was given by the spacecraft manager. This was accomplished without problem.

Reclaimed battery chassis from the *Mariner* Mars 1964 program were used for the *Mariner* Venus 67 project. No major problems were encountered.

The nine CC&S modules were completely reworked and refurbished. This consisted of removal and reinstallation of approximately 40 components. The systems were re-FA tested and qualified for the *Mariner* Venus 67 program. In the opinion of QA, the rework accomplished in this area was above average and extremely well organized. This type of endeavor is highly recommended for future programs.

The solar panel substrates were purchased from one supplier and delivered to another for assembly. Solar cells left over from the *Mariner* Mars 1964 program were also furnished to the second supplier. Five thousand new cells were procured to complete the project requirements. Flight solar panels were delivered to SAF promptly with complete documentation and certification.

The power conditioning systems were made up of the *Mariner* Mars 1964 hardware. Both systems were returned to the original supplier for refurbishment to the *Mariner* Venus 67 configuration. Delivered units displayed discrepancies (e.g., insulation damage, cold-flow conditions, holes in circuit boards, diode damage, contaminated connectors, and inadequacies in the conformal coating). Stycast spot bonding was broken in several areas where it was used to tie down and support wire bundles. All modules for both systems were reworked, cleaned, refurbished, re-Dow treated, and submitted for final inspection. The new documentation and certifications were delivered to SAF in proper order.

The two power regulator cases were also of *Mariner* Mars 1964 vintage and were reworked to the new *Mariner* Venus 67 configuration. Consistent with project control, QA personnel were assigned to the supplier to ensure compliance with requirements.

Because the planet sensor was a new addition to the spacecraft, hardware had to be designed, fabricated, and tested. QA problems arose because new contractor engineering personnel were assigned responsibility for this unit. Red-lined prints were utilized throughout fabrication of this unit without proper notification and authorization by responsible personnel. This failure to notify made the certification difficult.

The OSE transition in the attitude control section of the technical division was difficult because of continuing calibration problems. This was a constant problem throughout the *Mariner* Venus 67 program. It is recommended that a clearer definition and requirements be established at the beginning of all future programs to alleviate this problem.

*d. Engineering mechanics.* Two structures were selected after a mechanical inspection of all existing units; no major shifts from the *Mariner* Mars 1964 inspections of these structures was noted. The best two spacecraft buses of the lot were picked; all dimensions were within specifications. Minor modifications, consisting mainly of providing new locations for flight guidance sensors and harness damping hardware, were followed by cleaning. Insert problems arose because of the excessive usage of these buses in the past program. All inserts were inspected and replaced as necessary.

The temperature control louver assemblies were not redesigned for the *Mariner* Venus 67 mission, and the *Mariner* Mars 1964 assemblies were utilized after being repolished and requalified.

The high-gain antenna structure used the *Mariner* Mars 1964 reflector assemblies, which had been modified to accommodate a newly designed superstructure assembly for mounting on the spacecraft.

The low-gain antenna structure utilized existing *Mariner* Mars 1964 units with minor modifications.

Spacecraft cabling necessitated the modification and re-inspection of 42 *Mariner* Mars 1964 cables. Eighty-five new cables were fabricated for *Mariner* Venus 67 with a problem arising in the soldering of the cinch connectors. Poor solderability of this type of connector results in connections of poor quality. Inspection of the solder connections on the cinch connectors was difficult because of solder flow and gold amalgamation.

In the structures area, it was found that the units were subject to corrosion when in a high-humidity atmosphere. This problem arose at JPL and AFETR and is currently under investigation.

The metal thermal shields left over from the *Mariner* Mars 1964 program needed only to be re-polished and cleaned to meet the *Mariner* Venus 67 requirements.

The flexible blanket shields were of a new design, and inspection/surveillance was provided by QA during the manufacture of these units.

*e. Propulsion subsystem.* The midcourse correction propulsion system was of the *Mariner* Mars 1964 vintage with minor changes in design. The majority of components were *Mariner* Mars 1964 hardware. All units were re-inspected and re-certified prior to assembly. Valve assemblies, pressure transducers, and motor parts were cleaned, re-assembled, inspected and FA tested. Nitrogen tank assemblies for the fuel and oxidizer pressurizing system were a new procurement for *Mariner* Venus 67. Tanks were subjected to in-process source inspection, receiving inspection, and X-ray examination. Final assembly of the propulsion system was controlled by a detailed step-by-step QAI and checklist. FA testing was provided with QA monitoring in the division, at the remote test site, and at the environmental test laboratory.

A transducer failure in the midcourse propulsion system during laboratory testing at AFETR prompted a

failure analysis investigation which resulted in the detection of an out-of-control manufacturing process. Upon replacement of the oxidizer valve and transducers, tests were completed under the surveillance of QA for recertification. The valve and a new transducer were returned to AFETR for final assembly on the midcourse propulsion system.

*f. Environmental simulation.* QA personnel assigned to the Environmental Test Laboratory (ETL) provided test surveillance and monitoring of all activities performed (i.e., FA testing, TA testing, and environmental spacecraft system level tests).

Spacecraft system testing was performed on the STM, PTM, and two flight spacecraft (M67-1 and M67-2). Approximately 470 natural and induced environmental tests were performed at the assembly level. These tests included 216 FA, 78 TA, 170 development, and 5 life tests.

The verification and monitoring of the sequence of testing and the compliance with the detailed environmental test procedure was performed by QA personnel. Proper pre-test evaluations were conducted as applicable and included checking test equipment calibration and test tolerances, levels, and durations in accordance with the governing specifications and procedures. Verification of cleanliness of equipment as well as the test area was also accomplished.

The environmental test facilities at the Laboratory have improved overall cleanliness since the *Mariner* Mars 1964 project.

Responsibilities in the environmental facilities also included signing of the test results summary forms, which were an integral part of the certification requirements to SAF. This form basically stated whether the unit tested passed the environmental requirements.

No major problems were encounted at ETL.

*g. Systems test and launch operations.* The SAF QA function, which was organized during the *Ranger* series and expanded to encompass the *Mariner* Mars 1964 program, was re-instated for the *Mariner* Venus 67 project. The function of this group was to ensure the proper control, testing, and assembly of the flight vehicles. Additional responsibilities were to maintain a documentation control center consisting of all documentation related to the *Mariner* Mars 1964 project. This was necessary and extremely helpful for the *Mariner* Venus 67 program because of the similarity of the new hardware being fabricated and the utilization of old components. The assigned QA personnel were experienced in the SAF operations because of assignment on previous programs. Activities performed included monitoring of all activities on, or around, the flight vehicles, certification and inspection of all flight hardware (including mechanical assembly inspections and services), and maintenance of a flight hardware bonded store. In addition, QA was responsible for maintenance of a complete and up-to-date status of all hardware utilized in the *Mariner* Venus 67 program (including OSE), and the preparation of SAF PFR summary reports.

Certification of *Mariner* Venus 67 flight hardware, by the supplying technical division, was identical to the *Mariner* Mars 1964 program primarily because of hardware similarity. Several documents, such as certifications and procedures, were streamlined to dispose of any redundancy that existed in previous programs. Upon initial delivery to SAF, and when applicable, the hardware was subjected to a microscopic and mechanical inspection. This specific area will be more fully discussed in the concluding remarks of this section.

QA surveillance at SAF was provided 24 h per day when dictated by test schedule or operations. Documentation of all activities was accomplished and maintained throughout the program. This daily activity, in the form of a discrepancy log, depicted movement of hardware on and off the vehicles, and any other information considered pertinent and of interest. The daily activity report was reproduced and distributed to cognizant personnel.

Beginning with the initial hardware delivery and assembly at SAF through launch at AFETR, complete spacecraft status reports were issued and distributed for each major event performed on the vehicles. These status reports constitute a permanent record of all hardware installed on a specific vehicle for a specific event and are part of the SAF QA documentation control center.

Another service to engineering personnel performed by SAF QA was the issuance of the SAF PFR summary reports every 30 days to provide cognizant engineers with a PFR status of their respective equipment.

The bonded stores area in which the flight hardware was stored was operated and maintained exclusively by SAF QA personnel.

Mechanical inspection activities at SAF were related primarily to the assembly of the flight vehicles (i.e., verifying torques of all nuts, bolts, clamps, etc.). The safety requirements imposed by applicable procedures were also the responsibility of SAF QA. The alignment and verification of units such as the low-level positioner, overhead crane calibrations, and spacecraft handling equipment were additional services performed by SAF mechanical inspection.

Upon completion of the environmental testing, each spacecraft underwent a post-environmental teardown inspection. The spacecraft was disassembled and SAF QA performed the required inspection. The results of these inspections were as shown in Table IV-60 and Figs. IV-204 and IV-205. It should be noted that the discrepancies in the midcourse reference column of Table IV-60 were as reported during the same activity on the *Mariner* Mars 1964 program on the same basic spacecraft.

**Table IV-60. Post-environmental teardown inspection**

| Spacecraft | Total discrepancies | *Mariner C* reference |
|---|---|---|
| MV67-1 | 185 | 2/125 |
| MV67-2 | 114 | 3/107 |
| **General** | | |
| Contamination | 82 | 42 |
| Damage | 35 | 21 |
| Missed operation | 22 | 9 |
| Conformal coating | 28 | 26 |
| Spot bonding | 18 | 16 |

In summary, the significant problems encountered in the SAF activities were:

(1) Spacecraft Assembly and Test Procedures. This area caused QA problems because many procedures were not recognized as being a necessary requirement. An example of the trouble caused was during the environmental testing on the flight vehicle at JPL. There was no QA buy-off on the procedure, and the UV photometer desiccant cover was left on the spacecraft during the second chamber tests. This caused the loss of approximately two days. The problem of procedures was resolved by inclusion of QA buy-off in all applicable areas in the procedures.

(2) The movement of spacecraft in SAF was accomplished with the overhead crane. It is felt that a modification in the control system would greatly enhance the safety and handling.

(3) The previously mentioned receiving inspection performed by SAF QA has been changed since the *Mariner* Mars 1964 program. It was the project policy that a complete microscopic and mechanical inspection be performed as part of the certification to SAF. This was not the case for *Mariner* Venus 67, and subsystems that were delivered to SAF were not disassembled and inspected; only a cursory inspection of the exterior of subsystems could be performed. Because of this change in policy, the possible detection of discrepancies was postponed until the post-environmental teardown inspection. The photographic requirement was one of the other problems encountered. It was impossible to meet the project requirements of photographic documentation because the units could not be disassembled. This problem was resolved by taking the photographs during the post-environmental teardown inspection; however, this, in some cases, took place 4 or 5 months after initial delivery to SAF.

The QA effort performed at AFETR was essentially the same as that accomplished at SAF. Buildings AO, ESF, and launch pad 12 at AFETR were utilized by JPL in preparation of the *Mariner* Venus 67 for launch. Surveillance of all activities performed on flight hardware in these areas was provided by QA.

With the final system test on the spacecraft at the Laboratory completed, SAF QA began preparations to ship the spacecraft and all associated hardware and support equipment to AFETR. This activity included packing of flight hardware, preparing the spacecraft for shipment, road testing of trucks prior to loading, surveillance of the loading of each piece of hardware, OSE, and ground-handling equipment. All items were inventoried, manifested, and checked. The entire shipping operation was under the surveillance of SAF QA.

Hardware problems were encountered at AFETR with the Canopus sensor, radio subsystem, and the UV photometer.

The Canopus sensor was found to have noise in the system, and this necessitated a change in sensors between M67-1 and M67-2. The sensors were also returned to JPL for problem investigation and recalibration.

| SYSTEM | DAMAGED INSULATION | CONTAMINATION | UNPOTTED CONNECTORS | DAMAGED CONNECTORS | CONFORMAL COATING | DAMAGED INSERTS | LOOSE INSERTS | PIN RETENTION FAILURE | DAMAGED PAINT | SPOT BONDING | LOOSE CONNECTOR STANDOFFS | DOW TREAT SCRATCHES | LOOSE CONNECTIONS | ALUMINUM SCRATCHES | CONTAMINATED CONNECTORS | TARNISHED SURFACES | LOOSE NUTS OR BOLTS | CORROSION |
|---|---|---|---|---|---|---|---|---|---|---|---|---|---|---|---|---|---|---|
| 1. DAS (20A1–9) | | 9 | | | 9 | | | | | | | | | | | | | |
| 2. TRD (25A1) | | | | | | | | | | | 1 | | | | | | | |
| 3. PLASMA PROBE (32A1–4) | | 2 | | | | | | | 1 | | | | | | | | | |
| 4. HELIUM MAGNETOMETER (33A1–3) | | | | | | 2 | | | | 1 | | | | | | | | |
| 5. UV PHOTOMETERS (34A1, 34A2) | | 1 | | | 2 | | | | | | | | | | | | | |
| 6. DFR (35A1, 35A2) | | | | | | | | | | 1 | 1 | | | | 2 | | | |
| 7. SPACECRAFT RADIO SUBSYSTEM | | 3 | | | | | | | | | | | | | | 2 | 1 | |
| 8. STS (DATA ENCODER 6A1–6A13) | | | | | | | | | | | | | | | | | | NONE |
| 9. FLIGHT COMMAND SUBSYSTEM (3A1–3A7) | | | | | | | | | | 7 | | | | | | | | |
| 10. TRS (16A1–6) | | | | | | | | | | | | | | | | | | NONE |
| 11. HIGH-GAIN ANTENNA (2E 1) | DAMAGED DURING CHAMBER TEST AND REPAIRED | | | | | | | | | | | | | | | | | NONE |
| 12. LOW-GAIN ANTENNA (2E 2) | | | | | | | | | | 1 | | | | 2 | | 2 | | |
| 13. DRF ANTENNA, 425 MHz (15E 3) | | | | | | | | | | | | | | | | | | NONE |
| 14. DRF ANTENNA, 50 MHz (15E 2) | | | | | | | | | | | | | | | | | | NONE |
| 15. AC SUBSYSTEM (7A1) | | | | | 1 | | | | | | | | | | | | 1 | |
| 16. AC SUBSYSTEM (7A2) | | | | | | | | | | | | | | | | | | NONE |
| 17. AC GAS SYSTEM (7GA1 AND 2) | LEAKING VALVE WAS CHANGED OUT | | | | | | | | | | | | | | | | | NONE |
| 18. STRUCTURES | | 5 | | | | 4 | | | 2 | 1 | | 2 | | | | | | |
| 19. CANOPUS SENSOR (7CS8) | | 1 | | | | | | | | | | | | | | | | |
| 20. SUN SENSORS (7PS2, 6, 7SS2, 6) | | 1 | | | | | | | | | | | | | | | | |
| 21. SUN GATE SENSOR (7SG7) | | | | | | | | | | | | | | | | | | NONE |
| 22. EARTH SENSOR (7ED6) | | 1 | | | | | | | | | | | | | | | | |
| 23. PLANET SENSOR (7LS8) | | 1 | | | | | | | | | | | | | | | | |
| 24. TERMINATOR SENSOR (7TS2) | | 1 | | | | | | | | | | | | | | | | |
| 25. JVA (7JV5 AND 6) | | | | | | | | | | | | | | | | | | NONE |
| 26. CENTRAL COMPUTER AND SEQUENCER (5A1–9) | | | | | 4 | | 2 | | | 1 | | | | | | | | |
| 27. POWER SUBSYSTEM, BAY I (4A11–18) | | 1 | | | 8 | | | | | 1 | | | | | | | | |
| 28. POWER REGULATOR, BAY VIII (4A8) | | 1 | 2 | 1 | 1 | | | | | 1 | | | | | 6 | | 2 | |
| 29. BATTERY (4A14) | | | | | | | | | | | | | | | | | | NONE |
| 30. SOLAR PANELS (4A1, 3, 5, AND 7) | | | | | | | | | | | | | | | | | | NONE |
| 31. DEPLOYABLE SUN SHADE | | | | | | | | | | | | | | | | | | NONE |
| 32. TCR | | | | | | | | | | | | | | | | | | NONE |
| 33. SEPARATION INITIATED TIMER (8M1) | | | | | | | | | | | | | | | | | | NONE |
| 34. PAS (8AS1) | | | | | | | | | | | | | | | | | | NONE |
| 35. PIPS | | | | | | | | | | 2 | | | | | | | | |
| 36. PROTECHNICS SUBSYSTEM (8A1/2) | 1 | 2 | | | 1 | 5 | | | | | | | | | | | | |
| 37. SPACECRAFT CABLING | | | | | | | | 1 | | | | | | | | | | |
| 38. THERMAL CONTROL | | | | | | | | | | | | | | | | | | NONE |
| | | | | | | | | | | | | | | | | | | |

**Fig. IV-204. SAF disassembly inspection, M67-1**

| SYSTEM | DAMAGED INSULATION | CONTAMINATION | UNPOTTED CONNECTORS | DAMAGED CONNECTORS | CONFORMAL COATING | DAMAGED INSERTS | LOOSE INSERTS | PIN RETENTION FAILURE | DAMAGED PAINT | SPOT BONDING | LOOSE CONNECTOR STANDOFFS | DOW TREAT SCRATCHES | LOOSE CONNECTIONS | ALUMINUM SCRATCHES | CONTAMINATED CONNECTORS | TARNISHED SURFACES | LOOSE NUTS OR BOLTS | CORROSION |
|---|---|---|---|---|---|---|---|---|---|---|---|---|---|---|---|---|---|---|
| 1. DAS (20A1-9) | | | | 9 | | | | | | | | | | 2 | | | | |
| 2. TRD (25A1) | | | | | | | | | | 4 | | | | 2 | 1 | | | |
| 3. PLASMA PROBE (32A1-4) | | | | | | | 1 | | | | 1 | | | 2 | | | | |
| 4. HELIUM MAGNETOMETER (33A1-3) | | 2 | | 2 | | | | 1 | | | | | | | | 3 | | |
| 5. UV PHOTOMETERS (34A1, 34A2) | | | | 1 | | | | | | | 1 | | | 2 | 1 | | | |
| 6. DFR (35A1, 35A2) | | | | | | | | | | 4 | | | | | | | | |
| 7. SPACECRAFT RADIO SUBSYSTEM | | | 2 | | | | | | 2 | | | 3 | | | | | | |
| 8. STS (DATA ENCODER 6A1-6A13) | | | | 3 | | | | | | | | | | 13 | | | | |
| 9. FLIGHT COMMAND SUBSYSTEM (3A1-3A7) | | 3 | | | | 1 | | | 7 | | 3 | | | 7 | | | | |
| 10. TRS (16A1-6) | | | | 2 | | | | | | | | | | | | | | |
| 11. HIGH-GAIN ANTENNA (2E1) | | | | | | | | 1 | | | | | | | | | | |
| 12. LOW-GAIN ANTENNA (2E2) | | | | | | | | | | | | | | | 3 | | | |
| 13. DFR ANTENNA, 425 MHz (15E3) | | | | | | | | | | | | | | | | | | NONE |
| 14. DFR ANTENNA, 50 MHz (15E2) | | | | | | | | | | | | | | | | | | NONE |
| 15. AC SUBSYSTEM (7A1) | | | | 1 | | | | | | | | | | | | | | |
| 16. AC SUBSYSTEM (7A2) | | | | | | | | | | | | | | | | | | NONE |
| 17. AC GAS SYSTEM (7GA1/2) | | 2 | | | | | | | | | | | | | | | | |
| 18. STRUCTURES | | 6 | | 6 | 3 | 3 | | 9 | 9 | | 3 | | 2 | | 1 | | 5 | |
| 19. CANOPUS SENSOR (7CS8) | | | | | | | | | | | | | | | | | | NONE |
| 20. SUN SENSORS (7PS2, 6, 7SS2, 6) | | 4 | | | | | | | | | | | | | | | | |
| 21. SUN GATE SENSOR (7SG2) | | 1 | | | | | | | | | | | | | | | | |
| 22. EARTH SENSORS (7ED6) | | 1 | | | | | | 1 | | | | | 1 | | | | | |
| 23. PLANET SENSOR (7LS8) | | | | | | | | | | | | | | | 1 | | | |
| 24. TERMINATOR SENSOR (7TS2) | | 1 | | | | | | | | | | | | | | | | |
| 25. JVA (7JV5 AND 6) | | 2 | | | | | | | | | | | | | | | | |
| 26. CENTRAL COMPUTER AND SEQUENCER (5A1-9) | | 2 | | | | | | | | | | | | | | | | |
| 27. POWER SUBSYSTEM, BAY I (4A11-18) | | | | 4 | | | | | | | 2 | | | 8 | | | | |
| 28. POWER REGULATOR, BAY VIII (4A8) | | | 2 | | | | | 1 | | | | | | | | | | |
| 29. BATTERY (4A14) | | | | | | | | | | | | | | | | | | NONE |
| 30. SOLAR PANELS (4A1, 3, 5, AND 7) | | | | | | | | | | | | | | | | | | NONE |
| 31. DEPLOYABLE SUN SHADE | | 1 | | | | | | | | | | | | | | | | |
| 32. TCR | | | | | | | | | | | | | | | | | | NONE |
| 33. SEPARATION INITIATED TIMER (8M1) | | | | | | | | | | | | | | | | | | NONE |
| 34. PAS (8AS1) | | | | | | | | | | | | | | | | | | NONE |
| 35. PIPS | | | | | | | | | | | | | | | 2 | | | |
| 36. PYROTECHNICS SUBSYSTEM (8A1/2) | | 2 | | | | | | | | | | | | | | | | |
| 37. SPACECRAFT CABLING | | | | 2 | | | | | | | | | | | | | | |
| 38. THERMAL CONTROL | | 6 | | | | | | | | | | | | | | | | |
| | | | | | | | | | | | | | | | | | | |

**Fig. IV-205. SAF disassembly inspection, M67-2**

The relay problem encountered with the radio subsystem proved that the photographs taken by SAF QA were invaluable for investigative purposes. The relay change of hardware was accomplished without problem.

The anomaly encountered with the UV photometer at AFETR resulted in a change of units. During the final electrical test performed on the vehicle prior to shroud installation, the UV photometer exhibited a high count rate. It was felt that this problem may have been caused by the ionized air blower used to remove a static charge on the vehicle because of live pyrotechnic devices and post-injection propulsion systems being installed. The ionization gun, which contains a radioactive source, used by QA in checking for static electricity was also considered as a possible source.

The UV photometer was removed from M67-2 and returned to the calibration laboratory. After exhaustive tests had been performed (with negative results), the change was completed. The M67-1 UV photometer was installed on the M67-2.

An additional activity performed by QA was to supply personnel to the Pad 12, M67-2 purge watch. This consisted of monitoring the dry nitrogen purge of the spacecraft. A log was initiated and is part of the QA records. The shipment of the spare spacecraft, OSE, and ground-handling equipment to JPL was handled in the same manner as the shipment going to AFETR.

*h. Recommendations for future programs.* The following is a listing of recommendations which, if implemented, will minimize the minor problems encountered during the *Mariner* Venus 67 program:

(1) It would be desirable to station full-time QA engineers at each subsystem supplier. This would reduce the interface time for discrepancies as well as provide a higher degree of technical competence for hardware decision making.

(2) Each subcontractor should be required to detail its QA plan prior to award of contract. These plans should be reviewed by JPL QA early in the procurement cycle.

(3) The decision to rework or modify equipment built for previous programs should be thoroughly investigated in the area of process control and new technology. In many cases, present-day methods are noncompatible with existing hardware, and early resolution of these problems would alleviate decisions under schedule strain.

(4) QA should support its reports with some meaningful statistical data. This would increase the objectivity and engineering value of the QA function.

(5) A standard method of handling and routing units after arrival at JPL should be instituted. This should be a project requirement with enforcement provisions.

(6) The project should establish a method of shipping material from JPL to subsystem contractors. This requirement should be consistent with the concern for documentation and hardware integrity in light of the mission requirements.

## O. Parts Acquisition and Screening

The parts acquisition task team procured nearly 66,000 electronic components for the *Mariner* Venus 67 program. Approximately 86% of these parts were screened per JPL specifications with an overall average yield of 62%. The remaining 14% either did not require screening (i.e., breadboard), or the screening data are not available at this time.

*1. Approach.* The following policy for obtaining parts was established at the beginning of the project:

"When new or revised design requires electronic parts, the following shall be accomplished in order of preference:

(1) Standard parts shall be selected from the existing Approved Parts List (APL).

(2) Necessary standard parts (not listed in the *Mariner* 67 APL) shall be selected from the JPL Preferred Parts List (PPL).

(3) Nonstandard parts shall be selected from existing APL.

(4) Highest available commercial grade part shall be selected.

Subsystem usage acquired pa

| 20A2 | 35 | 20A1 | | 20A1 | 20A1 | 7CS8 | 4A1 | 34 | 05 | 16 | 04 | 4A14 | 06 | 2 |
|---|---|---|---|---|---|---|---|---|---|---|---|---|---|---|
| DAS logic AAAF | DFR AB-J | DAS power supply 3 AABF | A/PW AAHE | DAS power supply 1 AALF | DAS power supply 2 AAMC | Canopus tracker AC-E | Solar panel AD-E | UV photometer AE-J | CC&S AF-E | Tape recorder AG-D | Spacecraft power supply AHBE | Battery AI-E | Data encoder AJ-D | TR AK |
| 102 | | | | | | | | | 2 | | | | | |
| 3656 | 10 | 320 | 750 | 205 | 259 | 843 | | 556 | 6 | 656 | 182 | | 1033 | 52 |
| 6468 | 300 | 420 | 720 | 163 | 341 | 297 | 210 | 138 | 72 | 857 | 307 | | 2346 | 12 |
| | 100 | | | | | | | | 100 | 70 | 10 | 20 | 6 | 6 |
| | | | 100 | | | 10 | | | | | | | | |
| 16 | | | | | | | | | | | | | | |
| | | | | | | 12 | | | | 16 | 6 | | 3 | |
| | | | | 49 | | 24 | | | | 2 | 5 | | | 1 |
| | | | | | | | | | | | | | | 1 |
| | | | 120 | | | | | | | | | | | |
| 2913 | | 462 | 1412 | 107 | 172 | 35 | | 10 | | 747 | 61 | | 578 | 18 |
| 9002 | | 2109 | 2230 | 2259 | 812 | 579 | 277 | 387 | 1092 | 3356 | 674 | | 1052 | 191 |
| | | | | | | | | | | | | | | |
| 947 | 15 | | | 21 | 36 | 40 | | | 22 | 21 | 30 | | | |
| 5240 | | | | | 25 | | | | | | | | | |
| | | | | | 100 | 8 | | | | | | | | |
| 28344 | 425 | 3311 | 5332 | 2804 | 1745 | 1848 | 487 | 1091 | 1294 | 5725 | 1275 | 20 | 5018 | 28 |
| 4 | 4 | 1 | 4 | 1 | 1 | 0 | 8 | 0 | 0 | 1 | 0.6 | 0 | 1 | 1 |
| 0 | 0 | 0 | 24 | 0 | 0 | 4 | 0 | 3 | 4 | 5 | 3.4 | 10 | 3 | |
| NA | NA | NA | 0 | NA | NA | 2 | NA | 2 | 0 | 4 | 10 | 90 | 10 | 5 |

mple of total data.



FOLDOUT FRAME 1

FOLDOUT FRAME 2

## Table IV-61. Subsystem usage part type summary

| )7 | 08 | 10 | 7LS8 | 7TS2 | 02 | 03 | | 7A1 | 12 | Total acquired parts | Total screened parts | Average yield, % | Average procurement delivery time, weeks |
|---|---|---|---|---|---|---|---|---|---|---|---|---|---|
| tude trol N-E | Pyrotechnic control AOJH | PIPS AOKH | Planet sensor AP-E | Terminator sensor AQ-E | Radio AR-D | Command ASD | Suspect spares AT-D | Autopilot AU-H | Div. 35 mechanical AZ-H | | | | |
| | | | | | | | | | | 104 | 65 | 17.9 | 6 |
| 23 | | | 45 | | 128 | 30 | | | | 9,658 | 9,112 | 74.1 | 5 |
| 57 | | | 42 | | 15 | | 20 | | | 13,359 | 12,170 | 57.6 | 4 |
| | | | | | | | | | | 421 | 401 | 91.5 | 1 |
| | | | | | | | 10 | | | 120 | 126 | 59.7 | 3 |
| | | | | | | | | | | 16 | — | — | 1 |
| | | | | | | | | | | 37 | 35 | 76.7 | 3 |
| | | | | | 15 | | | | | 113 | 110 | 30.6 | 3 |
| | | | | | | | | | | 13 | 13 | 50.0 | 0.5 |
| | | | | | | | | | | 127 | 102 | — | 0.5 |
| 52 | 15 | 45 | 32 | 23 | 34 | 14 | 50 | | | 7,182 | 6,418 | 43.0 | 4 |
| 07 | | | 99 | 180 | 102 | | | 597 | 25 | 27,814 | 23,343 | 80.7 | 3 |
| | | | | | | | | | 50 | 50 | — | — | 0.5 |
| 00 | | | | | | | 20 | | | 1,252 | 1,184 | 56.5 | 7 |
| | | | | | | | | | | 5,265 | 3,425 | — | 9 |
| | | | | | | | | | | 111 | 11 | 100.0 | 0.5 |
| 49 | 15 | 45 | 218 | 203 | 294 | 44 | 100 | 597 | 75 | 65,642 | 56,515 | 61.5 | 3.2 |
| 0 | 0 | 0 | 4 | 4 | 0 | 1.5 | NA | 0 | NA | 86% of all the procured parts were screened | | | |
| 4 | 4 | 4 | 0 | 0 | 4 | 2.5 | NA | 4 | NA | 62.7% of the procured parts were obtained from vendors—18.7% from JPL stores and 18.6% from various other sources. | | | |
| 5 | 0 | 0 | NA | NA | 10 | 0 | NA | 2 | NA | | | | |



FOLDOUT FRAME

**Page intentionally left blank**

PRECEDING PAGE BLANK NOT FILMED.

When additional parts are required for *existing design:*

(1) Additional parts identically comparable to those used in *Mariner* 1964 would be used in existing designs.

(2) If this is not possible, parts will be selected in accordance with the above steps.

All parts acquired for new fabrication shall be subjected to 100% screening evaluation in accordance with approved specifications."

A task group was established to expedite the acquisition of the parts to meet the new subsystem requirements and modification to existing designs. During the initial phase of the task group activity, action was taken to make "speculation buys" of common part types with general circuit usage. These provided a preliminary list for meeting subsystem requirements. The *Mariner* Mars 1964 residual parts from all division stocks were pooled to meet the anticipated subsystem designs and changes.

A task group was organized into four subgroups which provided the controls for part acquisition, screening contract coordination, technical division interface, and screening vendor monitoring.

The original concept provided a single major screening contract for screening transistors, diodes, resistors, and capacitors. The concept was modified when the single screening contractor could not instrument and staff adequately to meet the part and schedule needs. The purchase order method was established utilizing four additional screening sources. This method proved workable but was slow and consumed more manpower to initiate screening purchase requisitions and follow-up. Parts quality assurance (PQA) support was used to monitor screening vendors, screen critical and difficult parts, review vendor screening reports, and verify the acceptance of parts supplied for use.

A semi-automatic status report system was developed to give fast, up-to-date information covering the procurement and screening progress. The system was also capable of sorting procurement problems and screening entries from the total status.

It was the intent of the parts acquisition group (PAG) to have a parts representative responsible for obtaining and defining part requirements and interfacing with the parts specialists, subsystem cognizant engineers, QA, stores, and receiving. The parts and screening coordination control was responsible for initiating procurements and establishing the screening requirements, obtaining technical inputs for procurement, and providing status relating to progress for all parts processing activities. The functional monitoring of screening activity was accomplished by screening vendor representatives who were responsible for interfacing with parts specialists, QA and parts and screening control.

The bonded stores activity was regulated by parts and screening coordination control, screening vendor control, and the parts representatives. All incoming parts from manufacturers were processed through receiving and stores. Stores prepared parts for shipment to screening vendors as directed by screening control. All incoming screened parts were received through stores and placed into bonded stock. Data books containing the visual and screening test data by lot, prepared by the screening vendors, were submitted to cognizant personnel for evaluation. Only lots with deficient yields were examined completely. Problems occurred with parts that initially were accepted and were later found nonconforming when delivery to the subsystem was attempted. In cases of this nature, a nonconforming material review was held.

All parts delivered for flight use were subject to, and approved by, the cognizant engineer, part representative, parts specialist, and QA prior to release for assembly.

Withdrawal of residual parts for use by other projects was regulated by the user division parts representative and cognizant engineer with concurrence by the project office.

Table IV-61 is a summary of the subsystem usage part type, and Table IV-62 is the parts acquisition and screening program summary.

***2. Electronic parts failure analysis.*** In support of the *Mariner* Venus 67 project, a variety of failure analysis type services was provided. In addition to laboratory analysis of failed or defective parts, these services included dynamic X-ray examination of certain critical parts and performance of special investigations aimed toward providing better definition of particular parts problems. A total of 118 of these failure analysis efforts was documented. Of these documented efforts, 105 were

**Table IV-62. Program summary—parts acquisition and screening**

| Item | Value |
|---|---|
| Total parts procured | 65,642 |
| Total parts screened | 56,515 |
| Percentage parts screened | 86% |
| Overall average yield | 61.5% |
| Percentage of parts procured from vendor | 62.7% |
| Percentage of parts obtained from JPL stores | 18.7% |
| Percentage of parts obtained from other sources | 18.6% |
| Average unit procurement cost | $ 5.37[a] |
| Average unit screening cost | $ 4.94[a] |
| Total cost per component part | $ 10.31[a] |
| Total cost of all procured parts | $244,665.57[a] |
| Total cost of all screened parts | $198,846.38[a] |
| Total parts cost | $443,511.95 |
| Average number of parts per screening lot | 32 |
| Average screening cost per lot | $ 158.00 |
| Total number of screening lots | 1,746 |

[a]Calculations based on a statistical sample of more than 70% of the total available data.

performed in response to PFRs (Table IV-63). The documented efforts which were not related to specific PFRs are listed in Table IV-64. The number of parts per type analyzed in response to PFRs is given below:

| | Flight | OSE | Total |
|---|---|---|---|
| Capacitors | 11 | 1 | 12 |
| Integrated circuits | 17 | 0 | 17 |
| Transistors | 7 | 37 | 44 |
| Diodes | 3 | 8 | 11 |
| Transformers | 4 | 2 | 6 |
| Resistors | 6 | 1 | 7 |
| Relays | 1 | 1 | 2 |
| Miscellaneous | 3 | 3 | 6 |
| Total | 52 | 53 | 105 |

| | Critical PFRs | Noncritical PFRs |
|---|---|---|
| Flight | 34 | 18 |
| OSE | 9 | 44 |

**Table IV-63. Part failure analyses arranged by PFR number**

| PFR No. | Part family | Part No. | Comments |
|---|---|---|---|
| 007862 | Capacitor | Type J | Pinholes in the tantalum oxide dielectric |
| 007865 | Capacitor | CK05 | Metal bridging between the plates |
| 008310 | Choke | 38161 | Damaged during equipment modification |
| 008311 | Resistor | ARS-2 | Damaged during equipment modification |
| 008323 | Transistor | 2N2658 | Shorted—probably because of electrical abuse |
| 008326 | Capacitor | 123D | Electrolyte lost through a leaky seal |
| 010424 | Integrated circuit | DAE 424 | Intermittently open bonds |
| 010628 | Capacitor | 123D | Electrolyte lost through a leaky seal |
| 010718 | Integrated circuit | DAE 424 | Failure not verified |
| 011033 | GM tube | 6213 | Cause of failure not determined |
| 011041 | Transformer | Special | Short due to sloppy workmanship during transformer assembly |
| 011044 | Integrated circuit | DAE 416 | Lid came off—probably because of mechanical abuse |
| 011047 | Integrated circuit | DAE 480 | Degradation probably because of electrical abuse |
| 011048 | Integrated circuit | DAE 424 | Lead bent during equipment troubleshooting |
| 011067 | Capacitor | CK05 | Capacitor was reported to have drifted; device was still within tolerance and contained no observed defects |
| 011073 | Integrated circuit | DAE 424 | Failure not verified |
| 011076 | Integrated circuit | DAE 416 | Device was within specification; suspect equipment margins are set too low |
| 011082 | Transistor | FSP 247-1 | Improperly placed bonds produced intermittent shorting |
| 011094 | Integrated circuit | DAE 731 | Failure not verified |
| 011096 | Resistor | CCB | Crack in coating due to unknown causes |
| 011099 | Integrated circuit | DAE 731 | Failure not verified |
| 011105 | Diode, varactor | MA4558 | Cause of failure not definitely determined |

## Table IV-63 (contd)

| PFR No. | Part family | Part No. | Comments |
|---|---|---|---|
| 011136 | Resistor | MEA-T2 | Erratic because of defective connection between the lead and resistance element |
| 011146 | RFI filter | GF-3708 | Bad solder joint inside the device |
| 011152 | Diode, zener | 48-29553 | Intermittently open because of thermal contraction of the S-spring |
| 011156 | Diode, zener | 48-29553 | Intermittently open because of thermal contraction of the S-spring |
| 011157 | Transistor | 2N834 | High $I_{EBO}$ because of a gold scrap |
| 011158 | Diode, zener | 1N746 | Diode installed backwards within the potted module |
| 011163 | Transistor | 2N652A | High-leakage current; cause not determined |
| 011165 | Transistor | 2N834 | Low gain (soft EB knee); cause not determined |
| 011166 | Transistor | 2N652A | Shorted probably because of electrical abuse |
| 011167 | Transistor | 2N834 | Open wire at post because of a manufacturing error |
| 011168 | Potted module | — | All parts found to be within tolerance; failure not verified |
| 011226 | Relay | Series 33 | Failure not verified |
| 011227 | Transistor | 2N1613 | Shorted because of electrical abuse |
| 011259 | Capacitor | 29F | Shorted because of electrolyte leakage through a defective internal seal |
| 011267 | Transistor | 108D030 | Shorted because of electrical abuse |
| 011284 | Transformer | SP66 | Open winding; cause not determined but probably related to known part deficiencies |
| 011285 | Transistor | 2N2082 | Shorted because of electrical abuse |
| 011286 | Relay | RP9896G17 | Broken lead; cause not determined |
| 011544 | Capacitor | 15K | Environmental tests caused breakage of internal leads; deficient part design |
| 011557 | Transistor | 2N2222 | Open base bond because of excessive bonding pressure |
| 011558 | Transformer | 25-33442 | Intermittent shorting because of part design deficiencies |
| 011594 | Transistor | 2N2639 | Lead corrosion because of the method of module assembly |
| 011702 | Diode, zener | ? | Intermittently open because of thermal contraction of the S-spring |
| 011704 | Transistor | 2N956 | Cause of failure not determined |
| 011705 | Capacitor | Mica | An unencapsulated capacitor had been used in the potted module and was shorting to a transistor |
| 011706 | Transistor | 2N956 | Shorted probably because of electrical abuse |
| 011707 | Transformer | SP66 | Open winding; probably related to known part deficiencies |
| 011723 | Transistor | 2N652A | Shorted probably because of electrical abuse |
| 011724 | Transistor | 2N652A | Shorted; cause not determined |
| 011725 | Transistor | 2N652A | Shorted probably because of electrical abuse |
| 011735 | Transistor | 2N1544 | Shorted due to unknown cause; produces secondary failures |
| 011747 | Transistor | 2N404 | Open collector because of electrical abuse |
| 011748 | Transistor | 2N404 | Open because of electrical abuse |
| 011803 | Diode | 980314 | Open because of electrical abuse |
| 011804 | Crystal | CR-50/U | Cold solder joint internally |
| 011805 | Diode | 980314 | Open because of electrical abuse |
| 011806 | Transistor | 2N404 | Shorted because of electrical abuse |
| 011807 | Transistor | 2N1605 | Open because of electrical abuse |
| 011809 | Transistor | 2N1544 | Shorted probably because of electrical abuse |
| 011810 | Transistor | 2N1375 | Shorted probably because of electrical abuse |

## Table IV-63 (contd)

| PFR No. | Part family | Part No. | Comments |
|---|---|---|---|
| 011811 | Transistor | 2N404 | Shorted because of encapsulated extraneous wire |
| 011812 | Transistor | 2N404 | Open because of electrical abuse |
| 011813 | Transistor | 2N1375 | High leakage current due to an undetermined cause |
| 011815 | Transistor | 2N1375 | Shorted probably because of electrical abuse |
| 011817 | Transistor | 2N1375 | Shorted probably because of electrical abuse |
| 011818 | Transistor | 2N404 | Shorted probably because of electrical abuse |
| 011820 | Transistor | 2N1375 | Shorted probably because of electrical abuse |
| 011822 | Transistor | 2N404 | Shorted probably because of electrical abuse |
| 011824 | Transistor | 2N404 | Intermittent short possibly because of included metallic contaminants |
| 011827 | Transistor | 2N1605 | Shorted probably because of electrical abuse |
| 011828 | Diode | 980302 | Open because of electrical abuse |
| 011832 | Transistor | 2N404 | Failure not verified |
| 011836 | Transistor | 2N404 | Shorted probably because of electrical abuse |
| 011837 | Transistor | 2N1537 | Shorted—cause undetermined |
| 011843 | Transistor | 2N1375 | Shorted probably because of electrical abuse |
| 011875 | Capacitor | 29F | Electrolyte leakage because of a defective seal |
| 011876 | Capacitor | 29F | Electrolyte leakage because of a defective seal |
| 011922 | Transistor | 2N941 | Shorted probably because of electrical abuse |
| 011971 | Resistor | ARS-2 | Damaged during equipment modification |
| 103901 | Integrated circuit | DAE 424 | Failure not verified |
| 103904 | Integrated circuit | DAE 424 | Lid came off; device was overheated during lid attach |
| 103919 | Integrated circuit | DAE 480 | Lid came off; device was overheated during lid attach |
| 103928 | Integrated circuit | DAE 180 | Device was destroyed by application of excessive voltage |
| 103930 | Transformer | PE6161 | Windings not soldered to external leads |
| 103945 | Integrated circuit | DAE 480 | Lid came off; device was overheated during lid attach |
| 103946 | Integrated circuit | DAE 424 | Package was chipped; device was electrically OK |
| 103947 | Integrated circuit | DAE 424 | Failure not verified |
| 105388 | Transistor | 2N930 | Open because of electrical abuse |
| 105388 | Transistor | 2N2907A | Shorted because of electrical abuse |
| 105454 | Transistor | 2N834 | Open because of electrical abuse |
| 105455 | Transistor | 2N834 | Degradation probably resulting from contamination |
| 105456 | Resistor | CG 1/8 | Wrong value built into potted module; assembly error |
| 105457 | Transistor | 2N652A | Open because of defective joint formed during manufacture |
| 105459 | Diode | 1N914 | Diode was installed backwards within the potted module |
| 105643 | Diode | FDH600 | Broken during installation |
| 105643 | Diode | FD306 | Shorted because of electrical abuse |
| 105646 | Resistor | MCE | High resistance because of an assembly-induced defective termination |
| 105647 | Capacitor | C11A682K | Hole in device encapsulation; should have been an initial visual reject |
| 105658 | Resistor | 10K | Defective connection between one lead and the element |
| 105683 | Transformer | C-311577 | Short because of inadequate insulation |

Table IV-63 (contd)

| PFR No. | Part family | Part No. | Comments |
|---|---|---|---|
| 105762 | Capacitor | 350D | Part meets all specifications; application problem |
| 105763 | Trigistor | 2N897 | High leakage due to undetermined causes |
| 105881 | Integrated circuit | SE480 | Degraded substrate diode |

**Table IV-64. Part failure analyses not related to specific PFR**

| Part family | Part No. | Comments |
|---|---|---|
| Transformer | SP Series | Investigation of winding corrosion due to Scotchcast 247 encapsulant |
| Integrated circuit | NE 180 | Device was destroyed by application of excessive voltage |
| Integrated circuit | DAE 156 | Gross leak testing of reject integrated circuits |
| Integrated circuit | various | Analysis of the effects of various contaminants on the appearance of an integrated circuit chip |
| Crystal | 443.406 kHz | Broken solder joints at the point of connection to the crystal |
| Switch, motor driven | M-566 | Brush and commutator wear resulted in failure |
| Capacitors | HMC-80 | Cracks in the ceramic dielectric allowed shorts to develop |
| Integrated circuit | NE 480 | Failure not verified |
| Integrated circuit | NE 116 | High leakage because of surface contamination |
| Integrated circuit | NE 180 | Device was destroyed by electrical abuse |
| Integrated circuit | various | Twelve devices destroyed by static discharge |
| Integrated circuit | NE 180 | Failure not verified |

*3. Approved electronic parts list.* The purpose of the approved electronic parts list was to exercise control in the selection and acquisition of electronic parts for any portion of the spacecraft which was new or updated, and to list in convenient categories all electronic components on the spacecraft. This list was periodically updated from schematic drawings and parts list information supplied by the cognizant engineers and electronic parts representatives.

Following initial design reviews, all subcontractors, or JPL cognizant engineers, submitted preliminary parts lists tabulating each different part intended for use on each subsystem. Parts engineering then reviewed these lists recommending, where applicable, use of alternate parts because of higher qualification and reliability or for standardization. All attempts were made to use parts already qualified and evaluated.

Table IV-65 shows the parts count for the spacecraft by subsystem, and Table IV-66 shows the reliability rating of the parts by subsystem.

*4. Recommendations.* The following is a listing of recommendations that should be considered for future projects:

(1) Provide a central facility at JPL where all parts can be physically examined.

(2) Inspect all incoming parts received from the manufacturer to verify correctness.

(3) Provide complete review of all screened parts to determine acceptability at the time screening is completed.

(4) Provide multiple screening contracts to handle the parts screening.

(5) Provide improved monitoring of screening contractors to ensure a keen awareness of facility loading.

(6) Supply a JPL stock room with common usage parts to promote standardization, cost reduction, and availability of long-lead-time parts.

(7) Provide a more effective method to follow up procurements.

(8) Provide a more flexible method of placing screening contracts by purchase order for parts not covered by screening contract.

(9) Restrict parts procurement to current manufacturers' stock.

(10) Procure parts directly from the manufacturer to improve yields.

## Table IV-65. Summary of spacecraft parts count by subsystem

| Subsystem | No. | Capacitors | Diodes | Resistors | Transistors | Other[a] | Total |
|---|---|---|---|---|---|---|---|
| Radio | (02) | 594 | 203 | 658 | 122 | 197 | 1774 |
| Command | (03) | 406 | 791 | 1030 | 338 | 50 | 2615 |
| Power | (04) | 145 | 293 | 395 | 134 | 97 | 1064 |
| CC&S | (05) | 257 | 728 | 1059 | 266 | 260 | 2570 |
| Data encoder | (06) | 1465 | 1464 | 3416 | 1055 | 185 | 7585 |
| AC | (07) | 227 | 291 | 523 | 119 | 101 | 1261 |
| Pyrotechnic | (08) | 42 | 48 | 114 | 4 | 32 | 240 |
| Wiring | (09) | | | | | | |
| Thermal | (11) | | | | | 3 | 3 |
| Mechanical | (12) | 6 | 4 | 6 | | 13 | 29 |
| Tape recorder | (16) | 232 | 331 | 686 | 197 | 33 | 1479 |
| DAS | (20) | 144 | 89 | 261 | 62 | 617[b] | 1173 |
| Trapped radiation | (25) | 94 | 38 | 206 | 61 | 18 | 417 |
| Plasma probe | (32) | 162 | 425 | 684 | 211 | 12 | 1494 |
| Magnetometer | (33) | 212 | 83 | 597 | 153 | 6 | 1051 |
| UV photometer | (34) | 203 | 148 | 665 | 155 | 52 | 1223 |
| DFR | (35) | 405 | 111 | 481 | 150 | 143 | 1290 |
| Total subsystem parts | | 4594 | 5047 | 10,781 | 3027 | 1819 | 25,268 |

[a]Does not include 518 connectors. "Other" includes inductors, relays, transformers, microcircuits, cores, silicon-controlled rectifiers and switches, crystals, thermistors, sensitors, fuses, and tubes.

[b]There are 566 microcircuits in the DAS.

## Table IV-66. Summary of spacecraft parts reliability ratings by subsystem

| Subsystem | Ratings[a] | | | | | | | | | | | | | | | |
|---|---|---|---|---|---|---|---|---|---|---|---|---|---|---|---|---|
| | BX1 | | BX2 | | BX3 | | BY | | T | | C | | R | | DS | |
| | Quantity | % | Quantity | % | Quantity | % | Quantity | % | Quantity | % | Quantity | % | Quantity | % | Quantity | % |
| Radio | 19 | 8.3 | 4 | 1.8 | 0 | 0 | 84 | 36.8 | 20 | 8.7 | 20 | 8.7 | 26 | 11.4 | 55 | 24.1 |
| Command | 3 | 13.6 | 0 | 0 | 0 | 0 | 6 | 27.2 | 0 | 0 | 1 | 4.5 | 4 | 18.1 | 8 | 36.3 |
| Power | 5 | 4.2 | 0 | 0 | 0 | 0 | 45 | 37.5 | 1 | 0.8 | 9 | 7.5 | 25 | 20.8 | 35 | 29.0 |
| CC&S | 3 | 4.7 | 1 | 1.6 | 1 | 1.6 | 22 | 34.9 | 1 | 1.6 | 11 | 17.5 | 9 | 14.2 | 15 | 23.8 |
| Data encoder | 6 | 8.1 | 1 | 1.4 | 1 | 1.4 | 20 | 27.0 | 1 | 1.4 | 7 | 9.4 | 18 | 24.3 | 20 | 27.0 |
| Attitude control | 6 | 4.4 | 3 | 2.2 | 0 | 0 | 32 | 23.3 | 1 | 0.7 | 8 | 5.8 | 25 | 18.2 | 62 | 45.2 |
| Pyrotechnic | 1 | 4.7 | 0 | 0 | 0 | 0 | 2 | 9.5 | 0 | 0 | 2 | 9.5 | 8 | 38.0 | 8 | 38.0 |
| System wiring | 0 | 0 | 0 | 0 | 0 | 0 | 3 | 33.0 | 0 | 0 | 0 | 0 | 2 | 22.0 | 4 | 44.0 |
| Thermal control | 0 | 0 | 0 | 0 | 0 | 0 | 3 | 100.0 | 0 | 0 | 0 | 0 | 0 | 0 | 0 | 0 |
| Mechanical devices | 0 | 0 | 0 | 0 | 0 | 0 | 0 | 0 | 0 | 0 | 1 | 9.0 | 0 | 0 | 10 | 91.0 |
| Tape recorder | 4 | 5.7 | 1 | 1.4 | 0 | 0 | 15 | 21.7 | 1 | 1.4 | 8 | 11.5 | 15 | 21.7 | 25 | 36.2 |
| DAS | 11 | 20.7 | 0 | 0 | 0 | 0 | 7 | 13.2 | 8 | 15.0 | 0 | 0 | 6 | 11.3 | 21 | 39.6 |
| Trapped radiation | 7 | 13.4 | 1 | 1.9 | 1 | 1.9 | 22 | 42.3 | 2 | 3.8 | 5 | 9.6 | 4 | 7.6 | 10 | 19.0 |
| Plasma probe | 3 | 5.8 | 2 | 3.4 | 4 | 6.9 | 18 | 31.0 | 2 | 3.4 | 4 | 6.9 | 8 | 13.7 | 17 | 29.3 |
| Magnetometer | 2 | 3.6 | 2 | 3.6 | 0 | 0 | 10 | 17.3 | 1 | 1.8 | 2 | 3.6 | 9 | 16.4 | 29 | 52.7 |
| UV photometer | 2 | 3.3 | 0 | 0 | 0 | 0 | 23 | 38.0 | 4 | 6.6 | 7 | 11.6 | 4 | 6.6 | 20 | 33.0 |
| DFR | 24 | 22.8 | 0 | 0 | 0 | 0 | 41 | 39.0 | 3 | 2.9 | 8 | 7.6 | 4 | 3.8 | 25 | 23.8 |

[a]In each section, parts are given one of the following reliability status ratings:

DS = Parts that are included in the preferred parts list and are recommended for spacecraft applications.

C = Parts that are not included in the preferred parts list but are considered reliable because they are members of a preferred parts list parts family.

R = Parts that have been deleted from the preferred parts list because of either standardization efforts or part obsolescence. These parts are not recommended for use in new equipment designs.

T = Parts that are currently being tested or are members of the same family as a part being tested.

BX1 = Parts that have marginal reliability. Consideration should be given to removal of these parts from critical flight equipment.

BX2 = Parts that have undesirable reliability characteristics. Consideration should be given to removal of these parts from all flight equipment.

BX3 = Parts that have extremely inferior reliability. These parts should not be used in flight equipment.

BY = Parts for which little or no reliability information is available.

## P. System Test Complex Data System

*1. Evolution from Mariner Mars 1964 system.* Because of the successful application of a computer-based data acquisition and processing system in *Mariner* Mars 1964 systems testing (Ref. 1), its continued use was decreed for the *Mariner* Venus 67 project. However, the computer data system used in *Mariner* Mars 1964 was committed to the *Surveyor* project and, therefore, unavailable for *Mariner* Venus 67 use. It would have been possible to procure an updated copy of the same system, thus retaining the capability to use some developed *Surveyor/Mariner* software; however, certain disadvantages became evident. Most important was that the computer equipment manufactured by the UNIVAC military division was not leasable, and that the *Mariner* Venus 67 project funding constraint and project duration indicated strong advantages to the use of leased versus purchased equipment. Also, a more complete selection of peripheral equipment, communication interfaces, and data display equipment was available from leased equipment sources. In addition, maintenance and modification services are provided with leased systems, therefore simplifying system operations, modification, and personnel training. A computer lease procurement was therefore conducted, resulting in selection of the CDC 3300 basic computer, together with peripheral tapes, console, card reader, punch, and line printers. Much of the special interface equipment between computer and peripherals used in the *Mariner* Mars 1964 system was thus not required. Teletype printers used for data printout on the STC, and their associated communications controllers, were also leased for the period of need.

Figure IV-206 shows the principal elements of the computer system. The principal differences between

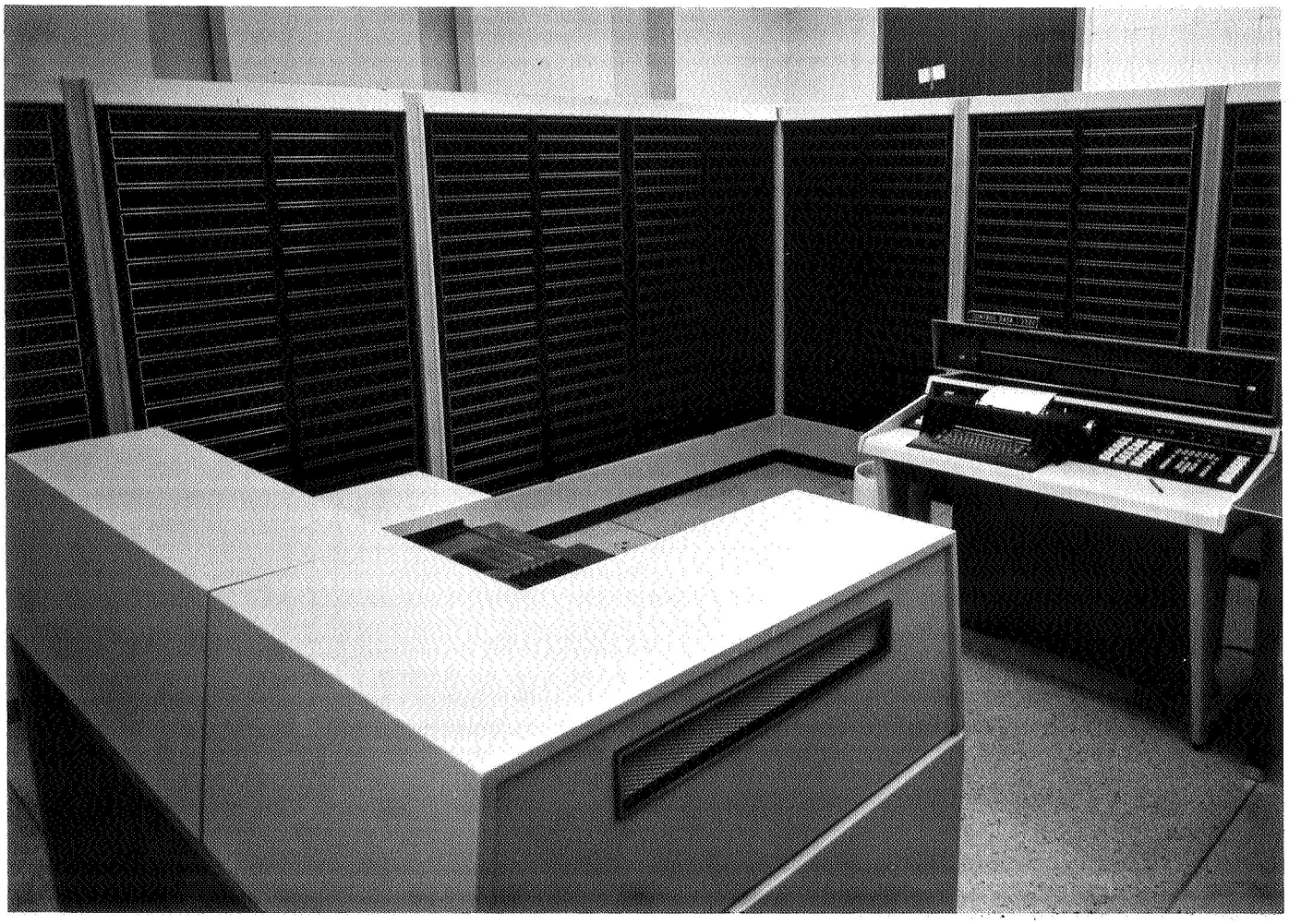


**Fig. IV-206. STCDS—CDC 3300 computer system**

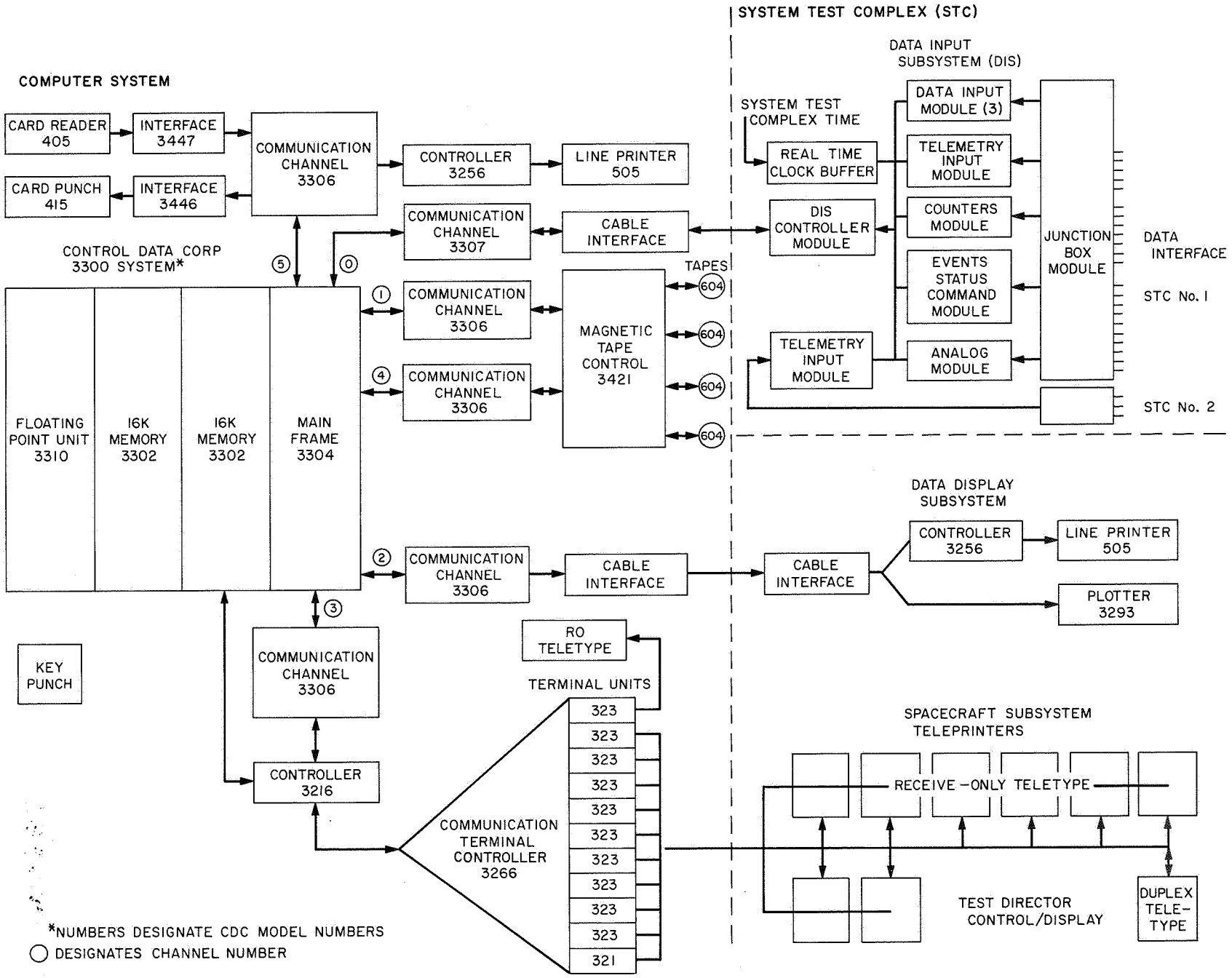



**Fig. IV-207. Block diagram—system test complex data system**

the 1967 and the 1964 computer system equipment were 24-bit rather than 18-bit word size, an increase from 16,000 to 32,000 word core memory, fully addressable memory with 1.25 $\mu$s rather than 4 $\mu$s cycle time, use of two line printers rather than one, inclusion of a hardware floating-point unit, and several additional teletype printers.

The selection of a new computer system did have the disadvantage of requiring the development of a completely new software system and support programs on a short time schedule.

*2. Configuration and system description.* A block diagram of the STC data system (STCDS) is shown in Fig. IV-207. It is functionally similar to that of *Mariner* Mars 1964 and the equipment was similarly arranged with the computer system located in the SAF, off the system test complex, with the data input subsystem and data display system located on the STC near the data sources and the spacecraft test team and data analysis. Data are acquired via data input subsystem (DIS) modules shown in Fig. IV-208.

An executive program routine (Fig. IV-209) controlled the operation of numerous separate programs associated with test data input and recording, processing control, data processing, data display, and interrupt processing and control of peripheral equipment. The executive program overhead is reduced by minimizing the length of tests required to determine whether there is a need for call-up of each particular program or routine.

Control of the program by input cards permits specifying the data streams to be processed, selection of the types of measurements and messages to be displayed on each TTY printer, and modification of data suppression and conversion constants, and limits. The real-time test support program and the nonreal-time data evaluation program are similar; however, the real-time program sacrifices processing and display functions, if necessary, to ensure that all available data are recorded, whereas the nonreal-time program ensures the completion of all processing and display functions to permit the evaluation of every recorded data sample.

All programs were written in CDC 3300 assembly language (COMPASS). The CDC real-time operating system (SCOPE) was not well adapted to STCDS executive program requirements, and was abandoned after initial attempts to use it.

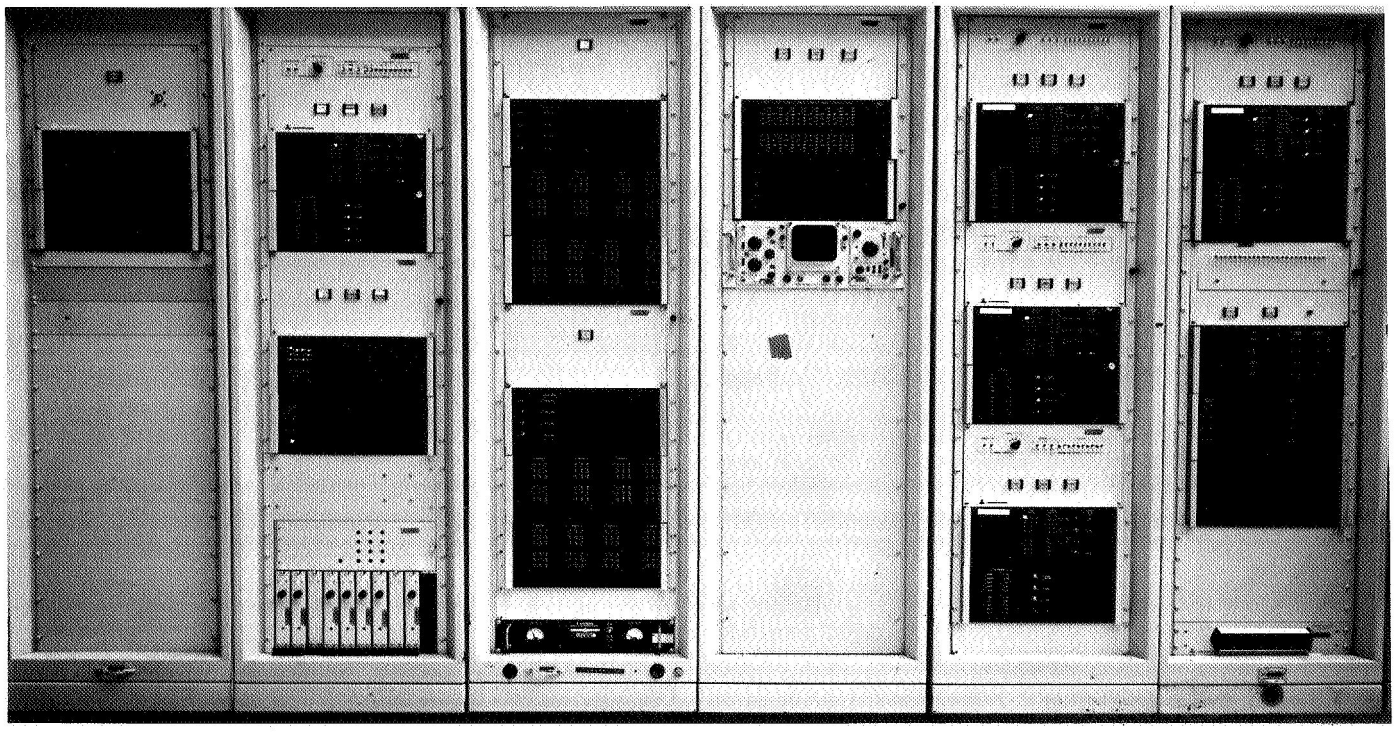


**Fig. IV-208. STCDS data input subsystem**

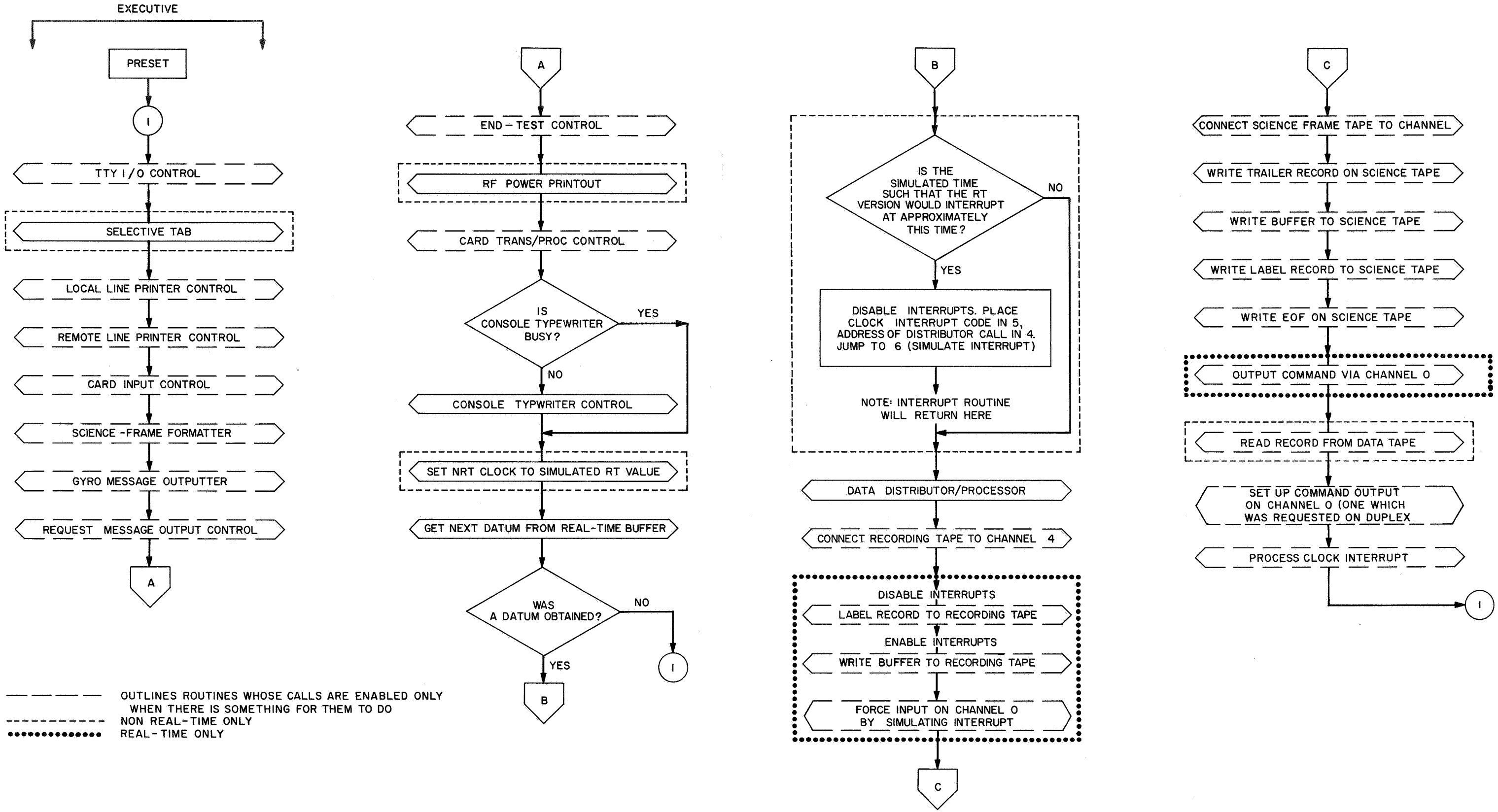



**Fig. IV-209. Executive control program flow chart**



FOLDOUT FRAME 1

FOLDOUT FRAME 2

**Page intentionally left blank**

PRECEDING PAGE BLANK NOT FILMED.

3. *Development and capabilities.* As in 1964, the *Mariner* Venus 67 STCDS objectives were limited to data acquisition, recording, processing, and display, with no spacecraft control functions exercised by the computer system. The general functional requirements of the STCDS were established by discussion with the Systems Test and Launch Operations Section. These requirements were based on experience with the *Mariner* Mars 1964 computer data system, and enabled the STCDS programmers to begin planning programming and buffer structures for data acquisition and recording, the decommutation routines for telemetry data, and the output processors for the line printer and teletype printers located on the system test complex. The standard processing requirements for telemetry and analog data, and for events and status data were well understood functionally since they were a carryover from the 1964 *Mariner* system and needed only to be adapted to the CDC 3300 computer system before coding. Subsequently, all special processing and additional requirements for processing the acquired data in real time or nonreal time were defined by a series of User Service Requests (USRs) which were approved by the system test and operations manager prior to implementation by the STCDS programming and hardware cognizant engineers. The most significant USRs were those established as new requirements for science DAS data acquisition, data recording, and processing for display on a separate STCDS line printer.

The developed system had the capability to decommutate simultaneously four data streams: GTS telemetry or data encoder hardline telemetry, DAS hardline data, DAS output to tape recorder track 1, and DAS output to tape recorder track 2. All decommutated DAS data and science telemetry were recorded on a system test experimenter's tape (STET) for off-line use in science subsystem analysis. This tape was provided to users together with experimenter's reformatting program test (XRPT) to allow generalized extraction and reformatting functions to be performed on the STET tapes. The science data also were printed on a line printer in a science analysis area located off the system test complex.

Capability was provided to handle the five *Mariner* telemetry modes, including the extraction of the equivalent of Mode 3 science data stream, from the Mode 4, Track 1 playback data. Because memory restrictions limited table sizes, only three of the four data streams listed above could be processed simultaneously for real-time display; however, this was not a particularly significant test-support limitation.

4. *Performance and problem summary.* Because of the tight procurement schedule, the approach to the design and procurement of the data input subsystem was modular; the primary data acquisition modules were obtained and integrated first, followed successively by those needed later in the test phase. As a result, integration of the later modules with the OSE on the system test complex was delayed several months because of conflicts with the spacecraft test schedule. In addition, OSE-STCDS interface circuits were late in definition, and trouble was experienced with the diverse types and levels of interfaces encountered, as was also true for *Mariner* Mars 1964.

The inability to conduct realistic tests of the low-speed analog data-input module after delivery delayed the investigation of a serious problem which prevented the use of this module in *Mariner* Venus 67 spacecraft system testing. Operation of the eight-channel high-speed analog module was satisfactory, and it was used at JPL and ETR for autopilot tests. The low-speed module problem was related to the use of reed-type relays in the multiplexer which were apparently unsuited to the actual switching application. Many of the reeds exhibited intermittent high contact resistance or failed to close at all. Even worse, there were several cases in which the contacts stuck closed, causing perturbation of all the many analog data channels being sampled by the particular section of the multiplexer in which the stuck contact was located.

A total of 35 USRs was approved. Eleven of these could not be implemented or were only partially implemented. The reasons for this deficiency were partly STCDS hardware problems including the lack of a functioning low-speed analog system, the lack of a proper interface with the RF counter in the radio subsystem OSE, and inability to input the CC&S OSE 1-pulse/s clock pulse to the computer system via an external interrupt channel. The inability to accommodate a real-time plot program in the computer because of core size limitations prevented full implementation of several USRs. Improper operation of the attitude control jet pressure transducers prevented the computer system from acquiring the data necessary to satisfy several other USRs.

The basic telemetry processing milestone was met, but software development for the subsequent capabilities, and especially checkout in the operational system configuration, was seriously hampered by unavailability of the STCDS because of test support commitments. The software schedule for later capabilities was perturbed

further by the additional science data processing and display requirements levied.

The performance of the system in terms of the computer system up-time, or availability to support system tests, is shown in Table IV-67. These performance samples were taken during continuous portions of system test support and show the improvement of computer system reliability as experience in maintenance and operation was gained and the early hardware and software failures were uncovered and fixed. By comparison, the computer data system used for *Mariner* Mars 1964 test support provided an up-time of 90% during 3730 total power-on hours. However, the up-time during periods of requested test support was 98.3%.

**Table IV-67. Computer system reliability (up-time)**

| Test phase | Failures | Down-time, h | Operating hours | Up-time, % |
|---|---|---|---|---|
| M67-1 simulator, Phase 1 | 39 | 5.4 | 176 | 97.0 |
| M67-1 simulator, Phase 2 | 21 | 1.7 | 82 | 98.0 |
| M67-2 simulator, Phase 1 | 11 | 1.7 | 168 | 99.0 |
| M67-2 simulator, Phase 2 | 2 | 0.1 | 86 | 99.9 |
| ETR operations | 19 | 0.7 | 231 | 99.8 |
| | | | 63[a] | |
| Total | 92 | 9.6 | 806 | 98.8 |

[a]Nonreal time support.

## Q. OSE Development and Use

*1. OSE system design changes.* The bulk of OSE ECRs for the conversion of *Mariner* Mars 1964 equipment to *Mariner* Venus 67 equipment was based on the new spacecraft design and correction of minor problems experienced with *Mariner* Mars 1964 equipment. Some of these problems were documented as PFRs with ECR corrective action following. Others were in the nature of upgrading changes, such as changes due to progress in technology, or changes in component availability, which normally are not related to PFRs.

Changes to the OSE system design were forced by spacecraft design changes, the availability of certain hardware required to test and communicate with the spacecraft, and the correction of problems from *Mariner* Mars 1964. These problems are briefly described in the following sections.

*a. Data input subsystem.* The computer data input subsystem (DIS) was re-designed to interface with a new computer (CDC 3300) because the *Mariner* Mars 1964 computer had been assigned to the *Surveyor* program. In addition, some DIS design changes were made as a result of a review of effectiveness of ranges and functions used on *Mariner* Mars 1964 and their compatibility with *Mariner* Venus 67 functions. This review resulted in the adoption of fewer input ranges. Consequently, fewer circuits had to be designed and procured.

*b. Science/data automation.* Design changes in this area reflected the spacecraft mission change from Mars to Venus. As a result, new science OSE evolved and television OSE was deleted.

*c. Telemetry and command processing computer.* The age of the existing TTY encoders, and the proven (on *Pioneer, Surveyor*) capability of the SDS 920 computers at the DSS sites caused the replacement of the TTY encoders with the telemetry and command processor (TCP). This change in ground handling of the data required familiarization with the new equipment before it could be used in support of the *Mariner* Venus 67 mission. Consequently, a TCP was located adjacent to the STC in SAF to act as a processor of data to be sent to SFOF for pre-mission program checkout and personnel training.

*d. Data encoder homing.* Synchronization problems with the data encoder launch complex equipment and the spacecraft data encoder were eliminated by providing individual returns to the blockhouse and eliminating the common returns in the data encoder OSE.

*e. Interface hardware.*

*System test complex.* Subsystem design changes resulted in 196 drawing changes in the STC interface hardware documentation based on 33 ECRs and 7 PFRs. A large majority of the changes were function nomenclature changes affecting drawings only; hardware changes were few. Hardware changes did, however, include new cables in the interface to the science, DIS, and TCP areas, re-wiring of STC junction boxes, and re-building of interface feed-through panels for use in the SAF,

space simulator, and checkout facility in Building AO at AFETR.

*Launch complex equipment.* Subsystem design changes resulted in 33 drawing changes in the launch complex equipment (LCE) interface hardware documentation. As in the STC, many of these changes were function nomenclature changes only, and did not affect hardware. Hardware changes, however, included several new test cables, re-wired junction boxes on the umbilical tower and in the blockhouse and launch pad OSE area, a re-wired spacecraft simulator and the addition of video pair and control line cabling to the launch complex for science and acoustic measurements.

As in *Mariner* Mars 1964, all design changes to interface hardware, such as junction boxes, were completed ahead of the LCE test schedule to allow checkout under simulated launch conditions before installation at the launch complex, thus minimizing validation time after installation.

Two umbilical catenary cables that were available from *Mariner* Mars 1964 were validated and determined acceptable for flight-support use. Design changes in this area were limited to drawing changes.

**2. *Grounding investigations.***

*a. Evaluation of instrumentation ground system.* During the testing of M67-1 and M67-2, unexplained transients caused an assortment of spacecraft performance anomalies. Included in the anomalies were data encoder deck skips and resets, noise on the medium deck readings, DAS status bit changes, DAS frame count changes, and PN bit changes.

In an attempt to isolate the source or sources of these transients, the instrumentation ground system (IGS) current was monitored. It was hoped that some correlation could be made between observed IGS transients and the spacecraft anomalies.

After the IGS was instrumented for reading of both the ac and dc levels, it became obvious that excessive currents did flow in the IGS. Moreover, the level of these currents fluctuated, adding more support to the premise that transients in the IGS resulted in spacecraft anomalies. Tests were performed on the OSE configurations at SAF, the space simulator vacuum chamber for M67-1 and M67-2, and at ETR in an attempt to lower the ground currents.

Initial ground current readings at SAF were as high as 3 A rms and 1 A dc. Sources of the ground currents were isolated and eliminated. They were:

(1) Neutral and instrumentation grounds were reversed on the secondary of the tape recorder OSE rack 116RC1 power isolation transformer.

(2) Alternating current neutral and instrumentation grounds were shorted together in the power cable of rack 116RC1.

Final ac and dc ground readings were 30 to 40 ms rms ac and 1 to 5 mA dc, respectively.

Ground currents during the space simulator tests on M67-1 were approximately 1.5 A rms and 1 A dc. No attempt was made to correct this situation.

Prior to the space simulator testing of M67-2, the OSE complex was checked in an attempt to isolate and eliminate the sources of the high ground currents. The anomalies were identified and corrected resulting in ac and dc ground currents of 25 mA rms ac and 1 to 5 mA dc, respectively. The sources of the ground current were as follows:

(1) The Franklin printer located at the test director's console.

(2) No isolation transformer on the data encoder rack 116RC1.

(3) The ground wire supplied with the commercial 3-phase power cable was connected to the power distribution OSE ground. This wire tied the OSE instrumentation ground to earth at a second point.

Because all the OSE equipment was repaired prior to shipment, no ground current problems occurred at ETR. In the ETR OSE configuration, the alternating and direct ground currents were approximately 60 mA rms ac and 1 mA dc, respectively.

With the ground currents in the 10- to 100-mA rms and 1- to 5-mA dc region, it was possible to note any major fluctuations in the IGS current levels.

*b. Summary.* As previously noted, monitoring of the IGS with the instrumentation used in the *Mariner Venus 67* program provided information about gross violations in the ground current levels. Little, if any, correlation between IGS transients and spacecraft anomalies was found because inadequacies in the IGS

instrumentation limited the system to gross rather than detailed current level readings. The major inadequacies of the IGS instrumentation were:

(1) The overall frequency response of the Hewlett Packard (HP) model 456A current probe, HP model 400E voltmeter, and the Midwestern Instruments model 102-150 galvanometer is approximately 150 Hz. A result of this low-frequency response is the loss of any recorded transients with frequency components greater than 150 Hz.

(2) The HP 456A probe has a maximum input current of 1 A rms or 1.5 A peak. As a result, all reported ground-current readings in excess of 1 A rms are questionable.

(3) The HP model 400E voltmeter reads an rms value that is proportional to the absolute average value of a sine wave. Since the ground currents were complex, not sinusoidal waveforms, the HP 400E did not give a true rms current value.

Early readings of the dc levels were in error since the HP model 428B milliammeter was subjected to ac levels that were in excess of the meter ac rejection ratio capability. The dc reading taken after the elimination of the high alternating currents reflected accurately the level and polarity of the dc current in the IGS.

*c. Recommendations.* The recommendations listed below should be implemented into any future IGS and IGS instrumentation to correct the *Mariner* Venus 67 deficiencies and improve the IGS capability as an analytic tool in the pursuit of spacecraft anomalies:

(1) A more thorough test of incoming OSE should be made to ensure compliance with JPL specifications. These tests should include the following:

  (a) Verify isolation transformer and proper isolation hook-up.

  (b) Verify that ac power neutral is isolated from OSE chassis ground.

  (c) Verify that the ac power neutral and OSE chassis ground are isolated in the power cable.

  (d) Verify that the teletypewriters have isolation transformers and that the isolation transformer shields are returned to building ground by a system other than the IGS.

(2) The HP model 400E voltmeter should be replaced by a true rms voltmeter. A better choice of meter would be the HP model 3400A rms voltmeter. This voltmeter responds to rms value (heating value) of the input signal for all waveforms.

(3) The instrumentation should monitor both the IGS cable from the spacecraft to the IGS star and the cable from the IGS star to building ground. This would help isolate the ground current transient source to the spacecraft or the OSE.

(4) The cable connecting the IGS star to building ground should not exceed 10 ft. At the thermal vacuum chamber, this cable was in excess of 30 ft.

(5) An oscilloscope and oscillograph recorder should be made an integral part of the IGS. The purpose of these instruments would be to extend the bandwidth capability of the system beyond the present 150-Hz limit.

# V. Launch Vehicle Integration

## A. Program Initiation and Definition

Program go-ahead was authorized on December 22, 1965. At the beginning of January 1966, JPL representatives visited LeRC to discuss the requirements on the launch vehicle. Preliminary agreements were reached, primarily that Lockheed Missiles and Space Company (LMSC) would be immediately authorized, under an existing LeRC contract, to develop the preliminary launch vehicle performance data needed for mission design. Spacecraft injection from a parking orbit was specified. Definition and analysis of the *Mariner* Venus 67 interface hardware was to be initiated under letter contract to LMSC, with *Agena* configuration studies to follow under routine contractual procedures. The *Mariner* Venus 67 Aerospace Ground Equipment (AGE) contract would be with LMSC/ETR as an amendment to the existing launch services contract.

The maximum available launch period, based on preliminary JPL estimates of *Atlas/Agena* capability, opened in late May and closed in late June 1967. This allowed 17 months from project go-ahead to launch. Based on the Lewis Research Center (LeRC) standardized launch vehicle procurement schedule (Fig. V-1), defining the mission-peculiar features of the launch vehicle and its interfaces with the spacecraft had to begin immediately.

While LeRC was generating work statements for LMSC and General Dynamics/Convair (GD/C), and working out the necessary contract changes, JPL was developing the detailed requirements and restraints (Ref. 16) to be placed on the launch vehicle system by the mission and spacecraft so that this information would be available in fully documented form prior to the start of interface hardware fabrication.

Preliminary LMSC vehicle performance data were provided to JPL in March 1966. Shortly thereafter, JPL mission design studies resolved the lower versus upper Venus aim point problem. The true, mission constrained, opening of the launch period was thereby established, corresponding to launch readiness on June 12, 1967. All participating agencies were so advised on March 23, 1966 by TWX (Appendix C).

*1. Ground rules and constraints.* The factors which primarily controlled the direction of launch vehicle system effort were:

(1) A firm launch readiness date of June 12, 1967 for all flight and ground-support systems.

(2) One launch vehicle.

(3) Minimum change to flight and ground equipment from the *Mariner* Mars 1964 configuration.

The influence of these constraints is pointed out later in the several areas where each had particular significance.

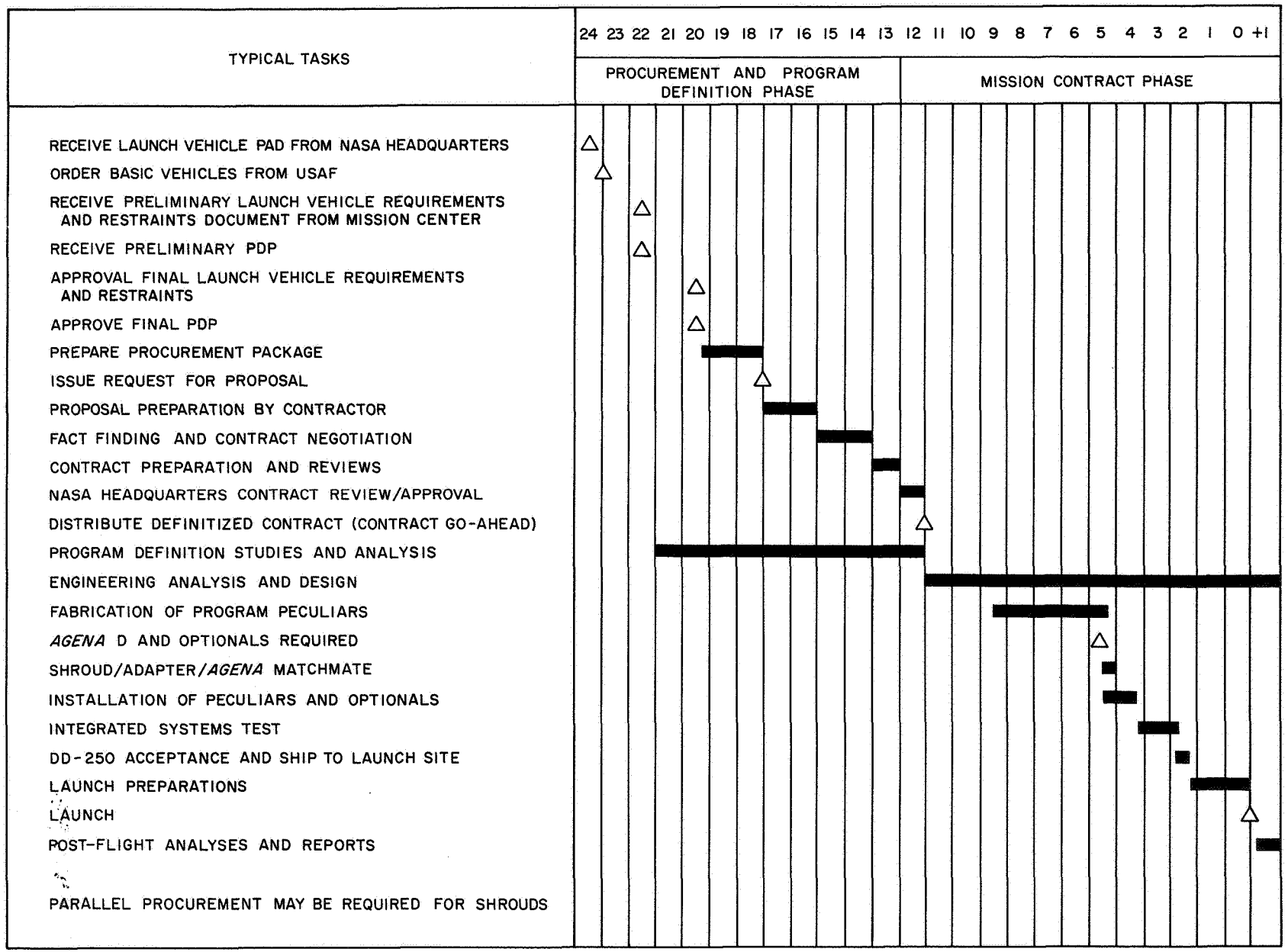



**Fig. V-1. Vehicle integration and *Agena* mission adaptation**

2. *Launch period and injection energy available.* By March 1966, JPL mission design studies showed that the useful launch period would begin on June 12, 1967, the date on which the injection energy required of the launch vehicle was near its minimum. Approximately 40% of the launch period available from the launch vehicle was therefore rejected in the interest of overall scientific value of the mission. The reason for this was an encounter constraint involving a Venus aim point dichotomy coupled with the corresponding differences in fly-by altitude and scientific yield at the planet. The 3-$\sigma$ launch vehicle energy limit would be reached 14 days later. A plot of launch vehicle energy in the standard and emergency configurations is shown in Fig. V-2 in terms of propellant reserves for each day of the launch period.

Therefore, early in 1966, the project faced a situation where no slack existed in the launch-vehicle procurement cycle, and only two weeks were to be available for launch, and only one launch vehicle would be peculiarized for the mission. A consequence of this situation was a decision by the project manager to hold weekly meetings of the system managers in addition to the weekly project meetings. A second consequence was the requirement for a contingency plan for the launch vehicle and the launch complex.

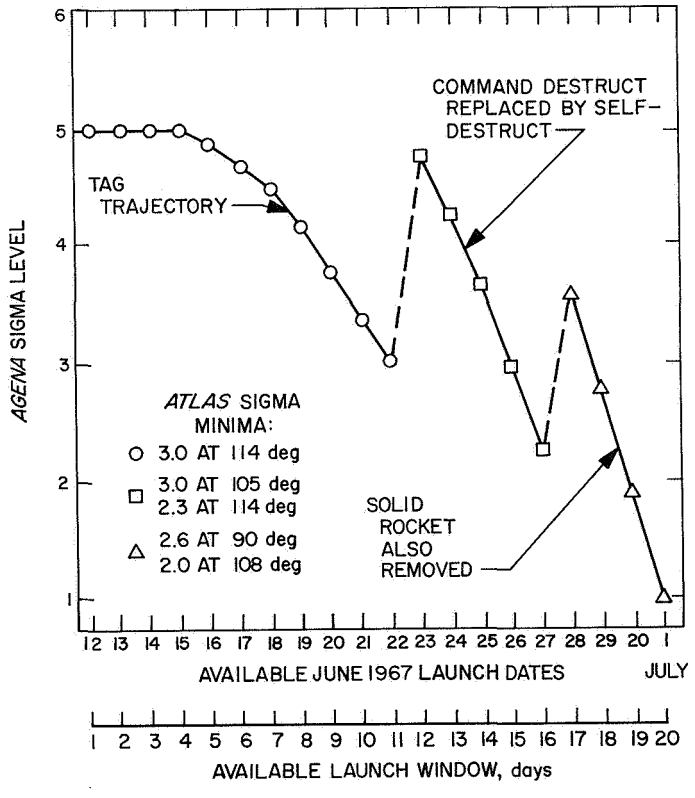



**Fig. V-2. Variation in *Agena* performance reserves—*Mariner* Venus 67**

3. *Launch readiness contingency plan.* To ensure launch within the available two-week period it was essential that the launch vehicle and its launch complex be ready on June 12, 1967, and that the inherent reliability of these systems be maximized within budgetary limits.

The first step was the establishment of a requirement for contingency planning for both of the above objectives. This action was followed by a contingency planning meeting at LeRC which included representatives from Kennedy Space Center (KSC) and JPL. Two specific stipulations by JPL were: (1) that the histories of all prior NASA *Atlas SLV-3/Agena D* launches be examined for failures and corrective actions, and (2) that an emergency extension of the 3-$\sigma$ *Mariner* Venus 67 launch period be developed, with the corresponding configuration and performance data to be published monthly by LMSC along with the 3-$\sigma$ performance.

Both LMSC and GD/C, and subsequently GE and Burroughs, were directed by LeRC to examine all aspects of their hardware and their operations to determine what should be done and what could be done to ensure launch readiness and to enhance system reliability.

Results of the studies by the four contractors and by KSC/ULO are contained in Refs. 17, 18, 19, and 20. Some of the key actions taken are summarized in Section V-F.

## B. Launch Vehicle

The basic launch vehicle provided for the *Mariner* Venus 67 mission was an *Atlas SLV-3* and an *Agena D* (SS-01B). The two *Atlas* stages for *Mariners III* and *IV* were *Atlas D* models tailored especially to meet injection energy requirements. The *SLV-3*, however, was a standardized version for use on all NASA missions using the *Agena* as the second stage.

The *SLV-3* had many subsystem level improvements, with the new transistorized autopilot as the outstanding example. Modular packaging of subsystems in the pods was substantially modified to facilitate peculiarizing the vehicle through selecting the set of peculiar and optional kits most suitable to a given NASA mission. This approach had been used on the *Agena* for many years as the result of its varying use by the USAF, both as a second stage and as an earth satellite.

The *Agena D* was the same model used for the first time by *Mariners III* and *IV*, the SS-01B. Only two *Agena* configuration changes were introduced for *Mariner*

Venus 67 in regard to mission-peculiar and optional kits: the retrorocket installation was different, and the continuous positive ullage control jet required by JPL for *Mariner* Mars 1964 was not considered necessary in view of the successful re-start history of the *Agena D* propellant containment system.

*1. Shroud.* The *Mariner* Venus 67 shroud (a nose fairing for the *Agena* and an encapsulating structure for the spacecraft) was adapted from the *Lunar Orbiter* shroud, which, in turn, was a structural refinement of the *Mariner IV* metal shroud. The latter was designed and fabricated by LMSC after the failure of the *Mariner III* fiberglass version.

The *Mariner* Venus 67 shrouds were manufactured by the Boeing Co. and modified by LMSC for the mission. LMSC patched over the *Lunar Orbiter* air conditioning door, installed an umbilical door, and provided a purge gas inlet fitting near the top of the cylindrical section. The umbilical door was designed by LMSC after closure problems were experienced on *Mariners III* and *IV*, but it had never been previously flown. The door functioned flawlessly in tests and in flight.

The basic Boeing shroud differed from the *Mariner IV* shroud primarily because it had (1) a slip joint at the intersection of the conical and ogival sections to accommodate differential expansion, (2) an improved method for retaining the polished aluminum thermal liners inside the shroud, and (3) a larger and stronger aerodynamic skirt above the shroud V-band. Eliminated from the *Mariner* Mars 1964 shroud design was the in-flight V-band tension monitoring system, and the parasitic slot antenna.

Prior to encapsulation of the spacecraft at AFETR, the shroud was cleaned for the last time in the new clean room adjacent to Building AE. This excellent KSC/ULO facility had not been available for *Mariner* Mars 1964.

*2. Adapter.* The *Mariner* Venus 67 adapters were provided by LMSC. The adapters were almost identical to the *Mariner* Mars 1964 adapter design. The diaphragm was improved by fabricating it from one sheet, however, instead of riveting two semicircular sections.

In the fall of 1966, JPL requested that brackets be added to the adapter as required to cover three protuberances which otherwise could cause the spacecraft sun shade to hang-up if it were inadvertently deployed prior to spacecraft separation. Two tests were conducted at JPL with the sun shade prematurely deployed. The second test, using LMSC-fabricated covers, demonstrated that positive spacecraft separation with noncatastrophic tip-off rates would result if the sun shade deployment springs were prematurely released.

Eliminated from the *Mariner* Mars 1964 adapter design were two of three vibrometers and the spacecraft separation rate sensing and measurement system. The separation rate system had not worked satisfactorily on previous missions. The pyrotechnic harnesses were of an improved design. A design improvement was also made in the spacecraft V-band tension readout system whereby two of the eight installation strain gages could be read on the pad by plugging in the readout console to an electrical connector installed in the outside conical wall of the adapter. As previously, the semiconductor strain gages in the two pyrotechnic release devices were wired into the *Agena* telemetry system.

The remaining flight instrumentation provided in the adapter was a vibrometer, an adapter temperature gage, and a shroud cavity pressure gage.

To reduce magnetic fields in launch vehicle interface hardware, magnetic surveys were made during the *Agena* systems test in Sunnyvale and during flight match mate tests in Pasadena. JPL demagnetization equipment was made available at ETR to ensure that flight hardware and the required assembly tools were as magnetically clean as feasible.

## C. Launch Vehicle Integration

The integration of the launch vehicle system and the spacecraft was accomplished by generating the requirements and constraints necessary for mission success.

In addition to essential daily contacts with the launch vehicle agencies involved, meetings were held periodically to resolve interface problems and to coordinate schedules. Several types of meetings were held, all of which involved the spacecraft/launch vehicle interface in some degree, as follows:

(1) Interface design and launch vehicle configuration.

(2) Launch vehicle performance.

(3) Interface planning and schedule coordination.

(4) AGE and launch complex facility modification design and scheduling.

(5) Launch vehicle design reviews.

In addition to these regularly scheduled meetings, *ad hoc* meetings were held as the occasion demanded. A contingency planning meeting was held at LeRC, and conferences at JPL were held to discuss strain gage monitoring equipment, sun shade deployment problems, and match mate test results.

Match mate tests, with both preliminary and flight hardware, were conducted at JPL and were intended to provide direct assurance of the compatibility of the hardware interface prior to encapsulation of the spacecraft at ETR. The tests were, of course, limited to measuring mechanical fit and electrical function, and hence were essentially static and continuity tests, except for pyrotechnic firings.

Assurance that other mission-peculiar modifications to the launch vehicle were adequate and compatible with the mission were not so easily obtained. Specified studies, analyses, and tests coupled with the launch vehicle design reviews, the NASA quarterly reviews, and the interface meetings at LMSC, were the primary means for developing assurance that launch vehicle hardware would meet design requirements and scheduled milestones.

## D. Launch Pad Selection and Planning

Introduction of the *Mariner* Venus 67 mission into the existing NASA launch schedules resulted in a continuing consideration of schedule adjustments and trade-offs. LeRC preferred Launch Complex 13 (LC13) for schedule reasons, but JPL preferred LC12 for operational reasons, discussed later. To immunize the *Mariner* Venus 67 launch against possible pad damage from the preceding launch, and to extend the option for either pad, LeRC directed LMSC to prepare mission-peculiar launch complex configuration drawings and to procure the necessary hardware for both LC12 and LC13.

LC12 was accepted as the primary pad with LC13 to remain as the back-up pad until ATS-A (the mission preceding *Mariner* Venus 67) was launched from LC12. If ATS-A did not damage LC12 excessively, then LC13 would be dropped as a back-up pad. If LC12 was severely damaged, then *Mariner* Venus 67 preparation would shift to LC13.

The ATS-A was launched successfully on schedule with minimum damage to LC12. The back-up pad option was thereupon dropped.

*1. Launch pad acoustic environment.* One of the technical considerations in launch pad selection was the comparative severity of the spacecraft acoustic environment as the launch vehicle lifted off and cleared the umbilical tower. LC12 has a flame bucket deluged with 26,000 gpm of water for protection, whereas on LC13, the bucket is protected by a layer of gunnite. The service tower on LC12 is rolled back in an L-shaped path before launch so that it is completely clear of the flame. The LC13 tower, however, is rolled straight back several hundred feet from the launcher, and the flame is diverted to protect the tower. The resulting effect is higher acoustic energy levels for LC13 because of the diverter and the absence of water.

Test results from the JPL instrumentation of external acoustic levels during the launch of *Mariners III* and *IV* revealed the acoustic energy differences between the two pads. Because existing *Mariner III* hardware was to be requalified to FA test levels, an adequate margin of safety would exist only if acoustic loadings during launch were no greater than would be experienced on LC12.

*2. Launch pad modifications and validation.* The *Mariner* Mars 1964 requirements on the launch complex largely satisfied *Mariner* Venus 67 requirements. The parasitic antenna in the shroud having been eliminated, the S-band parabolic antenna on the umbilical tower was changed from 10 ft in diam to 6. A second 4-ft dish was added to permit boresighting one antenna on Building AO and the other on DSS 71.

Science instruments checkout in Building AO required some changes to the video pair cabling from the launch complex. A new console was added to the JPL racks in the blockhouse for recording of acoustic levels at lift-off.

The *Mariner* Mars 1964 pad cable drawings were reviewed, corrected, and updated to incorporate *Mariner* Venus 67 requirements. Schedules were established early in the program and coordinated changes were periodically issued by LMSC. No significant problems were encountered except for a few deteriorated RF connectors in the 1⅝-in. pressurized coaxial cables.

All JPL electrical cables and connectors provided by GD/C and LMSC were re-checked and replaced where insulation resistances had fallen below specification levels. LC12 was re-validated, and no significant problems were encountered during pre-launch operations or countdown.

## E. Launch Vehicle System Problem Areas and Failures

Hardware problems were first encountered with the new Baldwin-Lima-Hamilton (BLH) V-band tension readout console during flight match mate tests in Pasadena. The BLH gear was newly procured and not yet debugged. Had the earlier test with nonflight hardware been truly a dress rehearsal as originally planned, these deficiencies plus operator problems might have become evident much sooner. The problem continued right up to launch, with much time being consumed by KSC/ULO, LMSC/ETR, and LeRC personnel in discussions of what the operational and environmental design deficiencies were, and what could be done to obtain the performance expected of the console.

The two flight shrouds and adapters were sufficiently mismatched when mechanically fit-checked at ETR that reassignment of matching articles and some rework was required, despite the fact that these articles had been matched and the fits certified as being within specification prior to shipment from Sunnyvale.

The *Agena* horizon sensor launch constraints due to sun-in-the-field-of-view were so severe, when finally analyzed, that the left head was disabled during the coast phase for every launch day targeted.

After final encapsulation of the spacecraft at ESF the shroud cavity leakage was measured at various $N_2$ flow rates. The rates were high enough so that JPL requested that the circumferential joint be taped in accordance with a prior agreement with LeRC that this option be available. Samples of the tape actually used were flown to JPL for evaluation by materials specialists. The test results showed deterioration at sufficiently low temperatures that the tape was removed from the encapsulated assembly at ETR just prior to mating the spacecraft to the *Agena*.

Launch vehicle subsystem failures occurred at ETR despite strong efforts by the involved agencies to ship top quality hardware to ETR. The guidance modules for the *Atlas* were relatively trouble-free, but severe problems with the *Agena* timer and velocity meter occurred in the final days before launch. The *Agena* propellant isolation valve seals were re-designed and successfully retested just prior to the onset of the timer and velocity meter problems.

A momentary interruption in *Agena* engine thrust had occurred on several flights prior to *Mariner* Venus 67 during either first or second burn. This anomaly was of concern to LMSC because it represented a possible failure mode. Therefore, each *Agena* flight was carefully monitored in an attempt to produce an explanation, and to evaluate the effectiveness of would-be remedies which were incorporated. Nevertheless, a momentary drop in thrust did occur in the *Mariner* Venus 67 flight during second burn.

A backup Mod III track transmitter had always been available, but had not been mechanized to permit switchover during a flight. This change was implemented under the contingency plan and tested prior to launch. The first test was unsuccessful; however, changes in the transmitter power transformer switching circuits corrected the problem as demonstrated in tracking tests using an airplane.

## F. Results

The results of the contingency planning effort are best revealed by the successful launch on the first attempt. Authorization of the contingency planning study allowed many marginal conditions to surface and become visible to system management. It also focused attention on continuing problem areas, such as spare parts provisioning and lack of adequate redundancy in the Mod III ground guidance system, for example. By no means were all of the improvements proposed by LMSC, GD/C, GE, Burroughs, and KSC/ULO authorized, but the many problem areas documented by these agencies were thoroughly discussed and the vital improvements were funded by LeRC.

The *Atlas* phase of flight was nominal, except for the late acquisition by the Mod III tracking system. A typographical error in the input data caused an erroneous setting in one of the acquisition cubes. An attitude transient was thereby induced in the vehicle, but it did not exceed the structural limits of the vehicle and was damped out.

The *Agena* phase of flight was also nominal except for the momentary (approximately 1 s) interruption in thrust mentioned previously. The timer, velocity meter, and propellant isolation valves (PIV) functioned within required tolerances. Guidance accuracy was greater than on any previous NASA *Agena* flight.

The disablement of the *Agena* left horizon sensor head after first burn and its re-connection after spacecraft separation did not cause excessive *Agena* attitude control perturbations.

Spacecraft tip-off rates at separation from the *Agena* were well within the design goals.

The *Agena* posigrade maneuver was executed within the accuracy limits established by planetary quarantine requirements.

The lift-off and flight environments were within the acoustic and vibrational limits for which the *Mariner* Venus 67 spacecraft was designed and tested.

Cleanliness of all interface hardware was demonstrated by a marked reduction in spacecraft roll transients during cruise as compared with *Mariner IV*.

The special efforts to provide magnetically clean interface hardware resulted in a significant improvement in magnetometer performance during the cruise phase.

## G. Recommendations

The following recommendations should be taken into account in future programs:

(1) More rapid means should be developed for initiating time-critical work by launch vehicle contractors in advance of a negotiated contract.

Even with Applications Technology Satellite (ATS), Orbiting Geophysical Observatory (OGO), and other contracts in existence between LeRC and the launch vehicle manufacturers (LMSC and GD/C), the most significant delays in executing the *Mariner* Venus 67 launch vehicle task were due to administrative problems associated with contract coverage. In several instances, LMSC initiated work in advance of firm contract coverage in order to avoid serious schedule slippages.

Because certain analytical studies normally performed by launch vehicle contractors are time-critical and are a necessary part of preliminary mission design due to the interplay between launch constraints and planet encounter constraints, an arrangement should be made with NASA whereby JPL would be authorized to contract directly for such studies.

(2) Continue to contract for modifications to the launch complex as done on *Mariner* Venus 67.

The new LeRC approach of contracting for *Mariner* Venus 67 AGE and launch complex facility modifications directly with LMSC/ETR rather than with LMSC/SV seemed to reduce interface problems and to accelerate the pad modification and validation schedules.

(3) Specify in top level project documentation the need for reliable spare parts and for their specific assignment to the mission.

Significant improvement was evident in the provisioning of *Agena* spare parts. The LeRC contract with LMSC specifically cited the mission-peculiar spares required. Therefore, the remaining area for improvement is to increase knowledge of, and confidence in, the standard spares which are stocked on a pooled, non-mission-identified basis.

(4) Launch vehicle agencies should make comprehensive measurements of the lift-off environment during every launch, and provide these data to mission agencies on a continuing basis.

The acoustic and vibrational environment experienced by the spacecraft during launch and during powered flight is a key factor in spacecraft design. The more accurately these loadings can be predicted, the less the conservatism which must be introduced into the flight qualification and FA tests which complex spacecraft subsystems must survive. The launch vehicle system normally provides both the sensors and the telemetry by means of which flight environmental parameters are obtained; however, the lift-off environment was measured by JPL.

Because of differences in opinion and interpretation of acoustic measurements, it is recommended that the Launch Vehicle Agency measure the external acoustic spectrum at lift-off for all launches so that the effect of changing launch vehicle configurations (*LV-3C, SLV-3, SLV-3A, SLV-3C*, etc.) can be correlated and more accurately predicted.

(5) Require more stringent FA testing of key subsystems and components.

Reliability of critical subsystems and components still remains a threat to "one-of-a-kind" missions. Even after approximately 200 *Agena* flights, new failure modes came to light in the propellant isolation valve seal, the timer, and the velocity meter. The deficiencies in design and in fabrication fortunately were identified and removed prior to launch, but under crisis conditions.

(6) Analyze incentive contracts for possible mission risks. The injection energy capability of the launch vehicle must be known within approximately one

$C_3$ unit early in a program so that the spacecraft weight budget and the launch period can be established. Prior to the generation of firing tables, however, this capability must be known with maximum feasible precision. Firing tables are generated, therefore, on the basis of tag values of stage weight and engine thrust.

Although the *Mariner* Venus 67 *Atlas* engines had been selected in September 1966, a significant decrease in guaranteed *Atlas* performance occurred in December 1966. In January 1967, a similar reduction in guaranteed *Agena* performance occurred. These reductions may have resulted from reconsideration of risks under the incentive launch contracts, rather than for such reasons as assignment of low-performance engines or measured stage weights being higher than predicted. An apparently ample contingency had been provided, and LeRC had confidently predicted that much of the contingency would eventually go toward increasing vehicle performance.

If performance incentives are included in future launch vehicle contracts, these provisions should be made known to all agencies concerned and fully understood and accepted by the principals so that spacecraft design and mission planning will not be unduly perturbed by possible reconsideration of the contractual risks and trade-offs involved.

# VI. Mission Operations System

## A. System Definition

The mission operations system (MOS) is composed of a combination of the earth-based mission-independent facilities and personnel provided by the tracking and data system, and the mission-oriented equipment, personnel, and procedures required to evaluate and direct the space flight operations of the *Mariner V* mission.

The pre-mission activities included the functional design and capabilities required, mission-related hardware and software development, development tests and personnel training, and the preparation of a flight operations plan. Post-launch operations include the analysis, decision making, and control processes for executing the required operations.

## B. System Concept and Configuration

The basic concepts of the *Mariner* Venus 67 MOS are extensions of the *Mariner IV* mission. The differences from *Mariner IV* reflect the changes in the supporting facilities (i.e., DSN) and the change in missions.

*1. Basic design guidelines.* The basic design guidelines were as follows:

(1) Use of *Mariner IV* mission-related hardware and software wherever possible.

(2) Use of new developments in the supporting facilities of the DSN such as communications processors and redesigned SFOF computers.

(3) Use of on-site (DSIF) computers to supplement and back-up SFOF computers.

(4) Use of the DSN's multi-mission support areas in the DSIF to provide flexibility in obtaining tracking support.

(5) Obtain test experience and analysis personnel training in conjunction with support of spacecraft checkout.

(6) Establish a single system for operating *Mariners IV* and *V* concurrently.

*2. MOS design team.* A design team was established to formulate and develop the MOS design and to provide the plans, procedures, and tests required. The activities of the team were coordinated by the space flight operations director (SFOD). The team consisted of: (1) SFOD, (2) spacecraft analysis and command (SPAC) director, (3) flight-path analysis and command (FPAC) director, (4) space science analysis and command (SSAC) director, (5) data processing operations director, (6) mission-related hardware (MRH) engineer, (7) DSN project engineer, and (8) other personnel as required.

The primary functions performed by the design team were:

(1) Establish and monitor the development and testing schedules.

(2) Prepare the NASA support instrumentation requirements document (SIRD) and supply inputs to the AFETR program requirements document.

(3) Prepare the space flight operations plan and space flight operations test plan.

(4) Assist in the preparation and review of appropriate inter-system interface documents.

(5) Coordinate and review requests for, and changes to, hardware and computer programs.

*3. Configurations.* Detailed discussions of the MOS operating configurations are presented in Sections VI-D and VII.

*4. Configuration control and monitoring.* Basic configuration control and monitoring were accomplished by using established change control and failure reporting techniques.

*a. Change control.*

(1) Mission-related hardware rework and refurbishment was handled under the spacecraft system engineering change requirement procedure under control of the spacecraft system engineer. A slight modification of this procedure was necessary when the MRH was transferred to the TDS for operations and maintenance.

(2) A procedure nearly identical to the DSN programming change requirements was used in computer program development. A three-phase freeze policy was adopted, that of first freezing the requirements (functional design), followed by a freeze of the detailed design, and subsequently freezing the entire program. This procedure was carried over after integration of the programs into the DSN. The procedure was controlled by the SFOD and administered by the DSN.

(3) Changes to DSN capabilities or configurations were handled by standard DSN change control procedures. These procedures were available for hardware and software in all DSN systems.

*b. Failure reporting.*

(1) The spacecraft PFR procedure was used for mission-related hardware development and checkout. After transfer of the hardware to the DSN, the appropriate DSN failure reporting procedure was used (SFOF or DSIF).

(2) The DSN/SFOF discrepancy reporting procedure was used for computer program checkout and general operations testing. After transfer of the on-site (DSIF) program to the DSN, the DSN/DSIF procedure was used for that particular program.

## C. Complementary Analysis Teams

The complementary analysis teams (CATs) provided a means for using the talents of personnel not directly assigned to flight operations, but who had detailed spacecraft or mission design knowledge. The CATs functioned as advisors to subsystem cognizant engineers in the SPAC.

The prime role of the CATs was to provide knowledgeable support on specific problem areas, with no specific operational function to perform. Secondary roles were:

(1) To provide a focal point for sustained interest and information on the part of the design, development, and management personnel during the flight operations phase.

(2) To provide some orientation and training for the design and development personnel on the problems encountered in flight.

(3) To provide potential replacements for operations personnel in SPAC.

Since the prime role of the CATs is to support individual analysts and not be a direct part of operations, this, in effect, dictates an organization based on technology and line organization discipline. For this reason, the CATs were associated with the line organizational structure. Each technical division manager appointed a CAT coordinator who was responsible for all planning activities and the direction of the CAT during the flight. The CAT coordinator also provided liaison between the CAT and the SPAC analysts.

Data handling and voice communications equipment similar to the SPAC equipment were provided to each technical division CAT area (Fig. VI-1).

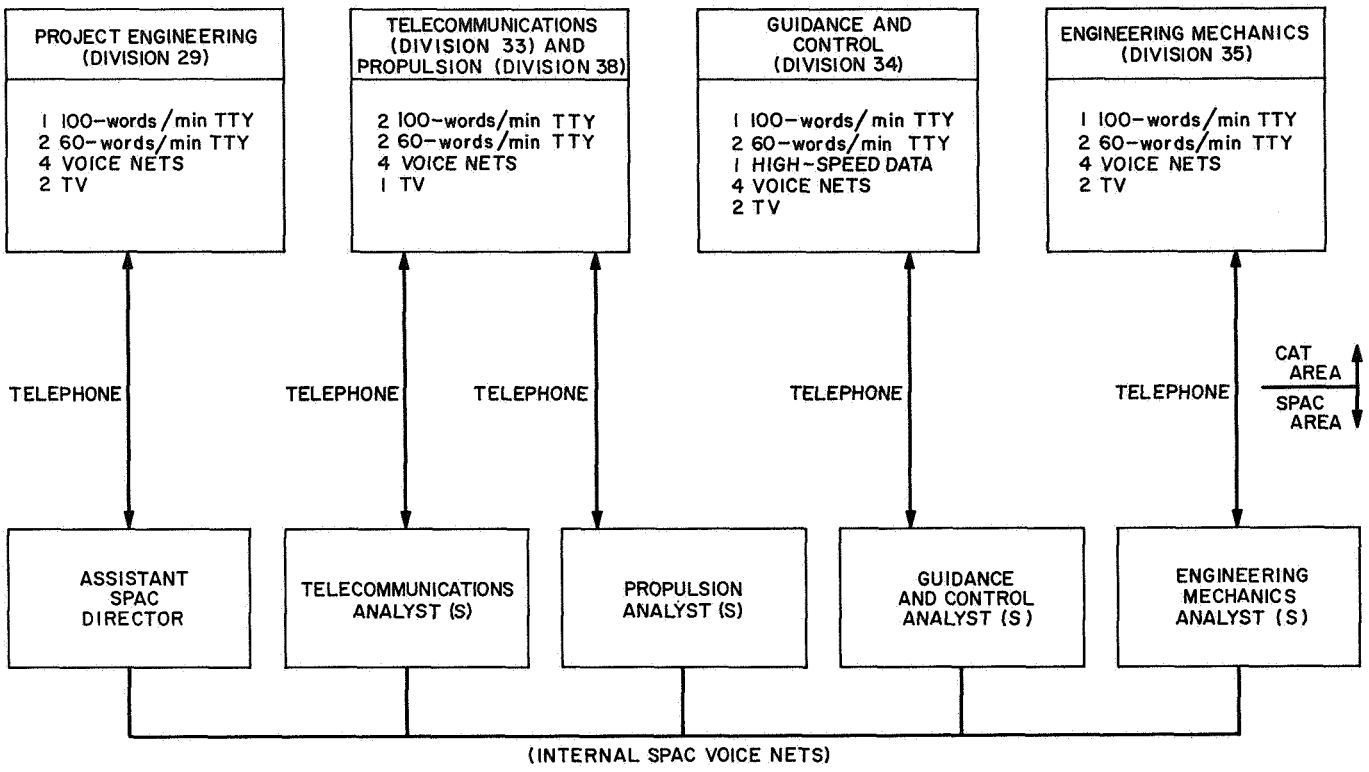



**Fig. VI-1. CAT equipment provision**

This equipment included the following:

(1) 100-words/min computer-driven TTY.

(2) 60-words/min standard TTY.

(3) Appropriate voice networks (listen only).

(4) TV displays.

(5) High-speed data line.

The TTYs were slaved to the subsystem (or divisional subsystem group) machines in the SPAC. The TV displays provided mission time and ground communications status. The high-speed data line fed a digital-to-analog converter for strip chart display in the guidance and control division CAT.

## D. Mission-Related Hardware Development

*1. Ground command subsystem.* The MRH from the *Mariner* Mars 1964 mission was returned by the various DSIF stations for refurbishment and modification as required to adequately support the *Mariner* Venus 67 mission. This section describes the ground command subsystem (RWV) equipment condition, incorporated modifications, refurbishment, new modifications, testing, and recommendations for the equipment's use, if required, for future missions.

*a. Equipment condition.* The equipment condition can be described by considering two primary aspects: physical and operational condition of the equipment. These aspects are described in the following paragraphs.

*Physical condition.* The physical condition is essentially the condition of the units when uncrated after receipt from the various locations. These statements may not apply to all units specifically, but, as generalizations, are applicable to the RWV refurbishing effort. The received physical condition indicated that little care was taken when the units were packed for shipment.

In general, the commercial equipment within the consoles was in operating condition, although all units required calibration. Most units had not had any preventative repair, maintenance, or calibration since 1965.

After completion of an initial inventory, it became apparent that parts had been removed from the RWVs

to supply equipment for other station requirements. Without considering spares, equipment shortages were as follows:

| *Equipment* | *Quantity* |
|---|---|
| Time display | 5 |
| Monitor receiver | 9 |
| Counter | 3 |
| Oscilloscope | 3 |

The monitor receivers were deficient in two areas. Each receiver has a front panel switch that allows selection of one of five different received frequencies. There appeared to be no standardization as to what these frequencies should be. Also, all units were out of specification on the signal/noise ratio measurement at the receiver front end, due to poor alignment of the receivers.

*Operational condition.* Upon receipt, the RWVs were given a basic operational check. This check showed the following conditions to exist in all units:

(1) Many front panel indicators were inoperative because light bulbs were burned out.

(2) Field modifications which were supposed to have been made were not.

(3) Wiring errors existed in some units.

(4) Seven of the thirteen RWVs were capable of transmitting commands. In the remaining six, command transmission was prevented by detector failure in three units, a wiring error in one unit, a power supply failure in one unit, and logic failure in one unit. The operating RWVs were not free of failures, but they were capable of transmitting commands.

*Incorporated modifications Mariner Mars 1964.* Results of the modification checks disclosed many *Mariner* Mars 1964 modifications were either incorrectly made or not made at all. These deficiencies were corrected during the *Mariner* Venus 67 refurbishment effort. During the detailed operational checks, the RWV modulator and detector were re-aligned, and the machine was exercised through all of its operating modes. During these checks, only a minimal number of wiring errors were found, but many component failures were located and repaired. These failures are shown in Table VI-1. No PFRs were written on burned-out front panel displays or on problems known to be caused by the operators.

**Table VI-1. Ground command subsystem PFR summary**

| PFR description | Quantity |
|---|---|
| System description | 13 |
| Shorted transistors | 18 |
| Open transistors | 5 |
| Degraded transistors | 1 |
| Contaminated transistors | 1 |
| Open clamping diodes | 4 |
| Open logic diodes | 5 |
| Shorted logic diodes | 2 |
| Logic indicator bulbs | 15 |
| Power supplies | 2 |
| Open crystals | 2 |
| Perforators | 2 |
| Open capacitor | 1 |
| Coaxial relay | 1 |
| Faulty PCB etch | 1 |
| Wiring | 2 |
| Faulty connector | 1 |

Upon completion of testing, all commercial equipment was removed from the RWVs and sent to Goldstone for preventative maintenance, calibration, and cleaning. Remaining mechanical and electrical deficiencies were repaired, and the commercial equipment was presented for QA inspection. At that time complete, unmodified, working RWVs existed.

*b. Refurbishment.* Refurbishment of the RWVs began with a detailed test of all units. This test had two primary objectives. The first was to verify that the 29 *Mariner* Mars 1964 modifications installed in the units previous to this effort were installed properly. The second was to verify that the modified RWV was operating correctly.

*Modifications.* Operation of the RWV and station reports indicated that there were areas where the RWV was deficient and needed modification. Modifications were incorporated in the RWV to alleviate the undesirable conditions that existed. All but one of the modifications incorporated were done on the authority of ECRs. The non-ECR modification involved the changing of the RWV monitor receiver's frequency coverage.

*Testing.* The completion of the refurbishment of the RWVs consisted of installing any missing commercial equipment and the running of two tests on each unit. These tests included an FA test and an RF check.

The FA tests were witnessed in all cases by a DSN-appointed representative. The purpose of this test was to show that the unit under test performed correctly.

RF checks were performed to prove that the phase of the RWV output was of the correct sign so that the flight system would lock to the received command modulation. If this signal was inverted, the command system would fail to lock and no commands could be transmitted to the spacecraft. These tests were performed using a command modulation checker (verified in SAF to simulate the spacecraft command detector). All units passed this test.

*Problem failure reports.* During the refurbishment effort for the RWVs, all component failures were documented through the JPL PFR system (67 reports were written). Table VI-1 groups the failures in categories. There are more failed components than PFRs because some PFRs accounted for multiple component failures.

Several of the groups of failures listed in Table VI-1 warrant additional discussion. These are the PFRs concerning shorted transistors, open logic indicator bulbs, and the power supplies. All transistors which have failed are of the alloy junction type, typical of the state-of-the-art in the mid 1950s. The mode of failure of these transistors is an over-voltage punch-through of the base, leaving a solder bridge connecting the collector and emitter junctions. The RWVs were investigated to find whether over-voltage conditions were present, but none were found, either in normal operation or during power switching. Even if power supply failures are postulated, which would allow maximum available voltage to be applied to the system power busses, the rated transistor voltages would not have been exceeded. Discussion of these failures with the components evaluation group indicates that component degradation with age could allow these failures to occur.

Two power supplies failed while in operation with the RWV. The cause of failure in both supplies was over-voltage punch-through of the series regulator transistor. As before, investigation showed no over-voltage conditions to exist. It is therefore postulated that component degradation of the transistors was at least the initial cause of the failures. These failures become important when it is realized that this type of failure does not blow the power supply fuse and does apply maximum voltage to the power bus. It is probable that these power supply failures have caused secondary failures within the systems by over-rating degraded components. Logic indicator bulbs are in general use within the RWV to show the state of flip-flops. These bulbs are actually implemented in the circuits as collector load resistors in the active portion of the flip-flops. These bulbs are run at lower-than-rated voltage to extend their operating life, but they do burn out. Each bulb failure disables some operating portion of an RWV.

*c. Test equipment.*

*Command modulation checker.* The command modulation checker is used to simulate the spacecraft for the purpose of verifying that command modulation is of the proper phase. This unit consists of a modified *Mariner R* transponder, flight command detector, and a command decoder. It was designed to operate from an internal battery or 110 V ac external power.

Investigation of this unit showed several problems. The first was in the voltage regulator. This unit, as wired, operated like a diode. When wired correctly, there was insufficient voltage across the series regulators (two existed) to allow proper regulation.

*d. Recommendations.* The success of the *Mariner* Venus 67 mission at times was dependent upon the command transmission capability of the DSIF stations. These, in turn, depended directly on the successful operation of the RWV. As such, the RWV should be a relatively reliable piece of equipment. There are many areas where the reliability of this machine can be improved. Recommendations covering these areas are discussed in the following paragraphs.

As previously discussed, the logic indicator bulbs are in the active portion of their respective circuits. These bulbs should be replaced with resistors or a new line of logic cards that would remove the indicator lamps from the active circuitry.

The transistors used throughout the RWV are of an alloy junction type that were state-of-the-art when the RWVs were first built. The PFRs written against these units seem to indicate that the transistor junctions are degrading. A study should be undertaken to determine whether this is the case and, if so, all transistors of these types used in the RWV should be replaced.

The 2N1544 transistor failures occurred in the RWV main power supply. As explained previously, when these transistors fail, excessive voltage is applied to the power buses which can cause secondary failures. If these failures occur in critical circuitry, a main power supply failure can disable emergency mode command capability of the RWV. The power supplies in the RWV should be replaced with units that have both over-voltage and high-current protection capabilities. High-current protection protects

the power supply while over-voltage protection protects the RWV circuits.

The emergency mode implementation of the RWV should be improved to allow error detection if a power supply failure occurs. This can be done by extending the capability of the emergency power supplies to cover the total system capacity. In the advent of power supply failure, power would be switched and command transmission would continue in a normal fashion.

With the elimination of logic indicator bulbs, a second emergency mode improvement becomes imperative. Some type of binary or octal display must be included to display the emergency register contents. There is no other check to verify the correct operation of this register.

Several of the potentiometer adjustments necessary to align the RWV modulator and detector are marginal. The adjustments should have higher resolution for more accurate alignment. These adjustments are of the threshold detector in the detector synchronization channel and the ratio adjustments of the modulator amplifiers.

**2. *Ground telemetry subsystem.*** The MRH from the *Mariner* Mars 1964 mission was returned by the various DSIF stations for refurbishment and modification as required to adequately support the *Mariner* Venus 67 mission. This section describes the ground telemetry subsystem (GTS) equipment condition, refurbishment, modifications and testing.

*a. Equipment condition.* The equipment condition can be described by considering two primary aspects: physical and operational condition of the equipment. These aspects are described in the following paragraphs.

*Physical condition.* The physical condition is essentially the condition of the units when uncrated after receipt from the various locations. These statements may not apply to all units specifically but, as generalizations, are applicable to the GTS refurbishing effort. The received physical condition indicates that little care was taken when the units were packed for shipment. The following are typical of the problems noted:

(1) Consoles were dented and paint was chipped.

(2) All units were very dirty.

(3) The drawer tracks on some consoles would not operate, or drawer locks would not catch.

(4) Protective caps were missing on many connectors.

(5) Light bulbs, switches, connectors, and cable clamps were loose.

(6) Some mounting screws and other small hardware items were missing.

(7) Some units had missing equipment.

*Operational condition.* There were three GTS configurations:

(1) Eight DSN/GTSs which consisted of one 2-bay rack of equipment that was used at the DSIF tracking stations to process the receiver output.

(2) Two STC/GTSs which consisted of five bays, two 2-bay racks, and one 1-bay rack of equipment that were used on the spacecraft test complex to check out the spacecraft before launch.

(3) An SFOF/GTS which consisted of a 1-bay rack of equipment that was used in SFOF to process data from the high-speed data lines as a backup for the 7044 computer.

Six of the eight DSN/GTSs would perform the basic functions of demodulating the composite signal and, in turn, decommutating the demodulator output and printing it out on the printer. Of the two GTSs that did not work, one had been damaged while in transit and the other had a data programmer problem.

The STC/GTSs were in approximately the same condition as the DSN/GTSs. For example, four 6122 amplifiers and mounts were missing from one of the STC/GTSs. This delayed the schedule on that particular GTS for several weeks until a replacement for the missing equipment was located. Also, the single-bay racks of each STC/GTS had unauthorized modified wiring. As a result, the wiring in these racks had to be re-installed.

Because the SFOF/GTS had been refurbished and modified separately from the other GTS units, there is very little information available regarding its initial condition.

The SFOF/GTS contains a decommutator, data programmer, and printer. It receives non-return to zero (NRZ) data, bit synchronization, and word synchronization from the digital-to-analog converter (green box) in SPAC which, in turn, receives its input from the high-speed data lines from the DSIF stations. Some modifications (such as the addition of the BCD time input) were performed on the

SFOF/GTS to make it compatible with the green box interface. No documentation existed on the inter-rack wiring for the SFOF/GTS, nor does any exist at this time. The mode 3 modification was incorporated into the decommutator and data programmer of the SFOF/GTS.

*b. Refurbishment.* The refurbishment of each GTS generally involved the following basic steps:

(1) A preliminary electrical check and preliminary QA inspections were made to determine the initial condition of the equipment.

(2) The equipment was then disassembled, cleaned, re-calibrated, modified and re-assembled.

(3) Electrical checks were then made to ensure proper operation of the equipment.

(4) After the electrical checks, QA made a final mechanical inspection of the equipment.

(5) The FA test was then performed on the equipment in the presence of a DSN representative.

After the initial inspection and checkout, each console was dismantled and given a thorough cleaning. The paint was touched up where required. The commercial equipment in the GTSs (such as oscilloscopes, counters, amplifiers, etc.) were calibrated. All of the digital printers were checked.

A major calibration effort was performed on all the data demodulators. All of the filters in the plug-in units were re-tuned. This was necessary in some cases so that the demodulator would pass the bit error tests. All other adjustments in the demodulator were checked and re-adjusted where necessary. During the calibration of the demodulators, it was found that the conformal coating on the demodulator printed circuit cards had run inside some of the potentiometers, causing the wiper to have intermittent contact with the resistor. As a result, all potentiometers in the demodulator were carefully checked for any intermittent conditions and changed when such a condition was found. The interrack wiring was verified on all DSN/GTSs to ensure compatibility with the documentation.

*Modifications.* Modifications were made to the DSN and STC GTSs to correct known deficiencies or problems. All modifications were made on the authority of ECRs.

*Testing.* Upon completion of the modification installation, each GTS was re-assembled, and checked out electrically. After the GTS was operating properly, QA made a final detailed inspection. Discrepancies found by the final QA inspection were corrected and the GTS was then given a final acceptance test.

*Problem/failure reports.* During the refurbishment effort, 34 PFRs were written on the GTSs (Table VI-2). The majority of the PFRs were written on failures discovered during the final acceptance tests. Several dozen transistors and light bulbs were discovered to be bad during the clean-up phase of the refurbishment, which was not under PFR control. Most of these failures occurred in the decommutator.

**Table VI-2. Ground telemetry subsystem PFR summary**

| PFR description | Quantity |
|---|---|
| Initial QA inspection results | 9 |
| Transistor failures | 9 (total: 26 transistors) |
| Diode failure | 1 |
| Miswiring | 3 |
| Bad solder joints | 3 |
| Lamps burned out | 1 |
| Power transformer shorted | 1 |
| Bad RFI filter | 1 |
| Card misalignment | 1 |
| Drawer misalignment | 1 |
| Wrong component in isolation switch (manufacturing error) | 1 |
| Broken wire | 1 |
| Extra resistors in lamp driver | 1 |
| Corrosion of transistor leads | 1 |

The last category in Table VI-2 (corrosion of transistor leads) refers to two dual transistors located on the phase detector cards in the demodulator. In several cases the corrosion was so severe that the leads would break with only a slight touch.

The transistors were mounted upside down with the leads bent down into the printed circuit board. The leads were insulated with Teflon sleeving. Failure analysis pointed out that, during the soldering process, flux vapors (probably ammonium chloride) were generated and rose into the Teflon tubing. The conformal coating when applied sealed off both ends of the tubing. The chlorine then reacted with the leads, causing them to deteriorate. All dual transistors on all phase detector cards were replaced and the tubing was left off of the leads.

*c. Spares.* The majority of spares for the *Mariner* Venus 67 MRH came from the *Mariner* Mars 1964 mission and were returned by the various DSIF stations for refurbishment and modification.

*Equipment condition.* The equipment condition can be described by considering two primary aspects: physical and operational condition of the equipment. These aspects are described in the following paragraphs.

*Physical condition.* Arrival inspection disclosed that the heavy equipment had torn lose within the shipping boxes, damaging both the equipment and the boxes. In some boxes with drawers, continual vibration had loosened screws holding the drawer sliders, causing the drawers to tilt, jam, and spill their contents. Much of the equipment was damaged, partially because of careless packing methods and partially because of careless handling during transit. Many of the GTS spare parts and cards were packed without protection between adjacent units.

*Operational condition.* The bulk of the spares effort centered with the spare printed circuit cards. Of the 2700 received, and as per spares criteria, 965 were tested electrically to determine their operational condition.

*Refurbishment procedure.* The printed circuit cards were inventoried as they arrived, and were placed systematically on holding racks. This arrangement made all cards quickly accessible and also protected them from further damage. A card file was generated to facilitate bookkeeping on each type of printed circuit card. This card file contained the printed circuit card assembly number, a list of *Mariner* Venus 67 MRH equipment in which the card was to be used, the quantity of cards required for spares, an inventory of cards received, the quantity of cards which had been electrically tested and determined "good," and the quantity of cards which had been electrically tested and determined "bad."

Approximately 2700 cards were received and inspected by QA as they were placed on the racks. Each printed circuit card was stamped "OK" if accepted by QA, and an inspection report (IR) was generated for any discrepancy. All discrepancies were corrected before the card was stamped by QA and accepted for use in the spares program.

There were 175 different types of printed circuit cards produced by six different manufacturers. Although 2700 cards were inventoried, only 965 cards were electrically tested and shipped to the overseas stations. Another set of spares was also generated for use in SAF.

Two additional spares kits were sent to the DSN at Goldstone. These two kits were to be tested by the DSN personnel at the Goldstone repair depot, and one set of spares was to be shipped by the DSN to DSS 51. The second set of spares was to remain at the Goldstone repair depot as back-up spares.

Although circuit cards made up the bulk of the spares effort, power supplies, transformers, amplifiers, etc., also required inspection and testing.

Another category of spares included small items such as connectors, crimping tools, inductors, small transformers, lamp bulbs, fans, etc. Because some of these items were not returned by the DSN, it was necessary to purchase new parts as replacements. Most of the purchased parts were received prior to the initial spares shipments to the DSN stations. Other parts arrived after the initial shipment and were then shipped to the stations for addition to the spares kits.

Resistors, small capacitors, transistors, diodes, etc., were not distributed. DSN stocks of piece parts were considered adequate for emergency repairs at the overseas stations. Normal repair procedure was to return failed units to the Goldstone repair depot where equipment and personnel were available for complete repairs.

An effective equipment maintenance program requires not only spares, but also an arrangement that permits the desired ones to be located and removed with ease, as the need arises.

To allow the DSN stations to organize the spares upon receipt, each part was identified by item number, part number, and the part nomenclature or description.

All RWV MRH spares were boxed separately from the GTS MRH spares. The packing operation was observed by QA and quantities of parts verified by them. Any shortage due to unavailability of parts was noted and these were sent in a later shipment to the stations.

*Testing.* Because no procedures or fixtures were available for testing of spare cards, it was necessary to devise some. The test fixture used was not elaborate or devoted to operator convenience because of the tremendous variety of cards involved, the small quantity of each type of card required, and the lack of time to design such a fixture. The fixture was comprised of a chassis with an

appropriate card connector mounted on it. Each terminal of the connector was accessible by banana jacks. Any signal could be placed on any pin with the use of commercially available test equipment. A separate test fixture was built to accommodate each type of card connection. About 90% of the MRH spare cards were tested in this manner, with the exception of a few of the analog type cards which could not be conveniently tested by this method and were tested by RWV and GTS equipment operators in the equipment itself.

Because of the inaccurate estimates at the beginning of the spares effort on the quantity of each card type required, a greater number of cards was tested than required. A total of 1683 cards of all types were electrically tested and 137 of these had electrical problems. This represents approximately 8.8% of the cards tested as being unacceptable.

*Recommendations.* The testing and shipping of spares could have been accomplished more efficiently. The primary disadvantages encountered were:

(1) Testing and shipping of spares was conducted at a location away from where MRH equipment personnel refurbished the equipment.

(2) A shortage in personnel existed at the beginning of the program.

(3) QA inspectors were shifted during the program. This required training of new personnel.

(4) Spares program was initiated before requirements were clearly defined.

(5) The spares card requirements of a MRH program were defined late during the program (this is particularly true of the GTS).

(6) Documentation of the GTS was incomplete (modifications were not fully documented on cards and only some of the manuals contained circuit operation theory).

**3. *MSA digital-to-analog converter.*** Real-time analog display of guidance and control spacecraft functions were required in the SPAC and Guidance and Control Analysis Team (GCAT) areas during critical portions of flight (i.e., launch, sun acquisition, star acquisition and identification, and trajectory correction maneuvers). Most of these engineering displays were required in real time to verify proper operation and to apply corrective action to the spacecraft if necessary. It was essential that these spacecraft critical measurements be available with minimum delay and with the highest probability of occurrence. For these reasons the digital-to-analog converter (D/AC) and recorder were supplied to SPAC and GCAT for support during the *Mariner V* flight (Fig. VI-2). The D/AC and recorder interfaced directly with the high-speed data line from each DSN site.

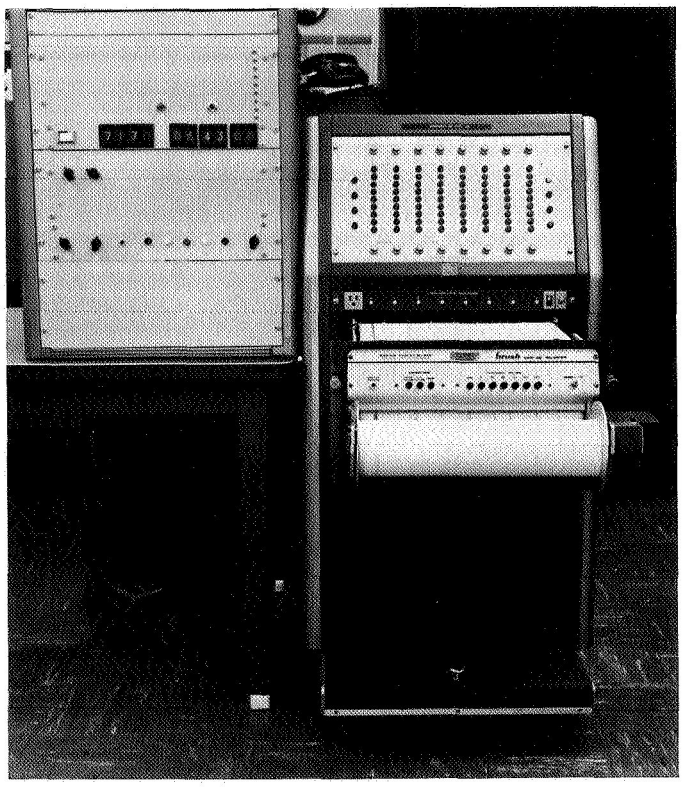


**Fig. VI-2. D/AC (left) and output recorder in GCAT facility**

As part of the *Mariner IV* CC&S project, a D/AC was designed to display certain engineering telemetry data channels on an eight-channel analog recorder. This analog display was implemented for the purpose of real-time, quick-look, spacecraft engineering status (particularly in regard to the AC subsystem during acquisition and midcourse maneuver phases of the flight). Since this display proved quite valuable during the *Mariner IV* flight, it was therefore incorporated into the *Mariner* Venus 67 project.

Because of a major change in the spacecraft data handling by the DSN, the D/AC designed for *Mariner IV* had to be redesigned for *Mariner* Venus 67 (Fig. VI-3). This redesign was so extensive that it was decided to build all new equipment rather than modify the existing unit. Also, since SPAC and GCAT were to be located in different buildings, an additional D/AC was needed.

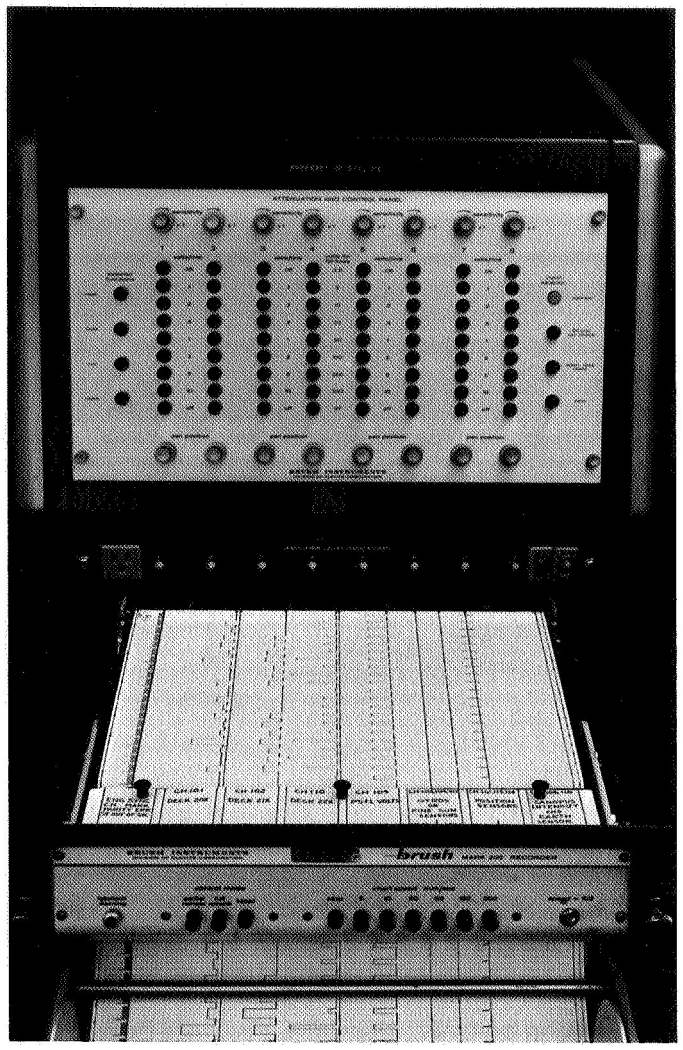



**Fig. VI-3. D/AC (close view)**

The D/AC was designed to provide:

(1) Analog recorded display of the engineering telemetry channels associated with:
   (a) The three subcommutated channels.
   (b) Pitch, yaw, and roll gyroscope outputs.
   (c) Pitch, yaw, and roll position sensor outputs.
   (d) Canopus intensity.
   (e) Earth sensor output.
   (f) Power switching and logic (PS&L) voltage.

(2) Digital recorded display of time when operating from the high-speed data line (HSDL).

(3) Recorded display of deck synchronizations and channel markers.

(4) Nixie display of event register status and time.

(5) Compatibility with both *Mariners IV* and *V* telemetry data.

(6) Word synchronization, bit synchronization, and information associated with the seven bits of spacecraft data to be used by external decommutating equipment, e.g., GTS and science.

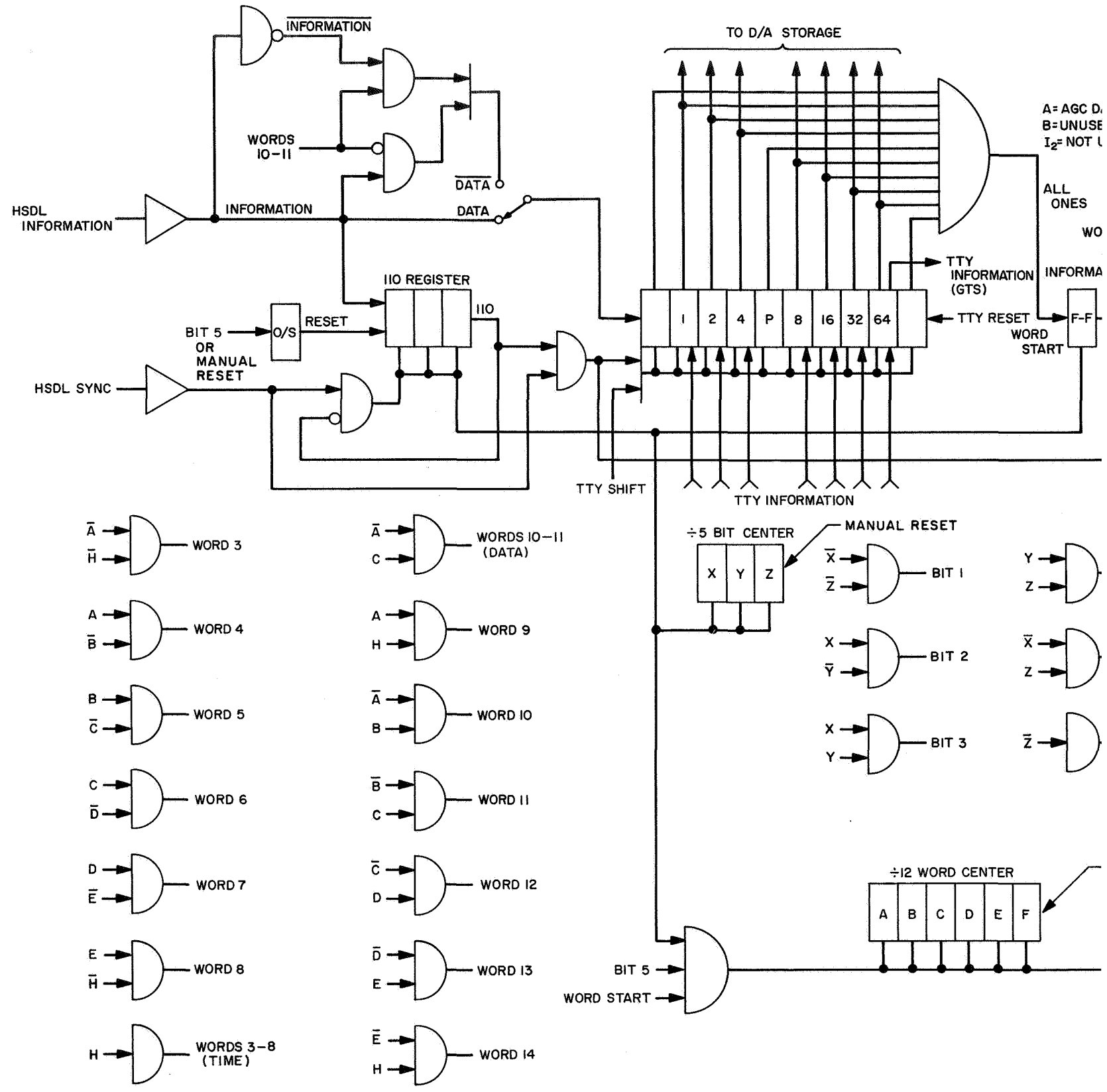
(7) HSDL station AGC as an analog output for remote recording.

*a. High-speed data line logic.* The primary mode of operation for the D/AC is associated with obtaining telemetry data from the HSDL from the DSN. The D/AC used in SPAC has the additional capability of operating from the TTY data if high-speed data are not available.

Figure VI-4 is a block diagram of the HSDL logic and illustrates the HSDL format for each data block associated with the spacecraft telemetry data. One HSDL data block is associated with each channel of spacecraft data. Each data block consists of 14 words of 5 bits, preceded by a 110-synchronization pattern. The first two words in this data block are all ones and are used as the data block synchronization, whereas the 110-synchronization pattern is used as the individual word synchronization. The HSDL has two outputs: digital information in accordance with Fig. VI-4 and a 1200-Hz-square wave synchronization signal.

After the first two words have been received as the data block synchronization, and the 110 pattern is recognized for each succeeding word, the 1200-Hz synchronization signal is used to count down a divide-by-five bit counter. Each state of this bit counter corresponds to one of the five information bits associated with each word. Each time the bit counter cycles through five bits, it steps a divide-by-twelve word counter. Each state of this word counter corresponds to one of the twelve data block words following the data block synchronization. By selecting the appropriate word and bit time from these counters, each bit of data within the data block can be extracted and processed as desired.

Word 3, bit 1 identifies the data block as either a spacecraft telemetry channel or as a station AGC measurement. If this particular bit is a "one," the AGC flip-flop is set; if it is a "zero," the spacecraft word flip-flop is set. Word 3, bit 2 is not processed by the D/AC. Bits 3 and 4 contain the BCD data for tens of hours. Bit 5 in each word is a






FOLDOUT FRAME 1

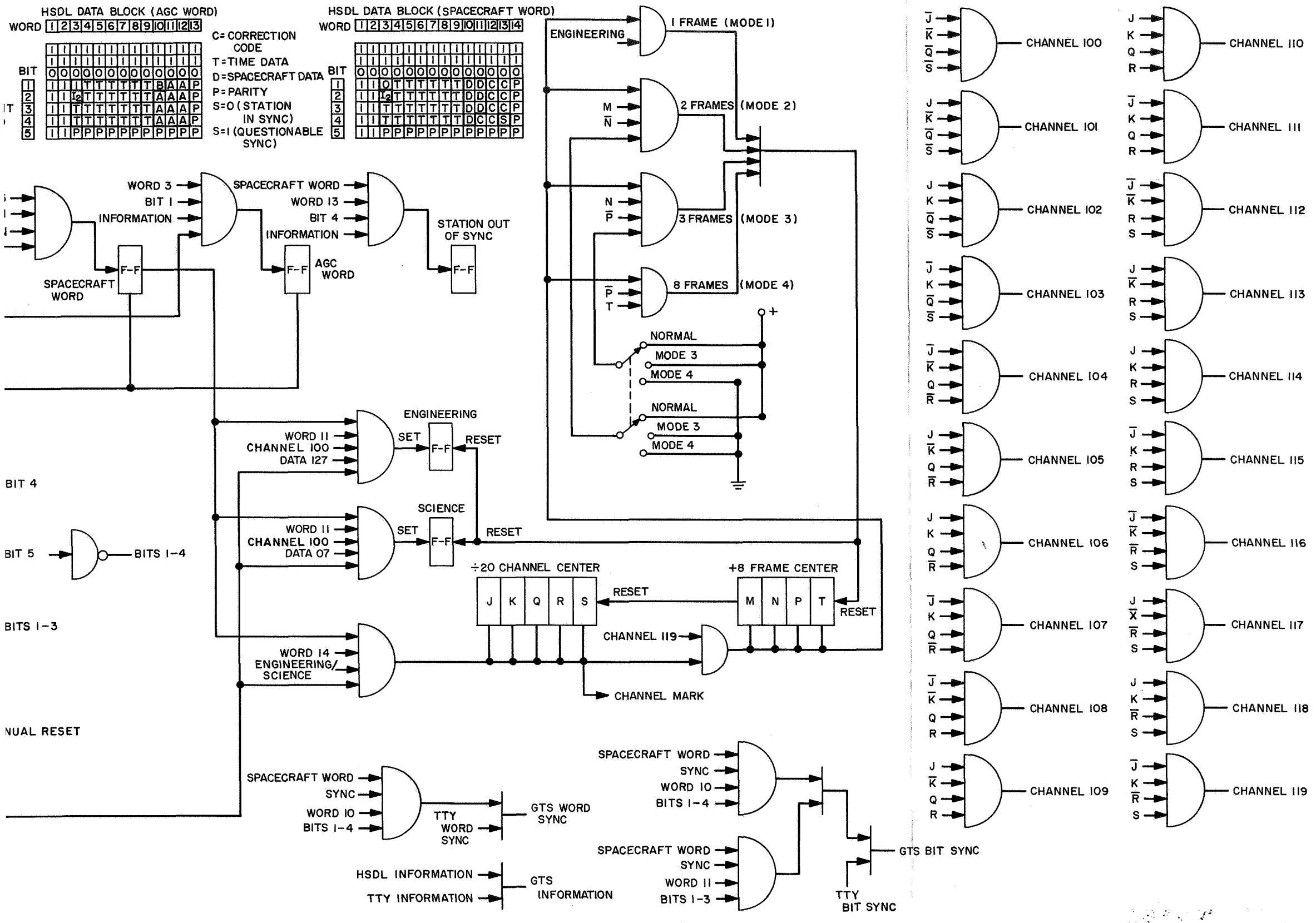
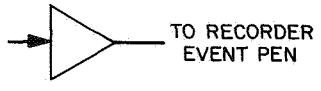



**Fig. VI-4. D/AC HSDL logic block diagram**

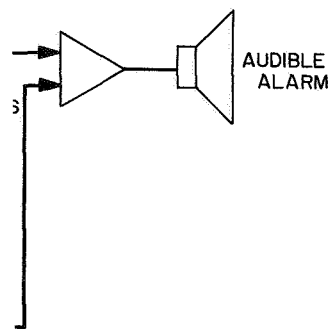


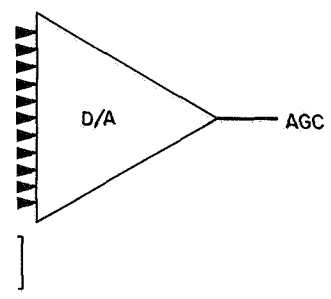
FOLDOUT FRAME 2

FOLDOUT FRAME 3


TO RECORDER
EVENT PEN


TO RECORDER
(CHANNEL 8)


AUDIBLE
ALARM


D/A
AGC

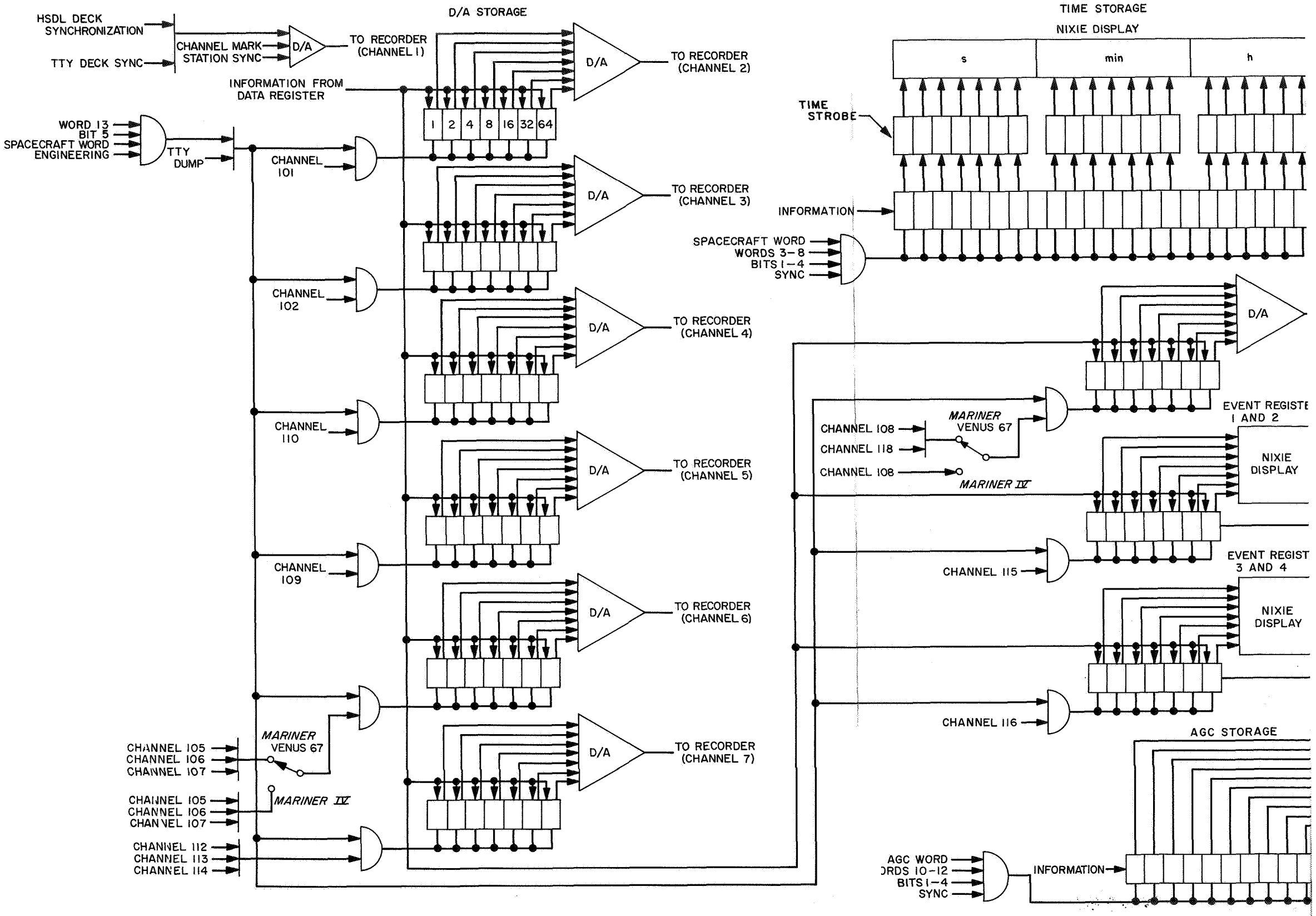



**Fig. VI-5. D/AC output control block diagram**





Fold out FRAME I

Fold out Frame I

PRECEDING PAGE BLANK NOT FILMED.

parity bit that is adjusted for an even number of "ones" in each word (except the first two data block synchronization words).

Words 4 through 9 are associated with BCD data for hours, tens of minutes, minutes, tens of seconds, seconds, and tenths of seconds, respectively. Tenths of seconds are not displayed by the D/AC.

Words 10 and 11 contain the 7 bits of spacecraft data. These bits are routed to a temporary storage register. If they are all ones (binary 127) corresponding to an engineering frame synchronization, the engineering flip-flop is set. The divide-by-twenty channel counter is now enabled, and steps once for each succeeding data block. Each state of this counter corresponds to one of the spacecraft telemetry channels. During normal operation (telemetry mode 1 or 2) after this counter divides by 20, it resets itself and the engineering flip-flop, and waits until another engineering frame synchronization or a science frame synchronization (binary 07) is received. If a science frame synchronization is received, the science flip-flop is set, the channel counter enabled, and the reset delayed until two cycles (frames) through the counter have occurred (40 spacecraft channels). In data mode 3, the reset is delayed until three cycles have occurred (60 channels) and in data mode 4, the reset is delayed for eight cycles (160 channels).

Connected to the temporary storage register is each of the storage registers associated with each channel on the analog recorder and its associated D/A amplifier (Fig. VI-5). The data are not transferred to any of the D/A storage registers until a strobe or transfer signal for each register is generated. These strobe signals are obtained from the channel counter when the engineering flip-flop is set (engineering data). Pre-selected spacecraft engineering data are thus stored, converted to a convenient analog voltage, and displayed on the analog recorder.

Similarly, the data bits are associated with time and AGC and are routed to their respective storage registers for Nixie display or recording.

The only remaining information bit processed by the D/AC is word 13, bit 4 which is associated with the DSIF data synchronization condition. If this bit is a "one" the station-out-of-synchronization flip-flop is set.

Each of the main control flip-flops is monitored by a light on the front panel for ease in determining the current data condition.

When operating from the HSDL, additional functions are available to aid in the display and readout of the data. A DATA function is available for displaying the data in the normal mode when the data on the HSDL are the complement of the actual spacecraft data. A derived synchronization function is available to automatically generate deck synchronizations if the spacecraft data bit error rate is high.

*b. TTY Logic.* Figure VI-6 is a block diagram of TTY logic. The TTY data line is entirely different from the HSDL. It consists of 6 bits of non-return-to-zero, single-line data (information only). A synchronization signal for processing the data must be generated internally. The signal level between words is always a "one" and the first bit of each word is always a "zero." Therefore, a transition from a "one" to a "zero" always occurs at the beginning of each word. This transition is used to generate the required synchronization signal. A gated synchronization generator is started at this transition and generates six synchronization pulses and stops until the next transition is sensed. These synchronization pulses are spaced in time coincident with the six information bits in the TTY data.

The TTY input buffer senses the transition from a "zero" to a "one" as well as the transition from a "one" to a "zero." A flip-flop is set or reset by the output of this buffer and, therefore, follows the data on the TTY line. The output of this "information" flip-flop and the internally generated synchronization are used to load the last five TTY information bits into a temporary storage register.

The five bits of data stored are binary-coded Baudot for operation with the teletype machines. It is therefore necessary to convert the data from Baudot to seven-bit binary. Two TTY words are required for each spacecraft telemetry word. These TTY words are designated digit 1 and digit 2. A flip-flop is used to keep track of the proper digit for each telemetry word. This flip-flop is initialized (digit 1) whenever a *0, 1,* or *2,* which are unique to the first digit, is sensed in the data. It is also initialized whenever a character other than a number is sensed (e.g., space, carriage return, line-feed, etc.)

After the five bits of TTY information are stored, a 2.5-kHz clock is started to further process these data. This clock generates 24 bit times for each TTY word. Figure VI-7 illustrates how each of these bits is used for processing the TTY word.

The 2.5-kHz clock is started by the last (sixth) synchronization pulse generated as the TTY word is sensed.

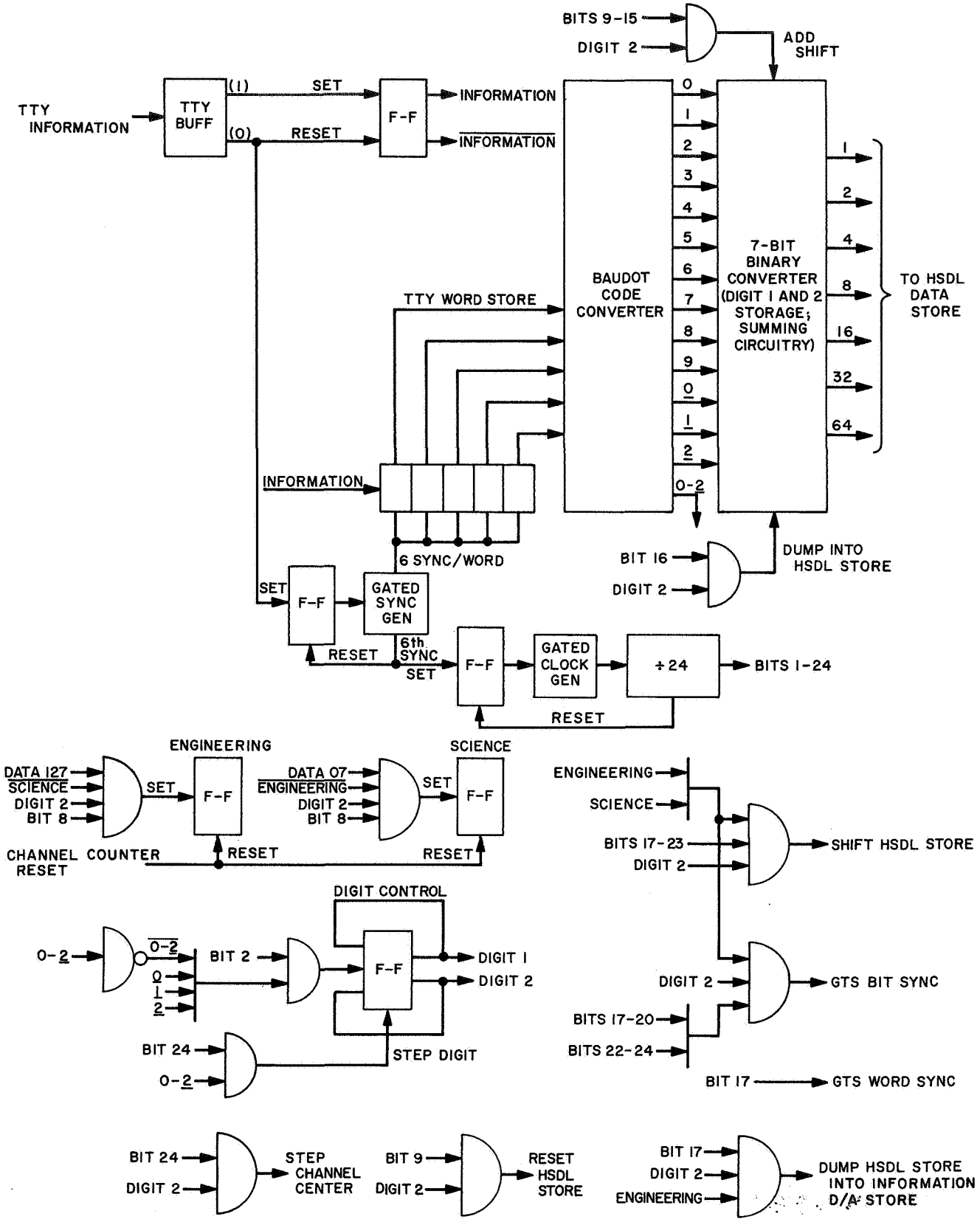



**Fig. VI-6. D/AC TTY logic block diagram**

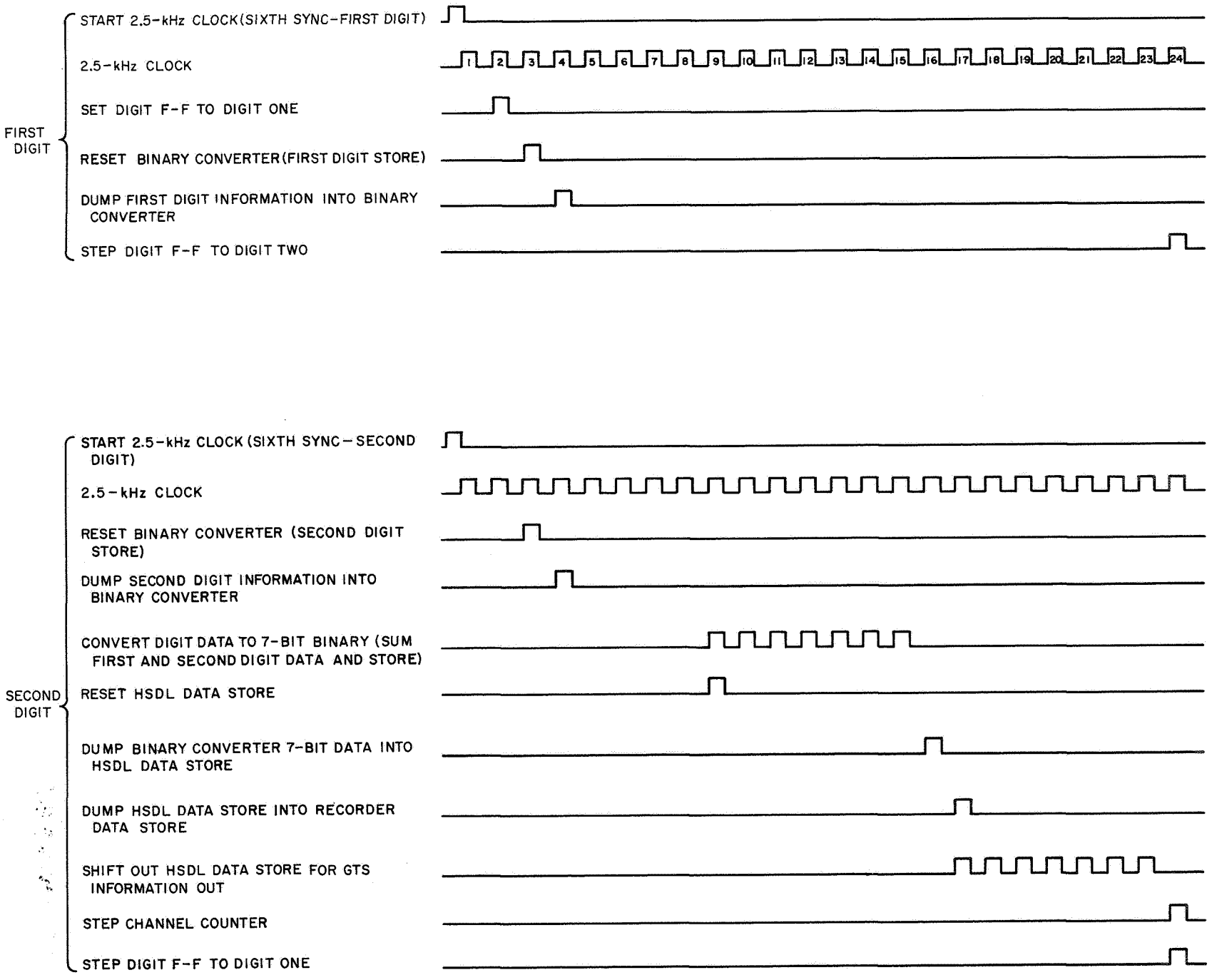



**Fig. VI-7. TTY conversion control timing diagram**

If the TTY word is decoded as a non-figure, *0*, *1*, or *2*, the digit flip-flop is set to digit 1 at bit time 2. At bit 3, the storage register within the binary converter used to store the digit 1 data is reset. At bit 4, the digit 1 data are dumped from the Baudot decoder into this digit 1 store. Bit 24 steps the digit flip-flop to digit 2 if digit 1 was a number. It remains in the digit 1 position if the TTY word was a space or some other non-number.

When the next TTY word is sensed, the last synchronization starts the 2.5-kHz clock again. If the TTY word is decoded as a number between 0 and 9, the digit flip-flop remains at digit 2. Bit 3 resets the digit 2 storage register within the binary converter. Bit 4 then dumps the digit 2 data into the digit 2 storage register. At bit 8 time, the contents of the digit storage registers within the binary converter are strobed for the presence of an engineering or science frame synchronization. If the two-digit word stored was a frame synchronization, the appropriate engineering or science flip-flop is set and the channel counter enabled. Bits 9 through 15 shift out the digit data from each register whereupon it is summed together and the result stored in the 7-bit digit 1 register. Bit 16 dumps these 7 bits of information (corresponding to the binary DN of one spacecraft telemetry channel) into the HSDL temporary storage register (Fig. VI-4). Bit 17 then dumps these data from the HSDL temporary store into the appropriate D/A storage register as discussed above under the HSDL logic description. Bits 17 through 23 shift the data out of the HSDL temporary store for use as the information output to the GTS equipment. Bit 24 steps the HSDL channel counter to the next channel, and the digit flip-flop to digit 1. The process is then repeated for the next two TTY words that correspond to a spacecraft telemetry data channel.

Event register status (telemetry channels 115 and 116) are Nixie tube displayed on the front panel, both for HSDL and TTY operation. An audible alarm is also provided to signal when any of the event registers change by an odd number.

*c. Recorder control.* Several functions are provided by the analog recorder which are used in displaying the telemetry data. They are:

(1) Eight analog channels.

(2) Two event-pens.

(3) Remote speed control.

The analog channels are used to display the telemetry data output from the D/A amplifiers. These D/A amplifiers consist of a weighting network and a 702A integrated circuit operational amplifier (Fig. VI-8). The analog output sensitivity from these amplifiers is 25 mV per DN. Switches are provided on the front panel of the D/A to increase this sensitivity to 50 mV per DN. At this increased sensitivity, however, the D/A amplifier will saturate at approximately 100 DN. The recorder input attenuator can be adjusted also to give the desired recorded scale factor. Normally, the data are recorded with a scale factor of 4 DN per small division on the record paper.

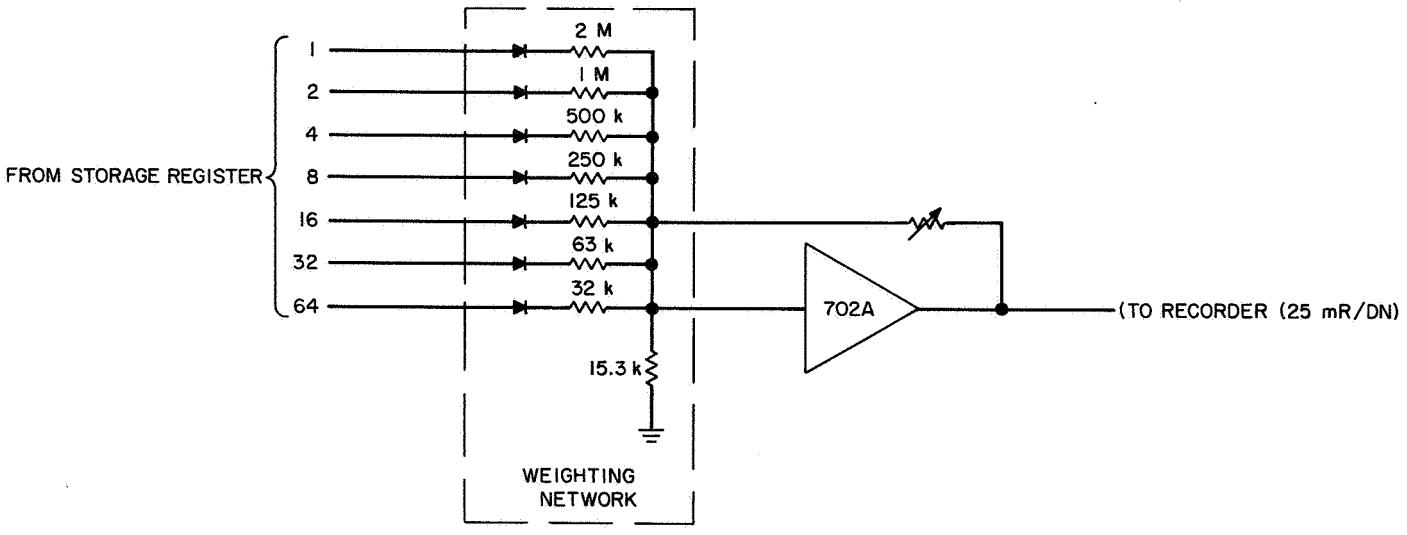



**Fig. VI-8. D/A amplifier**

Three modes of recording the telemetry data are available for selection:

(1) Non-return-to-zero display of all channels.

(2) Return-to-zero display of all channels.

(3) Return-to-zero display of all channels except return-to-64 display for gyroscope and position sensor channels.

Item (3) is the normally used mode for *Mariner* operations. Table VI-3 lists the recorder channel assignments for *Mariners IV* and *V*.

The left event pen on the recorder is utilized for recording time when operating from the HSDL. (Time is not displayed or recorded when operating from TTY.) This display consists of a marker pulse followed by appropriate pulses in BCD for hours, minutes, and seconds. Figure VI-9 illustrates this display.

The right event pen changes position when a station-out-of-synchronization indication occurs.

The remote recorder speed control is used to adjust the recording speed for optimum display, and to conserve paper when nothing is being recorded. Three different speeds are utilized during normal data recording:

(1) Adjustable speed for recording time.

(2) Adjustable speed for recording telemetry data.

(3) Fixed speed (slow) for non-recording (e.g., science or no data).

Speed switching is automatically controlled by the electronics within the D/AC. The actual speeds used for time and data recording can be selected from switches on the back of the D/AC.

**Table VI-3. Analog recorder channel assignments**

| Channel | Assignments |
|---|---|
| Recorder channel 1 | Deck synchronization; channel marker; station out of synchronization (HSDL only) |
| Recorder channel 2 | Spacecraft telemetry channel 101 |
| Recorder channel 3 | Spacecraft telemetry channel 102 |
| Recorder channel 4 | Spacecraft telemetry channel 110 |
| Recorder channel 5 | Spacecraft telemetry channel 109; or station AGC |
| Recorder channel 6 | Spacecraft telemetry channels 103, 104, and 107 (*Mariner V*)<br>105, 106, and 107 (*Mariner IV*) |
| Recorder channel 7 | Spacecraft telemetry channels 112, 113, and 114 |
| Recorder channel 8 | Spacecraft telemetry channels 108 and 118 (*Mariner V*)<br>108 only (*Mariner IV*) |
| Recorder left event pen | Time in BCD (HSDL only) |
| Recorder right event pen | Station out of synchronization (HSDL only) |

All logic within the D/AC is implemented by DTL integrated circuits (14 lead flat packs) mounted four to a board. A total of 344 of these devices are used in the D/AC containing both HSDL and TTY logic, and 244 devices in the D/AC containing only HSDL logic.

The D/A amplifiers utilize discrete components as well as an IC operational amplifier.

All buffer amplifiers required for input/output interfacing, other than with the analog recorder, utilize discrete components entirely.

All the electronics are incorporated into two 19-in. panels installed in a semi-portable (two-man) 3-ft cabinet. A third panel area is provided for HSDL station selection equipment.

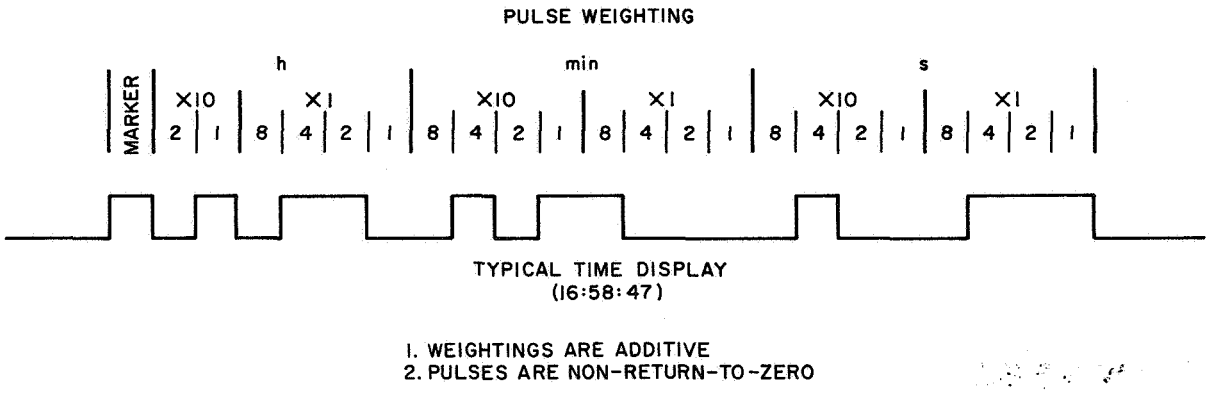



**Fig. VI-9. Recorded time**

## E. Computer Program Development

*1. Overall software development plan.* Control of the software efforts logically falls into two divisions: (1) *quality control,* and (2) *configuration control.* Quality control ensures that all elements work properly. Configuration control ensures that the overall development of the system follows anticipated schematics. Both are applications of common sense.

Figure VI-10 is a matrix summarizing the configuration control procedure decided upon for standardizing the software quality control procedures and the actual operating procedures that apply to flight operations programming.

The points of view displayed in Fig. VI-10 are the scheduling aspect, the actual tasks to be carried out, the documentation, and the emphasis of control. The matrix is not, in physical reality, so divided; but this division helps to clarify the formal issues.

The initial effort was the project definition. From this followed a variety of functional requirements for subtasks. The matrix shown concentrates on one task, but it should be remembered that in a project such as *Mariner* Venus 67 many similarly organized tasks proceeded in parallel.

Functional requirements outline the capabilities that are required of the task to be performed. The request for programming (RFP) is a document further elaborating the functional requirements and translating them into programming detail. It is no more than a first step to describing the programming task. The approach derives from the premise that infinite resources and infinite time will be available to carry out the task. This is clearly unrealistic, but it is a good starting point from which to progress.

After a request for programming has been produced, a design team or task force is established. The chairman gathers a group of people—the task force—that is to be directly concerned with, and have line accountability for, subsystems in the task.

The first step is to define the task. Starting with the RFP, a system design is developed by the members of the task force. The system design is fairly detailed. It includes a time schedule, a resource allocation schedule, and the subtask assignments to be carried out by various members of the task force; and it summarizes the findings and documents the work of the task force. This last effort is covered in a Division Engineering Planning Document (DEPD) which, when signed by all relevant levels of management up through the division office, becomes the commitment document for the task. The originator of the task request may not be completely cognizant of all the details that go into the implementation of the task. He may sometimes be insufficiently trained to recognize the possibilities and the impossibilities in programming. Therefore, the task force leader has the charter of interacting with the originator of the job request to iterate the requirements until they make sense, not only to the originator but also to the programmer. It is the converged concept which is documented in the DEPD.

From there, one proceeds through various stages of review to the actual implementation. This includes setting up programming schedules; presenting the actual design detail, which is generally done at the group level; and establishing the acceptance test detail. The acceptance test detail presents requirements for assessing the performance of the completed set of programs. After the programming has been carried out, the acceptance tests are performed on the completed set of programs under the eyes of a competent panel. If the acceptance tests are satisfactorily completed the system is *bought off* and becomes operational. The task is ended.

Various phases of operational procedures are mainly concerned with the manner in which the program is transferred from the programmers to the project or to the Space Flight Operations Facility (SFOF), and the manner in which long-term maintenance is to be carried out. Several peripheral jobs also must be attended to such as those of training operators, establishing operating procedures for personnel in the SFOF, and developing change control procedures.

*2. Software system description.* Figure VI-11 shows the hardware and software system used to support *Mariner* Venus 67. The system is divided into three major areas: the Deep Space Instrumentation Facility (DSIF), the Ground Communications System (GCS), and the Space Flight Operations Facility (SFOF). The software efforts to be discussed are shown in those blocks made up by dashed lines. The arrows show data routing. Solid arrows indicate incoming data flow to the SFOF; and the broken arrows are outgoing data flow from the SFOF.

*a. Telemetry and command processor.* The on-site system includes the ground telemetry system (GTS), and the telemetry and command processor (TCP) which consists of an SDS 920 computer and a communication buffer.

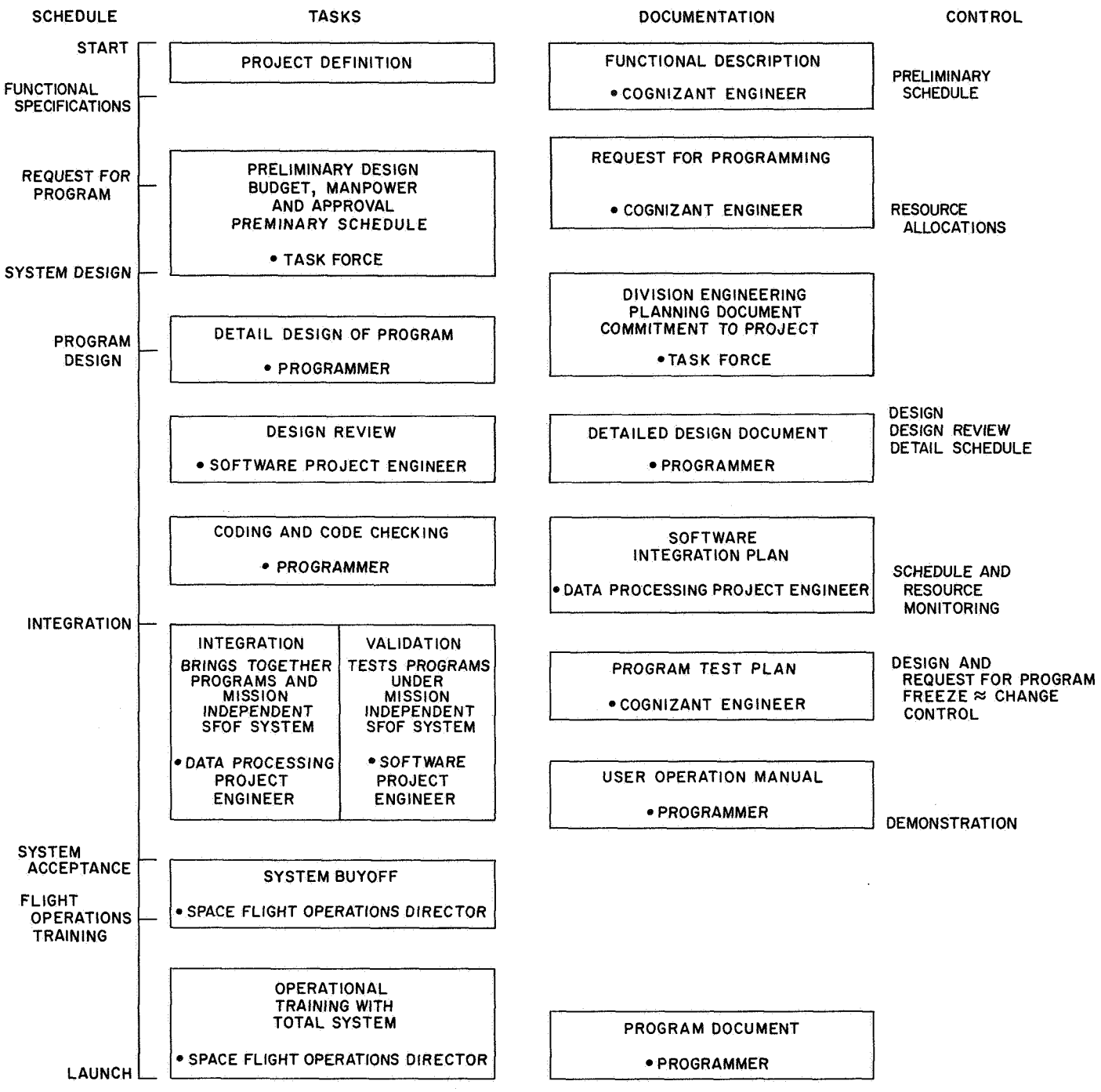



**Fig. VI-10. Elements of software development and control**

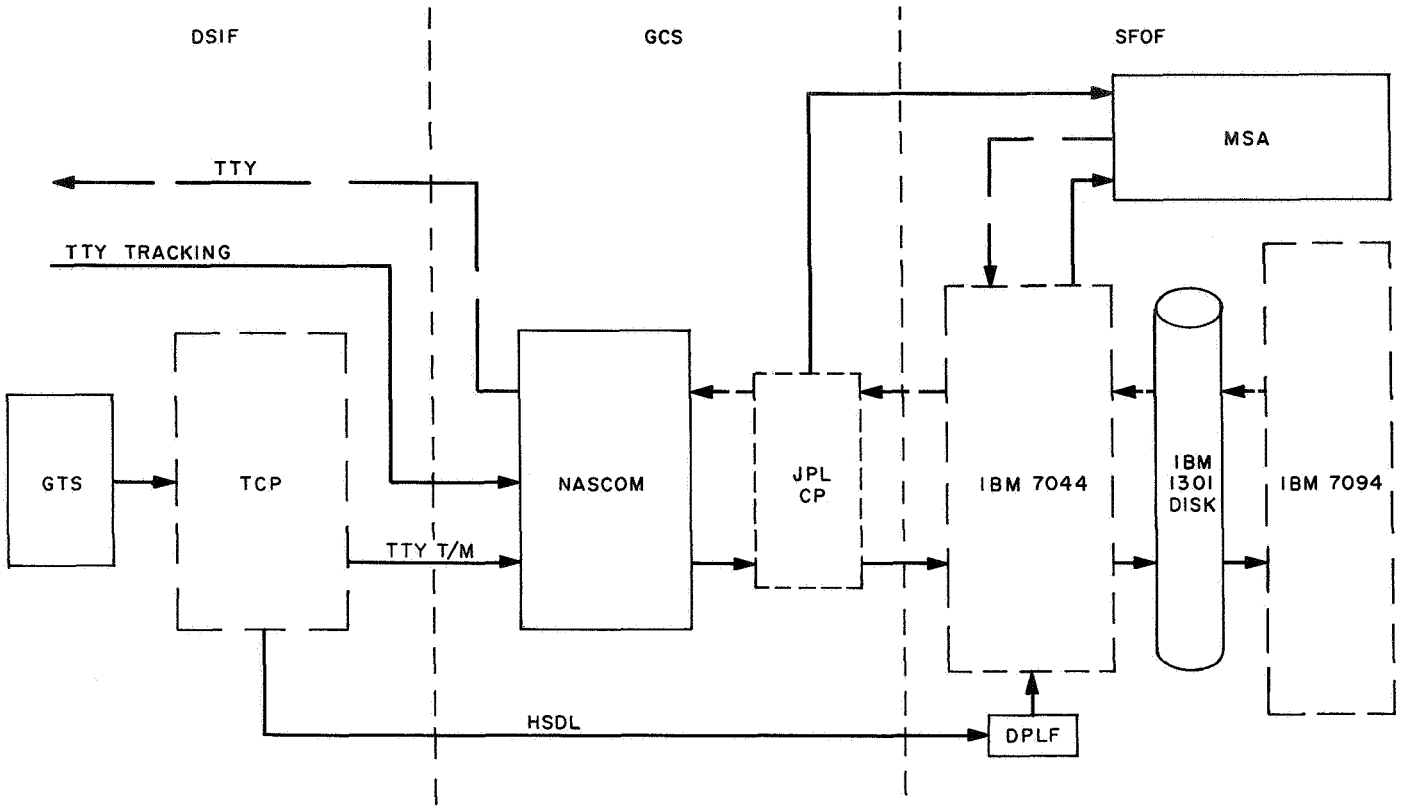



**Fig. VI-11. Data processing system for *Mariner* Venus 67 support**

The communication buffer is essentially the external, or output, interface. The primary function of the TCP program is to process *Mariner* spacecraft telemetry data by frame detection, engineering decommutation, science decommutation, teletype output, high-speed data output, and data logging.

Data from the GTS are received in the form of digital telemetry data, word sync, bit sync, ground receiver automatic gain control (AGC) data, and receiver in- and out-of-lock status. In addition, the station-time input is used in time-tagging the data. The TCP on-line typewriter provides control inputs to the program.

The output data are formatted for transmission through the communication buffer on various teletype lines and high-speed data lines, and for visual display of the spacecraft AGC and static phase error (SPE) at the DSIF station.

All data received by the TCP, except AGC data, are formatted and stored on a log tape.

*b. Communications processor.* The transmission of teletype data for the *Mariner* program was made via the NASA Communications Network (NASCOM). The software task in this area was primarily to define and operate a working interface between JPL and NASCOM.

The basic transmission scheme used is *message switching*. In this procedure, messages originating at DSIF stations are routed through communications processors (CP)

to desired terminal points in the SFOF by means of routing data contained in headers that are affixed to the body of the message. The JPL communications processor is also used for routing data originating within the SFOF. Terminal points include teleprinters in the *Mariner* support area, TV printers, and the data processing system (DPS). Messages are also routed from the SFOF to the DSIF.

*c. 7044 redesign system.* The teletype (TTY) data inputs to the SFOF data processing system from the various DSS sites enter the SFOF communications processor which transmits the data to the 7044 redesign system via input/output programs and the 7288 multiplexer. The 7044 system receives these inputs and stores the data in system buffers. The communications processor input processor program (IPP) extracts the data from input system buffers and sorts them into other system buffers according to spacecraft number, data type, Deep Space Station (DSS) number, and control inputs by operations personnel.

The 7044 system operates the mission-dependent processors, and the tracking residual programs when an appropriate number of inputs have been received or when an appropriate time has elapsed after the inputs have been received. The mission-dependent processors process the data by performing decommutation, identification, scaling, and alarm checking. The information is stored into system buffers to be formatted and sent out to SC 3070 printers, Milgo plotters, and teleprinters. The data sent from the 7044 system to the SC 3070 printers and Milgo plotters are sent directly by means of the 7288 multiplexer. However, all teletype data are sent to the communications processor which drives the teleprinters in the SFOF. No teleprinters are driven directly by the 7044 system.

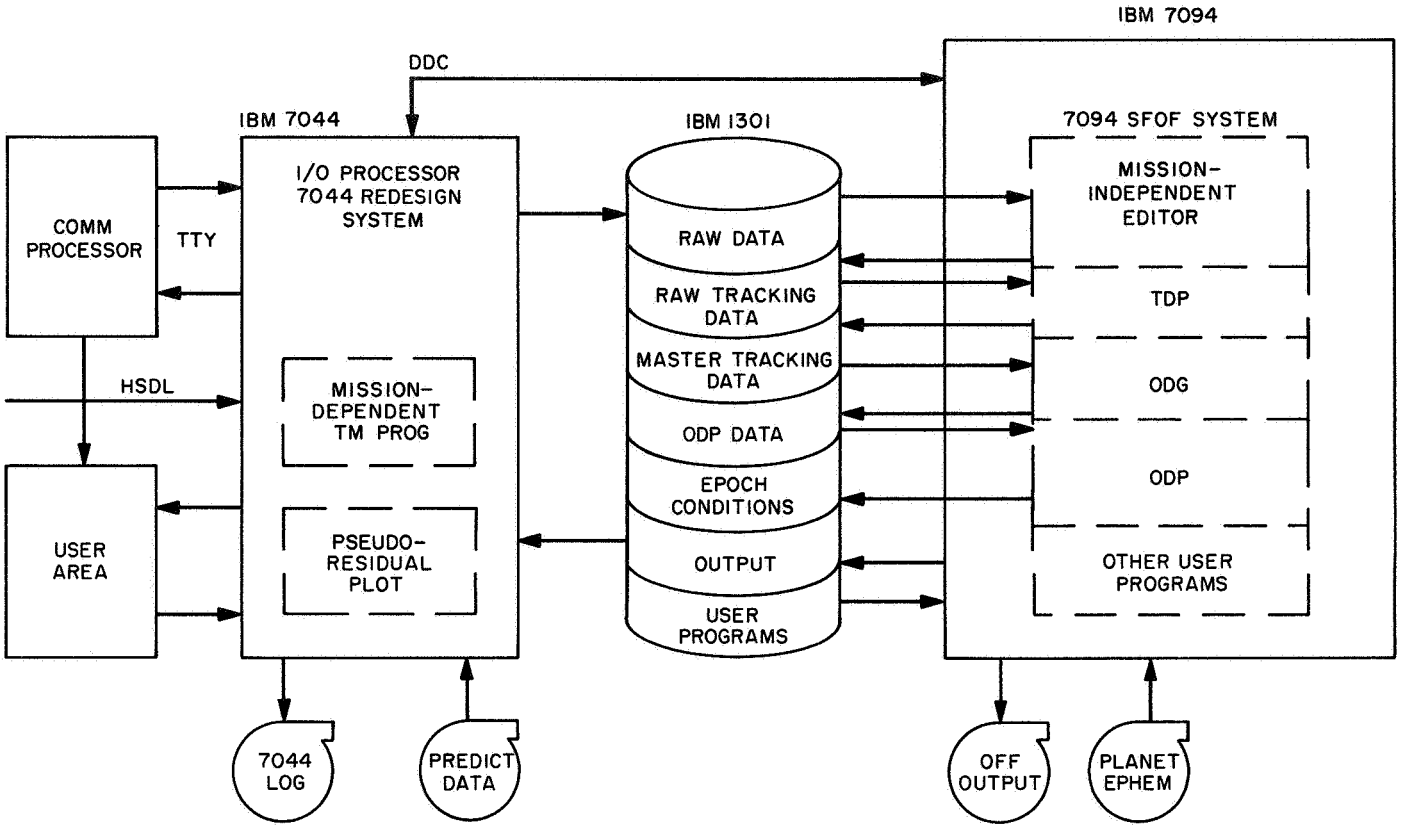
Data also come in from the telemetry processing stations (TPS) through the 7288 multiplexer and are stored in system buffers. The appropriate processors are operated and the data are extracted from the system buffers. Inputs from both the communications processors and the telemetry processing stations are stored on the 7044 log tape at the time they are received by the 7044 system. If the system is in mode 2, all inputs are stored on the disk for later processing by the 7094. When the data are stored on the disk raw file in mode 2, the 7094 is informed that the data are available by means of the direct data connection; and the 7094 communications processor editor extracts the raw data from the disk at its leisure, processes it, and stores it in the master data tables, making it available to user programs.

The operations personnel at the user I/O stations request various 7094 user programs to operate. These programs extract the data from the master data tables, process the data, and generate outputs for the SC 3070 printers, the Milgo plotters, and the teletype. These outputs are put on the disk, and the 7044 is informed that they are on the disk and available. The 7044 informs the operations personnel by means of an administrative printer that the information is available. At the request of the operations personnel, the 7044 extracts the data from the disk, and sends it to the 3070 printers and the Milgo plotters as requested. The teletype data on the disk that is requested for output are sent through the communications processor to the various teleprinters and DSS sites as required.

The 7044 tape units are used for logging data and reading-in predict information for tracking residual calculations. The 7044 also has an associated drum for storing programs and tables.

Access to this drum is possible through the I/O routines and the drum queueing routines. There are additional service routines in the 7044 system for conversion, turning programs on and off, system control, recovery, and special formatting of displays.

*d. 7094 redesign system.* Preceding sections have covered in detail the telemetry command processor, the communications processor, and the 7044 redesign system. A summary shows that teletype data are received from the NASCOM system by the communications processor and provided to the 7044; in addition, information generated by the 7044 or 7094 is routed to the communications processor for distribution to SFOF user areas or overseas sites. In the 7044 system, the mission-dependent telemetry program performs data processing functions similar to the telemetry command processor. It performs frame detection, decommutation, identification, and time tagging of spacecraft telemetry data. These data can then be transmitted by the 7044 to user areas, or to any place in NASCOM. The pseudo-residual plot program compares tracking data and prediction data obtained from the predict data tape. Residuals are computed from incoming tracking data and predicted tracking observables and then displayed as plots in the user areas. All data entering the 7044 system are logged on magnetic tapes.




| | |
|---|---|
| COMM | COMMUNICATIONS |
| TTY | TELETYPE |
| HSDL | HIGH-SPEED DATA LINE |
| TM | TELEMETRY |
| ODP | ORBIT DETERMINATION PROGRAM |
| ODG | ORBIT DATA GENERATOR |
| EPHEM | EPHEMERIS |
| TDP | TRACKING DATA PROCESSOR |
| DDC | DIRECT DATA CHANNEL |

**Fig. VI-12. 7094 user program environment**

The user program environment is illustrated in Fig. VI-12. A 7044, a 1301 disk, and a 7094 are operating together and communicating with one another. In addition, control inputs – usually from punched cards or switches – can be entered at the user areas, received by the 7044, and sent to the 7094 by way of the direct data channel (DDC).

*FPAC user programs.* As raw tracking data are received, they are placed on the disk by the 7044 system. The raw data on the disk are then accessible to the 7094 user programs.

There are four tracking data handling programs illustrated, but only one program operates within the 7094 SFOF system at one time. The mission-independent editor acquires the raw teletype data from the disk, which contains mixed tracking and telemetry data, and separates them by extracting the tracking data and storing them on the disk in the raw tracking data file.

The tracking data processor (TDP) program retrieves these data, edits and reformats them, and then places them back on the disk in the master tracking data file.

The orbit data generator (ODG) program uses this file to prepare a block of data for the orbit determination program (ODP). Essentially the ODG program extracts a subset from the master tracking data file and formats it by using control inputs that have been provided to the program.

The orbit determination program retrieves the block of ODP data compiled by the ODG program and, employing a least-squares curve fit and using an iterative technique, determines the orbit of the spacecraft. The injection, or epoch, conditions are placed on the disk and are available to other programs.

The area on the disk labeled *user programs* contains the actual programs called up by the system and brought into the 7094 for operation.

Trajectory computations are performed by the programs **TJ1M** and **POWM**. The epoch conditions and the planetary ephemeris are used by **TJ1M** to compute the spacecraft ephemeris and generate a trajectory *save* tape that consists of tabulated information computed at specified points along the trajectory.

These values include earth–sun–probe angles, clock angles, and velocities. Essentially **POWM** is a trajectory program except that it actually generates tracking predictions during the *burn* that are used for early acquisition and are based on predicted or actual lift-off time. The DSIF acquisition predictions are computed by the program **PRDX**. It also predicts viewing periods of the stations and voltage-controlled oscillator frequencies of the transmitter. This information is formatted for teletype and later transmitted to the DSIF stations for aid in spacecraft acquisition.

In addition, **PRDX** produces a predict data tape which is used as an input to the 7044 for computation of pseudo-residual plots. **PRDX** uses the epoch conditions and the planetary ephemeris as inputs.

The midcourse maneuver (**MC1M**) program provides the necessary information for selecting a midcourse maneuver which satisfies all trajectory constraints. In addition, it generates capability ellipse plots and formats the maneuver commands for transmission to the spacecraft.

Again, the inputs are the epoch conditions and planetary ephemeris.

*SPAC user programs.* The spacecraft performance analysis and command user programs are the star identification program (**SIPM**), the communication prediction program (**CPPM**), the attitude reference program (**ATTREF**), and the AGC calibration program (**AGCM**).

The SPAC programs receive telemetry data information from the user area. (The mission-independent editor has the system capability of extracting the telemetry data and storing them on the disk, as is done with the tracking data. However, this capability is not used by *Mariner*.) Another input for three of the SPAC programs (**SIPM, CPPM,** and **ATTREF**) is the trajectory *save* tape since, to accomplish their individual tasks, these programs require an exact knowledge of the location of the spacecraft in space.

The results of all 7094 user programs are available to the user area by means of the 7044 and the output area of the disk. Selected results are recorded on magnetic tape for later off-line processing.

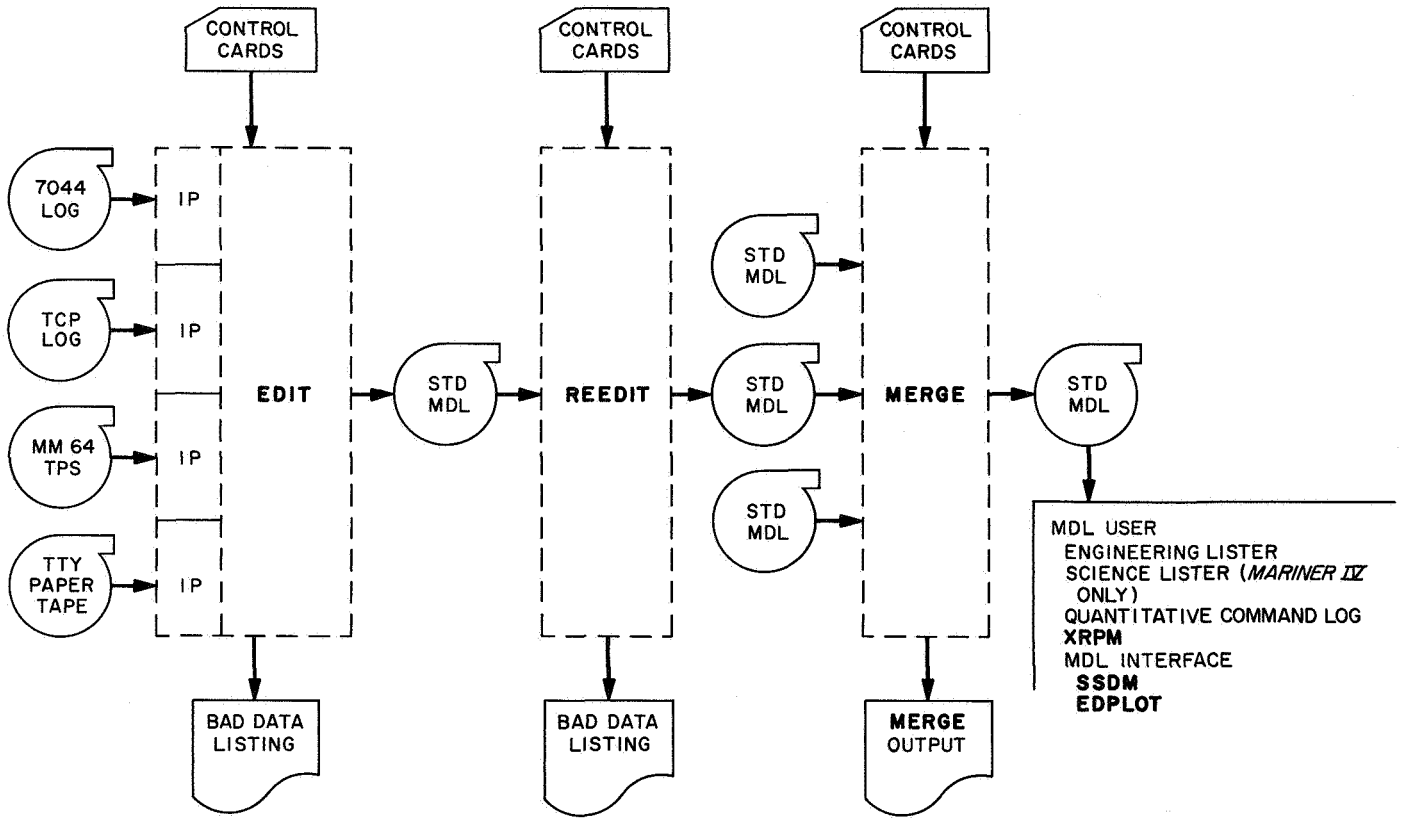
*e. Non-SFOF programs.* The master data library (MDL) programs (Fig. VI-13) for *Mariner* Venus 67 are identical to those used for *Mariner* Mars 1964 except for two additional input processors (IP) and the MDL interface user program.

The MDL programs do not operate in the SFOF software system, but in the standard International Business Machines System (IBSYS).

The purpose of the MDL programs is to generate, in non-real time, a tape containing the most accurate stream of telemetry data possible. This tape then becomes the basis for analysis by experimenters and spacecraft engineers. This processing of various input source tapes into a final tape is done by the three basic software programs of the MDL chain: **EDIT, REEDIT** and **MERGE.**

Data are recorded in various places and in various formats in the total data processing system. The tapes containing these data are the inputs to the MDL programs. The telemetry processing station and teletype paper tape inputs were used for *Mariner* Mars 1964. Their input capabilities will remain, but for *Mariner* Venus 67 they have been replaced by two new sources: the telemetry and command processor log tape, which was recorded at the telemetry and command processor; and the 44 log tape, recorded at the 7044.

Each tape input has an associated input processor (IP) specifically designed to handle a particular format. The input processors perform a translation function from the varied input tape formats to a standard format recognizable by **EDIT.** This program performs frame detection and evaluates the quality of each frame.




MM 64 *MARINER* MARS 1964
TPS TELEMETRY PROCESSING STATION
TCP TELEMETRY AND COMMAND PROCESSOR
TTY TELETYPE
STD STANDARD
MDL MASTER DATA LIBRARY
IP INPUT PROCESSOR

**Fig. VI-13. Master data library programs**

Included in the telemetry data stream is status information regarding the processing, recording, and receiving equipment such as receiver in- and out-of-lock and demodulator in- and out-of-sync. **EDIT** program recognizes this information and uses it in evaluating the data quality during the frame detection process.

In addition to the standard MDL tape, a bad data listing is recorded on magnetic tape. This listing is essentially an evaluation tool for determining the additional processing required to improve the MDL tape.

**REEDIT** provides a means to correct the MDL tape by supplying appropriate control cards whose information is based on the investigation of the bad data listing. **REEDIT** also produces a bad data listing which, if the correcting process has been done properly, will be appreciably shorter than that produced by **EDIT.**

**MERGE** processes a number of tapes (up to six) from various sources, covering the same period of transmission, and merges them into one *best possible* standard MDL tape. The tapes processed by **EDIT** and **REEDIT** are from a variety of sources. Consequently many tapes may contain telemetry data for identical tracking periods. This occurs during station overlaps, i.e., when more than one station is tracking the spacecraft at one time; and also during in-station overlaps when a switch is made from one tape to another during a pass, i.e., when the second recorder is started before the first has finished.

*MDL user programs.* The MDL user programs are used as tools in the evaluation process of the standard MDL tapes generated at any stage (i.e., **EDIT, REEDIT,** or **MERGE**).

The standard MDL tapes, regardless of the stage of processing, are in an identical format. Since **REEDIT** and **MERGE** refine the data stream without altering this format, any of the MDL user programs can use any MDL tape as an input.

The engineering lister extracts all the engineering data from an MDL tape and organizes them into a *quick look* format. The science lister does essentially the same thing with science data, but for *Mariner IV* only. **XRPM** is a selective extract program. For example, a magnetometer experimenter, by providing certain control inputs to **XRPM**, can extract all magnetometer data from a given MDL tape.

The MDL interface program acts as a common boundary between the MDL tape and two programs carried over from *Mariner IV*. In the discussion of SPAC user programs it was pointed out that telemetry data were not stored on the 1301 disk as were tracking data. *Mariner IV*, on the other hand, did store telemetry data on the disk and two very useful programs (**SSDM** and **EDPLOT**) made use of this feature. The MDL interface program allows these programs to operate from the standard MDL tapes. **EDPLOT** provides a plot of the engineering values recorded. **SSDM** is a suppressed data printout; that is, only values which violate certain constraints are printed out and repetitive values are ignored.

*Monitoring of program development.* Software development was monitored by the use of schedules and status reporting. The schedule shown in Fig. VI-14 gives an overall view of the progress of the various programs as of March 20, 1967. On that date most of the software was operational or was finishing final tests.

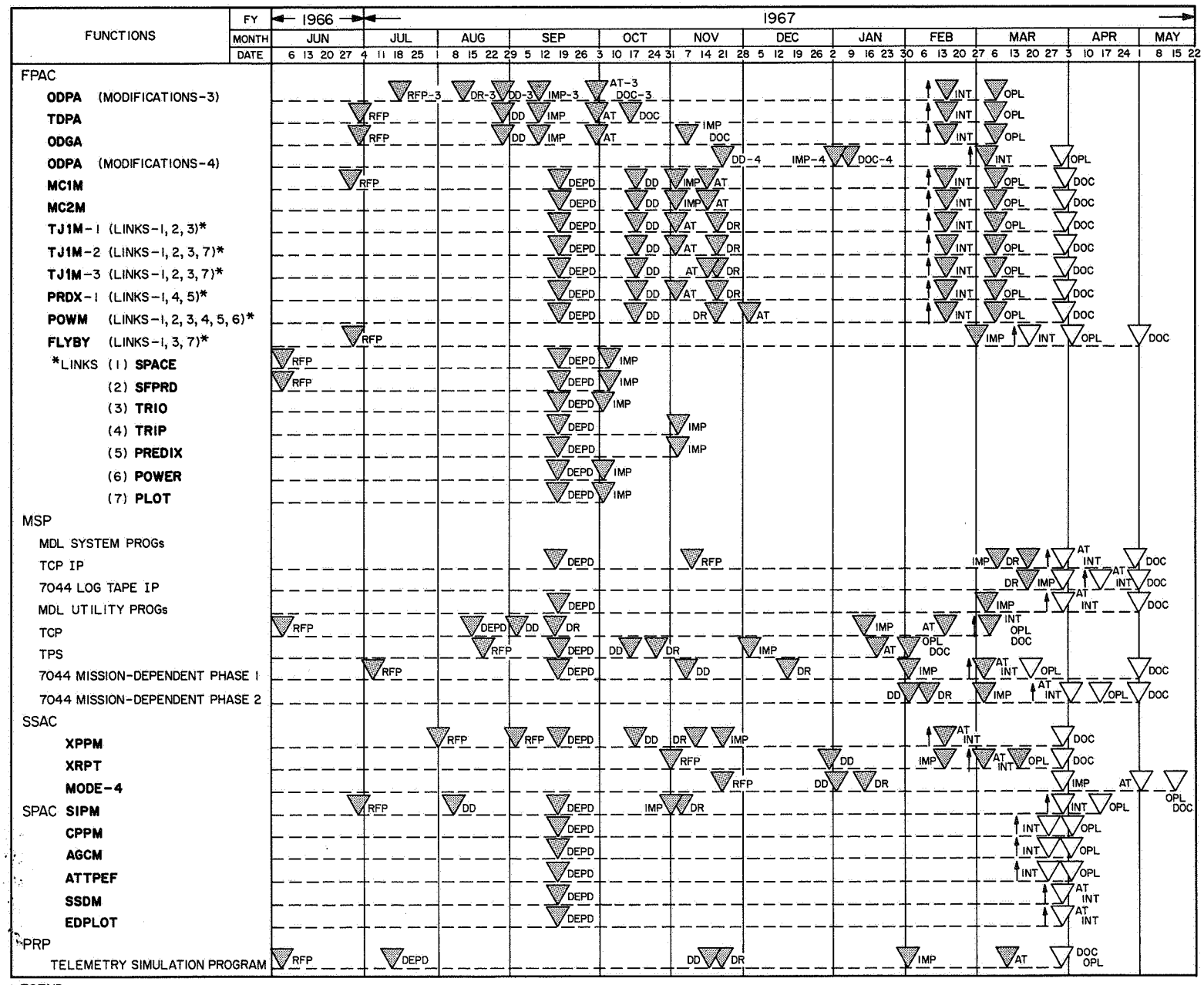
Control over changes to the software was put into effect almost as soon as development started. The software control underwent successive stages: (1) control over basic program design, (2) control over detail design, and (3) control over program code. A change control form approved by the DPPE, SFOD and MOS managers is required for changes to any program under one of the three levels of change control.

*Software testing.* A set of tests was performed on each of the four basic software subsystems: 7094 user programs, 7044 redesign system, communications processor, and telemetry and command processor. The following list is an example of the tests used on the 7094 user programs. The same types of tests were used on other software subsystems.

(1) Integration tests. These tests demonstrate that each set of user programs (source deck) operates properly in mode 4 using the 7094 redesign SFOF monitor, and the mission-independent editor.

(2) Compatibility tests, 1. These tests demonstrate that the user programs operate properly in mode 2 using the 7044 system.

(3) Compatibility tests, 2. These tests demonstrate compatibility between the user programs, the 7044 system, the communications processor, and the DSIF. Only those user programs which bound the communications processor or the DSIF are tested.




LEGEND

- ▽ ESTIMATED COMPLETE
- ▼ COMPLETE
- RFP REQUEST FOR PROGRAMMING
- DEPD DIVISION ENGINEERING PLANNING DOCUMENT
- DD DETAIL DESIGN
- DR DESIGN REVIEW
- OPL OPERATIONAL
- IMP CODING AND CHECKOUT
- AT ACCEPTANCE TEST
- INT SYSTEM INTEGRATION
- DOC FINAL DOCUMENT
- IP INPUT PROCESSOR

REVISED 3-20-67

**Fig. VI-14. Program development schedule**

(4) Demonstration tests. These tests are used to demonstrate to the DSN and the *Mariner* Project personnel that the entire Mission Operations System is ready to support *Mariner V* simulations. A sequence of events, in which all phases of the mission are covered, approximates the sequence to be used in the simulations.

*System performance to midcourse.* In general, the performance of the data processing system from launch to midcourse was excellent. During this 5-day period there were only a few data processing system problems, mostly caused by computer hardware malfunctions. The longest period of trouble-free operation extended beyond 50 h.

The system was in SFOF mode 2 on two computer strings for a total of 36 h during launch, as well as for several 8-h periods before midcourse. All user programs worked very well and the sequence of events met with no problems.

## F. Mission Operations Testing and Training

Operational readiness was accomplished by a four-phase test program: (1) development tests for mission related hardware (MRH) and computer programs, (2) compatibility testing and integration of hardware and software into tracking data system (TDS) facilities, (3) spacecraft–MOS compatibility, and (4) operations training and procedural tests.

*1. Development tests.* Development tests were conducted as part of the MRH and computer program development. Successful completion of the tests and demonstration of the element (command equipment package, telemetry equipment package, or computer program) indicated its readiness to be integrated into the final configuration. The hardware and software transferred to the DSN for maintenance were accompanied by test, change control, and failure report logs.

*2. MOS–TDS integration and compatibility tests.* By mutual agreement between the MOS and the TDS, the compatibility testing and integration of hardware and software into TDS facilities were accomplished under TDS auspices.

*3. Spacecraft–MOS compatibility tests.* The objectives of these tests were to train the SFO teams, to train the SPAC team in evaluating spacecraft flight sequence and data mode changes as the result of commanding the spacecraft, and to exercise the MOS hardware and software with live spacecraft data.

The tests were conducted using the telemetry data source from the spacecraft at the spacecraft assembly facility (SAF) and at Hangar AO (AFETR). The composite signal was sent through the MRH and the telemetry and command processor. The formatted teletype output of the telemetry and command processor was received at the SFOF and distributed in the mission support area on 60-wpm teletype machines. The high-speed data were received at the SFOF and sent to the 7044 and processed and sent to the communications processor, the $30 \times 30$ plotters, and the 3070 printers. The communications processor output was distributed to the 100-wpm teletype machines.

*4. Operations training and readiness.* The primary objective of these tests was to train SPAC and SSAC personnel in evaluating live spacecraft data in real-time while in their space flight operation environment. The live spacecraft data were made available by combining the training tests with selected in-going spacecraft testing. The spacecraft testing was conducted under the direction of the spacecraft test operations manager.

*a. SPAC and SSAC training tests.* SPAC and SSAC groups monitored the live spacecraft data on a noninterference basis. The training tests that were conducted included (1) parameter variation test—specific parameters varied to maximum/minimum tolerance; (2) space simulator tests—tests conducted in the space simulator to create the expected flight temperatures and vacuum environment; (3) system tests—tests conducted to ensure that all spacecraft systems performed according to design specifications; (4) simulated launch—final full scale checkout of all launch and operation systems before launch; and (5) failure mode tests—an exception in that the SPAC and SSAC groups under the direction of the SPAC director were allowed to generate and carry out command sequences, with the live spacecraft, that were designed to overcome anomalous conditions induced by the spacecraft test operations team. By appropriate reactions of the spacecraft test operations team to the commanded sequences, the resulting spacecraft performance simulated realistic spacecraft failure and recovery mode situations.

*b. FPAC tests.* Several FPAC tests were conducted with the objective of training FPAC personnel to accomplish those flight path functions necessary for the SFO.

Simulated tracking data sources were used to exercise the FPAC team in orbit determination, trajectory analysis, maneuver command generation, and predict generation through all critical phases of the mission. This included launch, maneuver, and encounter phases. Nonstandard, as well as standard, simulated flight sequences were used for these three critical mission phases.

*c. Combined operational tests.* A series of combined operational tests which did not involve the flight spacecraft was conducted before launch. The data source for these tests was composed of a combination of simulated data and spacecraft test tapes recorded during spacecraft tests in the spacecraft assembly facility.

The primary purpose of these tests was to ensure that all the elements of the MOS, including technical and operational personnel of the DSN, were prepared to support the spacecraft after launch.

These tests indoctrinated and exercised the MOS operational and technical personnel in the system, and in the procedures to be used for the mission. The first combined operational test was supported by the following facilities: (1) SFOF (mission support area, data processing system—mode 2, telemetry processing station, communication center, simulated data conversion center, and the track area); and (2) DSS 11, 14, and 61, forming an encounter configuration.

The test was conducted over a period of two days with Day 1 covering $MC$ −3 h to $MC$ +90 min, and 3.5 h of cruise data. Day 2 covered the periods from $E - 3$ h to $E + 2$ h (approximately 45 min of spacecraft mode 2) and $E + 14$ h to $E + 16$ h (2 h of mode 4). Simulated data packages which were transmitted to the participating Deep Space Stations before the test were processed by the on-site computer system and transmitted to the SFOF where they were analyzed in real time by the analysis teams in the mission support area and the flight path analysis area number 2.

The second combined operational test was supported by the same SFOF facilities, and DSS 11, 14, and 42. The first day of the test covered the periods from $L - 30$ min to $L + 6.5$ h, and 3 h of dual-mission cruise (*Mariner IV* and simulated data from the Deep Space Stations). The second day of the test covered the periods from $E - 6$ h to $E + 2$ h (approximately 45 min of spacecraft mode 2) and $E + 14$ h to $E + 16$ h (2 h of tape playback).

The third combined operational test was supported by the same SFOF facilities as the first and second, the AFETR, and DSS 42 and 51. Day 1 of the test covered the period from $L - 30$ min to $L + 90$ min, $L + 16$ h to $L + 18$ h, and $MC - 3$ h to $MC + 90$ min. Day 2 covered $MC - 3$ h to $MC + 2$ h, and 2 h of cruise.

*d. Operational readiness tests.* Two operational readiness tests were prepared for the launch of *Mariner V*. The first test was conducted over a two-day period and lasted for 23 h. The second and final test was conducted over a three-day period and lasted 32 h. The spacecraft tracking and telemetry data for the operational readiness tests were used to simulate the mission, in the same manner as in the combined operation test, by activating and exercising the equipment and systems of the Deep Space Stations to the greatest extent possible.

Participation of the AFETR in the test included simulating and providing *Atlas/Agena* booster launch countdown and boost phase flight events through injection; simulating and providing AFETR tracking data; calculating the parking orbit, transfer orbit, and orbital elements, injection criteria and DSIF look angles; and transmitting all these data to the SFOF by way of the communication system.

The Deep Space Stations at Goldstone, Woomera, Tidbinbilla, Madrid, Johannesburg, Cape Kennedy, and Ascension participated in the tests by processing the simulated tracking and telemetry data through the station equipment and transmitting the data to the SFOF by means of communication in keeping with established procedures and sequence of events. The stations also received and acknowledged receipt of commands and tracking predictions. The Deep Space Stations executed the commands and verified the execution times in accordance with the procedures established in the Tracking Instruction Manual. The tracking and telemetry data received at the SFOF was responded to in real time. The tracking data from the AFETR were processed and spacecraft tracking look angles and prediction data were transmitted to the appropriate Deep Space Stations. The tracking data from the stations were processed to establish the orbit of the spacecraft, and additional prediction data were transmitted to the appropriate stations. The tracking data were used to determine the orbit of the spacecraft and determine the requirements for the maneuver corrections. Maneuver commands were transmitted to the appropriate stations for simulated transmission to the spacecraft.

## G. FPAC Early Mission Performance

*1. Tracking data coverage.* During the nonpowered transfer flight period between $06^h29^m$ GMT, June 14, and $23^h07^m$ GMT, June 19, essentially continuous tracking coverage was obtained by DSS 11 (Goldstone, Pioneer), 41 (Woomera), 42 (Tidbinbilla), 51 (Johannesburg), and 61 (Madrid). DSS 41 and 51 participated only briefly in the early phase of this period, as Table VI-4 shows. The types of data used in determining the orbit of the spacecraft are as follows:

(1) HA, DEC (hour angle, declination): The pointing angle of the tracking antenna, in degrees, used only in the very early orbits.

(2) CC3 (S-band phase-coherent counted doppler): A measure of the topocentric radial velocity of the

**Table VI-4. DSIF tracking data used in computations of *Mariner V* premaneuver orbits**

| Orbit identification | DSS | Data type[a] | GMT Data | | Number of points[b] | Standard deviation[a] | RMS[a] | Mean error[a] | Remarks |
|---|---|---|---|---|---|---|---|---|---|
| | | | Beginning | Ending | | | | | |
| PROR XA | 51 | HA | 6/14 062932 | 6/14 065042 | 24 | 0.00887 | 0.00899 | −0.00141 | Biased DSS 51 angles |
| | 51 | DEC | 062932 | 065042 | 24 | 0.0538 | 0.0538 | −0.00178 | |
| PROR YA | 41 | HA | 070412 | 072702 | 27 | 0.0554 | 0.206 | 0.198 | |
| | 41 | DEC | 070412 | 072702 | 27 | 0.156 | 0.331 | −0.291 | |
| | 42 | HA | 071052 | 072602 | 55 | 0.0242 | 0.453 | −0.452 | Incorrectly computed DSS 42 angles |
| | 42 | DEC | 071052 | 072602 | 55 | 0.109 | 0.612 | 0.602 | |
| | 51 | HA | 070412 | 071651 | 79 | 0.280 | 0.179 | 0.177 | |
| | 51 | DEC | 070412 | 071651 | 79 | 0.517 | 0.367 | −0.364 | |
| | 51 | CC3 | 070417 | 071648 | 77 U | 0.290 | 0.291 | 0.142 | |
| ICEV XA | 41 | HA | 065342 | 082002 | 87 | 0.0515 | 0.0852 | 0.0678 | |
| | 41 | DEC | 065342 | 082002 | 87 | 0.0328 | 0.161 | −0.157 | |
| | 42 | HA | 065842 | 081902 | 42 | 0.247 | 0.644 | −0.594 | Incorrectly computed DSS 42 angles |
| | 42 | DEC | 065842 | 081902 | 42 | 0.303 | 0.811 | 0.752 | |
| | 51 | HA | 070402 | 081802 | 97 | 0.00719 | 0.0672 | 0.0669 | |
| | 51 | DEC | 070402 | 081802 | 97 | 0.0405 | 0.203 | −0.199 | |
| | 51 | CC3 | 070357 | 081732 | 94 U | 0.310 | 0.317 | 0.0671 | |
| ICEV YA | 42 | CC3 | 083632 | 085632 | 14 U | No summary printed | | | |
| | 51 | HA | 070412 | 090002 | 186 | 0.00659 | 0.00696 | 0.00223 | |
| | 51 | DEC | 070412 | 090002 | 186 | 0.00459 | 0.00464 | 0.0007 | |
| | 51 | CC3 | 070357 | 082932 | 162 U | 0.103 | 0.107 | −0.0296 | |
| ICEV XB | 42 | CC3 | 083432 | 092932 | 54 U | 0.0125 | 0.0131 | 0.00387 | |
| | 51 | CC3 | 070357 | 104532 | 132 U | 0.0303 | 0.0308 | −0.00564 | |
| MDPR YA | 42 | CC3 | 083632 | 085632 | 19 U | 0.00726 | 0.00727 | 0.000514 | |
| | 51 | CC3 | 070417 | 082932 | 152 U | 0.0574 | 0.0574 | −0.000437 | |
| PREL YA | 42 | CC3 | 083632 | 085632 | 19 U | 0.00680 | 0.0136 | 0.000185 | |
| | 51 | CC3 | 070417 | 082932 | 151 U | 0.0562 | 0.0567 | −0.00708 | |
| PREL YB | 42 | CC3 | 083632 | 092932 | 48 U | 0.0133 | 0.0133 | 0.000346 | |
| | 51 | CC3 | 070357 | 132032 | 228 U | 0.0325 | 0.0325 | −0.00135 | |
| | 61 | CC3 | 114032 | 123232 | 41 U | 0.0161 | 0.0162 | 0.00164 | |
| DACO YA | 51 | CC3 | 083632 | 174032 | 306 U | 0.0297 | 0.0297 | −0.00123 | |
| | 61 | CC3 | 114032 | 170932 | 149 U | 0.0163 | 0.0163 | 0.000934 | |
| GLPR YA | 42 | CC3 | 083632 | 092932 | 48 U | 0.0131 | 0.0131 | −0.000 | |
| | 51 | CC3 | 070357 | 182532 | 379 U | 0.0459 | 0.0460 | −0.00190 | |
| | 61 | CC3 | 6/14 114032 | 6/14 170932 | 149 U | 0.0164 | 0.0164 | 0.0008 | |

[a]Hour angle (HA) and declination (DEC) are expressed in degrees; and S-band phase-coherent counted doppler (CC3), in Hz (1 m/s $\simeq$ 15.3 Hz).

[b]C is *compressed*—data are averaged over 600-s intervals; *U* is *uncompressed*—data are counted over a period of 10 or 60 s.

[c]Data from here to end of table refer to CC3 data only.

spacecraft, and the primary type of orbit data. Units—1 m/s $\simeq$ 15.3 Hz.

*a. Summary.* Table VI-4 shows the tracking data available in the premaneuver orbits. Angle data, only, were obtained until $07^h03^m57^s$ GMT, approximately 40 min after injection into transfer orbit. The angles from DSS 51 were biased until this time, when it was discovered that the antenna had been tracking on a side lobe. Orbit PROR XA is corrupted by these biased angles. The DSS 42 angles in orbits PROR YA and ICEV XA are effectively biased because of an incorrect station latitude used in the computations of these orbits.

**Table VI-4 (contd)**

| Orbit identification | DSS | Data type[a] | GMT Data | | Number of points[b] | Standard deviation[a] | RMS[a] | Mean error[a] | Remarks |
|---|---|---|---|---|---|---|---|---|---|
| | | | Beginning | Ending | | | | | |
| DACO YB | 11 | CC3 | 6/14 185432 | 6/14 212532 | 87 U | 0.0206 | 0.0244 | 0.0132 | |
| | 42 | CC3 | 083632 | 6/14 092932 | 48 U | 0.0131 | 0.0154 | −0.00795 | |
| | 51 | CC3 | 070357 | 6/14 182532 | 379 U | 0.0464 | 0.0465 | −0.00275 | |
| | 61 | CC3 | 114032 | 6/14 170932 | 149 U | 0.0193 | 0.0194 | 0.00113 | |
| NOMA 1 | 11 | CC3 | 185432 | 6/15 015332 | 341 U | 0.0197 | 0.0204 | −0.00507 | |
| | 42 | CC3 | 083632 | 6/15 111332 | 553 U | 0.00978 | 0.00979 | −0.000441 | |
| | 51 | CC3 | 070357 | 6/14 182532 | 378 U | 0.0468 | 0.0470 | −0.00200 | |
| | 61 | CC3 | 114032 | 6/15 183032 | 538 U | 0.0114 | 0.0118 | 0.00286 | |
| NOMA 2 | 11 | 60001[c] | 6/14 223032 | 6/15 015332 | 191 U | 0.00855 | 0.0216 | −0.0198 | Estimated |
| | | 60002 | 6/15 193332 | 6/15 214228 | 116 U | 0.00700 | 0.0210 | −0.0198 | Station locations, solar pressure, and AU |
| | | 10002 | 6/15 214258 | 6/15 214407 | 7 U | 0.0240 | 0.0273 | −0.0130 | |
| | | 60003 | 6/16 193432 | 6/16 202532 | 52 U | 0.00804 | 0.0230 | −0.0215 | |
| | 42 | 60002 | 6/15 020532 | 6/15 111332 | 505 U | 0.00441 | 0.0205 | −0.0200 | Post roll data |
| | | 60003 | 6/16 002532 | 6/16 111332 | 515 U | 0.00530 | 0.0229 | −0.0223 | |
| | 61 | 60002 | 6/15 112532 | 6/15 192332 | 428 U | 0.00739 | 0.0210 | −0.0197 | |
| | | 60003 | 6/16 112832 | 6/16 191332 | 371 U | 0.00839 | 0.0244 | −0.0229 | |
| NOMA 3 | 11 | 60001 | 6/14 185432 | 6/15 015302 | 19 C, 168 U | 0.0157 | 0.0157 | 0.000473 | All data |
| | | 60002 | 6/15 193802 | 6/16 213702 | 13 C | 0.00232 | 0.00285 | −0.00165 | |
| | | 60003 | 6/16 193902 | 6/16 225032 | 6 C, 103 U | 0.00757 | 0.00816 | −0.00305 | |
| | 42 | 60001 | 6/14 083632 | 6/14 092932 | 48 U | 0.0135 | 0.0138 | −0.00252 | |
| | | 60002 | 6/15 021002 | 6/15 111302 | 57 C | 0.00217 | 0.00232 | 0.000822 | |
| | | 60003 | 6/16 003002 | 6/16 111102 | 61 C | 0.00359 | 0.00445 | −0.00263 | |
| | 51 | 10001 | 6/14 070422 | 6/14 070422 | 1 U | 0.000 | 0.0371 | 0.0371 | |
| | | 05001 | 6/14 071116 | 6/14 071811 | 7 U | 0.00742 | 0.00755 | −0.00140 | |
| | | 60001 | 6/14 072032 | 6/14 182532 | 273 U | 0.0158 | 0.0158 | −0.00164 | |
| | 61 | 60001 | 6/14 114032 | 6/14 170932 | 149 U | 0.0159 | 0.0161 | −0.00275 | |
| | | 60002 | 6/15 112532 | 6/15 192232 | 58 C | 0.00541 | 0.00551 | 0.00104 | |
| | | 60003 | 6/16 112832 | 6/16 191332 | 46 C | 0.00488 | 0.00495 | −0.000860 | |
| NOMA 4 | 11 | 60001 | 6/14 223032 | 6/15 015302 | 39 C | 0.00876 | 0.00905 | −0.00228 | Post roll data |
| | | 6002 | 6/15 193802 | 6/15 213702 | 13 C | 0.00165 | 0.00200 | −0.00113 | |
| | | 6003 | 6/16 193902 | 6/17 012332 | 6 C, 233 U | 0.00234 | 0.00239 | 0.000468 | |
| | | 6004 | 6/17 190532 | 6/17 195232 | 37 U | 0.00366 | 0.00526 | 0.00377 | |
| | 42 | 60002 | 6/15 021002 | 6/15 111302 | 57 C | 0.00278 | 0.00278 | 0.0000685 | |
| | | 60003 | 6/16 003002 | 6/16 111102 | 61 C | 0.00341 | 0.00342 | −0.000240 | |
| | | 60004 | 6/17 013632 | 6/17 111232 | 222 U | 0.00460 | 0.00483 | −0.00146 | |
| | 61 | 60001 | 6/15 112532 | 6/15 192232 | 58 C | 0.00511 | 0.00537 | 0.00166 | |
| | | 60002 | 6/16 112832 | 6/16 191332 | 47 C | 0.00501 | 0.00510 | 0.000925 | |
| | | 60003 | 6/17 120132 | 6/17 183632 | 207 U | 0.00749 | 0.00751 | −0.000646 | |

## Table VI-4 (contd)

| Orbit identification | DSS | Data type[a] | GMT Data | | Number of points[b] | Standard deviation[a] | RMS[a] | Mean error[a] | Remarks |
|---|---|---|---|---|---|---|---|---|---|
| | | | Beginning | Ending | | | | | |
| NOMA 5 | 11 | 60001 | 6/14 185432 | 6/15 015302 | 19 C, 168 U | 0.0141 | 0.0141 | −0.00004 | All data |
| | | 60002 | 6/15 193802 | 6/15 213702 | 13 C | 0.00212 | 0.00323 | −0.00244 | |
| | | 60003 | 6/16 193902 | 6/17 012132 | 51 C | 0.00227 | 0.00287 | −0.00175 | |
| | | 60004 | 6/17 190702 | 6/17 212932 | 5 C, 87 U | 0.00277 | 0.00277 | 0.00004 | |
| | 42 | 60001 | 6/14 083632 | 6/14 092932 | 48 U | 0.0135 | 0.0138 | −0.00248 | |
| | | 60002 | 6/15 021002 | 6/15 111302 | 57 C | 0.00214 | 0.00232 | 0.000917 | |
| | | 60003 | 6/16 003002 | 6/16 111102 | 61 C | 0.00355 | 0.00404 | −0.00194 | |
| | | 60004 | 6/17 014102 | 6/17 111202 | 26 C | 0.00250 | 0.00383 | −0.00291 | |
| | 51 | 10001 | 6/14 070422 | 6/14 070422 | 1 U | 0.000 | 0.0371 | 0.0371 | |
| | | 05001 | 6/14 071311 | 6/14 071811 | 6 U | 0.00811 | 0.00827 | −0.00163 | |
| | | 60001 | 6/14 072032 | 6/14 182532 | 273 U | 0.0158 | 0.0159 | −0.00155 | |
| | 61 | 60001 | 6/14 114032 | 6/14 170932 | 149 U | 0.0157 | 0.0159 | −0.00259 | |
| | | 60002 | 6/15 112532 | 6/15 192232 | 58 C | 0.00551 | 0.00572 | 0.00153 | |
| | | 60003 | 6/16 112832 | 6/17 120332 | 47 C | 0.00481 | 0.00481 | 0.00007 | |
| | | 60004 | 6/17 121402 | 6/17 183402 | 25 C | 0.00237 | 0.00304 | −0.00191 | |
| NOMA 6 | 11 | 60001 | 6/14 225502 | 6/15 015302 | 19 C | 0.00372 | 0.00376 | −0.00056 | Post roll data |
| | | 60002 | 6/15 193802 | 6/15 214228 | 14 C | 0.00175 | 0.00286 | −0.00227 | |
| | | 10002 | 6/15 214317 | 6/15 214402 | 2 U | 0.00171 | 0.00173 | −0.0002 | |
| | | 60003 | 6/16 193902 | 6/17 012132 | 51 C | 0.00248 | 0.00248 | 0.00005 | |
| | | 60004 | 6/17 191002 | 6/18 020832 | 14 C, 271 U | 0.00258 | 0.00259 | 0.000149 | |
| | | 60005 | 6/18 185132 | 6/18 190432 | 14 U | 0.00208 | 0.0158 | 0.0157 | |
| | 42 | 60002 | 6/15 021002 | 6/15 111302 | 57 C | 0.00285 | 0.00287 | −0.000291 | |
| | | 60003 | 6/16 003002 | 6/16 111102 | 61 C | 0.00329 | 0.00331 | −0.000408 | |
| | | 60004 | 6/17 014102 | 6/17 111202 | 26 C | 0.00221 | 0.00274 | −0.00162 | |
| | | 60005 | 6/18 021932 | 6/18 111232 | 443 U | 0.00443 | 0.00444 | 0.000312 | |
| | 61 | 60002 | 6/15 112532 | 6/15 192232 | 58 C | 0.00522 | 0.00543 | 0.00148 | |
| | | 60003 | 6/16 112832 | 6/17 120332 | 47 C | 0.00500 | 0.00505 | 0.000758 | |
| | | 60004 | 6/17 121402 | 6/17 183402 | 42 C | 0.00232 | 0.00274 | −0.00145 | |
| | | 60005 | 6/18 115232 | 6/18 183632 | 193 U | 0.00805 | 0.00821 | 0.00163 | |
| NOMA 7 | 11 | 60001 | 6/14 185432 | 6/15 015302 | 19 C, 168 U | 0.0141 | 0.0141 | 0.000324 | All data |
| | | 60002 | 6/15 193802 | 6/15 213702 | 13 C | 0.00192 | 0.00329 | −0.00267 | |
| | | 60003 | 6/16 193902 | 6/17 012132 | 51 C | 0.00227 | 0.00252 | −0.00109 | |
| | | 60004 | 6/17 191002 | 6/18 020702 | 44 C | 0.00209 | 0.00209 | 0.00010 | |
| | | 60005 | 6/18 185602 | 6/18 190302 | 2 C | 0.000732 | 0.0144 | 0.000208 | |
| | 42 | 60001 | 6/14 083632 | 6/14 092932 | 48 U | 0.0137 | 0.0139 | −0.00246 | |
| | | 60002 | 6/15 021002 | 6/15 111302 | 57 C | 0.00209 | 0.00233 | 0.00104 | |
| | | 60003 | 6/16 003002 | 6/16 111102 | 61 C | 0.00364 | 0.00402 | −0.00170 | |
| | | 60004 | 6/17 014102 | 6/17 111202 | 26 C | 0.00246 | 0.00363 | −0.00267 | |
| | | 60005 | 6/18 022402 | 6/18 110802 | 53 C | 0.00201 | 0.00202 | 0.00006 | |

## Table VI-4 (contd)

| Orbit identification | DSS | Data type[a] | GMT Data | | Number of points[b] | Standard deviation[a] | RMS[a] | Mean error[a] | Remarks |
|---|---|---|---|---|---|---|---|---|---|
| | | | Beginning | Ending | | | | | |
| NOMA 7 (contd) | 51 | 10001 | 6/14 070422 | 6/14 070422 | 1 U | 0.000 | 0.0371 | 0.0371 | |
| | | 05001 | 6/14 071311 | 6/14 071811 | 6 U | 0.00826 | 0.00857 | −0.00228 | |
| | | 60001 | 6/14 072032 | 6/14 182532 | 273 U | 0.0158 | 0.0159 | −0.00116 | |
| | 61 | 60001 | 6/14 114032 | 6/14 170932 | 149 U | 0.0157 | 0.0159 | −0.00234 | |
| | | 60002 | 6/15 112532 | 6/15 192232 | 58 C | 0.00570 | 0.00595 | 0.00168 | |
| | | 60003 | 6/16 112832 | 6/17 120332 | 47 C | 0.00493 | 0.00493 | 0.000135 | |
| | | 60004 | 6/17 121402 | 6/17 183402 | 42 C | 0.00206 | 0.00254 | −0.00149 | |
| | | 60005 | 6/18 115702 | 6/18 183302 | 23 C | 0.00300 | 0.00354 | 0.00189 | |
| LAMC | 11 | 60001 | 6/14 225502 | 6/15 015302 | 19 C | 0.00403 | 0.00443 | −0.00185 | Post roll data |
| | | 60002 | 6/15 193802 | 6/15 213702 | 13 C | 0.00161 | 0.00190 | −0.00101 | |
| | | 60003 | 6/16 193902 | 6/17 012132 | 51 C | 0.00248 | 0.00292 | 0.00154 | |
| | | 60004 | 6/17 191002 | 6/18 020702 | 44 C | 0.00167 | 0.00170 | 0.000344 | |
| | | 60005 | 6/18 185602 | 6/18 223132 | 2 C, 182 U | 0.00347 | 0.00351 | −0.000539 | |
| | 42 | 60002 | 6/15 021002 | 6/15 111302 | 57 C | 0.00283 | 0.00283 | 0.000188 | |
| | | 60003 | 6/16 003002 | 6/16 111102 | 61 C | 0.00347 | 0.00358 | 0.000856 | |
| | | 60004 | 6/17 014102 | 6/17 111202 | 26 C | 0.00272 | 0.00327 | −0.00182 | |
| | | 60005 | 6/18 022402 | 6/18 110802 | 53 C | 0.00239 | 0.00259 | −0.00100 | |
| | 61 | 60002 | 6/15 112532 | 6/15 192232 | 58 C | 0.00529 | 0.00585 | 0.00248 | |
| | | 60003 | 6/16 112832 | 6/17 120332 | 47 C | 0.00493 | 0.00518 | 0.00161 | |
| | | 60004 | 6/17 121402 | 6/17 183402 | 42 C | 0.00225 | 0.00281 | −0.00169 | |
| | | 60005 | 6/18 115702 | 6/18 183302 | 23 C | 0.00287 | 0.00315 | −0.00132 | |
| LAPM | 11 | 60001 | 6/14 220032 | 6/15 015302 | 19 C, 36 U | 0.00789 | 0.00794 | −0.000897 | Includes some roll data from DSS 11 |
| | | 60002 | 6/15 193802 | 6/15 213702 | 13 C | 0.00164 | 0.00164 | −0.000338 | |
| | | 60003 | 6/16 193902 | 6/17 012132 | 51 C | 0.00258 | 0.00305 | 0.00162 | |
| | | 60004 | 6/17 191002 | 6/18 020702 | 44 C | 0.00162 | 0.00169 | −0.000488 | |
| | | 60005 | 6/18 185602 | 6/19 025332 | 23 C, 189 U | 0.00292 | 0.00304 | 0.000849 | |
| | | 60006 | 6/19 185332 | 6/19 221732 | 198 U | 0.00396 | 0.00398 | 0.000343 | |
| | 42 | 60002 | 6/15 021002 | 6/15 111302 | 57 C | 0.00277 | 0.00301 | 0.00117 | |
| | | 60003 | 6/16 003002 | 6/16 111102 | 69 C | 0.00331 | 0.00356 | 0.00130 | |
| | | 60004 | 6/17 014102 | 6/17 111202 | 59 C | 0.00261 | 0.00286 | −0.00115 | |
| | | 60005 | 6/18 022402 | 6/18 110802 | 53 C | 0.00269 | 0.00367 | −0.00249 | |
| | | 60006 | 6/19 010532 | 6/19 110332 | 412 U | 0.00463 | 0.00475 | −0.00105 | |
| | | 60006 | 6/19 110432 | 6/19 111132 | 8 U | 0.00346 | 0.00117 | 0.0112 | |
| | 61 | 60002 | 6/15 112532 | 6/15 191432 | 55 C | 0.00389 | 0.00453 | 0.00232 | |
| | | 60003 | 6/16 112832 | 6/17 120332 | 46 C | 0.00403 | 0.00413 | 0.000934 | |
| | | 60004 | 6/17 121402 | 6/17 183402 | 42 C | 0.00216 | 0.00360 | −0.00288 | |
| | | 60005 | 6/18 115702 | 6/18 183302 | 29 C | 0.00214 | 0.00398 | −0.00335 | |
| | | 60006 | 6/19 113132 | 6/19 183632 | 389 U | 0.00839 | 0.00851 | −0.00146 | |

*b. Compressed data.* In Table VI-4, the number of doppler points are tagged with either a *U* or a *C*. The *U* indicates the data counted over a period of 10 or 60 s. The later orbits in Table VI-4 are identified with a pass number listed under data type. This always refers to CC3 data only. The first two digits indicate the sample time of the data, in seconds, and the last three digits identify the pass number from that station. If the number of points is tagged with a *C*, this means that the data have been *compressed*, or averaged, over 600-s intervals. This smoothing process is reflected in improved statistics for individual points.

*c. Controlled roll data.* The spacecraft was in a controlled roll mode until approximately $22^h50^m$ GMT, June 14. Since the antenna is offset from the center of mass of the spacecraft, this caused a sine curve in the observed-minus-computed doppler residuals, with amplitude of about 0.02 Hz. This sine curve may be seen in the DSS 11 residual curve (Fig. VI-15). In referring to Table VI-4, it must be remembered that statistics on this part of the doppler tracking data are corrupted by this effect.

*d. Time resolver doppler.* Normally, doppler cycles are counted to the nearest cycle at a fixed sample rate under control of the station clock. For this mission, however, the operators at DSS 11 used a special device for incrementing the sample time to the exact time of zero-phase delay between transmitter and receiver. This device has the advantage of eliminating counter truncation error. Table VI-4 shows, for example, that with this system DSS 11 doppler achieved a standard deviation of 0.00234 Hz for 6 points with 600-s count time and 233 points with 60-s count time in pass 3 of orbit NOMA 4. This compares favorably with pass 4 of DSS 42 doppler in the same orbit, of which the standard deviation is 0.00460 Hz for 222 points with 60-s count time. Only DSS 11 used a time resolver device in the premaneuver phase of the mission.

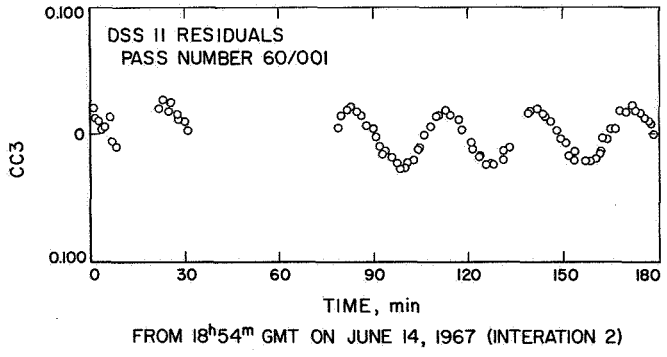



**Fig. VI-15. Doppler residuals during controlled roll**

*e. One-way doppler data.* Although not used in orbit reduction, one-way doppler data generated by the spacecraft oscillator is important to the encounter phase in the occultation experiment. Because of this importance, and also to establish the period of the CC&S cyclic, one-way doppler residuals are regularly computed by the ODP. Figure VI-16 shows the spacecraft oscillator warm-up curve with a discontinuity at $21^h57^m$ caused by the cyclic event, as seen in the one-way residuals. Note that spacecraft temperature is decreasing, a frequency drift effect that can be seen in the latter part of the curve.

**2. *Premaneuver orbit determination results.*** The Orbit Determination Program (ODP) uses a weighted least-squares technique for estimating up to 20 parameters and forming up to a $20 \times 20$ covariance matrix. The first 12 premaneuver orbits, through $19^h38^m$ GMT, June 15, estimated only geocentric equatorial position and velocity of the probe, with a corresponding $6 \times 6$ covariance matrix. Of these early orbits, PROR XA, PROR YA, and ICEV XA were degraded by biased angles, as was previously mentioned.

*a. Orbit state vector.* Table VI-5 shows the state vector solutions and associated standard deviations from the premaneuver orbits. Note that two epochs were used for

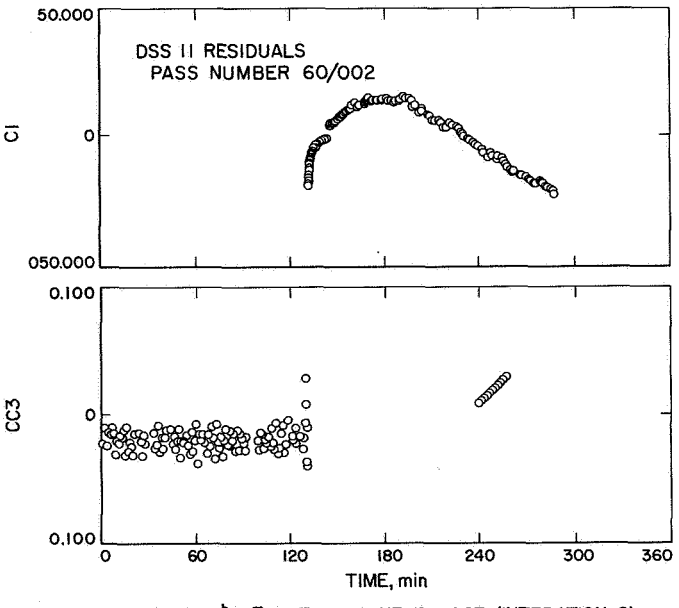



**Fig. VI-16. One-way warm-up curve showing cyclic event at $21^h57^m$ GMT**

## Table VI-5. Initial conditions of *Mariner V* premaneuver orbits

| Orbit identification | Epoch, GMT June 14, 1967 | Geocentric space-fixed position | | | Geocentric space-fixed velocity | | | Position uncertainties, 1 $\sigma$ | | | Velocity uncertainties, 1 $\sigma$ | | |
|---|---|---|---|---|---|---|---|---|---|---|---|---|---|
| | | x, km | y, km | z, km | x, km/s | y, km/s | z, km/s | $\sigma_x$, m | $\sigma_y$, m | $\sigma_z$, m | $\sigma_x$, m/s | $\sigma_y$, m/s | $\sigma_z$, m/s |
| PROR XA | 06:24:37.100 | 6430.7816 | −1160.2529 | −533.85299 | 1.7051417 | 9.6648580 | −5.7670747 | 9743.4 | 13897. | 5453.8 | 18.64 | 51.66 | 22.34 |
| PROR YA | | 6416.6756 | −1230.8562 | −731.91162 | 1.6219889 | 9.7114220 | −5.7422701 | 21435. | 45206. | 81177. | 23.42 | 30.59 | 38.50 |
| ICEV XA | | 6435.0075 | −1166.9439 | −523.24137 | 1.6985057 | 9.7519772 | −5.6694543 | 2938. | 7898. | 14923. | 9.853 | 6.898 | 7.800 |
| ICEV YA | | 6437.6896 | −1191.5500 | −534.17180 | 1.7101299 | 9.7199947 | −5.7073967 | 3147. | 9568. | 18419. | 11.75 | 10.15 | 12.09 |
| ICEV XB | | 6439.0375 | −1187.4443 | −537.59330 | 1.7017812 | 9.7221273 | −5.7049827 | 1056.8 | 3563. | 3497 | 0.9456 | 6.728 | 9.384 |
| MDPR YA | | 6438.9529 | −1186.4890 | −537.72921 | 1.7007203 | 9.7219321 | −5.7060349 | 2489.7 | 15015. | 7689.9 | 11.73 | 19.15 | 28.60 |
| PREL YA | | 6438.9480 | −1186.5558 | −537.74087 | 1.7007838 | 9.7218896 | −5.7060745 | 2489.5 | 15026. | 7672.8 | 11.73 | 19.16 | 28.61 |
| PREL YB | | 6439.0166 | −1187.2355 | −537.37487 | 1.7017861 | 9.7230284 | −5.7040332 | 761.3 | 518.5 | 629.2 | 0.6666 | 1.446 | 31.13 |
| DACO YA | | 6439.2577 | −1187.2355 | −537.37486 | 1.7017861 | 9.7225636 | −5.7043627 | 518.0 | 397.5 | 693.7 | 0.5347 | 0.7014 | 2.051 |
| GLPR YA | | 6439.2120 | −1187.3930 | −537.00825 | 1.7020798 | 9.7229566 | −5.7032949 | 1196.3 | 865.0 | 1505. | 1.046 | 1.612 | 4.645 |
| DACO YB | | 6438.9782 | −1187.1913 | −537.40764 | 1.7017661 | 9.7224742 | −5.7045916 | 287.9 | 373.7 | 428.2 | 0.3509 | 0.7723 | 1.055 |
| NOMA 1 | | 6439.0098 | −1187.2602 | −537.51488 | 1.7017203 | 9.7222863 | −5.7048408 | 68.76 | 108.5 | 130.3 | 0.0902 | 0.2164 | 0.2620 |
| NOMA 2 | | 6438.3870 | −1188.8097 | −536.31939 | 1.7035321 | 9.7224200 | −5.7047653 | 885.7 | 1526.7 | 922.5 | 1.623 | 0.5181 | 0.6515 |
| NOMA 3 | | 6439.0485 | −1187.3274 | −537.50841 | 1.7017447 | 9.7222307 | −5.7048470 | 30.23 | 46.54 | 33.63 | 0.0472 | 0.0529 | 0.0880 |
| NOMA 4 | 22:00:00.000 | −162050.57 | 155937.37 | −56185.187 | −2.6362289 | 2.1369942 | −0.69217914 | 1817. | 2135. | 2897. | 0.0203 | 0.0206 | 0.0433 |
| NOMA 5 | 06:24:37.100 | 6439.0489 | −1187.3289 | −537.50879 | 1.7017450 | 9.7222283 | −5.7048498 | 75.56 | 96.44 | 90.70 | 0.0803 | 0.1610 | 0.2012 |
| NOMA 6 | 22:00:00.000 | −162050.61 | 155937.28 | −56185.251 | −2.6362273 | 2.1369958 | −0.69218034 | 1611. | 1939. | 2779. | 0.0156 | 0.0170 | 0.0395 |
| NOMA 7 | 06:24:37.100 | 6439.0505 | −1187.3315 | −537.51215 | 1.7017435 | 9.7222240 | −5.7048541 | 74.91 | 94.08 | 88.51 | 0.0788 | 0.1568 | 0.1951 |
| LAMC | 22:00:00.000 | −162050.21 | 155937.31 | −56185.189 | −2.6362305 | 2.1369918 | −0.69218217 | 1611. | 1920. | 2772. | 0.0155 | 0.0168 | 0.0394 |
| LAPM | 22:00:00.000 | −162050.22 | 155937.32 | −56185.164 | −2.6362309 | 2.1369915 | −0.69218127 | 1537. | 1795. | 2706. | 0.0143 | 0.0154 | 0.0377 |

## Table VI-6. Target parameters of *Mariner V* premaneuver orbits

| Orbit identification | Time on computer | | Target statistics | | | | | | | | | | | Type solution | Encounter time |
|---|---|---|---|---|---|---|---|---|---|---|---|---|---|---|---|
| | GMT | day | B, km | B • T, km | B • R, km | $T_L$, days | SMIA, km | SMAA, km | $\theta$, deg | $\sigma_{B \cdot R}$, km | $\sigma_{B \cdot T}$, km | $\sigma_T$, s | $\sigma_S$, km | | GMT Oct 19, 1967 |
| PROR XA | 07:41:00 | 165 | 8608.9830 | 722810.36 | 467644.18 | 139.28 | 10351.4 | 3081917. | 162.72 | 915498. | 2942819. | 1675672. | 4628031. | 6 × 6 | Nov 1 01:58:43.431 |
| PROR YA | 08:42:00 | | 553321.70 | 452429.88 | −318546.85 | 123.09 | 24123. | 209929. | 27.15 | 98185. | 187114. | 106300. | 350763. | 6 × 6 | Oct 15 15:57:36.641 |
| ICEV XA | 08:56:00 | | 92462.993 | 63398.130 | −67305.878 | 126.7 | 6991.0 | 26896. | 46.01 | 19951. | 19344. | 25658. | 27790. | 6 × 6 | 02:27:56.082 |
| ICEV YA | 10:08:00 | | 103665.06 | 86031.496 | −57836.193 | 126.8 | 7445. | 29746. | 46.79 | 22274. | 21075. | 28906. | 88905. | 6 × 6 | 06:32:28.629 |
| ICEV XB | 11:49:00 | | 104715.86 | 81712.672 | −65486.255 | 126.7 | 2288.6 | 3398.8 | 178.63 | 2289.4 | 3398.2 | 2811.4 | 8670.3 | 6 × 6 | 03:50:01.188 |
| MDPR YA | 12:38:00 | | 103031.03 | 79941.151 | −64998.496 | 126.7 | 8585.9 | 21500. | 162.70 | 10395. | 20686. | 12917. | 39834. | 6 × 6 | 03:57:40.176 |
| PREL YA | 14:01:00 | | 103100.66 | 80043.522 | −64982.922 | 126.7 | 8583.7 | 21522. | 162.75 | 10389. | 20711. | 12899. | 39778. | 6 × 6 | 03:58:06.020 |
| PREL YB | 14:36:00 | | 104640.21 | 81534.246 | −65587.639 | 126.7 | 579.1 | 1902.0 | 73.68 | 1832.6 | 771.1 | 2246. | 6928. | 6 × 6 | 03:47:45.326 |
| DACO YA | 18:51:00 | | 104922.83 | 81680.620 | −65856.484 | 126.7 | 183.0 | 564.8 | 68.67 | 530.3 | 267.0 | 604.9 | 1865.6 | 6 × 6 | 03:43:10.051 |
| GLPR YA | 19:44:00 | | 104885.59 | 81661.791 | −65820.505 | 126.7 | 377.8 | 1347. | 70.77 | 1278.6 | 569.4 | 1465. | 4518. | 6 × 6 | 03:43:46.342 |
| DACO YB | 22:18:00 | | 104511.22 | 81482.685 | −65445.908 | 126.7 | 317.5 | 406.9 | 39.62 | 356.5 | 373.1 | 431.8 | 1131.5 | 6 × 6 | 03:50:20.814 |
| NOMA 1 | 19:38:00 | 166 | 104540.10 | 81532.887 | −65429.504 | 126.7 | 81.53 | 157.0 | 39.48 | 118.0 | 131.8 | 164.8 | 508.3 | 6 × 6 | 03:50:41.614 |
| NOMA 2 | 23:07:00 | 167 | 104422.43 | 81494.182 | −65289.677 | 126.7 | 171.2 | 192.3 | 96.49 | 192.0 | 171.5 | 221.7 | 683.7 | 14 × 14 | 03:53:54.728 |
| NOMA 3 | 00:33:00 | 168 | 104398.75 | 81459.476 | −65295.114 | 126.7 | 142.0 | 175.8 | 125.8 | 165.0 | 154.4 | 179.1 | 552.2 | 16 × 16 | 03:55:00.697 |
| NOMA 4 | 21:54:00 | 168 | 104382.47 | 81456.020 | −65273.405 | 126.1 | 131.5 | 196.3 | 59.75 | 182.0 | 150.6 | 253.0 | 780.3 | 14 × 14 | 03:55:27.945 |
| NOMA 5 | 23:00:00 | 168 | 104382.32 | 81450.270 | −65280.322 | 126.7 | 75.6 | 152.7 | 56.01 | 133.5 | 106.0 | 201.8 | 622.2 | 16 × 16 | 03:55:27.285 |
| NOMA 6 | 20:36:00 | 169 | 104395.13 | 81470.350 | −65275.753 | 126.1 | 78.2 | 202.8 | 94.80 | 202.7 | 178.4 | 235.1 | 724.9 | 14 × 14 | 03:55:19.402 |
| NOMA 7 | 22:20:00 | 169 | 104388.91 | 81454.418 | −65285.684 | 126.7 | 155.3 | 180.8 | 117.01 | 175.8 | 160.9 | 194.6 | 600.0 | 16 × 16 | 03:55:18.761 |
| LAMC | 23:51:00 | 169 | 104447.01 | 81483.270 | −65342.590 | 126.1 | 176.7 | 203.0 | 94.97 | 202.9 | 176.9 | 235.5 | 726.1 | 14 × 14 | 03:53:14.919 |
| LAPM | 22:30:00 | 178 | 104455.70 | 81486.744 | −65352.149 | 126.1 | 162.9 | 194.1 | 107.71 | 191.4 | 166.1 | 213.1 | 657.2 | 16 × 16 | 03:53:00.547 |

starting the trajectory integration. Orbits using an epoch of $06^h24^m37^s.100$ include data taken during the controlled roll period, whereas orbits with an epoch of $22^h00^m00^s.000$ did not include these data in the least-squares fit.

*b. Target point.* The ODP has the capability of mapping the covariance matrix from the epoch to the target planet at time of closest approach. These target parameters are expressed in the B-plane system (see section III for definitions). Target parameters and statistics are tabulated for each orbit in Table VI-6. The parameter $T_L$ is the time of flight linearized along the incoming asymptote of the planet-centered flight hyperbola. *SMIA* is the semiminor axis and *SMAA* the semimajor axis of the 1-$\sigma$ dispersion ellipse of the OD uncertainty in the B-plane. The angle $\theta$ gives the orientation of *SMAA*, measured counterclockwise from **T**. The vector **S** lies along the incoming asymptote and is normal to the B-plane. The target point of each orbit, except for PROR XA and PROR YA, is plotted in the B-plane in Figs. VI-17 and VI-18.

*c. Solar radiation pressure.* The perturbative spacecraft acceleration resulting from solar radiation pressure is modeled by

$$\ddot{r} = \frac{kA}{mr^2}(1 + \gamma_B)$$

where

$r$ = the sun–probe distance in kilometers

k = $1.031 \times 10^8$, a solar radiation constant

$A$ = the spacecraft effective area normal to $r$, nominally 6.60519 square meters

$m$ = the spacecraft mass, nominally 245.71 kilograms

$\gamma_B$ = the reflectivity coefficient of the spacecraft, nominally 0.40123054

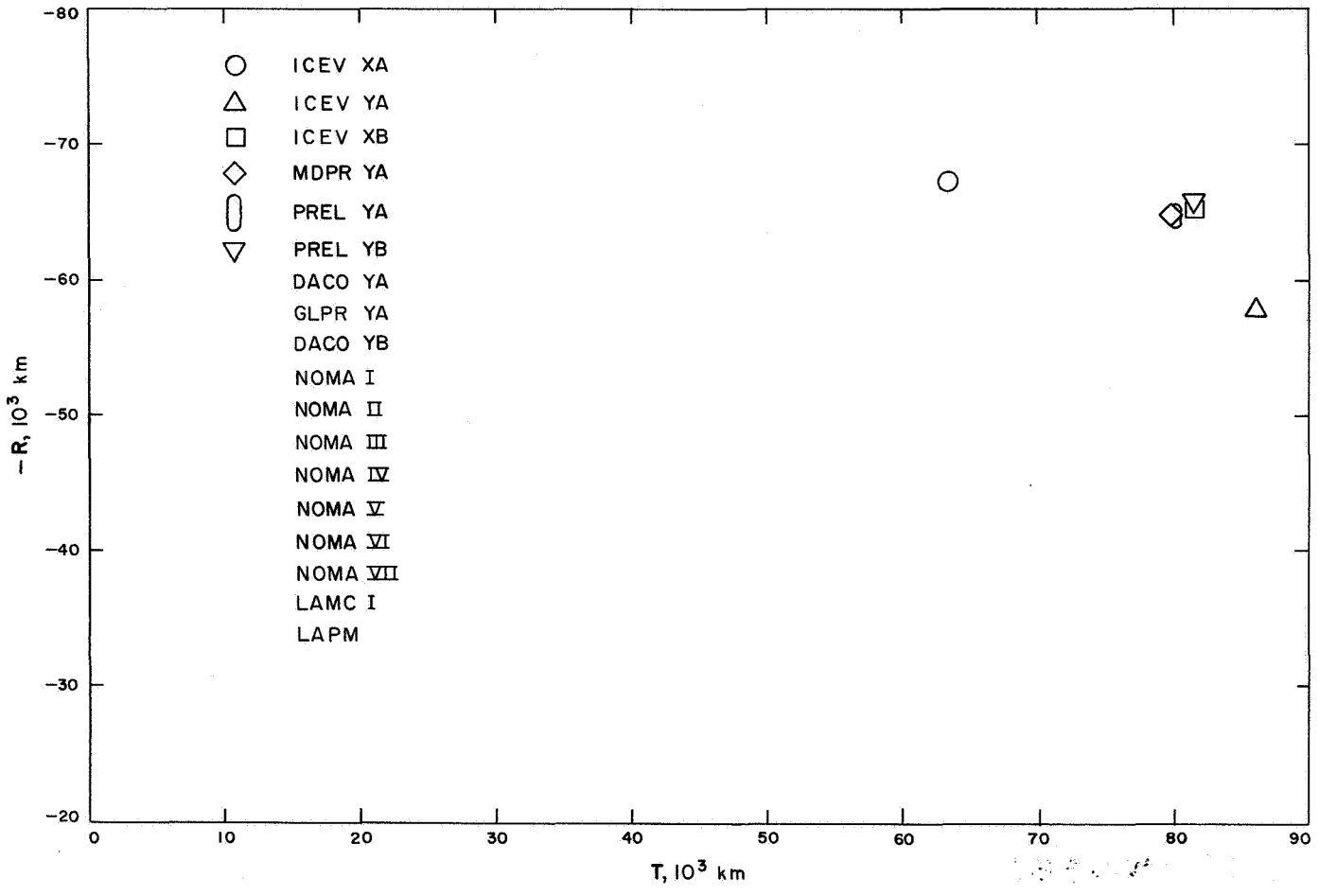



**Fig. VI-17. B-plane plot of *Mariner* Venus 67 premaneuver orbits showing origin at Venus**

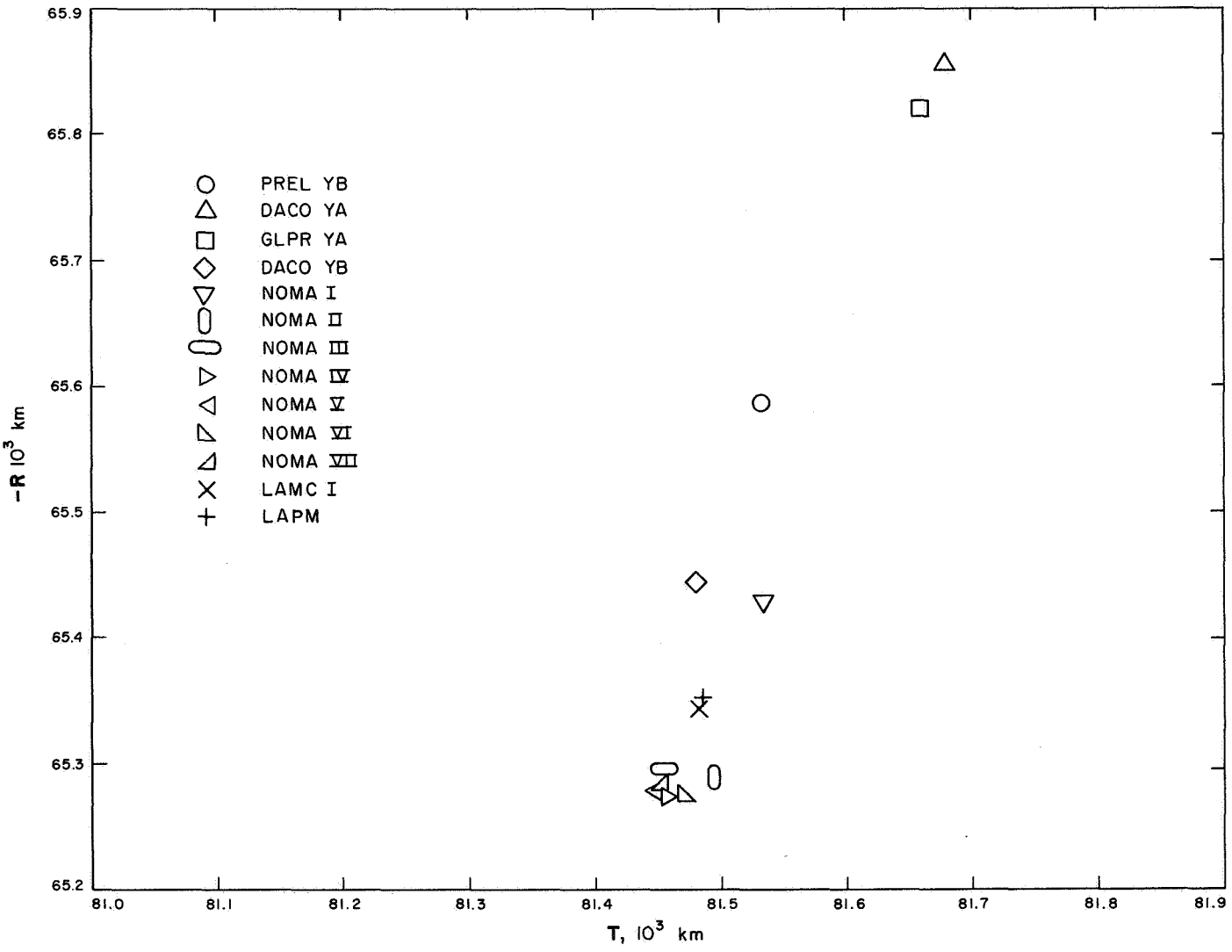



**Fig. VI-18. B-plane plot of *Mariner* Venus 67 premaneuver orbits with expanded scale**

**Table VI-7. Preliminary *Mariner V* solutions for solar radiation. Pressure, station locations and geocentric equatorial state vector at 23:08:20:650, June 19, 1967**

| Parameter | Nominal, $\sigma$ | | Premidcourse, $\sigma$ | Postmidcourse, $\sigma$ | Observed post minus pre[a] |
|---|---|---|---|---|---|
| $\gamma_B$ | 0.40123054 | ±0.0400 | 0.40864007 ±0.0288 | 0.37740661 ±0.0112 | −0.03123346 |
| $\rho_{11} \cos \phi_{11}$, m | 5206353.3 | ±20.0 | 5206331.4 ±12.4 | 5206327.1 ±3.5 | −4.3 |
| $\lambda_{11}$, deg | 243.15091 | ±0.00050 | 243.15101 ±0.00029 | 243.15070 ±0.00018 | −0.00031 |
| $\rho_{42} \cos \phi_{42}$, m | 5205341.6 | ±20.0 | 5205353.5 ±12.0 | 5205347.3 ±2.7 | −6.2 |
| $\lambda_{42}$, deg | 148.98148 | ±0.00050 | 148.98174 ±0.00029 | 1489.98141 ±0.00018 | −0.00033 |
| $\rho_{61} \cos \phi_{61}$, m | 4862604.5 | ±18.7 | 4862606.4 ±11.8 | 4862597.6 ±4.3 | −8.8 |
| $\lambda_{61}$, deg | 355.75113 | ±0.00050 | 355.75146 ±0.00029 | 355.75114 ±0.00018 | −0.00032 |
| | Nominal post+midcourse | Nominal post minus pre | | | |
| $x$, km | −1194559 | −0.013 | −1194557.7 ±6.3 | −1194553.1 ±3.3 | 4.6 |
| $y$, km | 986069.1 | −0.121 | 986069.08 ±6.49 | 986080.15 ±3.9 | 11.07 |
| $z$, km | −3196927 | −0.258 | −319692.25 ±16.95 | −319678.29 ±6.2 | 13.96 |
| $x$, m/s | −2280.931 | −0.741 | −2280.1899 ±0.0128 | −2280.8194 ±0.0067 | −0.6295 |
| $y$, m/s | 1842.512 | −6.849 | 1849.3605 ±0.0133 | 1842.7422 ±0.0071 | −6.6183 |
| $z$, m/s | −588.9205 | −14.5851 | −574.33642 ±0.03335 | −588.24114 +0.00567 | −13.90472 |
| $V$, m/s | | 16.1272 | | | 15.4123 |
| $l$ | | −0.045743 | | | −0.040844 |
| $m$ | | −0.42476 | | | −0.429416 |
| $n$ | | −0.90415 | | | −0.90218 |

[a]This was the orbit (LAPM) using all the data up to the time of motor ignition.

Table VI-7 shows the premaneuver and postmaneuver least-squares solutions for $\gamma_B$. It is apparent that the span of tracking data available in the premaneuver solution is not adequate for a strong solution, as the standard deviation has not significantly improved over the a prior standard deviation assigned to the nominal value. By contrast, the postmaneuver solution contains nearly a month of tracking data, including ranging data. Moreover, the ranging data are particularly effective in this type of solution.

*d. Station locations.* The ODP is capable of estimating tracking station locations to a high degree of precision where sufficient doppler tracking data has been obtained. In the premaneuver phase of the mission, solutions were obtained for the locations of DSS 11, 42, and 61. These are tabulated and compared with nominal values and postmaneuver solutions in Table VI-7: $\rho$ is the geocentric radius vector to the station, $\phi$ is the geocentric latitude, and $\lambda$ the longitude. The systematic differences in longitude of about 0°.0003 between the premaneuver and postmaneuver solutions are probably caused by the earth ephemeris error. This maps into an insignificant error at target, however. The cause of the systematic differences in $\rho \cos \phi$, the distance from the spin axis of the earth, is unknown; these are also very small (4.3–8.8 m).

*3. Midcourse maneuver analysis based on orbit information.* Orbit determination after spacecraft injection showed that a midcourse maneuver would be required to bring *Mariner V* within 8,200 km of Venus center at closest approach. Accordingly, pitch and roll turns, followed by a nominal 17.66-s motor burn, were planned to this end.

*a. Pitch and roll turns.* Figures VI-19 and VI-20 show that the premaneuver pitch and roll commands were successfully executed by the spacecraft preparatory to motor ignition. The amplitude of the observed doppler residuals depended upon the antenna offset from the center of gravity at the spacecraft and the time period over which the turns were executed.

*b. Comparison of state vectors.* Table VI-7 shows the geocentric equatorial state vectors of the best available premidcourse orbit (LAPM) and postmidcourse orbit (POST 16) at a common epoch of $23^h08^m20^s650$ GMT,

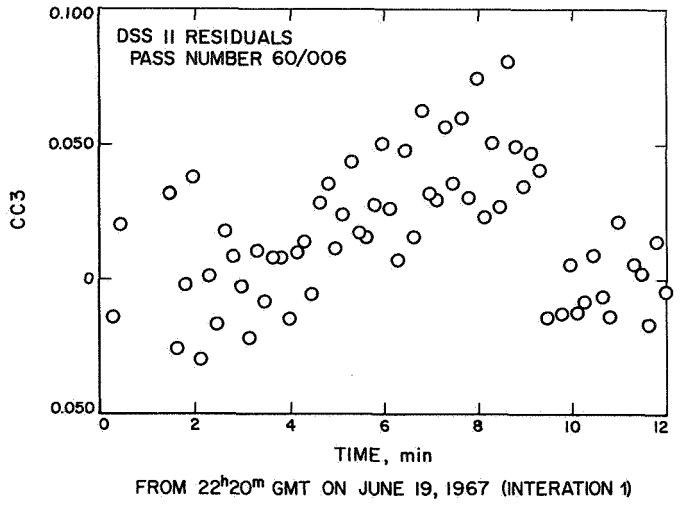



**Fig. VI-19. Doppler tracking residuals from DSS 11 during premaneuver pitch-turn**

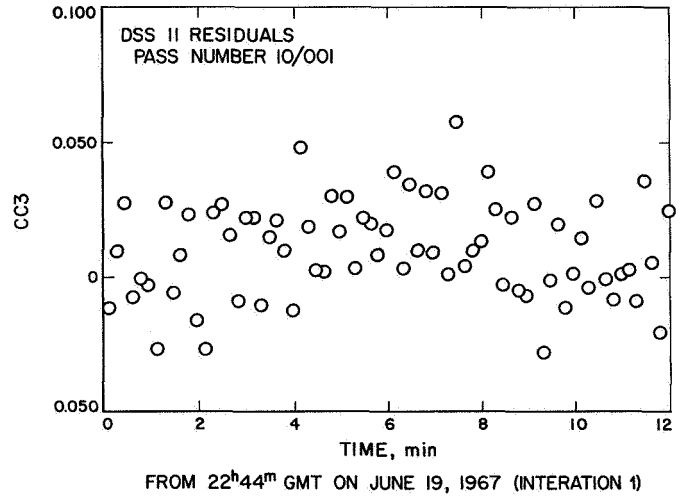



**Fig. VI-20. Doppler tracking residuals from DSS 11 during premaneuver roll-turn**

June 19, 1967. Since the epoch was chosen during the interval of midcourse motor burn, the difference between the orbit velocity vectors, tabulated on the right, is the observed velocity increment $V$ due to motor impulse. The magnitude of the nominal burn (based on orbit LAMC) have also been tabulated in Table VI-7 as well as the equatorial direction cosines $l$, $m$, and $n$ of the thrust vector. The observed positions have been tabulated only to show that they fall within their computed standard deviations. Positional errors of this magnitude do not map into significant target errors, nor do they affect the velocity calculations materially.

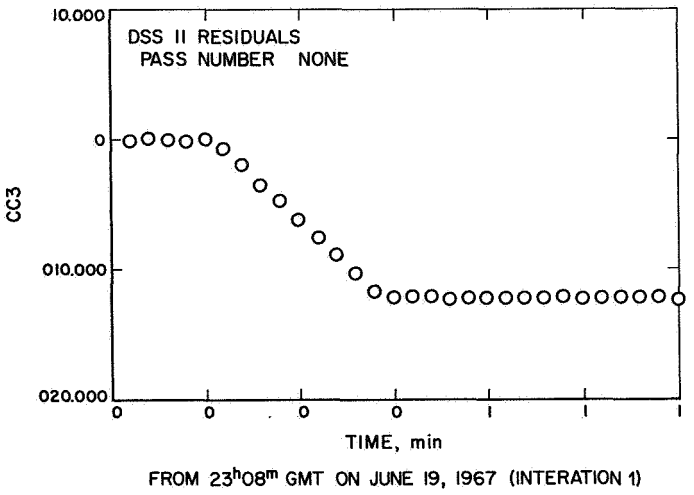



**Fig. VI-21. Doppler tracking residuals from DSS 11 during midcourse motor burn**

Figure VI-21 is a plot of DSS 11 tracking residuals during the maneuver, showing the topocentric radial velocity component of the burn.

*c. Conclusions.* Orbit results indicate that a 0.715 m/s error was made in the magnitude of the motor burn. The nominal and observed direction cosines agree strikingly, indicating a very small pointing error. If $\psi$ is the angle of the observed thrust axis from the nominal thrust axis, with subscripts used to denote observed and nominal direction cosines, then

$$\cos\psi = l_{observed}\, l_{nominal} + m_{observed}\, m_{nominal} + n_{observed}\, n_{nominal}$$
$$= 0.9999731, \text{ or } \psi \simeq 0.4^\circ$$

Interestingly, this is approximately the attitude control error at the maximum of the limit cycle, and telemetry shows the spacecraft to be in this position at the time the motor burn was executed.

***4. Trajectory analysis.*** During the *Atlas* sustainer and vernier stages, commands in vehicle attitude and engine cutoff times were given to adjust the altitude and velocity at *Atlas* vernier-engine cutoff. After the *Atlas/Agena* separation, a short coast period preceded the first *Agena* ignition. At a preset value of velocity increment, the *Agena* engine was shut off; at that time both the *Agena* and the attached spacecraft were moving in a circular parking orbit at a distance of approximately 185 km (115 mi) from the surface of the earth and were traveling at a speed of 7.8 km/s (4.8 mi/s; space-fixed). After a total

coasting time of 13.3 min in the parking orbit, the second *Agena* ignition was initiated.

At the end of *Agena* final cutoff (23 min, 19 s after liftoff) the *Agena*, with the spacecraft, was traveling at a speed of 11.4 km/s (7.08 mi/s; space-fixed). The latitude and longitude of injection (*Agena* cutoff) into the geocentric hyperbolic orbit were −4.7 deg and +351.5 deg, respectively, the injection taking place over the south Atlantic Ocean. The geocentric characteristics of the *Mariner* trajectory are listed in Table VI-8.

Within an hour after injection, the spacecraft was receding from the earth with decreasing speed in an almost radial direction. This reduced the geocentric angular rate of the spacecraft in inertial coordinates until the rotational rate of the earth exceeded the geocentric angular rate of the spacecraft. The direction of the earth track of the spacecraft then reversed from increasing to decreasing longitude over the surface of the earth.

**Table VI-8. Geocentric characteristics of *Mariner V* trajectory**

| Characteristic | Geocentric injection | Postmidcourse orbit |
|---|---|---|
| Parameter | | |
| Radius $R$, km | 6569.6304 | $1.5816147 \times 10^6$ |
| Altitude, km | 191.56854 | — |
| Inertial speed $V$, km/s | 11.400128 | 2.9906292 |
| Earth-fixed speed $V_E$, km/s | 10.989368 | 112.96145 |
| Geocentric latitude $\phi$, deg | −4.6930562 | −11.661060 |
| Longitude $\theta$, deg | 351.53082 | 245.89294 |
| Right ascension $\Theta$, deg | 349.55227 | 140.46110 |
| Path angle of inertial velocity $\Gamma$, deg | 1.8980037 | 89.328850 |
| Azimuth of inertial velocity $\Sigma$, deg | 119.97742 | 61.817802 |
| Path angle of earth-fixed velocity $\gamma$, deg | 1.9689745 | 1.5169653 |
| Azimuth of earth-fixed velocity $\sigma$, deg | 121.22208 | 270.00839 |
| Time of event $T$, GMT | 06:24:37.1 (June 14, 1967) | 23:08:20.650 (June 19, 1967) |
| Hyperbolic orbital element | | |
| Semimajor axis $a$, km | −46261.501 | −47228.655 |
| Eccentricity $e$ | 1.1418646 | 1.0784276 |
| Inclination of equator $i$, deg | 30.308785 | 30.313409 |
| Longitude of ascending node $\Omega$, deg | 161.47921 | 161.12944 |
| Argument of perigee $\omega$, deg | 185.77009 | 179.06218 |
| Perigee distance $q$, km | 6562.8713 | 3704.0325 |
| Time of perigee passage $T$, GMT | 06:24:01.322 (June 14, 1967) | 06:14:54.599 (June 14, 1967) |

Several months before the first launch readiness date, it was decided to bias the premidcourse aiming point by moving it outward from the design aiming point about 80,000 km. Since the spacecraft is injected into its escape hyperbola by the *Agena D* stage, a maneuver is necessary after separation to place the *Agena* in a different trajectory from that of the spacecraft to make sure that the *Agena* would not violate the contamination constraint. Owing to the sensitivities of the trajectories considered, an *Agena* maneuver after separation could not guarantee to displace the booster trajectory from that of the spacecraft with the required probability of $10^{-5}$ unless this biased aiming point was used.

The biased aiming point selected for a June 14, 1967 launch was a $B$ and $\theta$ of 103,425 km and −32.3 deg respectively.

When several hours of continuous tracking had taken place, it was estimated that the spacecraft would miss Venus with a $B$ of 104,467 km and a $\theta$ of −38.7 deg. The actual arrival time was October 19, 1967 $03^h52^m45^s.155$ GMT instead of the desired arrival time of October 19, 1967 $18^h00^m00^s$ GMT. A comparison of these results with the desired biased encounter of Venus showed that the injection guidance system of the launch vehicle had performed well within 3 $\sigma$ (three times the standard deviation) of the nominal values. The results also showed that no useful encounter data could be obtained, and that a midcourse maneuver would be required. This maneuver was expected, since the launch trajectory had been biased by 80,000 km at Venus encounter.

A midcourse maneuver was executed 5 days after launch, on June 19, 1967 at $23^h08^m06^s$ GMT. The spacecraft was then $1.58 \times 10^6$ km ($0.98 \times 10^6$ miles) from the earth and still moving under the influence of the earth in an earth-centered hyperbolic orbit. The speed of the spacecraft was 2.99 km/s (6692 mi/h) with respect to the earth and 27.02 km/s (60,452 mi/h) with respect to the sun. Postmidcourse orbit computations showed that the spacecraft aiming point had been changed to a $B$ and $\theta$ of 28,413 km and −31.5 deg respectively, with closest approach to occur October 19, 1967 at $17^h34^m$ GMT.

## H. SPAC Early Mission Performance

*1. Chronology.* The spacecraft performance covers the period from launch through the midcourse maneuver (i.e., June 14, 1967 through June 19, 1967). Table VI-9 is a chronological listing of events during this period.

## Table VI-9. Chronology of *Mariner V* performance

| Day | Event | GMT |
|---|---|---|
| 165 | Launch mode — mode 2 | 05:15:00 |
| | LCE relay hold release | 05:27:05 |
| | Switch to internal power | 05:55:00 |
| | Tape recorder on launch mode | 05:56:28 |
| | JPL ready-switch on | 05:57:10 |
| | CC&S inhibit release | 05:58:00 |
| | *Agena armed* | 05:58:45 |
| | *Atlas* to internal power | 05:59:21 |
| | Clear relay release | 05:59:59 |
| | *Liftoff* | 06:01:00.176 |
| | Mark 1 (booster cutoff) | 06:03:08.85 |
| | Mark 2 (booster jettison) | 06:03:11.75 |
| | Mark 3 (*start of Agena auxiliary timer*) | 06:05:41.90 |
| | Mark 4 (sustainer cutoff) | 06:05:56.84 |
| | Mark 5 (start of *Agena* standard timer) | 06:06:08.57 |
| | Mark 6 (*vernier cutoff*) | 06:06:17.93 |
| | Mark 7 (shroud ejection) | 06:06:20.24 |
| | Mark 8 (*Atlas/Agena* separation) | 06:06:22.28 |
| | Mark 9 (*first Agena ignition*) | 06:07:21.80 |
| | Mark 10 (first *Agena* cutoff) | 06:09:45.36 |
| | In parking orbit | 06:09:45.36 |
| | *DSS 72 acquisition* | 06:19:30 |
| | Out of earth shadow | 06:20:18 |
| | Mark 11 (second *Agena* ignition) | 06:23:01.2 |
| | Mark 12 (second *Agena cutoff*) | 06:24:35.50 |
| | Pyro armed by PAS. Deck skip on all 3 decks (attributed to PAS) | 06:27:16.90 |
| | Mark 13 (*Agena*/spacecraft separation) | 06:27:16.90 |
| | Science on | 06:27:17.57 |
| | Mark 14 (start of *Agena* yaw maneuver) | 06:27:20.1 |
| | Mark 15 (end of *Agena* yaw maneuver) | 06:27:28.9 |
| | DSS 51 acquisition | 06:28:55 |
| | Tape recorder off (seen in data) | 06:29:42 |
| | CC&S relay hold off (seen in data) | 06:29:42 |
| | RF power up (seen in data) | 06:29:42 |
| | Solar panels deployed | 06:30:19.01 |
| | Mark 16 (*Agena* posigrade maneuver) | 06:32:16.9 |
| | Acquisition sun in pitch | 06:33:50 |
| | Sun acquisition | 06:44:23 |
| | DSS 41 acquisition | 06:48:54 |
| | DSS 42 acquisition | 06:53:05 |
| | CC&S L1 | 06:53:56.6 |
| | CC&S L2 | 06:57:56.0 |
| | DSS 51 change to two-way | 07:03:00 |
| | DSS 71 end of track | 07:17:00 |
| | Two-way transfer from DSS 51 to 42 | 08:30:00 |
| | Station 72 end of track | 09:21:00 |
| | Two-way transfer from DSS 42 to 51 | 09:35:00 |
| | Station 61 acquisition | 11:11:20 |
| 165 | Two-way transfer from DSS 51 to 61 | 11:30:00 |
| | DSS 42 end of track | 11:20:57 |
| | DSS 41 end of track | 12:11:52 |
| | Two-way transfer from DSS 61 to 51 | 12:40:00 |
| | Two-way transfer from DSS 51 to 61 | 13:50:00 |
| | Two-way transfer from DSS 61 to 51 | 15:00:00 |
| | Two-way transfer from DSS 51 to 61 | 16:10:00 |
| | Two-way transfer from DSS 61 to 51 | 17:20:00 |
| | Two-way transfer from DSS 51 to 61 | 18:30:00 |
| | DSS 11 acquisition | 18:33:36 |
| | Two-way transfer from DSS 61 to 11 | 18:50:00 |
| | Two-way transfer from DSS 11 to 61 | 19:30:00 |
| | DSS 51 end of track | 19:41:51 |
| | Two-way transfer from DSS 61 to 11 | 20:10:00 |
| | DSS 61 end of track | 20:23:49 |
| | CC&S L3 | 22:38:00.5 |
| | Canopus sensor acquisition of earth (center of null) | 22:49:01 |
| | Gyros off | 22:50:00 |
| | Command modulation applied Normalization | 23:33:13 |
| | DSS 42 acquisition | 23:50:01 |
| 166 | DC-V21 transmitted | 00:30:00 |
| | DC-V21 received at spacecraft | 00:30:37 |
| | DC-V21 observed in data | 00:31:07 |
| | DC-V21 transmitted | 00:34:00 |
| | DC-V21 received at spacecraft | 00:34:37 |
| | DC-V21 observed in data | 00:35:07 |
| | Canopus acquisition | 01:09:02 |
| | Gyros off | 01:12:31 |
| | Command modulation removed | 01:20:00 |
| | Two-way transfer from DSS 11 to 42 | 02:00:00 |
| | DSS 11 end of track | 04:40:00 |
| | DSS 61 acquisition | 11:05:43 |
| | Two-way transfer from DSS 42 to 61 | 11:20:00 |
| | DSS 42 end of track | 11:55:07 |
| | DSS 11 acquisition | 18:31:29 |
| | Two-way transfer from DSS 61 to 11 | 19:30:00 |
| | DSS 61 end of track | 20:38:24 |
| | CC&S cyclic-1 — No. 1 observed on *schedule* | 21:58:07 |
| | DSS 42 acquisition | 23:57:53 |
| 167 | DSS 11 end of track | 04:53:00 |
| | DSS 61 acquisition | 11:03:00 |
| | Two-way transfer from DSS 42 to 61 | 11:20:00 |
| | DSS 42 end of track | 11:56:35 |
| | DSS 11 acquisition | 18:28:50 |
| | Two-way transfer from DSS 61 to 11 | 19:30:00 |
| | DSS 61 end of track | 20:46:27 |
| | DSS 42 acquisition | 23:55:00 |

Table VI-9 (contd)

| Day | Event | GMT |
|---|---|---|
| 168 | Two-way transfer from DSS 11 to 42 | 01:30:00 |
| | DSS 11 end of track | 04:47:56 |
| | DSS 61 acquisition | 10:57:49 |
| | Two-way transfer from DSS 42 to 61 | 11:20:00 |
| | DSS 42 end of track | 11:54:00 |
| | DSS 11 acquisition | 18:25:53 |
| | Two-way transfer from DSS 61 to 11 | 18:45:00 |
| | DSS 61 end of track | 20:41:59 |
| | DSS 42 acquisition | 23:52:00 |
| 169 | Two-way transfer from DSS 11 to 42 | 02:15:00 |
| | DSS 11 end of track | 04:46:22 |
| | DSS 61 acquisition | 10:55:13 |
| | Two-way transfer from DSS 42 to 61 | 11:20:00 |
| | CC&S cyclic-1—No. 2 occurred | 16:38:18.28 |
| | DSS 11 acquisition | 18:22:15 |
| | Two-way transfer from DSS 61 to 11 | 18:47:00 |
| | DSS 61 end of track | 20:38:05 |
| | DSS 42 acquisition | 23:51:22 |
| 170 | Two-way transfer from DSS 11 to 42 | 01:00:00 |
| | Two-way transfer from DSS 42 to 11 | 02:00:00 |
| | Two-way transfer from DSS 11 to 42 | 03:00:00 |
| | DSS 11 end of track | 04:43:59 |
| | DSS 62 acquisition | 10:51:28 |
| | Two-way transfer from DSS 42 to 61 | 11:20:00 |
| | DSS 11 end of track | 11:47:45 |
| | DSS 11 acquisition | 18:20:34 |
| | Two-way transfer from DSS 61 to 11 | 18:45:00 |
| | Command modulation applied | 19:35:00 |
| | QC-V1-1 (pitch turn duration) transmitted | 20:18:00 |
| | QC-V1-1 received at spacecraft | 20:18:42 |
| | QC-V1-1 observed in data | 20:19:13 |
| | QC-V1-2 (roll turn duration) transmitted | 20:23:00 |
| | QC-V1-2 received at spacecraft | 20:23:42 |
| | QC-V1-2 observed in data | 20:24:16 |
| | QC-V1-3 (motor burn duration) transmitted | 20:28:00 |
| 170 | QC-V1-3 received at spacecraft | 20:28:42 |
| | QC-V1-3 observed in data | 20:29:18 |
| | DSS 61 end of track | 20:35:00 |
| | DC-V29 (arm first prop maneuver) transmitted | 20:38:00 |
| | DC-V29 received at spacecraft | 20:38:42 |
| | DC-V29 observed in data | 20:38:58 |
| | DC-V14 (remove maneuver inhibit-remove prop inhibit) transmitted | 20:48:00 |
| | DC-V14 received at spacecraft | 20:48:42 |
| | DC-V14 observed in data | 20:48:50 |
| | DSS 61 end of track | 20:49:14 |
| | DC-V27 (initiate midcourse maneuver) transmitted | 21:23:59 |
| | DC-V27 received at spacecraft | 21:24:41 |
| | DC-V27 observed in data | 21:24:46 |
| | Data encoder to mode 1 | 21:24:46 |
| | Gyros on (observed in data) | 21:24:46.14 ±0.31 |
| | Pitch turn start | 22:24:10.9 |
| | Pitch turn stop | 22:29:13.9 to 22:29:15.4 |
| | Roll turn start | 22:46:10.3 to 22:46:12.6 |
| | Roll turn stop | 22:52:30.9 to 22:52:32.3 |
| | Motor burn start | 23:08:11.1 to 23:08:11.5 |
| | Motor burn stop | 23:08:26.4 to 23:08:29.5 |
| | Data encoder to mode 2 | 23:14:10.6 to 23:14:11.2 |
| | Start sun reacquition | 23:14:10.6 to 23:14:11.2 |
| | Sun acquired | 23:21:18.99 |
| | Canopus acquired | 23:32:27 |
| | DC-V21 No. 1 (roll override) transmitted | 23:33:15 |
| | DC-V21 No. 1 received at spacecraft | 23:33:57 |
| | DC-V21 No. 1 observed in data | 23:34:07 |

2. *Detailed spacecraft performance.* The complete spacecraft system performance was very good. The performance description lists in detail the minor deviations from the expected as well as the unexpected results.

*a. Radio subsystem.* The radio subsystem performed normally during the launch-through-midcourse phase of the mission. The cavity amplifier supplied spacecraft transmission power, and the spacecraft low gain antenna was used for transmitting and receiving. Spacecraft radio power-up occurred normally at spacecraft separation. The radio subsystem data were consistent with preflight predictions. Certain items of specific interest were noted.

(1) *Radio power-up.* Shortly after radio power-up, channel 213 (cavity power output to the low gain antenna) began to decrease from an initial data number (DN) of 75. After the radio subsystem temperatures stabilized, channel 214 stabilized at a DN of 70 to 71. Data obtained from the space simulator tests led to the conclusion that the cavity amplifier responded normally. The observed change

was attributed to a decreasing temperature in bay 6 and to the time required for the cavity power output to stabilize. Channel 300 (cavity cathode current) also responded normally.

(2) *Frequency predictions for first DSIF acquisition.* Predictions of DSIF acquisition frequencies for both uplink and downlink were based upon predicted spacecraft temperatures and curves of spacecraft transmitter and receiver frequencies vs temperature. The observed frequencies agreed with predictions.

During the midcourse maneuver, the radio subsystem temperatures increased by 8°F (within the predicted range). The spacecraft power switched from the solar panels to the battery during the pitch turn. While battery power was used, channels 214 (transmitter power output) and 300 (cavity cathode current) decreased by 1 DN. This decrease was the result of a slight drop of the cavity power supply voltage because of a lower primary input voltage from the spacecraft battery. After sun acquisition, channels 214 and 300 returned to their normal DN readings.

A DC-V9 command was transmitted to the spacecraft to turn on the ranging receiver. The following channels had changes in DN values to indicate that ranging was on:

(1) Channel 424 (spacecraft receiver VCO temperature) increased by 1 to 2 DN. This change was attributed to the increased power (0.7 W) dissipated in the ranging phase detector module when ranging is on.

(2) Channels 203, 205, 225, and 227 (spacecraft power subsystem current monitors) increased by 1 DN. An increase in these channels reflects the additional 0.7 W of power drawn when ranging is on.

*b. Command subsystem.* Telemetry data of the subsystems to which commands were sent showed that all commands were detected and decoded properly.

*c. Tape recorder subsystem.* Nineteen tape passes were accumulated during the launch phase. The tape recorder was turned off approximately 5⅓ s after separation of the spacecraft from the *Agena.*

*d. Data encoder subsystem.* One deck skip, which was a normal skip, was observed at the time of the spacecraft separation from the *Agena.*

*e. Attitude control subsystem.* The operation of the attitude control subsystem was normal.

(1) Gas subsystem. The spacecraft was launched with 5.18 lb of gas in the attitude control subsystem (2.58 lb in the $+X/-Y$ tank, and 2.60 lb in the $-X/+Y$ tank). Gas consumption during the phase from launch through midcourse appeared normal. A longer period of operation will be required to establish the rate of consumption, because so little gas was actually used.

(2) Inertial sensors. Performance of the gyros was normal. The launch caused saturation of all three axes. While the separation rates cannot be easily measured, they were no smaller than +7.0 mr/s (0.4 deg/s CW) in pitch, −15 mr/s (0.86 deg/s CCW) in yaw, and −2.65 mr/s (0.15 deg/s CCW) in roll. The decrease in angular velocity as the solar panels deployed was clearly visible at the time of the separation initiated timer (SIT) event. The panels were deployed in less than 12.6 s; the angular velocity decreased by 1.4 mr/s in pitch, 1.5 mr/s in yaw, and 0.3 mr/s in roll. Although the conservation of angular momentum predicts an increase in angular velocity in pitch and yaw at solar panel deployment, the increase of the moment arm of the gas jets (about 1 to 8 ft) more than offsets the corresponding increase in angular velocity by causing a decrease in the acquisition rates. The magnetometer calibrate spin rate was 78 DN or −3.72 mr/s (12.8 deg/min). The Canopus search rate was 73 DN or −2.13 mr/s (7.32 deg/min) based upon telemetry before acquisition. After acquisition of the earth, the spin rate was again 73 DN. After acquisition and subsequent deacquisition of the moon, however, the spin rate dropped to 71 DN or −1.86 mr/s (6.4 deg/min) until Canopus acquisition.

After the gyros were turned on, before the midcourse maneuver, the first gyro telemetry data showed readings of 63 DN in pitch, 65 DN in yaw, and 64 DN in roll. Since the pitch, yaw, and roll DN readings did not change when the gyros were turned on, it was concluded that the turn-on transient was minimal. The pitch and roll turn rates for the midcourse maneuver were in accord with those predicted. The CC&S was programmed for a 304-s pitch turn (desired magnitude, 55.3503 deg; commanded turn, 55.2672 deg, or 0.0831 deg short) and a 380-s roll turn (desired magnitude, 71.0248 deg; commanded turn, 70.946 deg, or 0.0788 deg short).

The data received following the turns showed that the turns were accurate, and that they were performed according to the specified polarity and duration. The pitch turn was 55.18 deg, and the roll turn was 70.93 deg. In terms of standard deviations, the turns were 0.2 $\sigma$ and 0.04 $\sigma$, respectively.

(3) Celestial sensors. After the spacecraft emerged from the shadow of the earth, all indications were that the earth sensor was apparently looking at the sun until sun acquisition was initiated. Earth sensor outputs were obtained during the magnetometer calibrate phase. An analysis of the apparent motion of the earth and its size will enable an accurate measurement of the spin rate. In addition, an earth sensor output was obtained during the roll search, verifying the search rate and aiding identification of the objects acquired by the Canopus sensor.

The sun sensor showed saturated outputs. The spacecraft was driven clockwise in pitch and counterclockwise in yaw to acquire the sun, but light from the earth illuminating the secondary sun sensors biased the electrical null approximately 78 mrad (4.5 deg) off the probe–sun line. The attitude control subsystem had acquired the false null in yaw and was in nonperiodic oscillation (limit-cycling) about the false null; however, the null also had to be acquired in pitch to trigger the sun gate because the sun gate field-of-view is about 5.1 deg. Fortunately, the location of the false null was such that all points of a normal limit cycle within the deadband placed the sun in the sun gate field-of-view so that the sun-gate event, when removing the power to the secondary sun sensors, also removed the false null.

Canopus sensor was turned on for the first time at L3. The expected acquisition of the earth was achieved. The maximum brightness noted of 30 DN corresponds to about 2.5 times that of Canopus; a brightness of about 0.75 times Canopus had been predicted. After the acquisition of the earth, two DC-V21s were transmitted to the spacecraft to override earth acquisition. The first DC-V21 was sent to the spacecraft to override acquisition on the first stable null of the earth. The second DC-V21 was timed to arrive at the spacecraft shortly after the second stable null of the earth was reached and before the gyros were turned off. The second command caused the spacecraft to roll off the earth and, shortly afterward, acquire the moon. (A limit cycle was not established because the moon apparently did not have a stable null.) The sensor moved off the moon in the search (CCW) direction, indicating a low-gate dropout of between 48 and 49 DN (0.22 to 0.19 times Canopus). The maximum brightness of the moon, that was observed, was 34 DN, about 1.6 times Canopus.

Roll search then continued until Canopus acquisition. The initial Canopus brightness reading of 37 DN persisted for about 6 h and then dropped to 38 DN, accompanied by a decrease in sensor temperature from 75 to 73 DN—about 3.25°F. The present and most stable value of 1 times Canopus appears to be 38 DN or 0.89 V and agrees closely with the calibration of 0.886 V made before delivery to the spacecraft assembly facility.

The Canopus, sun, and earth sensors performed normally during the cruise and maneuver periods. During the roll searches after the midcourse maneuver, a star map was made by the Canopus sensor that correlated with the a priori map produced by the *Mariner* star identification program. Several celestial objects were seen and identified in real time. The earth sensor viewed the earth during these roll searches and during the initial Canopus reacquisition.

(4) Control subsystem. The position deadbands of the attitude control subsystem are

| | | |
|---|---|---|
| Pitch | 34–35 DN | = +7.77 to +7.46 mrad |
| | 95–94 DN | = −7.97 to −7.67 mrad |
| Yaw | 34–35 DN | = +8.42 to +8.09 mrad |
| | 95 DN | = −8.69 mrad |
| Roll | 53–54 DN | = +6.87 to 6.42 mrad |
| | 75 DN | = −3.21 mrad |

Because of a 1.7-mrad null offset in the Canopus sensor, the roll limit cycle is unsymmetrical in position. Minimum rate increments have not been calculated, but some disturbance torques have been; the maximum torque observed thus far appears to be about 10 dyn-cm and some are as low as 1 dyn-cm. The role of derived rate in the initial sun acquisition is evident in that the rates were significantly reduced during the acquisition process.

During the motor burn, the autopilot performed its function of maintaining the thrust vector orientation of the spacecraft; the results were inferred from the postmidcourse analysis of the pitch and roll turns.

*f. CC&S subsystem.* The CC&S operation during this reporting period was completely normal. All events, L1 (deploy solar panels), L2 (turn on attitude control), and L3 (turn on Canopus sensor) occurred at their nominal times (within the resolution of the telemetry).

All maneuver events—DC-V27 received, gyros on and data mode 1, pitch turn start and polarity, pitch turn stop, roll turn start and polarity, roll turn stop, motor burn start, motor burn stop, reacquire start, maneuver counter overflow—occurred at their nominal times (within the resolution of the telemetry). The CC&S timing of events in telemetry channel 220 gave the correct number of overflows and the expected final readings for each of the turns and for the motor burn. The resolution of this channel is twice the word sync time (±0.42 s).

*g. Power subsystem.* The operation of the power subsystem during the launch and the magnetometer calibrate roll was nominal. All operating voltages and currents were within the expected ranges. A total of 4.3 A-h was removed from the battery during launch. A total of 50.7 A-h was available at sun acquisition indicating that an assumed nominal of 55.0 A-h was available at T − 7. By $21^h00^m$ GMT on June 18, 1967, 4.1 A-h had been returned to the battery. Because of the much lower charge rate used on the flight charger, a greater capacity will be returned to the battery than existed at launch. This is expected because the OSE charger cannot fully top off the battery at the constant current 1.9 A rate.

During the midcourse maneuver, a total of 2.33 A-h was removed from the battery. A total of 53.17 A-h was available at sun reacquisition. A calculated total of 55.5 A-h was available before the midcourse maneuver. The battery supplied somewhat more power during the maneuver than was originally estimated, but was within tolerance.

The shading of the solar panels by the spacecraft bus occurred as expected during the maneuver. Solar panel 4A7 was sufficiently shaded by the deployed sun shade after the pitch turn to preclude obtaining an output from that panel. This caused battery sharing to occur at a higher rate than expected. When the roll turn began, the shading moved from solar panel 4A7 to 4A5 which was only partially shaded at the end of the 70.93-deg turn.

*h. Temperature control subsystem.* Very little change was observed in the spacecraft temperatures during ascent and parking orbit. Temperatures at sun acquisition were within expected tolerances. The cooling of external items occurred during boost because of the gas expansion under the shroud. Further cooling occurred while the spacecraft was in the shadow of the earth. From the near-normal temperatures it can be inferred that the sun shade was properly deployed.

When the spacecraft entered the near-earth cruise configuration, the temperatures remained within design limits. The average spacecraft temperature was 2°F above the predicted level during pre-Canopus acquisition cruise and 1°F above the predicted level after Canopus acquisition. There were no bus temperatures that departed more than 4°F from prediction during pre-Canopus acquisition nor more than 2°F from prediction after Canopus acquisition. As expected, temperatures of equipment outside the bus show larger deviations from predictions.

During the midcourse maneuver, the bay 2 primary sun sensor reached a maximum temperature of about 98°F (12°F lower than that predicted). The difference between the predicted and actual ΔT is almost wholly attributed to considerably less severe *soakback* from the motor burn than had been expected. The majority of the temperature rise was attributed to solar heating. The thermal analysis which constrains the pitch angle for near-sun maneuvers considered only this heat factor; therefore, the constraints that were generated before launch appear to be realistic.

After the postmidcourse sun acquisition, an apparent anomaly in the $-Y$ pitch jet temperature (channel 425) was observed. A temperature of −21°F was observed 2 min before sun acquisition was completed. At 41 min after sun acquisition, a 1 DN decrease in temperature to −23°F was observed. Because of solar heating and a conduction heat input to the assembly 40 min before the anomalous reading, such a decrease in temperature was completely unexpected. The results of analysis suggested two possible explanations: (1) the pitch jets continued to release a considerable amount of $N_2$ at the time of the anomaly which caused cooling of the assembly because of gas expansion, and (2) at the time of sun acquisition the gas valves were subcooled approximately 10°F—because of gas expansion during acquisition—below the manifold temperature. If explanation (1) were a valid assumption, the average temperature of the assembly would have increased because of increased solar heating while the measured temperature would have decreased because

of heat losses to the cooler valves. The latter theory is more plausible, but both the test data and the flight data are insufficient to permit a positive conclusion.

During this reporting period, the structural and mechanical devices, the temperature control references, and the cabling performed as follows.

*Structural and mechanical devices.* The nominal spacecraft performance indicated that the spacecraft structure performed adequately through the critical launch and boost environments. The PAS actuated normally, and the SIT squib-firing current event occurred normally, allowing for a maximum of 7 s deployment time for solar panels. The corresponding SIT actuation time was 170 to 175 s (which corresponds to a SIT temperature of 74 ±4°F). This temperature range nearly agrees with the predicted value of 80°F; therefore, it can be concluded that the SIT operation was normal. The spacecraft performance was evidence that the spacecraft structure performed normally during the midcourse maneuver and the cruise.

*Temperature control reference (TCR).* The TCR data were obtained approximately ½ h after sun acquisition. All values were within predicted tolerances. A subsequent decrease in DN value of channels 413 and 432 over the following 3 h indicated a decreasing thermal input from the earth early in the mission. (There was a similar effect on the solar panels.) The lower equilibrium temperatures, apparently beyond earth influence, were still within tolerance.

The changes on the white TCRs (412 and 432) have permitted a resolution of change in solar absorptance (change only, not absolute value) of white coatings to an order of magnitude better than is possible in the laboratory. (The results of TCR performance are to a much finer degree than can be achieved in a lab.)

The results recorded during the second week of flight indicated that the temperature control coatings on the TCRs performed differently in space than in laboratory tests, and further support the results of the first week of flight. White S-13M continued to darken at a faster rate than was expected, black continued to bleach at a faster rate than was expected, and the white S-13M degraded faster than was predicted. A detailed description of TCR behavior is given below:

(1) Channel 412, S-13M White. The S-13 white coating was expected to degrade and be on scale within 10 to 15 h after launch. This did not occur until $L+30$ h, indicating either a lower initial solar absorptance or a slower initial degradation rate.

(2) Channel 432, S-13M White. Initial results were within predicted tolerances, but an increase in absorptance has been greater than expected. The first increase (0.5%) was evident within 5 h after launch.

(3) Channel 413, Black. The black TCR temperature decreased following sun acquisition (apparently as the earth influence decreased) and appeared to have reached equilibrium at 7 DN (140°F) 3 h after launch. At $T+20$ h, the DN changed to 6 (139°F). This change could be explained by assuming that the prior values of 7 DN were just above the switch point; however, the change to 5 DN at $T+83$ h and continuous readings of 5 DN after $T+83$ h indicate that a bleaching of the black reference was in process. A 1-DN reading change corresponds to less than 1% in the product $S\alpha/\epsilon$.

*i. Post-injection propulsion subsystem.* The telemetry data confirmed that the propulsion subsystem maintained a normal condition during launch. The thrust chamber pressure dropped to zero while the shroud cavity pressure dropped, as was expected, during the boost phase. After injection, the propulsion subsystem $\Delta V$ capability was about 92.1 m/s.

Following injection, propulsion subsystem temperatures decreased to within 2°F of the predicted values. As the temperatures decreased, the pressures decreased according to predictions. During this dynamic period from launch through injection, the propulsion subsystem remained leak-tight.

Data analysis showed that thermal equilibrium of the post-injection propulsion subsystem occurred during cruise, by day 169 (June 18, 1967). The temperature and pressure parameters were:

| Parameter | Post-launch | Cruise equilibrium |
|---|---|---|
| Thrust chamber pressure | 0 psia | 0 psia |
| Fuel tank pressure | 293 psia | 277 psia |
| Fuel tank temperature | 71°F | 56°F |
| Nitrogen tank pressure | 2961 psia | 2870 psia |
| Oxidizer pressure | 398 psia | 390 psia |
| Terminator sensor excitation | Off | Off |
| Nitrogen tank temperature | 67°F | 52°F |
| $\Delta V$ capability | 92.1 m/s | 91.9 m/s |

All parameters agreed with the tolerances of prelaunch predictions.

The propulsion subsystem performance during the motor burn of the midcourse maneuver appeared normal in all respects. There were deviations of 2 or 3 DN from the predicted chamber pressure. Previous experience made it possible to accept such small deviations from predictions rather than to consider them indicative of nonstandard subsystem performance.

After the midcourse motor burn, temperatures during *soakback* were not excessive. When cruise conditions were established following the maneuver, temperatures returned to within 1°F of premaneuver values. There were no indications of any leaks during or following the midcourse maneuver. The telemetered propulsion parameters during and immediately following the motor burn were as follows:

| Parameter | DN | EU |
|---|---|---|
| Thrust chamber pressure (during steady state) | 79–80 | 185–187 psia |
| Propellant tank pressure (during steady state) | 79 | 306 psia |
| Propellant tank temperature: | 37 | 59°F |
| Nitrogen tank pressure (at end of motor burn) | 79 | 2438 psia |
| Oxidizer pressure (at end of motor burn) | 93 | 362 psia |
| Nitrogen tank temperature | 47 | 69°F |

Postmaneuver tracking data established that the velocity increment imparted to the spacecraft during the maneuver was approximately 4.5% less than that planned. An extensive investigation was initiated in an attempt to determine if the cause of the deviation from the predicted trajectory lay in the velocity increment provided by the motor burn or in some other area.

*j. Pyrotechnics subsystem.* All pyrotechnic subsystem parameters remained normal during and after launch. Pyro was armed by the pyro arming switch at separation, and the event was recorded in register 3. Solar panel pinpullers were fired by the separation initiated timer at $06^h30^m19^s$ GMT, and events were recorded in register 1 and 3. No additional events were recorded when the CC&S L1 (solar panel deployment) occurred. The terminator sensor excitation remained off as expected.

During the midcourse maneuver, pyrotechnic events were recorded in registers 1 and 3 for both motor burn *start* and motor burn *stop*. It can be concluded from the telemetry data that both pyro units discharged and that all squibs probably fired when commanded.

The terminator sensor excitation remained off as expected.

*k. Science subsystem.* All science instruments maintained their normal condition during launch. Following spacecraft separation, the plasma probe high-voltage inhibit was removed; the magnetometer was saturated on all axes; and the magnetometer ignition backup, ultraviolet calibrate and drift check, trapped radiation detector, dual-frequency receiver calibrate, and data automation system functions were normal. The trapped radiation detector observed the Van Allen belts as expected. The magnetometer roll calibrate was normal.

The Stanford University antenna began sending signals to the dual-frequency receiver on the spacecraft shortly after *Mariner V* first rose over the Stanford horizon, and the dual-frequency receiver responded properly.

After the midcourse maneuver, two anomalies were observed in the ultraviolet photometer data. The ultraviolet photometer calibrate and drift-check sequence changed during the telemetry mode 1 period. In addition, the ultraviolet photometer C-tube readings decreased from approximately 20 DN before midcourse to approximately 6 DN following the maneuver and Canopus acquisition. Both anomalies are being evaluated.

### I. SSAC Early Mission Performance (Science Instruments)

***1. Helium magnetometer flight results.*** The period from launch through midcourse was successfully completed with no anomalous behavior. The magnetometer assisted in the spacecraft roll and acquisition phases as planned.

***2. Plasma probe flight results.*** The period from launch through midcourse was successfully completed with no anomalous behavior. As expected, no plasma was detected until the spacecraft left the magnetosphere. At this transition, the instrument showed the proper readings for the plasma shock wave.

No abnormal collector currents were measured at the steps corresponding to the highest modulator grid voltage.

*3. Ultraviolet photometer.* Following Canopus acquisition, day 166 $01^h09^m$ GMT, the ultraviolet photometer C-tube rest-state was approximately 20 DN. It was expected that this reading would be less than 10 DN. This was initially thought to be an indication of hydrogen in the ecliptic. As a result of the 20-DN readings the spacecraft was rolled, following the midcourse maneuver, to further evaluate the phenomenon.

Following the midcourse maneuver and the return to telemetry mode 2, all tubes showed an increase in readings which decreased to normal for tubes A and B, but to ~6 DN for the C-tube. Throughout the postmidcourse rolls, all tubes responded to the Milky Way and several stars. However, the C-tube response was lower than expected. After final Canopus reacquisition, the C-tube rest-state was approximately 6 DN rather than 20 DN as before the maneuver. This apparent drop in sensitivity is unexplained.

Following the switch to mode 2, another anomaly was observed. Before midcourse, the ultraviolet photometer calibrates occurred on fames divisible by 16, and drift checks occurred on frames divisible by 8. Following the midcourse, the calibrates occurred on frames divisible by 16 with a remainder of 7, and the drift checks occurred on frames divisible by 8 with a remainder of 7. All other science instruments were unchanged. The counters inside the UV photometer were somehow altered during the telemetry mode 1 part of the maneuver.

*4. Trapped radiation detector.* Following launch, the TRD observed the Van Allen belts near earth as expected, and observed variations in the proton and electron activity as well as changes in the solar x-ray activity. Overall TRD performance through midcourse was completely normal.

*5. Dual-frequency receiver.* The DFR flight performance through midcourse was completely normal. Stanford radiated to the *Mariner V* DFR approximately 25 h and the DFR locked on Stanford signals, responding as expected. Stanford reported that both carrier levels were within 1 dB of calculated values.

# VII. Mission Analysis Preparations and Activities During Countdown

The mission analysis preparations for and activities during the *Mariner* Venus 67 countdown and launch can be divided into three parts: (1) precountdown preparations, (2) countdown and launch activities, and (3) launch constraints planning and near-earth coverage analysis.

## A. Precountdown Preparation

The mission analysis precountdown preparations began shortly after project inception. The mission analysis representative (MAR) directed the efforts of the trajectory engineer and the launch phase mission analyst (LPA) toward determining a reasonable launch period design. A launch period was recommended that provided good arrival geometry by choosing the opening day of the launch period as June 12. The last day of the launch period was set for June 27. This 16-day launch period provided a probability of launch which was greater than 0.999. The last day of the launch period is always established by the final launch vehicle performance capability which in this mission was not known until a few months before launch. The final launch vehicle performance allowed for a launch period of 14 days (closing date June 25) with sufficient (3 $\sigma$) propellant reserves to assure a 99% probability of not running out of fuel. Although this 14-day period was judged adequate for launch, a study was performed to determine a strategy for extending the period beyond June 25 in case of emergency. A model was developed during this study to aid trading off launch vehicle propellant margins for added launch days and removing flight hardware such as the command destruct and retrofire rockets. The study resulted in an adaptive strategy which specified how the propellant margins were going to be allowed to drop in the emergency extension period. The final day of the extended launch period was July 1 and daily firing tables were prepared for each day from June 12 to July 1.

During the last few months before launch, the LPA prepared tradeoff studies that would prepare him for his responsibilities during the countdown and launch. In addition to his responsibility as the project launch constraints representative, the LPA assisted the mission director by providing information in real time concerning the risks to the mission from anomalies and failures during the countdown. In particular, certain pieces of flight hardware could fail without necessitating the aborting

of the mission. A problem arose concerning the advisability of launch should a non-abortive failure occur during the countdown. For example, if the launch had slipped to June 24, and if one of the flight experiments had failed, would the optimum strategy be to accept a degraded scientific mission and launch; or, to attempt repair and launch before the end of the period. The risk study established cutoff dates (depending on the type of failure or anomaly) beyond which the risk of not launching was so high that degraded mission performance would be preferable.

In a similar way, mission launch/hold criteria for the project class I data requirements were established. For the first few days of the launch period, the mission director decided to hold and, if necessary, slip launch one day rather than to accept either degraded mission performance or loss of a class I data requirement. This class I telemetry seemed to be the only available form of ground redundancy. In other words, if an anomaly developed in flight which required swift reaction (e.g., before the end of battery life), corrective commands could be sent only if telemetry indications of trouble were received. In this fashion, a set of project launch/hold criteria was established which took into account both the risk of not launching and the value of repairing each failure or anomaly.

To speed up the reaction time to failures and propagation difficulties that usually occur during the countdown, an order of priority was established for the class I data requirements. Thus one document, rather than many, provided the priority listing, the reason for the requirements, and the stations needed for prime and backup support. With this launch phase analyst's launch plan for *Mariner* Venus 67, Table VII-1, it was possible to quickly determine the effect of a tracking data system failure during the countdown.

Three weeks before launch the first launch date was slipped from June 12 to June 14 to optimize the value of the scientific mission. The value of the scientific data depended upon the distance of the aiming point from the center of the planet (**B** vector) and the distance of the probe at closest approach to the earth–Venus center line (**P** vector). Because of the relative positions of the Canopus and sun constraint regions a launch on June 14 rather than on June 12 would reduce the **B** vector about 500 miles and the **P** vector by several hundred km. This change in launch date increased the value of return of the science data about 30% from about 0.6 to 0.9. In addition, the value continued to increase to June 16 and stayed at a high level until June 21 when it began to drop. Thus, when the probability of launch was factored into this value tradeoff, June 14 turned out to be an optimal date for launch. June 14 had been recognized as a better launch date for mission value than June 12. However, since June 12 was an acceptable launch date, it was decided to provide as long a launch period as possible until close to launch when the increased risks produced by reduction of the period could be better judged against the full context of the readiness of the project.

Another part of the precountdown preparation was that of the TDS coverage estimates. To provide early coverage planning and support estimates, the TDS depends upon the project for early and accurate trajectory information. The AFETR required the receipt of the final trajectory data no later than 45 working days (L−9 weeks) before launch. Because of previously established schedules, the project was not able to meet this request and asked that the AFETR use preliminary trajectory data, data which was acceptable to the DSN and the MSFN. The project guaranteed the accuracy of these data to be better than $\pm 10$ s in mark event launch plus time, and $\pm 1$ deg in latitude and longitude of the earth track. The AFETR accepted this trajectory data for early planning but refused to guarantee that the project would receive commitments unless the trajectory data agreed closely with the final data which were to be supplied at $L - 6$ weeks. The project agreed to accept the increased risk if the TDS support data were made available 3 weeks before launch.

Unfortunately the TDS support coverage plans were not made available until roughly a week before launch and no support commitments were given by the AFETR. In addition, the project was notified by the TDS that one of the key tracking and telemetry ships which was to provide important support of the mission would not be supporting the mission during the full launch period. The final AFETR coverage plan showed large unexpected gaps in coverage. These events combined to force a reevaluation of the available launch period by the TDS analyst/LPA team. The TDS analyst developed a model which displayed various risks in launch when these gaps existed. The LPA mapped these TDS risks into the overall mission data risks from which the mission director selected his level of acceptable mission data risk. In this way, the daily launch windows were increased from 60 to 80 min a day. The windows for the first few days were judged adequate for launch (Table VII-2).

## Table VII-1. Launch phase analyst's launch plan for Mariner V

| Item | Priority | Class I requirement and need | Prime and backup supporting stations |
|---|---|---|---|
| A | 1.0 | RT[a] C-band post-injection/pre-posigrade maneuver tracking<br>Early spacecraft orbit determination<br>Early assessment of mission status<br>DSN post-injection predicts | Twin Falls (P)<br>Pretoria (BU)<br>Ascension (BU)<br>Three station coverage starting at about 104° azimuth. |
| B | 2.0 | RT[a] Spacecraft S-band separation to S+5 min<br>Monitor of critical spacecraft events<br>Assessment of mission status | Twin Falls (BU)<br>Johannesburg (BU)<br>Ascension DSN (P) |
| C | 3.0 | RT[a] Launch vehicle second burn VHF (mark events 11, and 12 and velocity meter readout and booster pressure)<br>Duration of second burn<br>Normalcy of second burn<br>Corroboration of initial orbit calculation | Twin Falls (P) 96–105<br>Ascension (P) 102–108<br>Coastal Crusader (P) 108–114 |
| D | 3.5 | NRT[b] Complete launch vehicle second burn VHF from burn −20 s to injection +20 s<br>Magnetic tape for non-real time evaluation of launch vehicle performance<br>NASA/Lewis future repairs | Twin Falls (P) 96–105<br>Ascension (P) 102–108<br>Coastal Crusader (P) 108–114 |
| E | 3.5 | RT and NRT Launch vehicle VHF from launch to parking orbit Insertion +25 s, mark events 1–10<br>Normalcy of launch vehicle<br>Performance from liftoff through first burn of *Agena*<br>*Assessment of mission status*<br>Magnetic tape to be used for post launch launch vehicle evaluation | Tel IV (P)<br>Antenna at AE (P)<br>Antigua (P) |
| F | 4.5 | RT Spacecraft S-band/channel F any continuous 3 min from launch to Antigua set<br>Monitor of spacecraft status<br>Assessment of mission status<br>One complete data commutation on mode 2 | Station Tel IV (P)<br>DSS 71 (P)<br>Antigua (BU)<br>*All launch azimuths.* |
| G | 5.0 | RT C-band post- parking-orbit insertion tracking<br>AFETR IRV and predicts<br>Determination of parking orbit | Antigua (P) |
| H | 6.0 | NRT *Post-posigrade maneuver, C-band*<br>Planetary quarantine requirements<br>Determine final *Agena* orbit | Carnarvon (P)<br>Pretoria (BU) |
| I | 6.0 | NRT VHF spacecraft S − 10 s to completion of yaw maneuver + 10 s and mark events 13, 14, 15.<br>Magnetic tape for non-real time evaluation | Pretoria (P) |
| J | 7.0 | Complete spacecraft S-band or channel F from L to parking-orbit insertion +25 s<br>Magnetic tape for non-real time evaluation | Tel IV (P)<br>DSS 71 (P)<br>Antigua (P) |
| K | 7.5 | Spacecraft S-band L+51 to L+58 | Johannesburg (P) |
| L | 8.0 | NRT Posigrade mark event 16. Start of posigrade −10 s to completion of posigrade +10 s | Carnarvon (P) |

[a]Real or near-real time.
[b]Non-real time.
[c]Prime.
[d]Backup.

**Table VII-2. Launch time report for June 14–17 as of June 7, 1967**

| Date of launch | Opening and closing of launch window | | | Duration of launch window |
|---|---|---|---|---|
| June | Launch azimuth, deg | Launch time, GMT h:min | plan | Time, min |
| 14 | Open 98.8 | 5:47 | 14F | 77 |
| | Close 114.0 | 7:04 | 14K | |
| 15 | Open 98.7 | 5:31 | 15F | 81 |
| | Close 114.0 | 6:52 | 15K | |
| 16 | Open 99.0 | 5:20 | 16F[a] | 80 |
| | Close 114.0 | 6:40 | 16K | |
| 17 | Open 98.0 | 4:59 | 17F | 90 |
| | Close 114.0 | 6:29 | 17K | |

[a]Denotes that window is open after the beginning of a launch plan.

## B. Countdown and Launch Activities

During the second part of the mission analysis activities, the countdown itself, the LPA received reports from the TDSA regarding the status of the support of the TDS. The LPA discussed this status with the launch vehicle data analyst in Building AE, the mission analyst at Pasadena, the SFOD, the data coordinator at the RTCS, and other key personnel to better evaluate both the constraints to the launch and certain risks to the mission. The LPA continually advised the mission director of the effect which these constraints (risks) had upon the launch window. These discussions with the mission director were carried on by personal communication since the LPA was seated next to the mission director during launch operations. During the countdown, the LPA was advised that communications with the downrange ship would be poor at launch owing to propagation problems. These problems could have caused loss of important class I tracking and telemetry data. Since these data were available from only one site, the LPA recommended a change in launch plan to enable two other sites to retrieve these data and the mission director concurred. To accomplish the change in launch plan, a launch hold of 14 min was called.

During the plus-count, the mission analysis activity focused upon evaluating the minute-by-minute status of the mission. Before launch, a network had been established between the LPA and various key off-line personnel (that is personnel who perform analysis functions rather than work directly in-line to the operations). This network had been established before launch and consisted of communications with several key analysts. In particular, the LPA was advised of the analysis of the launch vehicle telemetry by analysts stationed in Hangar AE, the exact position and velocity errors of the *Agena* at parking orbit insertion by analysts at the General Electric guidance lab, the quality of the tracking data by the coordinator at the real-time computer system and the status of the spacecraft telemetry by the spacecraft manager. The LPA, in turn, after combining these various inputs into a single overall picture of the mission, reported it to the mission director. Because of propagation and certain other problems, the real-time computing facility at Cape Kennedy was not able to produce a reliable post-injection orbit from AFETR data for several hours. Similarly, the SFOF had difficulty producing a reliable orbit from DSN data. In addition, the mark event times for start and stop of *Agena* second burn indicated a substantially short burn duration. However, launch vehicle telemetry during second burn was available. This telemetry included the *Agena* chamber pressure during second burn and a velocity meter read-out. Since the chamber pressure was high, thus explaining the short second burn, and the velocity meter read-out was as predicted for a nominal flight, the LPA team was able to report that the mission appeared to be nominal. This was, of course, confirmed by subsequent orbit determination solutions.

## C. Launch Constraints Planning and Near-Earth Coverage Analysis

The launch constraints planning took place in four stages. First, the non-TDS coverage launch constraints were defined. Second, the project specified a set of near-earth data requirements. Third, the total near-earth TDS coverage capabilities were examined to determine which project requirements could and could not be met. Fourth, whenever the TDS coverage capabilities could not satisfy a project requirement, a TDS launch constraint resulted. In other words, launch constraint = required coverage − available coverage.

To this list of launch constraints were added the constraints due to limitations other than those produced by the TDS:

(1) Limitation of the launch corridor to launch azimuths between 90–114 deg east of north caused by range safety.

(2) Limitation of last launch date of the launch period to June 25 because of insufficient available energy from the launch vehicle.

(3) Elimination of all launch days before June 12 because of poor arrival geometry at Venus.

These three non-TDS constraints defined what was called the available base launch period and base launch window. The base launch period was from June 12 to June 27 and the base launch window was from 90–114 deg or 2.2–2.8 h.

The second stage of the launch constraint planning included determining the project data requirements for the near-earth phase of the mission. Each system or other element of the project defined its near-earth data requirements which the launch constraints representative, upon approval from the project office, combined into one set (Fig. VII-1). The systems which placed most of the requirements were the spacecraft system and the launch vehicle system. However, requirements were placed by the project which did not come from any particular system (i.e., the requirement for post-posigrade maneuver tracking data was required to prove the project had met the planetary quarantine constraint).

To allow for differences in importance among the requirements, they were divided into three classes. Class I data was designated as the most important class (Fig. VII-2).

The TDS coverage capabilities were examined to determine which, if any, of the project requirements could not be met. To accomplish the analysis, graphs of earth tracks and station view periods were generated (Figs. VII-3 and VII-4) which provided a key visual aid in the near-earth coverage analysis. The capabilities of the various resources of the TDS are shown and the various gaps in coverage (and hence deficiencies in support of project requirements) can be identified. Because the *Mariner V* injection occurred over the Atlantic Ocean, the use of AFETR tracking ships was necessary to meet several of the class I requirements. After the land station coverage capabilities were shown on these graphs, ships were positioned to minimize the coverage gaps. The resultant gaps in coverage after the entire set of resources is considered are the TDS-produced launch constraints.

Because there are three agencies (AFETR, DSN, MSFN) which support the near-earth phase of the mission, the job of coordinating the support can be hazardous. In particular, the need for an AFETR ship to cover part of a requirement while the DSN supports another part with the MSFN as a backup produced several coordination problems. In fact, the project requirement for S-band spacecraft data from *Agena*/spacecraft separation ($S$) to $S+5$ min required just such a configuration because the AFETR ships did not have demodulators.

In addition, because of the limitation on the number of available demodulators, it was necessary to determine a strategy for distribution so that the maximum amount of data would be returned. To assist this tradeoff, a model was formulated by the constraints representative that employed a figure of merit as the variable to maximize. This figure of merit is called the *amount of critical view* (ACV) and is a measure of the value of the support from a given station.

This amount of critical view of a given station is defined as *the time that stations will view a particular interval on a particular day, summed over all possible azimuths for that day.* An example should help explain this meaning. Figure VII-5 is a plot of the station view periods as a function of the time from launch for the June 12 launch date. Only four stations are shown—Ascension, Johannesburg, Carnarvon, and Tidbinbilla. Figure VII-5 indicates the time at which various critical events occur. In particular, the class I data requirement intervals from $S$ to $S+5$ min and from launch $(L)+51$ to $L+58$ min are shown. The ACV of a station is defined as *the amount of view of that station in a critical class I data interval.* Only that portion of the view is considered in which the station in question would be the *only land station available.* For example, only that portion of the Carnarvon view of the $L+51$ to $L+58$ interval which could not be viewed by Tidbinbilla would be included in the Carnarvon ACV. Since the possible view varies with the launch azimuth, the ACV for a given day is determined by adding the amount of view for a given azimuth over all azimuths from 90–114 deg. Thus, the ACV has units of deg–min. For example, the ACV for Carnarvon on June 12 is 32 deg–min of view.

To arrive at a figure of merit for the entire launch period, and to take into account that launch is more likely in the early part of the launch period than in the late part, each ACV for a given day is multiplied by the probability of launching on that day. The results are then summed and normalized to provide the *normalized critical view* (NCV). The NCV for 3 stations—Ascension, Johannesburg and Carnarvon—is given in Table VII-3 for the $S$ to $S+5$ min and $L+51$ to $L+58$ min required data intervals.

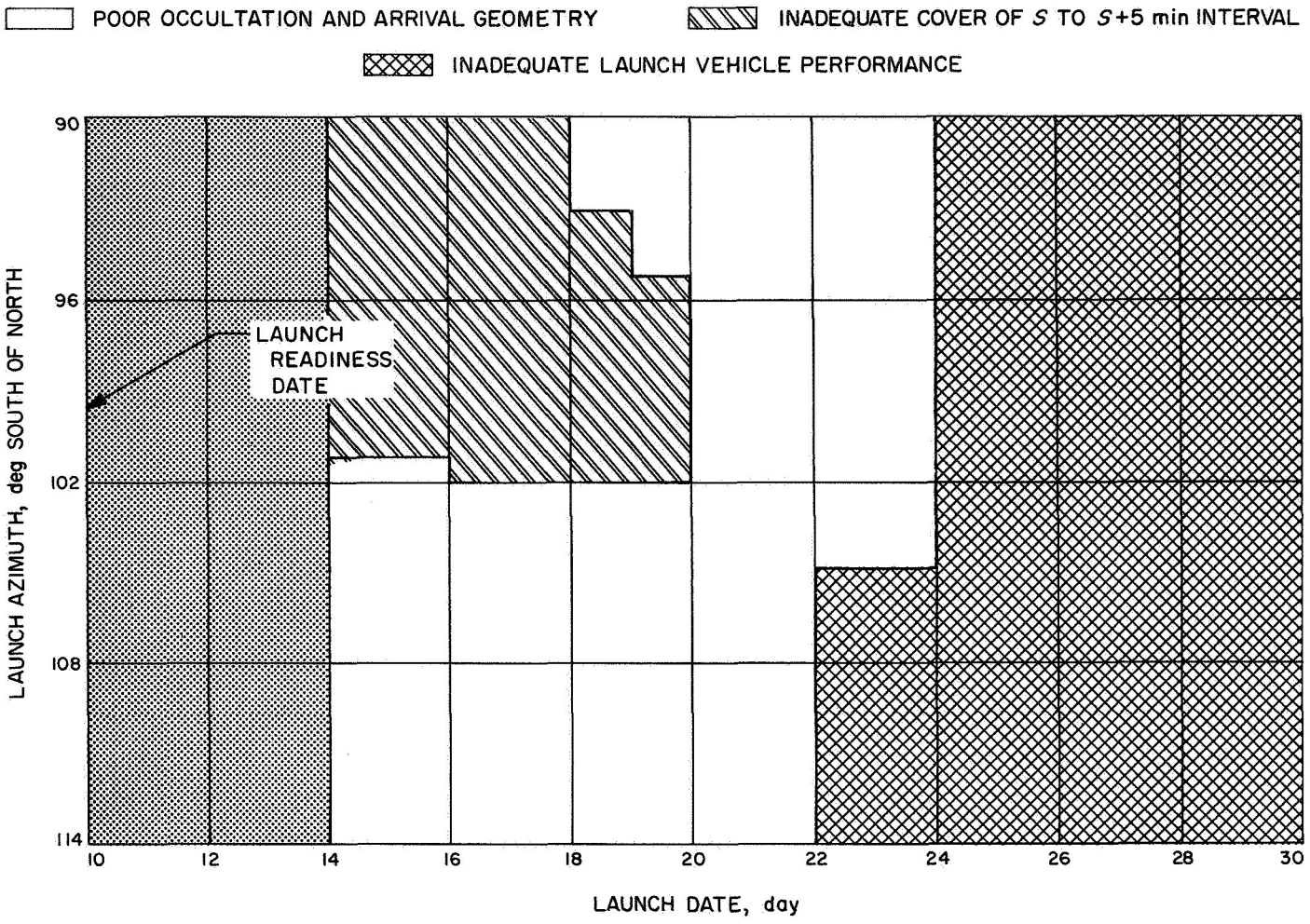



**Fig. VII-1. Summary chart of launch constraints**

This model clearly showed that placing two demodulators, one at Ascension and one at Johannesburg, was preferred to placing one demodulator at Carnarvon and the other at either Ascension or Johannesburg.

**Table VII-3. The figure of merit (NCV) for each station, taking into account the variation of probability of launch within the launch period**

| Station | Figure of merit Normalized critical view (NCV) |
|---|---|
| Ascension only | 58.2 deg-min |
| Ascension and Johannesburg only | 141.6 deg-min |
| Johannesburg only | 113.2 deg-min |
| Johannesburg and Carnarvon only | 113.2 deg-min |
| Carnarvon only | 21.6 deg-min |
| Carnarvon and Ascension only | 79.8 deg-min |

As the near-earth coverage analysis proceeded, a TDS configuration necessary to meet the project near-earth requirements began to emerge. The TDS analyst and the launch phase analyst worked together to insure that this TDS configuration was both acceptable to the project to meet class I requirements and feasible as sound configuration for the TDS. This TDS analyst/LPA team was established about three months before launch and played an important role in the final countdown and launch operations. The method of operation was for the TDS analyst to formulate a near-earth configuration and the LPA to analyze the effect of this configuration upon the mission. There was, of course, a good deal of necessary coordination between these two analysts so that often the LPA helped formulate a TDS configuration and the TDS analyst helped evaluate the effect of the configuration upon the mission. This interplay between the two analysts was extremely valuable and necessary for the successful support of the project requirements.

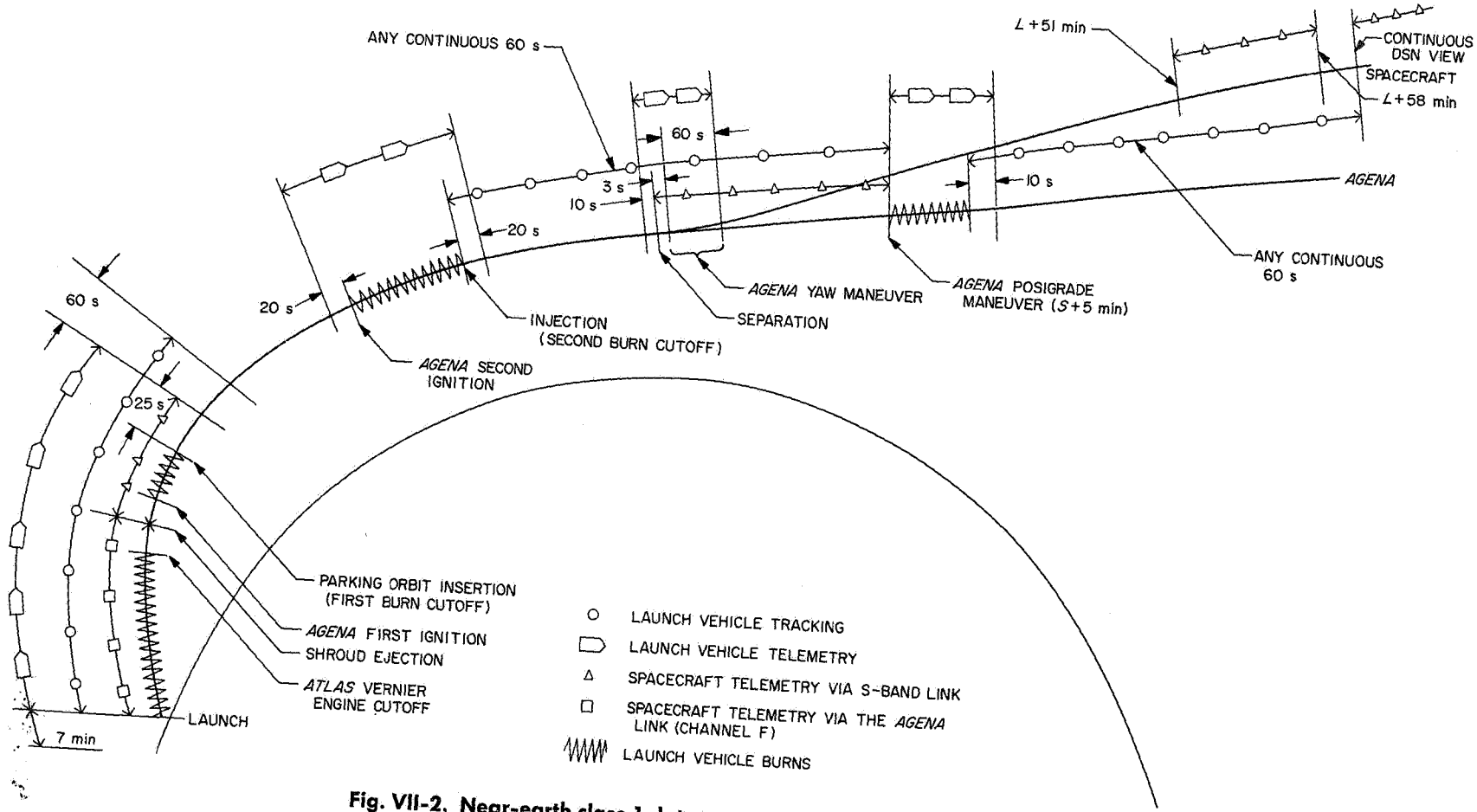



**Fig. VII-2. Near-earth class 1 data requirements for *Mariner* Venus 67**

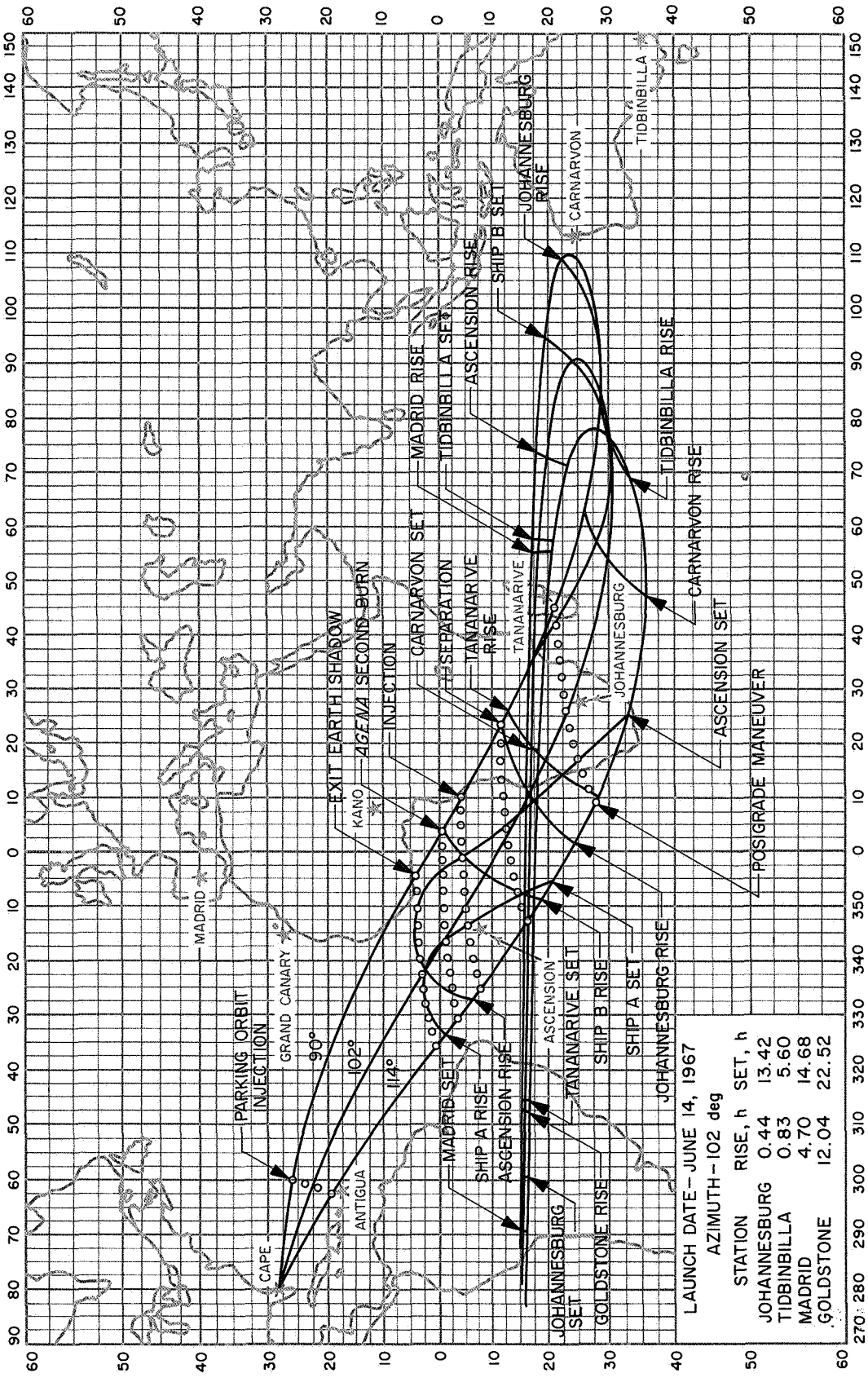



**Fig. VII-3. Earth tracks for June 14, 1967**

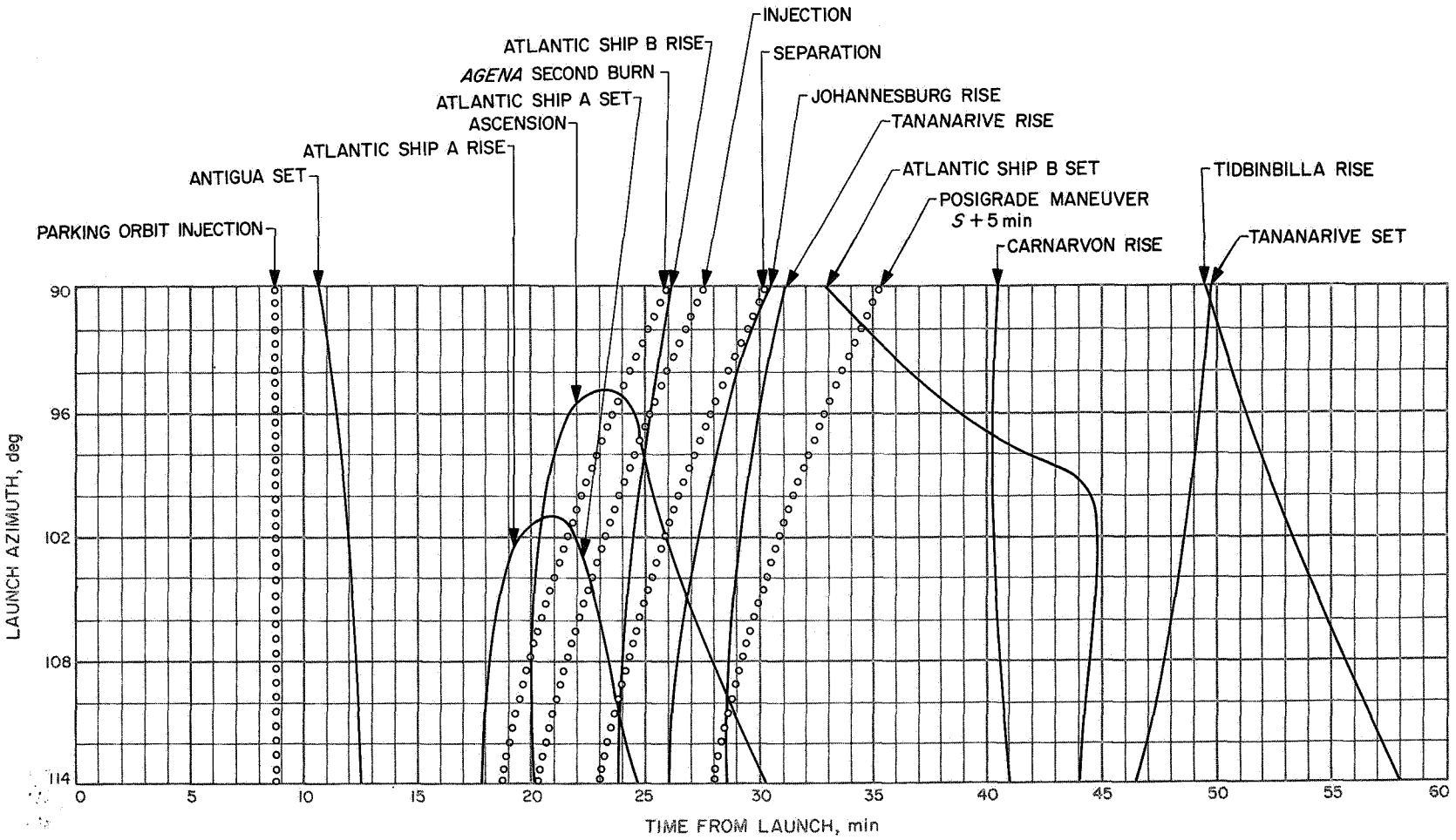



**Fig. VII-4. Station view periods for June 14, 1967**

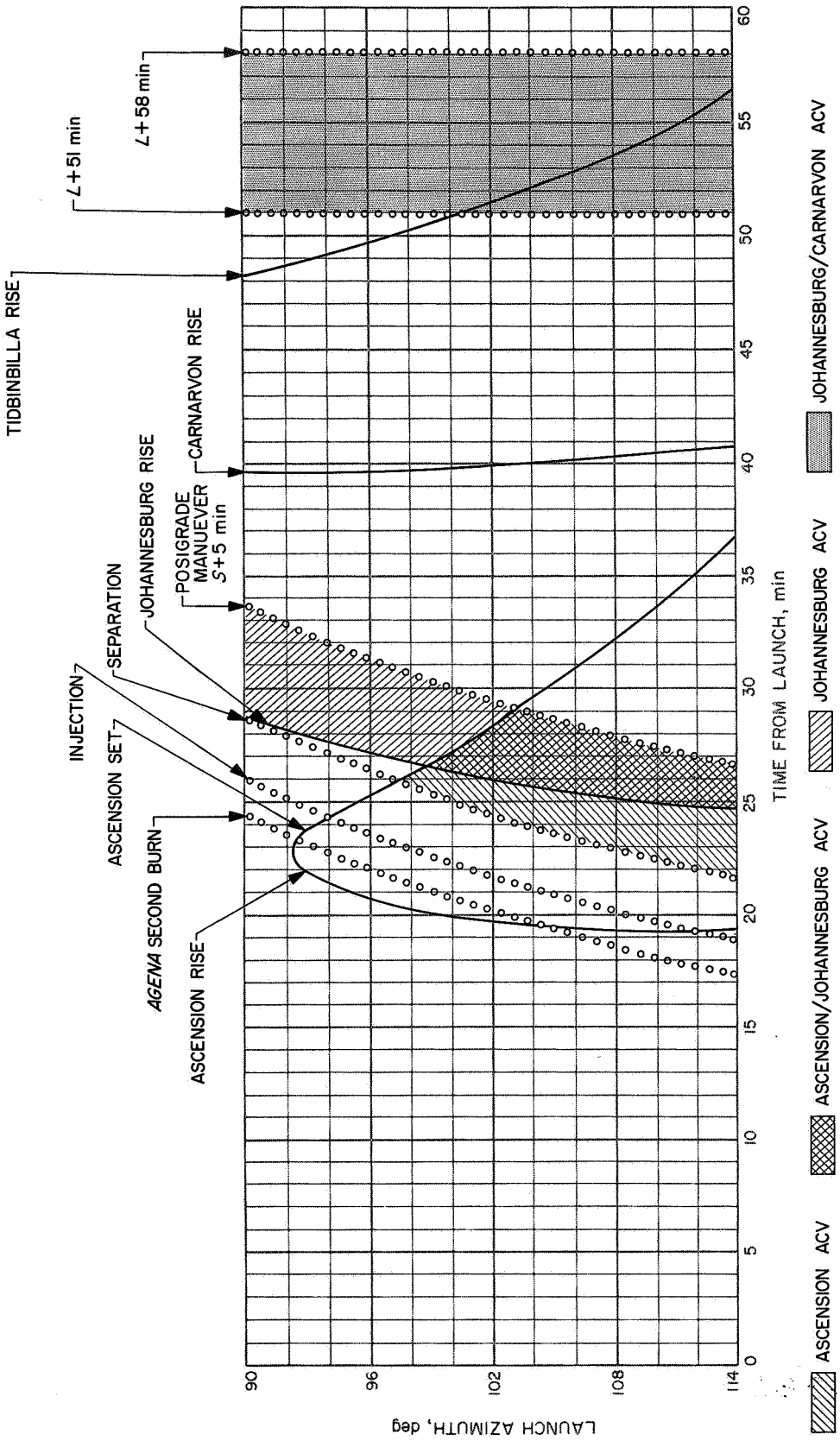
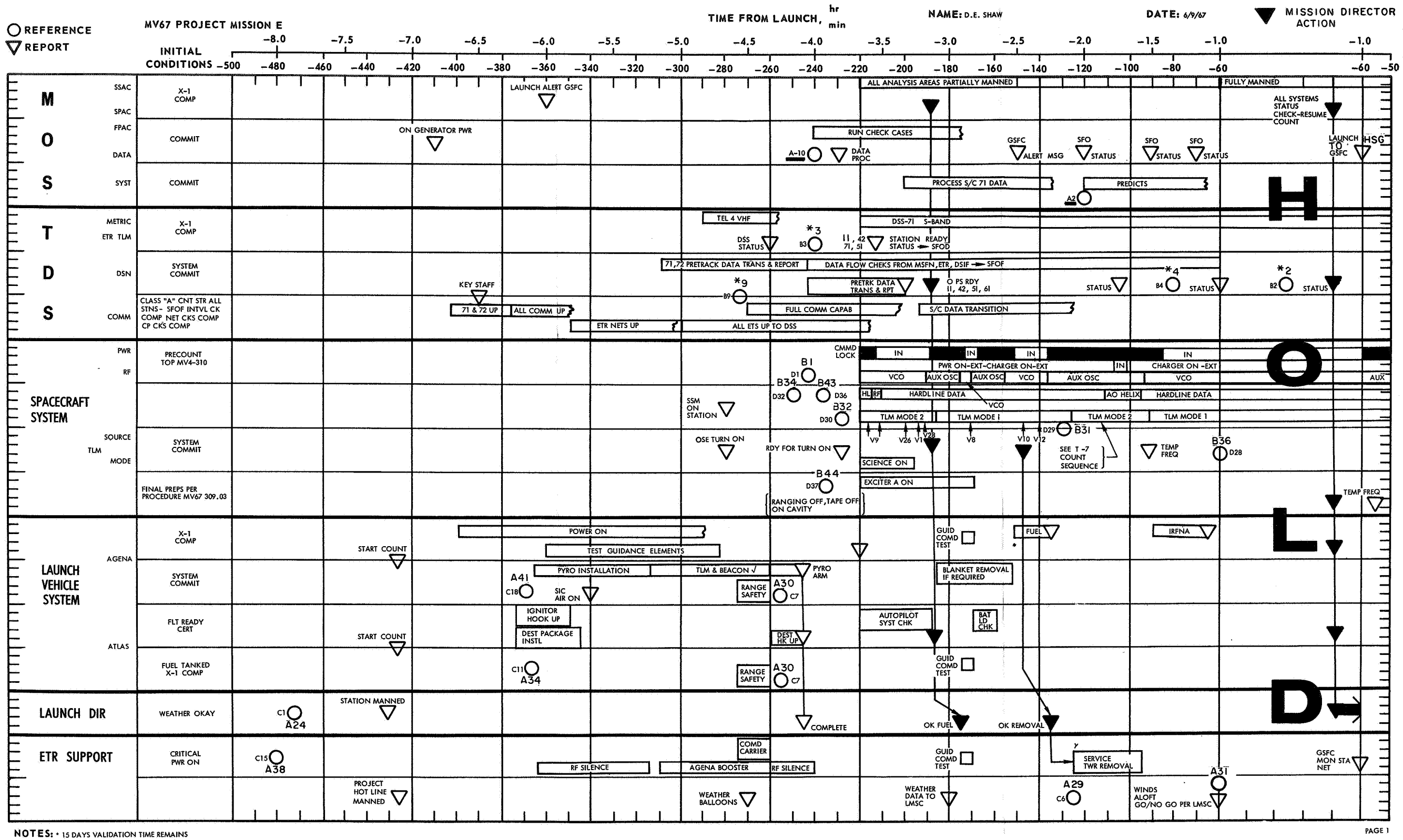



**Fig. VII-5. Station view periods for June 12, 1967**

# Appendix A

## Launch Sequence Document

PRECEDING PAGE BLANK NOT FILMED.




NOTES: * 15 DAYS VALIDATION TIME REMAINS
γ NO MORE ACCESS TO BLANKET OR UMBILICAL

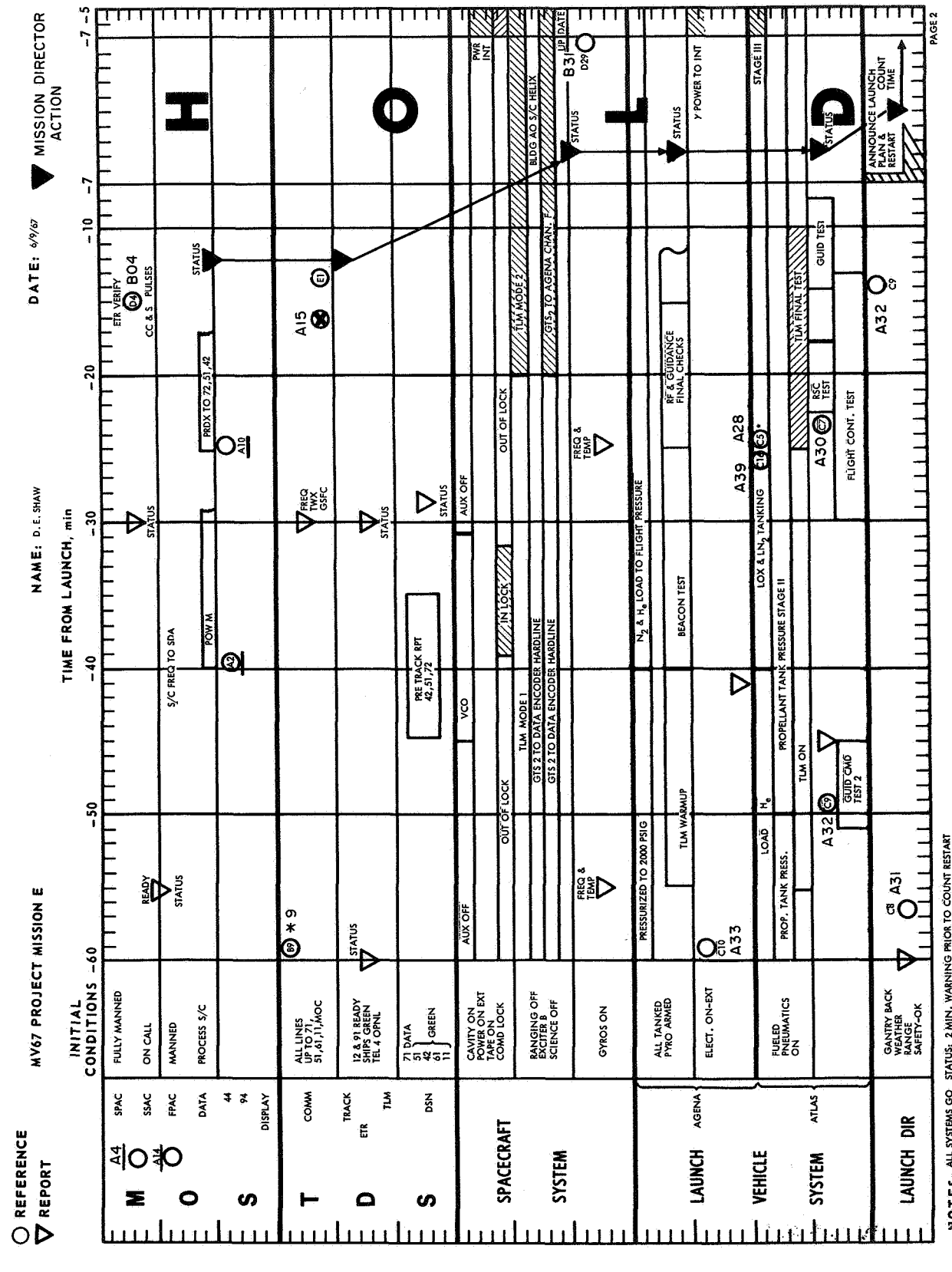
PAGE 1

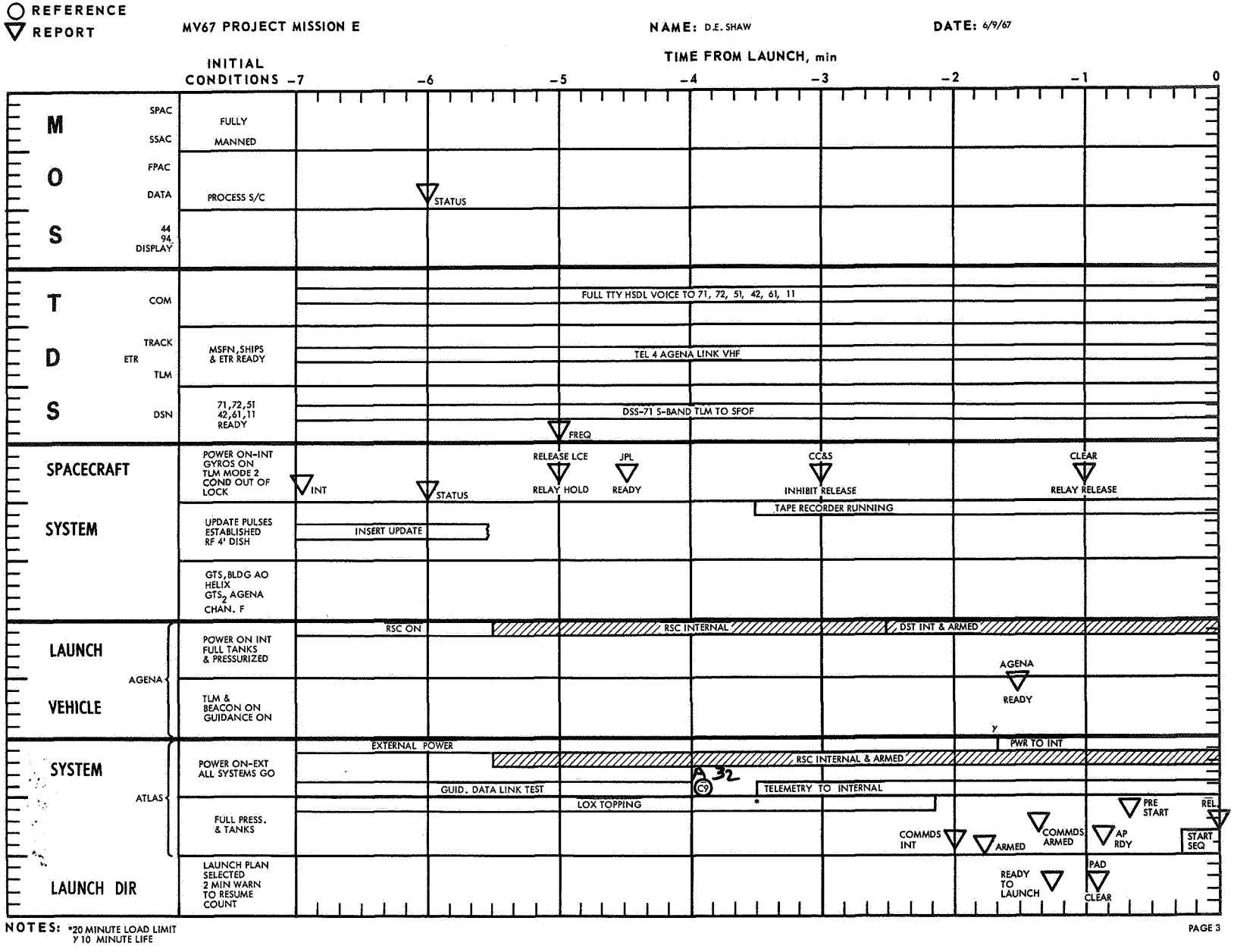
FOLDOUT FRAME 1

FOLDOUT FRAME 2

**Page intentionally left blank**

PRECEDING PAGE BLANK NOT FILMED.



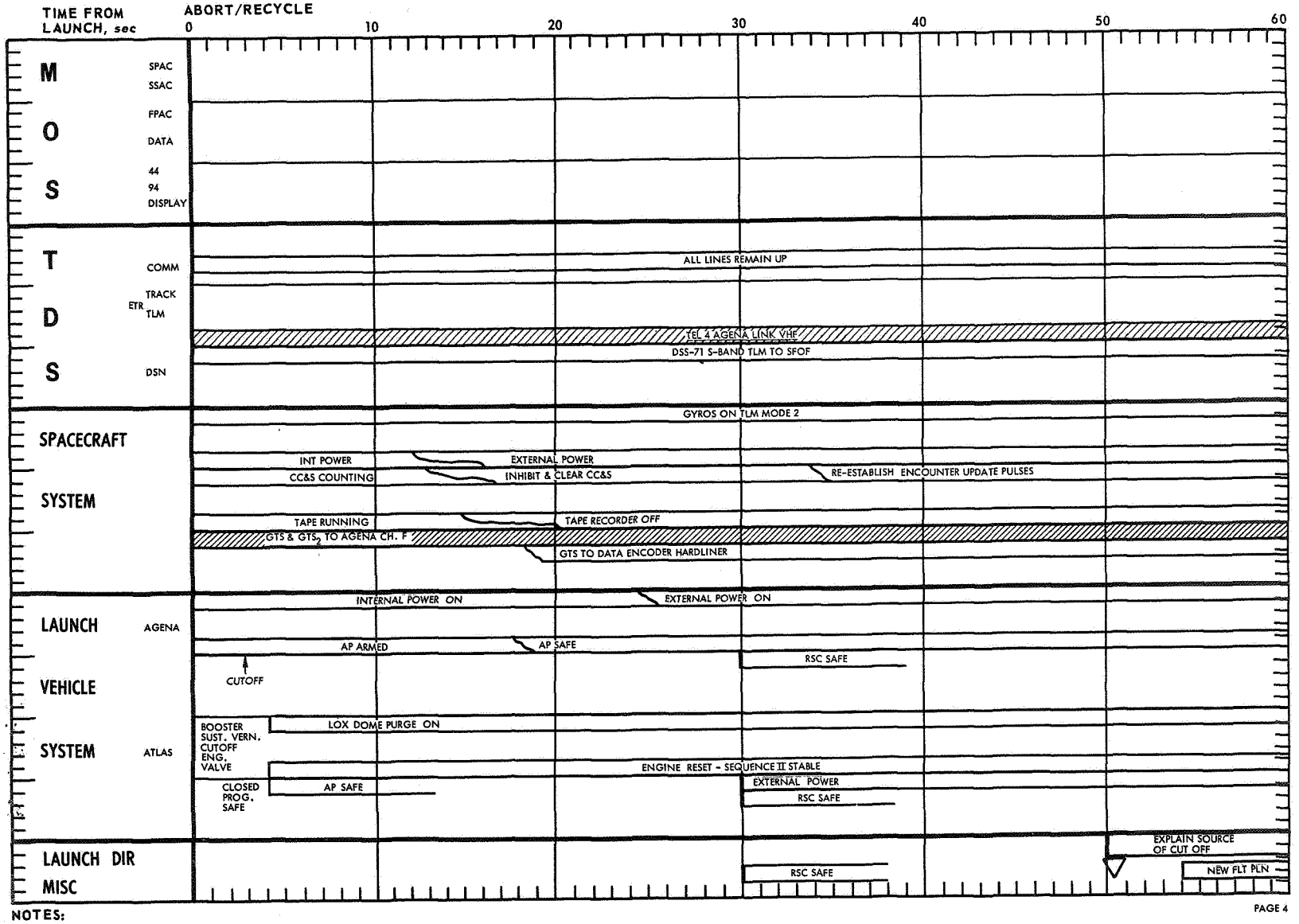

REFERENCE
REPORT
MV67 PROJECT MISSION E
NAME: D.E. SHAW
DATE: 6/9/67
INITIAL CONDITIONS
TIME FROM LAUNCH, min
-7
-6
-5
-4
-3
-2
-1
0
MOST
SPAC
SSAC
FPAC
DATA
44
94
DISPLAY
FULLY MANNED
PROCESS S/C
STATUS
COM
TRACK
ETR
TLM
DSN
MSFN, SHIPS & ETR READY
71,72,51
42,61,11
READY
FULL TTY HSDL VOICE TO 71, 72, 51, 42, 61, 11
TEL 4 AGENA LINK VHF
DSS-71 S-BAND TLM TO SFOF
FREQ
SPACECRAFT SYSTEM
POWER ON-INT GYROS ON TLM MODE 2 COND OUT OF LOCK
INT
STATUS
RELEASE LCE
RELAY HOLD
JPL
READY
CC&S
INHIBIT RELEASE
CLEAR
RELAY RELEASE
TAPE RECORDER RUNNING
UPDATE PULSES ESTABLISHED RF 4' DISH
INSERT UPDATE
GTS, BLDG AO HELIX
GTS2 AGENA CHAN. F
LAUNCH VEHICLE
AGENA
POWER ON INT FULL TANKS & PRESSURIZED
RSC ON
RSC INTERNAL
DST INT & ARMED
TLM & BEACON ON GUIDANCE ON
AGENA
READY
y
SYSTEM
ATLAS
POWER ON-EXT ALL SYSTEMS GO
EXTERNAL POWER
PWR TO INT
RSC INTERNAL & ARMED
A 32
C9
GUID. DATA LINK TEST
TELEMETRY TO INTERNAL
FULL PRESS. & TANKS
LOX TOPPING
*
COMMDS INT
ARMED
COMMDS ARMED
AP RDY
PRE START
REL
START SEQ
LAUNCH DIR
LAUNCH PLAN SELECTED 2 MIN WARN TO RESUME COUNT
READY TO LAUNCH
PAD
CLEAR
NOTES: *20 MINUTE LOAD LIMIT
y 10 MINUTE LIFE
PAGE 3

○ REFERENCE
▽ REPORT

MV67 PROJECT MISSION E

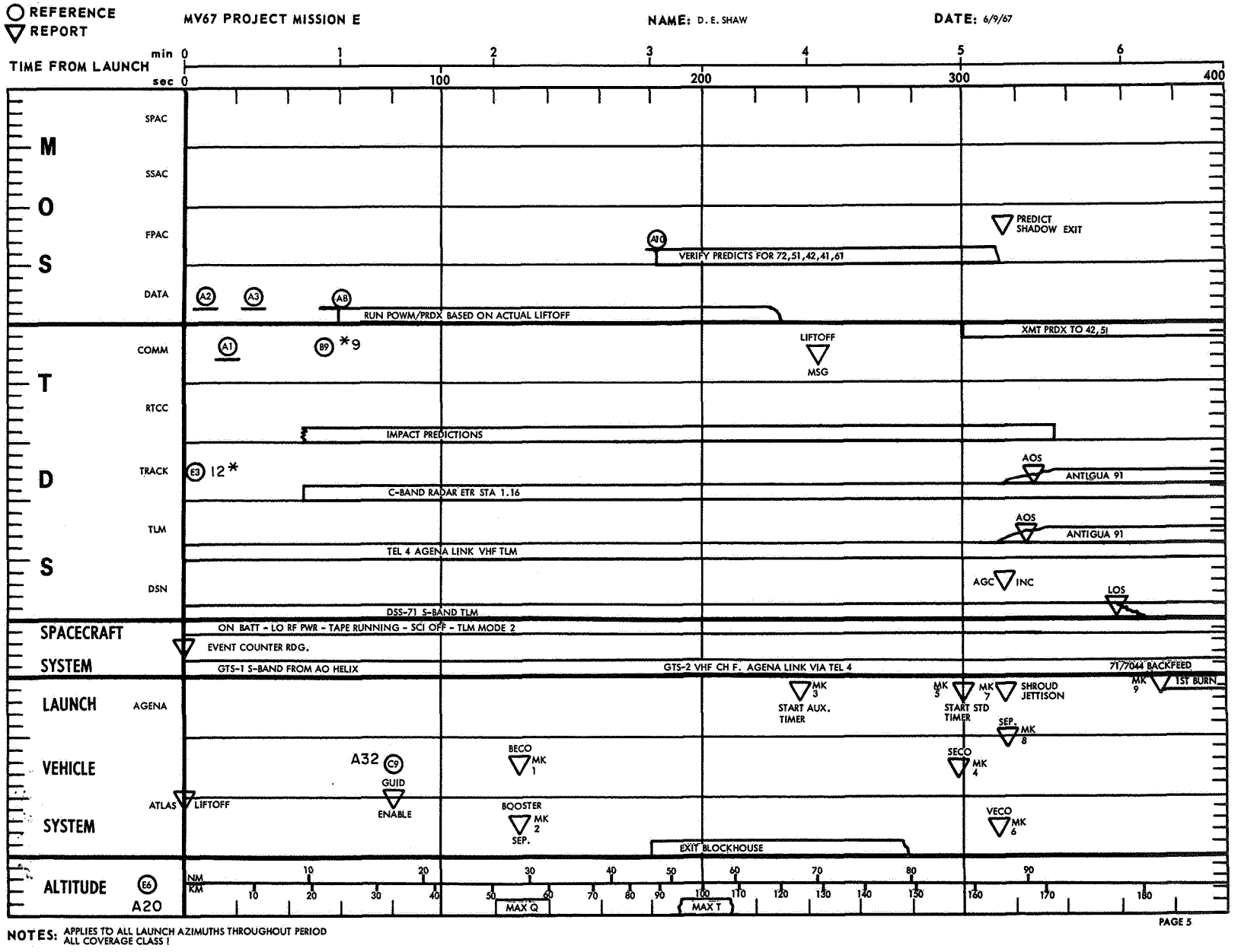
NAME: D. E. SHAW

DATE: 6/9/67



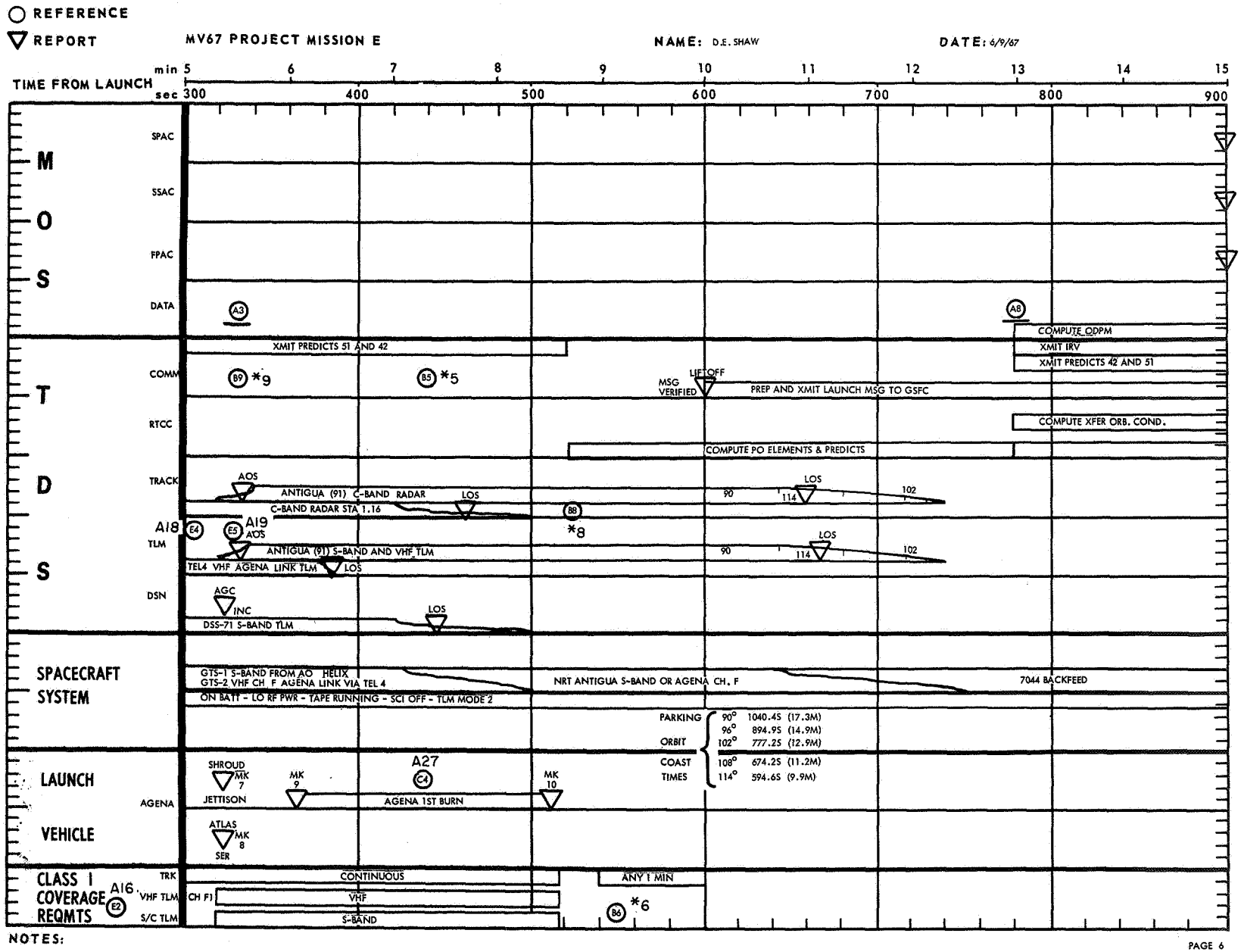

NOTES:

PAGE 4

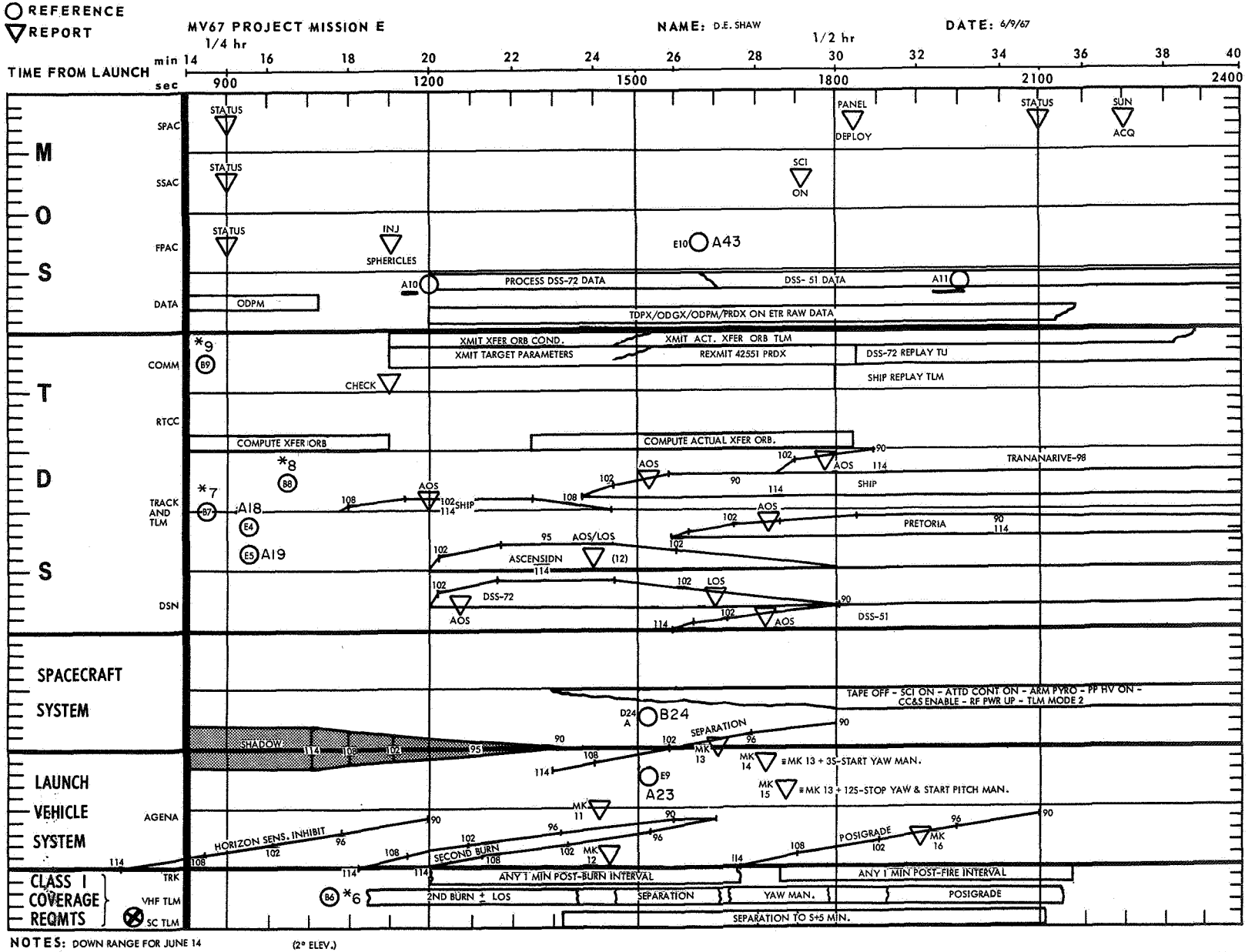



PAGE 5

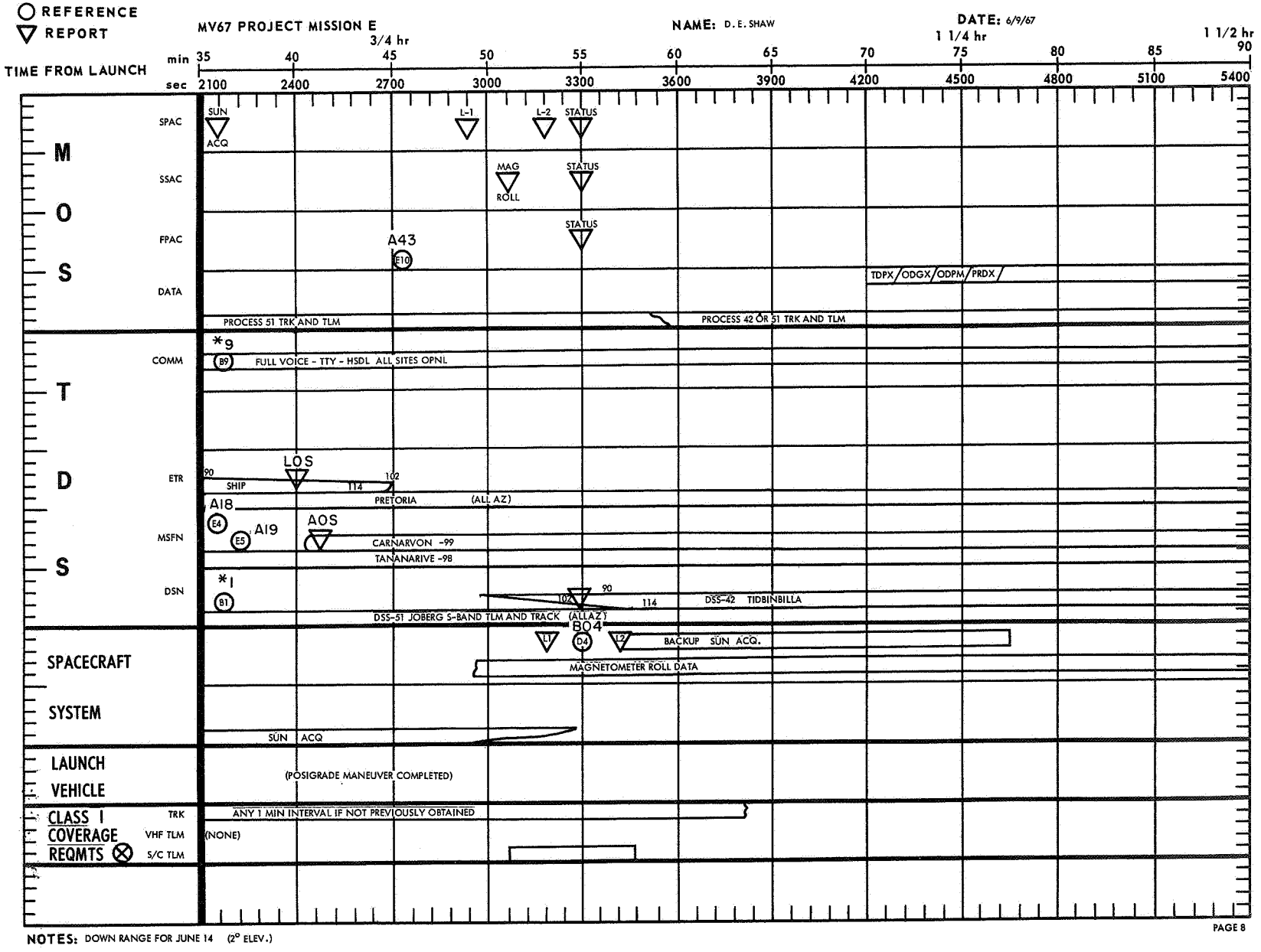
NOTES: APPLIES TO ALL LAUNCH AZIMUTHS THROUGHOUT PERIOD
ALL COVERAGE CLASS 1


REFERENCE
REPORT
MV67 PROJECT MISSION E
NAME: D.E. SHAW
DATE: 6/9/67
TIME FROM LAUNCH
min 5 6 7 8 9 10 11 12 13 14 15
sec 300 400 500 600 700 800 900
MOS
SPAC
SSAC
FPAC
DATA
A3
A8
COMPUTE ODPM
XMIT IRV
XMIT PREDICTS 42 AND 51
TDS
COMM
XMIT PREDICTS 51 AND 42
B9 *9
B5 *5
LIFT OFF
MSG VERIFIED
PREP AND XMIT LAUNCH MSG TO GSFC
RTCC
COMPUTE XFER ORB. COND.
COMPUTE PO ELEMENTS & PREDICTS
TRACK
AOS
ANTIGUA (91) C-BAND RADAR
LOS
C-BAND RADAR STA 1.16
B8 *8
90 114 102
A18 E4 E5 A19
TLM
AOS
ANTIGUA (91) S-BAND AND VHF TLM
TEL4 VHF AGENA LINK TLM
DSN
AGC INC
DSS-71 S-BAND TLM
SPACECRAFT SYSTEM
GTS-1 S-BAND FROM AO HELIX
GTS-2 VHF CH F AGENA LINK VIA TEL 4
NRT ANTIGUA S-BAND OR AGENA CH. F
7044 BACKFEED
ON BATT - LO RF PWR - TAPE RUNNING - SCI OFF - TLM MODE 2
PARKING 90° 1040.4S (17.3M)
96° 894.9S (14.9M)
ORBIT 102° 777.2S (12.9M)
COAST 108° 674.2S (11.2M)
TIMES 114° 594.6S (9.9M)
LAUNCH VEHICLE
AGENA
SHROUD JETTISON MK 7
MK 9
A27 C4
AGENA 1ST BURN
MK 10
ATLAS SER MK 8
CLASS I COVERAGE REQMTS
A16 E2
TRK
VHF TLM
S/C TLM
CONTINUOUS
CH F1
VHF
S-BAND
ANY 1 MIN
B6 *6

NOTES:




NOTES: DOWN RANGE FOR JUNE 14 (2° ELEV.)




NOTES: DOWN RANGE FOR JUNE 14 (2° ELEV.)

PRECEDING PAGE BLANK NOT FILMED.

# Appendix B

# Project Management Report

# OFFICE OF SPACE SCIENCE AND APPLICATIONS

## JET PROPULSION LABORATORY
## CALIFORNIA INSTITUTE OF TECHNOLOGY

## PROJECT MANAGEMENT REPORT

## *MARINER*

(*VENUS* 67 AND *MARINER IV*, AGENCY CODES 817 AND 813)

(NOTE: *THE MILESTONE AND RESOURCES DATA CONTAINED IN THIS ISSUE MAY NOT BE COMPLETE OR MAY NOT REFLECT FINAL FIGURES AT CONCLUSION OF THE PROJECT*

JET PROPULSION LABORATORY

# *MARINER VENUS* 67 AND *MARINER IV* PROJECTS

STATUS AS OF 4-17-67

## CONTENTS


NARRATIVE ANALYSIS (LEVEL 2) . . . . . 1
TECH PERFORMANCE DATA . . . . . 2
MV67 MASTER SCHEDULE (LEVEL 2) . . . . . 3
MV67 SPACECRAFT SYSTEM SCHEDULE (LEVEL 3) . . . . . 4
MV67 MISSION OPERATIONS SYSTEM SCHEDULE (LEVEL 3) . . . . . 5
MV67 TRACKING AND DATA ACQUISITION SYSTEM SCHEDULE (LEVEL 3) . . 6
MV 67 ATLAS/AGENA - AGENA PROCUREMENT (493) 7
NARRATIVE ANALYSIS (LEVEL 3) . . . . . 8
MV67 ATLAS/AGENA MASTER SCHEDULE (LEVEL 3) . . . . . 9
MV67 FINANCIAL STATUS . . . . . 10
MV67 MANPOWER . . . . . 11
MV67 COST TREND ANALYSIS . . . . . 12
MIV MASTER SCHEDULE . . . . . 13
MIV FINANCIAL STATUS . . . . . 14
MIV MANPOWER . . . . . 15


## HEADQUARTERS CONTROLLED MILESTONES

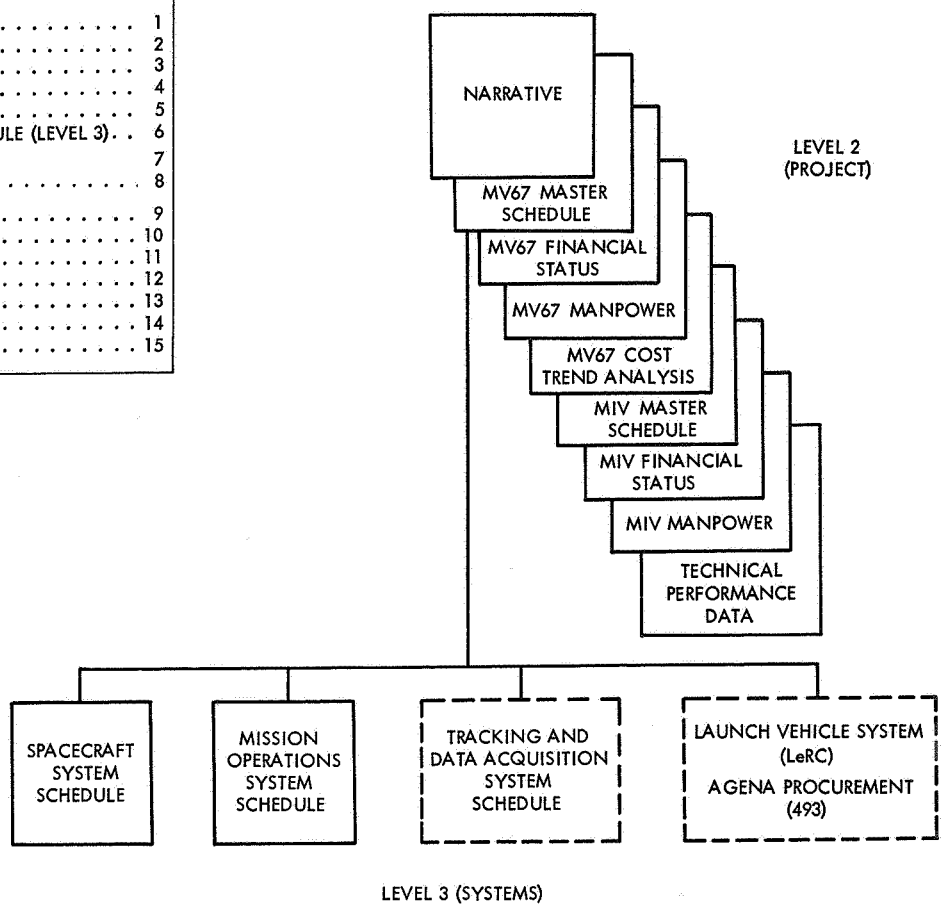
### *MARINER VENUS* 67 PROJECT

EXPERIMENTS SELECTED
PROJECT APPROVED (PAD ISSUED)
PDP SUBMITTED FOR APPROVAL
LAUNCH VEHICLE SHIPMENT DATES
SPACECRAFT PRESHIPPING REVIEW
MISSION READINESS REVIEW (LAUNCH READINESS)
QUARANTINE CRITERIA ESTABLISHED
CERTIFICATION OF QUARANTINE PROVISIONS

### *MARINER IV* PROJECT

PROJECT APPROVED (PAD ISSUED)
PDP SUBMITTED FOR APPROVAL
BEGINNING OF REACQUISITION PERIOD
END OF REACQUISITION PERIOD

## REPORTING STRUCTURE




RESOURCES STATUS REPORTED SEPARATELY - NOT INCLUDED WITH MV67 PROJECT INFORMATION PRESENTED HEREIN.

NARRATIVE

JET PROPULSION LABORATORY
RESPONSIBILITY: G. R. Ludecke
APPROVAL: R. LUDECKE
ACCOMPLISHMENT: D. SCHNEIDERMAN

# NARRATIVE ANALYSIS
## *MARINER* 1967 PROJECT

2 LEVEL

ORIGINAL SCHEDULE APPROVAL 4/28/66 (DATE)
LAST SCHEDULE CHANGE NONE (DATE) (INITIALS)
STATUS AS OF 6/12/67 (DATE) (INITIALS)

SUMMARY OUTLOOK

The final phases of MV67 launch preparations and operational readiness testing leading to a June 14 launch have been completed. Mariner IV spacecraft conditioning and data retrieval activities were resumed with return of DSS-14 to service.

SIGNIFICANT PROGRESS

Mariner IV - The Mariner IV spacecraft was contacted on June 7 with a received signal level of approximately -167 dbm. Telemetry was processed through DSS Stations 14/11 to the SFOF and through the comm processor and 7044 to outputs in the Mariner support area. This test was combined with the final ORT as part of the total Mariner Venus 67 launch readiness.

Mariner Venus 67 - The Mariner Venus 67 spacecraft was removed from the launch vehicle after a radio system problem was noted. A relay in the radio system was replaced and the spacecraft returned to L/C-12 and mated with the launch vehicle on 6/8/67--simulated launch was conducted on 6/9/67. All project systems have completed final testing--all are in launch support readiness.

| EXCEPTIONAL ACTIVITIES PLANNED FOR THIS REPORT INTERVAL | ACTUAL |
|---|---|
| Finalize Launch and Hold Criteria | Accomplished |
| Perform Combined Operational Tests | Accomplished |
| Conduct J-FACT and Simulated Launch | Accomplished |
| Hold Two Operational Readiness Tests | Accomplished |

EXCEPTIONAL EVENTS PLANNED FOR NEXT PERIOD

LAUNCH
Midcourse Maneuver
Begin Combined Mariner IV/Mariner Venus 67 Operations

FLASH REPORT

Mariner V was successfully launched from ETR at 02:01 EDT June 14, 1967. Midcourse maneuver requirements are nominal, basically correcting the aiming point bias. All spacecraft systems are operating normally and Canopus was acquired at 18:09 PDT on June 14, 1967.

JET PROPULSION LABORATORY
RESPONSIBILITY:
APPROVAL: A. R. LUEDECKE
ACCOMPLISHMENT: D. SCHNEIDERMAN

# TECHNICAL PERFORMANCE DATA FORM FOR *MARINER* 1967 SPACE FLIGHT PROJECT

(2 LEVEL)

STATUS OF 6/12/67 (DATE) (INITIALS)

| | | | | | |
|---|---|---|---|---|---|
| I. MISSION INFORMATION | Mariner E | Mariner IV | | | |
| A. DATE EXPERIMENT INTEGRATION | 9/1 - & 12/15-66 | ACCOMPLISHED | | | |
| B. RECOVERY PLANNED | NONE | NONE | | | |
| C. LIFETIME (MISSION DURATION) | MIN 124 days | 17 Mo. * | | | |
| II. FLIGHT CHARACTERISTICS | | | | | |
| A. APOGEE (APOLUNE, ETC.)(AU) | 1.0172 | 1.573037 | | | |
| B. PERIGEE (PERILUNE, ETC.)(AU) | 0.715959 | 1.103634 | | | |
| C. INCLINATION (°) | 2.92 | 2.54 | | | |
| D. PERIOD (DAYS) | 294.67 | 567.115 | | | |
| III. AVAILABLE S/C CAP. | | | | | |
| A. WT. AVAILABLE FOR EXPERIMENTS | 0.00 | 0.00 | | | |
| B. VOL. AVAILABLE FOR EXPERIMENTS | 0.00 | 0.00 | | | |
| C. POWER AVAILABLE FOR EXPERIMENTS | 0.00 | 0.00 | | | |
| D. TELEMETRY | PSK | PSK | | | |
| E. STORAGE | 0.00 | 0.00 | | | |
| F. INFORMATION RATE (BPS) | 8-1/3 or 33-1/3 | 8-1/3 or 33-1/3 | | | |
| G. ACCELERATION (G) | 16.4 GRMS SHAPED NOISE | 16.4 GRMS SHAPED NOISE | | | |
| H. THERMAL RANGE (°C) | +75 to -10 | +75 to -10 | | | |
| I. STABILIZATION: TYPE ACCURACY (°) | 3 AXIS GAS JET USING SUN (±0.48°) + CANOPUS (±0.25°) | 3 AXIS GAS JET USING SUN (± 0.48°) + CANOPUS (±0.25°) | | | |
| IV. ASSIGNED S/C PAYLOAD CAP. | | | | | |
| A. WT. ASSIGNED (LBS) | 63.5 | 77.1 | | | |
| B. VOL. ASSIGNED (CU. IN.) | 2309 | 2645 | | | |
| C. POWER ASSIGNED (WATTS) | 35.6 | 42.3 | | | |
| D. DATA STOR. CAP. ASSIGNED (BITS) | $1 \times 10^6$ | $5.24 \times 10^6$ | | | |
| V. MISSION MARGIN | | | | | |
| A. LIFTING CAPACITY OF L/V | 542. | NOT APPLICABLE | | | |
| B. SPACECRAFT WEIGHT | 541.76 | 574.74 | | | |
| C. MISSION MARGIN | 0 | - | | | |
| VI. OTHER INFORMATION (SEE INSTRUCTIONS) | | | | | |
| | | | | | |
| | | | | | |
| VII. REMARKS | | | | | |
| A. SEE INSTRUCTIONS | 12 DAY NOMINAL LAUNCH PERIOD AT $C_3$ of 10.1 $km^2/s^2$ | * TO A/C GAS DEPLETION | | | |

PAGE 2

2 YEAR

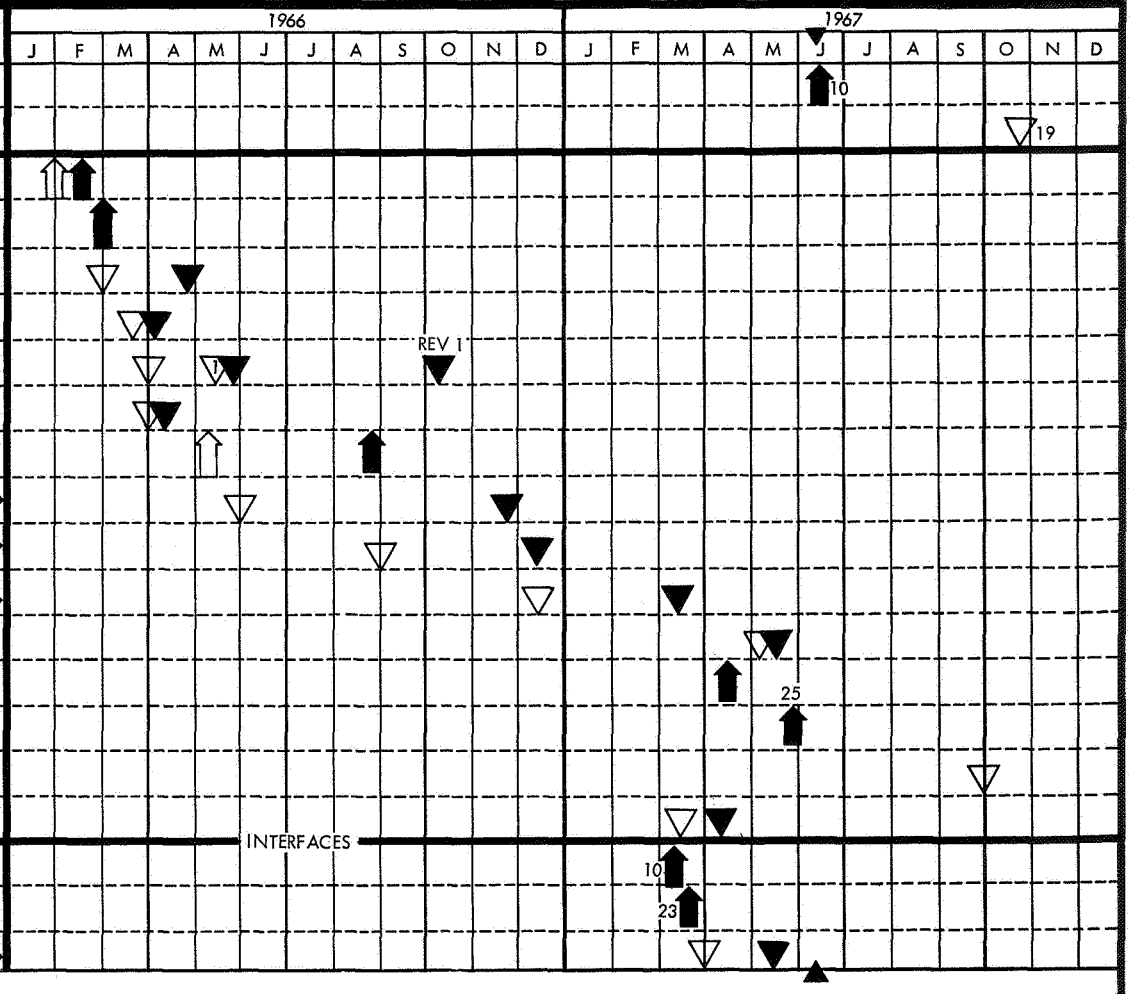
**JET PROPULSION LABORATORY**
RESPONSIBILITY:
APPROVAL: A. P. LUEDECKE
ACCOMPLISHMENT: O. SCHNEIDERMAN

# MASTER SCHEDULE
## *MARINER VENUS* 67 PROJECT

2 LEVEL

ORIGINAL SCHEDULE APPROVAL 4/28/66 (DATE)
LAST SCHEDULE CHANGE NONE (DATE) (NO.) (INITIALS)
STATUS AS OF 6/12/67 (DATE) DS/DSH (INITIALS)

| | MILESTONES |
|---|---|
| 1 | LAUNCH READINESS |
| 2 | ENCOUNTER |
| 3 | EXPERIMENTS SELECTED |
| 4 | PROJECT APPROVED (PAD ISSUED) |
| 5 | SPACECRAFT DESIGN ESTABLISHED |
| 6 | PRELIMINARY STANDARD TRAJECTORY PUBLISHED |
| 7 | SIRD PUBLISHED |
| 8 | PRD INPUTS TO ETR |
| 9 | PDP SUBMITTED FOR APPROVAL |
| 10 | REQMTS. AND RESTRAINTS DOCUMENT ISS. |
| 11 | FLIGHT SUPPORT S/C (67-1) DEL. TO SAF |
| 12 | FLIGHT SPACECRAFT (67-2) DELIVERY TO SAF |
| 13 | MOS FLIGHT OPERATIONAL |
| 14 | SPACECRAFT PRESHIPPING REVIEW |
| 15 | MISSION READINESS REVIEW |
| 16 | ENCOUNTER READINESS REVIEW |
| 17 | MOP/LOP PUBLISHED |
| | INTERFACES |
| 18 | SHIP ATLAS TO ETR |
| 19 | SHIP AGENA TO ETR |
| 20 | T&DA OPERATIONAL READINESS |




NOTES:

PAGE 3

2 YEAR

**JET PROPULSION LABORATORY**
RESPONSIBILITY:
APPROVAL: A. R. Luedecke R. LUEDECKE
ACCOMPLISHMENT: D. Schneiderman D. SCHNEIDERMAN

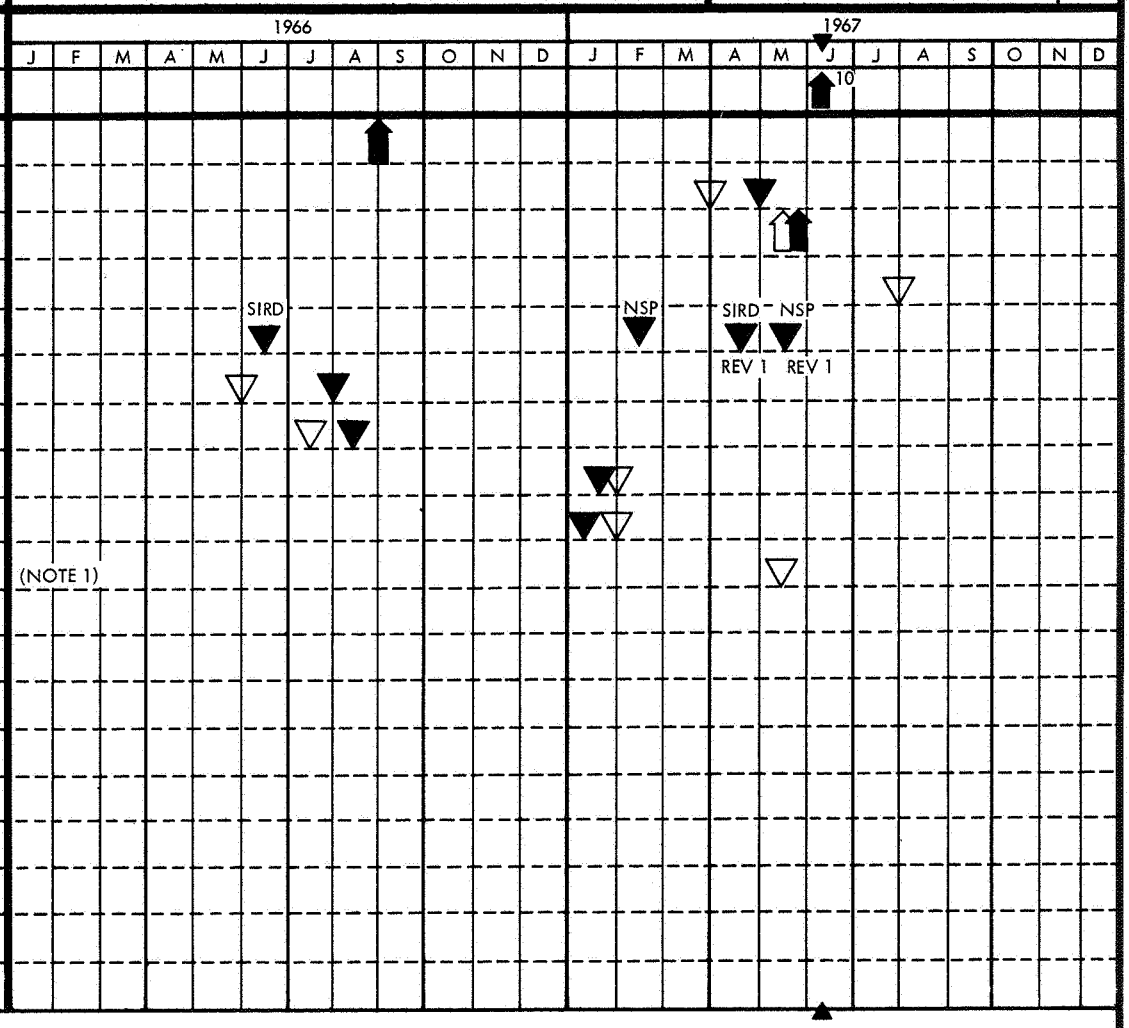
# MASTER SCHEDULE (CONT)

## *MARINER VENUS* 67 PROJECT

2 LEVEL

ORIGINAL SCHEDULE APPROVAL 6/22/66 (DATE)
LAST SCHEDULE CHANGE NONE (DATE) (NO.) (INITIALS)
STATUS AS OF 6/12/67 (DATE) DS/WEK (INITIALS)

| | MILESTONES |
|---|---|
| 1 | LAUNCH READINESS |
| 2 | QUARANTINE CRITERIA ESTABLISHED |
| 3 | PRELAUNCH CONTAMINATION PROB. ANALYSIS |
| 4 | QUARANTINE CERTIFICATION |
| 5 | POST MIDCOURSE CONTAMINATION REPORT |
| 6 | NASA HQ SIGNOFF SIRD AND NSP |
| 7 | CONIC VIEW PERIODS DOCUMENT PUBLISHED |
| 8 | FLIGHT PLAN APPROVAL DOCUMENT PUBLISHED |
| 9 | LAUNCH CONSTRAINTS DOCUMENT PUBLISHED |
| 10 | MISSION TARGETING SPECIFICATION PUBLISHED |
| 11 | FINAL POST INJECTION STANDARD TRAJECTORY DOCUMENT PUBLISHED |
| 12 | |
| 13 | |
| 14 | |
| 15 | |
| 16 | |
| 17 | |
| 18 | |
| 19 | |
| 20 | |




NOTES:
(1) TRAJECTORY CHARACTERISTICS HAVE REMAINED UNCHANGED FROM THOSE PUBLISHED IN PD 72 ON 4/1/66. HENCE THE NEED FOR THIS FINAL TRAJECTORY DOCUMENT HAS DISAPPEARED AND IT WILL NOT BE ISSUED.

PAGE 4

2 YEAR

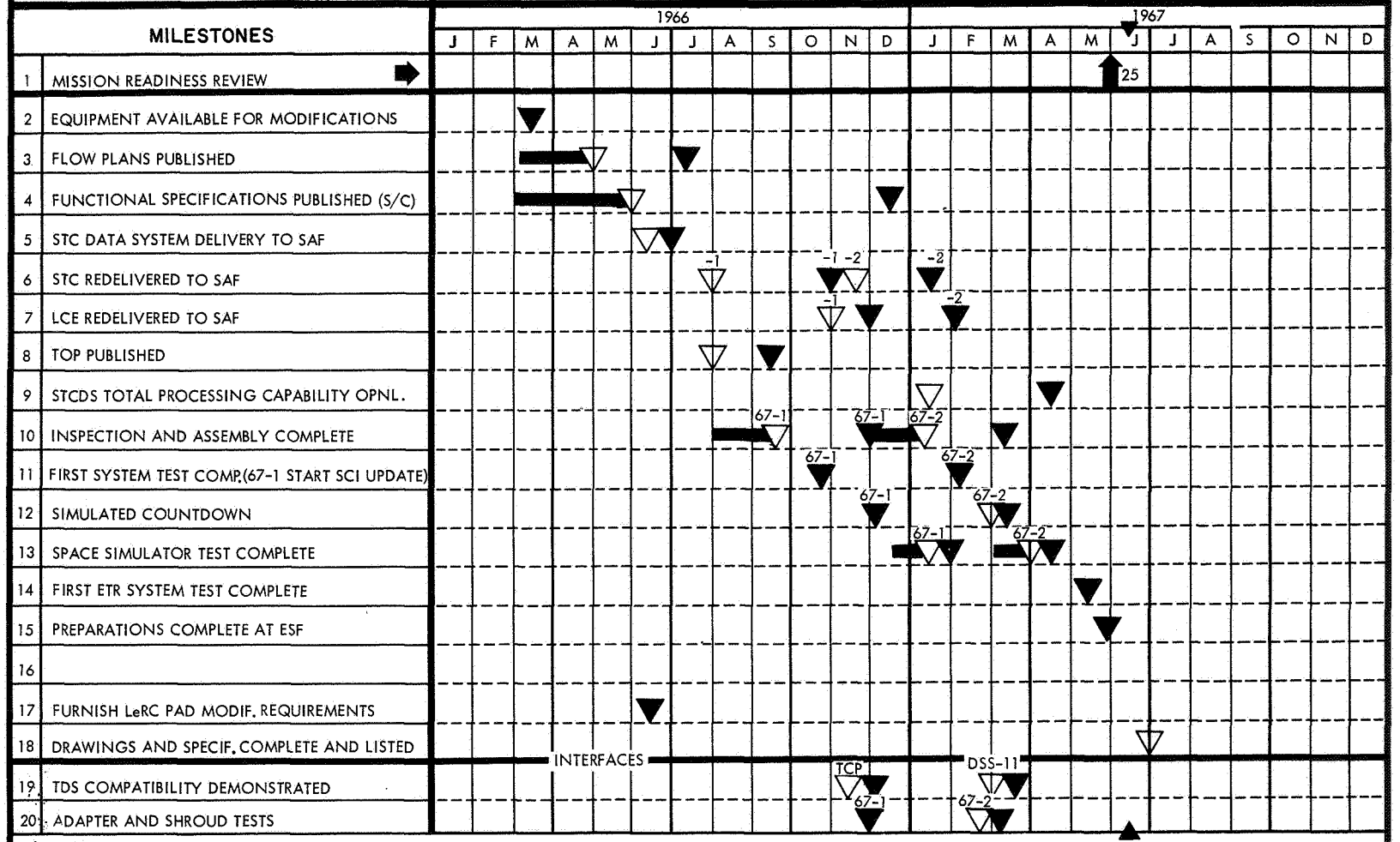
JET PROPULSION LABORATORY
RESPONSIBILITY:
APPROVAL: D. SCHNEIDERMAN
ACCOMPLISHMENT: A. E. WOLFE

# SPACECRAFT SYSTEM SCHEDULE

## *MARINER VENUS* 67 PROJECT

3 LEVEL

ORIGINAL SCHEDULE APPROVAL 5/20/66 (DATE)
LAST SCHEDULE CHANGE NONE (DATE)
STATUS AS OF 6/12/67 (DATE) (NO.) (INITIALS)




NOTES:

PAGE 5

2 YEAR

**JET PROPULSION LABORATORY**
RESPONSIBILITY:
APPROVAL: D. SCHNEIDERMAN
ACCOMPLISHMENT: D. W. DOUGLAS

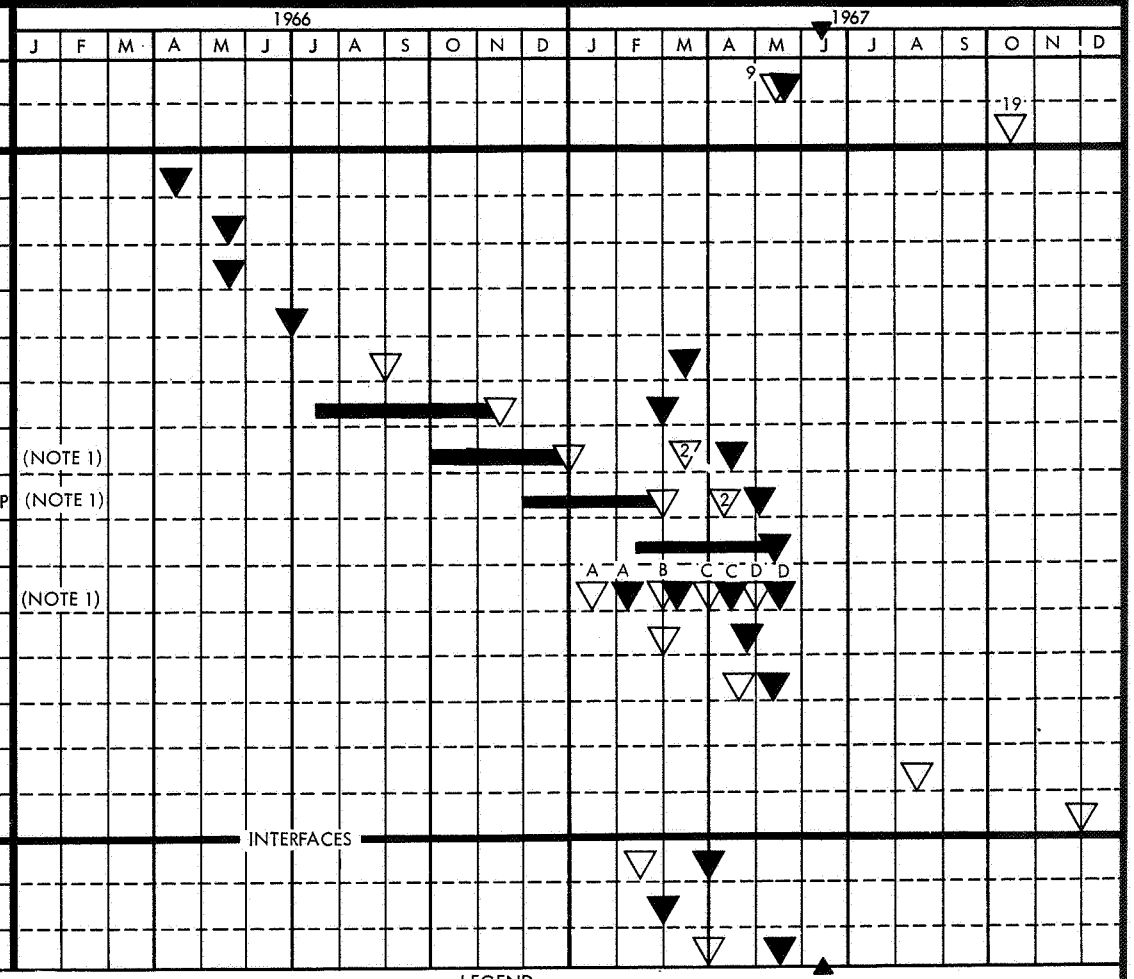
# MISSION OPERATIONS SYSTEM SCHEDULE

3 LEVEL

*MARINER VENUS* 67 PROJECT

ORIGINAL SCHEDULE APPROVAL 5/23/66 (DATE)
LAST SCHEDULE CHANGE 8/22/66 (DATE) 1 (NO.) (INITIALS)
STATUS AS OF 6/12/67 (DATE) (INITIALS)

| | MILESTONES |
|---|---|
| 1 | FLIGHT OPERATIONAL (READY FOR ORT) |
| 2 | ENCOUNTER |
| 3 | GROUND DATA HANDLING ELEMENTS DEFINED |
| 4 | HARDWARE DESIGN ESTABLISHED |
| 5 | PROGRAMMING DESIGN DEFINED |
| 6 | SPACE FLIGHT OPERATION PLAN PUBLISHED |
| 7 | SFO-TEST PLAN ISSUED |
| 8 | FINAL MRH DELIVERY |
| 9 | SUBSYSTEM DEVELOPMENT TESTS COMPLETE |
| 10 | INTEGRATION AND COMPATIBILITY TESTS COMP |
| 11 | OPERATIONAL TRAINING TESTS COMPLETE |
| 12 | SOFTWARE DELIVERIES |
| 13 | GROUND DATA HANDLING ACCEPTANCE |
| 14 | MOS-SPACECRAFT TRAINING COMPLETE |
| 15 | |
| 16 | ENCOUNTER CONVERSION COMPLETED |
| 17 | FINAL MDL DISTRIBUTED |
| | INTERFACES |
| 18 | CP & 7044 R SOFTWARE AVAIL |
| 19 | MSA OCCUPANCY DATE |
| 20 | T&DA OPERATIONAL READINESS |




NOTES:

(1) ONLY INCOMPLETED ITEM IS STAR IDENTIFICATION PROGRAM. EXPECTED OPERATIONAL DATE IS 5/20.

LEGEND

A. INTERIM TCP SOFTWARE PACKAGE TRANSFERRED TO DSN.
B. FINAL TCP SOFTWARE PACKAGE AVAILABLE FOR RELEASE TO DSN.
C. LAST REAL TIME DATA PROCESSING SOFTWARE RELEASED TO DSN.
D. LAST NON REAL-TIME DATA PROCESSING SOFTWARE RELEASED TO DSN.

PAGE 6

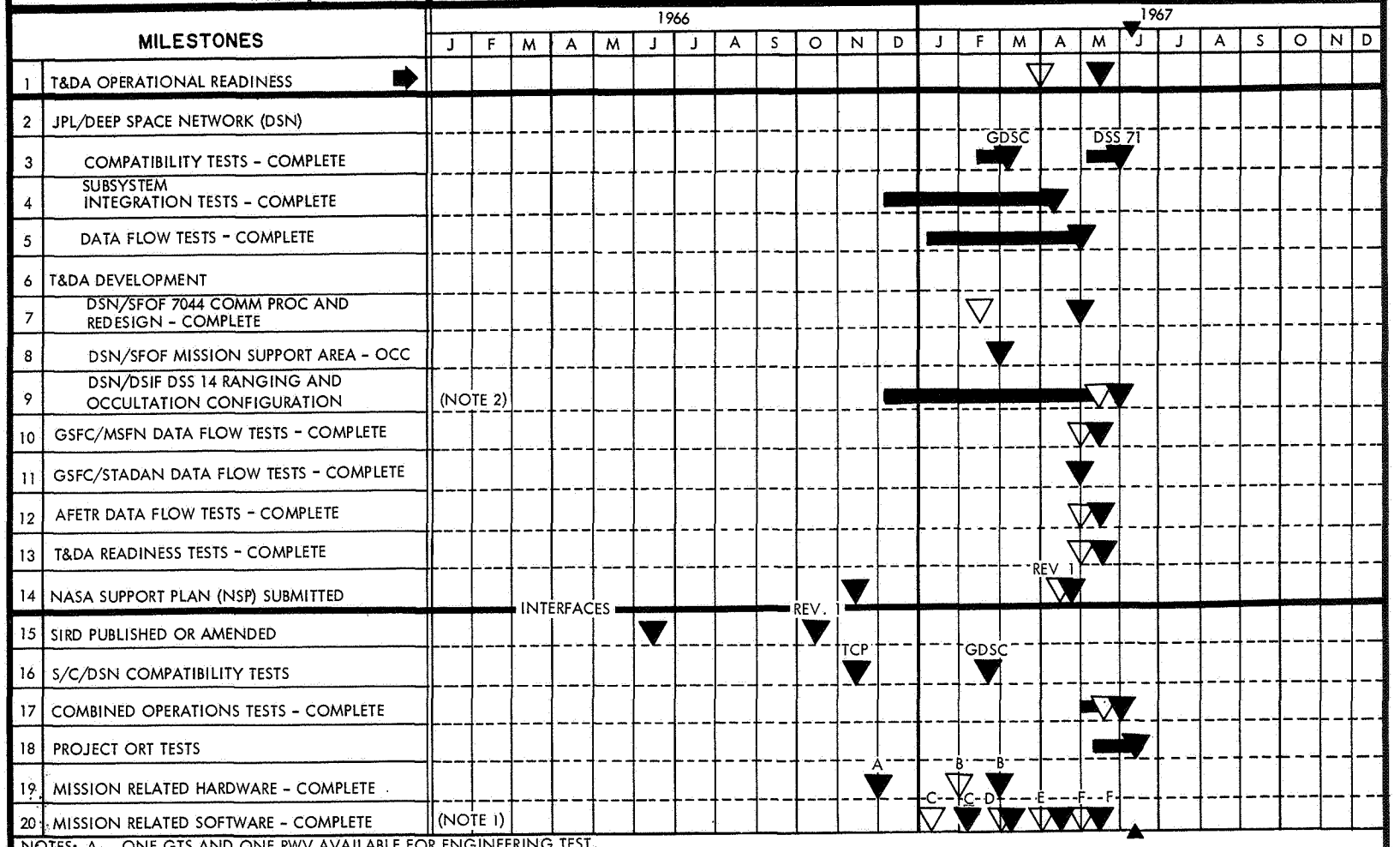
2 YEAR

**JET PROPULSION LABORATORY**
RESPONSIBILITY:
APPROVAL: D. Schneiderman D. SCHNEIDERMAN
ACCOMPLISHMENT: N. Renzetti N. RENZETTI

# TRACKING & DATA ACQUISITION SYSTEM SCHEDULE
## *MARINER VENUS* 67 PROJECT

3 LEVEL

ORIGINAL SCHEDULE APPROVAL 11/21/66 (DATE)
LAST SCHEDULE CHANGE 5/23/66 (DATE) M99 (NO.) (INITIALS)
STATUS AS OF 6/12/67 (DATE) MJS (INITIALS)




NOTES: A. ONE GTS AND ONE RWV AVAILABLE FOR ENGINEERING TEST.
B. LAST GTS AND RWV WITH DOCUMENTATION AND SPARES TRANSFERRED TO DSN.
C. INTERIM TCP SOFTWARE PACKAGE AVAILABLE FOR RELEASE TO DSN.
D. FINAL TCP SOFTWARE PACKAGE AVAILABLE FOR RELEASE TO DSN.
E. LAST REAL TIME DATA PROCESSING SOFTWARE RELEASED TO DSN.
F. LAST NON-REAL TIME DATA PROCESSING SOFTWARE RELEASED TO DSN.

(2) CONTINUING OPERATIONAL CHECKOUT TESTS

PAGE 7

| LEWIS RESEARCH CENTER | NARRATIVE ANALYSIS | ORIGINAL SCHEDULE APPROVAL (Date) |
|---|---|---|
| APPROVAL RESPONSIBILITY H. W. PLOHR | AGENA PROCUREMENT (493) 3 | LAST SCHEDULE CHANGE (Date) (No) (Initials) |
| ACCOMPLISHMENT RESPONSIBILITY L. W. CROTSER | ATLAS/AGENA LEVEL | STATUS AS OF 5-18-67 (Date) (Initials) |
| | MARINER '67 | |

SUMMARY OUTLOOK

Launch vehicle activities are scheduled to support launch readiness of Mariner Venus 67 June 9 (EST) for a launch period opening June 12, 1967.

STATUS VS. PLANS

Changes in Plan

None.

Progress During the Report Period

MAB testing of the Mariner '67 Agena, Atlas checks and installation and checkout of AGE are progressing on schedule at ETR.

Planned During the Next Report Period

The installation and checkout of LC-12 AGE is scheduled for completion May 26.

Mariner Venus '67 Atlas/Agena mate (VOS) is scheduled May 30.

Launch readiness is scheduled June 9, for a launch period opening June 12.

Problem Areas

Investigation of the ATS A Agena propellant isolation valve failure has resulted in modifications to the valve. These modifications were accomplished on the Lunar Orbiter D Agena in time to support the successful May 4 launch, and will be implemented for all Agena two-burn missions including Mariner Venus '67.

3 YEAR

LEWIS RESEARCH CENTER

APPROVAL RESPONSIBILITY H. W. Plotz by sea

ACCOMPLISHMENT RESPONSIBILITY Floyd K. W. Cotton

# MASTER PROGRAM/PROJECT SCHEDULE

3 LEVEL

ATLAS/AGENA PROCUREMENT
MARINER VENUS'67

ORIGINAL SCHEDULE APPROVAL JUN 66 (Date)

LAST SCHEDULE CHANGE ____ (Date)

STATUS AS OF 5/18/67 (Date) Part

| | MILESTONES | CY 1966 J F M A M J J A S O N D | CY 1967 J F M A M J J A S O N D | CY 1968 J F M A M J J A S O N D |
|---|---|---|---|---|
| 1 | LAUNCH READINESS DATES → | | 9 | |
| 2 | HARDWARE | | | |
| 3 | ATLAS AND GUIDANCE SYSTEM | 13 | 7 | |
| 4 | BASIC AGENA D | 13 | 17 | |
| 5 | TEST HARDWARE FOR JPL | 24 | 21 | |
| 6 | FLIGHT SHROUD SYSTEMS (2) | 15 | 26 | |
| 7 | AGENA D ADAPTATION | 11 | 22 | |
| 8 | AGENA AND S/C SUPPORT AGE | 11 | 7 | |
| 9 | LAUNCH MARINER VENUS 67 | | | |
| 10 | AGE I &C | | 10 | |
| 11 | BOS | | 14 | |
| 12 | AGENA CHECKS AND VOS | | 24 | |
| 13 | S/C MATE & LAUNCH READINESS → | | 9 | |
| 14 | | | EXTERNAL INTERFACES | |
| 15 | JPL DEFINE LV REQ'MTS | 31 | | |
| 16 | SELECT LAUNCH COMPLEX | 17 | | |
| 17 | RESOLVE MAR'67/ATS A CONFLICT | 27 | | |
| 18 | MAR'67 S/C READY FOR MATE | | 1 | |
| 19 | | | | |
| 20 | | | | |

NOTES

SCHEDULE DOES NOT INCLUDE NON-PACING "SOFTWARE" PROCUREMENTS, SUCH AS LAUNCH SERVICES, GUIDANCE EQUATIONS, PROGRAM SUPPORT AND STUDIES PRIOR TO AGENA ADAPTATION, SPACE VEHICLE ANALYSES AND SUPPORTING SERVICES.

NASA-C-931 (Rev. 6-66)

JET PROPULSION LABORATORY
RESPONSIBILITY:
APPROVAL: G. R. Luedecke (A. R. LUEDECKE)
ACCOMPLISHMENT: D. Schneiderman (D. SCHNEIDERMAN)

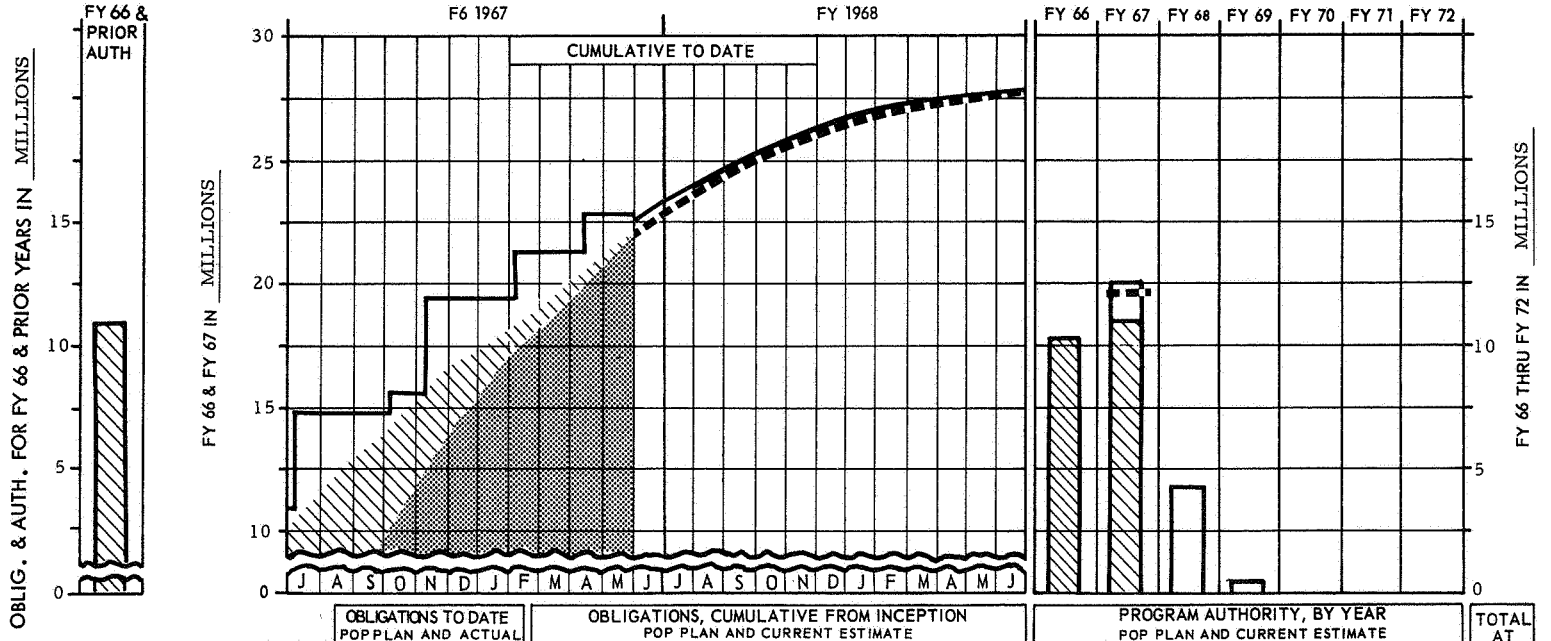
# PROJECT FINANCIAL STATUS

(2 LEVEL)

## *MARINER VENUS 67*

ACTUAL OBLIGATIONS AND COSTS AS OF 28 MAY 67 (DATE)

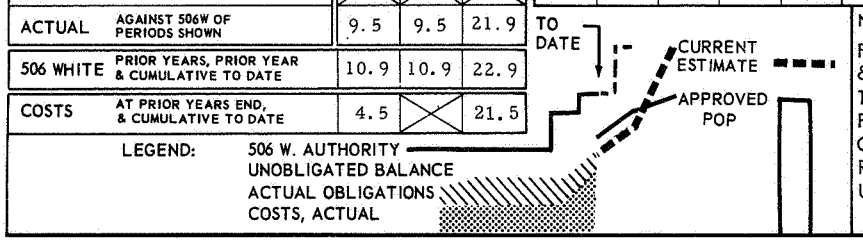
STATUS AS OF 12 JUN 67 (DATE) (INITIALS)




| FISCAL PERIODS | OBLIGATIONS TO DATE POP PLAN AND ACTUAL: FY 66 & PRIOR AUTH. | FY 66 AUTH. ONLY | CUM. TO DATE |
|---|---|---|---|
| APPROVED POP 67-1 | 9.5 | 9.5 | 22.7 |
| CURRENT ESTIMATE | | | |
| ACTUAL (AGAINST 506W OF PERIODS SHOWN) | 9.5 | 9.5 | 21.9 |
| 506 WHITE (PRIOR YEARS, PRIOR YEAR & CUMULATIVE TO DATE) | 10.9 | 10.9 | 22.9 |
| COSTS (AT PRIOR YEARS END, & CUMULATIVE TO DATE) | 4.5 | | 21.5 |

| OBLIGATIONS, CUMULATIVE FROM INCEPTION POP PLAN AND CURRENT ESTIMATE | | | | | | | |
|---|---|---|---|---|---|---|---|
| 30 JUN FY 1967 | | | | 30 SEP FY 1968 | 31 DEC FY 1968 | 31 MAR FY 1968 | 30 JUN FY 1968 |
| 23.4 | | | | 25.5 | 26.8 | 27.3 | 27.6 |
| 23.0 | | | | 25.1 | 26.4 | 26.9 | 27.2 |

| PROGRAM AUTHORITY, BY YEAR POP PLAN AND CURRENT ESTIMATE | | | | | | | TOTAL AT COMPLETION |
|---|---|---|---|---|---|---|---|
| FY 1966 | FY 1967 | FY 1968 | FY 1969 | FY 1970 | FY 1971 | FY 1972 | |
| 10.9 | 12.5 | 4.2 | 0.4 | | | | 28.0 |
| 10.9 | 12.1 | 4.2 | 0.4 | | | | 27.6 |




NOTES

FY 66 FY-END DATA, ADJUSTED THRU 5/28/67 ARE 9.484 OBLIGATED & 1.416 BALANCE AVAILABLE. THE FY 67 DATA INCLUDE 68K FOR KSC; THESE OBLIGATIONS ARE NOT REPORTED TO JPL. FY 68 AND FY 69 PLANS INCLUDE 360K AND 140K, RESPECTIVELY, FOR NASA HQ TO COVER POST-LAUNCH SCIENTIFIC DATA ANALYSIS.
REVISED ESTIMATE OF COST THROUGH COMPLETION BASED UPON CURRENT PROJECT STATUS.

PAGE 10

NARRATIVE

**JET PROPULSION LABORATORY**
RESPONSIBILITY:
APPROVAL: G. R. Luedecke A. R. LUEDECKE
ACCOMPLISHMENT: D. Schneiderman D. SCHNEIDERMAN

# MANPOWER

## *MARINER VENUS* 67 PROJECT

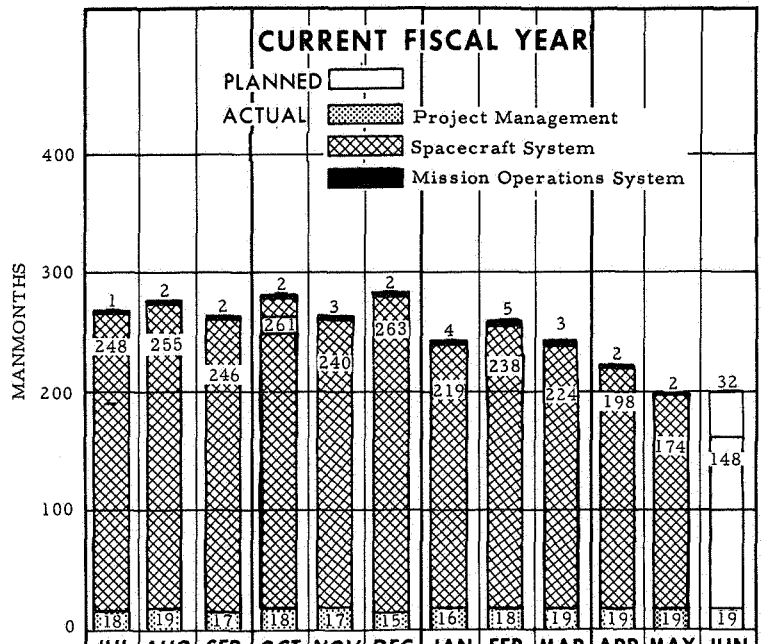
2 LEVEL

ORIGINAL SCHEDULE APPROVAL 2/25/66 (DATE)
LAST SCHEDULE CHANGE 10/30/66 (DATE) 2 (NO.) (INITIALS)
STATUS AS OF 12 JUN 67 (DATE) (INITIALS)

PERCENTAGE OVERTIME 18.5
(AVERAGE FOR REPORT PERIOD)

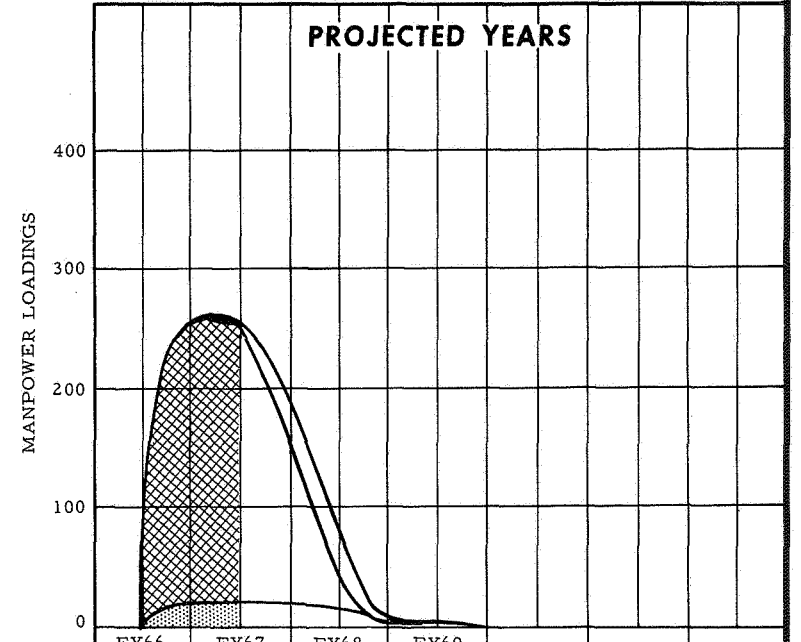
## DIRECT EQUIVALENT MANPOWER

### CURRENT FISCAL YEAR




| | JUL | AUG | SEP | OCT | NOV | DEC | JAN | FEB | MAR | APR | MAY | JUN |
|---|---|---|---|---|---|---|---|---|---|---|---|---|
| PLANNED | 240 | 245 | 249 | 252 | 254 | 255 | 243 | 235 | 233 | 222 | 212 | 199 |
| ACT./EST. | 267 | 276 | 265 | 281 | 260 | 280 | 239 | 261 | 246 | 219 | 195 | |
| CUM. PLANNED | 240 | 485 | 734 | 986 | 1240 | 1495 | 1738 | 1973 | 2206 | 2428 | 2640 | 2839 |
| CUM. ACT./EST. | 267 | 543 | 808 | 1089 | 1349 | 1629 | 1868 | 2129 | 2375 | 2594 | 2789 | |

### PROJECTED YEARS




| | | FY66 | | FY67 | | FY68 | | FY69 |
|---|---|---|---|---|---|---|---|---|
| PLANNED | | 255 | 249 | 193 | 83 | 9 | 6 | |
| ACT./EST. | | 255 | 253 | 216 | 83 | 9 | 6 | |
| CUM. PLANNED | | | | | | | | |
| CUM. ACT./EST. | | | | | | | | |

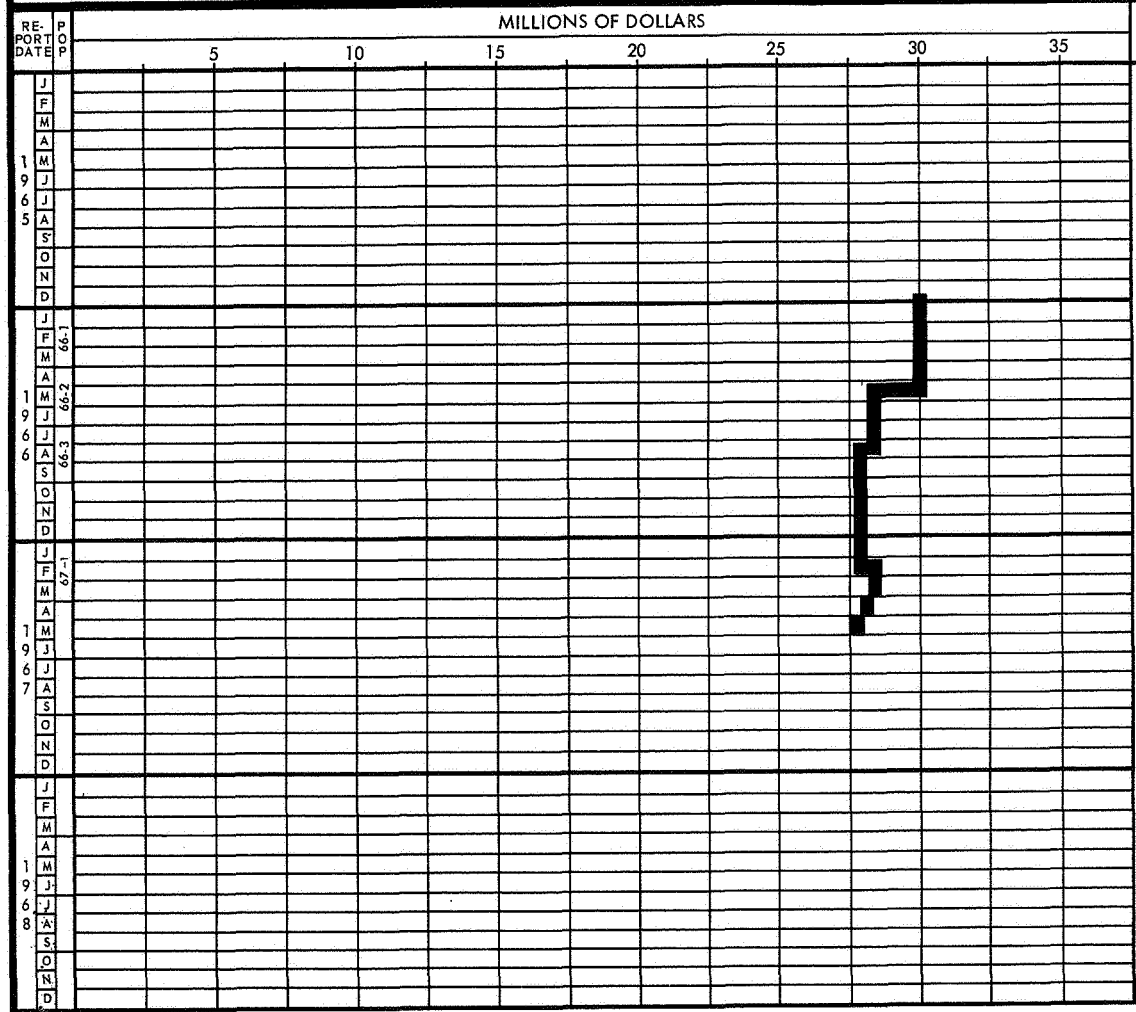
NOTES

JET PROPULSION LABORATORY
RESPONSIBILITY:
APPROVAL: A. R. LUEDECKE
ACCOMPLISHMENT: D. SCHNEIDERMAN

# COST TREND ANALYSIS
## *MARINER VENUS* 67 PROJECT

2 LEVEL

STATUS AS OF 12 JUN 67 (DATE/INITIALS)




REASON FOR PLANNED COST CHANGE

..... ESTIMATE BASED ON GUIDELINES AND PAST EXPERIENCE

..... ESTIMATE BASED ON ROUGH DIVISIONAL ESTIMATES AND COMBINED MARINER VENUS AND MARINER IV OPERATIONS

..... ESTIMATE BASED ON CURRENT DIVISIONAL DETAILED ESTIMATES TO COMPLETION

.....ESTIMATE BASED ON CURRENT ANALYSIS OF FY 67 COSTS VS WORK TO BE ACCOMPLISHED, WITH FUNDS ADDED FOR KSC AND HQ.

POP 67-1, AS APPROVED BY HQ.

REVISED ESTIMATE OF COST THROUGH COMPLETION BASED UPON CURRENT PROJECT STATUS.

NOTES:

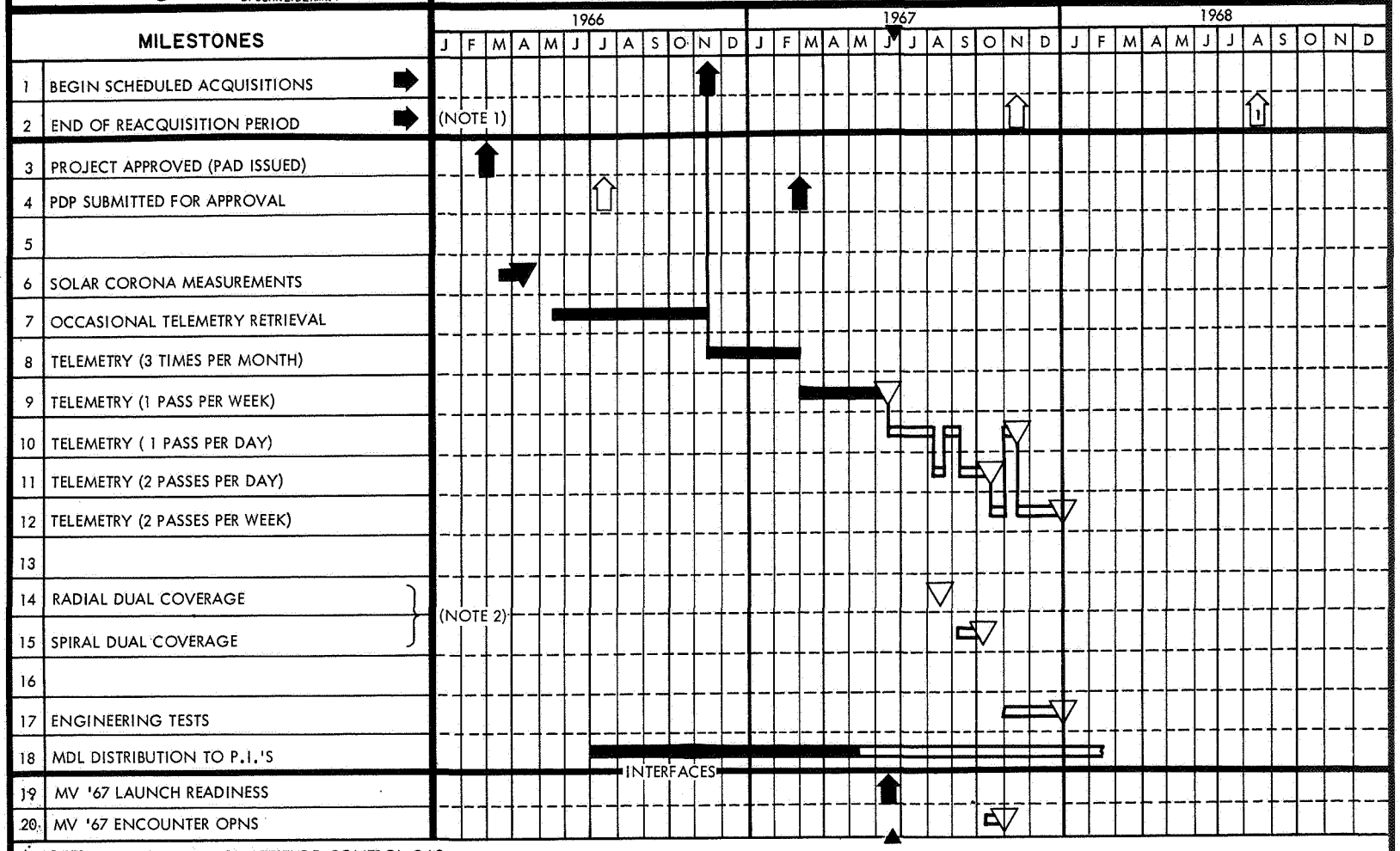
3 YEAR

**JET PROPULSION LABORATORY**
RESPONSIBILITY:
APPROVAL: A. R. LUEDECKE
ACCOMPLISHMENT: D. SCHNEIDERMAN

# MASTER SCHEDULE
## *MARINER IV* PROJECT

2 LEVEL

ORIGINAL SCHEDULE APPROVAL 1/7/66 (DATE)
LAST SCHEDULE CHANGE 1/23/67 (DATE) 1 (NO.) DS/DSL (INITIALS)
STATUS AS OF 6/12/67 (DATE) (INITIALS)




NOTES: (1) DEPLETION OF ATTITUDE-CONTROL GAS
(2) COMBINED MISSION WITH MV '67
(3) THE INDICATED TELEMETRY RECOVERY (LINE ITEMS 8-12) BASED ON HOLDING TO PLAN "A" OF THE 1/10/67 OSSA LEVEL 1 PROGRAM MANAGEMENT REPORT.

PAGE 13

JET PROPULSION LABORATORY
RESPONSIBILITY:
APPROVAL: A. R. LUEDECKE
ACCOMPLISHMENT: D. SCHNEIDERMAN

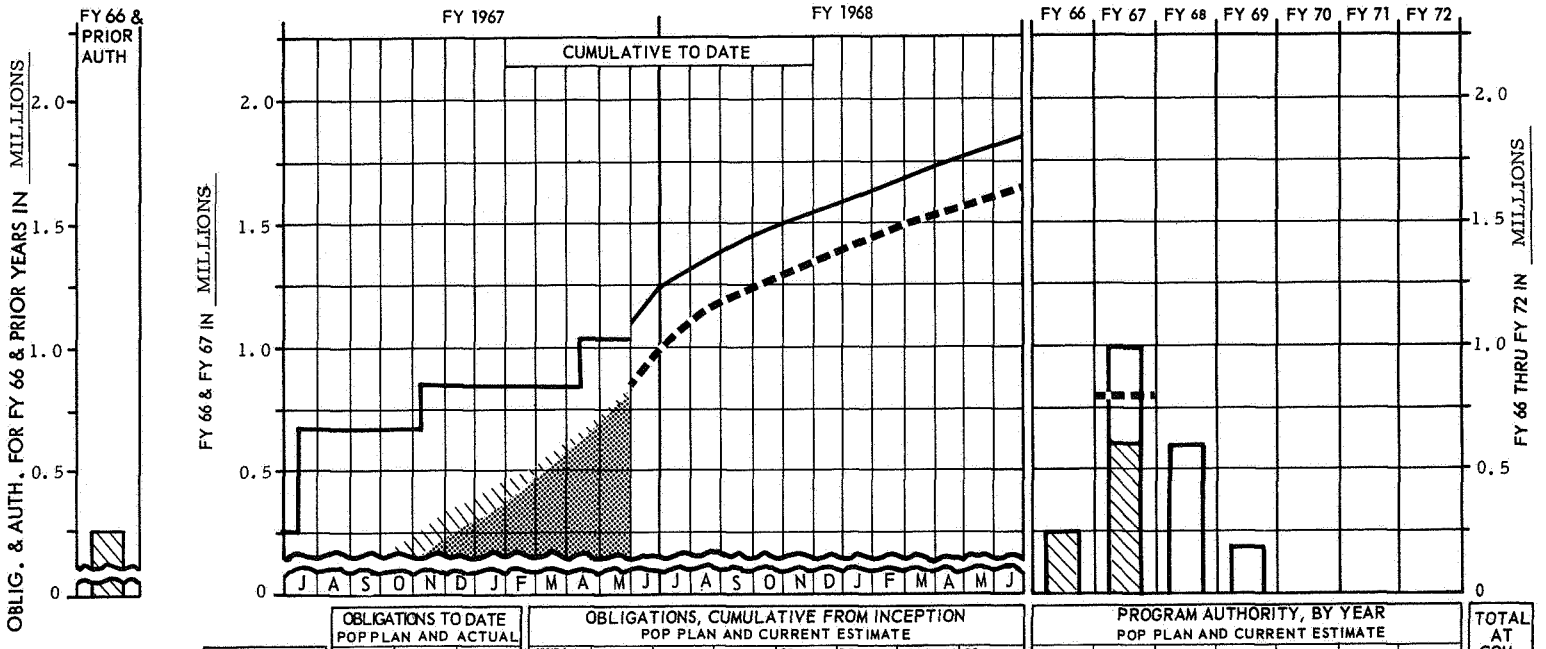
# PROJECT FINANCIAL STATUS

## *MARINER IV* PROJECT

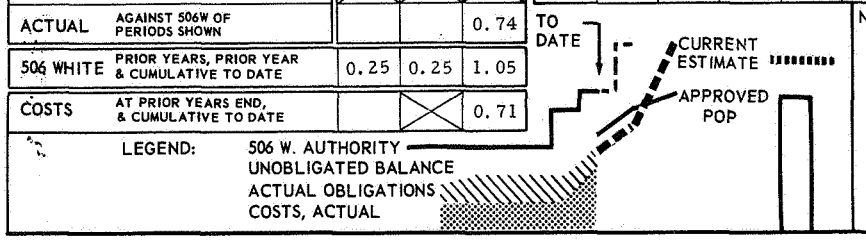
2 LEVEL

ACTUAL OBLIGATIONS AND COSTS AS OF 28 MAY 67 (DATE)

STATUS AS OF (DATE) 12 JUN 67 (INITIALS)




| FISCAL PERIODS | OBLIGATIONS TO DATE POP PLAN AND ACTUAL: FY 66 & PRIOR AUTH. | FY 66 AUTH. ONLY | CUM. TO DATE | OBLIGATIONS, CUMULATIVE FROM INCEPTION POP PLAN AND CURRENT ESTIMATE: 30 JUN FY 1967 | | | 30 SEP FY 1968 | 31 DEC FY 1968 | 31 MAR FY 1968 | 30 JUN FY 1968 | PROGRAM AUTHORITY, BY YEAR POP PLAN AND CURRENT ESTIMATE: FY 1966 | FY 1967 | FY 1968 | FY 1969 | FY 1970 | FY 1971 | FY 1972 | TOTAL AT COMPLETION |
|---|---|---|---|---|---|---|---|---|---|---|---|---|---|---|---|---|---|---|
| APPROVED POP 67-1 | | | 0.91 | 1.25 | | | 1.44 | 1.59 | 1.73 | 1.85 | 0.25 | 1.00 | 0.60 | 0.20 | | | | 2.05 |
| CURRENT ESTIMATE | | | | 1.05 | | | 1.24 | 1.39 | 1.53 | 1.65 | 0.25 | 0.80 | 0.60 | 0.20 | | | | 1.85 |
| ACTUAL AGAINST 506W OF PERIODS SHOWN | | | 0.74 | | | | | | | | | | | | | | | |
| 506 WHITE PRIOR YEARS, PRIOR YEAR & CUMULATIVE TO DATE | 0.25 | 0.25 | 1.05 | | | | | | | | | | | | | | | |
| COSTS AT PRIOR YEARS END, & CUMULATIVE TO DATE | | | 0.71 | | | | | | | | | | | | | | | |




NOTES

THE CURRENT ESTIMATE IS THE AMOUNT RECENTLY DISCUSSED WITH THE NASA HQ PROGRAM OFFICE.

PAGE 14

NARRATIVE

JET PROPULSION LABORATORY
RESPONSIBILITY:
APPROVAL: G. R. Luedecke G. R. LUEDECKE
ACCOMPLISHMENT: D. Schneiderman D. SCHNEIDERMAN

# MANPOWER

## *MARINER IV* PROJECT

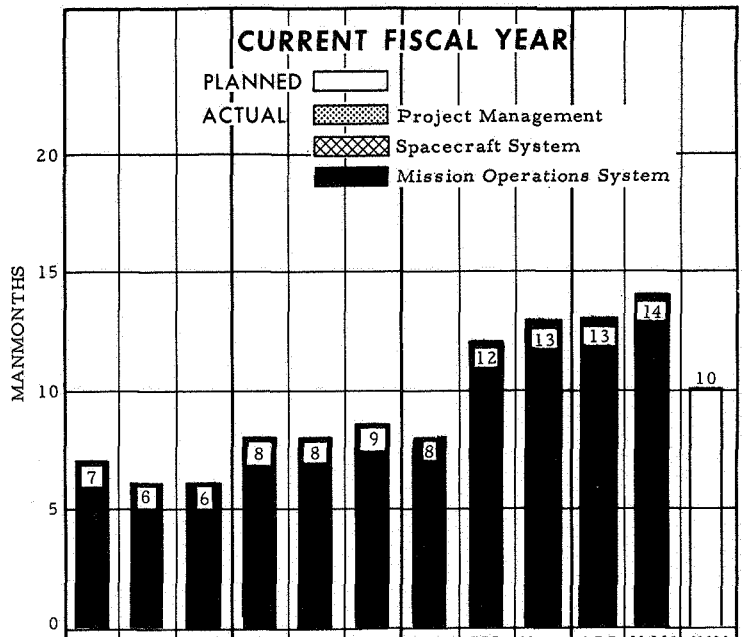
2 LEVEL

ORIGINAL SCHEDULE APPROVAL 2/25/66 (DATE)
LAST SCHEDULE CHANGE 10/30/66 (DATE) 2 (NO.) (INITIALS)
STATUS AS OF 12 JUN 67 (DATE) (INITIALS)

PERCENTAGE OVERTIME 10.8
(AVERAGE FOR REPORT PERIOD)

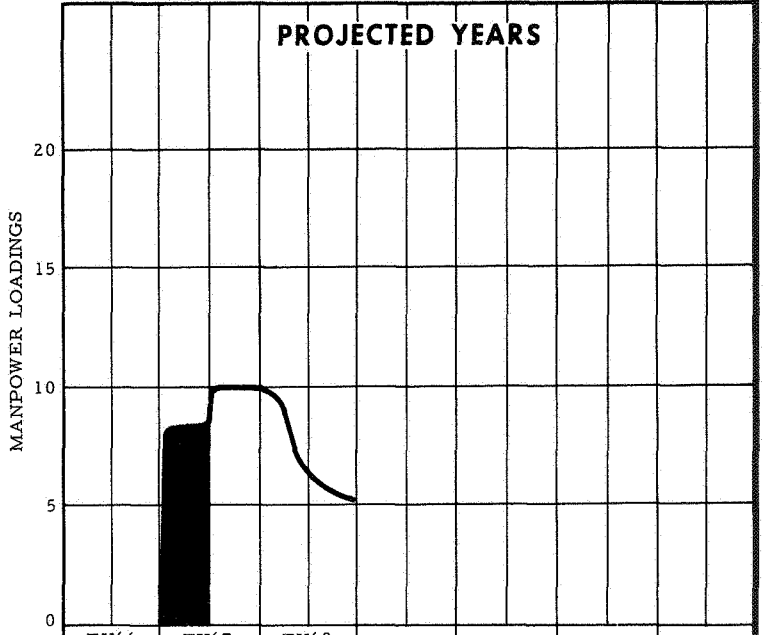
## DIRECT EQUIVALENT MANPOWER

### CURRENT FISCAL YEAR




| | JUL | AUG | SEP | OCT | NOV | DEC | JAN | FEB | MAR | APR | MAY | JUN |
|---|---|---|---|---|---|---|---|---|---|---|---|---|
| PLANNED | 8 | 8 | 8 | 8 | 8 | 8 | 10 | 10 | 10 | 10 | 10 | 10 |
| ACT./EST | 7 | 6 | 6 | 8 | 8 | 9 | 8 | 12 | 13 | 13 | 14 | |
| CUM. PLANNED | 8 | 16 | 24 | 32 | 40 | 48 | 58 | 68 | 78 | 88 | 98 | 108 |
| CUM. ACT./EST | 7 | 13 | 19 | 27 | 35 | 44 | 52 | 64 | 77 | 90 | 104 | |

### PROJECTED YEARS




| | FY66 | | FY67 | | FY68 | | | | | | | |
|---|---|---|---|---|---|---|---|---|---|---|---|---|
| PLANNED | | | 8 | 10 | 6 | | | | | | | |
| ACT./EST. | | | 8 | 14 | 6 | | | | | | | |
| CUM. PLANNED | | | | | | | | | | | | |
| CUM. ACT./EST. | | | | | | | | | | | | |

NOTES

# Appendix C

## *Mariner* Venus 67 Launch Constraints

UNCL

(CLASSIFICATION)

ADMINISTRATIVE MESSAGE CENTER — TELETYPE SERVICE REQUEST

☐ PRIORITY
☐ ROUTINE

☐ BOOK------ EACH ADDRESSEE SENT TEXT AS SEPARATE MESSAGE.
☒ MULTIPLE-- EACH ADDRESSEE SENT TEXT AND LIST OF OTHER ADDRESSEES.

ADDRESSEE(S)

H. W. Plohr
Agena Project Manager
Lewis Research Center
Cleveland, Ohio

S. C. Himmel
Lewis Research Center

E. H. Davison
Lewis Research Center

R. K. Hackbarth
Lewis Research Center

D. E. Forney
LeRC/FEB
c/o LMSC/SV

J. L. Shoenhair
LMSC/SV

J. Berggren
GDC/SD

R. H. Gray
KSC/ULO
USAFETR

G. A. Reiff
NASA HQS
Washington, DC

NOTE: REDUCE NUMBER OF WORDS TO MINIMUM NECESSARY FOR CLARITY.

JOB NO. 547-10204-1-2910

DATE March 23, 1966

TEXT:

Mar '67-91043 DS/ANW

Subject: Mariner Venus 1967 Launch Constraints

1. Launch period is tightly constrained by restrictions on aim point. These restrictions are dictated by many geometric considerations at encounter, by limitations on antenna degrees of freedom, and by science objectives. The dominant factor in establishing best launch day is RF occultation. Among mission objectives, this experiment is of primary importance. The opening day of the launch period is based on the quality of occultation data at encounter. Optimum antenna orientation at encounter changes each day. Each day the launch is delayed the quality of the occultation data degrades.

2. In order to maximize the value of the Venus 1967 mission I would like to launch on a preselected day early in the launch period. This does not mean that an extended launch period and a high probability of launching within that period are unimportant. Rather, it means that all mission planning, prelaunch operations, hard and software generation and checkout should be geared to a launch on a preselected date. At this time, the best date for planning purposes is June 12, 1967 GMT. However to ensure the necessary demonstrated launch capability on this date all systems within the Mariner Venus '67 Project shall have completed all launch readiness tests and be in a launch configuration by 10 June 1967. Having accomplished this objective we will wait until 12 June for the actual launch.

FROM: EXT.

JPL 1190-S AUG 64

(CLASSIFICATION)

UNCL
(CLASSIFICATION)

ADMINISTRATIVE MESSAGE CENTER — TELETYPE SERVICE REQUEST

☐ PRIORITY
☐ ROUTINE

☐ BOOK------ EACH ADDRESSEE SENT TEXT AS SEPARATE MESSAGE.
☐ MULTIPLE-- EACH ADDRESSEE SENT TEXT AND LIST OF OTHER ADDRESSEES.

ADDRESSEE(S)

NOTE: REDUCE NUMBER OF WORDS TO MINIMUM NECESSARY FOR CLARITY.

JOB NO. 547-10204-1-2910

DATE

TEXT:

3. This launch philosophy is tailored to the mission and to the ground rules within which the mission must be designed. As is apparent, it differs from Mariner Mars 1964. The difference is not due to having only one pad and one launch vehicle, but primarily is due to the greater mass of Venus and the correspondingly severe perturbations in the trajectory at encounter.

4. In consequence of these facts, planning by all elements of the Mariner Project should recognize the objective of readiness to launch with a high probability of success on the preselected date. I will appreciate your dedicated support of this launch-on-time objective.

Dan Schneiderman

D. Schneiderman
Mariner '67 Project Manager

DS/ANW:cjk
bc: J. N. James
J. McGee
H. J. Margraf
H. N. Levy, Jr.
T. H. Parker
J. Small
A. E. Wolfe
M. T. Goldfine
C. W. Snyder
J. Paulson
A. E. Conrad
A. N. Williams
D. W. Douglas
N. A. Renzetti

FROM: EXT.

JPL 1196-S AUG 64

(CLASSIFICATION)

PRECEDING PAGE BLANK NOT FILMED.

# Glossary

| | |
|---|---|
| AC | attitude control |
| ACV | amount of critical view |
| ADC | analog-to-digital converter |
| ADP | automatic data processing |
| AFETR | Air Force Eastern Test Range |
| AGC | automatic gain control |
| AGE | aerospace ground equipment |
| AO | auxiliary oscillator |
| APAC | antenna pointing angle change |
| APL | approved parts list |
| ATM | antenna test model |
| ATS | *Applications Technology Satellite* |
| BCD | binary-coded decimal |
| BECO | booster engine cutoff |
| BLH | Baldwin–Lima–Hamilton |
| B/R | booster-regulator |
| CAT | complimentary analysis teams |
| CC&S | central computer and sequencer |
| CCW | counterclockwise |
| CC3 | S-band phase-coherent counted (two-way) doppler |
| CDC | command data console |
| CDS | computer data system |
| C/E | control electronics |
| CKAFS | Cape Kennedy Air Force Station |
| CP | communications processor |
| CPV | Canopus probe near limb of Venus angle |
| CW | clockwise |
| D/AC | digital-to-analog converter |
| DAS | data automation system |
| DC-V | direct command—(*Mariner* Venus 67) |
| DDC | direct data channel |
| DE | data encoder |
| DEPD | Division Engineering Planning Document |
| DFR | dual-frequency receiver |
| DIS | data input subsystem |
| DN | data number |
| DPLF | data phone line formatter |
| DPPE | data processing project engineer |
| DPS | data processing system |
| DSIF | Deep Space Instrumentation Facility |
| DSN | Deep Space Network |
| DSS | Deep Space Station |
| DTM | developmental test model |
| *E* | encounter (+ time) |
| ECR | Engineering Change Requirement |
| EMC | electromagnetic compatibility |
| EMI | electromagnetic interference |
| EOT | end of tape |
| EP | electrical prototype |
| EPV | earth probe near limb of Venus angle |
| ESF | explosive safe facility |
| ETL | Environmental Test Laboratory |
| FA | flight acceptance |
| FET | field-effect transistor |
| FOV | field of view |
| FPAA | flight-path analysis area |
| FPAC | flight-path analysis and command |
| GCA | gyro control assembly |
| GCAT | guidance control analysis team |
| GCS | Ground Communications System |
| GD/C | General Dynamics/Convair |
| GE | General Electric Company |
| GMT | Greenwich Mean Time |
| GTS | ground telemetry system |
| HEPA | high-efficiency particulate air |
| HSDL | high-speed data line |
| HVC | high-voltage control |
| IBM | International Business Machines Corporation |
| IBSYS | International Business Machines System |
| IC | integrated circuit |
| IF | intermediate frequency |
| IGS | instrumentation ground system |
| I/O | input/output |
| IP | isolated pulse; input processor |
| IPP | input processor programs |
| IR | inspection report |
| IRV | interrange vector |
| IS | isolated step |

## Glossary (contd)

| | |
|---|---|
| J-FACT | joint flight acceptance composite test |
| JVA | jet vane actuators |
| KSC | Kennedy Space Center |
| *L* | launch (+ time) |
| LaRC | Langley Research Center |
| LASL | Los Alamos Scientific Laboratory |
| LCE | launch complex equipment |
| LeRC | Lewis Research Center |
| LMSC | Lockheed Missile and Space Center |
| LPA | launch phase mission analyst |
| L&PP | Lunar and Planetary Programs |
| MAR | mission analysis representative |
| MC | midcourse |
| MDL | master data library |
| MIED | mission-independent editor |
| MOS | Mission Operations System |
| MRB | material review board |
| MRH | mission related hardware |
| MRS | mission related software |
| MSA | mission support area |
| MSFN | Manned Space Flight Network |
| MSP | mission support program |
| MT | master timer |
| NAMG | narrow-angle Mars gate |
| NASCOM | NASA Communications Network |
| NCV | normalized critical view |
| NMI | NASA Management Instruction |
| ODG | orbit data generator |
| ODP | Orbit Determination Program |
| OGO | *Orbiting Geophysical Observatory* |
| ORT | operational readiness tests |
| OSE | operational support equipment |
| OSSA | Office of Space Science and Applications |
| PAG | parts acquisition group |
| PAS | pyro arming switch |
| PCA | pyrotechnics control assembly |
| PCE | power conditioning equipment |
| PDP | project development plan |
| PERT | Program Evaluation and Review Technique |
| PFR | Problem Failure Report |
| PIPS | post-injection propulsion system |
| PIV | propellant isolation valve |
| PMR | Project Management Reports |
| PN | pseudo-noise |
| PNG | pseudo-noise generator |
| PO | post orbit |
| PPL | Preferred Parts List |
| PQA | parts quality assurance |
| PRP | pseudo-random pulse |
| PS&L | power switching and logic |
| PSO | planet sensor output |
| PTM | proof test model |
| QA | quality assurance |
| QAI | quality assurance instructions |
| QC | quantitative command |
| RF | radio frequency |
| RFI | radio frequency interference |
| RFP | request for programming |
| RSS | radio subsystem |
| RTCS | real-time computer system |
| RWV | read-write-verify |
| S | separation (+ time) |
| SAF | spacecraft assembly facility |
| SC | spacecraft |
| SDCC | simulated data conversion center |
| SDS | Scientific Data Systems, Inc. |
| SECO | sustainer engine cutoff |
| SFO | Space Flight Operations |
| SFOD | Space Flight Operations Director |
| SFOF | Space Flight Operations Facility |
| SIRD | support instrumentation requirements document |
| SIT | separation initiated timer |
| SLV | Saturn launch vehicle |
| SMIT | simulated midcourse intersection test |
| SN | serial number |
| SPAC | spacecraft performance analysis and command |

## Glossary (contd)

| | |
|---|---|
| SPE | static phase error |
| SPV | sun probe near limb of Venus angle |
| SS | sun sensor |
| SSAC | space science analysis and command |
| STC | System Test Complex |
| STCDS | System Test Complex Data System |
| STET | system test experimenter tape |
| STM | structural test model |
| STP | standard temperature and pressure |
| STS | spacecraft telecommunications system |
| sync | synchronous; synchronizer; synchronization |
| TA | type approval |
| TCM | thermal control model |
| TCP | telemetry and command processor |
| TCR | temperature control reference |
| T&DA | tracking and data acquisition |
| TDP | tracking data processor |
| TDS | tracking data system |
| TE | trajectory engineer |
| TIM | Tracking Instruction Manual |
| TM | telemetry |
| TPS | telemetry processing station |
| TRD | trapped radiation detector |
| TRS | tape recorder subsystem |
| TSO | terminator sensor output |
| TSP | telemetry simulation program |
| TTY | teletype |
| TVCA | thrust vector control assembly |
| TWT | traveling wave tube |
| TWTA | traveling wave tube amplifier |
| ULO | unmanned launch operations |
| USR | user service request |
| UV | ultraviolet |
| VAC | volts ac |
| VCO | voltage-controlled oscillator |
| VECO | vernier engine cutoff |
| VHF | very high frequency |
| VSWR | voltage standing-wave ratio |
| wpm | words per minute |
| XTM | experimental test model |

### Computer Programs

| | |
|---|---|
| **AGCM** | automatic gain control calibration |
| **ATTREF** | attitude reference |
| **CPPM** | communication prediction |
| **EDPLOT** | engineering data plotting |
| **FLYBY** | flyby fine print |
| **MC1M** | midcourse maneuver |
| **POWM** | powered flight |
| **PRDX** | predicts |
| **ODGA** | orbit data generator |
| **ODPA** | orbit determination |
| **SIPM** | star identification |
| **SSDM** | systems suppressed data |
| **TDPA** | tracking data processor |
| **TJ1M** | trajectory |
| **XRPM** | experimenter's data reformatting |
| **XRPT** | experimenter's data reformatting program for system test data |

### Orbit Identifications

| | |
|---|---|
| DACO | data consistency |
| GLPR | Goldstone predict |
| ICEV | initial condition evaluation |
| LAMC | last maneuver calculation |
| LAPM | last premidcourse |
| MDPR | Madrid predicts |
| NOMA | nominal maneuver |
| POST | postmidcourse |
| PREL | preliminary evaluation |
| PROR | predict |
| X, Y | computer strings |

PRECEDING PAGE BLANK NOT FILMED.

## References


1. *Mariner Mars 1964 Project Report: Mission and Spacecraft Development, Vol. I. From Project Inception Through Midcourse Maneuver,* Technical Report 32-740. Jet Propulsion Laboratory, Pasadena, Calif., Mar. 1, 1965.
2. Luce, R., and Raiffa, H., *Games and Decisions,* John Wiley & Sons, London, 1957.
3. McKinsey, John C., *Introduction to the Theory of Games,* McGraw-Hill Book Co., Inc., New York, 1952.
4. *Voyager Planetary Quarantine Studies—Phase 1A, Task B,* Document D2-82733-2. The Boeing Company, Seattle, Wash., Aug. 1966.
5. *Voyager Phase 1A, Task C, Bi-Monthly Report 5,* Document Voy-CO-PR5. General Electric Company, Missiles and Space Div., Valley Forge, Pa., Feb. 1967.
6. *Mariner Mars 1964 Project Report: Spacecraft Performance and Analysis,* Technical Report 32-882. Jet Propulsion Laboratory, Pasadena, Calif., Feb. 15, 1967.
7. Schutz, F. L., et al, *Mariner-Mars Science Subsystem,* Technical Report 32-813, Jet Propulsion Laboratory, Pasadena, Calif., Aug. 15, 1966.
8. Koehler, R. L., *A Phase-Locked Dual Channel Spacecraft Receiver for Phase and Group Path Measurements,* Final Report SU-SEL-65-007. Stanford University, Stanford, Calif., Feb. 1965.
9. Eshleman, V. R., et al., "The Interplanetary Electron Number Density from Preliminary Analysis of the Pioneer 6 Radio Propagation Experiment," *J. Geophys. Res.,* Vol. 71, No. 13, July 1, 1966.
10. Nixon, Robert H., *Bipolar Analog-to-Pulse-Width Converter,* Technical Report 32-1034. Jet Propulsion Laboratory, Pasadena, Calif., Jan. 15, 1967.
11. *Space Exploration Programs and Space Sciences,* Space Programs Summary 37-23, Vol. VI. Jet Propulsion Laboratory, Pasadena, Calif., Oct. 31, 1963.
12. Schmuecker, J. D., and Spehalski, R. J., *Mariner Mars 1964 Basic Structure, Design and Development,* Technical Report 32-953. Jet Propulsion Laboratory, Pasadena, Calif., May 1, 1967.
13. Freeland, R. E., *Mariner Venus 67 Structural Developmental and Qualification Vibration Test Report,* Technical Report 32-1161. Jet Propulsion Laboratory, Pasadena, Calif., Nov. 1, 1967.
14. Keeler, Louis H., Nalbandian, Andrew J., and Olbeter, Albert A., *A Sensitive S-Band Noise Receiver Developed for the Mariner Mars 1964 Spacecraft Program,* Technical Report 32-1029. Jet Propulsion Laboratory, Pasadena, Calif., Nov. 15, 1966.
15. *Standard Procedures for the Microbiological Examination of Space Hardware,* NHB 5340.1. National Aeronautics and Space Administration, Washington, D.C., Aug. 1967.

## References (contd)

16. *Mariner Venus 1967, Launch Contingency Planning Study,* LMSC/A858101, Change Order 22. Mar. 17, 1967. Lockheed Missiles and Space Company, Sunnyvale, Calif., Mar. 17, 1967. Also available as NAS 3-8982.

17. *Mariner Venus 1967, Contingency Planning Study,* GD/C Report AA67-0004, General Dynamics Corp., Convair Div., San Diego, Calif. (un-dated).

18. *Mariner Venus 67, Contingency Planning Study,* Document GE 67E007, General Electric Co., Defense Electronics Div., Utica, N.Y., May 24, 1967.

19. *Mariner Venus 67, Contingency Planning Study,* No. 8607-67-410, Burroughs Corp., Detroit, Mich., May 12, 1967.